

CHEMICAL ANALYSIS

A SERIES OF MONOGRAPHS ON
ANALYTICAL CHEMISTRY AND ITS APPLICATIONS

Editors

P. J. ELVING, J. D. WINEFORDNER

Editor Emeritus: I. M. KOITHOFF

Advisory Board

Fred W. Billmeyer, Jr.

Eli Grushka

Barry L. Karger

Vivian Krizan

Victor G. Mossetti

A. Lee Smith

Bernard Tremillon

T. S. West

VOLUME 19

A WILEY-INTERSCIENCE PUBLICATION

JOHN WILEY & SONS

New York • Chichester • Brisbane • Toronto • Singapore

Thermal Analysis

THIRD EDITION

WESLEY WM. WENDLANDT

Department of Chemistry
University of Houston
Houston, Texas



A WILEY-INTERSCIENCE PUBLICATION

JOHN WILEY & SONS

New York • Chichester • Brisbane • Toronto • Singapore

...	518 096
	11111
	3 ed.
TCMBO 6820	

To my wife

Copyright © 1964, 1974, 1986 by John Wiley & Sons, Inc.

All rights reserved. Published simultaneously in Canada.

Reproduction or translation of any part of this work beyond that permitted by Section 107 or 109 of the 1976 United States Copyright Act without the permission of the copyright owner is unlawful. Requests for permission or further information should be addressed to the Permissions Department, John Wiley & Sons, Inc.

Library of Congress Cataloging in Publication Data

Wendlandt, Wesley William.
Thermal analysis

(Chemical analysis, 0069-2883; v. 19
..A Wiley-Interscience publication.)
Includes bibliographies and index.

1. Thermal analysis. I. Title. II. Series.

QD79T38W45 1985 543'086 85-12419
ISBN 0-471-88477-4

Printed in the United States of America

10 9 8 7 6 5 4 3

PREFACE

The primary goal of this book, as described in the preface to the second edition, is to serve as a *general* introduction to the field of thermal analysis. Due to the voluminous papers published during the past 10 years, it is not possible to make the book *comprehensive* for each technique. Indeed, separate volumes could easily be written on each one discussed here. Some degree of critical evaluation has been added, especially in chapters such as those on reaction kinetics, purity determination, and instrumentation.

Thermal analysis techniques have been applied to almost every science area, from archaeology to zoology, and to every type of substance, from alabaster to zeolites. Indeed, it is difficult to find an area of science and technology in which the techniques have not been applied. This truly universal use of thermal analysis is consistent with its early history in, for example, clays, mineralogy, metallurgy, and inorganic substances.

The main changes in this edition are as follows: (1) Numerous new applications of thermal analysis techniques have been added to the chapters on TG, DTA, DSC, EGD/EGA, and others. (2) Other techniques, not used as often, are described in greater detail, such as EGD/EGA, TMA, DMA, thermopometry, thermoelectrometry, thermosonimetry, and others. (3) The chapter on EGD/EGA has been rewritten, as has the chapter on miscellaneous techniques. (4) The determination of purity by DSC has been rewritten. (5) Commercially available instruments have been briefly described for each technique, including the application of microcomputers to many of these instruments.

It is a pleasure to acknowledge the generosity of the many individuals who sent me copies of their reprints in thermal analysis, particularly the Editorial Board members of *Thermochimica Acta*, also, the encouragement and assistance of the late Professor P. J. Elving, Professor I. M. Winefordner, and Mr. James L. Smith are much appreciated. The continued research support of the Robert A. Welch Foundation, Houston, Texas, is also acknowledged. The skilled typing of Miss Dieu-Hanh Nghiem Tran made possible the preparation of this manuscript.

WESLEY WM. WENDLANDT

Houston, Texas
December, 1985

PREFACE TO THE FIRST EDITION

The purpose of this monograph is to acquaint chemists and other investigators with the relatively new series of instrumental techniques which are broadly classified as "thermal methods." In the past, many of these techniques involved tedious, time-consuming, manual recording methods; however, all of them are now completely automatic and employ either analog (recorder) or digital readout devices. Thus, due to automation, the instruments become capable of self-operation, improving both the accuracy and precision of the measurements as well as relinquishing both the investigator's time and patience.

These thermal methods provide a new means of solving existing chemical problems, as well as creating new ones. It is difficult for the author to think of a modern chemical laboratory without a thermobalance or differential thermal analysis apparatus. The former instrument can provide rapid information concerning the thermal stability, composition of pyrolysis intermediates, and composition of the final product, as a compound is heated to elevated temperatures. The latter apparatus can provide information concerning the enthalpy changes occurring during thermal decomposition of the compound, as well as the detection of phase transitions of various types. Both techniques yield a wealth of information in a very short period of time.

This book is not intended to be a comprehensive survey of the literature on each thermal technique. Rather, it is a critical review, as far as space permits, on each method. It is felt that the investigator should be well informed on both the *advantages* and *limitations* of each thermal technique in order to use these techniques intelligently. It must be admitted that this book is written primarily for the analytical chemist, although the techniques are useful in other fields of investigation as well.

The author would like to acknowledge his gratitude to Professors P. I. Elving and I. M. Kolthoff for their helpful advice and guidance during the preparation of the manuscript, to helpful comments from his former colleague, Dr. Edward Sturm; to Professor J. Jordan and S. T. Zenchelsky for supplying him with their personal reprints; to Mr. Irwin Dosch and Dr. Robert L. Stone for their assistance in supplying several of the badly needed

photographs; and to his present and former students who made this work possible in the first place.

Also, the author would like to express his indebtedness to the Division of Research, U.S. Atomic Energy Commission; the Air Force Office of Scientific Research, U.S. Air Force; and to the Robert A. Welch Foundation, for their continual support of the author's work in this field.

And finally, because of their efforts above and beyond the call of duty, the author would like to acknowledge with thanks his typists, Miss Sallie Hardin, Miss Sue Richmond, and Miss Kathryn White.

WESLEY WM. WENDLANDT

Lubbock, Texas
January, 1964

CONTENTS

1. GENERAL INTRODUCTION	
2. THERMOGRAVIMETRY	9
A. Introduction,	9
B. Same Factors Affecting Thermogravimetric Curves.	12
1. Instrumental (Thermobalance) Factors,	13
a. Heating Rate,	13
b. Recording or Chart Speed,	17
c. Effect of Furnace Atmosphere,	18
d. Sample Holder,	25
e. Conditions for Optimum Sensitivity,	32
2. Sample Characteristics,	33
a. Sample Mass,	33
b. Sample Particle Size,	35
c. Miscellaneous Sample Effects.	37
C. Sources of Error in Thermogravimetry,	38
1. Sample-container Buoyancy,	38
2. Furnace Convection Currents and Turbulence,	41
3. Temperature Measurement,	41
4. Other Errors,	46
D. Self-Generated Atmosphere Thermogravimetry,	46
E. Derivative Thermogravimetry (DTG),	52
1. Separation of Overlapping Reactions,	54
2. "Fingerprinting" Materials,	55
3. Calculation of Mass Changes in Overlapping Reactions,	55
4. Quantitative Analysis by Peak Height Measurement,	55
F. Reaction Kinetics,	57
i. Nonisothermal Methods,	57
a. Newkirk Method,	60
b. Freeman and Carroll Method.	61
c. Horowitz and Metzger Method.	61

- d. Coats and Redfern Method, 61
- e. Doyle Method, 62
- f. Ingraham and Marier Method, 64
- g. Vachuska and Voboril Method, 64
- h. Master Data Method, 65
- i. Steady-State Parameter Jump Method, 66
- j. Reich and Stivala Method, 67
- k. Ozawa Method, 68
- J. Miscellaneous Methods, 70
- 2. Comparison of Different Methods, 71
- 3. Mechanism of Reaction from Nonisothermal Kinetics, 79
- 4. Critique, 80

References, 82

3. THERMOBALANCES AND ACCESSORY EQUIPMENT 87

- A. Introduction. 87
 - 1. Recording Balances, 89
 - 2. Cahn Electrobalances, 92
 - 3. Sample Holders. 93
 - 4. Furnaces and Furnace Temperature Programmers. 99
 - 5. Temperature Detection and Recording Systems. 99
- B. Thermobalances. 109
 - 1. Introduction. 109
 - 2. Du Pont Thennobalance, 112
 - 3. Derivatograph, 113
 - 4. Mettler Thermobalances. 114
 - 5. Perkin-Elmer Thennobalance. 118
 - 6. Stanton Redcroft Thennobalances, 119
 - 7. Rigaku Thennobalances, 121
 - 8. SETARAM Thermobalances. 123
- C. Miscellaneous Thermobalances. 125
 - 1. Quartz Balances. 126
 - 2. Automated Thermobalances. 127
 - 3. High-Pressure Thermobalances. 130
 - 4. Thermomolecular Beam Analysis. 131
 - 5. Vapor-pressure Methods Using a Thermobalance. 133
 - 6. Miscellaneous, 134

References. 134

4. APPLICATIONS OF THERMOGRAVIMETRY 137

- A. Introduction, 137
- B. Applications to Catalysis, 138
- C. Applications to Clays and Minerals, 139
- D. Applications to fuels, 143
 - 1. Coal, 143
 - 2. Oil Shale, 144
 - 3. Miscellaneous. 146
- E. Applications to Inorganic Materials, 147
 - 1. Alkaline Earth Halide Hydrates, 147
 - 2. Alkaline Earth Oxalates. 148
 - 3. Aluminum Oxide Precipitates, 151
 - 4. Alumina Whiskers, 152
 - 5. Ammonium Dichromate. 154
 - 6. Calcium Chromate, 156
 - 7. Calcium Silicate Hydrates. 158
 - 8. Copper (II) Acetate, 160
 - 9. Copper (II) Chloroacetates, 161
 - 10. Copper (II) and Cobalt (II) Tartrates, 163
 - II. Complexes. 164
 - a. $[\text{Pt}(\text{NH}_3)_4]\text{Cl}_2 \cdot \text{H}_2\text{O}$. 164
 - b. $\text{K}_2\text{Pt}(\text{CN})_4\text{Br}_2$, 165
 - c. $[\text{Co}(\text{NH}_3)_5\text{Cl}]\text{Cl}_2$ and $[\text{Co}(\text{NH}_3)_5\text{Br}]\text{Br}_2$, 166
 - d. Miscellaneous. 167
 - 12. Diamonds, 168
 - 13. Egyptian Blue. 168
 - 14. Mercury (I. II) Compounds. 170
 - 15. Nickel (II) Sulfide, 173
 - 16. Niobium Nitride, 175
 - 17. Potassium Permanganate, 176
 - 18. Potassium Hydrogen Phthalate, 177
 - 19. Basic Potassium Aluminum Sulfate, 178
 - 20. Platinum Group Oxides. 179
 - 21. Sodium Carbonate. 181
 - 22. Titanium Carbide, 184
- F. Applications to Pharmaceuticals, 184
 - 1. Analgesics, 184
 - 2. Antacids. 186
 - 3. Determination of Composition. 187
 - 4. Moisture Determination. 190
 - 5. Sulfa Drugs, 191

G.	Applications to Polymeric Materials, 191	
1.	Introduction, 191	
2.	Relative Thermal Stability, 193	
3.	Additive Content, 195	
4.	Composition of Polymer Blends and Copolymers, 199	
5.	Miscellaneous, 199	
H.	Miscellaneous Applications, 200	
1.	Analytical Applications, 200	
2.	Automatic Gravimetric Analysis, 201	
3.	Drying of Analytical Precipitates, 204	
4.	Applications to Vapor-pressure Determination, 205	
5.	Miscellaneous, 207	
	References, 208	
5.	DIFFERENTIAL THERMAL ANALYSIS AND DIFFERENTIAL SCANNING CALORIMETRY	213
A.	Basic Principles of DTA/DSC, 213	
1.	Introduction, 213	
2.	Historical Aspects, 216	
3.	Theoretical Aspects, 216	
4.	Factors Affecting the DTA/DSC Curve, 227	
a.	Heating Rate, 228	
b.	Furnace Atmosphere, 232	
c.	Sample Holders, 241	
d.	Thermocouples, 249	
e.	Thermocouple Location, 252	
5.	Sample Characteristics, 258	
a.	Sample Mass, 258	
b.	Sample-particle Size and Packing, 259	
c.	Effect of Diluent, 263	
6.	Critique of Operational Parameters, 264	
7.	Differences Between DTA and DSC, 266	
B.	Quantitative Aspects, 269	
1.	Introduction, 269	
2.	Calibration, 270	
3.	Calibration Standards, 276	
4.	Calculation of Enthalpy Changes, 278	
5.	Other Factors, 279	
6.	Precision and Accuracy of ΔH Measurements, 280	
C.	Reaction Kinetics, 282	
	References, 293	

6.	DIFFERENTIAL THERMAL ANALYSIS AND DIFFERENTIAL SCANNING CALORIMETRY INSTRUMENTATION	299
A.	Instrumentation Principles, 299	
1.	Introduction, 299	
2.	Sample Holders, 299	
3.	ΔT and T Detection, 305	
4.	T-Axis Calibration, 309	
5.	Furnaces and Temperature Programmers, 312	
6.	Low-level Voltage Amplifiers and Recorders, 319	
S.	DSC-DTA Instruments, 320	
1.	Introduction, 320	
2.	Sealed-tube Techniques, 320	
3.	High-pressure Systems, 325	
4.	High-temperature Systems, 329	
5.	Micro-sample Instruments, 332	
6.	Automation of DTA Instrumentation, 333	
7.	Differential Scanning Calorimetry with Reflected Light Measurement, 336	
8.	Multiple Sample Digital DTA Apparatus, 337	
9.	Miscellaneous Instruments, 338	
C.	Commercial Instruments, 345	
1.	Perkin-Elmer, 345	
a.	DSC-2C, DSC-4, and DSC7 Instruments, 345	
b.	OTA 1700 System, 347	
2.	Du Pont, 349	
3.	Mettler, 349	
4.	Stanton Redcroft, 351	
5.	SETARAM, 352	
6.	Netzsch, 353	
7.	Sinku Riko, 353	
8.	Eberbach, 353	
	References, 353	
7.	APPLICATIONS OF DIFFERENTIAL THERMAL ANALYSIS AND DIFFERENTIAL SCANNING CALORIMETRY	359
A.	Introduction, 359	
B.	Applications to Biological Materials, 363	
C.	Applications to Catalysts, 369	

D.	Applications to Clays and Minerals, 373	
E.	Applications to Fuels, 381	
F.	Applications to Inorganic Materials, 388	
G.	Applications to Organic Materials, 406	
H.	Applications to Pharmaceuticals, 419	
1.	Applications to Polymers, 424	
J.	Miscellaneous Applications, 442	
K.	References, 452	
8.	EVOLVED GAS DETECTION AND EVOLVED GAS ANALYSIS	461
A.	Introduction, 461	
B.	Definition of EGO and EGA, 461	
C.	Role of EGD-EGA in Thermal Analysis, 463	
D.	Historical Review, 465	
E.	Current EGO-EGA Techniques, 470	
F.	Intermittent and Continuous Sampling Modes, 474	
1.	Trapping, 475	
2.	Combined Intermittent and Continuous Modes, 475	
G.	Coupling with TG Technique, 477	
1.	TG-Photometric Analysis, 477	
2.	TG-TCD, 478	
3.	TG-GC, 478	
4.	TG-MS, 482	
H.	Coupling with DTA Technique, 489	
1.	DTA-TCD, 489	
2.	DTA-ETA, 489	
3.	DTA-GC, 490	
4.	DTA-MS, 490	
1.	Instrumentation and Measurement Parameters, 493	
1.	Typical EGO-EGA Apparatus, 493	
2.	Detectors, 494	
3.	Measurement Parameters, 495	
a.	Effect of Instrument Parameters on EGD Curves, 495	
b.	Effect of Operating Parameters On P-T and V-I Curves, 498	
c.	Baseline Stability, 499	
d.	Resolution of EGA Curve Peaks, 499	
e.	Temperature Calibration in EGD, 500	
1.	Other EGD-EGA Techniques, 501	

1.	DTGA, 501	
2.	Temperature Programmed Reduction (TPR), 503	
3.	Automatic EGD Apparatus, 504	
4.	EGA-MS, 508	
5.	Detection of Water Evolution, 509	
6.	Pyrolysis- Gas Chromatography, 510	
7.	Flame Ionization Detection, 512	
8.	Thin-Layer Chromatography, 514	
9.	Thermoparticulate Analysis, 515	
10.	Organic Particulate Analysis, 517	
11.	Titrimetric Methods, 518	
12.	Infrared Spectroscopy, 519	
13.	EGO Measurements at Subambient Pressures, 520	
14.	Emanation Thermal Analysis (ETA), 524	
a.	Introduction, 524	
b.	Instrumentation, 525	
c.	Applications, 530	
K.	Applications of EGD-EGA, 533	
	References, 552	
9.	THERMOPHOTOMETRY	559
A.	High-temperature Reflectance Spectroscopy and Dynamic Reflectance Spectroscopy, 559	
1.	Introduction, 559	
2.	High-temperature Reflectance Spectroscopy, 562	
3.	Instrumentation, 563	
4.	Applications of HTRS and DRS to Inorganic Compounds, 568	
a.	The Octahedral \rightarrow Tetrahedral Transition in $\text{Co}(\text{py})_2\text{Cl}_2$, 568	
b.	$[\text{Cu}(\text{en})(\text{H}_2\text{O})_2]\text{SO}_4$, 570	
c.	$\text{CuSO}_4 \cdot 5\text{H}_2\text{O}$, 573	
d.	$\text{CoCl}_2 \cdot 6\text{H}_2\text{O}$, 575	
e.	$\text{Ni}(\text{py})_4\text{Cl}_2$, 577	
f.	Thermochromism of $\text{Ag}_2[\text{HgI}_4]$, 577	
g.	Thermal Matrix Reaction, 580	
B.	Photometric Methods, 581	
C.	High-Temperature Infrared Spectroscopy, 583	
D.	Thermal Optical Microscopy Techniques, 584	
1.	Fusion Microscopy, 584	
2.	Depolarized Light Intensity and Photometric	

	Thermal Microscopy, 590	
E.	Thermoluminescence.. 596	
1.	Introduction, 596	
2.	The TL Process. 597	
3.	Kinetics of TL, 598	
4.	Instrumentation. 600	
5.	Applications. 602	
a.	Archaeological Dating, 607	
b.	Measurement of Ionizing Radiation. 609	
F.	Oxyluminescence, 610	
1.	Introduction, 610	
2.	Intensity and Spectral Distribution. 611	
3.	Mechanism of the OL Process. 612	
4.	Kinetics of Oxyluminescence. 615	
5.	Oxyluminescence in Polymer Stabilizer Studies, 616	
6.	Instrumentation, 618	
7.	Application of OL to Polymers. 620	
	References, 622	
10.	CRYOSCOPIC AND DIFFERENTIAL SCANNING CALORIMETRY PURITY DETERMINATION	627
A.	Cryoscopic Methods, 627	
1.	Introduction, 627	
2.	Theory, 629	
3.	Experimental Techniques, 635	
4.	Errors, Limitations, and Other Factors Affecting Results. 639	
a.	Limitations of the Dynamic Method. 640	
b.	Limitations of Static Method, 642	
c.	Comparison of Results Obtained by the Static and Dynamic Methods, 643	
d.	Recommendations, 644	
5.	Applications to Impurity Determinations and Other Problems, 645	
B.	Differential Scanning Calorimetry Methods. 651	
1.	Introduction. 650	
2.	Principles of Measurement, 653	
3.	The DSC Curve, 656	
4.	Thermal Lag and Undetermined Premelting, 658	
5.	Experimental Measurements, 662	
6.	Applications. 664	
7.	Assessment, 666	
	References. 668	

11.	MISCELLANEOUS THERMAL ANALYSIS TECHNIQUES	671
A.	Introduction, 671	
B.	Thermomechanical Methods, 671	
1.	Introduction, 671	
2.	Instrumentation, 673	
a.	TDA and TMA, 673	
b.	DMA, 678	
3.	Torsional Braid Analysis. 681	
4.	Applications. 682	
a.	TDA, 682	
b.	TMA, 686	
c.	DMA, 692	
C.	Thermoelectrometry, 697	
1.	Introduction, 691	
2.	Electrical Conductance., Current, and Resistance. 698	
3.	Dielectric Constant, 718	
a.	Instrumentation, 120	
b.	Applications, 724	
4.	Miscellaneous Electrical Techniques, 727	
a.	Current-Voltage, 727	
b.	Thermally Stimulated Discharge (TSD), 728	
c.	Current-Temperature and Voltage - Temperature, 728	
d.	Applied Electrical Fields, 133	
D.	Thermosonimetry, 134	
1.	Introduction, 734	
2.	Instrumentation, 734	
3.	Applications. 736	
E.	Thermomagnetometry, 740	
1.	Introduction, 740	
2.	Instrumentation, 740	
3.	Applications, 740	
F.	Accelerating Rate Calorimetry, 747	
1.	Introduction, 747	
2.	Instrumentation, 748	
3.	Theory, 751	
4.	Applications, 753	
G.	SEDEX System, 755	
1.	Introduction. 755	
2.	Instrumentation, 756	
3.	Theory and Applications. 758	
	References. 759	

12. THE APPLICATION OF DIGITAL AND ANALOG COMPUTERS TO THERMAL ANALYSIS,	765
A. Introduction. 765	
B. Thermogravimetry (TG). 765	
C. Differential Thermal Analysis (DTA) and Differential Scanning Calorimetry (DSC), 779	
D. Miscellaneous Thermal Techniques, 783	
E. Commercial Thermal Analysis Instrumentation, 786	
a. Perkin-Elmer Systems. 787	
b. Du Pont Model 1090 Thermal Analysis System, 792	
c. Mettler Tello TA Processor, 793	
d. Stanton Redcroft System, 795	
References, 795	
13. THERMAL ANALYSIS NOMENCLATURE	799
A. Introduction, 799	
B. General Recommendations, 800	
C. Terminology, 801	
D. Definitions and Conventions. 803	
1. General, 803	
2. Methods Associated with Weight Change. 803	
a. Static, 803	
b. Dynamic. 803	
E. Methods Associated with Energy Changes. 804	
F. Methods Associated with Evolved Volatiles. 805	
G. Methods Associated with Dimensional Change. 805	
H. Multiple Techniques. 805	
1. DTA. 806	
1. TG, 806	
K. DTA and TO. 806	
L. DTA. 807	
M. TG. 808	
References. 810	
INDEX	811

CHAPTER

GENERAL INTRODUCTION

The currently accepted definition of *thermal analysis*, as given by Mackenzie (1,2) and the International Confederation for Thermal Analysis (ICTA) is: "A group of techniques in which a physical property of a substance and/or its reaction products is measured as a function of temperature whilst the substance is subjected to a controlled temperature program." This definition implies that before a thermal technique can be regarded as thermoanalytical, three criteria must be satisfied:

1. A physical property has to be measured.
2. The measurement has to be expressed (directly or indirectly) as a function of temperature.
3. The measurement has to be made under a controlled temperature program.

Failure of any method to meet these criteria would exclude it as a method of thermal analysis.

The physical property measured and the corresponding thermal analysis technique are tabulated in Table 1.1 (3) and further elaborated on in Chapter 13. Notice that under the physical property of mass, thermogravimetry (TG), evolved gas detection (EGD), evolved gas analysis (EGA), emanation thermal analysis (ETA), thermoparticulate analysis, and others are included. Similar considerations can be included in the physical properties of optical characteristics, electrical characteristics, magnetic characteristics, and so on. The definitions of each individual technique are given in the chapter in which they are discussed. A select number of the thermal analysis techniques are summarized in Table 1.2. Each technique is tabulated in terms of the parameter measured, a typical recorded data curve, the instrumentation needed, and the chapter in which it is described.

Surveys of the types of thermal analysis techniques used and their applications to numerous areas of research have been published by Wendlandt (6), Liptay (7), and Dunn (8). The most widely used techniques are TG and DTA, followed by DSC and TMA. Inorganic materials are the most widely studied by thermal analysis techniques, followed by high polymers, metals and

Table 1.1. Physical Properties Measured in Thermal Analysis (3)

Physical Property	Derived Techniques ¹	Acceptable Abbreviation
Mass	Thermogravimetry	TG
	Isobaric mass-change determination	
	Evolved gas detection	EGD
	Evolved gas analysis	EGA
	Emanation thermal analysis	
Temperature	Thermoparticulate analysis	
	Heating-curve determination ²	
Enthalpy	Differential thermal analysis	DTA
Dimensions	Differential scanning calorimetry ³	DSC
Mechanical characteristics	Thermodilatometry	
	Thermomechanical analysis	TMA
Acoustic characteristics	Dynamic thermomechanometry	
	Thermosonometry	
	Thermoacoustimetry	
Optical characteristics	Thermooptometry	
Electrical characteristics	Thermoelectrometry	
Magnetic characteristics	Thermomagnetometry	

¹When the temperature program is in the cooling mode, this becomes cooling-curve determination.

²The confusion that has arisen about this term seems best resolved by separating two modes (power compensation DSC and heat flux DSC) as described in Chapter 5.

metallic alloys, and organic substances. Lombardi (3) has estimated that there are over 10,000 thermoanalytical instruments in use throughout the world at this time.

It should be noted that, in many cases, the use of only a single thermal analysis technique may not provide sufficient information about a given system. As with many other analytical methods, complementary or supplementary information, as can be furnished by other thermal analysis techniques, may be required. For example, it is fairly common to complement all DTA or DSC data with thermogravimetry. If one or more gaseous products result, evolved gas analysis may prove useful in solving the problem at hand. Simultaneous thermal techniques are helpful in this respect in that several types of data are obtained from the same sample under identical pyrolysis conditions.

The field of thermal analysis has grown rapidly during the 20 years since publication of the first edition of this book. One criterion of growth of a scientific area is the number of publications appearing in the literature.

Table 1.2. Some Thermal Analysis Techniques

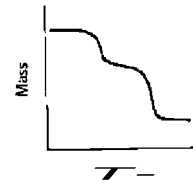
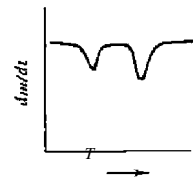
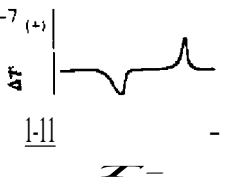
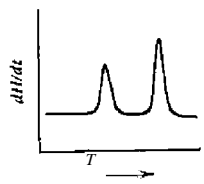
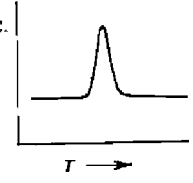
Technique	Parameter Measured	Instrument Employed	Chapter	Typical Curve
Thermogravimetry (TGI)	Mass	Thermobalance	2-4	
Derivative thermogravimetry (DTG)	dm/dt	Thermobalance	2	
Differential thermal analysis (DTA)	$T_s - T_r(\Delta T)$	DTA apparatus	5-7 (+)	
Differential scanning calorimetry (DSC)	Heat flow dH/dt	DSC calorimeter	7	
Evolved gas detection (EGD)	Thermal conductivity ⁴	TC cell ⁵	T.C.	

Table 1.2. Some Thermal Analysis Techniques

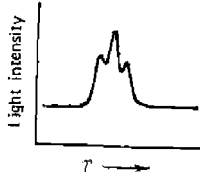
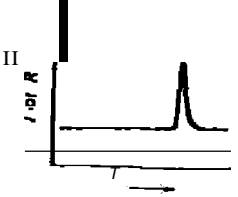
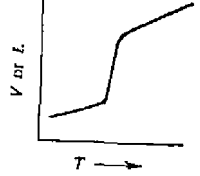
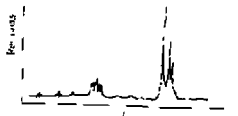

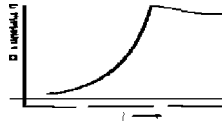
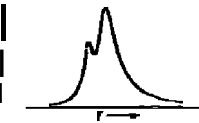
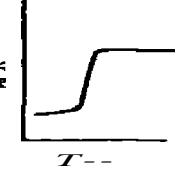

Technique	Parameter Measured	Instrument Employed	Chapter	Typical Curve
Thermoluminescence (TL)	Light emission	Photo detector ^b	9	
Electrical conductivity (EC)	Current or resistance	Electrometer Or bridge	11	
Thermomechanical analysis (TMA) (dilatometry)	Volume or length	Dilatometer	11	
Thermosonometry	Sound	TS Apparatus	11	
Dynamic mechanical analysis (DMA)	Frequency	DMA apparatus	11	

Table 1.2. Some Thermal Analysis Techniques

Technique	Parameter Measured	Instrument Employed	Chapter	Typical Curve
Dielectric constant	Dielectric constant	Capacitance bridge	11	
Oxyluminescence	Light emission	TL apparatus	9	
Dynamic reflectance spectroscopy (DRS)	Reflectance	Spectrophotometer	9	
Emanation thermal analysis (ETA)	Radioactivity	ETA apparatus	8	

^aOther detectors may be used.

^bMay be a photomultiplier tube, photodiode, photocell, or other instrument.

Prior to 1969 - 1970 thermal analysis papers were published in a large number of international scientific journals, making a literature search very time-consuming. In 1969 the *Journal of Thermal Analysis* was founded by Buzagit and Simon as editors, in Budapest, Hungary. This journal publishes nu-

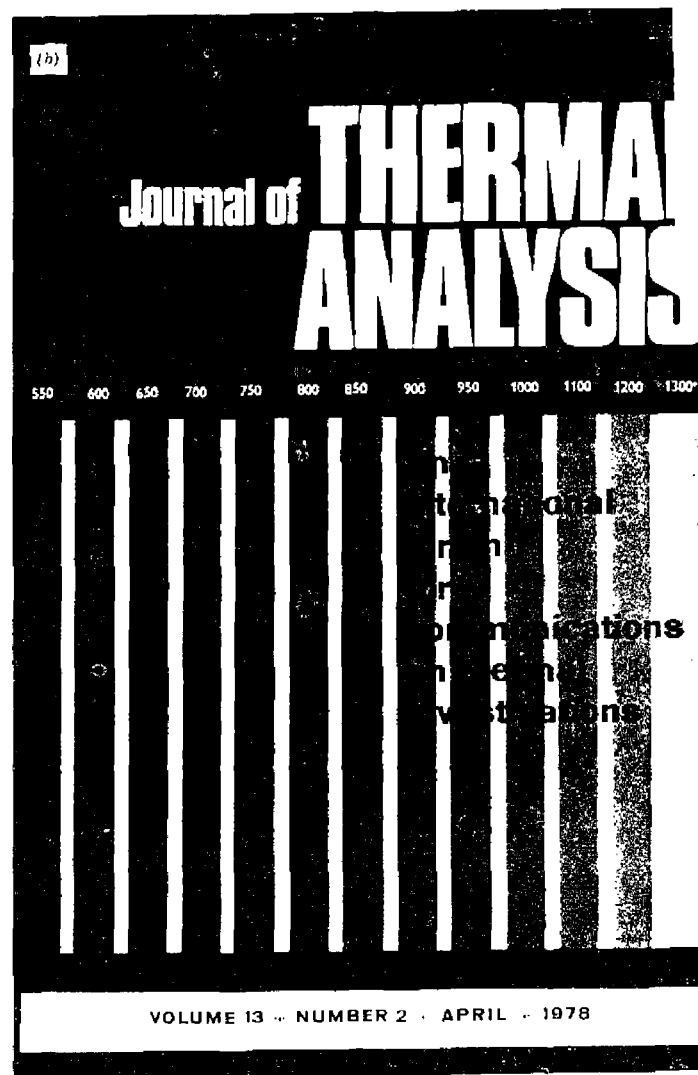
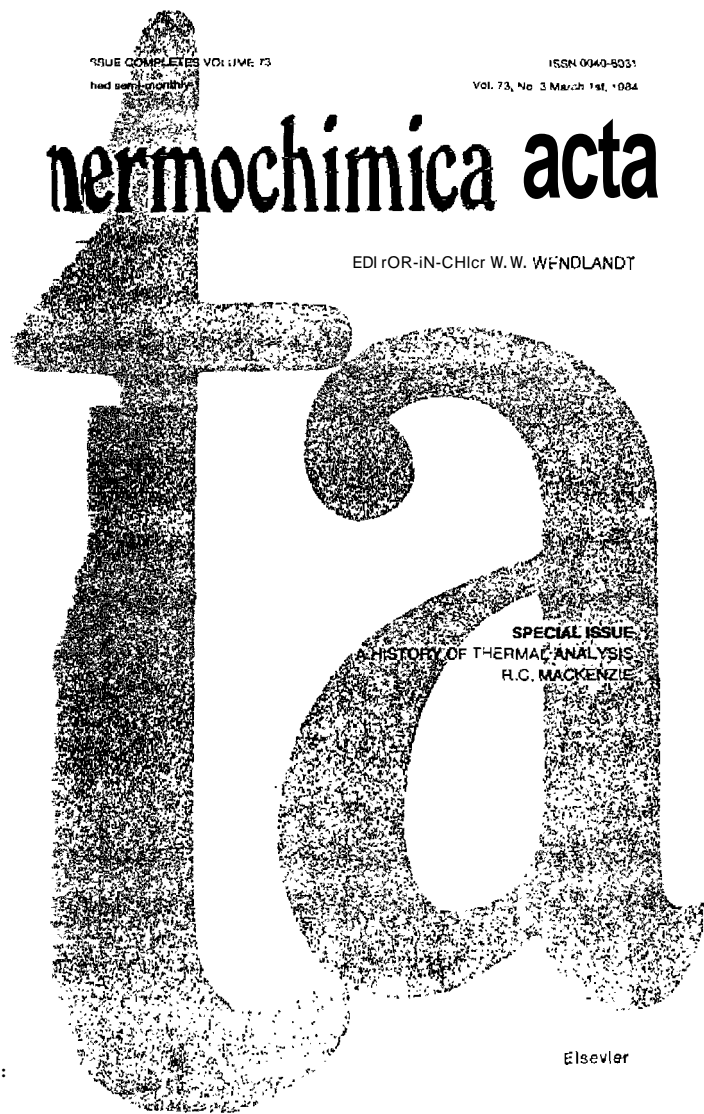


Figure 14 The two thermal analysis journals. (a) *Thermochimica Acta* (b) *Journal of Thermal Analysis*.

merous manuscripts on thermal analysis, of which a large proportion originate from Eastern European countries and Western Asia. *Thermochimica Acta*, a journal that publishes contributions in thermal analysis and calorimetry from workers throughout the world, was founded by Wendlandt in 1970 (4). To illustrate the growth of publications in thermal analysis, *Thermochimica Acta* has increased from about 400 pages in 1970 to over 3600 pages in 1983. The cover sheets of these two journals are illustrated in Figure 1.1.

Two useful abstracting journals are available: *Thermal Analysis Abstracts* (Heyden & Sons, London) and *Chemical Abstracts CA Selects: Thermal Analysis* (Chemical Abstracts Service, Columbus, OH). Numerous reviews on the many aspects of thermal analysis are published annually: A biennial review of the field is written by Wendlandt (5) in which all areas of thermal analysis are included.

REFERENCES

1. Mackenzie, R. C., *Thermochim. Acta*, 28, 1 (1979).
2. Mackenzie, R. C., [*sr. J. Chem.*, 22, 203 (1982)].
3. Lombardi, G., *For Better Thermal Analysis*, 2nd ed., ICFA, Rome, 1980.
4. Wendlandt, W. W., *Thermochim. Acta*, 50, 1 (1981).
5. Wendlandt, W. W., *Anal. Chem.*, 56, 250R (1984).
6. Wendlandt, W. W., *Thermochim. Acta*, 36, 393 (1980).
7. Liptay, G., *J. Thermal Anal.*, 25, 235 (1982).
8. Dunn, J. G., *Chem. Abstr.*, 47, 281 (1980).

CHAPTER

2

THERMOGRAVIMETRY

A. INTRODUCTION

The thermal analysis technique of thermogravimetry (TG) is one in which the change in sample mass (*mass-loss or gain*) is determined as a function of temperature and/or time. Three modes of thermogravimetry are commonly used, as illustrated in Figure 2.1: (a) *isothermal* thermogravimetry, in which the sample mass is recorded as a function of time at constant temperature; (b) *quasi-isothermal* thermogravimetry, in which the sample is heated to constant mass at each of a series of increasing temperatures; and (c) *dynamic* thermogravimetry, in which the sample is heated in an environment whose temperature is changing in a predetermined manner, preferably at a linear rate. Most of the studies discussed here will refer to dynamic thermogravimetry, which will be designated as thermogravimetry.

The resulting mass-change versus temperature curve (which has various synonyms such as *thermolysis curve*, *pyrolysis curve*, *thermogram*, *thermogravimetric curve*, *thermogravigram*, *thermogravimetric analysis curve*, and so on) provides information concerning the thermal stability and composition of the initial sample, the thermal stability and composition of any intermediate compounds that may be formed, and the composition of the residue, if any. To yield useful information with this technique, the sample must evolve a volatile product, which can originate by various physical and chemical processes such as those discussed in Chapter 4. Except for the mass-changes, much of the information obtained from the TG curve is of an empirical nature in that the transition temperatures are dependent on the instrumental and sample parameters. Thus, it is difficult to make meaningful comparisons between TG data obtained on different thermobalances in different laboratories. The use of commercially available thermobalances has done much to improve this situation, but it should still be noted that the curve transition temperatures are procedurally obtained temperatures and are not fundamental to the compound as are X-ray d -spacings and infrared absorption band minima.

The characteristics of a single-stage mass-loss curve are illustrated in Figure 2.1. Two temperatures may be selected as characteristic of any

THERMOGRAVIMETRY

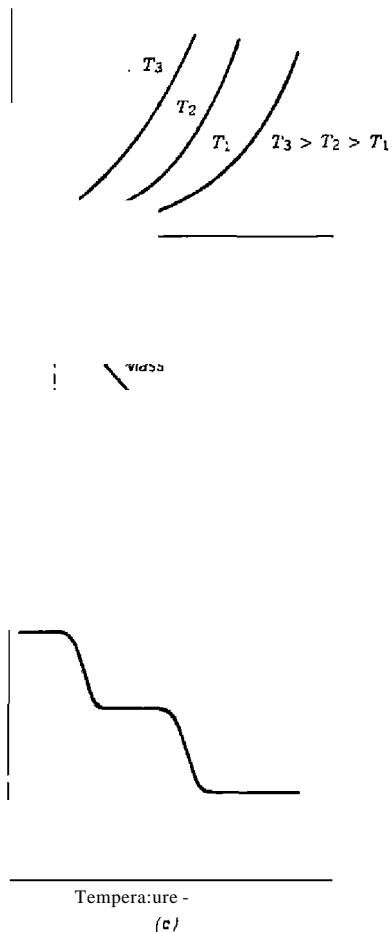


Figure 4.1. Three modes of thermogravimetry: (a) isothermal thermogravimetry; (b) quasi-isothermal thermogravimetry; (c) dynamic thermogravimetry.

single-stage nonisothermal reaction: T_i , the *initial temperature* or *procedural decomposition temperature* (pdt), which is the temperature at which the cumulative mass-change reaches a magnitude that the thermobalance can detect; and T_f , the *final temperature*, which is the temperature at which the cumulative mass-change first reaches its maximum value, corresponding to complete reaction. Although the T_i may be the lowest temperature at which

INTRODUCTION

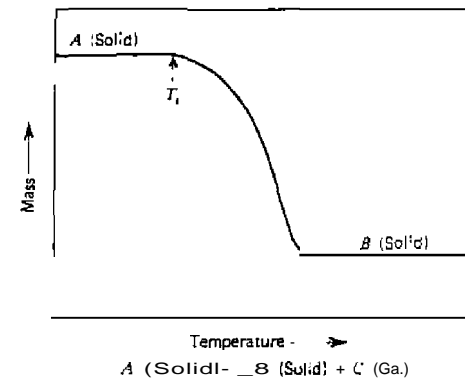


Figure 2.2. Characteristics of a single-stage reaction TG curve (1).

the onset of a mass-change may be observed in a given experiment, it is neither a transition temperature in the phase-rule sense nor a true decomposition temperature below which the reaction rate suddenly becomes zero. At a linear heating rate, T_f must be greater than T_i , and the difference, $T_f - T_i$, is called the *reaction interval*. For an endothermic decomposition reaction, T_i and T_f both increase with increasing heating rate, the effect being greater for T_f than for T_i .

The thermal stability is defined as a general term, (2) indicating the ability of a substance to maintain its properties as nearly unchanged as possible on heating. From a practical point of view, thermal stability needs to be considered in terms of the environment to be imposed on the material and the functions it has to perform. The thermobalance is a useful technique for studying the ability of a substance to maintain its mass under a variety of conditions.

The historical aspects of TG have been discussed by Duval (3-5), Wenglandt (7), Keatch (23), and others (107-109). Perhaps the first thermobalance was that described by Nernst and Riesenfeld (120), who used a Nernst quartz torsion microbalance, equipped with an electric furnace, to study the mass-loss on heating of Iceland spar, opal, zirconia, and other minerals. The Japanese Honda was apparently the first to use the term *thermobalance* for an instrument he described in 1915/191. The French school of thermogravimetry began with Urbain in 1912 when he modified a two-pan analytical balance into a crude thermobalance (24). This was followed by the work of Guichard (1923) (10), Vallet (1936), Chevillard (1936), Duval (1950), and many others. The first commercial thermobalance in the United States, which prompted further work in TG, was that described by Mauer (31) in 1954,

although Niagara Electronic Laboratories had such an instrument available as early as 1949. Early pioneers in TG in the United States were described by Wendlandt (7). The modern aspects of thermogravimetry began in the late 1950s with the work of Duval who used the thermobalance to create an interest in gravimetric analysis (3, 4, 106). High-quality, precision, commercially available thermobalances became widely used in the early 1960s (see Chapter 3).

B. SOME FACTORS AFFECTING THERMOGRAVIMETRIC CURVES

As with any instrumental technique, there are with thermogravimetry a large number of factors which affect the nature, precision, and accuracy of the experimental results. Thermogravimetry probably has a larger number of variables because of the dynamic nature of the temperature change of the sample. Duval (3, 4, 11) discussed in detail the precautions involved in using a thermobalance as well as the many other variables involved in thermogravimetry. "No attempt will be made to include all these in this discussion; only the most important parameters will be reiterated here. Basically, the factors that can influence the mass-change curve of a sample fall into the following two categories:

1. Instrumental (thermobalance) factors.
 - a. Furnace heating rate
 - b. Recording or chart speed.
 - c. Furnace atmosphere.
 - d. Geometry of sample holder and furnace.
 - e. Sensitivity of recording mechanism.
 - f. Composition of sample container.
2. Sample characteristics.
 - a. Amount of sample.
 - b. Solubility of evolved gases in sample.
 - c. Particle size.
 - d. Heat of reaction.
 - e. Sample packing.
 - f. Nature of the sample.
 - g. Thermal conductivity.

Unfortunately, definitive studies are lacking on some of these factors: if some type of study has been made, it has been limited to only one type of

thermodynamic or recording system and corrections cannot be easily made with other types of instruments. It is true, of course, that many of the foregoing factors, such as sample-holder geometry, recording speed, balance sensitivity, and sample-container air buoyancy, are fixed with any given thermobalance. Factors which are variable and difficult to reproduce are the sample-particle size, packing, the solubility of evolved gases in the sample, furnace convection currents, and electrostatic effects. In view of these variables, it is unfortunate that some type of standard sample is not available for comparing one given experimental apparatus with another. An insight into the use of standard compounds for temperature calibration, however, is given in Chapter 3.

1. Instrumental (Thermobalance) Factors

a. Heating Rate

The effect of heating rate change on the procedural decomposition temperatures of a sample has been widely studied. Perhaps the only other parameter that has been studied more is that of the effect of atmosphere on the TG curve. For a single-stage endothermic reaction, Simons and Newkirk (11) have pointed out the following changes for T_i and T_f , as a function of fast (F) and slow (S) heating rates. For the initial procedural decomposition temperature, T_i ,

$$(T_i)_F > (T_i)_S$$

For the final procedural temperatures, T_f ,

$$(T_f)_F > (T_f)_S$$

while the reaction interval, $T_f - T_i$, varies according to

$$(T_f - T_i)_F > (T_f - T_i)_S$$

For any given temperature interval, the extent of decomposition is greater at a low rate of heating than for a similar sample heated at a faster rate. If the reaction involved is exothermic, the sample temperature will rise above that of the furnace, and it has been shown (8) that the difference between the furnace temperature and the sample temperature is greatest for the faster rate of heating when a reaction is occurring. When successive reactions are involved, the rate of heating may well determine whether or not these reactions will be separated. The appearance of a point of inflection

in the TG curve at a faster heating rate may resolve itself into a horizontal plateau at a slow heating rate.

The effect of heating rate on the TG curve of a sample has been discussed by numerous authors. Mention should be made of the investigations or reviews by Duval (3, 4, II), Newkirk (12), Redfern and co-workers (6, S), Simmons and Wendlandt (13), DeVries and Gellings (14), Herbeli (15), and others.

Another study on the effect of heating rate on the T_i and T_f temperatures of siderite is illustrated in Figure 2.3. Kotra et al. (107) used furnace heating rates of 1-20°C/min, in a N_2 atmosphere, and observed that T_i varied from 400-480°C, whereas T_f ranged from 500-610°C under the same conditions. Similar behavior was noted for the mineral goethite. Dunn and Jayaweera (110) showed that if an oxidation reaction took place, the TO curve can change drastically with a change in heating rate. They found that in the oxidation of a nickel sulfide concentrate, the initial extrapolated onset temperature was 595°C at a 1°C/min heating rate. At 10°C/min, this value increased to 640°C, but then decreased to 470°C at a heating rate of 50°C/min. A mass-gain was first observed due to the formation of metal sulfates followed by a mass-loss, which was attributed to the oxidation of a sulfide phase.

It should not be inferred that the use of high heating rates in thermo-

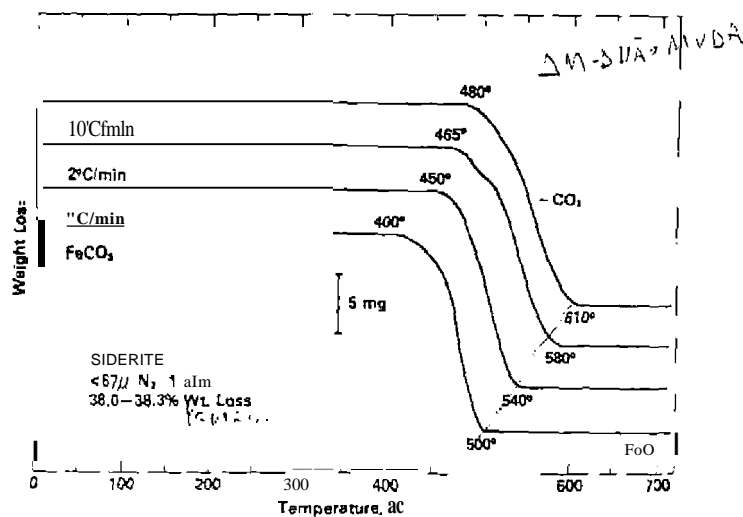


Figure 2.3. Effect of heating on the TG curves of siderite (107)

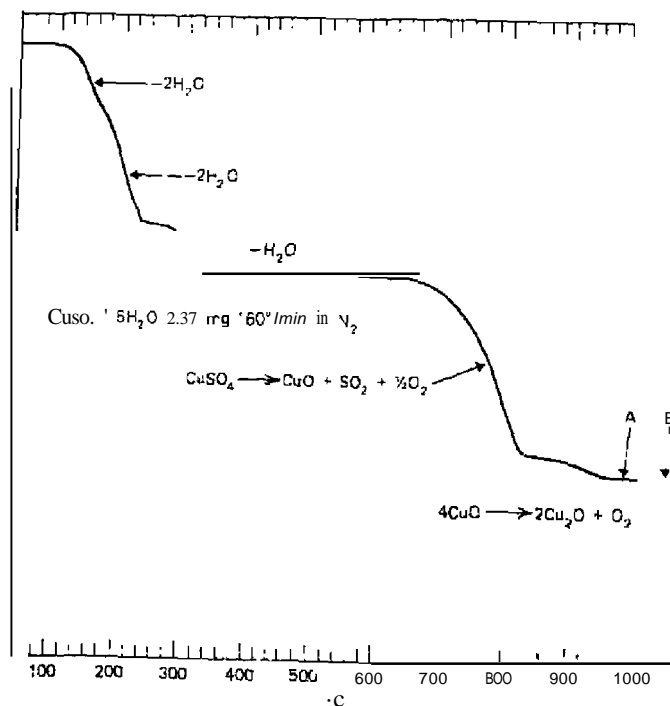


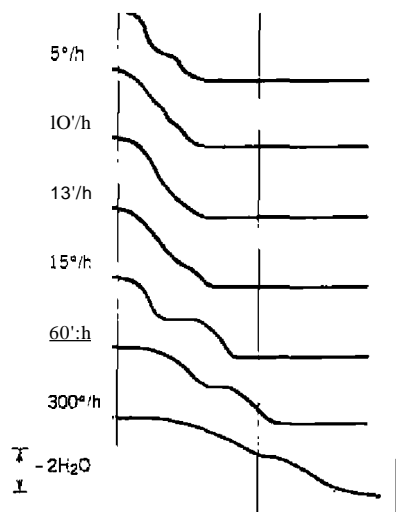
Figure 2.4. TO curve of $CuSO_4 \cdot 5H_2O$ obtained at a very fast heating rate (16).

gravimetry always has a deleterious effect on the TG curves obtained. If a small sample is used, very fast heating rates may be employed and one will still be able to detect the presence of intermediate compounds formed during the decomposition reaction. When a fast heating rate of 160°C/min was used, the TG curve of $CuSO_4$, shown in Figure 2.4, was obtained (16). The entire curve was recorded in 5.5 min, with the intermediate compounds indicated by either curve inflection points or horizontal mass plateaus.

The detection of intermediate compounds in the TG curve is also dependent on the heating rate. Fruchart and Michel (17) detected intermediate compounds, with the compositions 6-, 4-, 2-, and 1-hydrate, when $NiSO_4 \cdot 7H_2O$ was heated at a rate of 0.6°C/min. A previous study at 2.5°C/min revealed only the existence of the 1-hydrate (18). A similar situation was observed with the monosalicylaldoximezinc (II) chelate as studied by Rynasiewicz and Flagg (19) and DeClerq and Duyal (20). On heating at

300°C/h a wet precipitate containing a 250% excess of water, a horizontal mass region was obtained in the curve from 215-290°C (19). DeClerq and Ival (20), using a higher heating rate of 380°C/h, did not detect a horizontal mass level and hence rejected the method for the determination of zinc. Their results indicated that when samples containing a large amount of water are studied, a slow heating rate should be employed. It should also be noted that a sudden inflection in the mass-loss curve may be caused by a sudden variation in the rate of heating and thus be false (6). One method used to detect this phenomenon is always to record the furnace temperature as a function of time on a strip-chart recorder. Temperature perturbations are discussed further in Chapter 3.

At very slow heating rates, Nagase et al. (109) studied the dehydration of $\text{CuSO}_4 \cdot 5\text{H}_2\text{O}$ in a static air atmosphere, as shown in Figure 2.5. A heating rate of 15°C/h is the lower limit at which a fairly distinct two-step curve can be obtained. At slower heating rates, the kinetic component decreases and the



150

in static air at heating rates of 2-300°C/h (109).

equilibrium component ¹⁵increases. When the heating rate is decreased to 13°C/h or less, the [initial] dehydration temperature does not change appreciably. New curve inflections are observed in the 2°C/h curve that correspond to intermediate compositions of $\text{CuSO}_4 \cdot 4\text{H}_2\text{O}$ and $\text{CuSO}_4 \cdot 2\text{H}_2\text{O}$, respectively. However, X-ray diffraction data revealed only $\text{CuSO}_4 \cdot 3\text{H}_2\text{O}$ as the intermediate compound present. The appearance of the curves ¹⁴changed dramatically with change in furnace atmosphere from static air to flowing nitrogen at the same range of heating rates.

The recording of more pronounced horizontal mass plateaus in the TG curve is possible by use of a quasistatic heating rate mode, as previously mentioned. This method was first used by Honda (9) and also by Lukaszewski and Redfern (6) and Paulik and Paulik (21). With this technique, provision is made for the interruption of the linear temperature rise cycle and continuation of the heating at a constant fixed temperature. This method gives mass-loss curves that are, in general, ¹⁴steeper than those obtained under dynamic conditions and provides more accurate data on the final decomposition temperatures.

b. Recording or Chart Speed

The recording of the mass-loss curves for either rapid or slow reactions can have a pronounced effect on the shape of the curves. The effect of chart speed on the recording of the curves of various reactions is illustrated in Figure 2.6. In curve (a), there is a definite flattening of the curve as the chart speed is increased for a slow thermal decomposition reaction. In the case of a slow reaction followed by a rapid one, curve (b), the lower-chart speed curve shows less separation of the two steps than the higher-chart speed curve. For a fast reaction followed by a slower one, curve (c), an effect similar to that of curve (b) was observed, namely, shorter curve plateaus.

An excessive chart speed will tend to minimize differing rates of mass-loss. It is recommended that a chart speed of 6-12 in./h for a heating rate of 1-6°C/min be employed (6). With X-Y recorders, however, the chart speed on the temperature axis is controlled by the response of the instrument and the heating rate, while the mass axis is controlled by the responses of the recorder pen and the recording balance and the rate of the thermal decomposition reaction. Simons and Newkirk (1) have criticized the use of X-Y recorders for recording TG data because unexpected disturbances that can occur in the heating rate or thermocouple response can produce spurious perturbations in the mass-temperature record. Only a separate temperature-time record can disclose these adventitious effects and permit effects caused solely by changes in sample mass to be distinguished from them.

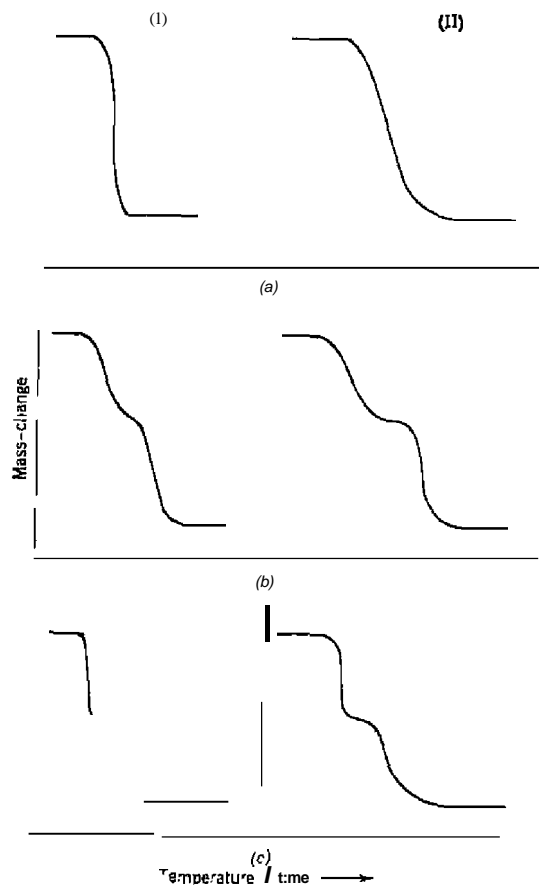
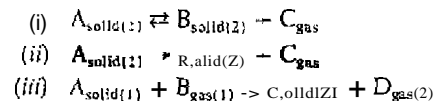


Figure 2.6. Effect of chart speed on the shapes of mass-loss curves. (I) low chart speed; (II) high chart speed (6).

c. Effect of Furnace Atmosphere

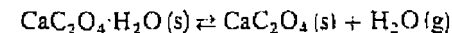
Perhaps the most widely studied instrument variable has been the effect of furnace atmosphere on the TG curve of a sample. The effect of the atmosphere on the mass-change curve depends upon (1) the type of reaction, (2) the nature of the decomposition products, and (3) the type of atmosphere employed. For (1), three types of reactions may be studied, either reversible

or irreversible:

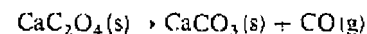


If an inert gas is employed, its function will be to remove the gaseous decomposition products in reactions (i) and (ii) and to prevent reaction (iii) from occurring. If the atmosphere contains the same gas as that evolved in the reaction, only the reversible reaction (i) will be affected and no effect will be observed on reaction (ii). In reaction (iii), if gas (1) is changed in composition, the effect on the reaction will depend on the nature of the gas introduced (e.g., an oxidizing or reducing gas will probably affect the mass-change curve). The preceding discussion concerns a dynamic (or flowing) gas atmosphere; in the case of a static (or fixed) atmosphere, the following behavior probably takes place. If the sample evolves a gaseous product reversibly, as the temperature of the furnaces (and sample) increases, it will begin to dissociate as soon as its dissociation pressure exceeds the partial pressure of the gas or vapor in its immediate vicinity. Since a dynamic temperature system is employed, the specific rate of the decomposition reaction will increase, as well as the concentration of the ambient gas surrounding the sample, due to the decomposition of the sample. If the ambient gas concentration increases, the rate of the reaction will decrease. However, due to convection currents in the furnace, the gas concentration around the sample is continuously changing, which is one of the reasons that static atmospheres are not recommended; for reproducible results, dynamic atmospheres under rigidly controlled conditions are used.

A good illustration of the effect of atmosphere on reversible and irreversible reactions, such as those illustrated in reactions (ii) and (iii), is shown in Figure 2.7 (1). The curves show the effect of heating $\text{CaC}_2\text{O}_4 \cdot \text{H}_2\text{O}$ in both dry N_2 and O_2 atmospheres. The dehydration step, which is reversible,



is unaffected because both gases are equally effective in sweeping evolved water vapor away from the sample surface. For the second reaction,



the curves diverge because the oxygen reacts with the evolved CO, giving a secondary oxidation reaction which raises the temperature of the unreacted

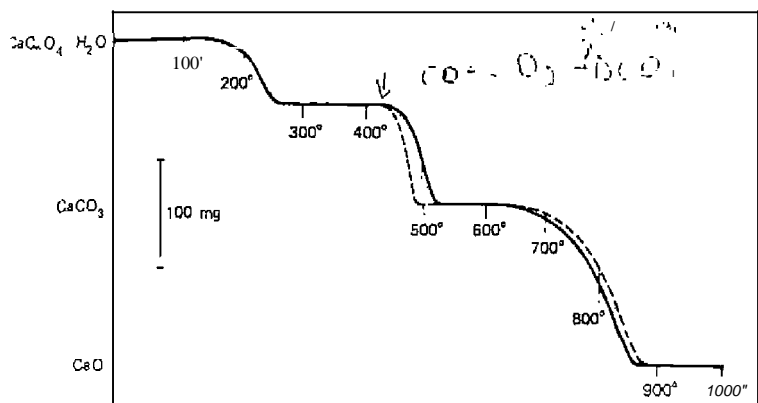
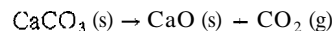


Figure 2.7. Effect of atmosphere on the mass-loss curve of $\text{CaC}_2\text{O}_4 \cdot \text{H}_2\text{O}$ (500-mg sample heated at $300^\circ\text{C}/\text{h}$) (1). • - - -, dry O_2 ; - - - -, dry N_2 .

solid. This higher temperature produces a marked acceleration in the decomposition rate. Thus, the decomposition of the compound occurs more rapidly and is completed at a lower furnace temperature in dry O_2 than in the inert atmosphere of dry N_2 .

The third step in the decomposition reaction,



is also a reversible reaction and hence should not be influenced by either the oxygen or the nitrogen. As can be seen, however, there is a slight difference in the composition of the CaCO_3 formed during the second step of the decomposition reaction. The CaCO_3 formed in an oxygen atmosphere is slightly different from that formed in nitrogen. This difference was not described (11), but it was stated that the mass-change curves cannot disclose differences in particle size, surface area, lattice defects, or other characteristics of the sample.

In the case of reversible reactions such as those previously described, increasing the partial pressure of carbon dioxide in the furnace atmosphere will increase the T_d of the curve, as shown in Figure 2.8. The initial decomposition temperature can range from about 400°C at reduced pressure to 900°C in a carbon dioxide atmosphere at a pressure of 760 Torr. These are rather pronounced changes, due to the extremes in furnace atmosphere used, but they illustrate dramatically the effect of the furnace atmosphere

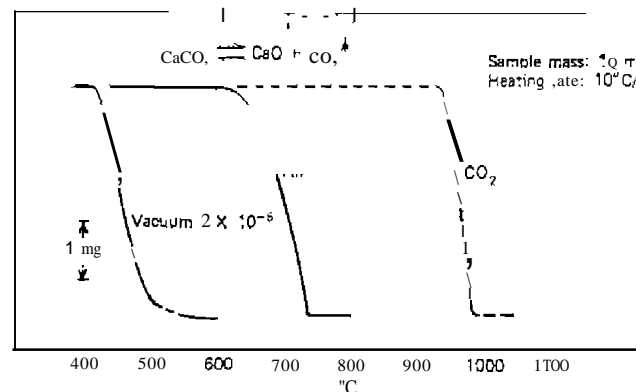


Figure 2.8. TG curves of CaCO_3 in various atmospheres.

on the TG curve. Paulik et al. (22) described a similar series of curves for the decomposition.

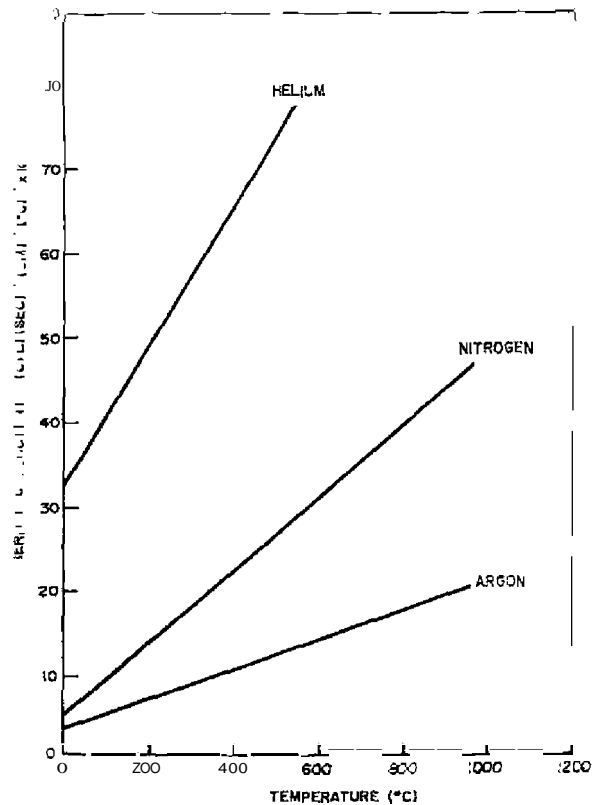
Caldwell et al. (115) found that the thermal decomposition of CaCO_3 occurred most rapidly in furnace atmospheres having the greatest thermal conductivity, which indicates that the rate of reaction is dependent on how quickly heat is supplied to the system. Figure 2.9 shows the thermal conductivity of He, N_2 , and Ar as a function of temperature. The rate of the inert decomposition of CaCO_3 was higher in He, followed by N_2 and then Ar.

Many of the problems involved in obtaining reproducible TG curves of a sample can be solved by using the technique of self-generated atmosphere. This technique is discussed later in this chapter.

The effect of water vapor in the furnace atmosphere has been rather widely studied (1), especially in reactions involving dehydration and hydration. Wendlandt and Simmons (25) studied the thermal decomposition of $\text{BaCl}_2 \cdot 2\text{H}_2\text{O}$ and $\text{BaBr}_2 \cdot 2\text{H}_2\text{O}$ in water-saturated atmospheres and in dry nitrogen atmospheres, whereas Herbell (15) studied the reduction of NiO with dry and water-saturated hydrogen. For $\text{CaSO}_4 \cdot 2\text{H}_2\text{O}$, gypsum, Wiedemann and Bayer (110) found that at a partial pressure of 20 Torr of water, the compound dehydrates directly to anhydrite. On cooling, rehydration to $\text{CaSO}_4 \cdot 0.5\text{H}_2\text{O}$ took place. The dehydration and rehydration behavior of $\text{CaSO}_4 \cdot 2\text{H}_2\text{O}$ is related to structural similarities and to the high mobility of the water molecules between the CaSO_4 layers.

The effects of reduced pressure on the TG curve of various compounds have been reported. Guenot and Manoli (26) reported the effect on the dehydration of $\text{CuSO}_4 \cdot 5\text{H}_2\text{O}$, whereas Nicholson (27) studied the effects of

THERMOGRAVIMETRY



Thermal conductivity of the He, N₂, and Ar according to Caldwell et al. (115).

SOME FACTORS AFFECTING THERMOGRAVIMETRIC CURVES

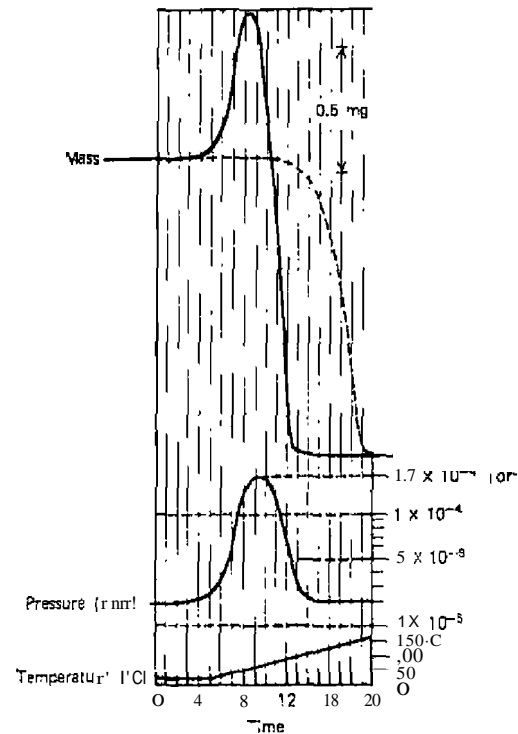


Figure 2.10. TG curves of CaC₂O₄ · H₂O dehydration at ---, nonnal pressure and — high-vacuum condition (29).

low pressure on the thermal decomposition of FeC₂O₄ · 2H₂O. Criado et al. (111) studied the kinetics of decomposition of MnCO₃ at CO₂ pressures from 2.6 × 10⁻⁴ Pa to 26.6 kPa. It was found that this reaction followed a first-order kinetic law independent of the CO₂ pressure employed. Criado and Morales (112) studied the TG of a sample of CaO · CaCO₃ at CO₂ pressures of 29–184 Torr.

Apparent mass gains are occasionally observed in the thermal decomposition of a sample under high vacuum conditions if the sample layer is of a critical thickness and if a certain type of sample holder is employed. Such an effect is shown for the dehydration of CaC₂O₄ · H₂O in Figure 2.10, as

recorded by Wiedemann (29). The broken-line curve shows the dehydration reaction under normal atmospheric pressure, whereas the solid-line curve is that recorded under high vacuum conditions. The "apparent" gain in sample mass at the beginning of the reaction is due to the collision of the water molecules with the sample container during pumping. For a better understanding of this effect, Wiedemann (113) placed equal amounts of sample in a ring sample holder located around the empty thermobalance crucible, and in another experiment, placed the sample inside the thermobalance crucible. Both experiments resulted in the same apparent mass increase. Thus, it was concluded that only a fraction smaller than 0.5% of the apparent mass increase can be attributed to the recoil of the molecules leaving the sample crucible; almost all of the effect is due to reimpact phenomena. It was also

found that this effect decreases with a decrease in heating rate and is absent when much larger pumping cross sections are used. Wiedemann employed his effect to construct a new apparatus for simultaneous X-ray-TG measurements; this technique was called *thermomolecular beam analysis* (TMBA) and is further described in Chapter 3.

Friedman (30) has discussed this effect in the thermal dissociation of tellurium *in vacuo*. He showed that the magnitude of this momentum-transfer effect is expressed by the equation

$$w = m - \frac{1}{g} \alpha v \left(\frac{dm}{dt} \right) \quad (2.1)$$

where w is the mass of the sample as determined by the thermobalance. m is the actual sample mass, g is the acceleration due to gravity, α is a geometric factor, v is the velocity of the ejected gas, and dm/dt is the rate of change of actual mass. Wiedemann and Bayer (113) found that the measured impact forces, in agreement with Maxwell's theory, are proportional to the square root of the absolute temperature and the mean velocity of the gas molecules. Thus, it is possible to measure an unknown temperature from the mass effect measured. The method is limited to the pressure region of $< 10^{-3}$ Torr, with a standard deviation in temperature measurement of ± 5 K at 1225 K.

The effect of an increase in pressure on the TG curve has been described by Brown et al. (28). High-pressure effects would be the opposite of those encountered in low-pressure atmospheres; the T_i for the reaction would be shifted to higher temperatures as well as the increase in the reaction interval,

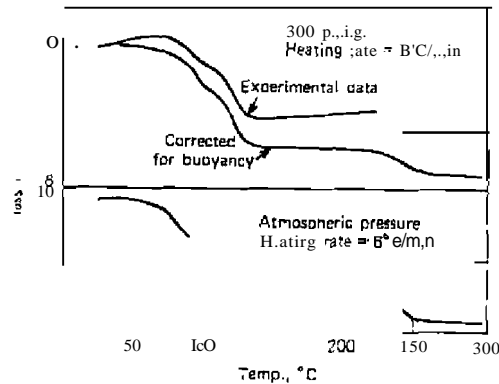
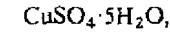


Figure 2.11. TG curves for the dehydration of $\text{CuSO}_4 \cdot 5\text{H}_2\text{O}$ (28).

$T_j - T_i$. When a high-pressure thermobalance was used, the



as shown in Figure 2.11, were obtained. The curve obtained at high pressure was similar to that recorded at atmospheric pressure. The correction for buoyancy effects. Procedural decompositions were almost identical to those obtained from the curve at 1 atm. This may be due to the limited pressure range studied. One effect of increased pressure is the large increase in buoyancy. This curve is usually corrected for this change.

Numerous other studies on the effect of furnace atmosphere on TG curves have been reported (12, 21, 32-41).

d. Sample Holder

The large number of sample holders used in thermogravimetry is described in Chapter 3. Sample holders range from flat plates to deep crucibles. Materials used in their construction may include alumina, and ceramic compositions to various metals and alloys.

Simons and Newkirk (1) have shown that for $\text{CaC}_2\text{O}_4 \cdot \text{H}_2\text{O}$ the geometry of the sample holder is immaterial if no interaction is observed between the sample and the gaseous atmosphere or products. As seen in Figure 2.12, the curves for $\text{CaC}_2\text{O}_4 \cdot \text{H}_2\text{O}$ heated in a car-

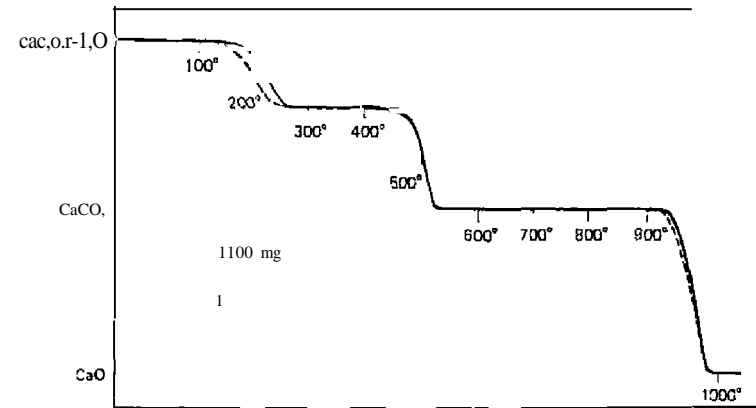


Figure 2.12. Effect of sample-holder geometry on the TG curve of $\text{CaC}_2\text{O}_4 \cdot \text{H}_2\text{O}$ in a dynamic CO_2 atmosphere; - - - quartz dish; — — — porcelain crucible (1).

where are identical above 275°C. As expected, the loss of water occurred more readily from the shallow quartz dish than from the crucible. The shape of the crucible had no effect upon the decomposition of anhydrous CaC_2O_4 . Because this reaction is not reversible, and in a CO_2 atmosphere no important diffusion-controlled reaction can occur. The geometry of the sample holder also had no effect on the dissociation of CaCO_3 because this reaction is reversible, and the atmosphere used was solely the gas involved in the reaction.

When the thermal decomposition reaction was carried out in a dynamic atmosphere of nitrogen, both the loss of water and the loss of carbon dioxide were affected by the geometry of the container. Likewise, the decomposition of CaC_2O_4 was unaffected. The marked effect of the geometry of the sample holder provides evidence that a significant pressure of water vapor and carbon

dioxide must have existed in the interior of the crucible during dissociation, even when the atmosphere that flowed over the crucible entered the thermobalance free from either water or carbon dioxide or from both (11).

The difference in TG curves for $\text{CuSO}_4 \cdot 5\text{H}_2\text{O}$ obtained using a crucible and the multiplate sample holder is illustrated in Figure 2.13 (42). Curve (I) was obtained by use of a crucible, while in obtaining curve (2) the sample was placed as a thin layer on the surfaces of a multiplate holder. The latter type of holder yielded better separation of overlapping reactions and also resulted in lower procedural decomposition temperatures. A similar effect was reported by Paulik and Paulik (21).

The effect of the size and the heat-sink properties of the sample holder has been illustrated by Gam (34). The effect is shown on the thermal decomposition of lead carbonate in Figure 2.14. The sample holder, which was placed on an aluminum block 1 in. in height with a cylindrical surface of 3.1 in.^2 , was employed. The shallow aluminum pan was of the same diameter but had an overall height of $\frac{1}{8}$ in. A factor of 16 in the area directly exposed to the heated furnace wall permitted more rapid heat transfer to the middle of the sample and hence more uniform temperature throughout. It should be noted that the sample on the massive sample holder decomposed over a smaller

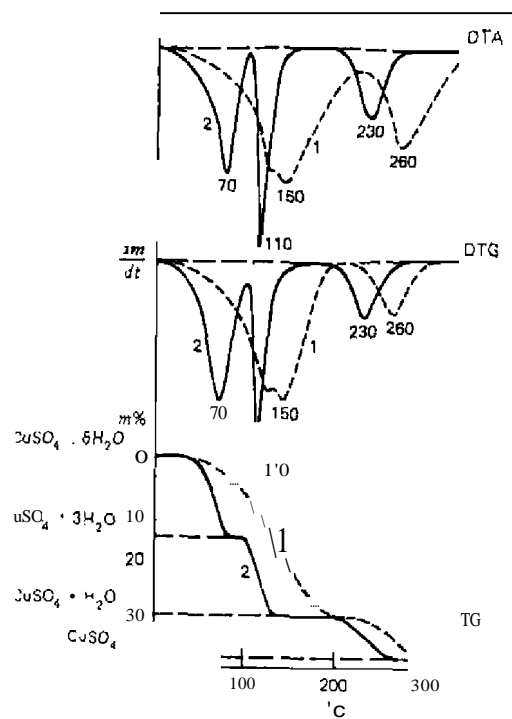


Figure 2.13. Effect of crucible and multiplate sample holder on TG curve of $\text{CuSO}_4 \cdot 5\text{H}_2\text{O}$ (24); ---, crucible, 500 mg; —, multiplate, 200 mg, heating rate of $10^\circ\text{C}/\text{min}$.

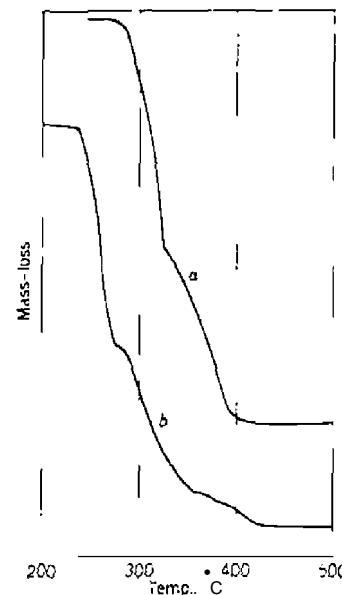


Figure 2.14. Effect of heat sink on the TG curves of lead carbonate. a, massive aluminum block; b, thin aluminum pan. Heating rate is about $450^\circ\text{C}/\text{h}$ (34).

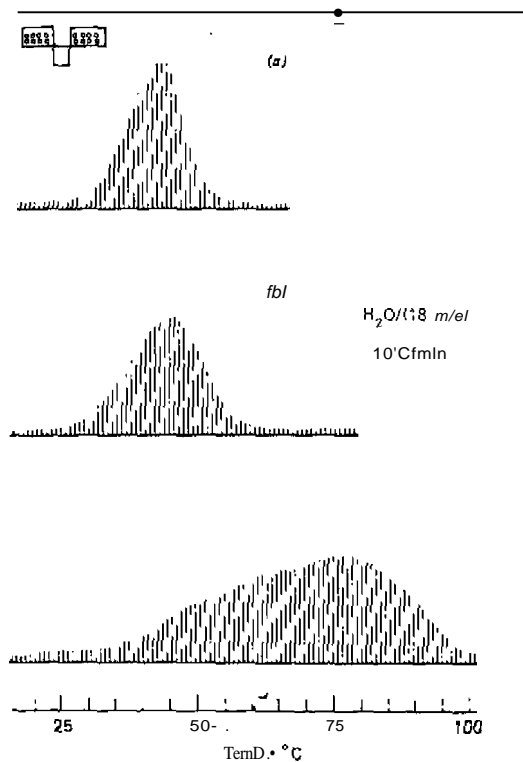


Figure 2.16. Effect of sample packing and sample-holder geometry on the evolution of water from $\text{CaC}_2\text{O}_4 \cdot \text{H}_2\text{O}$ (44).

zinc hydroxide carbonate during the thermal decomposition reaction. Using a flowing air atmosphere, a semispherical Pt/Rh crucible, and a heating rate of $15^\circ\text{C}/\text{min}$, they obtained the results shown in Figure 2.17. After reaching a temperature of 185°C , the sample was maintained isothermally at this temperature (or 5 h). This resulted in a 50% conversion of the sample to ZnO. After cooling to 25°C , concentric zones of the sample were taken out of the crucible and analyzed by X-ray diffraction. As shown by the X-ray photometer curves, the upper layer A had the highest proportion of ZnO (~70%); the middle zones B and C contained about 50% ZnO, and the bottom zone D showed only about 25% ZnO.

The material of construction of the sample holder should have little

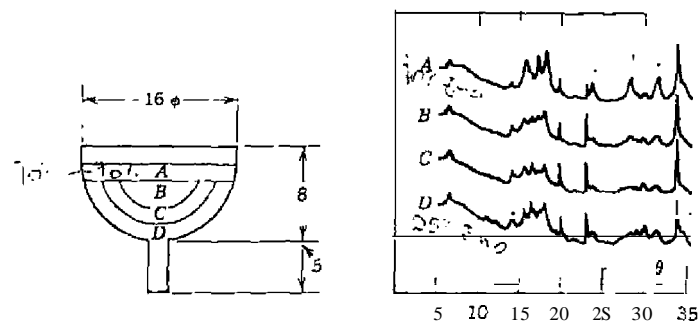


Figure 2.17. X-ray diagrams showing differences in composition of the various zones during heating of zinc hydroxide carbonate (113).

effect on the TG curves if it does not react with the sample. Newkirk and Aliferis (45) have shown that sodium carbonate can react with porcelain and alumina crucibles at high temperatures and hence reveal a mass loss in the TG curve (see Chapter 4). The catalytic properties of platinum may affect the TG curves of certain metal sulfides, as was shown by Ramakrishna, Udupa and Aravamudan (46). The platinum crucible catalyzed the oxidation of zinc sulfide to zinc sulfate, a process that did not occur in alumina crucible.

In the study of reversible reactions or of reactions in which a component of the atmosphere can react with either the original sample or a solid or gaseous decomposition product, the possible existence of partial pressure gradients throughout the mass of the powdered sample should be recognized (11). These gradients can affect both the shape of the TG curves and the magnitude of the thermal effects that accompany the reactions. They can be reduced by packing the powder loosely in a shallow container, using crucibles with microporous or macroporous walls, or passing a controlled atmosphere through the bed of the powdered sample.

Duval (3) suggested that since the walls of the crucible are heated more strongly than the center, the use of a plate and a thin layer of sample would be the best sample holder, whereas the high-walled crucible would be the worst. However, certain samples swell or spall when heated, so that the use of crucibles with high walls is necessary. Duval does not recommend covered crucibles, however, since this would cause the horizontal mass plateaus to be longer. This was illustrated with the pyrolysis of magnesium ammonium phosphate. In an open crucible, there appeared to be a discontinuity between the loss of water and that of ammonia, while in the covered crucible there appeared to be a short horizontal plateau at least a break as soon as the ammonia stopped coming off.

e. Conditions for Optimum Sensitivity

Mass sensitivity as a critical parameter in thermogravimetry has been considered by Cahn and Peterson (47). Greater sensitivity of the thermobalance permits the use of smaller samples, with improved determination of mass plateaus of intermediate compounds and the use of faster heating rates. However, thermobalances with sensitivities greater than $1 \mu\text{g}$ can be attained only under two conditions (48): (1) sample hangdown tubes of 9 mm inside diameter or less if used at atmospheric pressure and (2) larger-diameter tubes if used at reduced pressure (41 mm id at 150 Torr). Unfortunately, the use of the 9-mm tubes limits the sample size to 15–20 mg.

The effect of tube diameter on the mass noise level (peak-to-peak in μg) is shown in Figure 2.18 (47). At larger diameters substantial noise is observed, while at 9 mm there are only $3 \mu\text{g}$ of noise. At 16 mm, the noise is about $1.5 \mu\text{g}$ peak-to-peak, which is readable to $0.1 \mu\text{g}$.

A similar study was made of the effect of pressure and tube diameter on the noise level. For $1 \mu\text{g}$ peak-to-peak noise, the tube diameter varied, as shown in Figure 2.19, with the pressure. As can be seen, the lower the pressure employed is, the greater is the tube diameter that can be used for an equivalent amount of noise. With the larger tube diameter, it was found that for a given pressure, maximum noise usually occurred between 150 and 650°C . Higher temperatures were usually less noisy than the lower values studied. Noise as a function of tube diameter was about the same with flowing gases as with static atmospheres. With the former, the noise was nearly independent of gas velocity, at least from 5–500 ml/min; extremes of noise varied from 1–2 μg

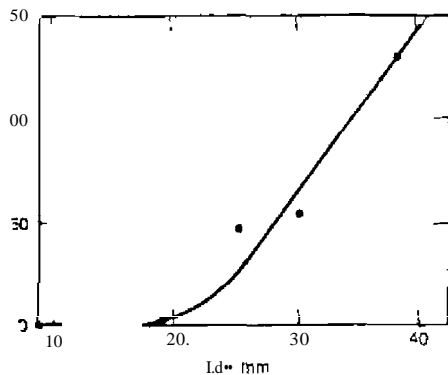


Figure 2.18. Mass noise, μg peak-to-peak versus inside diameter of sample tube, in air at atmospheric pressure (47).

SOME FACTORS AFFECTING THERMOGRAVIMETRIC CURVE

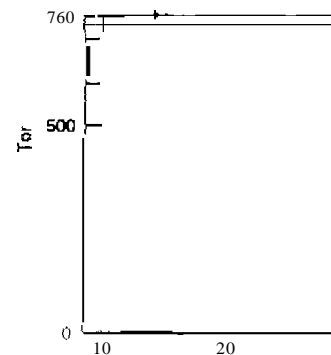


Figure 2.19. Pressure in Torr for $1 \mu\text{g}$ peak-to-peak noise versus Id.

peak-to-peak. The 16-mm-diameter tube appeared to be adequate for both static and dynamic gas applications, as well as a good choice for low-pressure operation, except where exceptionally large samples were accommodated.

2. Sample Characteristics

a. Sample Mass

According to Coats and Redfern (8), the sample mass can affect the thermogravimetric curve in three ways:

1. The extent to which endothermic or exothermic reaction of a sample will cause sample temperature to deviate from the programmed temperature change (the larger the sample mass is, the greater the deviation is).
2. The degree of diffusion of the product gas through and around the solid particles (under static conditions, the product gas immediately surrounding the reacting particles will be governed by the bulk of the sample).
3. The existence of large thermal gradients throughout the sample, particularly if it has a low thermal conductivity.

In order to detect the presence of intermediate compounds, experimenters prefer a small sample to a larger one, as seen by the curves in Figure 2.18.



sample masses in the TG of $\text{CuSO}_4 \cdot 5\text{H}_2\text{O}$ (48). Heating rate of

H_2O mass plateau is clearly indicated when a 18.00 mg sample is used, in contrast with the 18.00 mg sample. This is because samples as small as 0.426 mg are not

sample mass on the T_i and T_f values, Richer and others. Virtually constant for calcium carbonate in an inert nitrogen and carbon dioxide. On the other hand, when the decomposition reaction has begun (1), it generally does not proceed uniformly throughout the entire mass of the sample. In such cases, it would be expected that the time for the decomposition of a powdered solid would increase with sample mass. Because the furnace heating rate is linear, there is a corresponding increase in the observed value of T_f .

observed in the thermal decomposition of CaCO_3 (association of $\text{Ca}_2\text{O} \cdot 4\text{H}_2\text{O}$, as seen in Figure 2.21. increase in the T_f values for the dehydration reaction of CaCO_3 with increased sample mass. However, the reaction is exothermic, as is the case with the decomposition of CaCO_3 . the T_f values do not change with change in sample mass because the sample temperature increases more rapidly than does

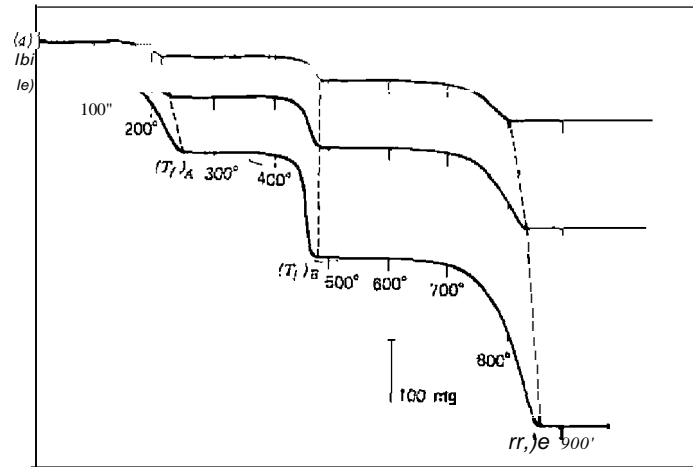


Figure 2.21. Effect of sample mass on the TG curves of $\text{CaC}_2\text{O}_4 \cdot \text{H}_2\text{O}$ in a static atmosphere at a heating rate of $300^\circ\text{C}/\text{h}$ (1). a, 126 mg; b, 250 mg; c, 500 mg.

the measured furnace temperature, and the resultant acceleration in specific reaction rate may compensate, at least in part, for the increase in sample mass. Simons and Newkirk (1) found that if the decomposition reaction was carried out in an inert nitrogen atmosphere, all three T_f values for $\text{CaC}_2\text{O}_4 \cdot \text{H}_2\text{O}$ were shifted to higher temperatures with an increase in sample mass.

The TG curves of large and small single crystals of calcite, 1.57045 g and 1.62 mg, respectively, are very different. These curves, as shown in Figure 2.22, were obtained by Wiedemann and Bayer (113). The smaller crystal exhibited a lower decomposition temperature than that found for the larger crystal of calcite. The effect is even more pronounced when it is noted that two different thermobalance recording sensitivities were used, 0.1 and 100 mg/in., respectively.

b. Sample Particle Size

The effect of sample particle size on the TG curve has been comparatively little studied. Various particle sizes will cause a change in the diffusion of product gases, which will alter the reaction rate and hence the curve shape. Most of the studies in this area that have been reported have been concerned with the effect of particle size on the kinetics parameters (8, 43). Large crystals

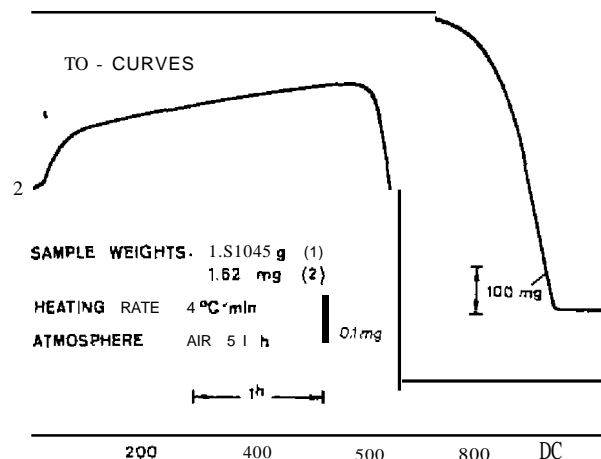


Figure 2.22. Effect of sample mass on the thermal decomposition curves of calcite (113).

of the sample may deprecitate, causing sudden mass-losses in the TO curve. The smaller the particle size is, the greater will be the extent to which equilibrium is reached, and at any given temperature, the greater the extent of decomposition will be (8).

In comparing the thermal decomposition curves of calcium carbonate and calcite, Richer and Vallet (32) found that the empirical decomposition temperatures obtained at the heating rate of 150°C/h in a stream of nitrogen gas were the following: powdered calcium carbonate, 783°C; powdered calcite, 802°C; cube of calcite weighing about 350 mg, 891°C.

Likewise, for a chrysotile sample, Martinez (49) found that the decomposition temperature decreased with a decrease in sample particle size. For the ground material, there was a continuous loss in mass from about 50-850°C, with the most rapid decomposition between 600 and 700°C. For the massive material, there was little mass-loss until a temperature of about 600°C was attained. Similar results were obtained for serpentine and a brucine-carbonate mixture. In general, a decrease in particle size of the sample lowers the temperature at which thermal decomposition begins, as well as the temperature at which the decomposition reactions are completed.

Generally speaking, a sample consisting of large crystals or particles, having a low ratio of surface area/mass, will often decompose more slowly than a sample of equal mass but consisting of very small particles. According to Wiedemann and Bayer (113), loosely packed, coarse materials have air spaces that can reduce the thermal conductivity of the sample, thus changing

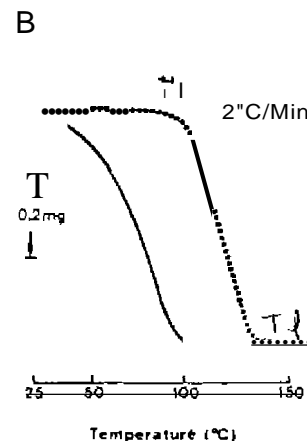


Figure 2.23. Effect of particle size on the dehydration of whewellite (113). — powdered (150 mesh); (.) single crystal.

the appearance of the TG curve. Smaller particles allow denser packing with a higher thermal conductivity. Packing density is not easy to reproduce regardless of the particle size of the sample. Figure 2.23 shows the difference in the TG curves of two samples of whewellite, $\text{CuC}_2\text{O}_4 \cdot \text{H}_2\text{O}$, in vacuum (113). When 6 mg samples are used, the powdered material dehydrates at a much lower temperature than does the single crystal.

c. Miscellaneous Sample Effects

The effect of the heat of reaction of the sample on the mass-loss curve has been studied by Newkirk (12). The heat of reaction will affect the difference between the sample temperature and the furnace temperature, causing the sample temperature to lead or lag behind the furnace temperature, depending on whether the heat effect is exothermic or endothermic. Since these temperature changes may be 100° or more, depending on the heating rate employed, the calculation of kinetic constants from mass-loss curves may be unavoidably and significantly in error. This effect is more thoroughly discussed in Section C.3 of this chapter.

The solubility of gases in solids imposes a serious limitation on the thermogravimetric method, as discussed by Guiochon (150). It is difficult to eliminate or even measure and is generally unknown. This was shown by the heating of solid ammonium nitrate initially containing 1% nitric acid at 200°C for 3 h. At the end of this period, the sample contained 0.6% nitric acid. This acid has no catalytic effect on the decomposition of the sample, which gives no nitric acid under these conditions, so that only the slowness of its evaporation

can explain these results, The concentration of this dissolved substance may be decreased to a small value by the use of wide crucibles without covers, a thin layer of sample, and a flow of inert gas through the furnace. According to Guiochon (50), this gas flow through the furnace is almost always necessary to facilitate the diffusion of gases to and from the sample.

C. SOURCES OF ERROR IN THERMOGRAVIMETRY

The sources of error in thermogravimetry can lead to considerable inaccuracies in the temperature and mass-change data obtained. Accurate thermogravimetry requires that a correction be applied for these errors or that at least some recognition be made of their magnitude. Many of these errors are interrelated and hence cannot be considered separately. Full consideration must be given to all these factors in thermogravimetry.

The possible sources of error in thermogravimetry are many; among them can be listed the following:

1. Sample-container air buoyancy.
2. Furnace convection currents and turbulence.
3. Random fluctuations in the recording mechanism and balance.
4. Furnace induction effects.
5. Electrostatic effects on balance mechanism.
6. Environment of the thermobalance.
7. Condensation on sample support.
8. Temperature measurement and calibration.
9. Weight calibration of recording balance.
10. Chart paper rulings,
11. Reaction of the sample with sample container.
12. Temperature fluctuations.
13. Momentum-transfer effects in vacuum TO.

I. Sample-container Buoyancy

The effect of air buoyancy changes on the sample holder and certain balance components has been studied (3, 4, 12, 15, 29, 37, 48, 51, 52). Most of the studies have used the Chevenard thermobalance (3, 4, 37, 51, 52), but other balances have been studied as well (12, 15, 29, 37, 48).

Wiedemann (29) discussed the effect of buoyancy on the sample and certain parts of the thermobalance as a function of temperature. It should be

kept in mind that the density of the gas phase decreases with temperature also. At about 300°C the density, and therefore the buoyancy exerted on the sample, is about one half as great as at 25°C. In air, this results in an apparent mass variation of about 0.6 mg/cm³. This variation in gas density and buoyancy (mg/cm³) versus temperature is shown in Figure 2.24. The area lying between the curves roughly corresponds to the normal pressure fluctuations expected while working at atmospheric pressure.

In another investigation, Wiedemann and Bayer (113) pointed out that buoyancy cannot be neglected for accurate TG measurements. Buoyancy not only affects parts of the balance system and sample crucible, but it also affects a sample that changes its mass and volume during its thermal decomposition reaction. The extent of the buoyancy effects and its corrections are shown in the TG curves obtained for a large sample of CaCO₃ in a CO₂ atmosphere in Figure 2.25. The top curve is not corrected for the buoyancy of the crucible and of the crucible holder; the second curve takes into account a correction for the buoyancy of the crucible and of the crucible holder; whereas the third corrects for the buoyancy change of the sample. In addition, the exact sample weights at room temperature, 800°C, and at 1000°C are indicated for the CO₂ atmosphere and after correction for vacuum. It is evident that accurate results are obtained only after corrections are applied for buoyancy corrections of the sample, crucible, and the crucible holder. At high temperatures, the nearly parabolic buoyancy correction curve may show a pronounced deviation starting from about 700°C (113). This effect is caused by thermal radiation and convection, which lead to heating certain parts of the balance system. This problem can be avoided by placing a cooling system between the furnace and the adjacent balance housing.

For a platinum sample holder, 0.7 cm², 0.5 cm deep, and weighing 1.6 g, Lukaszewski (37) found that the increase in mass from ambient to 350°C

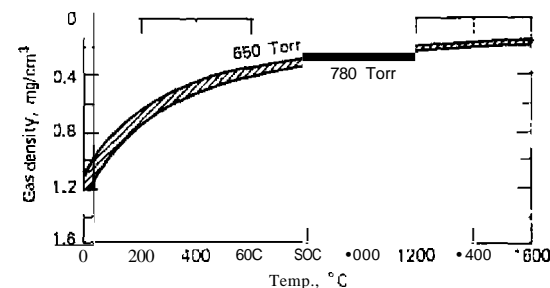


Figure 2.24. Changes in gas density or buoyancy versus temperature at various pressures (29). Curves are given for air.

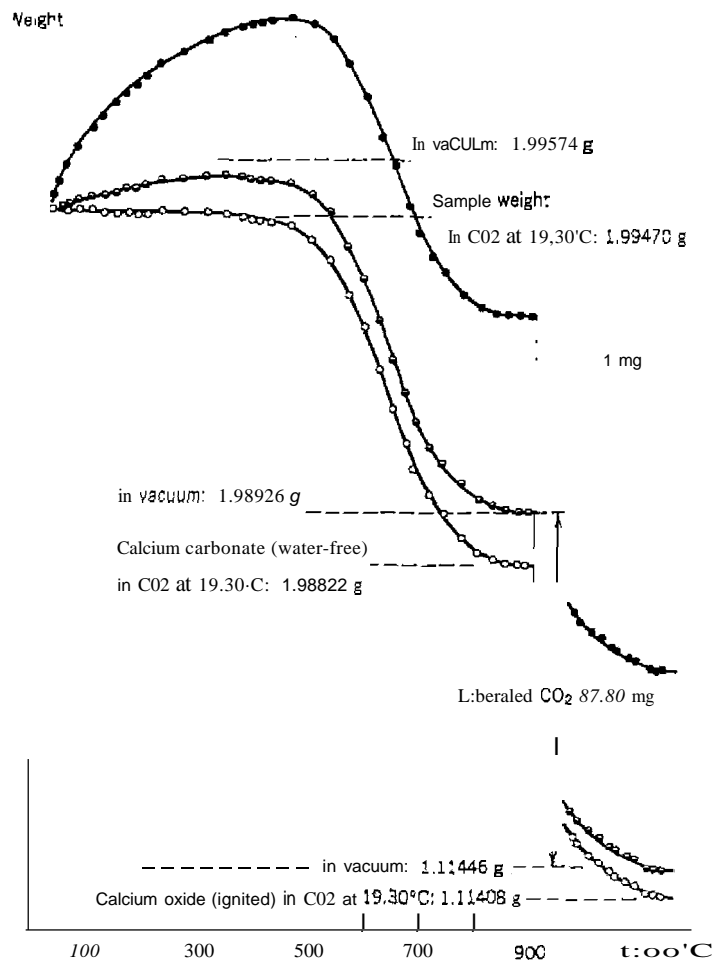


Figure 2.25. Buoyancy effect on the TG curves of a large sample of CaCO_3 (113). $- \cdot - \cdot - \cdot - \cdot - \cdot -$ uncorrected mass curve; $(-\circ-\circ-\circ-\circ-)$ corrected for buoyancy of crucible and holder; $(-\circ-\circ-\circ-\circ-)$ additional correction for sample.

was 0.1 ± 0.05 mg, and from $350-1400^\circ\text{C}$ was 0.2 ± 0.05 mg, at a heating rate of $1.3^\circ\text{C}/\text{min}$. The effects of different heating rates and load sizes were also studied.

Using the Cahn Model RG Electrobalance converted to a thermobalance, Cahn and Schultz (48) recorded the buoyancy curve for a platinum sample

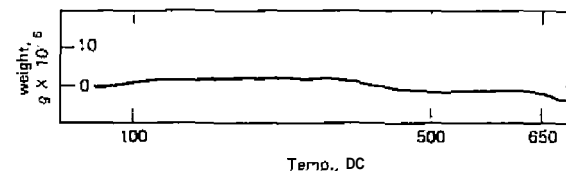


Figure 2.26. Change in mass of a platinum sample holder using the Cahn balance (48).

holder, as shown in Figure 2.26. The change in mass is very small ($\approx 2 \times 10^{-6}$ g) in the temperature range from $25-650^\circ\text{C}$, using an 8-mm-diameter bangdown tube. This correction is much smaller than that for the Chevenard balance, by a factor of a thousand or so.

The sample buoyancy changes using high-pressure thermogravimetric techniques have already been mentioned (28).

2. Furnace Convection Currents and Turbulence

The apparent mass-gain or mass-loss due to convection currents in the furnace has been studied by Newkirk (12) and by Lukaszewski (37). The apparent mass-loss caused by the upflowing stream of air on the sample container and the apparent mass-gain due to air turbulence are determined largely by the sample crucible size and shape (12). The apparent mass-changes as a function of furnace top openings are given in Figure 2.27. It was found that except for a large opening, there was always an initial mass-gain even when on further heating there was an overall mass-loss. It was not possible to choose an opening that would give no apparent mass-gain on heating over the entire temperature range. This effect is also dependent on the furnace heating rate. When using a flowing gas atmosphere in the furnace, Newkirk (12) found an additional apparent mass-gain, as shown in Figure 2.28. Its magnitude was governed by the molecular mass of the gas employed.

3. Temperature Measurement

If the temperature of the sample is taken as the temperature measured by a thermocouple located just above or below the sample container, then the true sample temperature will either lead or lag behind the furnace temperature. The magnitude of this difference depends on the nature of the reaction (whether it is endothermic or exothermic), the heating rate, the sample thermal conductivity, the geometry of the sample holder, and so on. This effect is illustrated by the curves for the sample and thermowell temperatures of $\text{CaC}_2\text{O}_4 \cdot \text{H}_2\text{O}$, as shown in Figure 2.29. There are definite inflections at

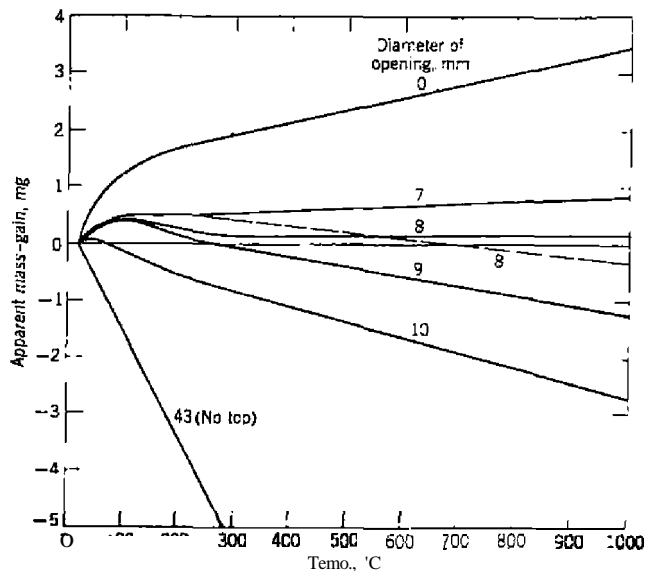


Figure 2.27. Effect of furnace top opening on apparent mass-change of Chevenard thermobalance at a heating rate of 300°C/h (1, 2); —, one porcelain crucible, Coors 230-000 (about 4 g); - - -, two crucibles.

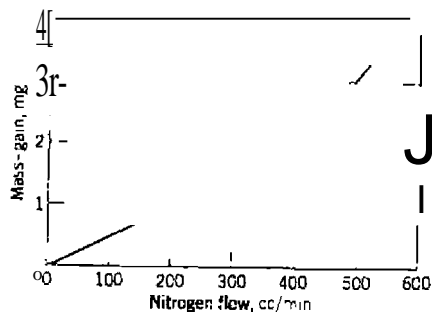


Figure 2.38. Effect of gas velocity on apparent mass-gain of a porcelain crucible at room temperature on the Chevenard thermobalance (12).

SOURCES OF ERROR IN THERMOGRAVIMETRY

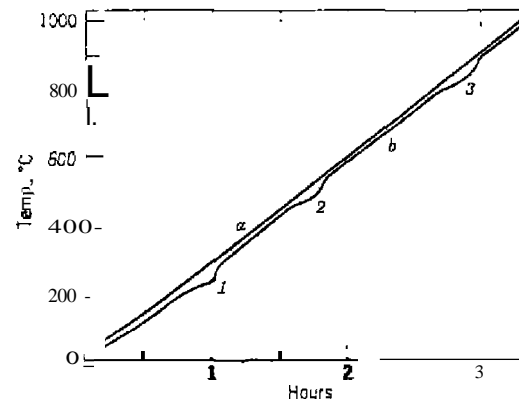
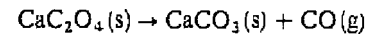


Figure 2.29. Thermowell and sample temperature in the decomposition of $\text{CaC}_2\text{O}_4 \cdot \text{H}_2\text{O}$ in nitrogen on a Chevenard thermobalance. One-gram sample heated at 300°C/h at a nitrogen flow rate of 400 cc/min. *a*, Thermowell temperature ($\sim 10^\circ$ ca.); *b*, sample temperature (36) (1) $\text{CaC}_2\text{O}_4 \cdot \text{H}_2\text{O} \rightarrow \text{CaC}_2\text{O}_4 + \text{H}_2\text{O}$; (2) $\text{CaC}_2\text{O}_4 \rightarrow \text{CaCO}_3 + \text{CO}$; (3) $\text{CaCO}_3 \rightarrow \text{CaO} + \text{CO}_2$.

three places on the sample temperature curve caused by the decomposition reactions of the compound.

The temperature difference between the sample and the furnace for $\text{CaC}_2\text{O}_4 \cdot \text{H}_2\text{O}$ has also been studied by Newkirk (12). The difference in temperature for this compound at a fairly high heating rate, 600°C/h, is illustrated in Figure 2.30. Curve (a) showed a 10-14" lag in the range of 100-1000°C. The endothermic loss due to water evolution resulted in a 25° lag at 200°C. With the larger sample, these effects are accentuated. It should be noted that Newkirk (12) observed an exothermic heat effect for the reaction



while Soulen and Mockrin (36) stated that it was an endothermic reaction. The discrepancy is that in an air atmosphere, which Newkirk presumably employed, carbon monoxide was oxidized to carbon dioxide by air, the oxidation reaction being highly exothermic. The latter investigators Lisen and nitrogen furnace atmosphere in which the oxidation reaction did not take place. This again emphasizes the importance of furnace atmosphere and its effect on the pyrolysis reactions. When the heating rate was lowered (to 600-150°C/h, the temperature difference between the sample crucible and the

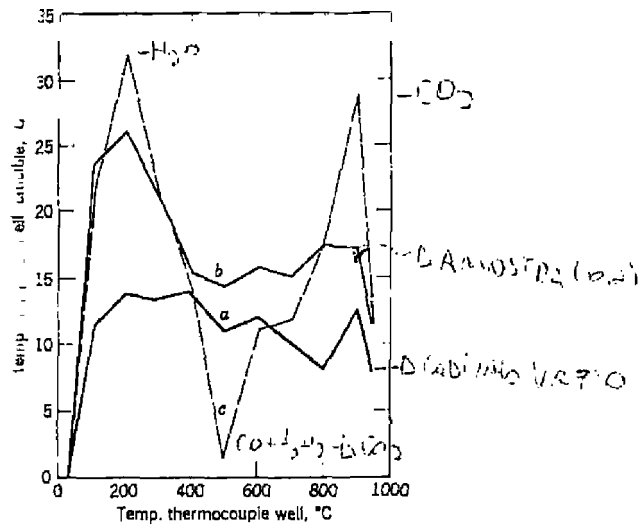


Figure 2.30. Temperature differences between sample and furnace for $\text{CaC}_2\text{O}_4 \cdot \text{H}_2\text{O}$ (12). a, crucible only; b, crucible + 0.2 g of sample; c, crucible + 0.6 g of sample.

furnace thermocouple decreased, as was shown by Newkirk (12). The effect of heating rate on this temperature difference is illustrated in Figure 2.31. The lag varied from 3–14° and was roughly proportional to the heating rate.

The uncertainty in the actual temperature of the sample can be greatly

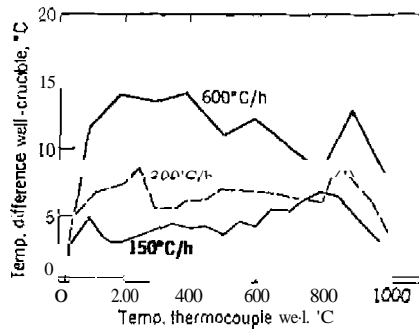


Figure 2.31. Effect of heating rate on sample-holder temperature (12).

reduced by use of a sample holder which contains a thermocouple as an integral part of it. Small temperature differences will still be observed, however, due to the size of the sample, the geometry of the sample holder and so on, but they will be far smaller than in the previous type of temperature detection. One approach which has been used with some success is to position the thermocouple very close to the sample but not in contact with it, as is done with the Du Pont thermobalance (53). The thermocouple is placed within the sample holder itself but does not touch it. A rapid temperature rise in the sample temperature can be detected by this method, as shown by the curves for $\text{CaC}_2\text{O}_4 \cdot \text{H}_2\text{O}$ in Figure 2.32. As has been previously shown, the decomposition of CaC_2O_4 in air is an exothermic reaction. This exothermic reaction causes the sample temperature to rise very rapidly: about 500°C (curve B) to a maximum value of 630°, where reaction is complete. The sample temperature then drops back to the temperature of the furnace, which is still slightly below 500°C.

Gayle and Egger (54) showed that the mode of heat rise is important in determining the amount of mass lost after a given time, but it is unimportant in its influence on the mass-loss rate and kinetic analysis. The symmetric temperature fluctuations do not result in a cancellation of errors when the rate behavior is an exponential rather than a linear function of temperature.

The calibration of the temperature axis in thermogravimetry is discussed in Chapter 3.

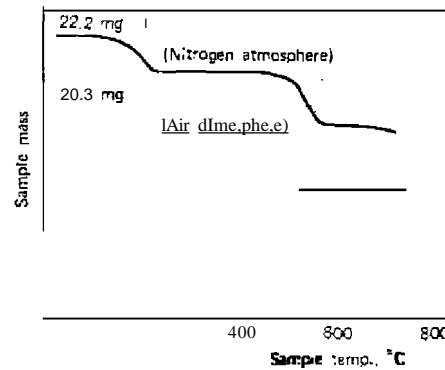


Figure 2.32. Detection of temperature change in sample with a close-proximity detector (53).

4. Other Errors

A well-designed thermobalance should reduce several of the other errors to negligible values. The errors caused by random fluctuations of the recording mechanism, furnace induction effects, electrostatic effects, changes in thermobalance environment, and so on can be eliminated by proper thermobalance design, construction, and location in the laboratory.

Newkirk (12) found that if the balance mechanism of the Chevenard thermobalance was not properly thermally shielded, the oil in the dash pots became warm, causing an apparent mass-gain due to the decreased buoyancy of the oil. In the latest model of this balance, the oil dash pots have been replaced by a magnetic damping device.

Condensation on the cool part of the sample-holder support rod is another source of error. The condensate may reevaporate as the temperature is increased and may again condense still lower on the support. This can lead to entirely false conclusions. Soulen and Mockrin (36) stated that this problem is intensified when a rapid inert gas flow is employed because the volatile materials are driven downward onto the support rod. The magnitude of this effect can be ascertained if the sample holder, the sample, and the support assembly are weighed both before and after each run. If they differ appreciably in mass, a correction must be applied. This, of course, gives no information about the correction during the course of the run. Soulen and Mockrin (36) eliminated this problem in the Chevenard thermobalance by placing a ceramic or Otckel sleeve around the crucible support. Without the sleeve, a completely erroneous mass-loss curve was obtained for this particular compound. Of course, for compounds involving noncondensable gaseous products, this will present no problem.

Cahn and Schultz (55) have discussed the elimination of weighing errors in the Cahn Model RG balance. The effects of temperature and a corrosive atmosphere, as well as electrical and magnetic effects, were considered.

Periodic calibration of the thermobalance will prevent errors on the mass axis of the recorder. Many investigators calibrate the instrument before each run by adding a known weight to the sample container.

D. SELF-GENERATED ATMOSPHERE THERMOGRAVIMETRY

A "self-generated" atmosphere is one which is composed of the gaseous decomposition products of the reaction and which is in intimate contact with the sample by virtue of the type of sample holder employed. The thermogravimetry of various compounds in such an atmosphere is of importance because of the reproducibility of the composition of the atmosphere,

and hence the mass-loss curve. This technique was suggested initially by Garn and Kessler (33) and Forkel (56), and has been the subject of an extensive review by Newkirk (57). The technique is not very widely used, especially since the introduction of high-quality commercial thermobalances in which a reproducible furnace atmosphere can be maintained.

The most important aspect of the technique is in the design of the sample holders, two of which are described in Chapter 3. Other sample-holder designs have been described by Newkirk (57, 58). The evolution of sample holders of use in self-generated atmospheres is illustrated in Figure 2.33. A listing of the different types of compounds that have been studied by the self-generated atmosphere technique is shown in Table 2.1 (57).

The primary influence of the use of the self-generated atmosphere technique is to increase the pressure of the gas evolution to 1 atm, which gives rise to favorable thermodynamic, physical, and kinetic effects. The control is not exact, and some investigators consider the use of the technique to be a makeshift or last resort (57). In many instances, however, precise atmosphere control is not available, or is difficult or impossible, because the reaction products are complex or unknown. The technique has a sound theoretical basis and, in such instances, would seem to be a good choice for the initial TG study of a complex solid-gas system.

The sample holder should have as small a vapor volume as possible. A large vapor volume allows gas pressure gradients in the sample, may result in different reactions, and, it is claimed, may cause nonstoichiometric mass-losses. A large vapor volume will also make it more difficult to locate T_i and hence more difficult to compare results by different investigators. Also, this

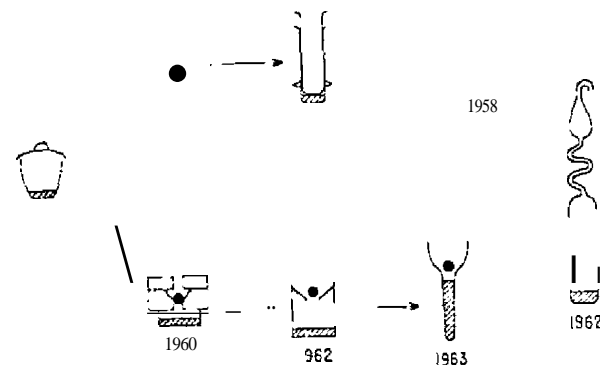


Figure 2.33 Evolution of sample holders for self-generated atmospheres (57)

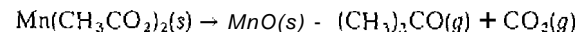
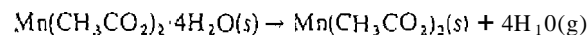
Table 2.1. Compounds Studied by the Self-generated atmosphere Technique (57)

Crucible* Type	Compound
P	Ammonium carbonate monohydrate
MR	Anthracite
P	Brucite [Mg(OH) ₂]
C	n-Butylammonium tetrachloroborate
C	n-Butylammonium tetrachloroborate
C	i-Butylammonium tetraphenylborate
C	s-Butylammonium tetraphenylborate
I'	Cadmium carbonate
BV	Cadmium(II) sulphate (8/3) hydrate
I'	Calcite (CaCO ₃)
BV	Cerussite (PbCO ₃)
MR	Charcoal (wood)
P	Chrysotile
MR	Coal
BY	Cobalt(III) acetate tetrahydrate
CC	Cobalt(II) oxalate dihydrate
P	Cobalt oxalate hydrate
BY	CuSO ₄ ·3Cu(OH) ₂ ·H ₂ O
BY	CuSO ₄ ·2Cu(OH) ₂
I', BV	Copper sulfate pentahydrate
C	Ethylammonium tetrachloroborate
BV	Gypsum (CaSO ₄ ·2H ₂ O)
DC	Iron(III) carbonate
I'	Lead(II) carbonate
C; powder; P, CC	Lead(II) carbonate
Ce, C	Lead(II) oxide
MR	Lignite
I'	Magnesite (MgCO ₃)
CC	Magnesium sulfate heptahydrate
Cc, C, P	Manganese(II) acetate tetrahydrate
DC, I'	Manganese(II) carbonate
C	n-Octylammonium tetrachloroborate
C	n-Propylammonium tetrachloroborate
C	n-Propylammonium tetraphenylborate
DC	Rhodochrosite (MnCO ₃)
DC	Siderite (FeCO ₃)
P	Silver carbonate
P	Sodium oxalate
I'	Talc
P	Thorium(IV) nitrate pentahydrate
P	Thorium(VI) oxalate hexahydrate
P	Uranyl sulfate hydrate
DC, BY	Zinc sulfate heptahydrate

*Key to crucibles: BV, bail valve; C, covered; CC, capillary crucible; DC, deep crucible; MR, micro-retort; P, piston.

technique, the atmosphere produced by the first reaction may have a beneficial or detrimental effect on the following reaction; for example, water can accelerate the decomposition of anhydrous CaC₂O₄.

The thermal decomposition of manganese(II) acetate 4-hydrate is discussed (57), to illustrate the use of the self-generated atmosphere. A two-step decomposition sequence has been proposed, similar to the following:



The mass-loss curves of Mn(CH₃CO₂)₂·4H₂O are illustrated in Figure 2.34(57). In curve A, the sample loses mass immediately at room temperature which is water containing some acetic acid, the latter being detected by its odor. The two major stages of mass-loss on heating correspond approximately to the loss of hydrate-bound water and the decomposition of the anhydrous salt to manganese(II) oxide. Both stages of mass-loss show curve inflections.

The effect of the self-generated atmosphere, curve B, is to increase the initial mass-loss temperature, T_i, and to decrease the reaction interval, t_i - T_i. The increase in T_i has the beneficial effect of eliminating the initial mass-loss at room temperature with its resulting uncertainty about the starting point of the curve. The inflection point during loss of water is located at about 135°C and a mass fraction of 0.9. The second stage of mass-loss

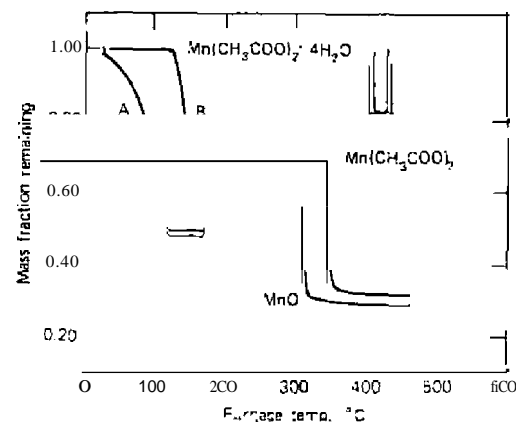


Figure 2.34. TG curves of Mn(CH₃CO₂)₂·4H₂O in a shallow dish containing 53.8 mg in dynamic N₂ and B piston crucible containing 102.6 mg in air. Heating rate was 150 C h (57).

occurs in two approximately equal parts, a very rapid and uniform initial mass-loss followed by a less rapid but still fairly uniform second loss. The nearly horizontal mass plateaus had to be corrected for a buoyancy effect which is observed for all self-generated atmosphere sample holders.

The two curves are compared in a quantitative manner in Table 2.2. An advantage of a close-fitting piston crucible is that a determination can be stopped at any point, the crucible cooled and removed, and the gas analyzed. The disadvantage of this type of crucible is that if the piston is in contact with the molten sample, it will stick, and then subsequently be expelled from the cylinder.

A rather dramatic effect of the use of the self-generated atmosphere technique plus the quasistatic heating-rate mode is shown in Figure 2.35. Paulik and Paulik (21) found that the thermal decomposition of $\text{Ni}(\text{NH}_3)_6\text{Cl}_2$ dissociated in three separate steps, at 180, 320, and 360°C, respectively. The slight overshoot of the curve during the first dissociation reaction was said to be due to an induction period caused by delayed nucleus formation. The sample holder employed is described in Chapter 3.

The advantages and the limitations of the self-generated atmosphere technique have been described by Newkirk (57); they are the following.

Limitations

1. Buoyancy corrections vary depending on the molecular weight of the gas filling the crucible.
2. Large, heavy crucibles will cause a greater uncertainty in sample temperature.

Table 2.2. Comparison of Self-generated and Dynamic N_2 Mass-loss Curves for $\text{Mn}(\text{CH}_3\text{CO}_2)_2 \cdot 4\text{H}_2\text{O}$ (57)

Reaction	Dynamic N_2		Self-generated Atmosphere	
	Obs.	Calc.	Dos.	
T_1 first stage, °C	25		112	
T_f first stage, °C	110		205	
Loss to $\text{Mn}(\text{CH}_3\text{CO}_2)_2$, %	30.6	29.40	29.0 ^a	(30.3) ^b
T_1 , second stage, °C	260		340	
T_f , second stage, °C	350		367	
Loss to MnO , %	71.8	71.06	70.6 ^a	(68.8) ^b

^aCorrected for buoyancy effect.

^bUncorrected for buoyancy effect.

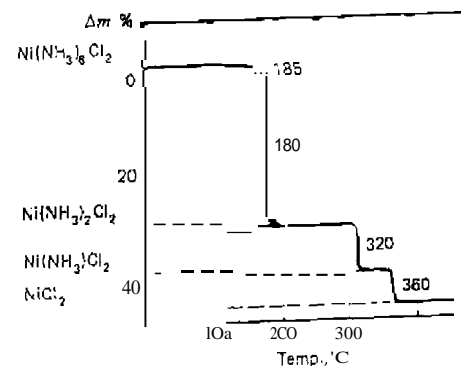


Figure 2.35. TG curve of $\text{Ni}(\text{NH}_3)_6\text{Cl}_2$ in self-generated sample holder and quasistatic heating (21).

3. In dehydration of hydrates, the chances of melting and the appearance of pseudo-plateaus may be enhanced.
4. poorer resolution may result if the first reaction is delayed to a temperature at which a subsequent reaction begins.
5. Secondary reactions with the evolved gas may make interpretation difficult

Advantages

1. The reaction interval will be narrower, overlapping reactions will be more clearly resolved, and intermediates will be more accurately identified.
2. New phases will be revealed.
3. Reactions will proceed, for the most part, at a fixed pressure of the gaseous products equal to atmospheric pressure. The course of reactions, except at the start, will not be affected by varying partial pressure.
4. The observed initial decomposition temperature will be more closely related to an equilibrium decomposition temperature.
5. Experiments can be performed on materials subject to oxidation at elevated temperatures with little interference from oxidation.
6. Very fast reactions can be studied without loss of solid product.
7. Better results will be obtained on materials with an appreciable vapor

pressure at room temperature. The sample can be weighed more accurately and will yield a horizontal baseline on the TG curve.

8. The effects of particle size difference will be reduced and the effects of crucible geometry standardized. This is particularly important with inhomogeneous materials such as rocks and minerals.
9. The recrystallizations of new phases from hydrates or hydroxides will be facilitated.
10. It has been claimed that irreversible decompositions will show better resolution and a smaller reaction interval in some instances, although it is not known why.

Recommended Uses

Thermogravimetry in self-generated atmospheres may be useful for studies of the following:

1. Consecutive reactions, and particularly for hydroxides, hydrates, ammoniates, carbonates, acetates, oxalates, and sulfates.
2. Inhomogeneous materials.
3. Compounds that decrepitate or explode.
4. Air-sensitive materials.
5. Volatile materials.
6. Materials that decompose to yield several gaseous products.
7. Destructive distillation.

E. DERIVATIVE THERMOGRAVIMETRY (DTG)

In conventional thermogravimetry, the mass of a sample, m , is continuously recorded as a function of temperature, T ; or time, t ,

$$m = J(T \text{ or } t) \quad (2.4)$$

Quantitative measurements of the mass-changes are possible by determination of the distance, on the curve mass axis, between the two points of interest or between the two horizontal mass levels. In derivative thermogravimetry, the derivative of the mass-change with respect to time, dm/dt , is recorded as a function of time (t) or temperature (T), or

$$\frac{dm}{dt} = J(T \text{ or } t) \quad (2.5)$$

In other cases, the derivative of the mass-change with respect to temperature, dm/dT , is recorded as a function of time (t) or temperature (T),

$$\frac{dm}{dT} = f(T \text{ or } t) \quad (2.6)$$

In either case, the resulting curve is the first derivative of the mass-change curve. A series of peaks are obtained, instead of the stepwise curve, in which the areas under the peaks are proportional to the total mass-change of the sample. A horizontal plateau in the TG curve gives a corresponding horizontal plateau in the DTG curve because $dm/dt = 0$. A maximum in the DTG curve is obtained when the TG curve has an inflection point where mass is being lost the most rapidly.

De Keyser (59, 60) first suggested DTG in 1953, followed by Erdey et al. (61) and Waters (62). Further work in this area has been by Erdey (63, 64), Paulik et al. (65), Waddams and Gray (66), Waters (67), Cambell et al. (68), and Erdey et al. (69).

A comparison between a conventional (a) and a derivative (b) mass-loss curve is given in Figure 2.36. The derivative curve may be obtained either from the TG curve by manual differentiation methods or by electronic differentiation of the TO signal. Accessory equipment is available for most

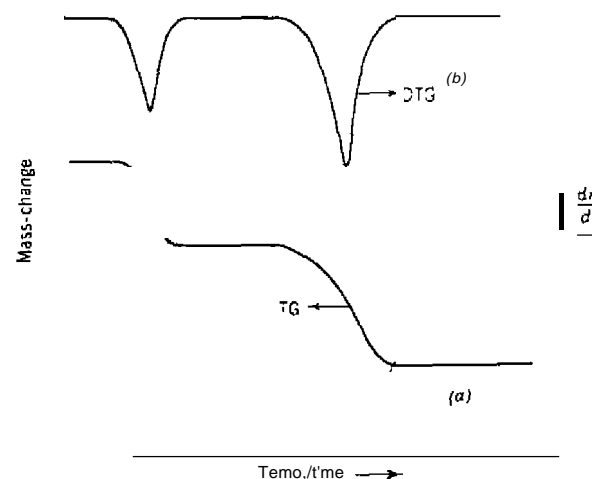


Figure 2.36 Comparison between (a) integral (TGI) and (b) derivative (DTG) mass-loss curves.

kinetic parameters for mass-loss under a particular set of experimental conditions. Empirical data treatments, no matter how augustly clothed in the trappings of kinetics, are still empirical, although admittedly on a higher level of sophistication (71). As a general rule, definitive kinetic parameters can be derived from mass-loss data only in the light of a large amount of additional evidence. In the case of polymers, there is usually not enough pertinent information available to warrant undertaking meaningful kinetic analysis. Thus, mass-loss data for these materials are commonly subjected to empirical kinetic treatments.

The advantages of determining kinetic parameters by nonisothermal methods rather than by conventional isothermal studies are (8) that (1) considerably fewer data are required; (2) the kinetics can be calculated over an entire temperature range in a continuous manner; (3) when a sample undergoes considerable reaction in being raised to the required temperature, the results obtained by an isothermal method are often questionable; and (4) only a single sample is required. A decided disadvantage of nonisothermal compared with isothermal methods is that the reaction mechanism cannot usually be determined, and hence the meanings of the activation energy, order of reaction, and frequency factor are uncertain. The use of nonisothermal kinetic methods has been seriously questioned (72) and much criticized (43, 73-79). As a result of this criticism, and also in order to keep within the scope of this book, the discussion of kinetic methods given here will only be superficial in nature. For more comprehensive treatments, the reader should consult other sources [71, 80-82, 121, 141, 146].

Bagchi and Sen (154) state the following as explicit advantages of nonisothermal methods over isothermal methods:

- I. It is possible to determine the reaction Onset temperature (T_0) very precisely by nonisothermal methods, which is almost impossible to do by the isothermal method. The zero-time error is therefore absent.
- II. A considerable portion of the sample is likely to undergo some reaction during initial heat-up of an isothermal experiment, particularly when the temperature of onset of reaction is lower than the isothermal temperature. In these cases, the values of α will not be zero at $t=0$ for an isothermal experiment. This is likely to bring in another correction for such errors under considerations that also tend to be arbitrary.
- III. For a nonisothermal experiment, a single sample is sufficient to scan the entire temperature range, whereas for the isothermal mode, a new sample is needed for each experiment. In the latter case, it would be almost impossible to ensure identical sample characteristics for each

isothermal experiment unless the sample is chemically pure, thus precluding the analysis of industrial samples.

The foundation for the calculations of kinetic data from a TG curve is based on the formal kinetic equation (43)

$$-\frac{dX}{dt} = kX^n \quad (2.8)$$

where X is the amount of sample undergoing reaction, n is the order of reaction, and k is the specific rate constant. This equation describes very well the kinetics of the thermal decomposition of solids, such as the endothermic reactions of metal oxalates, permanganates, perchlorates, and azides. The temperature dependence of the specific rate constant, k , is expressed by the Arrhenius equation

$$k = Ae^{-E/RT} \quad (2.9)$$

where A is the preexponential factor, E is the activation energy, and R is the gas law constant, which generally applies to only a narrow temperature range.

The mathematical treatment of kinetic equations makes use of one of the following three methods of evaluation: (1) differential, (2) integral, or (3) approximate.

As discussed by Sestak (431), the relationship of X to mass-loss, w , is given by the equation

$$-dX = \frac{m_0}{w_\infty} dw \quad (2.10)$$

where m_0 is the initial mass of the sample and w_∞ is the maximum mass-loss. By integration of the left-hand side of equation (2.10) from m_0 to X and by integration of the right-hand side from zero to w , the following is obtained:

$$X = \frac{m_0}{w_\infty} (w_\infty - w) \quad (2.11)$$

By substitution of equations (2.11) and (2.9) into equation (2.8), and by differentiating the logarithmic form, an expression is obtained which is one of the differential methods: the Freeman and Carroll (831) method.

Integral methods use the integrated form of equation (2.8) after the

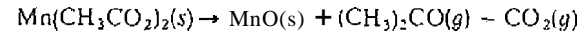
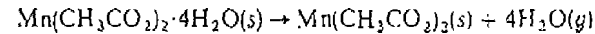
Table 2.1. Compounds Studied by the Self-generated atmosphere Technique (57)

Crucible Type	Compound
P	Ammonium carbonate monohydrate
MR	Anthracite
r	Bruceite [Mg(OH) ₂]
C	n-Butylammonium tetrachloroborate
C	r-Butylammonium tetrachloroborate
C	i-Butylammonium tetraphenylborate
C	s-Butylammonium tetraphenylborate
P	Cadmium carbonate
BV	Cadmium(II) sulphate (8/3) hydrate
P	Calcite (CaCO ₃)
BY	Cerussite (PbCO ₃)
/viR	Charcoal (wood)
P	Chrysotile
MR	Coal
BY	Cobalt(II) acetate tetrahydrate
CC	Cobalt(II) oxalate dihydrate
P	Cobalt(II) oxalate hydrate
BY	CuSO ₄ ·3Cu(OH) ₂ ·H ₂ O
BV	CuSO ₄ ·2Cu(OH) ₂
r, BV	Copper sulfate pentahydrate
C	Ethylammonium tetrachloroborate
BV	Gypsum (CaSO ₄ ·2H ₂ O)
DC	[Iron(III) carbonate]
r	Lead(II) carbonate
C (powder), p, CC	Lead(II) carbonate
CC, C	Lead(II) oxide
MR	Lignite
P	Magnesite (MgCO ₃)
CC	Magnesium sulfate heptahydrate
CC, C, P	Manganese(II) acetate tetrahydrate
DC, P	Manganese(II) carbonate
C	n-Octylammonium tetrachloroborate
C	n-Propylammonium tetrachloroborate
C	n-Propylammonium tetraphenylborate
DC	Rhodochrosite (MnCO ₃)
DC	Siderite (FeCO ₃)
P	Silver carbonate
P	Sodium oxalate
P	Talc
P	Thorium(IV) nitrate pentahydrate
P	Thorium(IV) oxalate hexahydrate
P	Uranyl sulfate hydrate
DC, BY	Zinc sulfate heptahydrate

Key to abbreviations: BV, ball valve; C, covered; CC, capillary crucible; DC, deep crucible; MR, micro-retort; P, piston.

technique, the atmosphere produced by the first reaction may have a beneficial or detrimental effect on the following reaction; for example, water can accelerate the decomposition of anhydrous CaC₂O₄.

The thermal decomposition of manganese(II) acetate 4-hydrate is discussed (57), to illustrate the use of the self-generated atmosphere. A two-step decomposition sequence has been proposed, similar to the following:



The mass-loss curves of Mn(CH₃CO₂)₂·4H₂O are illustrated in Figure 2.34 (57). In curve A, the sample loses mass immediately at room temperature which is water containing some acetic acid, the latter being detected by its odor. The two major stages of mass-loss on heating correspond approximately to the 1055 of hydrate-bound water and the decomposition of the anhydrous salt to manganese(II) oxide. Both stages of mass-loss show curve inflections.

The effect of the self-generated atmosphere, curve B, is to increase the initial mass-loss temperature, T_i, and to decrease the reaction interval, T_f - T_i. The increase in T_i has the beneficial effect of eliminating the initial mass-loss at room temperature with its resulting uncertainty about the starting point of the curve. The inflection point during loss of water is located at about 45°C and a mass fraction of 0.9. The second stage of mass-loss

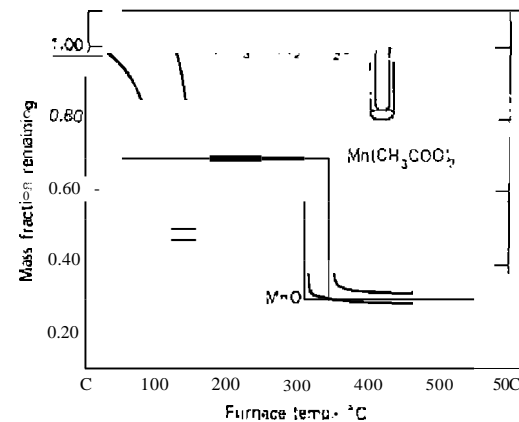


Figure 2.34. TG curves of Mn(CH₃CO₂)₂·4H₂O in a shallow dish containing 153.8 mg of dynamic N₂ and B piston crucible containing 102.6 mg in air. Heating rate was 150°C/h (57).

occurs in two approximately equal parts, a very rapid and uniform initial mass-loss followed by a less rapid but still fairly uniform second loss. The nearly horizontal mass plateaus had to be corrected for a buoyancy effect which is observed for all self-generated atmosphere sample holders.

The two curves are compared in a quantitative manner in Table 2.2. An advantage of a close-fitting piston crucible is that a determination can be stopped at any point, the crucible cooled and removed, and the gas analyzed. The disadvantage of this type of crucible is that if the piston is in contact with the molten sample, it will stick, and then subsequently be expelled from the cylinder.

A rather dramatic effect of the use of the self-generated atmosphere technique plus the quasistatic heating-rate mode is shown in Figure 2.35. Paulik and Paulik (21) found that the thermal decomposition of $\text{Ni}(\text{NH}_3)_6\text{Cl}_2$ dissociated in three separate steps, at 180, 320, and 360°C, respectively. The slight overshoot of the curve during the first dissociation reaction was said to be due to an induction period caused by delayed nucleus formation. The sample holder employed is described in Chapter 3.

The advantages and the limitations of the self-generated atmosphere technique have been described by Newkirk (57); they are the following.

Limitations

1. Buoyancy corrections vary depending on the molecular weight of the gas filling the crucible.
2. Large, heavy crucibles will cause a greater uncertainty in sample temperature.

Table 2.2. Comparison of Self-generated and Dynamic N_2 Mass-loss Curves for $\text{Mn}(\text{CH}_3\text{CO}_2)_2 \cdot 4\text{H}_2\text{O}$ (57)

Reactant	Dynamic N_2		Self-generated Atmosphere	
	Obs.	Calc.	Obs.	
T_i , first stage, °C	25		112	
T_f , first stage, °C	130		205	
Loss to $\text{Mn}(\text{CH}_3\text{CO}_2)_2$, %	30.6	29.40	29.0 ^a	(30.3) ^a
T_i , second stage, °C	260		340	
T_f , second stage, °C	350		367	
Loss to MnO , %	71.8	71.06	70.6 ^b	

^aCorrected for buoyancy effect.

^bUncorrected for buoyancy effect.

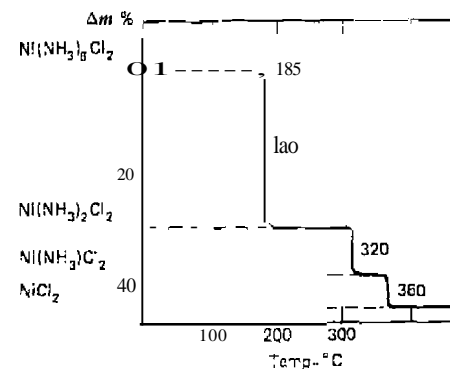


Figure 2.35. TO curve of $\text{Ni}(\text{NH}_3)_6\text{Cl}_2$ in self-generated sample holder and quasistatic heating (21).

3. in dehydration of hydrates, the chances of melting and the appearance of pseudo-plateaus may be enhanced.
4. Poorer resolution may result if the first reaction is delayed to a temperature at which a subsequent reaction begins.
5. Secondary reactions with the evolved gas may make interpretation difficult.

Advantages

1. The reaction interval will be narrower, overlapping reactions will be more clearly resolved, and intermediates will be more accurately identified.
2. New phases will be revealed.
3. Reactions will proceed, for the most part, at a fixed pressure at the gaseous products equal to atmospheric pressure. The course of reactions, except at the start, will not be affected by varying partial pressure.
4. The observed initial decomposition temperature will be more closely related to an equilibrium decomposition temperature.
5. Experiments can be performed on materials subject to oxidation at elevated temperatures with little interference from oxidation.
6. Very fast reactions can be studied without loss of solid product.
7. Better results will be obtained on materials with an appreciable vapor

pressure at room temperature. The sample can be weighed more accurately and will yield a horizontal baseline on the TG curve.

8. The effects of particle size difference will be reduced and the effects of crucible geometry standardized. This is particularly important with inhomogeneous materials such as rocks and minerals.
9. The recrystallizations of new phases from hydrates or hydroxides will be facilitated.
10. It has been claimed that irreversible decompositions will show better resolution and a smaller reaction interval in some instances, although it is not known why.

Recommended Uses

Thermogravimetry in self-generated atmospheres may be useful for studies of the following:

1. Consecutive reactions, and particularly for hydroxides, hydrates, ammoniates, carbonates, acetates, oxalates, and sulfates.
2. Inhomogeneous materials.
3. Compounds that decrepitate or explode.
4. Air-sensitive materials.
5. Volatile materials.
6. Materials that decompose to yield several gaseous products.
7. Destructive distillation.

E. DERIVATIVE THERMOGRAVIMETRY (DTG)

In conventional thermogravimetry, the mass of a sample, m , is continuously recorded as a function of temperature, T , or time, t ,

$$m = f(T \text{ or } t) \quad (2.4)$$

Quantitative measurements of the mass-changes are possible by determination of the distance on the curve mass axis, between the two points of interest or between the two horizontal mass levels. In derivative thermogravimetry, the derivative of the mass-change with respect to time, dm/dt , is recorded as a function of time (t) or temperature (T), or

$$\frac{dm}{dt} = f(T \text{ or } t) \quad (2.5)$$

In other cases, the derivative of the mass-change with respect to temperature, dm/dT , is recorded as a function of time (t) or temperature (T),

$$\frac{dm}{dT} = f(T \text{ or } t) \quad (2.6)$$

In either case, the resulting curve is the first derivative of the mass-change curve. A series of peaks are obtained, instead of the stepwise curve, in which the areas under the peaks are proportional to the total mass-change of the sample. A horizontal plateau in the TG curve gives a corresponding horizontal plateau in the DTG curve because $dm/dt = 0$. A maximum in the DTG curve is obtained when the TG curve has an inflection point where mass is being lost the most rapidly.

De Keyser (59, 60) first suggested DTG in 1953, followed by Erdey et al. (61) and Waters (62). Further work in this area has been by Erdey (63,64), Paulik et al. (65), Waddams and Gray (66), Waters (67), Cambell et al. (68), and Erdey et al. (69).

A comparison between a conventional (a) and a derivative (b) mass-loss curve is given in Figure 2.36. The derivative curve may be obtained either from the TG curve by manual differentiation methods or by electronic differentiation of the TG signal. Accessory equipment is available for most

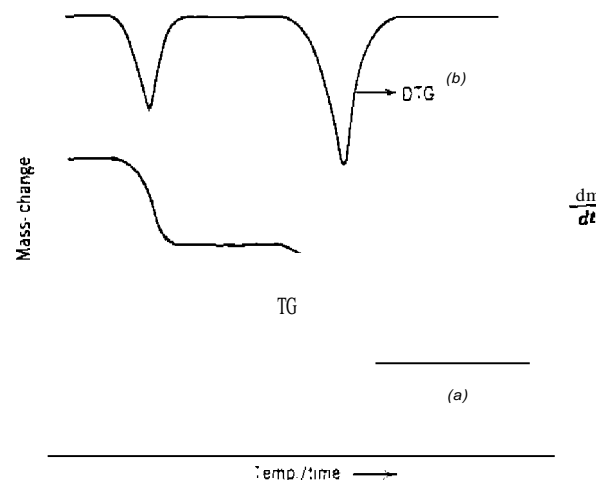


Figure 2.36. Comparison between (a) integral (TG) and (b) derivative (DTG) mass-loss curves.

thermobalances so that the DTG curve can be easily recorded along with the TG curve. The DTG curve, whether derived mathematically or recorded directly, contains no more information than does an integral TG curve obtained under the same experimental conditions; it simply displays the data differently (70).

Information obtainable from the DTG curve has been summarized by Dunn (116):

1. The DTG curve presents this information in a form that is more visually accessible, whereas the DTG curve contains no more information than does the TG curve.
2. The DTG curve allows the ready determination of the temperature at which the rate of mass-change is a maximum, T_{max} , and this provides additional information to the extrapolated onset temperature T_o and the extrapolated final temperature T_f . All three temperatures, however, respond to changes in experimental conditions, and T_{max} values are no more characteristic of a material than is T_o or T_f .
3. The area under the DTG curve is directly proportional to the mass-change.
4. The height of the DTG peak at any temperature gives the rate of mass-change at that temperature. These values can be used to obtain kinetic information since equations can be written of the form (117)

$$-\frac{dm}{dt} = A e^{-(E/RT)} f(m) \quad (2.7)$$

Dunn (116) has discussed the application of DTG curves to thermogravimetry; these applications include:

1. Separation of Overlapping Reactions

Reactions that occur within the same temperature range give TG curves that appear to consist of one continuous mass-loss. DTG curves, however, are discontinuous lines, and hence subtle mass-changes are emphasized. Four different TG curves and their corresponding DTG curves are shown in Figure 2.37. Curve (a) is a single reaction that occurs over a small temperature range; curve (b) consists of two reactions that are partially overlapping; curve (c) consists of two reactions, the first of which occurs slowly, followed by a fast reaction; and curve (d) is one in which minor reactions occur during or near a major reaction.

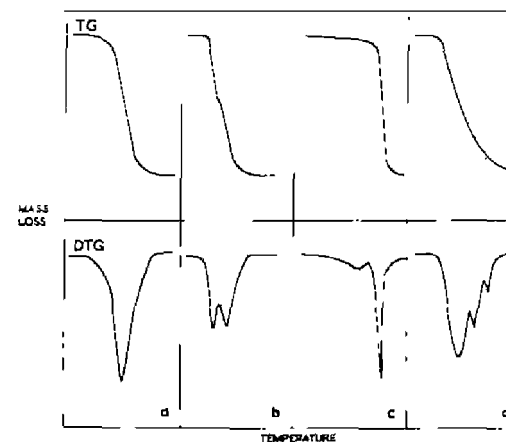


Figure 2.37. Comparison of TG and DTG curves, three of which exhibit overlapping reactions (116).

2. "Fingerprinting" Materials

Because the subtleties of the TG curve are visually emphasized in the DTG curve, the latter is frequently recorded as part of the characteristic information collected on new, unknown, or standard material.

3. Calculation of Mass Changes in Overlapping Reactions

When overlapping reactions occur, it is sometimes difficult to locate on the TG curve an unambiguous point where one reaction ends and the other starts. By use of the minima in the DTG curve, an extrapolation procedure such as that shown in Figure 2.38 can be used to determine approximately where the second reaction begins.

4. Quantitative Analysis by Peak Height Measurement

DTG curve peak heights may be used for quantitative purposes since when no mass-loss is occurring, $dm/dt = 0$. During a mass-loss reaction, $dm/dt > 0$, hence the DTG peak is proportional to the mass-loss of the sample. This approach has been used to analyze natural rubber and butadiene rubber in a blend (118) and also the degree of conversion of high alumina cement (19).

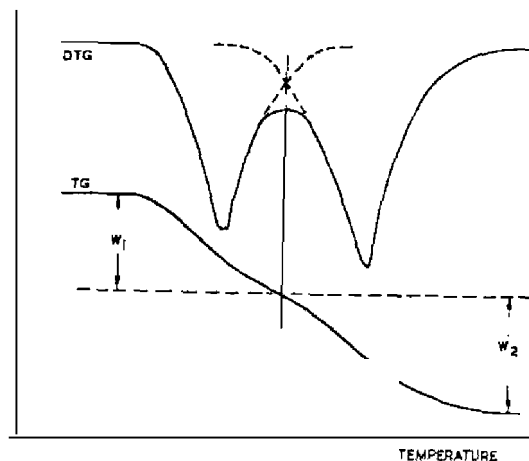


Figure 2.38. Idealized TG and DTG curves in which the minimum in the DTG curve is used to define the end of the first mass-loss and the onset of the second (116).

The advantages of derivative thermogravimetry have been summarized by Erdey et al. (61):

1. The curves may be obtained in conjunction with TO and DTA measurements.
2. The curves for OTA and derivative thermogravimetry (DTG) are comparable, but the results of the former method indicate even those changes of state that are not accompanied by loss in mass. The curves by the latter method are more reproducible.
3. Although the curves for OTA extend over a wider temperature interval, due to subsequent warming of the material after reaction, the DTG measurements indicate exactly the temperatures of the beginning, the maximum rate, and the end of the change.
4. On the TG curves, changes following each other very closely cannot be distinguished, as the corresponding stages coincide. The DTG curves or the same change indicate by sharp maxima that the thermogravimetric stages can be divided into two parts.
5. The DTG curves are exactly proportional to the derivatives of the TG curves; therefore, the area under the curves gives the change in mass precisely. Accordingly, DTG can give exact quantitative analyses.

6. The DTG method can be used for the investigation of materials which for some reason or another cannot be analyzed by DTA. For example, some organic compounds melt during heating, but even so the DTG method yields fairly good results.

The DTG technique has been criticized by Newkirk (58, 70), who claimed that the technique has not been subjected to extensive critical analysis. Some claims and comments of DTG compared to TG are given as follows (58):

Claim	Comment
1. DTG is more precise in showing onset of reaction accompanied by a small loss in mass.	1. Not unless a more sensitive balance is used.
2. DTG shows overlapping changes better.	2. This seems to be a real advantage to most people.
3. DTG permits reaction temperatures to be defined more exactly.	3. Only the temperature of the maximum rate.
4. Comparison of DTG and DTA enables distinction between DTA peaks due to mass-loss and those due to other thermal changes.	4. No advantage over TG.

The practice of designating the peak temperature of a DTG curve as the "decomposition temperature" should not be used. The peak temperature represents the temperature at which the rate of mass-change is at a maximum, and it clearly is not the temperature at which the sample begins to lose mass or T_i (70).

F. REACTION KINETICS

1. Nonisothermal Methods

Dynamic thermogravimetry has been widely used during the past 10 or so years to study the kinetics of thermal decomposition reactions. As pointed out by Doyle (71), one mass-loss curve is equivalent to a large number of isothermal mass-loss curves; also, this large amount of information is gained without sample-to-sample error, since the same sample is used throughout the determination. It should be pointed out, however, that thermogravimetric data are only narrowly definitive, and consequently, merely going through the motions of kinetic analysis can lead only to trial

transposition of the mass-loss, w , in equations (2.10) and (2.11),

$$\left(\frac{m_0}{w_\infty}\right)^{-n} \int_0^w (w_\infty - w)^n dw = \frac{A}{\phi} \int_{T_1}^{T_2} e^{-E/RT} dt \quad (2.12)$$

The right-hand side of this equation can be solved by various methods, and the final solution to the equation is an infinite series of which the first two terms are of interest generally. These methods are used by Doyle (84) and Coats and Redfern (85) as well as by others (86, 87).

In the approximation methods, the right-hand side of equation (2.12) is solved by an approximation using the temperature, T_i , corresponding to the maximum rate of decomposition. This method was used by Horowitz and Metzger (88) and others (87, 89-91).

a. Newkirk Method

From a single TG curve, Newkirk (12) obtained rate constants for the decomposition reaction, as illustrated in Figure 2.39. For a series of temperatures, T_1 and T_2 , the sample mass remaining, $a - x_1$ and $a - x_2$, and the reaction rates, (dx/dt) , and $(dx/dt)_h$ were obtained by tangents to the curve at points 1 and 2. If the reaction is of first order, then the logarithm of the reaction rate constant k , $dx/dt = k(a - x)$, when plotted against $1/T$, should yield a straight line. The results of measurements under isothermal and

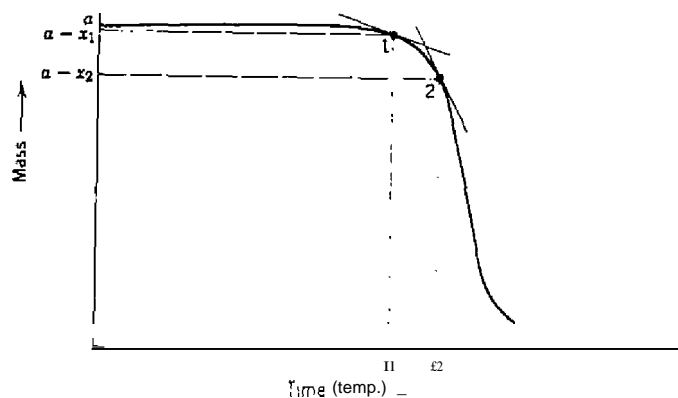


Figure 2.39. Determination of reaction rate and extent of reaction from a TG curve (12).

nonisothermal conditions yielded straight lines that were approximately parallel.

b. Freeman and Carroll Method

Perhaps the most widely used kinetics method is that developed by Freeman and Carroll (83) in 1958. The advantage of this method is that considerably fewer experimental data are required than in the isothermal method and that the kinetics can be obtained over an entire temperature range in a continuous manner without any missing regions. In addition, where a sample undergoes considerable reaction in being raised to the temperature of interest, the results obtained by an isothermal method are often questionable. The order of reaction, n , and the activation energy of the reaction are calculated from the equation

$$\frac{-(E/2.3R)\Delta(1/T)}{\Delta \log w_r} = -n + \frac{\Delta \log (dw/dt)}{\Delta \log w_r} \quad (2.13)$$

where $w_r = w_\infty - w$, in which w_∞ is the maximum mass-loss, and w is the total loss in mass up to time t .

c. Horowitz and Metzger Method

For the example in which the rate constant involves concentrations expressible as mole fractions and the total number of moles is constant, the expression (88)

$$\ln \ln \left(\frac{W_0 - W_f}{W - W_f} \right) = \frac{E\theta}{RT^2} \quad (2.14)$$

may be used, in which W is the mass remaining at a given temperature, W_0 and W_f are the initial and final masses, respectively, and θ is a reference temperature.

d. Coats and Redfern Method

for a reaction in which the order is unknown, Coats and Redfern (85) derived the following expression:

$$\log \left\{ \frac{1 - n(1 - x)^{1-n}}{1 - n(1 - x_1)^{1-n}} \right\} = \log \frac{AR}{nE} \left[1 - \frac{2RT}{E} \right] - \frac{E}{2.3RT} \quad (2.15)$$

where α is the fraction of the sample decomposed at time t , and a is the heating rate. A plot of either $\log[1 - (1 - \alpha)]^{1-n}/T^2$ (if $n > 1$) or, where $n = 1$, $\log[1 - \alpha]/T^2$ against $1/T$, should result in a straight line of slope $-E/2.3R$ for the correct value of n . The quantity $\log(AR/af) - (2RT/E)$ appears to be reasonably constant for most values of E and all the temperature range over which most reactions occur.

e. Doyle Method

The kinetics of volatilization of polymers have been discussed in detail by Doyle (71, 84). If w is the apparent residual mass fraction calculated on the initial mass, the apparent mass fraction volatilized, v , is

$$v = (1 - w) \quad (2.16)$$

The apparent volatilization rate is found by multiplying the TG curve slope, $-dw/dT$, by the constant heating rate, B ;

$$\frac{dv}{dt} = -B \frac{dw}{dT} \quad (2.17)$$

For a particular volatilization step, however, the appropriate residual mass fraction is the true one, h , calculated on the total reaction volatilized during the step, rather than on the total initial mass

$$h = \frac{w - G}{H} \quad (2.18)$$

where H is the total apparent mass fraction volatilized during the step and G is the apparent weight fraction remaining after the step has been completed. From equations (2.16) and (2.17),

$$\frac{dv}{dt} = -H \frac{dh}{dt} \quad (2.19)$$

It should be noted that H and G are seldom clearly defined; their estimation, in many cases, constitutes one of the major difficulties of kinetics calculations.

Another difficulty arises from the need to take into account the nature of the kinetic process. In general

$$-\frac{dh}{dt} = f(h) \quad (2.20)$$

where r is the empirical rate constant of volatilization and the specific form of $f(h)$ depends on the reaction order. The constant r must be treated as empirical because its value for a particular substance is not always uniquely determined by temperature, but may depend on the nature and geometry of the sample holder, the nature of the environmental atmosphere, and other factors. The potential triviality of r was constantly emphasized by Doyle (84) by use of the symbol r instead of the specific rate constant, k . Using this terminology, the Arrhenius equation for the volatilization process is

$$r = ae^{-b/RT} \quad (2.21)$$

The constant b , at least over part of the experimental temperature range, had the same value as the activation energy.

When evaluating the constants in equation (2.17), one usually employs only a small portion of the TG curve, the region where the slope is neither too shallow nor too steep to be measured with sufficient precision. In fact, in the range of volatilization rates that are small compared to the heating rate, the slopes found from the TG curve are not only imprecise, but they are also inherently inaccurate, being consistently greater than those found by an isothermal method. This effect is due to the fact that, in thermogravimetry, the dwell time at each temperature is so brief that no evidence of volatilization can accumulate in the range of small volatilization rates.

Zsako (94) has also attempted to simplify Doyle's trial-and-error method and to find new applications to TG curves. Starting with the basic equation previously described by Doyle (84),

$$g(x) = \frac{AE}{Rq} p(x) \quad (2.22)$$

and taking the logarithm, he obtained

$$\log \frac{AE}{Rq} = \log g(x) - \log p(x) = B \quad (2.23)$$

where B depends only on the nature of the compound studied and on the heating rate, but not on the temperature. The value of $g(x)$ for a given temperature can be calculated from the TG curve if $f(x)$ is known.

The method consists of the following: Presuming the validity of the function $f(x)$ and using TG data, the author calculated $g(x)$ values for different temperatures. By means of a trial-and-error method, the apparent activation energy can be estimated by finding the E value which ensures the maximum

constancy of

$$B = \log g(\alpha) - \log P(X) \quad (2.24)$$

f. Ingraham and Marier Method

For a reaction such as the thermal decomposition of calcium carbonate, which obeys linear kinetics, the rate constant may be expressed as

$$k = \frac{dw}{dt} \quad (2.25)$$

in which dw represents the loss in mass from unit area in period of time, dt . When the temperature of the sample is increased at a linear rate, the temperature at any time, t , is

$$T = b + at \quad (2.26)$$

where a is the heating rate and b the initial temperature. From this relationship, Ingraham and Marier (95) showed that if dt is replaced by dT/a , the following equation can be written:

$$\log \frac{dw}{dT} = \log T - \log a + \log C - \frac{E}{2.303R} \quad (2.27)$$

The activation energy is calculable from the slope of a plot of $[\log(dw/dT) - \log T + \log a]$ versus $1/T$. The logarithm of the heating rate, although constant for any particular experiment, was retained in the equation to permit correlation of TG curves carried out at different heating rates.

g. Vachuska and Voboril Method

In this method (96), the kinetic constants are calculated from the TG curve by a differential method. It takes into account also the thermal effects of reactions which result in a deviation of the sample temperature from the programmed values of the linear heating. Starting with the differential equation for the thermal decomposition of a solid,

$$\frac{d\alpha}{dt} = k(1-\alpha)^n \exp\left(-\frac{E}{RT}\right) \quad (2.28)$$

where α is the degree of transformation, one finds that the logarithm of this

equation is

$$\ln\left(\frac{d}{dt}\right) = \ln k + n \ln(1-\alpha) - \frac{E}{RT} \quad (2.29)$$

Considering that α and T are functions of time and differentiating with respect to time,

$$\frac{d^3\alpha/dt^3}{d\alpha/dt} = -\frac{n}{1-\alpha} \left(\frac{d\alpha}{dt}\right) + \frac{E}{RT^2} \left(\frac{dT}{dt}\right) \quad (2.30)$$

By rearrangement, a linear equation is obtained

$$\frac{(d^3\alpha/dt^3)T^2}{(d\alpha/dt)(dT/dt)} = -\frac{n}{1-\alpha} \frac{T^2}{dT/dt} + \frac{E}{R} \quad (2.31)$$

by means of which the reaction order, n , can be calculated from the slope and the intercept gives the activation energy.

1. Miscellaneous Methods

Simplified methods for the calculation of specific rate constants from TG curves have been described by various investigators. Dave and Chopra (97) calculated the specific rate constant by use of the equation

$$k = \frac{(Ajmo)^{n-1}(dx/dt)}{A - a^n} \quad (2.44)$$

where A is the total area under the derivative TG curve (DTG); a is the area for the reaction up to time t ; dx/dt is the height of the curve at time t ; m_0 is the initial mole fraction of the reactant; and n is the order of reaction.

A similar approach was employed by Papazian et al (98) and Adoniji (100) in which the specific rate constant was calculated from a DTG curve by use of the expression

$$k = \frac{dx/dt}{(a-x)^n} \quad (2.45)$$

where $(a-x)$ is the mass of reactant not decomposed. This simple method was said to yield kinetic results which were similar to those obtained from isothermal measurements.

Fanner (99) used the expression

$$\log(-\dot{w}w^{-n}) = \frac{-E}{R \ln 10} \left(\frac{1}{T}\right) + \log A \quad (2.46)$$

where w is the reactant mass fraction, calculating E and A from the slope and intercept of a parametric plot of $\log(-\dot{w}w^{-n})$ versus $1/T$.

Magnuson (101) discussed in detail the individual steps needed to calculate the kinetics of the thermal decomposition of a high molecular weight dimethylsiloxane polymer. Use was made of the simple first-order rate equation

$$-\frac{dW}{dt} = k_p W \quad (2.47)$$

where $-dW/dt$ is the rate at which sample mass is decreasing, k_p is the procedural rate constant, and W is the sample mass.

The method derived by Achar et al. (102) is a differential one and applies to all reaction mechanisms, provided that the correct mechanism is known (76). It is based on the use of the expression

$$\ln\left(\frac{1}{f(\alpha)} \cdot \frac{d\alpha}{dT}\right) = \ln \frac{A}{B} - \frac{E}{RT} \quad (2.48)$$

where α is the fraction of sample reacted in time t , and B is the heating rate. When the left-hand side of the equation is plotted against $1/T$, a straight line is obtained from which E and A can be determined. The form of $f(\alpha)$ depends on the nature of the reaction; for example, for the parabolic law, $\alpha^2 = kt$, which applies to many diffusion controlled reactions, $f(\alpha) = \frac{1}{2}\alpha$.

The method developed by Broido (103), which was applied to the pyrolysis of cellulose, is based on the equation

$$\ln \ln \frac{1}{Y} = -\left(\frac{E}{R}\right)\left(\frac{1}{T}\right) + \text{constant} \quad (2.49)$$

where Y is the number of initial molecules not yet decomposed. Thus, a plot of $\ln \ln (1/Y)$ versus $(1/T)$ should yield a straight line from which E and Z can be calculated from the slope.

h. Master Data Method

Jones et al. (122) used the reduced-time method of Sharp et al. (123) in which the experimental kinetics data are plotted against the master data in such a way as to produce a linear plot. The experimental data are first expressed in the form α_e as a function of $(t/t_{0.5})_e$, where e refers to the experimental data. Three equivalent plotting procedures are then possible:

1. The experimental value α_e at which $(t/t_{0.5})_e$ has the same value as that in the master data $(t/t_{0.5})_m$ is plotted against the master value of α (designated α_m). If $\alpha_e = \alpha_m$ the resulting plot will be a straight line through the origin with slope α_e/α_m equal to unity.
2. The experimental value $(t/t_{0.5})_e$ may be plotted against $(t/t_{0.5})_m$ for common values of α_e and α_m . The resulting plot should be a straight line through the origin with slope $(t/t_{0.5})_e/(t/t_{0.5})_m$ equal to unity for absolute correlation.
3. The experimental time t_e may be plotted against $1/(t_{0.5})_m$ for common values of α_e and α_m . For complete correlation the plot should be a straight line through the origin with slope equal to $(t_{0.5})_e$.

Any of the three methods will indicate the value of A in the general expression, $k = A/(t_{0.5})_e$, thus allowing k to be evaluated directly. Master values of $t/t_{0.5}$ as a function of α for common solid-state reaction expressions are presented (122).

i. Steady-state Parameter Jump Method

Flynn and Dickens (124) described a TG method in which the magnitude of a rate-forcing variable such as temperature, pressure, gaseous flow rate, gaseous composition, and so on is jumped by discrete steps. This method can be used to determine kinetic relationships between the rate of mass-loss and the jumped variable. The method avoids the disparate effects of separate experimental histories in methods in which two or more experiments are compared and also the necessity for guessing the complex rate versus the extent of reaction relationship.

The technique is illustrated schematically for temperature jump in Figure 2.40 (124), in which the rate of mass-loss, \dot{w} , is plotted as a function of time. The rate, at a constant temperature, T_1 , proceeds along a smooth curve until time, t_1 , when the temperature is jumped to a new value, T_2 . At T_2 , the mass-loss adjusts to the new temperature and as temporal lags dissipate, it follows

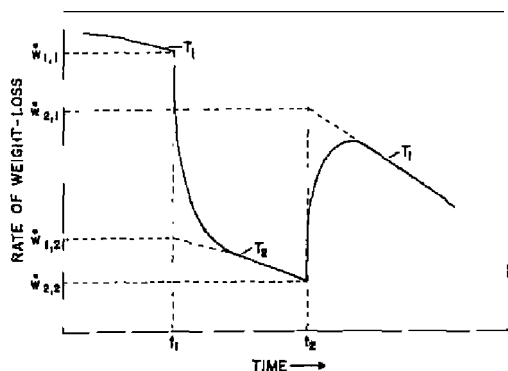


Figure 2.40. Schematic temperature jump experiment (124).

a new steady-state curve. At time, t_2 , the temperature is jumped from T_2 back to the original value, T_1 . The rates of mass-loss before and after (by extrapolation) the jump are $\dot{w}_{2,2}$ and $\dot{w}_{2,1}$, respectively.

The method was applied to the kinetics of the oxidation of polystyrene.

j. Reich and Stivala Method

In this method (125), values of E corresponding to various arbitrarily selected values of n are calculated for each two given pairs of values of α and T . The resulting arbitrary values of E may be plotted against corresponding n values, and the region bounded by intersecting curves used simultaneously to estimate actual values of E and n .

For two pairs of values of α and T ,

$$\ln \frac{1 - (1 - \alpha_1)^{1-n} \left(\frac{T_2}{T_1}\right)^2}{1 - (1 - \alpha_2)^{1-n}} = \frac{E}{R} \left(\frac{1}{T_2} - \frac{1}{T_1} \right) \quad (2.32)$$

values of E/R can be calculated for various arbitrarily selected values of n . Assuming uniqueness, only one pair of E, n values will be pertinent. By using other pairs of α and T values, one will obtain other sets of values of E and corresponding n . In all these sets, there should only be one pair of E, n values in common. This pair can be ascertained by plotting the various sets of E, n values. The region bounded by the intersecting curves will be common to all (or most) of the curves and from this region can be determined values of E and n simultaneously. The equation does not apply when $n = 1$; it is rare in practice for reactions to be exactly first order, and hence this equation is

considered to be of general utility. The frequency factor, A , can be calculated from

$$\ln K = \ln \left[\frac{1 - (1 - \alpha)^{1-n}}{y^2} \right] + \frac{E}{RT} \quad (2.33)$$

where

$$K = \frac{A(1-n)R}{(RH)E} \quad (2.34)$$

RH is the constant rate of heating. Various values of K (and hence of A) can be evaluated from values of α and corresponding values of T . From these values of K , an average value of A may be estimated.

Reich and Stivala (126) used the preceding method (R-S) and a double-log (D-L) method to distinguish one reaction mechanism from among 15 theoretical possibilities for heterogeneous solid-state reactions using theoretical TG data. With a certain degree of accuracy of TG data and for large E/RT values (718), the R-S method was shown to be superior to the D-L method and a good indicator of a most probable mechanism.

An iteration method for calculation of E and n using computer data reduction techniques was also described by Reich and Stivala (127) as well as various other algorithms (128-133, 137-139) and graphical methods to determine the reaction mechanism (134-136).

Criado and Ortega (140) concluded that Reich and Stivala's method makes possible the assignment of an "n order" to a reaction that follows quite a different mechanism. In such a case, the method gives erroneous values of E .

k. Ozawa Method

This is an approximate integral method similar to, but simpler than, that of Doyle (142). It is more widely applicable than some of the other methods and can be used for the random degradation of high polymers.

In this method (92), the fractional weight, W , of a reacting material is expressed as a function of the fraction of a structural quantity, such as a group, a constituent, a broken bond, and so on, which is represented by x :

$$W = f(x) \quad (2.35)$$

where x changes according to the kinetic equation

$$\frac{dx}{dt} = A \exp \left(-\frac{E}{RT} \right) g(x) \quad (2.36)$$

By integration,

$$-\int_{x_0}^x \frac{dx'}{g(x')} = A \int_{t_0}^t \exp\left(-\frac{E}{RT}\right) dt \quad (2.37)$$

where x_0 is the value of x at $t = t_0$.

When the temperature of the sample is increased at a constant rate, a , the change in x is given by

$$-\int_{x_0}^x \frac{dx}{g(x)} = \frac{A}{a} \int_{T_0}^T \exp\left(-\frac{E}{RT}\right) dT \quad (2.38)$$

where T_0 is the value of T at $t = t_0$. Ordinarily, the rate of the reaction is very low at low temperatures, thus

$$-\int_{T_0}^T \exp\left(-\frac{E}{RT}\right) dT = \int_0^T \exp\left(-\frac{E}{RT}\right) dT \quad (2.39)$$

The value of the right-hand side is expressed and tabulated by Doyle (41) as the function, p :

$$\frac{E}{R} p\left(\frac{E}{RT}\right) = \int_0^T \exp\left(-\frac{E}{RT}\right) dT \quad (2.40)$$

If E/RT is larger than 20, $p(E/RT)$ can be approximated by

$$\log p\left(\frac{E}{RT}\right) = -2.315 - 0.4567 \frac{E}{RT} \quad (2.41)$$

If the weight decreases to a given fraction at temperature, T_1 , for a heating rate of a_1 , at T_2 for a_2 , and so on, the equation obtained is

$$\frac{AE}{a_1 R} p\left(\frac{E}{RT_1}\right) = \frac{AE}{a_2 R} p\left(\frac{E}{RT_2}\right) = \dots \quad (2.42)$$

From equation (2.42) the linear equation is derived:

$$-\log a_1 - 0.4567 \frac{E}{RT_1} = -\log a_2 - 0.4567 \frac{E}{RT_2} = \dots \quad (2.43)$$

Thus, plots of $\log a$ versus $1/T$ for a given value of W must be a straight line.

the slope of which gives E . If the TO curves are given as plots of W versus $1/T$ for various heating rates, the curves can be superimposed upon each other by shifting them along the abscissa. The length of the lateral shift is proportional to the logarithm of the heating rate of the curve.

Ozawa has applied this method to DTO curves (93) and has also studied the effect of the heating rate on TA curves in greater detail (143).

2. Comparison of Different Methods

Sestak (43) compared the kinetic results calculated by five different methods for a system corresponding to the dehydration of $\alpha\text{-CaSO}_4 \cdot 0.5\text{H}_2\text{O}$. The five methods evaluated mathematically were: (1) Freeman and Carroll (83); (2) Doyle (84); (3) Coats and Redfern (85); (4) Horowitz and Metzger (88); and (5) Van Krevelen et al. (81). From these calculations it was found that the deviations of computed values of E did not differ by more than 10%. Thus, all the methods appear to be satisfactory for the calculation of E within the limits of accuracy required. The errors of each method due to the inaccuracy of visual deduction of values from the TO curves were also calculated. These errors, ϵ_E and ϵ_n (errors in calculation of E or n , respectively), were as follows: (1) Freeman and Carroll method, $\epsilon_E = 4\%$ and $\epsilon_n = 12\%$; (2) Horowitz and Metzger method, $\epsilon_E = 2\%$ (when the correct value of n is assumed); (3) Doyle method, $\epsilon_E = 4\%$. However, the magnitude of this error depends primarily on the position of the point on the TO curve on which the calculations are being performed. In the case of differential methods, the most accurate data are calculated from the medium-steep parts of the curve. For the approximation method, the accuracy depends on the determination of the curve inflection point temperature.

From the viewpoint of ease of computation, Doyle's method seems to be very simple because the kinetic data are obtained from a single point on the curve. The necessity of knowing the reaction order ahead of time appears to be a disadvantage which finds a partial remedy in the Coats and Redfern method.

Three kinetic methods were evaluated by Sharp and Wentworth (76) using the thermal decomposition of calcium carbonate under various conditions. The physical state of the sample was as a pellet, a powder, or as 1:1 molar ratios with α -aluminum oxide or α -iron(III) oxide. The three methods used were: Method I, Freeman and Carroll; Method II, Coats and Redfern; and Method III, Achar et al. (102). The kinetic data calculated by Methods II and III are presented graphically in Figure 2.41 and in Table 2.3. In every case a linear plot was obtained over a wide range of x with $n = \frac{1}{2}$. When these methods were applied with $n = \frac{2}{3}$, the range of x was less, especially in the case of Method III, which led to noticeable curvature at

THERMOGRAVIMETRY

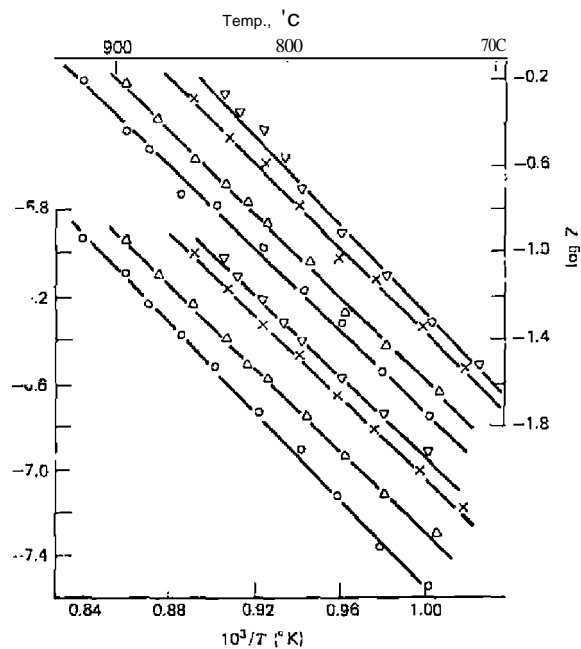


Figure 2.41. Data calculated from Methods II and III (76). \circ CaO, (pellet); Δ CaCO₃ (powder); \square CaCO₃·Al₂O₃; ∇ CaCO₃·Fe₂O₃.

high values of α . With $n = 1$, this curvature became more marked for both methods. Activation energies with $n = \frac{1}{2}$ averaged about 44 kcal/mole. The addition of iron or aluminum oxides did not affect the activation energy.

The results obtained by means of Method I, from a combination of data on the pellet and powder, are given in Figure 2.42 and Table 2.4.

The points are more scattered than those given in Figure 2.41, leading to much uncertainty in the value of E . The line shown is a theoretical line drawn to pass through the ordinate axis at -0.5 with a slope which leads to the values of 44 kcal/mole for the activation energy. Although this line seems satisfactory, other lines reading to different values for n and E could be easily drawn.

Methods II and III lead to substantially the same results; the latter has the advantages of leading directly to values for A from the intercept and being equally applicable to both diffusion-controlled and order-of-reaction kinetics. The disadvantage of this method is the necessity of determining

Table 2.3. Kinetic Parameters Using Methods II and III (76)

Material	Method II $n = \frac{1}{2}$		Method III $n = \frac{1}{2}$		Method II $n = \frac{1}{2}$		E kcal/mole	Range	E kcal/mole	Range
	Range	E kcal/mole	Range	E kcal/mole	Range	E kcal/mole				
Cu pellet CaCO ₃	0.03-0.08	46	0.01-0.08	43	0.03-0.08	49	0.0-0.8	45		
powder	0.05-0.06	43	0.01-0.06	44	0.05-0.06	44	0.0-0.79	47		
CaCO ₃ ·Al ₂ O ₃	0.06-0.07	43	0.03-0.07	44	0.06-0.07	44	0.0-0.67	46		
CaCO ₃ ·Fe ₂ O ₃	0.1-0.183	42	0.07-0.083	48	0.1-0.183	45	0.007-0.72	48		

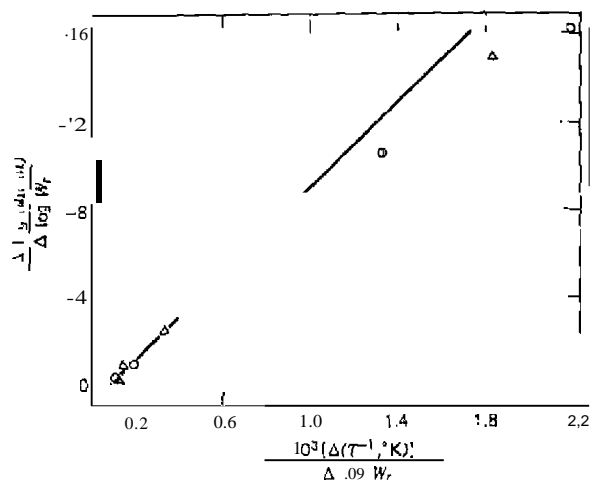


Figure 2.42. Data calculated from Method I (93). \circ CaCO₃ (pellet); Δ CaCO₃ (powder).

Table 2.4. Kinetic Parameters from Method I (76)

Number of Points Used	Range	n	E kcal/mole
8	0.25-0.84	± 0.55	43
14	0.05-0.84	-0.07	36

$d\alpha/dT$, the tangents to the TG curve, at a series of values for T . Method II is slightly less tedious to calculate than Method III and avoids the determination of tangents.

The greater scatter in the data obtained by Method I is due largely to the determination of three difference functions over short temperature intervals. One of these involves the tangents dW/dt ; therefore, any inaccuracy in determining a single value affects the position of two points in the plot used to determine the activation energy. As a result of these analyses, Method I was considered less satisfactory than the other two methods and was not recommended for use.

Carroll and Manche (104) criticized the use of trial-and-error methods of calculations, such as those previously described in Methods II and III. The question arises whether the criterion of constancy of kinetic parameters is appropriate even for the case of a simple chemical reaction, since a solid-

state reaction is a very complex process. They argued that in our present state of knowledge, constancy of kinetic parameters in general, for reactions in the solid state, is an unwarranted assumption. The Freeman and Carroll method can be used if the random errors in the slope measurements are smoothed out, particularly for the initial and final stages of the process. Precision of the method can be enhanced considerably by this simple procedure.

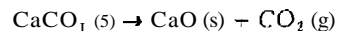
Johnson and Gallagher (145) compared the same three kinetic methods that Sharp and Wentworth (76) employed. Using the thermal decomposition of $\text{BeSO}_4 \cdot 4\text{H}_2\text{O}$, they tabulated the kinetic results as shown in Table 2.5. Plots for Method III generally showed a greater degree of nonlinearity for a poor fitting model than do those of equations of Method II. An attempt was made to adapt the Erofeev and power law models to the Method II analysis but it was found that this method was completely insensitive to these models. The effect of heating rate and sample size was also determined for these methods. It was found that [for variation in sample size, the kinetic parameters were reasonably constant (for E), whereas the apparent A showed a general downward trend with increasing sample size. In general, the same effects were noted for the change in heating rates. Method III was found to be the most useful nonisothermal kinetics method. Results from this method most

Table 2.5. Comparison of Standard Deviation for Several Kinetic Models for 11.2 mg of Reagent Beryllium Sulfate Heated at 4.9°/min; $\alpha = 0.1 - 0.9$ (145).

Method	Kinetic Model	Stand. Dev.	Activation energy (kcal/mol)	Preexp Term (sec ⁻¹)
II	Order $n = 0.50$		48	1.3×10^7
	Order $n = 0$	0.022	41	6.5×10^5
	$n = \frac{1}{2}$	0.002	48	1.3×10^7
	$n = \frac{2}{3}$	0.006	51	3.5×10^7
	$n = 1$	0.014	56	2.0×10^9
III	Order $n = 0$	0.0010	31	3.9×10^3
	$n = \frac{1}{2}$	0.0002	49	1.6×10^7
	$n = \frac{2}{3}$	0.006	54	2.1×10^8
	Order or Erofeev $n = 1$	0.0012	66	2.5×10^9
	Erofeev $n =$	0.0010	36	5.1×10^4
Isothermal order	$n =$	0.0030	26	2.5×10^2
	$n =$		52	4.0×10^8

consistently matched the isothermal results in terms of kinetic model, E and A .

In another investigation, Gallagher and Johnson (147) compared isothermal and nonisothermal methods to study the reaction kinetics of the thermal decomposition of CaCO_3 . According to isothermal kinetics studies, the reaction



fits the contracting geometry rate law as well as the Erofeev equation with $n = 2$. The former, however, is conceptually simpler and has the added advantage of being more compatible with nonisothermal techniques. A comparison study using the various nonisothermal techniques at different heating rates and sample sizes for this reaction is illustrated in Table 2.6. In general, the E values at any given heating rate decrease with a decrease in sample mass. The same trend is observed for $\log A$ values.

Galadla (146) compared the methods of Kissinger (148), Reich (149), Carroll and Manche (81), Coats and Redfern (85), and Satava and Skvara (150) to study the thermal decomposition kinetics of $\text{CaC}_2\text{O}_4 \cdot \text{H}_2\text{O}$, CaC_2O_4 , $\text{MgC}_2\text{O}_4 \cdot \text{H}_2\text{O}$, and MgC_2O_4 . Methods based on the maximum rate temperature such as those of Kissinger, Reich, and Carroll, and Manche were not suitable because they could not distinguish between overlapping reactions or mechanisms. Satava and Skvara's method is recommended since it gives the least number of possible operating mechanisms. The dehydration mechanisms are as follows: $\text{CaC}_2\text{O}_4 \cdot \text{H}_2\text{O}$, three-dimensional phase boundary movement; $\text{MgC}_2\text{O}_4 \cdot \text{H}_2\text{O}$, Avrami-Erofeev nuclei growth; CaC_2O_4 , Avrami-Erofeev nuclei growth A_2 ; and MgC_2O_4 , three-dimensional phase boundary migration mechanism.

Barbooti (151) compared the Coats and Redfern (85) and Horowitz and Metzger (88) methods for the kinetics of the decomposition of $M \text{ Mal} \cdot 3\text{H}_2\text{O}$ complexes ($M = \text{Mn, Co, Ni, and Cu}$ and $\text{Mal} = \text{malonate}$). It was concluded that multistep reactions may be investigated employing these methods and accurate isolation of the overlapping reactions can be obtained.

Rajeshwar (152) determined the kinetics of the thermal decomposition of Green River oil shale kerogen by using direct Arrhenius, Freeman and Carroll, and Coats and Redfern methods. The E , A , and n values are given in Table 2.7. Rajeshwar concluded that the ability to resolve multiple processes hinges on the efficacy of the particular kinetic analysis employed and is not an inherent difficulty with nonisothermal TG techniques in general. The direct Arrhenius and Coats and Redfern methods clearly indicate the presence of two reactions with distinctly different kinetic parameters. On the other hand, the Freeman and Carroll method is handicapped at low fractional

Table 2.6. Comparison of Kinetics Data Obtained on CaCO_3 in Oxygen by Different Nonisothermal Methods (147)

Temp. Rate (°C/min)	Weight (mg)	ABS ^a		CR ^b		FC ^c		n
		ΔH^{*d}	$\log A$	ΔH^{*d}	$\log A$	ΔH^{*d}	$\log A$	
73.6	1.25	53.4	908	55.5	9.54	58.4	10.04	0.63
	2.08	50.9	836	54.5	9.11	52.6	8.66	0.56
	4.07	44.2	6.58	48.3	7.42	47.5	7.18	0.61
	8.73	45.7	6.65	45.5	6.62	45.7	6.66	0.47
	16.05	44.2	6.11	37.5	4.81	45.0	6.26	0.52
18.2	0.77	56.6	10.18	61.6	11.30	59.9	10.83	0.58
	2.15	55.0	9.36	55.9	9.53	44.3	7.11	0.21
	4.39	51.2	8.20	51.4	8.23	48.5	7.65	0.40
	7.79	50.8	7.89	48.6	7.43	52.4	8.15	0.58
	16.72	45.7	6.54	42.7	5.92	47.4	6.84	0.55
4.45	0.01	60.5	11.32	66.5	12.75	70.6	13.42	0.79
	2.30	59.3	10.59	61.5	11.11	52.8	9.15	0.35
	4.20	59.0	10.28	58.1	10.04	50.1	8.32	0.25
	8.14	54.8	8.99	55.1	9.04	50.4	8.04	0.18
	16.16	52.5	8.20	50.8	7.82	47.6	7.18	0.38
1.16	1.09	63.4	11.80	62.0	11.46	62.5	11.58	0.48
	2.27	60.5	10.81	60.2	10.73	46.9	7.69	0.14
	2.81	58.3	10.04	56.3	9.66	53.4	8.95	0.38
	8.18	61.9	10.53	56.3	9.20	58.6	9.76	0.46
	16.34	56.1	9.04	52.3	8.18	44.5	6.51	0.17
0.29	0.96	54.8	9.74	55.1	9.89	34.3	4.69	-0.18
	2.11	60.2	10.82	56.9	10.00	67.3	12.45	0.69
	3.76	59.4	10.45	55.6	9.46	55.2	9.45	0.42
	7.81	55.3	10.04	51.4	9.08	42.5	7.00	0.11
	15.86	56.7	9.36	51.5	8.11	46.0	7.88	0.18

^aDifferential method of Achar, Brindley and Sharp (102), $n = 0.5$.

^bIntegrating method of Coats and Redfern (8), $n = 0.5$.

^cDifference-differential method of Freeman and Carroll (83).

^dIn kcal/mole.

n = order of reaction.

conversions where extraction of difference differentials from the raw TG data is prone to increasing error. Application of the latter on the TG data of oil shales would have led to incomplete information on the pyrolysis mechanism. The Coats and Redfern method yields somewhat lower values for E relative to the other methods employed.

Table 2.7. Kinetic Parameters for the Nonisothermal Decomposition of Green River Oil Shale Kerogen (152)

Method	Heating Rate (°C/min)	Kinetic Parameters ^a				n ^b
		E ₁	E ₂	A ₁	A ₂	
Direct Arrhenius [eq. (6) and Fig. 3]	5	82.96 (13.44)	187.71 (3.23) ^c	5 × 10 ⁴ (1.42)	5.9 × 10 ¹² (1.18)	
	10	74.75 (2.85)	162.57 (2.22)	2.9 × 10 ⁴ (1.18)	9.7 × 10 ¹⁰ (0.82)	
	20	108.10 (1.06)	209.50 (2.98)	9.78 × 10 ⁶ (1.18)	2.88 × 10 ¹⁴ (1.06)	
Freeman Carroll [eq. (12) and Fig. 4]	5, 20		138.27 (0.42)			
Coats-Redfern [eq. (8) and Fig. 5]	5	41.9 (0.92)	117.32 (2.18)			
	10	27.40 (1.05)	116.48 (1.59)			
	20	37.21 (1.76)	133.24 (2.31)			

^aUnits of E and A are in kJ/mole and min⁻¹, respectively.

^bA kinetic order of unity was assumed for the direct Arrhenius and Coats and Redfern methods (see text).

^cNumbers in parentheses represent standard deviation by least-squares analyses.

Ozawa (153) found that the Freeman and Carroll, Coats and Redfern, and Sharp and Wentworth methods cannot be applied to a second-order reaction, random scission in main chains of polymers, and a system of two parallel competitive first-order reactions. These three methods, nonetheless, yielded straight-line relationships and false unreal kinetic parameters were calculated. For the random scission reaction, Ozawa's method gives correct kinetic parameters. For the two parallel competitive first-order reactions, none of the earlier methods can be applied. One of the methods of avoiding false parameters is to observe a process at different heating rates. If the kinetic parameters estimated by analyzing the curves at different heating rates coincide with each other, the kinetic parameters are not false. Another technique is to utilize two or more methods and if the kinetic parameters coincide with each other, the kinetic parameters are not false. A third and most desirable way is to use a method based on a more fundamental kinetic equation, such as that of Ozawa (92).

3. Mechanism of Reaction from Nonisothermal Kinetics

Deduction of the mechanism of the reaction by use of nonisothermal kinetic methods has been discussed by Sestak and Berggren (73) and Satava (105). The procedure used by Satava is based on the assumption that the nonisothermal reaction proceeds in an infinitesimal time interval isothermally, where the rate may be expressed as

$$\frac{d\alpha}{dt} = A e^{-E/RT} f(\alpha) \quad (2.50)$$

where α is the fraction decomposed in time t , and $f(\alpha)$ depends on the mechanism of the process. With a constant temperature increase, $dT/dt = q$, integration of equation (2.50) leads to

$$\int_0^{\alpha} \frac{d\alpha}{f(\alpha)} = g(\alpha) = \frac{E}{Rq} p(x) \quad (2.51)$$

where $p(x)$ is defined as

$$p(x) = \frac{e^{-x}}{x} - \int_{-x}^{\infty} \frac{e^{-u}}{u} du = \frac{e^{-x}}{x} + Ei(-x) \quad (2.52)$$

where $u = E/RT$, $x = E/RT$, and T is the temperature at which the fraction α of the sample has reacted.

From the logarithmic form of equation (2.50),

$$\log g(\alpha) - \log p(x) = \log \frac{f(\alpha) E}{Rq} \quad (2.53)$$

it can be seen that the right-hand side is independent of temperature. While the left-hand side is temperature-dependent. To a first approximation, the function, $\log p(x)$ is a linear function of $1/T$, if x is sufficiently large, and thus $\log g(\alpha)$ must also be a linear function of $1/T$. For the correct mechanism, $\log p(x)$ versus $1/T$ should be a straight line. For other incorrect mechanisms, this will not be true. The sensitivity of this procedure for mechanism determination is not high, but still it yields useful information.

The types of mechanisms most frequently encountered are shown in Table 2.8, while the procedure used to evaluate the reaction mechanism from a TG curve is given in Figure 2.43. As can be seen, only the curve corresponding to the F_1 mechanism gives a straight-line curve.

Table 2.8. Commonly Used Reaction Mechanisms (105)

Function	Equation'	Rate-controlling Process
	$x^2 = kt$	One-dimensional diffusion
	$(1 - \alpha) \ln(1 - \alpha) + \alpha = kt$	Two-dimensional diffusion, cylindrical symmetry
	$[1 - (1 - \alpha)^{1/3}]^2 = kt$	Three-dimensional diffusion, spherical symmetry; Jander equation
D_*	$(1 - \frac{2}{3}\alpha) - (1 - \alpha)^{2/3} = kt$	Three-dimensional diffusion, spherical symmetry; Ginstling-Brounshtein equation
	$-\ln(1 - \alpha) = kt$	Random nucleation, one nucleus on each particle
	$[-\ln(1 - \alpha)]^{1/2} = kt$	Random nucleation; Avrami equation I
	$[-\ln(1 - \alpha)]^{1/3} = kt$	Random nucleation; Avrami equation II
	$1 - (1 - \alpha)^{1/2} = kt$	Phase boundary reaction, cylindrical symmetry
	$1 - (1 - \alpha)^{2/3} = kt$	Phase boundary reaction, spherical symmetry

Many other mathematical methods have been proposed to analyze non-isothermal kinetic data to determine unequivocally the exact kinetic model using functional forms of $g(\alpha)$ or $f(\alpha)$ of the rate-controlling step (154). Criado (155) found that it was impossible in the Coats and Redfern method to distinguish between an interface chemical reaction-controlled mechanism (R_j) and the Jander diffusion mechanism (D_3). Bagchi and Sen (156) also demonstrated the inadequacy of the Coats and Redfern method in identifying unambiguously the rate-controlling mechanism of the dehydroxylation of $Mg(OH)_2$.

4. Critique

Since the kinetics of homogeneous and heterogeneous reactions are fundamentally different, Arnold et al (157) have shown that the nonisothermal TG Curve provides insufficient information for the purpose of reaction kinetic calculations. Mathematical considerations prove also that the parameters of the Arrhenius model cannot be calculated correctly from the TG curve by curve-fitting methods and that there is no unique correlation between the estimated parameters and the measured curves. Also, the correlation between A and D described as a "compensation effect" is certainly a mathematical

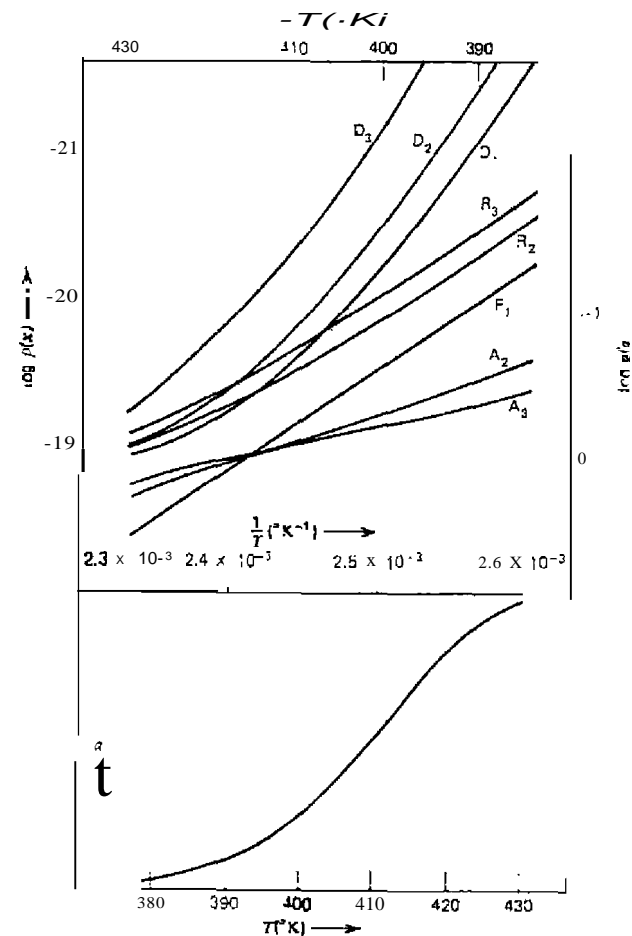


Figure 2.43. Procedure for obtaining the mechanism from a TG curve (105). Lower curve: compares with kinetic equation F , (see Table 2.6); $E = 30 \text{ kcal/mole}$; $Z = 10^{13.8} \text{ mole}^{-1}$, and $q = 1 \text{ C/min}$. Upper curves are plots of $\log g(\alpha)$ versus $1/T$, calculated from TG curve for various kinetic equations. The straight line for kinetic equation F , coincides with the plot of $-\log \rho(\alpha)$ versus $1/T$ for $E = 30 \text{ kcal/mole}$.

compensation effect, which is a trivial consequence of the badly conditioned parameter estimation.

On the basis of many experiments and theoretical considerations, Arnold et al. (158) showed that TG curves are strongly influenced by the experimental conditions, and hence the kinetic parameters calculated from these curves are fictitious and their determination is uncertain. The Arrhenius equation, taken from homogeneous kinetics, cannot be applied to nonisothermal heterogeneous reactions since the conditions of the equation are not fulfilled.

REFERENCES

1. Simons, E. L., and A. E. Newkirk, *Talanta*, 11, 549 (1964).
2. Newkirk, A. E., and E. L. Simons, private communication.
3. Duval, C., *Inorganic Thermogravimetric Analysis*, 2nd ed., Elsevier, Amsterdam, 1963.
4. Duval, C., *Inorganic Thermogravimetric Analysis*, ISI ed., Elsevier, Amsterdam, 1953.
5. Duval, C., *Anal. Chem.*, 23, 1271 (1951).
6. Lukaszewski, G. M., and J. P. Redfern, *Lab. Prac.*, 30, 469 (1961).
7. Wendlandt, W. W., *Am. Lab.*, Jun., 1977, p. 25.
8. Coats, A. W., and J. P. Redfern, *Analyst*, 88, 906 (1963).
9. Honda, K., *Sci. Rep. Tohoku Univ.*, 4, 97 (1915).
10. Guichard, M., *Bull. Soc. Chim. Fr.*, 2, 539 (1935).
11. Duval, C., *Anal. Chim. Acta*, 31, 301 (1964).
12. Newkirk, A. E., *Anal. Chem.*, 32, 1558 (1960).
13. Simmons, E. L., and W. W. Wendlandt, *Thermochim. Acta*, 2, 465 (1971).
14. DeVries, K. J., and P. J. Gellings, *J. Inorg. Nucl. Chem.*, 31, 1307 (1969).
15. Herbelle, T. P., *Thermochim. Acta*, 4, 295 (1972).
16. Perkin-Elmer Model TGS-1 Thermobalance Brochure. Perkin-Elmer Co., Norwalk, C.
17. Fruchart, R., and A. Michel, *Compt. Rend.*, 246, 1222 (1958).
18. Demassieux, N., and C. Malard, *Compt. Rend.*, 245, 1514 (1957).
19. Rynasiewicz, J., and J. F. Flagg, *Anal. Chem.*, 26, 1506 (1954).
20. DeClerq, M., and C. Duval, *Anal. Chim. Acta*, 5, 282 (1951).
21. Paulik, F., and I. Paulik, *Thermochim. Acta*, 4, 189 (1972).
22. Paulik, J. T., I. Paulik, and L. Erdey, *Anal. Chim. Acta*, 34, 419 (1966).
23. Keatich, C. J., *Anal. Proc.*, Mar. 1980, p. 77.
24. Urbain, G., *Compt. Rend.*, 154, 347 (1912).
25. Wendlandt, W. W., and E. L. Simmons, *Thermochim. Acta*, 3, 71 (1972).
26. Guenot, J., and J. M. Manoli, *Bull. Soc. Chim. Fr.*, 2663 (1969).
27. Nicholson, G. C., *J. Inorg. Nucl. Chem.*, 29, 1599 (1967).
28. Brown, H. A., E. C. Penski, and I. J. Callahan, *Thermochim. Acta*, 3, 271 (1971).
29. Wiedemann, H. G., *Chem. Congress paper*, Frankfurt, Jun. 26, 1964.
30. Fredman, H. L., *Anal. Chem.*, 37, 768 (1965).
31. Mauer, F. A., *Rev. Sci. Instrum.*, 25, 598 (1954).
32. Richer, A., and P. Vallet, *Bull. Soc. Chim. Fr.*, 148 (1953).
33. Garn, P. D., and J. E. Kessler, *Anal. Chem.*, 32, 1563, 1900 (1960).
34. Garn, P. D., *Anal. Chem.*, 33, 1247 (1961).
35. Rabatin, J. G., and C. S. Card, *Anal. Chem.*, 31, 1689 (1959).
36. Soulen, I. R., and I. Mockrin, *Anal. Chem.*, 33, 1909 (1961).
37. Lukaszewski, G. M., *Nature*, 194, 959 (1962).
38. Newkirk, A. E., and D. W. McKee, *J. Chem. Phys.*, 37, 370 (1962).
39. Macklen, E. D., *J. Inorg. Nucl. Chem.*, 29, 1229 (1967).
40. Sreger, H. F., *J. Inorg. Nucl. Chem.*, 34, 175 (1972).
41. Newkirk, A. E., *Thermochim. Acta*, 2, 1 (1971).
42. Paulik, F., J. Paulik, and L. Erdey, *Talanta*, 13, 1405 (1966).
43. Sestak, J., *Talanta*, 13, 567 (1966).
44. Wiedemann, H. G., in *Thermal Analysis*, R. F. Schwenker and P. D. Garn, eds., Academic, New York, 1969, p. 229.
45. Newkirk, A. E., and I. Aliferis, *Anal. Chem.*, 30, 982 (1958).
46. Ramakrishna Udupa, M. Aravamudan, and G. Aravamudan, *Curio Sci.*, 39, 206 (1970).
47. Cahn, L., and N. C. Peterson, *Anal. Chem.*, 39, 403 (1967).
48. Cahn, L., and H. Schultz, *Anal. Chem.*, 35, 1729 (1963).
49. Martinez, E., *Am. Mineral.*, 46, 901 (1961).
50. Guiochon, G., *Anal. Chem.*, 33, 1124 (1961).
51. Simons, E. L., A. E. Newkirk, and I. Aliferis, *Anal. Chem.*, 29, 48 (1957).
52. Mielenz, R. C., N. C. Schieletz, and M. F. King, *Clays and Clay Minerals*, NAS-NRC, Washington Pub. 327, 1954, pp. 289-296.
53. Sarasohn, I. M., and R. W. Taubling, *Pittsburgh: ConC. Anal. Appl. Spectr.*, Pittsburgh, PA., March 5, 1964.
54. Gayle, J. B., and C. T. Egger, *Anal. Chem.*, 44, 421 (1972).
55. Cahn, L., and H. R. Schultz, in *Vacuum Microbalance Techniques*, K. H. Bchrodt, ed., Vol. 3, Plenum, New York, 1963, p. 29.
56. Forkel, W., *Naturwissenschaften*, 47, 10 (1960).
57. Newkirk, A. E., *Thermochim. Acta*, 2, 11 (1971).
58. Newkirk, A. E., in *Proceedings of the First Toronto Symposium on Thermal Analysis*, H. G. McAdie, ed., Chemical Institute of Canada, Toronto, 1965, p. 29.
59. De Keyser, W. L., *Nature*, 172, 364 (1953).
60. De Keyser, W. L., *Bull. Soc. Fr. Ceram.*, 20, 1 (1953).
61. Erdey, L., F. Paulik, and J. Paulik, *Nature*, 174, 885 (1954).
62. Waters, P. L., *Nature*, 178, 324 (1956).
63. Erdey, L., *Period. Polytech.*, 1, 35, 91 (1957).
64. Erdey, L., *Chem. Zvesti*, 12, 352 (1958).
65. Paulik, F., J. Paulik, and L. Erdey, *Z. Anal. Chem.*, 160, 241, 321 (1958).
66. Waddams, J. A., and P. S. Gray, *Nature*, 183, 1729 (1958).
67. Waters, P. L., *J. Sci. Instrum.*, 35, 411 (1958).
68. Campbell, C. S., Gordon, and C. L. Smith, *Anal. Chem.*, 31, 1158 (1959).
69. Erdey, L., B. Liptay, G. Svehla, and F. Paulik, *Talanta*, 9, 489 (1962).
70. Newkirk, A. E., and E. L. Simons, *Talanta*, 13, 1401 (1966).

71. Doyle, C. D., in *Techniques and Methods of Polymer Evaluation*, P. E. Slade and L.T. Jenkins, eds., Marcel-Dekker, New York, 1966, Chap. 4.
72. Clarke, T. A., E. L. Evans, K. G. Robins, and I. M. Thomas, *Chem. Comm.*, 266 (1969).
73. Sestak, J., and G. Berggren, *Thermochim. Acta*, 3, 1 (1971).
74. Hill, R. A. W., *Nature*, 227, 703 (1970).
75. Simmons, E. L., and W. W. Wendlandt, *Thermochim. Acta*, 3, 498 (1972).
76. Sharp, I. H., and S. A. Wentworth, *Anal. Chem.*, 41, 2060 (1969).
77. Sestak, J., *Silikaty*, 11, 153 (1967).
78. MacCallum, J. R., and I. Tanner, *Eur. Polym. J.*, 6, 1033 (1970).
79. Draper, A. L., and L. Sveum, *Thermochim. Acta*, 1, 345 (1970).
80. Flynn, I. H., and L. A. Wall, *J. Res. Natl. Bur. Stand.*, 70A, 487 (1966).
81. Carroll, B., and E. P. Manche, *Thermochim. Acta*, 3, 449 (1972).
82. Reich, L., and S. Stivala, *Elements of Polymer Degradation*, McGraw-Hill, New York, 1971.
83. Freeman, E. S., and B. Carroll, *J. Phys. Chem.*, 62, 394 (1958).
84. Doyle, C. D., *J. Appl. Polym. Sci.*, 5, 285 (1961).
85. Coats, A. W., and J. P. Redfern, *Nature*, 201, 68 (1964).
86. Turner, R. C., J. Hofman, and D. Chen, *Can. J. Chem.*, 41, 243 (1963).
87. van Krevelen, W. C. van Heerden, and F. Hutjens, *Fuel*, 30, 253 (1951).
88. Horowitz, H. H., and G. Metzger, *Anal. Chem.*, 35, 1464 (1963).
89. FROSS, R. M., I. O. Sayler, and H. S. Wilson, *J. Polym. Sci.*, 2, 1147 (1964).
90. Berlin, A., and R. T. Robinson, *Anal. Chim. Acta*, 27, 50 (1962).
91. Reich, L., *J. Polym. Sci.*, B2, 621 (1964).
92. Ozawa, T., *Bull. Chem. Soc. Jpn.*, 38, 1881 (1965).
93. Ozawa, T., *J. Thermal Anal.*, 2, 301 (1970).
94. Zsako, J., *J. Phys. Chem.*, 72, 2406 (1968).
95. Ingraham, T. R., and P. Marier, *Can. J. Chem. Eng.*, 42, 161 (1964).
96. Vachuska, J., and M. voboril, *Thermochim. Acta*, 2, 379 (1971).
97. Dave, N. G., and S. K. Chopra, *Z. Physik. Chem.*, 48, 257 (1966).
98. Papazian, H. A., P. I. Pizzolato, and R. R. Orreil, *Thermochim. Acta*, 4, 971 (1972).
99. Farmer, R. W., Air Force Materials Lab. Tech. Report AFML-TR-65-246, 1967, Part 11.
100. Adonyi, Z., *Period. Polytech.*, 11, 325 (1967).
101. Magnuson, I. A., *Anal. Chem.*, 36, 1807 (1964).
102. Achar, B. N. N., G. W. Brindley, and I. H. Sharp, *Proc. Int. Chim. Conf., Jerusalem*, J, 67 (1966).
103. Broido, A., *J. Polym. Sci.*, Part A-2, 7, 1761 (1969).
104. Carroll, B., and E. P. Manche, *Anal. Chem.*, 42, 1296 (1970).
105. Satava, V., *Thermochim. Acta*, 2, 423 (1971).
106. Duval, C., "Thermal Methods in Analytical Chemistry," in *Comprehensive Analytical Chemistry*, G. Svehla, ed., Vol. VII, Elsevier, Amsterdam, 1976.
107. Kotra, R. K., E. K. Gibson, and M. A. Urbancic, *Curus*, 51, 593 (1982).
108. Dunn, I. G., and S. A. Jayweera, *Thermochim. Acta*, 61, 313 (1983).
109. Nagase, K., H. Yokobayashi, M. Kikuchi, and K. Sane, *Thermochim. Acta*, 35, 99 (1980).

- J10. Wiedemann, H. G., and E. Bayer, *Z. Anal. Chem.*, 276, 1 (1975).
- J11. Criado, J. M., F. Gonzalez, and M. Gonzalez, *J. Therm. Anal.*, 24, 59 (1982).
- J12. Criado, J. M., and J. Morales, *Thermochim. Acta*, 23, 257 (1978).
- J13. Wiedemann, H. G., and E. Bayer, *Topics in Current Chemistry*, Springer-Verlag, Berlin, Vol. 77, 1978.
- J14. Paulik, E., and I. Paulik, *J. Therm. Anal.*, 5, 253 (1973).
- J15. Caidwell, K. M., P. K. Gallagher, and D. W. Johnson, *Thermochim. Acta*, 18, 15 (1977).
116. Dunn, I. G., *Application Note 250*, Stanton Redcroft Ltd., London.
117. Chen, R., *J. Mater. Sci.*, 11, 1521 (1976).
118. Brazier, D. W., and G. H. Nickel, *Rubber Chem. Tech.*, 48, 661 (1975).
119. Barnes, P. A., and I. H. Baxter, *Thermochim. Acta*, 24, 427 (1978).
120. Nernst, W., and E. H. Riesenfeld, *Ber.*, 36, 2086 (1903).
121. Brown, M. E., D. Dollimore, and A. K. Galwey, in *Chemical Kinetics*, C. H. Bamford and C. F. H. Tipper, eds., Vol. 22, Elsevier, Amsterdam, 1980.
122. Jones, L. F., D. Dollimore, and T. Nicklin, *Thermochim. Acta*, 13, 240 (1975).
123. Sharp, J. H., G. W. Brindley, and B. N. N. Achar, *J. Am. Chem. Soc.*, 49, 379 (1966).
124. Flynn, I. H., and B. Dickens, *Thermochim. Acta*, 15, 1 (1977).
125. Reich, L., and S. S. Stivala, *Thermochim. Acta*, 24, 9 (1978).
126. Reich, L., and S. S. Stivala, *Thermochim. Acta*, 34, 257 (1979).
127. Reich, L., and S. S. Stivala, *Thermochim. Acta*, 36, 103 (1980).
128. Reich, L., and S. S. Stivala, *Thermochim. Acta*, 41, 391 (1980).
129. Reich, L., and S. S. Stivala, *Thermochim. Acta*, 52, 337 (1982).
130. Reich, L., and S. S. Stivala, *Thermochim. Acta*, 53, 121 (1982).
131. Reich, L., and S. S. Stivala, *Thermochim. Acta*, 55, 385 (1982).
132. Reich, L., and S. S. Stivala, *Thermochim. Acta*, 58, 383 (1983).
133. Reich, L., and S. S. Stivala, *Thermochim. Acta*, 61, 361 (1983).
134. Reich, L., and S. S. Stivala, *Thermochim. Acta*, 60, 251 (1983).
135. Reich, L., and S. S. Stivala, *Thermochim. Acta*, 59, 247 (1982).
136. Reich, L., and S. S. Stivala, *Thermochim. Acta*, 61, 129 (1983).
137. Reich, L., and S. S. Stivala, *Thermochim. Acta*, 68, 379 (1983).
138. Reich, L., and S. S. Stivala, *Thermochim. Acta*, 71, 231 (1983).
139. Reich, L., and S. S. Stivala, *Thermochim. Acta*, 13, 165 (1984).
140. Criado, J. M., and A. Ortega, *Thermochim. Acta*, 44, 239 (1981).
141. Gam, P. D., *CRC Crit. Rev. Anal. Chem.*, Sept. 1972, p. 65.
142. Doyle, C. D., *J. Appl. Polym. Sci.*, 5, 285 (1961).
143. Ozawa, T., *J. Thermal Anal.*, 9, 217 (1976).
144. Dickens, B., and I. H. Flynn, "Thermogravimetry Applied to Polymer Degradation Kinetics," in *Polymer Characterization*, C. D. Carter, ed., *Advances in Chemistry Series 203*, American Chemical Society, Washington, DC, 1983, Chap. 12.
145. Johnson, D. W., and P. K. Gallagher, *J. Phys. Chem.*, 76, 1474 (1972).
146. Gadala, A. M. M., *Thermochim. Acta*, in press.
147. Gallagher, P. K., and D. W. Johnson, *Thermochim. Acta*, 6, 67 (1973).
148. Kissinger, H. E., *J. Res. Natl. Bur. Stand.*, 57, 212 (1956).
149. Reich, L., *J. Polym. Sci.*, 2, 621 (1964).
150. Satava, V., and f. Skvara, *J. Am. Ceram. Soc.*, 52, 541 (1969).

151. Barbooti, M. M., *Thermochim. Acta*, 68, 363 (1981).
152. Rajeshwar, K., *Thermochim. Acta*, 45, 253 (1981).
153. Ozawa, T., J., *Thermal Anal.*, 7, 601 (1975).
154. Bagchi, T. P., and P. K. Sen, *Thermochim. Acta*, 70, 363 (1983).
155. Criado, J. M., J. Morales, and V. Rives, J., *Thermal Anal.* 14, 221 (1978).
156. Bagchi, T. P., and P. K. Sen, *Thermochim. Acta*, 51, 175 (1981).
157. Arnold, M., G. E. Veress, J. Paulik, and F. Paulik, *Anal. Chim. Acta*, 124, 341 (1981).
158. Arnold, M., G. E. Veress, J. Paulik, and F. Paulik, *J. Thermal Anal.* 17, 507 (1979).

CHAPTER

3

THERMOBALANCES AND ACCESSORY EQUIPMENT

A. INTRODUCTION

The thermobalance is an instrument that permits the continuous weighing of a sample as a function of temperature. The sample may be heated or cooled at some selected rate or it may be isothermally maintained at a fixed temperature. Perhaps the most common mode of operation is heating the sample at furnace heating rates from 5-10°C/min. Almost all modern thermobalances are automatically recording instruments, although manual recording is still used occasionally for long-term isothermal measurements (e.g., with helix-type thermobalances).

The modern thermobalance is illustrated schematically in Figure 3.1. It consists, generally, of the following component parts: (1) recording balance; (2) furnace; (3) furnace temperature programmer or controller; and (4) recorder, either of the strip-chart or X-Y function type. The specific details of each component depend on the particular application that is required of the instrument. For example, furnaces can be obtained that operate up to 2400°C or more, and employ air, inert gases, hydrogen, nitrogen, vacuum, and other atmospheres. Likewise, for the recording balance, sensitivities from as low as 0.02 mg full-scale deflection to 100 g or more are available.

Some factors that must be considered in the construction or purchase of an automatic thermobalance have been given by Lukaszewski and Redfern (1):

1. The instrument should be capable of recording the mass-loss or -gain of the sample as a function of temperature and time.
2. The thermobalance furnace should have a wide range of operation, such as from ambient temperature to 1000, 1600, or 2400°C.
3. The mass-loss of the sample should be recorded to an accuracy of better than $\pm 0.01\%$, while the temperature should be recorded to an accuracy of $\pm 1\%$.
4. The physical effects due to the normal functioning of the instrument.

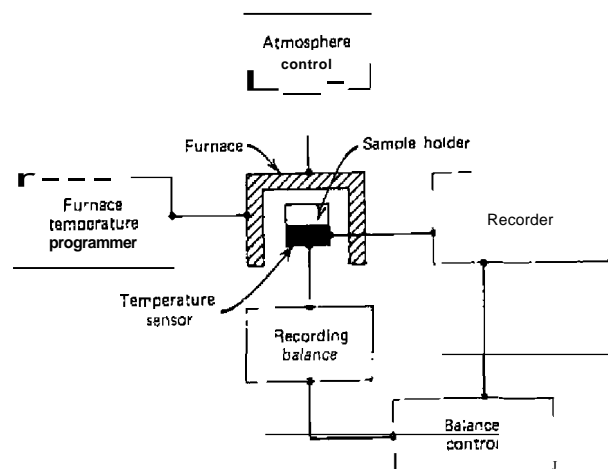


Figure 3.1. Schematic diagram of a modern thermobalance.

such as radiation and convection currents and the magnetic effects due to the furnace heaters, should not affect the accuracy of the balance. The latter effect does not interact with any conducting or magnetic materials that may be studied.

5. The position of the crucible within the furnace of the thermobalance should always be the same, so that the temperature recorded corresponds to the sample temperature.
6. The furnace should be equipped to allow for the heating of samples in various atmospheres.
7. The instrument should be as versatile as possible, providing for easy changes in heating rates together with automatic control of temperature programming.
8. The balance should be adequately protected from the furnace, and care should also be taken to keep the wear of the knife edges and other moving parts to a minimum to ensure accuracy or weighing.
9. The balance should be capable of simple periodic calibration to ensure accuracy of operation.
10. The chart used to record mass-loss and temperature rise should be capable of various speeds, and there should be provision for accurate recording or a suitable time interval.

Obviously, all these requirements cannot be met in every thermobalance. However, a number of commercially available instruments do incorporate these features.

1. Recording Balances

Perhaps the most important component of the thermobalance is the recording balance. The requirements for a suitable recording balance are essentially those for a good analytical balance, namely, accuracy, reproducibility, sensitivity, capacity, rugged construction, and insensitivity to ambient temperature changes. In addition (2), the balance should have an adjustable range of mass-change and a high degree of electronic and mechanical stability, be able to respond rapidly to changes in mass, be relatively unaffected by vibration, and be of sufficiently simple construction to minimize the initial cost and need for maintenance. From a practical viewpoint, the balance should be simple to operate and versatile in that it can be used for varied applications.

Recording balances can be divided basically into two general classifications, based on their mode of operation: (1) deflection-type instruments and (2) null-type instruments (2).

The automatic null-type instrument is based on the principle given in Figure 3.2. The balance incorporates a sensing element which detects a deviation of the balance beam from its null position: horizontal for beam balances and vertical for electromagnetic-suspension types. A restoring force, of either electrical or mechanical mass loading, is then applied to the beam through the appropriate electronic or mechanical linkages, restoring it to the null position. This restoring force, proportional to the change in mass, is recorded directly or through an electromechanical transducer of some type.

The various deflection-type balances are shown in Figure 3.3. These instruments involve the conversion of the balance-beam deflections about the fulcrum into the appropriate mass-change curves by III photographic



Figure 3.2. Null-type balance (2).

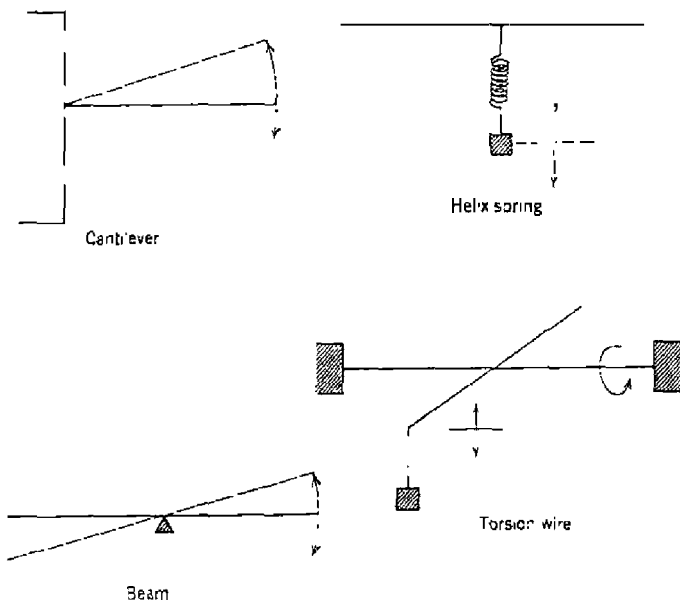


Figure 3.3. Deflection-type balance (2).

recording. (2) recording electrical signals generated by an appropriate displacement measurement transducer, and (3) using an electromechanical device. The types of deflection balances are the following:

1. The helical spring, in which changes of mass are detected by contraction or elongation of the spring and which may be recorded by suitable transducers.
2. The cantilevered beam, constructed so that one end is fixed and the other end, from which the sample is suspended, is free to undergo deflection.
3. The suspension of a sample by an appropriately mounted strain gauge that stretches and contracts in proportion to mass changes.
4. The attachment of a beam to a taut wire which serves as the fulcrum and is rigidly fixed at one or both ends so that deflections are proportional to the changes in mass and the torsional characteristics of the wire.

Gordon and Campbell (2) have summarized the various methods that have been employed to detect the deviation of a balance beam from its horizontal or vertical position in the null-point balances. They are the following:

Optical

1. Light source - mirror-photographic paper.
2. Light source-shutter-photocell.

Electronic

1. Capacitance bridge.
2. Mutual inductance; coil-plate, coil-coil.
3. Differential transformer or variable permeance transducer.
4. Radiation detector (Geiger tube).
5. Strain gauge.

Mechanical

1. Pen electromechanically linked to balance beam or coulometer.

After the departure of the beam from its rest position has been detected, some method of restoring the beam back to the rest position must be employed. These methods are the following (2):

Mechanical

1. Addition or removal of discrete weights; or beam rider positioning.
2. Incremental or continuous application of torsional or helical spring force.
3. Incremental or continuous chainomatic operation.
4. Incremental addition or withdrawal of a liquid (buoyancy).
5. Incremental increase or decrease of pressure (hydraulic).

Electromagnetic interaction

1. Coil-armature.
2. Coil-magnet.
3. Coil-coil.

Electrochemical

1. Coulometric dissolution or deposition of metal at electrode suspended from balance beam or coulometer.

The manner in which the weight-changes of the balance are recorded are summarized as follows (2):

Mechanical

1. Pen linked to potentiometer slider.
2. Pen linked to chain-restoring drum.
3. Pen or electric arcing-point on end of beam.
4. Pen(s) linked to servo-driven photoelectric beam-deflection follower.

Photographic

1. Light source-mirror-photographic paper using either a drum, time base, or flat bed; temperature base-mirror galvanometer.

Electronic

1. Current generated in a transducing circuit such as photocell, differential transformer, strain gauge, bridge, radiation detector, capacitor, or inductor.
2. Current passing through the coil of an electromagnet.

In general, electronic recording is more versatile and convenient than a mechanically linked system because of the many transducers that can be used to obtain the electrical signal proportional to the change in mass as determined by either the deflection-type or the null-type balance. The continuously recorded analog data from the primary curve can be simultaneously translated into other useful forms such as derivatives, integrals, logarithms, or any desired function, many of which lend themselves to the digital operations associated with automatic computation and automatic processes (2).

Ewing (57) has reviewed electronic laboratory balances. The various types of null detectors, such as optical, inductive, and capacitive types, as well as the electronic readouts are discussed.

2. Cahn Electrobalances

The Cahn electrobalance is a sensitive, accurate, reliable, and easily operated balance which is based on a D'Arsonval galvanometer, with the sample

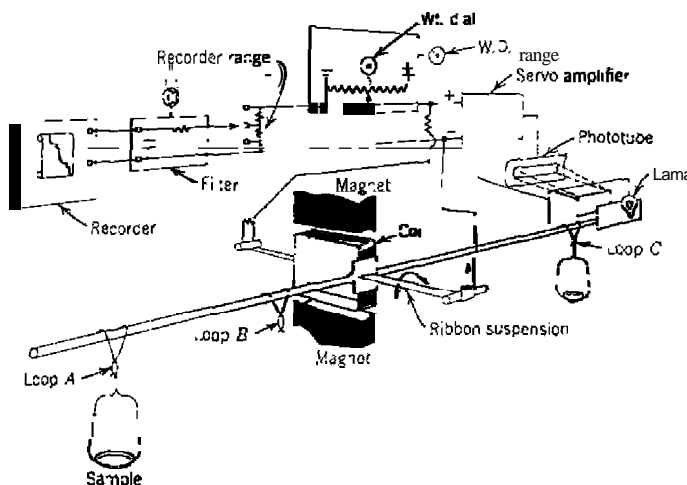


Figure 3.4. Schematic diagram of the Cahn electrobalance.

suspended from the indicating needle (beam). Changes in sample mass cause the beam to deflect, changing the photocell current, which is then amplified and applied to the coil attached to the beam. This coil is in a magnetic field so that current flowing through it exerts a moment on the beam restoring it to a null position. The coil current is thus an exact measure of sample mass. A schematic diagram of the balance is shown in Figure 3.4. The entire balance can be placed in a glass enclosure which can be used to pressures down to $\sim 10^{-6}$ Torr or lower. Various models are available, each differing in sensitivity, mass capacity, and other features.

The latest versions of the Cahn recording microbalance are the Models 1000 and 2000. The former has a mass capacity of 100 g with a sensitivity of $0.1 \mu\text{g}$ and is capable of operation at pressures of 10^{-7} Torr to 50 atm. The Model 2000 is similar, except that the mass capacity is 1.0 or 2.5 g with a mass sensitivity of 0.1 or $1.0 \mu\text{g}$ for the 1.0 or 2.5 g load, respectively. This microbalance is used in the Cahn 113 TG system. The furnace on this system has a maximum temperature of 1100°C with heating rates of $1-25^\circ\text{C}/\text{min}$.

3. Sample Holders

One of the most important components of a thermobalance is the sample holder. The geometry, size, and material of construction have a rather important effect on the mass-loss curve obtained. A large variety of sample holders have been described, a representative number of which are shown

in Figure 3.5. As in the case of DTA sample holders (Chapter 6), the type of holder used depends on the size and nature of the sample and the maximum temperature range to be employed. Materials of construction include glass, quartz, alumina, graphite, aluminum, stainless steel, platinum, and many others. Sample size may vary from 1 mg to hundreds of grams, but the most commonly used sample mass is from 5-100 mg.

A sample holder which is widely used with Cahn Electrobalance is shown in (a). It is 5-9 mm in diameter and is constructed of platinum or quartz with the geometrical shape of a hemisphere. Sample sizes from 1-20 mg

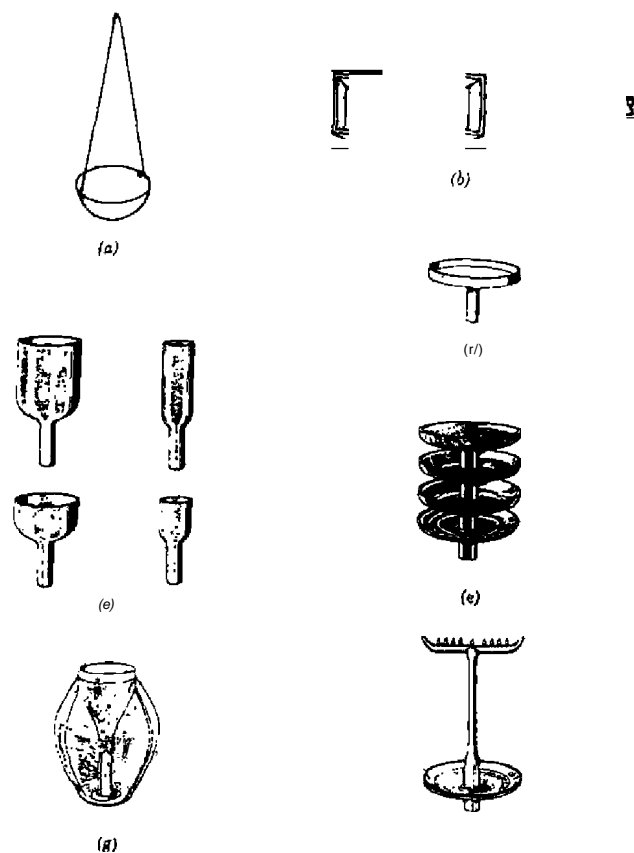


Figure 3.5. Representative sample holders for thermogravimetry.

may be investigated. The sample holder in (b) is used in horizontal thermobalances such as are available from Linseis or Netzsch and come in various sizes and materials of construction. A large number of sample holders are available for use in the Mettler thermobalance system (3), as shown by the examples in (d) (f). In (c), the open-type crucible, various sizes are available from 0.1-5 ml in volume; they are constructed from a platinum-rhodium alloy, alumina, quartz, and graphite. The flat-plate-type holder, (d), is used for high-vacuum studies. Thin layers of sample are used to prevent decrepitation during dissociation. Use of the polyplate sample holder, (e), provides a large surface area for the sample. Similar holders have been described by Erdcy et al. (4, 5) for use in the Derivatograph; one holder consisted of 10-20 plates spaced at 2-mm intervals, permitting the use of samples from

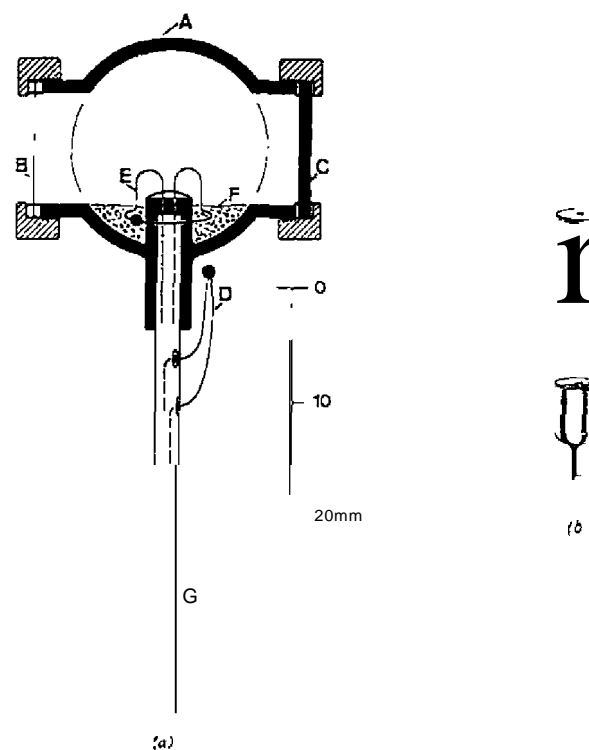


Figure 3.6. Sample holders for vapor-pressure measurements (6).

1.2-1 g in mass. Effervescent samples can be studied conveniently in the holder shown in (g), while strips of sample (e.g., metal foil strips) can be suspended on the sample holder illustrated in (f). For simultaneous TG-DTA measurements, the sample holders discussed in Chapter 6, Figure 3.2, may be employed.

For vapor-pressure measurements, the sample holders illustrated in Figure 3.6 may be used. The holder in (a) is a schematic cross section of a Knudsen cell described by Wiedemann and Vaughan (6). The main body of the cell, A, is constructed of aluminum and suspended on the thermobalance by a ceramic tube, G. A copper-constantan thermocouple, E, is brought into the cell through a vacuum-tight connection, detects the sample temperature, F, or the temperature of the vapor phase. A second thermocouple, D, serves to control the furnace temperature. The orifice, B, is made from 0.01-mm-thick Nichrome foil and contains a small hole. A screw fitting on the cell permits rapid removal or exchange of orifices of different hole diameters (1-3 mm in diameter). The other end plate, C, is used to load the sample into the cell. Both end plates are sealed to the body by Teflon O-rings. Sample volume is ≤ 1.5 ml and the cell can be used in the temperature range from -100-200°C. A simpler version of a vapor pressure cell, which contains a removable lid, is shown in (b).

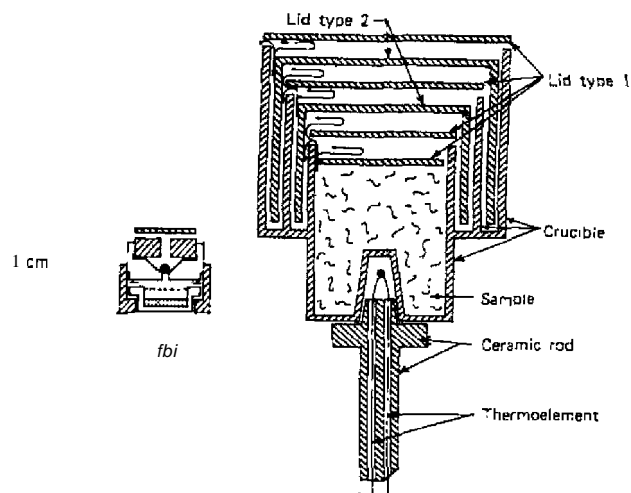


Figure 3.6. Sample holders for "self-generated" atmospheres (7-10).

For studies involving dissociation reactions in "self-generated" atmospheres (7), the sample holders in Figure 3.7 may be used. In the piston and cylinder arrangement, shown in (a), the clearance between the two provides a long diffusion path and effectively prevents contamination from the atmosphere. The Forkel crucible (8), as shown in (b), has a lid containing a ball valve to ensure separation of the sample atmosphere and the atmosphere in the furnace. Various other glass and quartz sample holders have been discussed by Newkirk (9). Perhaps the most elaborate sample holder is the one shown in (e), which was described by Paulik and Paulik (10). The sample crucible is covered with six close-fitting lids or covers in which the gaseous

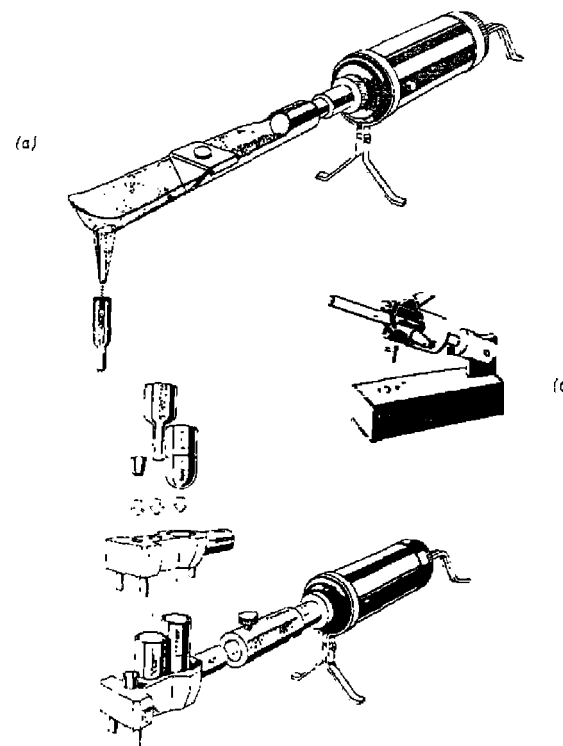


Figure 3.7. Sample-loading accessories. (a) Vibrator with spatula for loading small samples; (b) crucible vibrator for uniform packing of samples; (c) sample press for compressing low-density samples into the sample holder (10).

decomposition products are forced to escape through a long and narrow labyrinth.

Aids to ensure uniform sample packing are illustrated in Figure 3.8 (3). A vibrator with spatula attached, as shown in (a), is used to load small samples into the sample holder. In order to pack the samples in a uniform manner, one may employ the vibrator and sample holder device in (b). The packing of voluminous, low-density samples in the appropriate sample holder is accomplished by the small press illustrated in (c).

The loading of moisture- or oxygen-sensitive samples into the Mettler thermobalance sample holder is conveniently carried out by use of the controlled atmosphere enclosure shown in Figure 3.9 (3). The sample is introduced, via an enclosed sample holder, into the enclosure and loaded into the furnace chamber after the controlled atmosphere has been introduced. After loading, the furnace chamber is closed and the enclosure is removed.

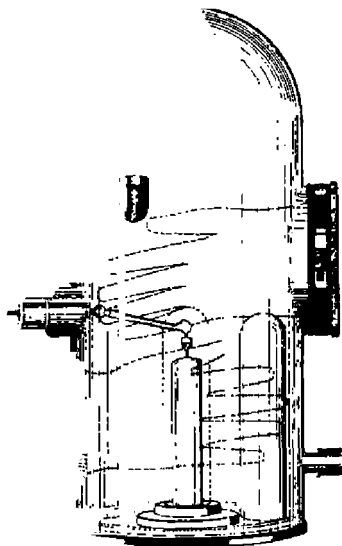


Figure 3.9. Enclosure for sample loading in controlled atmosphere (3)

4. Furnaces and Furnace Temperature Programmers

The types of furnaces employed in TG measurements are similar to those discussed in Chapter 6.A.4. The choice of furnace heating element and type of furnace depends on the temperature range desired. Furnaces have been described which operate in the temperature range from ambient room temperature to 1000, 1600, or even 2400°C. The furnace may be mounted vertically or horizontally and positioned either above or below the balance mechanism. Mounting above the balance is generally recommended because of a number of factors, most of them due to thermal gradients in the furnace chamber and temperature changes of the balance. Resistance heater element furnaces are the most widely used, the temperature limits of which are given in Chapter 6 (Table 6.2). Very few TG studies require low temperature furnaces, although low-temperature TG-magnetic susceptibility measurements may employ a low-temperature cryostat of some type.

The furnace thermal symmetry requirements are perhaps less stringent than those required with DTA measurements. It is desirable to know the temperature distribution curves of the furnace, such as are illustrated in Figure 6.6 in Chapter 6. There should be a zone of homogeneous temperature flux in the sample holder area.

The temperature rise of the furnace is controlled by a temperature programmer, the requirements of which are similar to those used in DTA (see Chapter 6). The heating rates should be linear and reproducible, since a nonlinear heating rate will influence the resulting TG curve, especially if a time-based recording system is used. The linearity requirements are not so important as in DTA, however. The heating rates used are generally from 5-10°C/min, although some measurements have been made at 160°C/min. An average value which is widely used is 5°C/min, but this can vary depending on the size of sample and the TG information desired.

5. Temperature Detection and Recording Systems

As previously mentioned, in thermogravimetry the mass-change of the sample is continuously recorded as a function of temperature. The temperature, in this definition, may be that of the furnace chamber, the temperature near the sample (i.e., in close contact with the sample container), or the temperature of the sample. These three sources of temperature detection are shown in Figure 3.10. In (a), the thermocouple is near the sample container but not in contact with it. There is a correlation between the temperature of the container and that detected by the thermocouple, but the thermocouple will either lead or lag behind the sample temperature, depending on the thermochemistry of the reaction. Most thermobalances use this type of

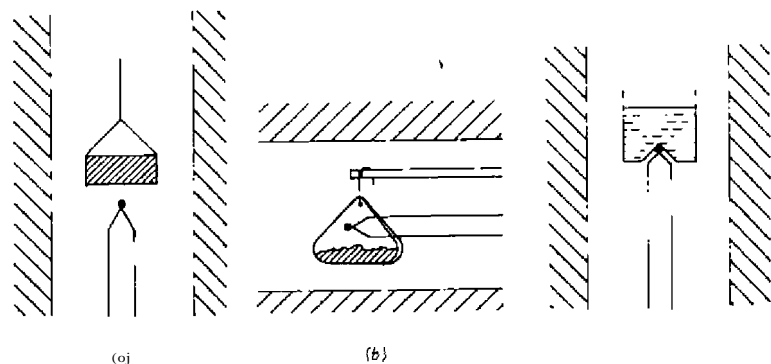


Figure 3.10. Location of temperature detection thermocouple in a thermobalance (12).

thermocouple arrangement even though it is a poor one. It is even worse when low-pressure atmospheres are employed, as in high-vacuum thermogravimetry; in this case, heat transfer is by radiation alone rather than by convection and conduction.

The thermocouple is in close proximity to the sample in (b) and is positioned inside, but not in contact with, the sample holder. This arrangement is better than (a) because the thermocouple will respond to small changes of sample temperature. The best method of sample temperature detection is to have the thermocouple either in contact with the sample or with the sample container, as shown in (c). In the latter, the temperature detected will be the integrated temperature. However, the main problem is that with sensitive recording balances the thermocouple leads can cause weighing errors, or at least interference with the balance mechanism. One way to detect the actual sample temperature and yet not interfere with the balance mechanism is to suspend an electronic device near the sample holder which will transmit the sample temperature to a fixed receiver located near the sample container. Manche and Carroll (13) described a unijunction transistor relaxation oscillator which used a thermistor as the temperature detector. The frequency of oscillation, which is a function of sample temperature, was transmitted via a mutual inductance between two suspended coils to a receiver and counter. The device was limited, however, to a maximum temperature of about 150°C.

The calibration of the temperature of the furnace and/or sample chamber has been discussed by Stewart (12) and Norem et al. (14, 15). Stewart (12) used a conventional thermobalance which contained a thermocouple mounted external to the sample, while Norem et al. (14, 15) calibrated a furnace which used a resistance element for temperature detection.

Stewart (12) discussed three approaches to temperature calibration:

1. The use of standard materials with reproducible mass-loss points that could be referred to the temperature.
2. The use of materials having known reproducible (and reversible) temperature transitions and direct measurement of temperature.
3. The use of materials with magnetic transitions which could be displayed on a mass-loss curve and referred to the temperature.

The first approach is the most appealing, but the evolution of a volatile product is dependent not only on the temperature and rate of temperature change, but also on the type and nature of the furnace atmosphere. The second method was used by Stewart (12) in his temperature calibration scheme but required that the thermocouple be in contact with the sample or the sample container during the calibration procedure. Compounds chosen for standards were those containing $solid_1 \rightleftharpoons solid_2$ or $solid \rightleftharpoons liquid$ type transitions, which were not atmosphere-dependent. The standards used and their transition temperatures were potassium nitrate (129.5 and 333°C), potassium chromate (665°C), and tin (231.9°C).

Norem et al. (14, 15) used the third method, as previously discussed, to calibrate the temperature of their type of furnace and/or sample container. A ferromagnetic material was placed in the sample container and suspended within a magnetic field. At the material's Curie point temperature, its equivalent magnetic mass diminishes to zero and the thermobalance indicates an apparent mass-loss. For calibration over the temperature range from ambient temperature to 1000°C, it is obvious that a number of ferromagnetic materials must be used. The criteria which were considered characteristic of an ideal standard were the following (15):

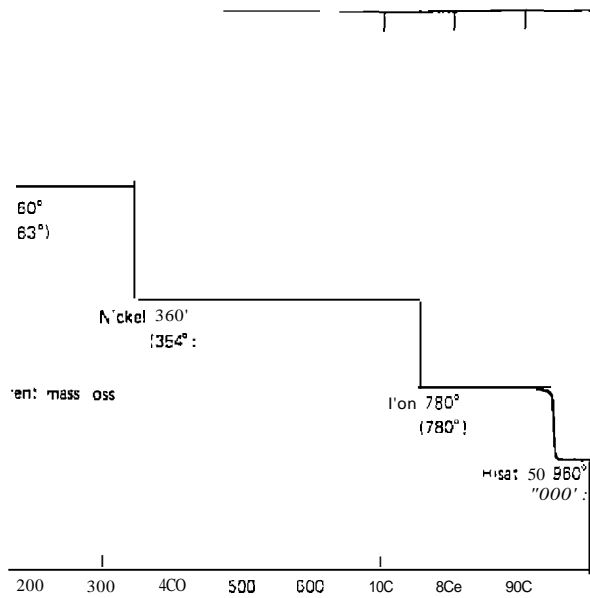
1. The transition must be sharp: that is, its natural or true width should extend over a small temperature range.
2. The energy required to effect the transition should be small (under the dynamic scanning conditions of TG, the "sharpness" of a transition is inversely proportional to transition energy).
3. The transition temperature should be unaffected by the chemical nature of the atmosphere and independent of pressure.
4. The transition should be reversible so that the sample can be run repetitively to optimize or check the calibration.
5. The transition should be unaffected by the presence of other standards so that several samples can be run simultaneously to obtain a multi-point calibration in a single experiment.

De readily observable using standard samples in
parable to normal sample sizes investigated

using four standard ferromagnetic samples is
actual transition temperatures are indicated in
st be used in the heating mode because they
on cooling. Transition temperatures are also
heating rate of the furnace, but this dependency
mm range. The effect of the heating rate on the
moerature is given by

$$(3.1)$$

thermal resistance between heat source and sample
heat capacity of the sample and its container,



Temperature calibration with ferromagnetic standards: heating rate of 10 °C

and \dot{T}_h is the heating rate. The parameter Re , is the instrumental time constant, a most important parameter characterizing the performance of the instrument (or any thermal analysis instrument).

[Elder (11) discussed the use of magnetic temperature calibration standards at high heating rates, 50-150°C/min. At these heating rates, the dynamic compensating factor, or rate parameter of the controller, must be employed. Using the four magnetic standards, alumina (1163°C), nickel (354°C), Perkalloy (596°C), and iron (780°C), Elder obtained the effective magnetic transition effective mass-loss curves as shown in Figure 3.12. Two different heating rates, 20 and 100°C/min, were employed as well as fixed and variable rate procedures. It was found that the T_s values for the magnetic materials were accurate to $\pm 2^\circ\text{C}$. According to Elder (11), the internal calibration procedure of the Perkin-Elmer System 4 controller appears to be of little value.

McGhie et al. (53, 54) proposed a new temperature calibration technique in which a small inert platinum weight is suspended within the thermobalance sample container by a fusible link composed of a temperature calibration material. When the temperature exceeds the fusible link melting point, the platinum weight is released. The weight is either caught in the sample container, producing an "action/reaction" response on the TG curve,

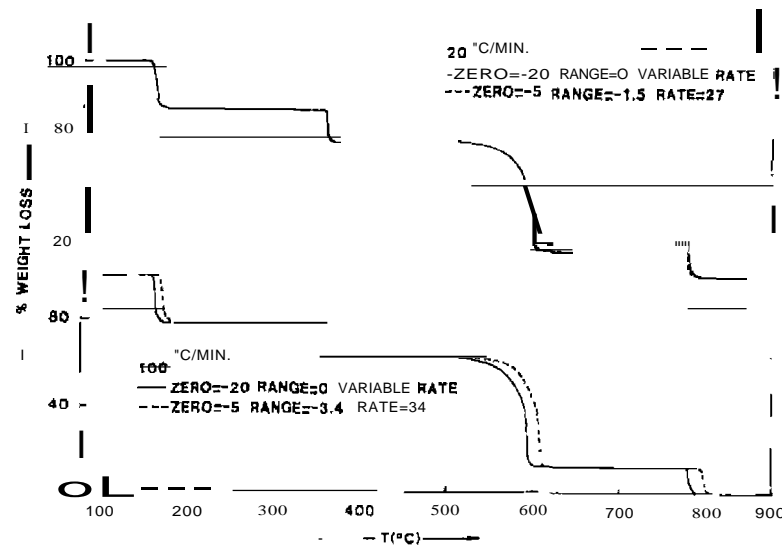


Figure 3.12. Magnetic transition effective mass-loss curves at heating rates of 20 and 100°C/min⁻¹ (11).

or dropped through a hole in the bottom of the sample container, producing a discontinuous weight-loss. The fusible links are constructed from wires of 0.25 mm or smaller diameter of indium, tin, lead, zinc, aluminum silver, or gold.

The sample container for the Du Pont Model 951 thermobalance was modified as illustrated in Figure 3.13. Holes were pierced in the sides of the container to hold the quartz rod or platinum wire support for the fusible link and weight. A rectangular hole was cut in the bottom of the sample container to permit the weight to fall when the fusible link wire melts. A typical weight-drop calibration curve, using a zinc fusible link, is shown in Figure 3.14. The corrected thermobalance temperature found was 419.68°C as compared to a literature temperature of 419.58°C. The calibration data for all metals using the weight-drop method is given in Table 3.1. Temperature calibration is claimed to be accurate to within $\pm 2^\circ\text{C}$ over the range 25-1200°C, with an individual measurement precision of $\pm 1.1^\circ\text{C}$.

Blaine and Fair (55) determined new estimates for the "true" magnetic transition temperatures of the IeTA Certified Magnetic Reference Materials GM761, using a Six-point calibration method. The results of the magnetic transition temperatures obtained are presented in Table 3.2. Experimental measurement precision varied from $\pm 0.81^\circ\text{C}$ for nickel to $\pm 3.2^\circ\text{C}$ for Permanorm 3. The narrowest magnetic transition temperature was 3.0°C for nickel, whereas the widest was 13.1°C for Permanorm 3. A pooled standard deviation of $\pm 2.0^\circ\text{C}$ could be calculated from these data. The experi-

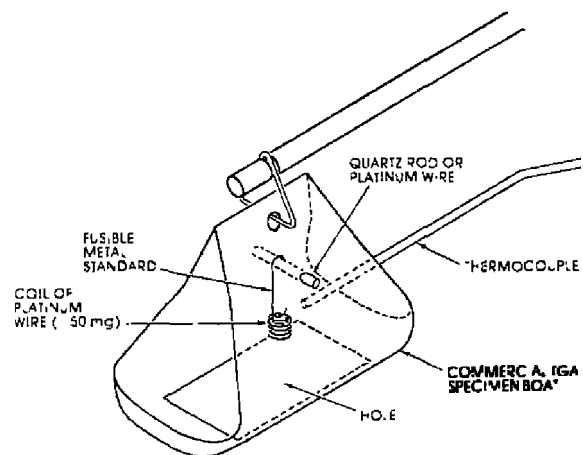


Figure 3.13. Fusible link temperature calibration. Modification of sample container (54)

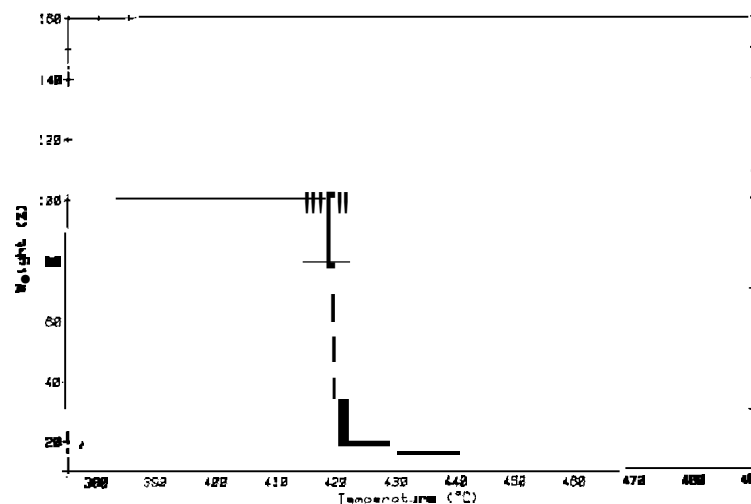


Figure 3.14. Typical fusible link weight-drop curve (54).

Table 3.1. Fusible Link Temperature Calibration Data. Dropping Weight Method (53)

Material	Obsd. Temp. ($^\circ\text{C}$)	Corrected Temp. ($^\circ\text{C}$)	Lit. Temp. ($^\circ\text{C}$)	Deviation from Lit. Value ($^\circ\text{C}$)
Indium	159.90 \pm 0.97	154.20	156.63	-2.43
Lead	333.02 \pm 0.91	331.05	327.50	3.55
Zinc	418.78 \pm 1.08	419.68	419.58	0.10
Aluminum	652.23 \pm 1.32	659.09	660.37	-1.28
Silver	945.90 \pm 0.52	961.25	961.93	1.68
Gold	1048.70 \pm 0.87	1065.67	1064.43	1.24

mental results in Table 3.2 were corrected, using a linear calibration curve, to produce the new estimates of the magnetic transition temperatures presented in Table 3.3. The precision of these values varies with the transition temperature range of each particular material but has a pooled standard deviation of $\pm 2^\circ\text{C}$.

Generally, three types of recording systems are used to record the output signals of mass and temperature from the thermobalance. They are: (1) strip-chart potentiometric recorders, (2) X-Y or X-Y₁Y₂ recorders, and (3) multipoint potentiometric recorders. These recording systems are sche-

Table 3.2. Observed Magnetic Transition Temperatures for Magnetic Standards GM 761 (55)

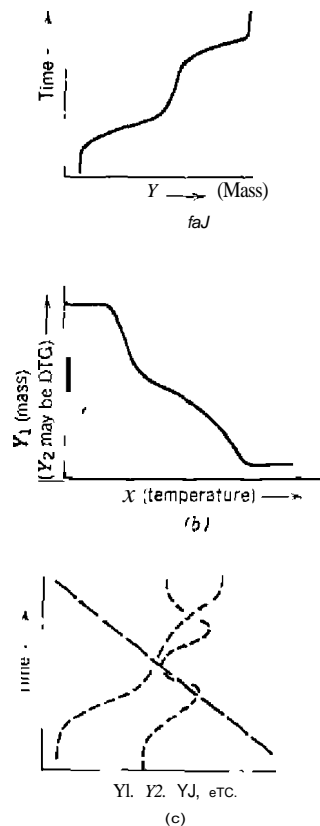
Material	No. of Determinations	Mean Temp. (°C)	SD (°C)
Permanorm 3	4	262.6	±3.2
Nickel	3	361.73	±0.8
Mumetal	3	402.5	±2.3
Permanorm 5	3	430.1	±1.1
Trafoperm	4	746.9	±1.2

matically illustrated in Figure 3.15. If the strip-chart potentiometric recorder is employed, two of them are required; one for mass versus time, the other for temperature versus time. The temperature recording will also serve as a visual check on the linearity of the temperature program (should be a straight line) or the progress of a temperature cycling experiment (heat, isothermal, or cool). The use of a X-Y or X-Y₁ Y₂ recorder is more convenient since mass is plotted directly against temperature. Using Y₂, the DTG or DTA, DSC curve may also be plotted simultaneously. If more than three parameters need to be recorded, the multipoint potentiometric recorder is useful. Thus, the TG, DTG, DTA, DSC, T, and gas pressure curves may all be simultaneously plotted. Different colored dots on the printout permit easy identification of the curve.

The effects of a temperature program perturbation on the mass-loss curves using both types of recording systems are shown in Figure 3.16. In (a), using a time-base recorder, the temperature perturbation occurred at A, resulting in the recording of the solid-line curve. The normal curve, if no change in the heating rate took place, is shown by the dashed-line curve. Similarly, for the

Table 3.3. New Estimates of Magnetic Transition Temperatures for Magnetic Standards GM 761 (55)

Material	Transition Temp. (°C)		
	Experimental	Lit.	Deviation (°C)
Permanorm 3	259.6 ± 3.7	266.4 ± 6.2	-6.8
Nickel	361.2 ± 1.3	354.4 ± 5.4	6.8
Mumetal	403.0 ± 2.5	385.9 ± 7.2	17.1
Permanorm 5	431.3 ± 1.6	459.3 ± 7.3	28.0
Trafopenn	756.2 ± 1.9	754.3 ± 11.0	2.1

Figure 3.13. Types of recording systems used in thermobalances. (a) strip-chart potentiometric recorder; (b) X-Y or X-Y₁ Y₂ recorders; (c) multipoint potentiometric recorder.

X-Y recorder, (b), the temperature perturbation occurred at A, resulting in the change to the dashed-line curve. The normal curve is indicated by the solid curve. However, in the time-base recorder, a curve of the system temperature was also recorded so that the change in heating rate could be immediately detected. With the X-Y recorder, this change in heating rate would probably not be detectable unless the curve was duplicated several times.

Another type of recorder that is a combination data acquisition and plotting system is the data center recorder. These recorders convert up to eight low-level analog signals to digital, store them on magnetic media such as a floppy disk, and then reprint the data at the convenience of the operator.

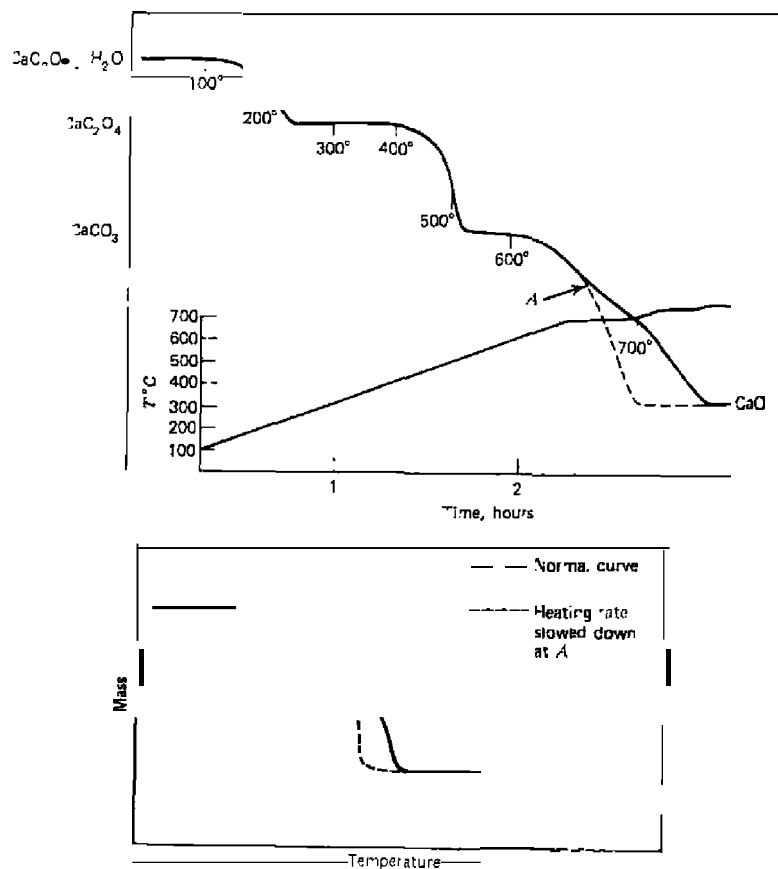


Figure 3.16. Effect of temperature perturbation on mass-loss curve. (a) Time base recorder; heating rate slowed down at A; (b) X-Y recorder.

One such data center recording system, the Bascom-Turner instrument, has been described by Kapiian et al. (58) and Wendlandt (59). The latter reference discusses the use of this recorder in thermal analysis. An example of the application of the recorder to TG is shown in Figure 3.17. The TG data of $\text{CaC}_2\text{O}_4 \cdot \text{H}_2\text{O}$ was recorded from a thermobalance and then replotted as: A, mass-time, scaled and offset; B, mass-temperature, scaled and offset; C, mass-time; D, mass-temperature; E, first derivative of TG curve or DTG; and F, temperature-time curve.

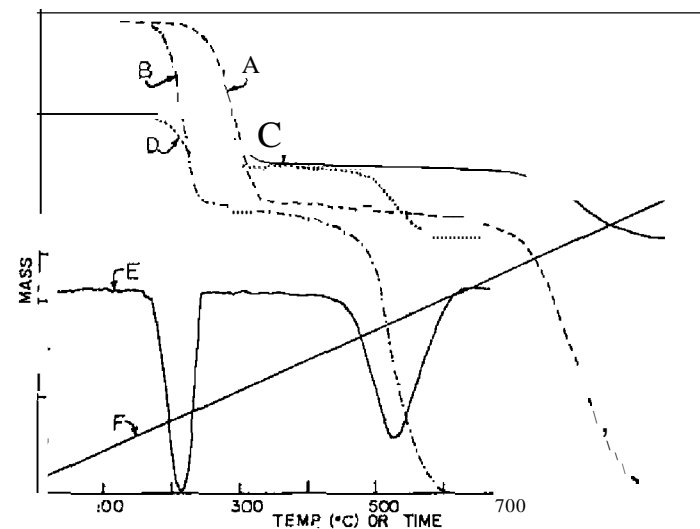


Figure 3.17. TG curves of $\text{CaC}_2\text{O}_4 \cdot \text{H}_2\text{O}$ as replotted on a data center recorder (59). Heating rate of $10^\circ\text{C min}^{-1}$ in N_2 . Data sampling rate was 1.0 sec. A, Mass-time, scaled and offset; B, mass-temperature, scaled and offset; C, mass-time; D, mass-temperature; E, first derivative-temperature; F, temperature-time.

Most of the commercial thermobalances now available use computer data reduction techniques to process the raw TG data (see Chapter 12). A dedicated microcomputer system plots the resultant data using a plotter or dot-matrix printer. Scaling and offset of the curve can be carried out as well as other mathematical operations such as differentiation, curve peak integration, and so on.

B. THERMOBALANCES

1. Introduction

A large number of reviews and books have been written describing various commercial and noncommercial thermobalances. Mention should be made of the reviews by Gordon and Campbell (2), Duval (16), Lewin (17), Jacque et al. (18), Saito (19), Vaughan (20), Wendlandt (21, 22), and others. Books containing descriptions of thermobalances include those by Duval (23, 24), Gam (25), Kcattch (26), Anderson (27), Wendlandt (28), Saito (29), and

others. Due to the limited space available, only those thermobalances containing novel or important features will be discussed here. Likewise, only a few of the many commercial instruments will be mentioned since these are adequately described elsewhere in recent reviews or books (21, 22, 28).

The first thermobalance was probably the instrument described by Honda (30) in 1915. This instrument, as shown in Figure 3.18, consisted of a balance with a quartz beam. The sample was placed in a porcelain or magnesia crucible, G, which was suspended in an electrically heated furnace, J. Attached to the opposite end of the balance beam was a thin steel wire helix, E, which was immersed in oil contained in a Dewar flask, H. The Dewar-flask-helix assembly was adjusted by a screw mechanism to maintain the balance beam in a null position. A rather low heating rate was employed, since it took 10-14 hours to attain a temperature of 1000°C. However, Honda used a quasi-isothermal heating cycle in that during a mass-loss transition the furnace temperature was maintained at a constant temperature until the transition was completed. This procedure alone sometimes required 1-4 hours. Convection currents were evident above 300°C, as might be expected from the furnace sample arrangement. A sample mass of about 0.6 g was normally employed.

The work of Honda did indeed lay the foundation for practically all of the future work in thermogravimetry. His thermobalance enabled the investiga-

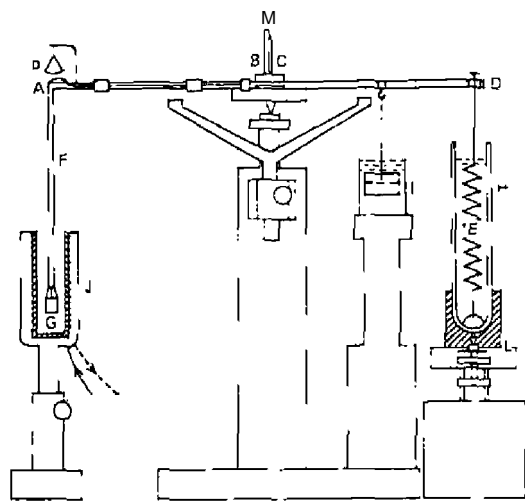


Figure 3.18. The thermobalance as described by Honda (30).

tor to weigh the sample continuously as it was heated and also employed the feature of quasi-isothermal heating. The latter technique cannot be carried out automatically by present-day thermobalances. He modestly concluded his paper by saying, "All of the results above given are not altogether original; the present investigation with the thermobalance has however revealed the exact positions of the change in structure and also the velocity of the change in respective temperatures. The investigation also shows the great convenience of using such a balance in similar investigations in chemistry."

Numerous other Japanese workers modified the Honda thermobalance and also developed new instruments. The results of their studies have been summarized in a monograph by Saito (19).

The French school of thermogravimetry was started by Guichard (31) in 1923. He apparently was unaware of Honda's work, but then he never claimed to be the discoverer of thermogravimetry. He improved the technique, brought it to a high state of development for that time, and critically examined each phase of it. His original thermobalance (23) contained a gas-fired furnace in which gas was metered to the burner via a constant-level device consisting of a valve with a float attached to it. The float rested on the surface of a tank filled with water. This water drained into another container via an adjustable valve, thus causing a slow but gradual opening of the gas metering valve and hence increasing the furnace temperature. Equally interesting is the manner in which the mass-change of the sample was detected by the balance. This was achieved with a hydrostatic device in which small amounts of oil were added to a "U" tube to compensate exactly for the mass-change. A loss of mass of 100 mg corresponded to the addition of 9 ml of oil. Mass-loss curves recorded on this balance agreed well with the results obtained by Duval (23) some 40 years later.

Guichard's work was followed by the investigations of Vallet (32), Dubois (33), and others (23). Perhaps the greatest impetus to the French school of thermogravimetry was the development of the Chevenard (34) recording thermobalance. This balance had been under development since 1936 and became commercially available in 1945; it was the first automatic (photographically) recording instrument. In the hands of Duval and co-workers (23, 24), it became the standard instrument for work in this field.

Two other important milestones in the development of the modern thermobalance occurred in 1958 and 1964. A multifunctional instrument, called the Derivatograph, was described by Pauik (35) et al. in 1958. The instrument could record not only the TG curve, but also its first derivative (DTG) and the differential thermal analysis (DTA) curve. In 1964, Weidemann (3) described the Mettler system, which was perhaps the most sophisticated thermobalance ever commercially available. This system is described in detail by Wiedemann and Bayer (8).

2. Du Pont Thennobalance

The Du Pont thennobalance has been described by Sarasohn and Tabeing (36). The balance, illustrated schematically in Figure 3.19, contains a null-balancing, torque-band electric meter movement with an optically actuated servoloop. The sample is placed in a container which is suspended directly on the balance beam. In normal operation, the temperature-sensing thermocouple is positioned within 1 mm of the sample, and hence indicates very close to the sample temperature. Mass changes of the sample are plotted as a function of temperature on an internal X-Y recorder. Balance sensitivity is reported to be $2 \mu\text{g}$. The horizontal beam-in-furnace design and the position of the sample container permit axial flushing of the furnace tube with various inert gases. The sample presents minimum cross section to the gas flow, which results in a negligible torque perpendicular to the beam. Hence, there is a minimum of turbulence and noise in the balance. A maximum furnace temperature of 1200°C is attainable.

An atmosphere control system for the thermobalance, as described by Williams (37), permits the rapid changing of the dynamic gas atmosphere between oxygen, hydrogen, and argon.

Enclosure of the Du Pont thermobalance in a high-pressure chamber has been described by Brown *et al.* (37) and Williams *et al.* (38). Pressures of up to 20 atm and a maximum temperature of 350°C were possible with the former, while the latter instrument could be operated up to 68 atm and a maximum temperature of 450°C . The modification by Williams *et al.* (38) also permitted simultaneous magnetic susceptibility measurements on the

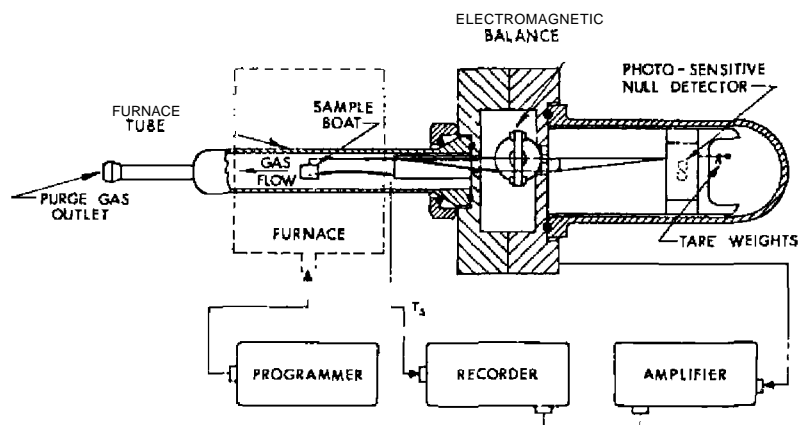


Figure 3.19. Du Pont Model 951 thermobalance.

sample (see Chapter 11). Chiu (39) described a modification of the Du Pont thermobalance in which concurrent TG, DTA, and ETA (electrothermal analysis) curves could be recorded. This instrument is described in Chapter II. Other combinations, such as the coupling of the balance to a gas chromatograph or mass spectrometer, are described in Chapter 8.

3. Derivatograph

The Derivatograph, which was first described by Paulik *et al.* (35) in 1958, is a multifunction thermal analysis system which can record the TG, DTG, DTA, and T curves of a sample on a single chart. By means of accessory attachments, the TD (thermal dilation) and DID (derivative of TD) curves may be recorded as well as the evolved gas curves (see Chapter 8).

The instrument, as shown in Figure 3.20, consists of an analytical balance, two furnaces, a furnace-temperature programmer, sample and reference crucibles, a voltage regulator, and a galvanometric light beam-photographic paper recorder. The balance is of the air-damped analytical type, with a basic sensitivity of $20 \pm 0.2 \text{ mg}$ full-scale deflection and a working mass range of 10 mg to 10 g. The derivative of the TG curve is obtained by means of a simple device consisting of a magnet and an induction coil. The former is suspended on one arm of the balance beam, with both of its poles surrounded

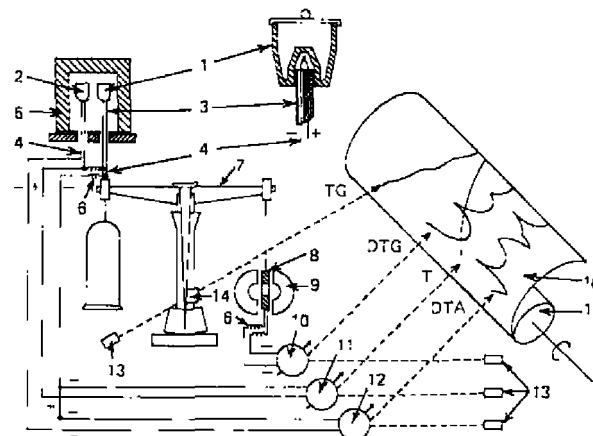


Figure 3.20. Schematic diagram of the Derivatograph. 1, crucible for the sample; 2, crucible for the inert material; 3, porcelain tube; 4, thermocouples; 5, electric furnace; 6, torsionless read; 7, balance; 8, coil; 9, magnet; 10, DTG-galvanometer; 11, T-galvanometer; 12, DTA-galvanometer; 13, lamps; 14, optical slit; 15, color-recording cylinder; 16, photographic chart.

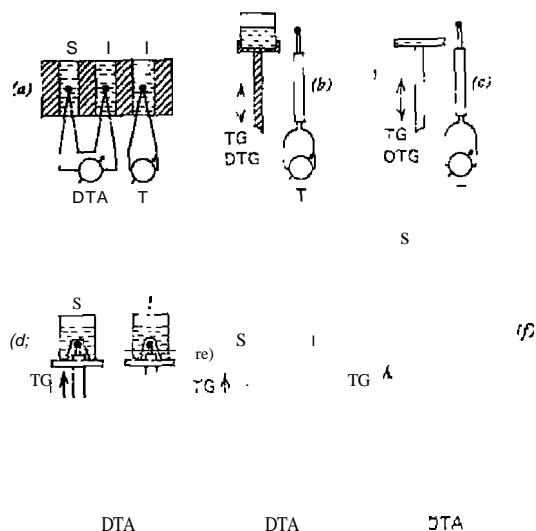


Figure 3.21. Sample holders for Derivatography (60). (a) Sample holder of DTA apparatus; (b) crucible of derivative thermobalance; (c) monoplate sample holder of the derivative thermobalance; (d) crucible of the D-graph; (e) monoplate holder of the D-graph; (f) polyplate holder of the D-graph.

by two induction coils. When a change of mass occurs, movement of the magnet induces a voltage in the coils which is proportional to the rate of mass change. This induced coil voltage is recorded on the chart as one of the curves. Maximum temperature of the furnace is 1100°C; N₂, CO₂, Ar, Oz. and so on may be used as the furnace atmosphere at atmospheric pressure only.

Various sample holders, several of which are illustrated in Figure 3.21, have been described (40) and their applications to specific problems discussed. The labyrinth, self-generated atmosphere type of sample holder has previously been examined (Chapter 2.)

4. Mettler Thermobalances

The Mettler TA1 thermoanalyzer, as developed by Wiedemann (3, 60), was perhaps the most elaborate and versatile of any thermobalance ever constructed. It is no longer available commercially, having been superseded by the Mettler TA 2000 and TA 3000 systems. However, because of its uniqueness, the Mettler TA1 is described here.

The instrument is shown schematically in Figure 3.22. The balance is of the aluminum beam-substitution type with sapphire knife edges and planes. Change in the sample mass causes a beam deflection which moves a light shutter, interrupting a light-beam display on two photodiodes. The balance in photo-diode current is amplified and fed back to a coil attached to the balance beam as a restoring force. The electrical mass indication has a dual weighing range with three different sensitivities as standard; a fourth is optional. Two consecutive sensitivities, in the ratio of 1:10, are always recorded. One range is 0-1000 mg, recorded as 100 mg in.; the second is also 0-1000 mg but is recorded as 100 mg full-scale deflection, or 10 mg in. A more sensitive mass range of 0-10 mg is recorded in an identical manner. A unique design feature is the gas flow control system. Corrosive and non-corrosive gases may be employed, with provisions in the case of the former to keep it from coming in contact with the balance mechanism. Two vacuum

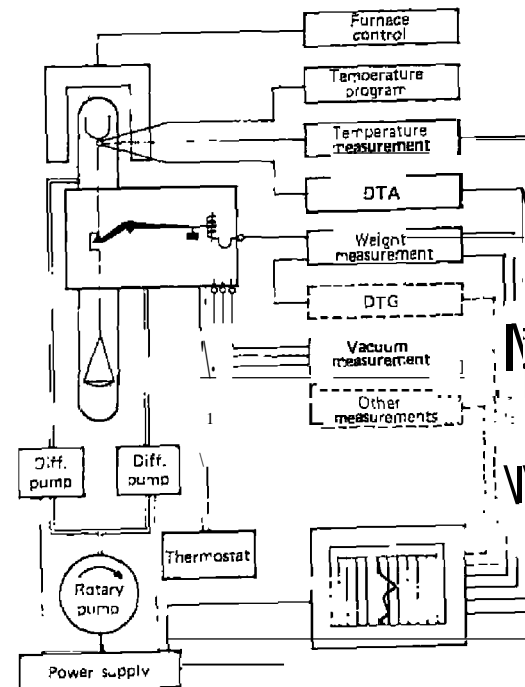


Figure 3.22 Schematic diagram of the Mettler thermoanalyzer (1).

and diffusion pumps are employed to evacuate the furnace chamber to pressures of the order 5×10^{-6} Torr.

Three furnaces are available: a low-temperature unit with a maximum temperature of 1000°C , a high-temperature unit for use up to 1600°C , and a super high-temperature model with a maximum temperature of 2400°C . These furnaces are illustrated in Chapter 6 (Figure 6.5). The sample holders are also discussed in Chapter 6 because of their simultaneous use for DTA and thermogravimetry.

Although a large number of different types of inert and oxidizing furnace atmospheres can be used with this system, a controlled vapor furnace system may also be employed, as shown in Figure 3.23. It replaces the standard Mettler 25 1000°C quartz tube furnace. In operation, the sample is placed in the sample holder, P, after which the furnace unit is put in place and sealed by ground glass joint, G. The sample chamber is heated by heater element, K, with the aid of reflector shield, S. A liquid (water or an organic compound) is heated to boiling at A by means of a small cartridge heater. Carrier gas (usually nitrogen) is introduced at D to transfer the vapor through inlet F.

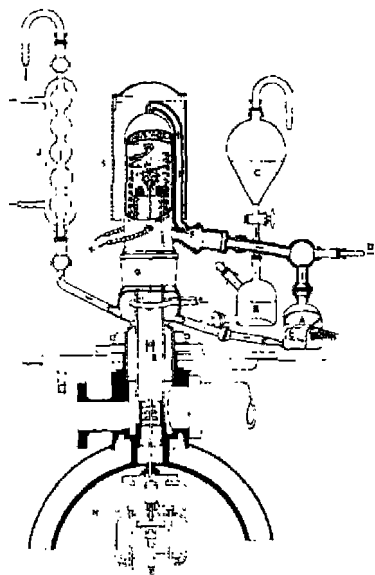


Figure 3.23. Vapor atmosphere furnace for the Mettler system.

Another gas stream, which is brought through the balance mechanism, H, and the baffle, R, is used to prevent vapors from condensing on the sample holder support rod or the balance chamber. Containers B and C are reservoirs for adding liquid to A. A water-cooled condenser at I condenses the vapor to a liquid which is then returned to boiler A.

The coupling of the Mettler thermobalance to a gas chromatograph or mass spectrometer is discussed in Chapter 8.

The Mettler TA 2000 C thermoanalyzer system permits simultaneous TG-DSC measurements from 25 – 1200°C at pressures from atmospheric to 10^{-5} mbar. With a special furnace, a corrosive gas atmosphere can also be used. A schematic diagram of the thermoanalyzer is shown in Figure 3.24.

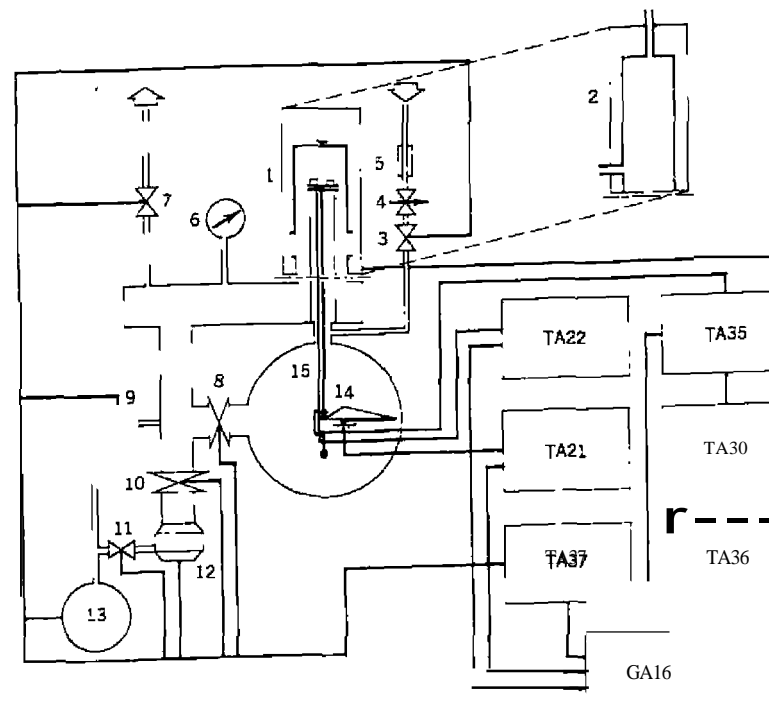


Figure 3.24. Mettler TA 2000 C thermoanalyzer schematic diagram. 1, furnace for regular gas atmosphere; 2, furnace for corrosive gas atmospheres; 3, inlet valve; 4, needle valve; 5, gas flow meter; 6, pressure gauges; 7, exhaust valve; 8, shut-off valve; 9, bypass valve; 10, plate valve; 11, fore-vacuum valve; 12, diffusion pump; 13, rotary pump; 14, balance; 15, sample cup holder.

One unique feature of the balance is the ability to use samples up to 6 g; however, the electrical weighing range is only -2 to $+2$ g. Reproducibility of the mass-measuring system is $10 \mu\text{g}$ with a linearity of 10^{-4} . Alumina cups, of $50 \mu\text{L}$ capacity, are used to contain the sample and reference materials. Calorimetric sensitivity of the DSC measurements is $\sim 2.5 \mu\text{V/mW}$, with an accuracy of $\pm 5\%$ and a reproducibility of $\pm 2\%$.

The Mettler TA 3000 is a modular TG, DSC, and TMA system in which the basic unit is the TeIO TA processor. All control and data processing are handled by the TC10 processor with software computer programs to calculate various functions (see Chapter 12). The Model TG50 thermobalance contains a 25 1000°C furnace with heating and cooling rates from 0 to $1000^\circ\text{C}/\text{min}$. Electrical weighing range is 0 to 150 mg, with a readability of $1 \mu\text{g}$ and a reproducibility of $\pm 1 \mu\text{g}$. Gaseous samples at atmospheric pressure may be passed through the furnace area.

5. Perkin-Elmer Thermobalance

The Perkin-Elmer Model TGS-2 thermobalance has been described by Cassel and Gray (56) and elsewhere. This instrument has been superseded by the Model TGA7, which is essentially the same thermobalance except for the external cabinet and computer control capability (see Chapter 12). The thermobalance uses a servo-operated balance system, such as that illustrated schematically in Figure 3.25, in which an electrical signal from an optical null-detector (57) is applied directly to control the current in a torque motor. The balance has provisions for digital mass readout using four-digit thumbwheels and a two digit vernier with three full-scale ranges of 10, 100, and 1000 mg.

The furnace and sample holder are shown in Figure 3.26. A unique feature of this instrument is the small thermal mass furnace, which consists of an aluminum oxide cylinder 0.5 in. in diameter by 0.75 in. in length, wound with platinum wire. The platinum wire functions as both a heater and a temperature sensor in a novel electrical design which "time shares" the wire at high frequency. Resistance (temperature) of the wire is sensed during one half of a cycle and compared with the desired program temperature. Power is then applied during the second half of the cycle to null the difference between actual and desired temperature. Thermal lags between heater and sensor are eliminated since they are the same element and coupling between the wire and furnace body is via a highly conductive material. Maximum temperature of the furnace is 1000°C . An automatic temperature calibration program is built into the system 4 microprocessor controller; the system can be calibrated in about 20 min.

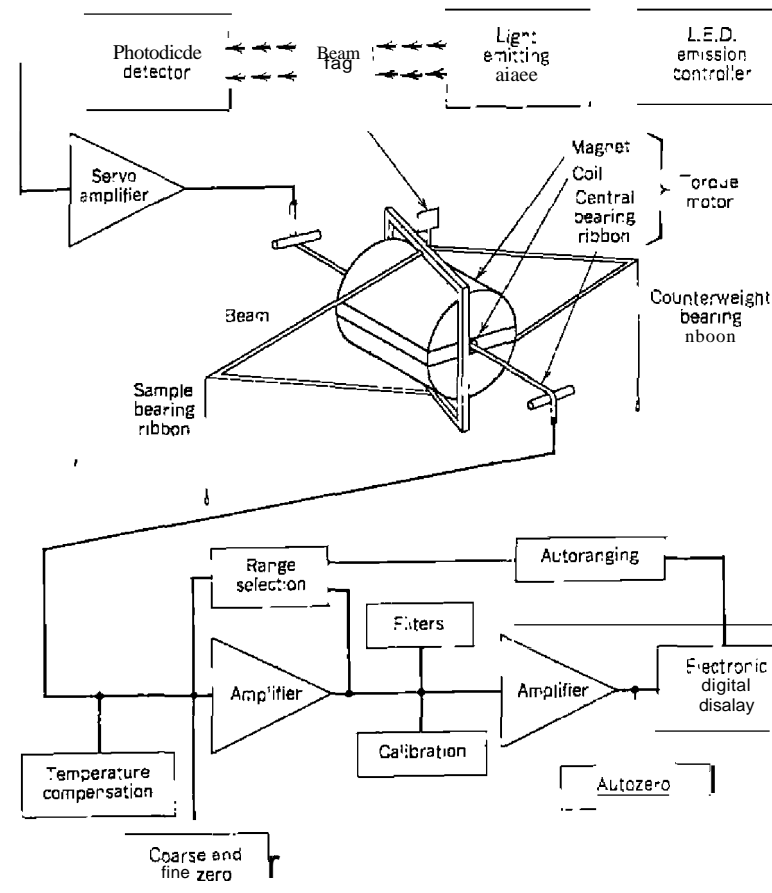


Figure 3.25. Perkin-Elmer TGS-2 servo-operated balance system.

6. Stanton Redcroft Thermobalances

The Model TG-750 thermobalance is illustrated in Figure 3.27. This instrument features a miniature water-cooled furnace in conjunction with an electronic microbalance, with mass sensitivities of 1-250 mg full-scale deflection on a potentiometric recorder. Heating rates of 1 to $100^\circ\text{C}/\text{min}$ are available with a maximum furnace temperature of 1000°C . The furnace will cool from 1000 to 50°C in about 4 min.

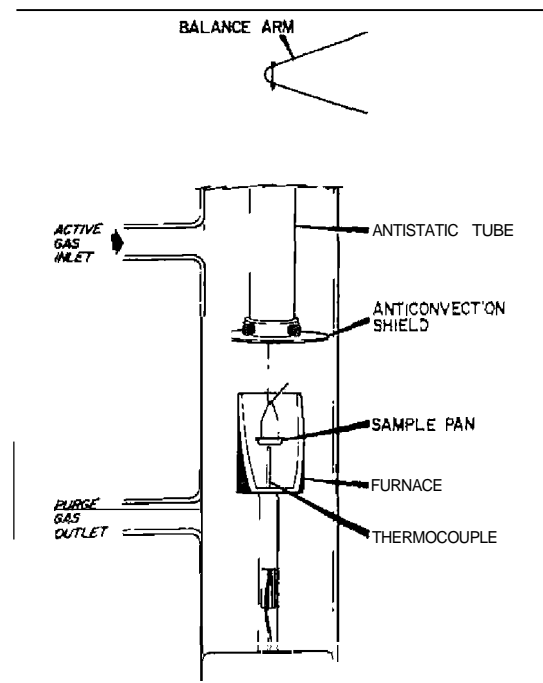


Figure 3.26. Perkin-Elmer TGS-2 furnace and sample holder (56).

Simultaneous TG and DTA may be performed on the Model STA-780 series of thermobalances. A cross section of the 1500°C furnace is shown in Figure 3.28. The sample and reference containers are flat-bottomed 6 mm in diameter platinum crucibles, O, supported on plate-type platinum-platinum-13% rhodium thermocouples, P. For use above 1000°C, alumina disks 0.1 mm thick are inserted between the crucibles and thermocouples to prevent high-temperature welding. The furnace is noninductively wound with platinum-rhodium alloy, W, wire permitting maximum temperatures of 1500°C. Cooling time for 1500–600°C is said to be approximately 10 min, if the furnace is lowered from around the sample container; programmed cooling at a 10°C/min rate can be maintained down to 120°C.

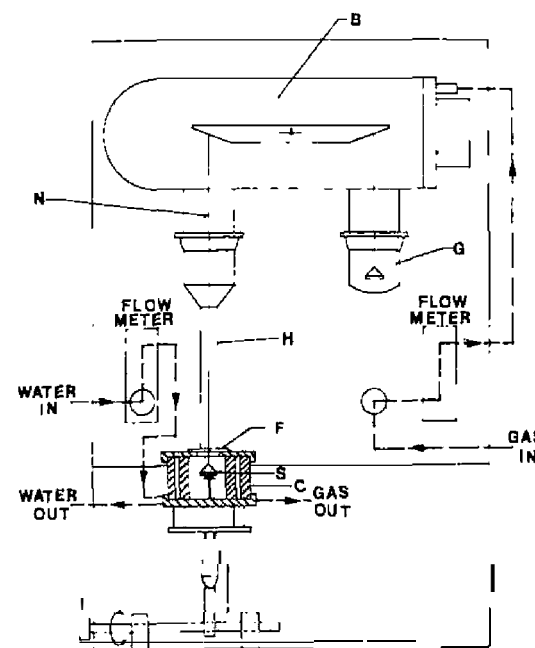


Figure 3.27. Schematic diagram of Stanton Redcroft Model TG-750 thermobalance.

7. Rigaku Thermobalances

Several models of thermobalances are available from Rigaku, the two of interest here are the DM TG/DTA system and the rapid heating thermobalance. The latter uses an infrared imaging furnace capable of heating rates of 1800°C/min. A schematic diagram of the OM TG/OTA system is shown in Figure 3.29. This system is based on a newly designed double beam balance which is said effectively to cancel buoyancy, convection, and thermomolecular flow effects, common to single beam balances. The balance has a maximum mass capacity of 200 mg with weighting ranges 0.5–200 mg full scale. Two furnaces are available with maximum temperatures of 1000 and 1500°C, respectively. Heating rates are 1999°C/min or h.

The rapid heating thermobalance employs a conventional single beam microbalance of the taunt-band suspension type. Maximum mass capacity is

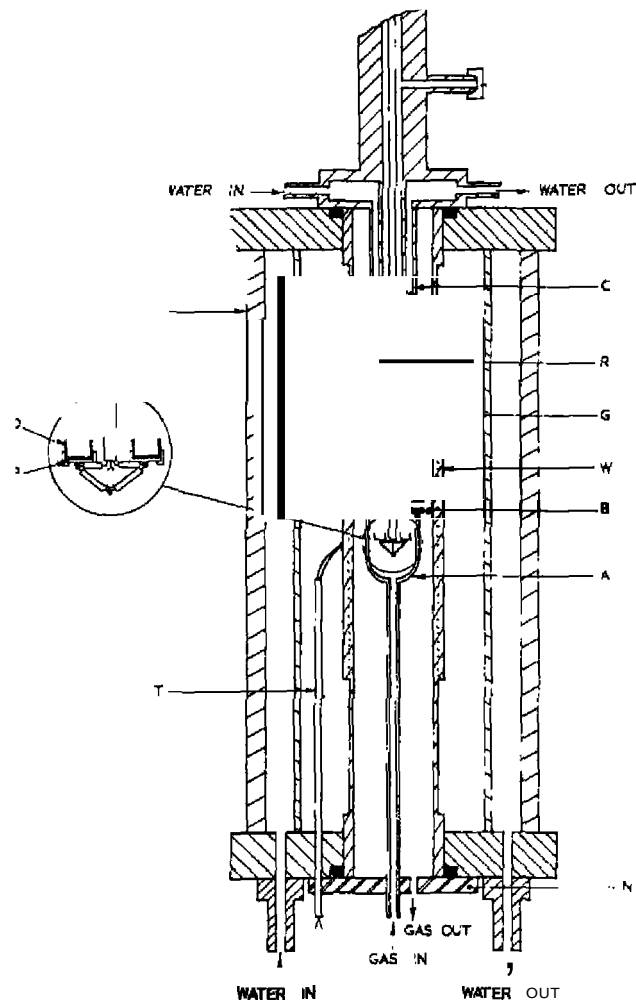


Figure 3.28. Cross section of Stallion Redcroft TG-DTA 1500°C furnace.

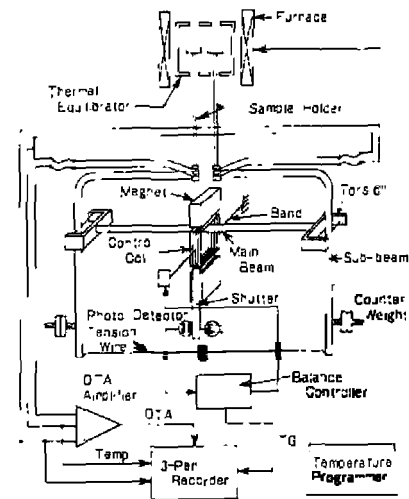


Figure 3.29. Schematic diagram of the Rigaku DM TG/DTA system.

5 g, with a sensitivity of $10 \mu\text{g}$. Full-scale mass ranges that can be employed is $\pm 500 \text{ mg}$. The maximum operational furnace temperature is 1200°C , using the infrared imaging principle, or heating or cooling rates of $1.999^\circ\text{C}/\text{min}$ or h, using the temperature programmer.

8. SETARAM Thermobalances

Perhaps the instrument manufacturer with the most models of thermobalances and other JA instruments is SETARAM. Thermobalances for simultaneous TG-DTG-DTA-EGA measurements in the temperature range from -196 - 2400°C are available, using either the Ugin-Eyraud B.70 balance or the MTH microbalance. These two balances are illustrated in Figure 3.30. The Ugin-Eyraud balance is a knife-edge beam type in which the sample is suspended on one end and a weight compensation system on the other. Maximum mass-load is 100 g with sensitivity of 10^{-5} - 10^{-6} g/g of load. Ten mass ranges may be recorded, 75-3200 mg full scale. The balance may be used at pressures from $5 \times 10^{-6} \text{ Torr}$ to 0.2 bar.

The MTB microbalance is cylindrical in shape and is mounted on a metal base that serves as a "pumping block." It has a symmetrical beam type suspended on a cantilever. Depending on the model, maximum mass capacity is 10, 50, or 100 g, with mass sensitivity of 0.4 - $10 \mu\text{g}$. The balance may be used at pressures from 1 atm to 10^{-6} Torr .

C. MISCELLANEOUS THERMOBALANCES

The conversion of *Cahn* electrobalances to thermobalances has been described by a number of investigators. For the Model RG balance, mention should be made of the instruments described by Gulbransen et al (41), Feldman and Ramachandran (42), Pedersen (43), Etter and Smith (47), and numerous others (52); the Model RM is described by Scott and Harrison (44); and the Model RTL is described by Bradley and Wendlandt (45) and others (46).

The hangdown tube and furnace assembly used by Etter and Smith (47) is illustrated in Figure 3.31. A small platinum resistance heater located inside a relatively short quartz sample tube is used as the furnace. The temperature-sensing thermocouple is located inside the furnace chamber with entry into the chamber from the bottom. This design is similar to that of the Perkin-Elmer thermobalance.

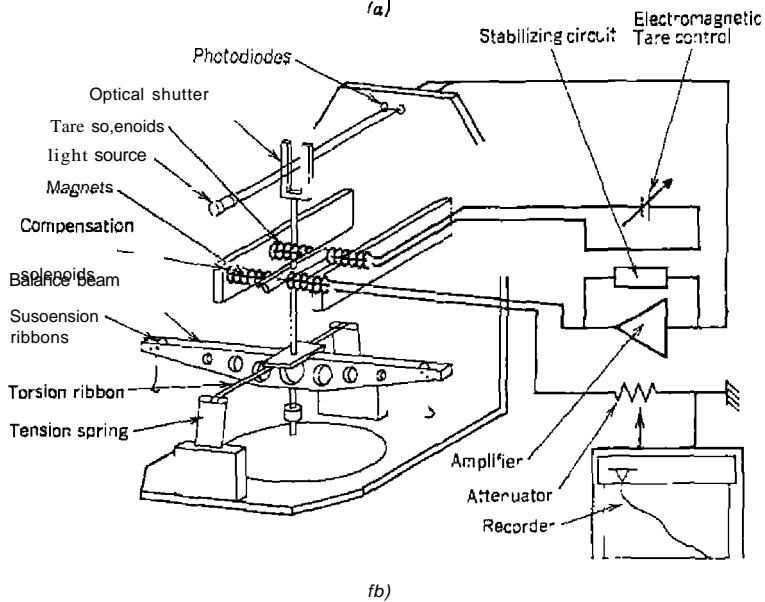
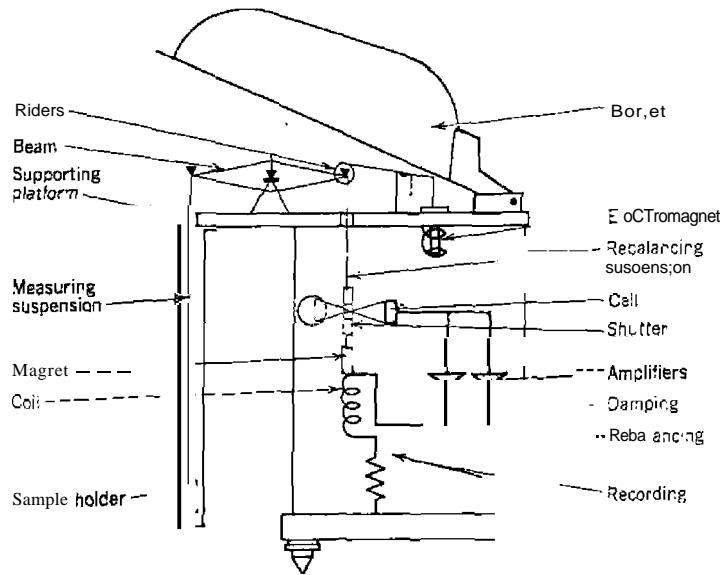


Figure J.J.D. Schematic diagram of SETARAM balances. (a) Uguine-Eyraud B.70 balance; (b) MTB microbalance.

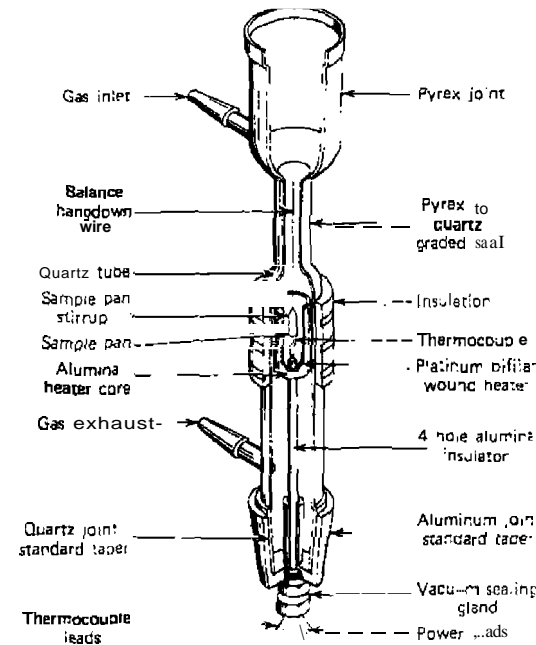


Figure 3.31. Microfurnace used in thermobalance described by Etter and Smith (47).

1. Quartz Balances

The use of resonating quartz crystals for mass-change determinations is very attractive because a sensitivity of about 10^{-12} g/cm² is feasible. Mass determinations with resonating quartz crystals have been discussed by Plant (48) and Van Empel et al. (49). The principle (49) of the determination is based on the relationship between the variation, Δf , of the resonant frequency, f , and the mass added, Δm , or

$$\frac{\Delta f}{f} = \frac{\Delta m}{m} \quad (3.2)$$

where m is the effective mass of the quartz between two electrodes. Measurement must be made at a fixed temperature due to the variation of the frequency with temperature. At relatively high temperatures, a variation of 1°C corresponds to a relative frequency change of 2×10^{-6} , which results in an apparent mass-change of 8×10^{-9} g. However, by use of a dual electrode system in which one electrode is used for temperature sensing and the other for mass-changes, a resonating quartz balance can be constructed (49).

Another approach is to use a thin quartz fiber, 5.20 μ in diameter and about 1 cm long, covered with a thin coating of evaporated gold (48). The fiber is held rigidly at one end and rests between two parallel metal plates to which a de potential is applied. When an audio frequency signal is applied to the fiber, it displays vibrating reed resonances whose frequency depends on the physical parameters of the fiber. If mass is added to the free end of the fiber, the resonant frequencies shift downward, being dependent on the amount of mass.

Other types of balances using quartz crystals have been described also (48).

The first application of a quartz crystal for use as a nonisothermal thermobalance was reported by Henderson et al. (66). This was accomplished through the use of a minicomputer to characterize the temperature-frequency relationship for the crystal and to correct numerically the frequency-temperature-mass relationship to obtain the TG curve of the sample. One advantage of such a system is that very fast heating rates may be employed due to small sample size (1-40 μ g typical) and high sensitivity. Thin films of sample exhibit rapid gas diffusion and thus permit thermal equilibrium to be maintained at heating rates of 100°C/min or greater. Applications of this thermobalance include the evaluation of thin films and coatings as well as various polymer studies of pyrolysis, flammability, and so on.

2. Automated Thermobalances

The modern thermobalance is an automatic instrument in that the mass-change of a sample can be recorded over a wide temperature range. Little attention has been given to the introduction of a new sample automatically into the furnace chamber or of studying multiple samples in a sequential manner. The automated instrument (45, 50) is capable of automatic sampling and temperature programming. Eight samples, contained in the rotatable sample holder disk, can be studied in an individual manner. A schematic diagram of the balance, furnace, and sample changer mechanism is shown in Figure 3.32a. While a diagram of the furnace and sample holder configuration is given in Figure 3.32b.

The thermobalance is conventional in design in that it consists of a tor-loading recording balance (Cahn Model RTL balance), a Leeds and Northrup four-channel multipoint potentiometric recorder (0-5 mV full scale), a small tube furnace, a sample-changer mechanism, and an automatic furnace-temperature programmer. Perhaps the most novel feature of the instrument is the automatic sample-changing mechanism, which operates in the following manner: The samples to be investigated are placed into small cylindrical platinum containers, Figure 3.32b. 5.0 mm in diameter by 2.00 mm in

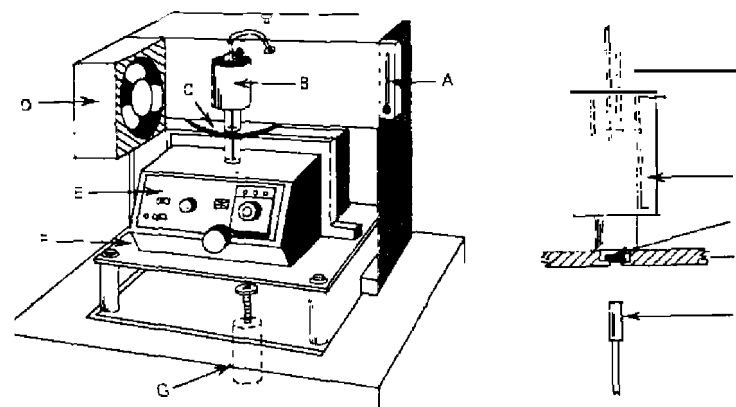


Figure 3.32. An automated thermobalance. (a) Balance, furnace, and sample change mechanism; (b) furnace and sample holder (50). (a) A, gas flow meter; B, furnace; C, sample holder disk; D, cooling fan; E, Cahn Model RTL recording balance; F, balance platform. (b) A, gas inlet tube; B, thermocouples; C, furnace heater windings and insulation; D, sample container; E, sample holder disk; F, ceramic sample probe.

height. Eight such containers are placed in the circular indentations cut in the periphery of the 0.25-in.-thick by 5.0-in.-diameter aluminum sample-holder disk, Figure 3.32*b* (E). The sample containers are positioned directly below the opening of the tube furnace, Figure 3.32*h* (e), by the rotation of a small electric motor connected to a microswitch which is tripped by an indentation in the circumference of the disk. The positioned sample is picked up by the ceramic sample probe, Figure 3.32*h* (F), which is attached to the beam of the balance. Movement of the entire balance and the balance platform, Figure 3J2a (E and F), is controlled by a motor-driven screw in the base of the platform. The motor is reversible so that the platform can be raised or lowered, with limits of movement in both directions controlled by microswitches. After the sample is positioned in the central part of the furnace, the furnace is flooded with nitrogen or some other gas and the furnace temperature programmer is activated. Once a preselected furnace maximum temperature limit is attained, the balance is lowered and the sample container is retained by the sample-holder disk. The disk then rotates to position a new sample at the base of the furnace. A cooling fan, Figure 3.32*a* (D), is activated, which cools the furnace to a preselected lower temperature limit, at which point the entire cycle is repeated, using a new sample. The heating and cooling cycles are performed on eight successive samples. Each sample is preweighed into the sample containers using a Mettler semi-microprinting balance. The individual sample containers are tared to within ± 1 mg (empty weight is about 130 mg); each sample is kept under 10.0 mg so that the recorded pen deflection remains on the recorder scale. The recorder mass range is 0-10 mg at 1.00 mg/in. on a 10-in.-wide chart; a chart speed of $\frac{1}{15}$ or $\frac{1}{2}$ in./min was normally used.

The obvious advantage of the automated thermobalance system over existing instruments is the ability to determine the mass-loss curves of eight successive samples. Operation of the instrument is completely automatic, and once the cycle is begun the instrument does not require the attention of the operator until the eighth sample curve is completed. The instrument should find use for the routine TG examination of a large number of samples, each to be studied under identical thermal conditions. Because the system is completely automated, data reduction or control by a small digital computer could easily be accomplished (see Chapter 14.)

A somewhat different approach was taken by Ferguson et al. (51) in which they described a multispecimen weighing device which was capable of studying samples over long periods of time. The samples were heated in flowing CO_2 - CO - O_2 atmospheres in the temperature range 620-770° K. The sample carrier, which is attached to the "carousel" beam of the balance and the carousel mechanism, are shown in Figure 3.33.

The carriers were constructed of punched sheet and were fitted with

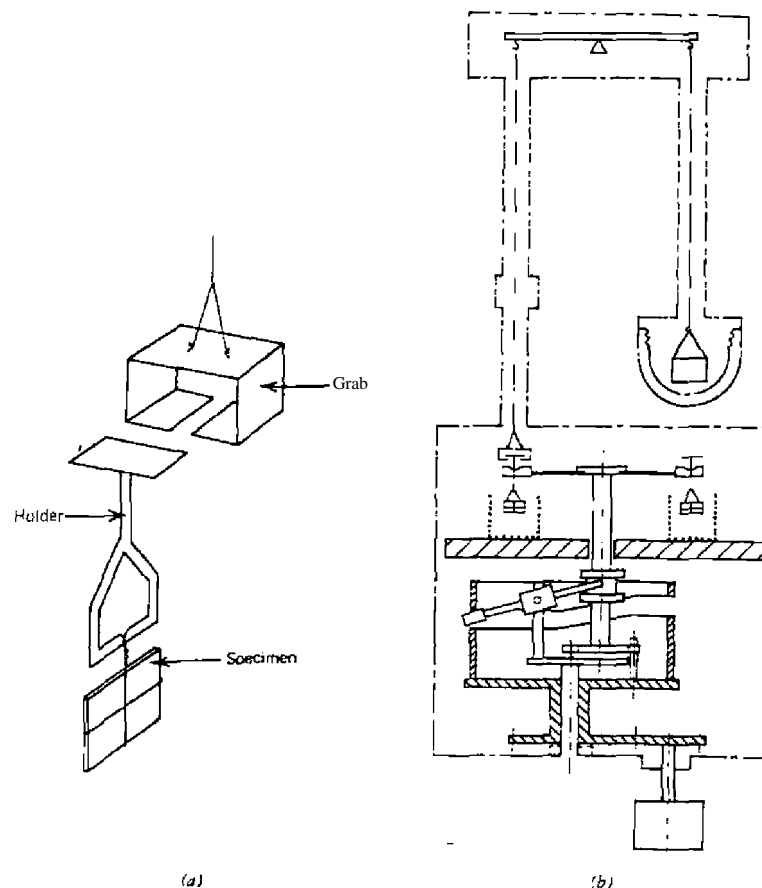


Figure 3.33. Multisample weighing balance of Ferguson et al. (51); (a) Sample carrier; (b) schematic diagram of balance.

flat horizontal heads by spot welding. The sample weighing is carried out by lifting a sample off the carousel beam by engaging the carrier with the grab. The carousel mechanism is mounted so that the sample carriers, which rest in V-blocks near the ends of the radial arms, pass through the grab at the appropriate stage of the weighing cycle. When six samples have passed through the grab the rotation of the carousel stops with the seventh sample in position for weighing. The radial arms are lowered so that the head of the

sample carrier is completely supported by the grab. This position is held for 90 sec while the balance settles and the sample mass is recorded. The radial arms are then raised to reengage with the sample holder and lift it clear of the grab before the carousel rotates once again to bring another sample to the weighing position. Twenty samples may be heated at one time in which each sample is weighed once in a complete cycle lasting 1.5 hours.

3. High-pressure Thermobalances

Ghods and Neumann-Tilte (63, 64) constructed an isothermal balance with two symmetrical pans for use in the hydrogenation of coal chars to pressures of 5 MPa. Provision was made for the trapping of coal tar and other pyrolysis products that could be analyzed by gas chromatography.

A similar symmetrical two-pan balance for use up to 3000 bar was described by Sabrowsky and Deckert (65).

Williams and Wendlandt (68) have described a high-pressure thermobalance based on the Du Pont Model 950 balance and capable of operation at temperatures of 500°C and 500 atm pressure. A schematic diagram of the balance enclosure is shown in Figure 3.34. The balance chamber was machined in the form of a cylinder from stainless steel. The furnace was insulated with Marinite which was machined to fit inside the pressure vessel and extend from the inner plate to the front of the balance housing. Provision was made for fitting the furnace within the insulated chamber and permitting

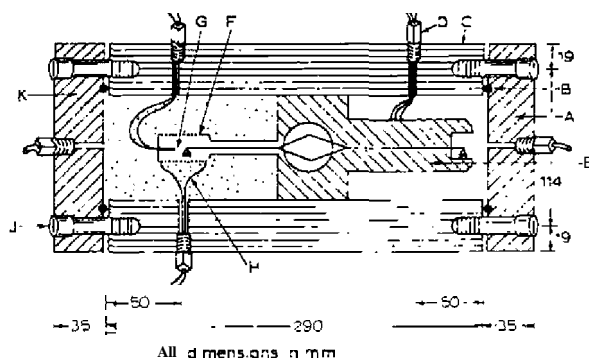


Figure 3.34. Schematic diagram of the high-pressure thermobalance enclosure. A, end plate with threaded opening for gas inlet fitting; B, Buna-N O-ring; C, pressure cell; D, high-pressure connector for control cable; E, balance movement; F, furnace chamber; G, furnace thermocouple; H, furnace heater wire in Marinite insulation; J, hexdrive bolts; K, end plate with threaded opening for gas outlet fitting (68).

free movement of the sample beam and container from the taunt-bane movement balance mechanism. Several procedures were described for correcting the change of buoyancy of the system as the pressure was changed within the chamber.

A high-pressure enclosure for the Cahn 1000 electrobalance, for use at pressures up to 1500 psi, is available from Cahn Instruments. The enclosure is machined from two pieces of stainless steel and contains no weld joints. Optional accessories include a reactor and counterweight chambers and a-ring sealed couplings.

4. Thermomolecular Beam Analysis

Combining a high-temperature X-ray camera with a thermobalance is difficult due to geometrical and focus problems. However, Wiedemann and Bayer (61) have described such a technique in which high-temperature X-ray diffraction patterns and information about its mass-loss can be obtained on a single sample. This new technique, which they called thermomolecular beam analysis (TMBA), is illustrated schematically in Figure 3.35.

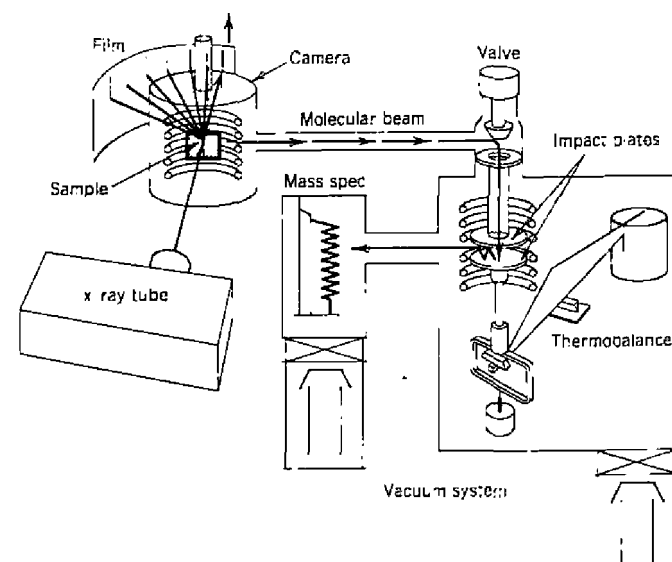


Figure 3.35. Thermomolecular beam analysis apparatus, as described by Wiedemann and Bayer (61).

powdered sample is mounted on a platinum wire mesh sample holder in the X-ray camera. On heating, the thermal decomposition gaseous products pass from the camera to the thermobalance via a vacuum-tight tube. The evolved gases form a molecular beam, which is directed at the empty sample container of the balance. Due to the special flat shape of the inlet orifice and of the balance pan, the arriving molecular bounce back and forth several times before they are removed through the vacuum system. The force of the impacting molecules is proportional to the first derivative of the mass change with time. Thus, the peak area of the recorded curves is directly proportional to the total mass-change of the sample. A mass spectrometer, connected to the system, is used to identify the gaseous molecules evolved from the sample.

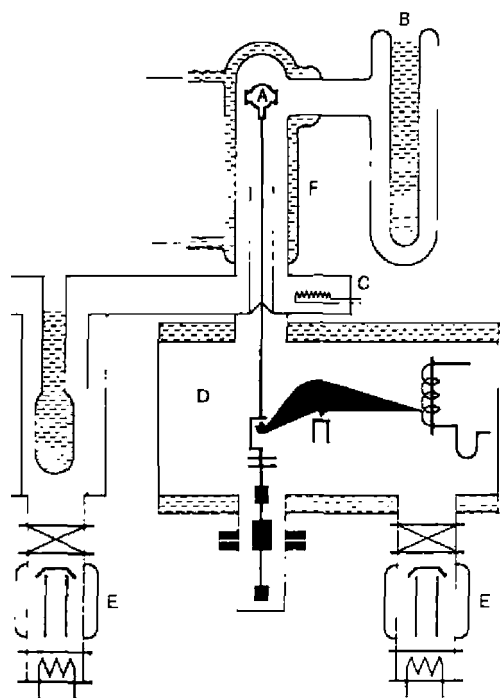


Figure 3.36. Apparatus used by Wiedemann (60) for Knudsen effusion vapor-pressure measurements. A, Knudsen cell; B, cold trap; C, ionization gauge; D, balance and housing; E, diffusion pumps; F, thermostatically controlled reaction chamber.

5. Vapor-pressure Methods Using a Thermobalance

The apparatus used by Wiedemann (60) to obtain the Knudsen effusion vapor pressures of various inorganic and organic substances is shown in Figure 3.36. The Knudsen effusion method is useful for the measurement of vapor pressures $1 \cdot 10^{-6}$ Torr. Using a thermobalance, one can obtain the effusion rate, $\Delta m/\Delta t$, directly from the change in mass of the sample, while the furnace is maintained at some isothermal temperature. The choice of effusion cell used (see Section A.3) depends on the temperature range to be studied, glass or aluminum cells at low temperatures and noble metals or ceramics at higher temperature. The system in Figure 3.36 uses a thermostated reaction chamber employing a heated liquid. For higher temperatures, this is replaced by a furnace that can be isothermally controlled.

Ferro et al. (67) used a coupled torsion-Knudsen effusion apparatus to measure the vapor pressures of *o*-, *m*-, and *p*-chlorobiphenyls. The apparatus, as shown in Figure 3.37, consists of a conventional torsion-Knudsen effusion

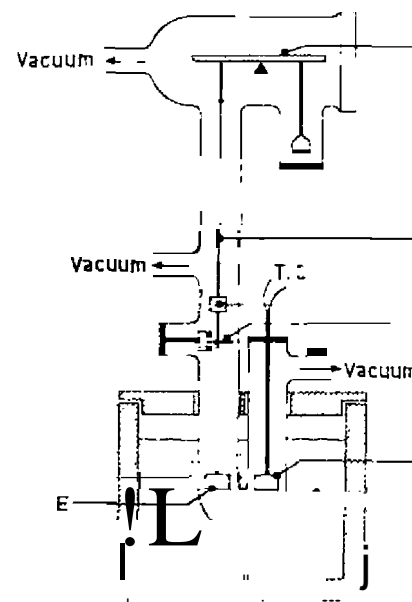


Figure 3.37. Coupled torsion-Knudsen effusion apparatus of Ferro et al. (67). A, electric balance; B, tungsten torsion wire; C, reflecting mirror; D, braking disc; E, torsion cell; F, ionization gauge; G, thermostatic sand bath.

apparatus, suspended under vacuum from one pan of a Cahn RH electrobalance. A thermostatic fluidized sand bath, controlled to $\pm 0.2^\circ\text{C}$, is used to heat the reaction chamber. The temperature of the cell was measured by a calibrated iron-copper thermocouple inserted in a cell similar to the effusion one and placed at the same position. The mass loss, determined by using the electrobalance, corresponded to vapor pressures of about 10^{-5} kPa.

6. Miscellaneous

Bart et al. (62) have described the enclosure of a Mettler TA-1 thermoanalyzer in a sealed system in order to permit the examination of samples containing alpha and beta/gamma emissions. Samples containing plutonium and uranium may be studied by TG with no radiation hazard to the operator. All balance components could be reached through glove ports.

REFERENCES

- Lukaszewski, G. M., and J. P. Redfern. *Lab. Pract.*, **10**, 469 (1961).
- Gordon, S., and C. Campbell. *Anal. Chem.*, **32**, 271R (1960).
- Wiedemann, H. G., *ACHEMA Congress*, Frankfurt, Germany June 26, 1964.
- Erdey, L., F. Paulik, and J. Paulik. *Mikrochim. Acta*, 1966, 699.
- Paulik, F., J. Paulik, and L. Erdey. *Talanta*, **13**, 1405 (1966).
- Wiedemann, H. G., and H. P. Vaughan. *Thermochim. Acta*, **3**, 355 (1972).
- Gam, P. D., and J. E. Kessler. *Anal. Chem.*, **32**, 1563 (1960).
- Forkel, W., *Naturwissenschaften*, **47**, to (1960).
- Newkirk, A. E., *Thermochim. Acta*, **2**, 1 (1971).
- Paulik, F., and J. Paulik. *Thermochim. Acta*, **4**, 189 (1972).
- Elder, J. P., *Thermochim. Acta*, **52**, 235 (1982).
- Stewart, L. N., *Proceedings of the Third Toronto Symposium on Thermal Analysis*, H. G. McAdie, ed., Chemical Institute of Canada, Toronto, February 25-26, 1969, p. 205.
- Mar-cite, E. P., and B. Carroll. *Rev. Sci. Instr.*, **35**, 1486 (1964).
- Norem, S. D., M. J. O'Neill, and A. P. Gray. *Proceedings of the Third Toronto Symposium on Thermal Analysis*, H. G. McAdie, ed., Chemical Institute of Canada, Toronto, February 25-26, 1969, p. 221.
- Norem, S. D., M. J. O'Neill, and A. P. Gray. *Thermochim. Acta*, **1**, 29 (1970).
- Duval, C., *Anal. Chem.*, **23**, 1271 (1951).
- Lewin, S. Z., *J. Chem. Educ.*, **39**, A575 (1962).
- Jacque, L., G. Guiochon, and P. Gendrel. *18th. Soc. Chim. France*, 1961, 1061.
- Saito, H., in *Thermal Analysis*, R. F. Schwenker and P. D. Garn, eds., Academic, New York, 1969, p. 1.
- Vaughan, H. P. *Am. Lrh. J.*, **10** (1970).
- Wendlandt, W. W., *Lab. Management*, Oct., 25 (1965).

- Wendlandt, W. W., *J. Chem. Educ.*, **49**, A571, A623 (1972).
- Duval, C., *Inorganic Thermogravimetric Analysis*, Elsevier, Amsterdam, 1953.
- Duval, C., *Inorganic Thermogravimetric Analysis*, 2nd ed., Elsevier, Amsterdam, 1963.
- Gam, P. D., *Thermoanalytical Methods of Investigation*, Academic, New York, 1965, Chap. 10.
- Keatch, C., *An Introduction to Thermogravimetry*, Heyden, London, 1969.
- Anderson, H. C., in *Technique and Methods of Polymer Evaluation*, P. F. Slade and L. T. Jenkins, eds., Marcel-Dekker, New York, 1966, Chap. 3.
- Wendlandt, W. W., in *Handbook of Commercial Scientific Instruments*, C. Veillon and W. W. Wendlandt, eds., Marcel-Dekker, New York, Vol. 2 (1973).
- Salta, H., *Thermobalance Analysis*, Gijitsll Shain, Tokyo, 1962.
- Honda, K., *Sci. Repts. Tohoku Univ.*, **4**, 97 (1915).
- Guichard, M., *Bull. Soc. Chim. France*, **33**, 258 (1923).
- Vaillet, P., *Bull. Soc. Chim. France*, **3**, 103 (1936).
- Dubois, P., *Bull. Soc. Chim. France*, **3**, 178 (1936).
- Chevenard, P., X. Wache, and R. de la Tullaye. *Bull. Soc. Chim. France*, **10**, 41 (1944).
- Paulik, F., J. Paulik, and L. Erdey. *Z. Anal. Chem.*, **160**, 241 (1958).
- Sarasohn, I. M., and R. W. Tabeling. *Pittsburgh Conference of Analytical Chemistry and Applied Spectroscopy*, March 5, 1964.
- Williams, H. W. *Thermochim. Acta*, **1**, 253 (1970).
- Williams, I. R., E. L. Simmons, and W. W. Wendlandt. *Thermochim. Acta*, **5**, 101 (1972).
- Chill, I., *Anal. Chem.*, **39**, 861 (1967).
- Paulik, J., F. Paulik, and L. Erdey. *Anal. Chim. Acta*, **34**, 419 (1966).
- Gulbransen, E. A., K. F. Andrew, and F. A. Brassart, in *Vacuum Microbalance Techniques*, Plenum, New York, 1965, Vol. 4, p. 127.
- Feldman, R. F., and V. S. Ramachandran. *Thermochim. Acta*, **2**, 393 (1971).
- Pedersen, E. J. *Sci. Instr.*, **1**, 1013 (1968).
- Scott, K. T., and K. T. Harrison. *J. Nucl. Mater.*, **8**, 307 (1963).
- Bradley, W. S., and W. W. Wendlandt. *Anal. Chem.*, **43**, 223 (1971).
- Cahn Electrobalance Model RTL. Instructions No. 2006, Cahn Instrument Co.
- Etter, D., and W. H. Smith. *J. Chem. Educ.*, **49**, 143 (1972).
- Plant, A. F., *Industrial Res.*, July, 361 (1971).
- Van Empel, F. J., E. C. Bailegooyen, F. Boersma, and J. A. Poullis. *Thermochim. Acta*, **5**, 129 (1972).
- Wendlandt, W. W., *Chimia*, **26**, 1 (1972).
- Ferguson, J. M., p. M. Livesey, and D. Mortimer. International Confederation of Thermal Analysis III, Davos, Switzerland, Aug. 1971, Paper 1.
- Wendlandt, W. W., *Anal. Chim. Acta*, **49**, 185 (1970).
- McGhie, A. R., *Anal. Chem.*, **55**, 987 (1983).
- McGhie, A. R., J. Chiu, P. G. Fair, and R. L. Blaine. *Thermochim. Acta*, **67**, 241 (1983).
- Blaine, R. L., and P. G. Fair. *Thermochim. Acta*, **67**, 233 (1983).
- Cassel, R. B., and A. P. Gray. *Thermochim. Acta*, **36**, 265 (1980).
- Ewing, G. W., *J. Chem. Educ.*, **53**, A252 (1976).

58. Kaplan, J., J. Marston, and D. Weise, *Amer. Lab.*, Sept. 1980, 107.
59. Wendlandt, W. W., *Thermochim. Acta*, 50,7 (1981).
60. Wiedemann, H. G., and G. Bayer. *Topics in Current Chemistry*, Vol. 77. Springer-Verlag, Berlin, (1978).
61. Wiedemann, H. G., and G. Bayer, *Z. Anal. Chem.* 266, 97-109 (1973).
62. Bart, G., F. Petrik, F. Sprunger, and P. Gritsch, *Thermochim. Acta*, 52, 169 (1982).
63. Ghodsi, M., and C. Neumano-Tilte, *Thermochim. Acta*, 62, 1 (1983).
64. Ghodsi, M., R. Drie, and J. P. Lempereur. *Thermochim. Acta*, 28, 259 (1979).
65. Sabrowsky, H., and H. G. Deckert, *Chem. Ing. Tech.*, 50, 217 (1978).
66. HenderSOEL, D. E., M. B. DiTaranto, W. G. Tonkin, D. I. Ahlgren. D. A. Gatenby, and T. W. Shym, *Anal. Chem.*, 54, 2067 (1982).
67. ferro, D., V. Piacente, and P. Scardala, *Thermochim. Acta*, 68, 329 (1983).
68. Williams, J. R., and W. W. Wendlandt, *Thermochim. Acta*, 7, 253 (1973).

CHAPTER

4

APPLICATIONS
OF THERMOGRAVIMETRY

A. INTRODUCTION

The method of thermogravimetry is basically quantitative in nature in that the mass-change can be accurately determined. However, the temperature ranges in which the mass-changes occur are qualitative in that they depend on the instrumental and sample characteristics. With the wide use of commercial thermobalances, TG data of a sample can be correlated from laboratory to laboratory if similar conditions of pyrolysis are employed.

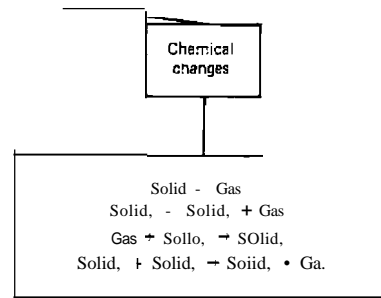
Thermogravimetry is widely used in almost all of the areas of chemistry and allied fields. In the early 1950s it caused a revolution in inorganic gravimetric analysis, and if a similar analogy can be used in the 1960s, the revolution occurred in the field of polymer chemistry. Equally important has been the application of TG techniques to applied science problems such as the characterization of various materials used in road construction, determination of moisture contents in a wide variety of materials, and numerous others. As will be seen, TG is almost universally applied to a large number of analytical problems in the fields of metallurgy, paint and ink science, ceramics, mineralogy, food technology, inorganic and organic chemistry, polymer chemistry, biochemistry, geochemistry, and others.

The application of thermogravimetry to a particular problem is possible if a mass-change is observed on the application of heat. If no mass change is observed, then other thermal techniques such as DTA, DSC, TMA, and so on, may have to be employed. If the mass-change is very small (< 1%), then perhaps other techniques such as evolved-gas analysis (EGA) may be more useful. Mass-changes (generally mass-losses) which can be detected by TG techniques are summarized in Figure 4.1.

Some of the many applications of thermogravimetry are listed as follows:

1. Thermal decomposition of inorganic, organic, and polymeric substances.
2. Corrosion of metals in various atmospheres at elevated temperatures.
3. Solid-state reactions.

APPLICATIONS OF THERMOGRAVIMETRY



Changes detectable by TG.

ROASTING AND CALCINATION OF MINERALS,

and evaporation of liquids.

coal, petroleum, and wood.

In moisture, volatiles, and ash contents.

Droptail and sublimation.

Many applications of thermogravimetry have been reviewed in numerous reviews and books. Mention should be made of the recent review articles by Gordon and Campbell (1), Duval (2), Coats and Redfern (3), Lukaszewski and Redfern (4) and biennial reviews by Murphy (5, 6), Toursei (7), and Wendlandt (88, 138, 139). Relevant books or book chapters include those by Duval (8, 9), Wendlandt and Smith (10), Wendlandt (11), Johnson (12), Doyle (13), Barrall (14), Liptay (15), Reich and Redemann and Bayer (72), Daniels (140), Kcattch and Dolli (11), Paulik and Paulik (142), and many others.

B. APPLICATION TO CATALYSIS

As described how TA techniques can be used to optimize the performance of various catalysts. The ability to study the effect of variables such as catalyst composition, temperature, and gas flow rates on the reaction rates can be obtained quickly and cheaply prior to large-scale studies. TG, for example, may be used to study the optimum methods for the preparation of the catalyst, as shown in Figure 4.2 (130). The catalyst is prepared by

APPLICATIONS TO CLAYS AND MINERALS

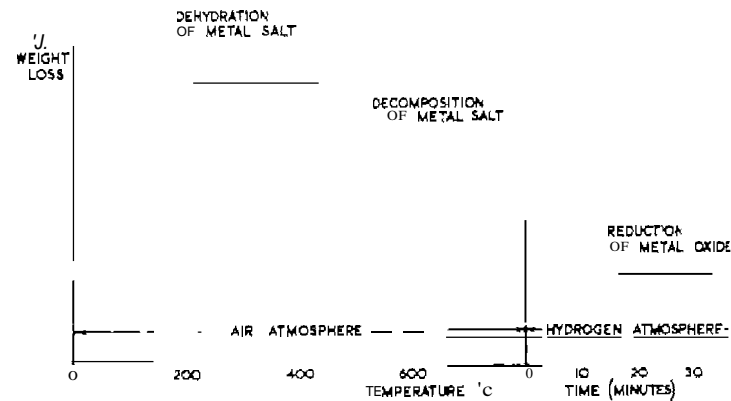


Figure 4.2. TG curve of the formation of a $\text{Ni}/\text{Al}_2\text{O}_3$ catalyst by direct reduction of $\text{Ni}(\text{NO}_3)_2/\text{Al}_2\text{O}_3$ at 1600°C (130).

impregnating the support material with a solution of the metal salt. After dehydration and calcination of the metal salt, the atmosphere of the furnace is changed to hydrogen to form the finely divided metal. Conditions of heating rate, gas flow rate, and temperature range associated with each step can be easily varied and the effect on the surface area determined.

The mass-gain of a catalyst as it absorbs a gas can be continuously monitored by TG. The gain in mass at any temperature is related to the number of occupied active sites. TG can also be used to determine the surface area of supported catalysts from the mass-gain at a temperature that gives monolayer surface coverage (130). Catalyst poisoning can also be monitored from the mass-gains of the catalyst. Reactions involving organic materials frequently deposit coke and sometimes sulfur on the catalyst surface. When deactivation has occurred by water adsorption, TG can be used to determine the mass-loss associated with reactivation.

Gallagher et al. (131) used TG and other TA techniques to study the preparation and performance of perovskite oxidation catalysts, $\text{La}_{1-x}\text{M}_x\text{MnO}_3$ where M is Pb, Ca, Sr, or Ba and $\text{LaMn}_{1-x}\text{Cu}_x\text{O}_{3+y}$ are catalysts (132). Patel et al. (133) studied the thermal decomposition and catalytic activity of $\text{Ba}_x\text{Ln}_{1-x}\text{CoO}_3$, where Ln is La, Nd, Sm, and Dy.

C. APPLICATIONS TO CLAYS AND MINERALS

Dunn (109) has summarized the major areas of application of TG and other TA techniques to clays and accessory minerals. These applications include

1. Assessment of raw material deposits through characterization, classification, and analysis.
2. Investigation of the changes in the raw materials resulting from industrial processing.
3. General problem-solving techniques used when difficulties are encountered through changes in raw material, new technology, or new specifications.

TG and DTG has the capability of providing accurate quantitative determinations, provided that a single stoichiometric reaction of the clay or mineral occurs in the temperature range of interest. Thus, the mass-loss due to the dehydroxylation of clays (see Figure 4.3) can be used to determine the clay content of a mixture. When overlapping mass-losses occur, isothermal intervals can be employed to resolve the separate reactions, as in the determination of alunite and kaolinite in alunitic clays (110) and $MgCO_3$ and $CaCO_3$ content in dolomites.

Kaolinite is one of the most important clays in industry. It is used as a filler in paper and is also extensively used in the rubber and ceramic industries. The clay is found as a secondary mineral formed by the weathering or hydrothermal alteration of aluminum silicates, particularly feldspars. Kaolinite occurs naturally in almost every country of the world.

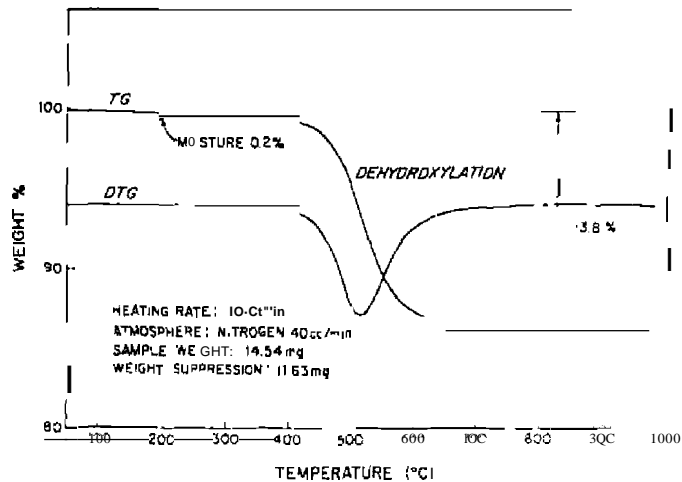


Figure 4.3. TG curve of kaolinite standard (II: 1).

The TG and DTG Curves of a kaolinite standard, as determined by Earnest (111), is shown in Figure 4.3. Sorbed water is evolved at temperatures up to 200°C; in this case, the amount is 0.2% of the total sample mass. The dehydroxylation reaction occurs in the temperature range of 400–700°C, resulting in a mass-loss of 13.8%. The DTG curve is similar in symmetry to the DTA curve peak. Experimental factors, such as heating rate, larger sample-particle size, and so on, can shift the peak minima temperatures.

Other kaolinite clays studied by Earnest (111) include hydrite UF, Dixie clay, and Peerless kaolin. Montmorillonite clay minerals have also been characterized by Earnest (112).

The application of the Derivatograph technique (TG, DTG, DTA, and T) to numerous minerals has been described by Selmececi (113). Paulik et al. applied the same technique to the determination of carbonate, sulfate, pyrite, and organic material in minerals, soils, and rocks (114). hydargillites (115,116).

Mackenzie and Caillere (117) described the use of TG and other TA techniques to the qualitative and quantitative determination of clay minerals in soils.

Hofman et al. (28, 29) studied the thermogravimetry of soils, relatively pure clays, crystalline carbonates, and soils to which known amounts of clays and carbonates were added. Sharp breaks were observed in the decomposition curves of relatively pure clay minerals at elevated temperatures, which suggested the use of thermogravimetry for the determination of pure clays and simple clay mixtures. The quantities that could be determined by this technique were water content, organic matter content, and inorganic carbonates.

The decomposition curves of most soils showed horizontal mass levels starting at 150–180°C and extending to 210–240°C, indicative of either hygroscopic moisture or hygroscopic moisture plus easily volatile organic compounds. In general, the mass-loss values fell between those obtained by the Karl Fischer method and oven drying at 105°C. The organic matter started to burn off between 210 and 240°C and was usually completely burned off at 500°C. In organic soils and those containing less than 15% clay, a relatively close estimate of the organic matter could be made from the mass-loss curve. When the clay content varied from 15–40%, the loss in mass at 500°C usually gave an estimate of the organic matter, which was in satisfactory agreement with dry-combustion and wet-oxidation data. When the clays contained more than 40% clay, it was not possible to distinguish between mass-losses due to decomposition of organic matter and those due to the elimination of the lattice water of clays. This work also suggests that the lattice water in the pure clay samples can be quantitatively determined. Because the lattice water came off at different temperatures with different

clays, it may be possible to use these temperatures as an additional means of identification and characterization.

Mulley and Cavendish (30) found that TG could be used to analyze mixtures of calcium hydrogen orthophosphate 2-hydrate (brushite) and anhydrous calcium hydrogen orthophosphate (monetite) based on their loss of water on heating. The water loss on the heating of brushite corresponds to 2.5 moles per mole of compound, while the monetite evolves 0.5 mole per mole of compound. The total mass-loss on heating a mixture of the two compounds is

$$\text{mass-loss due to } \text{CaHPO}_4 \cdot 2\text{H}_2\text{O} = b = 0.06620\% \quad (4.1)$$

and

$$\text{mass-loss due to } \text{CaHPO}_4 = a = 0.2617b\% \quad (4.2)$$

The total mass-loss is

$$T\% = 0.0662a + 0.2617b \quad (4.3)$$

but $b = (100 - a)$; therefore the total mass-loss is

$$T\% = 26.17 - 0.1955a \quad (4.4)$$

From a plot of T versus a , which is a straight line, the composition of the mixture can be read directly off the curve. By a similar series of calculations, the analysis of three component systems could be carried out.

High- and low-magnesium calcite minerals, in addition to aragonite and normal calcite, were analyzed by several different methods, including TG (31). The results obtained by TG compared favorably with X-ray diffraction and wet chemical analyses.

Paulik et al. (32) developed a Derivatographic method for the determination of pyrites content in bauxite and clay minerals. This method could be used to analyze the samples if they contained more than 0.2% pyrite. Use was made of the DTG curve, rather than the TG curve, for the determination.

D. APPLICATIONS TO FT/ELS

1. Coal

Thermogravimetry is apparently less frequently used to characterize coal than are DSC/DTA (118). The former has been found to be more useful as a rapid and convenient tool for screening and proximate analyses of coal samples. Use of TA techniques, including TG, in the characterization and analysis of coals, oil shales, and oil sands has been reviewed by Rajeshwar (19). A typical TG curve of an Ohio coal sample, in nitrogen and in oxygen, is shown in Figure 4.4 (118). In nitrogen, volatiles and moisture are lost at temperatures up to 1000°C; on changing the atmosphere to oxygen, fixed carbon is burned off leaving the ash as residue. Thus, from a single sample, usually 10–30 mg, the moisture and volatiles, fixed carbon, and ash can be determined. Typical analyses for these components on two coal samples are shown in Table 4.1 (118). These data agree within limits of experimental error with those determined by the ASTM method. Particle size changes did not result in systematic changes in the mass-loss plateau corresponding to the moisture/volatile matter and fixed carbon/ash contents.

The proximate analysis of coal samples has also been described by Fyans (122), Sadek and Harrell (23), Earnest and Fyans (124), Hassel (125), and others. Using TG, Serageldin and Pan (126) described the reaction kinetics of the thermal decomposition of coal.

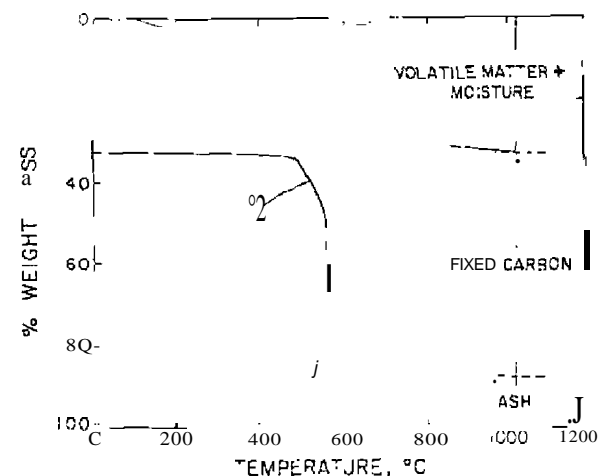


Figure 4.4. A typical TG curve of an Ohio coal sample. Sample mass of 22.14 mg (118)

Table 4.1. TG and DTG Analyses of Coal Samples (118)

Parameters	Sample Number					
	1231			1232 ₁		
	A ^b	B ^a	Reponed	A	B	Reported
Volatiles -						
moisture (wt.%) ^c	45.5	45.4	50.4	30.0	28.5	27.9
Fixed carbon						
(wt.%) ^c	47.0	48.5	42.4	23.0	29.5	22.1
Ash (wt.%)	7.5	6.0	7.2	47.0	42.0	50.0
DTG peak temp (°C)	445	445	445	460	460	460

^aHeating rate: 10°C min⁻¹.

^bParticle size: -250 - 300 mesh.

^cParticle size: - 10 - 16 mesh.

2. Oil Shale

Oil shale is a sedimentary rock that contains both inorganic (mineral) and organic (kerogen and bitumen) components. The oil is derived from the oil shale by destructive distillation. Most forms of organic matter in the shales belong to the *exinite* group of macerals. These are largely algal in origin with lesser contributions from spores, pollen, and cuticle of higher land plants (120). Since thermal retorting is one of the most common approaches to the processing of oil shales, TA methods, especially TG, are useful techniques for studying this process.

Earnest (120) described the TG behavior of a sample of Green River (Colorado) oil shale. The TG and DTG curves, shown in Figure 4.5, indicate a two-step mass-loss for shales from the upper and mahogany zones of the Green River formation. Notable exceptions to this behavior are in shales containing significant amounts of trona, dawsonite, and other minerals. The initial thermal decomposition in the 300-550°C temperature range is caused by the major kerogen plus bitumen pyrolysis. The second mass-loss stage, from 650-800°C, is due primarily to the evolution of carbon dioxide from the decomposition of carbonate mineral components. These mass-losses will vary with the amounts of organic and mineral components in the individual shales. Although the carbonate components may be calcitic, dolomitic, or ankeritic, they are not easily distinguished by TG in a nitrogen atmosphere.

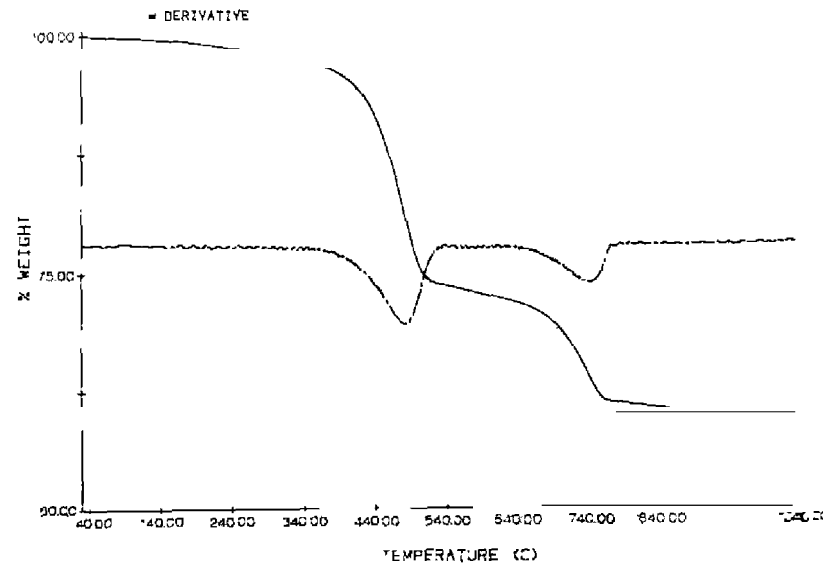


Figure 4.5. TG and DTG curves of a Green River (Colorado) oil shale (120).

The TG curve peak area can be correlated to the oil yield of the shale in (L/tonne); Table 4.2 shows this correlation, which is based on the relationship (120), DTG area (wt%) = 0.115 oil yield (L/tonne). It is interesting to note that a plot of DTG peak area versus oil yield extrapolates to within

Table 4.2. Correlation of DTG Peak Area with Oil Yield for Green River Shales (120).

Oil Yield (l Tonne ⁻¹)	DTG Peak Area (wt.%)
44.6	4.9
83.4	9.1
124.7	13.9
170.1	19.2
208.9	24.0
282.7	31.9

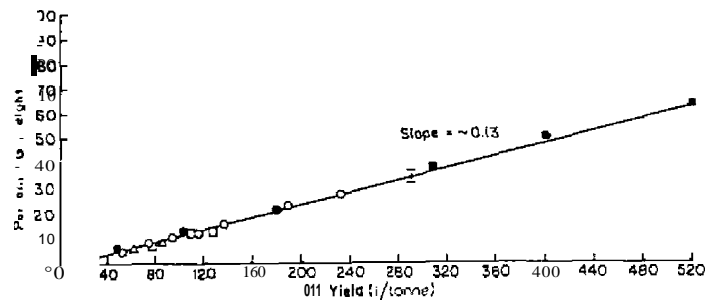


Figure 4.6. Correlation between TO mass-loss at 500°C with oil yield. Samples are: •, Poirts, Rille, CO; ○, Logan Wash, CO; □, Rock Springs, WY; △, Vermol, UT. The vertical bar denotes maximum mean deviation in TO values (121).

experimental error of zero oil yield for zero peak area. This implies that, for this set of samples, the contribution to the DTO peak area by interfering minerals was very minor. The variation of oil yield with the depth of oil shale seam can also be determined by this method.

Rosenvold et al. (121) proposed a similar TO assay method for oil shales in which the percent mass-loss at 500°C could be used to calculate potential oil yields in liters per tonne. The generality of the method is shown by the plot of % mass-loss versus oil yield in Figure 4.6. The four oil shale samples used came from different sources in Utah, Colorado, and Wyoming. A single line correlates the relationship between the two parameters regardless of the particular location from where the oil shale originates. This confirms the expectation that, for shales from the same formation, the indigenous kerogen should be characterized by comparable H/C ratios and, consequently, comparable oil/gas yield ratios. This curve also confirms the general validity of the proposed TO assay method.

Earnest (128) studied the oxidative profiles of several American and Australian oil shales using TG-D110. For American and Canadian oil sands, Rosenvold et al. (129) obtained TG and DSC curves of bitumen extracts. The extracts were heated in an inert atmosphere, yielding curves showing that thermal decomposition takes place in two distinct stages. The first stage reaches a maximum at about 350°C, whereas the second shows a rate maximum at 475°C.

3. Miscellaneous

The thermobalance can also be used as a microdistillation apparatus, as described by Cassel et al. (127). Three materials, crude oil, light oil, and

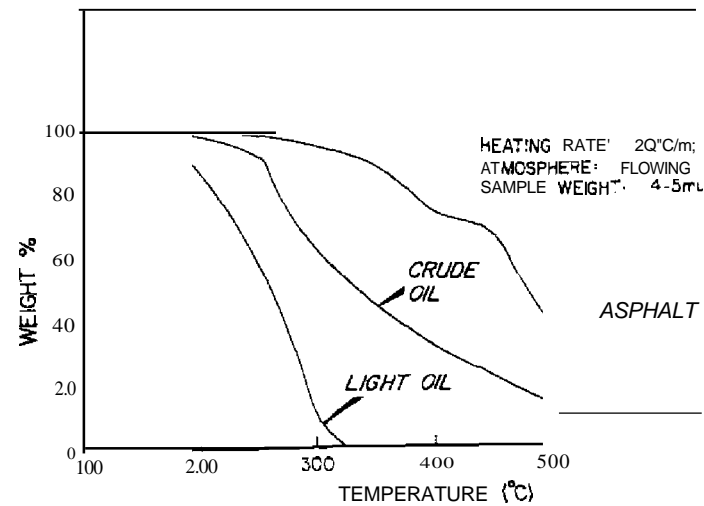


Figure 4.7. Microdistillation of petroleum products using TGA.

asphalt, were placed in sealed sample holders containing a pinhole vent cover, respectively. The TO curves obtained for these three samples are illustrated in Figure 4.7. As expected, the low molecular weight light oil distilled between 100 and 330°C; the crude oil from 300-600°C; and the asphalt in the temperature range 200-650°C. It was stated that by using a series of isothermal equilibration steps, one could obtain results that would be more reproducible and independent of experimental conditions of sample size, pinhole diameter, and nitrogen flow rate.

E. APPLICATIONS TO INORGANIC MATERIALS

1. Alkaline Earth Halide Hydrates

The alkaline earth halide hydrates and related salts have been studied by TO and other thermal techniques under a variety of atmospheric and instrumental conditions. Using the quasi-isothermal and quasi-isobaric techniques in different types of sample holders, Paulik et al. (61) found that various hydrate stoichiometries could be obtained. As shown in Figure 4.8, the inflection points in curve (1) indicate the presence of $\text{CaBr}_2 \cdot 2\text{H}_2\text{O}$ and $\text{CaBr}_2 \cdot \text{H}_2\text{O}$. In curves (2)-(4), the inflection points correspond to $\text{CaBr}_2 \cdot 3\text{H}_2\text{O}$ and

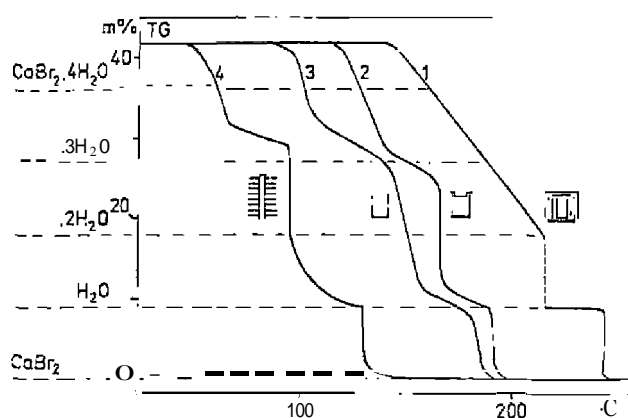


Figure 4.8. Quasi-isothermal-quasi-isobaric dehydration of $\text{CaBr}_2 \cdot 6\text{H}_2\text{O}$ in different sample holders (61).

$\text{CaBr}_2 \cdot \text{H}_2\text{O}$. The inflection point for the former stoichiometry shows slight variations from that of the theoretical stoichiometry for this compound. This is explained as follows: Since $\text{CaBr}_2 \cdot 6\text{H}_2\text{O}$ melts in its water of crystallization at 35°C , a compact crust is formed on the surface of the compound, frequently ruptured by the escape of water vapor. Thus, it is difficult to ascertain if a compound with the $\text{CaBr}_2 \cdot 3\text{H}_2\text{O}$ stoichiometry is actually formed or if it is an intermediate composition formed from the drying of a liquid phase. In each crucible type, the water evaporation took place under different conditions, and hence there is a variation in the curve inflection points.

Paulik et al. (62) also found that anhydrous CaBr_2 decomposed completely in an oxygen atmosphere between 500 - 1000°C with the formation of CaO and Br_2 . In a nitrogen atmosphere, 3% of the compound was evolved due to sublimation at temperatures between 700 and 1000°C .

The dehydration of $\text{CaX}_2 \cdot n\text{H}_2\text{O}$ and $\text{SrX}_2 \cdot n\text{H}_2\text{O}$, where $X = \text{Cl}^-$, Br^- and I^- were investigated by TG and DTA by Buzagh-Gere et al. (63), whereas Paulik and Paulik (64) examined the TG behavior of $\text{BaCl}_2 \cdot 2\text{H}_2\text{O}$ under quasi-isothermal and quasi-isobaric conditions.

2. Alkaline Earth Oxalates

The determination of calcium, strontium, and barium ions in the presence of one another has been carried out by thermogravimetry by Erdey et al. (35,36). The ions are precipitated in the form of mixed metal oxalate hydrates

and decomposed on the thermobalance. From the resulting mass-loss curves, the amounts of calcium, strontium, and barium can be determined.

The mass-loss curve and its first derivative (see Chapter 2) of a mixture of calcium, strontium, and barium oxalate hydrates are shown in Figure 4.9.

From the curve, it can be seen that the decomposition processes are going on independently of one another. Between 100 and 250°C , the water of hydration is evolved since each ion forms a metal oxalate 1-hydrate. According to the curves of individual compounds, the water contents are lost in the

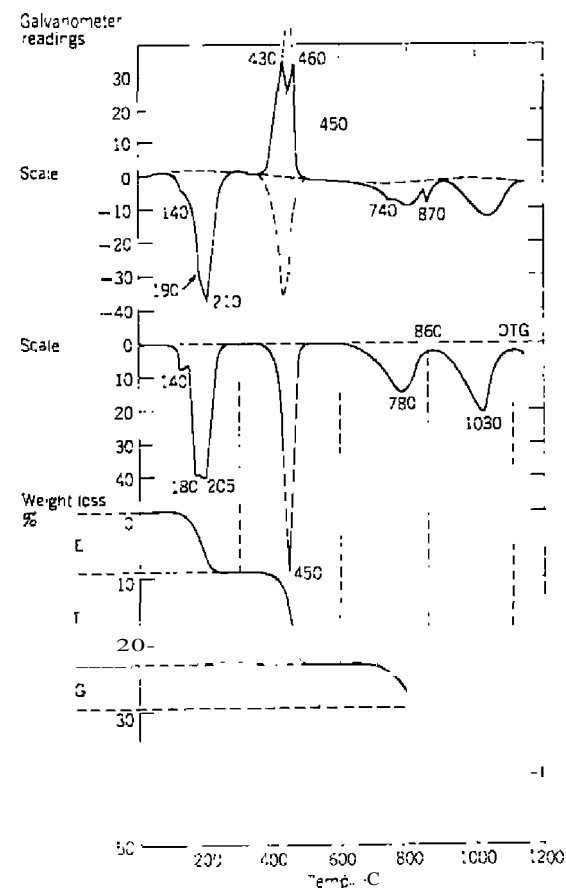


Figure 4.9. Mass-loss curves of calcium, strontium, and barium oxalate hydrates (35).

following order: barium, strontium, and calcium. However, under the conditions of mixed precipitates, the decomposition of strontium and calcium oxalates hydrates take place simultaneously.

After the loss of the water of hydration, the curve exhibited a horizontal mass level from 250–360°C, which corresponded to the composition for anhydrous metal oxalates. Decomposition of the three oxalates then took place simultaneously, the process being completed at about 500°C. The anhydrous metal carbonates were then stable from about 500–620°C, followed by strontium carbonate, which also began to decompose in this range and was completely decomposed at 1100°C, at which temperature barium carbonate began to decompose.

From the mass-loss curve, then, the following data are obtained: *D*, mass of dry precipitate at 100°C; *E*, mass of water of hydration; *F*, mass of carbon monoxide formed by the decomposition of the anhydrous metal oxalates; *G*, mass of carbon dioxide formed by the decomposition of calcium carbonate; and *L*, the mass of carbon dioxide formed by the decomposition of strontium carbonate. From these data, the amounts of calcium, *C*, strontium, *S*, and barium, *B*, can be calculated from

$$\text{Amount of calcium, } C = 0.91068 \cdot G$$

$$\text{Amount of strontium, } S = 1.9911 \cdot L$$

$$\text{Amount of barium, } B = 0.58603 \cdot D - 1.9457 \cdot G - 25788 \cdot L$$

Assuming that the amounts of *C*, *S*, and *B* are unity, the error of the determination was calculated as

$$\frac{\Delta D}{D} = \frac{\Delta E}{E} = \frac{\Delta F}{F} = \frac{\Delta G}{G} = \frac{\Delta L}{L} = 0.1\% \quad (4.5)$$

The simultaneous determination of calcium and magnesium by thermogravimetry has been described by Dupuis and Duval (37). Using the mass-loss curve of a typical dolomite sample, as illustrated in Figure 4.10, the amounts of calcium and magnesium can be calculated. Using the principles previously discussed under automatic thermogravimetric analysis, one finds that *EF* corresponds to a mixture of MgO and CaCO₃ and *GH* corresponds to a mixture of MgO and CaO. The difference, $w_1 - w_2$, is equal to the mass of carbon dioxide evolved between 500 and 900°C by the decomposition of calcium carbonate. The amount of calcium oxide is then given by

$$w(\text{CaO}) = (w_1 - w_2) \cdot \frac{56}{44} = (w_1 - w_2) \cdot 1.272 \quad (4.6)$$

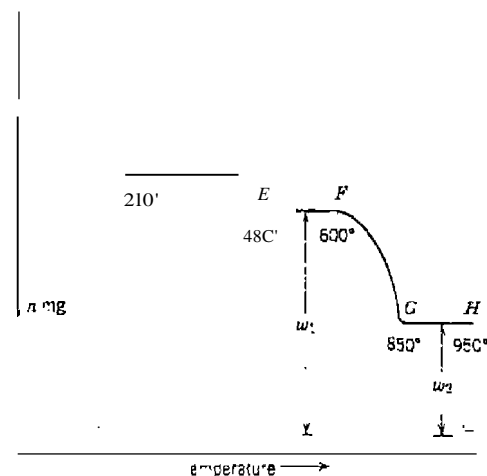


Figure 4.10. Mass-loss curve of a mixture of magnesium and calcium carbonate precipitate (wet) (37).

and the amount of magnesium oxide by the difference

$$\text{wtMgO} = w_1 - w(\text{CaO}) \quad (4.7)$$

3. Aluminum Oxide Precipitates

Although in 1949 Dupuis and Duval (24) studied the pyrolysis of hydrous alumina, $\text{Al}_2\text{O}_3 \cdot n\text{H}_2\text{O}$, prepared by using some 25 precipitating agents, more recent works by Erdey and Paulik (25) and Milner and Gordon (26) have raised questions concerning the low ignition temperatures obtained. The minimum temperatures for ignition to Al_2O_3 , as found by Dupuis and Duval (24), were 180 (for bromine), 1031°C (for aqueous ammonia). Little agreement was found with these results by Erdey and Paulik (25) in that most of the samples were still losing mass at 1000°C the maximum temperature of the Derivarograph. Milner and Gordon (16) recommended that a minimum temperature of 1100°C be used for aluminum oxide precipitates that are to be ignited and weighed by conventional techniques. The latter conclusion is based partially on the results in Table-U. The results show that the minimum conventional ignition temperature is 1 hour at 1100°C, following charring of the filter paper. If the sulfate ion is present, as in the basic sulfate method, an even higher temperature is indicated.

Duval (27) maintains that if the sample is to be heated, cooled, and weighed

Table 4.3. Effect of Ignition Temperatures on the Weights of Aluminum Oxide Precipitates Obtained by Different Methods (26)

Temp. ^a °C	Percent Excess Mass over Final Reference Value			
	Method A (Urea-Basic Sulfate Method)	Method B (Urea-Basic Succinate Method)	Method C (Urea Method) ^b	Method D (Ammonium Hydroxide Method)
	(%)	(%)	(%)	(%)
650	19.2	3.9	1.1	4.5
800	9.8	2.3	1.7	2.4
950	3.4	1.0	1.0	1.2
1100	0.6	0.0	0.0	0.2
1200	0.2	0.0	0.0	0.1
(2nd hour)	Ret. value	Ref. value	Ref. value	Ref. value

^aAfter charring of the filter paper, the precipitates were ignited at 500°C for 8 h before being ignited (or 1 h at each of the stated temperatures.

^bChloride, but not sulfate or succinate, was present.

outside the thermobalance, it is necessary to ignite the aluminum oxide to a higher temperature such that it will not be hygroscopic while it is being cooled and weighed on an analytical balance. It was stated that, using automatic thermogravimetric analysis, this source of error was eliminated, and that the lower temperatures can be employed. Duval (27), however, does not comment on the different curves presented by Erdey and Paulik (25). The latter concluded that the internal structure of the hydrous aluminum oxide is determined by such variables as the rate and temperature of precipitation, and only to a small extent by the nature of the precipitant. They also stated that the lower temperatures reported by Dupuis and Duval (24) were due to the variable precipitation conditions employed since these are difficult to reproduce. Even small variations would have a marked effect on the ignition temperatures.

4. Alumina Whiskers

Wiedemann et al. (71) employed a thermobalance to grow alumina (Al_2O_3) whiskers, using the volatilization and oxidation of aluminum in a wet argon/hydrogen atmosphere. A schematic view of the sample holder, showing the formation of the α - and γ -alumina whiskers, is given in Figure 4.11 (71). Starting material containing the aluminum was an iron-aluminum alloy,

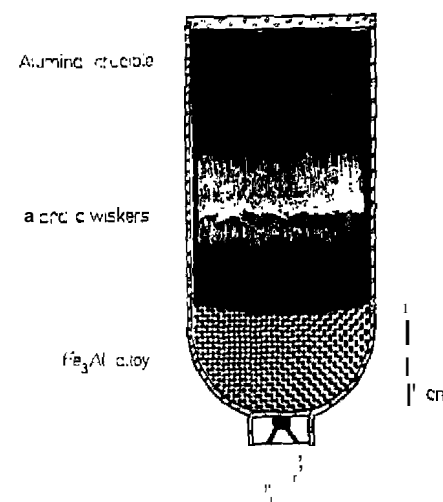


Figure 4.11. Cross section through an alumina crucible with Fe_3Al alloy and Al_2O_3 whiskers in typical orientation (atgrification of whiskers 10×1 (71).

Fe_3Al , while the total gas pressure in the thermobalance was 100 Torr. Formation of the alumina whiskers takes place at a growth rate of 0.04 mg/min at 1550°C, as shown in Figure 4.12 (72). Further interpretation of the reactions involved during the formation of the whiskers is illustrated in Figure 4.12b. The original sample weight of Fe_3Al is M_0 , x corresponds to the weight increase resulting from oxidation and deposition of the vaporizing aluminum, and y is the amount of vaporized aluminum. With a covered Al_2O_3 crucible, about 90% of the vaporized aluminum was oxidized to alumina and deposited within the crucible in the form of whiskers. The α -whiskers grow at the lower temperature of 1450–1500°C, whereas at higher temperatures, the hexagonal γ -whiskers are favored. No whisker growth was observed in a dry Ar/H_2 atmosphere. The effect of crucible material was noted in that alumina and thoria crucibles produced the best whiskers, a magnesia crucible gave the spinel, $MgAl_2O_4$, and a graphite crucible caused carburization of the Fe_3Al alloy. When Al-rich alloys were used, volatilization of the aluminum occurred above 1200°C without the formation of the whiskers. Using the alloy, Fe_3Al , one was able to control the growth rate and morphology of the alumina whiskers by variation of temperature and time. The thickness of the α -whiskers usually varied between 10–40 μm with lengths up to 500 μm . The longest α -whiskers were of the order of the crucible diameter (8 mm) with thicknesses from 200 Å to 5 μm .

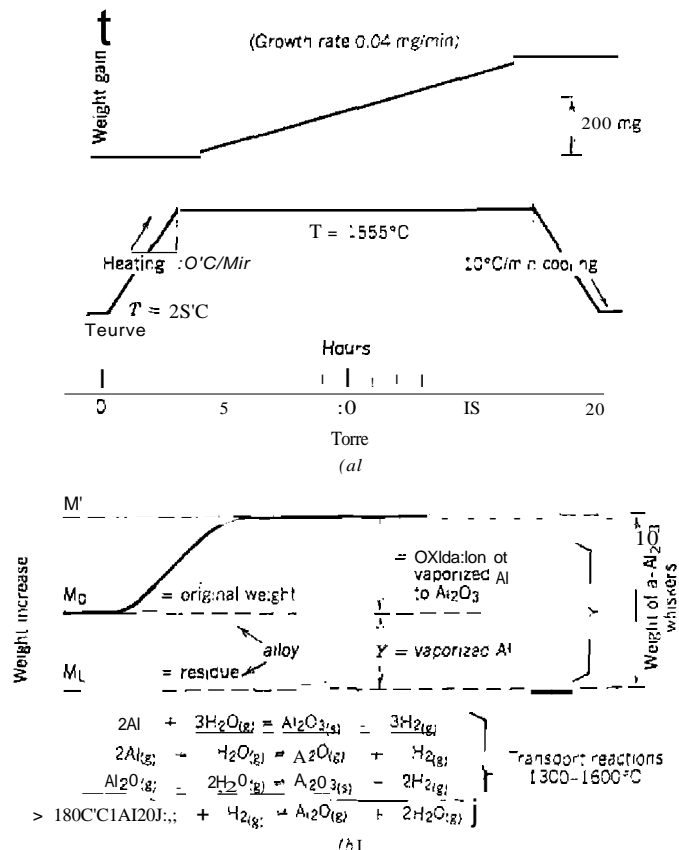
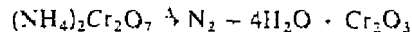


Figure 4.12. (a) TG curve showing formation of alumina whiskers in wet H_2 (2°) Ar atmosphere (72). (b) schematic representation of reactions occurring during whisker formation (72).

5. Ammonium Dichromate

The simplified thermal decomposition of $(\text{NH}_4)_2\text{Cr}_2\text{O}_7$ has often been represented by the equation



In a comprehensive thermal analysis study, Mahieu et al. (66) showed that

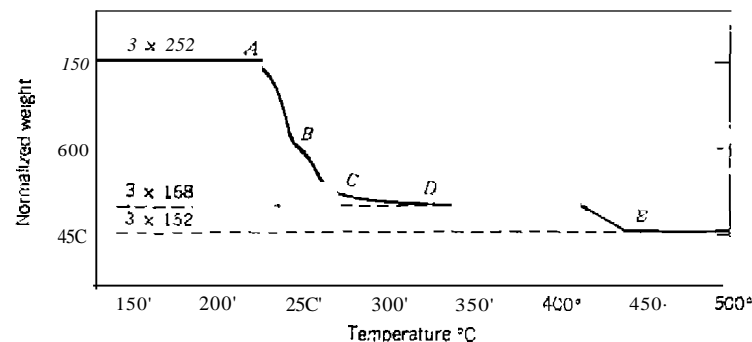
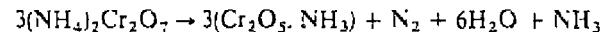


Figure 4.13. TO curve of $(\text{NH}_4)_2\text{Cr}_2\text{O}_7$ mixed with inert Al_2O_3 (1:4 ratio) at a heating rate of 2°C min^{-1} (66).

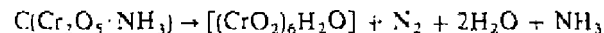
the actual reaction was far more complex than this. Using many TA techniques, including TG, as shown in Figure 4.13, they found that six compounds, labeled A to E, exist in the curve. All weights were normalized to three times the molecular weight of $(\text{NH}_4)_2\text{Cr}_2\text{O}_7$ (i.e., 756 g) to facilitate visualization of the reaction stoichiometry.

The first transition, A \rightarrow B, began at 235°C and involved a mass loss of 20% or 153 g when normalized at the second transition, B \rightarrow C, at 260°C ; the total mass loss was 31%. The third transition, C \rightarrow D, at 300°C , gave a further mass loss of 18 g, bringing the sum of mass losses to 33.5% of the original amount of $(\text{NH}_4)_2\text{Cr}_2\text{O}_7$. Finally, at 420°C , the last transition, D \rightarrow E, brought the total mass loss to 40%, giving a residue that corresponded to the stoichiometry for Cr_2O_3 . The reactions that occurred at the various transitions are as follows:

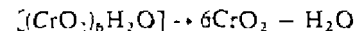
1. A \rightarrow B Transition. Reduction of Cr(VI) to Cr(V) occurs with loss of ammonia and nitrogen according to the equation



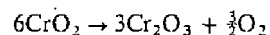
2. B \rightarrow C Transition. This transition can be represented by the equation



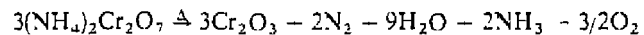
3. C \rightarrow D Transition. Dehydration of the compound, $[(\text{CrO}_2)_6\text{H}_2\text{O}]$, occurs, or



4. *D* → *E* Transition. This last transition corresponds to the reaction



Summation of all of the preceding transitions gives the overall reaction



6. Calcium Chromate

TG was used by Clark et al. (57) to analyze CaCrO_4 , which is used as the active cathode material in thermally activated voltaic cells of the type:



Methods of analyzing this material are time-consuming and, in certain cases, of uncertain accuracy. Approximately 14 hours are needed to complete the analytical procedures currently being used. TG, however, was found to be an effective quality control tool in screening out samples having an assay value below 97.0% CaCrO_4 .

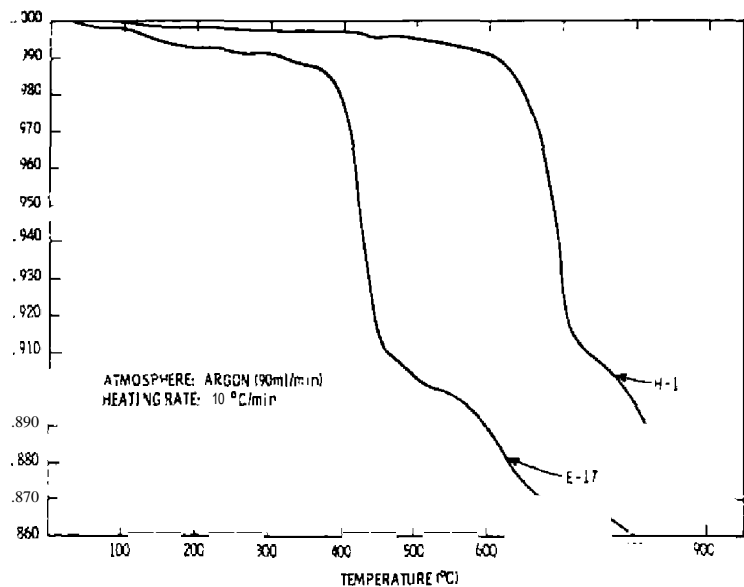


Figure 4.14. TG curves for two samples of CaCrO_4 in Ar (57).

Table 4.4. Comparison of TG and Chemical Analyses of CaCrO_4 (57)

Sample	Analyses from TG in Argon				Chemical Analyses		
	Total H_2O (%)	H_2O from Ca(OH)_2 (%)	CaO at 600°C (%)	CaCO_3 at 600°C (%)	CaCO_3 at 600°C (%)	CaCrO_4 at 600°C (%)	CaCrO_4 at 600°C (%)
E-3	2.2	0.4	1.3	0.0	0.06	0.14	98.6
E-13	3.1	0.4	1.3	0.5	0.3	0.7	97.7
E-12	4.2	0.3	1.0	0.9	0.35	0.8	97.6
G-1	4.1	0.3	4.2	0.5	0.25	0.6	95.8
E-2	4.0	0.6	1.9	0.9	0.2	0.4	95.2
H-1	2.6	0.9	2.9	4.4	1.4	3.3	90.1
I-1	2.0	0.5	4.8	5.1	2.1	4.8	87.4
I-1	5.7	3.4	11.2	2.7	0.9	2.2	86.3
H-1	0.9	0.1	0.3	17.9	7.7	17.6	82.4
E-17	0.5	0.1	31.6	6.6	2.3	5.9	62.7
CaCO_3	0.0	0.0	0.0	01.0	44.1	01.2	0.0
Ca(OH)_2	23.1	22.2	80.8	7.7	2.2	6.5	0.0

Typical TO curves of impure CaCrO_4 in Ar are shown in Figure 4.14 (57). The principal impurity is $\text{Ca}(\text{OH})_2$ in a sample whose assay was about 97% CaCrO_4 . When heated in air, the $\text{Ca}(\text{OH})_2$ loses water to form CaO, but some of the CaO reacts with CO_2 in the air to form CaCO_3 . The use of CO_2 -free Ar prohibits this interfering reaction. A comparison of the total H_2O , $\text{Ca}(\text{OH})_2$, and CaCO_3 contents by TO and chemical analysis are given in Table 4.4. Calcium oxide content at 600°C was calculated based on the $\text{Ca}(\text{OH})_2$ determination. CaCrO_4 content at 600°C was then calculated by assuming that the only significant impurities present at room temperature were H_2O , $\text{Ca}(\text{OH})_2$, and CaCO_3 and that, consequently, only CaO and CaCO_3 were present at 600°C . As can be seen, the agreement with chemical analyses is quite good. No values for $\text{Ca}(\text{OH})_2$ are reported since no reliable chemical method of determining hydroxide ion in the small quantities present was found.

7. Calcium Silicate Hydrates

The free lime [$\text{Ca}(\text{OH})_2$] and carbonate (CaCO_3) contents of calcium silicate hydrates, ranging from 1.0-20%, were determined by a thermogravimetric method by Biffen (33). The mass-loss curves for a series of calcium silicate hydrates, calcium silicate hydrates plus varying amounts of calcium hydroxide, and calcium silicate hydrates plus varying amounts of calcium carbonate are given in Figure 4.15.

The curves for the calcium silicate hydrates are all quite similar, show no sharp breaks, and exhibit a gradual slope for a straight line between 375 and 650°C . The curve breaks above 600°C are due to the decomposition of carbonate content in the sample.

When synthetic mixtures of calcium silicate hydrate and calcium hydroxide were used, the series of curves obtained all indicated curve breaks, at about 500°C . These were caused by calcium hydroxide decomposition, as was shown by authentic mass-loss curves for the pure compounds. By taking the vertical distance from the point at which the straight-line curve starts to change due to evolution of the combined water from the calcium silicate hydrate to the point where it resumes the calcium silicate decomposition drop, and calculating the calcium hydroxide from the loss in mass of water equivalent to this vertical distance, one obtained a good estimate of the amount of calcium hydroxide in all cases.

The decomposition of calcium silicate hydrate samples containing added amounts of calcium carbonate, and in some cases calcium hydroxide, is given in Figure 4.15. The presence of calcium carbonate is indicated by the curve break, due to the evolution of carbon dioxide, in the temperature range 700 – 900°C . If a vertical distance is measured between the points where this

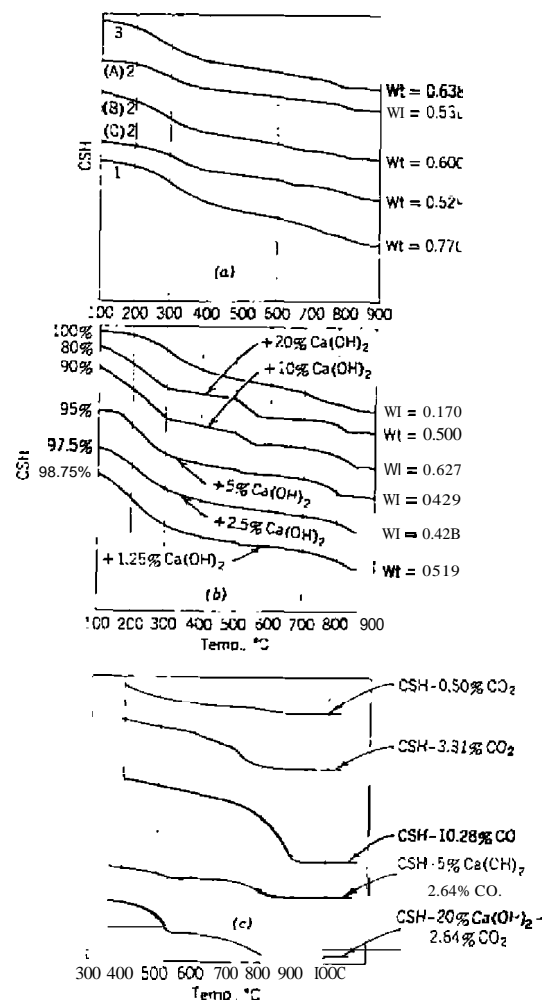


Figure 4.15 Mass-loss curve of (a) calcium silicate hydrate preparation; (b) calcium silicate hydrate preparation plus added $\text{Ca}(\text{OH})_2$; (c) calcium silicate hydrate preparations plus added amounts of CaCO_3 (33).

straight line begins to drop and then becomes horizontal, the carbon dioxide content of the sample can be easily obtained.

Good agreement with other accepted methods was reported for the determination of water, free lime, and carbonate in calcium silicate hydrates by the thermogravimetric method.

Ramachandran (34) determined the $\text{Ca}(\text{OH})_2$ content in calcium silicate mixtures by the water-loss between 450 and 550°C.

8. Copper (II) Acetate

Judd et al. (58) used TG and DTA to study the thermal decomposition of the acetates of sodium, calcium, copper, and silver. The TG curve of $\text{Cu}_2(\text{C}_2\text{H}_3\text{O}_2)_4 \cdot 2\text{H}_2\text{O}$, shown in Figure 4.16, is essentially a two-stage process but suggests that the process is more complicated than this. The first mass-loss occurs over the temperature range 100-180°C; the mass-loss of 9.3% found is slightly higher than the 9.0% calculated for the loss of 2 moles of water per mole of salt. Product analysis at this stage of the reaction indicated that small amounts of acetic acid were produced, although

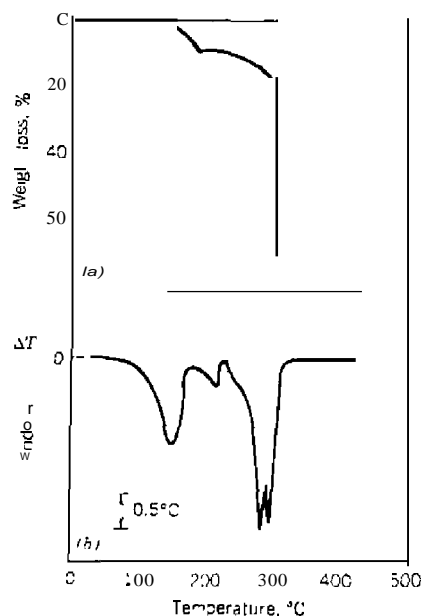
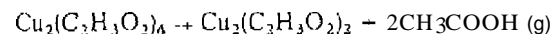
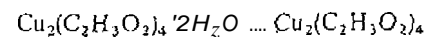
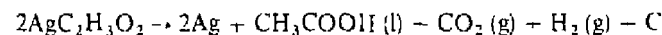
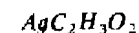
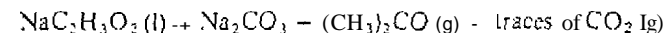
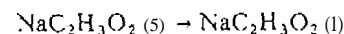
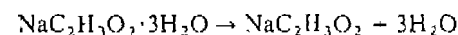
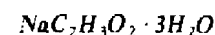
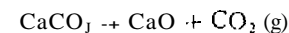
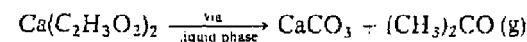
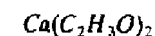


Figure 4.16. TG curve of $\text{Cu}_2(\text{C}_2\text{H}_3\text{O}_2)_4 \cdot 2\text{H}_2\text{O}$ (58)

this is probably due to the presence of some acetic acid adsorbed on the sample. The second stage began at about 200°C, proceeded slowly until 290°C, when the reaction became extremely rapid, leading to a final mass-loss of 70.0%. This value is much higher than that predicted for the formation of metallic copper (59.3%). On removing the furnace it was found that metallic copper was present on the cooler parts of the tube, indicating that part of the sample had volatilized during decomposition. The thermal decomposition reaction follows the stoichiometry:



The thermal decomposition reactions of other metal acetates are:



9. Copper (II) Chloroacetates

The thermal decomposition of copper (II) mono-, di-, and trichloroacetates was studied by TG and other techniques by Judd et al. (59). Magnetic moment and UV diffuse reflectance spectra data indicate that copper monochloroacetate 2-hydrate is dimeric, copper trichloroacetate 4-hydrate is monomeric, and copper dichloroacetate 4-hydrate forms an intermediate structure. The TG curve of copper trichloroacetate 4-hydrate is shown in Figure 4.17 (59). Its decomposition curve is not similar to that found for the other chloro-

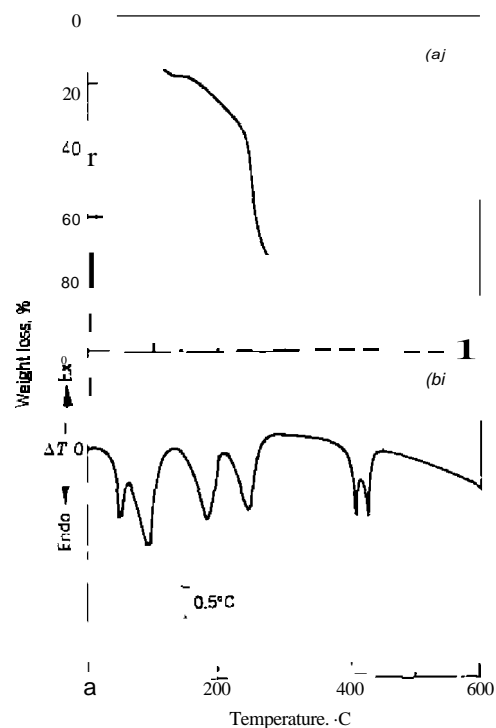
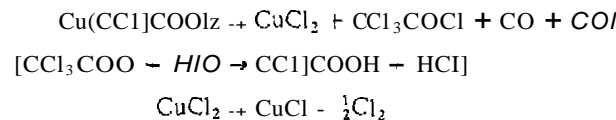
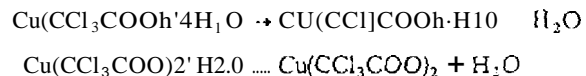
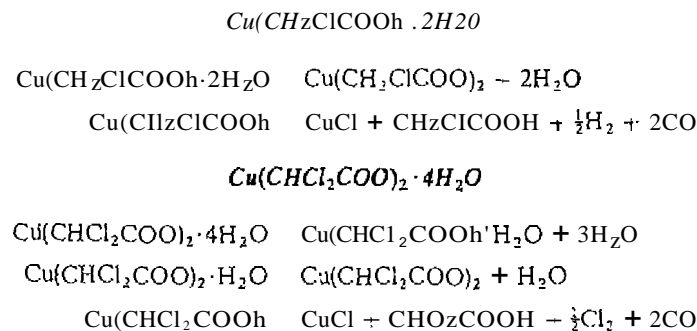


Figure 4.17. TG curve of $\text{Cu}(\text{CCl}_3\text{COO})_2 \cdot 4\text{H}_2\text{O}$ in N_2 (59).

acetates. Loss of water begins at about 65°C and a plateau on the curve is reached after a mass-loss of 11.5%. This corresponds to the loss of three moles of water per mole of salt (calculated mass-loss of 11.7%). Heating the compound above 140°C gave a further two-step mass-loss: 4.5% for the first stage and then rapid mass-loss to reach a final value of 70%. The final value corresponds to that expected for the formation of CuCl_2 (calculated value of 70.8%). Using data also obtained from DTA, one may represent the decomposition reaction as

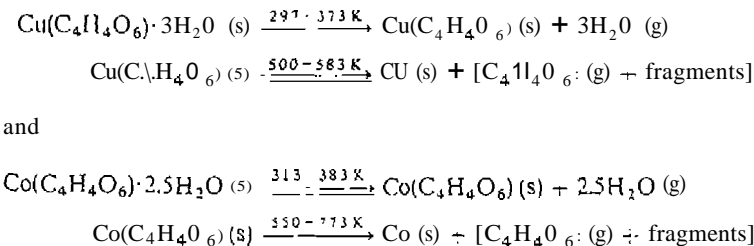


The thermal decomposition reactions of the other two salts are as follows:



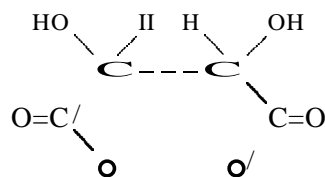
10. Copper (II) and Cobalt (II) Tartrates

The thermal decomposition of copper (II) tartrate, $\text{Cu}(\text{C}_4\text{H}_4\text{O}_6) \cdot 3\text{H}_2\text{O}$, and cobalt (II) tartrate, $\text{Co}(\text{C}_4\text{H}_4\text{O}_6) \cdot 2.5\text{H}_2\text{O}$, were investigated by use of TG, DTG, DTA, and MS techniques by Schmid and Felsche (69). In an argon atmosphere, the thermal dissociation reactions of both these compounds can be described by the equations



The existence of the very unstable $\text{C}_4\text{H}_4\text{O}_6$, a diradical formed in the course of the decomposition reaction of the anhydrous $\text{M}(\text{C}_4\text{H}_4\text{O}_6)$ compounds, indicates that this has a radical electron-transfer reaction mechanism.

Existence of a six-membered ring,



and other intermediate fragments is discussed (69).

II. Complexes

a. $[Pt(NH_3)_4]Cl_2 \cdot H_2O$

The thermal decomposition of the platinum complex, $[Pt(NH_3)_4]Cl_2 \cdot H_2O$, was studied in the derivatograph by Paulik et al. (77). Not only were the TO, DTG, and DTA curves recorded, but an analysis of the evolved gases was performed using thermal gas titrimetry (TGT) (see Chapter 8). The summation of seven curves for $[Pt(NH_3)_4]Cl_2 \cdot H_2O$ are shown in Figure 4.18. Each curve represents the analysis curve for a specific gaseous decomposition product except for curve (1), which is the TG curve. According to the

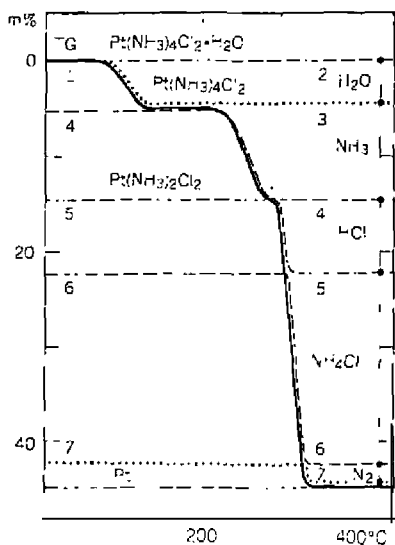
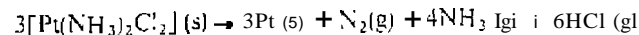
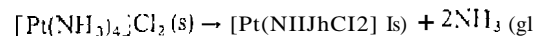
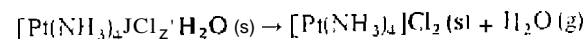


Figure 4.18. TG and TOT curves of $[Pt(NH_3)_4]Cl_2 \cdot H_2O$ in a N_2 atmosphere (77).

TG and TGT curves, the stoichiometry of the thermal decomposition can be represented by the equations



b. $K_2Pt(CN)_4Br_2$

The platinum nonstoichiometric mixed valence compound, $K_2Pt(CN)_4BrO_2 \cdot nH_2O$ is of great interest because of its unidimensional electrical conductivity. It has been shown that part of the ambiguity in published results may arise from the variability in the number of hydrate waters. Gallagher and Luongo (78) studied the fully oxidized analogous compound, $K_2Pt(CN)_4Br_2$, and the undioxidized $K_2Pt(CN)_4$ end members by TG and other TA techniques. The TG curves of these compounds are shown in Figure 4.19. Cyanogen, $(CN)_2$, was evolved during the decomposition and concomitant reduction in the oxidation number of platinum for both $K_2Pt(CN)_4Br_2$ and $K_2Pt(CN)_4$. Evolution of $(CN)_2$ began at about 360°C for the former compound, giving

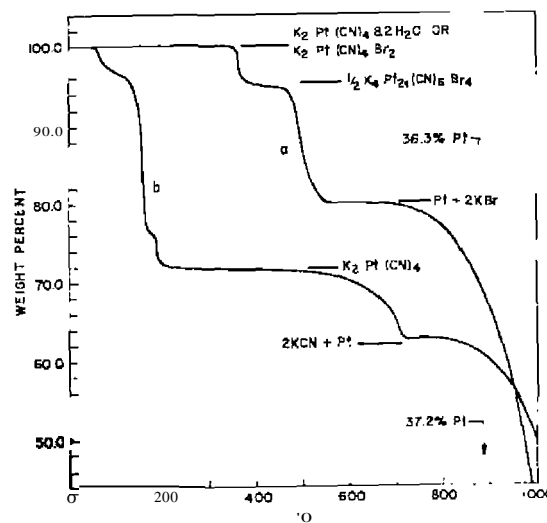
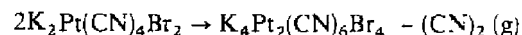


Figure 4.19. TG curves of $K_2Pt(CN)_4Br_2$ and $K_2Pt(CN)_4 \cdot 2H_2O$ in atmosphere N_2 , heating rate of 10°C/min (78).

an intermediate mass plateau from about 400-500°C. which corresponded to the stoichiometry of $K_4Pt_2(CN)_6Br_4$. Thus, the first stages of decomposition can be represented by the equation



This was followed by the decomposition reaction



Finally, the KBr vaporizes at temperatures above 700°C.

For $K_2Pt(CN)_4 \cdot 8H_2O$, the TG curve shows that water is readily evolved up to 200°C. The anhydrous $K_2Pt(CN)_4$ began to decompose at about 450°C to evolve CN_2 and form Pt metal and KCN at around 800°C. At still higher temperatures, KCN vaporizes or decomposes, leaving Pt metal as the residue.

c. $[Co(NH_3)_5Cl]Cl_2$ and $[Co(NH_3)_5Br]Br_2$

The TG curves of $[Co(NH_3)_5Cl]Cl_2$ and $[Co(NH_3)_5Br]Br_2$, as reported by Collins et al. (65), are shown in Figure 4.20. The $[Co(NH_3)_5Cl]Cl_2$ complex

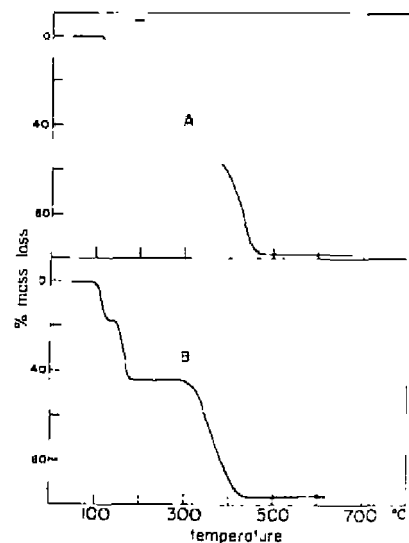


Figure 4.20. TG curves of $[Co(NH_3)_5X]X_2$ complexes. A. $[Co(NH_3)_5Cl]Cl_2$. B. $[Co(NH_3)_5Br]Br_2$. Pressure is 2×10^{-6} Torr (65)

began decomposing at 110°C to $trans-[Co(NH_3)_4Cl_2]Cl$ with the loss of one mole of ammonia per mole of complex. This intermediate compound produced the small plateau in the TG curve at about 8% mass-loss and was visually observed to have a green color. Decomposition of the $trans-[Co(NH_3)_4Cl_2]Cl$ to a 1:1 molar mixture of $CoCl_2 \cdot (NH_4)_2CoCl_4$ produced an inflection point in the TG curve at about 30% mass-loss. No horizontal mass level was observed since the $(NH_4)_2CoCl_4$ decomposed to $CoCl_2$ and NH_4Cl at a rate which was only slightly less than the rate of formation. The $CoCl_2$, which appeared as a stable intermediate compound at about 53% mass-loss, began to sublime at about 350°C with the sublimation continuing to a black residue, probably cobalt metal, at 98% mass-loss.

The dissociation reactions of $[Co(NH_3)_5Br]Br_2$ appear to be similar to those for $[Co(NH_3)_5Cl]Cl_2$ except for the first reaction step. The TG curve shows that a mass-loss corresponding to approximately 4 moles of ammonia per mole of complex occurs as the initial dissociation process. This can be interpreted as the direct dissociation of the complex to a 1:1 molar mixture of $CoBr_2 \cdot (NH_4)_2CoBr_4$. However, the sample was visually observed to have a green color during the course of this process which might indicate the presence of $trans-[Co(NH_3)_4Br_2]Br$ or $CoBr_2$. The $(NH_4)_2CoBr_4$ decomposed to $CoBr_2$ which sublimed at about 300°C, leaving a residue at 96% mass-loss.

d. Miscellaneous

Hill and co-workers studied the thermal decomposition of a large number of metal complexes of various alkyl derivatives of xanthic and dithiocarbamic acids. The complexes were studied by using TG, DSC, and other TA techniques. Compounds investigated included Ni(II) alkyl xanthates (79), Cu(II) dithiocarbamate complexes (80), dihalotin(IV) bisdiethylthiocarbamates (81), bis(diethylthiocarbamato) diphenyl tin(IV) (82), [etrakis(diethylthiocarbamato) tin(IV) (83, 84), and bisdiethylthiocarbamato tin(IV) (85).

Salas-Peregrin et al. (86) studied the thermal decomposition of some xanthine complexes of Co(II), Cu(II), and Cd(II), using TG and other TA techniques.

TG and other TA techniques were employed by Yoshikuni and co-workers to investigate the thermal properties of $trans-[CrCl_2(en)_2](H_2O)_2Cl_2$ (87); $[Cr(NH_3)_6]X_3$, $[CrX(NH_3)_5]Y_3$, and $trans-[CrX_2(NH_3)_4]Y$, where X and Y are Cl- and/or Br- (88); $trans-$ and $cis-[CrX_2(aa)_2]X \cdot nH_2O$, where X is Cl- and Br-, and aa is a diamine molecule (89); and octahedral nickel(II) complexes containing N,N- and N,N'-dialkylethylene diamines (90).

12. Diamonds

To simulate conditions of use in grinding and cutting tools, investigators have used TG to study the thermal properties of natural and synthetic diamonds (73). These studies are useful for diamond graphitization reactions as well as to test the compatibility and reactions between the diamonds and the binder materials. The TG curves of natural and synthetic diamonds, as determined by Wiedemann and Bayer (73), are given in Figure 4.21. In *vacuum* (1×10^{-5} Torr), graphitization occurs in natural diamond in the temperature region, 1700-1900°C. In contrast, synthetic diamond was graphitized between 1300-1600°C under the same conditions. The graphitization temperature is related to the formation and purity of the diamond samples. Synthetic diamonds contain small amounts of nickel, iron, and chromium, which may catalyze the transformation to graphite during heating. Also, synthetic diamonds are made by shockwave synthesis so that they may contain a larger amount of structural defects that could decrease the transformation temperatures.

Similar differences were found between natural and synthetic diamonds on oxidation in air atmospheres. The lower oxidation resistance of synthetic diamonds is probably due to the higher surface area, their polycrystalline character, and the presence of metallic ion impurities.

13. Egyptian Blue

The blue pigment used by the ancient Egyptians in their paintings and statuary has been the subject of modern thermoanalytical investigations by Bayer and Wiedemann (73-75). This blue pigment, called Egyptian blue,

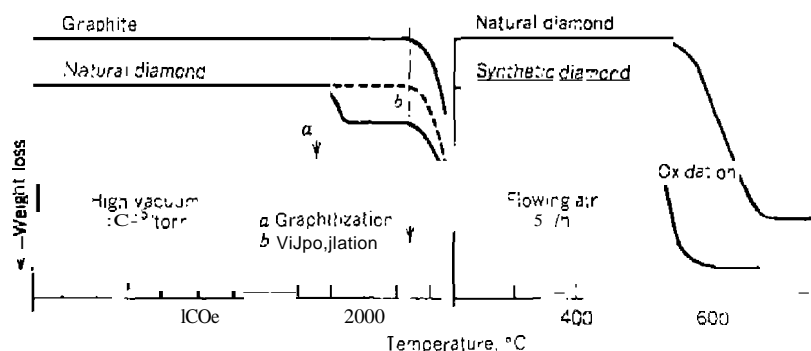


Figure 4.21. TG curves of graphitization, vaporization, and oxidation of natural and synthetic diamond (73).

has the formula, $\text{CaCu}[\text{Si}_2\text{O}_7]$, and is related to the isostructure; sheet silicates, $\text{SrCu}[\text{Si}_2\text{O}_7]$ and $\text{BaCu}[\text{Si}_2\text{O}_7]$. These compounds can be synthesized by use of the thermobalance, as shown in Figure 4.22, by heating quartz, CuO , calcite, and a fluxing agent such as Na_2CO_3 , borax, or PbO . Without such fluxing agents, the reaction proceeds very slowly, leading to a

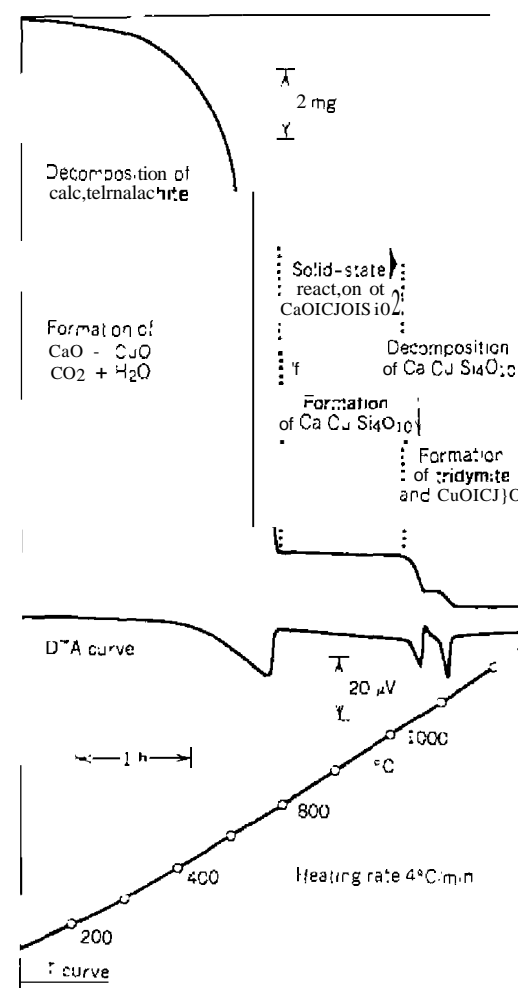


Figure 4.22. TG-DTA-T curves showing the formation of Egyptian blue from a calcite-CuO-quartz mixture (76).

finely crystallized, impure product which does not have the intense blue color of the pigment. With borax, the reaction mixture forms $\text{CaCu}[\text{Si}_4\text{O}_{10}]$ at about 900°C at a heating rate of $2^\circ\text{C}/\text{min}$ and remains stable in an oxidizing atmosphere to about 1000°C . Above this temperature, it decomposes due to the reduction of $\text{Cu}^{2+} \rightarrow \text{Cu}^+$, which is reversible. However, the initial compound does not form again on cooling in spite of the reoxidation, $\text{Cu}^+ \rightarrow \text{Cu}^{2+}$. The thermal stability of the isostructural compounds, $\text{SrCu}[\text{Si}_4\text{O}_{10}]$ and $\text{BaCu}[\text{Si}_4\text{O}_{10}]$, is greater than the calcium compound, decomposing at 1155 and 1170°C , respectively. It is interesting to note that the thermal decomposition of $\text{BaCu}[\text{Si}_4\text{O}_{10}]$ is completely reversible on cooling. Single crystals of the Ca, Sr, and Ba compounds can be grown by using borax, PbO , or Na_2CO_3 flux with heating cycles of 30 hours at about 900°C . These quadratic platelets with their characteristic intergrowth were similar to some of the original Egyptian blue samples. The latter were exceptionally pure and well crystallized and showed identical properties with the former synthetic samples. In inert or reducing atmospheres of N_2 or CO , the thermal decomposition reaction of Egyptian blue began at about 950 and 800°C , respectively, with the formation of the red-brown colored Cu_2O product.

14. Mercury (I, II) Compounds

The TG curves of yellow and red forms of mercury (II) oxides, as reported by Wendlandt (52), are shown in Figure 4.23. The yellow form has a lower initial procedural dissociation temperature (T_i) than the red form. Under the same conditions, $T_i = 400^\circ\text{C}$ for the yellow form (Curve A) and 460°C for the red form (Curve D). Likewise, the final procedural dissociation temperature (T_f) is higher for the latter, 660°C compared to 600°C . The reaction interval ($T_f - T_i$), however, is greater for the yellow (200°C) than for the red form (180°C). Only slight changes were observed for T_i values of the red form with variation in the heating rate. Values of T_i and T_f observed, were: $5^\circ\text{C}/\text{min}$ ($460, 660^\circ\text{C}$) (Curve E); $10^\circ\text{C}/\text{min}$ ($460, 660^\circ\text{C}$) (Curve D); and $20^\circ\text{C}/\text{min}$ ($470, 680^\circ\text{C}$) (Curve C). The T_f values increased with an increase in heating rate as did the reaction interval. On changing the furnace atmosphere from nitrogen to oxygen, the T_i value for the red form increased slightly from 460 - 480°C (Curve B), whereas the T_f value remained essentially unchanged. For both the yellow and red forms, the lower procedural dissociation temperatures for the yellow form are consistent with a decrease in particle size. It is well known that a reduction in particle size can lower the T_i values; the extent of the decrease, however, cannot be predicted.

The TG curves of some mercury (II) and (I) halides are shown in Figure 4.24. The mercury (II) chloride, bromide, and iodide compounds, in contrast

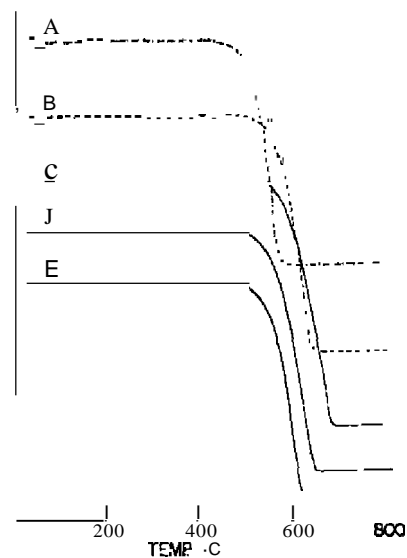


Figure 4.23. TG curves of yellow and red forms of mercury (II) oxide. A = yellow form, 20.4 mg, $10^\circ\text{C}/\text{min}$ in N_2 ; B = red form, 21.4 mg, $10^\circ\text{C}/\text{min}$ in O_2 ; C = red form, 22.0 mg, $20^\circ\text{C}/\text{min}$ in N_2 ; D = red form, 21.5 mg, $10^\circ\text{C}/\text{min}$ in N_2 ; E = red form, 19.2 mg, $5^\circ\text{C}/\text{min}$ in N_2 (52).

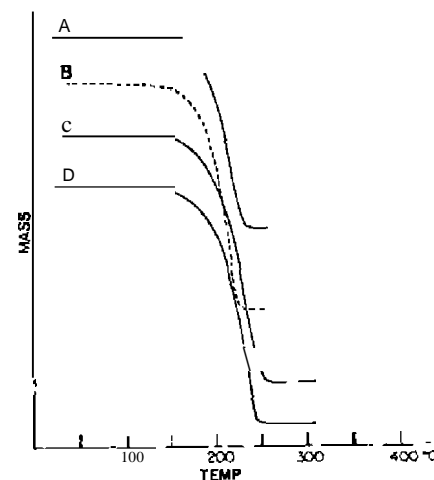


Figure 4.24. TG curves of some mercury (II) and (I) halides at $10^\circ\text{C}/\text{min}$ in N_2 . A = HgCl_2 , 9.9 mg; B = HgBr_2 , 10.3 mg; C = HgI_2 , 11.0 mg; D = Hg_2I_2 , 10.8 mg (52).

to the fluorides, show marked covalent character. Mercury (II) chloride crystallizes in an essentially molecular lattice, with the two short Hg-Cl distances being about the same length as the Hg-Cl bonds in gaseous HgCl₂. In HgBr₂, each mercury atom is surrounded by six bromide ions but two are so much closer than the other four that it can be considered that perturbed HgBr₂ molecules are present. Mercury (II) iodide has a layer structure with HgI₄ tetrahedra linked at some of the vertices. At 126-127°C, the red α -form is converted to a β -yellow molecular form. Because of their uses in analytical determinations, Duval (53) recorded the TG curves of Hg₂Cl₂ and HgI₂. The former compound is stable up to 130°C but sublimes at temperatures above this. For HgI₂, it was found to sublime at temperatures above 88°C. For all mercury (II) halides, the TG curves indicate only a one-step sublimation process. The T_i values found were 100°C for HgBr₂, 110°C for HgCl₂, and 135°C for HgI₂. Likewise, the T_f values also increased in this order. The T_i value for HgI₂ is somewhat higher than that reported by Duval (2).

Collins et al. (54) reported the TG curves *in vacuo* and the EGA of the evolved gases of other mercury (I) and (II) compounds. The TO curves of HgSO₄, Hg(SCN)₂, Hg(C₂H₃O₂)₂, Hg(NO₃)₂, and HgNO₃ are given in Figure 4.25. The most stable compound was HgSO₄ in which thermal decomposition, with the evolution of SO, SO₂, and O₂, occurs in the temperature interval from 500-750°C. The TG curve for the HgSO₄ indicates that the mass-loss occurs in one reaction step. However, the magnitude of the total mass-loss, combined with the evolved gas curves, suggests that more than one process is occurring simultaneously since the final mass level stabilizes with less than 1% of the original mass remaining. The anticipated solid-state product would be HgO, but data obtained for other compounds in this study indicate that HgO is unstable in the temperature range of

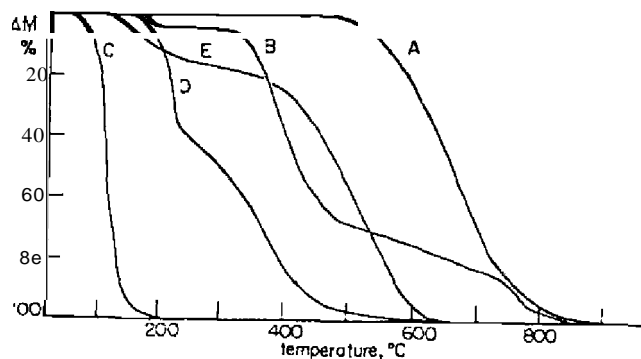


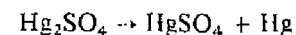
Figure 4.25 TG curves for A, HgSO₄; B, Hg(SCN)₂; C, Hg(C₂H₃O₂)₂; D, Hg(NO₃)₂; E, HgNO₃ · 1/2 H₂O *in vacuo* at a heating rate of 6°C min⁻¹ (54).

interest. If HgO is formed at all, it immediately decomposes to elemental mercury and oxygen. Elemental mercury, whether formed directly from HgSO₄ or through an HgO intermediate, would be vaporized and removed from the system since the vapor pressure of mercury is an appreciable value at temperatures in excess of 500°C.

The TG curve for Hg(SCN)₂ (Curve B) indicates that decomposition occurs as a multistep process over the temperature interval 150-800°C. Between 150 and 200°C a mass-loss of about 4% occurs, whereas at higher temperatures the mass-loss corresponds to about 65% of the total mass. In both reactions, CS₂ is the principal decomposition product.

Mass-loss of Hg(C₂H₃O₂)₂ begins at about 75°C and continues to 175°C and is probably due to the sublimation of this compound. For Hg(NO₃)₂, mass-loss begins at 150°C, and the EGA curve indicates the evolution of large quantities of NO, NO₂, and NO₂. The second stage of the decomposition reaction consists of the dissociation of HgO to Hg and O₂. In the case of HgNO₃, EGA curves indicate that this compound dissociates in three steps, although this is not evident from the TG curve. The first step is accompanied by the evolution of NO and NO₂, with small amounts of N₂O. This process occurs in the 100-200°C temperature interval and is followed by a gradual mass-loss until about 400°C, at which point the rate of mass-loss becomes more rapid. EGA curve peaks in the 350-475°C temperature range are due to the evolution of N₂O and NO. Decomposition of HgO occurs as the last step in the decomposition reaction giving O₂ as the final peak in the EGA curve.

Tariq and Hill (55) studied the thermal decomposition of Hg₂SO₄ and HgSO₄ by TG, as well as by using other techniques. Mercury (I) sulfate was found to disproportionate, in a N₂ atmosphere, according to the reaction



No intermediates were detected in the TG curve from 335-500°C, the temperature range of this reaction. Decomposition of HgSO₄ occurred then between 550-750°C, which compared with the decomposition range of 530-720°C for pure Hg₂SO₄. When HgSO₄ was heated *in vacuo*, MS of the decomposition gases indicated the presence of O₂, SO₂, and trace quantities of SO₃. There was no evidence for the presence of mercury or mercury compounds. However, when the temperature was raised to 680°C, the mass spectrum of the gaseous products showed the presence of Hg, SO₂, and O₂.

15. Nickel (II) Sulfide

The value and versatility of TG as an analytical technique when applied to

of inorganic compounds and materials was demonstrated by TG. TG is particularly useful when the sample of interest is in the single crystals that are too small to be analyzed by conventional methods. Such samples are quite common as a result of various low-yield processes. They are part of a low-volume multiphase product and are separated from the mixture. It was shown that the metal and sulfur contents of such samples could be determined using about 10-mg samples. Oxygen content could be determined also by oxidation of SrCrO₃ to SrCrO₄ while reduced to CrVO₃.

In the determination of sulfur, the TO curve of the oxidation of NiS is shown in Figure 4.26. The sulfur was removed in two regions, 390-490°C and 690-785°C. After cooling the system to 300°C, a hydrogen-argon atmosphere was introduced and the NiO was reduced to nickel metal.

Oxidation and decomposition of millerite, Ni_{0.994}S, was studied using TG, DTA, MS, and other techniques by Dunn and Kelby. The Ni_{0.994}S (henceforth abbreviated as NiS) with oxygen is shown in Figure 4.26. The TO curve is obtained if the sample crucible is covered in the furnace atmosphere. However, it is possible to suggest a mechanism for the oxidation of the NiS. Under the dynamic conditions of the TO curve, the oxidation takes place according to the reactions (tempera-

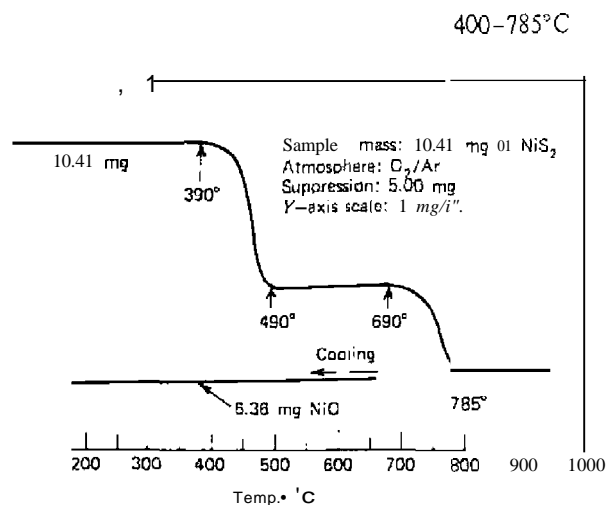
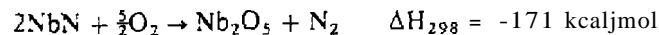


Fig. 4.26. TG curve of NiS₂ to determine sulfur content (57).

2. NiO + SO₂ + ½O₂ → NiSO₄ 500-785°C
3. NiS + ½O₂ → NiO + SO₂ 540-552°C and 682-692°C
4. 3NiS + 2NiSO₄ → Ni₃S₂ + 2NiO₂ + 3SO₂ 682-692°C
5. 10 NiS + 2O₂ → Ni₇S₆ + Ni₃S₂ + 2SO₂ 682-692°C
6. Ni₇S₆ + 9½O₂ → 7NiO + 6SO₂ 682-780°C
and/or
Ni₇S₆ + 12½O₂ → 6NiSO₄ + NiO
7. Ni₃S₂ (s) → Ni₃S₂ (l) 793°C
8. Ni₃S₂ (l) + 3½O₂ → 3NiO + 2SO₂ 793°C
9. NiSO₄ → NiO + SO₂ + ½O₂ 800°C

16. Niobium Nitride

Gallagher and Sinclair (93) studied the oxidation of niobium nitride, NbN_{0.9}, in a flowing atmosphere of 0.1% O₂ in air, using TG and other techniques. There was a pronounced tendency for thermal runaway near 600°C because of the highly exothermic nature of the reaction



The TO curves are given in Figure 4.27. Oxidation of the NbN is dependent on the heating rate and the oxygen concentration in the furnace atmosphere. In a 0.1% O₂ in air atmosphere, oxidation begins at about 400°C; in air, at 20°C/min, the oxidation began at about 500°C but exhibited the thermal

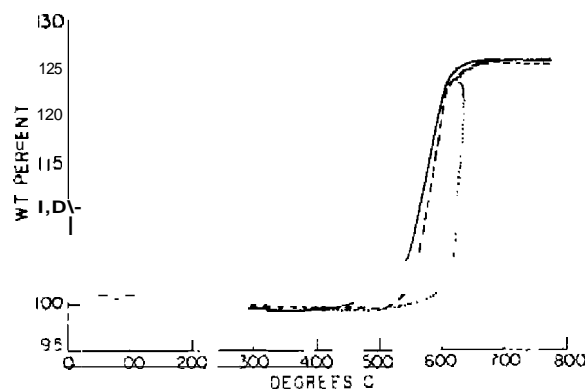
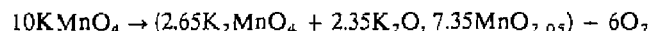


Figure 4.27. TG curves for the oxidation of δ-NbN_{0.9}. (a) 10°C/min in 0.1% O₂/Ar. (b) 20°C/min in air. (93).

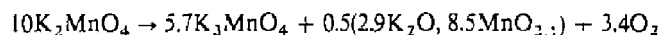
runaway mentioned previously. Obviously, the self-healing nature of the reaction can lead to errors in the evaluation of the reaction kinetics. Kinetic analysis was attempted only on those curves obtained at a heating rate of 1°C/min and in the O₂/Ar atmosphere. Isothermal TG experiments were also obtained in the temperature range 817- 897K.

17. Potassium Permanganate

The thermal decomposition of potassium, rubidium, and cesium permanganates was studied by using TG and DTA by Booth et al. (56). The TG curves of these compounds, in air, N₂ and O₂ atmospheres, are given in Figure 4.28. For KMnO₄ decomposition in air, the reaction followed the stoichiometry



In the temperature range 300-500°C, a small gradual mass-loss (1-2%) was observed for all compounds in air, O₂, or N₂ atmospheres. The effect of changing the atmosphere altered the decomposition temperatures only slightly. It was found that when heating to higher temperatures, 600°C, the mass-loss was dependent on the atmosphere. In all cases, the total mass-loss was found to be between 5 and 6%. The stoichiometry of this reaction was assumed to be



Similar observations were found in the case of Rb and Cs salts for the first

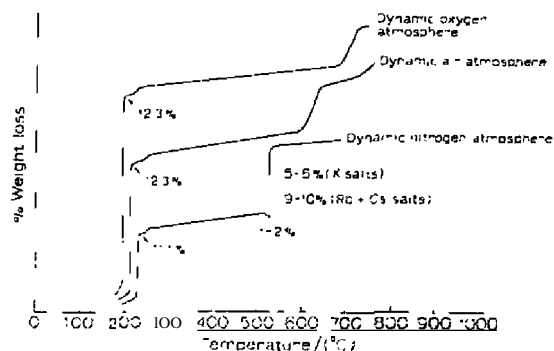


Figure 4.28. A typical TG plot of some group I permanganates in different atmospheres (O₂, N₂, and air). Heating rate: 1) C min⁻¹. Note: weight loss axis is not to scale (56)

stage, but the initial reaction temperatures were higher, in the order of Cs > Rb > K. The effect of atmosphere on the decomposition temperatures followed the order: T_{O₂} > T_{air} > T_{N₂}, with about 40° difference in decomposition temperature when O₂ replaced N₂ as the atmosphere.

The TG-DTA curves of KMnO₄ and KMnO₄/Sb mixtures have also been reported by Beck and Brown (67).

18. Potassium Hydrogen Phthalate

Although the use of the thermobalance was supposed to eliminate the confusion concerning drying and decomposition temperatures of analytical precipitates and reagents, in many cases it has only contributed to this confusion. In comparing four different investigations concerning the drying and decomposition temperatures of potassium hydrogen phthalate, investigators obtained four different results, not to mention the drying temperatures recommended by nonthermogravimetric methods. Dupuis and Duval (38) first reported that the decomposition of KHC₈H₄O₄ began at 172°C; Duval (39), in a later study, found a decomposition temperature of 240°C at a 150°C/h heating rate, and 236°C at a 300°C/h heating rate. Belcher et al. (40) reported that the compound began to decompose at 200°C and recommended a drying temperature of 100-150°C. Lastly, Newkirk and Laware (41) reported a procedural decomposition temperature of about 260°C. In view of the previous discussion on the limitations of thermogravimetry, these conclusions are perhaps not unusual. It is believed (41) that these studies have little value in determining the safe, long-term drying temperature for a primary standard substance.

The mass-loss curves of KHC₈H₄O₄, under various atmospheric conditions, are given in Figure 4.29.

There are four major decomposition reactions that take place during the pyrolysis: curve 1, water and phthalic anhydride volatilize and a residue of dipotassium phthalate is formed, K₂C₈H₄O₄; curve 2, the latter compound decomposes to form potassium carbonate and carbonaceous material; curve 3, the carbonaceous material loses mass slowly and finally burns giving a residue to K₂CO₃; and curve 4, the potassium carbonate decomposes with the evolution of carbon dioxide, while the K₂O formed reacts with the porcelain crucible sample holder.

The various conditions under which the thermal decomposition takes place are illustrated by the curves in Figure 4.29. The slight mass increase between 425 and 450°C, noted on the dashed curve, was caused by the evaporation of phthalic anhydride from the furnace walls with increasing temperature and its condensation on the crucible support rod.

Newkirk and Laware (41) found that the initial isothermal rate of decom-

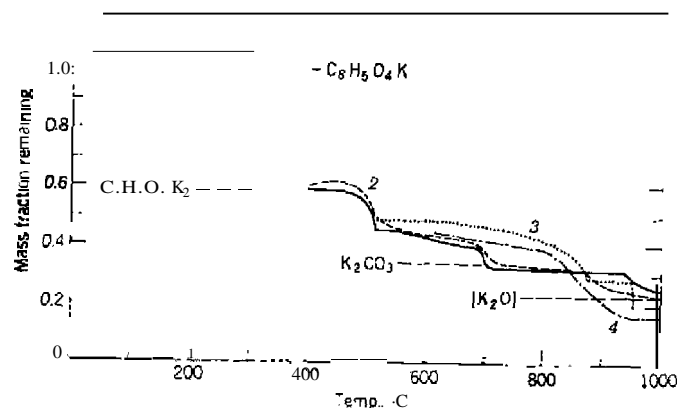


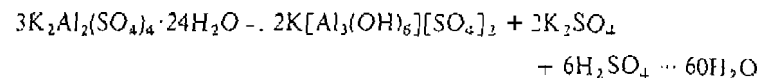
Figure 4.29. Thermal decomposition of 0.1 g samples of $\text{KHC}_8\text{H}_4\text{O}_4$ at a heating rate of $300^\circ\text{C}/\text{h}$, under various conditions: — — — air atmosphere, Pt crucible; - - - air atmosphere, porcelain crucible, without protective sleeve on crucible support rod; nitrogen atmosphere, porcelain crucible; - · - · - nitrogen atmosphere, preheated sample to 300°C (4).

position of $\text{KHC}_8\text{H}_4\text{O}_4$ in carbon dioxide at 235°C was about 15 mg/g/h. This compares with an extrapolated value of 7 mg/g/h previously reported. However, Duval (39) found no observable mass-loss from isothermal runs at 150, 160, and 170°C , respectively. If a sample mass of 0.5 g is assumed for his experiments, Newkirk and Lawarc (41) calculated that the mass-changes expected would be 0.004, 0.011, and 0.030, respectively. Since these changes are too small to be detected by the Cbevenard thennoblance, it is not surprising that Duval observed no mass-changes.

Smalley et al. (160) proposed the use of potassium hydrogen phthalate as a TG standard. Using DTG, they observed six peaks in the curve when this compound was heated in air from 25– 1000°C at a heating rate of $280^\circ\text{C}/\text{h}$. The peak minimum temperatures found were $300 \pm 10^\circ$, 400° , 510° , 565° , 680° , 700° , and 850°C , respectively. Since this compound is available in a high purity form as a pH standard, it is proposed for use as a TG standard as well. The peak temperatures are said to provide convenient reference points.

19. Basic Potassium Aluminum Sulfate

In the final purification processing of aluminum oxide by the Bretsznajder method, the principal product, basic aluminum ammonium sulfate, is contaminated with basic aluminum potassium sulfate. The latter is formed by the hydrolysis of aluminum potassium alum according to the equation



Thermal decomposition of the preceding two basic salts finally yields foundry quality Al_2O_3 . Using TG and other TTA techniques, Pysiak and Glinka (168) studied the thermal decomposition of basic aluminum potassium sulfate and determined the intermediate products and the reaction kinetics.

The TG curve of basic aluminum potassium sulfate (BAPS) is given in Figure 4.30. No distinct curve plateaus were observed but on the basis of other TA techniques, three regions of mass-loss could be observed: (1) loss of 3 moles of water per mole of BAPS with retention of alunite structure; (2) loss of OH water and disruption of alunite structure giving $\text{KAl}(\text{SO}_4)_2$, $\text{Al}_2(\text{SO}_4)_3$, and $\gamma\text{-Al}_2\text{O}_3$; (3) both $\text{KAl}(\text{SO}_4)_2$ and $\text{Al}_2(\text{SO}_4)_3$ dissociate, evolving SO_3 ($\text{SO}_2 + \frac{1}{2}\text{O}_2$) and yielding $\gamma\text{-Al}_2\text{O}_3$. The intermediate products of the decomposition of $\text{KAl}(\text{SO}_4)_2$ are $\text{Al}_2(\text{SO}_4)_3$ and K_2SO_4 . Detailed reactions for all the steps in the TG curve have been proposed (68).

20. Platinum Group Oxides

The platinum group metals, Pt, Ir, and Ru, form solid oxides with the formulas PtO , IrO_2 , and RuO_2 , which volatilize at elevated temperatures in an oxygen atmosphere. Most of the gaseous oxides are stable only at high

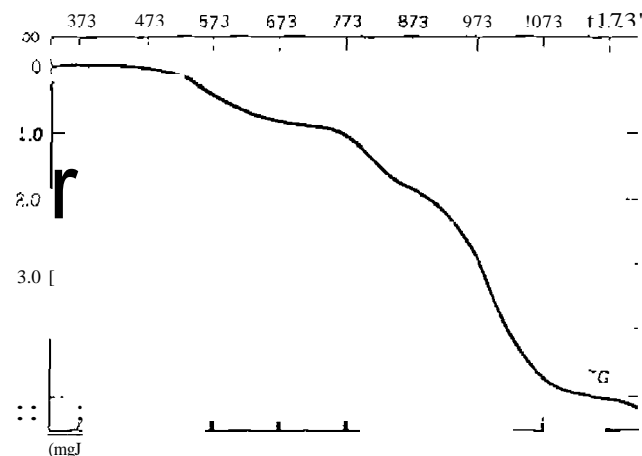
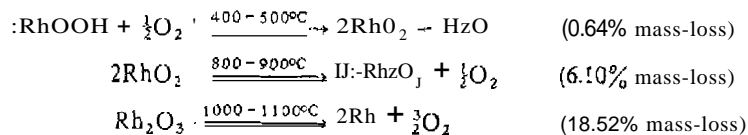


Figure 4.30. TG curve of basic aluminum potassium sulfate. Pressure is 1×10^{-6} kPa at a heating rate of $2\text{K}/\text{min}$ (68).

temperatures and usually contain the metals in the highest oxidation state. Palladium is an exception in that it dissolves oxygen in the solid state and forms PdO, which dissociates above 800°C.

The TG curves of the Pt group metal oxides are given in Figure 4.31 (70). The curves were obtained in an atmosphere of oxygen at 100 Torr and a heating rate of 10°C/min. Formation and dissociation of the oxides depend on the oxygen pressure, the heating rate, and the surface area of the metal powders. A decrease in oxygen pressure favored the complete oxidation of the metal powders. A plot of dissociation temperatures versus the equilibrium oxygen pressures permitted the calculation of the thermodynamic quantities of ΔH_{298}° , ΔS_{298}° , and $T_{diss}(P_{O_2} = 1 \text{ atm})$.

The thermal decomposition and interconversion between orthorhombic RhOOH and tetragonal RhO₂ have been investigated by Moran-Miguelcz and Alario-Franco (91). According to the TG and DTA curves in Figure 4.32, the decomposition of RhOOH proceeds in the following steps:



Calculated values for the mass-losses are 0.73, 5.93, and 18.90%, respectively. In vacuum ($\sim 1 \times 10^{-4}$ Torr), the thermal treatment of RhOOH at 400°C

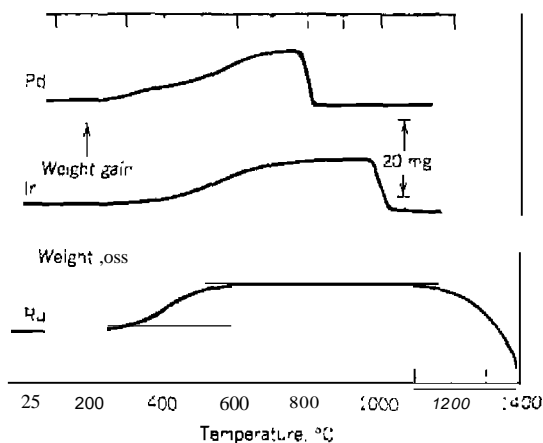


Figure 4.31. TG curves of PdO, IrO₂ and RuO₂ showing formation and dissociation reactions (70).

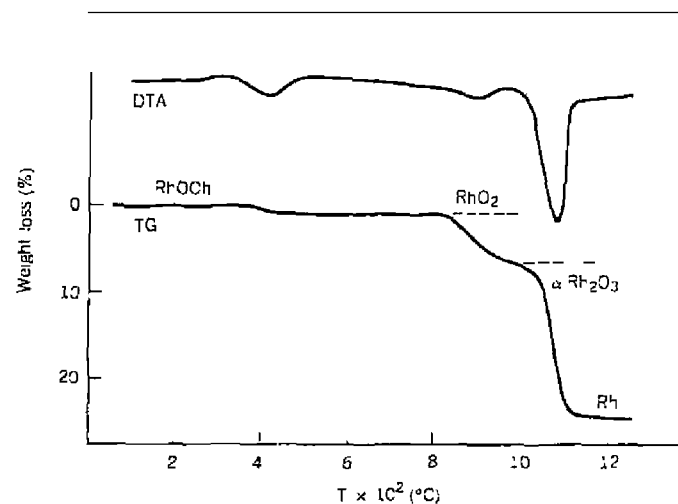
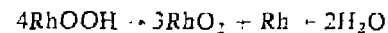
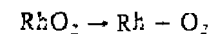


Figure 4.32. TG and DTA curves of RhOOH in air. Heating rate of 10°C min⁻¹, (91).

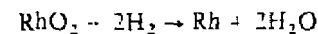
gives



On increasing the temperature to 500°C, the RhO₂ dissociates according to



In hydrogen, RhO₂ is converted to Rh metal and water at 170°C according to the equation



The experimental mass-loss of 23.90% is in good agreement with the calculated value of 23.70%.

21. Sodium Carbonate

The drying of sodium carbonate is important in the standardization of acids for various types of acidimetric titrations. The recommended drying temperature range is 250–300°C, although Duval (22) stated that a horizontal mass level was obtained from 100–840°C. In a more recent study, Newkirk and Aliferis (23) found that the decomposition temperature of anhydrous

sodium carbonate was dependent on the type of crucible container the sample was heated in. The results of this study are illustrated in Figure 4.33 and described in Table 4.5.

When the sodium carbonate was heated in platinum or gold sample holders, the mass-loss was much less rapid and was probably due to the decomposition of the sample to form sodium oxide and carbon dioxide. As seen in curve 6, the presence of a nitrogen gas stream resulted in a faster rate of mass-loss, while when water was present (curve 7) the observed mass-loss rate was less. A sample of sodium carbonate dried at 350°C showed no further mass change on further heating for 12 hours at 600°C and 4 hours at 650°C in a platinum crucible in air. The reaction of sodium carbonate with coarse silica sand occurred rapidly at 800–850°C as shown by curve 9. On grinding the silica mixture, the first evidence of mass-loss was at about 500°C (curve 10) or somewhat less than the temperature in curve 9.

It was recommended that sodium carbonate for analytical use be dried by heating in dry air or carbon dioxide using a platinum or other inert sample container in the temperature range of 250 to at least 700°C.

Table 4.5. Data for Figure 4.33

Curve ^a	Crucible	Atmosphere	Sample
1	Porcelain	Air	Na ₂ CO ₃
2	Porcelain	Air	Na ₂ CO ₃ ^b
3	Porcelain	Dry N ₂ ^c	Na ₂ CO ₃
4	Alumina	Air	Na ₂ CO ₃
5	Platinum	Air	Na ₂ CO ₃
6	Platinum	Dry N ₂ ^c	Na ₂ CO ₃
7	Platinum	Wet N ₂ ^c	Na ₂ CO ₃
8	Platinum	CO ₂ ^c	Na ₂ CO ₃
9	Platinum	Dry N ₂ ^c	Na ₂ CO ₃ + SiO ₂
10	Platinum	Dry N ₂ ^c	Na ₂ CO ₃ - SiO ₂ ^d
11	Gold	Dry N ₂ ^c	Na ₂ CO ₃ ^e

^aHeating rate 300°C/h. except runs 9 and 10.

^bCrucible covered.

^cGas flow rate 250 ml/min.

^dHeating rate 300°C/h to 520°C. then 50°C/h.

^eMaximum temperature 922°C. but sample cooled and held at 915°C after reaching 922°C.

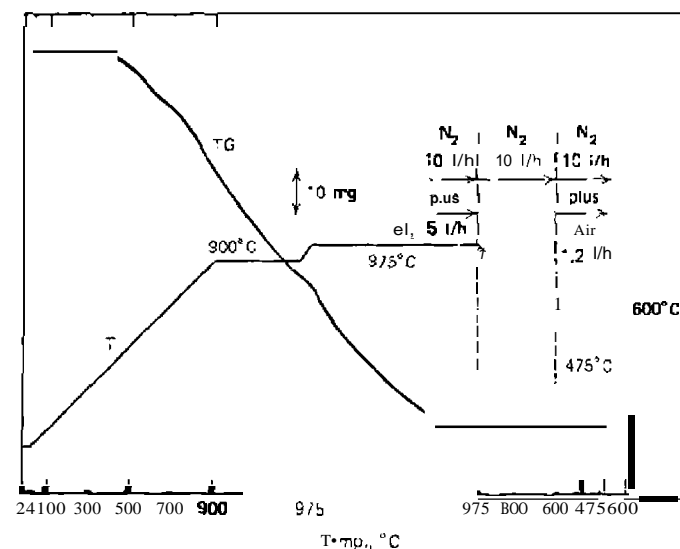


Figure 4.34. TGA method for the determination of T and C in a nonstoichiometric titanium carbide (4.3).

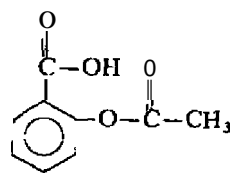
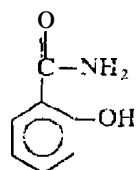
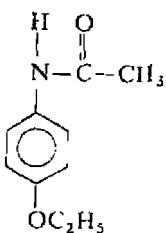
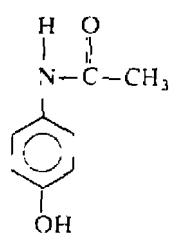
22. Titanium Carbide

Wiedemann (143) determined the titanium content of a nonstoichiometric titanium carbide by a multistep, variable atmosphere, variable temperature program, TO method. The sample was first heated in a chlorine atmosphere to 975°C. This converted the titanium to volatile titanium chloride, leaving a residue of carbon in the sample container. The amount of carbon residue was then determined by heating from 475-600°C in an air atmosphere, resulting in the oxidation of carbon to carbon dioxide. These processes are illustrated in the TG curve in Figure 4.34.

F. APPLICATIONS TO PHARMACEUTICALS

1. Analgesics

There are numerous nonprescription preparations that possess analgesic properties. These preparations, which relieve pain arising from organic disorders or of psychosomatic origin, contain various analgesic agents, the most common of which are the following:

I
Acetylsalicylic acid (aspirin)II
SalicylamideIII
PhenacetinIV
N-Acetyl-p-aminophenol
(acetaminophen)

Aspirin (I) is effective in musculoskeletal pain and headache but less effective for pain such as toothache and sore throat. N-Acetyl-p-aminophenol (IV) has a reasonable antipyretic effect and may be used as a substitute for aspirin in cases where fever reduction is important; it is second only to aspirin for use as a nonprescription analgesic. Acetanilide and phenacetin (III) are also effective as analgesic and antipyretic agents. Most of the acetanilide is metabolized to (IV), which is thought to be the active agent. However, compounds (III) and (IV) are less toxic than acetanilide so that the latter is no longer widely used. Salicylamide (II) is used for its analgesic as well as its slight sedative properties.

The most commonly used analgesic is acetylsalicylic acid (I) (aspirin). It is generally dispensed in 5-grain (325 mg) tablets which contain a small amount of binder, such as starch, and other components. The TO and DSC curves of aspirin preparations are, essentially, those of pure acetylsalicylic acid. A small black, charred residue is usually obtained at 500°C, if heated in a nitrogen atmosphere, of the binding agent. The TG curves of 12 commercially available analgesics are shown in Figure 4.35 (97). Although more useful information can be obtained from the DSC curves, TO curves are also valuable for the identification of the different analgesics. No horizontal mass plateaus were observed in any of the TG curves, even though regions of decreased rate of decomposition or sublimation could be observed. In the case of acetylsalicylic acid, the first mass-loss began at an initial temperature

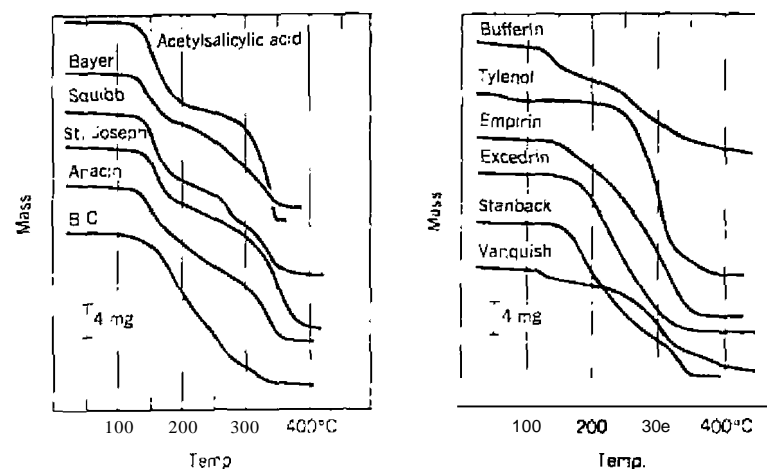


Figure 4.35. TG curves of commercially available analgesics as determined by Wendlandt and Collins (97).

(T_i) of 125°C. The rate of mass-loss increased greatly above 150°C but then decreased in the 225 - 300°C temperature range. This was followed by another region of rapid mass-loss, which terminated at 360°C. The sample container was empty at the latter temperature, indicating complete loss of the sample. As in the case of the DTA curves, the Bayer, Squibb, and St. Joseph aspirin preparations all gave similar TG curves. A residue of the charred binder was present in each of the preparations. The preparations, Empirin, Excedrin, and Stanback, yielded similar TG curves. Bufferin and Vanquish also gave similar TG curves, perhaps because of the presence of aluminum and magnesium hydroxy compounds, Tylenol, since it has a composition that does not contain acetylsalicylic acid, gave an entirely different type of TG curve. Hence, it is probably the simplest to identify of all the analgesics studied here.

2. Antacids

Wendlandt (98) used TG and DSC techniques to identify qualitatively 12 nonprescription antacids. These preparations are widely used to treat mild gastrointestinal disturbances. A large number of these preparations is commercially available, each differing in the ability to neutralize stomach acids. The active component of most antacids consists of compounds such as calcium carbonate, sodium hydrogen carbonate, aluminum hydroxide, magnesium trisilicate, dihydroxyaluminum aminoacetate, and so on. Perhaps the most popular component is calcium carbonate, mainly because it is more effective than various brands of aluminum hydroxides and is also inexpensive and rapid in neutralization action. It is not without adverse side effects, however, in that chronic use can cause constipation and the formation of urinary calculi. Another antacid frequently used is sodium hydrogen carbonate (NaHCO_3), which is rapid in action and effective in inducing gastric emptying belching. Chronic use can be harmful in that the gastric fluids are raised to high pH values, which stimulate the production of more hydrochloric acid. Also, its high basicity can cause alkalosis while the high sodium content can create problems for patients on a low salt diet. Still another antacid that is widely employed is aluminum hydroxide, either by itself or mixed with various magnesium compounds. In addition to its antacid properties, it may be effective in the treatment of peptic ulcer due to the ability to absorb pepsin. Aluminum hydroxide has more adverse side effects than calcium carbonate if used for prolonged periods of time. A somewhat more effective antacid than aluminum hydroxide for treatment of peptic ulcer is magnesium trisilicate, which has a greater capacity for pepsin adsorption. For short observation periods, however, this compound is less effective than the other antacids previously discussed. It will not produce alkalosis and large excesses will not raise the pH of gastric fluids much above

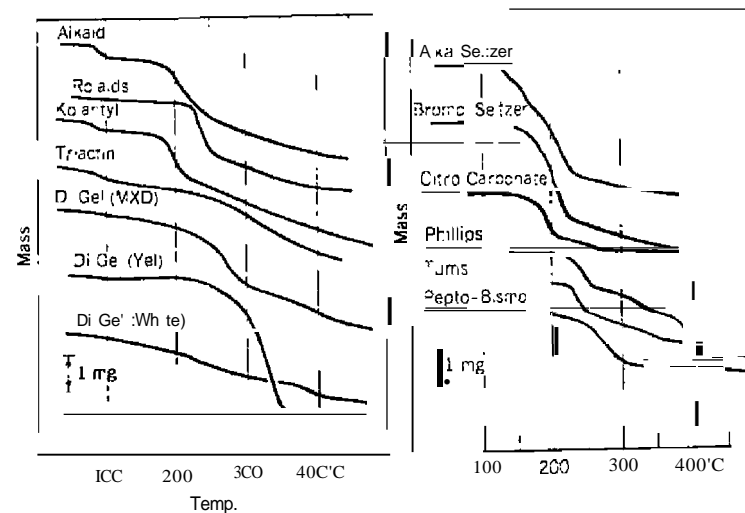


Figure 4.36. TG curves of nonprescription antacids (98).

7. Other effective antacids, which are used separately [or with aluminum hydroxide or magnesium trisilicate, include dihydroxyaluminum aminoacetate, hydrated magnesium aluminate, dihydroxyaluminum sodium carbonate, and others. Each of these compounds has been demonstrated to be as useful as antacids but has not been so popular as calcium carbonate or aluminum hydroxide.

The TG curves of the antacids are given in Figure 4.36. As expected, the TG curves are not so helpful for qualitative identification purposes as are the DSC curves. Similar features, such as the T_i values, were observed for Alka Seltzer, Bromo-Seltzer, and Citrocarbonate. Likewise, T_i values for Phillips, Tums, and Rolaids were similar. There were enough differences in the TG curves of Alkaid, Rolaids, Koiantyl, and Triactin to be useful for qualitative identification purposes.

3. Determination of Composition

Radecki and Wesolowski (95, 96) used TG and DTA to evaluate the influence of various tablet components on the thermal decomposition of pure pharmaceuticals. The resulting features of the TA curves could then be used to aid in the identification of the pharmaceutical and the quantitative control of the dosage. Thermal processes suitable for the determination of the principal

components of a pharmaceutical include (95):

1. *Dehydration.* The loss of constitutional or crystallization water accompanied by the formation of an intermediate compound of known composition and structure. These processes occur mainly in the temperature range 60-300°C.
2. *Decarboxylation.* Loss of CO₂ from substituents such as NaHCO₃ or CaCO₃. The former occurs over the temperature range 60-200°C, whereas the latter occurs at much higher temperatures, 600-800°C.
3. *Weight-losses* due to reactions between components of an effervescent mixture.
4. *Weight-losses* resulting from the formation of reaction intermediates that yield inflections in the TO curves.
5. *Weight-losses* due to total evaporation, sublimation, and combustion of a component in the pharmaceutical.

The quantization of results of the thermal decomposition of pharmaceuticals, using TG and DIG, is rapid and simple in that no calibration is required and time-consuming calculations are not necessary. Moreover, the results are less dependent on the experimental conditions. The relative errors for the determinations are listed in Table 4.6 (95).

Table 4.6. Relative Errors of Determinations of Components of Pharmaceutical Preparations. Based on Appropriate Processes of the Thermal Decompositions (95)

Process	Number of Preparations	Average Relative Error (%)
1. Dehydration. Loss of:		
A. Crystallization water	7	2.6
B. Constitutional water	2	6.1
2. Decarboxylation:		
A. Of sodium hydrogen carbonate	1	2.9
B. Of calcium carbonate	15	2.9
3. Weight loss due to chemical reaction between components of effervescent mixture	3	6.9
4. Weight loss corresponding to inflections in the TG curve. The composition and structure of an intermediate:		
A. Were established	13	5.5
B. Could not be established	10	2.6
5. Weight loss due to complete evaporation, sublimation or combustion of the component	11	5.0

Table 4.7. Results of the Quantitative Analysis of Thermal Decomposition of Model Tablet Containing Selected Pharmaceutical (96)

Tablet Mixture No.	Pharmaceutical	Stage of Thermal Decomposition ^a	Avn. (%)	Avn. (%)	Avn. (%)
TM-1	Phenyl salicylate	Volatilization	80	220	43.5
	Salicylamide	Volatilization	100	280	45.5
	Acetylsalicylic acid	Thermal decompn.	80	210	14.0
TM-2	Nitrofurantoin	Thermal decompn.	190-230		Undeterminable
	Ca pantothenate	Decarboxylation	640-740	4.0	31.6
TM-7	Antipyrine	Thermal decompn.	130	320	28.0
	Carbromal	Thermal decompn.	110	230	43.7
	Pyrazinamide	Thermal decompn.	140	210	Undeterminable
TM-3	Ca gluconate	Decarboxylation	580	710	4.5
	Al phosphate	Dehydration	40	210	45
	Mg trisilicate	Dehydration	40	30	Undeterminable ^c
TM-4	Isomiazid	Volatilization	160	350	Undeterminable ^c
	Novalgin	Dehydration	40	100	Undeterminable ^c

^aStage from which pharmaceutical content was evaluated.

^bTheoretical weight loss; experimental values in body of table.

^cLoss in weight after subtraction of the loss in weight due to dehydration of tablet was in good agreement with pharmaceutical content in the mixture.

The thermal decomposition of 14 model mixtures of drugs excipients was determined by TG, DTG, and DTA by Wesolowski (96). Qualitative determination of pharmaceutical preparations containing various amounts of phenyl salicylate, nitrofurantoin, and calcium gluconate was carried out by use of DTA. Wesolowski, by the TG method, determined the quantitative analysis of these mixtures by using the relationship

$$\text{Component Content} = \frac{\Delta m \text{ from TG Curve of mixture} \times 100}{\Delta m \text{ from TG curve of pure component}} \quad (4.8)$$

The results of these determinations for various pharmaceuticals are given in Table 4.7 (96).

4. Moisture Determination

TG is one of the most commonly used TA methods for the determination of moisture and other volatiles in pharmaceutical preparations. Two kinds of moisture can be determined: (1) surface or free moisture and (2) hydrate or bound moisture. The TG Curve in Figure 4.37, as determined by Daly (94), shows how the two types of moisture are found from a single TG curve. With a suppression of 50% of the total sample mass, the surface or free water is evolved at temperatures up to 120°C. The hydrate or bound water is evolved from 120-150°C. Amounts of moisture found are 8% surface or free water and 13.0% hydrate or bound water.

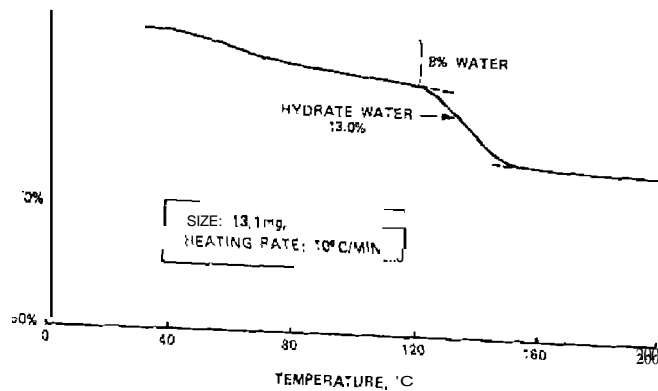


Figure 4.37. TG determination of surface or free moisture and hydrate or bound moisture (94).

5. Sulfa Drugs

Cook and Hildebrand (99) use TG for the qualitative identification of 12 sulfa drugs in the temperature range 25-800°C.

G. APPLICATIONS TO POLYMERIC MATERIALS

1. Introduction

Perhaps the greatest number of applications of thermogravimetry during the past 10 years has been in the characterization of polymeric materials. These studies have been useful not only in the applied areas but also in the theoretical aspects of high polymers. Applications of TG include comparisons of the relative thermal stability, the effect of additives on the thermal stability, moisture and additive contents, studies of degradation kinetics, direct quantitative analysis of various copolymer systems, oxidation stability, and many others. In studies of thermal oxidative degradation (42), TG can reveal the molecular structure and arrangement of repeating units, existence of cross-links between chains, side groups in homopolymer and copolymer chains, and so on. Rate constants, reaction orders, frequency factors, and activation energies of degradation can also be obtained (16).

A number of methods have been used to classify polymers according to their thermal stability. As discussed by Fock (42), classification is difficult because of the wide variety of possible thermal reactions at elevated temperatures. For example, the onset of decomposition may be the degradation of a side chain with the main polymer chain remaining intact; at some higher temperature, further decomposition could occur, resulting in drastic changes in the properties of the material. One substance may degrade completely in a single step, while a second substance under identical furnace conditions may leave a residue at the upper temperature limit.

Since the usual decomposition temperatures obtained from TG are highly dependent on the experimental procedure employed, Doyle (43) has used the expression "procedural decomposition temperature" as a precaution against mistakenly regarding such trivial data as definitive. Two types of procedural decomposition temperatures were defined by Doyle (43). The first of these was called the "differential procedural decomposition temperature" (dpdt) which was used to define the location of "knees" in normalized TG curves. The second type was called "integral procedural decomposition temperature" (ipdt) and was a means of summing up the entire shape of the normalized mass-loss curve.

The ipdt values are determined from a mass-loss curve as follows: The

curve, as shown in Figure 4.38, is divided into small squares. The area under the curve is integrated by weighing a paper cutout of the curve on an analytical balance. The mass of the crosshatched region in Figure 4.38 divided by the mass of the total rectangular plotting area is the total curve area, A^* , normalized with respect to both residual mass and temperature. The quantity A^* is converted to a temperature T_{A^*} , by

$$T_{A^*} = 875A^* - 25 \quad (4.9)$$

In T_{A^*} , it is presumed that all materials volatilize below 900°C and do so at a single temperature. Thus, T_{A^*} represents a characteristic end-of-volatilization temperature, rather than an ipdt having practical significance. However, it does serve as a measure of refractoriness, but is not very satisfactory.

To put all materials on an equal basis with respect to experimental temperature range, as in A^* , but also with respect to their individual refrac-

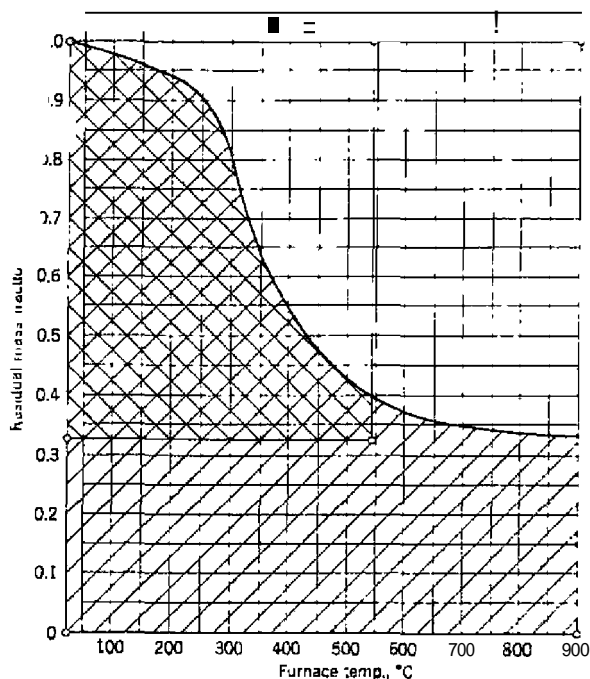


Figure 4.38. TO curve areas, A^* and R_0 (43)

Table 4.8. Integral Procedural Decomposition Temperatures of Some Common Polymers (43)

Polymer	ipdt (°C)
Polystyrene	395
Maleic-hardened epoxy	405
Plexiglas	345
66 nylon	419
Teflon	555
Kcl-F	410
Viton A	460
Silicone resin	505

tory contents, consider a second curve area, K^* , the ratio between the doubly crosshatched area and the rectangular area bounded by the characteristic end-of-volatilization temperature, T_{A^*} , and the residual mass fraction at the fixed end-of-test temperature of 900°C.

Doyle (43) showed that the product A^*K^* represented a comprehensive index of intrinsic thermal stability for 54 polymers of widely different basic types. It was also shown that by substituting A^*K^* for A^* in equation (4.9) the ipdt obtained had a practical meaning as a half-volatilization temperature. Unlike ordinary half-volatilization temperatures, defined as the temperature at which half the ultimate volatilization has occurred, the ipdt based on the residual mass fraction of 900°C was appropriate whether decomposition occurred in a single step or in several consecutive steps.

As a quantity derived from curve areas, the ipdt was highly reproducible and its value was only slightly affected by small vagaries or systematic errors in the data curve, especially as contrasted with indices derived on the basis of residual mass fraction end points alone. Even small variations in heating rate do not affect it appreciably. The ipdt of several polymeric materials are given in Table 4.8.

2. Relative Thermal Stability

A comparison of the relative thermal stability of a number of different polymers was described by Newkirk (44). The TG curves, as shown in Figure 4.39, were heated rapidly in nitrogen to about 340°C and then more slowly. An order of stability is readily observable: poly(methyl methacrylate) < polystyrene < Mylar and nylon < polyethylene < Lexan.

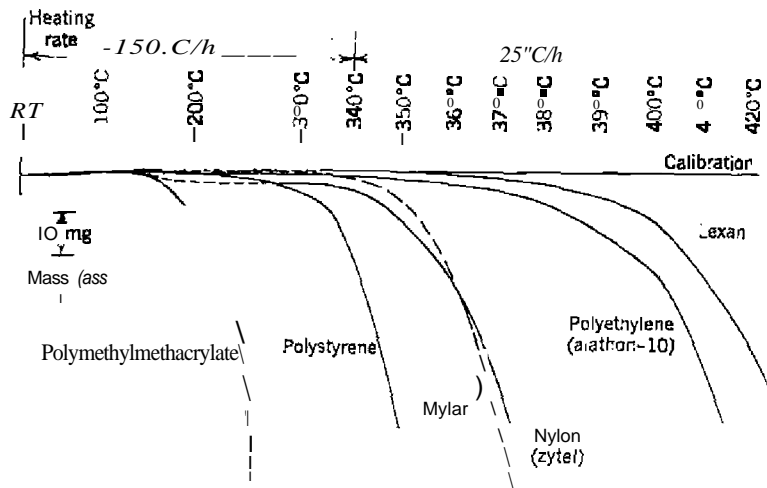


Figure 4.39. Comparison of thermal stabilities of various polymers according to Newirk (44).

In another TG study, Chiu (45) compared the relative thermal stabilities of five polymers, as shown in Figure 4.40. These polymers, poly(vinyl chloride) (PVC), poly(methyl methacrylate) (PMMA), high-pressure polyethylene (HPPE), polytetrafluoroethylene (PTFE), and an aromatic polyromellitimide (PI), were all heated under identical conditions in the

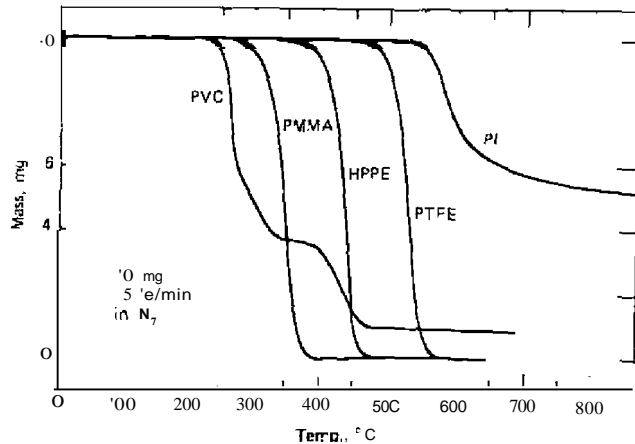


Figure 4.40. Relative thermal stability of polymers by TG (45).

same thermobalance. Each polymer showed its characteristic mass-loss curve in a specific temperature region. This type of information can be used as a guide for further studies on decomposition mechanisms.

3. Additive Content

Plasticizers are monomeric components that are added to plastics and elastomer formulations to modify the viscoelastic properties of the blend to make it more flexible, deformable, and processable. These additives are generally lower in thermal stability than the polymer components and can generally be separated from the polymers by heating to moderate temperatures in a N₂ atmosphere. The determination of a plasticizer, in this case petroleum, in a rubber shoe heel formulation, is shown by the TGA curve in Figure 4.41 (100). The rubber formulation contains the components of extender, polymer, and filler, each of which can be determined from the curve. The temperature program is as follows: fast heating rate in an inert atmosphere with brief dwell times at 310 and 450°C to allow for the oils and polymer, respectively, to volatilize. The furnace atmosphere is then changed to air and the amount of carbon black or polymer pyrolysis products is determined. The total time elapsed during the analysis is about 20 min.

Cassel and Gray (100) have developed a TG procedure for the determination of dioctyl phthalate (DOP) plasticizer in polyvinyl chloride. As illustrated in Figure 4.42, the DOP plasticizer is evolved from the sample by fixing the furnace temperature at 200°C in a N₂ atmosphere. When the

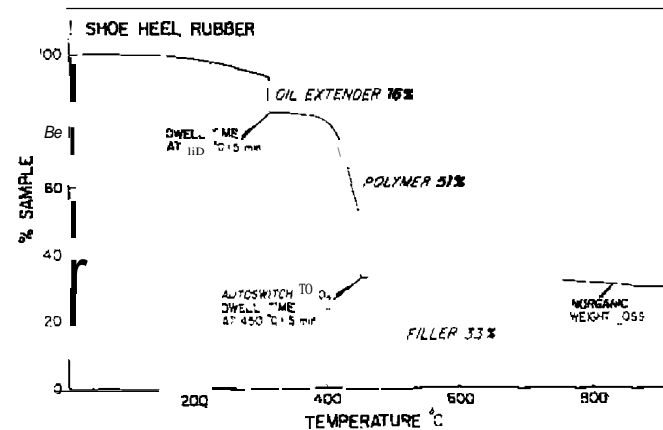


Figure 4.41. Determination of extender, polymer, and filler in elastomer (100).

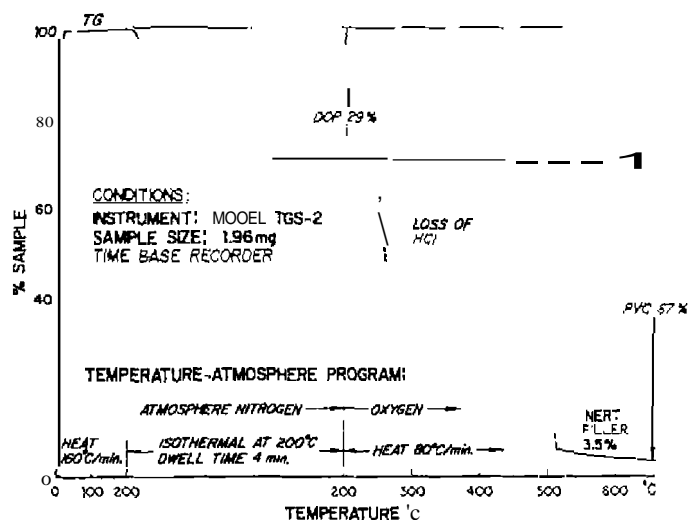


Figure 4.42. Determination of diethyl phthalate plasticizer in polyvinyl chloride (100).

atmosphere is changed to O_2 and the furnace is programmed at $80^\circ C/min.$, the PVC is decomposed into HCl and other pyrolysis products. The inert filler can be obtained by noting the amount of residue or ash remaining at $600^\circ C$. In the determination of the DOP, if this procedure is carried out on a series of identical samples at different isothermal temperatures, the half-life for the residency time for DOP can be obtained as a function of temperature. Plotting the data on a semilog plot (T versus $\log t$), the life expectancy of the plasticizer can be predicted at the end-use temperature (101).

In most cases, the organic material in a formulation can be separated from the inorganic filler components by heating to $500-600^\circ C$ in N_2 or oxidizing atmospheres. The total filler content can be determined from the TG chart. For some polymers, such as certain epoxy resins, these conditions will result in pyrolytic reduction of the polymer to carbon, which would preclude simple separation from carbon fillers. In this case, it is necessary to prepare unfilled polymer samples and run these under the desired separation conditions to determine the residue left by pyrolysis. The filled polymer can then be corrected for this effect. Once the organic material has been removed, the remaining filler can be further separated by either adding heat or changing the composition of the furnace atmosphere. This has been illustrated by the determination of MoS_2 in a polytetrafluoroethylene polymer formulation (100).

A few inorganic fillers can be identified and determined quantitatively in the presence of other fillers through the decomposition of the filler into its component substances, one of them being volatile. Such is the case with a $CaCO_3$ filler; the $CaCO_3$ decomposes into CaO (s) and CO_2 (g). This is illustrated by the TG curve of an inorganic-compound-filled thermoset polyester (100), as illustrated in Figure 4.43. The determination involves heating the polymer in air to $420^\circ C$, a brief dwell time to assure polymer combustion, then rapid heating to $750^\circ C$, with a brief dwell time to allow for $CaCO_3$ decomposition to occur, and finally, a brief heating above $750^\circ C$ to ascertain the absence of any further inorganic filler mass-loss. The mass-loss between $600-750^\circ C$ is due to the loss of CO_2 from the $CaCO_3$ and is calculated to be 15% of the original sample weight. From the decomposition stoichiometry and the molecular weight, the weight of $CaCO_3$ in the polymer is calculated to be 32%. By subtraction, the other inorganic filler is determined to be 30%.

Occasionally, it is difficult to pyrolyze completely or oxidize other components in the polymer matrix without decomposing the less stable metal carbonates. In order to prevent the overlapping of these reactions, Cassel and Gray (100) carried out the pyrolysis in an atmosphere of CO_2 to which a small amount of oxygen was added. The CO_2 atmosphere will suppress the metal carbonate decomposition to over $850^\circ C$. This procedure was illustrated by the decomposition of a limestone filler. In air, the peak temperatures of the DTG curve occurred at 475 and $750^\circ C$: in a CO_2-N_2 atmosphere,

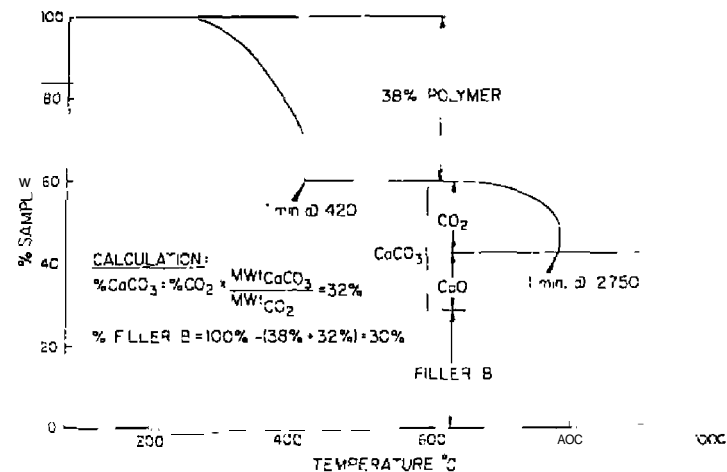


Figure 4.43. TG curve of an inorganic-compound-filled thermoset polyester polymer (100).

only a single peak was found at about 850°C. With pure CO₂, a shoulder peak was observed at about 900°C and another peak at about 925°C.

Charsley and Dunn (102) and Dunn (103) have applied TG to the characterization and quantitative determination of carbon black in rubber. The analysis involves volatilization of the oil and pyrolysis of the polymer in an inert atmosphere followed by oxidation of free carbon black in the rubber.

A typical TG curve in nitrogen and air for an oil extended ethylene-propylene terpolymer (EPDM) rubber compound is shown in Figure 4.44 (103). In N₂, the first mass-loss is due to the volatilization of the oil extender, although other volatile materials such as water, stabilizers, and cure residues may be lost as well. The second mass-loss is due to polymer decomposition, which for nonchar-forming polymers leaves carbon black and inorganic fillers. The atmosphere is then changed to air at 600°C and the carbon black is oxidized to gaseous carbon oxides. The residue is inert inorganic filler or ash. Graphite may also be determined as present by cooling the furnace to 300°C, changing the atmosphere to air, and reheating. Carbon black decomposes at a lower temperature than graphite. When the inorganic ash content is low (<0.1%), the determination of carbon black can be carried out directly in nitrogen. After loss of oil and polymer, the carbon black remains as a residue. This procedure can be carried out in 10 min. The total analysis for oil, polymer, carbon black, and inorganic filler takes about 20 min.

The variables affecting the T_{15} values have been elucidated by Charsley and Dunn (102). The T_{15} value is the temperature at which 15% of the total carbon black is oxidized, as determined by the TO mass-loss curve in an air

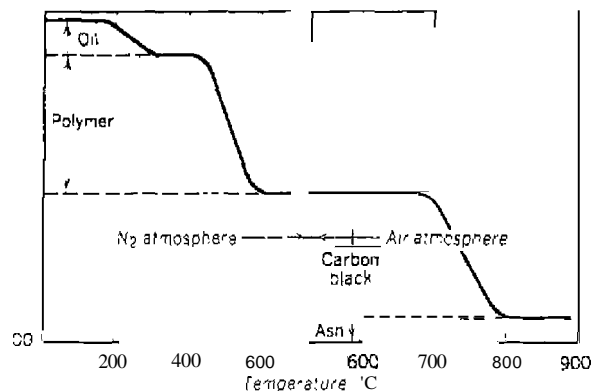


Figure 4.44. TG curve for EPDM rubber (103).

atmosphere. The T_{15} value variables investigated include the maximum temperature achieved during the pyrolysis step, heating rate, surface area of the carbon black, and so on.

4. Composition of Polymer Blends and Copolymers

Numerous TG studies have been made on the characterization of copolymer systems. In general, the thermal stability of a copolymer falls between those of the two homopolymers and changes in a regular fashion with the copolymer composition (45). In the case of ethylene-vinyl acetate copolymer, acetic acid is evolved rapidly and quantitatively during the initial stage of thermal decomposition. Only at higher temperatures (in inert atmosphere) do the residual hydrocarbon segments decompose. A typical TG curve of an ethylene-vinyl acetate copolymer is shown in Figure 4.45. The copolymer composition can be estimated from the initial mass loss. Compared to chemical, infrared, and nmr methods, TG is both rapid and accurate. Typical results for six copolymer samples with vinyl acetate contents ranging from 4.3-30% are given in Table 4.9. These results are compared with a chemical saponification method (45).

S. Miscellaneous

The determination of the thermal life rating of a magnet wire enamel by the customary method, ASTM 0-2307, is very time-consuming since it requires the heating of several wire samples at each of several temperatures and the periodic testing of each sample until electrical failure occurs. David (46)

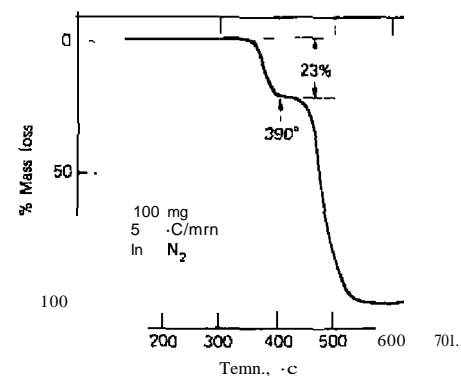


Figure 4.45. TO curve of ethylene-vinyl acetate copolymer (45).

Table 4.9. Correlation Between TG and Chemical Analyses of Ethylene-Vinyl Acetate Copolymer (45)

Vinyl Acetate (%) (Chemical)	Mass-loss Due to Acetic Acid (%)	Vinyl Acetate 1% (1G)	Absolute Deviation (%)
4.3	3.2	4.6	0.3
8.3	5.8	8.3	0.0
11.2	7.6	10.9	0.3
14.9	10.2	14.6	0.1
27.1	18.9	27.1	0.0
31.1	21.7	31.1	0.0

observed a correlation between the temperature of initial deflection (extrapolated to zero heating rate) of a TG curve of a magnet wire and the $T_{20,000}$ of the wire. Brown et al. (144) demonstrated correlations between TG (and DTA) data and $T_{20,000}$ for 15 commercial magnet wires. The wire samples were heated in a dynamic oxygen atmosphere, and the temperature at which 5% of the enamel mass had been lost correlated well with the $T_{20,000}$ value determined by the standard method. The kinetics of the decomposition was also determined (145).

Application studies that include the use of TG and other TA techniques to polymeric materials are numerous. Several illustrative studies include the following: applications to the electronics industry (104, 105); automotive industries (106); industry and research (107); and foam research and development (108).

H. MISCELLANEOUS APPLICATIONS

1. Analytical Applications

Duval (2, 8, 9) has discussed these in detail, as have Palei et al. (17); the applications given by the latter are as follows:

1. New weighing compositions in gravimetric analysis and the determination of their temperature stability ranges.
2. For weighing substances which are unstable at ambient temperatures, such as those which absorb CO_2 and H_2O from the air.
3. For studying the behavior of materials in atmospheres of various gases.

4. For determining the purity and thermal stability of analytical reagents, including primary and secondary standards.
5. For determining the composition of complex mixtures.
6. For systematically studying the properties of materials in relation to the methods used for their preparation.
7. For automatic gravimetric analyzing.

Duval (2) has also discussed these topics in addition to others, such as the following:

1. Various analytical techniques such as the ignition of filter paper.
2. Should a precipitate be dried or ignited?
3. Use of the thermobalance for discovery of new methods of separation and in gasometry.
4. The study of the sublimation of various substances.
5. Correction of errors in analytical chemistry.
6. Use of thermogravimetry in functional organic analysis.

2. Automatic Gravimetric Analysis

It was Duval (18) who envisioned the ability to determine the amount of a specific metallic ion in 15–20 min with the precision usually attainable in gravimetric procedures and independently of the skill of an operator. He also suggested the possibility of being able to determine simultaneously two or three different ions without having to carry out a preliminary separation. With these ideas as goals, Duval developed the technique known as *automatic gravimetric analysis*, in which a determination for a given metallic ion or mixture of ions could be rapidly carried out using the thermobalance. Selection of the gravimetric method to be used must be based on the following requirements:

1. Quantitative and immediate precipitation.
2. Immediate filtration with no need to age the precipitate.
3. Immediate drying.
4. Production of a TG constant weight plateau at the lowest temperature possible.

The principle of this technique, for the single-component system shown in Figure 4.46, is based on the following description. Using a clean and dry crucible, one can determine the baseline of the thermobalance, as indicated

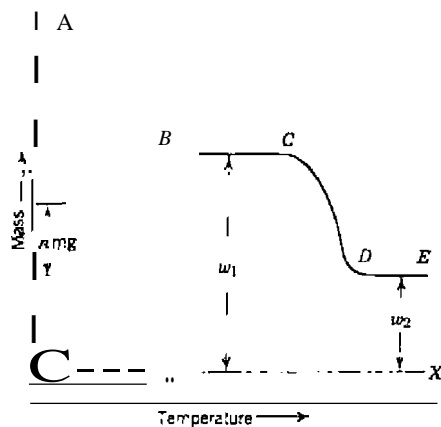


Figure 4.46. Automatic gravimetric analysis for a single-component system (18).

by the dashed line X. The crucible is removed from the balance, loaded with the wet precipitate, and then replaced on the balance. The precipitate is heated and the mass-loss curve recorded in the usual manner. From the horizontal mass plateau *BE*, the mass w_1 can be obtained, and from *DE* the mass, w_2 is taken. Since the mass levels indicate that a definite stoichiometry of the precipitate has been attained, multiplication of w_1 or w_2 by the appropriate gravimetric factor gives the mass of metal ion present. The metal ion content obtained by calculation from w_1 will probably be the most accurate because of the greater accuracy in mass measurement and the smaller gravimetric factor of the precipitate.

For certain precipitates, the entire operation—filtration, drying, and recording on the thermobalance—takes only 12 min (18).

In the case of a binary mixture, the procedure is similar. Take the case of the mixture as illustrated in Figure 4.47. The mass-loss curves for the pure individual components, *MX* and *NY*, are given, as well as the curve for a mixture of $MX + NY$. Component *MX* decomposes from *D* to *E*, while *NY* decomposes from *B* to *C*. In the mixture curve, horizontal mass levels are formed at the same temperatures as were present on the two initial component curves. Thus, from the mixture curve, the amount of *NY* can be obtained by determining the value of *BC*, the amount of *MX* from the value of *DE*. Thus, in one simple operation, the analysis of certain binary or ternary mixtures can be obtained with reasonable accuracy.

Duval (18) used this technique for the analysis of a binary mixture con-

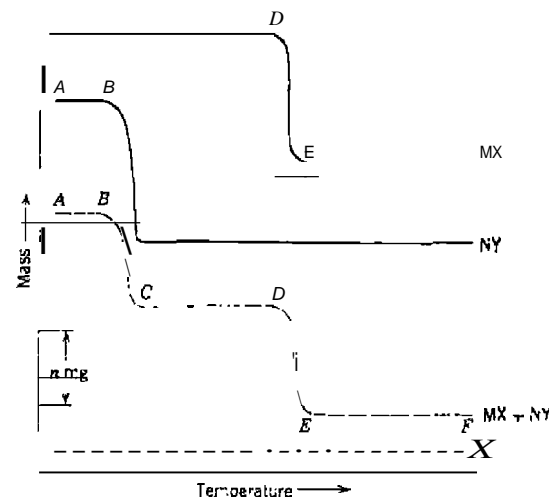


Figure 4.47. Automatic gravimetric analysis of a binary mixture (18).

taining calcium and magnesium ions. These two ions were precipitated as oxalates and the TG curve so obtained compared with curves for the individual metal oxalates. If x and y are the mass of calcium and magnesium, respectively, and m and n are the known masses (from the TG curve) of the mixtures present at 500 ($MgO - CaCO_3$) and 900 ($MgO + CaO$), then

$$\frac{100x}{40} - \frac{40.32y}{24.32} = m \quad (4.10)$$

$$\frac{56x}{40} - \frac{40.32y}{24.32} = n \quad (4.11)$$

hence,

$$x = \frac{m - n}{1.1} \quad (4.12)$$

A synthetic mixture containing 0.1541 g of $CaC_2O_4 \cdot H_2O$ and 0.053 g of $MgC_2O_4 \cdot 2H_2O$ gave $x = 0.0427$ g, compared with a theoretical value of 0.0422 g. A similar determination was carried out for the determination of copper-silver alloy from a mixture of the metal nitrates.

3. Drying of Analytical Precipitates

One of the first modern applications of the thermobalance to problems in analytical chemistry was the determination of the drying temperatures and weighing forms of analytical gravimetric precipitates. Duval (19) was impressed by the fact that authors were very specific about details concerning the conditions of precipitation, such as concentration of the reagents, volume of reagents, pH of the solution, time of aging precipitate, and other factors, but very vague about drying or pyrolysis temperatures. General statements such as "ignite to constant weight," "heat not above a dull red," and so on, were entirely inexcusable when it came to gravimetric precipitates. With the aid of 17 collaborators, Duval prepared and heated about 1200 precipitates which had been prepared for use in inorganic gravimetric analysis. Only a small number of these were judged to be suitable for the gravimetric determination of various metal ions, based on the ease of precipitation and the drying or ignition temperatures.

One of the early TG curves which was used in the gravimetric determination of calcium is that shown in Figure 4.48 (20). As is commonly known, the curve plateau at temperatures from 25 to 100°C corresponds to the composition for the initial compound; from 226 to 346°C, to CaC_2O_4 ; from 420 to 660°C, to CaCO_3 ; and from 840 to 980°C, to CaO . Thus, the drying and ignition temperatures and the composition of the compound at any temperature can be determined. The question of drying temperatures and the non-existence of a TG curve plateau (horizontal) have been discussed by numerous investigators, especially Simons and Newkirk (21). For a multistage thermal decomposition reaction, which would include most of the analytical precipitates studied, the following general conclusions can be drawn (21):

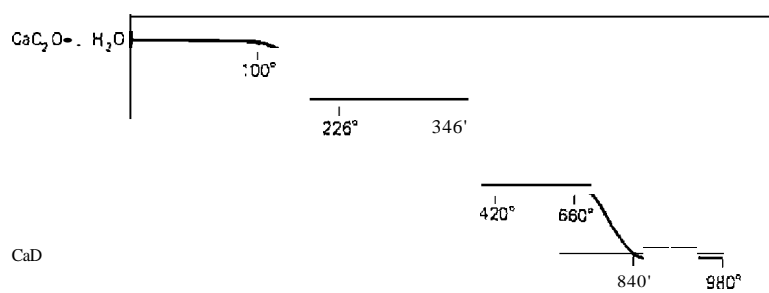


Figure 4.48. TG curve of $\text{CaC}_2\text{O}_4 \cdot \text{H}_2\text{O}$ by Feiler and Duval. (20)

1. The appearance of a plateau for a compound on a TG curve does not necessarily imply that the compound is isothermally stable, in either a thermodynamic or practical sense, at all or any temperatures that lie on that plateau.
2. If the curve obtained for a multistage reaction has no intermediate portion in which the mass remains constant with time over a range of temperature, one can make the reasonable inference that the reactions leading to the formation and to the subsequent decomposition of the intermediate are not independently sequential, but overlap at least partly.
3. In the absence of a true plateau, one cannot determine from a curve for successive reactions exact values for either the initial or final temperatures of the plateau (T_i or T_f), or the stoichiometric mass level, although a reasonable inference as to the latter can often be made.

Thus, the transfer of drying or ignition temperatures from a TG curve plateau to isothermal measurements appears to be questionable, although it is a widely used practice.

4. Applications to Vapor-pressure Determination

The vapor pressure or the sublimation behavior of organic compounds can be determined conveniently using thermogravimetry. Ashcroft (48), using the Langmuir equation

$$m = \alpha \left(\frac{M}{2\pi RT} \right)^{1/2} P \quad (4.13)$$

where M is the molar mass of the gaseous substance, T is the Kelvin temperature and α is the sublimation coefficient (assumed unity), determined the enthalpy of sublimation of a number of organic compounds and inorganic chelates. Application of the Clausius-Clapeyron equation to a sublimation process during which the surface area of the sample is constant shows that a plot of $\log [m(T)^{1/2}]$ against $10^3/T$ has a slope of $-0.0522 \Delta H_{\text{sub}}$, from which ΔH_{sub} may be calculated in kJ. Rates of mass-loss of powdered 50-100-mg samples, contained in a platinum boat, were recorded at a series of five or six temperatures over a 20-30° range. By choosing the temperature to give low rates of mass-loss and low (< 2%) overall loss, good straight-line plots were obtained from which the slopes, as calculated by the least-squares method, were reproducible to about 5%. Enthalpies of sublimation obtained by this method are shown in Table 4.9. There was good agreement between the

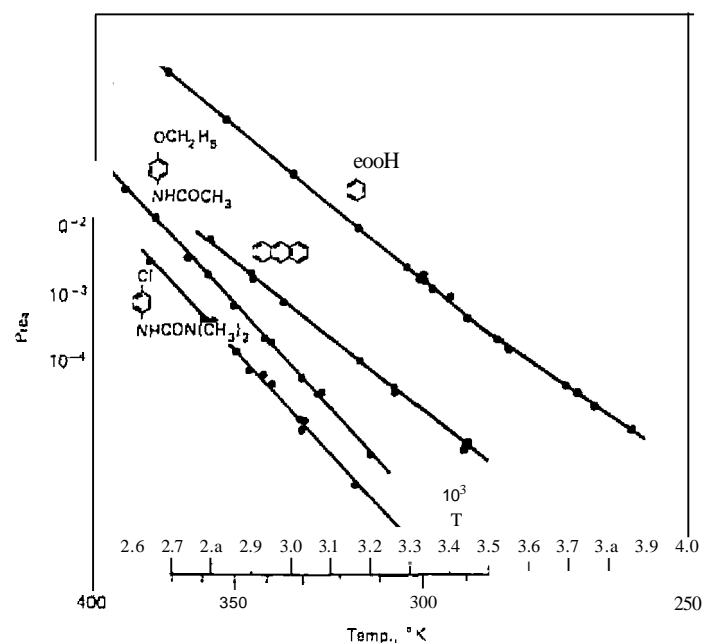


Figure 4.49. Vapor-pressure curves obtained by TO using the Knudsen effusion method (49).

two series of values for the first five compounds, although some variations may be expected from the different temperature ranges of measurement.

The determination of the vapor pressure of various compounds was reviewed by Wiedemann (49). He discussed the determination of vapor pressure by TG techniques based on the Knudsen effusion method. The sample holder that was employed is illustrated in Chapter 3 (Figure 3.6). For some measurements, a Pyrex glass cell having a diameter of about 15 mm was used. Four organic compounds were studied: *p*-chlorophenyl-*N,N'*-dimethyl urea (Monuron, a herbicide), *p*-phenacetin, anthracene, and benzoic acid, in the temperature range of 250-400 K. The vapor-pressure curves of these compounds, in the range from $0.1 \cdot 10^{-6}$ Torr, are shown in Figure 4.49. The ΔH values calculated were: Monuron, 27.4; *p*-phenacetin 27.6; anthracene, 20.1; and benzoic acid, 20.7 kcal/mole.

Adolji ISO developed a method in which the Derivatograph could be used for vapor-pressure determinations. The method is similar to that discussed by Ashcroft (48).

5. Miscellaneous

Probably the most important characteristic of military and commercial explosives and solid rocket propellants is performance as related to end use and safety. Performance can be described by a variety of conventional properties such as thermal stability, shock sensitivity, friction sensitivity, explosive power, burning, or detonation rate, and so on. Thermal analysis methods, according to Maycock (51), show great promise for providing information on both these conventional properties and other parameters of explosive and propellant systems. The thermal properties have been determined mainly by TG and DTA techniques and isothermal or adiabatic constant-volume decomposition. Physical processes in pseudostable ma-

Table 4.10. Enthalpies of Sublimation of Various Compounds in kJ mole⁻¹ (48)

Compound	ΔH_{sub}	Temp. Range (K)	Literature (ΔH_{sub})	Lit Temp. Range(K)
Anthraquinone	105.9	335-355	112.0	298
			127	470-590
			106.1	428
1,4-Dihydroxyanthraquinone	94.5	324-351	103.5	408
1,8-Dihydroxyanthraquinone	96.5	335-356	105.9	405
1-Aminoanthraquinone	90.9	361-385	113.8	451
Benzoic acid	89.1	299-329	91.5	343-387
			100	420-480
			91.3	420-480
Thymol	69.0	229-312	67.0	273-313
Sc ^{III} (acac) ₃	97.2	335-361	159	445-555
			99.6	389
			49.8	377-387
Cr ^{III} (acac) ₃	85.9	335-355	125	490-595
			110.9	397
			27.8	189-397
Al ^{III} (acac) ₃	117.3 ^b	335-355	77.8	383-391
Fe ^{III} (acac) ₃	114.9	335-355	116	452-535
			99.0	391
			55.3	378-388
Co ^{III} (acac) ₃	85.3	335-361	23.4	393
Cu ^{II} (acac) ₂	106.1	335-361	57.3	378-393

^aacac refers to acetylacetonate.

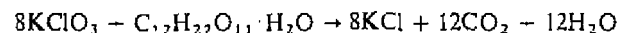
^bProbably a maximum value.

materials, which may be observed by DTA, can often be interpreted only with a knowledge of TG or gas evolution data.

The correct interpretation of the large amount of experimental data obtained by these techniques is a problem not to be taken lightly, since many important decisions relative to the use of a particular material may be based on these interpretations. It is obvious that these techniques can be used both for quality control and as an approach to the basic science of pseudostable materials.

TG and other TA techniques and their applications to cements and alloys have been reviewed by Baker (134). Gal et al. (135) described how the Derivatograph can be used to investigate the complex system of dust. The uses of TG and other TA techniques to archaeometry has been discussed by Bayer and Wiedemann (136).

Pyrotechnic compositions containing $KClO_3$ and lactose have been studied by TG and other TA techniques by Scanes (137). Oxidation of the lactose by the $KClO_3$ may be represented by the equation



REFERENCES

1. Gordon, S. and C. Campbell, *Anal. Chem.*, **32**, 271R (1960).
2. Duval, C. *Anal. Chem.* **23**, 1271 (1951).
3. Coats, A. W., and J. P. Redfern, *Analyst*, **88**, 906 (1963).
4. Lukaszewski, G. M., and J. P. Redfern, *Lab. Pract.*, 10,552 (1961).
5. Murphy, C. B., *Anal. Chem.*, **42**, 268R (1970).
6. Murphy, C. B., *Anal. Chem.*, **44**, 513R (1972).
7. Toursel, W., *Z. Chem.*, **7**, 265 (1967).
8. Duval, C., *Inorganic Thermogravimetric Analysis*, Elsevier, Amsterdam, 1953.
9. Duval, C., *Inorganic Thermogravimetric Analysis*, 2nd ed., Elsevier, Amsterdam, 1963.
10. Wendlandt, W. W., and J. P. Smith, *Thermal Properties of Transition Metal Ammine Complexes*, Elsevier, Amsterdam, 1967.
11. Wendlandt, W. W., in *Chelates in Analytical Chemistry*, H. A. Flaschka and J. A. Barnard, eds., Vol. 1, Marcel-Dekker, New York, 1967, Chap. 5.
12. Anderson, H. C., in *Techniques and Methods of Polymer Evaluation*, P. E. Slade and L. T. Jenkins, eds., Marcel-Dekker, New York, 1966, Chap. 3.
13. Doyle, C. D., in *Techniques and Methods of Polymer Evaluation*, P. E. Slade and L. T. Jenkins, eds., Marcel-Dekker, New York, 1966, Chap. 4.
14. Barrall, E. M., in *Guide to Modern Methods of Instrumental Analysis*, F. H. Guuw, ed., Wiley-Interscience, New York, 1972, Chap. 12.
15. Liptay, G., ed., *Atlas of Thermanalytical Curves*, Akademiai Kiado, Budapest, Vol. 1, 1971.

16. Reich, L., and S. S. Stivala, *Elements of Polymer Degradation*, McGraw-Hill, New York, 1971.
17. Palai, P. N., I. G. Sentyurin, and I. S. Sklyarenko, *Zh. Anal. Khim.*, **12**, 329 (1957).
18. Duval, C., Ref. 9, p. 84.
19. Duval, C., Ref. 9, Chap. VIII.
20. Peltier, S., and C. Duval, *Anal. Chim. Acta*, **1**, 345 (1947).
21. Simons, E. L., and A. E. Newkirk, *Talanta*, **11**, 549 (1964).
22. Duval, C., *Anal. Chim. Acta*, **13**, 32 (1955).
23. Newkirk, A. E., and I. Alfiferis, *Anal. Chem.* **30**, 982 (1958).
24. Dupuis, T., and C. Duval, *Anal. Chim. Acta*, **3**, 19 (1949).
25. Erdey, L., and F. Paulik, *Acta Chim. Acad. Sci. Hung.*, **7**, 45 (1955).
26. Milner, O. I., and L. Gordon, *Talanta*, **4**, 115 (1960).
27. Duval, C., Ref. 8, pp. 227-228.
28. Hoffman, I., M. Schnitzer, and I. R. Wright, *Chem. Ind. (London)*, **26** (1958).
29. Hoffman, I., M. Schnitzer, and I. R. Wright, *Anal. Chem.*, **31**, 440 (1959).
30. Mulvey, V. L., and C. D. Cavendish, *Analyst*, **95**, 304 (1970).
31. McCaleb, S. B., *Quesr* (Sun Oil Co.), **24** (1966).
32. Paulik, F., S. Gal, and L. Erdey, *Anal. Chim. Acta*, **29**, 381 (1963).
33. Biten, F. M., *Anal. Chem.*, **28**, 1133 (1956).
34. Rameshchandra, V. S., *Thermochim. Acta*, **2**, 41 (1971).
35. Erdey, L., F. Paulik, G. Svehla, and G. Liptay, *Z. Anal. Chem.*, **182**, 329 (1961).
36. Erdey, L., F. Paulik, G. Svehla, and G. Liptay, *Tafanw.*, **9**, 489 (1962).
37. Dupuis, T., and C. Duval, *Mikrochim. Acta*, **1**, 86 (1958).
38. Dupuis, T., and C. Duval, *Chim. Anal.*, **33**, 189 (1951).
39. Duval, C., *Anal. Chim. Acta*, **13**, 32 (1955).
40. Belcher, R., L. Erdey, F. Paulik, and G. Liptay, *Talanta*, **5**, 531 (1960).
41. Newkirk, A. E., and R. Laware, *Talanta*, **9**, 169 (1962).
42. Fock, J., *Some Applications of Thermal Analysis*, Mettler Instrument Corp., Griefensee, Switzerland, 1968.
43. Doyle, C. D., *Anal. Chem.*, **33**, 77 (1961).
44. Newkirk, A. E., *Proceedings of the First Toronto Symposium on Thermal Analysis*, H. G. McArdie, ed., Chemical Institute of Canada, Toronto, 1965, p. 33.
45. Chiu, J., in *Thermoanalysis of Fiberglass Fiber-Forming Polymers*, R. F. Schwenker, ed., Interscience, New York, 1966, p. 25.
46. David, D. L., *Insulation*, **13**, 38 (1967).
47. Williams, H. W., *Thermochim. Acta*, **1**, 253 (1970).
48. Ashcroft, S. L., *Thermochim. Acta*, **2**, 512 (1971).
49. Wiedemann, H. G., *Thermochim. Acta*, **1**, 355 (1972).
50. Adony, Z., *Period. Polytech.*, **10**, 325 (1966).
51. Maycock, J. N., *Thermochim. Acta*, **1**, 389 (1970).
52. Wendlandt, W. W., *Thermochim. Acta*, **10**, 101 (1974).
53. Duval, C., *Inorganic Thermogravimetric Analysis*, Elsevier, Amsterdam, 1953, p. 439.
54. Collins, L. W., E. K. Gibson, and W. W. Wendlandt, *Thermochim. Acta*, **11**, 177 (1975).
55. Tariq, S. A., and I. O. Hill, *J. Thermal Anal.*, **23**, 277 (1981).

56. Booth, J. S., D. Dollimore, and G. R. Heai, *Thermochim. Acta*, **39**, 281 (1980).
57. Clark, R. P., P. K. Gallagher, and B. M. Dillard, *Thermochim. Acta*, **33**, 141 (1979).
58. Judd, M. D., B. A. Plunkett, and M. I. Pope, *J. Thermal Anal.*, **6**, 555 (1974).
59. Judd, M. D., B. A. Plunkett, and M. I. Pope, *J. Thermal Anal.*, **9**, 83 (1976).
60. Smalley, I. J., G. O. Lill, S. P. Benley, and D. R. Wood, *Can. Mineral.*, **15**, 30 (1977).
61. Paulik, J., F. Paulik, E. Buzagh-Gere, and M. Arnold, *Thermochim. Acta*, **31**, 93 (1979).
62. Paulik, F., I. Paulik, E. Buzagh-Gere, and M. Arnold, *J. Thermal Anal.*, **15**, 271 (1979).
63. Buzagh-Gere, F., J. Szlatisz, and S. Gai, *J. Thermal Anal.*, **10**, 89 (1976).
64. Paulik, J., and F. Paulik, *Hung. Sci. Instrum.*, **34**, 15 (1976).
65. Collins, I. W., W. W. Wendlandt, and F. K. Gibson, *Thermochim. Acta*, **8**, 303 (1974).
66. Mahicu, B., D. J. Apers, and P. C. Capron, *J. Inorg. Nucl. Chem.*, **33**, 2857 (1971).
67. Beck, M. W., and M. J. Brown, *Thermochim. Acta*, **65**, 197 (1983).
68. Pysiak, I., and A. Glinka, *Thermochim. Acta*, **44**, 21 (1981).
69. Schmid, R. L., and J. Felsche, *Thermochim. Acta*, **59**, 1051 (1982).
70. Bayer, G., and H. G. Wiedemann, *Thermochim. Acta*, **11**, 79 (1975).
71. Wiedemann, H. G., E. Starzenegger, G. Bayer, and R. Wessicken, *Naturwissenschaften*, **61**, 65 (1974).
72. Wiedemann, H. G., and G. Bayer, *Topics in Current Chemistry*, Vol. 77, Springer-Verlag, Berlin, 1978, p. 122.
73. Wiedemann, H. G., and G. Bayer, *Z. Anal. Chem.*, **276**, 21 (1975).
74. Bayer, G., and H. G. Wiedemann, *Naturwissenschaften*, **62**, 181 (1975).
75. Bayer, G., and H. G. Wiedemann, *Sandoz Bull.*, **40**, 19 (1976).
76. Wiedemann, H. G., and G. Bayer, *Chem. Tech.*, Jun. 1977, p. 381.
77. Paulik, I., F. Paulik, and E. Czaran, *Anal. Chim. Acta*, **101**, 409 (1978).
78. Gallagher, P. K., and J. P. Luongo, *Thermochim. Acta*, **12**, 159 (1975).
79. Cavell, K. J., C. G. Sceney, J. O. Hill, and R. J. Magee, *Thermochim. Acta*, **5**, 319 (1973).
80. Sceney, C. G., J. O. Hill, and R. J. Magee, *Thermochim. Acta*, **11**, 301 (1975).
81. Bratspies, G. K., J. F. Smith, J. O. Hill, and R. J. Magee, *Thermochim. Acta*, **19**, 335 (1977).
82. Bratspies, G. K., J. F. Smith, J. O. Hill, and R. J. Magee, *Thermochim. Acta*, **19**, 349 (1977).
83. Bratspies, G. K., J. F. Smith, J. O. Hill, and R. J. Magee, *Thermochim. Acta*, **19**, 361 (1977).
84. Bratspies, G. K., J. F. Smith, and J. O. Hill, *Thermochim. Acta*, **19**, 373 (1977).
85. Bratspies, G. K., J. F. Smith, J. O. Hill, and R. J. Magee, *Thermochim. Acta*, **27**, 307 (1978).
86. Salas-Peregrin, J. M., E. Colacio-Rodriguez, J. D. Lopez-Gonzalez, and C. Valenzuela-Calahorra, *Thermochim. Acta*, **63**, 145 (1983).
87. Yoshikuni, T., R. Tsuchiya, A. Uehara, and E. Kyuuo, *Bull. Chem. Soc. Jpn.*, **51**, 113 (1978).
88. Veno, H., A. Uehara, and R. Tsuchiya, *Bull. Chem. Soc. Jpn.*, **54**, 1821 (1981).

89. Tsuchiya, R., A. Uehara, and T. Yoshikuni, *Inorg. Chem.*, **21**, 590 (1982).
90. Ihara, Y., E. Izumi, A. Uehara, R. Tsuchiya, S. Nakagawa, and F. Kuno, *Bull. Chem. Soc. Jpn.*, **55**, 1028 (1982).
91. Moran-Miguelez, E., and J. A. Alario-Franco, *Thermochim. Acta*, **60**, 81 (1983).
92. Dunn, J. G., and C. E. Kelly, *J. Thermal Anal.*, **12**, 43 (1977).
93. Gallagher, P. K., and W. R. Sinclair, *Isr. J. Chem.*, **22**, 222 (1982).
94. Day, K. F., *Am. Lab.*, Jan. 1975, p. 10.
95. Radecki, A., and M. Wesolowski, *J. Therm. Anal.*, **17**, 73 (1979).
96. Wesolowski, M., *Mikrochim. Acta*, **199** (1980).
97. Wendlandt, W. W., and L. W. Collins, *Thermochim. Acta*, **71**, 411 (1974).
98. Wendlandt, W. W., *Thermochim. Acta*, **10**, 93 (1974).
99. Cook, L. E., and H. Idebrand, *Thermochim. Acta*, **9**, 129 (1974).
100. Cassel, R., and A. P. Gray, *Thermochim. Acta*, **36**, 265 (1980).
101. Cassel, R., and A. P. Gray, *Plast. Eng.*, **33**, 5 (1977).
102. Charsley, E. L., and J. G. Dunn, *Plast. Rubber Process. Appl.*, **1**, 3 (1981).
103. Dunn, J. G., *Tech. Inform. Sheet No. 114*, Slanton Redcroft, London.
104. Blaine, R. L., *Educational Seminar*, Palo Alto, CA, June 28, 1974, Du Pont Co., Wilmington, DE.
105. Brennan, W. P., and R. B. Cassel, *Thermal Analysis Application Study 25*, Perkin-Elmer Corp., Norwalk, CT.
106. Brennan, W. P., *Thermal Analysis Application Study 26*, Perkin-Elmer Corp., Norwalk, CT.
107. DiYolo, M. P., W. P. Brennan, C. M. Earnest, and R. L. Fyans, *Pittsburgh Conf. Paper No. 972*, Atlantic City, N.J., March 1983.
108. Breakey, N. W., and R. B. Cassel, *Thermal Analysis Application Study 29*, Perkin-Elmer Corp., Norwalk, CT.
109. Dion, J. G., *Tech. Inform. Sheet No. 130*, Stanton Redcroft, London.
110. Pekenc, E., and J. H. Sharp, *Proc. 4th Int. TA. I. Buzas, ed.*, Vol. 2, Akademiai Kiado Budapest, 1975, p. 85.
111. Earnest, C. M., *Thermal Analysis Application Study 3D*, Perkin-Elmer Corp., Norwalk, CT.
112. Earnest, C. M., *Thermal Analysis Application Study 31*, Perkin-Elmer Corp., Norwalk, CT.
113. Selmecci, B., *Hung. Sci. Instrum.*, **21**, 39 (1971).
114. Paulik, I., F. Paulik, and M. Arnold, *J. Thermal Anal.*, **25**, 327 (1982).
115. Paulik, F., I. Paulik, R. Naumann, K. Kohnke, and D. Petzold, *Thermochim. Acta*, **64**, 1 (1983).
116. Naumann, R., K. Kohnke, P. Paulik, and F. Paulik, *Thermochim. Acta*, **64**, 15 (1983).
117. Mackenzie, R. C., and S. Caljere, "5011 Components, Vol. 2, Inorganic Components," J. E. Gieseking, ed., Springer, New York, 1975, Chap. 16, 529.
118. Rosenfeld, R. J., J. B. Dubow, and K. Rajeshwar, *Thermochim. Acta*, **53**, 321 (1982).
119. Rajeshwar, K., *Thermochim. Acta*, **63**, 97 (1983).
120. Earnest, C. M., *Thermochim. Acta*, **58**, 271 (1982).
121. Rosenfeld, R. J., K. Rajeshwar, and J. B. Dubow, *Thermochim. Acta*, **57**, 1 (1982).

122. Fyans, R. L., *Thermal Analysis Application Study 21*, Perkin-Elmer Corp., Norwalk, CT.
123. Sadek, F. S., and A. Y. Herrell, *Am. Lab.*, 16, 75 (1984).
124. Earnest, C. M., and R. L. Fyans, *Thermal Analysis Application Study 32*, Perkin-Elmer Corp., Norwalk, CT.
125. Hassel, R. L., *Thermal Analysis Application Brief No. TA-54*, Du Pont Co., Wilmington, DE.
126. Serageldin, M. A., and W. P. Pan, *Thermochim. Acta*, 71, 1 (1983).
127. Cassel, B., W. P. Brennan, and R. L. Fyans, unpublished results, Perkin-Elmer Corp., March 1978.
128. Earnest, C. M., *Thermochim. Acta*, 60, 171 (1983).
129. Rosenfold, R. L., J. B. Dubow, and K. Rajeshwar, *Thermochim. Acta*, 58, 325 (1982).
130. Dunn, I. G., *Tech. Inform. Sheet No. 103*, Stanton Redcroft, London.
131. Gallagher, P. K., D. W. Johnson, and F. Schrey, *Mater. Res. Bull.*, 9, 1345 (1974).
132. Vogel, E. M., D. W. Johnson, and P. K. Gallagher, *J. Am. Ceram. Soc.*, 60, 31 (1977).
133. Pati, S. B., A. Bandyopadhyay, D. K. Chakrabarty, and H. V. Keer, *Thermochim. Acta*, 61, 269 (1983).
134. Baker, K. F., *Am. Lab.*, Jan. 1978, 51.
135. Gal, S., F. Paulik, E. Pell, and H. Puxbaum, *Z. Anal. Chem.*, 282, 291 (1976).
136. Bayer, G., and H. G. Wiedemann, *Thermochim. Acta*, 69, 167 (1983).
137. Scanes, F. S., *Combust. Flame*, 23, 363 (1974).
138. Wendlandt, W. W., *Anal. Chem.*, 54, 97R-105R (1982).
139. Wendlandt, W. W., *Anal. Chem.*, 56, 250R-261R (1984).
140. Daniels, T., *Thermal Analysis*, Kogan Page, London, 1973.
141. Keatch, C. L., and D. Dollimore, *Introduction to Thermogravimetry*, 2nd ed., Heyden, London, 1975.
142. Paulik, F., and I. Paulik, "Simultaneous Thermoanalytical Examinations by Means of the Derivatograph," in Wilson and Wilson's *Comprehensive Analytical Chemistry*, G. Svehla, ed., Vol. XII, Part A, Elsevier, Amsterdam, 1982.
143. Wiedemann, H. G., *Mettler Technique Series, Tech. Bull. No. T-103*.
144. Brown, G. P., D. T. Haarr, and M. Metlay, *Proc. 9th Electron. Insul. Conf., IEEE* 32, C3-23, t60 (1965).
145. Brown, G. P., D. T. Haarr, and M. Metlay, *Thermochim. Acta*, 1, 441 (1970).

CHAPTER

5

DIFFERENTIAL THERMAL
ANALYSIS AND DIFFERENTIAL
SCANNING CALORIMETRY

A. BASIC PRINCIPLES OF DTA/DSC

1. Introduction

Differential thermal analysis (DTA) is a thermal technique in which the temperature of a sample, compared with the temperature of a thermally inert material, is recorded as a function of the sample, inert material, or furnace temperature as the sample is heated or cooled at a uniform rate. Temperature changes in the sample are due to endothermic or exothermic enthalpic transitions or reactions such as those caused by phase changes, fusion, crystalline structure inversions, boiling, sublimation, and vaporization, dehydration reactions, dissociation or decomposition reactions, oxidation and reduction reactions, destruction of crystalline lattice structure, and other chemical reactions. Generally speaking, phase transitions, dehydration, reduction, and some decomposition reactions produce endothermic effects, whereas crystallization, oxidation, and some decomposition reactions produce exothermic effects.

The temperature changes occurring during these chemical or physical changes are detected by a *differential* method, such as is illustrated in Figure 5.1. If the sample and reference temperatures are T_s and T_r , respectively, then the difference in temperature, $T_s - T_r$, is the function recorded. Perhaps a better name for this technique would be *differential/thermometry*; the term "differential thermal analysis" implies that it has something to do with analysis, which, as with any other analytical technique, may or may not be the case. In *thermal analysis* (another misnomer?), the temperature of the sample T_s , is recorded as a function of time (see Chapter 10), and a heating or cooling curve is recorded. Small temperature changes occurring in the sample are generally not detected by this method. In the *differential* technique, since the detection thermocouples are opposed to each other, small differences between T_s and T_r can be detected with the appropriate voltage amplification devices. Thus, small samples (down to several μg in mass)

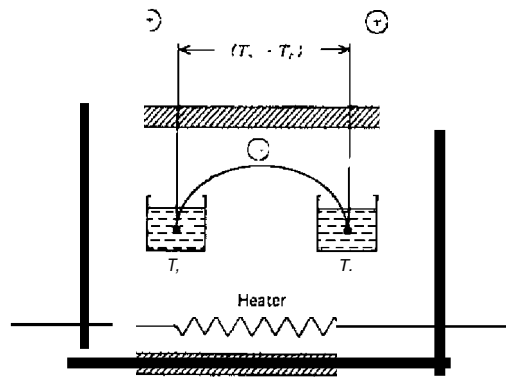


Figure 5.1. Basic OTA system.

may be employed and are, as a matter of fact, more desirable.

A comparison between the two techniques is shown in Figure 5.2. In parts (a) and (b), the sample temperature is recorded as a function of time as the system temperature is increased at a linear rate. However, the difference between the curves in (a) and (b) is that no enthalpic transition takes place in the sample in (a), while in (b) exothermic and endothermic changes occur. Since no other temperature changes take place in the sample in (a), no deviation from the linear temperature rise is detected in the sample temperature. However, in (b) deviations occur at the procedural initial reaction temperature, T_i , due to temperature changes caused by endothermic or exothermic changes. These changes are essentially completed at T_f and the temperature of the sample returns to that of the system. In the curves in (c), the difference in temperature, $T_s - T_f$, is recorded as a function of system temperature, T . At T_i , the curve deviates from a horizontal position to form a peak in either the upward or the downward direction, depending on the enthalpic change. The completion of the reaction temperature, T_f , does not occur at the maximum or minimum of its curve but rather at the high-temperature side of the peak. Its exact position depends on the instrumental arrangement. Thus, in the differential method, small temperature changes can be easily detected while the peak area is proportional to the enthalpic change ($\pm \Delta H$) and sample mass.

A typical DTA curve is illustrated in Figure 5.3. Four types of transitions are illustrated: (I) second-order transition in which a change in the horizontal baseline is detected; (II) an endothermic curve peak caused by a fusion or

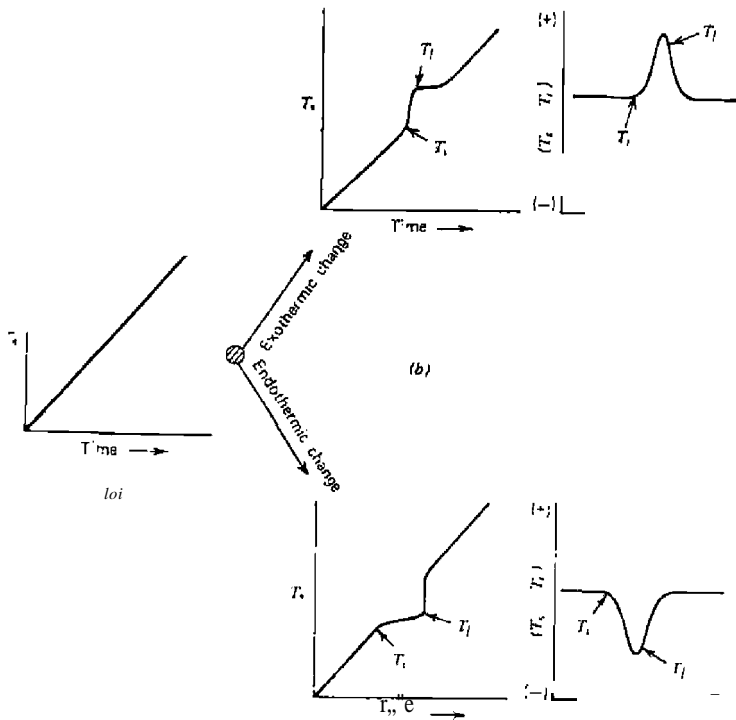


Figure 5.2. Comparison between thermal analysis and differential thermal analysis.

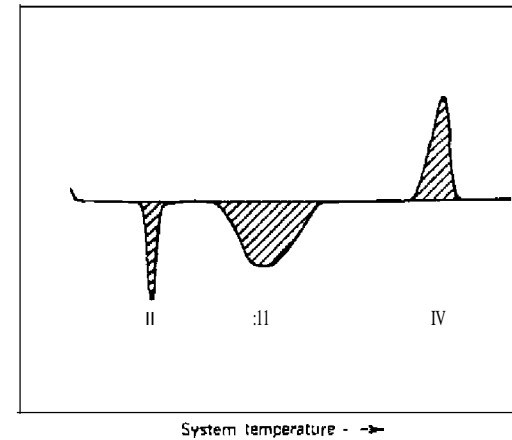


Figure 5.3. Typical OTA curve.

melting transition; (III) and endothermic curve peak due to a decomposition or dissociation reaction; and (IV) an exothermic curve peak caused by a crystalline phase change. The number, shape, and position of the various endothermic and exothermic peaks with reference to the temperature may be used as a means for the qualitative identification of the substance under investigation. Also, since the area under the peak is proportional to the heat change involved, the technique is useful for the semiquantitative or, in some cases, quantitative determination of the heat of reaction. Since the heat of reaction is proportional to the amount of reacting substance, DTA can be used to evaluate quantitatively the amount of substance present if the heat of reaction is known. Thus, the technique finds much use in the qualitative and semiquantitative identification of organic and inorganic compounds, clays, metals, minerals, fats and oils, polymeric materials, coal and shales, wood, and other substances. It can also be used to determine the radiation damage of certain polymeric materials, the amount of radiation energy stored in various minerals, heats of adsorption, effectiveness of catalytic materials, heats of polymerization, and others. Quantitatively, it can be used for the determination of a reactive component in a mixture, or the heat of reaction involved in physical or chemical changes.

2. Historical Aspects

The history of differential thermal analysis and differential scanning calorimetry, as well as thermal analysis, has been described in great detail by Mackenzie (10.11).

Numerous review articles, book chapters, and books have appeared on the techniques of DTA/DSC. Murphy has written biennial reviews on the subject from 1958 to 1982 (25, 26) when it was taken over by Wendlandt (12, 13). Book chapters and/or books includes those by Smothers and Chiang (27, 28), Wendlandt (23, 24), Garu (29), Mackenzie (30), Gordon and Campbell (32, 33), Kissinger and Newman (31), Barrall and Johnson (34), David (35), Barrall (36), Schultze (37), Ramachandran (38), Wunderlich (39), Porter and Johnson (40,41), Schwenker and Gam (42), Smykatz-Kloss (4), Pope and Judd (5), Paulik and Paulik (6), Jespersen (7), Sestak (8), and others. A bibliography of all the books written on DTA/DSC and other TA techniques since 1937 has been compiled by Lombardi (9).

3. Theoretical Aspects

There have been a number of different theories concerning the theoretical interpretation of the DTA curve. All the theories relate, in some manner, the area of the differential curve peak to the various parameters of the sample

and apparatus. The equations representing these parameters were developed through the use of conventional heat transfer relationships and the geometry of the sample and sample holder. The derivation of each of these theories is beyond the scope of this discussion, so only the final mathematical expressions will be presented.

In the theory developed by Speil et al. (2) and modified by Kerr and Kulp (3), the area enclosed by the differential curve is

$$\frac{m(\Delta H)}{gk} = \int_{t_1}^{t_2} \Delta T dt \quad (5.1)$$

where m is the mass of reactive sample, ΔH is the heat of reaction, θ is a geometrical shape constant for the apparatus, k is the thermal conductivity of the sample, ΔT is the differential temperature, and t_1 and t_2 are the integration limits of the differential curve. This expression is perhaps one of the simplest and relates the heat of reaction of the sample to the peak area through use of the proportionality constants or near-constants, θ and k . It neglects the differential terms and the temperature gradients in the sample and also considers the peak area to be independent of the specific heat of the sample. It is basically only an approximate relationship.

Voigt (143) derived the expression

$$\frac{\Delta H}{C_s} \left(\frac{df}{dt} \right) = \left(\frac{dY}{dt} \right) + A(r - Ys) \quad (5.2)$$

where C_s is the heat capacity of the cell plus its contents, f is the fraction of the sample transformed at any time t , ψ is the differential temperature, Y_s is the steady-state value of the differential temperature achieved a sufficiently long time after the initial condition $Y = Y_l$ at $t = t_1$, and A is a constant.

The inherent limitations of this theory are: (1) the assumption of a constant value of the heat capacity of the sample and (2) the assumption that the sample temperature is uniform throughout at each time instant. The heat capacity of the sample is that of the cell plus that of the transformed amount of the sample plus that of the untransformed amount. These amounts change during the course of the reaction. Thus, in practice, if the heat capacity of the cell is made large, this fluctuation is considered minor, although sensitivity is reduced. The nonuniformity of the sample temperature is not considered important enough to vitiate the method, although it does affect the transformation temperature rather than the calculation of the heat effects. Reduction of the heating rate, measurement of the sample temperature at its outside surface nearest the furnace wall, and various extrapolation procedures all reduce the error but do not eliminate it entirely (4).

Using a sample block constructed from an infinitely-high-thermal-conductivity metal such as nickel, in which the sample holder geometry is a cylinder, Boersma (44) found that the peak area was equal to

$$\int_{t_1}^{t_2} \Delta T dt = \frac{qa^2}{4\lambda} \quad (5.3)$$

where t_1 and t_2 are the times at the beginning and end of the peak, q is the heat of transformation per unit volume, ΔT is the differential temperature, a is the radius of the cavity filled with sample, and λ is the thermal conductivity of the sample material.

For a spherical metal sample container

$$\int_{t_1}^{t_2} \Delta T dt = \frac{qa^3}{6\lambda} \quad (5.4)$$

and for a one-dimensional case of a flat plate

$$\int_{t_1}^{t_2} \Delta T dt = \frac{qa^2}{2\lambda} \quad (5.5)$$

Lastly, for an infinitely large ceramic block, there are no finite solutions for the one- and two-dimensional cases; however, there is a solution for a spherical bolder:

$$\int_{t_1}^{t_2} \Delta T dt = \frac{qa^2}{6} \left(\frac{2}{\lambda_c} + \frac{1}{\lambda_s} \right) \quad (5.6)$$

where λ_c is the thermal conductivity of the ceramic material and λ_s is the thermal conductivity of the sample.

In the preceding equations as applied to a conventional DTA apparatus, the sample is used for two entirely different purposes: (1) as a producer of heat and (2) as a heat measuring resistance in which the flow of heat develops a temperature difference to be measured. To separate these two functions, Boersma (44) recommended the use of meta; sample and reference cups in which the temperature difference was measured from outside the sample and reference materials. The peak area then depended on the heat of reaction by

$$\int_{t_1}^{t_2} \Delta T dt = \frac{mq}{G} \quad (5.7)$$

where m is the mass of the sample, and G is the heat transfer coefficient between the nickel cup and the surrounding nickel shield. Although no data were presented, Boersma (44) claimed that measurements on the dehydration of $\text{CuSO}_4 \cdot 5\text{H}_2\text{O}$ confirmed equation (5.7) quantitatively. The samples were said to differ widely in packing density.

Lukaszewski, in a series of 11 papers, discussed the complex heat transfer problem in various types of DTA systems (45-55). These problems were simplified into three categories (53):

1. Heat transfer between the heat source (furnace wall or heater) and the block calorimeter by conductive, convective, and radiative mechanisms.
2. Heat conduction between the block calorimeter and some medium within it (reference or sample materials).
3. The active sample in the system may periodically undergo heat-absorbing (endothermic) or heat-generating (exothermic) phenomena as functions of time, temperature, and position in the medium. These involve complex heat transfer between the sample and the calorimeter under conditions where the physical properties of the sample are undergoing rapid change.

The main problems, those of (2) and (3), can be represented mathematically as

$$C_s \phi_s \left(\frac{\partial T}{\partial t} \right)_s = \text{div } k_s \text{ grad } T + A_s(P, t) \quad (5.8)$$

where C_s and ϕ_s are the specific heat and density of sample, respectively; the heat absorption or generation term can be represented as

$$A(P, t) = Qb(1-x)^n \quad (5.9)$$

where Q is the heat of reaction, b is the velocity constant ($2 \exp(-E/RT)$, x is the fraction of sample transformed, and n is the order of reaction. Imposing the condition that k_s is position- and temperature-independent, equation (5.8) reduces to

$$\left(\frac{\partial T}{\partial t} \right)_s = d_s \nabla^2 T + \frac{A_s(P, t)}{C_s} \quad (5.10)$$

where d_s is the thermal diffusivity of the sample and C_s is the heat capacity of

the sample per unit volume. Similarly, for the reference material, which exhibits no heat absorption or generation effects [so that $A/P, t) = 0$], equation (5.10) becomes

$$\left(\frac{\partial T}{\partial t}\right)_r = d_r \nabla^2 T \quad (5.11)$$

where d_r is the thermal diffusivity of the reference material.

The heat transfer problem for a DTA system containing ring thermocouples has been treated by David (56, 57). In order to obtain a mathematical expression for C_p , the heat capacity of the sample (or reference), one must consider two factors: (1) the effects of the system on the differential thermocouple and (2) the effects of the system plus sample on the differential thermocouple. The heat capacity of the sample holder containing a sample which is undergoing exothermic or endothermic changes can be expressed as

$$C_{p,s} dT_s = K_s (T_s - T_2) dt + dH \quad (5.12)$$

and for the reference side

$$C_{p,r} dT_r = K_r (T_r - T_1) dt \quad (5.13)$$

where T_1 is the reference temperature and a_r is the thermal diffusivity of the thermocouples, respectively, and $C_{p,s}$ and $C_{p,r}$ are the total heat capacities of the sample holder and sample and the reference holder and reference material, respectively.

Pacor (58) derived an expression for the relationship between the area of a DTA curve peak and the total amount of heat produced or absorbed for the DuPont DTA block-type sample holder. For the reference, which is not subject to chemical reaction,

$$\frac{1}{a_r} \left(\frac{\partial T_r}{\partial t}\right) = \nabla^2 T_r \quad (5.14)$$

where T_r is the reference temperature and a_r is the thermal diffusivity of the reference. Likewise, for the sample, in which chemical reaction (or transition) can occur,

$$\frac{1}{a_s} \left(\frac{\partial T_s}{\partial t}\right) = \nabla^2 T_s + \frac{1}{\lambda} q \quad (5.15)$$

where T_s is the sample temperature, a_s is the thermal diffusivity of the sample,

t is the thermal conductivity, and Q is transition heat per unit volume. Introducing the differential temperature, ΔT , and multiplying both sides by de and integrating over a time interval large enough to make all the transient terms negligible, the following expression is obtained:

$$\int_{t_1}^{t_2} \left(\frac{1}{a_s} \frac{\partial T_s}{\partial t} - \frac{1}{a_r} \frac{\partial T_r}{\partial t} \right) de = \nabla^2 \int_{t_1}^{t_2} \Delta T dt + \frac{Q}{\lambda} \quad (5.16)$$

The peak area in DTA is the area enclosed by the curve line and the baseline, so the area between the zero line and the baseline must be subtracted; thus,

$$\int_{t_1}^{t_2} \Delta T dt = \int_{t_1}^{t_2} \left(\frac{1}{a_s} \frac{\partial T}{\partial t} - \frac{1}{a_r} \frac{\partial T_r}{\partial t} \right) de \quad (5.17)$$

Subtracting equation (5.17) from equation (5.16) and defining the heating rate, $\alpha = dT/dt$,

$$\nabla^2 \int_{t_1}^{t_2} (\Delta T - \Delta T^1) dt = \frac{Q}{\lambda} = \nabla^2 \frac{S}{2} \quad (5.18)$$

where S is the surface of the peak. In the case of a cylinder of infinite length, with the boundary condition $\nabla^2 T = 0$ for $r = R$ (thus $S = 0$), the solution with the thermocouple in the center is

$$S = \frac{\alpha R^2}{4} \frac{Q}{\lambda} = \frac{\alpha R^2}{4} \frac{Q_w \rho}{\lambda} \quad (5.19)$$

where R is the radius of the sample holder, Q_w is the transition heat per unit mass, and ρ is the density.

The temperature distribution within the sample and the influence of the sample parameters on the DTA curve has been discussed in detail by Melling et al. (59). The temperature distribution in the sample obeys the well-known diffusion equation

$$\frac{\partial T}{\partial t} - \nabla^2 T = \frac{\alpha}{K} \frac{\partial q}{\partial t} \quad (5.20)$$

where $\alpha = K/\rho c$, and ρ is the density, c the specific heat, K the thermal conductivity, and $\partial q/\partial t$ the rate of internal heat generation per unit volume,

If the sample has the form of a cylinder of radius r and length l , then

$$\nabla^2 T = \frac{\partial^2 T}{\partial r^2} + \frac{1}{r} \frac{\partial T}{\partial r} - \frac{1}{r^2} \frac{\partial^2 T}{\partial \theta^2} + \frac{\partial^2 T}{\partial z^2} \quad (5.21)$$

If it is assumed that the distribution of temperature of the outer surface of the sample is independent of position, that is, far from the ends of the cylinder, then equation (5.16) reduces to

$$\nabla^2 T = \frac{1}{r} \left[\frac{\partial}{\partial r} \left(r \frac{\partial T}{\partial r} \right) \right] \quad (5.22)$$

Further use is made of these and other equations in a later section of this chapter.

A general theory for describing DTA curves (and DSC and TG) was developed by Gray (60) which employs the same initial equations and assumptions as previously discussed (43, 44) and others. The essential components of a thermal analysis cell are shown schematically in Figure 5.4. They consist of the sample and its container, at temperature T_s ; a source of heat energy, at temperature T_p ; and a path having a certain thermal resistance, R , through which the heat energy flows to or from the sample at a rate of dq/dt . It is assumed that (1) the sample temperature, T_s , is uniform and equal to that of the container; (2) the total heat capacity of the sample plus container, C_s , and the controlling thermal resistance, R , are constant over the temperature range of interest; and (3) the heat generated by the sample per unit time, dH/dt , is positive, and the heat absorbed is negative.

At any instant, the sample is generating heat at a rate dH/dt . Heat gene-

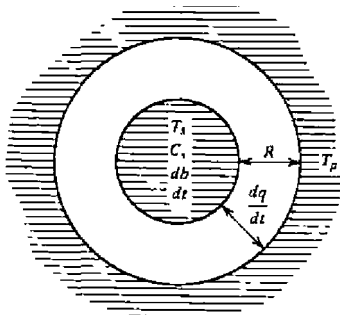


Figure 5.4. Schematic diagram of a thermal analysis cell (60).

rated by the sample can either increase the sample temperature or be lost to the surroundings. Since heat must be conserved, the sum of these two effects must equal dH/dt . Therefore,

$$\frac{dH}{dt} = C_s \left(\frac{dT_s}{dt} \right) + \frac{dq}{dt} \quad (5.23)$$

The rate of heat loss to the surroundings is controlled by the thermal resistance and the temperature difference between the sample and surroundings. According to Newton's Law,

$$\frac{dq}{dt} = \frac{T_p - T_s}{R} \quad (5.24)$$

and, substituting into equation (5.13), we have

$$\frac{dH}{dt} = C_s \left(\frac{dT_s}{dt} \right) + \frac{T_p - T_s}{R} \quad (5.25)$$

In a DTA apparatus, two cells as used as illustrated except one of them is the reference, where $dH/dt = 0$. Writing an equation similar to equation (5.25), we can express the instantaneous rate of heat generation by the sample as

$$R \left(\frac{dH}{dt} \right) = (C_s - C_r)(T_p - T_s) + RC_s \left(\frac{dT_s}{dt} \right) + RC_r \left(\frac{dT_r}{dt} \right) \quad (5.26)$$

It is assumed that R for the reference cell is the same as that for the sample cell. The heat capacity of the reference, C_r , will not be equal to that of the sample, C_s . The heating rate for the reference, dT_r/dt , is the same as that for the sample, dT_s/dt , and is therefore a constant.

From equation (5.26), at any time, RdH/dt can be considered as the sum of three terms in units of temperature (see Figure 5.5):

- Part (I): $T_s - T_r$, which is the differential temperature of the recorded curve.
- Part (II): $R(C_s - C_r)(dT/dt)$, which is the baseline displacement from the zero level.
- Part (III): $RC_s d[(T_s - T_r)/dt]$, which is the slope of the curve at any point multiplied by a constant, RC_s . The term RC_s is called the time constant of the system and has the units of time.

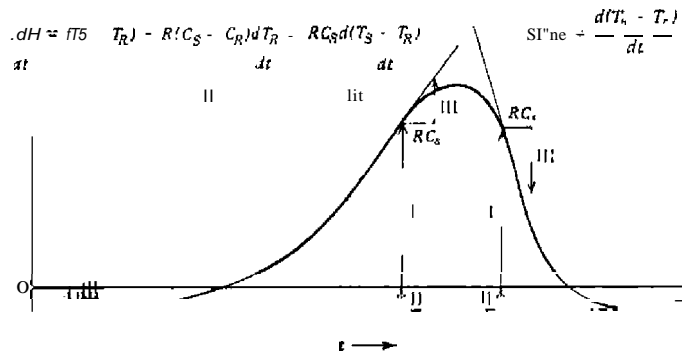


Figure 5.5. Determination of $R \frac{dT}{dr}$ from a DTA curve (60).

At any point on the curve,

$$R \left(\frac{dH}{dt} \right) = I + II + III \quad (5.27)$$

or if the tangent has a negative slope,

$$R \left(\frac{dH}{dt} \right) = I - II - III \quad (5.28)$$

Thus, knowing RC_s , a curve can be graphically constructed which directly reflects the instantaneous thermal behavior of the sample.

The theory of the Perkin-Elmer calorimeter has been presented by O'Neill (129), Gray (60), and Flynn (134), while that of the DuPont and Stone instruments has been discussed by Baxter (130) and David (131), respectively. The theory of the latter two instruments has been discussed previously in this chapter.

Using the DSC curve in Figure 5.6, Gray (60) developed the basic equation relating dH/dt to the measured quantities, as in the case of DTA.

$$\frac{dH}{dt} = - \frac{dq}{dt} + (C_s - C_r) \frac{dT_p}{dt} - RC_s \frac{d^2q}{dt^2}$$

The expression for dH/dt again involves the sum of three terms, as was described in the DTA theory. Two differences are noted between DSC and DTA: (1) the thermal resistance, R , occurs only in the third term in the equation and (2) the area under the curve peak is $\Delta q = - \Delta H$. A calibration

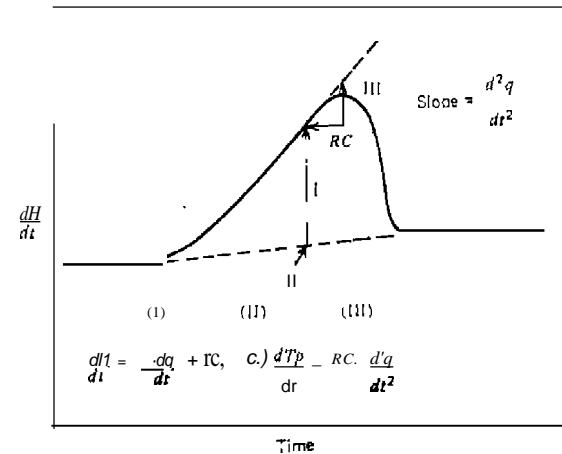


Figure 5.6. Application of equation (5.86) to a DSC curve (60).

coefficient is still required, but it is used to convert area to calories and is an electrical conversion factor rather than the thermal constant used in DTA.

A somewhat more sophisticated treatment is that given by Flynn (134) which concerns three critical parameters of the DSC curve:

1. The steady slope of the curve caused by a linearly increasing temperature increment and proportional to an interfacial conductivity term.
2. An onset temperature of the transition, T_i , obtained from the intersection of this slope with the baseline.
3. A decay constant, k_i , back to the baseline at the completion of the transition.

The slope of the curve can be described by Newton's law of cooling,

$$\frac{dq}{dt} = Ah(T_2 - T_1) \quad (5.30)$$

where h is the interfacial thermal conductivity, A is the area of the interface, and $T_2 - T_1$ is the temperature difference between the sample and the holder. The temperature of the sample, T_1 , is described by

$$T_1 = T_0 + \frac{1}{mc} \int \frac{dq}{dt} dt \quad (5.31)$$

where T_0 is the initial temperature, m is the sample mass, and e is the heat capacity of the sample. At a transition, T_i will remain at the transition temperature, T_i , for a residence time, t_i , determined from

$$\int_0^{t_i} \frac{dq}{dt} dt = m \Delta H_i \quad (5.32)$$

where ΔH_i is the heat of transition.

From these equations, for a constant heat capacity, the steady slope during the melting transition is

$$\text{slope} = j\beta hA = k_m \beta cm \quad (5.33)$$

The onset temperature, T_i , is

$$T_i = T_m + \frac{\beta cm}{hA} = T_m + \frac{\beta}{k_m} \quad (5.34)$$

and the decay constant at the termination of the transition is

$$\text{decay constant} = \frac{hA}{em} = k_m \quad (5.35)$$

In DSC curves it is usually assumed that the rate of change of the reference material temperature is equal to the programmed temperature. Brennan et al. (135) have considered this problem mathematically and found that the rate of change is controlled by the time constant of the reference material. If the time constant is about 1 sec, the assumption is valid after a few seconds. However, if it is much larger, the assumption will not apply.

Claudy et al. (14, 15) used an electrical analog model of a heat flux DSC apparatus with the numerical values of the resistors computed using a Mettler TA 2000B DSC apparatus.

A model system for DSC was developed by Flynn (16) in which the electronic response of the instrument is coupled with the heat flow across an interface. Equations are derived that relate the time constants for this two-step process with the thermal properties of the sample and the amplitudes, areas, slopes, and dwell time of the DSC curves. Flynn (17) has also developed a simple theory to utilize DSC for the determination of heat capacities, glass transition, and enthalpies of transition.

Shishkin (18) developed an equation on the role of the reference material in DTA. Two cases are presented: first the time constants of the sample and reference material cells do not change in the course of the experiment and (2)

these constants change continuously during the course of the

An analysis of differential and average heater power control a thermal transition in DSC was made by O'Neill (19). The heater power is uninfluenced by the average temperature control system applicable equally to exothermic or endothermic transitions.

4. Factors Affecting the DTA/DSC Curve

Differential thermal analysis, since it is a dynamic temperature measurement, has a large number of factors which can affect the resulting curves. These factors, which are similar to those discussed in gravimetry (Chapter 2), are more numerous in DTA and can have a pronounced effect on the curve. If the DTA curve is used for quantitative purposes, the shape, position, and number of endothermic or exothermic peaks is important. By a simple change of conditions, such as furnace atmosphere, the positions (with reference to the baseline) can be changed, and perhaps the number of curve peaks as well. For quantitative studies, the area enclosed by the curve is of interest, so the effect of the experimental parameters on the area must be known. When DTA is used for specific heat measurements, deviations become important and such conditions as particle size and diluent, system symmetry, sample packing, and so on must be accounted for if accurate and reproducible results are to be obtained.

A generalized DTA curve which will be used for purposes of illustration is shown in Figure 5.7. An endothermic peak is illustrated

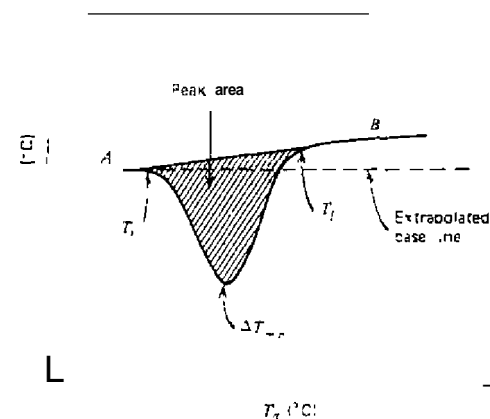


Figure 5.7 Generalized DTA curve

pretransition (or prereaction) baseline, B is the posttransition baseline, T_i is the procedural initial deviation temperature which the instrument can detect, ΔT_{min} is the procedural peak minimum temperature, and T_f is the procedural final temperature of the curve peak. For the temperature axis, T_n is the temperature of the reference (T_r), sample (T_s), or furnace (external) (T_a). The Y axis is that of the differential temperature, $T_s - T_r$ or ΔT .

As with the technique of thermogravimetry, the DTA curve is dependent on two general categories of variables: (i) instrumental factors and (ii) sample characteristics. The former category includes:

1. instrumental factors.
 - a. Furnace atmosphere.
 - b. Furnace size and shape.
 - c. Sample-holder material.
 - d. Sample-holder geometry.
 - e. Wire and bead size of thermocouple junction.
 - f. Heating rate.
 - g. Speed and response of recording instrument.
 - h. Thermocouple location in sample.

whereas the latter consists of

2. Sample characteristics.
 - a. Particle size.
 - b. Thermal conductivity.
 - c. Heat capacity.
 - d. Packing density.
 - e. Swelling or shrinkage of sample.
 - f. Amount of sample.
 - g. Effect of diluent.
 - h. Degree of crystallinity.

a. Heating Rate

Although the effects of heating rate on the ΔT_{min} temperatures and peak areas have been known for a number of years, only recently have these changes been explained in detail. In general, an increase in heating rate, say, from 2 to 20°C/min, will increase the T_i , ΔT_{min} , and T_f temperatures. As for peak area, the effect of heating rate depends on the T_n temperature used. If $T_s - T_r$ is plotted against T_s , the peak area will be proportional to the heating rate if the latter remains constant during the reaction (59), if

the peak area is measured as $T_f - T_i$ versus time, then it is independent of heating rate. The conclusion reached by Garn (61) that the area of the peak increases with heating rate because of "the problem of heat transfer" was not substantiated by Melling et al. (59). A higher heating rate will also decrease the resolution of two adjacent peaks, thereby obscuring one of the peaks. At very low heating rates, the peak areas become very small or nonexistent on certain types of instruments, depending on the type of sample holder.

Kissinger (62, 63) has shown that the ΔT_{min} temperature is dependent on the heating rate, according to

$$\frac{d[\ln(\beta/\Delta T_{min}^2)]}{d(1/\Delta T_{min})} = \frac{E}{R} \quad (5.36)$$

where β is the heating rate, ΔT_{min} is the peak minimum temperature, E is the activation energy, and R is the gas law constant. A plot of $\ln \beta/\Delta T_{min}^2$ versus $1/\Delta T_{min}$ should yield a curve whose slope is E/R . The dependency of ΔT_{min} on heating rate was confirmed by Melling et al. (59), but the determination of E/R was found to be invalid in a practical experiment.

Speil et al. (62) first pointed out that the actual peak temperature is the point at which the differential heat input equals the rate of heat absorption and therefore

$$\Delta T_{min} = \left(\frac{dH}{dt} \right)_{max} \frac{m}{gk} \quad (5.37)$$

as given in equation (j.1). A high rate of heating will cause dH/dt to increase because more of the reaction will take place in the same interval of time, and therefore the height or the apex or the differential temperature, ΔT_{min} , will be greater. Since the return to the baseline is a time function, as well as a temperature-difference function, the return will occur at a higher actual temperature with more rapid heating. This is illustrated for kaolin in Figure 5.8. The peak areas were reported to be equal to within $\pm 3\%$, although there seemed to be a slight tendency toward smaller areas with low heating rates.

Langer and Kerr (65) studied the effect of heating rate on peak temperatures for both the dehydroxylation reaction and the phase transition of kaolinite. These changes to the peak temperature at various heating rates are given in Table 5.1. Both peaks are increased by an increase in heating rate although the dehydroxylation reaction peak is more affected than the other peak.

The effect of heating rate on T_i , ΔT_{min} , and T_f temperatures of sodium hydrogen carbonate, as determined by BarraH and Rogers (64), is shown in Figure 5.9. This compound showed two endothermic peaks between [10

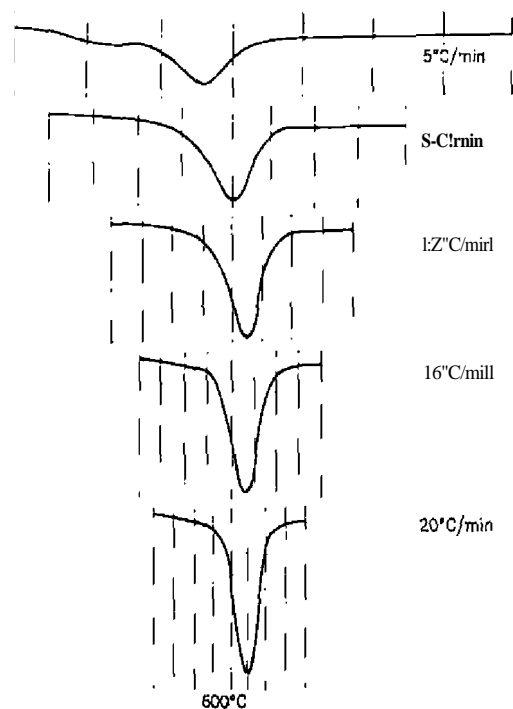


Figure 5.8. Variation of peak temperature with heating rate (2).

and $14D/C$. According to the least-squares extrapolations to zero heating rate, NaHCO_3 began to dissociate at $111.8 \pm 0.2^\circ\text{C}$, and attained the first ΔT_{\min} at $123 \pm 1^\circ\text{C}$ and the second ΔT_{mid} at $131.7 \pm 0.2^\circ\text{C}$.

The variation in ΔT_{\min} is fairly small if the differential temperature is measured against the sample temperature rather than the reference. In a careful investigation, Vassallo and Harden (66) studied the variation of ΔT_{\min} for the fusion of benzoic acid and Marlex 50. The results are shown in Table 5.2. The sample temperature, C_{sample} ($^\circ\text{C}$), was essentially constant over the entire range of heating rates studied. Using the reference temperature, A_{ref} (fl.), we found that the ΔT_{\min} values for benzoic acid varied about 4.0°C over the heating-rate ranges. Similar results were obtained for Marlex 50.

The effect on the resolution of two adjacent peaks in a DTA curve with heating rate is shown in Figure 5.10. At heating rates of 2.5 – $10^\circ\text{C}/\text{min}$,

Table 5.1. Effect of Heating Rate on Peak Temperatures (65)

Heating rate	10	20	30	40	$50^\circ\text{C}/\text{min}$
<i>Dehydroxylation Peak</i> ($^\circ\text{C}$)					
Curve set (II)	535 ^a	555	568	574	589
(2)	549	564	572	584	596
(3)	561	584	596	601	608
(4)	549	566	572	589	596
Average	549 ± 6	570 ± 6	580 ± 7	587 ± 7	597 ± 4
<i>Phase Transition Peak</i> ($^\circ\text{C}$)					
Curve set (I)	1013 ^b	1023	1035	1040	1045
(1)	1018	1031	1036	1040	1049
(3)	LOD	1023	1033	1040	1035
(4)	1015	1028	1033	1047	1049
Average	1015 ± 2	1025 ± 2	1034 ± 1	1041 ± 3	1044 ± 3

^a ΔT_{\min} peak temperatures.

^b ΔT_{\max} peak temperatures.

Table 5.2. Variation of ΔT_{\max} for Some Fusion Reactions with Heating Rate (66)

ϕ^a ($^\circ\text{C}/\text{min}$)	ΔT_{\max} ($^\circ\text{C}$)			
	Benzoic Acid		Marlex 50	
	A_{ref}^b	C_{sample}^c	A_{ref}^b	C_{sample}^c
5	121.5	121.8	136.0	134.2
10	121.6	121.7	138.0	134.4
15	122.1	121.9	138.7	134.2
25	124.0	121.9	139.5	134.2
40	125.5	121.9		134.2
80		121.8		134.4

^a ϕ = heating rate.

^b A_{ref} = ΔT plotted against reference material temperature.

^c C_{sample} = ΔT plotted against sample temperature.

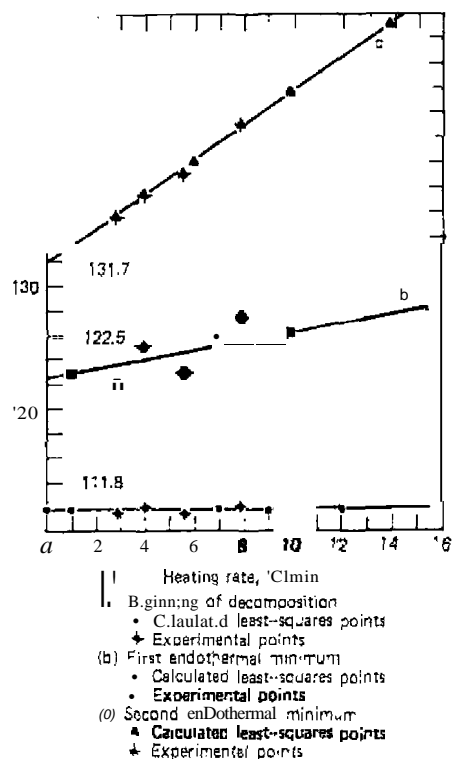


Figure 5.9. Least-squares extrapolation of peak temperatures to zero heating rate (64).

Johnson and Miller (67) showed that cholesteryl propionate gave a curve with three transitions: crystal \rightarrow smectic at 99°C; smectic \rightarrow cholesteric at 110°C; and cholesteric \rightarrow isotropic at 110°C. However, on changing the heating rate to 30°C/min, they no longer detected the 110°C peak, but detected a new, *small* endothermic peak at about 64°C.

They suggested the use of high heating rates to detect small transitions which would not be detected at lower heating rates. Another effect of heating rate increases on the curve peaks observed in this study was to increase the peak amplitude. This is illustrated in Figure 5.11.

b. Furnace Atmosphere

In the case of a reaction which involves the evolution or absorption of a

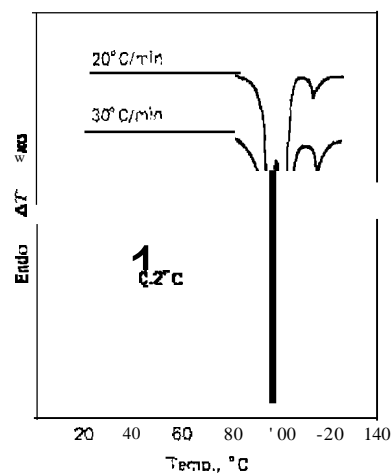


Figure 5.10. Effect of heating rate on curve peak resolution (67). Compound used was cholesteryl propionate.

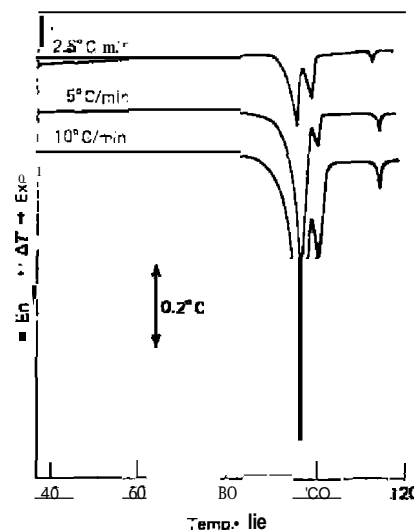


Figure 5.11. Effect of heating rate on the peak amplitude (67). Compound used was cholesteryl propionate.

gaseous component, the peak temperature and the shape of the peak will be affected by the gas pressure of the system. If the gaseous environment is identical to the evolved or absorbed gas, the changes will be more pronounced, as can be shown thermodynamically. The relationship between transition temperature and pressure is expressed by the well-known Clapey-

ron equation which gives the rate of change of vapor pressure with temperature,

$$\frac{dp}{dT} = \frac{\Delta H}{T \Delta V} \quad (5.38)$$

where p is the vapor pressure, ΔH is the heat of transition, and ΔV is the change in volume of the system due to the transition. For reversible volatilization processes, several assumptions may be made leading to the familiar Clausius-Clapeyron equation, the integrated form of which is

$$\ln p = -\frac{\Delta H_v}{RT} + C \quad (5.39)$$

where p is the vapor pressure in atm, ΔH_v is the heat of vaporization in cal/mole, R is the gas constant, T is the temperature, and C is a constant related to the entropy of transition.

The Clausius-Clapeyron equation may be considered a special case of the more general van't Hoff equation

$$-d \ln K_p = \frac{\Delta H}{RT^2} \quad (5.40)$$

where K_p is the equilibrium constant for a reversible and ideal equilibrium process. For a *solid-gas-type* process, which is frequently studied by DTA,

$$A_{\text{solid}} \rightleftharpoons B_{\text{solid}} + C_{\text{gas}}$$

an approximate form of the van't Hoff equation can be used,

$$\ln \frac{(K_p)_2}{(K_p)_1} = \ln \frac{(P_c)_2}{(P_c)_1} - \frac{\Delta H(T_2 - T_1)}{R(T_2 T_1)} \quad (5.41)$$

where $(P_c)_2$ and $(P_c)_1$ are the partial pressures of C_{gas} in the system at temperatures T_2 and T_1 .

This relationship not only provides a convenient method for determining the heat of volatilization processes, but also explains the response of volatilization peaks in DTA curves to changes in purge-gas flow rates exhibited in dynamic-gas DTA systems. Under dynamic flow conditions, increasing the flow rate generally reduces the peak temperature at which volatilization occurs when the purge gas is noninteracting with the sample (and is different

from the effluent gas). When the purge and effluent gases are identical, the volatilization peak either shifts to higher temperatures or remains unchanged relative to zero flow rate, depending on the operating conditions. This behavior is a reflection of the changes in partial pressure of the effluent gas in the immediate vicinity of the sample surface. When the purge gas dilutes the effluent gas, the partial pressure of the effluent diminishes with increasing flow rate, and the peak moves to lower temperatures. Thus, the peak position can be shifted merely by controlling the partial pressure at the sample surface using the purge gas as a diluent (68).

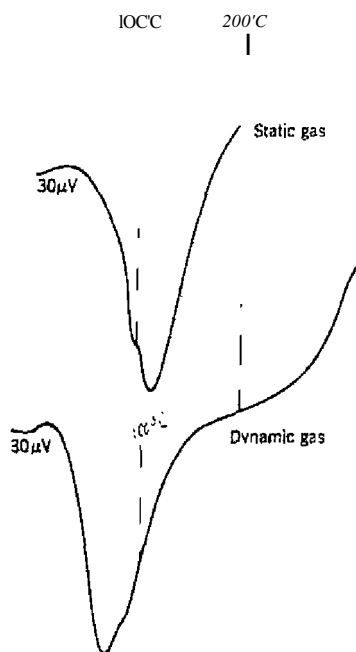
In an atmosphere containing a fixed partial pressure of the evolved gas, a substance will not begin to dissociate to an appreciable extent until the dissociation pressure of the decomposition reaction equals or exceeds the partial pressure of the gaseous component in the surrounding atmosphere. The higher the partial pressure of the surrounding gas is, the higher will be the dissociation temperature of the substance. Thus, the surrounding gaseous environment has a pronounced effect on the DTA curves so obtained. Furthermore, the reaction of the gaseous atmosphere with the sample can also produce peaks in the curve; for example, oxygen in the air causing an oxidation reaction and hence an exothermic peak.

Generally, two types of gaseous atmospheres are employed: (1) a static gaseous atmosphere, usually in an enclosed system; and (2) a dynamic gaseous atmosphere in which a gas flow is either maintained through the furnace or through the sample and reference materials. The first type is the most difficult to reproduce since the atmosphere surrounding the sample is continually changing in concentration due to gas evolution by the sample and by furnace convection currents. Under controlled conditions, the dynamic atmosphere is the simplest to maintain and reproduce.

In a comprehensive study, Stone (69) compared the results obtained in static and dynamic gas atmospheres, as well as the effect of various gas atmospheres at different pressures, on certain decomposition reactions. A comparison between static and dynamic gas atmospheres on the thermal decomposition of illitic shale is given in Figure 5.12. As can be seen, the peak minimum temperature, T_{min} , is shifted to lower temperatures in the dynamic-gas technique. The shapes of the curves are similar in the two techniques.

The effect of two different gaseous atmospheres on the curve obtained for lignite is illustrated in Figure 5.13. In the dynamic nitrogen atmosphere, the lignite pyrolyzes and distills off volatile matter; in oxygen, the lignite oxidizes, giving rise to exothermic instead of endothermic peaks.

The effect of the introduction of an atmosphere of the evolved gas on the DTA curves is shown in Figure 5.14. In an oxygen atmosphere, the rhombic to hexagonal transition of SrCO_3 and the decomposition peak overlap each



Fluxa Resonance, Inc.

Figure 5.12. Difference between DTA curves in static and dynamic atmospheres (69). Sample is an illitic shale.

other. On introducing an atmosphere of carbon dioxide, one finds that the transition peak remains at a ΔT_{min} of 927°C but the decomposition peak



is shifted to much higher temperatures (70).

The choice of sample-holder shape will affect the interaction of the gas atmosphere with the sample. If a glass capillary-tube-type holder is used, the changing of the furnace atmosphere will have little effect on the DTA curve due to the long gas diffusion path between the sample and the furnace atmosphere. A flat-dish-type holder is perhaps ideal for control of the gas-solid reaction but may cause loss of ΔT sensitivity due to radiant heat loss. For reactions in which the gas atmosphere plays no part, a spherical sample holder might be ideal, but would cause difficulty in introducing the sample.

The effect of pressure changes on the DTA curve has been studied by numerous investigators. Increasing the pressure in the system, even with an inert gas, increases the transition temperatures, T_i , ΔT_{min} , and T_f . At low pressures, < 1 Torr, the product gases are removed rapidly; hence the

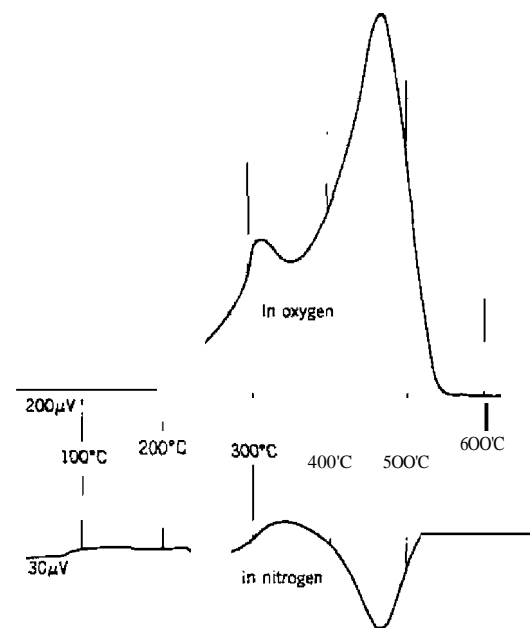


Figure 5.13. Effect of O_2 and N_2 atmospheres on the DTA curve of a mixture of 2.5% lignite in Al_2O_3 (69).

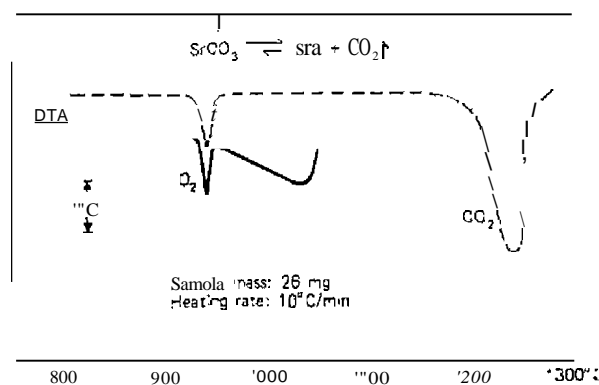


Figure 5.14. Effect of atmosphere on the thermal decomposition of SrCO_3 (70). The solid-solid transition at 927°C is not affected.

transition temperatures are shifted to lower temperatures and there is also a decrease in peak resolution. The effect of pressure changes from 5×10^{-6} Torr to 2300 p.s.i.g. on the DTA curves of $\text{MgSO}_4 \cdot 7\text{H}_2\text{O}$ are shown in Figure 5.15 (71). Resolution of the curve peaks is very poor for the low-pressure curve in that only a single endothermic peak is observed plus a

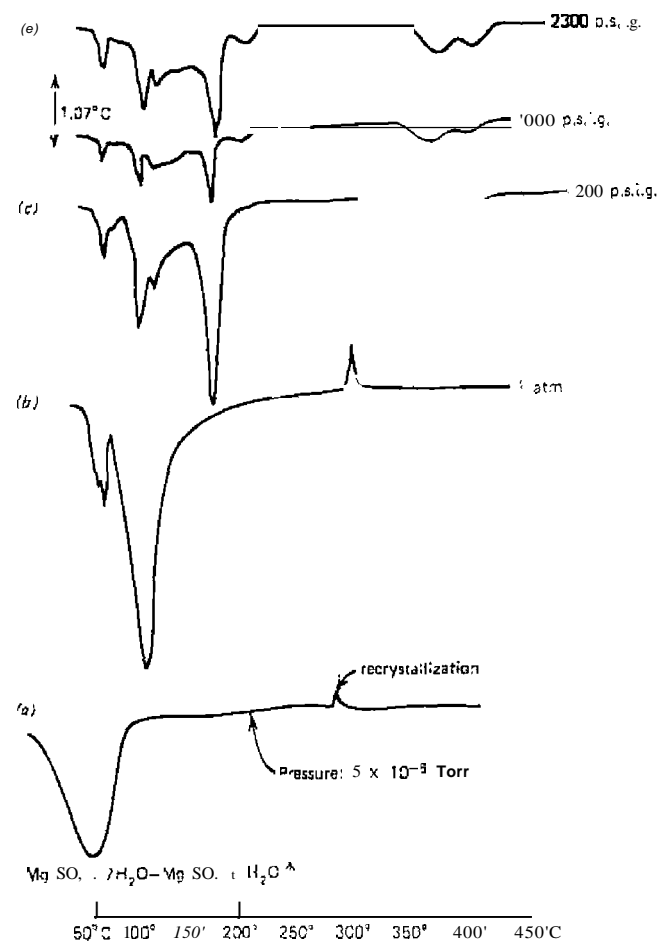


Figure 5.15. Effect of pressure on the DTA curves of $\text{MgSO}_4 \cdot 7\text{H}_2\text{O}$ (71); Nitrogen gas pressure; heating rate of $10^\circ\text{C}/\text{min}$.

small exothermic recrystallization peak. When the pressure is increased, new endothermic peaks appear in the dehydration process. Unfortunately, the origin of the peaks was not discussed. Similar effects were shown by Locke (72), Gam (73), Levy et al. (74), David (75), and others.

Williams and Wermlandt (20) determined the effect of pressure (1–69 atm) on the dehydration of a number of meta salt hydrates. The DTA curves of $\text{CoSO}_4 \cdot 7\text{H}_2\text{O}$ at various elevated pressures are shown in Figure 5.16. At 1 atm of pressure, two endothermic peaks are observed in the DTA curve: a small endothermic peak at a ΔT_{min} temperature of 55°C and a large endothermic peak at a ΔT_{min} of 115°C . As the pressure is increased, the 55°C peak remains essentially unchanged, indicating that it is some type of a phase transition that is pressure-independent. The 115°C peak, however, splits into two peaks as the pressure is increased to 69 atm. This peak splitting is thought to be due to the two reactions: (1) deaquation and the evolution of a liquid water phase and (2) vaporization of the liquid water phase. The first step is independent of pressure, whereas the second step is pressure-dependent.

Kamphausen et al. (21) determined the effect of pressure changes from ambient atmospheric to 2 kbar on the DSC curves of heneicosane, $\text{n-C}_{21}\text{H}_{44}$.

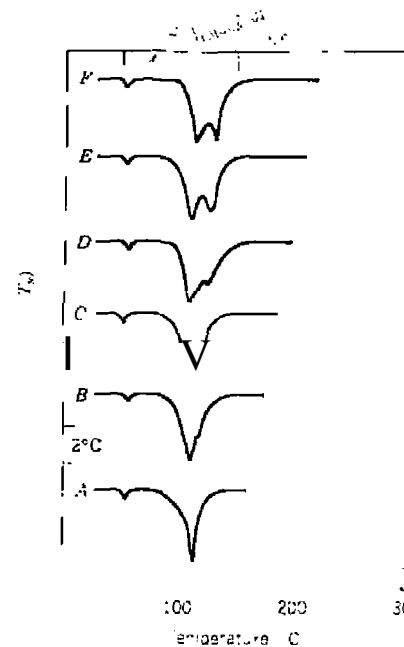


Figure 5.16. DTA curves of $\text{CoSO}_4 \cdot 7\text{H}_2\text{O}$ at various nitrogen pressures: (a) 1 atm; (b) 15 atm; (c) 21 atm; (d) 28 atm; (e) 35 atm; (f) 69 atm (20).

Two peaks were observed up to pressures of 1.5 kbar; at 2 kbar, only one DSC peak was observed. The lower temperature peak was due to a solid-solid phase transformation, whereas the other peak was caused by the fusion of the compound. Similar studies were made using cyclopentanone, cyclopentanol, and cyclohexanone up to 3 kbar applied pressure (136).

The effect of CO_2 pressure on the shape of the DTA curve of dolomite has been discussed by Bandi and Krapf (137). At pressures of less than 200 Torr, a one-step decomposition to CaO and MgO was observed; at higher pressures of CO_2 , a two-step process was found. It was concluded that the reaction mechanism was different at the lower pressures from that at higher pressures. Criado (138) has derived several equations proving that this is not the case but is merely the effect of pressure change on the fraction of sample reacted, α . He showed that between 500 and 1000 Torr the decomposition of CaCO_3 can be fitted closely by the equation

$$P_{\text{eq}}(\text{Torr}) = 1.4 \times 10^1 \exp(-39/RT) \quad (5.42)$$

Since the same decomposition mechanism has been reported for dolomite, the fraction decomposed of dolomite as a function of time, $d\alpha/dt$, in vacuum can be expressed as

$$d\alpha/dt = A \exp(-E/RT)(1 - \alpha)^{2/3} \quad (5.43)$$

The reaction, however, is carried out at some partial pressure of CO_2 , so

$$d\alpha/dt = A \exp(-E/RT) \left[1 - \frac{P_{\text{CO}_2}}{P_{\text{eq}}} \right] (1 - \alpha)^{2/3} \quad (5.44)$$

Substituting equation (5.42) into (5.44) and using $E = 39$ kcal/mole and $A = 2 \times 10^8 \text{ min}^{-1}$, one obtains equation

$$d\alpha/dt = \left(2 \times 10^8 \exp(-39/RT) - \frac{2 \times 10^8}{1.4 \times 10^{10}} P_{\text{CO}_2} \right) (1 - \alpha)^{2/3} \quad (5.45)$$

If the reaction rate were recorded at a heating rate of $\beta = dT/dt$, then equation (5.45) becomes

$$\frac{d\alpha}{(1 - \alpha)^{2/3}} = \frac{2 \times 10^8}{\beta} \exp(-39/RT) dT - \frac{1.4 \times 10^{-2}}{\beta} P_{\text{CO}_2} \text{Pen}, dT \quad (5.46)$$

Integrating equation (5.46), as described by Coats and Redfern (189), using as a lower integration limit of temperature, T_0 , previously calculated from equa-

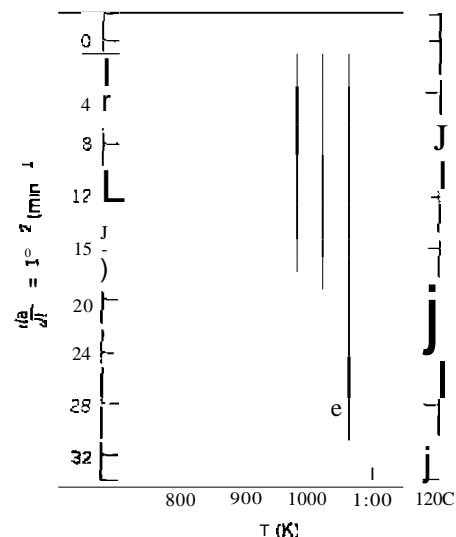


Figure 5.17. Plots of reaction rate of the thermal decomposition of CaCO_3 versus temperature. P_{CO_2} is: A. 0; B. 20; C. 100 Torr (138).

tion (5.42), one has

$$3[1 - (1 - \alpha)^{1/3}] = \frac{2 \times 10^8 RT^2}{39} \exp(-39/RT) - \frac{1}{39} \times \frac{10^8 RT^2}{\beta} \exp(-39jRT_C) - \frac{1.4 \times 10^{-2}}{\beta} P_{\text{CO}_2} (T - T_0) \quad (5.47)$$

Using equations (5.45) and (5.47), curves were plotted at pressures of 0, 20, and 100 Torr of CO_2 at a heating rate of $10^\circ\text{C}/\text{min}$, as shown in Figure 5.17. Thus, the abrupt narrowing of the DTA curve peaks is due to a change in pressure and not reaction mechanism.

c. Sample Holders

Since the shape of a DTA curve is influenced by the transfer of heat from the source to the sample and by the rate of internal generation or absorption

of heat by the reactive sample, the sample holder plays an extremely important part in the OTA experiment. The specific effects of the sample-holder design on the DTA curve have been discussed in detail by Wilburn et al. (76) and Melling et al. (59). Using an analog computer, the latter generated DTA curves employing various time constants, RC , for the sample holder. These results are shown in Figure 5.18. As the sample-holder time

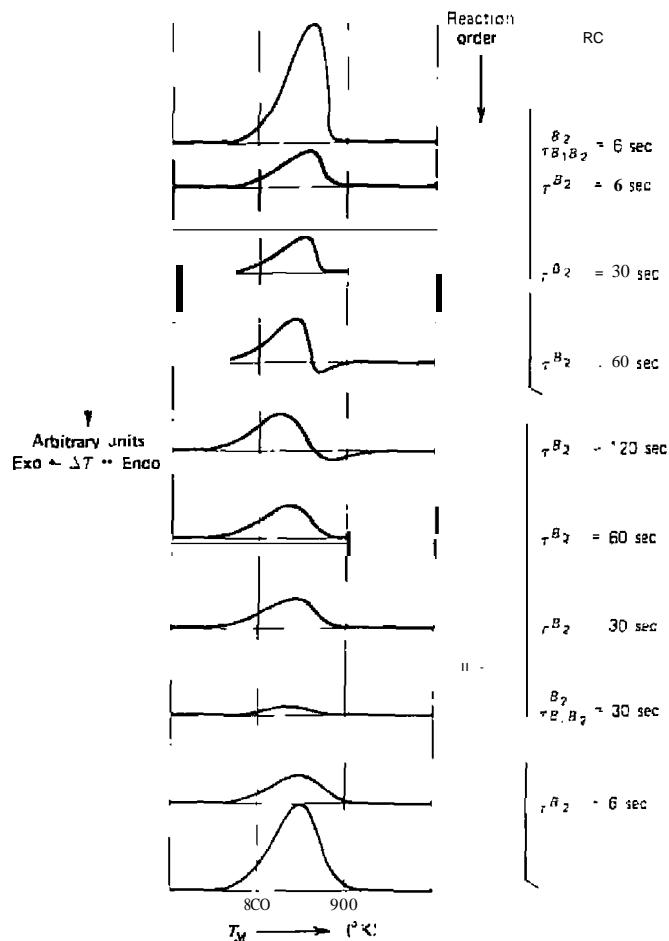


Figure 5.18. Effect of sample-holder diffusivity on the shape of the DTA peak (76).

constant is increased, the shape of the curve becomes distorted: this is the same as saying that as the holder diffusivity decreases and/or the heat capacity increases, the shape of the curve will be markedly changed. Low-diffusivity, block-type holders cause the DTA peak to overshoot the zero baseline and so produce what appears to be an exothermic peak after an endothermic peak. This could lead to erroneous conclusions in the interpretation of the OTA curve, but is due, in fact, to the use of a low-diffusivity block.

At high temperatures, transfer of heat will be mainly by radiation,

$$\frac{dH}{dt} = f(T_1 - T_2)^4 \tag{SA8}$$

so that heating will be more rapid. This is equivalent to reducing the diffusivity of the holder.

Wilburn et al. (76) state that to prevent the adverse distortion of OTA curves, the sample size should be small, heat leakage between the samples should be kept to a minimum, and heat transfer to the samples must be rapid.

OTA curves for identical samples show a change in shape with increasing sample radius (59) because of the development of a difference temperature at the beginning while the return to the baseline at the end of the reaction is delayed. With increasing radius, the "S" form of the leading edge becomes more pronounced, and distortion of peak shape is more noticeable. If the peak shape is to be used for the determination of any reaction parameter, samples of small radius must be employed.

As the sample radius is increased, the peak temperature increases for both reference and sample materials but the increase in sample temperature is much less than that occurring in the reference material. Hence, for minimum variation between samples of different radii, curves are best plotted using sample temperature as the abscissa. Also, to ensure that the heating rate in the sample remains reasonably constant during the reaction, one must use samples having small radii.

The time constant of the sample holder has previously been discussed by Gray (60) in equation 15.26. It is obviously an advantage in any sample holder to make RC_s as small as possible and ideally so small that the distance III in Figure 5.5 is negligible compared to I + II. The smaller and more constant RC_s is, the more accurately will the instrument record the instantaneous thermal behavior of the sample. Obviously, an R value equal to zero in a DTA sample holder would result in no curve peaks at all. For high sensitivity, a large R is required, which is therefore incompatible with the requirement for fast response or high resolution that RC_s be small. In

an instrument where the sample itself makes a major contribution to the thermal resistance, R, so that R is not constant during the transition, the curve peak area will not be proportional to the heat of transition.

Dosch (77) developed a simple electrical technique which could be used to measure both heat sensitivity and response time of a sample holder without interaction. Using the electrical analog for an isolated sample holder, as shown in Figure 5.19, Dosch placed a small electrical heater in the sample container and used it in the measurements. The heater sensitivity was calculated by relating the temperature change at equilibrium to the input power, and the response time was determined by measuring the time constant. The latter is the time required for the exponentially changing signal to reach 63.2% of its equilibrium value.

The thermal resistances and time constants for a number of different sample holders are shown in Figure 5.20. The resistance values obtained in C and D were not very reproducible due to the positioning of the heater in the sample area. The time-constant values, however, were much less affected. It is well known that the heat sensitivity of an isolated container-type holder decreases with increasing temperature. This effect, which is due to the increase in thermal conductivity, k, results in a reduced value for the thermal resistance.

The geometry of the sample holder has a large effect on the intensity of the peak and the peak areas obtained. In Boersma's (44) equations for peak area, the value of $qa^2/4\lambda$ was obtained for a cylindrical metal sample holder and $qa^2/6\lambda$ for a spherical holder. Experimentally, the spherical holder is

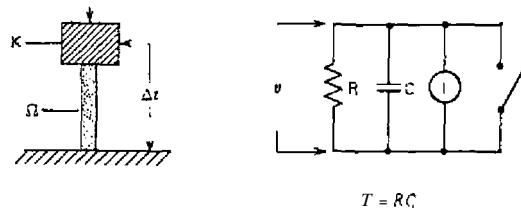


Figure 5.19 Hypothetical isolated DTA sample holder and its approximate electrical analog circuits; in both cases, the time, T, is the time required for the dependent variable (T or I) to reach 1-e or 63.2% of its final value (77). Equivalent quantities:

Time, seconds	T	T	Time, seconds
Thermal resistance	Ω	R	Resistance, ohms
Heat capacity	K	C	Capacitance, farads
Power	P	I	Current, amperes
Temperature	t	V	Potential, volts

	$\Omega, \text{ }^\circ\text{C/mW}$	t, sec
(a)	0.274	36
(b)	0.147	26.2
(c)	0.129	12.5
(d)	0.0784	16.5

Figure 5.20. Sample-holder configurations and the resulting values of Ω and T (77).

difficult to construct, although an approach to a sphere has been made by Lehmann et al. (78), who used a cylindrical holder with a rounded bottom. In a spherical arrangement, the thermal effects from all parts of the sample arrive "in phase" at the centrally located thermocouple junction (79),

In general, a sample holder, of either the block or the cup type, constructed of a low-thermal-conductivity material will give better peak resolution for an endothermic reaction than one constructed of a high-thermal-conductivity material (79-81); for exothermic reactions, the solution is worse for a low-thermal-conductivity material. Since most reactions studied by DTA are endothermic, it would appear that the low-thermal-conductivity sample holders would be preferred. In actual practice, however, the metal sample holders (high thermal conductivity) are more widely used, perhaps because of the ease of their fabrication and their durability,

A comparison between ceramic and metal sample holders has been made by Webb (82), Mackenzie (83), Arens (80), and Gerard-Hirne and Lamy (81). Webb found that for reactions involving the evolution of a gas, the ceramic sample holders gave peaks with maxima shifted to lower temperatures. However, for a crystalline phase transition such as the $\alpha \rightarrow \beta$ quartz transformation, the results were identical for metal and ceramic containers. Thus, it was concluded that the difference was caused by the ceramic holder allowing the gaseous decomposition products to diffuse into the furnace atmosphere, lowering the concentration of the gas in the sample, and so leading to a more rapid completion of the reaction. By using silica liners in the ceramic holder, Webb found that this gaseous diffusion did not take place, and hence the results were identical for ceramic and metal containers.

A comparison of the two types of sample holders (82) for endothermic reactions, such as the decomposition of $\text{Ca}(\text{OH})_2$, CaCO_3 , and MgCO_3 , showed that the nickel block was only slightly less sensitive than a ceramic sample holder. At temperatures of about 500°C , it gave peak areas which were about 80% of those for the ceramic, and at about 900°C , about 70%. The metal holder yielded peaks which were sharper and also increased the resolution of adjacent peaks. Webb (82) explained this as follows: An endothermic reaction begins in the portion of the sample nearest the walls of the sample well, and in the case of the metal (nickel, in this case) holder, heat is readily available from the large mass of metal of high thermal conductivity in contact with the cooler decomposing material. Rapid heat flow into this superficial layer masks the early part of the reaction by neutralizing the endothermic effect before it can affect the thermocouple junction. It is for this reason that the endothermic reaction appears to start at a higher temperature. When the temperature reaches a value at which the rate of decomposition becomes so rapid that the heat from the metal can no longer penetrate the increasingly thick layer of decomposed material of low thermal conductivity sufficiently rapidly enough to neutralize the endothermic effect, the reaction quickly manifests itself, reaching, for the rest of the reaction period, a rate comparable with that prevailing in the ceramic holder.

Comparing a ceramic (porous alumina) and a metal (nickel) sample holder, Mackenzie (83) found that for the endothermic peak in kaolinite, the peak was smaller in the metal holder (about 75% that of the ceramic) and was shifted about 6% higher in temperature.

The two basic types of sample holders, the block and isolated-container types, are compared in Table 5.3 (84).

Dollimore and co-workers made a comprehensive investigation of the effect of sample holders on the DTA curves of several reactions (139, 140). Using commercially available cell types illustrated in Figure 5.21, they found that the corresponding DTA curves for the decomposition of $\text{UO}_2\text{C}_2\text{O}_4 \cdot 3\text{H}_2\text{O}$,

Table 5.3. Comparison of Block and Isolated Container Sample Holders (84)

Advantages	Disadvantages
<i>Block type</i>	
1. Good temperature uniformity	1. Poor exchange with atmosphere
2. Good thermal equilibration	2. Poor calorimetric precision
3. Good resolution	3. Difficult sample manipulation
4. Good for b.p. determinations	4. Sensitive to sample density change
<i>Isolated container type</i>	
1. Good exchange with atmosphere	1. Poor resolution
2. Good calorimetric precision	
3. Good for high-temperature use	

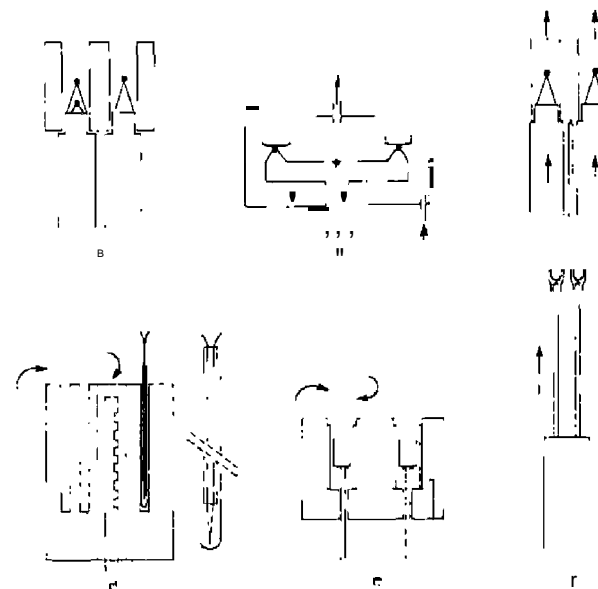
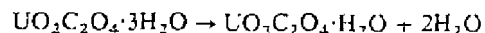


Figure 5.21. Commercial DTA sample holders evaluated by Dollimore et al. (139). (a) Netzsch Standard cell (nickel block, wells approx. 8 mm in diameter); (b) Stanton Redcroft cell (aluminum pans, approx. 6 mm in diameter); (c) Netzsch catalytic cell (ceramic sleeves, approx. 8 mm in diameter); (d) Du Pont intermediate temperature cell (sample tube approx. 1 mm in diameter); (e) Witburn cell (nickel block, wells approx. 9 mm in diameter); (f) Du Pont high-temperature cell with platinum liners in place (sample holder approx. 5 mm in diameter). Arrows indicate normal direction of gas flow.

dissociates according to the reaction



The splitting of the dehydration peak was due to the efficiency of the removal of water vapor from the DTA sample holder (see Figure 5.22). Specific details on the sample holders are as follows:

Netzsch Model 404. Using the standard cell (a), the complete removal of water vapor was not achieved. With the catalytic cell (b), with airflow over the cell, the splitting effect was less pronounced. The splitting effect could be completely eliminated using an airflow through the sample (c).

Stanton Redcroft DTA 671. With an undiluted sample (d), the peak splitting is apparent. Using a diluted sample (e), the splitting is reduced

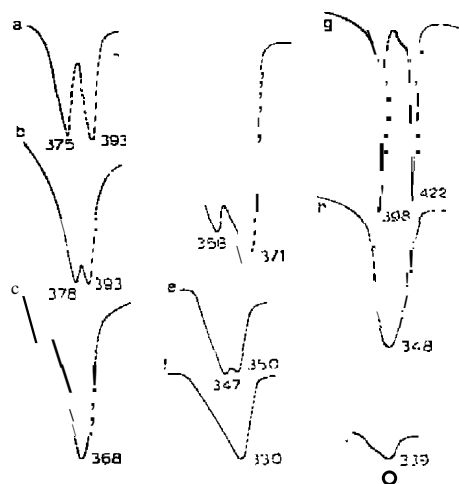


Figure 5.22. DTA curves for the dehydration of $\text{UO}_2\text{C}_2\text{O}_4 \cdot 3\text{H}_2\text{O}$ using various DTA sample holders (139). a, Netzsch standard cell, diluted sample, 300 mL min⁻¹, nitrogen over sample; b, Netzsch catalytic cell, diluted sample, 500 mL min⁻¹, air over sample; c, Netzsch catalytic cell, diluted sample, 5 mL min⁻¹, air through sample; d, Stanton Redcroft cell, undiluted sample, 25 mL min⁻¹, air over sample; e, Stanton Redcroft cell, diluted sample, static air; f, Stanton Redcroft cell, diluted sample, 10 mL min⁻¹, nitrogen; g, Du Pont intermediate temperature cell, undiluted sample, 400 mL min⁻¹, nitrogen over sample; h, Du Pont high-temperature cell, undiluted sample, *in vacuo* (1.9 kN m^{-2}); i, Du Pont high-temperature cell, with liner, diluted sample, 500 mL min⁻¹, air over sample; j, Du Pont high-temperature cell, without liner, diluted sample, 500 mL min⁻¹, air over sample. Diluted samples, 20% w/w with Al_2O_3 , peak temperatures in K.

even if no gas flow was used. Use of a flowing gas atmosphere completely eliminated the splitting effect (f).

Du Pont 910 intermediate cell. Undiluted samples gave two peaks for the dehydration reaction (y). Flow rates as high as 2 L/min gave similar results. Continuous evacuation of the cell (h) for an undiluted sample *in vacuo* gave complete elimination of the splitting. The high-temperature cell with liners produced only a single peak (i); in the absence of the liners, curve (j) indicated only a single peak. Similar changes in the DTA curve for the decarboxylation reaction of $\text{UO}_2\text{C}_2\text{O}_4 \cdot \text{H}_2\text{O}$ were observed.

From the preceding discussion, it is seen that the correct choice of sample holder is essential for certain types of reactions (139). For reversible reactions or reactions where product gases can either react with the residue or form an inert "blanket" (e.g., decomposition or metal oxysalts where reducing gases are formed during decomposition), it is necessary to establish whether proper atmosphere control is achieved using any particular DTA cell design. Since many investigators have access to only one apparatus, often used as a "universal" instrument for a variety of studies, it is clear that the required conditions (e.g., flow rate, sample weight, etc.) needed to eliminate secondary reactions must be established for the particular instrument and cell available.

In those cases where gas flow is not directly through the bulk sample, an important factor during decomposition in controlled atmospheres is the geometry or the sample holder rather than the sample size, flow rates, and so on, used. Thus, small thinly spread samples lead to efficient product gas removal but small samples contained by narrow, restricted tubes lead to a serious loss in efficiency of product removal.

Dollimore et al. (111) also investigated the effect of sample container composition on the DTA curve of magnesium formate 2-hydrate. Sample containers constructed from Al, Cu, and Pt metals were compared and discussed.

d. Thermocouples

Boersma (44) has shown by theoretical considerations that the heat loss by conduction along the thermocouple wires is fairly large and can have a considerable effect on the area of the peak obtained. Since the temperature in the sample center is measured by means of a thermocouple, part of the heat produced in the sample is carried away by the thermocouple wires and therefore too low a sample temperature is measured.

Figure 5.23 illustrates a spherical sample-filled cavity in a nickel block containing a thermocouple junction of radius r_1 . During a reaction, a

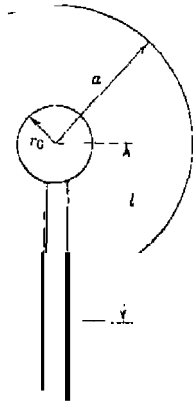


Figure 5.23. Heat leakage through thermocouple wires (44).

temperature gradient exists in the wires over length l . It is assumed that at the distance l , which is slightly larger than a , the radius of the sample cavity, the wires have attained the temperature of the nickel block. If the area of the thermocouple wires is A and O_0 is the thermojunction temperature, the amount of heat carried away by the thermocouple leads is

$$Q = \int_{t_1}^{t_2} \frac{A \lambda_p}{l} \theta_0 dt \quad (5.49)$$

where λ_p is the thermal conductivity of the wires. By various mathematical manipulations, the peak area for a spherical sample holder becomes

$$\int_{t_1}^{t_2} \theta_0 dt = \frac{qa^2}{6\lambda} \cdot \frac{\alpha}{1 - (\Lambda/\lambda)} \quad (5.50)$$

where α , which is very nearly unity, comes from the altered geometry of the holder and is equal to

$$\alpha = 1 - \frac{r_0^2}{a^2} \left(3 - 2 \frac{r_0}{a} \right) \quad (5.51)$$

and Λ is the heat leakage through the wires, or

$$\Lambda = \lambda_p \frac{r_0}{l} \frac{A}{4\pi r_0^2} \left(1 - \frac{r_0}{a} \right) \quad (5.52)$$

For low-thermal-conductivity samples, $(\lambda/\Lambda) \ll 1$, the peak area will become independent of the sample conductivity λ , whereas a high sample conductivity will cause an inversely proportional relationship.

For cylindrical holders, the expression is

$$\int_{t_1}^{t_2} \theta dt = \frac{qa^2}{4\lambda} \cdot \frac{1 - (r_0^2/a^2)[1 + 2 \ln(a/r_0)]}{1 - (\Lambda/l)(\lambda_p/\lambda)[\ln(a/r_0)/2\pi h]} \quad (5.53)$$

For most samples, the thermal conductivities are about $0.3 \text{ J/ms}^\circ\text{C}$, which makes λ/Λ about equal to unity. Therefore, according to equation (5.50), the heat leakage through the wires reduces the peak area to less than 50% of its theoretical value.

Hauser (88) also studied the effect of wire and thermojunction size on the peak shapes. He concluded that the larger wire size (No. 22 compared to No. 28 gauge) and the larger bead size (1.43 mm compared to 0.8 mm) gave the more pronounced peaks on the thermal decomposition curves. In considering the electrical resistance characteristics of the thermocouple wires, he found that No. 28 gauge wires have too high a resistance for proper electrical properties without too great a thermal conductivity. A 1A3-mm thermojunction diameter was much more efficient in maintaining the emf than the smaller junctions, but still the mass of the junction was not great enough to absorb an excessive amount of heat.

The effect of thermocouple wire size on the transition temperature of benzoic acid and toluene was studied by Vassallo and Harden (66). For No. 28 gauge wire, at a heating rate of $\text{W}^\circ\text{C}/\text{min}$, the melting point (mp) of benzoic acid was 121.7°C . The effect was also observed for a heating rate of $40^\circ\text{C}/\text{min}$. For the No. 40 gauge wire, the peak heights were about 15% less than those obtained for the larger wire. The difference in peak shapes and intensities for the sample and reference temperatures using the various wire gauges is illustrated in Figure 5.24. The shapes of the curves are entirely different for the different size wires.

Heat leakage due to thermocouple leads can be expressed by the equation (59)

$$\frac{dh}{dt} = K_H(T_s - T_A) \quad (5.54)$$

where dh/dt is the rate of heat loss, T_s is the temperature at the center of the sample, T_A is the ambient temperature, and

$$K_H = \frac{k_w a_w}{l} \quad (5.55)$$

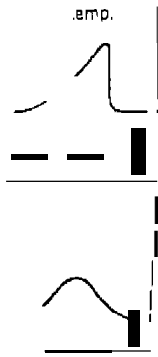


Figure 5.24. Character of boiling endotherm using sample and reference temperature measurements at a heating rate of 10°C/min (66).

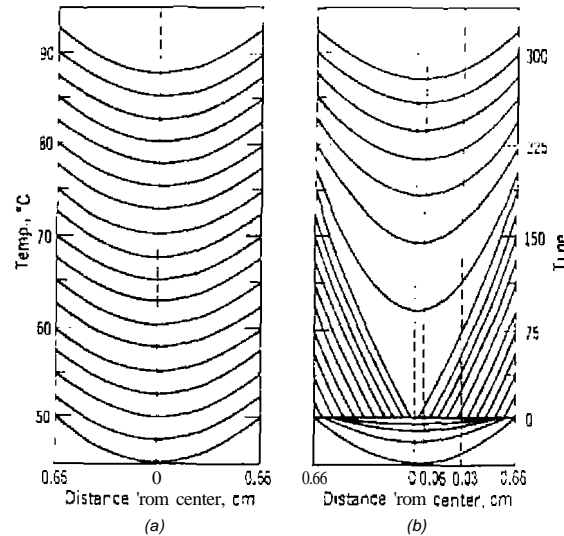


Figure 5.25. Temperature distribution, at 18.75-sec intervals, of (a) reference materials (b) sample material (85).

loss factor, κ_w is the thermal conductivity of the wire. A is the area of the wire, and l_w is the length of wire from ambient temperature. As would be expected, increasing thermocouple wire causes the area under a typical DTA curve to increase. It is also interesting to note that the peak temperature of the curve will only be zero if the reference and sample are identical and if heat leakage from both thermocouples is the same. If heat leakage differs, the differential temperature will be non-zero. A nonlinear baseline change may be due to the dependence of the heat-leakage factor. Heat leakage from the sample leads reduces the time for the quasisteady state to be reached as the rate of heating.

The temperature-axis thermocouples is discussed in

Thermocouple Location

The distribution in reference and sample materials has been discussed in (85) and is illustrated in Figure 5.25. The distribution in reference material are at all instants of time identical parabolas.

(5.56)

where T_c is the temperature, t is the time, x is the distance in the direction of

heat flow, α is the heating rate, α is the diffusivity of the material, and T_c is a constant having the dimensions of a temperature.

The sample material curve starts out as a parabola: as the outer layers reach the inversion temperature, so much heat is required to change them from the low to the high form that the heat supply is interrupted. The rate of heating at the center of the sample material slows up before the material at the center has reached the inversion temperature. As soon as the rate of heating at the center starts decreasing, the differential temperature curve will start to deviate from its baseline. At this point, neither the center of the sample material nor the center of the reference material is at the inversion temperature. Smyth (85) states that not too much importance can be attached to this point of initial deviation.

When the sample material inversion is completed, the distribution curve comes to a sharp point at its center. Since such a sharp point corresponds to a very high value of the second derivative of the equation

(5.57)

it would be expected that there would be a rapid rise in temperature at the

center. This rapid rise gradually slows down, until after more than 300s the sample material has caught up with the reference material, causing the differential temperature to become zero again.

The manner in which the differential temperature curve deviates as a function of reference temperature is presented in order to show more clearly the applications of Smith's (85) calculations. In DTA, the shape of the curve and also the peak maxima temperatures are variable depending on the source of the reference temperature. This is illustrated by the curves in Figure 5.26 in which the differential temperature is plotted against the temperature of the center of the reference material, the surface of the sample material, and the center of the sample material.

Curve (a) departs from zero some distance below the 50°C inversion temperature and reaches its peak some 20°C above the inversion temperature. In curve (b), the sample material surface temperature would correspond to the temperature of the metal block in which the sample and reference cavities are located. This curve starts deviating from the baseline at the inversion temperature, which, if this temperature could be accurately determined, would have useful significance on such a curve. If the differential temperature is plotted against the temperature at the center of the sample material, as shown in curve (c), the peak maximum temperature would be equal to the inversion temperature.

Smyth (85) illustrated the type of DTA curve obtained if the sample and

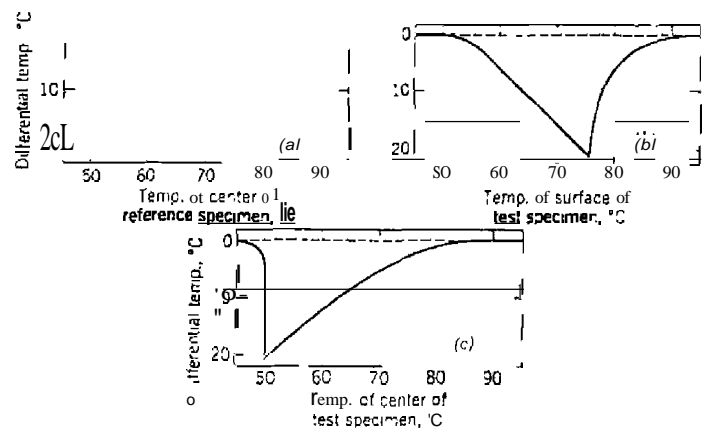


Figure 5.26. Differential temperature plotted against the temperature (a) at the center of the reference material; (b) of the surface of the sample material; and (c) at the center of the sample material (85).

reference thermocouples are not symmetrically located in their respective chambers. This asymmetry effect is shown in Figure 5.17.

Curve (a) shows the differential temperature curve if the thermocouple is 0.06 cm from the center, instead of at the center, of the sample material. In curve (b), a rather extreme case is presented in which the sample thermocouple is 0.30 cm from the sample center. In both curves, the peak maxima temperatures are completely different from those of the symmetrically centered thermocouples.

Barrall and Rogers (86) also determined the effect on the baseline of the and the deviation of the differential temperature baseline. The effect of the location of the thermocouple whose output is recorded against the differential temperature is illustrated in Figure 5.28.

In case (1), the system or X axis thermocouple was located directly in the middle of the sample-holder block. As seen from curves u, b, and c, the ΔT_{min} temperature increases rapidly with an increase in the heating rate. For case (2), the thermocouple was located in the center of the reference sample, and the resulting curves, d and e, showed a less pronounced change ΔT_{min} with heating rate. In case (3), in contrast to the first two cases, there was no change in heating rate. It was also stated that the endothermic peak was more symmetrical and the recorded melting range was narrower for case (3).

Barrall and Rogers (86) also determined the effect on the baseline of the differential curve if the thermocouples were not located symmetrically in the sample and reference chambers. The irregularities observed were even more pronounced when the sample packing was altered. These effects are shown in Figure 5.29.

Curve (1) illustrates the type of curve obtained with careful packing of the sample such that the thermocouples were symmetrically located not only with respect to the walls of the sample-holder block, but also with respect to the top and bottom of the material in the sample and reference chambers.

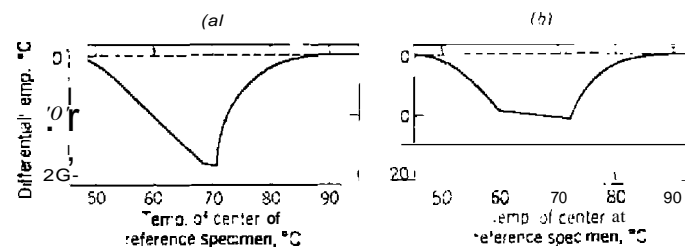


Figure 5.27. Effect of having an asymmetric arrangement of sample and reference thermocouples. (a) Thermocouple 0.06 cm from center of sample, (b) thermocouple 0.30 cm from center of sample (85).

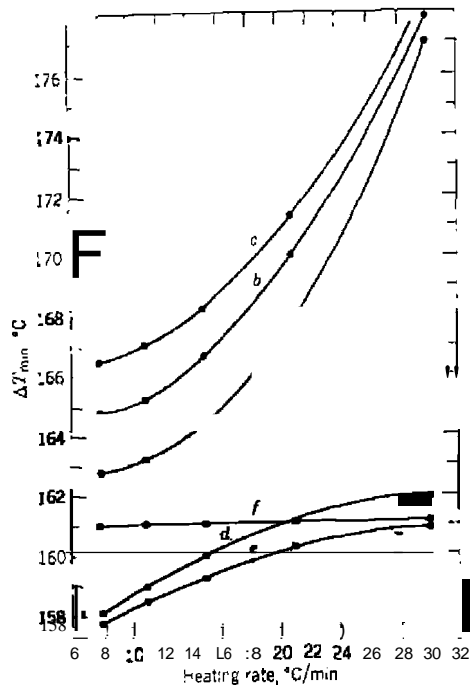


Figure 5.28. Effect of location of system thermocouple and heating rate on temperature at ΔT_{min} using successive runs on different sample weights of 8.3% salicylic acid on carborundum (86). Case 1: a, 0.0952 g; b, 0.1125 g; c, 0.1555 g. Case 2: d, 0.0952 g; e, 0.0822 g. Case 3: f, 0.0952 g.

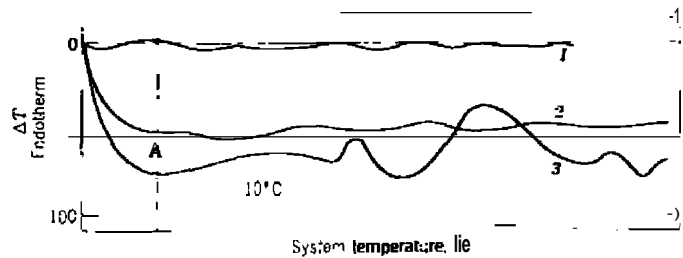


Figure 5.29. System temperature versus ΔT for carborundum in both cells (86). Curve 1, symmetrically located thermocouples; curve 2, unsymmetrically located thermocouples in uniformly packed samples; curve 3, unsymmetrical thermocouples in a nonuniformly packed sample.

If one thermocouple was displaced approximately 2mm toward the side, top, or bottom of the sample chamber, curve (2) was obtained. It can be seen that the displaced thermocouple heats up more quickly than the symmetrically located thermocouple, thus causing the deviation of the curve up to A. After the temperature difference has been established, the curve remains essentially constant for the remainder of the run. In curve (3), it is seen that loose packing leads not only to a displacement of the curve, but also to maxima and minima, presumably due to the shift of support particles as they expand during the heating process.

Melling et al. (59) found that the positioning of the thermocouple in a sample of small radius does not affect the measured peak temperatures. In samples of large radius, the shift of peak temperatures for the sample is significant, whereas the peak temperature of the reference material remains reasonably constant. The introduction of a measuring thermocouple does, however, affect the temperature distribution in the sample.

David et al. (87) made a comprehensive investigation of the use of furnace temperature (mode 1) or sample temperature (mode 2) as the temperature axis. A comparison of these two modes on the DTA curves of polyethylene, a material having a rather large specific heat, showed that the ΔT_{min} temperatures occurred at lower temperatures when mode 2 was used. The effect of the mode of temperature measurement on the various peak temperatures of pure metals is illustrated in Table 5.4. The extrapolated leading edge of the peak is taken normally as the transition temperature when furnace temperature

Table 5.4. Peak Temperature Measurements as a Function of Temperature Axis (87)

Sample ^a	Furnace Temp. (°C)			Sample Temp. (°C)		
	1st Deviation	Peak	Extrapolated	1st Deviation	Peak	Extrapolated
Indium	149 ^b	152 ^c	157 ^c	151 ^c	157 ^c	151 ^c
Indium	150 ^b	152 ^c	156 ^c	152 ^c	157 ^c	153 ^c
Indium	150 ^b	150 ^c	157 ^c	151 ^c	158 ^c	151 ^c
Tin	226	234 ^c	228 ^c	226	234 ^c	229 ^c
Tin	225	234	227	229 ^c	232 ^c	231
Tin	225 ^b	233	228	229 ^c	232 ^c	231
Aluminum	646	664	649	644	661	647
Aluminum	644	664	648	643	660 ^c	646
Aluminum	644	662 ^c	648	643	660 ^c	646
Aluminum	644	665	647	645.6 ^b	661.6 ^b	
Silver				958	961	

^a Known values: Indium, 156.6°C; tin, 231.8°C; aluminum, 660.1°C; and silver, 960.8°C.
^b Determined with higher chart speed.

ture is employed. Results of the three methods showed that peak temperature is an accurate measure of the transition temperature when the sample temperature is used. The extrapolated temperatures are low in this case, and if they are used, a calibration procedure is necessary.

5. Sample Characteristics

a. Sample Mass

According to the various theories on DTA, the area under the curve peak is proportional to the heat of reaction or transition, and hence, the mass of reactive sample. In general, the peak area is inversely proportional to the thermal conductivity, k ; directly proportional to the density, ϕ , and the heat of reaction, ΔH ; and independent of the specific heat (59). The relationship can be expressed as

$$A \propto \frac{\phi r^2 \Delta H}{k} \quad (5.58)$$

where A is the peak area ($\Delta T \times \text{time}$), r is the sample radius, and l is the length of sample. Then

$$A = \frac{\phi V \Delta H}{k} \quad (5.59)$$

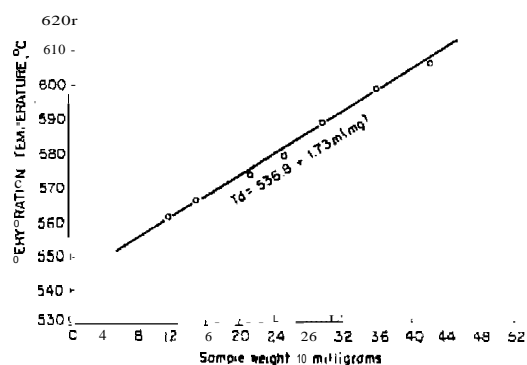


Figure 5.30. The change in peak temperature with change in sample mass for the dehydration of kaolinite (65).

where V is the volume of sample, and hence

$$A = \frac{Gm \Delta H}{k} \quad (5.60)$$

where G is a calibration factor and m the sample mass.

The effect of sample mass on the peak area will be discussed in greater detail in the sections on quantitative DTA and DSC.

Langer and Kerr (65) studied the effect of sample mass on the dehydroxylation peak of kaolinite. As shown in Figure 5.30, an increase in sample mass causes an increase in the peak minimum temperature (T_d), all determined at a heating rate of $25^\circ\text{C}/\text{min}$. The phase transition peak maximum temperature was only slightly affected (5°C) in contrast to the change for the dehydroxylation peak temperatures (45°C).

b. Sample-particle Size and Packing

There are a number of conflicting studies concerning the effect of particle size and particle-size distribution of the sample on the peak areas and ΔT_{min} values. Spiel et al. (2) found that the peak areas under the kaolin dehydration peak varied from 725–2080 mm^2 over the particle-size range of 0.05–0.1 to 5–20 μ . It was also found that the ΔT_{min} values varied from 580–625 $^\circ\text{C}$. However, Norton (89) found that the ΔT_{min} values remained essentially constant but that the temperature at which the dehydration reaction was completed varied from 610–670 $^\circ\text{C}$ over a particle-size range of < 0.1 to 20–44 μ . Grimshaw et al. (90) agreed with the latter study in that, with particle sizes down to 1 μ , the thermal characteristics of the kaolin samples were independent of particle size. This effect is illustrated in Table 5.5.

Carthew (91), who also studied the decomposition of kaolinite, in the particle-size range of > 2 to 0.25–0.1 μ , agreed with the work of Norton (89) and Grimshaw et al. (90). For particle sizes from 2–1 μ to 0.25–0.1 μ , the peak areas were essentially constant, as were the ΔT_{min} values. The disagreement with Spiel et al. (2) was attributed to the fact that they obtained their particle-size fractions by a grinding process, which could reduce the degree of crystallinity of the kaolin.

Barrall and Rogers (92) found that in a blank run of small glass beads against large beads, the baseline displacement indicated that the large beads did not transmit heat as well as the small beads. The baseline gradually decreased with increasing temperature and a large fraction of the displacement remained at 200 $^\circ\text{C}$.

Langer and Kerr (65) found that an increase in the particle size of kaolinite produced a peak temperature increase for the dehydration reaction. There

Table 5.5. Effect of Particle Size on the Thermal Characteristics of Kaolin (90)

Average particle size (μ)	Endothermic Reaction		Exothermic $\Delta T_{m,ex}$ ($^{\circ}\text{C}$)
	$\Delta T_{m,endo}$ ($^{\circ}\text{C}$)	Finishing Temp. ($^{\circ}\text{C}$)	
10-44	600	670	980
0.5- 1.0	605	650	980
0.25-0.5	605	630	980
0.10-0.25	600	615	980
<0.10	600	610	945, 990 ^a
<0.10 dialyzed	605	610	955, 986 ^a

^aTwo peaks.

was no significant shift in the phase-transition exothermic peak. An increase in sample packing density was said to increase heat transfer through the sample and cause changes in the baseline slope.

Rather dramatic changes in the DTA curves of silver nitrate were indicated (93) on change in particle size. These curves, as shown in Figure 5.31, indicate a change in the peak shape as well as the peak minimum temperature. The $\Delta T_{m,endo}$ for the original sample was 161°C , which shifted to 166.5°C in the finely ground sample. After melting, the three samples all gave identical DTA curves. According to Negishi and Ozawa (93), the effect of grinding on the transition is a kinetic one, namely, the formation of a barrier to the fusion transition.

A pronounced effect on the DTA curves of CdO due to grinding was also observed by Wada et al. (94). The origin of the DTA peaks, which became more pronounced as the time of grinding increased, was due to the presence of $\text{Cd}(\text{OH})_2$ contamination.

For the dehydration of $\text{CuSO}_4 \cdot 5\text{H}_2\text{O} \rightarrow \text{CuSO}_4 \cdot \text{H}_2\text{O}$, which proceeds in three stages, Pope and Sutton (142) found the appearance of certain endothermic peaks was dependent on the particle size of the sample. As illustrated in Figure 5.32, with the largest particles (-14 to 18 BS mesh), the first stage of decomposition occurred comparatively slowly, due to the small surface:mass ratio and the time taken for the evolved water to diffuse to the particle surface. The corresponding endothermic peak then tends to merge with that due to boiling of the evolved water. Samples having smaller mean particle size (-52 to 72) showed three distinct and separate endothermic peaks. Using even smaller particles (-72 to 100), Pope and Sutton observed only two endothermic peaks.

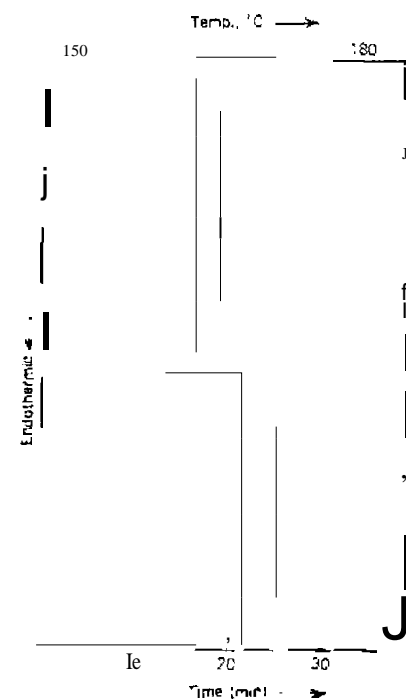


Figure 5.31. DTA curves of silver nitrate (193). (a) the original sample; b) the slightly ground sample; c) the finely ground sample.

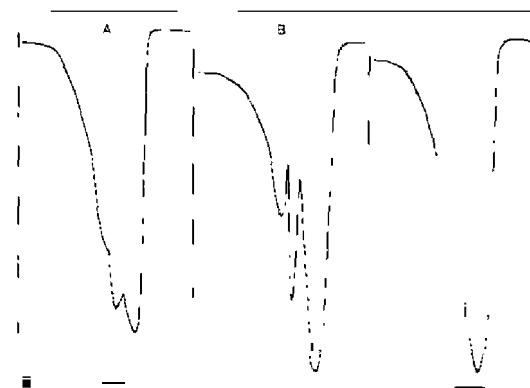


Figure 5.32. DTA curves of $\text{CuSO}_4 \cdot 5\text{H}_2\text{O} \rightarrow \text{CuSO}_4 \cdot \text{H}_2\text{O}$ in static air (142). 80 mg samples at a heating rate of $10^{\circ}\text{C min}^{-1}$: A) - 14 to 18; B) - 52 to 72; C) - 72 to 100 BS mesh sieve fraction.

The influence of grinding (hence, a reduction in particle size) on the DTA curves of thenardite is given in Figure 5.33. Wiedemann and Smykatz-Kloss (143) showed that a single crystal of thenardite gave narrow, reproducible DTA curve peaks. The powdered sample « ISO mesh) gave a completely different DTA curve. The transitions shifted to somewhat higher temperatures and showed a kind of "smear-over" effect, appearing over a temperature range much larger than in the case of the single crystal. Apparently, the powdered material partially recrystallizes as seen in the increase of the III \rightarrow I phase-transition peak on reheating.

As discussed previously, the area of the DTA peak is inversely proportional to the thermal conductivity of the sample, which in turn is dependent on the particle-size distribution and packing of the sample (59).

The effect of sample packing on the DTA curve has been illustrated by Gruver (95) as shown in Figure 5.34. In curve (A), the kaolin sample was placed in the sample crucible and settled by a slight tapping action; in Curve (B), the sample was tamped in place by use of a small glass rod. The curves obtained turned out to be identical. Admittedly, this is rather a crude method of testing this effect.

Bollin and Bauman (96) described a simple sample-packing technique which is capable of accurate reproduction of sample-packing density. The

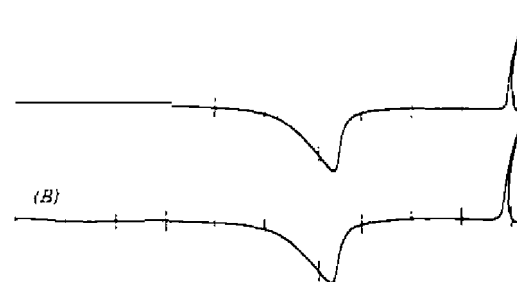


Figure 5.34. Effect of packing of the sample (kaolin): A, tapping; B, tamping (95).

sample is packed around the thermocouple by means of a machined loading die. The result of this packing procedure is an equidimensional sample placed immediately around the thermocouple and surrounded by 60-mesh-size aluminum oxide. This type of sample-loading procedure was said to produce a more efficient geometry than the planar "sandwich" method of Barshad (97).

The effect of crystallinity of the sample is rather difficult to evaluate because of the definition of the term "degree of crystallinity." Carthew (91) defined the latter, in the case of kaolin samples, as the perfection of crystal orientation and not the size of the crystal. Using five different samples of kaolin, he found that the area of the endothermic dehydration peak decreased with a decrease in sample crystallinity. The peaks appeared to be sharper as the degree of crystallinity of the sample increased. This effect of crystallinity was said to be similar to that of change in particle size, and could probably be explained in a similar manner.

c. Effect of Diluent

If samples are sufficiently diluted with a diluent (inert material), the physical properties of all tested materials will be more nearly the same, so that the peak area will be directly proportional to the heat of reaction or transition (59). Dilution will, however, reduce the heat effect, which in turn will reduce the peak area. The diluent must not, of course, react with the sample during the heating process.

The effect on the peak ΔT_{min} values for various concentrations of kaolinite and halloysite diluted with alumina has been studied by Dean (71). For the former substance, the ΔT_{min} values ranged from 525°C for a 10% mixture to 570°C for a 60% mixture. Similar results were found for the halloysite mixtures. De Jong (98) found that there was a direct relationship between

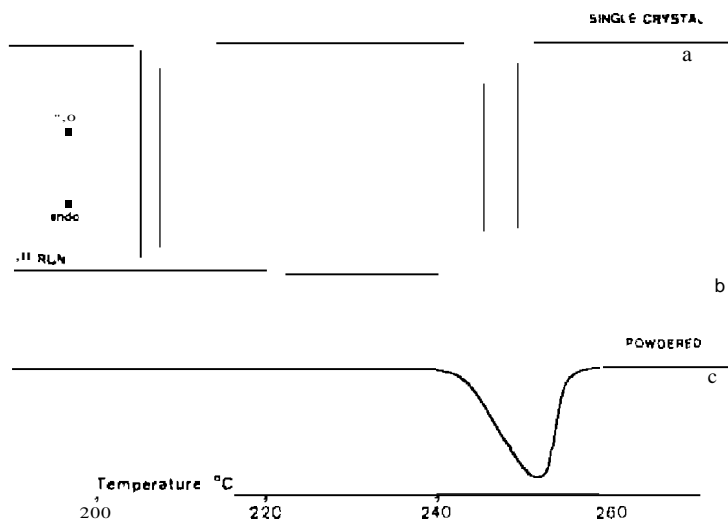


Figure 5.33. DTA curves of the thenardite from Wadi El-Natrun (143): (a) single crystal; (b) mesh « ISO mesh) sample; (c) second heating.

peak area and weight fraction of kaolinite diluted with alumina, provided that the density of the mixtures did not change drastically. For illite-alumina mixtures, however, with a tendency for greater peak areas for higher illite concentrations, a linear relationship was not found.

In a comprehensive study, Barra] and Rogers (92) determined the effect of diluents such as carborundum, iron metal, and iron(III) oxide on the peak caused by the fusion of salicylic acid. This effect is illustrated in Table 5.6. The variation in thermal conductivity of the diluent is probably the main cause of the peak area variation. Higher conductivity allows the thermal effect to be more efficiently conducted to the thermojunction in the center of the sample. It should be noted, however, that the diluent high thermal conductivity may decrease the peak area when the diluted sample is in direct contact with a metal sample block.

A "masking" effect has been noted (92) for certain peaks when the diluent reacts with the sample. This is illustrated in the case of 8-quinolinol diluted with carborundum and alumina, as shown in Figure 5.35. When carborundum is used, the ΔT_{min} obtained was 76.3°C; with an alumina diluent, no endothermic peak was observed in this temperature region. Apparently, a complex had been formed between the alumina and 8-quinolino!.

6. Critique of Operational Parameters

The key operational parameters for DTA (or DSC), as given by Sarason (84), are shown in Table 5.7. If a large sample size is chosen, lower heating rates are required. This in turn decreases the ΔT sensitivity and peak resolution. Small samples are perhaps the most convenient to use, especially with

Table 5.6. Peak Area Obtained by 0.01 g Salicylic Acid Diluted with Various Materials* (92)

Diluent	Salicylic Acid (%)	Area/0.01 g of Acid (mm ²)
Carborundum	6.87	306
Iron metal	8.82	710
Iron(III) oxide	3.40	280
Glass beads, 0.029 mm	4.57	322
Glass beads, 0.29 mm	5.58	289
Alumina	8.60	313
Nujol	20.00	92

* ΔT sensitivity of 67 μV per in.; heating rate of 7.9 C/min.

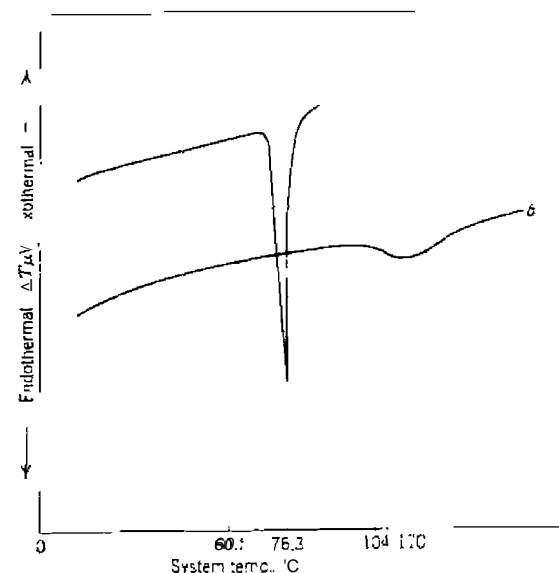


Figure 5.35. Masking effects of sample peaks caused by the diluent: a, 8-quinolinol diluted to 6.9% with carborundum; b, 8-quinolinol diluted to 6.9% with alumina (92).

Table 5.7. Key Operational Parameters (84)

Sample size	
Large:	Useful for detecting low-level transitions. Useful for nonhomogeneous samples. Curve peaks are broad; low resolution and temperature accuracy. Requires slow heating rate.
Small:	Good resolution of curve peaks. Peaks are sharp; transition temperatures need equilibrium values for zero-order reactions. Permits fast heating rate.
Heating rate	
	Increases sensitivity.
	Decreases resolution.
	Decreases temperature accuracy.
Atmosphere	
	Can react with sample.
	Dynamic preferred over static.

Table 5.8. Summary of Operational Parameters (84)

Parameter	Maximum Resolution	Maximum Sensitivity
Sample size	Small	Large
Heating rate	Slow	Fast
Sample holder	Block	Isolated container
Surface/volume of sample	Large	Small
Atmosphere	High k^a (He, Hz)	Low k (vacuum)

^aCompeting reversible volatilization reactions can frequently be resolved using dynamic gas atmosphere.

present-day commercial instruments. They also permit higher heating rates and give better peak resolution.

A summary of the operational parameters is given in Table 5.8 (84).

7. Differences Between DTA and DSC

The term *differential scanning calorimetry* has become a source of confusion in thermal analysis. This confusion is understandable because at the present time there are several entirely different types of instruments that use the same name. These instruments are based on different designs, which are illustrated schematically in Figure 5.36 (157). In DTA, the temperature difference between the sample and reference materials is detected, $T_S - T_R$ (a, b, and c). In power-compensated DSC (f), the sample and reference materials are maintained isothermally by use of individual heaters. The parameter recorded is the difference in power inputs to the heaters, $d(\Delta Q)/dt$ or dH/dt . If the sample is surrounded by a thermopile, such as in the Tian-Calvet calorimeter, heat flux can be measured directly (e). The thermopiles surrounding the sample and reference material are connected in opposition (Calvet calorimeter). A simpler system, also the heat-flux type, is to measure the heat flux between the sample and reference materials (d). Hence, dq_{si}/dt is measured by having all the "hot junctions" in contact with the sample and all the "cold junctions" in contact with the reference material. Thus, there are at least three possible DSC systems, (d), (e), and (f), and three derived from DTA (a), (b), and (c), the last one also being found in DSC. Mackenzie (157) has stated that the Boersma system of DTA (c) should perhaps also be called a DSC system.

Watson et al (128) apparently first used the term *differential scanning calorimetry* (DSC) to describe the instrumental technique developed (1963) by the Perkin-Elmer Corporation. This technique maintained the sample and reference materials isothermal to each other by proper application of

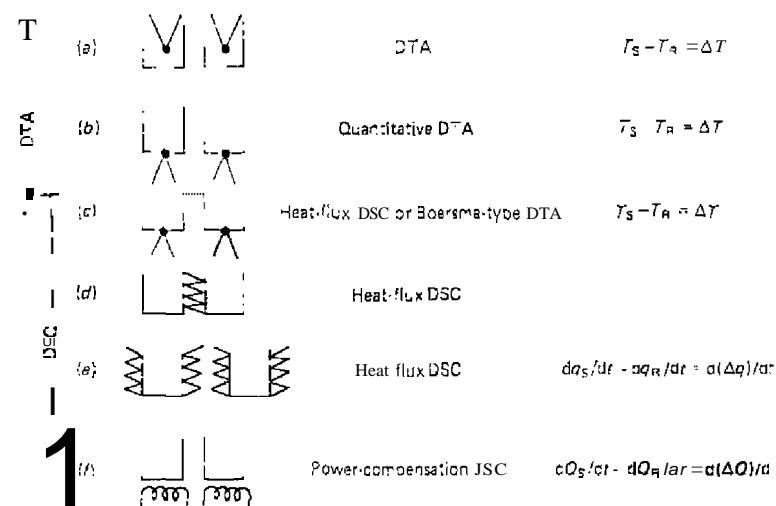


Figure 5.36. DTA/DSC principles schematically illustrated (157).

electrical energy, as they were heated or cooled at a linear rate. The curve obtained is a recording of heat flow, dH/dt , in meal/sec. as a function of temperature. A typical DSC curve is shown in Figure 5.37. In the true thermodynamics sense, an endothermic curve peak is indicated by a peak in the upward direction (increase in enthalpy), while an exothermic peak is recorded

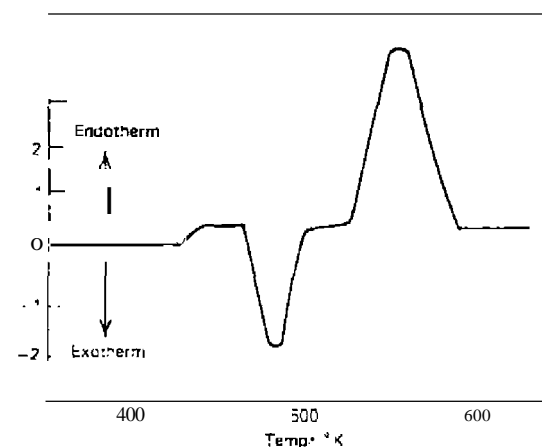


Figure 5.37. Recommended presentation of a DSC curve.

in the opposite direction. In all appearances, the DSC Curve looks very similar to that of a DTA curve except for the ordinate axis units. As in DTA, the area enclosed by the DSC curve peak is directly proportional to the enthalpy change.

$$\text{Area} = \Delta H m / K \quad (5.61)$$

except that K is independent of temperature.

The basic difference in the DSC instruments is schematically illustrated in Figure 5.38. The DSC instrument shown is that described by O'Neill (129). While the heat flux diagram, which is a Boersma DTA system, is that described by Baxter (130) or David (131). The basic difference between the two units is

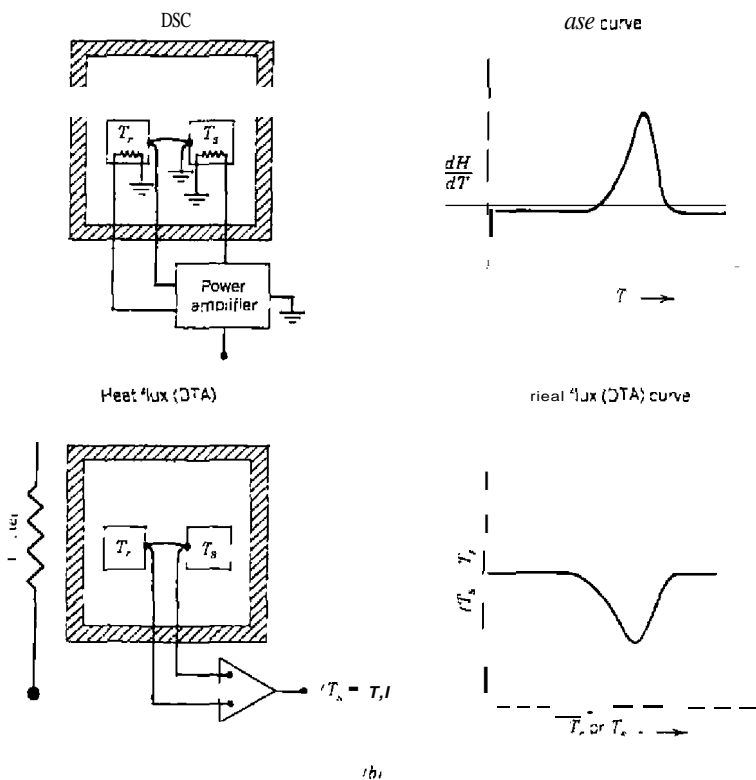


Figure 5.38. Difference between (a) DSC and (b) heat flux DTA techniques (129)

easily seen although the curves are similar in appearance. Much the same type of information is available from the curves; however, until recently, the DSC sample holder has been limited to about 500°C, while DTA holders have been capable of much higher operation. For quantitative measurements, ΔH , for example, the DSC technique is easier to use since the calibration coefficient, K , does not change with temperature. For overlapping curve peaks, there is only one value for K , which simplifies calculations.

Other types of calorimeters, such as the Calvert, Deltatherm, and others, have been reviewed by Wilhoit (132). A bibliography of DSC applications from 1964 to 1970 is available (135).

B. QUANTITATIVE ASPECTS

1. Introduction

The determination of the heat of transition (or reaction) or the mass of the reactive sample from the area of the curve peak is a widely used procedure in DTA and DSC. Expressed very simply,

$$\Delta H m = K A \quad (5.62)$$

where ΔH is the heat of transition (or reaction), m is the mass of reactive sample, K is the calibration coefficient, and A is the curve peak area. The calibration constant is related to the geometry and thermal conductivity of the sample holder and is usually determined by calibration of the system with compounds having known heats of transition (or reaction).

The use of DTA/DSC for determining the heat of transition has been reviewed by Bohon (99), Ozawa (100), and many others. The primary advantages of DTA or DSC techniques over classical calorimetry have been given as the following:

1. Rapidity of the determination; a wide temperature range can be investigated in minutes or hours.
2. Small sample masses: sample size may range from several milligrams to several hundred milligrams.
3. Versatility; samples may be either liquids or solids.
4. Simplicity and ease of procedure and analysis of data.
5. Applicable to cooling processes and to measurements under high pressure.
6. Ability to be used to study many different types of chemical reactions.

Disadvantages of the method include the following:

1. Relative low accuracy and precision of the method, 5-10% in most cases.
2. Inability to be used very conveniently to determine the ΔH of overlapping reactions.
3. The need for calibration over the entire temperature range of interest because K is a function of temperature (DTA only).
4. Inaccuracies in determining peak areas due to baseline change during the transition or reaction.

In many cases, the investigators have been perhaps somewhat optimistic about the results obtained and have not taken into account all the variables of the method. No great accuracy can be obtained unless all these variables are rigidly controlled, which in many cases is extremely difficult.

One of the first to determine the ΔH of fusion of several organic acids was Void (43), who used equation (5.2). The value of A was obtained by plotting $\log(y - Y)$ versus time, t . Thus, no calibration with standards was required.

In another very early investigation, Wittels (101) found that the area enclosed by the curve peak was proportional to the heat absorbed in the decomposition of calcite, CaCO_3 . A linear relationship was found, using sample weights from 0.30 to 3.00 mg. In another study, Wittels (102) elucidated the effect of heating rate and sample mass on the peak areas obtained by the thermal decomposition of tremolite, $\text{Ca}_2\text{Mg}_5\text{Si}_8\text{O}_{22}(\text{OH})_2$. The relationship

$$\Delta H = \frac{A}{\ln \ln [R(R - c)/m]} \quad (5.63)$$

was derived in which R is the heating rate, A is the peak area, and m and c are the constants. The best response of the instrument was obtained at a heating rate of 30 C/min, and fell off rapidly below 15 C/min.

The more recent investigations will be discussed later in this section.

2. Calibration

The calibration coefficient, K , is determined by use of compounds having known heats of transition. Most of the standards used involve the heat of fusion, ΔH_f or a solid \rightarrow solid $_2$ heat of transition. The standards, obviously, must meet certain qualifications such as chemical stability during the transition, low vapor pressure so the heat of vaporization does not contribute to the heat effect, and so on.

The expression used for K depends on the type of instrument employed and the method of recording the DTA or DSC curves. If the variables of ΔT sensitivity and recorder chart speed are included, the expression for K can be written as (103)

$$K = \frac{\Delta H}{m \cdot A \cdot \Delta T} \quad (5.64)$$

where ΔH is the heat of transition in cal/g, m is the sample mass in mg, C is the chart speed in in./min, A is the peak area in in.², and ΔT is the differential temperature sensitivity in deg/in. With these units, K is expressed in cal/min²C. A similar expression was used by David (104). For systems having a large heat capacity, Bohon (105) calculated K from the expression

$$K = t_h C_h \quad (5.65)$$

where t_h is the apparent heat transfer coefficient and C_h is the heat capacity of the sample holder, where $C_h \cong \bar{c}_h w_c / c$ is the specific heat of sample container and w_c its mass. The heat transfer coefficient can be obtained from

$$\log(\Delta T) = \frac{t_h}{2.303} t - t \quad (5.66)$$

In many of the methods of quantitative differential thermal analysis, the calibration coefficient can be mathematically determined and no experimental procedures are necessary. For example, Kronig and Snoodijk (104) calculated K for a cylindrical sample holder as

$$K = \frac{\phi a^2}{4} \quad (5.67)$$

and for spherical symmetry

$$K = \frac{\phi a^2}{8\pi a} \frac{M}{8\pi a} \quad (5.68)$$

where ϕ is the sample density, a is the radius of the sample holder, and h is the height of the sample. These equations describe the temperature difference between the center of the reference material and the sample material, assuming very small thermocouple junctions and leads. The quantity, $4\pi h$ or $8\pi a$, is the geometrical shape factor f in Spitzer's theory. These results were similar to those obtained by Boersma (44) in whose work the influence of the heat

loss through the thermocouple wires was taken into account. Void (43) obtained K by an analysis of the exponential decay of the curve after the reaction had ceased. The relaxation time must have such a large value that after the reaction or transition is completed, the temperature relaxes over a range large enough to be interpretable. Other attempts at calculating K were made by Ozawa (100), Pacor (58), and others.

The temperature dependence of K for the DuPont DTA sample holder is illustrated in Figure 5.39 (106). As can be seen, the calorimetric sensitivity of the apparatus decreases with temperature; that is, more heat is required per unit area. In differential scanning calorimetry, such as with the Perkin-Elmer instrument, K is independent of temperature; hence, only a one-temperature calibration is required. The problem of multitemperature calibration in DTA is also eliminated in the technique of constant-sensitivity DTA proposed by Wendlandt and Williams (107).

The calibration coefficient is also dependent on other instrumental variables such as furnace atmosphere. David (104) determined K as a function of temperature while varying the composition of the furnace atmosphere air, N_2 , or He) and also the pressure (5×10^{-6} Torr to 147 atm). The effect of different gaseous atmospheres on the value of K is shown in Figure 5.40 (104). The difference between the curves can be related to the different thermal conductivities of the gases studied. It was found, as expected, that K was independent of heating rate in the range from 2-40°C/min.

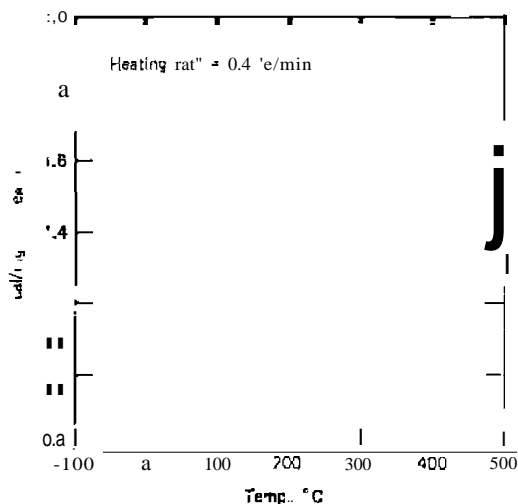


Figure 5.39 Temperature dependence of K (106).

QUANTITATIVE ASPECTS

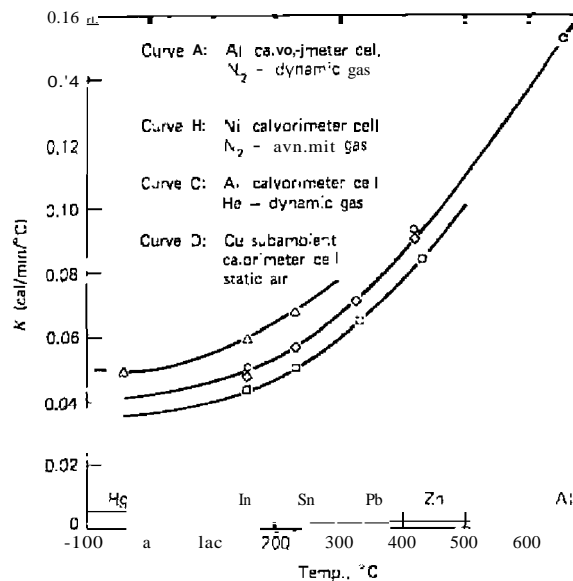


Figure 5.40. Effect of different furnace atmospheres on K (104).

In many cases, the curve for K was expressed in equation form. Currier (108) expressed the values for K as

$$K = -1.3 \times 10^{-4}T + 0.2200 \tag{5.69}$$

while Ozawa (100) found that the smoothed curve was fitted by the expression

$$K = 1.507259 - 8.782709 \times 10^{-3}T - 1.808468 \times 10^{-5}T^2 + 6.324056 \times 10^{-14}T^4 \tag{5.70}$$

The use of a DTA apparatus in which a substance having a known heat of fusion is employed as the reference material rather than an inert substance, was described by Wiedemann and van Tets (109, 110).

Ramachandran and Sereda (111) described the calibration of a DTA system using an internal standard of $AgNO_3$. The peak height was used rather than peak area for all calculations. The peak height was also used in the determination of quartz in a mixture by Davis and Holdridge (112), for calcium silicate (113) and other determinations.

According to Reichelt and Hemminger (144), the values of the calibration constant of a DSC apparatus obtained by means of heat of fusion standards are different from those of well-known heat capacity standards. Varying the container geometry, they were able to show that there was no influence of the disturbance of steady-state conditions of heat flux on the calculated value of the enthalpy of fusion of indium. An error of 20% in the enthalpy may result if incorrectly closed containers are employed.

Hohne (145) pointed out that the function principle of DSC can give rise to calibration errors in case of phase transitions disturbing the steady-state conditions. The cause of this problem is the temperature dependence of the coefficients of heat transfer, leading to weak nonlinearity of the calorimeter. This results in a dependence of the calibration factor on parameters such as mass and thermal conductivity of the sample, heating rate, peak shape, and temperature. By theoretical considerations and calculations, the uncertainty of the calibration factor due to the variation of sample parameters can be 1-5%, depending on the temperature and the instrument involved.

Ortiz and Rogers (146) described a procedure for different temperature calibration using the Perkin-Elmer DSC-1B. This method is based on emission balancing and also makes possible the simplification of emittance measurements, previously described by Rogers and Morris (141).

The calibration of the Perkin-Elmer DSC-2 instrument yields a constant used to convert recorded power units to calorimetric units of joules or calories. Generally, calibration is performed at only one temperature (i.e., the melting point of indium, 156.6°C). The precision and accuracy of this and other calibration measurements are discussed in Section B.6.

Since the specific heat of sapphire is known to within $\pm 0.2\%$ over a wide temperature range, Brennan and Gray (156) developed a specific heat method to calibrate the Perkin-Elmer DSC-2 instrument. As shown in Figure 5.41, a baseline is first established with the empty sample container, and then the curve for the sapphire sample is obtained, both over the same temperature interval. The differences between the two curves is due to the heat capacity of the sapphire; hence, the calibration constant at any temperature is equal to this difference times the heating rate. This requires that the heating rate of the instrument be accurately known. To minimize this problem, Brennan and Gray suggested that the area enclosed by the two curves rather than the displacement be used. This area is equal to the total change in enthalpy for the standard sapphire sample over the temperature range studied. Such a calibration procedure would not depend on the accuracy of the heating rate or the linearity of the temperature scale but only on the initial and final temperatures which are easy to determine.

A comparison between the value of K determined by fusion standards and by the specific heat standard is illustrated in Figure 5.42 (156). The specific

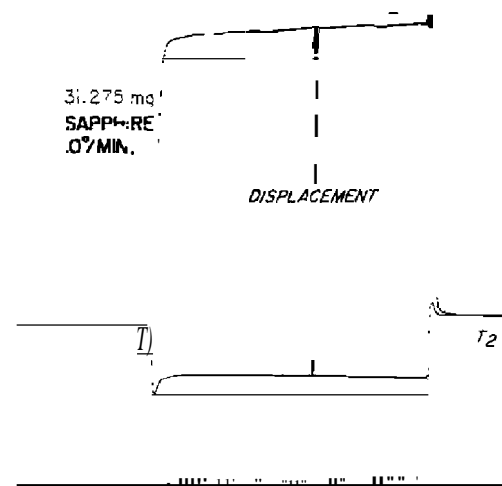


figure 5.41. Calibration of DSC with a specific-heat standard (156).

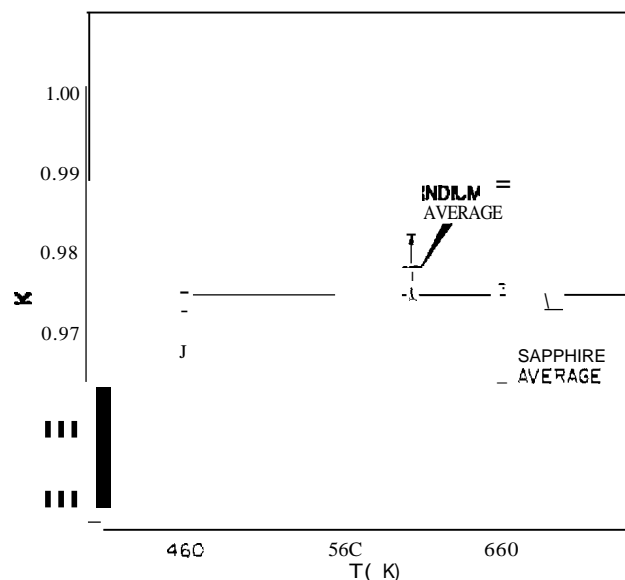


Figure 5.42. Comparison of calibration constant K determined by heat of fusion (indium) and specific-heat (sapphire) standards (156).

heat value of K is drawn as a solid line, whereas the fusion standards values (ΔH_f of indium) are indicated as dashes. Consideration of the precision of the two means indicates that the difference between them, $\approx 0.5\%$, is statistically significant.

Van Dooren and Muller (158) studied the peak width, peak height, and shape index of the melting peak of indium used as a calibrant in DSC.

3. Calibration Standards

Numerous compounds have been proposed to calibrate the DTA and DSC sample holders for quantitative determinations. Most of the standards used are pure metals, although many organic compounds of high purity have also been employed. The heat of fusion is the thermal transition normally used, although dehydration and decomposition reactions have also been recommended by numerous investigators. A list of standard materials used for calibration purposes is given in Table 5.9.

Most of the ΔH values given in Table 5.9 are those obtained at constant pressure. If the calibration is carried out at constant volume, such as was described by Bohon (105), the ΔH values must be corrected by the approximate relation

$$\Delta H(v) \cong \Delta H(p) - RT\Delta n \quad (5.71)$$

where $\Delta H(v)$ is the ΔH at constant volume, $\Delta H(p)$ is the ΔH at constant

Table 5.9. Standards Used for DTA/DSC Calibration

Substance	Temperature (°C)	ΔH_f
<i>National Physical Laboratory Standards (148)</i>		
Naphthalene	80.22	19.05 ^a
Benzil	94.8	23.35
Acetamide	114.3	21.65
Benzoic acid	122.3	18.09
Diphenylacetic acid	148.0	31.27
Indium	156.6	3.252
<i>Stanton Redcroft (149) results</i>		
Indium	156.6	28.47 ^b
Tin	231.9	60.6L
Lead	327.5	22.99
Zinc	419.4	115.79
Aluminum	660.2	398.1

Table 5.9. (Continued;

Substance	Temperature (°C)	tH_f	ΔH_f
<i>Stanton Redcroft (149) results (Cont.)</i>			
Silver	960.8	110.6	
K ₂ SO ₄	583	45.98	
K ₂ CrO ₄	665	54.34	
<i>Other calibrants</i>			
Azobenzene	34.6	21.6'	
C ₃ H ₆	44.9		2.59 ^a
CS ₂	47		4.81
Benzophenone	48.2	23.5	
Palmitic acid	62.5	51.2	
Stearic acid	69	47.5	
Biphenyl	69.8	28.7	
Phenanthrene	99.3	25.0	
o-Dinitrobenzene	114	32.3	
NH ₄ NO ₃	125		12.6
KNO ₃	128		12.86
BaCl ₂ ·2H ₂ O	130	116.6(-211.0)	
NH ₄ Br	137.2		(882 cal/mole)
CuSO ₄ ·5H ₂ O	150	228.5(-4H, O)	
KCN	177.0	25.72	
Ag ₂ S	179		4.08
CaSO ₄ ·2H ₂ O	180	157.2(-2H ₂ O)	
NH ₄ Cl	183.1		11873 cal/mole}
Pentaerythritol	187.8	77.1	
AgNO ₃	212	17.7	
LiNO ₃	252	885	
KeO"	299.8		23.7
NaNO ₃	306.2	44.2	
KNO ₃	337	28.1	
CdCO ₃	350	134.5(-CO ₂)	
K ₂ Cr ₂ O ₇	398		28.9
PbCl ₂	498	20.9	
LiBr	553	36	
LiSO"	575	62	
Na ₂ WO ₄	588.8		28.57
CaCO ₃	850	427.1(-CO ₂)	
^a kJ/mole.			
^b mJ/mg.			
^c cal/g.			

pressure, and Δn is the change in number of moles of gas formed in the reaction.

The sublimation enthalpy of benzoic acid has been suggested as a calibration standard by Murray et al. (150). The mean ΔH_{sub} obtained from 25 measurements was 133.48 ± 3.31 kJ/mole in the temperature range 328–329 K.

Richardson and Savill (151) reexamined the heat of fusion of indium and found that the ΔH_f was 3.35 ± 0.03 kJ/g-at (19.2 ± 0.3 J/g), some 2.5% higher than the value normally accepted (3.13–3.37 kJ/g-at).

4. Calculation of Enthalpy Changes

Once the DTA or DSC cell is calibrated and the calibration coefficient determined in the temperature range of interest, the ΔH of an unknown sample thermal transition can be calculated by use of the simple expression

$$\Delta H_x = \frac{K \cdot A}{m} \quad (5.72)$$

ΔH_x may be expressed in calories or joules per gram, calories or joules per mole, or millicalories or millijoules per milligram. The sample curve peak area may be obtained by a number of methods. They are: (1) cutting out and weighing the peak; (2) integrating the curve peak by use of a planimeter; (3) calculating the area from peak height \times width at 0.5 height; (4) integrating the curve peak by use of a recorder integrator; and (5) computer calculation. Most of the modern commercial instruments use method (5) (see Chapter 12).

Due to changes of heat capacity of the sample during the thermal transition, the instrument baseline often undergoes large displacements in the Y axis direction. This effect is not so prominent in modern DTA/DSC instruments as with older ones, due to the use of smaller samples, higher sensitivity, as well as better instrument design. If large baseline displacements occur, integration of the peak area is difficult or, at best, highly inaccurate. Also, if overlapping peaks are present in the curve, the curve may be integrated in parts, as shown in Figure 5.43 (106). For each of the various peak areas, a different K value must be used to calculate the ΔH (if DTA is used); the total ΔH is thus the sum of each area. With power-compensated DSC, however, one calibration constant is valid over a wide temperature range so that only a single K may be employed for the calculation.

Guttman and Flynn (154) suggested that the correct baseline can be obtained by extrapolating the heat capacities of the initial and final temperature state to the thermodynamic transition temperature. The heat of transition is then the area under the differential power-time curve using this baseline.

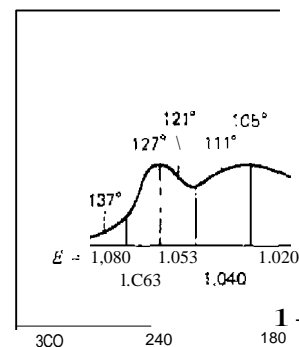


Figure 5.43. Integ...

Goldberg and Prosen (155) have proposed a method and have applied it to other...

Van Dooren and Muller investigated in great detail the effects of apparatus, test substance, reference material, as well as heating rate and particle size (153, 159). In the DSC, the influence of experimental factors, such as instrument characteristics; if the curve is described using standard deviations should be taken into account. Also, heat balance considerations, is

$$\Delta T = \frac{\beta}{A} (C_R - C_S) - \frac{\beta}{A \alpha} [C_S \exp(-A \alpha / C_S t) - C_R \exp(-A \alpha / C_R t)]$$

where β is the heating rate; A is the area for heat transfer; C_R and C_S are the heat capacities of the reference and sample, respectively. From the DSC curves, the following were determined: ΔU_0 is the initial baseline deflection (isothermal \rightarrow heating); δ is the baseline drift (cooling \rightarrow heating); and $\tau \Delta T$ is the lag time. Sample particle-size distribution did not affect the results, as did dilution, in a nonsystematic manner. Generally, no effect occurred in ΔU_0 if helium was used as the purge gas, or oxygen, or nitrogen.

For adipic acid (153), an increase in heating rate decreased the onset temperatures. There was also a significant effect on the specific enthalpy; at the intermediate heating rate of 0.08 K/sec, it is 2% higher than at the lower and higher rates. There was no increase in peak area with increasing heating rate, as was found by BarraH and Rogers (92). For large particle sizes, the onset temperature was decreased and the onset interval and total interval were significantly greater, especially at the highest heating rate. Also, the ΔH_f of large particles was significantly lower than that of the sample with a wider particle-size distribution. These effects may be accounted for by a greater thermal resistance in the large particle-size sample than in the sample with the smaller particles. Diluting agents with high thermal resistance decrease heat transfer and diminish the thermal effect and the peak area.

6. Precision and Accuracy of ΔH Measurements

Despite the present advanced development of statistical methods, the great majority of investigators still present numerical data without qualification as to precision and accuracy. Generally, when a new method or instrument appears, measurements are made on an arbitrary number of samples with data points obtained by an arithmetic mean approach. The resulting numbers, according to Schwenker and Whitwell (114), take on a disconcerting absolutism and are frequently cited as definitive values. Using the technique of DSC, these authors evaluated the resulting data using statistical methods.

The variables of heating rate, sample size, instrument sensitivity level, and metal standard used were incorporated into a factorial, 3×2^3 design. To keep the number of runs within reasonable limits, Schwenker and Whitwell used only three metals, indium, tin, and lead, as standards.

The predicted influence of the number of peak area measurements on calibration coefficient precision is shown in Table 5.10 (114). These data indicate that the best procedure is to replicate samples rather than planimeter area measurements. The standard errors show that no significant improvement in precision results from making four area measurements instead of two, whereas precision is markedly improved by increasing the number of samples.

The effect of the number of samples used to determine K and the number of samples for determining the ΔH of an unknown transition on precision, at the 95% confidence limits, is shown in Table 5.11. These results indicate that for the higher levels of precision, several samples are required for calibration.

From a practical viewpoint, very few calorimetric studies are reported in which 30 samples are used to calibrate K and to determine ΔH values. Hence, the precision expected is certainly greater than 1%, as indicated in Table 5.11. Since most of the measurements are of the first two types, the precision expected is from 4-7%, if not greater.

Table 5.10. Predicted Precision of Calibration Constants (114)

No. of Measurements		Standard Error	Estimated c.L. (%) (95% CL.1)
Samples	Area		
2		0.0286	
		0.0277	
		0.0202	
4		0.0196	± 3.9
		0.0168	
	2	0.0139	± 2.8
8	4	0.0137	
	1	0.0101	
	2	0.0098	± 2.0
	4	0.0096	

Table 5.11. Predicted Confidence Limits on ΔH (114)

No. of Samples		Estimated 95% C.L. (%)
Calibration	Unknown	
4	2	± 6.51
	4	± 6.22
	8	± 5.90
	2	± 5.56
	4	± 4.30
	8	± 4.36
	2	± 4.86
	4	± 3.96
30	3	± 3.42
	2	± 4.40
	4	± 3.46
	8	± 2.80
	30	± 1.10

Brennan and Gray (156) discussed the calorimetric precision and accuracy of DSC measurements (the Perkin-Elmer DSC-21). They stated that the operating principle and the design of the DSC-21 instrument provides no fundamental reason for it to be limited to a precision of $\pm 1\%$, as commonly reported. They examined the effects of sample mass, heating rate, and instrument sensitivity on the calibration of the instrument by a factorial design similar to that of Schwenker and Whitwell (114). It was found that no system-

matic variation or interactions with respect to the preceding three factors could be detected. They also stated that deliberately altering the thermal resistance between the sample pan and the sample holder had no detectable influence on the calibration constant.

Sturm (115) has described a systematic error in quantitative DTA that is caused by the change in the apparent heat transfer coefficient and the apparent heat capacity of the sample and sample holder. The logarithm of the peak area furnished an approximate measure of these changes; the ratio of the logarithms of the areas of the standard and sample provided a correction factor for K .

C. REACTION KINETICS

Almost all the kinetic methods used in DTA and DSC are based on the equation 159)

$$\frac{d\alpha}{dt} = f(\alpha, T) \quad (5.74)$$

where $d\alpha/dt$ is the rate of reaction, $f(\alpha, T)$ is a function of the amount reacted, and T is the absolute temperature at time t . It is also assumed that the rate of heat generation, H , is directly proportional to $d\alpha/dt$, or

$$H = B\rho \left(\frac{d\alpha}{dt} \right) \quad (5.75)$$

where B is the heat per unit volume and ρ is the sample density. Although the kinetic equation used depends on the reaction mechanism, one expression which excludes diffusion-controlled, fusion, and inversion-type reactions is

$$\frac{d\alpha}{dt} = A(1 - \alpha)^n e^{-E/RT} \quad (5.76)$$

where A is the preexponential factor, α is the fraction of sample reacted ($0 \leq \alpha \leq 1$), and n is the "order of reaction." This type of equation has been criticized by Clarke et al. (116) as being unusable for solid-state decomposition reactions. They stated that it is misleading, if not meaningless, to use the concept of reaction order; also, the activation energy is not very well defined because it is not known to which of the many processes it applies.

Although the results of kinetic studies by DTA may be questionable, much effort has been expended to derive expressions from which E and n can be calculated employing DTA or DSC data. Reviews of the determination of kinetics by DTA have been given by Friedman (117), Sestak and Berggren (118), Bohon (99), Murphy III, Sestak et al. (161, 162), and others.

One of the early methods used to obtain kinetic data from a DTA curve was that of Murray and White (119). They developed theoretical DTG curves and found that: (1) the shapes of DTA and DTG curves were similar and (2) the maximum temperature difference, ΔT_{\max} , occurred near $(d\alpha/dt)_{\max}$. Using $n = 1$ for a series of clay samples and by taking the second derivative of the temperature form of equation (5.76), they obtained

$$\frac{d^2x}{dT^2} = \left(\frac{A}{\beta} \right) e^{-E/RT} (1 - x) \quad (5.77)$$

and setting $d^2x/dT^2 = 0$, and substituting T_{\max} , they obtained

$$\frac{E}{RT_{\max}^2} = \left(\frac{A}{\beta} \right) e^{-E/RT_{\max}} \quad (5.78)$$

They also integrated equation (5.76) using the approximation

$$\int_{T_0}^{T} e^{-E/RT} dT \approx \left(\frac{RT^2}{E} \right) e^{-E/RT} \left(1 - \frac{2RT}{E} \right) \quad (5.79)$$

and equation (5.77) to give

$$-\ln(1 - x_{\max}) \approx 1 - \frac{2RT_{\max}}{E} \quad (5.80)$$

Kissinger (62) differentiated equation (5.77) and obtained

$$\frac{d \left[\ln \left(\frac{\beta}{1 - x_{\max}} \right) \right]}{dT_{\max}} = \frac{E}{RT_{\max}^2} \quad (5.81)$$

where β is the heating rate. For any value of n (63)

$$\frac{E}{RT_{\max}^2} = \left\{ \frac{An}{\beta} \right\} (1 - x_{\max})^{n-1} e^{-E/RT_{\max}} \quad (5.82)$$

which was developed instead of equation (5.77), and for $n \neq 0$ or 1

$$n(1 - \alpha_{\max})^{n-1} \approx 1 + (n-1) \left(\frac{2RT_{\max}}{E} \right) \quad (5.83)$$

Since $(n-1)(2RT_{\max}/E) \ll 1$, equation (5.81) may be further approximated by

$$n(1 - \alpha_{\max})^{n-1} \approx 1 \quad (5.84)$$

Substitution of equation (5.84) into equation (5.83) gives an approximate equation that is the same as equation (5.77). Thus, Kissinger concluded that equation (5.81) was independent of order. The order of reaction, n , was obtained from the shape index, S , defined as the absolute value of the ratio of the slopes of the tangents to the curve at the inflection points.

$$n \approx 1.26S^{2/3} \quad (5.85)$$

Reed et al. (120) used Kissinger's method in their investigation of the kinetics of the decomposition of benzenediazonium chloride and found that the E value so obtained differed from other methods by about 42%. By this criterion, they judged the method as unacceptable. Similar conclusions were made by Melling et al. (59) because the slopes they calculated from the computed DTA curves were all low when using the peak sample temperature. Hence, the method by which Kissinger evaluated E/R was invalid in a practical experiment. Piloyan et al. (121) cited the disadvantages of this method: (1) It requires the determination of several DTA curves at different heating rates and (2) it was necessary to use a special programming device to control the temperature. However, provided that the appropriate experimental conditions are used, Akita and Kase (122) concluded that the peak minimum of the DTA curve did agree with the maximum rate of reaction, in agreement with Kissinger.

Piloyan et al. (121) developed a kinetic method which was also based on equation (5.76). By substitution of $\Delta T = S(dx/dt)$, where S is the peak area they obtained

$$\ln \Delta T = C - \ln f(x) - \frac{E}{RT} \quad (5.86)$$

where C is a constant. If x lies between 0.05 and 0.8 (about up to the peak minimum), $\ln f(x)$ can be neglected and equation (5.86) can be approximated to

$$\ln \Delta T = C - \frac{E}{RT} \quad (5.87)$$

Estimated errors of the values of E obtained were between 15 and 20%.

Perhaps the most widely used kinetic method in DTA has been that derived by Borchardt and Daniels (185) in 1957. The method is based on the following assumptions: (1) The temperature in the sample and reference materials is uniform; obviously, this only can be applied to stirred liquids and not to solids; (2) the heat is transferred by conduction only, a condition easily met with liquids and the temperature ranges usually employed (the heat transfer through the thermocouple is neglected); (3) the heat transfer coefficients are identical for the sample and reference materials; and (4) the heat capacities of the sample and reference materials must also be identical, a condition approached if dilute sample solutions are investigated.

The actual rate of reaction at any temperature in terms of the slope of the curve ($d\Delta T/dt$) and the height ΔT is

$$-\frac{dN}{dt} = \frac{N_0}{KA} \left[C_p \frac{d\Delta T}{dt} + K\Delta T \right] \quad (5.88)$$

where N is the number of moles of reactant present at any time and is equal to the initial number of moles, N_0 , minus the number of moles that have reacted, or

$$N = N_0 - \int_0^t -\frac{dn}{dt} dt \quad (5.89)$$

By various manipulations, the rate constant, k , was shown to be equal to

$$k = \left[\frac{KA}{N_0} \right]^{n-1} \frac{C_p(d\Delta T/dt) + K\Delta T}{[K(A-a) - C_p\Delta T]^n} \quad (5.90)$$

where V is the volume, A is the total peak area, a is the area up to time t , and n is the order of reaction. In the case of a first-order reaction, $n = 1$,

$$k = \frac{C_p(d\Delta T/dt) + K\Delta T}{K(A-a) - C_p\Delta T} \quad (5.91)$$

For differential scanning calorimetry, where $\Delta T = 0$, the total heat is equal to the peak area, A ,

$$\Delta H = A \quad (5.92)$$

It is assumed that the heat evolved is directly proportional to the number of moles reacted. It follows that

$$\frac{dN}{dt} = \frac{N_0}{A} \left(\frac{dH}{dt} \right) \quad (5.93)$$

and the rate constant is given by

$$k = \frac{(AV/N_0)^{n-1} (dH/dt)}{(A-a)^n} \quad (5.94)$$

It was stated that this equation was not limited to DSC but could apply to any procedure where the rate of change of any physical property is measured as a function of temperature and time under conditions where the temperature is changing. The physical property should be nearly independent of temperature.

Equation (5.91) has been simplified by numerous investigations; since the quantities $C_p(d\Delta T/dt)$ and $C_p\Delta T$ are an order of magnitude smaller than the quantities to which they are added and subtracted, they may be neglected to obtain

$$k = \frac{\Delta T}{(A-a)} \quad (5.95)$$

for a first-order reaction, or

$$k = \frac{(AV/N_0)^{n-1} \Delta T}{(A-a)^n} \quad (5.96)$$

for the general case.

Padrnanabhan et al. (123) and Agarwala and Naik (124) have used the simplified expression, as shown by equation (5.95), to determine the kinetics of a thermal decomposition reaction involving a powdered solid. The use of this expression for solid-state reactions does not appear to be valid in view of the original assumptions made in the derivation of the original equation.

Also neglecting $C_p(d\Delta T/dt)$, Borchardt (125) made the approximation

$$\frac{d(N/N_0)}{dt} \approx \frac{dx}{dt} \approx \frac{\Delta T}{A} \quad (5.97)$$

The kinetic method of Borchardt and Daniels (185) was subjected to an exhaustive examination by Reed et al. (120) in 1965. The equations were

integrated numerically, producing theoretical DTA curves which agreed well with the corresponding experimental curves. The effects of the various parameters, such as heating rate, reaction order, E , and so on, on the DTA curves were also established by numerical integration.

Using the decomposition of benzenediazonium chloride, Reed et al. (120) compared the kinetic results obtained by several different methods; these comparisons are shown in Table 5.12. They concluded that the Borchardt and Daniels method can be used for the quantitative determination of kinetic parameters if the experimental conditions closely approximate the assumptions of the theory, namely, reaction order n , with respect to only one component, and the absence of temperature gradients and overlapping peaks.

Reich (126) modified equation (5.97) to give

$$k = \left(\frac{A}{W_0} \right)^{n-1} \frac{\Delta T}{\bar{a}^n} \quad (5.98)$$

where k is the rate constant, ΔT is the peak height, W_0 is a function of the initial sample mass, and

$$A = \int_0^{\infty} \Delta T dt$$

$$\bar{a} = \frac{\int_0^x \Delta T dt}{\int_0^x \Delta T da} \quad (5.99)$$

Table 5.12. Kinetic Constants for the Decomposition of Benzenediazonium Chloride (120)

Method	E , kcal/mole	$\log A$, min ⁻¹
<i>DTA</i>		
Reed et al. (120), using Borchardt and Daniel's method	28.7	18.4
Reed et al. (120) using Kissinger's method	16.7	10.8
Borchardt and Daniels (185)	28.3	18.1
	29.1	
	28.5	
	30.6	
<i>Wada (186)</i>		
Conventional		
Crossley et al. (187)	27.2	17.3
Moelwyn-Hughes and Johns (188)	27.025	17.26

A difference method was developed in which the values from two DTA curves, obtained at two different heating rates, were used to calculate E and n .

Maycock (127), using the DSC curves shown in Figure 5.44, and assuming a linear Arrhenius plot, found that E could be calculated by the expression

$$E = \frac{R \ln d_1 - \ln d_2}{1/T_1 - 1/T_2} = \frac{4.58 \log(\alpha_1/\alpha_2)}{1/T_1 - 1/T_2} \quad (5.100)$$

where d_1 and d_2 are rates of heat evolution at T_1 and T_2 , respectively.

Reich and Stivala extended their previous TG nonisothermal kinetics method (163) to DTA curves for the calculation of E and n (164). Using TG, they derived the following expression;

$$\ln \frac{1 - (1 - \alpha_2)^{1/n} \left(\frac{T_2}{T_1}\right)^2}{1 - (1 - \alpha_1)^{1/n} \left(\frac{T_2}{T_1}\right)^2} = \frac{E}{R} \left(\frac{1}{T_2} - \frac{1}{T_1}\right) \quad (5.101)$$

where α is the degree of conversion, T the absolute temperature, E the activation energy, and n the order of reaction. Assuming that the heat evolved in a small temperature interval is directly proportional to the mass of reacting material during the temperature rise, and that the heat capacity terms are

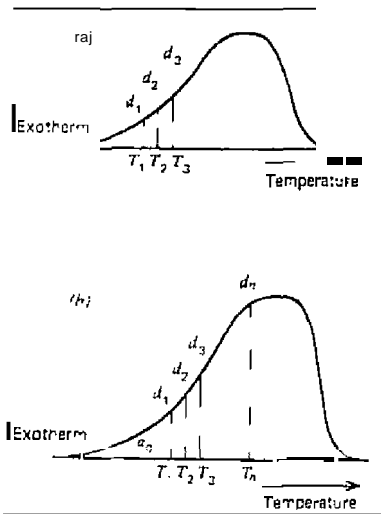


Figure 5.44. DSC curves used in kinetic analysis by Maycock (127).

negligible in comparison with other terms, they obtained the following:

$$(1 - \alpha) = \frac{\bar{a}_T}{A_T} \quad (5.102)$$

where

$$\bar{a}_T = \int_T^{T_\infty} \Delta T dT \quad \text{and} \quad A_T = \int_{T_0}^{T_\infty} \Delta T dT \quad (5.103)$$

with ΔT being obtained from the DTA curve. Substituting equation (5.102) into (5.101), the authors obtained

$$\ln \frac{1 - \left(\frac{\bar{a}_{T,1}}{A_T}\right)^{1-n} \left(\frac{T_2}{T_1}\right)^2}{1 - \left(\frac{\bar{a}_{T,2}}{A_T}\right)^{1-n} \left(\frac{T_2}{T_1}\right)^2} = \frac{E}{R} \left(\frac{1}{T_2} - \frac{1}{T_1}\right) \quad (5.104)$$

For two pairs of given values of \bar{a}_T/A_T and T , values of E and n can be calculated from equation (5.104) for various arbitrarily selected values of n . However, assuming uniqueness, only one pair of E and n values will be pertinent. Equation (5.104) does not apply if $n = 1$, but Reich and Stivala state that this value is rare in practice, and hence the equation is considered to be of general validity. An iteration method was also presented whereby values of E and n are computer calculated using a single DTA curve (165).

A simplified method for determining rate constants by DSC was introduced by Rogers (166). The deflection of the DSC curve above the baseline, b , is directly proportional to the rate of energy evolution or absorption of the sample, dq/dt , which in turn is directly proportional to the rate of reaction, $d\alpha/dt$. Therefore,

$$\alpha b = \beta \frac{dq}{dt} = \frac{d\alpha}{dt} = k(1 - \alpha) \quad (5.105)$$

where α and β are proportionality constants and k is the rate constant. Hence,

$$\ln b = \ln k/\alpha + \ln(1 - \alpha) \quad (5.106)$$

For a first-order reaction

$$-\ln(1 - \alpha) = kt \quad (5.107)$$

where c is a constant. Substituting equation 15.107 in (5.106) and combining constants gives

$$\ln b = C - kt \quad (5.108)$$

Thus, rate constants for first-order reactions can be obtained directly from a plot of $\ln b$ versus t .

For reactions that melt with decomposition, another DSC method was developed by Rogers (167) in order to determine the kinetic constants of such a system. Still another method was described by Rogers and Daub (168, 169) for the determination of kinetics for vapor phase reactions.

In a DTA curve, ΔT at any given instant can be approximated by being proportional to the instantaneous mass reacting rate:

$$\Delta T = k_1 y \quad (5.109)$$

According to Yang and Steinberg (170), the equation is approximate because k_1 is affected by the heat and mass transport processes that do not remain strictly constant during the reaction. For "first-order" reactions

$$\Delta T = k_1 r_0 \exp(-E/RT)(1-x)m_0 \quad (5.110)$$

where $y = m_0$, the instantaneous mass. The peak temperature, T_p , is obtained by setting $d(\Delta T)/dT = 0$ and solving for T_p . Murray and White (119) had previously used the following expression:

$$\frac{r_0}{k_1} \exp(-E/RT_m) = \frac{E}{RT_m^2}$$

where k_2 is the heating rate. The temperature at the inflection points (T_1), that is, at the maximum and minimum slopes, can be obtained by setting $d^2(\Delta T)/dT^2 = 0$ and solving for T_1 . The following is then obtained:

$$\frac{r_0}{k_1} \exp(-E/RT_1) \left(\frac{3E}{RT_1^2} - \frac{E}{k_2} \exp(-E/RT_1) \right) = \left(\frac{E}{RT_1^2} \right)^2 - \frac{3E}{RT_1^3} \quad (5.112)$$

In this equation, there exist two solutions for T : (T_{11} and T_{12}) that correspond to the two inflection points. E and r_0 can be calculated by solving equations (5.111) and (5.112) simultaneously with T_m and either one of the T_1 's, or by solving equation (5.112) with T_{11} and T_{12} .

Blecic et al. (171) developed a method for the determination of the reaction kinetics using one DTA curve, with the condition that the function character-

izing the reaction mechanism be determined from isothermal data

A method has been developed in which the DTA curve is obtained under pseudo-isothermal conditions: that is, both sample and reference materials are not heated: the temperature remains as isothermal as possible (172, 173).

Davies et al. (174) found that the polymorph transition kinetics of the changes of vaterite to calcite and aragonite to calcite could be followed using DTA and the equation

$$\frac{dx}{dt} = \frac{4}{3} k [-\ln(1-x)]^3 (1-x) \quad (5.113)$$

The crystal nucleation of glasses were studied using a DTA kinetics method developed by Marotta et al. (62, 175, 176).

Van Dooren and Muller studied the effects of sample mass and particle size on the determination of kinetic parameters by the Ozawa and Kissinger methods (177) as well as the Freeman and Carroll method (178), all using DSC. It was found that both sample mass and particle size could influence the kinetic parameters, but the extent of these effects are different for each substance. Kissinger's method did not have any practical advantages over the Ozawa method. For the Freeman and Carroll method, narrow peaks gave rise to very high E values and large errors. Even negative reaction orders were found that were indicative of the explosive character of the transition. Since the kinetic parameters differ considerably during the peak, it was not justified to attribute any physical meaning to them.

Quantitative correlations between kinetic parameters and sample mass and heating rate as well as dependent variables were derived for DTA and DSC by Krishnan et al. (179).

Anderson et al. (180) compared the most popular kinetics method (the DTA versions of them; for the TG methods see Chapter 2) using a homogeneous, irreversible first-order model reactor, with the following parameters:

$$\begin{aligned} \Delta H &= 40 \text{ kcal/mole} & q &= 3.75^\circ\text{C/min} \\ E &= 20 \text{ kcal/mole} & V &= 0.005 \text{ L} \\ A &= 10^{12} \text{ min}^{-1} & C_p &= 5.714 \text{ cal/deg} \\ \rho &= 0.1 \text{ mole/L} & K &= 4.0 \text{ cal/deg min} \end{aligned}$$

where

$$\frac{dx}{dt} = \frac{c}{K A} \left[C_p \frac{d\Delta T}{dt} - K \Delta T \right] \quad (5.114)$$

$$A = \int_0^{\tau} \Delta T dt \quad (5.115)$$

and

$$\frac{dx}{dt} = k_0 e^{XPI-E/RT} (C - x)^n \quad (5.116)$$

Using these data, the authors calculated a theoretical DTA curve with a mean error in ΔT of 8%. The theoretical curve was calculated to within $\pm 0.1\%$ of ΔT_{max} , but values down to $\pm 10\%$ of ΔT_{max} were generally involved in the comparison.

The results of the kinetic parameters calculations employing the different methods is presented in Table 5.13. DTA curves (1), (2), and (3) represent theoretical curves calculated with different errors in ΔT_{max} . From the table,

Table 5.13. Comparison of Different DTA Kinetics Methods (180)
(Theoretical Value of $E = 20$ kcal/mole)

	DTA Curve 1 (%)	DTA Curve 2 (%)	DTA Curve 3 (%)
Kissinger	18.76 (6.2)		
Piloyan et al.	18.74 (6.3)		
Borchardt-Daniels	20.00 (0)	19.96 (0.2)	21.5 (5.7)
Freeman-Carroll	19.86 (0.7)	15.60 (22.0)	59.68 (198.4)
Coats-Redfern	20.00 (0)	18.49 (7.51)	19.15 (4.1)
Škvara-Salava	20.00 (0)	19.30 (3.5)	19.50 (2.5)
Horowitz-Metzger	22.03 (0.2)	18.29 (8.5)	20.24 (11.2)
Gyulai-Greenhow	20.00 (0)	19.21 (4.0)	17.93 (110.41)
Székegy-Lengyel	20.00 (0)		

Table 5.14. Comparison of Kinetics Methods for the
Thermal Decomposition Kinetics of AIBN (183)

Method ^a	E (kcal/mole)	
Ozawa	22.6	28.6
Kissinger	22.2	27.9
ASTM-E698	22.2	21.2
Single scan DSC method ^b	31.4	35.2
Classical method	30.8	35.0

^aAll reaction orders assumed to be 1.

^bReaction order of $n = 0.95$.

it is seen that the methods of Borchardt and Daniels, Coats and Redfern, and Salava and Skvara gave the best results, even under extreme conditions. The Freeman and Carroll method is a sensitive indicator for deviations from the theoretical DTA curve.

A comparison of the kinetic parameters for the thermal decomposition of 2, 2'-azobis(isobutyronitrile) (AIBN) obtained by different DSC methods is given in Table 5.14 (184). The ASTM E-698 method is a modification of the Ozawa method (181), whereas the single scan DSC method is that described by Prime (182,183).

REFERENCES

- Murphy, C. B., *Miner. Sci. Eng.*, 3, 51 (1970).
- Speil, S., L. H. Berkelhamer, J. A. Pask, and B. Davis, *U.S. Bur. Mines, Tech. Papers*, 664 (1945).
- Kerr, P. F., and J. L. Kulp, *Am. Mineral.*, 33, 387 (1948).
- Smykatz-Kloss, W., *Differential Thermal Analysis*, Springer-Verlag, Berlin, 1974.
- Pope, M. I., and M. D. Judd, *Differential Thermal Analysis*, Heyden, London, 1977.
- Paulik, J., and F. Paulik, "Simultaneous Thermoanalytical Examinations by Means of the Derivatograph," in Wilson and Wilson's *Comprehensive Analytical Chemistry*, W. W. Wendlandt ed., Vol. XII, Part A, Elsevier, Amsterdam, 1981.
- Jespersen, N. D., "Biochemical and Clinical Applications of the Thermogravimetric Thermal Analysis," in Ref. 6, 1982.
- Sestak, J., *Thermophysical Properties of Solids*, in Ref. 6, 1984.
- Lomhardi, G., *For Better Thermal Analysis*, 2nd ed., CFA, Rome, 1980.
- Mackenzie, R. C., *Thermochim. Acta*, 73, 251 (1984).
- Ref. 10, p. 307.
- Wendlandt, W. W., *Anal. Chem.*, 54, 97R (1982).
- Wendlandt, W. W., *Anal. Chem.*, 56, 250R (1984).
- Claudy, P., I. D. Commercon, and J. M. Letoff, *Thermochim. Acta*, 68, 305 (1983).
- Ref. 14, p. 317.
- Flynn, J. B., in *Analytical Calorimetry*, R. S. Porter and J. F. Johnson, eds., Vol. 3, Plenum, New York, 1982.
- Flynn, J. H., *Thermochim. Acta*, 8, 69 (1974).
- Shishkin, Y. L., *J. Thermal Anal.*, 27, 113 (1983).
- O'Neill, M. I., *Anal. Chem.*, 47, 630 (1975).
- Williams, J., and W. W. Wendlandt, *Thermochim. Acta*, 1984.
- Kamphausen, M., G. M. Schneider, W. Spratte, and A. Wurlinger, *Proc. 4th Int. Conf. Chem. Thermodynamics*, Montpellier, France, Aug. 26-30, 1975.
- Borchardt, H. J., and F. Daniels, *J. Am. Chem. Soc.*, 79, 41 (1957).
- Wendlandt, W. W., in *Technique of Inorganic Chemistry*, H. B. Jonassen and A. Weissberger, eds., Vol. 1, Interscience, New York, 1963, p. 209.
- Wendlandt, W. W., *J. Chem. Educ.*, 49, A623 (1972).

25. Murphy, C. B., *Anal. Chem.*, 30,867(1958).
26. Murphy, C. B., *Anal. Chem.*, 44, 513R (1972).
27. Smothers, W. I., and Y. Cbiang., *Differential Thermal Analysis: Theory and Practice*, Chemical Publishing Co., New York, 1958.
28. Smothers, W. J., and Y. Chiang, Ref. 27, 2nd ed., 1966.
29. Gam, P. D., *Thermaanalytical Methods of Investigation*, Academic, New York, 1965.
30. Mackenzie, R. C., ed., *Differential Thermal Analysis*, Academic, London, Vol. 1, 1970.
31. Kissinger, H. E. and S. B. Newman, in *Differential Thermal Analysis in Analytical Chemistry of Polymers*, G. M. Kline, ed., Vol. XII, Part II, Interscience, New York, 1962.
32. Gordon, S., in *Encyclopedia of Science and Technology*, Vol. 13, McGraw-Hill, New York, 1960, pp. 556-559.
33. Gordon, S., and C. Campbell, in *Handbook of Analytical Chemistry*, L. Meites, ed., McGraw-Hill, New York, 1963.
34. Barrall, E. M., and J. F. Johnson, in *Techniques and Methods of Polymer Evaluation*, P. E. Slade and L. T. Jenkins, eds., Vol. 1, Marcel-Dekker, New York, 1966, Chap. 1.
35. David, D. J., Ref. 34, Chap. 2.
36. Barrall, E. M., in *Guide to Modern Methods of Instrumental Analysis*, F. H. Gow, ed., Wiley-Interscience, New York, 1972, Chap. 12.
37. Schultze, D., *Differentialthermoanalyse*, Deutscher Verlag der Wissenschaften, Berlin, 1969.
38. Ramachandran, V. S., *Differential Thermal Analysis in Cement Chemistry*, Chemical Publishing Co., New York, 1969.
39. Wunderlich, B., in *Physical Methods of Chemistry*, A. Weissberger and B. W. Rossiter, eds., Vol. 1, Part V, Wiley-Interscience, New York, 1971, Chap. VIII.
40. Porter, R. S., and J. F. Johnson, eds., Vol. I, *Analytical Calorimetry*, Plenum, New York, 1968.
41. Porter, R. S., and J. F. Johnson, eds., Ref. 40, Vol. 2, 1970.
42. Schwerker, R. F. and P. D. Gam, eds., Vols. 1, 2, *Thermal Analysis*, Academic, New York, 1969.
43. Void, M. J., *Anal. Chem.*, 21,683(1949).
44. Boersma, S. L., *J. Am. Ceram. Soc.*, 38, 281 (1955).
45. Lukaszewski, G. M., *Lab. Pract.*, 14, 1277 (1965).
46. Ref. 45, p. 40.
47. Lukaszewski, G. M., *Lab. Pract.*, 15, 75 (1966).
48. Ref. 47, p. 82.
49. Ref. 47, p. 187.
50. Ref. 47, p. 302.
51. Ref. 47, p. 431.
52. Ref. 47, p. 551.
53. Ref. 47, p. 664.
54. Ref. 47, p. 762.
55. Ref. 47, p. 861.

56. David, D. J., *Anal. Chem.*, 36, 2162 (1964).
57. David, D. J., *Lab. Equip. Dig.*, Jun. Aug., 1968, p. 10.
58. Pacer, P., *Anal. Chim. Acta*, 37, 200 (1967).
59. Melling, R., F. W. Wilbur, and R. M. McIntosh, *Anal. Chem.*, 41, 1275 (1969).
60. Gray, A. P., in *Analytical Chemistry*, R. F. Porter and J. M. Johnson, eds., Plenum, New York, 1968, p. 209.
61. Gam, P. D., Ref. 29, p. 60.
62. Kissinger, H. E., *J. Res. Nat. Bur. Stand.*, 57, 217 (1956).
63. Kissinger, H. E., *Anal. Chem.*, 29, 1702 (1957).
64. Barrall, E. M., and L. B. Rogers, *J. Inorg. Nucl. Chem.*, 28, 41 (1966).
65. Langer, A. M., and P. F. Kerr, *Du Pont Thermogram*, 3, No. 1, 1 (1968).
66. Vassallo, D. A., and J. C. Harden, *Anal. Chem.*, 34, 132 (1962).
67. Johnson, J. F., and G. W. Miller, *Thermochim. Acta*, 1, 373 (1970).
68. Sarasohn, I. M., *Du Pont Thermogram*, 2, No. 1, 1 (1965).
69. Stonc, R. L., *Anal. Chem.*, 32, 1582 (1960).
70. *Mettler Thermal Technique Series*, Tech. Bull. No. T-106.
71. Dean, L. A., *Soil Sci.*, 63, 95 (1947).
72. Locke, C. E., in *Proceedings of the Third Toronto Symposium on Thermal Analysis*, H. G. McAdie, ed., Chemical Institute of Canada, Toronto, 1969, p. 251.
73. Gam, P. D., *Anal. Chem.*, 37, 771 (1965).
74. Levy, P., G. Nieuweboer, and L. C. Semanski, *Thermochim. Acta*, 4, 429 (1960).
75. David, D. J., *Anal. Chem.*, 37, 82 (1965).
76. Wilbur, F. W., J. R. Hesford, and J. R. Flowers, *Anal. Chem.*, 40, 777 (1968).
77. Dosch, E. L., *Thermochim. Acta*, 3, 367 (1970).
78. Lehmann, H., S. S. Das, and H. H. Pae1sch, *Tennid.-Ztg. u. Keram. Rundschau* (1954), 1.
79. Bayliss, P., and S. St. J. Warne, *Am. Mineral.*, 47, 775 (1962).
80. Arens, P. L., *A Study of the Differential Thermal Analysis of Clays and Clay Minerals*, Excelsiors Foto-Offset, The Hague, 1951.
81. Gerard-Hirne, J., and C. Jamy, *Bull. Soc. Fr. Ceram.*, 26 (1951).
82. Webb, T. T., *Nature*, 174, 686 (1954).
83. Mackenzie, R. C., Ref. 82, p. 688.
84. Sarasohn, I. M., ACS Short Course, American Chemical Soc., Washington, DC, 1969.
85. Smyth, H. T., *J. Am. Ceram. Soc.*, 34, 221 (1951).
86. Barrall, E. M., and L. B. Rogers, *Anal. Chem.*, 34, 1101 (1962).
87. David, D. J., D. A. Nirke, and B. Duncan, *Am. Lab.*, Jan. 1971, p. 51.
88. Hauser, R. E., B. S. thesis, N.Y. State College of Ceramics, Alfred, NY, 1951.
89. Norton, F. H., *J. Am. Ceram. Soc.*, 22, 54 (1939).
90. Grimshaw, R. W., E. Heaton, and A. L. Roberts, *Trans. Br. Ceram. Soc.*, 44, 76 (1945).
91. Carthew, A. R., *Am. Mineral.*, 40, 107 (1955).
92. Surrah, E. M., and L. B. Rogers, *Anal. Chem.*, 34, 1106 (1962).
93. Nagishi, A., and T. Ozawa, *Thermochim. Acta*, 2, 89 (1971).
94. Wada, M., Y. Iida, and S. Ozaki, Jr., *J. Appl. Phys.*, 8, 1569 (1949).
95. Gruver, R. M., *J. Am. Ceram. Soc.*, 31, 323 (1948).

96. Bolin, E. M., and A. J. Bauman, in *Analytical Calorimetry*, R. F. Porter and J. M. Johnson, eds., Vol. 2, Plenum, New York, 1970, p. 339.
97. Barshad, I., *Am. Mineral.*, 37, 667 (1952).
98. deJong, G. J., *J. Am. Ceram. Soc.*, 40, 42 (1957).
99. Bohon, R. L., *Proceedings of the First Toronto Symposium on Thermal Analysis*, H. G. McAdie, ed., Chemical Institute of Canada, Toronto, 1965, p. 63.
100. Ozawa, T., *Bull. Chem. Soc. Jpn.*, 39, 207L (1966).
101. Witel's, M., *Am. Mineral.* 36, 615 (1951).
102. Ref. 101, p. 760.
103. Collins, W. E., in *Analytical Calorimetry*, R. S. Porter and J. M. Johnson, eds., Vol. 2, Plenum, New York, 1970, p. 353.
104. David, D. J., Ref. 103, p. 369.
105. Bohon, R. L., *Anal. Chem.*, 35, 1845 (1963).
106. Chiu, J., in *Analytical Calorimetry*, R. F. Porter and J. M. Johnson, eds., Vol. 2, Plenum, New York, 1970, p. 171.
107. Wendlandt, W. W., and J. R. Williams, International Confederation of Thermal Analysis III, Davos, Switzerland, Aug. 1971, paper I.
108. Currell, B. R., in *Thermal Analysis*, R. F. Schwenker and P. D. Garn, eds., Vol. 2, Academic, New York, 1969, p. 1185.
109. Wiedemann, H. G., and A. van Tets, *Z. Anal. Chem.*, 233, 161 (1968).
110. Wiedemann, H. G., and A. van Tets, *Thermochim. Acta*, 1, :59 (1970).
111. Ramachandran, V. S., and P. J. Sereda, *Nature, Phys. Sci.*, 233, 134 (1971).
112. Davis, C. F., and D. A. Holdridge, *Clay Miner.*, 8, 193 (1969).
- Ramachandran, V. S., *J. Thermal Anal.*, 3, 181 (1971).
- Schwenker, R. F., and I. C. Whitwell, in *Analytical Calorimetry*, R. F. Porter and J. M. Johnson, eds., Vol. 1, Plenum, New York, 1968, p. 249.
115. Sturm, E., *Thermochim. Acta*, 4, 461 (1972).
116. Clarke, T. A., E. L. Evans, K. G. Robbins, and J. M. Thomas, *Chem. Commun.*, 266 (1969).
117. Friedman, H. L., *Proceedings of the Third Toronto Symposium on Thermal Analysis*, H. G. McAdie, ed., Chemical Institute of Canada, Toronto, 1969, p. 127.
118. Sestak, J., and G. Berggren, *Svavak*, 64, 695 (1970).
119. Murray, P., and J. White, *Trans. Br. Ceram. Soc.*, 54, 204 (1955).
120. Reed, R. I., L. Weber, and B. S. Gottfried, *Ind. Eng. Chem. Fundam.*, 4, 38 (1965).
121. Poloyan, G. O., I. D. Ryabchikov, and O. S. Novikova, *Nature*, 212, 1229 (1966).
122. Akita, K., and M. Kase, *J. Phys. Chem.*, 72, 906 (1968).
123. Padmanabhar, V., S. C. Saraiya, and A. K. Sundaram, *J. Inorg. Nucl. Chem.*, 12, 356 (1960).
124. Agarwala, R. P., and M. C. Naik, *Anal. Chim. Acta*, 24, 128 (1960).
125. Borchardt, H. L., *J. Inorg. Nucl. Chem.*, 12, 252 (1960).
126. Reich, L., *J. Inorg. Nucl. Chem.*, 28, 1329 (1966).
127. Maycock, J. N., *Thermochim. Acta*, 1, 389 (1970).
128. Watson, E. S., M. J. O'Neil, J. Justin, and N. Brenner, *Anal. Chem.*, 36, 1233 (1964).
129. O'Neil, M. L., Ref. 128, p. 1238.
130. Baxter, R. A., in *Thermal Analysis*, R. F. Schwenker and P. D. Garn, eds., Academic, New York, 1969, p. 65.

131. David, D. J., *J. Thermal Anal.*, 3, 247 (1971).
132. Wilhoit, R. C., *J. Chem. Educ.*, 44, A57 (1967).
133. Perkin-Elmer Corp., Norwalk, Conn., May 1970.
134. Flynn, J. H., in *Status of Thermal Analysis*, O. Menz, ed., NBS Special Publication 338, U.S. Gov't. Printing Office, Washington, DC, Oct. 1970, p. 119.
135. Brennan, W. P., D. Miller, and J. C. Whiteil, *Thermochim. Acta*, 2, 354 (1971).
136. Wurfinger, A., and J. Kreutzenbeek, *J. Phys. Chem. Solids*, 39, 193 (1978).
137. Bandi, W. R., and G. Krapf, *Thermochim. Acta*, 14, 221 (1976).
138. Criado, J. M., *Thermochim. Acta*, 19, 129 (1977).
139. Dollimore, D., L. F. Jones, and T. Nicklin, *Thermochim. Acta*, 11, 307 (1975).
140. Dollimore, D., and J. Mason, *Thermochim. Acta*, 43, 183 (1981).
141. Dollimore, D., J. P. Gupta, and D. V. Nowell, *Thermochim. Acta*, 30, 339 (1979).
142. Pope, M. I., and D. I. Sutton, *Thermochim. Acta*, 23, 188 (1978).
143. Wiedemann, H. G., and W. Smykal-Kloss, *Mettler Application No. 3465*, Mettler Instrument Corp., Griefensee, Switzerland.
144. Reichelt, J., and W. Hemminger, *Thermochim. Acta*, 69, 59 (1983).
145. Hohe, G. W. H., *Thermochim. Acta*, 69, 175 (1981).
146. Ortiz, L. W., and R. N. Rogers, *Thermochim. Acta*, 3, 383 (1972).
147. Rogers, R. N., and E. D. Morris, *Anal. Chem.*, 38, 110 (1966).
148. Charsley, E. L., J. A. Rumsey, and S. B. Warrington, *Anal. Proc.*, Jan. 1984, p. 5.
149. *Tech. Inform. Sheer*, No. 15, Stanton Redcroft Ltd., London.
150. Murray, J. P., K. J. Cavell, and J. O. Hill, *Thermochim. Acta*, 36, 97 (1980).
151. Richardson, M. J., and N. G. Savill, *Thermochim. Acta*, 12, 221 (1975).
152. Van Dooren, A. A., and B. W. Muller, *Thermochim. Acta*, 49, 163 (1981).
153. Van Dooren, A. A., and B. W. Muller, *Thermochim. Acta*, 54, 115 (1982).
154. Guttman, C. M., and J. H. Flynn, *Anal. Chem.*, 45, 408 (1973).
155. Golberg, R. N., and E. J. Prosen, *Thermochim. Acta*, 6, 1 (1973).
156. Brennan, W. P., and A. P. Gray, *Thermal Analysis Application Study 9*, Perkin-Elmer Corp., Norwalk, CT.
157. Mackenzie, R. C., *Inst. Proc.*, June 1980, 217.
158. Van Dooren, A. A., and B. W. Muller, *Thermochim. Acta*, 49, 151 (1981).
159. Ref. 158, p. 175.
160. Ref. 158, p. 185.
161. Sestak, I., V. Satava, and W. W. Wendlandt, *Thermochim. Acta*, 7, 333 (1973).
162. Sestak, I., "Thermophysical Properties of Solids," in Wilson and Wilson's *Comprehensive Analytical Chemistry*, W. W. Wendlandt, ed., Vol. XII, Part D, Elsevier, Amsterdam, (1984).
163. Reich, L., and S. S. Stivala, *Thermochim. Acta*, 24, 9 (1978).
164. Reich, L., and S. S. Stivala, *Thermochim. Acta*, 25, 367 (1978).
165. Reich, L., and S. S. Stivala, *Thermochim. Acta*, 66, 383 (1983).
166. Rogers, R. N., *Anal. Chem.*, 44, 1336 (1972).
167. Rogers, R. N., *Thermochim. Acta*, 3, 437 (1972).
168. Rogers, R. N., and G. W. Daub, *Anal. Chem.*, 45, 596 (1973).
169. Rogers, R. N., *Thermochim. Acta*, 9, 444 (1974).
170. Yang, R. T., and M. Steinberg, *J. Phys. Chem.*, 80, 965 (1976).
171. Blacic, O., Z. D. Zivkovic, and M. Martinovic, *Thermochim. Acta*, 60, 61 (1983).

172. Matsuda, H. and S. Goto, *Can. J. Chem. Eng.*, 62, 101 (1984).
 173. Ref. 172, p. 108.
 174. Davies, P., D. Dollimore, and G. R. Ieal, *J. Thermal Anal.* 13, 473 (1978).
 175. Marotta, A. A. Bun, and F. Branda, *J. Mater. Sci.* 16, 341 (1981).
 176. Marotta, A. A. Buri, and F. Branda, *J. Thermal Anal.*, 21, 227 (1981).
 177. Van DiOren, A. A., and B. W. Muller, *Thermochim. Acta*, 65, 257 (1983).
 178. Ref. 177, p. 269.
 179. Krishan, K., K. N. Ninan, and P. M. Madhusudaran, *Thermochim. Acta* 71, 305 (1983).
 180. Anderson, H., W. Besch, and D. Haberland, *J. Thermal Anal.*, 12, 59 (1977).
 181. Ozawa, T., *J. Thermal Anal.* 2, 30 (1970).
 182. Prime, R. B., *Anal. Calorim.*, 2, 201 (1970).
 183. Prime, R. B., *Polym. Eng. Sci.*, 13, 365 (1973).
 184. Provder, T., R. M. Holsworth, T. H. Grentzer, and S. A. Kline, *Polymer Characterization*, C. D. Craver, ed., American Chemical Society, Washington, DC, 1983, p. 233.
 185. Borchardt, H. J., and F. Daniels, *J. Am. Chem. Soc.*, 79, 41 (1957).
 186. Wada, G., *Nippon Kagaku Zasshi*, 1956 (1960).
 187. Crossley, M. L., R. H. Kienle, and C. H. Berbrook, *J. Am. Chem. Soc.*, 62, 1400 (1940).
 188. Moelwyn-Hughes, E. A., and P. Johnson, *Trans. Faraday Soc.* 36, 948 (1940).
 189. Coats, A. W., and I. P. Redfern, *Nature*, 201, 68 (1964).

CHAPTER

6

DIFFERENTIAL THERMAL ANALYSIS AND DIFFERENTIAL SCANNING CALORIMETRY INSTRUMENTATION

A. INSTRUMENTATION PRINCIPLES

1. Introduction

As for thermogravimetry, there are a large number of different types of instruments for DTA. Perhaps the reason for this multiplicity is that before the advent of reliable commercial DTA instruments, each investigator designed and built his or her own apparatus. Needless to say, each apparatus varied widely in the type of components employed. Various types of sample holders, furnaces, ΔT amplifying devices, temperature programmers, and recorders were described. Because of this, there was little agreement in the DTA curves obtained for identical materials from instrument to instrument or from laboratory to laboratory. In fact, it was almost impossible to duplicate exactly the results obtained by another instrument in another laboratory, and this, at times, led to much controversy. Since the advent of good commercial DTA instruments in the late 1950s, some standardization has taken place, so that it is now possible to duplicate DTA data, providing, of course, that identical pyrolysis conditions are employed.

A typical DTA apparatus is illustrated schematically in Figure 6.1. The apparatus generally consists of (1) a furnace or heating device, (2) a sample holder, (3) a low-level de amplifier, (4) a differential temperature detector, (5) a furnace temperature programmer, (6) a recorder, and (7) control equipment for maintaining a suitable atmosphere in the furnace and sample holder. Many modifications have been made of this basic design, but all instruments measure the differential temperature of the sample as a function of temperature or time assuming that the temperature rise is linear with respect to time).

2. Sample Holders

One of the most important components of a DTA apparatus is the type of sample holder (and identical reference material holder) employed. There

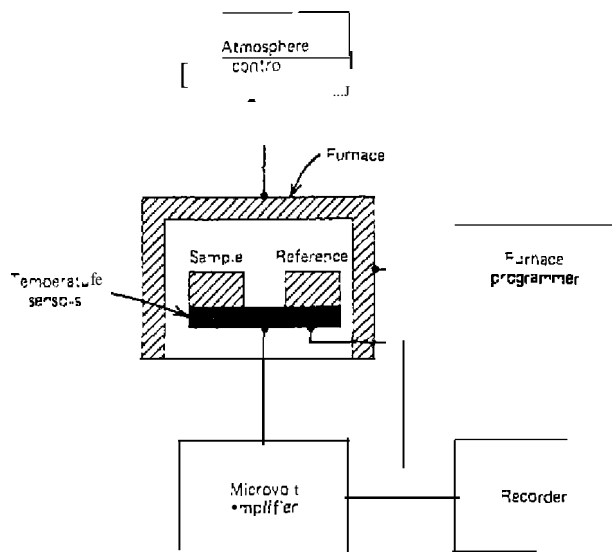


Figure 6.1. Schematic diagram of a typical UTA apparatus.

are a wide variety of sample holders available, in commercial instruments or that have been described in the literature. The type of sample holder (1) used depends, of course, on the nature and quantity of the sample and also on the maximum temperature to be investigated. Sample holders have been constructed from alumina, zirconia (ZrO_2), borosilicate glass, Vycor glass, fused quartz, beryllia, boron nitride, graphite, stainless steel, nickel, aluminum, platinum or platinum alloys, silver, copper, tungsten, the sample itself, and numerous other materials. Some typical sample holders used in DTA are shown in Figure 6.2. In (a), the sample (~ 100 mg) is pressed into a closed-end tube and the tube is placed over the ceramic insulator tube containing the thermojunction (2). This type of sample holder will permit the sample to dissociate in a self-generated atmosphere. It cannot be used with samples that fuse on heating, however. For determining heats of explosion for a number of explosive materials, the isochoric sample holder in (b) was used by Bohon (3). It consisted of a stainless steel body and cap that was sealed with a screw cap and a copper gasket. The internal volume was about 0.085 ml and contained about 25 mg of sample. By means of a loading chamber, the sample holder could be charged with a gas at pressures up to 1000 psig. Mazieres (4) developed the microsample holder in (c) for use with samples from 1-200 μ g in mass. The sample was contained in a chamber

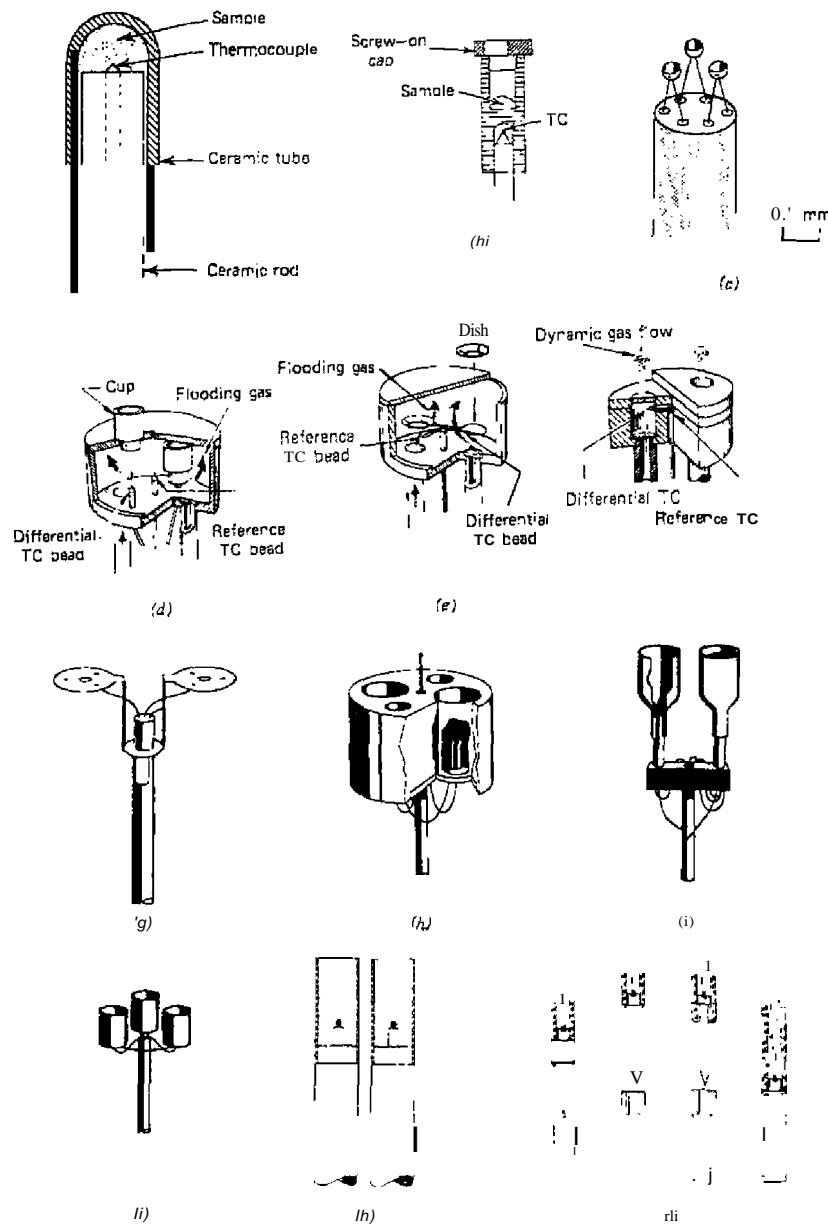


Figure 6.2. DTA sample holders.

drilled in the thermojunction itself. A similar cup-type holder was also described which could be used for samples from 0.1 to 10 mg in mass. Some difficulty would certainly be experienced in the handling of microgram quantities of sample.

Sample holders used in the Stone instruments are shown in (d)-(f). Small cups are used in (d) to contain samples from 10 to 200 mg in mass; the cups are constructed from aluminum, stainless steel, nickel, or platinum and or palladium alloys. For smaller samples, 0.1 to 20 mg, the highly sensitive ring thermocouple holder, as shown in (e), is used. The sample dishes can be made from aluminum, stainless steel, or platinum by the investigator using a simple press and die. True dynamic gas atmosphere control is featured in the sample holder in (f). The gas flow is through the sample and reference materials; it cannot be used with samples that fuse, however.

Sample holders illustrated in (g)-(j) are used in the Mettler thermo-analyzer system. In (g), the sample is placed in a small cup or crucible and placed on the small circular discs which contain the thermojunction. A block-type sample holder is shown in (h) in which an alumina block is employed. The sample is contained in a crucible which may be constructed from platinum or other metals. For macro amounts of sample, the holder in (i) may be used. The containers are constructed of alumina or of different metals. If only small amounts of sample are to be studied, the micro crucible sample holder in (j) may be used.

The sample holders in (k) are used in Linseis DTA equipment. In (k), removable sleeves made of metal or ceramic are used to contain the sample. This type of sample holder is convenient for cleaning purposes as the sleeve may be easily removed, leaving the exposed sample. A disadvantage of this type of sample holder is that the thermocouple is in direct contact with the sample and may be attacked by corrosive sample materials, thus changing its EMF output characteristics. A similar disadvantage is present for the probe-type sample holders in (l) and (m), in which the thermocouple is immersed in the interior of the sample. The glass sample container in (l) is usually a disposable capillary tube 1-2 mm in diameter. A sample holder for horizontal use is illustrated in (m).

A sample holder for use at very high temperatures (2200 C) is illustrated in (n). It is constructed of tungsten-tungsten, 26% rhenium, and is for use in the Mettler instruments.

The unique sample holder illustrated was developed by Miller for use in the study of textile filaments and yarns. The filament sample is wound in the grooves cut in the outer surface of an aluminum cylinder. Three identical cylinders are mounted symmetrically in the center of a vertical furnace. Two are used for the sample and reference materials, while the third is used to monitor the furnace temperature.

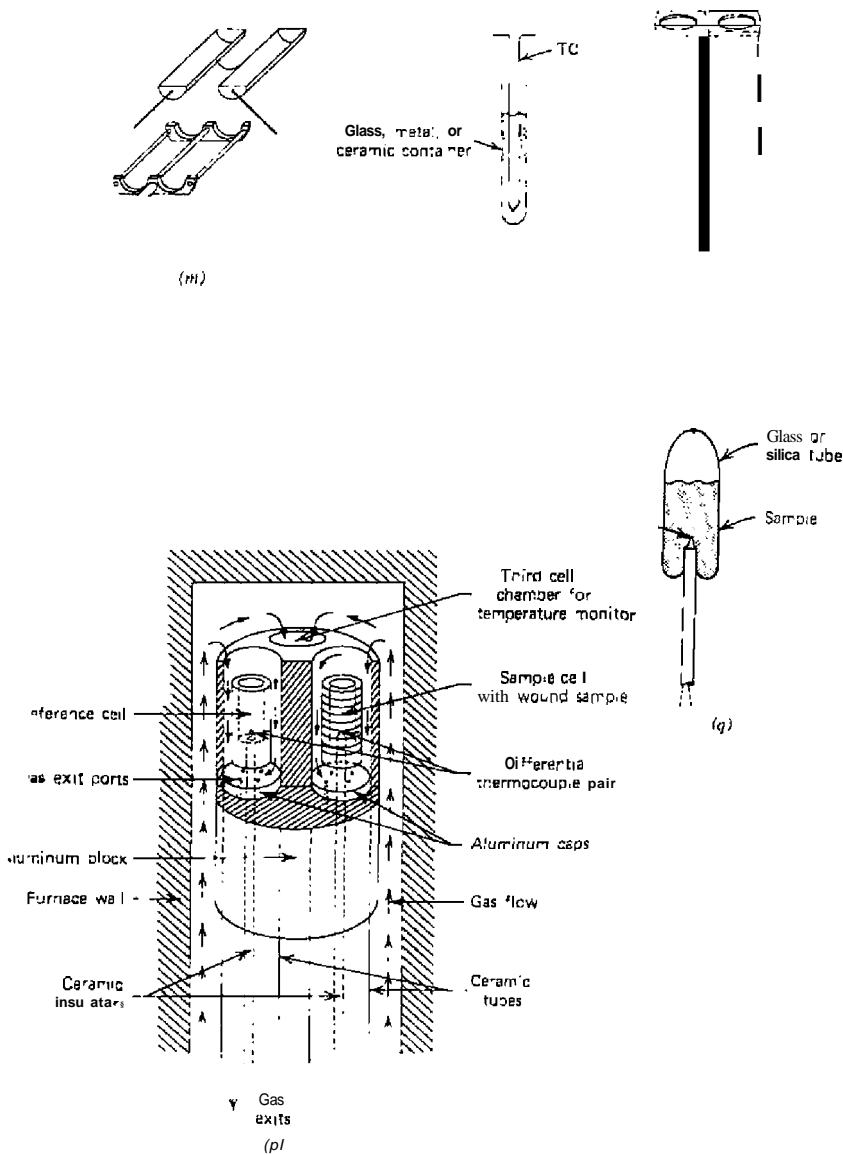


Figure 6.2 (Cont'd)

Brunskill et al. (73) used the sample holder shown in figure 6.3. The crucible, machined from an annealed platinum rod, was placed in direct contact with the thermocouple. In order to prevent mass-loss during decomposition reactions, one could seal the crucible with a high-temperature Turner flame.

The DTA curves of samples in sealed tubes can be determined by use of the sample holder in (g). Sealed tube holders are described in a later section of this chapter.

To increase the number of samples that can be studied at anyone given time, experimenters have described various multiple sample holders capable of studying three, four, five, or six samples simultaneously. Several arrangements of these holders are illustrated in Figure 6.4.

The arrangement in (a), which is due to Kulp and Kerr (6,7), contained six sample wells and three reference wells. Each sample and reference well was $\frac{1}{8}$ in. in diameter and $\frac{3}{8}$ in. deep, drilled in a nickel metal block. A multipoint recorder was used to record the temperature differences for each sample-reference combination.

The multiple sample holder, as shown in (b), contains four separate sample-reference pairs, as well as a monitor thermocouple. Slits are cut at various radial intervals in the block to prevent thermal gradients from one sample interfering with an adjacent reference well. Four separate dc amplifiers are used in conjunction with a four-channel recorder.



Figure 6.3. Platinum sample holder of Brunskill et al. (73)

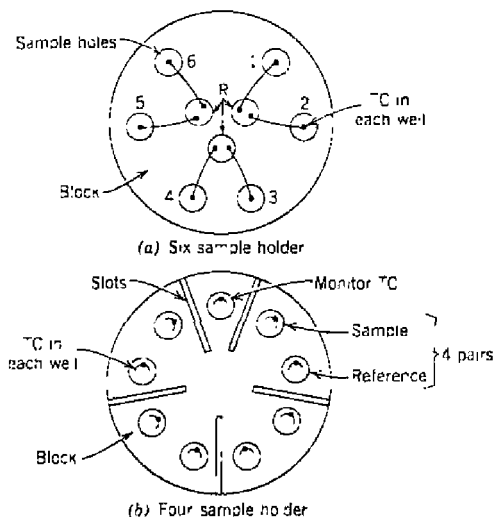


Figure 6.4. Multiple sample-holder arrangements.

A five-sample multiple sample block has also been described by Cox and McGlynn (8). A somewhat different approach was employed by Burr (9) in which five samples, contained in an aluminum block, were recorded using a multichannel recorder. The ΔT signals of the samples were recorded at 36-sec intervals.

3. ΔT and T Detection

The choice of a temperature detection device depends on the maximum temperature desired, the chemical reactivity of the sample, and the sensitivity of the dc amplifier and the recording equipment. The most common means of differential temperature detection is with thermocouples, although thermopiles, thermistors, and resistance elements have been employed. For high-temperature studies, an optical pyrometer may also be practical.

A thermocouple generates an electrical potential which is roughly proportional to the difference in temperature between the two junctions (Seebeck effect), and is well suited for differential temperature measurements (10). It may also be used for absolute and relative temperature measurements by keeping one junction, the reference junction, at constant temperature. Thermocouples normally used in DTA instruments are shown in Table 6.1. The temperature limits listed are for relatively accurate measurements with

Table 6.1. Characteristics of Some Typical Thermocouples at 25°C (10)

ISA Type	Metal No. 1 (Positive)	Metal No. 2 (Negative)	Maximum Temp. (°C)	Thermoelectric Power ($\mu\text{V}/^\circ\text{C}$)
S	Platinum	Platinum-10% Rhodium	1600	5.5
T	Copper	Constantan	250	40
Y	Iron	Constantan	450	51
E	Chromel	Constantan	1000	59
K	Chromel	Alumel	1000	41
	Tungsten	Tungsten-26% Rhenium	2200	3.3

20-gauge wire in air. The copper-constantan thermocouple is the most popular for use from - 150 to 250°C and is highly stable and reproducible over this temperature range. Noble metal thermocouples, especially the platinum-platinum, 10% rhodium, are preferred for applications requiring high accuracy in the range 500-1200°C. The Platinel-type thermocouples are also useful in this range and have the advantage of a larger thermoelectric power ($\sim 40 \mu\text{V}/^\circ\text{C}$). For temperatures up to 3000°C, tantalum carbide versus graphite has been suggested (11).

To increase the output signal from the different thermocouples without the use of an amplifier, experimenters have employed thermopiles (8, 12, 13). The advantage of such a system is the greater output signal with a lower noise level, due to lack of electronic amplification. A five-thermocouple ΔT thermopile, used in the Mettler TA 3000 system, is shown in Figure 6.5. The ΔT sensitivity is $115 \mu\text{V}/^\circ\text{C}$ and it is usable in the temperature range from - 170 to 600°C. To prevent electrical shorting when an aluminum sample

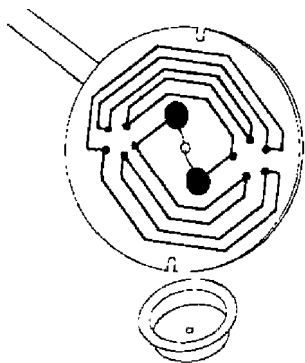


Figure 6.5. Five thermocouple thermopiles used in the Mettler TA 3000 DSC system.

container is placed over the thermocouples, the entire disk is coated with a thin layer of vapor-deposited silicon dioxide.

The usual mechanical configuration of the thermocouple is two wires welded together to form a thermojunction. Other types of thermocouple configurations that have been proposed are the thin-film type (17) and the disc (17, 18) type. The thin-film thermocouples eliminate the need of attempting to match the thermojunctions formed from wire wires. The former can be made light in weight, and can be exactly matched by evaporation of thin films of dissimilar metals which overlap to form a thermojunction. Preparation of nickel-gold thin-layer thermocouples is illustrated in figure 6.6 (15, 16). Gold was vacuum evaporated on thin plates, followed by electroplating of the nickel. Aluminum samples were then used to contain the samples in the temperature range from - 500°C. The thermoelectric power of the thermocouples increased from $10 \mu\text{V}/^\circ\text{C}$ at 25°C to about $25 \mu\text{V}/^\circ\text{C}$ at 200°C.

Audiere et al. (122) described a thin-film micro-DTA apparatus which permitted the study *in situ* of thin-film materials. The samples are prepared by evaporation, cathodic sputtering, and sputtering on to a substrate of metallic films, which constitute the thermocouples of the DTA.

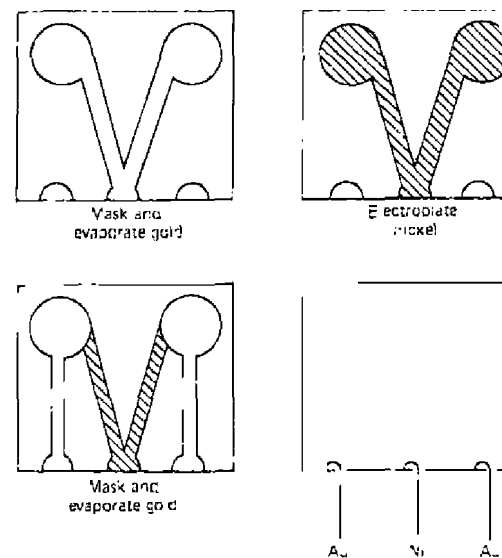


Figure 6.6. Preparation of thin-film thermocouples (13, 14)

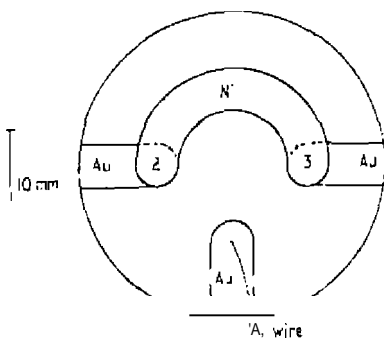


Figure 6.7. Thin-film thermocouple arrangement of Audiere et al. (122).

holder, as shown in Figure 6.7, consists of a Au-Ni thermocouple system deposited on a sapphire disk, 100 μm thick by 25.4 mm in diameter. Aminiuro wires were ultrasonically welded to the 1- μm thick gold films for electrical contacts. The thermoelectric power of the Au-Ni thermocouple was found to be about 23 $\mu\text{V}/^\circ\text{C}$ in the temperature range 20-300 $^\circ\text{C}$. The disk-type thermocouple and sample holder (18) are shown in Figure 6.8. The disk is made of constantan and serves as the major path of heat transfer to and from the sample and also as one half the ΔT -measuring thermocouple. A Chromel wire is connected to each raised indentation, thus forming a Chromel-constantan differential thermocouple system. This system is usable in the temperature range from -150 to 600 $^\circ\text{C}$. Yamamoto et al. (17) used a dumbbell-shaped piece of Chromel which consisted of two circular

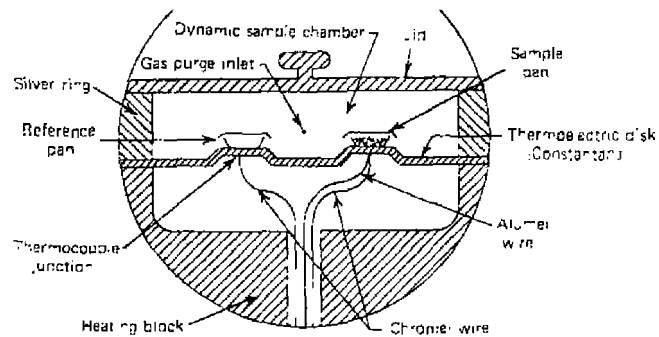


Figure 6.8. Disk-type thermocouple described by Baxter (16).

disks connected by a narrow strip. Alumel wire, welded to the center of each disk, served as the other thermocouple junction. Other thermoelectric disks are shown in Section 2.

4. T-Axis Calibration

As with many other analytical techniques, the temperature axis used in differential thermal analysis (DTA) must be calibrated with materials having known transition temperatures. The International Confederation of Thermal Analysis (ICTA) has been very active in developing a set of standard materials for this purpose (19) and has worked with the U.S. National Bureau of Standards to have these materials made commercially available (20). The U.S. National Bureau of Standards GM 754-GM 760 DTA temperature standards are listed in Table 6.2. They cover the temperature range from -83 to 925 $^\circ\text{C}$. The results of an ICTA "round-robin" study with 24 cooperating laboratories have been reported by Menis and Sterling (20).

Freezing temperature standards are also available from the National

Table 6.2. U.S. Bureau of Standards DTA Temperature Standards

GM	Material	Peak Temp. ($^\circ\text{C}$)	Unit
754	Polystyrene	$\sim 105^\circ\text{C}$	10 g
757	1,2-Dichloroethane	$\sim -33^\circ\text{C}$	4 mL
	Cyclohexane (transition melting)	$\sim -83^\circ\text{C}$ $\sim -7^\circ\text{C}$	4 mL
	Phenyl ether	30 $^\circ\text{C}$	4 mL
	o-Terphenyl	58 $^\circ\text{C}$	5 g
758	Potassium nitrate	$\sim 128^\circ\text{C}$	10 g
	Indium	157 $^\circ\text{C}$	3 g
	Tin	232 $^\circ\text{C}$	3 g
	Potassium perchlorate	300 $^\circ\text{C}$	10 g
	Silver sulfate	430 $^\circ\text{C}$	3 g
759	Potassium perchlorate	300 $^\circ\text{C}$	10 g
	Silver sulfate	$\sim 430^\circ\text{C}$	3 g
	Quartz	$\sim 573^\circ\text{C}$	1 g
	Potassium sulfate	$\sim 583^\circ\text{C}$	10 g
	Potassium chromate	$\sim 665^\circ\text{C}$	10 g
760	Quartz	573 $^\circ\text{C}$	3 g
	Potassium Sulfate	$\sim 583^\circ\text{C}$	10 g
	Potassium chromate	$\sim 665^\circ\text{C}$	10 g
	Barium carbonate	$\sim 810^\circ\text{C}$	10 g
	Strontium carbonate	$\sim 925^\circ\text{C}$	10 g

Physical Laboratory, Teddington, England, U.K. These substances and their respective freezing points are given in Table 6.3.

Judd and Pope (123) proposed the use of $(\text{SrBa})\text{CO}_3$ mixtures as temperature standards in the temperature range 780–930°C. These double carbonates undergo an *orthorhombic-hexagonal* transition at a temperature that is dependent on the composition of the double carbonate. This transition temperature for the various double carbonates is shown in Table 6.4. In each case, a single narrow endothermic DTA peak is obtained with a peak

Table 6.3. Freezing-Point Temperature Standards Available from the National Physical Laboratory

Substance	Freezing Temperature (°C)
4-Nitrotoluene	51.5
Naphthalene	80.2
Benzil	94.8
Acetanilide	114.3
Benzoic acid	122.3
Diphenylacetic acid	147.0
Anisic acid	182.8
2-Chloroanthraquinone	209.6
Carbazole	245.6
Anthraquinone	284.5

Table 6.4. Transition Temperatures of Double Carbonates, $(\text{SrBa})\text{CO}_3$ (123)

Mole % BaCO_3 in $(\text{SrBa})\text{CO}_3$	Transition Temperature (°C) (±2°C)
0	930
10	872
20	831
30	808
40	788
50	780
60	776
70	779
80	786
90	797
100	810

temperature corresponding to that shown in the table. Reheating the same sample gave the same endothermic peak with a temperature reproducibility of ±2°C.

The calibration of the temperature axis of the Perkin-Elmer DSC-2 has been discussed by O'Neill and Fyans (24). Temperature readout in this particular instrument can be in °C, K, or °F from 00.0 to 999.9°, and is switch-selected. A calibration curve obtained at a heating rate of 40°F/min is shown in Figure 6.9. Since many industrial processes operate in terms of °F, it is often convenient to use this scale in DSC studies.

The accuracy of temperature calibration, using the same metals shown in Figure 6.9, is illustrated in Table 6.5. Temperatures given are the indicator

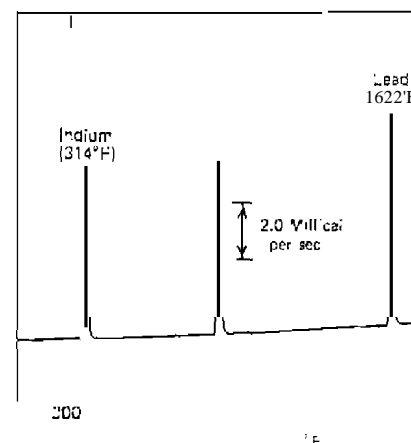


Figure 6.9. Typical temperature calibration.

Table 6.5. Accuracy of Temperature

Standard	Literature M.P. (°C)
Indium	156.63
Tin	231.97
Lead	327.50
Zinc	419.58
Aluminum	660.37

onset temperatures obtained by extrapolating the curve peak leading edge to the extrapolated baseline. This was calculated by a computer analysis to eliminate subjective bias.

Fairly high-resistance thermistors, 100,000.Ω at ambient temperature, connected in a bridge circuit have been used to detect the differential temperature (22, 23). This method does not normally require the use of an amplifier. Because their resistance decreases rapidly with increase in temperature, thermistors are generally only useful up to about 300°C (23).

S. Furnaces and Temperature Programmers

Again, as in the preceding section, the choice of furnace heating element and type of furnace depends on the temperature range under investigation. DTA furnaces have been described which operate in the range from -190 to 2800°C. The furnace may be mounted vertically or horizontally; it may be heated by either a resistance element, infrared radiation (25, 26), high-frequency rf oscillation (11, 27), or a coil of tubing through which a heated or cooled liquid or gas is circulated (28).

Resistance elements are perhaps the most widely used in furnace construction. Some resistance elements and their approximate temperature limits are given in Table 6.6. These temperature limits are, of course, dependent on the furnace design and insulation.

The wide variety of DTA furnace configurations is shown in Figure 6.10.

Table 6.6. Maximum Temperature Limits for Furnace Resistance Elements

Element	Approximate Temperature (°C)
Nichrome	1100
Kanthal	1350
Platinum	1400
Platinum-10% rhodium	1500
Rhodium	1800
Tantalum	1330
Globar	1500
KanthaJ Super	1600
Molybdenum	2200
Platinum-20% rhodium	1500
Chrome! A	1100
Tungsten	2800

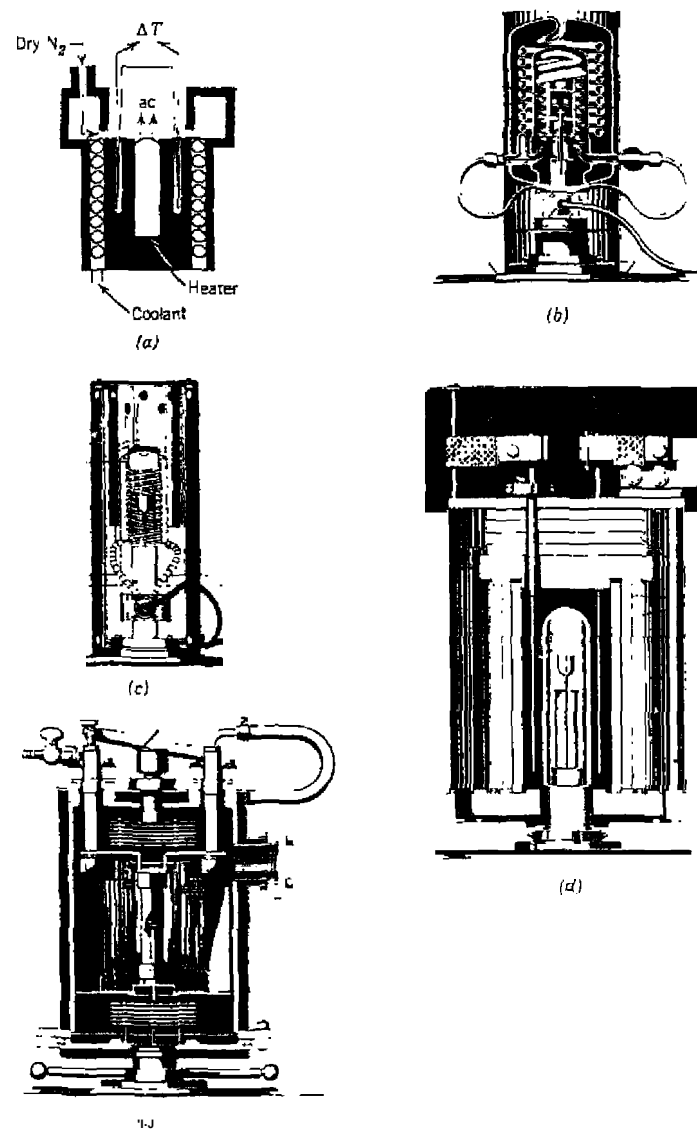


Figure 6.10. DTA furnace configurations.

In (a), a design described by Vassallo and Harden (29), the furnace is heated by a heater cartridge. It has provision for rapid cooling or for use below room temperature by passing a coolant through the cooling coils which surround the furnace. Sample and reference materials are placed in glass capillary tubes.

More sophisticated furnaces, for use in the temperature range from -150 to 2400°C, are shown by the Mettler thermoanalyzer furnaces in (b)–(e). The furnace in (b) is for use from -150 to 400°C and uses a Kanthal resistance wire heater element. For use from 25 to 1000°C, the furnace in (c) is employed. This furnace also uses Kanthal heater elements and features high-vacuum operation. The high-temperature furnace (d) is for use from 25 to 1600°C, also under high-vacuum conditions. It contains a furnace winding composed of super-Kanthal. Recently introduced was the super-high-temperature furnace (e), which can be used in the temperature range from 400 to 2400°C. The furnace heater elements are constructed of tungsten. The sample holders described in Section 2 can be used with the Mettler furnaces described here.

The requirements for a good DTA furnace include symmetry in heating and the ability of the heater elements to heat uniformly. The furnace temperature distribution must be uniform in the area of the sample holder for good results. Wiedemann (30) has reported the temperature distribution curves of the Mettler furnace, as illustrated in Figure 6.11. The gray area indicates the zone of homogeneous temperature in relation to the position of the sample holder. A temperature distribution study has been given by Yamamoto et al. (17) for a furnace used in the DTA apparatus they designed.

For operation at low temperature, the furnace may be surrounded by a Dewar flask and precooled with liquid nitrogen. The furnace is then heated by the furnace element using a heating-mode program. Another method is to use a gas as a heat exchange medium, such as is illustrated in Figure 6.12 (31). Most temperature programmers do not function efficiently unless a

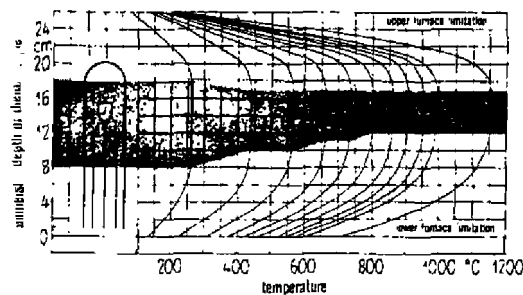


Figure 6.11: Temperature distribution in a DTA furnace (39).

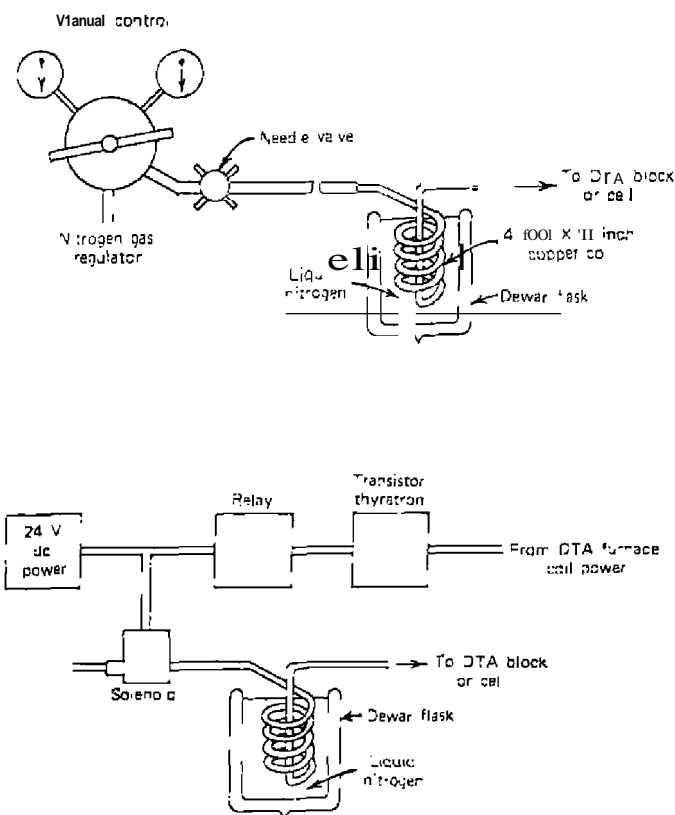


Figure 6.12: Simple cooling systems for DTA apparatus (38).

thermal reservoir at least 30°C below the program temperature is available. The ultimate low-temperature limit should perhaps be thermoelectric cooling.

Arndt et al. (24) found that controlled cooling based on natural convection currents could not be used in the temperature range 30–120°C at cooling rates of 10°C/min. They proposed the use of the simple controlled cooling apparatus shown in Figure 6.3. The jacket consisted of an aluminum cylinder of about 8 cm in diameter in which ice water from a cryogenic bath was circulated by means of a pump. The entire jacket was covered by a PVC

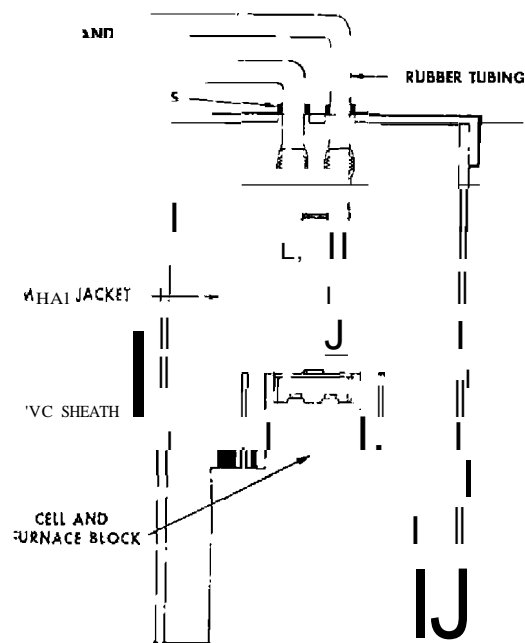


Figure 6.13. Controlled cooling system of Arndt et al. (124).

neath to eliminate condensation problems. Subambient temperature cycling could also be used if the iced water were replaced with a dry ice-ethanol mixture.

In an attempt to control the atmosphere within the furnace and sample holder, various techniques have been employed. They include (1) flooding the furnace with a gaseous atmosphere (32-35); (2) vacuum furnaces (32, 33, 35-41); and (3) a dynamic gas flow atmosphere (32, 33, 42, 43). An elaborate high-vacuum system for DTA furnaces has been described by Wiedemann (30).

Although most DTA instruments have only one furnace, to increase the number of samples that can be run each day several furnaces may be used in conjunction with the sample holder, amplifier, and recording system. In fact, an instrument that contains four different furnaces (44) has been described.

The rate of temperature increase of the furnace is controlled by a temperature programmer. This programmer should be capable of linear temperature

programming over a number of different temperature ranges, and hence must be compatible with several different thermocouple types. The heating rates should be linear and reproducible, since a nonlinear heating rate influences the DTA curves. As shown by Theall (145), programmer power cycling will cause variations in the DTA curve peaks as well as spurious peaks. Another characteristic of the programmer is that it should be stable with respect to line voltage and ambient temperature variations. The programmer control thermocouple should be compensated electrically or by an ice bath.

The type of temperature programmer varies from the simple voltage transformer coupled to a synchronous motor to the more sophisticated feedback, proportional-type programmer. On-off-type programmer cannot be used because of the fluctuating power outputs which give severe thermal gradients in the furnace and sample holder systems. A solid-state, feedback-type, proportional programmer used in the DTA thermal analysis instruments is shown in Figure 6.14. In a proportional type programmer, when the error signal between the command voltage

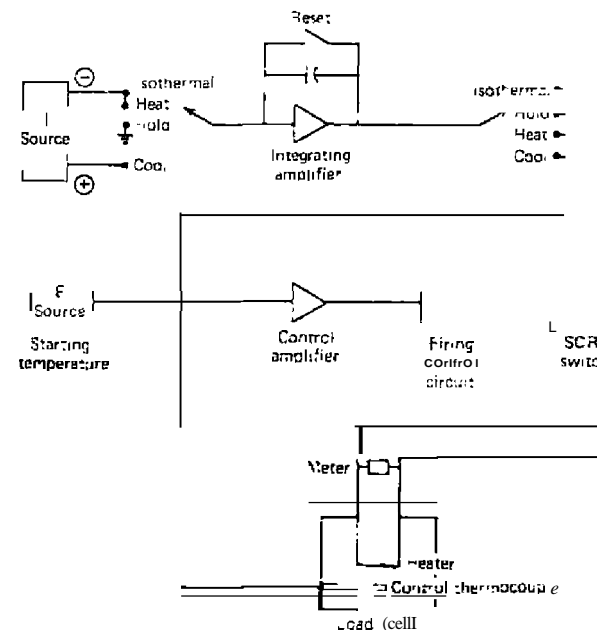


Figure 6.14. Du Pont temperature programmer.

the output of the control signal differs by an amount more than the "dead band" of the control amplifier, the error signal is amplified, and this power is applied to the heater. The power applied to the heater is proportional to the error signal at the input to the control amplifier. The heating-rate accuracy of this programmer is said to be $\pm 5\%$ or $0.1^\circ\text{C}/\text{min}$, whichever is greater. The accuracy is governed mainly by the output of the control thermocouple. In the programmer itself, the limiting factor is the adjustment and drift of the power supply that controls the current which is integrated by the integrating amplifiers. The reproducibility is $0.1^\circ\text{C}/\text{min}$, while the heating-rate linearity is $\pm 1\%$ or $0.01^\circ\text{C}/\text{min}$. The former is dependent on the drift of the power supply and amplifier bias, while the latter depends on the output linearity of the control thermocouple.

In the Stone instruments, a stepper motor is used to control the rate at which nonlinear ramp functions of the output of the four most common types of thermocouples are generated. This nonlinear generated curve is

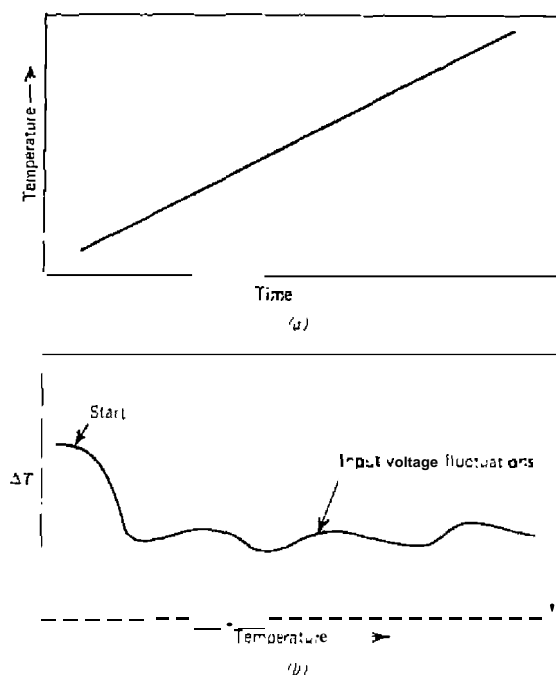


Figure 6.15. Heating rate curves: (a) Temperature versus time curve; (b) DTA curve of unbalanced system.

compared with the nonlinear thermocouple output and the signal difference led to an error amplifier which triggers an SCR circuit which controls the furnace voltage. The linearity is said to be better than 0.25% for any 100°C interval or 0.5% full scale.

The accurate determination of the linearity of the furnace heating rate is not an easy matter. From a plot of temperature versus time, as shown in Figure 6.15a, the heating rate can be estimated to $\pm 5\%$ or better. To determine minute fluctuations of the furnace heating-rate curve, the curve in Figure 6.15b is used. A DTA curve is recorded with the reference chamber filled with an inert material (α -alumina, for example) while the sample chamber is empty. In this unbalanced condition, the fluctuations in the power input voltage are easily seen. This type of behavior is also seen if the ΔT thermocouples are unsymmetrically located in the furnace chamber (46). It should be noted that it is even more difficult to measure accurately heating rates of $1^\circ\text{C}/\text{min}$ or less.

The heating rates of most commercial DTA furnaces can be varied from 0.5 to $50^\circ\text{C}/\text{min}$. Most DTA curves, however, are recorded at heating rates of 10 to $20^\circ\text{C}/\text{min}$. The higher heating rates are convenient for preliminary examination of the thermal behavior of a sample.

6. Low-Level Voltage Amplifier and Recorders

The output voltage from the differential thermocouple is of the order of 0.1 to $100\ \mu\text{V}$, depending on the type of thermocouples used (see Table 6.1) and the temperature difference between them. Hence, unless a very sensitive recording system is used ($< 100\ \mu\text{V}$ full scale), the ΔT signal must be amplified by a low-level microvolt amplifier. The amplifier must have low noise, low drift, and high stability to be useful for DTA instrumentation. Instability of the amplifier will result in an unstable baseline (45), while drift by either input voltage or ambient temperature changes will cause output fluctuations. Pickup of 60 Hertz ac by the input wiring can cause output noise as well as an unstable baseline.

Many times, in an effort to reduce amplifier noise, capacitors are added across the output of the amplifier, and occasionally at the input (45). These capacitors frequently reduce the response time of the amplifier, which causes a shift in the curve peaks and also a loss of peak resolution. A proper value of capacitor must be used, if noise is a problem, to form a compromise between noise reduction and loss of peak resolution. Amplifier impedance mismatch can also cause nonlinear output voltages, which can distort the curve peaks.

Various recorders have been described, from photographic light-beam galvanometer types to modern electronic potentiometric recorders. Burgess

(47) gives an excellent discussion of some of the earlier recording devices. Probably the first to use modern potentiometric recorders, especially the multipoint type, were Kerr and Kulp (7) and Kaulfman and Dilling (48). This type of recorder, plus the use of multiple sample holders, increased the usefulness of DTA for the qualitative identification of geological materials. Another technique, using a two-channel recorder, is to record both the differential temperature and the reference material temperature as a function of time on the same chart paper. $X-Y$ and $X-Y_2$ recorders, such as those illustrated in Chapter 3, are also used. Data center recorders may also be employed. Most of the modern commercial DTA and DSC systems utilized some type of computer data reduction and plotting or printing systems, such as those described in Chapter 12. Dedicated microcomputers or mini-computers are used to process the raw data, which can be replotted in a variety of formats.

B. DTA INSTRUMENTS

1. Introduction

The modern DTA instrument is derived from the two-thermocouple design suggested by Roberts-Austen (49) in 1899. Many instruments have been designed and constructed since that time, each slightly different in the design of the furnace, temperature programmer, recording equipment, sample-holder design, and so on. Smothers and Chiang (50) in 1958 described in detail some 155 DTA instruments located throughout the world. This list was deleted in the second edition of their book (51), which, however, included a bibliography of some 4248 references to the DTA literature, many of them describing the instrumentation employed by the investigators. Modern equipment is adequately summarized in various textbooks (52-54), while specifications on commercially available instruments are described elsewhere (56-58).

A number of DTA instruments are described here; an attempt is made to include only those instruments which possess some novelty in design or that have made important contributions to the development of DTA instrumentation.

2. Sealed-tube Techniques

The enclosure of the sample in a sealed and sometimes evacuated chamber or tube is an old technique. The technique is useful for phase-diagram investigations (59), especially those involving corrosive materials (chalco-

genide reactions, for example), and in other areas such as organic reactions (60, 61), metal salt hydrates (62), metallurgical problems (63), molten salt equilibria (64), and numerous other problems.

A simple sealed-tube sample holder is shown in Figure 6.2(q). Other sealed-tube sample and reference holders are shown in Figure 6.16 (59). In one case, (a), the thermocouples were sealed directly into the tubes, and this presented problems with metal-to-glass seals. Heat transfer from the sample to the sensing thermocouple is fairly low in most of the examples given. The system in (e) is much better than most of the others because the

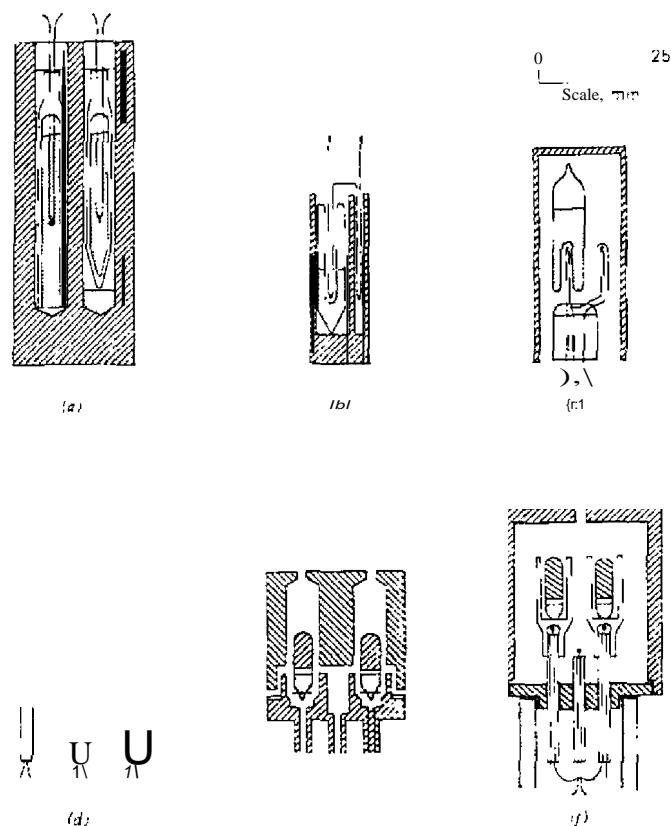


Figure 6.6 Sealed-tube sample holders in which the containers are evacuated. (a) Roberts (65); (b) Jensen (69); (c) Kracek (66); (d) Ballin and Kerr (57); (e) Ballin (55), Faktor and Hanks (68).

ring thermocouple provides a high-thermal-conductivity contact over an appreciable area. None of the sample holders illustrated exhibit very high-resolution DTA curves, due to the thermal inertia of the system. The preparation of the evacuated type of sealed-tube sample holders has been described in detail (67).

A glass ampoule sample holder, as described in Chiu (1251), is shown in Figure 6.17. Such a sealed sample container has been found to withstand an internal pressure of up to 1800 psi and is suitable to be used as a microreactor to study most chemical reactions. An ampoule holder, constructed from silver or aluminum metal, is used to support the ampoule in the DSC sample chamber. Liquid or solid samples are introduced into the ampoules by a syringe. The ampoule sealing technique has been described elsewhere (126).

Schouteten et al. (127) described a simple stainless steel DSC sample cell that is sealed by a resistance welding technique. The welded capsule could withstand pressures of over 80 atm.

A high-pressure sample holder, capable of withstanding a maximum internal pressure of 150 atm, was described by Earnest et al. (128). The cell, constructed of stainless steel that could be gold plated, had a capacity of 40 μ L and could be used to a maximum temperature of 400°C.

A sample holder, to be used for ignition studies, was described by Charsley et al. (129). The sample and reference materials were placed in flat-bottomed quartz crucibles, 6 mm in diameter and 20 mm in length. The crucibles were supported by plate-type Chromel-Alumel thermocouples, fitted with locating pins and having 0.5-mm-diameter wire leads.

A miniature Li/SO₂ battery was enclosed in a nickel-plated steel can containing a thermocouple well so that it could be studied by DTA ([30).

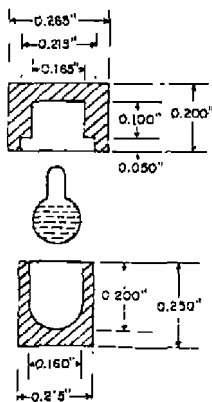


Figure 6.17. Glass ampoule sample holder for DSC studies (25).

DTA curves could be obtained during electrical discharge of the cell.

A sealed-tube sample holder for milligram quantities of sample has been described by Wendlandt (62). The tubes employed were standard glass-capillary melting point tubes, which are used in the furnace and sample holder shown in Figure 6.18. Samples are enclosed in the 0.9-1.4-mm-od capillary tubes that are placed in thin aluminum heat transfer sleeves. An identical empty tube was used for the reference thermocouple. After placing the sample (from 5-7 mg) in the tube, the author sealed it off using a small oxygen-gas flame to a length of about 20 mm.

The sample-loading procedure used by Barrett et al. (60,61) was similar to that given previously except that special precautions had to be taken due to the volatility of the organic samples. The capillary tube containing the sample was cooled by inserting it into a cooled aluminum block (dry ice-acetone bath coolant) and then sealing off the tube with a micro gas torch. Some precaution must be observed concerning the size of the sample; large samples may generate excessive pressure if gaseous decompositions are involved, and this may lead to minor explosions. The sample size should be adjusted so that the gas pressure will not exceed about 45 atm.

A sealed-tube DTA apparatus has been described by Gilparick et al. (64) for phase studies of the molten salt system, NaF-KF-BF₃. The sample holder, as shown in Figure 6.19, contains about 4 g of sample which is continuously agitated to avoid segregation and compositional changes during the heating and cooling cycles. Nickel was used as the material of construction for the

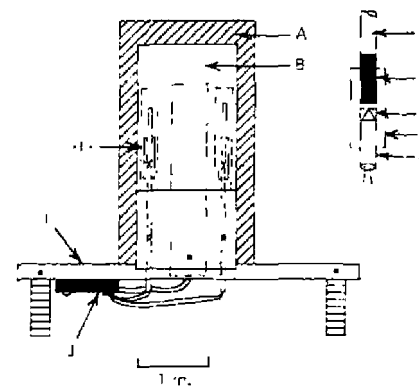


Figure 6.18. Sealed-tube DTA furnace and sample holder (62). A, insulated cover; B, aluminum block; C, glass capillary tube; D, sample; E, sample thermocouple; F, aluminum heat transfer sleeve; G, ceramic insulator tube; H, reference chamber; I, transit platform; J, terminal strip.

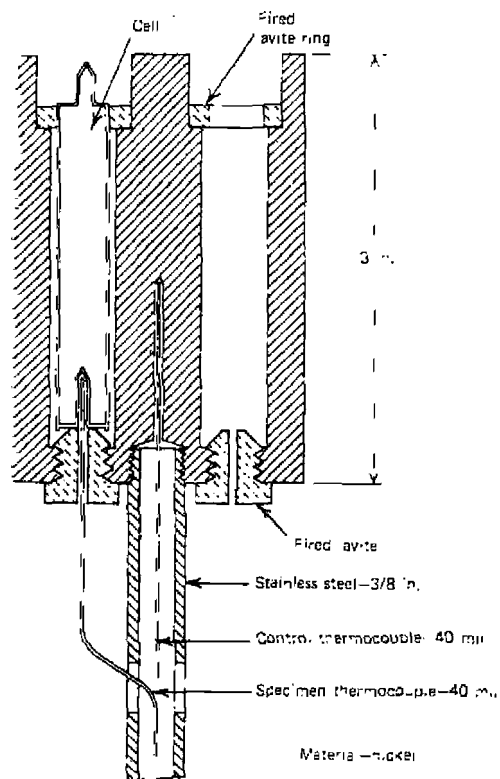


Figure 6.19. Sample holder for molten salt phase studies (64).

capsules, which were evacuated and sealed under vacuum. The enclosed thermocouples gave reproducible results for the resulting phase transitions at ΔT sensitivities of 25–100 $\mu V/cm$ of chart displacement. A similar metal sample-holder capsule was described by Etter et al. (63); the capsules were constructed of tantaleum.

Barral and Rogers (70) described a constant-pressure device (not a sealed-tube type sample holder) which is illustrated in Figure 6.20. Total cell volume was about 0.8 ml; a glass capillary tube provides a reservoir for the gases released during a reaction and prevents significant dilution of the sample atmosphere with air or the loss of gas. The small mercury seal provides for sample atmosphere expansion and maintains an essentially constant pressure in the cell.

DTA INSTRUMENTS

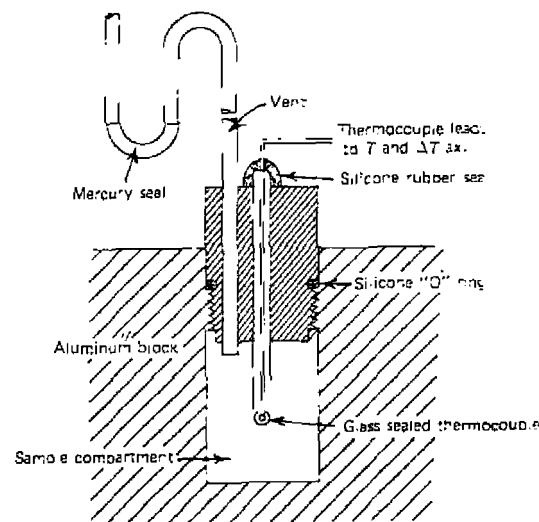


Figure 6.20. Sample holders for constant pressure in a self-generated atmosphere (11).

Mention has already been made of the high-pressure metal sample holder employed by Bohon (3) for his DTA studies on explosive materials. A similar type of sample holder constructed from a Swagelok stainless steel fitting has been described by David (11).

3. High-pressure Systems

High-pressure DTA has been reviewed briefly by Locke (72). The previous studies have been concerned mainly with the effect of pressure on solid-liquid and solid₁ → solid₂ equilibria. The equipment used in high-pressure studies employs piston-cylinder pressure-generating systems in the 60–800 kbar range, while lower-pressure equipment involves external pressurization by gases.

Harker (73) described an apparatus in which the sample and reference materials were sealed in platinum capsules. Wires welded to the capsules were led from the pressurized microreactor through a pressure packing. Nitrogen was used as the pressurization gas, although argon is to be preferred because the former causes severe embrittlement of platinum alloys. Several melting points in the CaO-Ca(OH)₂-Ca₃SiO₄ system at 15,000 psig were obtained.

Cohen et al. (74) described a piston-cylinder apparatus which could be

used up to 50 kbar at temperatures to 1200°C. They discussed in detail the components of the high-pressure furnace, sample holder, and pressure transmission. A typical thermocouple assembly is shown in Figure 6.21. All wires, with the exception of the tip which is in contact with the sample container, are insulated with alundum cement. Sample capsules used were made of tantalum, niobium, platinum, graphite, and so on; they were in the shape of a cup $\frac{1}{8}$ in. in diameter by $\frac{1}{8}$ in. in length. The cap is made of the same material as the capsule body. Pressure is transmitted to the sample by the furnace assembly, a combination of pans made of talc, graphite, pyrophyllite, thermocouple tubing, thermocouples, sample container, boron nitride, and so on. The determination of the pressure on the sample is not a straightforward problem.

A DTA apparatus that could be used up to a pressure of 4000 bar and temperatures to 500°C was described by Kuballa and Schneider (75). This apparatus, which is illustrated in Figure 6.22, contained a DTA cell that was constructed of stainless steel; a maximum pressure of 4000 bar and a maximum temperature of 500°C were possible. The cell was enclosed by two Bridgman pistons which contained the thermocouples. Cell wells for the sample and reference materials were made from a 97% platinum-3% iridium alloy; they were suspended on the sheathed thermocouple junctions. Upper and lower sides of the sample-holder area were thermally heated by ZrO_2 blocks. A furnace placed around the pressure vessel permitted linear heating rates from 0.2 to 10°C/min.

DTA instruments for high-pressure hydrogenation reactions have been described by various Japanese investigators (76, 77). Bousquet et al. (78) described a high-pressure DTA furnace and sample holder which could be

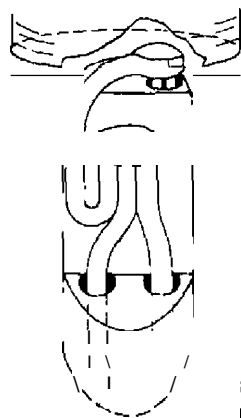


Figure 6.21. Three-wire thermocouple assembly (1); high-pressure DTA apparatus (74).

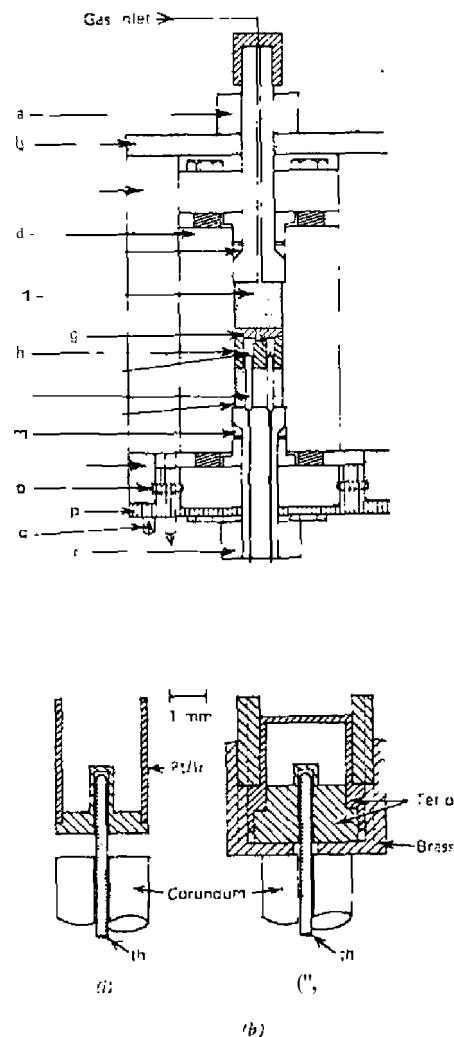


Figure 6.22. High-pressure DTA apparatus of Kuballa and Schneider (75) (a) a, r = coolers; b, n = pyrophyllite insulating disk; c = heating block; d = high-pressure vessel; e, m = copper seals; f, l = ZrO_2 blocks; g = copper shield; h, j = calorimeter block; i = thermocouple; k = corundum capillary; o = fastening screw; p = support; q = inlet and outlet of refrigerant; (b) (i) open Pt/Ir well; (ii) closed Pt/Ir well with brass holder (th = steel-sheathed thermocouple).

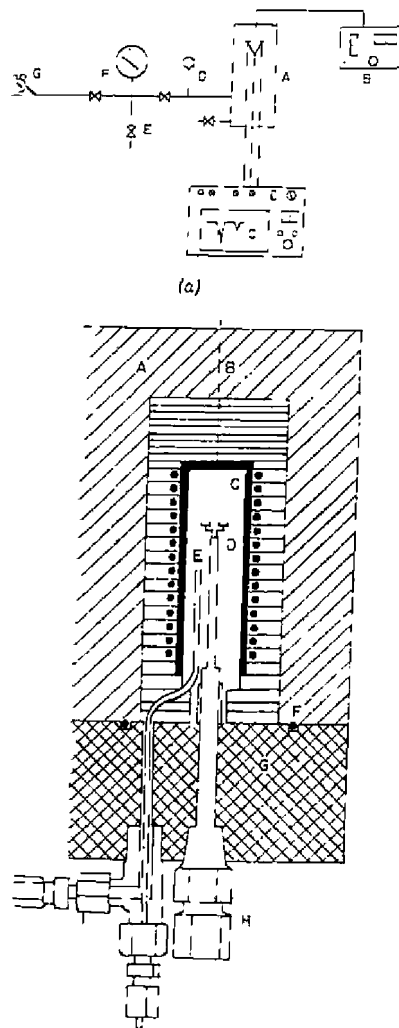


Figure 6.23. High-pressure DTA system described by Williams and Wendlandt (131). (a) Schematic diagram of apparatus. A, high-pressure DTA cell; B, T & T Controls Company Model No. TPC-2000 temperature programmer; C, Du Pont Model 900 recording module; D, relief valve; E, valve; F, pressure gauge; G, gas pressure regulator; H, gas cylinder. (b) Schematic diagram of DTA cell. A, furnace chamber; B, high-pressure connectors for furnace wires and thermocouples; C, furnace; D, DTA sample and reference holders; E, gas outlet tube; F, Buna-N O-ring; G, base plate; H, Conax connector for thermocouple wires; I, gas inlet-outlet connector.

328

used up to 500 bar and a maximum temperature of 500 C. This apparatus is available from Netzsch-Geratebau GmbH. The Stone high-pressure DTA sample holder has been described by Locke (*n*). It can be used at pressures up to 3000 psig and at a maximum temperature of 500°C.

A schematic diagram of the high-pressure DTA system described by Williams and Wendlandt (131) is shown in Figure 6.23. It consisted of a high-pressure DTA cell and enclosure [A] complete with relief valve (D), pressure gauge (F), a furnace temperature programmer (E) and the Du Pont Model 900 Recording Module (C). The high-pressure DTA cell consisted of two 104-mm-od cylindrical segments of type 316 stainless steel secured together with six stainless steel bolts, each 13 mm in diameter. The upper portion of the enclosure (A) contained a 26-mm-id furnace house in an insulated body. A threaded opening was provided at the top of the chamber for the heater wire entry through a Conax high-pressure connector. The gas-tight seal between the upper portion of the chamber and the base (G) was obtained by the use of a Buna-N O-ring (F) contained in a groove cut in the base. The base contained two threaded openings for high-pressure gas inlet-outlet fittings (I) and a Conax wire connector (H) for the thermocouple wires. The sample probe (D) consisted of a 5-mm diameter four-holed ceramic tube containing the differential thermocouple and furnace thermocouple wires. The reference and sample containers consisted of 1 × 2 mm in diameter platinum cups welded to the thermojunctions of the thermocouples. The top of the probe was enclosed by a removable machined aluminum cap to ensure even heat distribution to the sample.

The sample was capable of operation to a maximum temperature of 500°C and a maximum pressure of 600 atm.

High-pressure DTA and DSC systems have been described by Vurflinger et al. (132-135). These instruments can be used in the temperature range -200-150°C at up to 3 kbar pressure. The DTA cell is a cylindrical pressure vessel made of copper-beryllium, closed at the top by a Bridgman piston. From the bottom, two steel-sheathed thermocouples were introduced into the inner volume of the vessel where identical DTA wells were fastened onto the two thermocouple junctions and inserted into a symmetrical calorimeter block.

Kamphausen (136) described a high-pressure DSC system using the Perkin-Elmer DSC-1B sample holder and electronic circuitry. The sample holder is enclosed by two Bridgman pistons, permitting pressures of up to 2000 bar in the temperature range -20-200°C.

4. High-temperature Systems

The problems of a DTA apparatus for operation above 1200 C are quite different from those that operate below this temperature. The electrical

leakage from the increased electrical conductivities of the refractory components and of the air in the furnace becomes important. Adequate shielding of the low-level thermocouple circuits is much more critical. The high temperatures often cause melting of the sample, which destroys the thermocouple assembly as well as the sample holders. Even with these problems, DTA instruments which operate up to 3000°C or higher have been described.

A DTA apparatus capable of operation up to 1575°C is shown in Figure 6.24 (79).

The furnace consisted of an aluminum core, which was wound with platinum-20% rhodium resistance wire. A booster coil of Nichrome wire was also wound on the two ends of the core; this was used only for the very high-temperature work. The differential temperatures were detected with platinum versus platinum-10% rhodium thermocouples, inserted in the indentations of the platinum sample and reference cups. To shield the thermocouple wires, platinum foil was wound around the ceramic insulating tubes used to bring them into the furnace hot zone.

A commercially available temperature programmer, dc amplifier, and two-point recorder were employed. Furnace heating rates of from 0 to 30°C/min were possible.

A high-temperature DTA furnace and sample holder which does not use thermocouples as temperature sensors has been described by Nedumov (80). A critical assessment of various instruments that do employ thermocouples found that they were unsatisfactory for quantitative DTA studies of metals and metallic alloys. Temperature detection in this apparatus is by use of tungsten resistance thermometers. The apparatus can be used to temperatures over 3000°C.

A multifunctional apparatus that permits the determination of the thermal analysis, derivative thermal analysis, DTA, and thermal derivative thermal analysis (temperature versus derivative of temperature) curves has been described by Rupert (81-83). This apparatus is shown schematically in Figure 6.25 (81). The sample is contained in crucible A located within the eddy current concentrator B. The current concentrator receives power from the induction heater K, whose output is controlled by the induction power heater control I. Light from the sample emerges through a 0.070-in.-diameter hole in the top of the crucible, and travels upward through a Pyrex or quartz window into the lower end of the beam splitter. Part of the light is reflected at approximately a right angle to the axis of the beam splitter, by the partially aluminized bottom mirror, to the optical pyrometer D used to measure the temperature of the sample. The light that passes through the bottom mirror is reflected outward by the top mirror and is focused by the 27.5-cm-focal-length achromatic lens into a 0.067-in.-diameter aperture in front of a photomultiplier tube, which was used at temperatures above 1400°C. While for

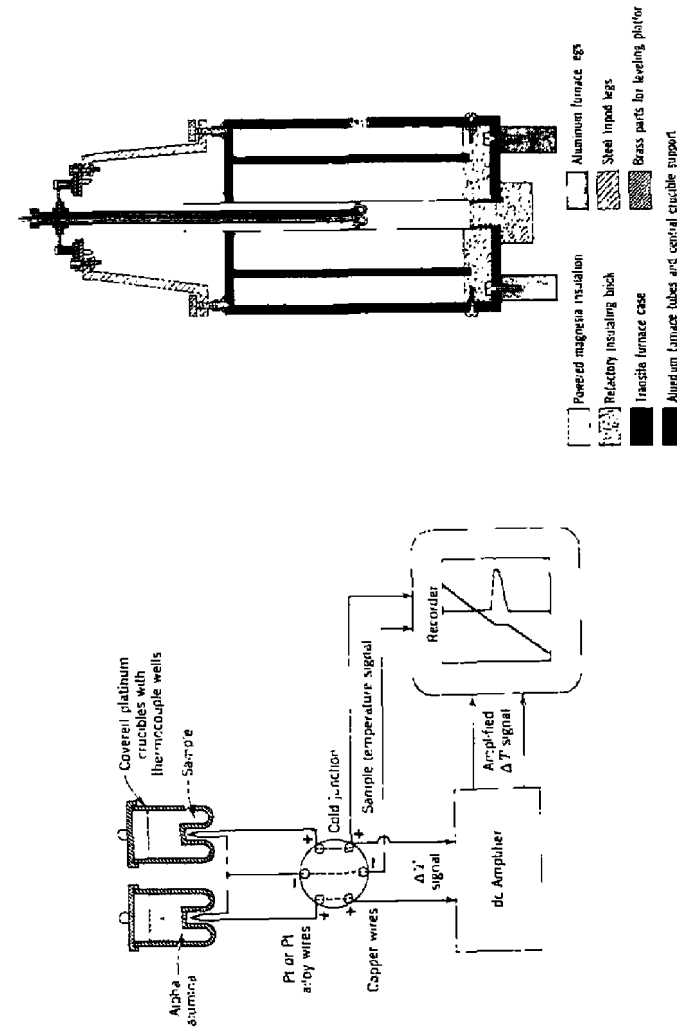


Figure 6.24 High temperature DTA apparatus of Newk

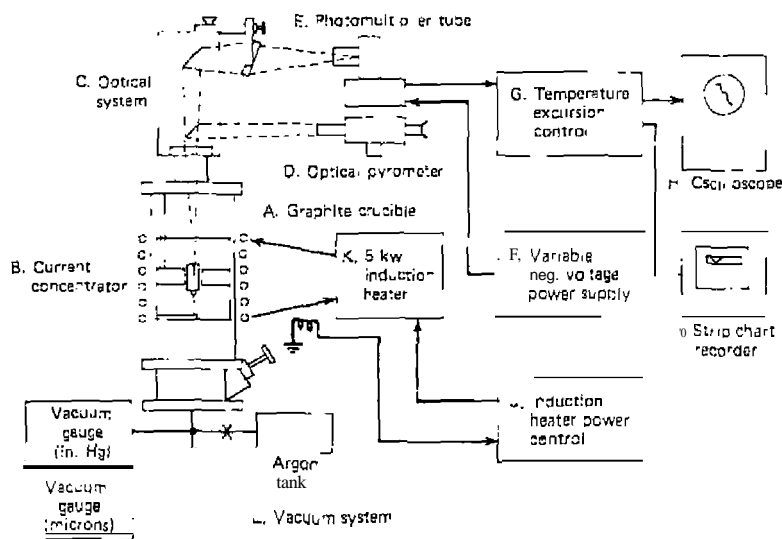


Figure 6.25. High-temperature multifunctional apparatus described by Rupert (81).

lower temperatures a IP21 tube was used. Further modification of the instrument has been described (82).

Kocherzhinsky (137) described a DTA apparatus, using a special type of thermocouple, that is capable of operation in argon atmospheres to temperatures up to 2480°C. The thermocouples did not use ceramic insulation in the high-temperature furnace area.

5. Micro-Sample Instruments

The determination of DTA curves from microgram quantities of sample has previously been described by Mazieres (41). A more comprehensive review of micro-DTA instrumentation is that by Sommer and Jochens (84). In this review, the entire area of high-temperature microscopy, coupled with DTA measurements, is discussed in detail. In most of the instruments described, the thermocouple junction acts as a heater and temperature detector, as well as the sample holder.

The micro-DTA apparatus developed by Müller and Sommer (185) is shown in Figure 6.26. The circuit used a motor-driven variable voltage regulator and was capable of heating rates from 5°C/min to 1000°C/sec. Recordings

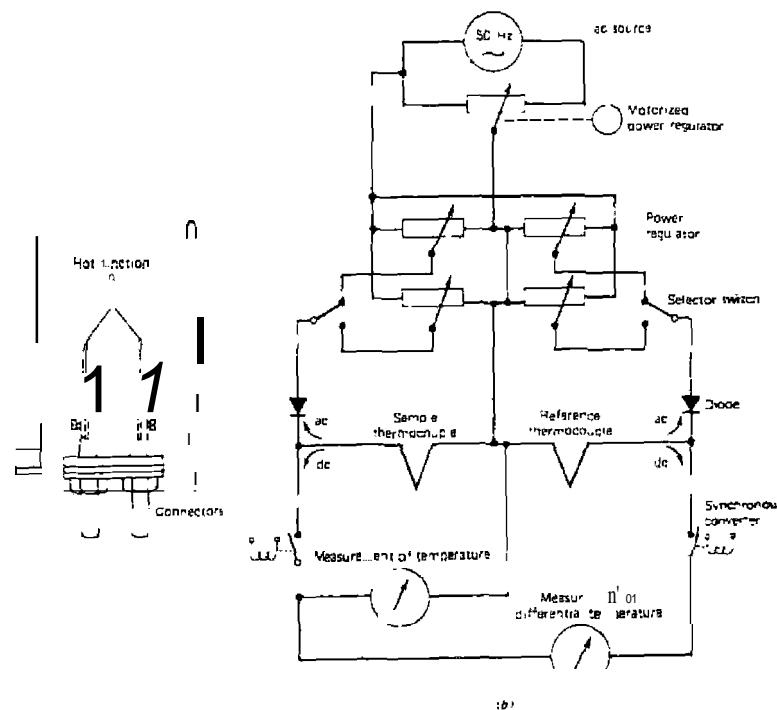


Figure 6.26. Micro DTA apparatus (2). (a) sample holder; (b) electrical circuit (85, 36).

of the sample temperatures and the ΔT were made on a high-speed recorder. In an improvement of this apparatus, the sample and reference thermocouples were placed in individual cells and only the cell housing the sample was retained in the optical system of the microscope (86).

A similar DTA apparatus has been described by Proks and Zlatovskiy (187) in which the sample is contained in the thermojunction. The thermocouple is heated by a high-frequency current, which has been amplitude-modulated by a low-frequency signal.

6. Automation of DTA Instrumentation

Present-day DTA instruments are capable of automatic operation in that after the sample has been manually inserted the temperature rise is controlled by a temperature programmer which will turn off the instrument after a preselected temperature limit is attained. When the furnace has been cooled

back to room temperature, the pyrolyzed sample is removed from the sample holder, a new sample is introduced, and the heating cycle is repeated.

Wendlandt and Bradley (88, 89) have described an automated instrument which is capable of studying eight samples in a sequential manner. The samples are automatically introduced into the furnace, pyrolyzed to a preselected temperature limit, and then removed. After the furnace has cooled back to room temperature, the cycle is repeated. Operation of the sample-changing mechanism, furnace-temperature rise and cooling, recording, and so on is completely automatic.

A line drawing of the sample-changing mechanism and the furnace platform is shown in Figure 6.27.

The powdered samples are contained in glass capillary tubes, D, or 1.6-1.8-mm id, which are placed in the circular sample holder plate, A.

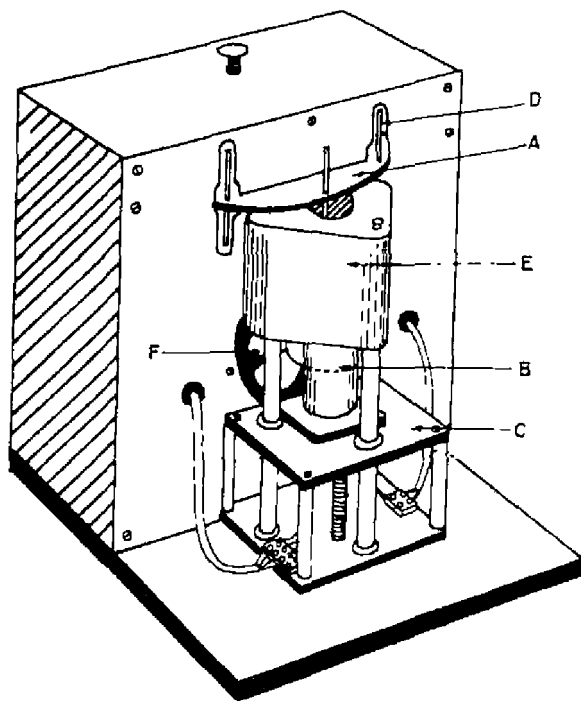


Figure 6.27. Automated DTA apparatus of Wendlandt and Bradley (88). A, sample holder plate; B, furnace; C, furnace platform assembly; D, sample capillary tube; E, furnace block; F, cooling fan.

The aluminum sample holder plate is 8.0 in. in diameter by $\frac{1}{8}$ in. thick and has provision for retaining eight glass capillary tubes. The glass tubes are held in their respective positions by means of small spring clips. The plate is rotated by a small synchronous electric motor equipped with an electromagnetic clutch. The rotation of the plate by the motor is controlled by a lamp-slit-photocell arrangement. Adjacent to each sample-holder position is a 0.50 x 0.06-in. slit cut in the aluminum plate. Alignment of the plate slit between the lamp and photocell by the drive motor permits exact positioning of each capillary tube with the furnace cavity.

After the sample capillary tube is in position, the furnace platform, C is raised so that the tube is positioned into the aluminum heat transfer sleeve, located on the sample thermojunction. Movement of the furnace platform is controlled by a reversible electric motor connected to the platform by a screw drive. Upper and lower limits of travel are controlled by two microswitches. The furnace is insulated from the platform by a 0.25-in. layer of transite and, while in the heating position, by a Marinite sleeve, E. The rotation interval for sample changing is 15 sec, while it takes 50 sec to raise the furnace platform to the full upper limit.

After the sample has been heated to the upper temperature limit, the furnace is lowered, the sample-holder plate rotates to a new position, and a cooling fan is activated to direct air on the hot furnace. Cooling time for the furnace, from 450°C to room temperature, takes about 20 min. After the furnace has been cooled to room temperature, the above cycle is repeated with a new sample.

A schematic diagram of the furnace and sample chamber is shown in Figure 6.28. The cylindrical furnace (E) is 1.5 in. in diameter by 3.3 in. in

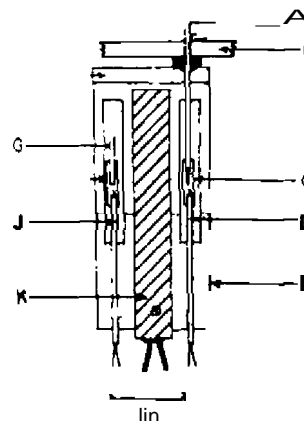


Figure 6.28. Furnace and sample chamber. A, glass capillary tube for sample; B, sample holder plate; C, sample heat transfer sleeve; D, sample thermocouple; E, furnace block; G, reference capillary tube; H, reference heat transfer sleeve; J, reference thermocouple; K, heater cartridge.

length, and is heated by a 210-watt stainless steel heater cartridge (K). The upper temperature limit of the furnace is about 500°C. The sample and reference cavities are about 0.25 in. in diameter by 1.5 in. in length. Thermal contact between the sample and reference capillary tubes (A and G) is made by the aluminum heat transfer sleeves (e and H). The cylindrical sleeves are about 0.7 in. in length. The ends of the sleeves are drilled out so that the sample tube and the $\frac{1}{8}$ -in.-diameter ceramic insulator tube (D or J) fit closely within the sleeve. To minimize heat leakage from the furnace to the sample-holder plate (B) a transit cover (F) is used to enclose the top of the furnace.

Since the automated DTA apparatus has an upper temperature limit of about 500°C, its use has been restricted to intermediate temperature applications such as the deaquation of metal salt hydrate systems. It should find wide use in the routine DTA examination of both organic and inorganic samples. The automated features should permit convenient computer interfacing so that reaction temperatures, peak areas, purity calculations, ΔH calculations, and so on can be easily carried out.

7. Differential Scanning Calorimetry with Reflected Light Measurement

Haines and Skinner (138) modified a Perkin-Elmer DSC-IB instrument to permit simultaneous observation and recording of optical changes in the sample as well as to obtain DSC data. This modification is illustrated schematically in Figure 6.29. Reflected light measurements were made using a

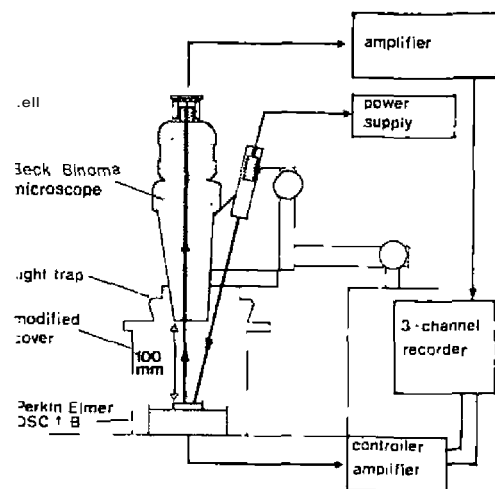


Figure 6.29. Combined DSC-RLI apparatus as described by Haines and Skinner (138).

Beck Binoma stereomicroscope mounted over the DSC sample holder. The light detector was a Vickers CdS photoconductive cell which had a large light-sensitive area and a maximum response at 545 m μ . The signal from the detector was amplified by a operational amplifier. Both DSC and light detector cell signals were recorded on a strip-chart recorder.

8. Multiple Sample Digital DTA Apparatus

A multiple sample DTA system coupled to a digital control system was described by Seyler and Kalbfleisch (139) for use in high-volume testing of industrial samples. The furnace assembly, as shown in Figure 6.30, consisted of eight thermocouples and a 30 W cartridge heater mounted in a 2.54-cm-diameter silver block. Seven sample thermocouples were wired in opposition to the eight (reference) thermocouples. The latter also serves as the control thermocouple for the temperature programmer. Controlled atmospheres of air or an inert gas are possible at pressures from 20-760 Torr. with furnace

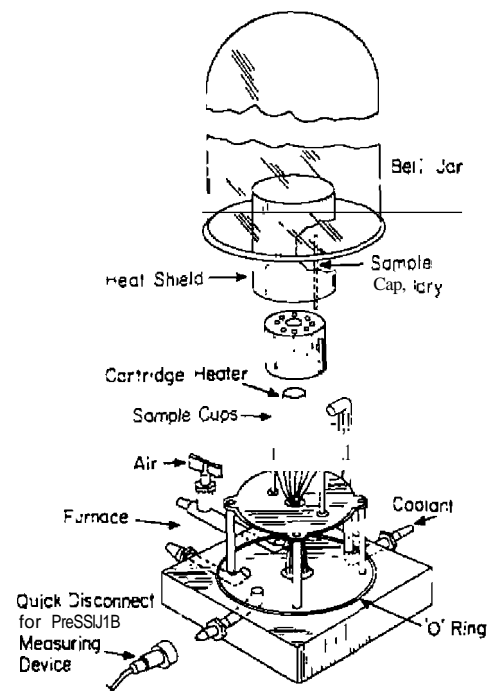


Figure 6.30. Multiple digital DTA apparatus (139).

temperatures up to a maximum temperature of 300°C. A multiplexer sequentially connects the T and ΔT preamplifier outputs to the digitizer input at 333 msec intervals. The alternating T - ΔT signal sequence is maintained via a decoder from the memory address counter.

9. Miscellaneous Instruments

One of the first precise vacuum or inert-atmosphere instruments was designed and constructed by Whitehead and Breger (37). The furnace was constructed from an alundum core, 9 in. in length by 2 in. 10, wound with Chromel resistance wire. The core was shielded by four sheet-nickel cylinders, mounted on three posts, and the entire assembly was placed inside a 12 × 24-in. Pyrex bell jar. All electrical connections were made through the bottom of the bell jar mounting base. The sample block was made in the dimensions shown from Type 446 or 309 stainless steel. The furnace heating rate was controlled by a Leeds and Northrup Micromax controller; the differential temperatures were recorded on a Beckman Photocell recorder.

Wendlandt (39) has also described a simple vacuum or controlled atmosphere DTA furnace and sample holder. The furnace tube was 19 cm in length, 2.5 cm in diameter, and partially constructed of fused silica. The lower end of the tube contained two Pyrex glass 25-mm-ID a-ring joints, which were attached to the fused silica tube by a Nylon seal, machined to the dimensions of the glass a-ring joint, and attached to it by a compression clamp. The Chromel-versus-Alumel thermocouple wires were brought into the furnace zone by use of 10-mm-diameter, two-holed ceramic tubing. The sample and reference cups made of Inconel were 7 mm in diameter and 10 mm in length, and had a volume of 0.8 mL. The cups fit snugly on the insulator tube and were in intimate contact with the thermojunctions. The furnace was wound, on either the insulated fused silica tube or an external ceramic tube, which fit closely about the silica tube, with Nichrome resistance wire. The furnace temperature programmer consisted of a variable-voltage transformer driven by a synchronous motor. The differential temperature signal was amplified by a de microvolt amplifier and recorded against temperature on an X-Y recorder.

A low-temperature DTA apparatus, capable of operation in the temperature range -190-400°C, has been described by Reisman (40). With the Dewar container filled with liquid nitrogen, the heating rate of the sample block was controlled by increasing the voltage into the heater coils, while cooling was accomplished by varying the pressure of the gas present in the outer chamber. Commercially available de amplifiers and recorders were employed in the apparatus to record the DTA curve.

An extremely rugged DTA furnace and sample holder has been described

by Bohon (35). In this apparatus, the differential thermocouples are isolated from the sample to avoid destruction from explosions or chemical reaction with the sample. This was accomplished by employing Chromel-versus-Alumel thermocouples encased in an Inconel sheath. The furnace tube and auxiliary pressure manifold were made from Monel metal. Pressures up to 1000 psig have been sustained in the furnace tube assembly at 350°C, and 400 psig at temperatures up to 500°C.

A highly sensitive DTA apparatus which permitted the determination of phase-transition temperatures of $\pm 0.5^\circ\text{C}$ over a wide range of heating rates has been described by Vassallo and Harden (29). The sample holder and heating block are illustrated in Figure 6.9(A). The apparatus is conventional in the differential temperature-measuring circuit, but in the furnace-temperature-measuring circuit a dc amplifier and zero-suppressing circuit are used when temperature accuracies of better than $\pm 0.5^\circ\text{C}$ are required. The heating block permits the use of 1.5-2.0 × 30-mm melting point capillary tubes as sample and reference material containers, with the thermocouples inserted into the sample through the top of the tube. The block was heated by a 30-W cartridge heater placed in the center of the block. The double coil of copper tubing served as a cooling line. One coil was immersed in a coolant contained in the lower part of the flask, while the second coil surrounded the block. The block was cooled by a flow of air or nitrogen through the lower coil, then to the coil surrounding the block. A temperature range - 150-450°C could be covered by the apparatus.

For studying the kinetics of homogeneous reactions in solution, Borchardt and Daniels (91) used the glass apparatus illustrated schematically in Figure 6.31. The cells consisted of two Pyrex tubes, 1.25 in. in diameter and 5 in.

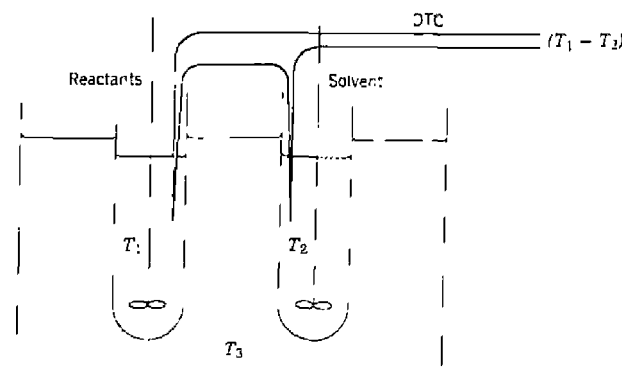


Figure 6.31. Solution DTA apparatus used by Borchardt and Daniels (91).

in length, each having a volume of about 60:nl. The thermocouples, contained in Kel-F covered copper tubes, were inserted into the tube contents from the top. The bath temperature, and hence the sample and reference materials, was gradually increased by use of a heater connected to a variable-voltage transformer.

A DTA apparatus containing thermistors as the differential temperature detection devices has been described by Pakulak and Leonard (22) and is illustrated in Figure 6.32a, while the thermistor bridge circuit is shown in Figure 6.32b. The matched thermistors, 100,000 Ω at 25°C, were contained in glass tubes and centered in each of the sample and reference tubes. A third thermistor was used to detect the temperature of the furnace. All thermistors and tubes were placed into a furnace constructed of aluminium. The heating rate of the furnace was controlled by increasing the furnace-windings voltage by means of a variable-voltage transformer. A heating rate of 2°C/mm was normally employed.

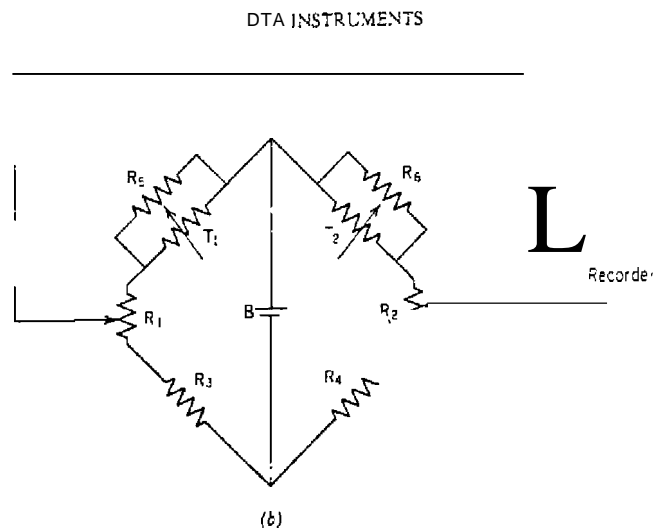
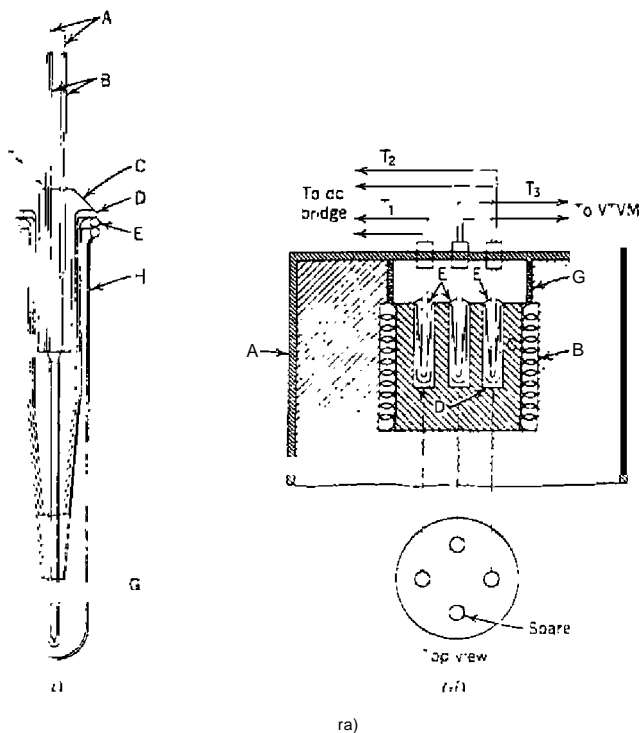


Figure 6.32. Thermistor DTA apparatus of Pakulak and Leonard (22): (a) (i) sample holder and furnace; (ii) thermistor bridge circuit. (b) (i) A, output leads; B, teflon sleeving; C, electrical resistor cement; D, 1.5-mm centrifuge tube; E, 1.5-mm centrifuge tube; F, two-hole ceramic tube; G, thermistor; H, test tube. (ii) A, furnace; B, furnace coil; C, block, aluminum; D, sample tubes; E, thermistor containers; F, T₁, T₂, T₃, thermistors; G, glass ring 1 in. × 3/4 in. (iii) R₁, R₂, 100 Ω potentiometer; R₃, R₄, 1000 Ω ± 1%; R₅, R₆, 2000 Ω ± 1%; F₁, F₂, thermistors-100,000 Ω at 25°C; B, 1 1/2 V dry cell.

It should be noted that an amplifier was not required since the bridge unbalance voltage signal was large enough to be recorded by the recorder.

One of the first controlled-atmosphere-controlled-pressure DTA instruments was described by Stone in 1960 (42, 43). A schematic diagram of the furnace and sample holder is shown in Figure 6.33. The sample holder permits a gas flow through the sample and reference materials during the heating cycle. Gas enters through the sample-holder manifold and diffuses through the porous disks in order to provide a minimum of turbulence and a maximum of gas uniformity in and around the sample. The gas composition may be changed at any time during the heating process or may be cycled between two or more gases. Pressure within the furnace chamber may vary from a -2 Torr to 100 psig.

An oven (15, 16) in which the thin-film thermocouples, previously described in Sections 3, are used is shown in Figure 6.34. It permitted programmed temperature operation from -120 to 500°C. For cooling, previously cooled nitrogen was flowed through the coil surrounding the oven chamber. Linear temperature programming was possible by controlling the flow of nitrogen gas.

DTA has been described (97, 98). An earlier apparatus has been described by Stone and Rase (42).

Radio-frequency heating of large samples of rubber has been described by Wald and Winding (99). The sample is placed between two parallel plates which are connected to a rf generator. Sample temperature is detected by a thermocouple located in the center of the sample.

A new DSC cell, based on the DTA principle (as is the Du Pont DSC cell previously discussed) has been described by David (110). The calorimeter cell, as shown in Figure 6.36, contains a differential thermocouple of a new thin-form design that is isolated from the cell wall and bottom to provide greater sensitivity. This thermocouple consists of a sheet of negative Platinel II type thermocouple alloy coupled to a positive Platinel II alloy. Flat shallow containers are employed for the sample and reference materials. Two addi-

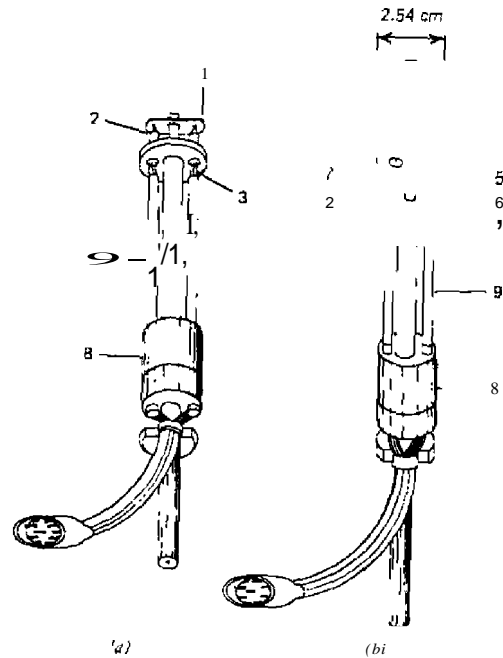


Figure 6.36. DSC cell by David (110). 1, thermocouple for x axis or system temperature readout; 2, limit switch thermocouple; 3, programming or furnace thermocouple; 4, dynamic gas port entry; 5, dynamic gas port exit; 6, sample side of differential thermocouple; 7, reference side of differential thermocouple; 8, ceramic thermal insulator; 9, ceramic support rods; 10, sample pans.

tional thermocouples are used for measuring the temperature of the cell and for the furnace programmer, limit switch, and temperature readout. The maximum temperature of the cell is 1000°C.

Other calorimeters described include a microcalorimeter (111) similar to the Calvet instrument (112), high-temperature differential calorimeters (113-117), and others (118-121).

C. COMMERCIAL INSTRUMENTS

1. Perkin-Elmer

a. DSC-ZC, DSC-4, and DSC7 Instruments

The most widely used DSC instruments are the Perkin-Elmer differential scanning calorimeters, the first model of which (DSC-I) was introduced in 1963 (100, 101). The Model DSC-2 was introduced in 1973 (24, 102, 103) followed by the DSC-4, and in 1984, the DSC7 system. The DSC-2 featured an extended maximum temperature limit of 725°C (as do the DSC-4 and DSC7), as well as improved baseline repeatability and linearity, and higher-temperature sensitivity.

A comparison (24) of the sample holders used in the DSC-I, DSC-IB, and DSC-2 instruments is shown in Figure 6.37. In the DSC-I cell, the sample and reference holder consisted of a stainless-steel cup and support, a platinum-wire sensor, an etched Nichrome heater, and other thermal parts. All these components were mechanically crimped together in a very tight sandwich. This sample holder operated well over the temperature range -125 to 500°C. In the DSC-2 sample holder, the materials of construction used are a platinum-iridium alloy for the body and structured members of the holder, a platinum wire for both the heater and sensor, and α -alumina for electrical insulation. All parts of the holder are spot-welded together.

A schematic diagram of the calorimeter is shown in Figure 6.38. The apparatus, unlike DTA, maintains a sample temperature isothermal to a reference substance (or furnace block) by supplying heat to the sample or reference material. The amount of heat required to maintain these isothermal conditions is then recorded as a function of time (or temperature). In addition to recording the enthalpy curve, if the sample evolved a volatile material during the heating process, the gas evolved by the sample is recorded.

The instrument contains two "control loops," one for the average-temperature control and the other for the differential-temperature control. In the former, a programmer provides an electrical output signal proportional to the desired temperature of the sample and reference holders. The pro-

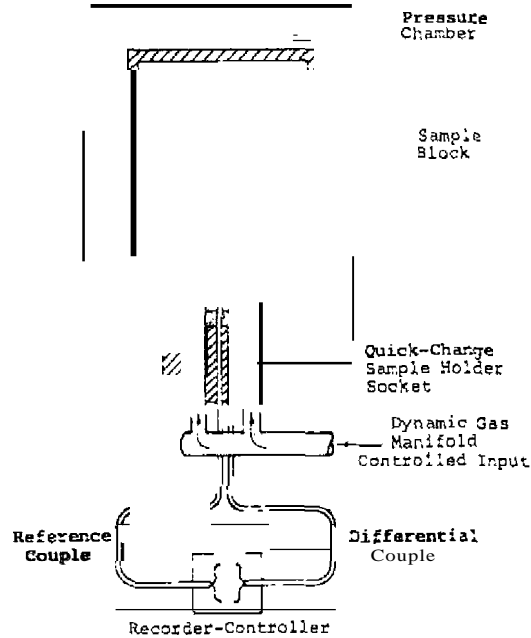


Figure 6.33. Stone's DTA apparatus, schematic (42, 43).

It is frequently necessary to isolate the DTA furnace and sample holder from the control console because of explosion hazards, radioactivity, toxic environments, and so on. The remote DTA sample holder and furnace must be capable of normal operation and must be easily loaded with the sample. Such a remote system has been described by Graybush et al. (93) in which a DuPont standard DTA cell was modified for remote operation for the study of primary explosives. The need to protect samples from the slightest oxidizing environment necessitated the cell being evacuated to 10^{-6} Torr. This required removal of the porous disk and redesign of the support and also, resealing of the electrical and gas connectors. Thermocouple connections were protected from the development of thermal gradients by shielding with glass tubing.

Several DTA instruments have been described by Barrall et al. (94, 95). A DTA calorimeter cell in which the ΔT -sensing thermocouples are attached to the sample container is shown in Figure 6.35. In this apparatus, copper-constantan thermocouples are soldered to a 4-mm-OD copper cup fitted with a copper lid. The thermocouples and sample cups are supported on ceramic insulator tubes which are attached to a metal base. All the cups were heated by thermal radiation received from the blackened copper radiation shield; this prevented radiation hot spots due to furnace winding. The entire DTA cell was enclosed by a glass bell jar which provided a controlled atmosphere from reduced pressures to about 2 atm.

A controlled-pressure system for a DTA apparatus has been described by Kemme and Kreps (96). This apparatus permitted the determination of sample vapor pressures by DTA.

Instrumentation used to evaluate the catalytic properties of a material by

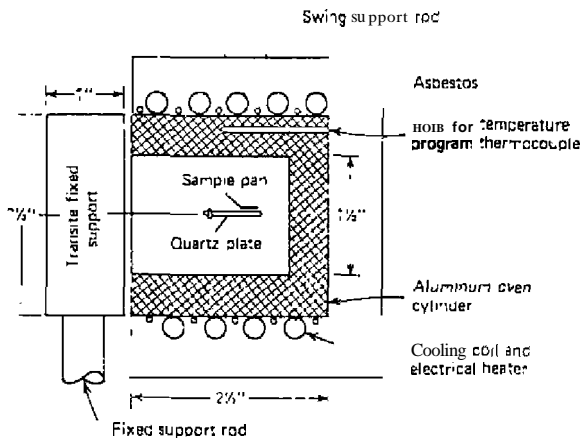


Figure 6.34. Over, for use with thin-film thermocouples (18, 16).

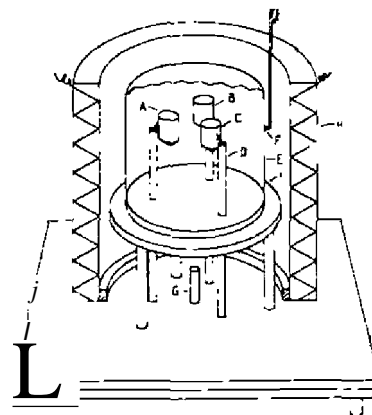


Figure 6.35. DTA calorimeter cell described by Barrall et al. (94). A, copper sample cups, 4-mm O. D. by 6 mm; C, J-pet reference cup; D, two-conductor ceramic supports, 3-mm diameter by 5 mm; E, copper radiator shield, 35-mm diameter by 53 mm; F, program-sensing thermocouple; G, liquid CO₂ cooling gas jet; H, electric furnace, 45-mm id by 100 mm; I, copper base plate, 38-mm diameter.

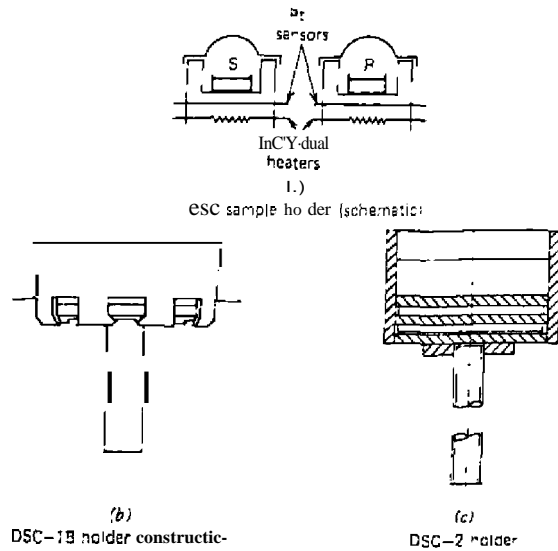


Figure 6.37. Sample-holder construction used in the Perkin-Elmer DSC instruments (24)

grammer signal which reaches the average temperature amplifier is compared with signals received from platinum-resistance thermometers permanently embedded in the sample and reference holders via an average-temperature computer.

In the differential-temperature loop, signals representing the sample and reference temperatures, as measured by the platinum-resistance thermometers, are fed to the differential-temperature amplifier via a comparator circuit, which determines whether the reference or the sample temperature is greater. The differential-temperature-amplifier output then adjusts the differential-power increment put into the reference and sample heaters in the direction and magnitude necessary to correct any temperature difference between them. A signal proportional to the differential power is also transmitted to the pen of a recorder, giving a curve of differential power versus time (temperature). The area under a peak, then, is directly proportional to the heat energy absorbed or liberated in the transition.

The DSC-2 features a temperature readout accuracy of $\pm 1.0^\circ\text{C}$ with a precision of $\pm 0.1^\circ\text{C}$. Calorimetric sensitivity ranges from 0.1 to 20.0 mcal sec^{-1} full-scale deflection using a 10-mV recorder. The furnace atmosphere may be N_2 or Ar, static or dynamic, at a pressure of 0.5 to 3 atm. Helium gas is required for low-temperature operation.

Specifications for the DSC7 are given in Table 6.7. As with the other DSC instruments, the data storage and processing is done by an external computer system with printout on a dot matrix printer or pen plotter, as discussed in Chapter 12.

Various sample holders have been described for the Perkin-Elmer DSC instrument. A sealed metal cell with a removable screw-on cap has been described by Freckberg and Alleman (104). Metals used were brass, stainless steel, and aluminum. Wendlandt (105) described a capillary-tube sample holder that used L6-1.8-mm-diameter glass capillary tubes. The tubes were contained in aluminum holders which were set in the sample and reference cells of the calorimeter. Sample holders for measuring the vapor pressure of a liquid (106) as well as for heats of mixing (107) have been described. Enclosure of the sample-holder chamber in a vacuum chamber has been described by Morie et al. (108). Other sample holders are described in Section B.2. For the DSC7 system, standard sample holders are constructed of aluminum, gold, platinum, copper, and graphite. Sealed and high-pressure sample holders for use up to 150 atm are constructed of aluminum, gold, and stainless steel.

b. DTA 1700 System

The Perkin-Elmer DTA 1700, which was introduced in 1980, conditions the

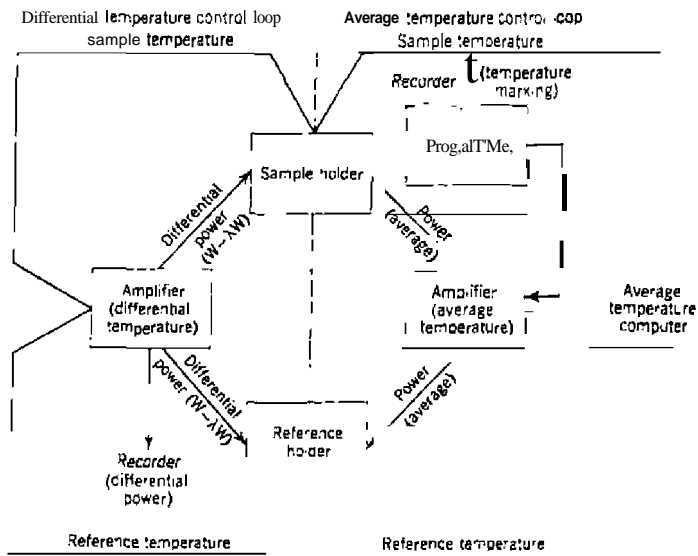


Figure 6.38. Schematic diagram of the Perkin-Elmer DSC instrument.

Table 6.7. Specifications of the Perkin-Elmer DSC7 System

DSC type	Power compensated temperature null principle. Measures energy directly, not differential temperature (ΔT).
DSC cell	Independent dual furnaces constructed of platinum-iridium alloy with independent platinum resistance heaters and temperature sensors.
Maximum sensitivity	$8 \mu\text{W}/\text{cm}$
Dynamic range	$8 \mu\text{W}/\text{cm}$ to $0.28 \text{ mW}/\text{cm}$
Noise (RMS)	0.002 mW
Calorimetric accuracy	Better than $\pm 1\%$
Calorimetric precision	Better than $\pm 0.1\%$
Temperature precision	$\pm 0.1^\circ\text{C}$.
Temperature accuracy	$\pm 0.1^\circ\text{C}$.
Temperature display	0.1°C increments
Heating and cooling rates	$0.1\text{--}5^\circ\text{C}/\text{min}$ in 0.1°C increments
Controlled (program) cooling	Ambient: $10^\circ\text{C min}^{-1}$ to 50°C $20^\circ\text{C min}^{-1}$ to 65°C $50^\circ\text{C min}^{-1}$ to 100°C $100^\circ\text{C min}^{-1}$ to 170°C Liquid N_2 : $10^\circ\text{C min}^{-1}$ to -180°C ; $50^\circ\text{C min}^{-1}$ to -165°C $100^\circ\text{C min}^{-1}$ to -135°C $200^\circ\text{C min}^{-1}$ to -85°C $300^\circ\text{C min}^{-1}$ to -30°C
Cooling times	Ambient: From $725\text{--}100^\circ\text{C}$ in under 4 min Liquid N_2 : From $+200\text{--}-150^\circ\text{C}$ in under 2 min
Temperature range	Standard unit allows operation from ambient to 725°C . With optional cooling accessories, the range may be extended to -170°C .
Temperature sensors	Distributed, platinum resistance thermometers.
Atmosphere	Static or dynamic including nitrogen, argon, helium, carbon dioxide, air, oxygen, or other inert or active gases.

ΔT signal by two modes, as shown in Figure 6.39. Mode (1) is the DTA mode in which the ΔT signal is linearized in degrees Centigrade, whereas Mode (2) is the DSC heat-flux mode with the ordinate output signal expressed in mcal/sec . Temperature programming is provided by the System 7/4 controller, which is incorporated in the instrument. Maximum furnace temperature of the system is 1500°C .

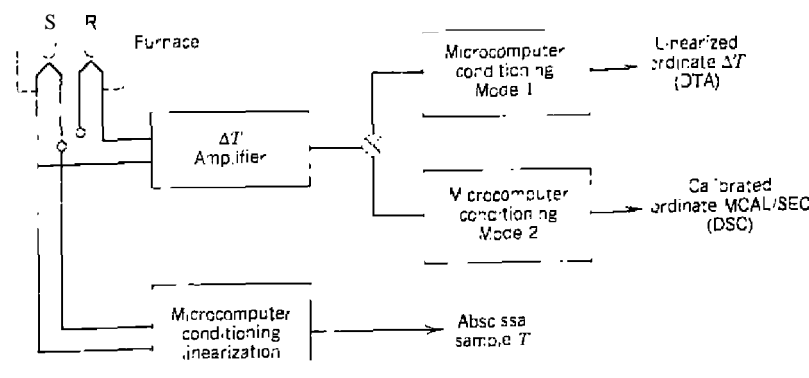


Figure 6.39. Signal conditioning for the Perkin-Elmer DTA system.

2. Du Pont

Two systems are available from Du Pont, the Model 1090 system (see Chapter 12) and the lower cost Series 99 system. Both require the use of modular cells, which for DSC-DTA consist of a one- and two-sample DSC cells, a high-pressure DSC cell, and several high-temperature DTA cells. A discussion of the theory and operational characteristics of the Du Pont DSC cell has been given by Baxter (18). The DSC cell, which has been illustrated in Figure 6.8, is based on a thermoelectric disk made of constantan which serves as the major path of heat transfer to and from the sample and also is one half the ΔT -measuring thermocouples. A Chromel wire is connected to each platinum, thus forming the Chromel-constantan differential thermocouple. The temperature range of the instrument is $150\text{--}600^\circ\text{C}$. A schematic diagram of the high-pressure DSC cell is given in Figure 6.40 (19). The pressure chamber is capable of pressures to 67 atm.

Miller and Wood (92) described the calorimetric accuracy and performance of the Du Pont high-temperature (1700°C) DTA cell. This furnace and sample holder are shown in Figure 6.41. Samples are contained in platinum cups inserted over platinum-platinum, 10% rhodium thermocouples and are surrounded by an alumina tube which is heated with a Kanthal-wire-wound furnace.

3. Mettler

The Mettler TA 2000C thermoanalyzer is a simultaneous 16-DSC instrument that has been previously described in Chapter 3. The data reduction

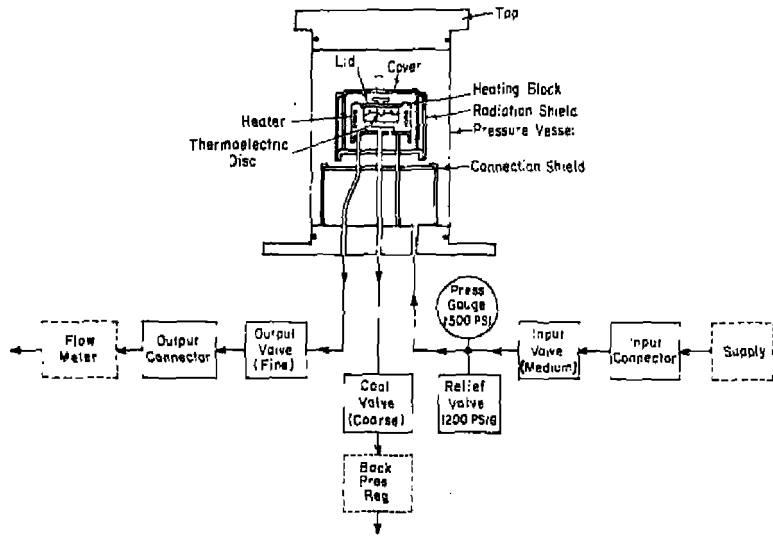


Figure 6.40. Du Pont high-pressure DSC cell.

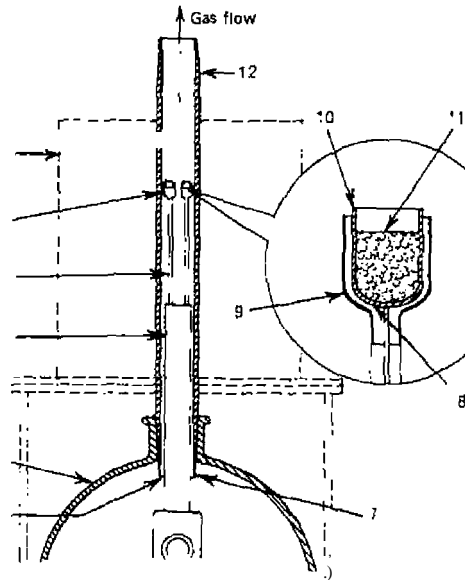


Figure 6.41. Du Pont 1200C DTA cell. according to Miller and Wood (92): 1. furnace; 2. alumina furnace tube; 3. shoulder; 4. ceramic insulator; 5. ceramic support; 6. tapered join; 7. thermocouple junction; 8. platinum cup; 9. platinum cup; 10. liner; 11. sample; 12. alumina furnace tube.

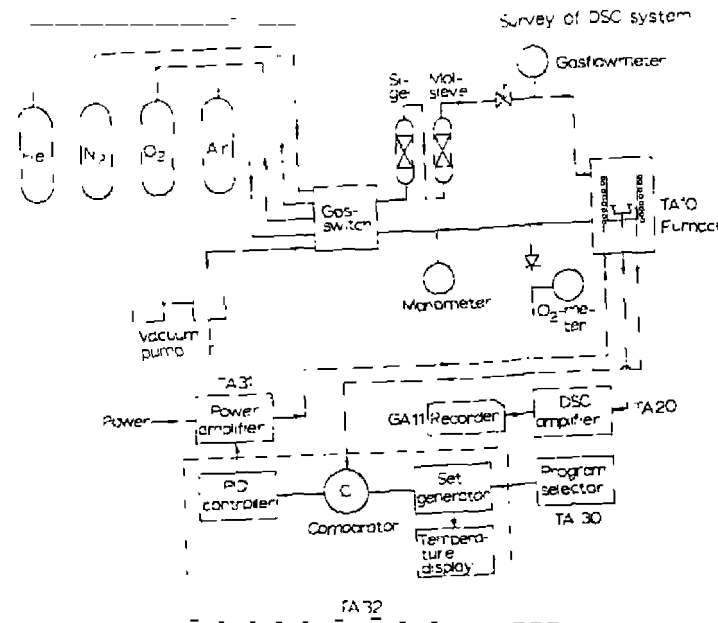


Figure 6.42. Mettler TA 2000 system (140).

system. Mettler TA 2000Z, is discussed in Chapter 12. A schematic diagram of the instrument, as described by Van Dooren and Muner (140), is shown in Figure 6.42. The baseline stability, calibration, and other characteristics of the system were also given (140).

The Mettler TA 3000 is a modular measuring and data reduction system incorporating the TC10 TA processor and DSC, TG, and TMA cells. Two DSC cells are available, the DSC 20 and DSC 30, usable in the temperature range from -20 to 600°C and -170 to 600°C, respectively. The accuracy of enthalpy measurements is $\pm 2\%$ with a precision of $\pm 0.5\%$.

4. Stanton Redcroft

The Model STA-700 series of instruments for TG and simultaneous TG-DTA have been described in Chapter 3. The systems have maximum furnace temperatures of 1000 or 1500°C. Also available are the DTA 670 series DTA instruments for use in the temperature range of -150 to 1650°C, and the TA 680 series usable in the temperature range from 25 to 1650°C. A wide variety of sample holders and furnaces are available for each series.

5. SETARAM

A large number of DSC and DTA instruments, several of which are combined with TG (see Chapter 3), are available from this manufacturer. Since it is not possible to discuss all of them here, only the Model DSC 111 will be described. The manufacturer's literature should be consulted for the other DTA systems that cover the wide temperature range of from -196 to 2400°C.

The sample holder and furnace of the DSC 111 is shown in Figure 6.43. It consists of a small thermostatically programmed block (1) arranged in an external enclosure (2). Two thin refractory tubes (3) contain the sample holder in their middle section, which is surrounded by a calorimetric fluxmeter (4). The fluxmeter detects the transfer of heat between the sample and the block, using the Tian-Calvet principle. The extremities of the refractory tubes permit the introduction and removal of samples and atmosphere control. A high precision electronic temperature programmer controls the furnace temperature. Maximum furnace temperature is 827°C with a heat-flux measurement of <15 to <30 μW absolute. Numerous sample-holder geometries are available.

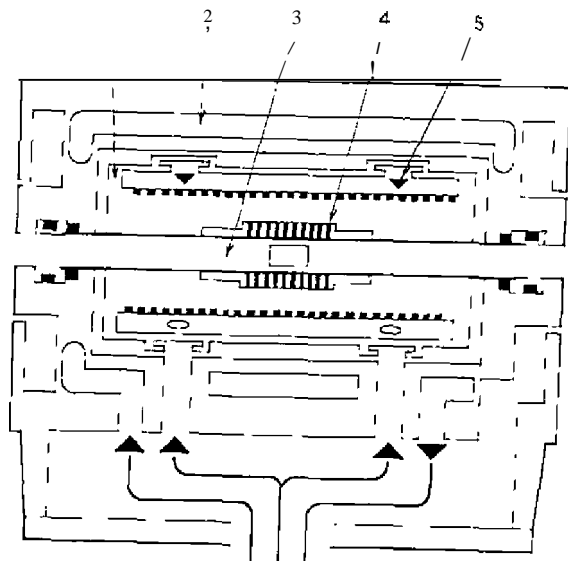


Figure 6.43. SETARAM DSC 111 system: sample holder and furnace arrangement.

6. Netzsch

As with the SETARAM instruments, many different DSC and DTA systems are available, including simultaneous TG-DTA systems. The latter have furnaces usable in the temperature range from -160 to 2400°C. For DTA, the Model 404 series covers the temperature range from -160 to 1700°C in 12 different models. A heat-flux system, the Model DSC 444, is based on the Tian-Calvet principle. It is operable from -140 to 500°C.

7. Sinku Riko

The C[vac-Riko thermal analysis equipment includes a number of DSC and DTA systems covering a wide temperature range. The DT-1500 series of DTA instruments is usable in the temperature range from -150 to 1500°C. For DSC, the DSC-1500 series covers the temperature interval from -170 to 550°C. Temperature programmers and infrared image furnaces are also available.

8. Eberbach

One of the earliest commercial DTA systems, a field portable unit, is still available from this manufacturer. It is used extensively in bauxite exploration and provides qualitative data in about 20 min. The complete apparatus is housed in a metal case, 21" L x 8.5" W x 9" H, containing the insulated base supporting the crucibles, pyrometer, galvanometer, and small tools.

REFERENCES

1. Wendlandt, W. W., "Differential Thermal Analysis," in *Technique of Inorganic Chemistry*, H. B. Jonassen and A. Weissberger, eds., Vol. 1, Interscience, New York, 1963, Chap. 6.
2. Gam, P. D., *Anal. Chem.*, **37**, 77 (1965).
3. Bohon, R. L., *Anal. Chem.*, **35**, 1845 (1963).
4. Mazieres, C., *Anal. Chem.*, **36**, 602 (1964).
5. Miller, B., *Thermochim. Acta*, **2**, 225 (1971).
6. Kulp, J. L., and P. F. Kerr, *Science*, **105**, 413 (1947).
7. Kerr, P. F., and J. L. Kulp, *Am. Mineral.*, **33**, 387 (1948).
8. Cox, D. B., and I. F. McGlynn, *Anal. Chem.*, **29**, 960 (1957).
9. Burr, J. T., in *Thermal Analysis*, R. F. Schwenker and P. D. Garn, eds., Vol. 1, Academic, New York, 1969, p. 3D1.
10. Wilhoit R. C., *J. Chem. Educ.*, **44**, A571 (1967).
11. Brewer, L., and P. Zavisanos, *J. Phys. Chem. Solids*, **2**, 284 (1957).

12. Lodding, W. and E. Sturm. *Am. Mineral.* 42:78(1957).
13. Jonich, M. J. and D. R. Bailey. *Anal. Chem.* 32:1578 (1960).
14. Van Tets, A., and H. G. Wiedemann. in *Thermal Analysis*, R. F. Schwenker and P. D. Garn, eds., Vol. 1. Academic, New York, 1969, p. 121.
15. King, W. H., C. T. Camilli, and A. F. Findeis. *Anal. Chem.* 40, 1330 (1968).
16. King, W. H., C. T. Camilli, and A. F. Findeis, in *Analytical Calorimetry*, R. S. Porter and J. F. Johnson, eds., Plenum, New York, 1968, p. 261.
17. Yamamoto, A. K., Yamada, M. Maruta, and J. Akiyama., in *Thermal Analysis*, R. F. Schwenker and P. D. Garn, eds., Vol. 1, Academic, New York, 1969, p. 105.
18. Baxter, R. A. in *Thermal Analysis*, R. F. Schwenker and P. D. Garn, eds., Vol. 1. Academic, New York, 1969, p. 65.
19. McAdie, I. G., in *Thermal Analysis*, R. F. Schwenker and P. D. Garn, eds., Vol. 1, Academic, New York, 1969, p. 693.
20. Menis, O., and J. T. Sterling, *Status of Thermal Analysis*, O. Menis, ed., Natl. Bur. Stand. Spec. Publ. 338, Washington, DC, Oct. 1970.
22. Pakulak, J. M., and G. W. Leonard, *Anal. Chem.* 31:1037 (1959).
23. Weaver, E. E., and W. Keim, *Proc. Indiana Acad. Sci.*, 70, 123 (1960).
24. O'Neill, M. L. and R. L. Fyans, *Eastern Anal. Symposium*, New York, Nov. 1971.
25. Hia, I. A., and C. B. Murphy, *Anal. Chem.*, 31, 1443 (1959).
26. Hogan, V. D., and S. Gordon, *Anal. Chem.*, 32:5731 (1960).
27. Campbell, C., and G. Weingarten, *Trans. Faraday Soc.*, 55, 2221 (1959).
28. Clappitt, B. H., *Anal. Chem.*, 35:577 (1963).
29. Vassallo, D. A. and I. C. Harden, *Anal. Chem.*, 34, 132 (1962).
30. Wiedemann, H. G., *Chem. Ing. Tech.* 36, 1105 (1964).
31. Barrall, E. M., in *Guide to Modern Methods of Instrumental Analysis*, T. H. Gow, ed., Wiley-Interscience, New York, 1972, Chap. 12.
32. Lodding, W., and L. Hammell, *Rev. Sci. Instrum.* 30, 885 (1959).
33. Lodding, W. and L. Hammell, *Anal. Chem.* 32, 657 (1960).
34. Rudin, A., H. P. Schreiber, and M. H. Waldman, *Ind. Eng. Chem.*, 53, 1371 (1961).
35. Bohon, R. L., *Anal. Chem.* 33, 1451 (1961).
36. Martin, A. J., and K. L. Edwards, *J. Sci. Instrum.* 36, 170 (1959).
37. Whitehead, W. L. and I. A. Breger, *Science*, 111, 279 (1959).
38. Stone, R. L., *J. Am. Ceram. Soc.*, 35, 76 (1952).
39. Wendlandt, W. W., *J. Chem. Educ.* 40, 428 (1963).
40. Reisman, A., *Anal. Chem.*, 32, 1566 (1960).
41. Chihara, H., and S. Seki, *Bull. Chem. Soc. Jpn.*, 26, 88 (1953).
42. Stone, R. L., and H. F. Rase, *Anal. Chem.*, 29, 1273 (1957).
43. Stone, R. L., *Anal. Chem.*, 32, 1582 (1960).
44. Levandowsky, J., and N. Sacovy, *Inst. Fr. Petro.* XI, 818 (1956).
45. Theall, G. G., in *Thermal Analysis*, R. F. Schwenker and P. D. Garn, eds., Vol. 1. Academic, New York, 1969, p. 97.
46. Barrall, E. M., and L. B. Rogers, *Anal. Chem.*, 34, 1101 (1962).
47. Burgess, G. K., *U.S. Bur. Stand., Bull.* 5, 199 (1908).
48. Kauffman, A. J., and E. D. Dilling, *Econ. Geol.*, 45, 22 (1950).
49. Roberts-Austen, W. C., *Metallographist*, 2, 1861 (1899).

50. Smothers, W. J., and Y. Chiang, *Differential Thermal Analysis: Theory and Practice*, Chemical Publishing Co., New York, 1958, pp. 294-399.
51. Smothers, W. J., and Y. Chiang, *Differential Thermal Analysis: Theory and Practice*, 2nd ed., Chemical Publishing Co., New York, 1966.
51. Gam, P. D., *Thermoanalytical Methods of Analysis*, Academic, New York, 1965, Chap. IX.
53. Barrall, E. M., and I. F. Johnson, in *Techniques and Methods of Polymer Evaluation*, P. E. Slade and L. T. Jenkins, eds., Marcel-Dekker, New York, 1966, Chap. L.
54. Mackenzie, R. C., and B. D. Mitchell, in *Differential Thermal Analysis*, R. C. Mackenzie, ed., Academic, Gordon, 1970, Chap. III.
55. Anon., *Ind. Res.*, Nov. 25, 1969.
56. Wendlandt, W. W., *Thermal Analysis Techniques*, in *Handbook of Commercial Scientific Equipment*, C. Veillon and W. W. Wendlandt, eds., Vol. 2, Marcel-Dekker, New York, in press.
57. Wendlandt, W. W., *Lab. Manage.*, Oct., 26 (1965).
58. Wendlandt, W. W., *J. Chem. Educ.* 49, A571, A623 (1972).
59. Boilin, E. M., in *Differential Thermal Analysis*, R. C. Mackenzie, ed., Academic, London, 1970, Chap. VII.
60. Barrell, E. L. H., W. Hoyer, and A. V. Santoro, *Mikrochim. Acta*, 1122 (1970).
61. Santoro, A. V., E. L. Barrett, and H. W. Hoyer, *J. Thermal Anal.* 2, 461 (1970).
62. Wendlandt, W. W., *Thermochem. Acta*, 1, 4:9 (1970).
63. Eller, D. E., P. A. Tucker, and L. J. Wittenberg, in *Thermal Analysis*, R. F. Schwenker and P. D. Garn, eds., Vol. 2, Academic, New York, 1969, p. 8:9.
64. Gilpatrick, L. O., S. Cantor, and C. J. Barton, *Thermal Analysis*, R. F. Schwenker and P. D. Garn, eds., Vol. 1, Academic, New York, p. 85.
65. Roberts, H. S., *J. Am. Chem. Soc.*, 57, 1034 (1935).
66. Kracek, F. C., *Trans. Am. Geophys. Union*, 27, 364 (1946).
67. Boilin, E. M., and P. F. Kerr, *Am. Mineral.* 46, 823 (1961).
68. Fakror, M. M., and R. Hanks, *Trans. Faraday Soc.* 63, 1122 (1967).
69. Jensen, L., *Am. J. Sci.*, 240, 695 (1942).
70. Barrall, E. M., and L. B. Rogers, *J. Inorg. Nucl. Chem.* 28, 41 (1966).
71. David, D. L., *Anal. Chem.*, 37, 82 (1965).
72. Locke, C. E., *Proceedings of the Third Torolco Symposium on Thermal Analysis*, I. G. McAdie, ed., Chemical Institute of Canada, Toronto, 1969, p. 251.
73. Brunskil, I. H., P. Tissol, and H. Schmid, *Thermochem. Acta*, 49, 351 (1981).
74. Cohen, L. H., W. Klement, and G. C. Kennedy, *J. Phys. Chem. Solids*, 27, 1196 (1966).
75. Kubaila, M., and G. M. Schneider, *Ber. Bunsen Ges. Phys. Chem.* 75, 513 (1971).
76. Takeya, G., T. Ishii, K. Makino, and S. Ueda, *Kogyo Kagaku Zasshi*, 69, 1654 (1966).
77. Ueda, S., S. Yokoyama, T. Ishii, and G. Takeya, *Kogyo Kagaku Zasshi*, 74, 1377 (1971).
78. Bousquet, J., J. M. Blanchard, B. Bonnetot, and P. Claudy, *Bull. Soc. Chim. Fr.*, 1841 (1969).
79. Newkirk, T. F., *J. Am. Ceram. Soc.* 41, 409 (1958).

80. Nedumov, N. A. in *Differential Thermal Analysis*, R. C. Mackenzie, ed., Academic, London, 1970, p. 168.
81. Rupert, G. N., *Rev. Sci. Instr.*, **34**, 11831 (1963).
82. Rupert, G. N., *Rev. Sci. Instr.*, **36**, 1629 (1965).
83. Rupert, G. N., *proc. 1st ICTA*, J. P. Redfern, ed., Macmillan, London, 1965, p. 9.
84. Sommer, G., and P. R. Jochens, *Miner. Sci. Eng.*, **3**, 3 (1971).
85. Miller, R. P., and G. Sommer, *J. Sci. Instrum.*, **43**, 293 (1971).
86. Sommer, G., P. R. Jochens, and D. D. Howat, *J. Sci. Instrum. Ser. 2*, **1**, 1116 (1968).
87. Proks, I., and I. Zlatovskiy, *Chem. Zvesti*, **23**, 620 (1969).
88. Wendlandt, W. W., and W. S. Bradley, *Anal. Chem. Acta*, **52**, 397 (1970).
89. Wendlandt, W. W., *Chimia*, **26**, 2 (1972).
90. Wendlandt, W. W., *J. Chem. Educ.*, **38**, 571 (1961).
91. Borchardt, H. J., and F. Daniels, *J. Am. Chem. Soc.*, **79**, 41 (1957).
92. Miller, G. W., and J. L. Wood, *J. Thermal Anal.*, **2**, 71 (1970).
93. Graybush, R. J., F. G. May, and A. C. Forsyth, *Thermochim. Acta*, **2**, 53 (1971).
94. Barrall, E. M., I. F. Gernert, R. S. Porter, and J. F. Johnston, *Anal. Chem.*, **35**, 1837 (1963).
95. Barrall, E. M., R. S. Porter, and J. F. Johnston, *Anal. Chem.*, **36**, 2172 (1964).
96. Kemme, H. R., and S. I. Kreps, *Anal. Chem.*, **41**, 1869 (1969).
97. Macak, J., and J. Malecha, *Anal. Chem.*, **41**, 442 (1969).
98. Dimitrov, R., *Compt. Rend. Acad. Bulbare Sci.*, **23**, 1215 (1970).
99. Wald, S. A., and C. C. Winding, *Anal. Chem.*, **37**, 1622 (1965).
100. O'Neill, M. J., *Anal. Chem.*, **36**, 1238 (1964).
101. Watson, E. S., M. I. O'Neill, J. Justin, and N. Brenner, *Anal. Chem.*, **36**, 1233 (1964).
102. *Perkin-Elmer Thermal Analysis Newsletter*, No. 10, Feb. 1972.
103. O'Neill, M. I., and A. P. Gray, *ICTA III, Davos, Switzerland*, Aug. 23-28, 1971, paper 1-24.
104. Freeberg, F. E., and T. G. Alleman, *Anal. Chem.*, **38**, 1806 (1966).
105. Wendlandt, W. W., *Anal. Chim. Acta*, **49**, 187 (1970).
106. Farritor, R. E., and L. C. Tao, *Thermochim. Acta*, **1**, 297 (1970).
107. Milta, I., I. Imal and H. Kambe, *Thermochim. Acta*, **2**, 337 (1971).
108. Morie, G. P., T. A. Powers, and C. A. Glover, *Thermochim. Acta*, **3**, 2591 (1972).
109. Levy, P. F., G. Nieuweboer, and L. C. Semanski, *Thermochim. Acta*, **1**, 429 (1970).
110. David, D. I., *J. Thermal Anal.*, **3**, 247 (1971).
111. Evans, W. J., E. J. McCourtney, and W. B. Carney, *Anal. Chem.*, **40**, 2621 (1968).
112. Calvel, R., *Compt. Rend.*, **226**, 1702 (1948).
113. Sale, F. R., *J. Phys. E: Sci. Instr.*, **3**, 646 (1970).
114. Thomasson, C. N., and D. A. Cunningham, *J. Sci. Instrum.*, **41**, 3081 (1964).
115. Berger, C., M. Richard and L. Eyraud, *Bull. Soc. Chim. Fr.*, 1491, 1965.
116. Raux, A., M. Reebaid, L. Eyraud, and J. Elston, *J. Phys. Phys. Appl.*, **25**, 51A (1974).
117. Nicholson, P. S., *Lawrence Radiation Lab. Report*, UCR-L-17320, Sept. 1967.
118. Speros, D. M., and R. L. Woodhouse, *J. Phys. Chem.*, **67**, 2164 (1964).
119. Speros, D. M., and R. L. Woodhouse, *J. Phys. Chem.*, **72**, 2346 (1968).
120. Garski, H., *Z. Angew. Chem.*, **24**, 206 (1968).

121. Muller, W., and D. Schuller, *Ber. Bunsen Ges. Physik. Chem.*, **75**, 79 (1971).
122. Audiere, J. P., C. Malieres, J. C. Carballes, and B. de Cremoux, *J. Phys. E: Sci. Instrum.*, **7**, 355 (1974).
123. Judd, M. D., and M. J. Pope, *Thermochim. Acta*, **7**, 247 (1973).
124. Arndt, P. E., J. G. Dunn, and B. Willix, *Thermochim. Acta*, **48**, 237 (1981).
125. Chiu, I., *Thermochim. Acta*, **26**, 57 (1978).
126. Chiu, J., in *Analytical Calorimetry*, R. S. Porter and J. F. Johnson, eds., Vol. 2, Plenum, New York, 1970, p. 171.
127. Schouteten, C. J. H., S. Bakker, B. Kiazema, and A. J. Peijnenburg, *J. Anal. Chem.*, **49**, 522 (1977).
128. Earnest, C. M., R. L. Fyans and W. Kunze, *Proc. 1st N. IT IS Conf.*, New Orleans, LA, October 1981.
129. Charsley, E. I., C. T. Cox, M. R. Ottaway, T. J. Barton, and J. M. Jenkins, *Thermochim. Acta*, **52**, 321 (1982).
130. Dey, A. N., *J. Electrochem. Soc.*, **127**, 1000 (1980).
131. Williams, I. R., and W. W. Wendlandt, *Thermochim. Acta*, **7**, 269 (1973).
132. Wurflinger, A., and G. M. Schneider, *Ber. Bunsen. Phys. Chem.*, **77**, 121 (1973).
133. Wurflinger, A., and G. M. Schneider, *Ber. Bunsen. Phys. Chem.*, **75**, 513 (1971).
134. Wurflinger, A., C. Josellak, and G. M. Schneider, *High Temp. High Pressures*, **8**, 645 (1976).
135. Wurflinger, A., and G. M. Schneider, *Ber. Bunsen. Phys. Chem.*, **79**, 1195 (1975).
136. Kamphausen, M., *Rev. Sci. Instrum.*, **46**, 668 (1975).
137. Kocherzhinsky, A., *Colloq. Int. C.N.R.S.*, **205**.
138. Haines, P. I., and G. A. Skinner, *Thermochim. Acta*, **59**, 343 (1982).
139. Seyler, R. J., and E. Kaiblich, *Am. Lab.*, Jan. 1978, p. 15.
140. Van Dooren, A. A., and B. W. Muller, *Thermochim. Acta*, **49**, 151 (1981).

APPLICATIONS OF DIFFERENTIAL THERMAL ANALYSIS AND DIFFERENTIAL SCANNING CALORIMETRY

A. INTRODUCTION

As previously discussed in Chapter 5, the DTA or DSC curve consists of a series of peaks in an upward or downward direction on the ΔT or heat-flow axis. The positions (on the temperature or X axis), shape, and number of peaks are used for purposes of qualitative identification of a substance, while the areas of the peaks, since they are related to the enthalpy of the reaction, are used for quantitative estimation of the reactive substance present or for thermochemical determinations. Because of the various factors which affect the DTA or DSC curve of a sample, the peak temperatures and the shape of the peak are rather empirical. Generally, however, the curves are reproducible for any given instrument, so that they can be useful in the laboratory. By use of various calibration substances, the areas enclosed by the curve peaks can be related to heats of reaction, transition, polymerization, fusion, and so on. Or, if the heat of the reaction is known, the amount of reacting substance can be determined.

Some origins of the endothermic or exothermic curve peaks are summarized in Table 7.1. Any phenomenon that produces an enthalpic change or a change in heat capacity (second-order transitions) can be detected by DTA or DSC techniques provided that the instrument has the required sensitivity. These phenomena are caused by fundamental changes in state, chemical composition, molecular reactivity of the substances, and so on. The shape of the peaks, and also the peak maximum ($\Delta T_{m.}$) and peak minimum ($\Delta T_{m.in.}$) temperatures, are controlled basically by the reaction kinetics, although they are also influenced by the sample packing and geometrical parameters, the heating rate, the furnace atmosphere, and the reference temperature source. Even more subtly, the changes of the baseline can be related to the change in specific heat of the sample; this is an important parameter in the detection of glass transition temperatures, T_g , in polymers. The area of the peak is determined by the enthalpic change and also by the instrumental factors such as the size, thermal conductivity, and the specific heat of the sample.

Table 7.1. Physicochemical Origin of DTA and DSC Curve Peaks (57)

Phenomena	Enthalpic Change	
	Endothermal	Exothermal
<i>Physical</i>		
Crystalline transition	x	
Fusion	x	
Vaporization	x	
Sublimation	x	
Adsorption		
Desorption	x	
Absorption		
Curie point transition	x	
Glass transition	Change of baseline, no peaks	
Liquid crystal transition	x	
Heat capacity transition	Change of baseline, no peaks	
<i>Chemical</i>		
Chemisorption		x
Desorption	x	
Dehydration	x	
Decomposition	x	x
Oxidative degradation		x
Oxidation in gaseous atmosphere		x
Reduction in gaseous atmosphere	x	
Redox reactions	x	x
Solid-state reaction	x	x
Combustion		x
Polymerization		x
Pre-curing (resins)		x
Catalytic reactions		x

The technique of DTA has been employed by geologists, ceramicists, and metallurgists for many years. DTA proved to be a rapid analytical tool for the determination and identification of clays and other minerals, phase transitions and phase diagrams, high-temperature kiln reactions, and so on. Normally, the technique is supplemented by X-ray diffraction, dilatometry, thermogravimetry, electrical conductivity, and other techniques. Only in fairly recent times has the chemist become interested in this technique, although many classical chemical studies were carried out in the 1930s. Mention should be made of the early studies by Kracek (58, 59). The list of applications to chemical problems has grown very rapidly, with applications

being made to all the sciences. Specific areas of investigation are summarized in Tables 7.2 and 7.3. Indeed, nearly every chemical field has been touched by this technique, although much of the recent emphasis has been in the area of polymer chemistry. Perhaps the largest: use of DSC has been in some phase of polymer characterization.

Because of the large number of applications of the techniques of DTA and DSC, the applications described here will be concerned mainly with analytical chemistry problems. In this area, DTA and DSC can be used as a control or a routine tool for comparing similar but not identical materials. As a control technique, it may be used to distinguish between raw materials quickly and easily in those cases in which the treatment of the material must be modified if slight changes in the material are encountered. As a comparison technique, DTA and DSC may be used in some cases to detect materials that yield anomalous results by other tests. Lastly, by suitable calibration of the instruments, these techniques may be used for the quantitative estimation of a substance or mixture of substances, or for purity determinations (see

Table 7.2. Specific DTA and DSC Applications in Chemistry

Materials	Types of Studies
Catalysts	Decomposition reactions
Polymeric materials	Phase diagrams
Lubricating greases	Reaction kinetics
Fats and oils	Solid-state reactions
Coordination compounds	Dehydration reactions
Carbohydrates	Radiation damage
Amino acids and proteins	Calorimetry
Metal salt hydrates	Heats of adsorption
Metal and nonmetal oxides	Heats of reaction
Coal and lignite	Heats of polymerization
Wood and related substances	Heats of sublimation
Natural products	Heats of transition
Organic compounds	Desolvation reactions
Clays and minerals	Desolvation reactions
Metals and alloys	Solid-gas reactions
Soil	Curie point determinations
Biological materials	Purity determinations
Pharmaceuticals	Thermal stability
	Oxidation stability
	Glass transition determinations
	Comparison

Chapter 10). An attempt is made here to include only illustrative types of applications, and it is not intended to be comprehensive.

B. APPLICATIONS TO BIOLOGICAL MATERIALS

Most of the applications of DTA to biological materials have been for identification and characterization. However, perhaps this is to be expected because of the complexity and heterogeneity of these materials: compare a sample of peat with benzoic acid or other simple organic compounds. The DTA curves are frequently quite broad and are devoid, in many cases, of narrow endothermic and exothermic peaks. Many of the older investigations in this area were done under rather uncontrolled conditions of furnace atmosphere and heating rates, so they cannot be compared with data obtained with modern instrumentation.

The application of DTA (and other thermal analysis techniques) to biological materials has been reviewed recently by Mitchell and Birnie (118) and Pfeil (119). The former is mainly concerned with the DTA studies of fresh plant material, bacteria, partially decomposed plant material, peat, and soil organic matter. Pfeil (119) discussed the application to human materials such as the liver, endema in burns, bones, and so on.

A summary of some of the applications of DTA and DSC to biological materials is given in Table 7.4.

Labowirz (138) reponed a phase transition in anhydrous cholesterol at 37°C which had $\Delta H = 0.66$ kcal/mole and $\Delta S = 2.1$ cal K⁻¹. This transition has been discussed by others.

The heat capacity of anhydrous ovalbumin and p-Iactoglobulin was determined using DSC by Berlin et al. (137). A linear relationship was found between the specific heat and moisture content with hydrated samples which contained 0.03-0.21 g sorbed water per gram of protein. Berlin et al. (139) also determined the heat of desorption of water vapor from amorphous and crystalline lactose by DSC.

Olafsson and Bryan (141) determined the thermal stability of 19 amino acids using DSC. They used the ΔT_{min} temperatures as the decomposition temperatures of the acids. In some cases, the unique shape of the curves and the number of peaks into which it could be resolved were used to characterize the compound.

The DTA curves of several bacterial dextrans have been determined by Morita (142) in order to study certain relationships between the OTA curve peaks and their molecular constitution.

The characterization of starch and related polysaccharides by DTA has been carried out by Morita (143). The OTA curves obtained for several

Table 7.3. Some Industrial Uses of DTA and DSC

	Carbo- nates	Car- bon oxi- des	Chro- m- ium ox- ide	Blasto- merit	Explo- sives	Chro- m- ium nitry	Fuels	Glass	Inks	Metals	Min- erals	Pharm- aceuti- cals	Phos- phor- ous	Fluor- ides	Proper- ties	Scaps	Spills	Tex- tiles	
Composition	✓	✓	✓	✓	✓	✓	✓	✓	✓	✓	✓	✓	✓	✓	✓	✓	✓	✓	✓
Quantitative	✓	✓	✓	✓	✓	✓	✓	✓	✓	✓	✓	✓	✓	✓	✓	✓	✓	✓	✓
Phase diagrams	✓	✓	✓	✓	✓	✓	✓	✓	✓	✓	✓	✓	✓	✓	✓	✓	✓	✓	✓
Solvent retention	✓	✓	✓	✓	✓	✓	✓	✓	✓	✓	✓	✓	✓	✓	✓	✓	✓	✓	✓
Hydration, dehydration	✓	✓	✓	✓	✓	✓	✓	✓	✓	✓	✓	✓	✓	✓	✓	✓	✓	✓	✓
Thermal stability	✓	✓	✓	✓	✓	✓	✓	✓	✓	✓	✓	✓	✓	✓	✓	✓	✓	✓	✓
Oxidative stability	✓	✓	✓	✓	✓	✓	✓	✓	✓	✓	✓	✓	✓	✓	✓	✓	✓	✓	✓
Polymerization	✓	✓	✓	✓	✓	✓	✓	✓	✓	✓	✓	✓	✓	✓	✓	✓	✓	✓	✓
Curing	✓	✓	✓	✓	✓	✓	✓	✓	✓	✓	✓	✓	✓	✓	✓	✓	✓	✓	✓
Purity	✓	✓	✓	✓	✓	✓	✓	✓	✓	✓	✓	✓	✓	✓	✓	✓	✓	✓	✓
Reactivity	✓	✓	✓	✓	✓	✓	✓	✓	✓	✓	✓	✓	✓	✓	✓	✓	✓	✓	✓
Catalytic activity	✓	✓	✓	✓	✓	✓	✓	✓	✓	✓	✓	✓	✓	✓	✓	✓	✓	✓	✓

Table 7.4. Applications of DTA and DSC to Biological Materials

Material	Techniques	References
Fats, Oils, and waxes	DTA, DSC	120-122,132,133
Human bone and hemoglobin	DTA	123
Tobacco	DTA	124
Polynucleotides	DTA	125
Protein denaturation and others	DSC	126, 137
Skin, skin constituents	DTA	127
Biopolymers	DTA	128,129
Yeast and blood cryobiology	DTA	130, 131
Human liver-hepatoma	DTA, EGA, TG	119
Edema in burns (human skin tissue)	DTA, TG, MS	119
Grain (corn, wheat, oats, etc.)	DTA, TG	119
Fresh plant material	DTA	118
Bacteria and actinomycetes	DTA	118
Peat and partially decomposed plant material	DTA	118
Soil organic matter	DTA	118
Wood	DTA	134
Cellulose	DTA	135
LiChens	DTA	136
Cholesterol	DTA, DSC	138
Lactose	DTA, DSC	139

samples of potato and corn starch are given in Figure 7.1. The samples were prepared into a compressed "sandwich"-type packing prepared by placing 150 mg of sample between two 200-mg layers of (calcined alumina and compressing at 200 psi.

The DTA curves of the starches were characterized by endothermic peaks in the 135-310°C region, followed by two distinct exothermic peaks in the 375-520°C range. The curves illustrate very nicely the effect of pretreatment on the starches.

Since starch is a polymeric glucoside composed of α -1,4- and α -1,6-linked glucopyranosidic units, it was of interest to examine the thermal properties of the linear polymeric fraction of starch, namely, that of amylose. The DTA curves for various amylose fractions, prepared from the same starches, have been reported. Examination of the three fractions reveals three distinct features: the endothermic peaks with ΔT_{min} of about 150 and 225°C, and a shoulder peak with a ΔT_{min} of 315°C. There were pronounced exothermic peaks in the 490-510°C temperature range.

The mechanism of the thermal degradation reactions is not known and is

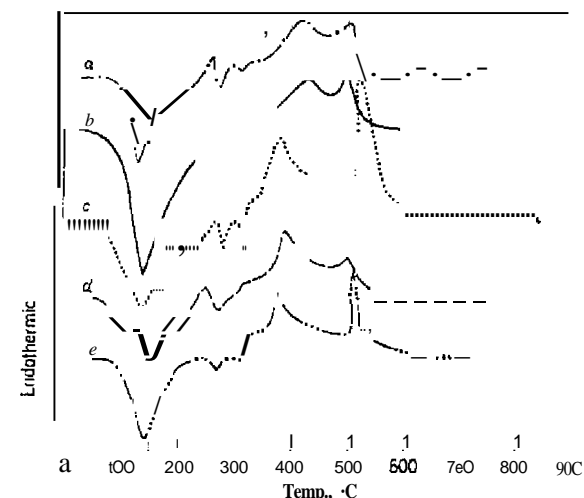


Figure 7.1. DTA curves of potato and corn starch. *a*, potato starch; *b*, potato starch, duplicate run; *c*, corn starch; *d*, methanol-extracted corn starch; *e*, ammonia-pregelatinized corn starch (143).

probably quite complicated. The DTA curves serve not merely to characterize or identify these carbohydrates, but will eventually lead to information, pertaining to the relationship between molecular composition and chemical properties.

Morita (144) also studied the DTA of several α - and β -linked polyglucosans, as well as rice starch. An interesting feature of this investigation was the study of the effect of moisture on the DTA curves obtained. This was illustrated by the study of rice starch stored in various types of atmospheres such as vacuum, 100% relative humidity water vapor, and so on. The presence of moisture altered the endothermic peak with a ΔT_{min} of 130°C but not the 275 or 310°C peaks. The results suggest that the original 130°C peak is not entirely due to the loss of residual moisture and that the dehydration process is not completely reversible.

The technique of DTA has been used to study the thermal degradation of balsam fir wood by Arseneau (134). Using air-dried wood and also various samples of wood that had been extracted with several reagents, Arseneau attributed the various DTA curve peaks to the reactions summarized in Table 7.5.

Blankenhorn et al. (219) studied aspen wood specimens that contained either white- or brown-rot fungal degradation using DSC and adiabatic

Table 7.5. Summary of DTA Curve Peaks for Air-dried Wood (134)

Peak (°C)	Compound
(1) Endotherm at 145	Alcohol-water extract
(2) Endotherm at 163	Alcohol-water extract
(3) Exotherm at 210	Unaccounted
(4) Exotherm at 265	Possibly acid lignin
(5) Exotherm at 285	Benzene-alcohol extract
(6) Exotherm at 300	Sum of benzene-alcohol extract and acid lignin
(7) Endotherm at 330	Cellulose
(8) Exotherm at 360	Same as (6)

oxygen bomb calorimetry, The DSC curve peaks of nondegraded and fungal-degraded wood differed from each other at all levels of mass-loss.

Edible fats and oils have been extensively studied by DSC. Information obtained is concerned with the crystallization from melt, heat of fusion, oxidative stability, characterization of glyceride groups, adulteration, solids content, and polymorphism of the fat or oil (220).

In the oxidative stability of an edible oil or fat (221, 222), the temperature at which oxidation begins is illustrated in Figure 7.2 (221). A regression line is drawn that follows the DSC curve before the start of oxidation. A second line is drawn as a tangent to the deflected curve through a measuring point which is at a defined value on the baseline. The intersection *b* of the two lines is the oxidation temperature. In addition, point *c* on the curve is useful. Some examples of dynamically measured oxidation temperatures are given in Table 7.6 (221).

Bihari-Varga (223) used DSC for the assay of glycosaminoglycans (GAG) and for the characterization of the stability of crosslinked proteins in intact human and animal tissues. By this method, age-related and pathological changes and repair reactions could be studied in various connective and vascular tissues. A typical DSC curve of human serum low-density lipoprotein (LDL) and of an aortic-GAG-LDL complex is given in Figure 7.3. A reversible endothermic transition took place in the LDL molecule at 33°C. Cholesterol esters within the LDL core existed as an isotropic solution above this temperature and in the form of the smectic liquid crystals below it. When LDL was converted to GAG-LDL complexes, the transition temperature was increased to 40°C.

Deckelbaum et al (224) found that this behavior requires the presence of a region rich in cholesterol ester within the lipoprotein.

The heats of denaturation of myoglobin, lysozyme, and chymotrypsin

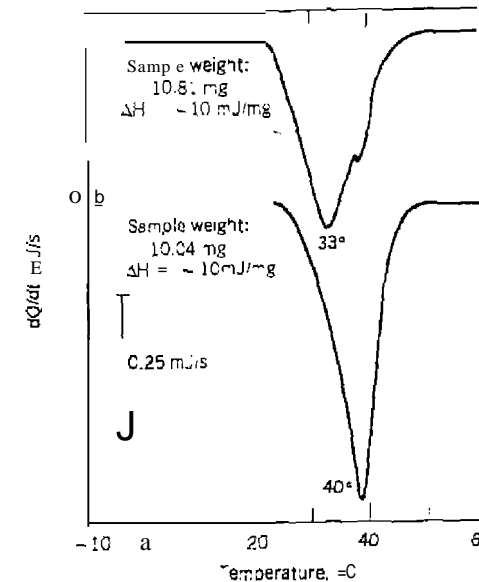


Figure 7.2. Schematic diagram of the determination of the oxidation temperature (221).

Table 7.6. Dynamically Measured Oxidation Temperatures in Oxygen of Some Edible Fats and Oils Between 90 and 190°C (221)

Product	Weight (mg)	Oxidation Temperature (°C)	Temperature at Threshold Value (mW/m²) (°C)
Sunflower oil	9.73		
Cooking oil (high temperature resistant)	10.86		
Used cooking oil	10.07		
Butter	11.46		162.6
Lard	10.70	138.1	155.0
Reproducibility*	9.11		0.7

*Standard deviation, determined on five sample runs of sunflower oil.

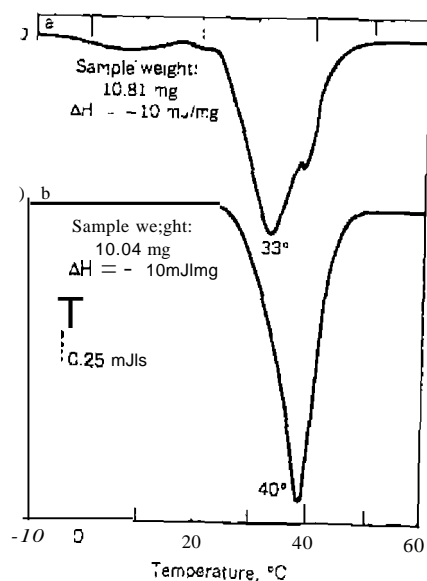


Figure 7.3. DSC curves of human serum LOL (a) and orotic-GAG-LOL complex (b) (223).

were determined by DSC by Cassel (225). Also, using high-resolution DSC, Cassel (226) measured the thermal transitions in dipalmitoyllecithin.

Bilhadens (227) recently reviewed the use of DSC in food research.

Raemy and Lambelet (228) used DSC to determine the specific heat of coffee and chocolate products and to study their thermal behavior above 20°C. Intensive exothermic reactions were evident when measurements were made in sealed cells. The thermal behavior of cereals above 20°C were also studied by DSC by Raemy and Loliger (229). The roasting and carbonization of the cereals above 170°C were attributed to their carbohydrate content.

Brennan reviewed the application of DSC and other TA techniques in the food, dairy, and agricultural industries (230) and in biology and biochemistry (231).

Joseph et al. (232) studied a series of *rae-1*, 2-diglycerides with substituted phenyl groups or a benzyl group on the 3-position by DSC. This technique showed that the compounds existed in different polymorphic forms. In all cases, solvent crystallized forms were different from those obtained by cooling the molten compound.

A method for determining the heat of transition of lipids was developed by Baker (233).

C. APPLICATIONS TO CATALYSTS

Locke and Rase (281) pointed out in 1960 that DTA is both a rapid and inexpensive method for screening potential catalysts, evaluating the effects of various pretreatments, and determining the poisoning tendencies of substances added to either the gas stream or catalyst. This speed and simplicity provided opportunities for extensive surveys that are otherwise inconvenient.

More recently, Gallagher et al. (282) and Dunn (283) reviewed the applications of DTA/DSC for the study of catalytic activity and other processes. The technique is used to optimize the performance of a catalyst system; to study the effects of variables such as catalyst composition, temperature, and gas flow rates on reaction rates; to prepare catalysts; to determine the most effective catalyst for a reaction; and to find the effects of poisoning on the catalytic activity (283).

rshii et al. (284) used DTA to study the effectiveness of a series of V_2O_5 /alkali salt catalysts on the oxidation of SO_2 to SO_3 .

The use of DTA to screen catalysts and to rank them in order of activity for a given reaction is illustrated in Figure 7.4. The catalytic activity is related to the area under the reaction exothermic peak; the larger the area is, the greater will be the activity.

The amount of metallic nickel in catalysts was determined by a DTA method by Macak and Malecha (84). Nickel produced by the reduction of nickel oxide was reoxidized by oxygen and the ΔT of the oxidation reaction was determined by the apparatus. The maximum value of ΔT between the reactor for catalytic reaction and that with inert SiO_2 packing was proportional to the amount of nickel in the catalyst sample. Accuracy of the method was about $\pm 4\%$.

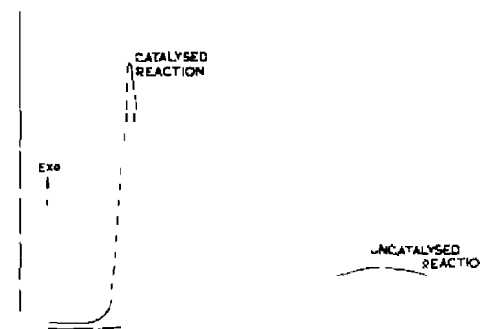


Figure 7.4. The addition of a catalyst to a reaction mixture (283).

Reaction of hydrogen, under pressure in a DSC cell, was used as a method for the determination of platinum or palladium in various catalysts (85). About 5 mg of catalyst are introduced into a DSC pan and the cell is pressurized to 150 psig with helium. The temperature is then increased to 75°C and the helium gas replaced with hydrogen at 200 psig. From the area of the DTA curve peak (versus time), the amount of platinum or palladium can be calculated.

Pressure DSC was used by Hassel (285) to evaluate catalyst activities. Hydrogen gas was added to a DSC cell containing the PdO/carbon catalyst, previously pressurized at 150 psig with helium. As the hydrogen replaced the helium gas, an exothermic reaction was observed, the peak area of which was proportional to the heat of reaction. The average heat of reaction, as obtained from six runs, was 19.5 ± 0.25 mcal/mg of catalyst.

DTA was used by Johnson and Gallagher (286) to detect the onset temperature and the extent of the catalytic oxidation of 1% hexane and to a lesser extent, 3% CO, in air. The onset or lowest temperature of reaction for the catalyst, $La_{0.5}Pb_{0.5}MnO_3$, for 1% hexane in air, is illustrated by curve (a) in Figure 7.5. This temperature, 140°C, was deemed too subjective for purposes of comparison so the ΔT maximum temperature of 365°C was chosen. However, the peak does not always occur at the same temperature for each material so the temperature at which a 2°C rise in ΔT was employed. This temperature is 306°C for curve (a). Using these criteria for catalytic activity, the effects of surface area, acid treatment, variation of M in $La_{0.7}M_{0.3}MnO_3$, and so on, were evaluated. The activity of some rare earth

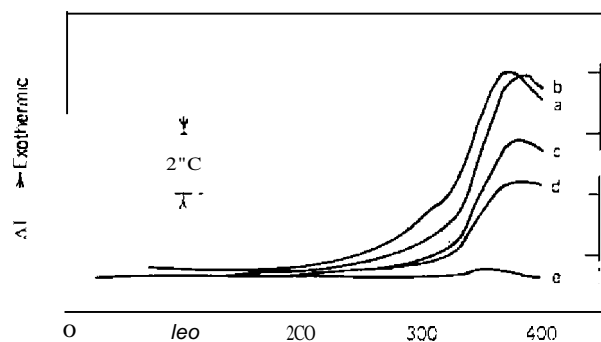


Figure 7.5 DTA curves of $La_{0.5}Pb_{0.5}MnO_3$ derived from coprecipitated hydroxides calcined at 540°C for 16 hours in air and diluted with varying amounts of alumina. Atmosphere: 1% hexane in air, a, 0% Al_2O_3 ; b, 50% Al_2O_3 ; c, 75% Al_2O_3 ; d, 87.5% Al_2O_3 ; e, 100% Al_2O_3 (286)

Table 7.7. Activity of Rare Earth Transition Metal Compounds Prepared from Cyanide Complexes (29) (Atmosphere is 1% hexane in air)

Compound	T of Calcination (C)	Heating (°C)
LaCoO ₃	500 [050]	277 350
PrCoO ₃	500 [050]	344 343
LaMnO ₃	900 1050	352 359
LaCrO ₃	1050	375

$\Delta T < 2^\circ C$.

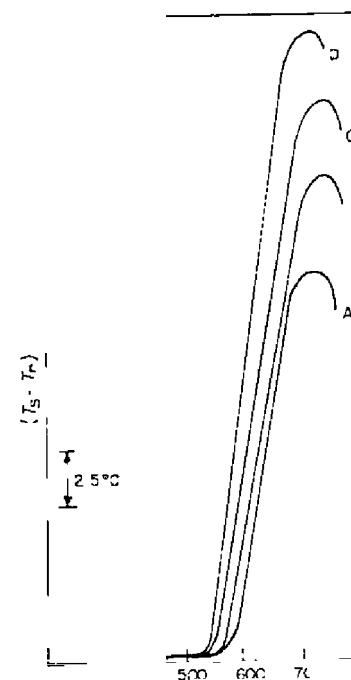
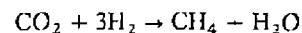


Figure 7.7. Methanation reaction on $NiMO_3$ (A) and $NiCrO_3$ (B, C, D) catalysts. Atmosphere: 1% hexane in air, A: 0% Al_2O_3 ; B: 20% Al_2O_3 ; C: 30% Al_2O_3 ; D: 40% Al_2O_3 (29)

transition metal compounds prepared from cyanide complexes is shown in Table 7.7. They all indicate some activity, however, LaCoO_3 exhibits greater hysteresis than do others.

Reddy et al. (291) used DTA to study the methanation reaction



using NiMoO_4 catalysts. This reaction, using one of the catalysts investigated, is shown in Figure 7.6. All the DTA curves showed that NiMoO_4 catalyzed the methanation reaction. Since the reaction is highly exothermic, $\Delta H_{500} = -218 \text{ kJ mol}^{-1}$, all the curve peaks are exothermic and very large in magnitude. The initial deviation from the baseline varies with change in composition (Hz:CO ratio), flow rate, and composition of the catalyst. Also, the curve peak maxima vary with the same parameter. They tend to be largest with the greatest flow rate but there are some exceptions. The initial curve deviations (T_i) and peak maxima temperatures (ΔT_m) are listed in Table 7.8. As shown by these data, the T_i values tend to decrease with an increase in flow rate for each Hz:CO ratio and catalyst composition. The same appears to be true in the case of ΔT_m values. A complicating factor with all the catalyst composition and Hz:CO ratios was the deposition of carbon. All the catalysts were

Table 7.8. NiMoO_4 Catalyst Methanation Reaction Temperatures (29J)

Flow Rate H ₂ :CO (ml min ⁻¹)	NiMoO ₄ Catalyst (°C)			
	No. 1120-135		No. 1140-110	
10:10	569 ^a	697 ^b		
20:20	541	706		
30:30	564	702		
40:40	508	654		
50:50	515	711		
10:20			560	716
20:40			550	737
30:60			532	735
40:80			528	709
20:10				532 685
40:20				518 692
60:30				508 687
80:40				504 687

^a T_i temperatures.

^b ΔT_m temperatures.

black in color at the termination of the DTA run, which necessitated the use of fresh catalyst for each run.

Catalytic oscillations were detected for various catalysts using DTA techniques by Gallagher and Johnson (287). The rapid response and high sensitivity of DTA make it suitable for the study of these oscillations which may be more difficult to detect by other techniques.

O. APPLICATIONS TO CLAYS AND MINERALS

One of the early fields of application of DTA was in the area of clays and minerals. These compounds, which gave birth to the theory and instrumentation of the technique, have been widely investigated. DTA was used to identify clays from various locations throughout the world and was widely used to determine the free quartz content of minerals. Numerous other applications were made of DTA; DSC was little used due to the low-temperature capability of the latter. Most of the interesting thermal behavior of clays and minerals occur above 500°C, and frequently above 1000°C. The applications of DTA to these materials is discussed by Mackenzie et al. (62, 186-188) and many others.

Using the DTA technique for quality control purposes, Gam and Flaschen (113) studied the thermal decomposition of different samples of magnesium carbonate and talc. The curves for the magnesium carbonate samples showed distinct differences due to their different thermal histories. Each of the talc curves exhibited a strong exothermic peak, starting at about 850°C. The magnitude of the reaction was about the same in each case, but differences in impurities caused pronounced differences in the curves. The Montana and Sierramic talcs gave a small endothermic peak at about 570°C, while the latter talc gave a pronounced endothermic peak at about 700°C.

The determination of goethite ($\alpha\text{-FeO}\cdot\text{OH}$) and gibbsite $[\text{Al}(\text{OH})_3]$ by themselves, and in mixtures, has been carried out by a DTA method by Lodding and Hammell (114). If goethite is heated in the controlled atmosphere DTA apparatus in a reducing atmosphere (hydrogen), it dehydrates below 300°C and the iron(III) ion present is immediately reduced to amorphous Fe_3O_4 which recrystallizes to magnetite between 300 and 360°C. If the hydrogen atmosphere is now replaced by nitrogen after reaching 400°C, and then by air, an exothermic peak is formed due to the oxidation of magnetite to maghemite, $\gamma\text{-Fe}_2\text{O}_3$. A second exothermic peak, due to the conversion of $\gamma\text{-Fe}_2\text{O}_3$ to $\alpha\text{-Fe}_2\text{O}_3$, occurs at 775-836°C. This peak is usually a doublet and the integrated area under it is proportional to the amount of newly formed hematite, which is, therefore, equal to the amount of hydrated iron oxide present in the original sample. The amount of gibbsite can then be

determined by the difference from the area under the dehydration peak. The hematite or magnetite present in the sample was said to have a negligible influence on the area of the conversion peaks.

The calibration curves of peak area to amounts of goethite and gibbsite present in the mixtures are given in figure 7.7. A similar curve for the $\gamma \rightarrow \alpha$ -Fe₂O₃ conversion was also presented by Liddard and Hammell (114).

Berg and Rassonskaya (115) proposed the use of a high-heating-rate DTA apparatus for rapid analysis of minerals and clays. The high heating rate, 80-100°C/min, was obtained by placing the sample holder into a previously heated furnace, preferably 300°C higher than the final sample temperature desired. It was claimed that the peak temperatures at this high heating rate for melting and boiling transitions were the same as those obtained at the 3-6°C/min. heating rate. Judging from previous studies, it is difficult to see how this could be true. Similar results were found for the peaks resulting from the dissociation of metal carbonates and for solid-state crystallizing phase transition. The advantages claimed for this technique are: (1) speed of investigation, 3-10 min; (2) small quantities of sample required, 20-100 mg; (3) simple regulation of heating rate; and (4) cheapness of analysis.

Using sealed glass or fused silica tubes for sample holders, Bollin et al. (116) followed the reaction of two or more solid substances by the technique of DTA. The procedure they used, which was later elaborated on by Bollin and Kerr (117), was called pyrosynthesis.

The technique of DTA can be used to determine the amount of uncalcined gypsum (CaSO₄·2H₂O) in plaster of Paris (CaSO₄·0.5H₂O). From the curve

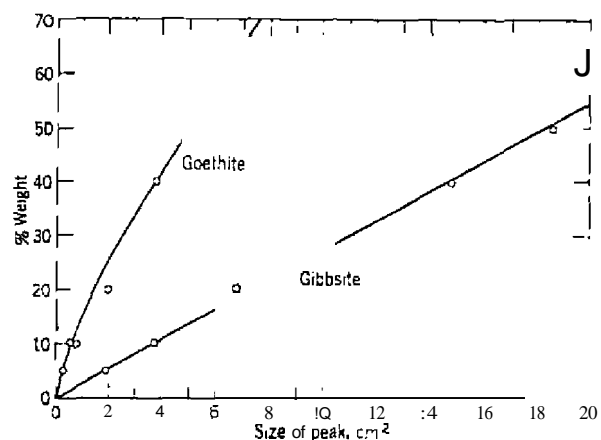
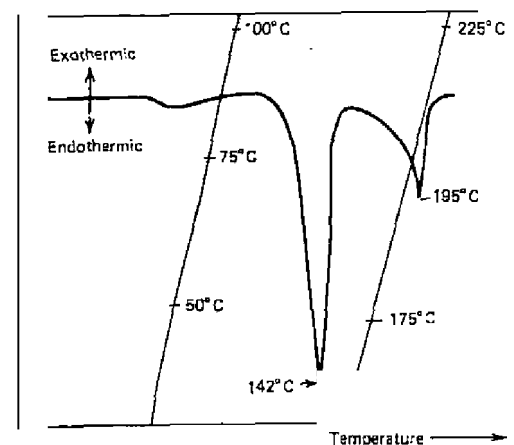
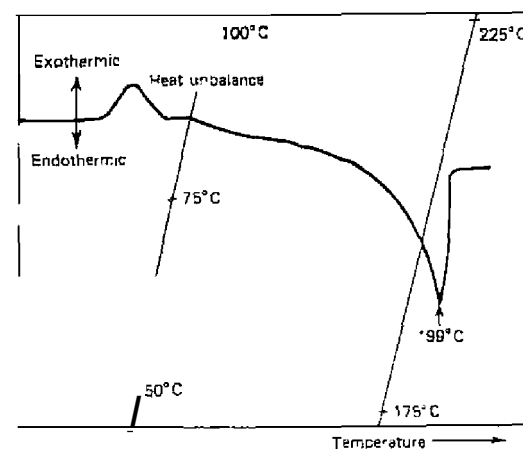


Figure 7.7. Calibration curves of peak areas for dehydration of gibbsite and goethite (111).

for the dehydration of gypsum in figure 7.8a, it is seen that the peak at ΔT_{\min} of 142°C is due to the dehydration of the first 1.5 moles of water per mole of salt. The second endothermic peak, at ΔT_{\min} of 198°C, is due to the evolution of the remainder of the water. Thus, the presence of gypsum in plaster of Paris could be determined from the DTA curve in figure 7.8b if a



(a)



(b)

Figure 7.8. (a) DTA curve of gypsum. (b) DTA curve of plaster of Paris (116).

peak at about 142°C appeared. The peak area would be proportional to the amount of gypsum present in the sample (106).

Gill (50) determined the gypsum content in a plaster of Paris-gypsum mixture from the ΔH of the 142°C endothermic peak. The relationship between the ΔH (meal/mg) and weight percent of gypsum was a straight line.

Dunn et al. (195) described a DSC analytical method for the determination of set plaster for gypsum and lime, using 1–2 mg size samples. A plot of the area of the gypsum dehydration endothermic peak is shown in Figure 7.9 versus the mass of $\text{CaSO}_4 \cdot 2\text{H}_2\text{O}$ in standard samples. The coefficient of variation for gypsum was 3.65%, whereas that for lime was 5.9%. The results for both gypsum and lime indicate that the DSC method can provide a rapid and accurate method of analysis for samples as small as 0.5 mg.

Ramachandran and Polomark (196) developed a DSC-DTA combination

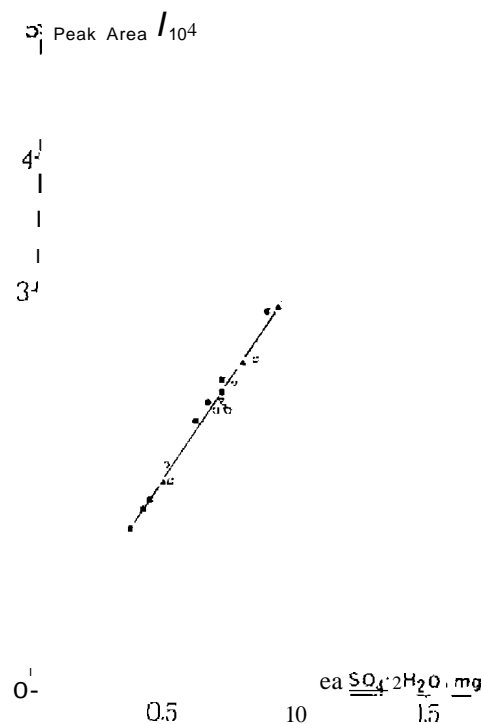


Figure 7.9. Calibration curve for gypsum in standard samples (195).

technique to estimate the concentration of $\text{CaSO}_4 \cdot 2\text{H}_2\text{O}$, $\text{Mg}(\text{OH})_2$, $\text{Ca}(\text{OH})_2$, CaCO_3 , and MgO in white coat plasters.

The quantitative analysis of the clay minerals, kaolinite, gibbsite, and goethite was described by Davis and Holbridge (109). The heats of dehydroxylation (dehydration) of two kinds of alunites were determined by DTA by Cohen Arazi and Krenkel (110). Reddick (111) determined the ΔH of decomposition for calcite, magnesite, rhodochrosite, and siderite as well as for ankerite. The relationship between the magnesite peak temperature and the magnesite content for various mixtures was reported by Warner and Mackenzie (112). The lowering of the peak temperature on dilution is virtually identical whether the diluent of the magnesite is alumina or other carbonates.

Hectorite was investigated by DTA by Eames (189) using furnace atmospheres of dynamic nitrogen, air, carbon dioxide, and static air. Hectorite specimens found in California are always associated with large amounts of calcite and, in some cases, varying amounts of dolomite. Thus, most published DTA curves reflect not only the thermal behavior of hectorite but also that of the carbonate contaminant. A typical DTA curve of hectorite is shown in Figure 7.10. An endothermic peak at ΔT_{min} of 121°C is caused by the inter/ave:

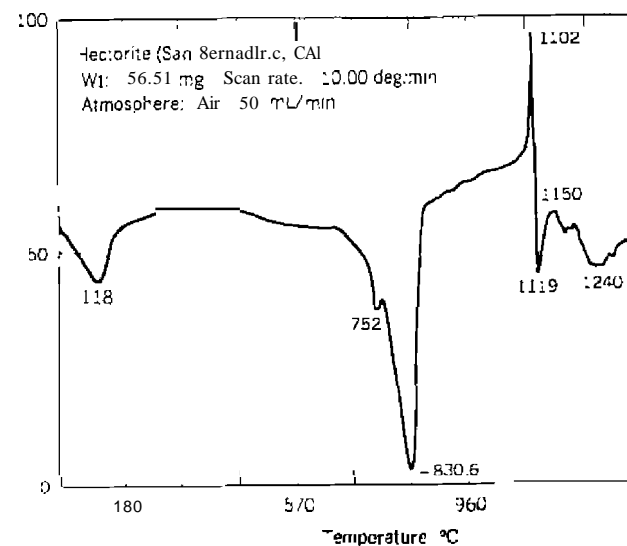


Figure 7.10. DTA curve of hectorite in a dynamic air atmosphere.

water loss, whereas the 829°C peak and 752°C shoulder peak are due to the dehydroxylation/carbonate decomposition reactions. A narrow exothermic peak at 1098°C is followed by endothermic peaks at 1119 and 1240°C. The latter are probably due to the formation of clinoptilolite.

One of the first clays to be studied by DTA was kaolinite, and it still is being investigated by modern OTA and other TA techniques. A typical DTA curve of kaolinite, as determined by Earnest (190), is shown in Figure 7.11. In general, the DTA curve peaks are due to the following processes:

1. *Desorption of Water-Ambient to 110°C-Endothermic-Minor.* Seldom observed by DTA except in highly disordered species. Easily observed by TG and DTG.
2. *Dehydroxylation of Crystal Lattice-450-700°C Endothermic-Major.* The main endothermic peak. Observed in all members of the group except allophane. Peak temperature, symmetry, and magnitude are diagnostic tools.
3. *Structural Organization-900-1000°C-Exothermic-Major.*
4. *Structural Organization and Rearrangement-1150°C up-Exothermic-Minor (Variable).* This represents the formation of mullite and cristobalite. The intensity varies with impurities or additives as well as particle size.

The DTA curve does not have an endothermic peak for the loss of desorbed water which, in this case, amounts to 0.2% by mass. Many studies have been concerned with the effect of particle size on the DTA curve peaks.

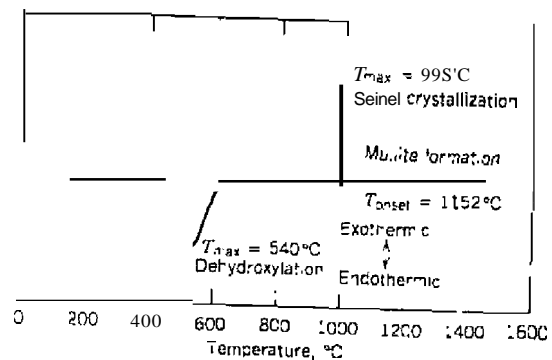


Figure 7.11. Typical DTA curve of kaolinite (190).

In general, the smaller the particle size is, the lower will be the ΔT_{min} for a given peak, and the narrower will be the peak.

Dunn (191) described the application of OTA to clays and minerals. Application of the Derivatograph to rock analysis, clays, and minerals has been described by Selmezi (192) and Paulik and Paulik (193).

The oxidation of natural pentlandite, (FeNi)₉SS, has been studied by OTA and other TA techniques by Dunn and Kelly (194). DTA curves of two samples of this mineral, one heated in oxygen and the other in air, are illustrated in Figure 7.12. The exothermic peak at 790°C and the endothermic peak at 830°C appear to be independent of oxygen partial pressure, but the exothermic peaks at 575 and 725°C both changed in an air atmosphere. The various reactions that take place in this mineral, as determined by DTA, TG, MS, and XRD are summarized in Table 7.9. Because of the complexity of this system, some of the reaction assignments must be considered tentative.

Crystalline quartz, when heated, undergoes a *solid* → *solid*₁ phase transition ($\alpha \rightarrow \beta$ quartz) at about 573°C. Keith and Tuttle (107) found that in a study of 250 quartz samples, the inversion temperature range was 38°C in natural quartz, although most of the samples were within 2.5 of 573°C. This

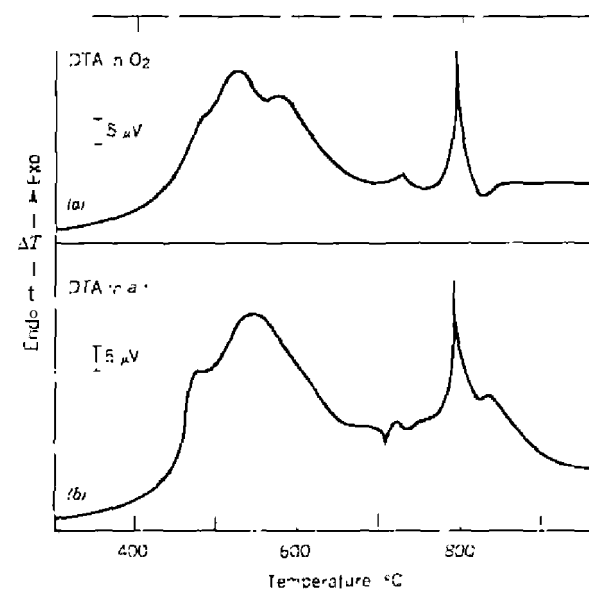


Figure 7.12. DTA curves of pentlandite (194).

Table 7.9. Oxidative Reactions of Pentlandite, (FeNi)₉S₈ (194)

Temperature (°C)	Reaction
<460	Pn1 → Pn2 + NiS + FeS
460-640	FeS + 2O ₂ → FeSO ₄
460-715	NiS + 2O ₂ → NiSO ₄
520 ^a	2FeS + 3.5O ₂ → Fe ₂ O ₃ + 5SO ₂
575 ^b	Pn2 + O ₂ → Ni ₂ FeO ₄ + SO ₂ + NiO + Fe ₂ O ₃
640-760	2FeSO ₄ → Fe ₂ O ₃ + (2SO ₂ + 0.5O ₂)
700-740	Pn1 → Ni _{3-x} S ₂ - Pn2 Pn2 + O ₂ → Ni ₂ FeO ₄ + SO ₂ NiS + 1.5O ₂ → NiO + SO ₂
775-805	Ni _{3-x} S ₂ $\xrightarrow{O_2}$ NiO + (5O ₂ + 0.5O ₂)
>800	NiSO ₄ → NiO + (SO ₂ + 0.5O ₂)

^aIn these cases the reaction temperature range is difficult to determine from the curves, and the DTA peak temperature alone is quoted.

inversion temperature was attributed to solid solution of varying amounts of other ions in the quartz. Since the amount of solid solution is influenced by the temperature during formation, the inversion temperature can be used as a criterion of formation temperature for samples crystallized under similar chemical environments.

Rouse and Jepsen (288) used DTA to determine the quartz contents (4 wt % maximum) of four clay materials and tourmaline. The sample was first heated to 700°C, which dehydroxylated the kaolinite. A DTA Curve was then recorded at a cooling rate of 10°C/min during which the $\beta \rightarrow \alpha$ quartz transition was observed at 573°C. Some eight different methods were used to determine the peak area and/or peak height of the quartz transition; the peak height method, illustrated in Figure 7.13, was finally adopted. The peak height, *h*, was proportional to the amount of quartz, *x*₀, in the mixture by use of the equation

$$h = B[q(1 - x_0) + x_0] \quad (7.11)$$

where *q* is a known weight of quartz added to the sample and *B* is a constant. Results of the determination are shown in Table 7.10. The DTA method is time-consuming but is superior to the X-ray and chemical analysis methods and gives the best experimental precision. Typically, the relative standard error is about 10% on an *x*₀ value of 0.04.

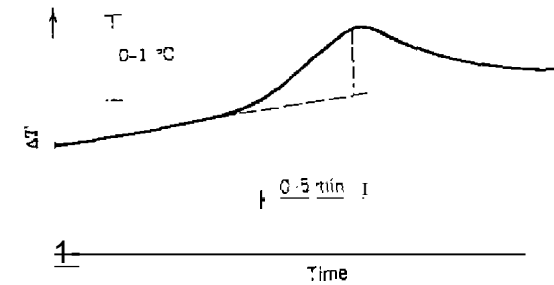


Figure 7.13. DTA cooling curve showing how peak height is determined (288).

Table 7.10. Determination of Quartz Content in Clays by DTA (288)

Sample	DTA		Chemical Analysis	
	<i>x</i> ₀	<i>x</i> ₀	<i>x</i> ₀	<i>x</i> ₀
A	2.15 ± 0.05	-0.002 ± 0.003	0.0094, 0.0092, 0.0090, 0.0084	
B	2.26 ± 0.07	0.003 ± 0.002	0.024	
C	2.03 ± 0.07	0.035 ± 0.003	0.052, 0.050, 0.050, 0.050	
D	1.98 ± 0.05	0.001 ± 0.002	0.0036, 0.0024, 0.0020	
E	2.34 ± 0.04	0.037 ± 0.002	0.234, 0.177, 0.122	

E. APPLICATIONS TO FUELS

Oil shales were characterized using DSC by Rajeshwar et al. (235); a typical DSC curve of a Green River oil shale is shown in Figure 7.14. The endothermic peak in the 250–450°C temperature range corresponds to the thermal decomposition of oil shale kerogen. The area under this peak, the enthalpy value, was found to be directly proportional to the amount of kerogen in the shale in the absence of minerals that are thermally active in this temperature range. A least-squares fit of the ΔH obtained experimentally follows the equation

$$\Delta H = -0.90 + 0.25 (Oy) \quad (7.2)$$

where *Oy* is the oil yield of the shales. A precision of oil yield of ± 8 L metric ton is estimated.

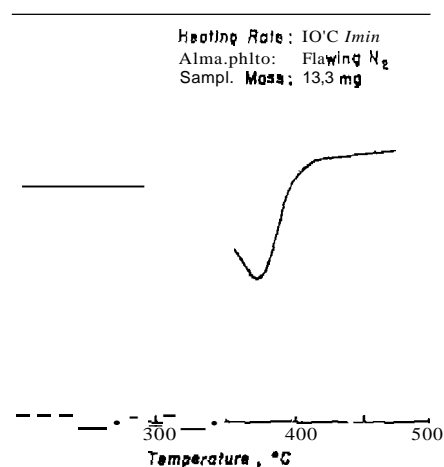


Figure 7.14. Typical DSC curve of a Green River oil shale, of yield of 316 L/metric ton. Open Al sample container (235).

Also, using DSC, the specific heats of Colorado oil shales were determined (237).

The heat of combustion of an oil shale was determined by DSC by Cassel *et al.* (236). It was necessary to grind the sample to 100 mesh prior to pyrolysis. The area under the curve gave the calorific content directly.

Yang *et al.* (289) used DTA to characterize the reactivities of three carbonaceous materials toward oxygen and carbon dioxide. A pseudo-third-order reaction can give a bifurcated peak in the DTA curve. The idea of the existence of two kinds of carbonaceous materials based on a bifurcated peak, as has often appeared in the literature, should be asserted with caution.

Noel and Corbett (90) applied DSC to the study of glass and melting transitions in asphalts. The T_g values obtained agreed well with those previously determined by dilatometry. Heats of fusion of the asphalt waxes ranged from 26 to 32 cal/g.

Pitches were characterized by DSC and TMA by Barr and Lewis (238). The DSC curves of a typical petroleum pitch, which had a Mettler softening point of 152°C, are illustrated in Figure 7.15. An endothermic peak in the vicinity of the expected T_g point was found in the initial DSC curve. A second run of the sample, after cooling it rapidly from 240 to 10°C, showed a well-defined T_g with an onset temperature of 83°C. The endothermic peak was no longer visible in the curve. Glass transition temperatures and softening

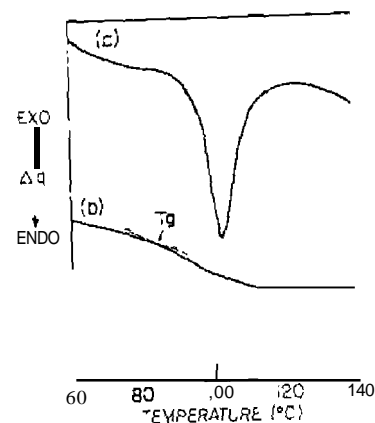


Figure 7.15. OSC curve for isotropic petroleum pitch, (a) first heating; (b) second heating on quenched sample (238).

points for isotropic pitches are listed in Table 7.11. For each of these pitches, changes in the softening point are paralleled by changes in the T_g temperature. The T_g ranged from 18 to 43°C for the pitches studied.

DTA studies on coal and related substances have been carried out by a large number of investigators, including Breger and Whitehead (37) and Camel and Smothers (1).

Breger and Whitehead (37), using a vacuum DTA apparatus, studied the

Table 7.11. Softening Points and Glass Transitions (DSC) for Isotropic Pitches (238)

Pitch	Mettler Softening Point (T_s) (°C)	Glass Transition (T_g) by DSC (°C)	
		Onset	Span
Coal tar	110	34	38
	126	38	28
	151	60	43
	173	83	30
Petroleum	122	50	18
	130	55	20
	152	83	20
	178	102	21
	188	108	21
Acenaphthylene	202	103	29
	234	134	29

thermal properties of cellulose, wood, lignite, and various coals. It was found that the low-temperature peaks for lignin disappeared or were masked in peat and then reappeared in the lignites. The decomposition peaks for lignin were suppressed in bituminous coals and were absent in the curves for anthracites.

Gamel and Smothers [1] related the areas under the decomposition peaks to the concentration of a Utah Mine coal in a coal-alumina mixture. A linear area versus concentration curve was obtained for 0-12.0% coal mixtures. They also found that the area under the curve peak was directly proportional to the BTU/lb values for the coal. This relationship is illustrated in Table 7.11.

Rosenvold et al. (239) used DSC to study the thermal decomposition of 21 bituminous coal samples from Ohio. Representative DSC curves of the coal samples are illustrated in Figure 7.16. Three regions of endothermic reactions are observed (1) a dehydration peak in the range 25-150°C; (2) a second very broad endothermic peak that spans the range from 150°C to yield a noticeable peak between 400 and 500°C; and (3) a narrower endothermic peak at temperatures $\geq 550^\circ\text{C}$. The broad reaction from 150-500°C probably corresponds to pyrolytic fragmentation of the carbon skeletal structure in coal with the third endothermic peak due to cracking reactions of the products evolved in the pyrolysis process.

The net area of the endothermic peak in the 150-500°C temperature range should be directly related to the volatile matter content of the coal. However, the correlation is not linear with widely scattered data points.

Fyans (240) also characterized coal samples by TG and DSC and compared the results with standard ASTM methods. As shown in Table 7.13, the calorific contents obtained by DSC compared favorably with the ASTM values with agreement within $\pm 3\%$.

Hassel (241) used pressure DSC (oxygen at 500 psig) to determine the heat of combustion of selected coal samples. The results were in good agreement with adiabatic bomb calorimeter results.

Table 7.12. Heating Values of Selected Arkansas Coals as Measured DTA and Peroxide Bomb Methods in BTU/lb (t)

Sample	Area Under Curve, (ir.,l)	Btu/lb Coal
Paris mine	0.345	13,347
Utah mine	0.460	14,476
Jerome mine	0.415	13,994
Quality excelsior mine	0.470	14,531

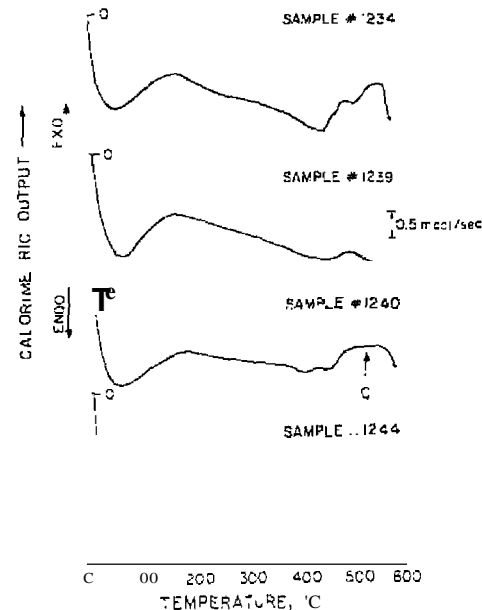


Figure 7.16. Representative DSC curves of selected Ohio coal samples. Open C

Table 7.13. Calorific Contents Obtained by DSC and the ASTM Method (241)

ASTM Value ^a	DSC Values ^a	
	Sample #217	
	20' min	40' min
	12,586	13,217
	12,924	
	13,244	
	Sample #417	
	20' min ⁻¹	
12,927	12,649	13,066
	Sample #917	
	20' min	40' min
12,518	12,350	12,713

^aAll quantities in BTU/lb

Differential thermal analysis has been applied to the degradation of hydrocarbon liquids (50-52) and has also been proposed for the quality control of grease (53, 54). Noël (55) showed that OSC could be used to characterize petroleum products and that the results could be correlated with some ASTM tests. The advantages of DSC over previous tests to characterize petroleum products are as follows:

1. Information is obtained quickly and reproducibly.
2. Very small samples are required (milligram quantities versus quart samples).
3. The equipment has multiple uses rather than the ability to do only one test.
4. The information is fundamental and low on empiricism; thus, it has research value as well as use for control and troubleshooting.

More recently, Noël and Cranton (242) reviewed the application of DSC and other TA techniques to petroleum research. The DSC applications are listed in Table 7.14.

Walker and Tsang (243) used pressure DSC to characterize lubricating oils, and virgin and re-refined lubricating base stocks. At pressures of 0.7-3.4 MPa (100-500 psig) air or oxygen and temperature near 200°C, degradation occurs with liberation of heat.

The oxidation of an automotive brake fluid and a motor oil was studied by high-pressure NSC (38). At an air pressure of 600 psig, indicated, the relative oxidative stability of each of the types of materials was determined.

Blaine (244) also used pressure DSC to study the oxidative stability of lubricating oils and greases.

Moynihan et al. (245) studied the melting and freezing behavior of jet and diesel fuels in the temperature range -60 to -20°C by DSC. None of the fuel samples failed to crystallize on rapid cooling on the DSC, and the degree of supercooling was quite small. Freezing points, as determined by DSC, tended to be several degrees lower than those measured by ASTM test D 3117-72.

The thermal degradation of cellulose in air was studied by Doilimore and Hoath (246) using DTA. Although the combustion of cellulose is a highly complex group of reactions, it is generally agreed that the degradation scheme in Figure 7.17 applies. In the degradation reaction, oxygen is shown as having an effect of the final products but not on the overall reactions. Varying the atmosphere may cause a different pathway to be favored, but the general scheme remains the same. Other factors that can affect the reaction pathway are temperature, period of heating (heating rate), and the physical and

Table 7.14. Applications of OSC to Petroleum Research (242)

A. Types of Studies

Melting and boiling points
 RotmOn transitions in hydrocarbons
 Heats of fusion, ΔH_f
 Purity determination using van't Hoff equation
 Homogeneous oxidation of hydrocarbons
 Heats of vaporization, ΔH_v
 Glass transitions of hydrocarbons
 Oxidation reactions
 Thermal degradation
 Adduct and complex formation
 Heats of mixing
 Heats of sublimation
 Critical temperatures

B. Materials Studied

Hydrocarbons of all types
 Catalysts
 Asphalts
 Petroleum waxes
 Lubricating oils
 Greases
 Soaps
 Fuels
 Crude oil

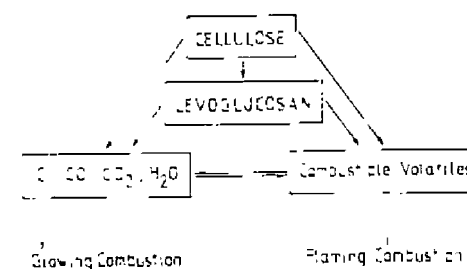


Figure 7.17. Reaction pathways for the degradation of cellulose (246)

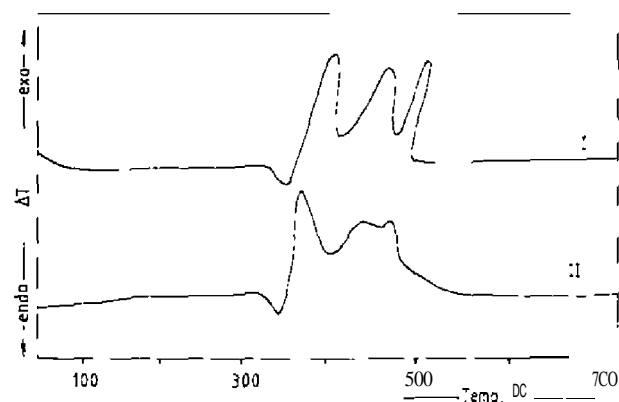


Figure 7.18. DTA curves of cellulose. (I) T axis is sample temperature; (II) T axis is reference temperature (246).

chemical properties of the cellulose. DTA curves of pure cellulose are given in Figure 7.18 (246). The curve consists of an endothermic peak at 349°C followed by three exothermic peaks at 404, 465, and 507°C. The DTA curve for a cellulose sample diluted with alumina was more difficult to interpret; it consisted of a single peak with two shoulder peaks. The three exothermic curve peaks in Figure 7.18 are thought to result from pyrolytic and oxidation processes. In a nitrogen atmosphere, there is an endothermic peak at 350°C followed by an exothermic shift of the baseline.

The DTA of cellulose, cellulose nitrate, pentaerythritol, pentaerythryl trinitrate, and other compounds of this type has been studied by Pakulak and Leonard (135). When a thermistorized DTA apparatus was used, the upper temperature limit of the instrument was only about 200°C; hence, cellulose and cellulose acetate did not give any peaks, while cellulose nitrate gave an exothermic peak with a ΔT_{max} of 180°C. Similar results were noted for the pentaerythritol series.

F. APPLICATIONS TO INORGANIC MATERIALS

The applications of DTA and DSC to inorganic compounds are similar to those discussed for organic compounds. Endothermic and exothermic peaks are caused by phase transitions (melting, boiling, polymorphic changes), dehydration, dissociation, isomerization, oxidation-reduction reactions, and so on. These applications are summarized in Figure 7.19. A

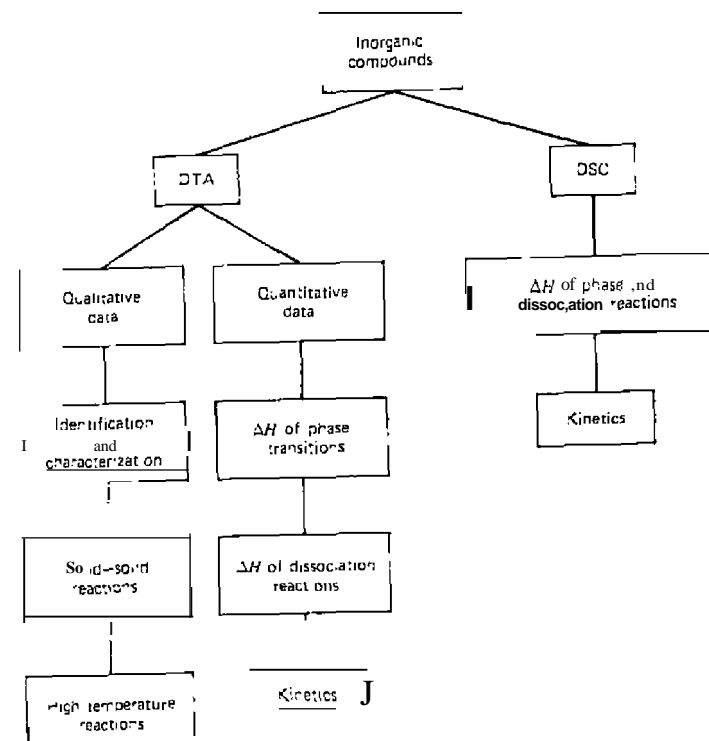


Figure 7.19. Some applications of DTA and DSC to inorganic compounds.

large number of DTA applications to inorganic compounds are reviewed by Mackenzie et al. (62) and DoUimore and Heal (185).

The effect of potassium chlorate impurity on the thermal stability of ammonium perchlorate has been studied by PencNam et al. (98). The effect of this impurity on the DTA curve of ammonium perchlorate is illustrated in Figure 7.20.

The curves clearly illustrate the presence of an increasingly large exothermic reaction after the 244°C lattice transition of the ammonium perchlorate. In the 0.1% KClO_3 region of impurity, the heat evolved after the lattice transition was great enough to initiate complete thermal decomposition of the sample. This represents an effective ISO lowering of the thermal decomposition temperature of the pure material, which normally decomposes

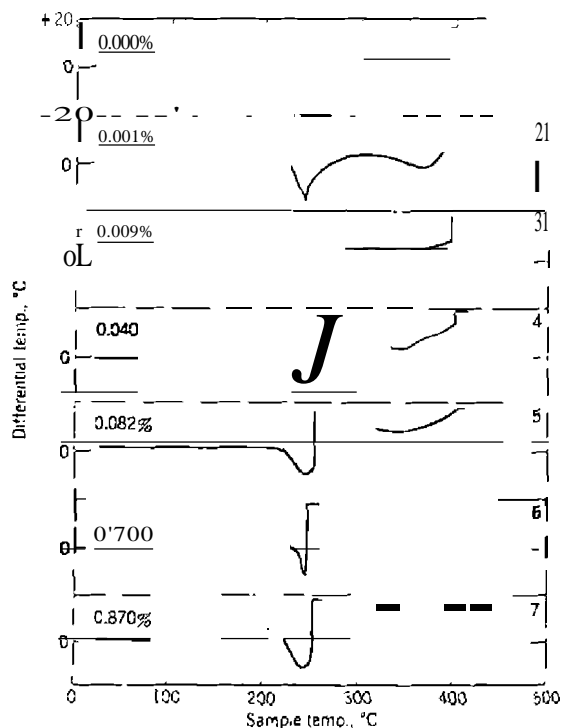


Figure 7.20 DTA curves of NH_4ClO_4 containing various amounts of KClO_4 (98).

at about 400°C. The DTA technique could be used to detect the approximate amount of impurity in the ammonium perchlorate.

furuichi et al. (64) studied the effect of additives on salts of halogen oxoacids, metal oxalates, and other compounds, using DTA and other TA techniques. The thermochemical changes to these compounds may be due to: (1) a chemical reaction occurring between reactant and additive to form intermediate stable compounds or (2) the catalytic action of additives accelerating or decelerating the reaction. DTA is an especially useful technique for this type of study because it gives extensive information on the reaction covering a wide temperature range in a single experiment.

DTA curves of KClO_4 and KClO_3 , in the pure state and also with various additives, are shown in Figure 7.21. The endothermic peak at 310°C (curves 11-3) is due to crystalline phase transitions of KClO_4 . Addition of $\alpha\text{-Al}_2\text{O}_3$

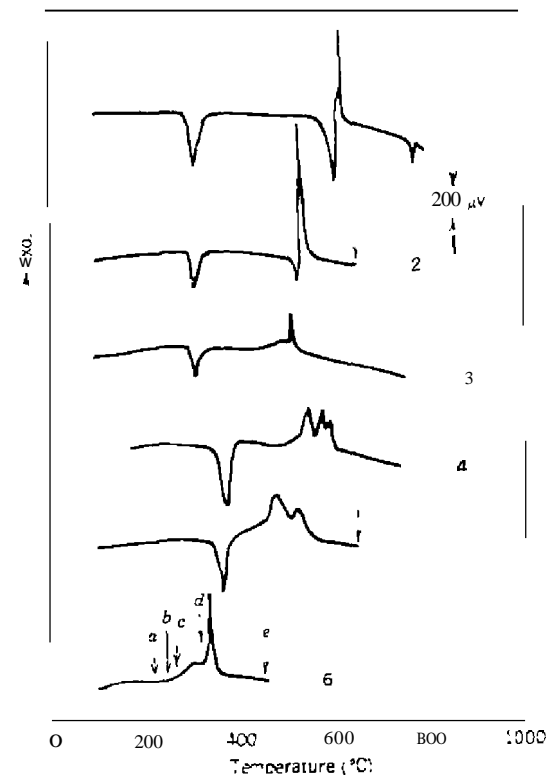


Figure 7.21. DTA curves of KClO_4 and KClO_3 systems in static air (164). 1. KClO_4 ; 2. $\text{KClO}_4 + \alpha\text{-Al}_2\text{O}_3$; 3. $\text{KClO}_4 + \alpha\text{-Fe}_2\text{O}_3$; 4. KClO_3 ; 5. $\text{KClO}_3 + \alpha\text{-Al}_2\text{O}_3$; 6. $\text{KClO}_3 + \alpha\text{-Fe}_2\text{O}_3$. Heating rate = 5°C min^{-1} ; mixing ratio "1 sample to addit." = 1:1 by weight. Arrows on the curves show temperatures at which the X-ray samples were taken.

and $\alpha\text{-Fe}_2\text{O}_3$ additives had no effect on these processes. KClO_4 showed two endothermic peaks at 605 and 780°C respectively, and a narrow exothermic peak at 615°C. The 605 and 780°C peaks are due to the fusion of KClO_4 and KCl , respectively, whereas the 615°C peak is caused by the decomposition of KClO_4 to KCl in the fused state. Addition of $\alpha\text{-Al}_2\text{O}_3$ lowers the peak temperatures of the 605 and 780°C peaks to 525 and 535°C, respectively. Although $\alpha\text{-Fe}_2\text{O}_3$ accelerates the decomposition of KClO_4 , no chemical reaction occurred between them.

For KClO_3 (curve 4), the endothermic peak at 375°C corresponds to the

melting or this compound, whereas the broad exothermic peak between 500° and 600°C is due to the decomposition of the molten salt. With the addition of α -Al₂O₃, the peak temperatures are shifted from 375° to 365° for the fusion reaction and from 500 to 600°C to 450° to 550°C for the exothermic reaction. In the case of the α -Fe₂O₃ additive, the fusion peak disappears and two exothermic peaks appear in the 250-350°C temperature range. Similar behavior was noted for the other reactions.

Rajeshwar et al. (180) used DSC to determine the enthalpy of crystal structure transformations of MClO₄ salts, where M = Na, K, Rb, Cs, and NH₄. As illustrated in Table 7.15, inconsistencies in the literature data are striking, especially with M = Na, K, Rb, and Cs. Most of the earlier studies used DTA techniques to determine the enthalpy changes. However, the literature values for NH₄ClO₄ are in good agreement with the author's results.

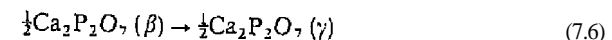
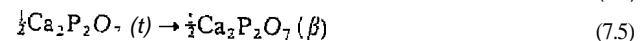
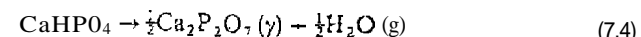
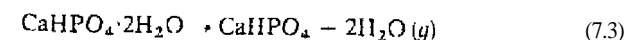
Erdey and Paulik (100), in a simultaneous DTA-TG study, investigated the thermal decomposition of barium, strontium, manganese(VI), calcium, magnesium, and zinc oxalates in air and nitrogen atmospheres. It was found that the evolved carbon dioxide formed in the reaction played an important part in that it may inhibit the progress of the reaction and shift the peak temperatures to higher values.

The changes in enthalpy which occur when CaHPO₄·2H₂O is heated up to 1300°C were determined by a DTA method by Mesmer and Frani (73). An

Table 7.15. Heats of Transformation of MClO₄ Compounds by DSC (180)

Compound	Present Study	Literature		
	Heats of Transformation (cal g ⁻¹)	Heats of Transformation (cal g ⁻¹)	Measurement Technique	Reference
NaClO ₄	3.88 ± 0.04	6.6	DTA	32
KClO ₄	24.49 ± 1.10	4.9 ± 1.6	DTA	33
		16.80	DTA	32
RbClO ₄	20.87 ± 0.05	23.75	DTA	33
		36.9	DTA	32
CsClO ₄	10.16 ± 0.25	16.22 ± 0.54	DTA	33
		8.61 ± 0.43	DTA	33
NH ₄ ClO ₄	19.34 ± 0.10	26.1	DTA	32
		19.58 ± 1.70	DTA	33
		19.58	DTA	34
		20.3 ± 0.6	OSC	35

internal standard of CaCO₃ was used to calculate the enthalpy changes which occurred during the reaction



Results of these enthalpy changes are given in Table 7.16.

Heats of transition of a number of inorganic compounds were determined using several new methods of quantitative DTA (74, 75). Results for one of the methods are summarized in Table 7.17 (75). It is interesting to note that a value of 25.2 cal/g was obtained for the melting transition in KNO₃, which agrees fairly well with the 27.7 cal/g reported previously (76). The value obtained with the Du Pont DSC cell was 22.7 cal/g, which is in agreement with another literature value, 22.7 cal/g (77).

An investigation was made by Barral and Rogers (78) to determine whether the precision of DTA measurements could be increased by using a reference compound as a thermochemical standard. The reference standard, in this case, was silver iodide. The ΔH of transition found was 216 ± 20 cal which is compared with a literature value of 205 ± 30 cal. Using an inert substance as the reference, a ΔH of 200 ± 90 cal was obtained. Thus, there was some improvement in the calorimetric accuracy obtained using this method.

Wendlandt (79) found that by using the sealed-tube technique, heats of dehydration of metal salt hydrates could be obtained which would be impossible using conventional open tubes or crucibles. This approach is illustrated by the DTA curves for CuSO₄·5H₂O. In the open-tube curve, the peaks are

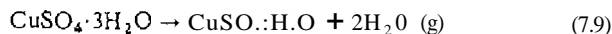
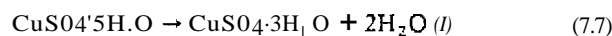
Table 7.16. Enthalpy Changes for CaHPO₄·SH₂O (73)

Reaction	Heating Rate	1/1 Cl	ΔH_x (kcal/mole)
	(C m ⁻¹)		
1	4	135	21.3, 20.9
2	4	430	6.9, 7.5
3	10	850	-0.17, -0.23
4	10	1220	0.85, 0.68

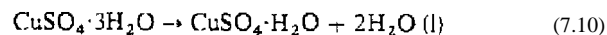
Table 7.17. Heats Of Transition Obtained by Ozawa et al. (75)

Sample	Present Work		Literature	
	Temp. (°C)	ΔH (cal/g)	Temp. (°C)	ΔH (cal/g)
Benzoic acid	122	38.0		35.2 34.8
KNO ₃	129	13.2	128	13.8
			127.5	11.78
			127.9	12.83
			127	12.05
KNO ₃	336	25.3	338	27.7
			334.3	22.75
				27.20
			331	28.1
AgNO ₃	161	3.42	160	3.9
			160	3.44
			158.9-160.6	3.49
			164	3.03
AgNO ₃	206	17.7	211	16.2
			210	17.57
			207	17.0
Al	658	1025	659	95.2
			660	96.3

due to the following reactions:



For the sealed-tube curve, the first peak is due to reaction (7.7), while the origin of the second peak is not known but may be due to the reaction



Thus, the sealed-tube sample holder permitted the determination of the ΔH of reaction (7.7), which was 12.9 ± 0.6 kcal/mol.

Similar studies were carried out on the deaquation of $[\text{Cr}(\text{NH}_3)_5\text{H}_2\text{O}]\text{X}_3$ (80) and $[\text{Co}(\text{NH}_3)_5\text{H}_2\text{O}]\text{X}_3$ (81) complexes.

The DTA curve of sulfur, as recorded by Chiu (82), is shown in Figure 7.22. The enantiotropic change from the *rhombohedral* to the *monoclinic* form is indicated by the 113°C peak, while melting was observed during the 124°C peak. Further transformations in liquid sulfur were observed at 179°C, and finally the boiling peak at 446°C.

Detection of organic contamination in ammonium nitrate is shown by the two DTA curves in Figure 7.23 (83). The exothermic peak begins at a low temperature in the sample with organic material contamination.

Brown et al. (51) used DSC to determine the ΔH of dehydration $\text{MnC}_2\text{O}_4 \cdot 2\text{H}_2\text{O}$ and the ΔH of decomposition of MnC_2O_4 in nitrogen and in oxygen. The DSC curve of this compound in nitrogen is shown in Figure 7.24. There are two endothermic peaks present that are identified as due to dehydration and decomposition. In an oxygen atmosphere, the high temperature peak becomes exothermic rather than endothermic. The ΔH of dehydration, both in nitrogen and oxygen, was determined to be 130 kJ/mole or, an average of 65 ± 5 kJ/mole H_2O . The ΔH of decomposition (or oxidation) was found to be 250 ± 25 kJ/mole in nitrogen and -300 kJ/mole in oxygen. The thermochemical evidence supports the claim that the decomposition residue is nonstoichiometric.

Rajeshwar and Secco (52,53) used DTA and other TA techniques to study the solid-state synthesis of 13 ammonium fluorolanthanates from NH_4F reaction mixtures. Two types of fluorolanthanates are formed in the reaction products, NH_4LnF_4 and $(\text{NH}_4)_3\text{Ln}_2\text{F}_9$.

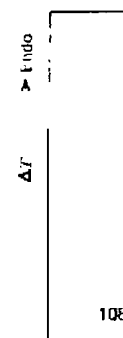


Figure 7.22. DTA curve ..

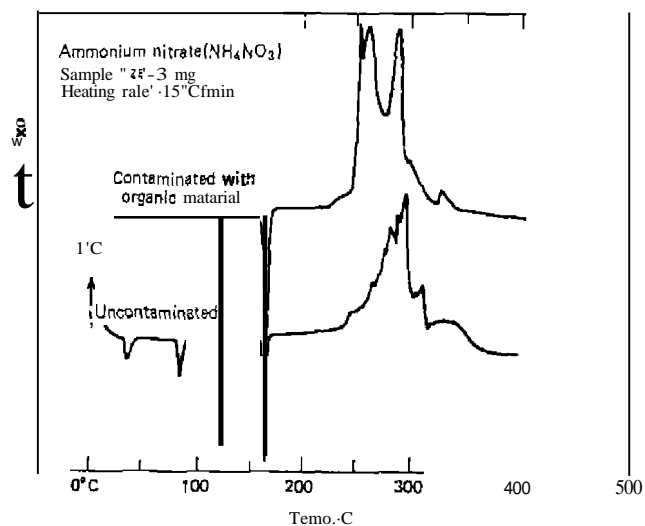


Figure 7.23. DTA curves of NH_4NO_3 in the pure state and contaminated with organic material (IS).

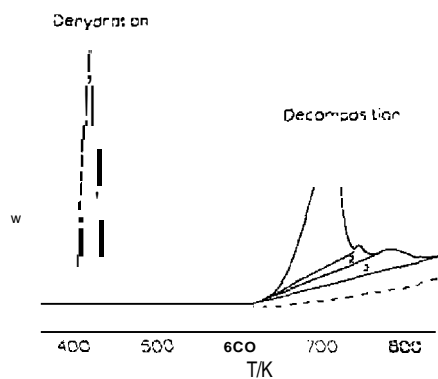


Figure 7.24. A representative DSC curve for the dehydration and decomposition reactions detected on heating rate 20 K min^{-1} a 5.21-mg sample of manganese (II) oxalate dihydrate in nitrogen using a gold sample pan. Water loss and anion breakdown are distinct and separate processes. The latter reaction is complex; the three areas marked are in the ratio 63:8:29 for 1:2:3, respectively; the dotted line indicates the baseline trace during sample run (51).

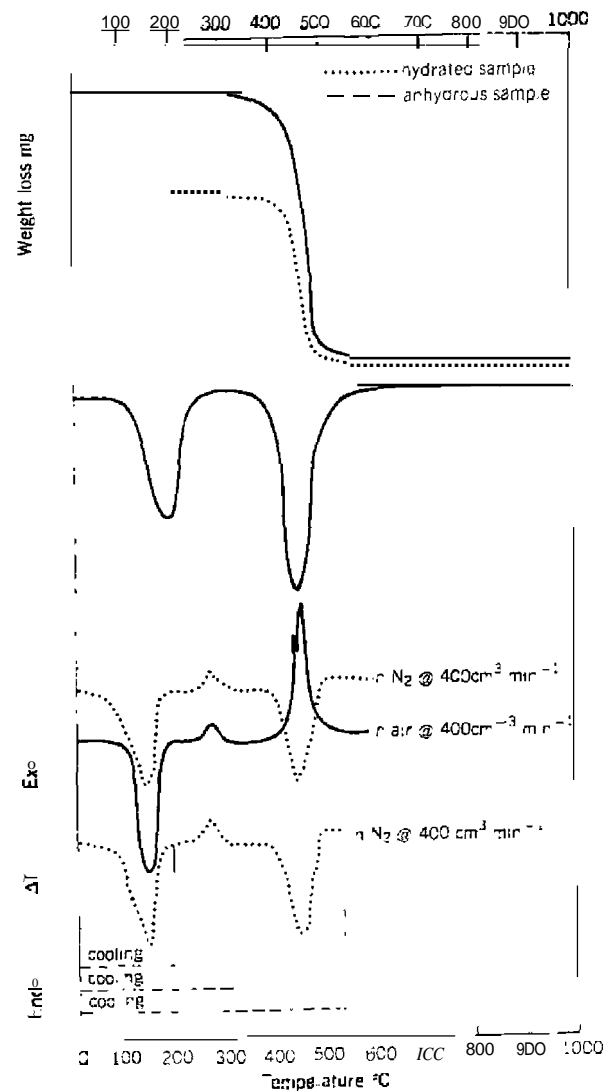


Figure 7.25. DSC and other TA curves of $\text{MgC}_2\text{H}_3\text{O}_4 \cdot 2\text{H}_2\text{O}$ (54).

The thermal decomposition of magnesium formate 2-hydrate was studied by DSC and other TA techniques by DoJJimore et al. (54). As illustrated in Figure 7.25, the DTA, TG, and DSC curves are dependent on the furnace atmosphere. An exothermic peak with a ΔT_{max} of 265°C occurred in a temperature range at which no mass-loss was observed on the TG curve. This peak was not altered when the furnace atmosphere was changed. Increasing the heating rate from 0.2 to 10°C/min had no effect on the curves. A schematic diagram for the decomposition of this compound is shown in Figure 7.26.

An unusual phase transition was observed in $\text{Ba}(\text{TO}_3)_2$ by Biswas et al. (55) at 422°C, which on cooling did not show an exothermic transition, indicating that the transition is irreversible. However, when the sample is cooled and then stored over P_2O_5 for a few hours, an endothermic peak is observed on reheating. In the latter case, the peak temperature is 378°C and the shape of the curve is quite different from that observed at 422°C.

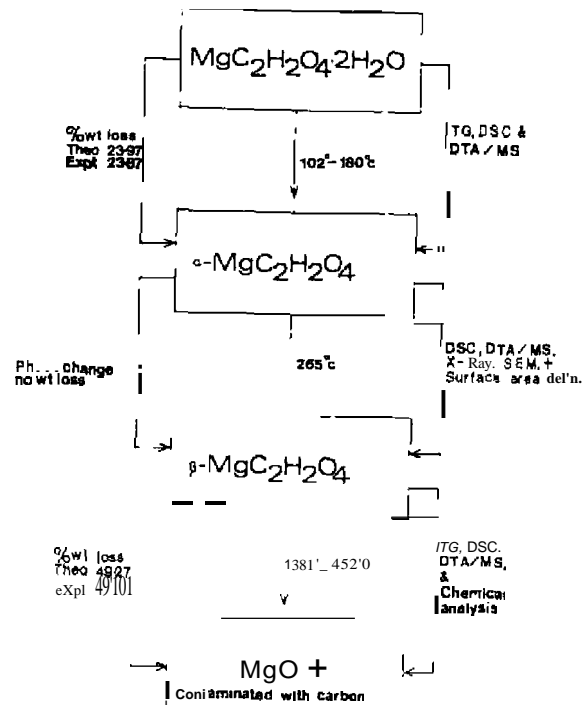
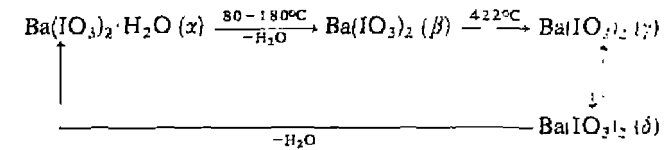
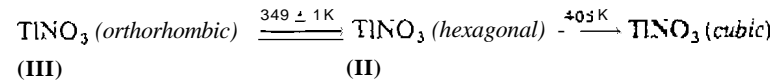


Figure 7.26. Schematic diagram of the thermal decomposition of $\text{MgC}_2\text{H}_2\text{O}_4 \cdot 2\text{H}_2\text{O}$ (54)

On cooling and storage over P_2O_5 again, the same 378°C peak appears on heating. Moisture absorption by the compound was found to increase the transition temperature. This transition and others can be explained by the reaction scheme



Ganguli et al. (56) reinvestigated the phase transitions of TlNO_3 using DSC and other techniques. The transitions observed were



The curve peak maximas depend on the particle size, moisture content, and thermal history of the sample. For the hexagonal-cubic transition, two peaks at ~ 409 and 413 K, respectively, were observed.

The decomposition temperatures of NaNO_3 , KNO_3 , $(\text{Na, K})\text{NO}_3$, NaNO_2 , and KNO_2 were determined by DSC (63). Sodium nitrate began to decompose at 840 ± 10 K, potassium nitrate at 820 ± 20 K, sodium and potassium nitrites at 800 ± 10 K. The sodium/potassium nitrate was more stable than the simple salts in that it did not begin to decompose below 990 K, the upper temperature limit of the investigation.

The phase transformations of potassium nitrate have been studied by DSC (65-67). The heat of transition of the phase change $\text{II} \rightarrow \text{I}$ at 129.7°C, is dependent on the thermal history of the sample, since it involves two steps. $\text{II} \rightarrow \text{III}$ and $\text{III} \rightarrow \text{I}$, at 2 degree intervals. Phase II has an orthorhombic structure, whereas phase I is trigonal. DSC curves of KNO_3 , as determined on a Perkin-Elmer DSC-2, are illustrated in Figure 7.27 (65). Curve III is the first experimental run of the sample that had a measured ΔH of 11.89 cal/g. Reheating the sample, curve (2), results in a sharper, more symmetrical curve peak. After fusion of the KNO_3 , cooling, and then reheating, curve (3) was obtained which has a sharper peak with a peak area about 50% of the other two peaks. The ΔH of this transition was about 5.95 cal/g, and corresponds to the transformation of the metastable $\text{III} \rightarrow \text{I}$. Shock cooling of the sample from 142-25°C, and then reheating of it gave curve (4). The area of the curve peak was about twice that of curve (3). This transition corresponded to the change from form II to I with a ΔH of 11.9 ± 0.1 cal/g.

Calorimetric data on the various phase transitions are given in Table 7.18.

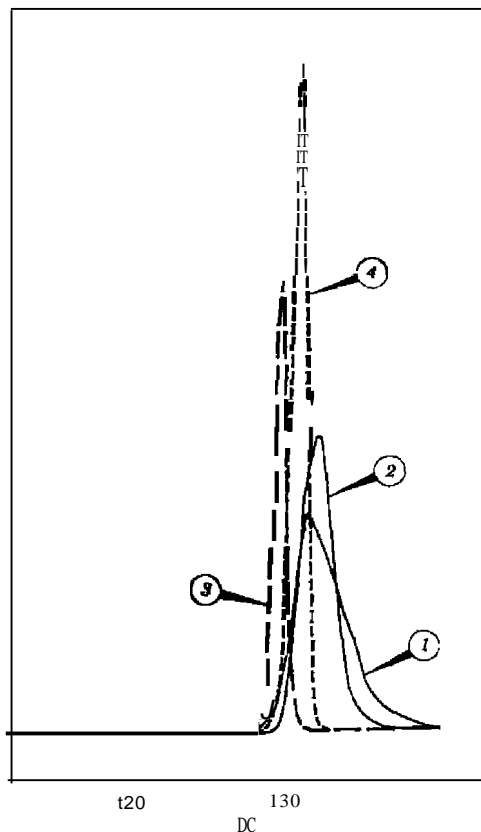
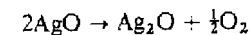


Figure 7.27. DSC curves of KNO_3 under various conditions (65).

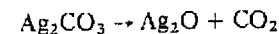
Table 7.18. Calorimetric Data for KNO_3 Crystalline Transitions

Transition	Temp. (°C) (10)	ΔH	
		Gray (65)	Wang 1671
$n \rightarrow I$	129.7	$11.82 \pm 0.0g$ cal/g	1291 ± 13 cal/mole
$III \rightarrow I$	128.8	5.96 ± 0.05	
$I \rightarrow III$	120	-6.02 ± 0.15	720 ± 7
$I \rightarrow$ melt	334.4	23.50 ± 0.22	
$III \rightarrow II$	94		571 ± 6

Barnes and Tomlinson (68) used DTA to analyze a mixture for silver(I) carbonate in the presence of silver(II) oxide. The method, as based on the DTA curve in Figure 7.28, is applicable quantitatively for mixtures containing more than 20% Ag_2CO_3 and semiquantitatively for 5%. The first curve peak is caused by the exothermic dissociation of AgO , or



whereas the second, which is endothermic, is due to the first step of the thermal decomposition of Ag_2CO_3 :



A least-squares method gave a straight-line calibration graph with the relationship

$$x = 0.498y - 2.52 \tag{7.11}$$

where y = the peak area of Ag_2CO_3 peak and x = the percentage of Ag_2CO_3 in the mixture. The mean deviation from the line was 3.0% above a level of 20% Ag_2CO_3 . Below this limit, because of the decreasing size of the silver carbonate peak, the results were less reproducible.

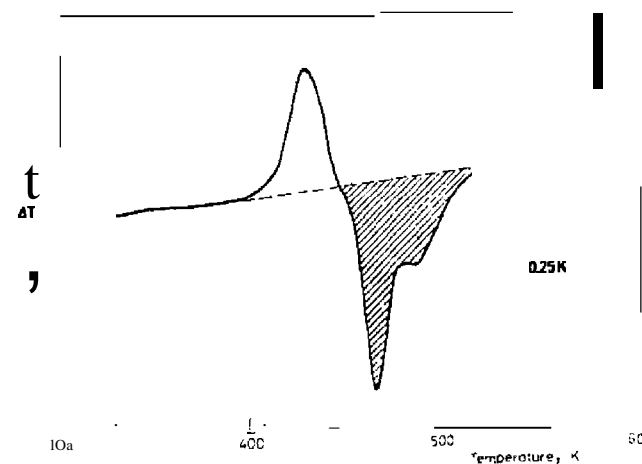


Figure 7.28. DTA curve of a mixture of 40% Ag_2CO_3 and 60% AgO . Heating rate of 15 K/min in a nitrogen atmosphere (67).

Other DTA studies were carried out on "active" and "inactive" forms of silver carbonate by Barnes and Stone (69).

Wendlandt (290) studied various mercury(I, II) compounds using DTA/DSC and other TA techniques. The DTA/DSC curves of the yellow and red forms of mercury(II) oxide are shown in Figure 7.29. The initial procedural ΔT deviation temperature (ΔT_i) was about 475°C for the yellow form and, as expected, 550°C for the red form. The minimum procedural ΔT temperatures (ΔT_m) were 575 and 655°C for the yellow and red forms, respectively. Using the DSC data, ΔT_i and ΔT_m values of 450 and 550°C, respectively, were found for the yellow form. In both the TG and DTA/DSC curves of the yellow and red forms of mercury (II) oxide, the lower procedural dissociation temperatures for the yellow form are consistent with a decrease in particle size. It is well known that a reduction in particle size of a compound such as this lowers the T_i (or ΔT_i) values. The extent of the lowering, however, cannot be predicted.

The DSC curves for the mercury(I, II) halides are illustrated in Figure 7.30 (290). Except for α -HgI₂, all the compounds exhibited a single endothermic peak in the DSC curves indicative of a sublimation process. The ΔT_i and ΔT_m values for the halides are: HgCl₂ (100, 185°C); HgBr₂ (125, 185°C); Hg₂Cl₂ (125, 200°C); and HgI₂ (140, 207°C). A small endothermic peak, due to the $\alpha \rightarrow \beta$ crystalline phase transition in HgI₂, is observed at ΔT_i and ΔT_m values of 125 and 127°C, respectively. All the curves were obtained using aluminum sample containers except for that of HgCl₂ where a platinum container was used due to a displacement reaction between the aluminum and this compound that resulted in an exothermic peak.

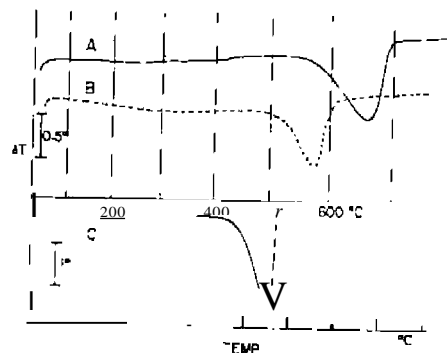


Figure 7.29. DTA/DSC curves of yellow and red forms of mercury(II) oxide at 10°C/min in N₂. a, red form; b, yellow form (by DTA); c, yellow form (by DSC) (290).

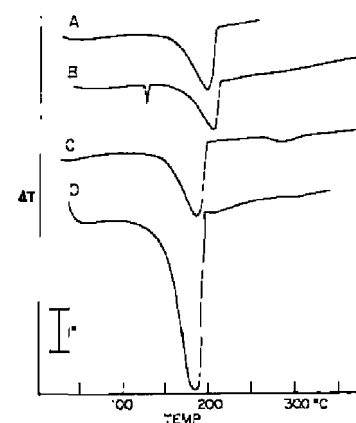


Figure 7.30. DSC curves of mercury (I, II) halides at 10°C min⁻¹ in N₂ (290). A, Hg₂I₂; B, HgI₂; C, HgBr₂; D, HgCl₂.

The sealed-tube DTA (see Chapter 6) curves of the mercury (I, II) halides are given in Figure 7.31 (290). Only the first-order phase transitions are observed by this technique, which in the case of these compounds, involves the fusion transitions. Since it is a sealed system, sublimation (or vaporization) of the compounds does not occur as was found in the case of DSC cell studies. The fusion endothermic peak temperatures agree fairly well with the melting point values reported in Table I. The ΔT_i and ΔT_m values found are: HgCl₂ (252, 257°C); HgBr₂ (235, 240°C); and α -HgI₂ (252, 257°C). In the case of the $\alpha \rightarrow \beta$ transition in HgI₂, the peak temperatures are somewhat higher, 135 and 140°C, respectively. Boiling points of the compounds, of course, could not be determined by this technique.

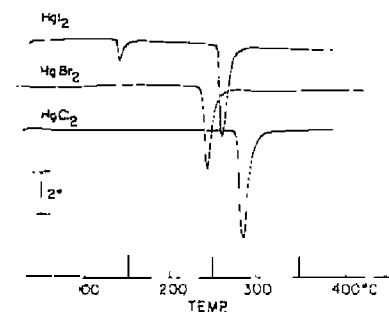
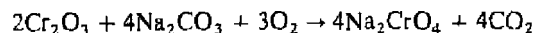


Figure 7.31. Sealed-tube DTA curves of HgI₂, HgBr₂, and HgCl₂ (290).

DTA was used to study the thermal decomposition of boracites. $M_j B_2 O_{13} X$, where M is Mg, Cr, Mn, Fe, Co, Ni, Cu, Zn, or Cd, and X is OH, F, Cl, Br, I, or NO_j , by Tissot et al. (70) and Gallagher (71).

Pyrotechnic compositions containing inorganic compounds have been investigated by DTA by numerous workers. Among the pyrotechnics studied were those containing titanium (109); $KClO_3$ and lactose (110); boron-silicon- KNO_3 (III); tungsten and $K_2Cr_2O_7$ (112); and boron- MoO_3 (177).

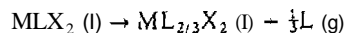
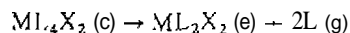
The reaction



was studied by DTA and other techniques by Sastri and Hill (178).

Deuterium isotope effects in thermal stabilities and enthalpy changes in the thermal dehydration of $CuSO_4 \cdot 5H_2O$ were studied by DSC by Tanaka (179).

The thermochemistry of a large number of transition-metal complexes of the type ML_nX_2 have been investigated using DSC by Beech et al. (89-91). These results as well as others are discussed in a book by Mortimer and Ashcroft (93). The overall decomposition reactions of the complex ML_nX_2 are as follows:



The decomposition reactions are recorded by DSC for the reaction (89)



The area, $(a + b)$, is a measure of this reaction, at a mean temperature, T_m . In the absence of a sample, no additional heat is required to raise the temperature of the empty sample pan, compared with the reference pan, as indicated by the horizontal baseline marked "empty pan." With a sample of mass m_{react} and specific heat $C_{p,react}$ present in the pan, the baseline is displaced by an amount corresponding to $m_{react} \cdot C_{p,react}$, the product of the mass and specific heat of ML_nX_2 . The ligand, L , of mass m_L and specific heat $C_{p,L}$, has been lost as a gas during the reaction. The mean temperature, T_m , is equal to $\frac{1}{2}(T_f - T_i)$. Total heat absorbed is represented by the area $(a + b - c - d)$,

so that the heat ΔH_{T_i} at temperature T_i of the reaction is given by

$$\Delta H_{T_i} = (a + b - c + d) - (T_f - T_i)[m_{prod} \cdot C_{p,prod} + \frac{1}{2}m_L \cdot C_{p,L}] \quad (7.12)$$

Only one half the term $m_L \cdot C_{p,L}$ is included because the ligand is liberated from the system, between T_i and T_f at a rate which is approximately constant. The heat, ΔH_{T_m} at some other temperature, T_m is given by

$$\Delta H_{T_m} = \Delta H_{T_i} + (T_m - T_i)[m_{prod} \cdot C_{p,prod} + m_L C_{p,L} - m_{react} \cdot C_{p,react}] \quad (7.13)$$

since

$$(T_m - T_i)[m_{prod} \cdot C_{p,prod}] = \frac{1}{2}d \quad (7.14)$$

$$(T_m - T_i)[m_L C_{p,L}] = \frac{1}{2}(T_f - T_i)[m_L C_{p,L}] \quad (7.15)$$

$$(T_m - T_i)[m_{react} C_{p,react}] = \frac{1}{2}(b + c + d) \quad (7.16)$$

and $b = c$ (approximately), the heat, ΔH_{T_m} , can be written as

$$\Delta H_{T_m} = a + b \quad (7.17)$$

Thermochemical data for the compounds $Co(py)_2X_2$ are given in Table 7.19.

Differential scanning calorimetry has been used to measure the heats of transition of some sodium, potassium, and silver compounds (94). The agreement of the experimental values with the literature for $KSCN$ and KNO_2 was very poor.

Table 7.19. Thermochemical Data for $Co(py)_2X_2$ Complexes (89)

Parameter	Cl	Br	
M.P., K		440	450
ΔH_i , kcal/mole	28.5 \pm 0.5 ^a	27.3 \pm 0.9	12.3 \pm 0.3 ^b
Heat rate, K min ⁻¹	8	16	16
T_i , K	420	overlaps	590
		m.p.	
	510	520	610
	600	540	630

^aRefers to blue form; transition of violet \rightarrow blue is $\Delta H = 3.02 \pm 0.07$ kcal/mole.

^bHeat of fusion of $Co(py)_2Cl_2$ is 6.3 ± 0.3 kcal/mole.

Stmchen (95) pointed out that the dissociation temperature of NaHCO_3 of 270°C commonly reported in many handbooks, is grossly in error. By use of DSC, the decomposition temperature was found to be about 100°C .

Block (96) reported an analytical method for chloride-bromide mixtures utilizing DSC. The fact that the heat of fusion of an ideal solid solution of the type $\text{A}_m\text{X}_n - \text{B}_m\text{X}_n$ or $\text{A}_m\text{X}_n - \text{A}_m\text{Y}_n$ is directly proportional to the concentration of solute ion was used to determine chloride-bromide mixtures in the concentration range 0-100%. Solutions containing both chloride and bromide are precipitated with silver nitrate, forming solid solutions of silver chloride-bromide. The heat of fusion of the mixed crystal is then determined, and the percent chloride or bromide obtained from a previously prepared standard curve.

Numerous other metal complexes were studied by DTA/DSC and other TA techniques including Ni(II), Cu(I) and Co(II), and Co(II) diethyldithiocarbamate complexes (72); bis(2,4-pentanedionato)beryllium (II) and tris(2,4-pentanedionato)aluminum (III) complexes (101); dihalogendi(tertiary-phosphine) cobalt (I) complexes (102); bis(trispyrrolidinophosphine oxide)-tetraniuranyl(IV) (103); Co(II), Cu(II), and Cd(II) xanthine complexes (104); and alkali and alkaline earth monomethyl violurates (105,108).

G. APPLICATIONS TO ORGANIC MATERIALS

The applications of DTA and DSC techniques to organic compounds are quite diverse, as is seen in Figure 7.32. It is difficult to point to one of the applications as the most important, or, for that matter, the most widely used. In the pharmaceutical and organic compound manufacturing industries, purity determination is perhaps the most important application. In other areas, identification only may be of vital interest. Only recently, due to the use of sealed-tube DTA and DSC sample holders, the study of organic reactions has assumed some importance. Information can be obtained from a single run which would normally take hours or days to complete by standard methods.

The enthalpic changes which occur in organic compounds are considerably less complex than those for organic polymers. However, they may exhibit various polymorphic changes which can be detected by DTA and DSC. The main sources of endothermic and exothermic enthalpic changes in organic compounds are fusion, vaporization, solid-solid transitions, sublimation, dehydration, decomposition, and combustion.

The applications of these techniques to organic compounds have been extensively reviewed (2-8). Specific DTA applications are reviewed by Mitchell and Birnie (2), while DSC techniques are discussed by Gray (4).

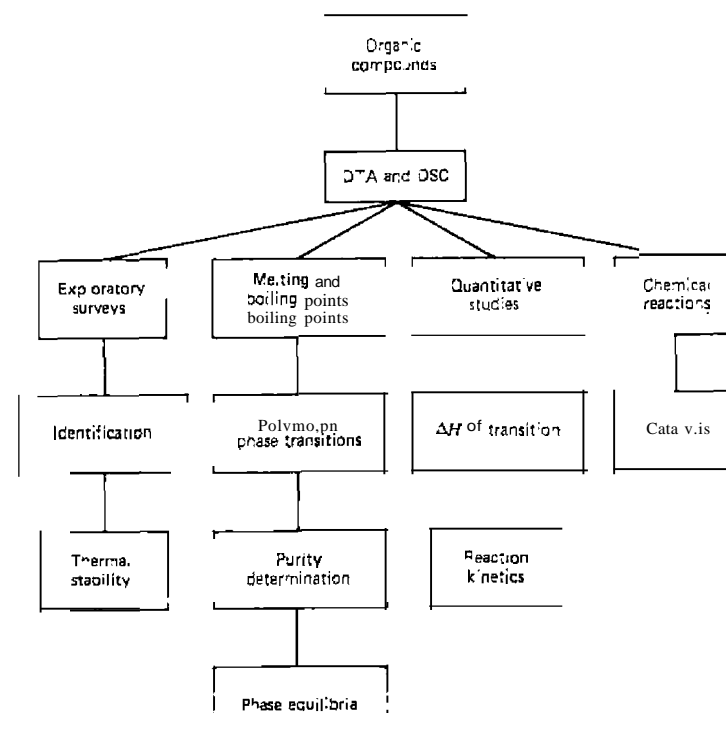


Figure 7.32. DTA and DSC applications to organic compounds.

The thermal decomposition of a number of organic acids has been studied by DTA by Wendlandt and Hoiberg (60, 5). Since the acids were decomposed in an argon atmosphere, only endothermic peaks were observed in the DTA curves. These peaks were caused by such reactions as dehydration, decarboxylation, sublimation, decomposition, and phase transitions from the solid to the liquid state. The maximum peak temperatures for the phase transitions were 10 to 30°C higher than the reported melting-point temperatures. The DTA curves for some of the acids are given in Figure 7.33.

The DTA curve for oxalic acid dihydrate, the only acid studied containing water of hydration, had dehydration peaks with ΔT_{m} values of 110, 120, and 125°C , respectively. All other curve peaks for the organic acids were caused by fusion and decomposition reactions. For example, the second endothermic peak in the succinic acid curve was probably caused by dehydration reaction.

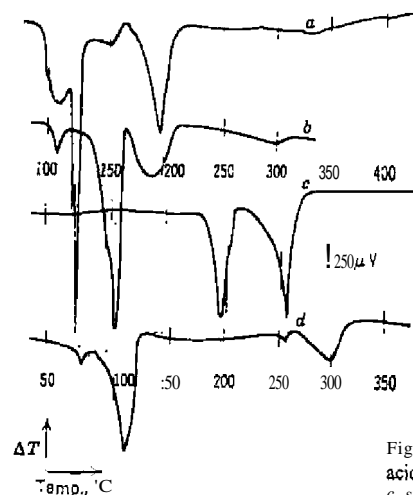
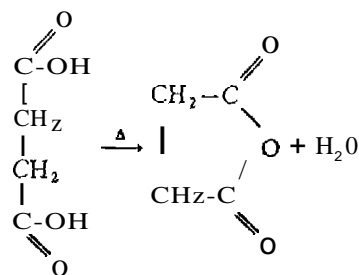
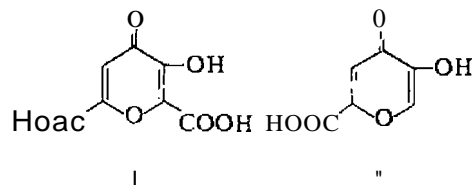


Figure 7.33. DTA curves of some organic acids; a, oxalic acid dihydrate; b, malonic acid; c, succinic acid; d, glutaric acid (60).

resulting in anhydride formation, of the type.



It has long been known that meconic acid (I) (3-hydroxy-4-oxo-4H-pyran-2,6-dicarboxylic acid) can be heated in air to 120-220°C to form comenic acid (II) (60). DTA was used to establish the best preparative



conditions for this reaction. It was found that comenic acid is formed by decarboxylation of meconic acid in a reaction giving an exothermic peak at ΔT_{max} of 240°C. At and above this temperature the product sublimes.

The boiling point of benzoic acid is shifted to higher temperatures by use of high-pressure DTA. Levy et al. (38) obtained the DTA curves of pure benzoic acid at ambient pressure and at a pressure of 2000 psig, as shown in Figure 7.34. Curve (a) indicates that benzoic acid melts at about 122°C. Under 2000 psig nitrogen pressure [curve (b)], the melting-point endothermic peak remains unchanged while the boiling point is elevated to 378°C. In order to avoid sublimation and evaporation and to ensure equilibrium conditions the samples were run in a small hermetically sealed aluminum pan which contained a small hole (~0.002 in.) punched in the top to equalize the pressure.

The precise determination of melting and boiling points by DTA was first discussed in detail by Vassallo and Harden (10). They obtained a precision of $\pm 0.3^\circ\text{C}$ over a wide range of heating rates and were able to make determinations in the temperature range from -150 to 450°C. The temperatures estimated for melting point, T_m , or boiling point, T_b , were selected from the most often recommended portions of the DTA peak, as shown in Figure 7.35. Point A is the intersection of the extrapolated straight-line portion of the low-temperature side of the peak with the baseline, and point B is the inflection point of the low-temperature side. Point C is the extrapolated temperature, while D is the extrapolated return to the baseline. The start and reference temperatures at which the various points occurred during melting of benzoic acid and the boiling of toluene are shown in Table

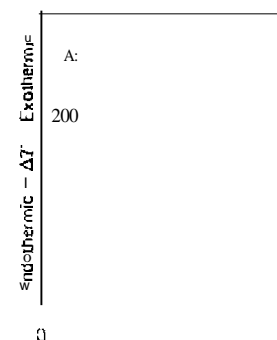


Figure 7.34. DTA curves of benzoic acid at ambient pressure (a) and 2000 psig of nitrogen (b) (38).

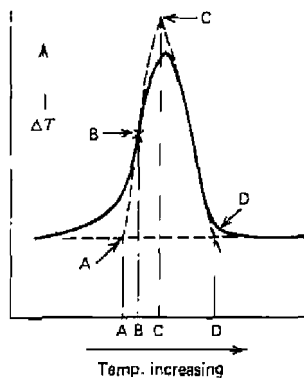


Figure 7.35. Transition temperature estimation methods (10).

Table 7.20. Comparison of Various Methods for Transition Temperature Measurement (10)

Temperature Measured	Benzoic Acid,* Melting Point (°C)			
	A	H	C	D
Reference	121.1	125.0	128.0	131.0
Sample	120.3	121.0	121.7	131.9
Method	Toluene [†] Boiling Point (°C)			
	A	B	C	D
Reference	112.5	114.2	115.9	116.2
Sample	114.6	113.2	111.2	118.8

*NBS, mp = 121.8°C.

[†]Merck, bp = 110° boiling range including 110.6°C.

With the exception of *D*, T_m estimates using the sample temperature are generally close to the true value. The closest estimates of T_m were achieved by use of the sample temperature at point C or the reference temperature at point A. The T_m estimated for toluene at points A, B, and D were higher than at point C, and this is probably due to superheating effects.

A low-temperature DTA curve of *n*-butane (10) is shown in Figure 7.36.

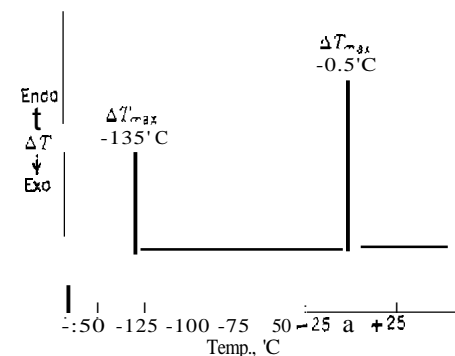


Figure 7.36. Low-temperature DTA curve of *n*-butane (10).

Table 7.21. Transition Temperatures Determined by DTA (10)

Compound	Melting point (T°C)		Boiling Point (T°C)	
	Found	Reported	Found	Reported
<i>n</i> -Butane	-135.0	-135.5	-0.5	-0.55
<i>n</i> -Pentane	-129.5	-129.7	36.2	36.0
<i>n</i> -Hexane	-94.5	-95.3	69.0	68.8
<i>n</i> -Heptane	-90.3	-90.6	98.2	98.4
<i>n</i> -Octane	-51.0	-56.8	125.6	125.6
<i>n</i> -Nonane			150.2	150.7
<i>n</i> -Decane			173.0	174.0
<i>n</i> -Dodecane			215.5	216.0
Benzoic acid	121.8	121.8		
Water	0.0	0.0	100.0	100.0
Toluene			111.1	110.6
Benzene	5.1	5.5	80.5	80.1
Acetic acid	16.5	16.6	118.4	118.1
Alathon 10 polyethylene resin	110.5	110.5 ^a		
Marlex 50 polyethylene resin	134.2	134.5 ^a		
Teflon TFE fluorocarbon resin	327.5	327.7 ^a		
Teflon FEP fluorocarbon resin	272.0	272.5 ^a		
Deirin acetal resin	170.5	171.0 ^a		

^aMelting points taken with Kofler hot stage microscope, or by X-ray techniques.

In the temperature range -150°C to 10°C , the endothermic peaks for boiling ($\sim 0.5^{\circ}\text{C}$) and melting ($\sim 13^{\circ}\text{C}$) are narrow and well defined. Melting and boiling points of a number of organic compounds are given in Table 7.21 (10).

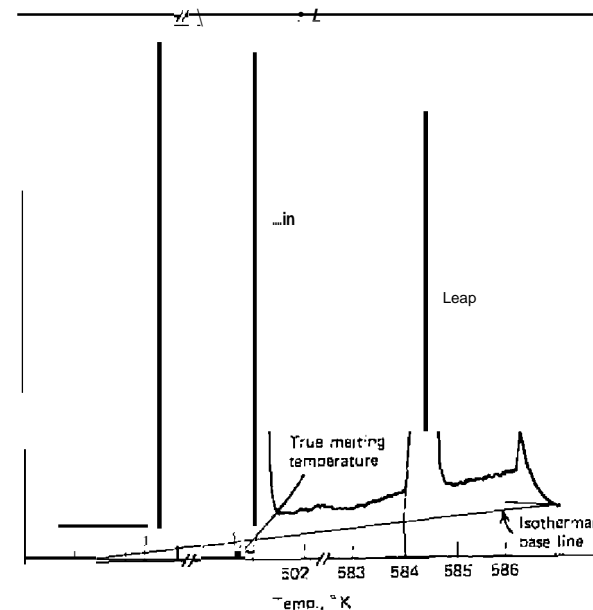
Banall (39) has discussed in great detail the precise determination of melting and boiling points by DTA and DSC. Many different methods are available for these determinations; however, BarraJl's method gives a consistent technique which is readily adaptable to commercial instruments and will cover a wide range of organic and inorganic materials. The data obtained are more consistent than those measured with the hot-stage, oil-bath, or capillary-tube techniques. Boiling-point data obtained by DTA and DSC are far more reproducible and usually more closely comparable to equilibrium-still results than data from microbullimetry, and they are certainly more rapid.

The experimental conditions of DTA necessitate that the ΔT parameter be plotted as a function of sample temperature, while in DSC the differential power curve is recorded as a function of time. For melting-point determinations, the sample may be encapsulated; in the case where the thermocouple must be inserted into the sample, a sample diluent mixture must be employed. The encapsulations are usually in a tightly sealed metal container of high thermal conductivity. In the case of boiling-point determinations, provision must be made for (1) equilibration of liquid and vapor and (2) control of atmospheric pressure. BarraH (39) described in detail how these two criteria can be met.

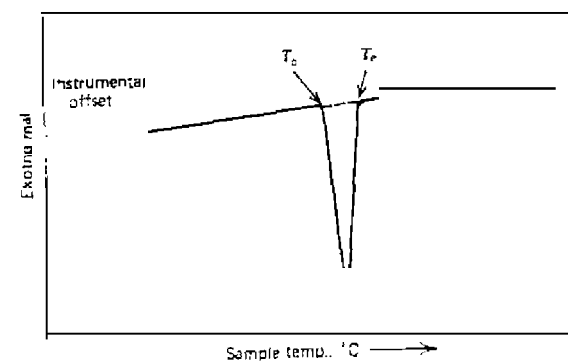
If an encapsulation procedure is employed for determining the melting point, an extrapolation procedure is used to correct for the thermal lag in the system, as shown in Figure 7.37a. The true melting point of the compound is obtained by the extrapolation of the leading edge of the peak curve to the isothermal baseline. If the sample is in direct contact with the thermocouple, the true melting point is T_b in Figure 7.37b. Other terms to be defined in the latter are the minimum in the peak, T_m , and the temperature at the end of the peak, T_e . The range between T_b and T_e is a function of the purity of the sample. Due to baseline drift, T_b is occasionally difficult to locate in impure samples.

In boiling-point measurements, T_e is of little significance. It is a function only of various instrument parameters, the rate of vapor diffusion, and the amount of sample present at the onset of boiling. The temperature at the beginning of the curve, T_b , corresponds to the boiling point of the compound (after suitable corrections).

A microboiling and melting point procedure using DTA was described by Kerr and Landis (11). The $2\text{-}\mu\text{l}$ samples were trapped at the exit port of a GC column and transferred with a $10\text{-}\mu\text{l}$ syringe to a capillary tube for DTA



(a)



(b)

Figure 7.37. Melting-point temperature determination: (a) encapsulated samples (199.9% pure); (b) thermocouple embedded directly in the sample (39)

study. Examples of boiling points of various organic compounds are illustrated in Figure 7.38. Micromelting point determinations permitted the estimation of the relative purity (>90%) of *m*- or *p*-xylenes.

Differential scanning calorimetry was used by Merrill and co-workers (43-45) to elucidate *solid* → *solid* phase transitions in a large number of organic compounds. First-order transitions were reponed for tetrahedral compounds of the type $CR^1R^2R^3R^4$, where R is methyl, methylol, amino, nitro, and carboxy, as well as for octahedral-type compounds. This technique was also used to detect phase transitions in alkali metal stearates (46), some dibenzazepines, carbazoles, and phenothiazines (16), and the half esters of O-phthalic acid (31). The solid-state decomposition kinetics and activation parameters of N-aryl-N'-tosyl-oxydi-imide N-oxides were determined using DSC by Dorko et al. (49).

Calorimetric heats of transition for other physical processes (melting, boiling, solid-solid, and so on) have been reponed by several investigators (22-25,31). Very careful calibration is necessary to obtain accuracies of the order of $\pm 5\%$.

Chiu (48) investigated the formation of an organic derivative by DTA.

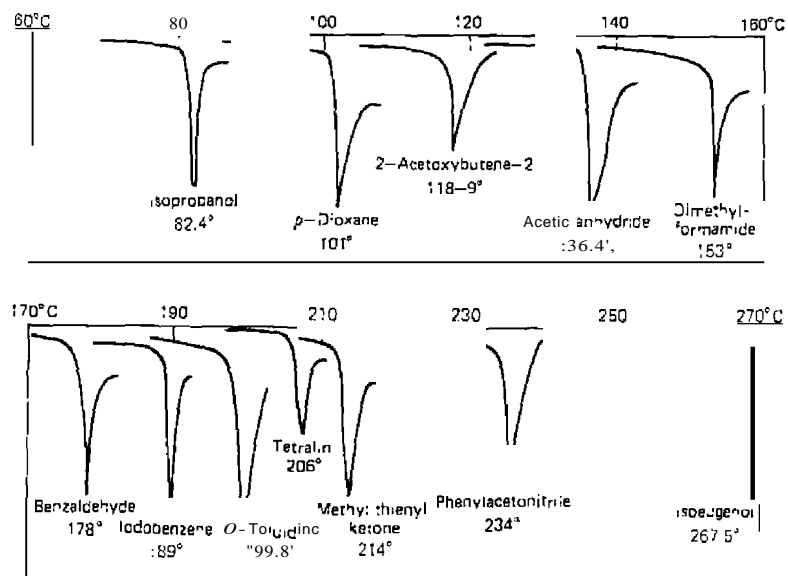


Figure 7.38. DTA curves of 2-5- μ l samples of various organic compounds (11).

He replaced the traditional method of preparing *the* derivative from the sample and reagent with a one-step process. The sample was heated with a specific reagent at a programmed heating rate in a selected atmosphere. The DTA curve showed the derivative forming reaction, the physical transitions of the sample or the reagent in excess, and the physical transitions of the intermediates and products. Glass capillary tubes were employed as the sample holder.

The formation of the acetone hydrazone derivative with *p*-nitrophenylhydrazine is illustrated in Figure 7.39. Curve (a) shows the endothermic peak for the boiling of acetone, with a ΔT_{max} of 58°C. For *p*-nitrophenylhydrazine, the endothermic peak at a ΔT_{max} of 160°C was caused by the fusion of the compound. A mixture of acetone and *p*-nitrophenylhydrazine, however, in the 54-80°C temperature range, gave a complex endothermic peak which was attributed to the net result of evaporation of excess acetone, solution of *p*-nitrophenylhydrazine in acetone, and hydrazone formation. The fusion of the hydrazone was indicated by the endothermic peak with a ΔT_{max} of 153°C. A rerun of the residue gave only a single endothermic peak, with a ΔT_{max} of 153°C. The reported melting point of the hydrazone

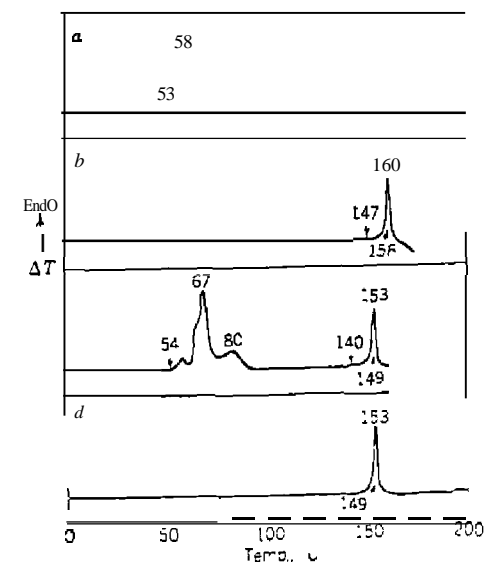


Figure 7.39. DTA curves showing formation of *p*-nitrophenylhydrazone of acetone. *a*, acetone; *b*, *p*-nitrophenylhydrazine; *c*, reaction mixture of acetone and *p*-nitrophenylhydrazine; *d*, rerun of residue from (c) (48).

derivative is 153°. Similar examples, such as the reactions of triethylamine with picric acid and dextrose with propylamine, were illustrated.

The method described is rapid and dynamic in nature, and requires that (1) a specific reagent should form a derivative with the sample rapidly; (2) the derivative so produced should show a discernible physical transition or a characteristic DTA curve; (3) one reactant more volatile than the other should be used in excess; (4) one reactant should serve as the solvent for the other; and (5) a catalyst may be used.

A Diels-Alder diene synthesis, using maleic anhydride and anthracene, was carried out using DTA by Harmelin et al. (26). This technique permits the determination of the temperature at which reaction occurs, the melting point of the adduct formed, and the decomposition of the adduct.

Chiu (234), using the sealed ampoule sample holder (microreactor) described in Chapter 6, studied a number of organic compounds and their reactions. The reaction between an unsaturated perfluorocarbon (PFHC) and methanol to form a perfluoroether is illustrated in Figure 7.40. A weighed amount of methanol was placed in the ampoule and then various amounts of PFHC were added using a metering device. The reaction occurred exothermically (curve D) in the temperature range from -50 to 90°C. Using DSC, the ΔH of the reaction was determined to be about 26 kJ/mole in a ten-fold excess of methanol. GC was used to analyze the contents of the ampoule at the end of the reaction.

Using sealed-tube sample holders, Santoro and co-workers (32-35) investigated a wide variety of organic reactions. Examples are the cis \rightarrow trans isomerization of stilbene and oleic acid, polymerization of styrene, Diels-Alder reactions, and others. Unstable intermediates in an organic reaction have been detected using DTA techniques by Koch (36). If a solution of an unstable compound is heated, temperature changes characteristic of reactions of the intermediate can be detected. Conversely, the absence of thermal effects indicates that no unstable product is present.

The determination of the relative purity of an organic compound by DTA and DSC methods will be discussed in Chapter 10. Most of the analytical methods are based on the DSC technique, although DTA may also be used.

Transition temperatures for a series of cholesteryl esters (13) are shown in Table 7.22. These temperatures are compared with those obtained by Gray (21). Temperatures observed by DTA endothermic peak minima agree to within $\pm 2^\circ$ with those observed visually. The absolute accuracies of the temperatures determined was $\pm 0.1^\circ$ in all cases, while the reproducibility was $\pm 0.05^\circ\text{C}$ for an individual sample on successive remeltings.

Heats of transition for liquid crystals have been determined by a number of investigators (14-16). These heats of transition are very small, ranging from 0.5 to 1.8 cal/g in most cases.

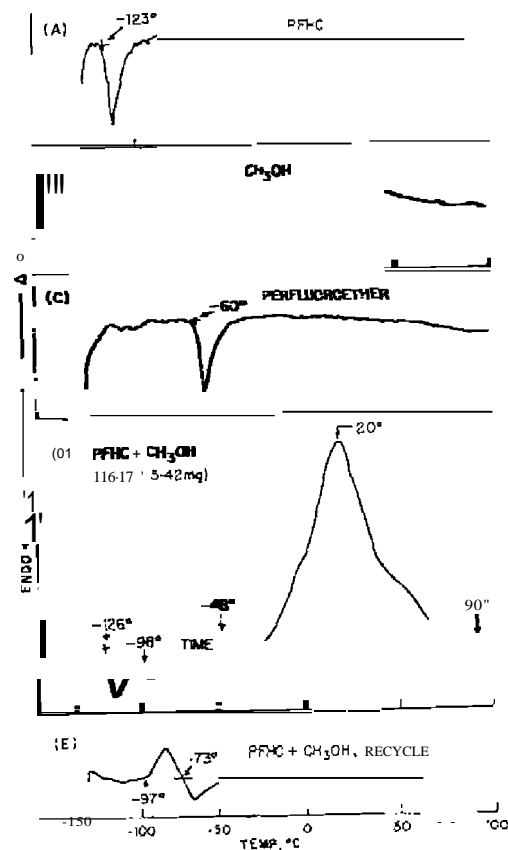


Figure 7.40. DSC curves of the reaction of PFHC-methanol in open (A, B, C) and sealed ampoules (D, E) (234).

Transition-temperature determinations for liquid crystals have been the subject of numerous investigations (17, 20). Not only can the melting points be determined, but also the liquid-crystal transitions. One of the first such determinations was that by Barrall et al. (12) on anisaldazine, which is illustrated in Figure 7.41. A stable, linear heating rate is necessary because a 1°C sudden departure for linearity can appear as a "glass transition point" on the DTA curve. The two curves in Figure 7.41 illustrate the use of temperature-axis amplification in order to separate closely spaced peaks. In

Table 7.22. Transition Temperatures for Cholesteryl Esters (13)

Cholesteryl Ester	DTA ^a			Gray ^a		
	T ₁	T ₂	T ₃	S	C	I
Formate			97.3		(60.5)	97.5
Acetate	44	81-87	118.4		(94.5)	116.5
n-Propionate	99 ± 1	110?	115.3		102	116
n-Heptylate			114.1	(<92.5)	(95.5)	114
n-Nonanoate	74.0	80.8	93.0	(77.5)	80.5	92
n-Decanoate		85.7	91.2	(81.5)	85.5	92.5
Myristate	73.6	79.7	85.5	71	81	86.5
Palmitate		79.7		(78.5)	779	83
Stearate			85.1	(75.5)	(79.5)	83

^aS = smectic; C = cholesteric; I = isotropic liquid; T₁ = lowest transition; T₂ = intermediate transition; T₃ = transition to isotropic liquid; parentheses indicate isotropic metastable transition.

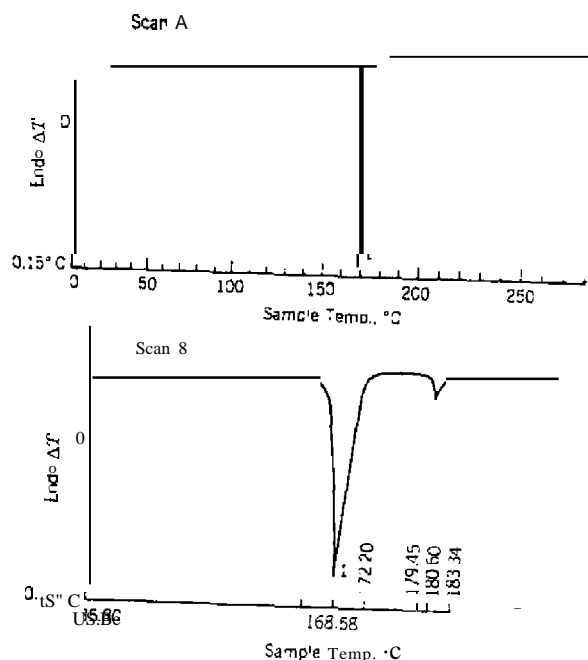


Figure 7.4. DTA curves of anisaidaz. (1) Fusion point. Curves A and B at ΔT = 0.05°C. In... T in curve A = 1 mV per in.; T in curve B = 8 mV per 8 in.

(A), the temperature span is 0 to 280°C, while in (B) it is from 135.80 to 183.34°C. The temperature scale in (B) was amplified about eight times over that in (A). Amplification of up to 1000 times in any 300° interval was possible in the temperature range from -100 to 500°C.

Other reviews of DSC and DTA investigations of liquid crystals are by Gray (247). Brennan and Gray (248) and others.

H. APPLICATIONS TO PHARMACEUTICALS

DSC has been applied to numerous problems in pharmaceutical science, a representative list of which is presented in Table 7.23.

Radecki and Wesolowski (268) determined the compositions of 117 pharmaceutical preparations using DTA and TG. They included powders, dusting powders, capsules, granulates, tablets, suppositories, ointments, and others. (See also Chapter 4.)

DSC can be used to "fingerprint" sodium penicillins although Tomassetti et al. (269) state that it was impossible to identify melting processes. Nine sodium penicillins were examined by DSC, as shown in Figure 7.42. The DSC curves contained mostly exothermic peaks, as expected, whose origin was not discussed due to the reaction complexity.

Khattab (270) investigated the thermal behavior, using DSC, of phenacetin, cholesterol myristate, sulfathiazole, sulfadiazine, sulfadimethyloxazole, sulfamerazine, and sulfadimidine. The DSC curve of sulfathiazole is illustrated in Figure 7.43. This drug had two endothermic curve peaks with peak temperatures of 166.4 and 200.2°C, respectively. It was observed that the first peak is composed of three stages, the main reaction is the middle one. Calculations of the heat of reaction gave 8.93 kJ/mole for the first peak and 24.1 kJ/mole for the second peak. The purity of this compound could not be

Table 7.23. Applications of DSC to Pharmaceutical Problems

Application
Melting points
Purity determination by melting point
Polymorphism
Moisture determination
Drug-excipient interactions
Determination of inorganics
Climate stability
Shelf-life

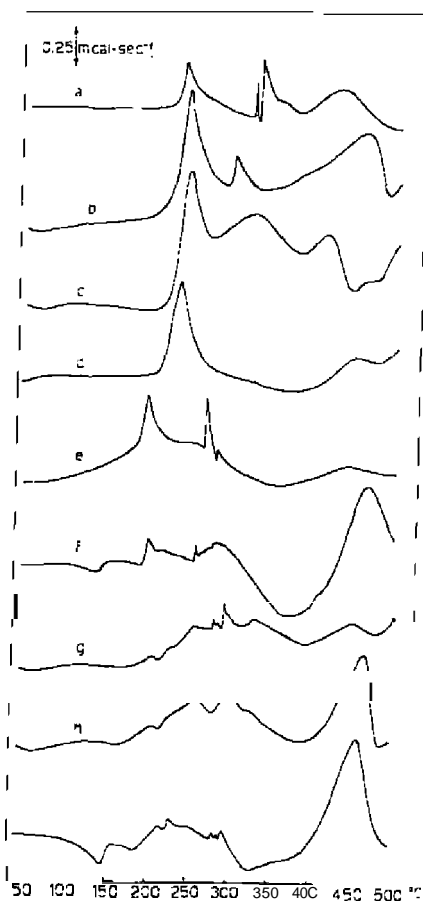


Figure 7.42. DSC curves of sodium penicillins, Heating rate of $10^{\circ}\text{C min}^{-1}$ in oxygen. a, benzylpenicillin; b, ampicillin; c, amoxycillin; d, epicillin; e, carbenicillin; f, methicillin; g, oxacillin; h, cloxacillin; i, dicloxacillin (270).

determined by DSC because of the presence of more than one crystal form and the fact that the fusion peak (second peak) is followed immediately by an exothermic decomposition peak. A summary of the DSC data on the sulfonamides is given in Table 7.24.

Wesolowski (271) used DTA/DSC and other TA techniques to determine the active ingredient, both qualitatively and quantitatively, in pharmaceutical preparations containing anti-inflammatory agents and formulations used for

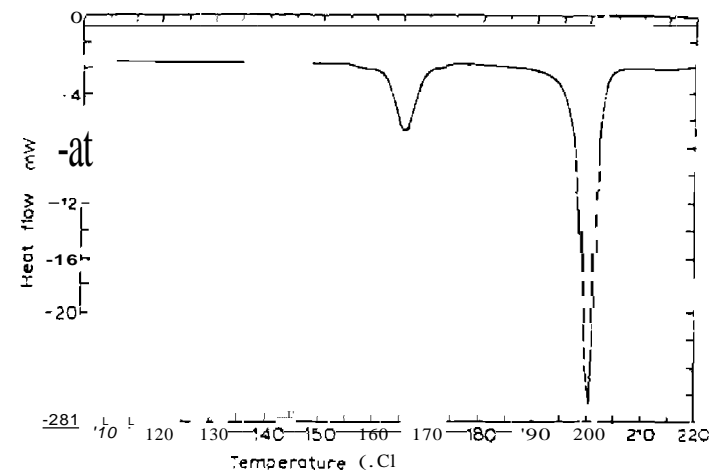


Figure 7.43. DSC curve of sulfathiazole. Heating rate of $10^{\circ}\text{C min}^{-1}$ on a sample size of 5.11 mg (270).

Table 7.24. DSC Data on Sulfonamides (270)

Sample	First Reaction		Heat of reaction (kJ mole ⁻¹)	Second Reaction		Purity by DSC Method (mole%)
	Temp. (°C) Start	Temp. (°C) Peak		Temp. (°C) Start	Temp. (°C) Peak	
Sulfathiazole	15.3	166.4	8.93	195	200.2	24.1
Sulfadiazine	248.0	257.0	43.30			
sulfadimethyloxazole	170.0	195.0	17.28	201	208	11.6
Sulfamerazine	229.2	233.2	45.80			99.81
Sulfadimidine	180.0	195.4	44.80			98.16

treatment of gastric and duodenal ulcers, gastritis, and mineral deficiencies. The advantages of these analyses is the elimination of time-consuming separation of the active components from the vehicles or additives. The disadvantage of the method is that it cannot be used for the determination of active components that have no distinct thermal decomposition stages, or which constitute less than 10% of the total contents. It is also difficult to analyze a sample for two or more active components.

Kuhnert-Brandstatter and Proll (272) used DSC and EGA to study: (1) single-stage and multistage desolvation (dehydration) reactions; (2) desolvation to a hydrate of lower water content and with subsequent congruent

fusion; and (3) single fusion as a hydrate. Examples of (1) are alpha-acetaminocinnamic acid \cdot 2H $_2$ O, 4,4-bipyridyl \cdot 2H $_2$ O, aceclidine hydrochloride \cdot H $_2$ O, terpine hydrate, D(+)-trehalose \cdot 2H $_2$ O, and Na $_2$ dimethylglyoxime \cdot 8H $_2$ O. For (2), examples studied were ethyl morphine HCl \cdot 2H $_2$ O, and codeine HCl \cdot 2H $_2$ O; and for (3), pecazine HCl \cdot 2E $_2$ O, and cyproheptadine HCl \cdot H $_2$ O (273).

The DTA curves of a number of pharmaceutical compounds have been described by Brancone and Ferrari (9) in which qualitative information concerning purity, solvation, structural configuration, and polymorphism were obtained. The DTA curve of triamcinolone diacetate (9), as shown in figure 7.44, aided in the establishment of its proper drying temperature. The solvent peaks at ΔT_{min} of 142 and 166°C, respectively, disappear on drying.

For routine drug-excipient interaction studies. DSC and an isothermal stress test are normally employed. According to van Dooren (274), DSC curves are difficult to evaluate and positive conclusions are rarely obtained; thus, the latter test is still necessary. Van Dooren claims that numerous considerations must be made before a positive identification of drug-excipient interaction by DSC can be made.

The DSC curves of methaqualone, 2-methyl-3-o-tolyl-4-(3H)-quinazolinone, were investigated by Warkentin et al. (292) to determine whether or not

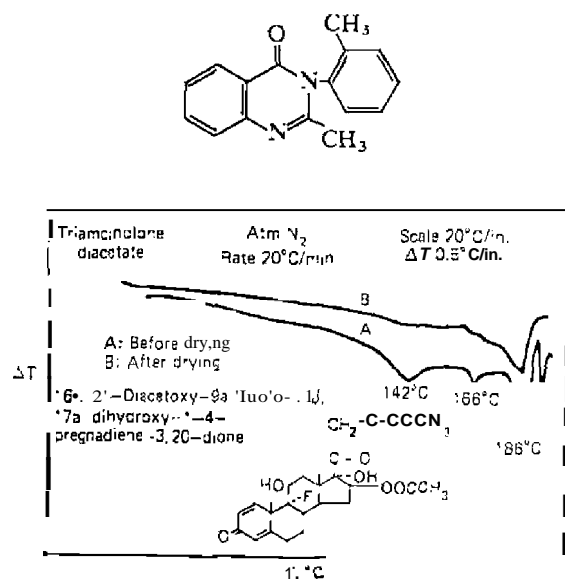


Figure 7.44. DTA curves of triamcinolone diacetate (9)

this technique could be used to identify the source of the commercial preparations of this drug. The DSC curves of four samples are shown in Figure 7.45. The curves for the first three samples were almost identical, whereas the fourth possessed an entirely different curve, indicating a different composition in the filler or binder material. As can be seen in curves A-C, all three contained a narrow endothermic peak with a ΔT_{min} of 115°C, a broad endothermic peak with a ΔT_{min} of about 210°C, and then another broad peak or peaks with a ΔT_{min} of about 375°C. The first endothermic peak is due to the fusion

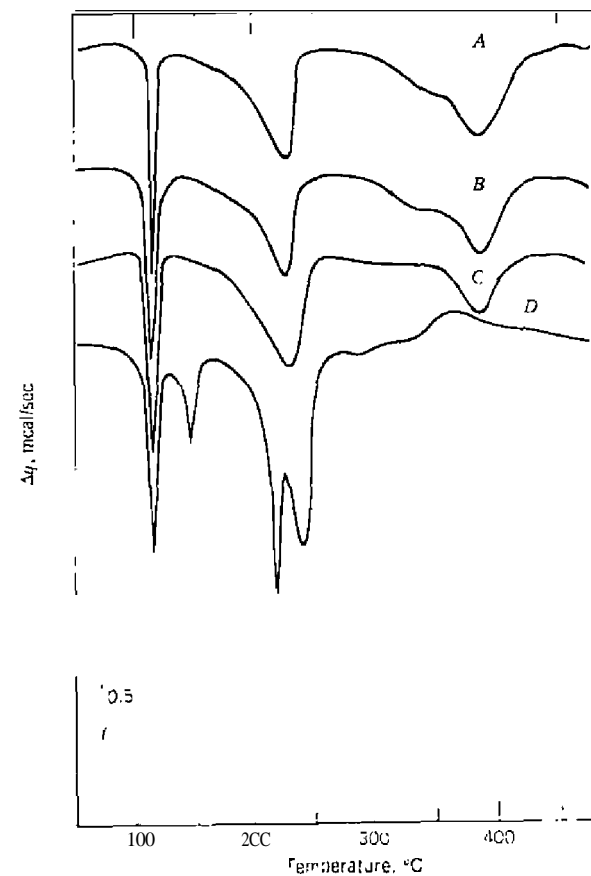


Figure 7.45. DSC curves of methaqualone (292), *u*, Mandrax, *h*, Quaalude (Mexico), *c*, Quaalude Roré 714 (USA); *d*, Sopar. Sample sizes were 3.2-3.6 mg

of the methaqualone (mp 114°C), the second is caused by its subsequent vaporization and/or decomposition, whereas the third region in the curve is due to the decomposition of the filler or binder material. Unfortunately, DSC could not be used to establish unequivocally the country of manufacture of the methaqualone.

Wendlandt and co-workers used DSC and TG to characterize analgesics (293), antacids (294), and nonprescription vitamin preparations (295) (see Chapter 4).

Other applications of DSC and other TA techniques to the pharmaceutical industry include physico-chemical interactions (275), polymorphism in triglyceride suppository formulations (276); drug-excipient interactions (277), and many more. Reviews of the applications of DTA/DSC and different techniques to pharmaceuticals include those by Brennan (27B), Daly (279), and others (280).

J. APPLICATIONS TO POLYMERS

Perhaps the greatest number of applications of DTA and DSC in recent years has been in the area of polymeric materials. These two techniques are routinely used to measure glass transition temperatures, T_g ; melting points, T_m ; degree of crystallinity; heats of fusion and/or crystallization; decomposition temperatures; and numerous other parameters. Several commercial

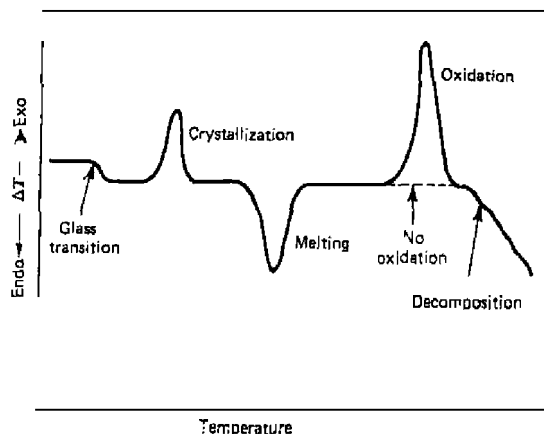


Figure 7.46. Schematic DTA curve of a typical polymer (145).

DTA and DSC instruments were developed mainly for use in polymer measurements.

The DTA curve in Figure 7.46 illustrates how the various thermal processes appear on a DTA curve (145). In actual practice, however, all these transitions are not so well defined on the same curve. It is necessary to make slight variations in procedure in order to show the transition of particular interest to best advantage. For example, oxidation is measured on a sample of smaller than normal size, and the run is carried out in the presence of either oxygen or air. For other measurements, nitrogen or low pressures are normally employed. The DTA or DSC equipment must be designed for

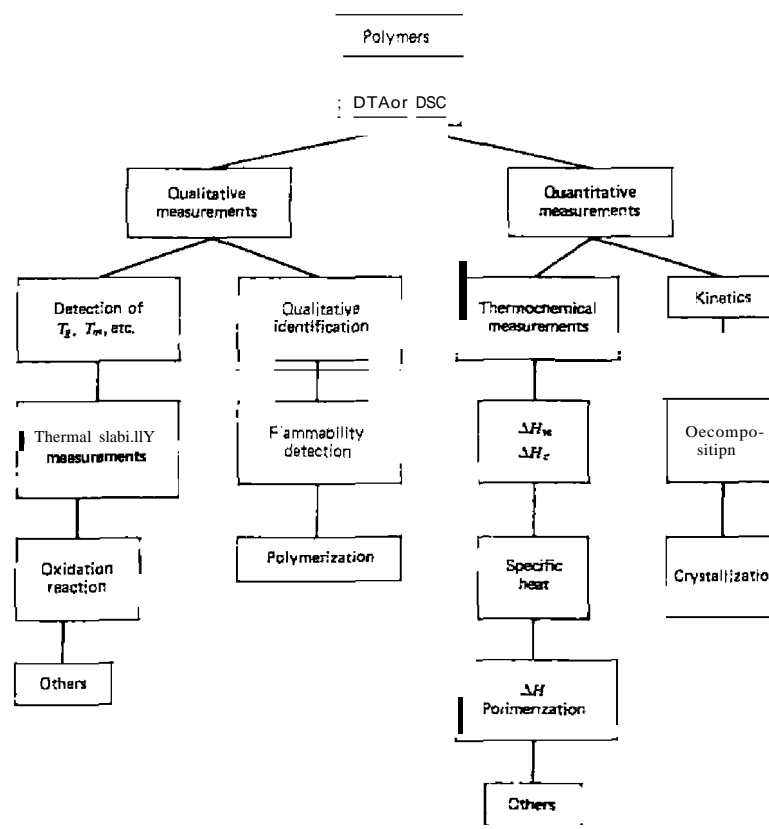


Figure 7.47. Applications of DTA and DSC to polymers.

programmed cooling so that the crystallization temperature on cooling can be measured.

The applications of these two techniques are schematically shown in Figure 7.47. Excellent reviews on these applications are given in books by Ke (146), Slade and Jenkins (147), Schwenker (148), Porter and Johnson (149, 150), Reich and Stivala (151), Schwenker and Gam (152), and others, and review articles by Murphy (5-8, 153) and numerous others.

The identification of polymer blends is illustrated by the DTA curve in Figure 7.48. Chiu (154) studied a physical mixture of seven commercial polymers: high-pressure polyethylene (HPPE), low-pressure polyethylene (LPPE), polypropylene (PP), polyoxymethylene (POM), Nylon 6, Nylon 66, and polytetrafluoroethylene (PTFE). Each component shows its own characteristic melting endothermic peak, at 108, 127, 165, 174, 220, 257, and 340°C, respectively. Polytetrafluoroethylene also has a low-temperature crystalline transition at about 20°C. The unique ability of DTA to identify this polymer mixture is exceeded by the fact that only 8 mg of sample was employed in the determination.

Anderson (162) studied the DTA of six different epoxides, both reacted and unreacted, with various amines and anhydride polymerizing agents. The samples, varying in mass from 1 to 3 g, were intimately mixed with equal amounts of aluminum oxide. After the mixture was placed in the sample tube, the tube was weighed before and after the heating cycle so that the loss in mass of the sample could be obtained.

The DTA curves of three catalyzed and uncatalyzed epoxides are given in Figure 7.49. The epoxides studied were Epon 1310 [tetraglycidyl ether or tetrakis (hydroxyphenyl)ethane], Diepoxide AG-13E (bis-epoxydicyclopentyl ether or ethyleneglycol), and UC Endo isomer (dicyclopentadiene dioxide). All the uncatalyzed epoxides, except the LC Endo isomers, exhibited exo-

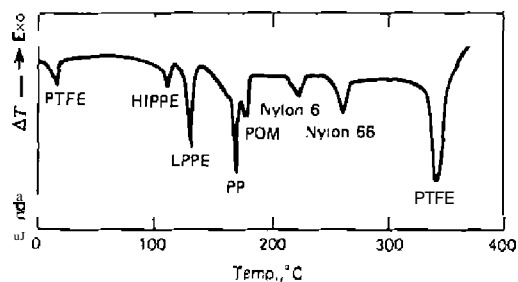


Figure 7.48 DTA curve of a seven-component polymer mixture (154).

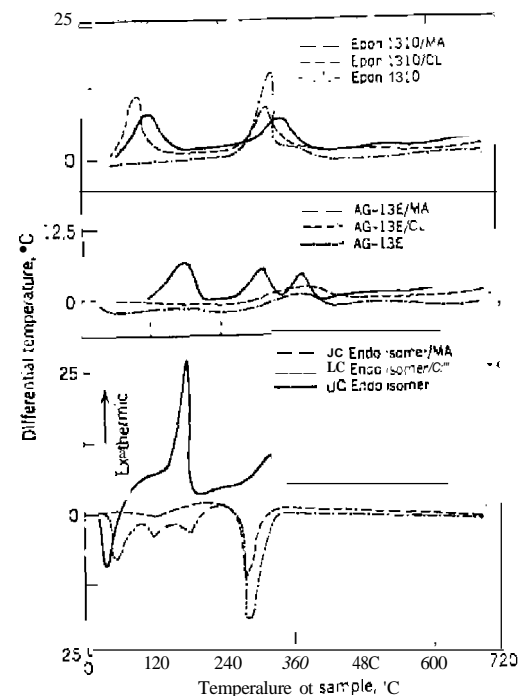


Figure 7.49. DTA curves of catalyzed and uncatalyzed epoxides. MA is maleic anhydride; CL is *m*-phenylenediamine; heating rate of 2.5°C min⁻¹ (162).

thermic peaks in the 300–400°C region. These peaks were believed to be due to the isomerization of the epoxy group to carbonyl groups (aldehydes for primary epoxides and ketones for secondary epoxides). The appearance of vapors in the tubes indicated that volatilization and decomposition also occurred simultaneously with isomerization and polymerization. The Endo isomer showed an endothermic peak because of the heat absorbed by volatilization, and decomposition masked any heat resulting from the slower rate of isomerization and etherification polymerization of its epoxy groups. The peak at ΔT_{min} of 184°C corresponded to the melting point of the Endo isomer.

When the preceding three epoxides were mixed with the catalysts (maleic anhydride or *m*-phenylenediamine), except for the AG-13E/CL and UC Endo isomer/CL, all the mixtures exhibited two exothermic peaks and only one

endothermic peak. This latter peak corresponded to the boiling points and/or decomposition points of both the epoxide and the catalyst.

The DTA curves obtained on the previous system may be used confidently as a characterization index. This technique offers unique advantages over other instrumental methods, especially those involving insoluble and amorphous crosslinked epoxy systems which exhibit diffuse X-ray patterns and which, because of their inherent intractable physical state, do not give reproducible infrared spectra.

Murphy et al. (163) studied the DTA of Vibrin 135 resins, the results of which are shown in Figure 7.50. Three samples of resin were studied; two of them contained 2% tert-butylperbenzoate catalyst, the other 0.5%. Each catalyst-resin mixture was then heated (cured) for a definite period of time. The DTA curves in (1) and (2) showed that two low-temperature exothermic peaks were observed, with ΔT_{\max} values of 150 and 180°C, respectively. This first peak was missing from the post-baked (180°C for 24 hours) sample, although the 320°C peak was found in all three curves. The presence

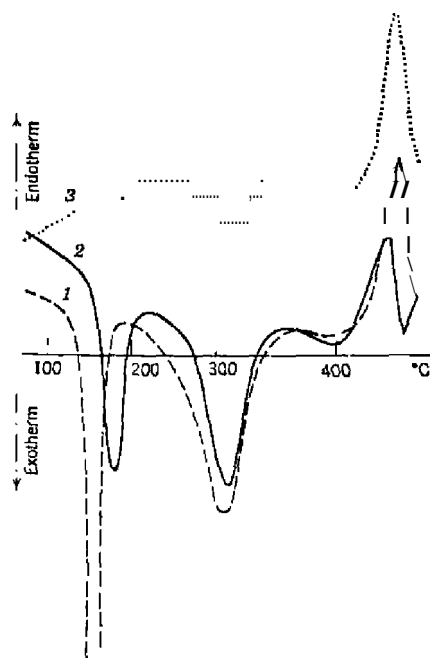


Figure 7.50. DTA curves of Vibrin 135 resins (163).

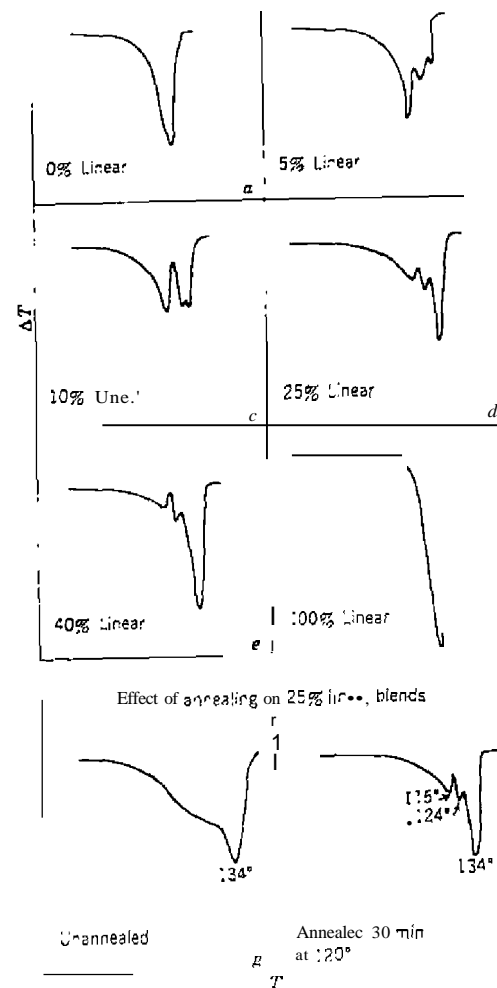


Figure 7.51. DTA curves of linear high-pressure polyethylene blends (10)

of the low-temperature exothermic peak was attributed to the further polymerization of the undercured resin, especially the polyester portion of the resin. The high-temperature exothermic peak was caused by the curing of the triallyl cyanurate portion of the resin.

Murphy et al. (164) further demonstrated the effect of different catalysts on the curing of Vibrin 135 resin by a DTA method. The catalyst, benzoyl peroxide, effected the most complete cure for the resin.

The technique of DTA has been used by Clampitt (165) for the estimation of the linear content of polyethylene blends. The DTA curves for several polyethylene blends are given in Figure 7.5L

Careful examination of the unannealed polyethylene sample curve indicated a peak with a ΔT_{min} of 134°C , and also a shoulder peak. On annealing the sample 30 min at 120°C , the shoulder peak was resolved into two peaks, with ΔT_{min} values of 115 and 124°C , respectively. When the preceding annealing procedure was used, varying the percentage of the linear content of the samples, the DTA curves in Figure 7.5I were obtained. The curves contained endothermic peaks with ΔT_{min} values of 115 , 124 , and 134°C , respectively. For the pure components, however, only one peak was obtained with high-pressure polyethylene, with a ΔT_{min} of 115°C peak decreased and the area under the 134°C peak increased as the amount of linear polymer increased. The 115°C peak was associated with the presence of crystals of high-pressure polyethylene, while the 134°C peak presumably was due to crystals of linear content.

Schwenker and Beck (166) studied by DTA the thermal degradation of polymeric materials used in textile manufacturing in air and nitrogen atmospheres. The polymers studied were dacmn, nylon 66, neoprene W, and orlon. From the results obtained, the reactions, such as rearrangements, cross-linking, and depolymerization taking place in the polymers on thermal degradation can be detected and identified. DTA can detect relatively small changes in polymer composition or the presence of substituents on the polymer backbone, as well as prove quite valuable for thermal degradation mechanism studies.

The DTA curves of nylon 66 fabric and neoprene W, in air and in nitrogen, are given in Figure 7.52.

At about 100°C , a weak endothermic peak due to the loss of sorbed water was observed in the nylon 66 curve. In air there was an exothermic reaction initiating at about 185°C and forming a small endothermic peak at a ΔT_{min} of about 250°C , the latter being caused by the fusion of the polymer (mp about 255°C). In nitrogen, the exothermic peaks were not present, suggesting that the air reactions were due to an oxidation reaction. The two endothermic peaks in the nitrogen curve were due to the fusion of the polymer and to the

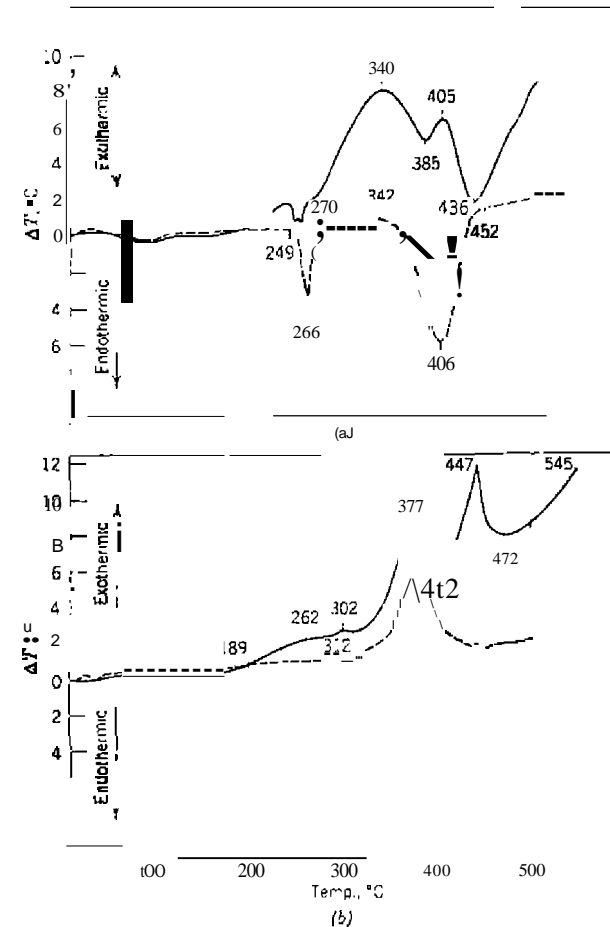


Figure 7.52. DTA curves of polymeric materials (166): (a) nylon 66; (b) neoprene W, in air (—) and in N_2 (---).

depolymerization reaction. It is obvious that the thermal degradation mechanisms are different for the air and nitrogen atmospheres.

In the DTA curves for neoprene W, both curves exhibited an exothermic peak with a ΔT_{min} of about 377°C . This peak was attributed to the elimination of HCl and the cross-linking of the residue,

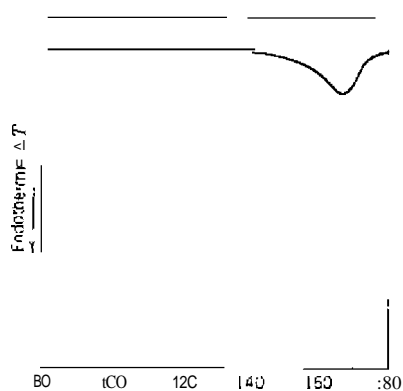
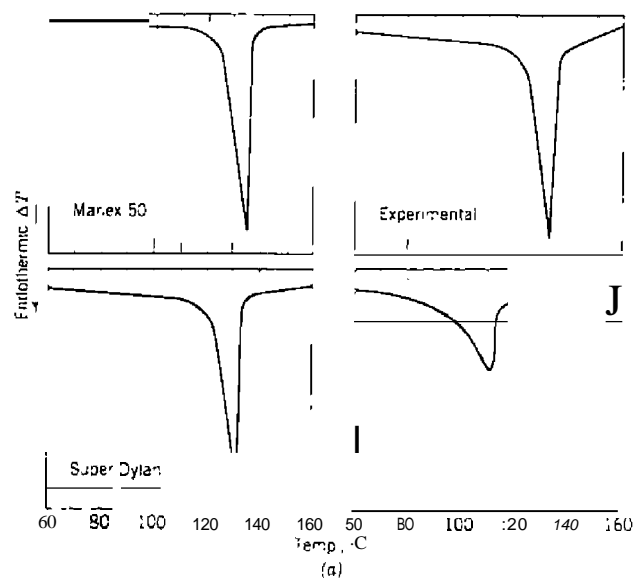


Figure 7.5.3. DTA curves of polyolefins (167). (a) Polyethylenes; (b) polypropylene.

The melting points and degree of crystallinity of a number of polyolefins have been studied by OTA by Ke (167). Five polyolefins are given in Figure 7.5.3.

From the curves, the peak maximum temperature, ΔT_{min} , was used for the determination of the polymer melting point. Results obtained by DTA were within $\pm 1^\circ\text{C}$ of the reported literature values, although several of them had a 15°C melting-point range, as indicated by the distance between the initial departure from the baseline and the peak. Isotactic polypropylene gave a somewhat broader endothermic peak at ΔT_{min} of 169°C . The end point of the transition was somewhere beyond the peak at a point not known exactly.

Ke (167) also determined the OTA curve of mixtures of polyolefins and found that the components could be identified if the melting points were sufficiently far apart. The peak areas were proportional to the amount of each component present in the mixture.

The degree of crystallinity of polyethylenes was calculated by comparing the area of the respective endothermic peak with the double peak of dotriacontane. The curve contains two peaks, the first of which is due to a chain-rotational transition a few degrees below the melting point. The resulting degree-of-crystallinity values agreed well with the literature values, as shown in Table 7.25.

The effect of diluents on the melting behavior of polyethylenes has also been studied by Ke (168). A comparison between the melting transitions of solution and melt-crystallized polyethylene has been made. The measurement of the melting and second-order transitions of polyethylene terephthalate by OTA has been studied by Scott (169). Rudin et al. (170) measured the oxidation resistance of various polymers and rubbers by a OTA method. A comparison of the melting and freezing curves before and after oxidation provided the indication of the extent to which the polymer had been damaged or oxidized.

Table 7.25. Degree of Crystallinity of Polyethylenes (167)

Polyethylene	Crystallinity (%)	
	Found	Literature
Marlex 50	91	93
Super Dyan	81	65-85
Experimental (polyethylene)	86	87
DYNH	52	40-60

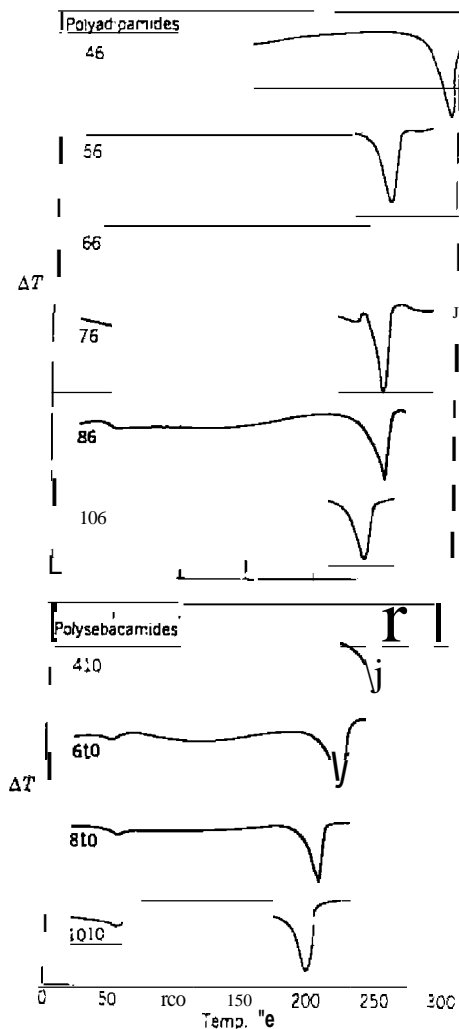


Figure 7.54. DTA curves of some polyadipamides and polysebacamides (17).

The melting and glass transitions in commercial Nylons and both homo- and copolyamides prepared by interfacial polycondensation have been studied by DTA by Ke and Sisko (171). The DTA curves for a number of the polyadipamides and polysebacamides are given in Figure 7.54.

The polyadipamides were made from diamines containing both even and odd numbers of carbon atoms and the polysebacamides from diamines containing an even number of carbon atoms. All curves exhibited a peak caused by the melting of the polymer, the melting point of which decreased with an increase in the number of carbon atoms in the diamine chain.

The application of DTA to the detection of changes induced in biphenyl, polyvinyl chloride, Teflon, and Versalube F-50 has been reported by Murphy and Hill (172). The curves for biphenyl and irradiated biphenyl are shown in Figure 7.55.

The nonirradiated sample gave a curve with two endothermic peaks which were caused by the fusion (70°C peak) and volatilization (175°C peak) of the compound. The irradiated sample gave the first two peaks, as well as an exothermic peak at about 370°C. The melting peak occurred at a slightly lower temperature. It was assumed that the 370°C exothermic peak was caused by air oxidation of the nonvolatile, radiation-induced biphenyl polymer remaining in the sample holder after volatilization of low-molecular weight materials. The lowering of the melting point was also caused by the irradiation of the sample. Similar results were noted for polyvinyl chloride samples. It was noted that by proper selection of materials on the basis of the relationship of peak area to radiation dose, DTA might be applied to dosimetry over a wide range of energy levels.

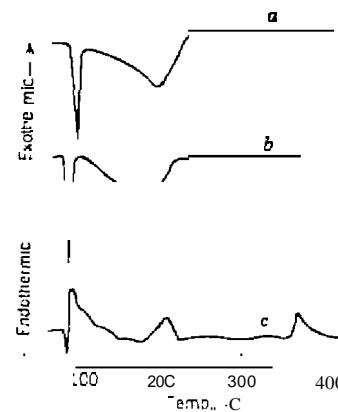


Figure 7.55. DTA curves of biphenyl: *a*, non-irradiated; *b*, irradiated; and *c*, irradiated versus nonirradiated samples (172).

A common application of DSC is the determination of the weight fraction of crystalline material in semicrystalline polymers. The method is based on the measurement of the polymer sample's heat of fusion, ΔH_f , and the plausible assumption that this quantity is proportional to the crystalline content. If by some process of extrapolation the heat of fusion, ΔH_f^c , of a hypothetical 100% crystalline sample is known, then the weight fraction of crystallinity is $\Delta H_f/\Delta H_f^c$ (155). The determination of polymer crystallinity has been reviewed by Gray (156) and Dole (157, 158).

Thus, the crystallinity of a polymer sample can be determined by measuring the total energy absorbed by the sample per gram and subtracting the amount of energy which would be absorbed by one gram of totally amorphous sample in the same temperature interval, and then dividing by the heat of fusion of 1 g of a perfectly crystalline sample. The DSC curves obtained for a semicrystalline polymer are shown in Figure 7.56. Use is made of the equation

$$x = \frac{\Delta H_{2,1} - \Delta H_{a(2,1)}}{\Delta H_f^c} \quad (7.18)$$

where x is the weight fraction at any temperature, ΔH_f^c is the heat of fusion of the perfectly crystalline sample, and $\Delta H_{2,1}$ and $\Delta H_{a(2,1)}$ are the heats of fusion of the sample and amorphous material, respectively. From the curve, $\Delta H_{2,1}$ is area ACDEF, $\Delta H_{a(2,1)}$ is area ABEF, and the difference is BCDG. Note that the correct baseline under the peak is the extrapolation of the recorded baseline from above the final melting point. It should not be drawn tangent to the pre- and postmelting lines, as is the common practice. Other procedures have been discussed by Bray (155, 156) for determining the values of the curve areas, extrapolation procedures, and so on. A computer program was also developed to aid in the crystallinity calculations.

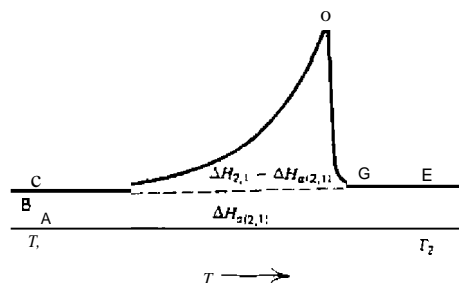


Figure 7.56. Typical DSC polymer melting curve and instrumental baseline (156).

Another method for the determination of polymer crystallinity is discussed by Duswail (159). It is based on the ability to cool a molten sample rapidly and reproducibly to a temperature where isothermal crystallization is allowed to occur. A series of crystallization curves for polyethylene obtained isothermally at various crystallization temperatures are shown in Figure 7.57. Differences in crystallizability that may be caused by branching, nuclear weight effects can be observed. The sensitivity and speed in detecting pellet-to-pellet variations in a lot of polymer are improved.

The quantitative measurement of the effect of annealing on the crystallinity of a polymer near the glass transition temperature was described by McKinney (160). The method is based on the use of the polymer as the reference material; the DSC curve for the sample is compared to the difference in heat energy between the sample and the reference material. By this technique it is possible to measure small energy differences that would appear as minor inflections on the usual procedure or as irregularities prior to the start of crystallization.

Activation energies for styrene polymerization were determined by Hoyer et al. (161). The DTA curve for the polymerization of pure styrene consists of a single exothermic peak corresponding to the onset of polymerization at 140°C. An E_a of 21.3 ± 0.6 kcal/mole was calculated.

The oxidative stability of polyethylene has been measured by Wendlandt (197), Charsley and Dunn (198, 199), and others. The most common measurements of the oxidative stability of a polymer is the oxidative induction time (OIT) utilizing DSC. The

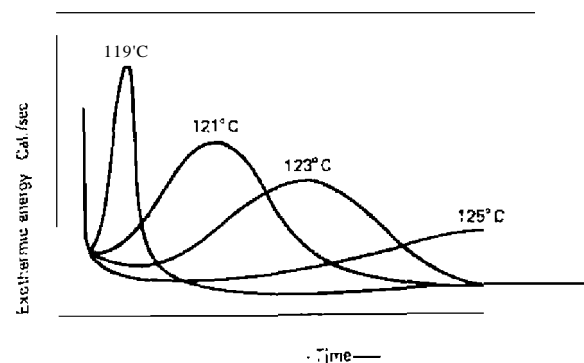


Figure 7.57. Isothermal crystallization curves for polyethylene (159).

of the test procedure that may be followed for this determination but all of them include determination of the time for which a sample is stable in an oxygen atmosphere, at an elevated temperature (197). Basically, the procedure selected for this study required heating the sample from 50°C to 200°C at a rate of 320°C/min in a dynamic oxygen atmosphere with a flow rate of 50 cm³/min and then switching to the isothermal mode. The strip-chart recorder used to receive the DSC output was activated immediately upon switching the instrument to the isothermal mode. The resulting DSC trace was characterized by a brief period during which thermal equilibrium was established followed by a flat, stable baseline during the isothermal interval until the oxidation chain reaction commenced to produce an exotherm. The residence time of the resin at 200°C prior to the onset of the exotherm is referred to as the oxidative induction time. Thus, this test has been interpreted as a titration of the surface antioxidant with oxygen gas using the DSC as a thermal indicator. Polyethylene samples containing various amounts of antioxidant additives are compared with each other using the OIT technique in Figure 7.58. The unstabilized resin failed to establish a baseline and exhibited immediate exothermicity. The induction time generally increased as the antioxidant concentration increased for the stabilized samples, as expected.

Another DSC measurement commonly used to judge the thermal or

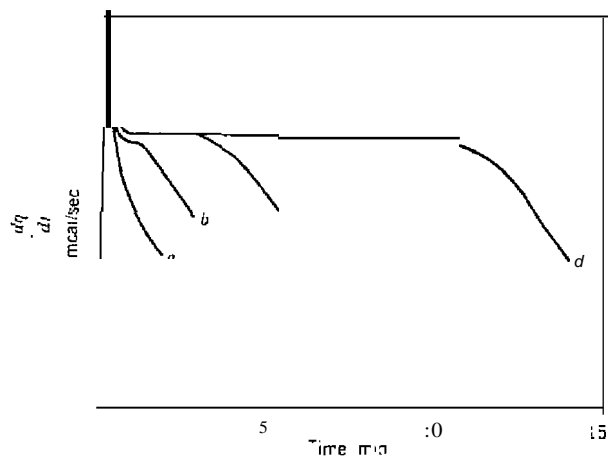


Figure 7.58. Oxidative induction time (OIT) curves for polyethylene samples containing (a) no stabilizer, (b) 0.005%, (c) 0.02%, (d) 0.05% Irganox 1010 measured by DSL. Sample weights were 5 = 1 mg (197).

oxidative stability of a resin is the onset temperature of the oxidation exotherm obtained from a standard scanning mode DSC curve of the sample, in an oxygen atmosphere. This technique offers the advantage of shorter analysis times for well-stabilized resins, whereas the effect of the antioxidant would be very persistent during the isothermal test. The DSC curves obtained for the standard polyethylene samples are shown in Figure 7.59. The onset temperatures of the exothermic peaks for these samples vary directly with the antioxidant concentrations in a relatively linear manner. Modification of such results to specific conditions for a particular resin is sometimes more difficult for this procedure than for the isothermal OIT procedure.

DSC is widely used, along with other TA techniques, to measure the glass transition, T_g , of polymers. This measurement using the DSC technique is illustrated in Figure 7.60(201). The T_g is taken as the midpoint in the curve as measured from the extensions of the pre- and posttransition baselines. The choice is somewhat arbitrary in that some investigators take the T_g as the first evidence of the displacement of the DSC curve from the pretransition baseline.

The DSC determination of many polymers has been described by numerous studies; illustrative examples are those for plasticizers such as dioethyl phthalate in poly(vinyl chloride) (202); brominated bisphenol A resin (203); cured epoxy resin (204); polystyrene (205); and others.

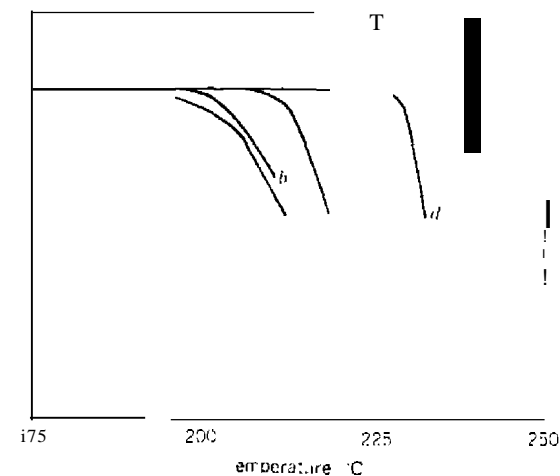


Figure 7.59. DSC curves for polyethylene with (a) no stabilizer, (b) 0.005%, (c) 0.02%, (d) 0.05% Irganox 1010 in a dynamic oxygen atmosphere with a heating rate of 10°C/hr. Sample weights were 5 = 1 mg (197).

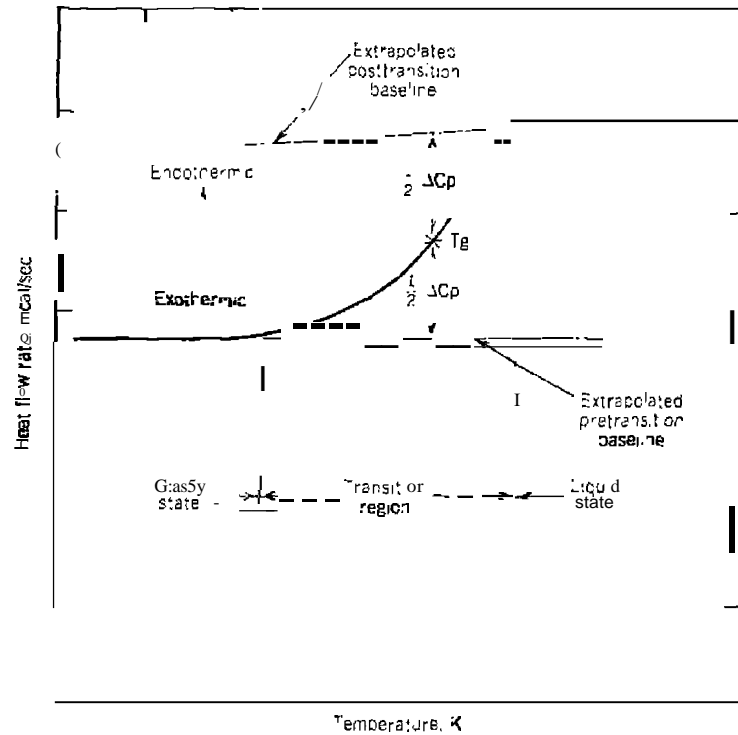


Figure 7.60. Measurement of T_g from the DSC curve (201).

DSC is widely used to predict the potential explosive hazard of materials in an ASTM method. The basis of the method, developed by Committee E 27, is the determination of the reaction kinetics using Ozawa's procedure (206). Ozawa employs a plot of the logarithm of the DSC heating rate versus the peak maxima temperatures; E , Z , k , and r can be calculated from this plot. The ASTM method has been used to evaluate the thermal stability of trinitrotoluene (207), nitrocellulose (208), and many other substances.

The determination of clustered water and water molecule clusters trapped in polyethylene have been described by Baker (209). This water has been related to a loss in the dielectric properties of polyethylene used in a submarine cable core. When DSC is employed, as shown by the curve in Figure

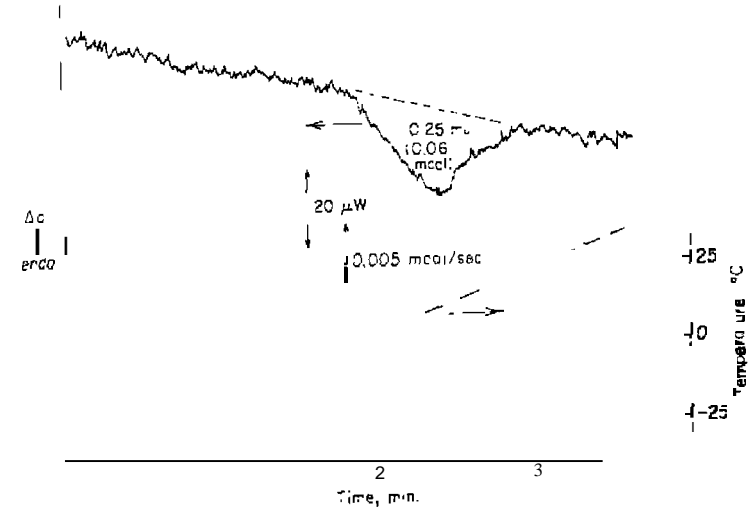


Figure 7.61. DSC curve of clustered water in polyethylene (209).

7.61, the amount of water in the clusters, C , is equal to

$$C = \frac{\Delta H_{tr}}{m\Delta H_f} \times 10^6 = \mu\text{g/g} \quad (7.19)$$

where ΔH_{tr} is the heat of transition in millijoules, m is the sample mass in milligrams, and ΔH_f is the heat of fusion of water (340.6 J/g). The DSC method is rapid and accurate, and measures only the clustered water since the sorbed water does not freeze when the polymer's temperature is lowered below the freezing point of water. Water in the clusters, however, can form sufficient bonds with other water molecules to form ice crystals when the temperature is lowered sufficiently.

The use of DSC and other TA techniques in assessment of polymer flammability has been discussed by Cullis and Hirschler (210), Haines et al. (211), and many others. DSC cannot, however, accurately represent the very complex process of polymer combustion. There is no correlation between the inflammability of different organic polymers and their thermal stability, even if the latter property is represented by an improved parameter such as the temperature at which 10% of the polymer has decomposed (210). The

technique can be useful, however, for evaluating the effects of an additive on the polymer substrate.

DSC and DTA have been widely used to study a wide variety of polymer substances. Among them are rubber (212); molding resins (113); printed circuit boards (214,215); fiber systems (216); polymer films (217); engineering thermoplastics (218); and others.

J. MISCELLANEOUS APPLICATIONS

The specific heat of a substance can be determined conveniently and rapidly using the techniques of DTA and DSC (173, 88). The method (173) is illustrated by the DuPont DSC curves for α -alumina, as given in Figure 7.62. A curve for the empty sample container is first run, as indicated by the upper curve. The sample is then placed in the sample container and its curve recorded, using the same instrument adjustments. The relationship between the "blank" (empty container) and the "sample" (empty container plus sample) then is

$$(C_p)_T \left(\frac{\text{meal}}{\text{mg}^{\circ}\text{C}} \right) = \frac{(\Delta T_x + \Delta T_{\text{blank}}) E_T}{Ma} \quad (7.20)$$

$(C_p)_T$ is the specific heat at temperature T ; ΔT_x is the absolute differential temperature for sample in $^{\circ}\text{C}$; ΔT_{blank} is the absolute differential temperature for empty container; E_T is the calibration coefficient at temperature

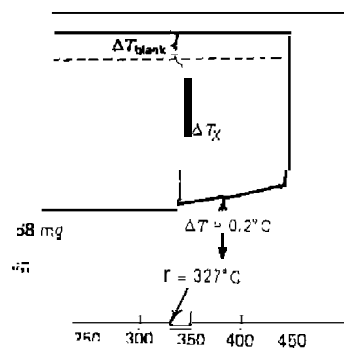


Fig. 7.62. Determination curves of α -alumina (73). $(C_p)_{327} = 0.279 \text{ meal/mg}$.

T in $\text{meal/}^{\circ}\text{C min}$; M is the sample mass in mg ; and a is the heating rate in uC/min . The $(C_p)_{327}$ of α -alumina found was 0.279 meal/mg .

DTA and DSC can be used to construct simple phase diagrams, as shown by the naphthalene-benzoic acid phase diagram in Figure 7.63.

An eutectic melting point is formed at a 50-50 mixture of the two components. The phase diagram was constructed from the melting endothermic peaks of the various mixtures, also shown in Figure 7.63. The melting temperatures in the phase diagram are the extrapolated temperatures for the onset of the melting (174, 175).

Vapor-pressure and heat-of-vaporization measurements are easily carried out using DTA (176) or DSC (99, 97) techniques. The heat of vaporization and heat of mixing of various organic liquids were obtained using DSC (97) by a small modification of the sample holder. The metallic cover on the holder was replaced by a glass cover with a glass tube at its center. This glass tube was designed to hold a microsyringe which contained the liquid sample. By this device, liquid sample could be added to the sample holder without any disturbance of the system temperature.

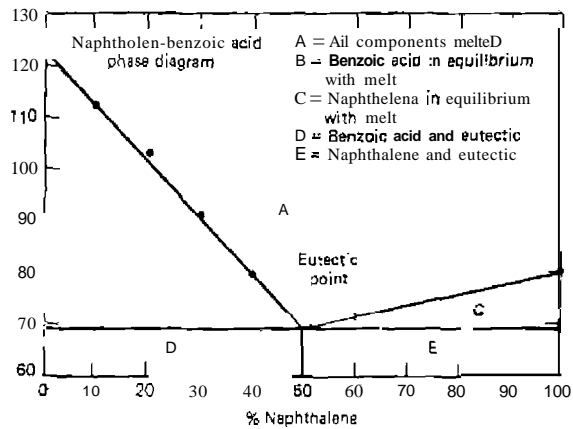
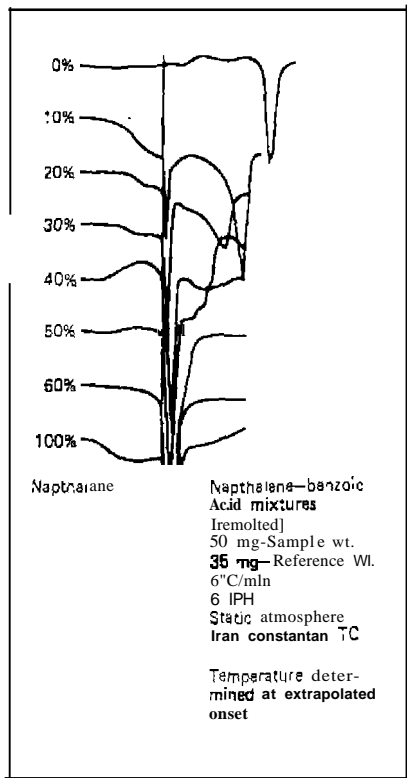
The curves for the endothermic mixing of benzene-ethanol obtained by operating the DSC cell isothermally are shown in Figure 7.64. Successive amounts of $2.4 \mu\text{l}$ of ethanol were added to $40 \mu\text{l}$ of benzene contained in the sample; the higher the ethanol concentration in the benzene is, the smaller will be the heat of mixing for the addition of the same quantity of ethanol. The molar heats of mixing

$$\Delta H_M = \Delta H_{\text{exp}}(n_1 - n_2) \quad (7.21)$$

where n_1 and n_2 are moles of ethanol and benzene, respectively, are plotted in figure 7.65. Agreement with previously reported values appears to be satisfactory.

A similar procedure was used (97) to determine the heat of vaporization of a liquid organic sample. The sample was added to the sample cell by means of the microsyringe and the curve area is proportional to the heat of vaporization. The relative standard deviation obtained for live determinations of the heat of vaporization of benzene was about $\pm 2\%$. This method cannot be used to determine ΔH_v at the boiling point of the sample, however. Boiling point values can be obtained by extrapolation procedures.

Heats of sublimation can also be obtained by the DSC technique (86). Samples were placed in aluminum pans and the space between the bottom and the domed aluminum cover was filled with powdered aluminum. The cover contained a small hole to permit evolved gases to escape. For heat-of-fusion measurements, the cover did not have a hole in it. Results of these measurements are illustrated in Table 7.26.



7.63. Phase diagram of the naphthalene-benzoic acid mixture (174, 175). Points in diagram taken from eight DTA curves.

MISCELLANEOUS APPLICATIONS

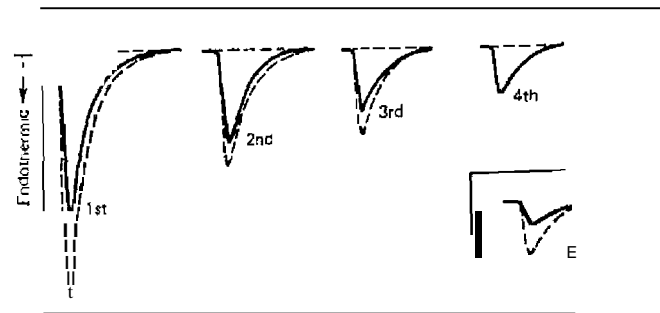


Figure 7.64. Successive additions of 4 µl of ethanol to 40 µl of benzene. Low benzene added (97).

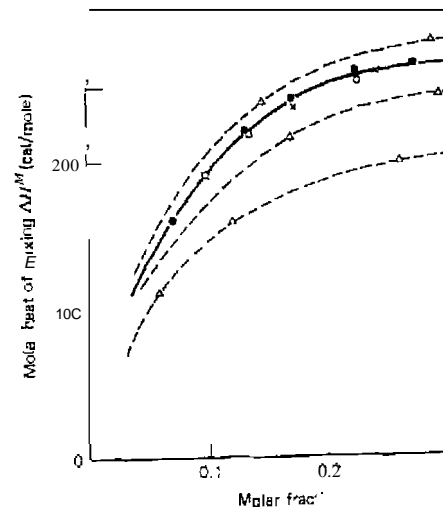


Figure 7.65. Molar heat of mixing of ethanol with benzene. --- 95 liter.

Critical temperatures of organic liquids can be determined by the method if sealed sample holders are used (87). The determination is done by use of cooling curves; a discontinuity in the curve is observed at the critical temperature, T_c . The sample, 20-50 µL, was sealed in 4-mm-diam capillary tubes and heated to a preselected temperature T_0 and then cooled while recording the ΔT signal as a function of sample temperature.

Table 7.26. Heats of Fusion, Vaporization, and Sublimation Determined by DSC (86)

Compound	Heating Rate K min ⁻¹	ΔH_{fus}	Temp. Range of Vaporization (K)	Literature Value, ΔH_{sub} (kJmol ⁻¹)	Quoted Temp. or Temp. Range of Literature Value Measurement (K)
Benzoic acid	8, 16, 32	∞		91.5	343-387
Anthraquinone		127 ± 3	470-590	89.1	299-329
Phthalic anhydride		$81 \pm 1(0.5)$	390-470	112.0	298
Thymol	2 ^o -5	46.5 ± 3.0	420-480	88.7	303-333
Ferrocene	8.5 + ^o	$65.5 \pm z$		91.3	273-313
Anthracene		84 ± 2		69.0	299-312
Naphthalene	8.9 \pm 0.2	26 ± 4		73.4	298
8-Hydroxy quinoline	22.1 \pm 0.4	78 ± 2		85.3	298
	6	78 ± 2		97.6	338-353
		68 ± 3		98.6	342-359
		95 ± 4		62.0	298
				72.7	298
				109	308-328

A sharp break in the curve corresponded to a point on the coexistence curve. The temperature corresponding to the coexistence point was determined as a function of increasing sample volume until a constant temperature (critical temperature) was achieved. The average deviation from literature value for compounds studied was $\pm 0.16^\circ\text{C}$.

Curie point temperatures can also be determined by DTA and DSC techniques. As illustrated in Figure 7.66, the specific heat of nickel, increases gradually up to the Curie point at 357°C , making a sudden change at this point. The sample size used was 75 mg.

Williams and Chamberland (140) discussed the application of DSC to the determination of Curie temperatures of ferromagnetic materials and Néel temperatures of antiferromagnetic and ferrimagnetic materials.

One of the more recent and interesting applications of DTA and DSC is to problems in archaeology. Pope (249) and Bayer and Wiedemann (250) have reviewed the many investigations that have been made to date. These studies have been concerned with applications to medieval glass, Egyptian papyrus, sands and clays found at archaeological sites, Nabatean pottery, Egyptian pigments, ancient wax binders in paint pigments, and others. One example of these studies is illustrated by the DTA curves of pressed and beaten papyrus sheets, as illustrated in Figure 7.67 (251). The difference between the lignin peaks or the pressed and beaten papyrus is caused by mechanical destruction of the material, which results in a lowering of the heat of combustion. The small endothermic peak at 140°C is caused by the dehydration of calcium oxalate I-hydrate. This observation agrees with the well-known fact that sedge, reed, and papyrus contain oxalic acid that can form calcium oxalate with calcium from the soil.

The use of DTA and DSC to study reactions in the formation of the pigment, Egyptian blue, have been previously discussed in Chapter 4 [252,

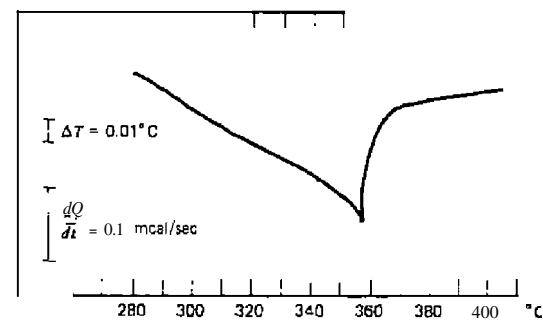


Figure 7.66. Curie point determination of nickel.

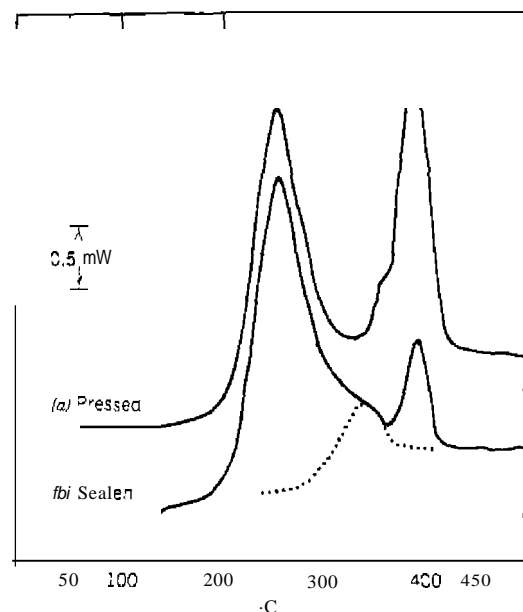


Figure 7.67. DTA curves of (a) pressed and (b) beaten papyrus sheets (2511).

The surface and bulk crystallization of $\text{Li}_2\text{O}\cdot 2\text{SiO}_2$ glass has been studied by DTA by Marotta and co-workers (253-255). DTA curves of as-quenched and nucleated $\text{Li}_2\text{O}\cdot 2\text{SiO}_2$ glasses are shown in Figure 7.68, whereas the peak temperatures and kinetics parameters are presented in Table 7.27. In fine and coarse powdered samples, surface nucleation is dominant (large peak) due to the high specific surface area of the samples and the short time of bulk nucleation. In the bulk sample, the small number of bulk nuclei is comparable with that of the surface nuclei due to the very low specific area of the sample. The DTA peak is thus narrower and shifted toward higher temperatures than those of powdered glasses. After a long heat treatment at the temperature of maximum nucleation rate, bulk nucleation is dominant in the bulk sample. These samples are comparable to the surface of the coarse powdered sample in which the DTA peaks are narrower and shifted toward lower temperatures than those of the as-quenched samples. In the fine powdered samples, the shape and peak temperatures are not changed by heat treatment.

The application of DTA and TG to glass has been briefly reviewed (256).

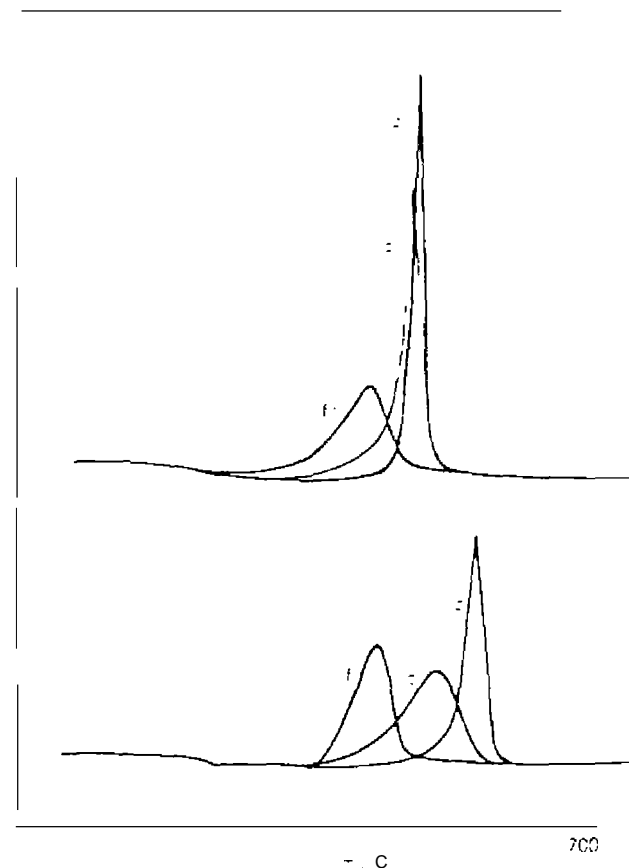


Figure 7.68. DTA curves of $\text{Li}_2\text{O}\cdot 2\text{SiO}_2$ glass at $5^\circ\text{C}/\text{min}$. (f) fine powder; (b) bulk powder; (b) bulk samples; (f) nucleated samples (253).

DSC was used to evaluate materials for latent heat thermal energy storage. The screening method, as described by Takakashi et al. (257), is outlined in Figure 7.69. Relationships connected by solid lines are usually investigated first. Among them are data concerning temperatures of transition and fusion and the latent heats involved. Some 3000 thermodynamic data have been listed in order of temperature, as well as the promising latent heats and transitions, in the temperature range from 100 to 1000°C and latent heat range 200 kJ/kg for fusion and 100 kJ/kg for transition (258).

Table 7.27. DTA Peak Temperatures and Kinetics Plottings for $\text{Li}_2\text{O} \cdot 25\text{SiO}_2$ Glass (253)

Samples	Q			N		
	T_p	E	n	T_p	E	n
Fine powder	583	70	1.2	579	63	1.0
Coarse powder	620	61	1.0	609	72	2.7
Bulk	650	40	2.7	614	59	3.9

Q = as-quenched samples; N - nucleated samples.
 T_p = DTA (5°C min^{-1}) peak temperature ($^\circ\text{C}$).
 E - activation energy (kcal mole⁻¹); n - JMA equation parameter.

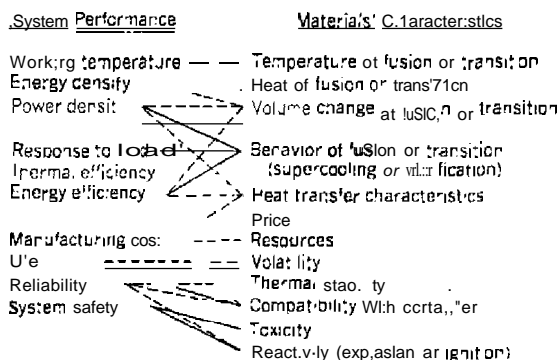


Figure 7.69. Relationship between the performance of the thermal energy storage system and the characteristics of the materials (257).

Promising materials for thermal energy storage include polyethylene (257) and others listed in Table 7.28 (259).

The thermal properties of explosives and propellant compositions are widely studied by DTA and DSC. Fauth (47) recorded the DTA curves of some hydrazine, guanidine and guanidinium picrates, styphnates, and sulfates. The decomposition temperatures found were generally considerably lower than those reported in the literature. Other picrates, those with thallium, ammonium, tetramethylammonium, and tetraethylammonium, were studied by Stammler (27). David (28) and Bohon (29) examined the thermal behavior of explosives and propellants under various external pressures up

Table 7.28. Promising Materials for Thermal Energy Storage in the Lower Temperature Range (259)

Materials	Melting Temp.	Heat of fusion		
	($^\circ\text{C}$)	(J/g)	(J/cm ³)	
Hydrocarbons	$\text{C}_{14} \sim \text{C}_{16}$ paraffine	2 ~ 7	152	119 ^a
	$\text{C}_{15} \sim \text{C}_{15}$ paraffine	4 ~ 10	153	119 ^a
	I-decano!	5 ~ 7	206	171 ^a
Cathrate compounds	C_{14} paraffine	2 ~ 5	165	127 ^a
	C_{15} paraffine	14 ~ 18	201	156 ^a
	$\text{SOI} \cdot 6\text{H}_2\text{O} (> 1 \text{ atm})$	7	247	
Inorganic salt hydrates	$\text{C}_2\text{H}_6\text{O} \cdot 17\text{H}_2\text{O}$	4.4	255	
	$(\text{CH}_3)_2\text{N} \cdot 10\frac{1}{2}\text{H}_2\text{O}$	5.9	239	
	$(\text{C}_4\text{H}_9)_4\text{NCHO}_2 \cdot 32\text{H}_2\text{O}$	12.5	184	
	$(\text{C}_4\text{H}_9)_4\text{NCHICO}_2 \cdot 32\text{H}_2\text{O}$	15.1	209	
	$\text{Na}_2\text{SO}_4 \cdot 10\text{H}_2\text{O} / \text{NaCl} / \text{NH}_4\text{Cl}$	13	180	
	$\text{CaCl}_2 \cdot 6\text{H}_2\text{O}$	29	180	301 ^b
	$\text{Na}_2\text{SO}_4 \cdot 10\text{H}_2\text{O}$	32.4	251	389 ^b
	$\text{Na}_2\text{CO}_3 \cdot 10\frac{1}{2}\text{H}_2\text{O}$	32.0	247	355 ^b
	$\text{Na}_2\text{HPO}_4 \cdot 12\text{H}_2\text{O}$	36	280	423 ^b
	$\text{Ca}(\text{NO}_3)_2 \cdot 4\text{H}_2\text{O}$	43	142	259 ^b
Inorganic eutectic mixtures	$\text{Na}_2\text{S}_2\text{O}_3 \cdot 5\text{H}_2\text{O}$	48.5	200	342 ^b
	$\text{NaCH}_2\text{COO} \cdot 3\text{H}_2\text{O}$	58	251	364 ^b
	$\text{Ba}(\text{OH})_2 \cdot 8\text{H}_2\text{O}$	78	293	640 ^b
	$\text{Sr}(\text{OH})_2 \cdot 8\text{H}_2\text{O}$	88	352	670 ^b
	$\text{Mg}(\text{NO}_3)_2 \cdot 6\text{H}_2\text{O}$	89	160	234 ^b
	$\text{KAl}(\text{SO}_4)_2 \cdot 12\text{H}_2\text{O}$	91	232	406 ^b
	$\text{NH}_4\text{Al}(\text{SO}_4)_2 \cdot 12\text{H}_2\text{O}$	94	251	409 ^b
	$\text{MgCl}_2 \cdot 6\text{H}_2\text{O}$	117	172	271 ^b
	$\text{KNO}_3 - \text{LiNO}_3$	100	138	332 ^b
	$\text{KNO}_3 - \text{LiNO}_3 - \text{NaNO}_3$	118	165	365 ^b
Polymers	High-density polyethylene	120 - 140	184 ~ 209	176 - 193

^aLatent heat per unit volume of melt.
^bLatent heat per unit volume of solid.

to 3000 psig using DTA. Heats of explosion and/or decomposition were determined. Decomposition of primary explosives employing a remotely operated DTA cell was described by Graybush et al. (30).

The phase transitions and dissociation reactions of organic explosive materials have been extensively investigated by DTA and DSC. Hall (40)

studied the processes of solid phase transition, fusion, and decomposition in several nitramines by DSC. Compounds investigated include .V-picryl-N-methylnitramine, 1,3,5-trinitroso-1,3,5,7-tetraazacyclooctane, and others. Rogers and Smith (41) studied a similar group of compounds and estimated the preexponential factor from the DSC curve. Rogers and Dinegar (42) determined the heat of fusion and other parameters of pentaerythritol tetranitrate (PETN) by DSC.

The application of DTA to criminalistics has been described by Helmitz (261),

Earnest (260) described a number of experiments involving DTA for undergraduate chemistry laboratories.

Reviews of applications of DTA, DSC, and other TA techniques, to various technological areas include: cements (262-264); electrical and electronics industries (265); automotive industries (266); and industrial raw materials (267).

REFERENCES

1. Gamel, C. M., and W. J. Smothers, *Anal. Chim. Acta*, 6,442 (1952).
2. Mitchell, B. D., and A. C. Bimie, in *Differential Thermal Analysis*, R. C. Mackenzie, ed., Academic, London, 1970, Chap. 22.
3. Manning, M., *Ind. Res.*, Feb. 1966, p. 18.
4. Gray, A. P., *Am. Lab.*, Jan. 1971, p. 43.
5. Murphy, C. B., *Anal. Chem.*, 38, 443R (1966).
6. Murphy, C. B., *Anal. Chem.*, 40, 380R (1968).
7. Murphy, C. B., *Anal. Chem.*, 42, 268R (1970).
8. Murphy, C. B., *Anal. Chem.*, 44, SUR (1972).
9. Brancone, L. M., and H. I. Ferrari, *Microchem. J.*, 10, 370 (1966).
10. Vassallo, D. A., and J. C. Harden, *Anal. Chem.*, 34, 1321 (1962).
11. Kerr, G., and P. S. Landis, *Anal. Chem.*, 44, 1176 (1972).
12. Barrall, E. M., I. F. Gernert, R. S. Porter, and J. F. Johnson, *Anal. Chem.*, 35, 837 (1963).
13. Barrall, E. M., R. S. Poner, and I. F. Johnson, *J. Phys. Chem.*, 70, J8S (1966).
14. Barrall, E. M., R. S. Porter, and I. F. Johnson, *J. Phys. Chem.*, 68, 2810 (1964).
15. Johnson, J. F. and G. W. Miller, *Thermochim. Acta*, 1, 373 (1970).
16. Gipstein, E., E. M. Barrall, K. Bredfeldt, and O. U. Need, *Thermochim. Acta*, 1, 253 (1972).
17. Ennujat, R. D., in *Analytical Calorimetry*, R. S. Porter, and I. F. Johnson, eds., Plenum, New York, 1968, p. 219.
18. Young, W. R., E. M. Barrall, and A. Aviram, in Ref. 17, Vol. 2, p. 1-3.
19. Barrall, E. M., Ref. 18, p. 12L.
20. Gipstein, E., E. M. Barrall, and K. E. Bredfeldt, Ref. 18, p. 127.
21. Gray, G. W., *J. Chem. Soc.*, 3733, 1956.
22. Barrall, E. M., R. S. Porter, and I. F. Johnson, *Anal. Chem.*, 36, 2172 (1964).

23. Ozawa, T., *Bull. Chem. Soc. Jpn.*, 39, 2071 (1966).
24. Pacor, P., *Anal. Chim. Acta*, 37, 200 (1967).
25. David, D. J., *Anal. Chim. Acta*, 36, 2162 (1964).
26. Harmelin, M., C. Duvaux, and N. D. Xuong, *Proc. Jrd. Anal. Chem. Conf.*, Budapest, 1970, Akademiai Kiado, 1970, p. 325.
27. Stamerler, M., *Explosivstoffe*, 7, 154 (1968).
28. David, D. J., *Anal. Chem.*, 37, 82 (1965).
29. Bohon, R. L., *Anal. Chem.*, 35, 1845 (1963).
30. Graybush, R. J., F. G. May, and A. C. Forsyth, *Thermochim. Acta*, 2, 153 (1971).
31. Barrall, E. M., *Thermochim. Acta*, 3, 55 (1972).
32. Barrett, E. I., H. W. Hoyer, and A. V. Santoro, *Mikrochim. Acta*, 121, 1970.
33. Santoro, A. V., E. J. Barrett, and H. W. Hoyer, *J. Thermal Anal.*, 2, 461 (1970).
34. Barrett, E. J., H. W. Hoyer, and A. V. Santoro, *Tetrahedron Lett.*, 5, 603 (1968).
35. Sanwro, A. Y., E. I. Barrett, and H. W. Hoyer, *Tetrahedron Lett.*, 19, 2297 (1968).
36. Koch, L., *Angew. Chem. Int. Educ.*, 9, 288 (1970).
37. Breger, I. A., and W. L. Whitehead, *Fuel*, 30, 247 (1951).
38. Levy, P. F., G. Nieuweboer, and L. C. Semanski, *Thermochim. Acta*, 1, 429 (1970).
39. Barrall, E. M., *Thermochim. Acta*, 5, 377 (1973).
40. Hall, P. G., *Trans. Faraday Soc.*, 67, 556 (1971).
41. Rogers, R. N., and L. C. Smith, *Anal. Chem.*, 39, 1024 (1967).
42. Rogers, R. N., and R. H. Dinegar, *Thermochim. Acta*, 3, 367 (1972).
43. Murrill, E., and L. Breed, *Thermochim. Acta*, 1, 239 (1970).
44. Ref. 43, p. 409 (1970).
45. Murrill, E., M. E. Whitehead, and L. Breed, *Thermochim. Acta*, 3, 1-11 (1972).
46. Ripmeester, J. A., and B. A. Dunell, *Can. J. Chem.*, 49, 2906 (1971).
47. Fauth, M. I., *Anal. Chem.*, 32, 655 (1960).
48. Chiu, J., *Anal. Chem.*, 34, 1841 (1962).
49. Dorko, E. A., R. S. Hughes, and C. R. Downs, *Anal. Chem.*, 42, 253 (1970).
50. Giil, P. S., *Application Brief No. T4 38*, Du Pont Co., Wilmington, DE.
51. Brown, M. E., D. Dollimore, and A. K. Galwey, *Thermochim. Acta*, 21, 103 (1977).
52. Rajeshwar, K., and E. A. Sacco, *Can. J. Chem.*, 55, 2620 (1977).
53. Ref. 52, p. 2628.
54. Dollimore, D., J. P. Gupta, and D. V. Nowell, *Thermochim. Acta*, 30, 339 (1979).
55. Biswas, P. K., A. Roy, and K. Nag, *Thermochim. Acta*, 42, 91 (1980).
56. Garguli, P., R. M. Iyer, and U. R. K. Rao, *Thermochim. Acta*, 45, 55 (1981).
57. Gordon, S., *J. Chem. Educ.*, 40, A87 (1963).
58. Kracek, F. C., *J. Phys. Chem.*, 11, 1281 (1929).
59. Kracek, F. C., *J. Phys. Chem.*, 34, 225 (1930).
60. Wendlandt, W. W., and J. A. Hoiberg, *Anal. Chim. Acta*, 28, 506 (1963).
61. Wendlandt, W. W., and J. A. Hoiberg, *Anal. Chim. Acta*, 29, 539 (1963).
62. R. C. Mackenzie, ed., *Differential Thermal Analysis*, Academic, New York, 1970, Chaps. 7-15.
63. Kramer, C. M., A. Munir, and J. V. Volpone, *Thermochim. Acta*, 55, 11 (1982).
64. Furuchi, R., T. Ishii, Z. Yamanaka, and M. Shimokawa, *Thermochim. Acta*, 51, 245 (1981).

65. Gray, A. P. *Thermal Analysis Application Study 1*, Perkin-Elmer Corp., Norwalk, CT.
66. Deshpande, V. V., M. D. Kirlkhanavala, and U. R. K. Rao, *J. Thermal Anal.* 6, 613 (1974).
67. Wang, E. Y., *J. Electrochem. Soc.*, 123,435(1976).
68. Barnes, P. A. and M. R. Tomlinson, *J. Thermal Anal.*, 7, 469 (1975).
69. Barnes, P. A., and F. S. Stone, *Thermochim. Acta*, 4, 105 (1972).
70. Tissot, P. J. Painot, J. P. Rivera, and H. Schmid, *Thermochim. Acta*, 56, 359 (1982).
71. Gallagher, P. K., *Thermochim. Acta*, 29, 165 (1979).
72. Cavell, K. J. J. O. Hill, and R. J. Magee, *Thermochim. Acta*, 33, 3831(1979).
73. Mesmer, R. E. and R. R. Irani, *J. Chem. Eng. Data*, 8, 530 (1963).
74. Ozawa, T., M. Momota, and H. Isozaki, *Bull. Chem. Soc. Jpn*, 40, 1583 (1967).
75. Ozawa, T., H. Isozaki, and A. Negishi, *Thermochim. Acta*, 1, 545 (1970).
76. Kelley, K. K., *Bull. U.S. Bur. Mines*, 584, (1960).
77. Sokolov, V. A., and N. F. Schmidt, *Izv. Sek. Fiz. Khim. Anal., Inst. Obshch. Neorg. Khim., Akad. Nauk. SSSR*, 27, 217 (1956); *Chem. Abstr.*, 50, 15200h (1956).
78. Barrall, F. M., and L. B. Rogers, *Anal. Chem.*, 36, 1405 (1964).
79. Wendlandt, W. W., *Thermochim. Acta*, 1, 419 (1970).
80. Wendlandt, W. W., G. D'Ascenzo, and R. H. Gore, Ref. 79, p. 488.
81. Wendlandt, W. W., G. D'Ascenzo, and R. H. Gore, *J. Inorg. Nucl. Chem.*, 32, 3404 (1970).
82. Chiu, J., *Anal. Chem.*, 35, 933 (1963).
83. *Du Pont DTA Apparatus Bulletin*, Du Pont Co., Wilmington, DE.
84. Macak, I., and I. Malecha, *Anal. Chem.*, 41, 442 (1969).
85. *Du Pont Application Brief*, No. 900831, July 1970.
86. Beech, G., and R. M. Lintonbon, *Thermochim. Acta*, 2, 86 (1971).
87. Hoyer, H. W., A. V. Salltoro, and E. J. Barrett, *J. Phys. Chem.*, 72, 4312 (1968).
88. Gray, A. P., *Perkin-Elmer Instrument News*, 16, No. 2 (1970).
89. Beech, G., C. T. Mortimer, and E. G. Tyler, *J. Chem. Soc.*, (A) 925 (1967).
90. Beech, G., S. J. Ashcroft, and C. T. Mortimer, Ref. 89, p. 929.
91. Beech, G., C. T. Mortimer, and E. G. Tyler, Ref. 89, p. 111.
92. Ashcroft, S. J., *J. Chem. Soc.*, (A) 10201(1970).
93. Ashcroft, S. J. and C. T. Mortimer, *Thermochemistry of Transition Metal Complexes*, Academic, London, 1970.
94. Adams, J. J., and J. E. House, *Trans. III. State Acad. Sci.*, 63, 83 (1970).
95. Simchen, A. E., *Isr. J. Chem.*, 9, 613 (1971).
96. Block, J., *Anal. Chem.*, 37, 1414 (1965).
97. Mita, I., I. Imai, and H. Kambe, *Thermochim. Acta*, 2, 337 (1971).
98. Peercciani, J. C., S. E. Wimberley, W. H. Bauer, and T. W. Clapper, *J. Phys. Chem.*, 64, 1309 (1960).
99. Farrator, R. F., and L. C. Tao, *Thermochim. Acta*, 1, 297 (1970).
100. Erdy, L., and F. Pallik, *Acea Chim. Acad. Sci. Hung.*, 7, 27 (1955).
101. Murray, J. P., and J. O. Hill, *Thermochim. Acta*, 63, 211 (1983).
102. Allen, E. A., and J. Del Gaudio, *J. Chem. Soc., Dalton Trans.*, 1356 (1975).
103. Brown, M. E., C. P. J. Van Vuufen, and A. I. thauer, *Thermochim. Acta*, 49, 247 (1981).

104. Salas-Peregrin, J. M., E. Colacio-Rodriguez, J. D. Lopez-Gonzalez, and C. Valenzuela-Calahorro, *Thermochim. Acta*, 63, 145 (1983).
105. Salas-Peregrin, J. M., M. A. Romero-Molina, C. Valenzuela-Calahorro, and I. D. Lopez-Gollale, *Thermochim. Acta*, 61, 307 (1983).
106. *Fisher DTA Instrument Bulletin*, Fisher Scientific Co., Pittsburgh, PA.
107. Keith, M. L., and O. F. Tuttle, *Am. J. Sci., Bowen Vol.*, 203(1952).
108. Salas-Peregrin, J. M., C. Valenmela-Calahorro, and F. Girela Vilchez, *Thermochim. Acta*, 58, 61 (1982).
109. Collins, I. W., *Combust. Flame*, 41, 325 (1981).
110. Scanes, F. S., *Combust. Flame*, 23, 3631(1974).
111. Charsley, E. L., C. T. Cox, M. R. Ollaway, T. J. Bar: on, and M. Jenkins, *Thermochim. Acta*, 52, 321 (1982).
112. Boddington, T., P. G. I. aye, H. Morris, C. A. Rosser, E. L. Charsley, M. C. Ford, and D. F. Tolhurst, *Combust. Flame*, 24, 137 (1975).
113. Gam, P. D., and S. S. Flaschen, *Anal. Chem.*, 29, 271 (1957).
114. Loddig, W., and L. Hammel, *Anal. Chem.*, 32, 657(1960).
115. Berg, I. G., and I. S. Rassonskaya, *Dokl. Akad. Nauk. SSSR*, 73, 113 (1950).
116. Bollin, E. M., J. A. Dunne, and P. F. Kerr, *Science*, 131, 661 (1960).
117. Bollin, E. M., and P. F. Kerr, *Am. Mineral.*, 46, 823 (1961).
118. Mitchell, B. D., and A. C. Birnie, in *Differential Thermal Analysis*, R. C. Mackenzie, ed., Academic, London, 1970, Chap. 24.
119. Pfeil, R. W., in *Proceedings of the Third Toronto Symposium on Thermal Analysis*, H. G. McAdie, ed., Chemical Institute of Canada, Toronto, 1969, p. 187.
120. *Du Pont Application Brief No. 20*, Du Pont Co., Wilmington, DE, 1968.
121. Haighton, A. J., and I. Hannewijk, *J. Am. Oil Chem. Soc.*, 35, 457 (1958).
122. Currell, B. R., and B. Robinson, *Talanta*, 14, 421(1967).
123. Gam, P. D., *Thermoanalytical Methods of Investigation*, Academic, New York, 1965, p. 124.
124. Edmonds, M. D., M. T. Core, A. Bauley, and R. F. Schwenker, *Tobacco Sci.*, 9, 48 (1965).
125. Hoyer, H. W., and E. J. Barrett, *Anal. Biochem.*, 17, 344 (1966).
126. Sleim, M., *Perkin-Elmer Instrument News*, 19, No. 2 (1968).
127. Puett, S., *Biopolymers*, 5, 327 (1967).
128. Hoyer, H. W., *J. Am. Chem. Soc.*, 90, 2480 (1968).
129. Hoyer, H. W., *Nature*, 216, 997(1967).
130. Moore, R., in *Thermal Analysis*, R. F. Schwenker and P. D. Garn, eds., Vol. 1, Academic, New York, 1969, p. 615.
131. Greaves, R., and J. Davies, *Ann. N. Y. Acad. Sci.*, 125, 548 (1965).
132. Luebke, H. W., and B. G. Breidenbach, *J. Am. O. [Chem. Soc.]*, 46, 60 (1969).
133. Cross, C. K., *J. Am. Oil Chem. Soc.*, 47, 229 (1970).
134. Arseneau, D. F., *Can. J. Chem.*, 39, 1915 (1961).
135. Pakulak, J. M., and G. W. Leonard, *Allal, Chem.*, 31, 5037 (1959).
136. Mitchell, B. D., and Birnie, A. C., *Analyst*, 91, 783 (1966).
137. Berlin, E., P. Kliman, and M. J. Pallansch, *Thermochim. Acta*, 4, 11 (1972).
138. Labowitz, L. C., *Thermochim. Acta*, 14(1911)72),

139. Berlin, E., P. G. Kijman, B. A. Anderson, and M. J. Pallansch. *Thermochim. Acta*, 2, 143 (1971).
140. Williams, H. W., and B. L. Chamberland. *Anal. Chem.*, 41, 2084 (1969).
141. Olafsson, P. G., and A. M. Bryan. *Mikrochim. Acta*, 871 (1970).
142. Morita, N. *J. Am. Chem. Soc.*, 78, 1197 (1956).
143. Morita, H. *Anal. Chem.*, 28, 64 (1956).
144. Morita, H. *Anal. Chem.*, 29, 1095 (1957).
145. Schulken, R. M., R. E. Roy, and R. H. Cox. *J. Polymer Sci.*, Part C, 6, 1725 (1964).
146. Ke, B., ed. *Thermal Analysis of High Polymers*, Wiley-Interscience, New York, 1964.
147. Slade, P. E., and L. T. Jenkins, eds. *Techniques and Methods of Polymer Evaluation*. Marcel Dekker, New York, 1966.
148. Schwenker, R. F., ed. *Thermoanalysis of Fibers and Fiber-Forming Polymers*, Wiley-Interscience, New York, 1966.
149. Porter, R. S., and I. F. Johnson, eds. *Analytical Calorimetry*, Plenum, New York, 1968.
150. Ref. 149, Vol. 2, 1970.
151. Reich, L. and S. S. Slivala. *Elements of Polymer Degradation*, McGraw-Hill, New York, 1971.
152. Schwenker, R. F. and P. D. Garn, eds. *Thermal Analysis*, Academic, New York, 1969. Vol. 1. Section 2.
153. Murphy, C. B., in *Differential Thermal Analysis*, R. C. Mackenzie, ed., Academic, London, 1970. Chap. 23.
154. Chlu, J. *Du Pont Thermogram*, 2, No. 1, 9 (1965).
155. Gray, A. P., *Perkin-Elmer Instrument News*, 20, No. 2, 8 (1969).
156. Gray, A. P., *Thermochim. Acta*, 1, 563 (1970).
157. Dole, M., *J. Polym. Sci., Part C*, 18, 57 (1967).
158. Dole, M., *Fortschr. Hochpolym. Forsch.*, 2, 221 (1960).
159. Duswalt, A. A., *Hercules Chem.*, No. 57.51 (1968).
160. Foltz, C. R., and P. V. McKinney. *Anal. Chem.*, 41, 687 (1969).
161. Hoyer, H. W., V. Santoro, and E. A. Barrett. *J. Polym. Sci., Part A-1*, 6, 1033 (1968).
162. Anderson, H. C., *Anal. Chem.*, 32, 1592 (1960).
163. Murphy, C. B., J. A. Palm, C. D. Doyle, and E. M. Curtiss. *J. Polym. Sci.*, 28, 447 (1958).
164. Ref. 163, p. 453.
165. Clampton, B. H. *Anal. Chem.*, 35, 577 (1963).
166. Schwenker, R. F., and L. R. Beck. *Tex. Res. J.*, 30, 624 (1960).
167. Ke, B. *J. Polym. Sci.*, 42, 1511 (1960).
168. Ke, B. *J. Polym. Sci.*, 50, 79 (1961).
169. Scott, N. D., *Polymer*, 1, 1141 (1960).
170. Rudin, A., H. P. Schreiber, and M. H. Waldman, *Ind. Eng. Chem.*, 53, 117 (1961).
171. Ke, B., and A. W. Sisko. *J. Polym. Sci.*, 50, 87 (1961).
172. Murphy, C. B., and J. A. Hill. *Nucleonics*, 18, 78 (1960).
173. *Du Pont Thermal Analysis Application Brief*, No. 1, Jan. 15, 1968.
174. *Fisher DTA Instrument Bulletin*, Fisher Scientific Co.

175. Visser, M. J., and W. H. Wallace. *Du Pont Thermogram*, 3, No. 19 (1966).
176. Kemmer, H. R., and S. I. Kreps. *Anal. Chem.*, 41, 1869 (1969).
177. Charsley, E. L., J. M. Jerkins, and P. G. Laye. *Application Note 251*, Stanton Redcroft, London.
178. Sastri, M. N., and I. O. Hill. *J. Thermal Anal.*, II, 323 (1977).
179. Tanaka, H. *Thermochim. Acta*, 43, 289 (1980).
180. Rajeshwar, K., V. R. Pai Yrnekker, and J. Kubow. *Combust. Flame*, 37, 25 (1980).
181. Syal, S. K., and S. R. Yoganasimhan. *Inorg. Nucl. Chem. Lett.*, 9, 119J (1973).
182. Markowitz, M. M., D. A. Boryta, and M. Harris. *J. Phys. Chem.*, 65, 261 (1961).
183. Pearson, G. S., *Oxid. Combust. Rev.*, 4, 1 (1969).
184. Kishore, K., V. R. Pai Verneker, and V. K. Mohan. *Thermochim. Acta*, 13, 277 (1975).
185. Dollimore, D., and G. R. Heal. *Lab. Practice*, 30, 221 (1981).
186. Mackenzie, R. C., *Eighth Conf. Clay Mineral. Petrol.*, Teplice, 1979, p. 9.
187. Mackenzie, R. C., and S. Cailere. *Soil Components*. J. E. Gieseking, ed., Vol. 2, Springer-Verlag, New York, 1975. Chap. 16.
188. Mackenzie, R. C., *Proc. 10th IETA Conf.*, B. Miller, ed., Vol. 1, Wiley, New York, 1982, p. 25.
189. Earnest, C. M., *Thermochim. Acta*, 63, 291 (1983).
190. Earnest, C. M., *Thermal Analysis Application Study 10*, Perkin-Elmer Corp., Norwalk, CT.
191. Dunn, J. G., *Technical Information Sheet No. 139*, Stanton Redcroft Ltd., London.
192. Selmezi, B., *Hung. Sci. Instr.*, 21, 39 (1971).
193. Pauik, I., and F. Paulik, *Simultaneous Thermoanalytical Examination by means of the Derivatograph*, W. W. Wendt, ed., Vol. XII, Elsevier, Amsterdam, 1981, Chaps. 13, 14.
194. Dunn, J. G., and C. E. Kelly. I. *Thermal Anal.*, 18, 147 (1980).
195. Dunn, J. G., B. T. Sturman, and W. Van Bronswijk. *Thermochim. Acta*, 37, 317 (1980).
196. Ramachandran, V. S., and G. M. Pojornark. *Thermochim. Acta*, 25, 611 (1978).
197. Collins, L. W., and W. W. Wendt, *J. Chem.*, 22, 233 (1982).
198. Charsley, E. L., and J. G. Dunn. *J. Thermal Anal.*, 17, 535 (1979).
199. Charsley, E. L., and J. G. Dunn. *Application Note 252*, Stanton Redcroft Ltd., London.
200. Blaine, R. L., *Application Brief/So. TA 40*, Du Pont Co., Wilmington, DE.
201. Brennan, W. P., *Thermal Analysis Application Study 7*, Perkin-Elmer Corp., Norwalk, CT.
202. Brennan, W. P., *Thermal Analysis Application Study II*, Perkin-Elmer Corp., Norwalk, CT.
203. Riesen, R., *Mettler Application No. 3402*, Mettler Instrument Corp., Greifensee, Switzerland.
204. Riesen, R., and H. Wyden. *Mettler Application No. 3408*, Mettler Instrument Corp., Greifensee, Switzerland.
205. Richardson, M. J., and N. G. Savill, II, *J. Thermal Anal.*, 11, 123 (1979).
206. Ozawa, T., *J. Thermal Anal.*, 9, 217 (1976).
207. Baker, K. F., *Application Brief No. TA 43*, Du Pont Co., Wilmington, DE.

208. Corssel, R. S., *Perkin-Elmer Thermal Analysis Application Study 28*, Perkin-Elmer Corp., Norwalk, CT.
209. Baker, K. F., *Application Brief No. TA 70*, Du Pont Co., Wilmington, DE.
210. Cuijis, C. F., and M. M. Hirschler, *Polymer*, 24, 834 (1983).
211. Haines, P. J., T. J. Lever, and G. A. Skinner, *Thermochim. Acta*, 59, 331 (1982).
211. Dunn, I. G., *Tech. Inform. Sheer No. 104*, Stanton Redcroft Ltd., London.
213. Riesen, R., and H. Sommerauer, *Am. Lib.*, Jan. 1983, p. 28.
214. Fruh, P., and G. Widmann, *Am. Lab.*, Jan. 1982, p. 93.
215. Fruh, P., and G. Widmann, *Mer/ler Applicatioll No. 3406*, Mettler Instruments Corp., Griefensee, Switzerland.
216. Brennan, W. P., *Thermal Analysis Application Study 6*, Perkin-Elmer Corp., Norwalk, CT.
217. Brennan, W. P., *Thermal Analysis Application Study 15*, Perkin-Elmer Corp., Norwalk, CT.
218. Brennan, W. P., *Thermal Analysis Application Study 22*, Perkin-Elmer Corp., Norwalk, CT.
219. Blankenhorn, P. R., R. C. Baldwin, W. Merrill, and S. P. Ottone, *Wood Sci.* 13, 26 (1980).
220. Anon., *Tech. Inform. Sheet No. 9*, Stanton Redcroft Ltd., London.
221. Anon., *Mettler Application No. 3001*, Mettler Instruments Corp., Griefensee, Switzerland.
222. Hassel, R. L., *Application Brief No. TA 48*, Du Pont Co., Wilmington, DE.
223. Bihara-Varga, M., *J. Thermal Anal.*, 23, 7 (1982).
224. Deckelbaum, R. J., G. G. Shipley, D. M. Small, R. S. Lees, and P. K. George, *Science*, 190, 392 (1975).
225. Cassel, R. S., *Thermal Analysis Application Study 5*, Perkin-Elmer Corp., Norwalk, CT.
226. Cassel, R. B., *Thermal Analysis Application Study 4*, Perkin-Elmer Corp., Norwalk, CT.
227. Biliaderis, C. G., *Food Chem.*, 10, 239-119g31.
228. Raemy, A., and P. Lambellet, *J. Food Technol.*, 17, 45L (1982).
229. Raemy, A., and J. Lolger, *Cereal Chem.*, 59, 189 (1982).
230. Brennan, W. P., *Thermal Analysis Application Study 16*, Perkin-Elmer Corp., Norwalk, CT.
231. Brennan, W. P., *Thermal Analysis Application Study 18*, Perkin-Elmer Corp., Norwalk, CT.
232. Joseph, I. T., A. Hybl, and J. H. Flynn, *Chem. Phys. Lipids*, 22, 239 (1978).
233. Baker, K. F., *Application Brief No. TA-53*, Du Pont Co., Wilmington, DE.
234. Chlu, J., *Thermochim. Acta*, 26, 57 (1978).
235. Rajeshwar, K., D. B. Jones, and J. B. DuBow, *Anal. Chem.*, 53, 121 (1981).
236. Cassel, B., W. P. Brennan, and R. L. Fyans, Preprint paper No. 570, Pittsburgh Conference, March 1978.
237. Jones, D. B., K. Rajeshwar, and J. B. DuBow, *Ind. Eng. Chem. Prod. Res. Dev.*, 19, 125 (1980).
238. Barr, J. B., and I. C. Lewis, *Thermochim. Acta*, 52, 297 (1982).

239. Rosenvold, R. J., J. B. DuBow, and K. Rajeshwar, *Thermochim. Acta*, 53, 321 (1982).
240. Fyans, R. L., *Thermal Analysis Application Study 21*, Perkin-Elmer Corp., Norwalk, CT.
241. Hassel, R. L., *Application Brief No. TA-55*, Du Pont Co., Wilmington, DE.
242. Noel, F., and G. E. Cranton, *Am. Lab.*, June 1979, 27.
243. Walker, J. A., and W. Tsang, *Society of Automotive Engineers, Inc.*, Fuels and Lubricants, Baltimore, MD, Oct. 20-23, 1980, No. 801383.
244. Blaine, R. L., *Application Brief No. TA 41*, Du Pont Co., Wilmington, DE.
245. Moynihan, C. T., M. R. Shahriari, and T. Bardakei, *Thermochim. Acta*, 52, 131 (1982).
246. Doilimore, D., and J. M. Hoath, *Thermochim. Acta*, 45, 87 (1982).
247. Gray, G. W., *Tech. Inform. Sheet No. 14*, Stanton Redcroft Ltd., London.
248. Brennan, W. P., and A. P. Gray, *Thermal Analysis Application Study 13*, Perkin-Elmer Corp., Norwalk, CT.
249. Pope, M. I., *Second European Symposium on Thermal Analysis*, D. Dollimore, ed., Heyden, London, 1981, 603.
250. Bayer, G., and H. G. Wiedemann, *Thermochim. Acta*, 69, 167 (1983).
251. Wiedemann, H. G., *Anal. Chem.*, 55, 1220A (1983).
252. Wiedemann, H. G., and G. Bayer, *Anal. Chem.*, 54, 619A (1982).
253. Marotta, A., A. Buri, and F. Branda, *Thermochim. Acta*, 40, 397 (1980).
254. Marotta, A., A. Buri, and F. Branda, *J. Thermal Anal.*, 21, 227 (1981).
255. Marotta, A., A. Buri, and F. Branda, *J. Mater. Sci.*, 16, 341 (1981).
256. Anonymous, *Technical Information Sheet No. 3*, Stanton Redcroft Ltd., London.
257. Takahashi, Y., R. Sakamoto, M. Kamimoto, K. Kanari, and T. Ozawa, *Thermochim. Acta*, 50, 31 (1981).
258. Kamimoto, M., K. Sabuta, T. Ozawa, and R. Sakamoto, *Circ. Elecrotech. Lab. No.* 196 (1978).
259. Ozawa, T., *Third Japan Symposium on Thermophys. Prop.*, 531 (1982).
260. Earnest, C. M., *J. Clem. Educ.*, 9, A 33 (1978); 10, A 373 (1978).
261. Helmitz, G., *Experim. Tech.*, 37, 343 (1979).
262. Whitehead, M. B., and G. A. Russell, *Am. Lab.*, Jan. 1979, p. 37.
263. Brown, R. A., and B. Cassel, *Am. Lib.*, Jan. 1979, p. 45.
264. *Tech. Inform. Sheer No. 6*, Stanton Redcroft Ltd., London.
265. Brennan, W. P., and R. B. Cassel, *Am. Lab.*, Jan. 1979, p. 80.
266. Brennan, W. P., unpublished communication, March 1978.
267. Earnest, C. M., W. P. Brennan, and M. P. DiVito, *PilCSBllrgh Conf. Pap.* 975, Atlantic City, NJ, March 7-11, 1983.
268. Radecki, A., and M. Wesolowski, *J. Thermal Anal.*, 17, 73 (1979).
269. Tomassetti, M., G. D'Ascenzo, and R. Currini, *Thermochim. Acta*, 60, 1 (1983).
270. Khattab, F. I., *Thermochim. Acta*, 61, 253 (1983).
271. Wesolowski, M., *Mikrochim. Acta*, 1982, 451.
272. Kuhner-Brandst3neL M., and F. Proli, *Wirochim. Acta*, 463 (1983).
273. Ref. 272, p. 287.
274. van Dooren, A. A., *Drug Dev. Ind. Pharm.*, 9, 43 (1983).

275. Gram, D. J. W., and I. K. A. Abovgela. *Anal. Proc.* Dec. 1982, p. 545.
276. Liversidge, G. G. D. J. W. Grant, and J. M. Padfield. *Anal. Proc.* Dec. 1982, p. 549.
277. Smith, A., *Anal. Proc.* Dec. 1982, p. 559.
278. Brennan, W. P., *Thermal Analysis Application Study 17*, Perkin-Elmer Corp., Norwalk, CT.
279. Daiy, K. F., *Am. Lab.*, Jan, 1975, p. 35.
280. *Mettler Application No. 201*, Mettler Instrument Corp., Griefensee, Switzerland.
281. Locke, C. E., and H. F. Rase, *Ind. Eng. Chem.* 60, 515 (1960).
282. Gallagher, P. K., D. W. Johnson, and E. M. Vogel, *Caralysis in Organic Syntheses*-1976, Academic, New York, 1976, 113.
283. Dunn, J. G., *Tech. Inform. Sheet No. 103*, Stanton Redcroft Ltd., London.
284. Ishii, T., R. Furuchi, and K. Kobayashi, *Thermochim. Acta*, 9, 39 (1974).
285. Hassel, R. L., *Application Brief No. TA-31*, Du Pont Co., Wilmington, DE.
286. Johnson, D. W., and P. K. Gallagher, *Thermochim. Acta*, 7, 303 (1973).
- 187, Gallagher, P. K., and D. W. Johnson, *Thermochim. Acta*, 15, 238 (1976).
288. Rowse, J. R., and W. B. Jepson, *J. Thermal Anal.* 4, 169 (1972).
289. Yang, R. T., M. Steinberg, and R. Smol, *Anal. Chem.* 48, 1696 (1976).
290. Wendlandt, W. W., *Thermochim. Acta*, 10, 101 (1974).
291. Reddy, M. R., R. A. Geanangel, and W. W. Wendlandt, *Thermochim. Acta*, 25, 117 (1978).
292. Warkentin, R. H., A. M. Wynne, and W. W. Wendlandt, *Thermochim. Acta*, 14, 99 (1976).
293. Wendlandt, W. W., and L. W. Collins, *Thermochim. Acta*, 100, 4111 (1974).
294. Wendlandt, W. W., *Thermochim. Acta*, 10, 93 (1974).
295. Collins, L. W., and W. W. Wendlandt, *Thermochim. Acta*, 11, 253 (1975).

CHAPTER

8

EVOLVED GAS DETECTION AND
EVOLVED GAS ANALYSIS

A. INTRODUCTION

The detection or analysis of the gases evolved during a chemical reaction, as a function of temperature, constitute the techniques of thermal analysis called evolved gas detection (EGD) and evolved gas analysis (EGA), respectively. These techniques, which paralleled the development of modern thermal analysis instrumentation, are currently used to solve many types of problems in thermal analysis. They are not so widely employed as DTA, DSC, TG, or perhaps other thermal analysis techniques, but they may be very useful in solving many types of TA problems. Although there are no reliable data available as to the number of publications pertaining to EGD-EGA techniques during the past several years, the number appears to be increasing greatly. According to a list of books published by Lombardi (3), there appears to be only one book available on EGD-EGA, Lodding's *Gas Effluent Analysis* (4), published in 1967. There are a number of book chapters such as those by Wendlandt (5, 6), Kenyon (7), Kiran and Gilham (8), Chiu (9), and Langer (128). Reviews have been written by Murphy (10, III), Chiu and Palemo (12), Ware (13), Redfern (14), Mackenzie (15), Friedman (16), Paulik and Paulik (129), and Holdiness (166).

B. DEFINITION OF EGD AND EGA

The International Confederation of Thermal Analysis (ICTA) nomenclature committee (17) defined EGD and EGA as:

Evolved Gas Detection (EGD). This term covers any technique of detecting whether or not a volatile product is formed during thermal analysis.

Evolved Gas Analysis (EGA). A technique of determining the nature and amount of volatile product or products formed during thermal analysis.

There are numerous other names for EGD and EGA in the literature.

CHEMICAL ANALYSIS

A SERIES OF MONOGRAPHS ON
ANALYTICAL CHEMISTRY AND ITS APPLICATIONS

Editors

P. J. ELVING, J. D. WINEFORDNER

Editor Emeritus: I. M. KOITHOFF

Advisory Board

Fred W. Billmeyer, Jr.

Eli Grushka

Barry L. Karger

William Krivan

Victor G. Mossotti

A. Lee Smith

Bernard Tremillon

T. S. West

VOLUME 19

A WILEY-INTERSCIENCE PUBLICATION

JOHN WILEY & SONS

New York / Chichester / Brisbane / Toronto / Singapore

Thermal Analysis

THIRD EDITION

WESLEY WM. WENDLANDT

*Department of Chemistry
University of Houston
Houston, Texas*



A WILEY-INTERSCIENCE PUBLICATION

JOHN WILEY & SONS

New York • Chichester • Brisbane • Toronto • Singapore

275. Grant, D. I. W. and I. K. A. Abovgeia, *Anal. Proc.*, Dec, 1982, p. 545.
 276. Liversidge, G. G., D. J. W. Grant, and J. M. Padfield, *Anal. Proc.*, Dec, 1982, p. 549.
 277. Smith, A., *Anal. Proc.*, Dec, 1982, p. 559.
 278. Brennan, W. P., *Thermal Analysis Application Study 17*, Perkin-Elmer Corp., Norwalk, CT.
 279. Daly, K. T., *Am. Lab.*, Jan. 1975, p. 35.
 280. *Mettler Application No. 801*, Mettler Instrument Corp., Griesensee, Switzerland.
 281. Locke, C. E., and H. F. Rase, *Ind. Eng. Chem.*, **60**, 515 (1960).
 282. Gallagher, P. K., D. W. Johnson, and E. M. Vogel, *Catalysis in Organic Syntheses—1976*, Academic, New York, 1976, 1:3.
 283. Dunn, J. G., *Tech. Inform. Sheet No. 103*, Stanton Rectror: Ltd., London.
 284. Ishii, T., R. Furuchi, and K. Kobayashi, *Thermochim. Acta*, **9**, 39(1974).
 285. Hassel, R. L., *Application Brief No. TA-31*, Du Pont Co., Wilmington, DE.
 186. Johnson, D. W., and P. K. Gallagher, *Thermochim. Acta*, **7**, 303 (1973).
 287. Gallagher, P. K., and D. W. Johnson, *Thermochim. Acta*, **15**, 2381(1976).
 288. Rowse, J. B., and W. B. Jepson, *J. Thermal Anal.*, **4**, 169 (1972).
 289. Yang, R. T., M. Steinberg, and R. 50101, *Anal. Chem.*, **48**, 1596 (1976).
 290. Wendlandt, W. W., *Thermochim. Acta*, **10**, 101 (1974).
 291. Reddy, M. R., R. A. Geanangel, and W. W. Wendlandt, *Thermochim. Acta*, **25**, 117 (1978).
 292. Warkentin, R. H., A. M. Wynne, and W. W. Wendlandt, *Thermochim. Acta*, **14**, 99 (1976).
 293. Wendlandt, W. W., and L. W. Collins, *Thermochim. Acta*, **10**, 411 (1974).
 294. Wendlandt, W. W., *Thermochim. Acta*, **10**, 93 (1974).
 295. Collins, L. W., and W. W. Wendlandt, *Thermochim. Acta*, **11**, 253 (1975).

CHAPTER

8

EVOLVED GAS DETECTION AND
EVOLVED GAS ANALYSIS

A. INTRODUCTION

The detection or analysis of the gases evolved during a chemical reaction, as a function of temperature, constitute the techniques of thermal analysis called evolved gas detection (EGD) and evolved gas analysis (EGA), respectively. These techniques, which paralleled the development of modern thermal analysis instrumentation, are currently used to solve many types of problems in thermal analysis. They are not so widely employed as TGA, DSC, TG, or perhaps other thermal analysis techniques, but they may be very useful in solving many types of problems. Although there are no reliable data available as to the number of publications pertaining to EGD-EGA techniques during the past several years, the number appears to be increasing greatly. According to a list of books published by Lombardi (3), there appears to be only one book available on EGD-EGA, Lodding's *Gas Effluent Analysis* (4), published in 1967. There are a number of book chapters such as those by Wendlandt (5, 6), Kenyon (7), Kiran and Gilham (8), Chiu (9), and Langer (128). Reviews have been written by Murphy (10, 11), Chiu and Palemo (12), Ware (13), Redfern (14), Mackenzie (15), Friedman (16), Paulik and Pallik (129), and Holdiness (166).

B. DEFINITION OF EGD AND EGA

The International Confederation of Thermal Analysis (ICTA) nomenclature committee (17) defined EGD and EGA as:

Evolved Gas Detection (EGD). This term covers any technique of detecting whether or not a volatile product is formed during thermal analysis.

Evolved Gas Analysis (EGA). A technique of determining the nature and amount of volatile product or products formed during thermal analysis.

There are numerous other names for EGD and EGA in the literature.

Names rejected by the IeTA committee were effluent gas detection, effluent gas analysis, thermovaporimetric analysis, and thermohygroscopic analysis. Also, terms such as mass spectrometric thermal analysis (MTA) and mass spectrometric differential thermal analysis (MDTA) should be avoided. Unfortunately, new names for the techniques are constantly being created, such as thermal evolution analysis (TEA). The technique of TEA, according to Chiu (18), includes all techniques that monitor continuously the amount of volatiles thermally evolved from the sample upon programmed heating.

The techniques of EGD and EGA are almost always used in conjunction with other thermal analysis techniques or multiple techniques. In multiple techniques, two options are possible: (1) One sample may be employed for all the measurements or (2) two or more samples, one for each technique, may be employed. To distinguish between the two modes, the terms *simultaneous* will be used for the application of two or more techniques to the same sample at the same time. The term *combined* will indicate the use of separate samples for each technique. Multiple techniques are indicated by the acceptable abbreviation for each technique such as TG-EGD, TG-DTA-EGD-MS, EGA-MS, and so on. Other terms that may be employed by the EGD-EGA techniques are:

1. *Sample*. The actual material investigated, whether diluted or undiluted.
2. *Heating Rate*. The rate of temperature increase, which is customarily quoted in degrees per minute using either Celsius ($^{\circ}\text{C}$) or Kelvin (K) scales. The heating rate is said to be constant when the temperature-time curve is linear.

McAfee (19) listed the IeTA recommendations for reporting EGD and EGA data. These recommendations are:

1. An identification of all substances (sample, reference, diluent) by a definitive name, an empirical formula, or equivalent compositional data.
2. A statement of the source of all substances, and the details of their histories, pretreatments, and chemical purities, so far as these are known.
3. A clear statement of the temperature environment of the sample during reaction.
4. A measurement of the average rate of linear temperature change over the temperature range involving the phenomena of interest. Non-linear temperature programming should be described in detail.

5. A statement of the dimensions, geometry, and materials of the sample where applicable.
6. An identification of the abscissa scale in terms of time or temperature at a specified location. Time or temperature should be plotted to increase from left to right.
7. An identification of the ordinate scale in specific terms where possible. In general, increasing concentration of *evolved* gas should be plotted upward. For gas density detectors, increasing gas density should also be plotted upward. Deviations from these practices should be clearly marked.
8. A statement of the methods used to identify intermediate or final products.
9. A faithful reproduction of all original records.
10. An identification of the sample atmosphere by pressure, composition, and purity, and by whether the atmosphere is self-generated or dynamic through or over the sample. The flow rate, total volume, construction, and temperature of the system between the sample and detector should be given, together with an estimate of the time delay within this system.
11. An identification of the apparatus used by type and commercial name, together with details of the location of the temperature-measuring thermocouple and the interface between the systems for sample heating and detecting or measuring evolved gases.
12. The relationship between signal magnitude and concentration of species measured should be stated in the case of EGA. When exact units are not used. For example, the dependence of the flame ionization signal on the number of carbon atoms and their bonding, as well as on concentration, should be given.

C. ROLE OF EGD-EGA IN THERMAL ANALYSIS

One of the original uses of modern EGD was to aid in the interpretation of OTA data. Using simultaneous OTA-EGD, Ayres and Bens (20) found that if an EGD peak was absent, while the DTA curve contained an endothermic or exothermic peak, it could be concluded that some type of phase transition had occurred in the sample. If curve peaks were found over the same temperature region for both EGD and OTA curves, some type of decomposition reaction involving volatile reaction products had occurred. A comparison of EGD and DTA curves is given in Table 8.1. Note that fusion and solid \rightarrow

Table 8.1. EGD and DTA Curve Peaks During Chemical or Physical Transition (20)

Chemical or Physical Transition	DTA Peak	EGO Peak	
		Yes	No
Decomposition	X ^b	X	X ^a
Fusion	X		X
Solid ₁ → Solid ₂	X ^b		X
Desorption	X	X	X
Vaporization			
Desolvation	X	X	
Effluvia	X	X ^c	
Sublimation	X	X ^c	

^aProduct may be solid or condense before reaching detector.

^bMay be exothermic or endothermic peak.

^cPossible condensation before reaching detector.

solid₂ transitions do not normally evolve volatile products and hence would not produce a peak in the EGD curve. Decomposition and desorption reactions may or may not yield EGD peaks depending on the nature of the reaction products. There is always the possibility, of course, that the evolved products will not reach the detector due to condensation. This was circumvented by use of heated exit lines and also an in-line heated CuO combustion chamber to fragmentize large molecular mass compounds.

The use of an inexpensive EGD detector system was of great use in interpreting DTA and DSC curves and many commercial instruments included the latter as an accessory. Since TG data are mainly concerned with the evolution of volatile products, EGD is not a useful accessory for this technique. However, the TG curve cannot normally give unequivocal answers as to the composition of the evolved gaseous products and this is where the role of EGA becomes important. By analyzing the evolved gaseous products by some analytical technique such as titrimetric, chromatographic, gas density, mass spectrometry, infrared, and so on, one can usually deduce the reaction pathway. For example, take the case of the thermal dissociation of $[\text{Cu}(\text{NH}_3)_4]\text{SO}_4 \cdot \text{H}_2\text{O}$. Since water and ammonia have similar molecular masses, 18 and 17 amu, respectively, it is difficult to distinguish between them on the basis of TG data alone. When the EGA technique employing mass spectrometry (MS) is used, however, the MS data can easily distinguish between the two compounds. Likewise, if a complex mixture of reaction

products is evolved, a preliminary separation by gas chromatography might be carried out followed by positive identification of each of the products by mass spectrometry (GC-MS). Unfortunately, the coupling of MS or GC-MS to the thermobalance does not fall into the classification of an "inexpensive" addition such as was advocated for the DTA-EGD combined technique. A less expensive alternative might be a chemical detector based on titrimetry or a specific ion electrode. Also, a relatively inexpensive gas density detector may be employed.

The principal role of EGD and EGA is mainly as complementary techniques for other thermal analysis data. Samples are studied by TG, DTA, DSC and other thermal analysis techniques first and if the decomposition reactions are unknown, EGA is usually called on to determine the composition of the reaction products. With these known, as well as the other physico-chemical data, the chemical pathway of the reaction can usually be elucidated. As mentioned earlier, the EGO-EGA data can often be obtained simultaneously with the other thermal data using multiple techniques with a substantial saving of time and effort.

O. HISTORICAL REVIEW

According to Mackenzie (21), the first evolved gas analysis experiments were carried out by Wedgwood (22) between 1782-1786. Wedgwood developed a pyrometer based on the firing of a triangular shaped piece of china clay. After firing, the shrinkage of the clay permitted him to calculate the temperature of the furnace in degrees Wedgwood. Unfortunately, his method gave highly erroneous results since the melting point of cast iron was determined to be about 10,000°C. Despite its inaccuracy, his pyrometer enabled numerical values to be assigned to high temperatures.

Not only did this illustrious pioneer develop a pyrometer and temperature scale, but he had also foreseen the development of the thermal analysis techniques of dilatometry, thermogravimetry, and evolved gas analysis. Of most interest here is EGA in which he took one of the china clay pieces and heated it in a sealed vessel attached to a bladder. The contents of the bladder were then analyzed for any evolved gases. Unfortunately, water vapor was not detected during the heating of the clay.

The development of EGD-EGA closely paralleled the introduction of controlled furnace atmosphere DTA and other thermal analysis techniques. In 1927, Oreel and Caillere (23) pointed out the importance of controlling the furnace atmosphere in DTA experiments on metallic chlorides. Some 20 years later, Berg (24) described perhaps the first EGD apparatus in which he

measured the volumes of the various gases evolved in the stepwise heating of a substance.

The most rapid period of growth of the technique, especially in the United States, began in the early 1950s and continued through the mid-1960s. In 1949, Rowland and Jones (25) developed a DTA apparatus with atmosphere control and used it to study the thermal dissociation of clays. This apparatus was perhaps the inspiration for Stone (26) who developed his dynamic gas DTA apparatus in 1952. Stone (27) probably envisioned the EGD technique but unfortunately did not monitor the composition of the evolved gases from the enclosed furnace chamber. Thus, he narrowly missed being the father of this useful technique. In 1960, Lodding and Hammell (28) placed a thermal conductivity detector on the gas outlets of a DTA apparatus (29). This apparatus is shown in Figure 8.1. The furnace was constructed of alumina and could be used at pressures up to 500 psig at a temperature of 1200°C. Gases introduced into the furnace chamber flowed through the sample and the reference material and exited the chamber separately. It was stated that the gas detection and analysis system permitted determination of the origins of the DTA curve peaks. No continuous EGD curves were described, however, but absorption tubes placed in the gas outlets were used to analyze the evolved gases.

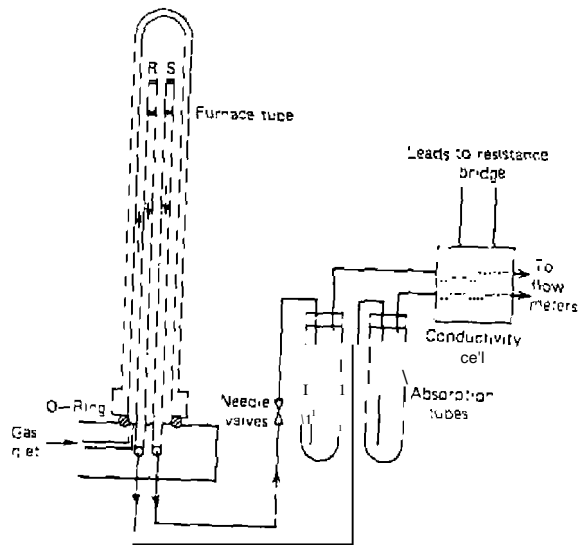


Figure 8.1. Combined DTA-EGA apparatus of Lodding and Hammell (28).

The simple pyrolysis apparatus described by Rogers et al. (30) in 1960 led to the birth of the modern EGD technique. The apparatus they developed, as shown in Figure 8.2, is based on three primary sections: (1) an electrically heated pyrolysis chamber, (2) a combustion tube, and (3) a thermal conductivity cell. The pyrolysis chamber contained a rather long gas inlet tube that served as a preheater for the carrier gas. It was heated by two 240-W cartridge heaters whose voltage input was controlled by a variable-voltage transformer. The combustion tube was a 5-in. segment of nickel tube that was heated by a resistance wire heater. It was filled with a mixture of fire brick and copper (III) oxide which was maintained at a temperature of 650-750°C. The purpose of this tube was to convert all volatile products into simple gases so that they would not condense in the tubes before reaching the detector. The thermal conductivity detector used model airplane glow plugs as detector elements; it was isolated from the pyrolysis chamber and combustion tube and maintained at room temperature. Voltage output from the detector was recorded on the Y axis of an X-Y recorder, whereas the temperature, as detected by a Chromel-Alumel thermocouple, was recorded on the X axis.

The EGD curves obtained on this apparatus resemble the derivative of TG curves. Results are not normally comparable to those obtained with DTA where products are contained. The qualitative effects of the operating vari-

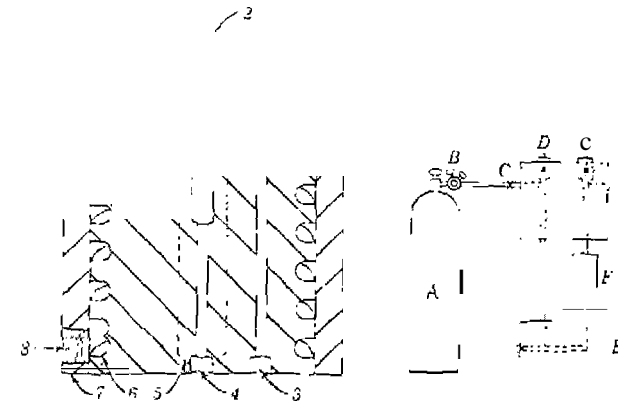


Figure 8.2. Pyrolysis block and accessory apparatus as described by Rogers et al. (30). Pyrolysis chamber: 2, nickel plug; 1, carrier gas inlet; 4, carrier gas outlet; 2, cartridge heater wires; 6, helical threads cut in inner body of block; 7, outer shell of block; 8, cooling jacket inlet; 9, cooling jacket outlet. A, carrier gas supply; B, pressure regulator; C, flow-control needle valve; D, reference thermal conductivity; E, pyrolysis chamber; F, combustion tube; G, active cell; H, manometer; I, pressure-control needle valve; J, rotameter.

abies (flow rate, heating rate, sample mass, thermal conductivity cell sensitivity, pressure, and carrier gas) on the nature of the EGD curves were determined. These variables, with the exception of the variation in thermal conductivity cell sensitivity, affected the peak maximum temperatures and peak heights.

In 1961, an apparatus similar to that of Rogers et al. (30) was described by Vassallo (31) for studying the pyrolysis of various polymeric materials. The detection system consisted of a thermistor thermal conductivity cell, rather than the model airplane glow plugs previously employed. It was stated that EGD cannot replace TG, but for comparing polymers of similar structure, it had more discrimination and was rapid. A mass-loss of 0.2 mg could be detected at much faster heating rates than those used in TG.

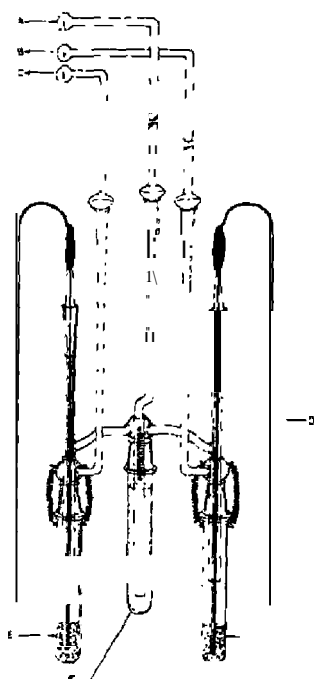


Figure 8.3. Sample and reference cell used by Ayres and Bens (5). A, sweeping gas inlet; B, gas strain to detector, sample; C, gas train to detector, reference; D, thermocouple probe leads; E, reference cell with glass beads; F, sweeping gas preheater, with glass wool; G, sample cell, with sample and glass beads.

One of the first systems for determining simultaneous EGD-DTA curves of a sample was that described by Ayres and Bens (20). This apparatus, as shown in Figure 8.3, permitted the continuous monitoring of the evolved gases and also selective sampling of any desired portion of the gases, as well as providing for obtaining the DTA curve. The sample and reference holders were all constructed of Pyrex glass and were connected to a glass manifold by standard taper glass joints. Evolved gases were detected with a thermal conductivity cell. Glass beads (0.1 mm in diameter) were used as the sample diluent and inert reference material.

Ayres and Bens (20) pointed out that difficulties were observed in their system because of increased vaporization of the sample due to the gas flow and the occasional condensation of this vapor in the cool part of the exit tube. The vaporization of the sample below the boiling point made boiling-point determinations difficult, whereas the condensation of sample before passage through the gas detector presented difficulties, since later the gas stream may become hot enough to decompose the condensate.

In 1962, Wendlandt (32) described a more robust EGD-DTA system in which the furnace system was constructed of nickel or stainless steel. The sample and reference substances were placed in small Inconel cups, which seated directly onto the differential thermojunctions, as shown in Figure 8.4. Helium was used as the carrier gas and the evolved gases were detected with a thermistor thermal conductivity cell.

Langer and Gohlke (33) described the first modern coupling of EGA with mass spectrometry in 1963. They heated the sample, by means of a small furnace in the vacuum chamber of a time-of-flight mass spectrometer and recorded the mass spectra of the decomposition products at selected inter-

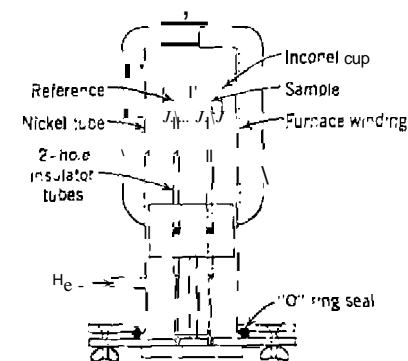


Figure 8.4. Combined EGD-DTA apparatus described by Wendlandt (32).

vals. Combining the preceding technique with DTA, Gohlke and Langer (34) described the first EGD-DTA-MS apparatus in 1966. They coined the term *mass spectrometric differential thermal analysis* to describe this technique. Simultaneously, Wendlandt et al. (35) described an EGD-OTA-MS apparatus that permitted the MS data to be obtained simultaneously with the EGO and OTA curves.

The first combination of thermogravimetry (TG) and a mass spectrometer was by Zitomer (36) in 1968 who coupled a Ou Pont thermobalance with a time-of-flight mass spectrometer. He applied the technique to the thermal decomposition of various polymers. Lastly, Wiedemann (37) described an elaborate TG-OTA-EGO-MS system in 1969. The system consisted of a Mettler thermoanalyzer couple to a Balzer quadrupole mass spectrometer that permitted the sample to be studied at low (10^{-6} Torr) or normal (1 atm) pressures.

E. CURRENT EGO-EGA TECHNIQUES

There are many different instrumental techniques presently being used for EGO and EGA. Almost any technique for determining the amount or composition of a gaseous substance can or has been employed. Perhaps the most widely used detector for EGO is the thermal conductivity detector (TCD), whereas for EGA, it is mass spectrometry. A large number of different types of mass spectrometers has been employed, including time-of-flight, magnetic sector, quadrupole, and others. A partial list of current techniques that are used in EGO and EGA is given in Table 8.2.

There are numerous other types of special identification detectors that can be used for EGO or EGA. These detectors, which are used widely in gas

Table 8.2. Techniques Used in EGD and EGA

Technique	Type	Reference	Comments
Differential thermal gas analysis	EGA	(38)	Concentration change of gas in a reactor gas stream
Elemental analysis IPyrochromJ	EGA	(49)	Functional group and C, H, N, & ar.alysis
Evolved radioactive gas	EGD	(48)	Evolution thermal analysis
Flame ionization detection	EGD	(55)	Sometimes called thermal evolution analysis
Gas chromatography	EGA		Many different columns and detectors are used

Table 8.2.

Technique	Type	Reference	Comments
Gas density detector	EGD or EGA		Use is difficult for mixtures
Infrared spectroscopy	EG, \	(53)	Either direct or indirect detection
Mass spectrometry	EGA	(34)	Use of many different types of mass spectrometers
Molecular weight chromatography (mass chromatography)	EGA	(16)	Gives molecular masses, absolute quantities, and GC retention times
Piezoelectric detection	EGA	(42)	Specific detection of SO ₂ , NO ₂ , and NH ₃
Photometric detector	EGO	(39)	Detects smoke density
Pressure changes	EGD	(41)	Various pressure transducers may be used
Pyrolysis-gas chromatography	EGA		Identification of separate pyrolysis fragments usually not made
Specific gas detector	EGA		Thermal response due to reaction with liquid or solid reagents
Specific ion electrodes	EGA	(52)	Has been used for F ⁻ and Cl ⁻ determinations
Special identification detectors	EGA		See Table 8.3
Thermal conductivity detector	EGD	(47)	May be thermistor or hot wire type
Thermal energy analyzer	EGA	(45)	Specific for N-nitroso functionality
Temperature programmed reduction	EGD	(46)	Catalyst reduction can be studied
Thermoparticulate analysis	EGO or EGA	(43) (44)	Detection of particulate matter; ion chamber detector may be employed
Thermal volatilization analysis	EGA	(51)	PiranL gauge used for pressure measurement
Thin-layer chromatography	EGA	(56)	Good for separation of mixtures of large organic molecules
Titrimetry	EGA	(50)	Titration with various reagents
Volume change	EGO	(40)	Constant pressure system employed

Table 8.3. Special Identification Detectors (57)

Entity	Technique
Elements	
1. Halides, P, S, and N	Microcoulometric titration
2. Certain elements	Flame photometric detector
3. Phosphorus compounds	Thermionic detector
4. Halogens, P, and S	Microwave emission detector
Organic compounds with high electron affinity (alkyl halides, conjugated carbonyls, nitriles, organometallic, many sulfur compounds)	Electron capture detector
Aromatic compounds	Spectrofluorimetric detector

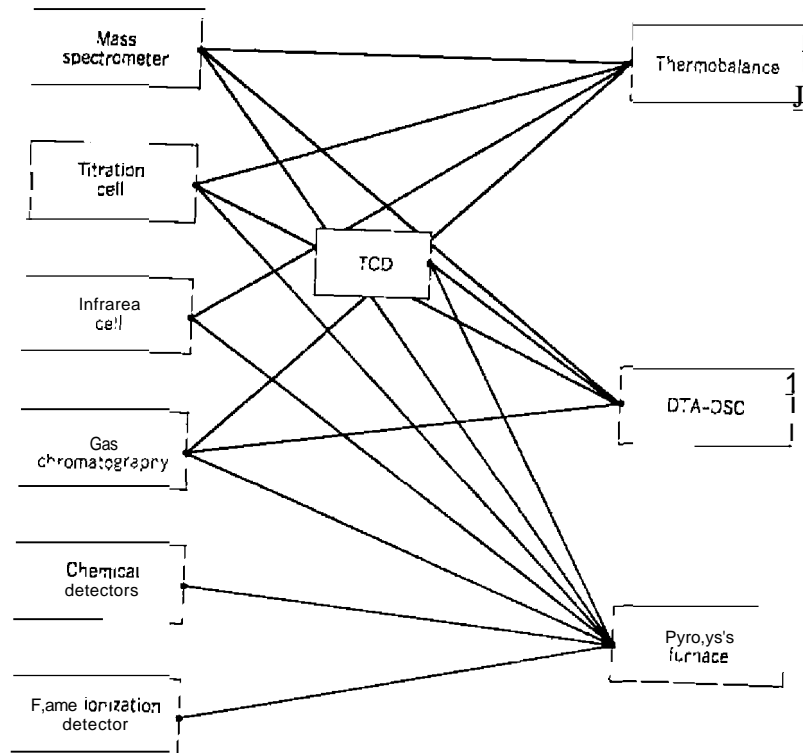


Figure 8.5. Examples of common multiple techniques

chromatography, are listed in Table 8.3. It should be noted that the detectors are specific for a given functionality-molecular weight, structural features, conformation, and so on of an evolved substance. Many of the detectors have not yet been applied to EGD or EGA instrumentation.

The usefulness of the EGD-EGA techniques can be extended by combining the various types of detectors, as given in Figure 8.2, with other thermal analysis methods. These multiple techniques offer a savings in time and effort, and since data are taken at the same time on the same sample, the results are more likely to be comparable than if they are taken separately on two or more different samples. Examples of the more common multiple techniques are given in Figure 8.5 and Table 8.4.

Besides the multiple techniques given here, a few of the EGD-EGA techniques listed in Table 8.2 are used by themselves and have not been coupled to other thermal analysis techniques. Some of them will no doubt be coupled to TG and OSC techniques in the future. Several of the EGD-EGA techniques will probably never be coupled to other thermal analysis techniques due to the uniqueness of the experimental parameters involved such as thin-layer chromatography.

Table 8.4. Multiple Techniques Employing EGD-EGA

Techniques	Comments
EGD-DTA	One of the first multiple techniques
EGA-MS	
EGD-EGA-MS	
DTA-EGD-MS	One of the early multiple techniques
TG-EGA-MS	
TG-DTA-EGA-MS	A commercial instrument is available for this technique
TG-pressure	
TG-GC	Instrument built for detection of Martian atmosphere
TG-GC-MS	
DTA-EGA-GC	
TG-T-TG-DTA	Developed for dermalography.
TG-IR	
TG-Photometry	Smoke evolution, measured with photodetector
ETA-DTA-dilatometry	
	Dilatometry not always employed. ETA-DTA is generally called emanation thermal analysis

F. INTERMITTENT AND CONTINUOUS SAMPLING MODES

There are two general sampling modes for coupling a pyrolysis chamber (furnace, thermobalance, DTA-DSC furnace, etc.) to an EGD-1:GA detector (TCD, FID, GC, MS, etc.). They are: (1) *intermittent* or batch sampling mode and (2) *continuous* mode. These modes are illustrated in Figure 8.6. For the continuous sampling mode, the gaseous products are introduced directly into the detector system via an interface coupling (see Sections G and H). The products are continuously sampled by the detector with the appropriate readout being proportional to their concentrations or composition. In the intermittent mode, the gaseous products are trapped by a low temperature or absorbent chamber and then introduced into the detector either at selected temperature intervals or after the heating cycle is completed. Both modes have their advantages and disadvantages. The intermittent (batch) mode has been used in the case of gas chromatography-mass spectrometry (58) and infrared spectroscopy (59). Its major advantage is that the detector system need not be extensively modified; this is important when a rather expensive instrument such as a mass spectrometer is shared by several groups of workers. Also, intermittent sampling permits the investigator to optimize the detector parameters to make the best use of each sample. The disadvantages of this mode are that each product must first be trapped (58), a process that may be inefficient. Once trapped, it must be stored for various periods of time and then introduced into the detector system. During this

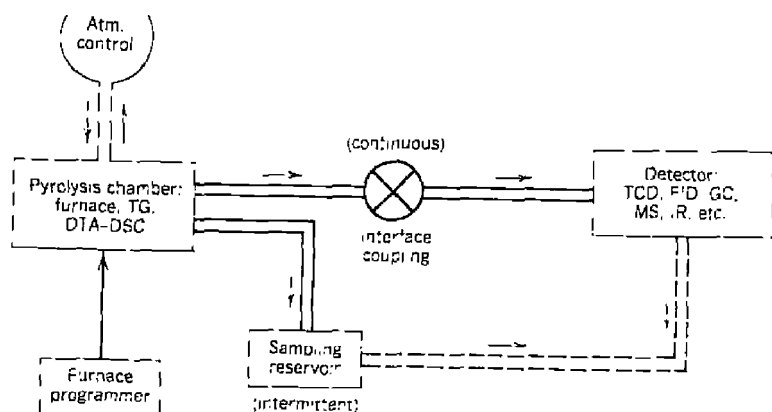


Figure 8.6. Intermittent and continuous sampling modes.

procedure, the sample is subject to decomposition, evaporation, and contamination. If a large number of samples are taken, these factors may become quite serious.

The continuous mode has the advantage of direct introduction into the detector system, with or without an interface coupling. The product is in a gaseous form that results in little if any loss or change in composition of the sample. There are no storage or manipulation losses with this type of arrangement. Also, this mode is less time-consuming than the intermittent mode and, in many cases, provides analytical data immediately. The disadvantages are that for some detectors, an elaborate interface is sometimes required, especially if there is a pressure differential between the pyrolysis chamber and the detector. Also, if a carrier gas is employed, the interface may require a concentrator or separator to increase the concentration of the products per unit volume. The detector should be as close to the pyrolysis chamber as possible to keep the sample introduction delay small. If the concentration of products is too large, a splitter must be introduced with most of the sample being discarded.

1. Trapping

The volatility of the sample determines the choice of trap to be employed. There are many different refrigerants available but the choices are usually ice water, dry ice solvent, and liquid nitrogen, which cover the temperature range from 0° to -196°C. The volume of the trap is also determined by the amount of sample desired; they range in size from microliters to several hundred milliliters. The smaller the sample is, the greater the trapping efficiency must become. Once trapped, the sample must be protected from degradation and contamination. The most obvious causes of decomposition of labile materials is exposure to air and light while the chances for decomposition, evaporation, polymerization, or absorption into rubber or plastic lined vessels increase with storage times. A gaseous sample can be collected without the use of coolant by means of glass bulbs connected to a manifold. Such a system has been described by Wendlandt (32). If three or four bulbs are employed, gaseous samples can be taken at selected temperature intervals and the contents analyzed later by the operator. Of course, the bulbs must be designed so that the contents can be connected to the detector system without contamination.

2. Combined Intermittent and Continuous Modes

Both intermittent and continuous sampling modes can be incorporated into a system, which was the case with one of the earliest systems described. The

Lodding and Hammell (28) system incorporated a DTA, a TeD, and gas absorption tubes. The absorption tubes selectively removed certain gaseous products from the DTA furnace effluent gases. Likewise, Wendlandt (32) employed a DTA, TeD, and glass sample bulb manifold. Gaseous products were collected in glass bulbs, which are later analyzed by a mass spectrometer.

Barnes and Kirton (60) developed a technique for both quantitative and qualitative determinations using a katharometer and differential freezing technique. This technique resulted in a greater increase in sensitivity when compared with DTA or conventional EGA using hot wire TeD. A schematic diagram of the apparatus, which employed a Stanton Redcroft Model 671H DTA instrument, is shown in Figure 8.7. All volumes were kept as small as possible using small diameter tubing; the swept volume was about 10 cm^3 . The freezing points of the product gases to be separated by the trap determine the choice of coolant. The coolant must provide a temperature

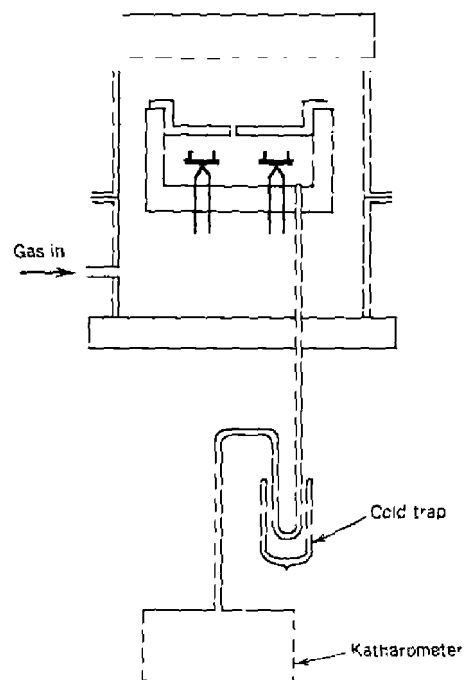


Figure 8.7. DTA apparatus and selective freezing of evolved gases (60).

such that the vapor pressure of the product to be stored is negligible, whereas that of the other evolved components and the carrier gas should be sufficiently high for them to pass unhindered. They found that carbon dioxide was effectively removed from the gas stream using liquid nitrogen as the coolant in the trap.

G. COUPLING WITH TG TECHNIQUE

I. TG-Photometric Analysis

There is considerable interest in determining the amount of smoke produced in burning materials, especially those used for thermal and sound insulation in aircraft. Loehr and Levy (61) devised a technique for characterizing materials as to their flammability properties using a thermobalance connected to a known volume flow cell installed in a precision photometer. The system, which is shown in Figure 8.8, consists of a Du Pont Model 950 thermobalance coupled to a Du Pont Model 410 precision photometer. The latter consisted of a split beam, sample reference system using a tungsten-iodine light source and S-5 photocells to detect light absorption caused by

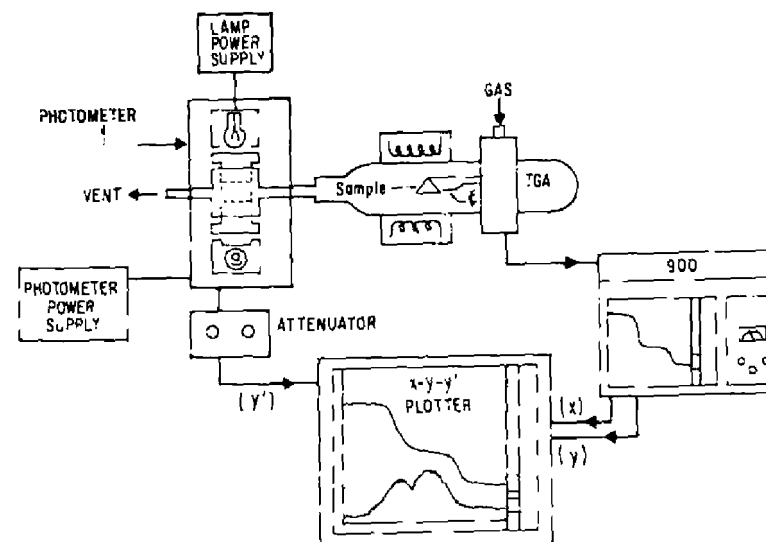


Figure 8.8. TG-photometer system of Loehr and Levy (61).

the evolved smoke. Smoke measurements were accomplished by employing a 1-cm³ stainless steel sample chamber with sapphire windows in the optical path. This chamber was coupled directly to the effluent end of the furnace tube. The voltage signals from the thermobalance and photometer were plotted as a function of furnace temperature on a X-y recorder.

2. TG-TCD

There are few examples of coupling a thermal conductivity detector to a thermobalance. One such system, as shown in Figure 8.9, which also contained a DTA apparatus, has been described by Krug (62). The carrier gas enters one side of the TCD, passes through the furnace chamber, and then exits from the other side. This system permitted recording of the TG, DTG, DTA and EGD curves.

3. TG-GC

Chiu (63) described a multiple TG-GC technique in which a thermobalance was coupled to a gas chromatograph by means of four Pyrex glass switching stopcocks. This apparatus, as shown in Figure 8.10, permitted following

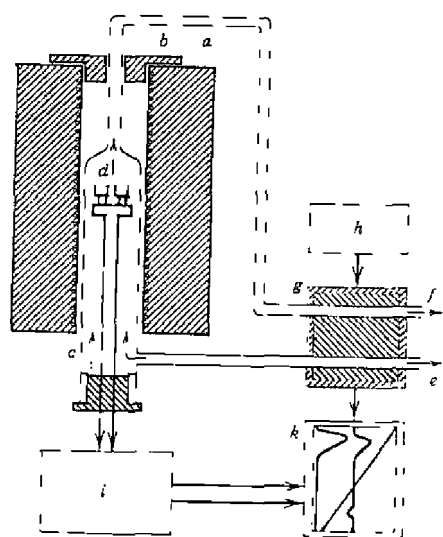


Figure 8.9. TG-TCD coupled system described by Krug (62).

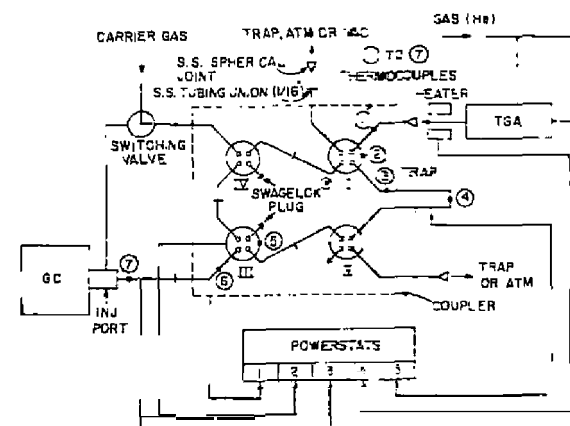


Figure 8.10. TG-GC coupler developed by Chiu (64).

the sample mass changes as it was heated on the thermobalance and also collected the evolved products at various stages and analyzed them intermittently by GC. This approach was similar to pyrolysis-GC except that the pyrolysis was monitored quantitatively by the thermobalance. Accordingly, the TG-GC technique possesses many advantages and disadvantages of the pyrolysis-GC technique, such as:

1. More expensive equipment is required.
2. Total time for analysis is greater.
3. Production of secondary pyrolysis products is reduced due to lower temperatures.
4. Interaction between impurities and decomposition products can be minimized.
5. Quantitative information on the components in the sample can be obtained from the TO curve.
6. Large samples can be accommodated so that trace amounts in a polymer matrix can be determined.
7. Temperature of the sample can be carefully controlled.
8. Both effluent and residue at any mass-change step can be recovered for studies by other techniques.

The first apparatus developed by Chiu (63) was superseded by an all metal semiautomatic coupler (64) in which the glass switching stopcocks

were replaced with four stainless steel microvolume valves. The switching operation was performed in a semiautomatic manner by solenoid valves. All the necessary plumbing connections were placed into a heated steel box. One switching valve was used to switch the carrier gas to either the coupler for TG-GC operation or the GC directly for normal GC operation. An additional purge gas inlet added at the end of the thermobalance enclosure was used to flush out the pyrolysis products. A small Dewar flask, cooled with liquid nitrogen, was used for trapping evolved volatiles.

A less complicated TG-GC coupling has been described by Cukor and Persiani (65) for on-column collection of pyrolyzates with the use of cold traps. This apparatus coupled a Du Pont Model 950 thermobalance to a Perkin-Elmer Model 900 gas chromatograph by means of a female Pyrex baH-joint attached to the quartz thermobalance furnace tube. The opposite end of the pyrex tube was connected through a graded seal to $\frac{1}{8}$ in. od stainless steel tubing, which was connected via a Swagelock fitting to the injector insert of a gas sampling valve. The exit portion of the furnace tube, which is outside the oven, and the adjoining connecting tubes were maintained at 250°C by use of heating tape. Two separate helium gas supplies were required—one for the GC and the other for the TG purge gas.

The apparatus used by Wiedemann (37) is shown in Figure 8.11. In order to keep the time delay in gas transfer to a minimum, he reduced the furnace volume to about 35 cm³. Gases were introduced into the gas chromatograph by means of a gas sampling valve that could be opened at specific intervals. Wiedemann commented that compared to a mass spectrometer the gas chromatograph is slower, but as far as the quality of results is concerned the methods are about equal.

An elaborate vapor-phase thermal analysis laboratory system, which incorporated a TG-GC coupling as well as other techniques, has been described by Uden et al. (66). The on-line apparatus, as illustrated schematically in Figure 8.12, permitted the separation and identification of evolved volatile species. Samples could be thermally degraded under slow temperature gradient conditions (4-40°C min⁻¹) in a flowing gas medium or pyrolyzed under ultra rapid rise-time conditions of up to 20,000°C sec⁻¹. Evolved volatiles were transferred to the master trap manifold where precolumn reactors and selective traps were available to meet the needs of the specific analysis. In many cases, the volatiles were directed from the manifold to the master gas chromatograph for separation followed by on-line vapor phase infrared spectroscopy. In addition or as an alternative to IR, on-line elemental analysis for C, H, N, O and S and functional group fragmentation by thermal cracking or mass spectrometry may be applied. The overall system was interfaced to a laboratory minicomputer for data acquisition, reduction, and instrumental control.

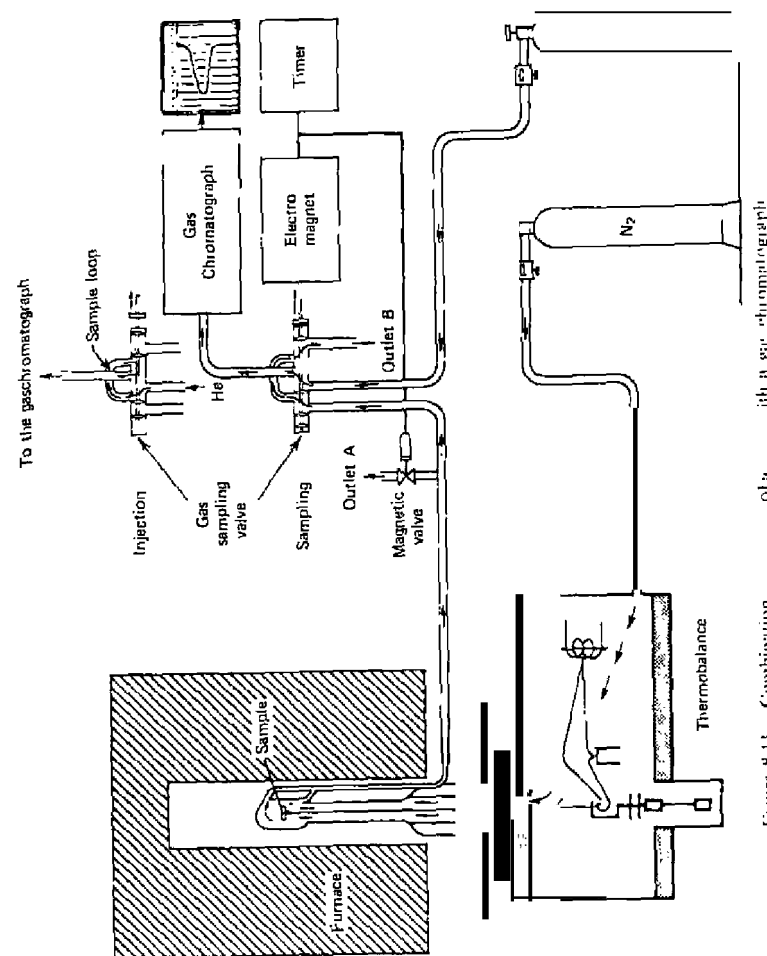


Figure 8.11. Combination of a thermobalance with a gas chromatograph Wiedemann (37).

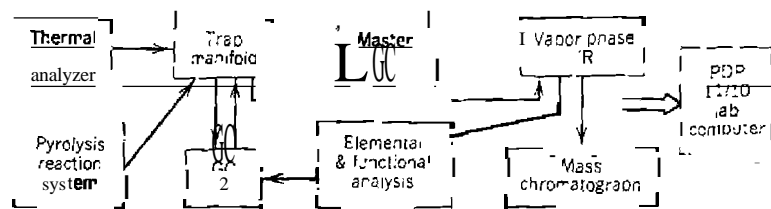


Figure 8.12. Vapor-phase thermal analysis system according to Uden et al. (66).

4. TG-MS

Zitomer (67) was the first to describe the coupling of a thermobalance to a time-of-flight mass spectrometer and a magnetic sector mass spectrometer. This technique eliminated the practice of collecting or trapping fractions for subsequent analysis and also permitted careful control of the furnace atmosphere. One of the important features of the TG-MS system is its relatively short "dead" time, that is, the time between product evolution and introduction into the mass spectrometer ion source. Under proper flow conditions, this time is of the order of seconds. There is also less probability of the formation of secondary reaction that can lead to products other than those initially evolved.

A schematic diagram of the TG-MS apparatus is shown in Figure 8.13. The Du Pont Model 950 thermobalance is coupled to a Bendix lime-of-flight mass spectrometer by a three-way and a metering diaphragm valve. The connecting tubing is a 0.25-in.-od stainless steel tubing that is connected to the exit port of the thermobalance by a 0.25-in. Swagelok union containing Teflon or silicone rubber ferrules. As in TG-GC, the most critical dimension is the length of tubing between the exit port and the metering valve. This should be as short as possible for the best resolution and least holdup. For this apparatus, the distance was less than 8 cm. The distance of the line between the diaphragm (metering) valve and the MS source is not critical. Ideally, it should be short and of wide diameter, negligible dead times can be realized, however, with a line as long as several feet. In the apparatus described here, satisfactory results were obtained with $\frac{1}{8}$ -in.-od stainless steel tubing.

Another system, which coupled a Cahn Model RH thermobalance to a Bendix time-of-flight mass spectrometer, has been described by Kleinberg and Geiger (68). The balance was connected to the ion source of the mass spectrometer by a valve and capillary tubing. The capillary tubing employed was 900 mm in length and had an id of about 0.25 mm. In order to yield a total gas pressure inside the ion source of $2-3 \times 10^{-5}$ Torr when the balance chamber was at atmospheric pressure, the authors had to crimp carefully the lip

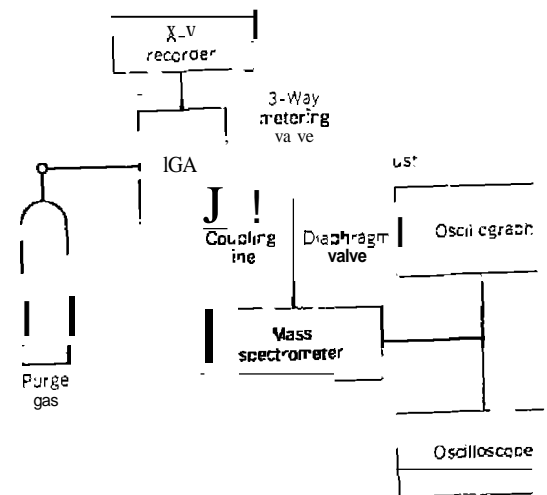


Figure 8.13. TG-MS apparatus developed by Zitomer (67)

of the capillary tube to form a suitable restriction. The mean free path of the sample of the sample molecules entering the restricted orifice at the tip of the capillary was small compared to the diameter of the restriction so that viscous flow conditions existed and no mass discrimination occurred.

Perhaps the most widely used TG-MS system, which includes DTG, DTA, and gas pressure measurements, is the Mettler thermoanalyzer. The system, which consists of a precision thermobalance, a high-vacuum system, a mass spectrometer, and a DTA measuring system, has been described in detail by numerous investigators (68-73).

In almost every system, the Mettler Thermoanalyzer was coupled to a quadrupole mass spectrometer, such as is illustrated in Figure 8.14 (37, 69). The sample may be studied under vacuum ($\sim 10^{-6}$ Torr) or under higher pressures to 1 atm. The reaction chamber, R, is surrounded by the furnace and separated from the balance by a diffusion barrier. The evolved gases pass directly to the mass analyzer, F, which is connected to a recorder, I, through the mass spectrometer control panel. Total pressure is determined by an ionization gauge, S, which also permits the recording of the TGD curve (in this case, due to the pressure change in the system). The relation between measured total pressure and the ion current of the calibration gas permits calibration of the mass spectrometer in absolute partial pressure units or A. Torr.

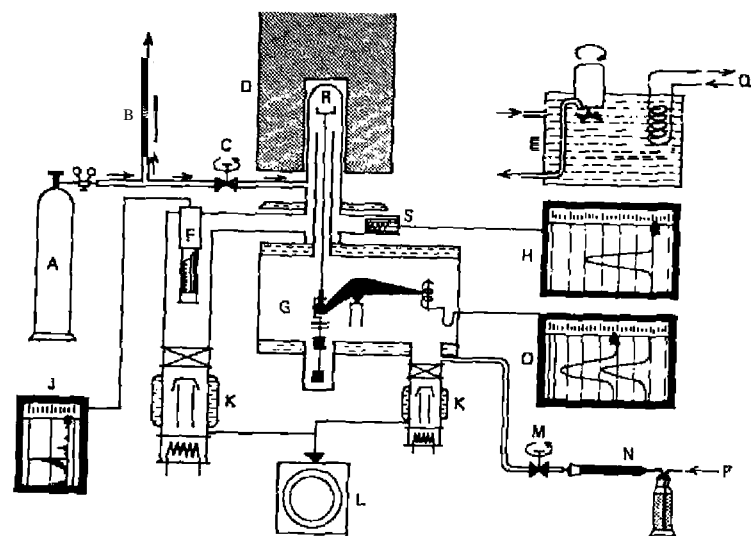


Figure 8.14. Mettler thermobalance-quadrupole mass spectrometer system (37, 69).

Gibson and co-workers (69, 101-103) used the preceding apparatus to study gas evolution from geochemical and lunar soil samples. All the calculations of mass spectral data were made by a dedicated minicomputer system. Smith and Johnson (104, 105) described a multipurpose apparatus that permitted the determination of the TG, DTA, EGD, and MS curves to oil-shale research problems. Chang and Mead (106) described a TG-gas chromatograph-high-resolution mass spectrometer system and its application to the degradation of polymers.

Moi (70) used a "flexible glass-end tubing" made of stainless steel lined with Pyrex glass on one end which served as the interface between the UTI 100C precision mass analyzer (quadrupole mass spectrometer) and the quartz furnace of the thermoanalyzer. The distance between the sample pan and the MS mounting flange was 20 cm. The interconnecting orifice was 2.3 mm i.d. which, along with its short length, resulted in a negligible dead time. The ability of the quadrupole mass filter to accept ions over a relatively large inlet energy spread and at varying entrance angles made it well suited for use in this application.

In the system developed by Clinckemaele and Hofmann (71), the quadrupole mass filter was inserted directly into the vacuum system of the thermoanalyzer. The gaseous decomposition products formed during pyrolysis of

the sample were continuously pumped by a diffusion pump. A system pressure of not more than 1×10^{-4} Torr was maintained to assure normal working conditions of the mass spectrometer. It was also possible to carry out TG measurements at atmospheric pressure if a separate vacuum system was maintained for the mass spectrometer. A small fraction of the decomposition gases was permitted to leak into the vacuum chamber and was analyzed with the mass spectrometer in the usual manner. Gas condensation effects were avoided to a large extent by heating the furnace outlet tubing to about 200°C. By proper adjustment of the carrier gas flow in conjunction with the pumping rate, the response time of the gas inlet system could be made less than 0.1 sec.

Szekely and Till (73), in attempting to solve some of the problems inherent in coupling a TG furnace to a quadrupole MS in the high-vacuum mode, developed the heated system coupling shown in Figure 8.15. They found that:

1. The connecting tube to the mass spectrometer must be short and have a diameter of at least 40 mm.
2. All of the system including the pump has to be heated to about 250°C to remove most of the residual gases.
3. Separate pumping systems must be employed for the thermoanalyzer and mass spectrometer if kinetics measurements were to be made. For measurements at atmospheric pressure, the arrangement given in Figure 8.15b is used.

The main problem in (3) is to obtain representative sampling into the quadrupole MS in spite of the atmospheric pressure of the balance and the extremely large excess of the carrier gas. As in the high-vacuum condition, the system must be heated carefully but smaller diameter tubes can be used because the mean free path of the gas molecules is quite low.

The two major disadvantages of coupling a thermobalance to a mass spectrometer can operate at pressures up to 1 Torr. The Mettler Thermo-thermobalance, the sample must be pyrolyzed under vacuum conditions and (2) if the thermobalance is operated at atmospheric pressures, a pressure-reducing interface must be employed. Baumgartner and Nachbaur (74) circumvented both these problems by using a quadrupole mass spectrometer equipped with chemical ionization (CI). The purge gas or the thermobalance was simultaneously used as the reaction gas in the chemical ionization source. This type of coupling eliminated all interface problems and restricted the fragmentation of the released volatile compounds. It permitted the identification of volatiles and the determination of their sequence of release even in very complex decomposition reactions.

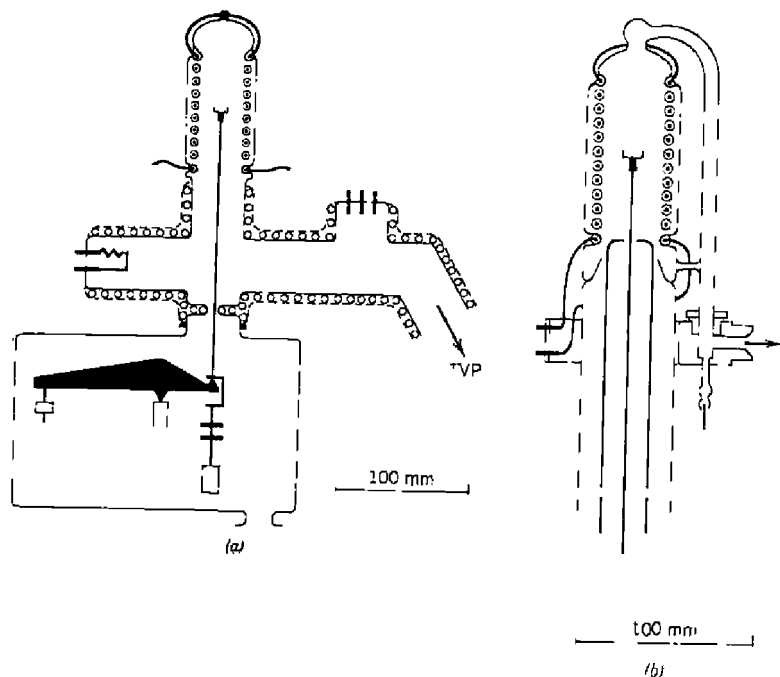


Figure 8.15. TG-MS system developed by Szekeley and Ti. (73). (a) For high vacuum; (b) for atmospheric pressure.

The TG-MS system, as shown schematically in Figure 8.16, consisted of a thermobalance connected to a mass spectrometer. The ion source of the mass spectrometer can operate at pressures up to 1 Torr. The Mettler Thermoanalyzer TA-2 was coupled to a Finnegan quadrupole mass spectrometer with a combined EI-CI source by means of $\frac{1}{8}$ -in.-od stainless steel tubing. The tubing length, which was about 60 cm, was terminated by a three-way metering valve to permit adjustment of the gas pressure in the ion source. Gases used for the CI studies included the noble gases of helium and argon as well as nitrogen and methane. The applicability of methane is limited due to its reaction with the samples at high temperatures.

Oyszal (151) has described a combined TG atmospheric pressure chemical ionization mass spectrometry system. A Perkin-Elmer IGS-2 thermobalance was connected to a Sciex TAGA 300 mass spectrometer. An initial ionization occurs with the electron bombardment of nitrogen and the N_2^+ ion then undergoes a charge transfer reaction with oxygen forming O_2^+ . This species

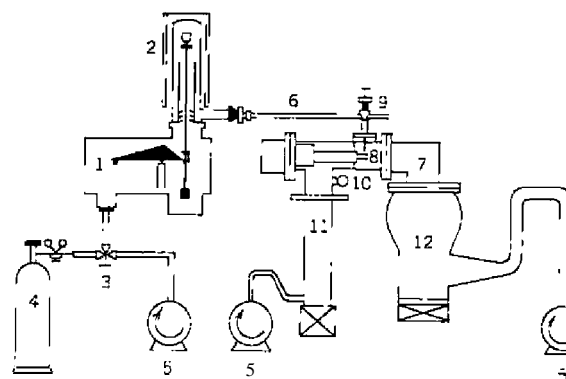


Figure 8.16. TG-MS with a chemical ionization source as described by Baumgardner and Nachbaur (74). 1, thermobalance; 2, furnace; 3, 3-way valve; 4, reaction gas cylinder; 5, rotary pumps; 6, coupling line; 7, quadrupole mass spectrometer; 8, CI-ion source; 9, metering valve; 10, ionization gauge; 11, analyzer diffusion pump; 12, CI diffusion pump.

then forms a cluster with gaseous water in the air and by a series of reactions forms the hydrated proton, H_3O^+ . As volatile products enter the ion source from the thermobalance, they react with H_3O^+ and either a proton or H_3O^+ is transferred to each molecule. These ionized molecules then pass through the quadrupole analyzer.

Chiu and Beattie (147-149) have described the coupling of a thermobalance to a mass spectrometer so that simultaneous TG-MS data can be obtained. They used different techniques to sample the evolved gaseous decomposition products ranging from differential trapping (147), total condensation of the pyrolyzate (149), to continuous sampling or monitoring of the evolved products (148), mainly from heated polymeric samples.

In the differential trapping method (147), the sample was heated under continuous vacuum at a programmed rate, condensing the evolved gases in traps maintained at different temperatures, continuously monitoring the pressure changes at strategic locations, and analyzing the trapped products by MS. One of the primary objectives was to explore the possibility of using EGO peaks to derive quantitative information on the basis of pressure-change detection. Using a Pirani gauge (a TeO detector), the pressure curve was S-shaped in the range from 10^{-4} to 1 Torr and higher. This type of curve is not ideal for quantitative work although the peak area plot appears to be linear except at very small amounts of materials.

A schematic diagram of the TG-MS system using a six-port microvalve is shown in Figure 8.17 (149). The valve was connected to a U-shaped liquid

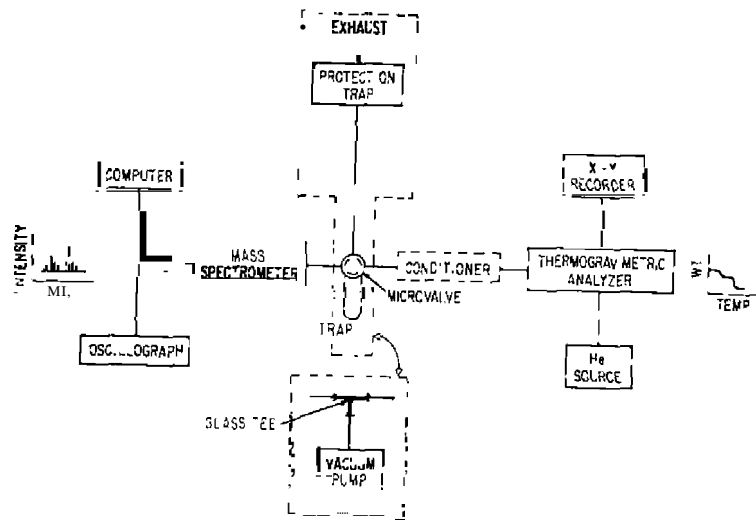


Figure 8.17. Schematic diagram of TG-MS system of Chiu and Beattie (149).

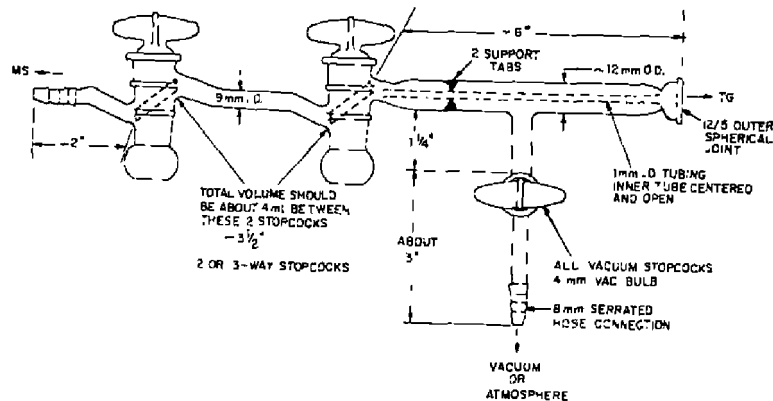


Figure 8.18. Schematic diagram of TG-MS interface of Chiu and Beattie (148).

nitrogen trap constructed of stainless steel or glass tubing, Provision was also made for direct sampling of the evolved gases to the mass spectrometer by means of a T-shaped glass or stainless steel tube interface. The evolved gases could either be trapped or introduced directly into the mass spectrometer.

In the third method, Chiu and Beattie (148) used an interface constructed from a T-shaped glass tube and a constant volume sampler, such as is shown in Figure 8.18. One arm of the tee was connected to the furnace tube of the thermobalance, whereas the other was welded to the stopcock of the sampler. The third arm was either vented into the atmosphere or connected to a vacuum pump. The sampler was connected to the heated inlet of the mass spectrometer. A 3-L gas reservoir and a gold leak tube were placed between the inlet and the ion source. To achieve the highest sensitivity, one can directly connect the sampler to the ion source through a direct probe attachment.

H. COUPLING WITH DTA TECHNIQUE

1. TGA-TeD

As mentioned earlier, the first simultaneous EGD technique was that involving a DTA system. Since these systems have been adequately described elsewhere (5, 6), they will not be discussed here. Several of the more recent systems will be described, the first of which is by Emmerich and Bayreuther (75). This system, which coupled a Netzsch Model 404M DTA apparatus to a TeD, is shown in Figure 8.19. No details on the coupling was presented but it was pointed out that the carrier gas flow rate must be well stabilized and the TeD must be thermostatically controlled for good results. DTA measurements could be carried out in the temperature range of 25 to 1600°C.

A similar system was described by Wist et al. (76) in which either EGO measurements or simultaneous DTA-EGD data could be made. Samples were placed on an Inconel disk which was supported in the furnace chamber by three ceramic posts.

2. DTA-ETA

The simultaneous measurement of emanation thermal analysis (ETA) with DTA has been described by Emmerich and Bolick (77). ETA is further described in Section 14 of this chapter.

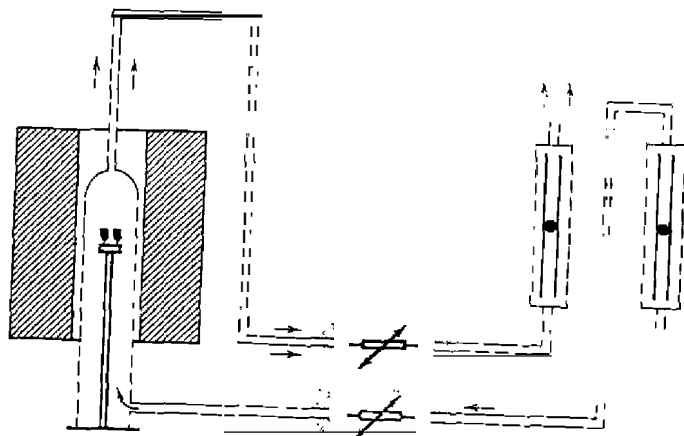


Figure 8.19. DTA-TeD system described by Emmerich and Bayreuther (75).

3. DTA-GC

Compared to DTA-MS, DTA-GC is less expensive to assemble and ensures better resolution in certain situations. Its disadvantage is that since it takes longer for the GC analysis time, the sampling rate is considerably less than that in DTA-MS. To eliminate or at least reduce the latter problem, Yamada et al. (78) samples the evolved gases at desired points on the DTA Curve and stored them until the GC analysis was carried out.

A schematic diagram of this DTA-GC apparatus is shown in Figure 8.20. The evolved gases from the sample, contained in the DTA sample holder, were carried by the purge gas to the trapping tube. Multiple trapping can be carried out by changing the trapping tube at the desired interval. The trapping tube in which the evolved gases are absorbed is stoppered at both ends and can be removed from the cooling block. It is then stored at room or sub-ambient temperatures until it is inserted in the heating block attached to the injection port of the gas chromatograph. After the tube stabilizes at the elevated temperature, the sample components are flushed into the GC column and eluted in the normal manner.

4. DTA-MS

Although many of the systems described in TG-DTA apply to DTA-MS, a system for DTA-MS only has been discussed by Asplund et al. (79). This

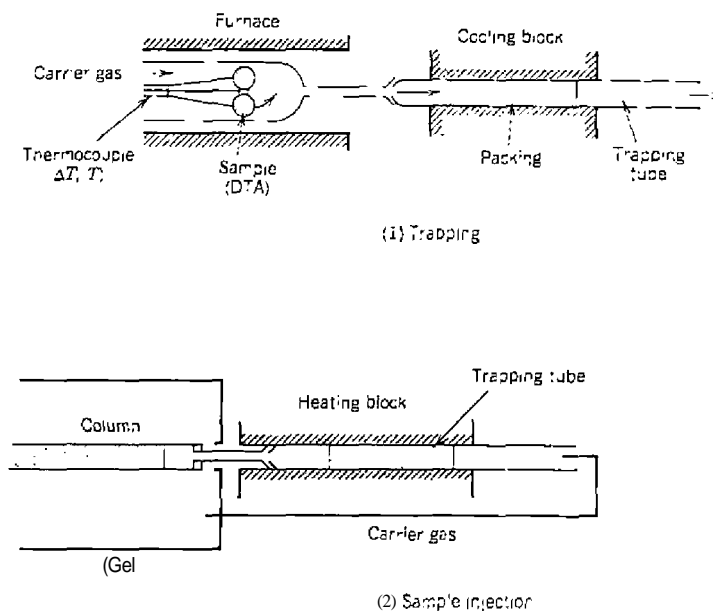


Figure 8.20. Simultaneous DTA-GC technique described by Yamada et al. (78).

apparatus, which is illustrated schematically in Figure 8.21, coupled a Stanton Redcroft 67-IB DTA sample chamber to an AEI QMS 40 quadrupole mass spectrometer. Two coupling techniques were used for the interfacing between the DTA and the mass spectrometer: (a) continuous inlet with by-pass and (b) a membrane separator. In (a), a 180-cm long, 0.3-mm-id stainless steel capillary tube was used to connect the two units. This tubing, which is covered with a PTFE sleeve and can be heated to 300°C, is connected to the mass spectrometer by a sintered silicon carbide leak which has a conductance of 0.01-1 Torr sec⁻¹. The pressure in the interspace is normally 3 Torr, and the flow of gas into and out of it is viscous in character and molecular through the leak. This interface is used for the analysis of water vapor and a wide range of gaseous products when their concentration is high. It is not suitable for low volatility decomposition products.

The membrane separator (b) had a greater sensitivity for organic substances and is less likely to be affected by condensation and decomposition products of low volatility. It has a 100 permeability toward carrier gases such as argon and helium but evolved volatiles, both inorganic and organic, are readily transported through the membrane. Gas leaving the DTA sample chamber can follow one of two routes, the first, (a) being the route to air that

allows for the larger fraction of the gas to escape. The second fraction will pass through the membrane (roLite B) with an increased proportion of evolved volatiles to carrier gas. The separator unit, enclosed in a small oven (O) that has a maximum operating temperature of 250°C, was linked through a glass-to-metal seal to a heated stainless steel capillary (S) of 0.8 mm id. The capillary tube is connected to the mass spectrometer through a bakable valve. With the mass spectrometer pumped down at a rate of 22 L/sec, and atmospheric pressure in the sample chamber, the vacuum achieved was 2 x 10⁻⁵ Torr.

1. INSTRUMENTATION AND MEASUREMENT PARAMETERS

1. Typical EGD-EGA Apparatus

A "typical" EGO-EGA apparatus cannot be described because of the variety of detectors that are employed. If certain restrictions are placed on the latter, plus other operating parameters, a general type apparatus can be depicted, such as is illustrated in Figure 8.22. The pyrolysis unit is a simple furnace or other thermal analysis device such as a thermogravimetric analyzer (TGA), DTA, DSC, or so on. A temperature programmer provides

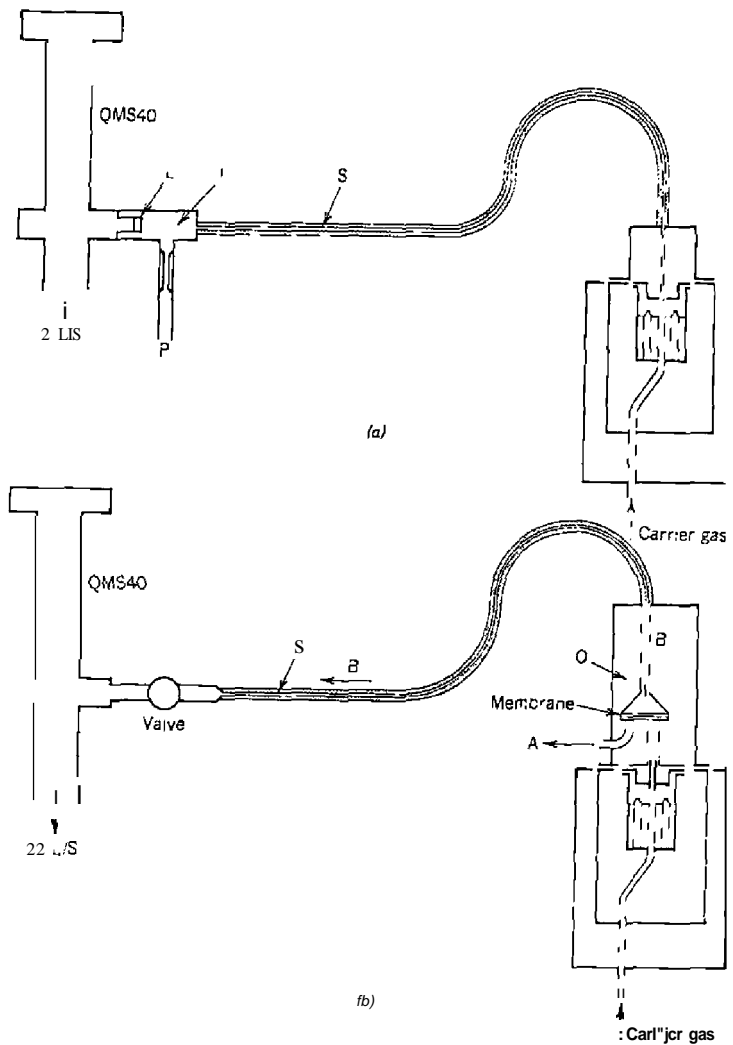


Figure 8.21 Two interface techniques used for DTA-MS by Aspöck et al. (79). Interface (a) is continuous inlet system with bypass; (b) membrane separator.

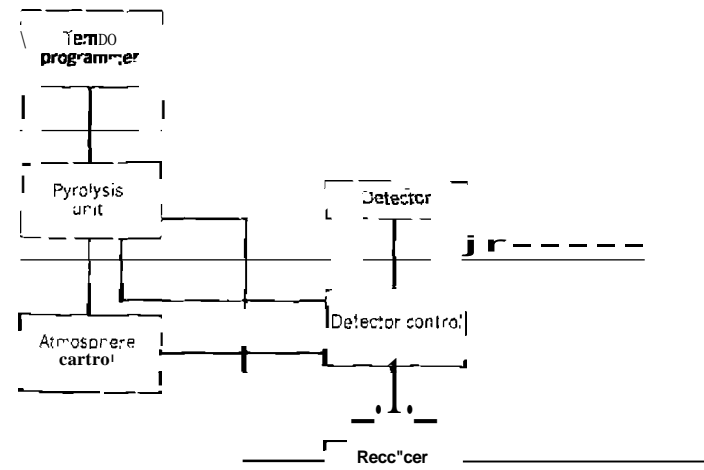


Figure 8.22. Typical EGD-EGA apparatus.

furnace temperature increase, generally in a linear manner, and an atmosphere control unit provides the proper gaseous atmosphere and flow conditions. The primary detector may be a simple thermal conductivity detector (TCD), a gas density, flame ionization, or other type of device. A control system converts the detector output to electrical signals so that they may be recorded on a recorder, as either a function of time (strip chart recorder) or temperature (X-Y function recorder). If the presence of an evolved gas only is detected, then the apparatus may be designated as EGD. On the other hand, if the amount or quantity of evolved gas is measured quantitatively, then the apparatus is EGA. The apparatus is more useful and versatile if it is coupled to an auxiliary analytical detector. This detector may be a gas chromatograph, mass spectrometer, titrimeter, IR cell, and so on. The additional information is quantitative and thus determines the amount and/or composition of the evolved gases. If these data are correlated with other thermal analysis data from the pyrolysis unit, then a large amount of information is available concerning the system under investigation. As pointed out by Wendlandt (169), the use of a single thermal analysis technique does not yield enough information to characterize a decomposition reaction. If a gaseous reaction product is evolved, EGA-EGA data may well provide the necessary complementary or supplementary information needed.

2. Detectors

Just as it is almost impossible to represent a typical EGD-EGA apparatus, it is equally difficult to describe the wide variety of detectors that have been employed. Using the techniques listed in Table 8.2, the type of detector employed for each method is listed in Table 8.5. As can be seen, there are a number of different types of detectors used, from simple thermal conductivity detectors to more sophisticated ion current detectors in mass spectrometry. It is, of course, impossible to discuss each one in detail here, although the complete apparatus is described in certain cases.

Thermal conductivity detectors have been discussed in detail by Ingraham (107), who also described their application to thermodynamic and kinetic measurements. In this same book, Lodding (4) describes the gas density detector as well as several ionization detectors, such as the argon ionization detector, the electron capture detector, and others. Flame ionization detectors have been described in detail by Brody and Chaney (108) and Johnson (109). The latter also discusses other types of detectors. Malone and McFadden (110) described many different types of special identification detectors, such as those listed in Table 8.3. Numerous texts on gas chromatography describe a wide variety of detectors, many of them useful in EGD and EGA.

The use of infrared absorption techniques to monitor EGA and EGA gas

Table 8.5. Types of Detectors Used in EGD-EGA Techniques

EGD-EGA Technique	Detector (or comments)
Differential thermal gas analysis	Thermal conductivity detector (TCD)
Elemental analysis (pyrochrom); Evolved radioactive gas	
Flame ionization detection (Thermal Evolution Analysis)	Flame ionization detector (FID)
Gas chromatography (GC)	Wide variety of detectors such as TCD, FID, etc.
Gas density detection	Gas density detector
Infrared spectroscopy	Infrared photometric detector system
Mass spectrometry	Various types of ion current detectors
Molecular weight chromatography (mass chromatography)	
Piezoelectric detection	
Photometric detection	Photocell-lamp system
Pressure changes	Pressure transducers of various types
Pyrolysis-GC	Same as gas chromatography
Specific gas detectors	
Specific ion electrodes	Specific ion electrode in solution containing evolved gas See Table 8.3
Special identification detectors	May be hot wire or thermal type
Thermal conductivity detector	
Thermal energy analyzer	
Temperature-programmed reduction	TCD
Thermoparticulate analysis	Particulate matter detector
Thermal volatilization analysis	Pirani gauge
Thin-layer chromatography	TLC plate with different coatings
Titrimetry	Titration cell
Volume changes	Variable volume system

stream has been discussed by Low (111) and Freeman (59). A wide variety of infrared techniques have been employed.

3. Measurement Parameters

a. Effect of Instrument Parameters on EGD Curves

In one of the earliest investigations on the use of the EGD technique, Rogers et al. (10) determined the qualitative effects of the system operating parameters on the EGD curves. The parameters studied included the carrier gas

flow rate, heating rate, sample mass, TCD sensitivity, and pressure and nature of the carrier gas. Many of the effects found were similar to those found for other thermal analysis techniques, such as TG and DTA/DSC (6). The instrument parameter variables, with the exception of the variation in TCD sensitivity, affected the peak maximum temperatures and peak heights; TCD sensitivity only affected the peak heights. To illustrate these effects, Figure 8.23 gives the effect of sample mass of PETN, an explosive, on the curve peak maxima and magnitude. The peak maximum temperatures varied from 160°C for a 1.4 mg sample to 178°C for a 20.5 mg sample. The larger the sample was, the greater the magnitude of the peak observed, which is of course expected. Thus, judicious control of sample size appears to be necessary for reproducibility of peak temperatures.

The observed changes in the EGD curve with operating parameters are listed in Table 8.6.

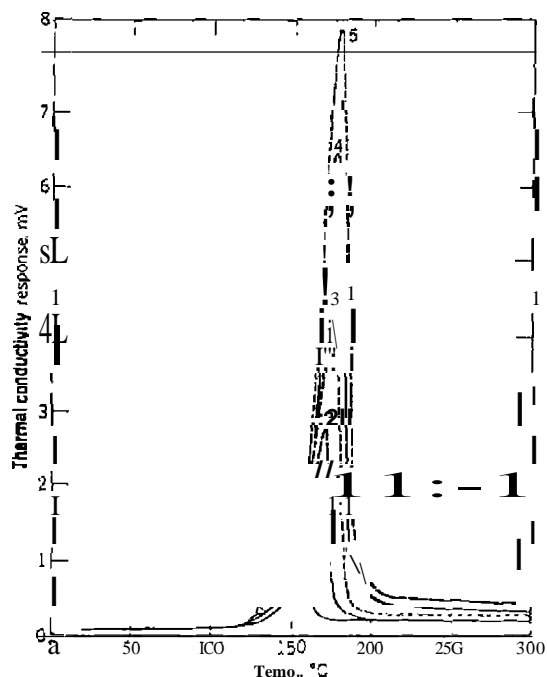


Figure 8.23. Effect of sample size on the EGD curve of PETN (30). 1. 1.4 mg PETN; maximum at 160°C; 2. 5.0 mg PETN; maximum at 167°C; 3. 9.7 mg PETN; maximum at 177°C; 4. 15.0 mg PETN; maximum at 178°C; 5. 20.5 mg PETN; maximum at 178°C.

Table 8.6. Observed Changes of EGD Curve Peaks with Operating Parameters (30)

Operating Parameter	Effect on	
	Peak Temp.	Peak Height
<i>Flow rate of carrier gas</i>		
L. Slow	No effect	Increase
Fast	No effect	Decrease
<i>Heating rate</i>		
Slow	Increase	Increase
Fast	Decrease	Decrease
<i>Sample mass</i>		
1. Large	Increase	Increase
Small	Decrease	Decrease
<i>TCD Bridge sensitivity</i>		
1. High	No effect	Increase
Low	No effect	Decrease
<i>Pressure</i>		
1. 1 atm → 2 atm	Increase	Decrease
<i>Atmosphere</i>		
1. He → air	No effect	Decrease

Krug and Hadrich (112) found that the EGD curve peak, like DTG, was proportional to the rate of reaction. As a rule, they found that the observed peak was quantitatively proportional to the quantity of sample, and that deviations from this were an indication of peculiarities in the reaction mechanism.

Emmerich and Bayreuther (75) found that in their simultaneous TG-EGD apparatus, the EGD peak area was proportional to the sample mass for the evolution of H_2O , CO , and CO_2 from the thermal decomposition of $CaC_2O_4 \cdot H_2O$. This proportionality is shown by the curves in Figure 8.24, which have a linearity of within $\pm 2\%$. They also studied the effect of gas flow quantity and peak height, half-width, and peak area using calibrated amounts of air injected into the carrier gas stream. The peak area and half-width decreased, whereas the peak height increased with an increase in gas flow. Thus, better

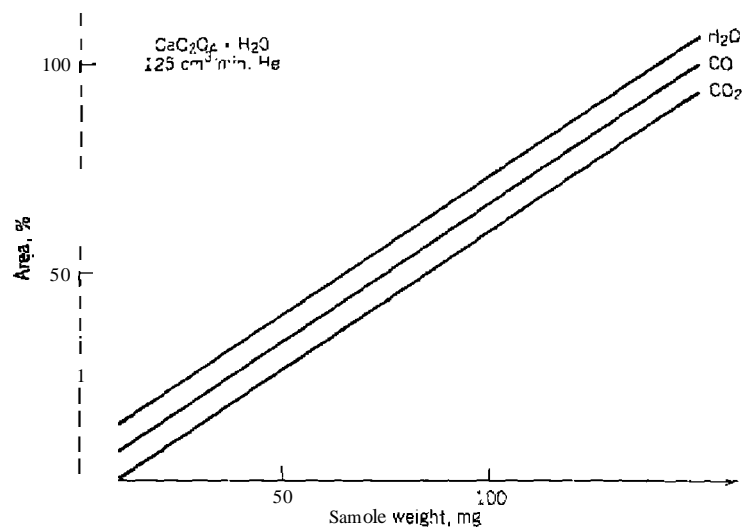


Figure 8.24. Relation between peak area and sample mass for $\text{CaC}_2\text{O}_4 \cdot \text{H}_2\text{O}$ (75).

resolution is obtained but lower sensitivity is observed on increasing the gas flow rate.

Barnes and Kirton (60), in their EGA study of the evolution of CO_2 from Ag_2CO_3 , found that the peak area was directly proportional to the quantity of CO_2 evolved.

b. Effect of Operating Parameters on P-T and V-T Curves

The effect of sample size on the magnitude of the P-T curve was studied by Wendlandt (13). Using the thermal decomposition of KHCO_3 , he found that the larger the sample mass is, the greater is the pressure increase observed. This is illustrated in Figure 8.25. There were slight changes in the T_i (initial temperature) and T_j (final temperature) values and also the reaction interval ($T_j - T_i$). Values for T_i (145°C) did not change substantially with sample mass but T_j values did increase slightly: 200°C (73 mg), 205°C (111 mg) and 210°C (149 mg). The initial pressure, P_i , was < 1 Torr in all cases, at a heating rate of 10°C min⁻¹. With heating rate, there were changes in the T_j and $T_j - T_i$ values but not those for T_i . Values for T_j reported were: 5°C min⁻¹ (190°C), 10°C min⁻¹ (210°C), and 20°C min⁻¹ (220°C).

Dekok et al. (114) found that the total area of the low pressure < 10 Torr dissociation curves of the alkaline earth carbonates was approximately

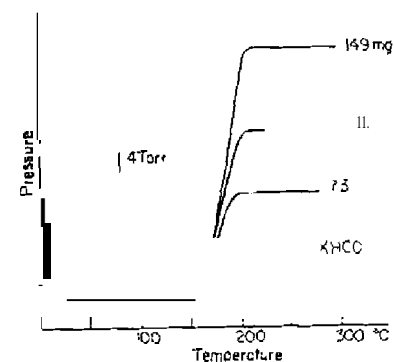


Figure 8.25. Effect of sample mass on P-T curves (113).

proportional to the product of the rate of heating and sample mass. Mutual deviations from this proportionality did not exceed 20%.

For V-T curves, Wendlandt (115) found that the heating rate had little effect on the T_i values for KHCO_3 but it did change the T_j values to some extent. The T_i value found was about 165°C for which the T_j values were 205°C (5°C min⁻¹), 215°C (10°C min⁻¹), and 240°C (20°C min⁻¹). There was, naturally, an increase in the ($T_j - T_i$) values with an increase in heating rate.

c. Baseline Stability

In DTGA (see Section II, Mizutani and Kalo (38) found that the following experimental variables affected the curve baseline stability. These factors are: (1) irregular heating or cooling of the furnace, (2) imperfect gas mixing, (3) temperature fluctuations of the TCD, (4) Gas leakage in apparatus connections, and (5) water or other condensable gases condensing in the gas train. Many of these factors could cause baseline fluctuations in other EGD-EGA systems, especially (3), (4) and (5).

d. Resolution of EGA Curve Peaks

The usefulness of the DTA-EGA technique is further increased by the resolution of the total EGA curve peaks into its component parts, using a curve resolver to deconvolute the overlapping peaks. Bardi and co-workers (116) (18) have demonstrated the usefulness of this approach, as shown in Figure 8.26. The curve resolution shows that both Cr_2C and $\text{Cr}_2(\text{C}, \text{N})$ are present in the sample. This approach could probably be applied to other studies as well.

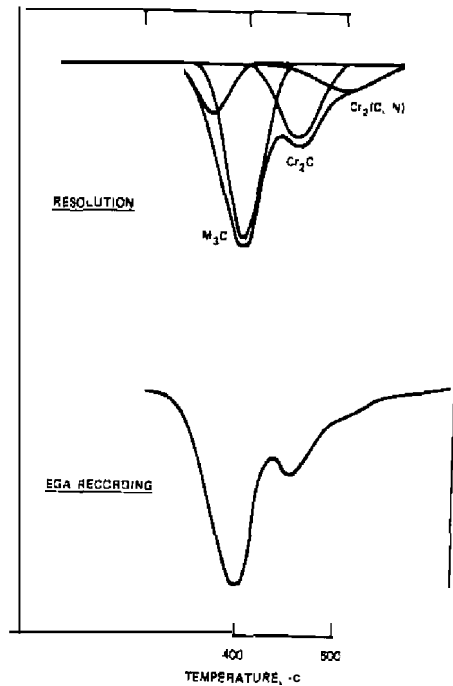


Figure 8.26. Resolution of EGA curve for sample containing Cr_2C and $C_1(C, N)$ (116).

e. Temperature Calibration in EGD

Ware (119) developed a material having a thermal transition, which could be used for the temperature calibration of an EGD apparatus. It was found that potassium sulfate, containing a small amount of dissolved carbon dioxide, released the latter substance during fusion so that the evolved gas peak coincided with the melting process and was independent of the heating rate and oxygen content of the atmosphere. The sample holder, shown in Figure 8.27, was used to contain the sample during the calibration run. It consisted of a platinum crucible placed in an alumina holder which was enclosed with a platinum metal cover. Carrier gas flows between the platinum cover and the alumina sample holder, up to the top of the sample holder, and impinges on the top of the sample. The gas then passes around the crucible and through a small hole in the center of the holder to a gas-density detector. It was estimated that the time lag between the sample and the detector for a gas flow

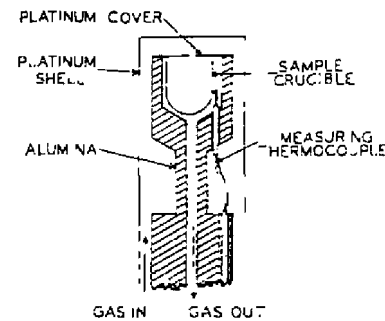


Figure 8.27. EGD temperature calibration sample holder (120).

detector for a gas flow rate of 30 mL/min was less than 6 sec. The preliminary results obtained using this system indicated that the gas evolution was not influenced by various furnace heating rates from 3-lace/min, nor was it appreciably affected by oxygen present in the gas atmosphere. It should be considered as a possible system for EGD temperature calibration; however, a wider range of conditions are required before final acceptance is obtained.

J. OTHER EGD-EGA TECHNIQUES

1. DTGA

In 1975, Mizutani and Kato (38) proposed a new EGA technique called differential thermal gas analysis (DTGA). The technique consists, basically, of a modified EGA method and a high-precision gas-mixing apparatus, which is able to detect not only evolved gases but also gas absorption due to reaction between the sample and a reactor gas. Gases absorbed or evolved by the sample subjected to a programmed temperature change, are determined with the aid of a thermal conductivity detector. It is interesting to note that an almost identical technique was developed for studying catalysts by Cveta-novic and Amenomiya (157) who proposed the name, temperature-programmed reduction (TPR). In TPR, the change in hydrogen gas concentration in a carrier gas, after passing through a temperature programmed reactor containing the test catalyst, was also detected by a thermal conductivity detector.

In DTGA, the gas stream consists of a mixture of an "active gas" which interacts with the heated sample, and an "inert gas" which does not. The sample is heated or cooled at a constant rate in gas mixtures such as $He-O_2$, $He-CO_2$, $He-H_2$, and the like. When interaction, such as absorption or

chemical reaction between the active gas and the sample occurs. the concentration of the active gas in the gas stream decreases. When the active gas is evolved from the sample, its concentration in the gas stream increases. Thus, the displacement of a recorder curve corresponding to absorption and evolution of the active gas appears on opposite sides of the baseline. In comparing this technique with TG, one finds that DTGA corresponds to mass-gain as well as to mass-loss.

A schematic diagram of the DTGA apparatus is illustrated in Figure 8.28. The apparatus consists of gas-mixing equipment (i), reactor (b), TCD (a), recorder (h), temperature controller (g), sample container (c), trap (d) and furnace (e). The mixed gases pass into the reference cell of the TCD and then through the reactor. Exit gases from the reactor pass through the sample side of the TCD and any unbalance in gas concentration is detected and recorded. It is interesting to note that the maximum temperature of the furnace is 1600°C.

A cross-sectional detail of the reactor is shown in Figure 8.29. The sample container (b) is placed at the top of a platinum tube (c), and the reactor gas introduced from the inlet (k) runs between an outer alumina tube (e) and an inner alumina tube (d). The gas stream over the sample (a) passes through the

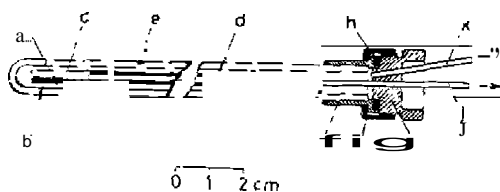


Figure 8.28. Schematic diagram of DTGA apparatus described by Mizutani and Kala (8). a. Thermal conductivity detector; b. reactor; c. sample container; d. trap; e. electric furnace; f. temperature controller; g. thermocouple; h. pen recorder; i. gas-mixing equipment.

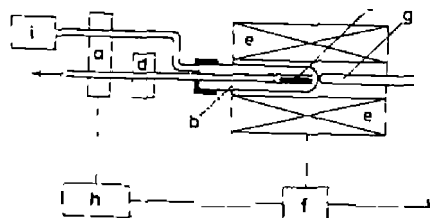


Figure 8.29. Cross-sectional detail of DTGA reactor (38). a. Sample; b. sample container; c. platinum pipe; d. alumina pipe; e. outer alumina pipe; f. fixed device; g. stainless steel cap; h. O-ring; i. screw joint; j. k. stainless steel pipe (inner diameter: 2 mm).

inner alumina tube and stainless steel tube (j) to the detector. The inlet and outlet tubes (j, k) are joined with solder to the stainless steel cap (g), whereas the outer alumina tube (e) is fixed to the stainless steel fixed device (f) with an adhesive to prevent gas leakage. Two metallic devices (f, g) are connected by a screw joint (i) and sealed with an O-ring (h). Sample changes are easily made by unscrewing the housing and replacing the sample holder. The metallic devices (f, i, g) are stable even when the system is heated to 1600°C.

The gas mixing greatly affects the baseline stability of the recorder. It is best to use a premixed gas mixture but the precision gas-mixing equipment described permits the use of many different types of gas mixtures. The baseline stability is also affected by the temperature changes of the TCD and the gas stream flowing through it. Accordingly, this part of the system was placed in a thermostat ($\pm 0.5^\circ\text{C}$). A trap is used for the separation or analysis of the evolved gases. Selective separation from the gas stream is achieved by use of a cold trap or an absorption trap containing *pzOs*, ascarite, and so on. The DTGA apparatus is described as very sensitive, usable, and trouble-free compared to other thermal analysis techniques.

2. Temperature Programmed Reduction (TPR)

The TPR technique consists of passing a 5% hydrogen in a nitrogen gas mixture over a catalyst sample and monitoring the change in hydrogen content of the effluent gas as the temperature is continuously increased. A continuous record of the rate of reduction of the catalyst is obtained, which usually contains several peaks. These peaks are related to the different catalyst components and are useful for studying the preparation, activation, and deactivation of catalysts particularly in cases in which the active catalyst components interact with the support or with each other as in alloying. The technique thus permits a profile or "fingerprint" of the catalyst reduction reaction to be obtained. It is eminently suitable for studying low-loaded highly dispersed systems whose characterizations are beyond the limits of detectability by most other direct methods of structural analysis such as X-ray diffraction, and so on.

A schematic diagram of the apparatus is shown in Figure 8.30. The catalyst sample, contained in a quartz tube, is surrounded by a small electric furnace whose temperature is controlled by a linear temperature programmer. The inert helium carrier gas is replaced by a 5% hydrogen-in-nitrogen reducing gas mixture, and the change in hydrogen concentration is monitored with the thermal conductivity detector. Since the gas flow is constant, the change in hydrogen concentration is proportional to the rate of hydrogen consumption or rate of catalyst reduction. The gas leaving the catalyst sample passes through small absorption tubes that remove water and other reduction

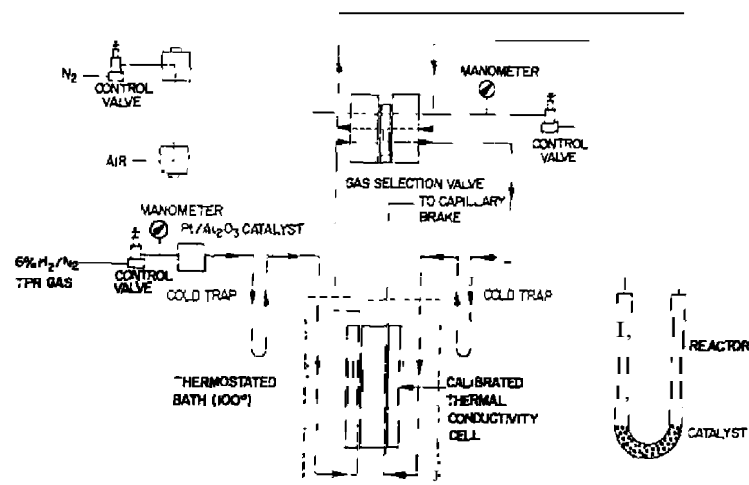


Figure 8.30. Schematic diagram of TPR apparatus described by Robertsor, et al. (120).

products that otherwise would interfere with the hydrogen analysis. A nitrogen-filled sample loop can be switched into the gas flow to calibrate the apparatus. The recorder is equipped with an integrator to measure the hydrogen gas peak areas; the integrator response can be calibrated directly in terms of the amount of hydrogen consumed.

Typically, 0.5 g of catalyst is used with a reducing gas flow rate of 600–1200 mL hr⁻¹. The reactor is heated at a linear rate of 4.5–10°C min⁻¹ over the temperature range of -80–700°C. A reduction peak in a TPR curve is typically 50°C wide, so in principal, 10 or more different components can be resolved.

Similar systems have been described by Tsuchiya et al. (152, 153), Smut7.ek et al. (154), Chan and Anderson (155), and Luengo et al. (using a GC detector) (156).

3. Automated EGD Apparatus

An automated EGD apparatus has been described by Nesbitt and Wendlandt (123,124). The term *automation* refers here to a system that is capable of automatically introducing, heating, and ejecting the sample without the attention or assistance of an operator. A number of samples, usually eight, are preloaded in sample containers and placed in the appropriate positions on the sample tray. These are sequentially introduced into the furnace,

undergo a preselected heating cycle, and are then removed, all automatically. After cooling the furnace to a preselected starting temperature, a new sample is introduced and the cycle is repeated.

A schematic diagram of the automated EGD apparatus is shown in Figure 8.31. Basically, the apparatus consists of a sample-changing mechanism and furnace, a programmer to control the rate of furnace temperature change, a thermistor thermal conductivity cell and bridge circuit, a two-channel strip-chart potentiometric recorder, and a helium supply and gas flowmeter. The electronic circuits for the sample changer mechanism were the same as previously described for the automated DTA apparatus (121).

The principal component of the EGD apparatus is the sample changer mechanism, which permits the automatic loading and removal of the samples. It is illustrated in Figures 8.32 to 8.34.

The sample, which is contained in an aluminum cup on a Pyrex glass rod centered in a sample lift disc, is elevated into the furnace and positioned directly below a pair of thermocouples. An O-ring, seated in a groove in the lift disc, seals the furnace so that the carrier gas entering the furnace base continuously circulates through it. The upper limit of travel of the lift disc platform is set by a microswitch which controls the reversible motor driving the platform elevation screw. As the furnace is sealed, the furnace programmer, on a relay delay circuit, is powered. The furnace is a Vycor tube, 25 mm in diameter and 6.4 cm in length, which is wound with 15 ft of Nichrome II resistance wire and covered with suitable asbestos insulation. As the furnace is sealed, the chart drive of the 2-pen strip-chart recorder is also powered. When the furnace temperature reaches a preselected maximum limit, the sample lift disc is lowered from the furnace and set back in to its place on the sample table tray. This tray is rotated by a small synchronous electric motor

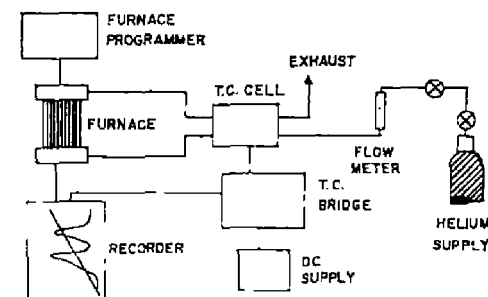


Figure 8.31. Schematic diagram of automated EGD apparatus of Nesbitt and Wendlandt (123, 124).

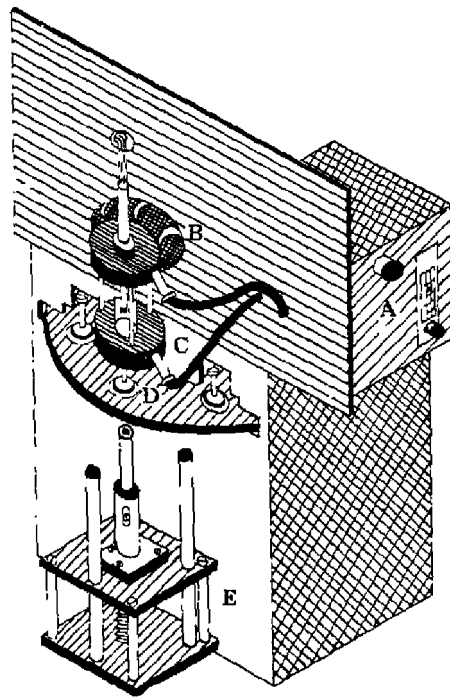


Figure 8.32. EGO sample changer mechanism. A, gas-metering valve and TeD chamber; B, cooling fan; C, furnace assembly; D, lift disc; E, platform (123, 124).

equipped with an electromagnetic clutch. The rotation of the tray by the motor is controlled by a lampslit-photocell arrangement. As the tray rotates, the furnace programmer is automatically reset, and the cooling fan is activated. When the furnace temperature decreases to a preset minimum (normally room temperature), a meter relay controlled by one of the furnace thermocouples starts the next cycle of operations, replicating what has just been described. The cycle is repeated eight times, after which a groove cut into the sample table tray intercepts a roller type microswitch that cuts off all power to the instrument.

The gas flow to the furnace is controlled by a two-stage gas regulator, a metering valve, and a valved flowmeter. Gas leaving the flowmeter passes first through one port of the thermoslatted thermistor-type thermal conductivity cell, and then exhausts to the atmosphere. The two-pen recorder

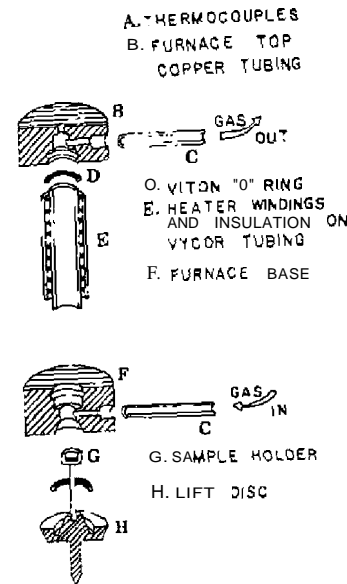


Figure 8.33. Exploded view of EGD sample changer (123, 124).

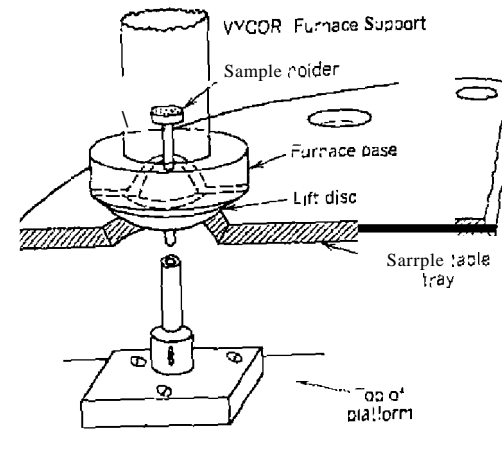


Figure 8.34. Detailed view of EGD sample chamber (123, 124).

simultaneously records both the furnace temperature and the imbalance of the thermal conductivity cell Wheatstone bridge circuit.

The obvious advantage of this apparatus is the automatic changing of the eight samples contained in the sample tray. Operation is completely automatic and once started, it does not require the attention of the operator. By the addition of a suitable data-logging system, the apparatus can be made semiquantitative if carefully calibrated.

4. EGA-MS

Gallagher (150) has described a system capable of mass spectrometrically analyzing the gaseous species evolved from a sample when heated either isothermally or at a programmed rate in the temperature range 100–1300°C. The apparatus is highly sensitive to both condensable and noncondensable gases, and provides: (1) linear heating rates from 0–400°C/m; (2) a short diffusion path so that time lag, condensation, and reactions with the environment are minimal; (3) data collection and presentation can be accomplished in a variety of modes. A block diagram of the apparatus is shown in Figure 8.35.

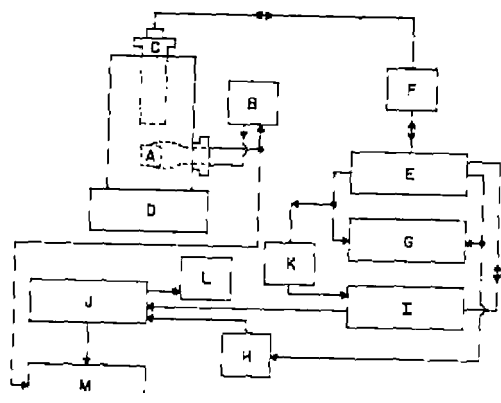


Figure 8.35. Block diagram of EGA apparatus (150). A. Furnace, RADAC-X; Luxel Co.; B. furnace controller, Speedomax, SCR, stepdown transformer, Leeds and Northrup Co.; C. quadrupole mass spectrometer head 100C, UTI Co.; D. turbomolecular pump 2404 D, Sargent Welch Co.; E. Control unit mass spectrometer 100C, UTI Co.; F. RF unit mass spectrometer 100C, UTI Co.; G. scope 130C, Hewlett Packard Co.; H. relay; I. MS programmer QPC10, Balzar Co.; J. integrator CR5-204, Columbia Scientific Co.; K. voltage divider, 1:10; L. teletype 33, Teletype Co.; M. recorder 3000 2 per., Houston Instrument Co.

The sample is heated in a molybdenum furnace containing a 1-cm³ volume alumina or Pt crucible. The furnace is inserted into a vacuum chamber through a quick connect port that includes the electrical feedthrough for the thermocouple (Pt-Pt, 0% Rh) and for the low temperature-high current required by the furnace. An upper flange supports the quadrupole mass spectrometer, positioned about 2.5 cm above the furnace. Included in this flange are a thermocouple gauge, a toggle valve to the atmosphere, and a bellows valve used for back-filling the system with helium gas. The chamber is evacuated by a turbomolecular pump to a pressure of $\leq 1 \times 10^{-6}$ Torr. An output of 0–10 V from the mass spectrometer is proportional to the range of atomic mass number selected from 0–300 amu. This signal is used for the oscilloscope display and its return to 0V is used to trigger a relay that signifies the beginning of a new scan in the data collection system.

5. Detection of Water Evolution

The detection and determination of water (or moisture) in a wide variety of industrial and chemical products is of great interest. Analytical techniques for water determination include chemical, spectroscopic, thermal, electrical, gravimetric, and physical techniques. One of the most versatile techniques is based on coulometry (130). This technique generally involves absorption of the water onto a hygroscopic material, from which it is subsequently electrolyzed. The current required for the electrolysis is directly proportional to the water absorbed. One such commercially available instrument based on this principle is the Du Pom 902 moisture evolution analyzer (MEA), illustrated in Figure 8.36.

The sample is weighed and placed in the oven where the water is vaporized. Nitrogen carrier gas flows through the molecular sieve dryer into the oven, where it absorbs the water vapor and transports it to the electrolytic cell.

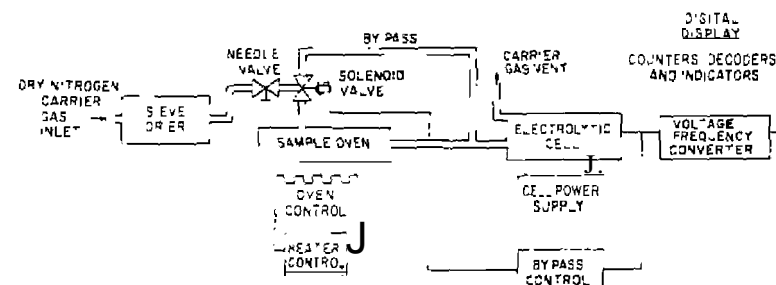


Figure 8.36. Du Pont 902 moisture evolution analyzer (130)

The electrolytic cell contains a V-shaped tube with two parallel, helically wound, platinum electrodes. A thin film of P_2O_5 is deposited between the electrodes; this substance readily absorbs the water from the carrier gas. The absorbed water transforms the P_2O_5 to H_3PO_4 , a conductor. A voltage on the platinum electrodes then electrolyzes the absorbed water to H_2 and O_2 . The current required for this electrolysis is integrated, scaled, and displayed on a digital readout device. Water levels as low as 1 ppm or as high as 10,000 ppm can be determined.

This instrument has been used to determine the water contents of many substances, included among them are polymers (131-137) pharmaceutical products such as penicillin, vitamins (138) effervescent tablets (139). Nuclear fuels, pulping black liquor, minerals (141) and coal (140) have also been studied.

Kristofet al. (142-144) have described a water detector in which the water in a carrier gas is absorbed on a hygroscopic material contained on a sintered glass filter. The liberated heat of absorption is detected by means of a coiled resistance thermometer. This apparatus, connected to a derivatograph, is shown in Figure 837. The liberated gases from the derivatograph furnace are transferred by a dry carrier gas (10 Lib) into the detector cell. The gas enters the detector cell through tube 1 and leaves it through tube 2. A hygroscopic material in the detector cell absorbs the water from the carrier gas resulting in the evolution of heat. The heat liberation can be determined by the resistance thermometer, connected in a Wheatstone bridge circuit. The output voltage from the bridge circuit is proportional to the water content of the carrier gas stream. Curve peaks from an injection of 50 mL of water-saturated air into the carrier gas stream are shown in Figure 8.38a. This results in a linear relationship between the area of the curve peak and the amount of water present, as given in Figure 8.38b.

6. Pyrolysis-Gas Chromatography

Onodera (145) has described an EGA apparatus in which the evolved product gases are led directly into a gas chromatograph. This arrangement, called pyrolysis-gas chromatography--was used to study the thermal decomposition products of some cobalt (III) ammine complexes. The apparatus consisted of a pyrolysis chamber, furnace, a furnace temperature programmer, a temperature recorder, and a gas chromatograph equipped with a TCD. Column packing used was silicone oil on Fluoropak-80 in a teflon tube. The pyrolysis chamber consisted of a U-shaped Pyrex glass tube, 15 cm long by 0.4 cm in diameter, which was terminated on both ends by an O-ring joint. The O-ring connectors were used to join the tube to the gas-sampling valve of the gas chromatograph. Heating of the tube was provided by a Nichrome

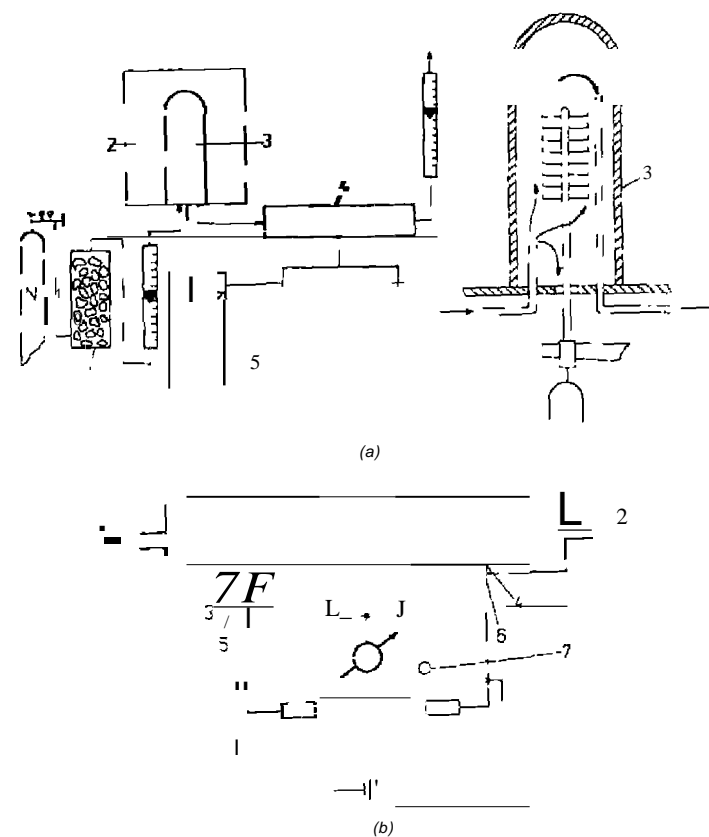


Figure 8.37. a Schematic diagram of water detector apparatus; b schematic diagram of the detector cell (144).

wire coil wound around the tube. During pyrolysis of the samples, helium gas was used to sweep the pyrolysis products into the gas chromatograph.

Another more elaborate pyrolysis-chromatography apparatus was described by MacLaury and Schroll (146), which permitted heating rates from $5^{\circ}C/min$ to $5000^{\circ}C/S$. It consisted of a Chemical Data Systems geological sample and analysis system and a gas chromatograph. This system is a self-contained bench-top instrument that provides a means of trapping volatiles from a DSC100 Pyroprobe solids pyrolyzer. The Pyroprobe uses a platinum

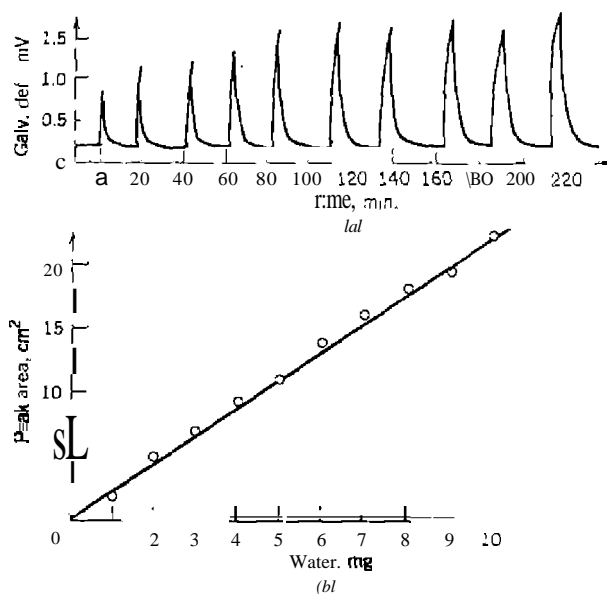


Figure 8.38. (a) Curve peaks obtained by an injection of 50 mL of water saturated air: (b) linear relationship between the curve peak areas and the amount of water present (142).

wire as both the heater element and the temperature detector. A maximum temperature of 1000 and 2°C can be achieved at heating rates from 5°C/m to 20°C/ms. The evolved gases can be monitored with a FID as well as a TeD. Volatiles can be monitored by splitting the evolved gas flow between one FID and a trap filled with Tenax-GC, a highly absorbent polymer for trapping most organic compounds.

7. Flame Ionization Detection

A flame ionization detector has been used by Eggerlsen and co-workers (96-100) to detect carbon-containing compounds in gaseous pyrolysis products. The apparatus consists of a small sample furnace coupled to a high-temperature flame ionization detector. A dynamic carrier gas transports the evolved gases from the pyrolysis furnace to the detector. The essential components of the apparatus are shown in Figure 8.39. The sample furnace and detector jet are constructed of Vycor tubing as a single unit. Due to the unitized construction and the high temperature of the flame

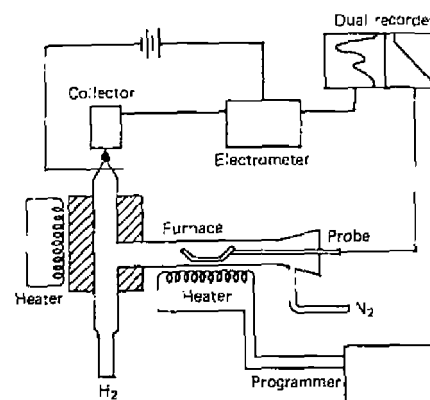


Figure 8.39. Schematic diagram of flame ionization detector system (100).

ionization detector (FID), normally 500°C, complete recovery of the volatile products is possible. The furnace is heated with a resistance wire heater element which is controlled by a precision temperature programmer. The flame jet is heated by a stainless steel block. Provision is made for injecting standard gas samples from a syringe, via a septum inlet, for convenient calibration of the detector response. The sample boat is made of aluminum, gold, or platinum and is held in a stainless steel wire frame attached to a sheathed thermocouple.

The FID method possesses high sensitivity, uses smaller samples than TG, can routinely detect decomposition rates of 0.01%/min, and can detect rates down to 0.001%/min if desired. The lowered limit of detection is of the order of 1×10^{-4} μg of carbon per minute. However, as found in previous work on the thermal stability of polymers (97), it is hardly feasible to utilize this high sensitivity because of the heating blank obtained even with a well-cleaned system (burnout with air at 550°C). The high sensitivity of the detector makes it possible to obtain meaningful thermal data curves with as little as a few micrograms of material. Vapor-pressure measurements can be made below the level of 1 mTorr (96).

A FID curve of polyvinyl chloride polymer formulation yielded four peaks corresponding to: a pesticide (79°), a plasticizer (179°), a stabilizer (275°), and the polyvinyl chloride (438°).

Trace amounts of organic carbon compounds in water can also be determined by this technique (99). The sample is heated in a nitrogen carrier gas in two stages to determine volatile (150°C) and nonvolatile (150–550°C) organic carbon. The water evaporated in the first stage changes the detector response

to some extent, but this can be taken care of by proper the calibration technique. The lower limit of detection is about 0.2 ppm. The method is especially effective for determining trace organic material that is volatile or steam-distillable under the conditions of the analysis. Results for the nonvolatile portions are sometimes low, particularly for natural organic material such as carbohydrates and proteins. In some cases, however, this can be compensated for by proper calibration techniques.

8. Thin-layer Chromatography

Although not a very widely used technique in this application, thin-layer chromatography (TLC) has been used to analyze evolved gaseous products and also for kinetics studies. Permanent-type gases, of course, cannot be handled by this technique, but high molecular weight compounds, which may be difficult to identify by other methods, can be separated and characterized. In addition, the equipment required for TLC is much less expensive than that required for any of the other methods.

The technique used by Rogers (93, 4) involved the heating of the sample under a flowing carrier-gas stream at a programmed rate (or isothermally) while impinging the carrier-gas stream containing the decomposition products onto the surface of an activated TLC plate. The plate is transported across the orifice of the pyrolysis stream as a function of sample temperature. Therefore, any position along the zone of application of the plate corresponds to a specific sample temperature. The plate can then be developed by the usual chromatographic techniques to separate the individual products of the reaction. The final plate yields two types of data: R_f data in the direction of development, and temperature data along the zone of application.

A developed TLC plate for TNT (93) showed that the TNT and volatile impurities begin to vaporize and appear on the TLC plate between 125 and 135°C, corresponding to the first appearance of gas in the pyrolysis curve. Most of the TNT vaporizes, and is collected undecomposed since it is a relatively stable compound thermally. Within the temperature range where TNT dissociates exothermally, as indicated by the DTA curve, the following products appear: 2,4,6-trinitrobenzyl alcohol (TNB-OH); 4,6-dinitroanthranil (DNA); 1,3,5-trinitrobenzene (TNB); 2,4,6-trinitrobenzoic acid (TNB-a); and a trace of an unidentified compound. The combination of the precision of the TLC method with the characteristic colors of the spray reagent make it relatively simple to identify all the major components found.

The TLC technique has also been applied to the study of reaction kinetics by Rogers and Smith (94).

Stahl (95) described a pyrolysis procedure that also used TLC to identify

the decomposition products. The sample was introduced into a glass cartridge with a conical tip and heated rapidly for a short period of time. The emerging gases were deposited as a spot on a TLC plate and developed with suitable reagents. He described numerous variations of the standard procedure and demonstrated its application of the analysis of drugs, food additives, and residues, and to phytochemistry.

Rogers (93) concluded his investigation of this technique by stating that it will probably be most useful for the study of polymeric materials. It should be possible to study large repeating units rather than just the simplest ultimate pyrolysis products. Because no thermal conductivity, flame ionization, or other detector is used, it is not necessary to employ specific carrier gases for best results. Mechanisms and interactions can be studied in any gas or vapor system, for example, oxygen, air, nitrogen, helium, hydrogen, carbon dioxide, or mixtures containing water vapor, acids, ammonia, and SO₂.

9. Thermoparticulate Analysis

The technique of thermoparticulate analysis (TPA) consists of the detection of evolved particulate material in the evolved gases as a function of temperature. In the presence of supersaturated water vapor, these particles provide condensation sites for water, and hence can be detected by light-scattering techniques. Water droplets grow very rapidly on the particulate matter (condensation nuclei) until they are of a sufficient size to scatter light. The scattered light, as detected by a phototube in a dark-field optical system, is proportional to the number of condensation nuclei initially present. It is an extremely sensitive measurement, with the capability of detecting one part of material in 10¹⁵ parts of air. The technique was first employed by Doyle (90) and has been reviewed by Murphy (91, 92).

A schematic diagram of the apparatus for TPA measurements is shown in Figure 8.40. The polymer samples, 1 × 0.125 × 0.014 in., were heated in a copper tube furnace that was programmed for a temperature rise of 50°C/h. Hydrogen was passed over the sample at a 3 mL/sec flow rate, but because the condensation nuclei counter required a gas flow of 100 mL/s, additional amounts of nitrogen were added beyond the furnace and heat exchangers. Some materials studied by this technique are shown in Table 8.7.

Murphy (91) has also described a converter that will generate condensation nuclei from a reactant that would normally not be detected by TPA. For example, ammonia can be detected by passing it through a flask containing a small amount of hydrochloric acid. The gaseous HCl above the solution reacts with the ammonia to form condensation nuclei of ammonium chloride. Other gases and the conversion processes employed are shown in Table

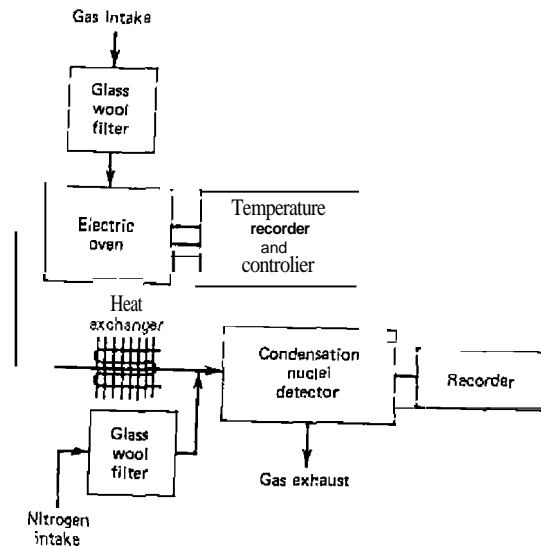


Figure 8.40. Schematic diagram of TPA apparatus (92).

Table 8.8. Gases Detected by Condensation Nuclei Techniques (93)

Compound	Conversion Process	Easily Detected Conc. (ppm)
Ammonia	Acid base	0.005
Benzene	Photochemical	2
Carbon dioxide	Electrochemical	5
Carbon monoxide	Chemical	1
Chlorine	Chemical	1
Ethyl alcohol	Reverse photochemical	5
Freon :2:21	Pyrolysis	2
Hydrogen chloride	Acid base	0.5
Hydrocarbon	Photochemical	11.1
Methyl mercaptan	Oxidation-photochemical	0.01
Ethylamine	Acid-base	0.5
Mercury	Photochemical	0.001
Nitrogen dioxide	Hydrolysis	0.5

8.8. The TPA method is continuous, capable of gas analysis through conversion techniques, and able to detect condensation nuclei. It is the only thermal technique with the last named capability.

10. Organic Particulate Analysis

In 1976, Phillips and Smith (158, 159) described a technique called *organic particulate analysis* (OPA) in which the particulate or aerosol matter emitted by a heated organic compound was detected and recorded. This technique is essentially identical to that of thermoparticulate analysis [TPAI, discussed previously]. The apparatus employed an ion chamber to detect the submicron particles by their influence on the output current of the instrument. Small ions were produced by a low-level radiation source containing the particulate matter. In the absence of particulate matter, almost all the ions are collected which results in a maximum output current of a magnitude determined by the strength of the radiation source and the ionization properties of the gas stream. When particles are present in the ionized gas stream, some ion-particle combinations take place. Because the particles are much larger than the ions, the mobility of the resultant charged particle is less, and only a few of the species are collected in the ion chamber. The result is a decrease in the output current of the ion chamber, this decrease being a function of the particle concentration and particle size. Concentrations as low as 2×10^{-10} g/L can be detected. When temperature and ion current are monitored, this

Table 8.7. Decomposition Temperatures of Polymeric Materials by Thermoparticulate Analysis (91)

Material	Atm.	Heating Rate (°C/h)	Decomposition Temp. (°C)
Poly(methyl methacrylate)	H ₂	50	310-320
	Air	50	242
	Air	180	237
Polystyrene	H ₂	50	337
	H ₂	50	337
Phenol-formaldehyde resin	H ₂	50	432
Polychlorinated ethylene	N ₂	180	340
Copper phthalocyanine	N ₂	180	230
Zinc 4,4'-bis(3-thiophenyl)pyridine	N ₂	180	255
	N ₂	180	255
	Air	180	350

results in an organoparticulation pattern for a specific organic compound. Temperatures that are significant from the data include: (1) threshold temperature, which corresponds to the onset of organoparticulation and (2) temperature at which there is a 50% decrease in the ion current. These values enabled an *organoparticulation temperature range* to be determined for each compound. Mass spectrometry was used to characterize the organoparticulate matter emitted by the organic compounds.

The OPA technique has been applied to isocyanate compounds (160, (61)), malonic acids (162), metal acetylacetonates (163), and diazonium compounds (164). There are also numerous industrial uses of the technique.

II. Titrimetric Methods

The amount of an evolved gas can be determined by a continuous titration method. A carrier gas removes the evolved gas from the furnace chamber and transports it to an aqueous-absorbing solution where it is continuously titrated. The titrant used will depend on the type of evolved gas to be determined. For example, ammonia is titrated with dilute hydrochloric acid, whereas water is determined by the Karl Fischer method. Compounds that can be determined include water, hydrogen chloride, ammonia, sulfur dioxide, carbon dioxide, and chlorine (80).

Paulik and co-workers (80-86) described the combination of titration analysis with the Derivatograph. By means of a continuous titrator, a curve of the evolved gas can be made, which they call the *thermo-gas-titrimetric* (TGT) curve, or the derivative of it, the *derivative thermo-gas-titrimetric* (DTGT) curve. This apparatus is illustrated in Figure 8AL. The sample in the furnace is surrounded by a silica chamber that can be flushed with an inert carrier gas. Evolved gases are transported by the carrier gas to the absorbing solutions, where they are titrated with a suitable reagent. The amount of titrant used is recorded as a function of time by means of a recording buret.

Fischer and Chiu (165) described the coupling of a thermobalance to an automatic titrator. A schematic diagram of the apparatus is given in Figure 8.42. A DuPont 951 thermobalance was coupled to a Radiometer RTS 822 titration system through a glass joint interface, as shown in Figure 8.43. An autoburet delivers titrant to the titration cell as determined by the sensing electrodes. The volume of titrant added as a function of time or temperature is recorded by a recorder. The interface capillary tube must be the proper diameter to provide optimum recovery of the eluted components. It was found that this diameter should be 0.125 in. with a length of about 4.5 in. A gas flow of 100 ml./min is recommended with a furnace heating rate of 10 °C/min. However, for certain samples, a slower heating rate of 2 °C/min is utilized to attain complete recovery.

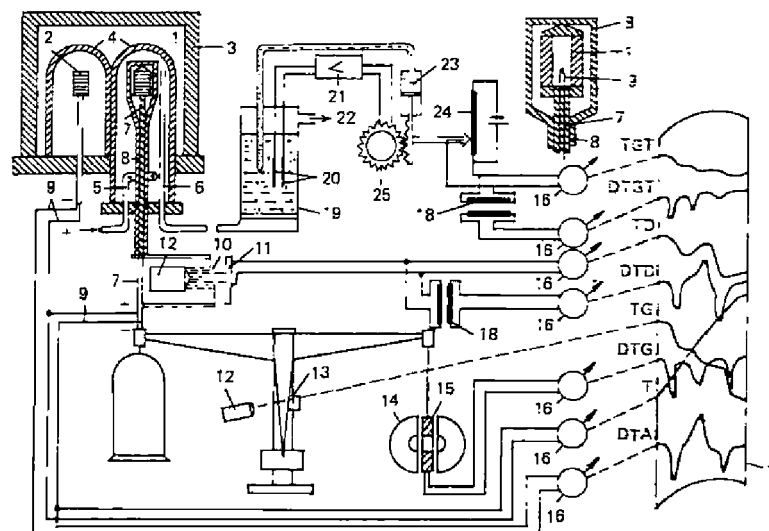


Figure 8AL. Apparatus for the parallel recording of DTA, T, TG, DTG, TGT, and DTGT curves (86). 1, compressed test piece; 2, compressed reference substance; 3, furnace; 4, silica bell; 5, inlet tube for carrier gas; 6, tube for gas extraction; 7, silica tube; 8, silica tube with stirrup-shaped end; 9, thermocouple; 10, diaphragms; 11, light cell; 12, lamps; 13, optical slit; 14, magnet; 15, coil; 16, galvanometer; 17, photographic paper; 18, derating transformer; 19, absorber; 20, electrodes; 21, amplifier; 22, vacuum pump; 23, automatic burette; 24, potentiometer; 25, servomotor.

12. Infrared Spectroscopy

Infrared spectroscopic techniques have long been used to analyze gas streams in industrial chemical processes. Recently, with the advent of fast-scan infrared spectrometers, they have been used as gas chromatograph detectors. One requirement of their use, needless to say, is that the compound must possess one or more infrared absorption bands. By means of a carrier gas, the evolved gas sample from a pyrolysis chamber can be readily passed through an infrared cell for analysis. Infrared systems that can be employed include (1) nondispersive analyzers, (2) dispersion spectrometers, (3) band-pass filter-type instruments, and (4) interference spectrometers; all these techniques have been adequately reviewed by Low (87).

Kiss (88, 89) coupled a Chevenard-type thermobalance with a type UR10 spectrophotometer; the evolved gases from the thermobalance were passed through a 10-cm-ID infrared cell. A method was developed in which either

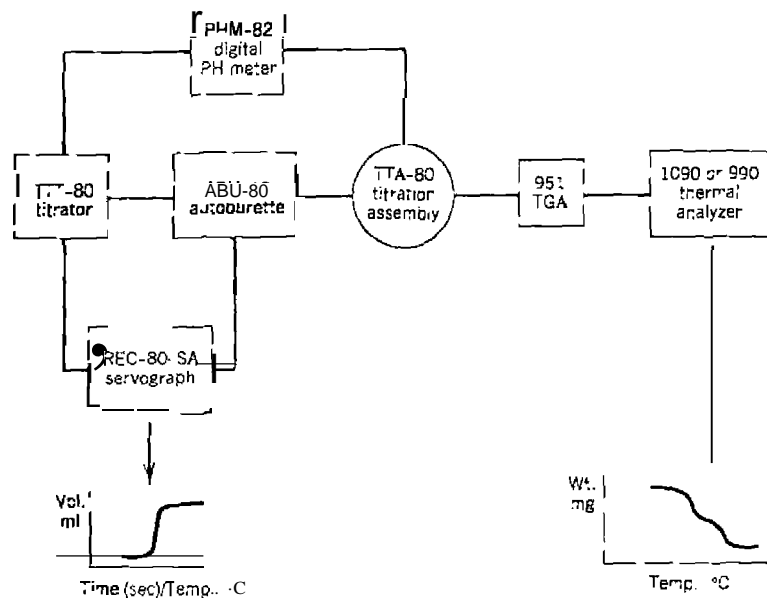


Figure 8.42. Schematic diagram of coupled TG-titration system of Fischer and Chiu (165).

the ammonia or the water (via C_2H_2 generation) content of the evolved gases could be determined. Water was not measured directly because the presence of hydrogen bonding in the molecule greatly diminished the sensitivity of the absorption measurement. However, by passing the evolved water over calcium carbide, acetylene was generated which could be detected by means of an absorption peak at 728.0 cm^{-1} . Other compounds investigated include ammonium paramolybdate and ammonium paratungstate. In a later investigation, binary mixtures of ammonia and water (C_2H_2) were determined by this technique (89).

13. EGD Measurements at Subambient Pressures

A standard method for determining solution kinetics of compounds that evolve gaseous products is to measure the amount of gas given off at constant pressure as a function of the amount of liquid displaced from a volumetric buret. Alternatively, it is possible to monitor the change in pressure at constant volume. Timberlake and Martin (125) have described an apparatus that

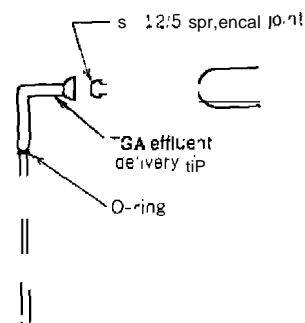
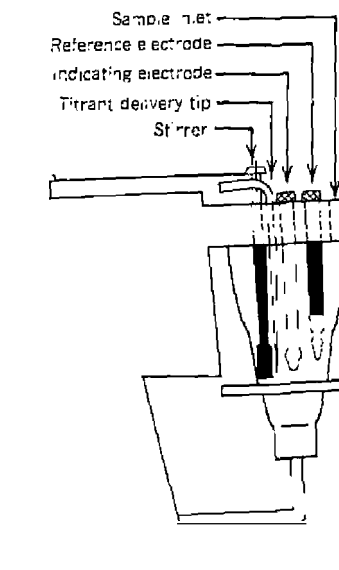


Figure 8.43. Interface of the TG-titration system of Fischer and Chiu (165).

records pressure changes automatically and continuously. Good precision was obtained for total pressure changes of 0.1 atm with pressure changes as small as 10 microns can be detected. This apparatus has been used to study the decomposition of a number of azoalkanes, which thermally evolve nitrogen in a first-order process, although the apparatus could be used to study any reaction that generates CO , CO_2 , SO_2 , hydrocarbons, and so on.

A schematic diagram of the apparatus is shown in Figure 8.44. The apparatus is constructed of 2 mm id capillary glass tubing, which is filled with mercury (shaded portion). The liquid sample solution is placed in flask B and attached to the glass system at D with a spring clamp. The gaseous products exert a pressure on the mercury at E, raising the level at G until mercury touches the electrical contact I, which has been inserted into H. This closes the mercury switch and activates the mercury filled buret, N, driving mercury into the system at N and L. Deactivation occurs when the pressure in the closed air system at L and B are equal and contact is broken at G. A strip-chart recorder continually records these "activations" (approximately 50-75/min) through a potentiometer attached to the piston-driven shaft on the buret. The difference between the recorder pen deflection after complete reaction and the various time intervals during the reaction is directly proportional to the pressure difference $P - P'$.

According to Bouwknegt et al. (126, 127), there is very little good data on the dissociation pressures of the alkaline earth carbonates below a pressure of 10 Torr. They thus developed two systems that could be used to measure heterogeneous dissociation reactions at low pressures and reliably determine the dissociation temperature, the rate of dissociation, and the dissociation pressure. A schematic diagram of the two systems are shown in Figure 8.45.

The systems illustrated permit dissociation pressure measurements in the 10^{-3} and $10^{-3} - 10^{-5}$ Torr (*b*) pressure ranges. In the former, the pressure

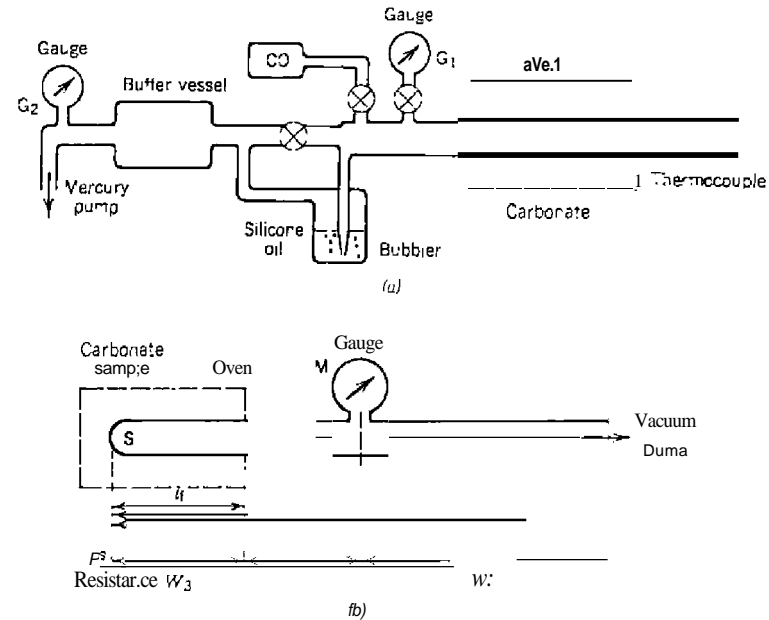


Figure 8.45. EGO systems for low-pressure dissociation measurements: (a) 10^{-3} Torr range (126); (b) $10^{-3} - 10^{-5}$ Torr range (126).

equalizer is a washing bottle or bubbler partly filled with silicone oil. The level of the oil determines the pressure during the measurement. It is operated against a low-pressure side. Pressure inside the system is measured by gauge G_1 , whereas gauge G_2 measures the mercury diffusion pump side. The sample, which is contained in a nickel boat, is pumped continuously by the diffusion pump.

The other apparatus (*b*), consists of a tube, with a circular cross section of diameter d and length L , which is connected to a vacuum pump. The sample is placed at $X = 0$, the end of the tube, which is heated over length l , by an electric furnace. The pressure at $X = l_m$ is indicated by gauge M and is related to the pressure just above the sample S . The equations required to calculate this pressure are given by the authors (31).

A simple technique was used by Wendlandt (1131) to record the changes of pressure in a system. The apparatus, which is illustrated in Figure 8.46, consisted of a vacuum system whose pressure is determined by a mercury-filled manometer tube containing a resistance wire. This wire is connected as one

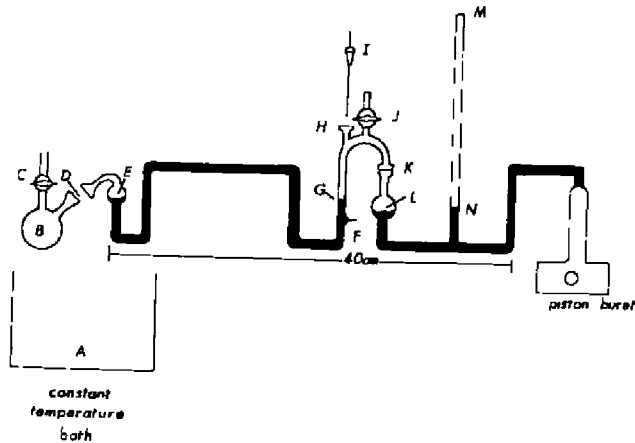


Figure 8.44. Constant-volume variable pressure kinetic apparatus of Tishbake and Martin (125).

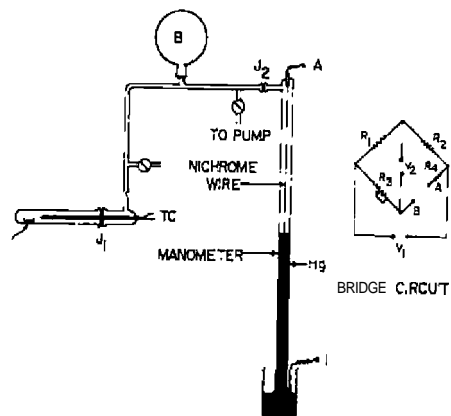


Fig. 1. Variable pressure apparatus as described by Wendlandt (113). $R_1 = 1200 \Omega$; $R_2 = 50 \Omega$, to turn; $R_3 = 10 \Omega$; $V_1 = 1-4V$; V_2 is bridge output voltage. V_3 50-500 mL.

... or a wheatstone bridge. As the mercury column rises and falls in the manometer, the resistance of the wire causes an unbalance voltage in bridge. This voltage is recorded as a function of temperature (EMF of thermocouple) on a recorder. The pressure range in the system can be varied by a change in more of the following parameters: (1) sample size, (2) system volume, (3) bridge voltage, V_1 , or (4) recorder sensitivity.

14. Emanation Thermal Analysis (ETA)

a. Introduction

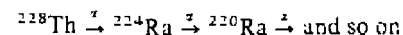
The technique of emanation thermal analysis (ETA) is a method by means of which information about the solid state and its changes are obtained on the basis of the amount of gas release from solids, measured at various temperatures (182). Inert gas atoms are used as trace indicators of the solid state and its changes but do not react with the solid in which they are incorporated. Their release is controlled by physico-chemical processes in the solid such as structural changes, interaction of the solid sample with the surrounding atmosphere, and the establishment of chemical equilibrium of reactions taking place in the solid. ETA is not a method of analysis, strictly speaking; the amount of gas release is used for the characterization of the solid state. Both radioactive and nonradioactive (stable) inert gas isotopes can be used although the former are more useful owing to their simple and sensitive detection.

Release of the radioactive gas makes possible the monitoring of various types of changes taking place during the thermal cycle. These include chemical reactions such as dehydration, thermal dissociation, synthesis, polymorphic transformations, melting, conversion of metastable amorphous structures into crystalline compounds, and changes in the concentrations of lattice defects. The ETA technique possesses several advantages over conventional TG and DTA. Under dynamic conditions, it permits the study of structural changes of compounds even when these changes are not related to a thermal effect (e.g., second-order phase transformations). In other cases, when finely crystalline or amorphous phases are formed, ETA is more sensitive than X-ray methods.

ETA is not a new technique; Rutherford (183) and Kolovrat-Chervmskii (184) working in the laboratory of M. Curie in Paris in the early 1900s showed that the release of radioactive emanation from radium salts depends on temperature. In the 1920-1930 period, Hahn and his co-workers in Berlin developed the emanation method which was used to investigate surface properties of precipitates used in analytical chemistry. Numerous investigators from all over the world used the method in the 1940s and 1950s to study a wide variety of problems in solid-state chemistry, metallurgy, physical chemistry, catalysis, colloid chemistry, and so on. The use of ETA with other thermal analysis methods was first studied by Balek and his co-workers in Czechoslovakia, beginning in the late 1960s. Balik recently reported the results of his work and that of others in a monograph (185) published in 1984. The growth of papers in this area is shown by the bar chart in Figure 8.47 (186). Starting in 1900, the number of papers published during each decade up to 1970 are recorded. Reviews on ETA of interest to thermal analysis also include those by Balik (187-192).

b. Instrumentation

Labeling of Solids. The classical emanation method used natural radioactivity (radon isotope emanation). During preparation of the solid, the inert gas is usually incorporated by coprecipitation of trace amounts (10^4 counts/g of substance) of the parent isotope of the gas (e.g., ^{228}Th and/or ^{224}Ra) from solution (190). When this is not possible, the sample is impregnated with a solution containing ^{228}Th and ^{224}Ra nuclides. The inert radioactive gas is formed in the substance due to the nuclear reactions



Other methods of sample labeling are based on the introduction of the gas itself into the solids without use of the parent isotope. These methods

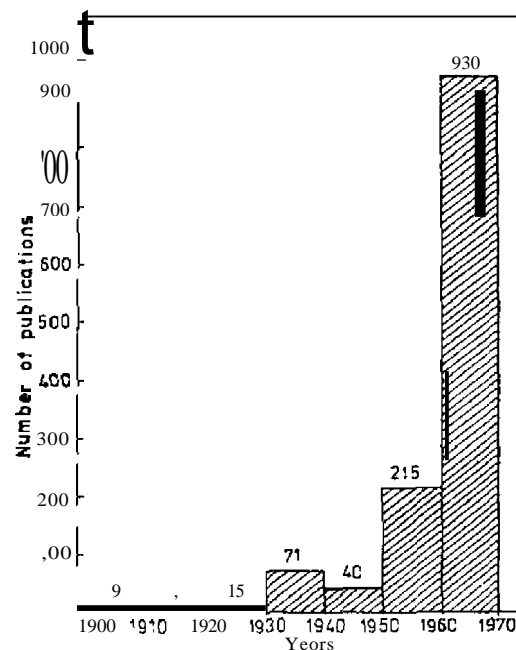


Figure 8.47. Number of emanation papers (including ETA) in each decade from 1900 to 1970 (196).

include: (1) recoil energy of nuclear reactions, (2) accelerated inert gas ion introduction, (3) diffusion process at a higher temperature and pressure in an inert gas atmosphere, and (4) crystallization of solids from melts or sublimation of solids in an atmosphere of radioactive gas.

All the preceding techniques yield products in which the incorporated gas is more or less stable, [open gas atoms are situated in interstitial positions in the crystal lattice.

Measurement of Inert Gas Release. Generally, it is possible to measure either the radioactivity of the gas remaining in the solid or the quantity of the gas released. A typical apparatus, for measurement of the latter and also DTA and TDA, is shown in Figures 8.48 and 8.49 (187). A labeled sample (generally 100 mg), a DTA reference material (Al_2O_3), and a sample for dilatometric measurements are placed in the sample holder. Temperature measurement is by thermocouples embedded directly into the samples. A

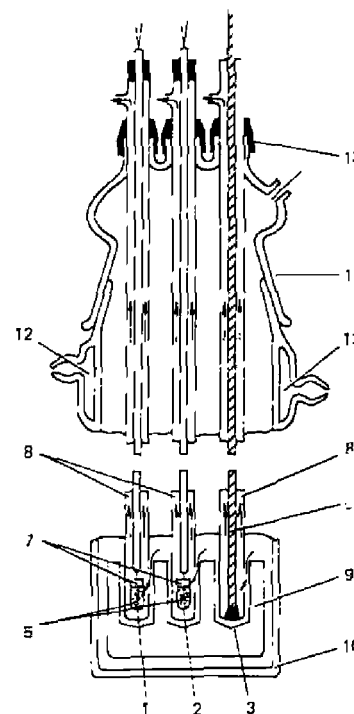


Figure 8.48. Reaction chamber for concurrent ETA, DTA, and dilatometric measurements (after Balek, 187). 1, activated sample; 2, DTA standard; 3, dilatometer sample; 5, composite thermocouple; 6, quartz dilatometer rod; 7, quartz vessels; 8, supporting pipes; 9, metal block; 10, quartz outer vessel; 11, ground glass joint; 12, coolant tube.

heating rate of 8-10°C/min is normally used since this is an optimum rate for DTA as well as ETA measurements. The radioactive gas released from the solid sample is carried by a carrier-gas stream that flows at a constant rate into the cells for gas radioactivity measurements (Figure 8.49). The apparatus simultaneously registers the α -activity of radon and the α -activity of xenon, introduced by ion bombardment. An ETA curve is recorded together with the DTA and dilatometric curves using a multipoint recorder.

Another apparatus, which permits the recording of Simultaneous ETA, DTA, and TG DTG, is shown in Figure 8.50 (192). The system consists of a commercial DTA apparatus and thermobalance manufactured by Netzsch-Geratebau, Selb, West Germany. For ETA measurements, an inert carrier-gas is passed over the sample S and the standard material 1 situated in the isothermal region of the furnace F. The radioactive emanation released from the sample is carried into a measuring cell. The alpha-activity of the emanation is counted by means of a silicon surface barrier detector D connected

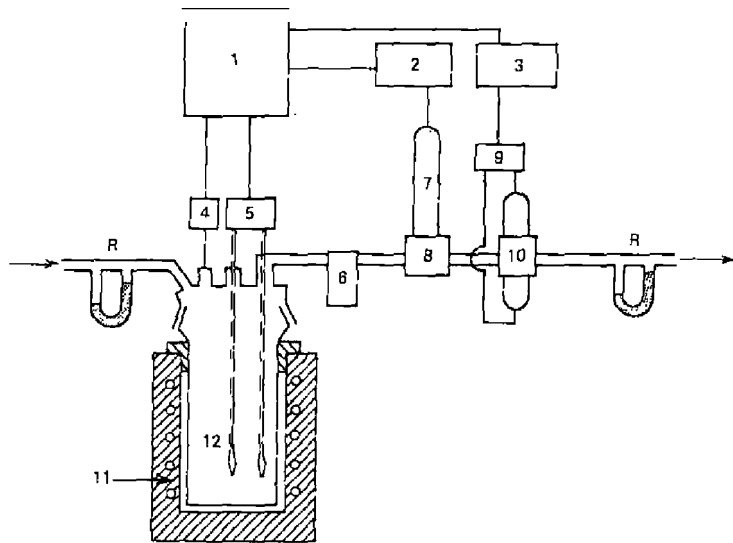


Figure 8.49. ETA apparatus (187). 1, electronic potentiometer; 2, alpha count integrator; 3, beta integrator; 4, dilatometer pickup; 5, thermocouple; 6, gas dryer; 7, photomultiplier; 8, scintillation chamber; 9, cathode repeater; 10, emission measurement chamber; 11, electric heater; 12, quartz reaction vessel; R, rheometer.

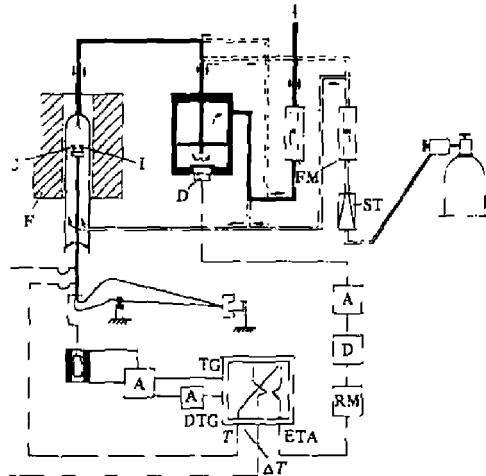


Figure 8.50. Apparatus for simultaneous ETA, DTA, and TG/DTG measurements (194). A, amplifier; D, silicon surface barrier detector; F, furnace; I, standard material; S, sample; FM, flow meter; ST, flow stabilizer; RM, count-rate meter.

to a count-rate meter. The ETA signal is recorded simultaneously with the DTA, TG, and DTG signals as a function of time t or temperature T of the sample. Experimental conditions were: heating rate of $10^\circ\text{C}/\text{min}$; sample mass of 100–200 mg; inert N_2 gas flow rate of 80 mL/min; and Al_2O_3 as the DTA reference material.

Inert Gas Release from Solids. The inert gas incorporated into a solid can be evolved as a result of chemical reaction, physical transformation or of damage to the crystalline state, inert gas diffusion, or the recoil of inert gas atoms (190, 191). The gas release is dependent on the technique used for labeling, that is, if the inert gas itself or its parent nuclide was introduced into the solid. If the inert gas is a result of the former, the gas atom may escape from the solid in one of the following pathways, as shown in Figure 8.51 (190). When the parent atom lies close to the surface of the solid, the recoil energy (of the order of 100 keV) which the inert atom gains during the decay of the parent may be sufficient to eject it from the solid, or it may escape by diffusion before it decays.

According to the theories of both the recoil and the diffusion processes (194), the release rate of the inert gas is given by

$$E = E_r + E_d = (r_0/4)(S/M)\phi + (D/\lambda)^{1/2}(S/M)\phi \quad (8.1)$$

where E_r is the part of emanation release due to recoil, E_d is the part of emanation release due to diffusion, r_0 is the range of recoiling atoms, S is the surface area, M is the grain mass, ϕ is the density, and λ is the decay constant of emanation. E_r is temperature-dependent and at room temperature is usually larger than E_d . At elevated temperatures, E_d rises because

$$D = D_0 \exp(-\Delta H/RT) \quad (8.2)$$

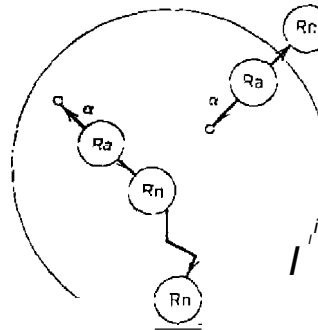


Figure 8.51. The recoil and diffusion processes of inert-gas release from a spherical grain (190).

where D_0 is the preexponential term, ΔH is the activation enthalpy of diffusion of emanation in the solid, R is the gas constant, and T is the absolute temperature.

When an inert gas is incorporated into a solid without its parent nuclide, the inert gas can be released by various diffusion processes, depending on the diffusion mechanisms.

All the theoretical considerations are valid assuming that no chemical or physical transformations take place in the solid during heating. If a change in the structure or surface of the solid takes place, discontinuities occur in the ETA curve.

c. Applications

Two types of information can be obtained from ETA measurements. The first is indirect information about processes occurring in the solid. Any process proceeding within a solid and leading to a change in either the surface to volume ratio or the diffusivity of the emanation atoms becomes directly observable. This is the basis of the numerous qualitative ETA applications to the study of solid-state processes such as aging, recrystallization, modification changes, dissociation, solid-state reactions, and so on.

The second is the fact that it is possible to obtain direct information about specific surface or diffusion parameters of the inert gas in the solid. The experimental conditions must be maintained so that a state of radioactive equilibrium is not destroyed during measurement of the emanation release rate. Labeling samples becomes extremely important since any theoretical approach starts with the assumption of some well-defined distribution of the immediate parent throughout the solid. The diffusion coefficient, D , and the activation enthalpy, ΔH , of diffusion of emanation can be determined. From a plot of $\log Ed$ versus $3/T$ obtained during the heating or cooling of the sample, the Tamman temperature can be calculated; the temperature, T , estimated from the ETA cooling curve, indicates the temperature at which the defect equilibrium achieved by previous heating is frozen.

The temperature dependence of the rate of emanation release from Fe_2O_3 is shown in Figure 8.52a. Alternatively, a semilogarithmic curve of the form $Ed J(1/T)$ may be constructed, as shown in Figure 8.6, the quantity Ed being evaluated from E (emanation power at the relevant temperature) and E_r (value of E measured at room temperature). In Figure 8.52b, two slopes may be seen in the curve—a low-temperature section with a low value of $2 \log E_d/2T$ and a high-temperature section with a larger value of $2 \log E_d/2T$. The discontinuity on the curve lies at 693°C , that is, 0.53 of the absolute melting point of Fe_2O_3 . With other crystalline, powdered inorganic substances, the discontinuity on the curve corresponds to 0.5–0.6 of their

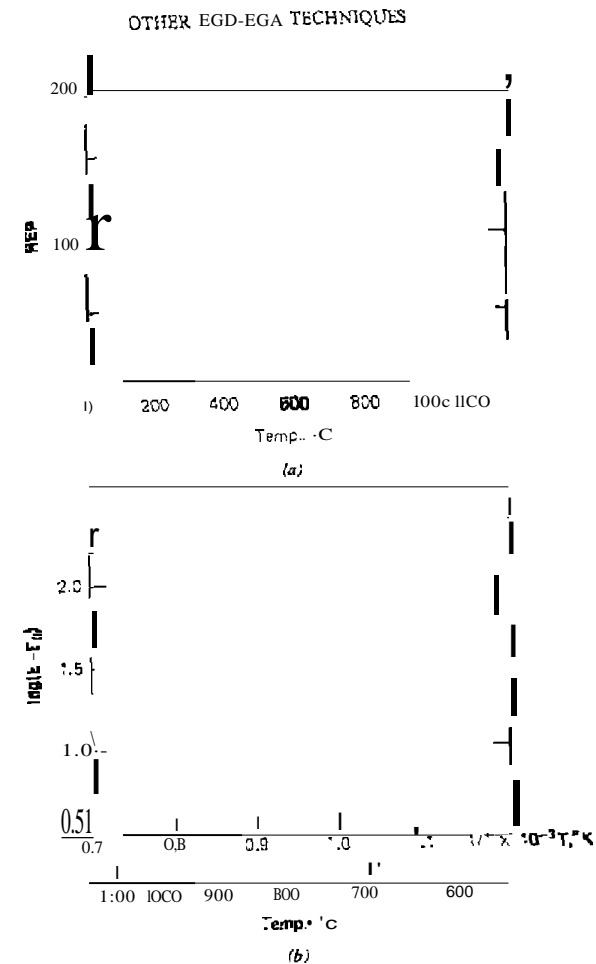


Figure 8.52. ETA curve of Fe_2O_3 . (a) $\ln E_r \cdot I(T)$ coordinates; (b) $\ln \{E - E_r\} = I(T)$ coordinates. E_r is the value of E at room temperature (204).

absolute melting point. This temperature is related to the beginning of sufficiently intensive motion of atoms or ions in the crystal lattice to cause an effective diffusion rate in the solid.

Based on the classical emanation method, it is therefore possible to determine this temperature range, which is of great practical importance since above this approximate temperature the solid-state reaction can occur

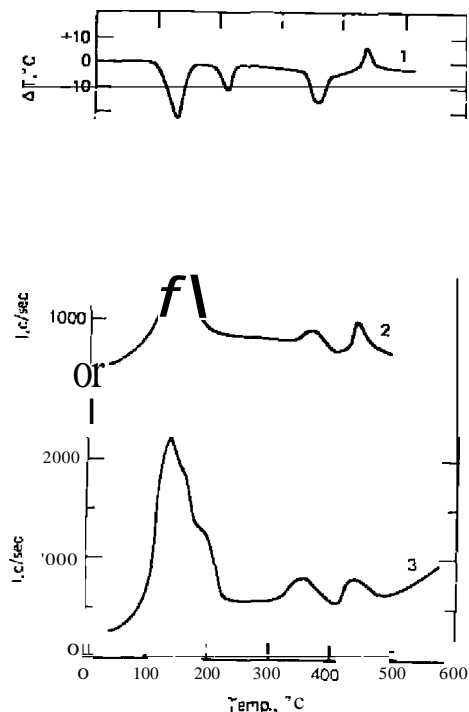


Figure 8.53. The thermal decomposition of $\text{Th}(\text{C}_2\text{O}_4)_2 \cdot 6\text{H}_2\text{O}$. 1, DTA curve; 2, temperature dependence of xenon release; 3, ETA curve (87).

by diffusion mechanisms. The slope of individual sections of the curve can be used to determine the activation energy of the emanation process in a solid for a specified temperature range. The E of random diffusion in Fe_2O_3 was evaluated as $Q = 15 \pm 3$ kcal/mole in the range 600–700°C and $Q = 40 \pm 5$ kcal/mole in the range 850–1100°C.

The ETA and DTA curves (187) of $\text{Th}(\text{C}_2\text{O}_4)_2 \cdot 6\text{H}_2\text{O}$ are illustrated in Figure 8.53. The ETA curve reveals three processes taking place: (1) stepwise dehydration in the temperature range 40–220°C (the DTA curve shows only two endothermic peaks in this range for the transitions of $6\text{H}_2\text{O} \rightarrow 2\text{H}_2\text{O}$ and $2\text{H}_2\text{O} \rightarrow 1\text{H}_2\text{O}$); (2) the flat peak in the 300–400°C range corresponds to decomposition of $\text{Th}(\text{C}_2\text{O}_4)_2 \cdot \text{H}_2\text{O}$; (3) the last peak, at 400–500°C, is due to the conversion of amorphous ThO_2 to crystalline. The curve of the rate of release of xenon that had been incorporated into the sample by ionic bom-

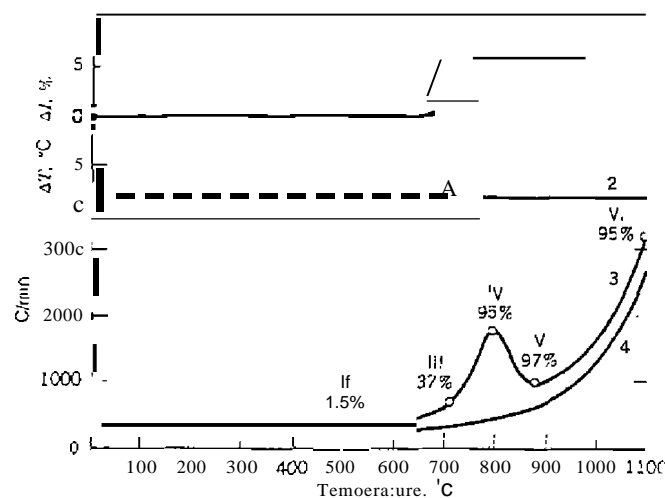


Figure 8.54. ETA, DTA, and TDA curves of $\text{ZnO} + \text{Fe}_2\text{O}_3$ mixture (196). 1, DTA; 2, TDA; 3, ETA; 4, reheating ETA. Percentage of ZnO reacted indicated for samples I-IV.

bardment fully confirms the reaction sequence indicated by the ETA curve:

The ETA, DTA, and TDA curves of $\text{ZnO}-\text{Fe}_2\text{O}_3$ mixture are shown in Figure 8.54 (195, 196). The ETA curve is of exponential form, being determined by the diffusion of ^{220}Rn from zinc ferrite. From the emanation rate, $\log ED$ can be plotted as a function of $1/T$, and the activation energy, ΔH_f determined for the diffusion process. The ETA curve reflects all the processes occurring during the solid-state reaction between the $\text{Fe}(\text{III})$ and $\text{Zn}(\text{II})$ oxides. A peak temperature of 790°C can be used to characterize the reactivity of this mixture.

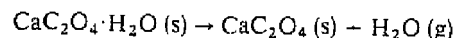
Numerous other applications of ETA have been described (182, 188, 189). Compounds or materials studied by this technique include barium salts of phthalic, isophthalic, terephthalic, benzoic, salicylic, 1,4-aminobenzoic, 1,2-dichlorobenzoic and 1,1-diodobenzoic acids (197); uranyl gels (198, 204); ferric oxide (199); cement (200, 201); powder metallurgy (192); $\text{Ge}_{0.25}\text{Te}_{0.80}\text{Se}_{0.15}$ (202); anatase (TiO_2), gibbsite, and kaolinite (193); thoria (ThO_2) powder (204); and many others.

K. APPLICATIONS OF EGD-EGA

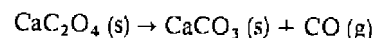
One of the most studied inorganic compounds for TG and DTA is calcium oxalate I-hydrate, $\text{CaC}_2\text{O}_4 \cdot \text{H}_2\text{O}$. This compound has been used to deter-

mine the instrument and sample parameters that affect TG (167) and DTA curves (37). Numerous EGD and EGA curves have been reported for $\text{CaC}_2\text{O}_4 \cdot \text{H}_2\text{O}$; however, only several will be discussed here.

A comparison of the EGA curve with the corresponding TG and DTA curves has been given by Emmerich and Bayreuther (75); these curves are illustrated in Figure 8.55. The $\text{CaC}_2\text{O}_4 \cdot \text{H}_2\text{O}$ was studied in a dynamic argon atmosphere in the temperature range from 25° to 800°C. The DTA curve peak between 150 and 250°C corresponds to the dehydration reaction



whereas that between 450 and 500°C is due to calcium carbonate formation, according to the reaction



The curve peak between 650 and 780°C is due to the dissociation of CaCO_3 by the reaction

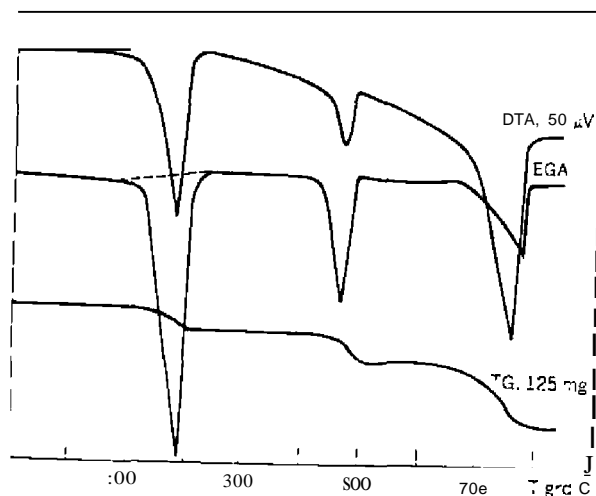
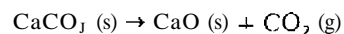
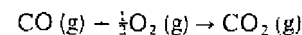


Figure 8.55. EGA, TG, DTA, curves of $\text{CaC}_2\text{O}_4 \cdot \text{H}_2\text{O}$ in argon (75). Dashed line indicates absorption of evolved water.

If the decomposition reactions are carried out in air rather than argon, the gaseous product in reaction (2) is CO_2 rather than CO due to the reaction



Using chemical trapping in DTGA, Mizutani and Kala (38) selectively removed reaction products such as water and carbon dioxide formed during the thermal decomposition of $\text{CaC}_2\text{O}_4 \cdot \text{H}_2\text{O}$. In the curves shown in Figure 8.56, curve (A) was obtained with no trapping and shows three peaks, the first for water, the second for CO and CO_2 , and the third for CO . In curve (B), an Ascarite trap was placed in the system to remove the water (first peak) and carbon dioxide (third peak) from the decomposition products. The second peak, which is in the opposite direction, appears as the reverse of the second peak in curve (A). This is caused by the CO reacting with the He-O_2 reactor gas reducing the concentration of the O_2 due to reaction (4). As a result of this gas composition change, the thermal conductivity of the gas decreases. The CO_2 that is formed is, of course, absorbed by the Ascarite trap.

The increase in pressure due to the evolution of gaseous decomposition products has also been measured for $\text{CaC}_2\text{O}_4 \cdot \text{H}_2\text{O}$ by Wendlandt (40) and Ashby et al. (168).

Using low-pressure techniques, Bouwknecht et al. (126, 127) studied the dissociation pressure of calcium, strontium, and barium carbonates. The pressure curve of a dissociating mixture of 36% (mole ratio) CaCO_3 , 34% SrCO_3 , and 30% BaCO_3 is shown in Figure 8.57. It is seen that the separation between the dissociation range of CaCO_3 and the other two carbonates

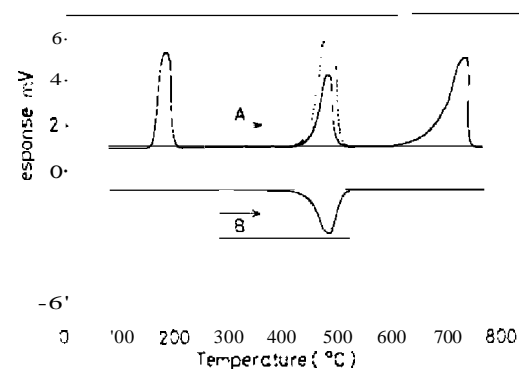


Figure 8.56. Selective trapping of decomposition products of $\text{CaC}_2\text{O}_4 \cdot \text{H}_2\text{O}$ (38). A, no trap; B, ascarite trap.

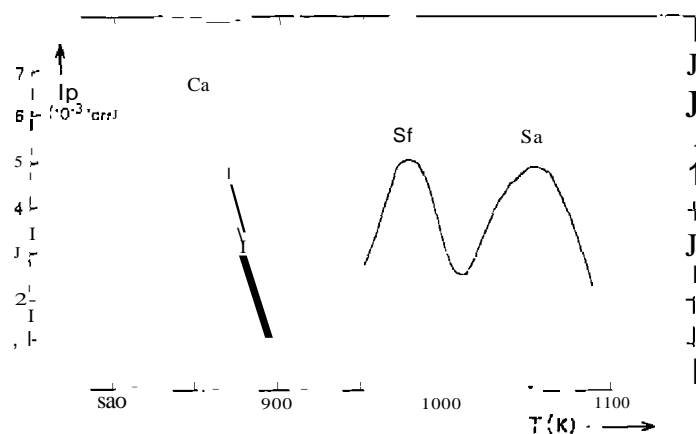


Figure 8.57. Pressure over a dissociating mixture of CaCO_3 , SrCO_3 , and BaCO_3 , (27).

is almost complete, where a fairly broad overlap occurs between SrCO_3 and BaCO_3 . Due to the approximate linearity of the system, the areas under the peaks, assuming no interaction between them, is proportional to the mole content of each component. The authors concluded that the EGO technique at low pressures is a quantitative and relatively precise thermal analysis method, which is rather simple to apply. It is a useful technique in investigations of the kinetics of heterogeneous reactions at these pressures.

The cobalt (III) ammine complexes have been extensively studied by Wendlandt (170) and co-workers. Recently, the cobalt (III) ethylenediamine complexes have been investigated, by EGA (mass spectrometry) and other TA techniques. Several of these studies, as well as those by other investigators, will be discussed briefly.

The EGA curves of $[\text{Co}(\text{en})_2]\text{Cl}_2$ (171) are shown in Figure 8.58. The curves indicate that the evolution of gaseous products occurs in two distinct stages below 400°C with a broad region of gas evolution at higher temperatures. The ethylenediamine evolution curves shows that essentially all of it is evolved in the region under the first peak in the gas evolution curve. Since this reaction is carried out *in vacuo*, the first decomposition step corresponds to the $[\text{Co}(\text{en})_2 - \text{Cl}] \rightarrow \text{CoCl}_2 \cdot (\text{NH}_4)_2\text{CoCl}_4$ transition. Ammonia, which is a fragmentation product of ethylenediamine, is also evolved in the first decomposition step as is shown in the ammonia evolution curves. A second peak in the ammonia evolution curve falls in the region under the second peak of the gas evolution curve. This smaller peak results from the dissociation of $(\text{NH}_4)_2\text{CoCl}_4$, with the evolution of NH_4Cl . The evolution of the

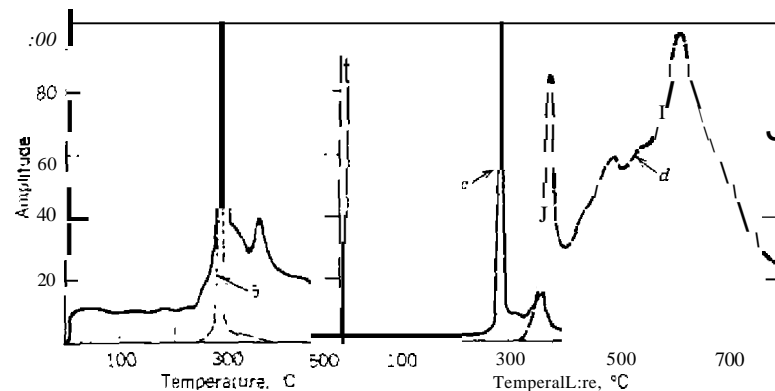


Figure 8.58. EGA curves for $[\text{Co}(\text{en})_2]\text{Cl}_2$ (171). a. gas evolution; b. ethylenediamine evolution; c. ammonia evolution; d. HO evolution.

latter gives the second ammonia peak in the HCl evolution curve which exactly superimposes on the ammonia peaks. The relative peak intensities between these product evolution curves are meaningless since each curve is separately normalized to 100% for the most intense peak. The HCl curve shows that evolution occurs over the entire region above 400°C , due mainly to the decomposition of CoCl_2 intermediates. The thermal behavior of $[\text{Co}(\text{en})_3]\text{Br}_3$ was similar to the chloride complex.

The thermal decomposition of $[\text{Co}(\text{en})_3](\text{NO}_3)_3$ and $[\text{Co}(\text{en})_3](\text{HSO}_4)_3$ (172) was decided much more complex than the corresponding chloride and bromide compounds. The EGA and MS curves for $[\text{Co}(\text{en})_3](\text{NO}_3)_3$ are shown in Figure 8.59. The EGA curve shows two distinct peaks between 100 and 200°C followed by a broad region of gas evolution to over 700°C . The two sharp peaks are due to the initial decomposition step in which $[\text{Co}(\text{en})_3](\text{NO}_3)_3$ decomposes to $\text{Co}(\text{NO}_3)_2$. All of the ethylenediamine and most of the ammonia formed by ethylenediamine fragmentation is evolved in this step. The broad region of gas evolution between 200 and 600°C is due to the release of trapped residues and to the decomposition of the $\text{Co}(\text{NO}_3)_2$. The third small peak in the ammonia evolution curve falls into this region and is due to the release of NH_4NO_3 , which was trapped in the residue during the initial decomposition step. The mass spectrum of gases evolved from the $[\text{Co}(\text{en})_3](\text{NO}_3)_3$ complex at 410°C *in vacuo* shows that very little of the organic residues remains in the system. The peaks that appear are due primarily to the decomposition of $\text{Co}(\text{NO}_3)_2$ and are therefore expected to be products formed from the nitrate ion. The base peak occurs at $m/e = 28$ and is probably due to nitrogen gas. The second most intense peak is at $m/e = 18$,

EVOLVED GAS DETECTION AND EVOLVED GAS ANALYSIS

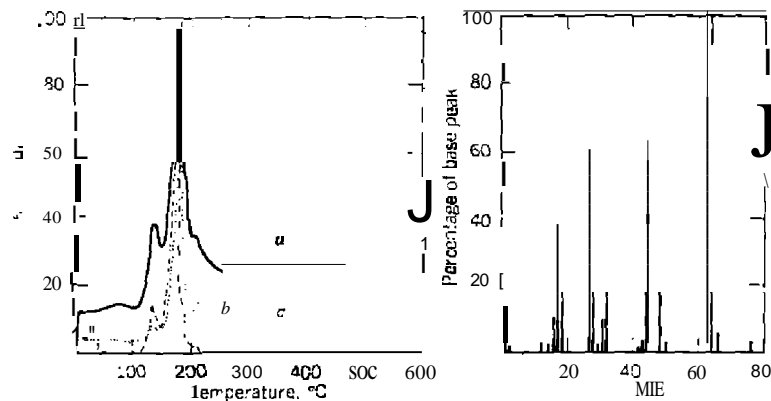


Figure 8.59. EGA and MS curves of $[\text{Co}(\text{en})_3](\text{NO}_3)_3$ (172). *a*, total gas evolution; *b*, ethylenediamine evolution; *c*, ammonia evolution. Spectrum on right is that of gases evolved at 410°C .

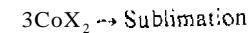
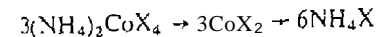
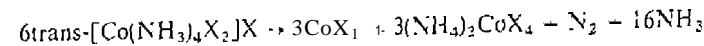
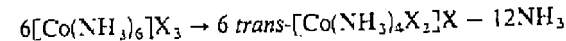
which could be either water or the ammonium ion. The peak of medium intensity at $m/e = 44$ is due to N_2O and the weaker peaks at $m/e = 30$ and 32 are due to NO and O_2 , respectively. The mass spectra of gases evolved at higher temperatures are similar except that the peaks due to trapped organic impurities are much weaker.

The gas evolution curves for the thermal dissociation of $[\text{Co}(\text{en})_3](\text{SCN})_3$ (1172) shows that gas is evolved in three phases. The first large peak arises from the initial dissociation of the complex to the $\text{NH}_4\text{Co}(\text{SCN})_3$ intermediate. The second smaller peak is due to the dissociation of this compound, whereas dissociation of the compound, $\text{Co}(\text{SCN})_3$, is responsible for the gaseous products released between 300 and 800°C . The first step in the dissociation process involves the release of most of the ethylenediamine. This was anticipated since this first step is thought to be the conversion of $[\text{Co}(\text{en})_3](\text{SCN})_3$ to $\text{NH}_4\text{Co}(\text{SCN})_3$ with the evolution of ethylenediamine. However, small quantities of ethylenediamine remain in the system to temperatures in excess of 500°C .

The evolution of ammonia as a function of temperature occurs in essentially two steps. The first large peak in the ammonia gas evolution curve superimposes exactly over the first peak in the ethylenediamine gas evolution curve. Therefore, most of the ammonia is probably due to the fragmentation of the evolved ethylenediamine. The second peak, which extends from about 175 to 250°C , is due to the dissociation of $\text{NH}_4\text{Co}(\text{SCN})_3$. This compound dissociates by first releasing ammonia followed by thiocyanate or thio-

cyanate dissociation products. This can be seen by comparing the ammonia evolution curve with the gas evolution curve for carbon disulfide, a product from the decomposition of the thiocyanate ion. These two curves will not superimpose on each other since the ammonia peak occurs about 15°C below the first carbon disulfide peak. If these two products were the result of the dissociation of an ammonium complex or of NH_4SCN , the two peaks would be superimposable, as in the case of the chloride and bromide complexes. This is another indication that the intermediate is an ammine complex.

The thermal dissociation of the $[\text{Co}(\text{NH}_3)_6]\text{X}_3$ ($\text{X} = \text{Cl}, \text{Br}$) (173) and $[\text{Co}(\text{NH}_3)_5\text{X}]\text{X}_2$ ($\text{X} = \text{Cl}, \text{Br}$) (174) complexes have also been investigated by EGA and other thermal analysis techniques. Although the reaction stoichiometry of the dissociation of $[\text{Co}(\text{NH}_3)_6]\text{X}_3$ ($\text{X} = \text{O}, \text{Br}$) complexes appears to be the same *in vacuo* as in air, the mode of decomposition seems to be somewhat different. The TG-EGA-MS data that has been presented indicates that dissociation *in vacuo* is accomplished according to the following reactions:



Onodera (145) recently studies the thermal decomposition of the $[\text{Co}(\text{NH}_3)_6]\text{Cl}_3$, $[\text{Co}(\text{NH}_3)_5\text{Cl}]\text{Cl}_2$ and $\text{trans-}[\text{Co}(\text{NH}_3)_4\text{Cl}_2]\text{Cl}$ using a GC technique for the separation of the evolved product gases. The EGA curves of the complexes, from 25 – 400°C , are shown in Figure 8.60. For $[\text{Co}(\text{NH}_3)_6]\text{Cl}_3$, the evolution of ammonia began at about 200°C , the maximum intensity for gas evolution being obtained at 250°C . This was followed by a second broad peak in the temperature range of 280 – 340°C . The EGA curves for $[\text{Co}(\text{NH}_3)_5\text{Cl}]\text{Cl}_2$ and $\text{trans-}[\text{Co}(\text{NH}_3)_4\text{Cl}_2]\text{Cl}$ were similar to that of $[\text{Co}(\text{NH}_3)_6]\text{Cl}_3$.

Next to $\text{CaC}_2\text{O}_4 \cdot \text{H}_2\text{O}$, $\text{CuSO}_4 \cdot 5\text{H}_2\text{O}$ has been perhaps the most widely studied by thermal analysis techniques. This compound undergoes a series of interesting dehydration, decomposition, and fusion reactions, if studied to high enough temperatures. All these reactions are shown by the EGA-DTA curves in Figure 8.61, as given by Emmerich and Bayreuther (75). The first three EGA curve peaks are due to the evolution of water, whereas the next three are due to the evolution of a SO_2 , SO , and O_2 equilibrium mixture.

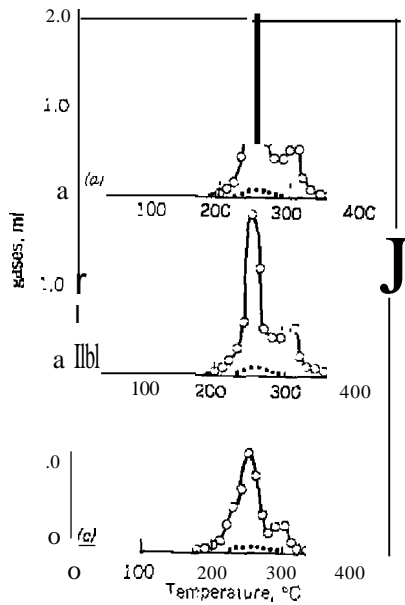


Figure 8.60. EGA curves of cobalt (II) ammine complexes as determined by GC (146). (a) $[\text{Co}(\text{NH}_3)_6]\text{Cl}_2$; (b) $[\text{Co}(\text{NH}_3)_4\text{Cl}_2]\text{Cl}$; (c) $[\text{Co}(\text{NH}_3)_4\text{Cl}_2]\text{Cl}$. (.....) NH_3 , (-----) NH_4^+

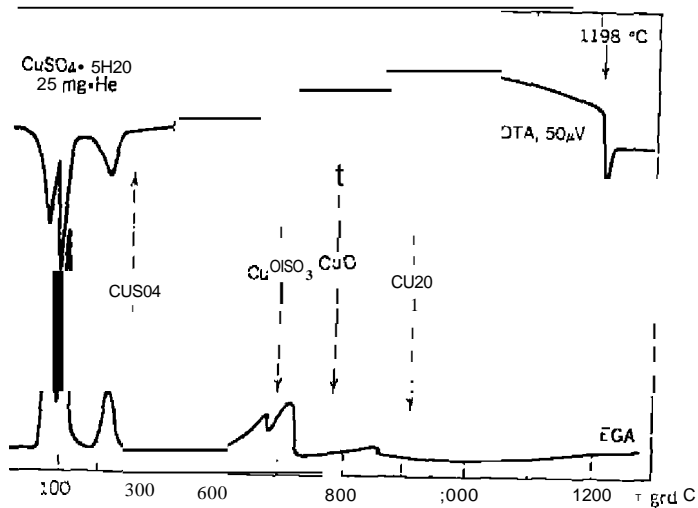
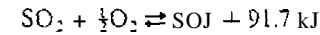


Figure 8.61. EGA, DTA curves of $\text{CuSO}_4 \cdot 5\text{H}_2\text{O}$ (75).

Notice that the fusion of Cu_2O at 1198°C can be seen on the DTA curve but is absent from the EGA curve.

The question of whether SO_2 or SO_3 is the primary decomposition product of anhydrous CuSO_4 was resolved by Baumgartner and Nachbaur (74) using chemical ionization (CI) mass spectrometry coupled to TG-DTA. A plot of the *m/e* 64 (for SO_2) and *m/e* 80 (for SO_3) intensities [or the decomposition composition of CuSO_4 is shown in Figure 8.62. Both SO_2 and SO_3 are indicated in the figure, the presence of which obeys the reaction



Thus, in the thermal decomposition of CuSO_4 , SO_2 and SO_3 must occur simultaneously in a ratio corresponding to the state of equilibrium at a given temperature. A similar conclusion was reached by Collins et al. (175) using a simultaneous TG-MS technique.

The EGA curves of $[\text{Al}_2(\text{SO}_4)_3 \cdot 18\text{H}_2\text{O}]$, as determined by Collins et al. (173), are given in Figure 8.63.

Although large quantities of water were lost during the initial pump-down, these curves show that a substantial amount of water remained strongly attached and was lost in the temperature region of 200–500°C. The dehydration is followed by dissociation of $\text{Al}_2(\text{SO}_4)_3$ between 700 and 900°C. As in the CuSO_4 decomposition, the primary product appears to be SO_3 with SO_2 , SO , and O_2 resulting from dissociation or fragmentation. These data agree with and support the following mechanism which has been proposed

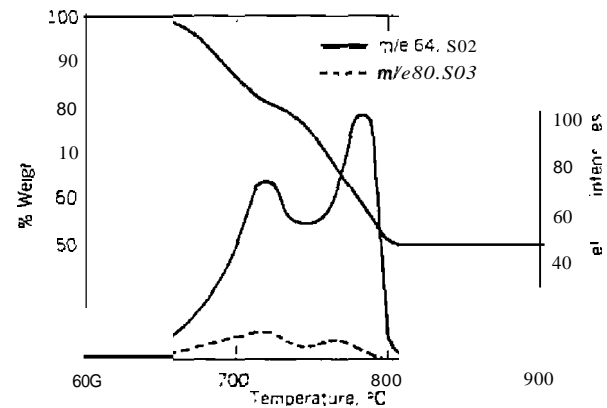


Figure 8.62. TG and MS profile curves for the decomposition of CuSO_4 (74).

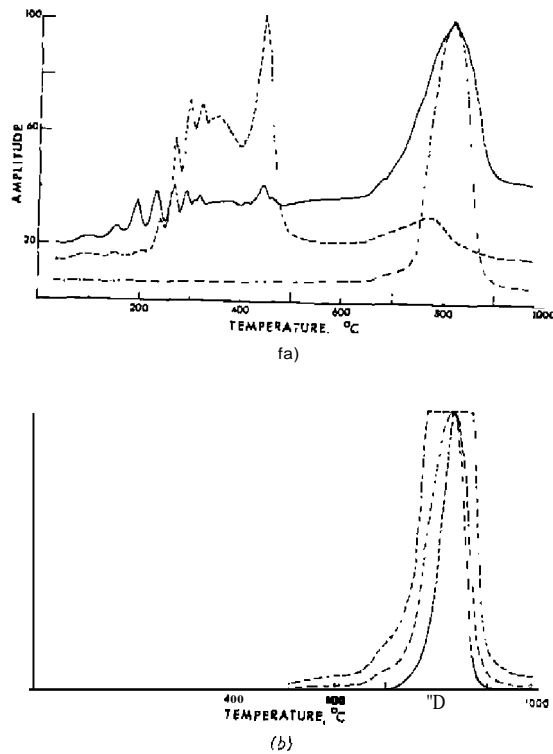
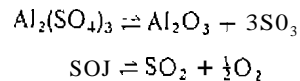


Figure 8.63. MS curves for Al₂(SO₄)₃. 18H₂O (175). (a) EGA curves. (—) total pressure; (---) H₂O; and (- · - · -) O₂. (b) MS curves. (—) SO₂; (---) SO; (- · - · -) SO₃.

previously by Johnson and Gallagher (176):



Intensity measurements of the *m/e* = 80 peak in selected spectra in the sulfate dissociation region yielded values ranging from 2.09-21.48. The lower values are probably more realistic since the high values were obtained during periods of detector saturation. However, in both cases the intensity was of sufficient amplitude to indicate that the peak actually existed and was not due to background noise. Also, the P + 2 peak was observed in some

cases. Previous investigations indicated that the SO₃ peak will always be relatively small even when it is the parent product. The SO₂/SO ratios were approximately the same for the Al₂(SO₄)₃ spectra as for the CuSO₄ spectra.

Collins et al. (177) studied the thermal decomposition of Hg(SCN)₂, HgSO₄, Hg(C₂H₃O₂)₂, Hg(NO₃)₂ and HgNO₃·H₂O using MS and other thermal analysis techniques. Due to space limitations, only the thermal decomposition of HgSO₄ and HgNO₃·H₂O will be discussed here.

The EGA curves of HgSO₄, as illustrated in Figure 8.64, show that decomposition occurs in the temperature interval from 500 to 750°C with the evolution of SO, SO₂, and O₂. No SO₃ could be detected in any of the mass spectra related to the decomposition process. Although this does not preclude the possibility of SO₃ being formed in small quantities that decompose to other sulfur oxides and oxygen, this process seems unlikely as shown in a recent study that indicates that sulfate compounds can decompose through at least two different mechanisms (175).

The EGA curves for HgNO₃·H₂O, as shown in Figure 8.65, indicate that this compound dissociates in three steps. The first step is accompanied by the release of substantial quantities of NO and NO₂ with a small amount of N₂O. This process lies in the temperature interval from 100 to 200°C and represents a mass-loss until about 400°C, at which point the rate of mass-loss becomes more rapid. The second set of evolved gas curve peaks occur between 350 and 475°C and contain large N₂O and NO peaks with only traces of NO₂. No mechanism can be suggested to account for the two sets of nitrogen oxide peaks occurring below 400°C when related to the TG curve data. However, the end product is probably HgO which dissociates between 450 and 600°C, as indicated by the final oxygen peak. The presence of the Hg²⁺

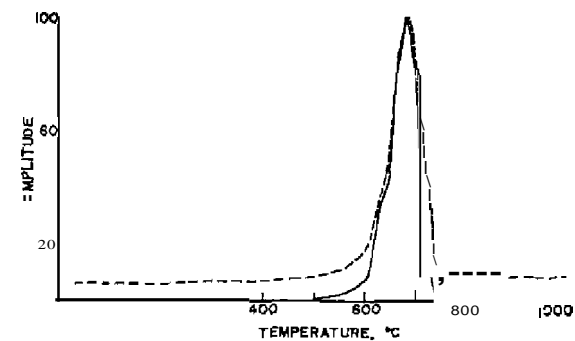


Figure 8.64. EGA curves of HgSO₄ (178): (—) SO₂; (---) O₂.

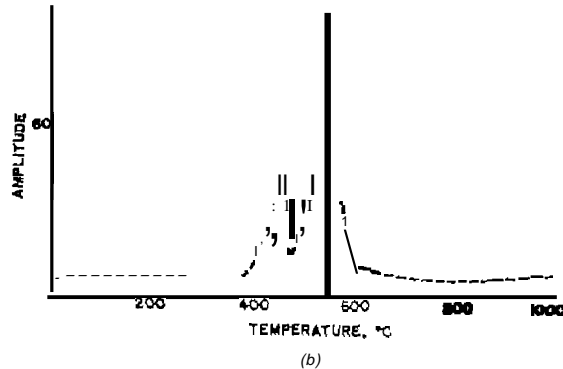
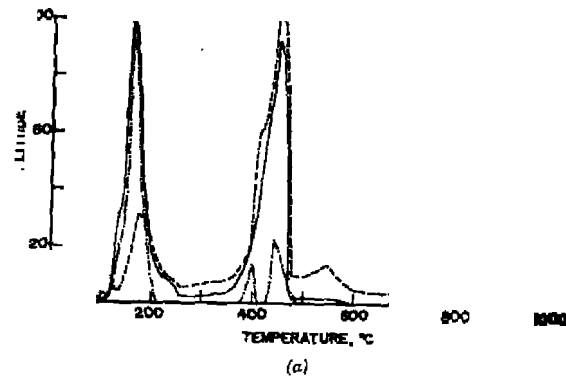


Figure 8.65. EGA curves of $Hg(NO_3)_2 \cdot H_2O$ (178); (a) (—) NO_2 ; (---) N_2O ; (---) NO_2 ; (b) (—) Hg ; (---) O_2 .

ion in this interval suggests that sublimation might also occur. No sample remains in the balance sample holder at temperatures in excess of 600°C. No water was detected during the initial decomposition process since it was removed by low-pressure conditions below 50°C and did not appear on the TG curve either.

Over a decade, Bandi and co-workers have employed EGA-DTA techniques to determine second-phase compounds isolated from steels by selective chemical or anodic dissolution of the matrix. This method has been used qualitatively to identify and quantitatively to determine approximately 35 carbides, carbonitrides, and nitrides, some of which could not be identified

by any other method (see reference 116 for a bibliography). These procedures have also been used in studies of chemical methods used in the isolation of pure Fe_3C from steel, in studies showing changes in carbonitride composition with heat treatment, and to show the change in types of carbides and nitrides formed in steel as the heat treatment of the steel is changed. Such changes are important because the type of precipitate formed is known to have a profound effect on the mechanical properties of the steel.

Quantitative analysis for these compounds is accomplished by monitoring the evolved gas from the programmed combustion or decomposition of an aliquot mass of the residue heated in a dynamic atmosphere of oxygen. From the composition of the gas, it is possible to calculate the amount of nitride or carbide in the steel. The application of EGA is based on the assumption that each metal carbide and nitride has a characteristic combustion or decomposition temperature range, an assumption that is nearly always valid. The usefulness of the method is limited by the difficulty in finding chemical reagents that will attack the steel matrix without destroying the compound to be determined. Also, the particle size of the nitrides and carbides may be so small that it becomes difficult to retain them on the finest pore-size organic membrane (118).

EGA-UTA has been applied to the analysis of Fe_3C , amorphous carbon, and graphite in steel and cast iron (178). In general, the previous claims for isolation of these compounds have been correct. Different amounts of Fe_3C are isolated by various chemical treatment, which explains the contradictions in the literature.

A comparison of the EGA CO_2 curves for residues isolated from highly alloyed cast iron is shown in Figure 8.66. Curve A is the bromine-methyl acetate treated matrix, whereas curve B is the residue from HNO_3 treatment. The curves indicate that both forms of elemental carbon (graphite and amorphous) are easily distinguishable. After combustion in the EGA apparatus, less than 20% of the sample mass of residue isolated by bromine-methyl acetate remained in the sample pan. This indicated that the residue was nearly 90% carbon, and the remainder was Fe_2O_3 from the iron present. Resolution of the EGA with a curve resolver showed that some Fe_3C was not dissolved in bromine-methyl acetate. The iron equivalent of the amount of CO_2 evolved at 380°C fits the microchemical iron value obtained for the isolated residue. This is further proof that the 380°C EGA peak is the result of the combustion of Fe_3C .

Three polymorphous crystalline ferric hydroxides, α -, β -, and γ - $FeOOH$ are known as the major components of naturally occurring oxidized products of iron, which, together with Fe_2O_3 and various amounts of amorphous hydrated oxides, constitute rust on steel surfaces. The properties of each component and the state of the composite formed from the small crystal

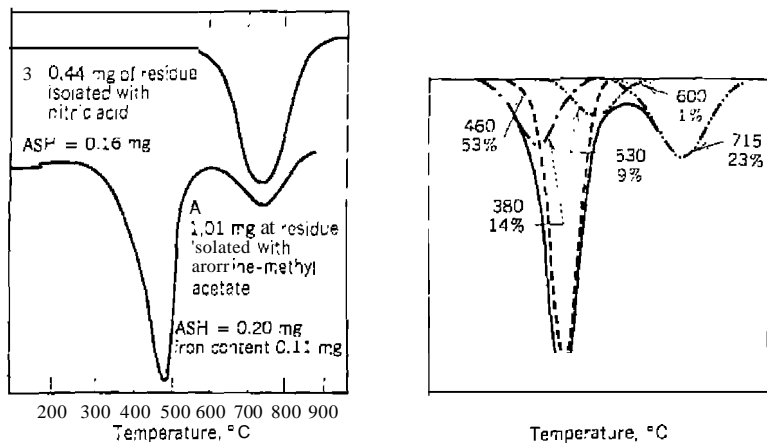
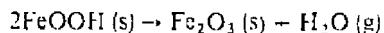


Figure 8.66. EGA curves of residues isolated from cast iron (178). A, treatment of residue with bromine-methyl acetate; B, treatment with HNO_3 . Right curve—resolution of EGA curve.

appear to govern the nature of a steel surface exposed to various environments and whether the steel continues to corrode or is protected from further progression of the corroding reaction. Ishikawa and Inouye (179) subjected the various forms of FeOOH to EGA in order to determine the nature of the adsorbed water on the crystal faces and the mechanism of the formation of water from OH groups on the crystal surface or inside the crystal.

The EGD curves for α -, β - and γ - FeOOH , as given in Figure 8.67, each show three peaks at approximately 70, 180, and 260°C. These peaks correspond to the evolution of water because they disappear when a cold trap is placed in front of the TCD. For β - FeOOH , an additional peak is observed at 370°C, which remains unchanged even when a cold trap of -20°C is inserted in the TCD line. The amounts of water evolved were determined by measurement of the peak areas. In addition to other differences between the samples, the amounts of water evolved from γ - FeOOH at 180°C are larger than the corresponding values for the other samples. In contrast, the value for γ - FeOOH at 260°C is comparatively small. The total amount of water evolved at 180 and 260°C may be considered as fundamentally of structural origin, arising from the decomposition reaction



The water desorbed below 100°C consists of molecules adsorbed physically on the crystal.

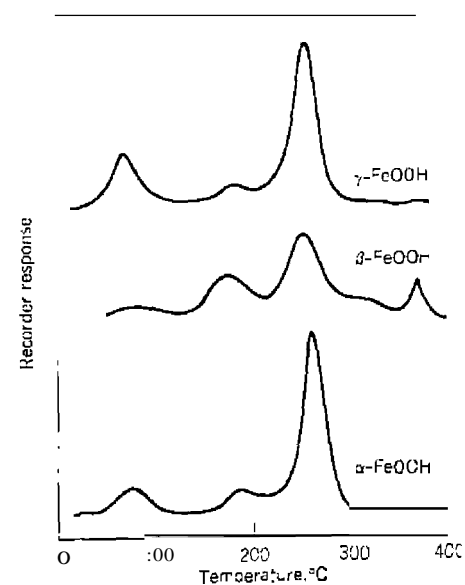


Figure 8.67. EGD curves of α -, β - and γ - FeOOH (179).

The techniques of DTA, and to some extent TG, have long been used by geochemists and others to study the thermal behavior of clays and minerals. Since many simultaneous reactions occur in clays, as well as solid-state reactions that alter the decomposition reaction, the use of other methods such as EGA, X-ray, IR, and so on, are used to supplement conventional thermal analysis techniques. Consequently, there has recently been an unusual amount of interest in the use of EGA (MS) in the study of these compounds.

The EGA and other thermal parameters of opalinuston has been reported by Muller-Vonmoos and Müller (72). In addition to the clay minerals kaolinite and illite, opalinuston contains some chlorite, various carbonate, quartz, micas, feldspars, pyrite, and organic material. Of particular interest are pyrite, organic material and siderite, all of which has a strong influence on the DTA curve. The thermal curves of opalinuston are given in Figure 8.68. Of interest here are the EGA (MS) curves of which curves for molar values of 18 (H_2O), 44 (CO_2), and 64 (SO_2) are presented. This particular sample contained about 1% organic carbon and 1.2% pyrite, both of which were evident from the EGA curves. At 335°C, the organic matter decomposed with the formation of H_2O and CO_2 , and at 412 and 469°C, the pyrite de-

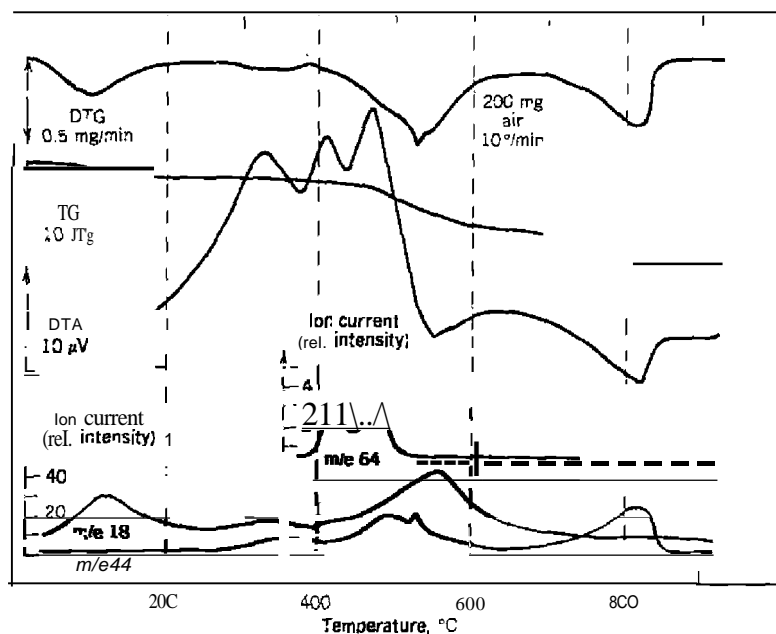


Figure 8.68. EGA and other thermal curves of opalinuston (72).

composed, yielding $5O_2$ as the product gas. The H_2O content of the evolved gases is greatest at about $550^\circ C$. The relatively spontaneous evolution of CO_2 indicates the decomposition of siderite, while the area of the CO_2 peak corresponds to a concentration of this material of 0.4–0.5%. A broad evolution of CO_2 was observed from 400 to $625^\circ C$, caused by the decomposition of higher molecular mass organic material and dolomite and calcite.

The EGA curves of siderite, as determined by GC techniques, were reported by Kubas and Szalkowicz (180). Figure 8.69 gives the EGA, as well as the TG and DTA curves, of siderite, which was heated in a dynamic helium atmosphere. The CO_2 curve peak, as determined by use of Gc, corresponded very well with TG and DTA curve temperatures. There is a small delay in the evolution of CO , which is present even in high-vacuum studies. On the basis of these curves, the decomposition sequence follows the reactions



Morgan (181) studied the thermal decomposition of several natural mineral

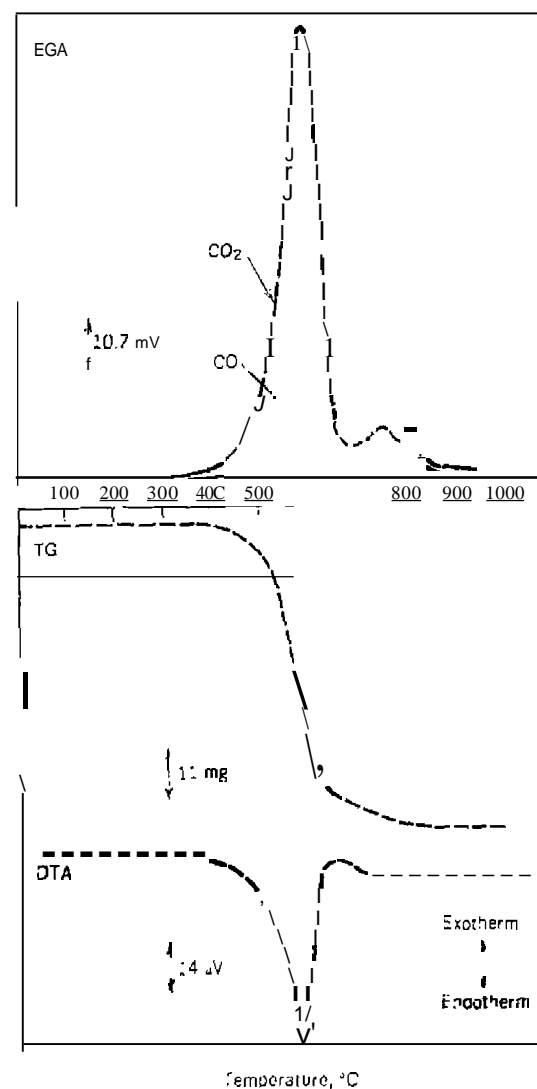
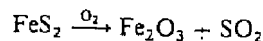


Figure 8.69. EGA-TG-DTA curves of siderite in a helium atmosphere (180)

n mixtures using DTA and commercially available H₂O, CO₂, and SO₂ detectors. These detectors consisted of a nondispersive infrared gas analyzer for H₂O and CO₂ and an electrochemical cell for the SO₂ detector. The EGA-DTA curves of Cambrian shale from Harlech Dome, Wales, are illustrated in Figure 8.70. The shale, which contains both pyrite and organic matter, gives EGA curve peaks for H₂O, CO₂, and SO₂ evolution. It is interesting to note that the two SO₂ peaks occur at the same temperature ranges as the DTA exothermic peaks, probably due to the reaction



and

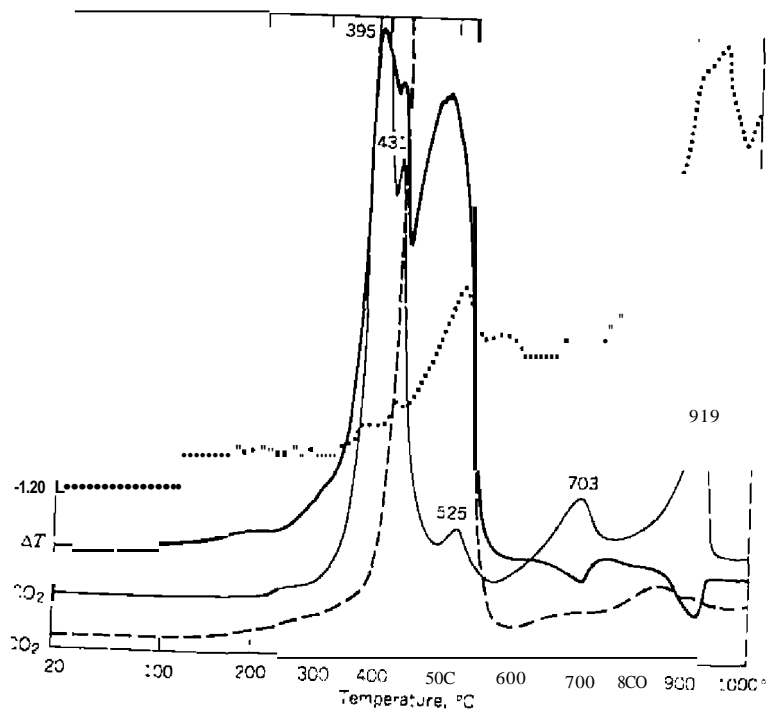


Figure 8.70. EGA-DTA curves of Cambrian shale, Harlech Dome, Wales (181).

Most of the FeS formed during the second reaction is immediately oxidized to Fe(II) and Fe(III) sulfates, although decomposition of a small amount of unchanged FeS is probably the cause of the SO₂ peak at 525°C. Iron (II) sulfate dissociates near 700°C into Fe₂O₃ and SO₃, the latter gas emits SO₂ + 1/2 O₂, thus giving rise to the SO₂ peak at 703°C.

EGA techniques have been widely used in polymer thermal stability and degradation studies, the analysis of trace impurities and additives, and in the elucidation of polymer structures (12). They are also used in vapor-pressure measurements and toxicity studies of constituents in polymer systems. Langer (128) has reviewed the applications of EGA techniques to polymers as well as numerous other compounds. Only a few illustrative examples will be discussed here.

The TG-MS of a polyacetal resin is shown in Figure 8.71 (149). The TG curve indicated two mass-loss steps involving 75 and 21%, respectively. MS of the two cuts corresponding to the two mass-loss steps showed mainly formaldehyde for the first cut and tetrafluoroethylene for the second cut. Since polyoxymethylene and polytetrafluoroethylene are known to depolymerize almost completely into their respective monomers, the resin part probably consists of 75% of the former and 21% of the latter by weight.

The TG-MS of polyvinyl acetate, as studied by Chiu and Beattie (148), is given in Figure 8.72. The first major mass-loss occurs at about 250°C and

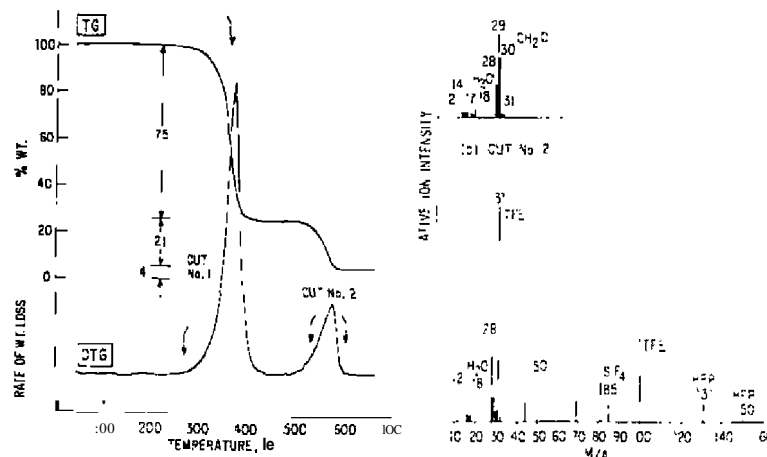


Figure 8.71. TG and MS curves of a polyacetal resin as determined by Chiu and Beattie (149).

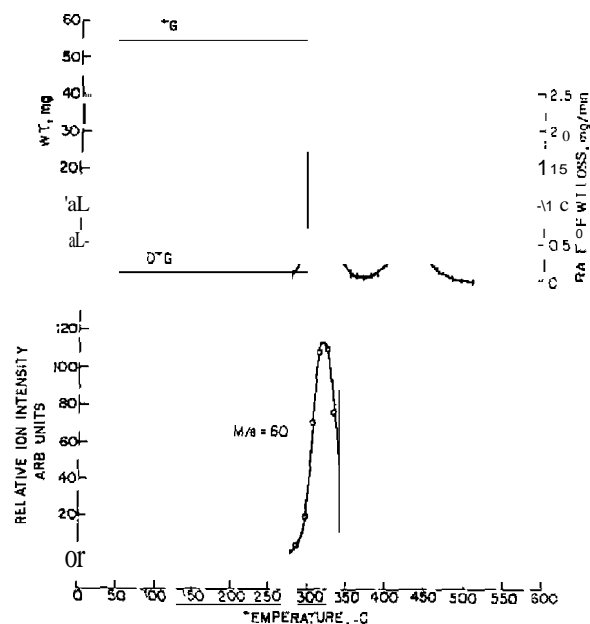


Figure 8.12. TG-DTG-MS curves of polyvinyl acetate (148).

involves the liberation of acetic acid. When the relative ion intensity of mass peak 60 of acetic acid is plotted versus temperature, the integrated peak area is a measure of the total amount of acetic acid evolved. A linear correlation was found for the acetic acid peak area versus the mass of acetic acid in four polymer standards. Such a technique is useful for the determination of a selected component without interference from other substances.

REFERENCES

1. *Thermochimica Acta*. W. W. Wendlandt, ed., Elsevier, Amsterdam.
2. *Journal Of Thermal Analysis*. E. Buzagh, and I. Simon, eds. Akademiai Kiado Budapest, Hungary.
3. Lombardi, G., *For Better Thermal Analysis*, ICTA, Univ. of Rome, 1977.
4. Lodding, W., ed., *Gas Effluent Analysis*, Marcel-Dekker, New York, 1967.
5. Wendlandt, W. W., *Thermal Methods of Analysis*, Wiley-Interscience New York, 1964.

6. Ref. 5, 2nd ed., 1974.
7. Kenyon, A. S., *Techniques and Methods of Polymer Evaluation*, p. E. Slade and L. T. Jenkins, eds., Marcel-Dekker, New York, 1966.
8. Kiran, F. and I. K. Gilham, *Polymer Characterization by Thermal Methods of Analysis*, J. Chiu, ed., Marcel-Dekker, New York, 1974.
9. Chiu, J., *Ref. 8*, 1974.
10. Murphy, C. B., *Anal. Chem. Ann. Rev.*, 46, 451 R (1974).
11. Murphy, C. B., *Anal. Chem. Ann. Rev.*, 48, 341 R (1976).
12. Chiu, J. and E. F. Palermo, *Anal. Chim. Acta*, 81, 1119 (1976).
13. Ware, R. K., *Characterization of Ceramics*, L. L. Hoch and R. W. Gould, eds., Marcel-Dekker, New York, 1971, Chap. 9.
14. Redfern, I. P., *Analyst*, 99, 849 (1974).
15. Mackenzie, R. C., *Ref. 14*, p. 900.
16. Friedman, H. L., *Thermochim. Acta*, 1, 199 (1970).
17. Mackenzie, R. C., *Talanta*, 16, 1227 (1969).
18. *Ref. 8*, p. 17.
19. McAdie, H. G., *Anal. Chem.*, 44, 640 (1972).
20. Ayres, W. M., and E. M. Bens, *Anal. Chem.*, 33, 568 (1961).
21. Mackenzie, R. C., *Differential Thermal Analysis*, R. C. Mackenzie, ed., Academic, New York, 1970, 17.
22. Wedgwood, J., *Phil. Trans. R. Soc. (London)*, 72, 305 (1782); 76, 390 (1786).
23. Orce, I., and S. Caillere, *Bull. Soc. Fr. Mineral.*, 50, 75 (1927).
24. Berg, G., *Izv. Sekr. fic. Khim. Anal. Inst. Obshch. Yeorgan. Khim. Akad. Nauk SSSR*, 19, 249 (1949).
25. Rowland, R. A., and E. C. Jones, *Am. Mineral.*, 34, 550 (1949).
26. Stone, R. L., *J. Am. Ceram. Soc.*, 35, 76 (1952).
27. Stone, R. L., *Anal. Chem.*, 32, 1582 (1960).
28. Lodding, W., and L. Hammell, *Anal. Chem.*, 32, 657 (1960).
29. Lodding, W., and L. Hammell, *Rev. Sci. Instrum.*, 30, 885 (1959).
30. Rogers, R. N., S. K. Yasuda, and I. Zinno, *Anal. Chem.*, 32, 672 (1960).
31. Vassallo, O. A., *Anal. Chem.*, 33, 1823 (1961).
32. Wendlandt, W. W., *Anal. Chim. Acta*, 27, 309 (1962).
33. Langer, H. G., and R. S. Gohike, *Anal. Chem.*, 35, 1301 (1963).
34. Gohike, R. S., and H. G. Langer, *Anal. Chim. Acta*, 36, 510 (1966).
35. Wendlandt, W. W., T. M. Southern, and J. R. Williams, *Anal. Chim. Acta*, 35, 254 (1966).
36. ZilOmer, F., *Anal. Chem.*, 40, 1091 (1968).
37. Wiedemann, H. G., *Thermal Analysis*, R. F. Schwenker and P. D. Garn, eds., Vol. 1, Academic, New York, 1969, p. 229.
38. Mizutani, N., and M. Kato, *Anal. Chem.*, 47, 1389 (1975).
39. Loehr, A. A., and P. F. Levy, *Am. Lab.*, 1972.
40. Wendlandt, W. W., *Thermochim. Acta*, 9, 951 (1974).
41. *Ref. 40*, p. 7.
42. Webber, L. M., and G. G. Guilbault, *Anal. Chem.*, 48, 2244 (1976).
43. Murphy, C. B., *Gas Effluent Analysis*, W. Lodding, ed., Marcel-Dekker, New York, 1967, p. 195.

44. Smith, J. B. D., D. C. Phillips, and T. D. Kaczmarek. *Anal. Chem.*, **48**, 89 (1976).
45. Fine, D. H., F. Ruleh, D. Lieb, and D. P. Rounbchler. *Anal. Chem.*, **47**, 1188 (1975).
46. Robertson, S. D., B. D. McNicol, J. H. De Baas, S. C. Kloet, and I. W. Jenkins, *J. Catal.* **37**, 424 (1975).
47. Ingraham, T. R. Ref. 43, p. 25.
48. Balek, Y., *Analysis*, 1,445 (1972).
49. Liebman, S. A., D. H. Ahistrom, T. C. Creighton, G. D. Prudcr, and E. J. Lev. *Thermochim. Acta*, **5**, 403 (1973).
50. Paulik, J., and F. Paulik. *Thermochim. Acta*, **3**, 13 (1972).
51. McNeill, I. C. *Eur. Polym. J.*, **3**, 409 (1967); *J. Thermal Anal.*, **1**, 389 (1969).
52. Fenner, T. R. F. W., G. J. Knight, and W. W. Wright. *Thermal Analysis*, H. G. Wiedemann, ed., Vol. 3, Birkhauser, Basel, 1971, p. 245.
53. Low, M. J. D., Ref. 43, p. 155.
54. Langer, H. G., and R. S. Gohlke, Ref. 43, p. 71.
55. Eggertsen, F. T., and F. H. Stross, *Thermochim. Acta*, **1**, 451 (1970).
56. Rogers, R. N., and L. C. Smith, *J. Chromatogr.*, **48**, 268 (1970).
57. Malone, C. T., and W. H. Mc Fadden in *Ancillary Techniques of Gas Chromatography*, I. S. Ettre and W. H. Mc Fadden, eds., Wiley-Interscience, New York, 1969, Chap. 10.
58. Flath, R. A., *Guide to Modern Methods of Instrumental Analysis*, T. H. Gow, ed., Wiley-Interscience, New York, 1972, Chap. 9.
59. Freeman, S. K., *Ancillary Techniques of Gas Chromatography*, L. S. Ettre and W. H. Mc Fadden, eds., Wiley-Interscience, New York, 1969, Chap. 6.
60. Barnes, P. A., and E. Kirton in *Analytical Calorimetry*, R. S. Porter and J. F. Johnson, eds., Vol. 3, Plenum, New York, p. 57.
61. Loehr, A. A., and P. F. Levy, *Am. Lab.*, Jan. 1972, p. 11.
62. Krug, D., *Chem. Ing. Tech.*, **46**, 839 (1974).
63. Chiu, J., *Anal. Chem.*, **40**, 1516 (1968).
64. Chill, J., *Thermochim. Acta*, **1**, 231 (1970).
65. Cukor, P., and C. Persian. *Polymer Characterization by Thermal Methods of Analysis*, J. Chill, ed., Marcel-Dekker, New York, 1974, p. 107.
66. Uden, P. C., D. E. Henderson, and R. J. Lloyd in *Proceedings of First European Symposium on Thermal Analysis*, D. Doilimore, ed., Heyden, London, 1976, p. 29.
67. Zitomer, F., *Anal. Chem.*, **40**, 1091 (1968).
68. Kleiberg, G. A., and D. L. Geiger. *Proc. 3rd ICTA Conf.* H. G. Wiedemann ed. Vol. 1, Birkhauser, Basel, 1971, p. 325.
69. Gibson, E. K., and S. M. Johnson, *Thermochim. Acta*, **4**, 49 (1972).
70. Mol, G. J., *Thermochim. Acta*, **10**, 259 (1974).
71. Clinckemillie, A., and C. Hofmann. *Proc. 3rd ICTA Conf.* H. G. Wiedemann, ed., Vol. 1, Birkhauser, Basel, 1971, p. 33.
72. Muller-Vonmoos, M., and R. Muller. *Proc. 4th ICTA Conf.*, I. Buras, ed. VDI, Heyden, London, 1975, p. 521.
73. Szekey, T., and F. Til, Ref. 72, Vol. 3, p. 917.
74. Baumgartner, F., and E. Nachbaur, *Thermochim. Acta*, **19**, 3 (1977).
75. Emmerich, W. E., and K. Bayreuther. *Proc. 4th ICTA Conf.*, I. Buzas, ed., Akademiai Kiado, Budapest, Vol. 3, p. 1017.

76. Wist, A. J. Fum. and J. Magill. Ref. 75, p. 259.
77. Emmerich, W. E., and V. Baick. *Proc. 3rd ICTA Conf.* H. G. Wiedemann, ed., Vol. 1, Birkhauser, Basel, 1971, p. 475.
78. Yamada, K., S. Orta, and T. Haruki in *Proc. 4th ICTA Conf.* I. Buzas, ed., Vol. 3, Heyden, London, 1975, p. 1029.
79. Espinal, M. L., fl. J. Madoc-Jones, E. L. Charsiey, and J. P. Redfern. *Proc. 3rd ICTA Conf.* H. G. Wiedemann, ed., Vol. 1, Birkhauser, Basel, 1971, p. 303.
80. Paulik, J., and F. Paulik, *Thermochim. Acta*, **4**, 189 (1972).
81. Paulik, J., F. Paulik, and L. Erdey. *Mikrochim. Acta*, **886** (1966).
82. Paulik, J., and F. Paulik. *Talanta*, **17**, 1224 (1970).
83. Paulik, J., and F. Paulik. *Proc. 3rd Anal. Chem. Conf.* Budapest, 1970, p. 225.
84. Wendlandt, W. W. *Anal. Chim. Acta*, **27**, 23; (1962).
85. Gal, S., J. Simon, and L. Erdey. Ref. 84, p. 243.
86. Paulik, F., and J. Paulik. *Thermochim. Acta*, **3**, 13, 17 (1971).
87. Law, M. J. D., in *Gas Effluent Analysis*, W. Lodding, ed., Marcel-Dekker, New York, 1967, Chap. 6.
88. Kiss, A. B., *Acta Chim. Acad. Sci. Hung.*, **61**, 207 (1969).
89. Kiss, A. B., *Aera Chim. Acad. Sci. Hung.*, **63**, 243 (1970).
90. Doyle, C. D., WADD Tech. Rept. 60-283, U.S. Air Force, Wright-Patterson Air Force Base, OH, May 1960.
91. Murphy, C. C., in *Gas Effluent Analysis*, W. Lodding, ed., Marcel-Dekker, New York, 1967, Chap. 1.
92. Murphy, C. B., F. W. Van Luik, and A. C. Pitsas, *Plast. Des. Process.*, Jilly 1964, p. 16.
93. Rogers, R. N., *Anal. Chem.*, **39**, 130 (1967).
94. Rogers, R. N., and L. C. Smith, *J. Chromatogr.*, **48**, 268 (1970).
95. Stahl, E., *Analyst*, **723** (1969).
96. Eggertsen, F. T., and F. H. Stross, *J. Appl. Polym. Sci.*, **10**, 1471 (1966).
97. Eggertsen, F. T., H. M. Joki, and F. H. Stross, in *Thermal Analysis*, R. F. Schwenker and P. D. Gam, eds., Academic, New York, 1969, p. 341.
98. Eggertsen, F. T., E. E. Seibert, and F. H. Stross, *Anal. Chem.*, **41**, 1175 (1969).
99. Eggertsen, F. T., and F. H. Stross, *Anal. Chem.*, **44**, 709 (1972).
100. Eggertsen, F. T., and F. H. Stross, *Thermochim. Acta*, **1**, 451 (1970).
101. Gibson, E. K., *Thermochim. Acta*, **5**, 243 (1973).
102. Gihson, E. K., and S. M. Johnson, *Proc. 2nd Lunar Sci. Conf.*, MIT Press, Cambridge, MA, 1971, Vol. 2, p. 1351.
103. Gibson, E. K., and G. W. Moore, *Thermochim. Acta*, **10**, 153 (1974).
104. Smith, I. W., and D. R. Johnson, in *Thermal Analysis*, R. F. Schwenker and P. D. Gam, eds., Vol. 2, Academic, New York, 1969, p. 1251.
105. Smith, J. W., and D. R. Johnson, *Am. Lab.*, Jan. 8, 1971.
106. Chang, T. L., and T. E. Mead, *Anal. Chem.*, **43**, 534 (1971).
107. Ingraham, T. R., in *Gas Effluent Analysis*, W. Lodding, ed., Marcel-Dekker, New York, 1967, Chap. 2.
108. Brody, S. S., and J. E. Chaney, *J. Gas Chromatogr.*, **4**, 42 (1966).
109. Johnson, L. J. F., in *Guide to Modern Methods of Instrumental Analysis*, T. H. Gow, ed., Wiley-Interscience, New York, 1972, Chap. 1.

110. Malone, C. T., and W. H. Mc Fadden in *Ancillary Techniques of Gas Chromatography*. L. S. Ettre and W. H. Mc fadden. eds., Wiley-interscience. New York, 1969, Chap. 10.
111. Low, M. J. D., *Thermochimica Acta*, W. W. Wendlandt, cd., Elsevier, Amsterdam, Author supply date.
112. Kug, D. and W. Hadrich. *Thermochim. Acta*, 15, 179 (1976).
113. Wendlandt, W. W., *Thermochimica Acta*, 9, 7 (1974).
114. De Kok, J., J. A. W. De Kock, and A. Bouwknecht *Thermochim. Acta*, 9, 409 (1974).
115. Wendlandt, W. W., *Thermochim. Acta*, 9, 95 (1974).
116. Bandi, W. R. and G. Krapf, *Anal. Chem.*, 49, 649 (1977).
117. Krapf, G., E. G. Buyok, and W. R. Bardi, *Thermochim. Acta*, 13, 47 (1975).
118. Bandi, W. R., E. G. Buyok, G. Krapf, and L. M. Meinick, in *Thermal Analysis*, R. f. Schwenker and P. D. Gam, eds., Vol. 2, Academic, New York, 1969, p. 1363.
119. Ware, R. K., *Thermochim. Acta*, 3, 49 (1972).
120. Rohertson, S. O., B. D. McNicol, J. H. De Baas, S. C. Kloet, and J. W. Jenkins, *J. Catal.*, 37, 424 (1975).
121. Wendlandt, W. W., and W. S. Bradly, *Anal. Chim. Acta*, 52, 391 (1970).
122. Wendlandt, W. W., *Climica*, 36, 1 (1912).
123. Neshitt, L. E., and W. W. Wendlandt, *Thermochim. Acta*, 10, 85 (1974).
124. Nesbitt, L. E. and W. W. Wendlandt in *Proc. 4th ICTA Conf.*, I. Buzas, ed., Vol. 2, Heyden, London, 1975.
125. Timberlake, J. W., and J. C. Martin, *Rev. Sci. Instrum.*, 44, 151 (1973).
126. De Kok, J., J. A. W. De Kock, and A. Bouwknecht, *Thermochim. Acta*, 9, 409 (1974).
127. Bouwknecht, A., J. De Kok, and J. A. W. De Kock, Ref. 126, p. 399.
128. Langer, H. G., in *Treatise on Analytical Chemistry*, 2nd ed., P. J. Elving, ed., Vol. 12, Part I, Wiley, New York, 1983.
129. Paulik, F., and I. Paulik, *Analysr*, 103, 417 (1978).
130. Hassel, R. L., *Am. Lab.*, Jan. 1976.
131. Blaine, R. L., *Du Pont Application Brief No.* TA 49.
133. fair, P. G., *Du Pont Application Brief No.* TA 47.
134. Blaine, R. L., *Du Pont Application Brief No.* TA 52.
135. Hassel, R. L., *Du Pont Application Brief No.* TA 67.
136. Blaine, R. L., *Du Pont Application Brief No.* TA 82.
137. De Francis, J. II., *Du Pont Application Brief No.* TA 87.
138. Glaine, I. H., *Du Pont Application Brief No.* TA 72.
139. Baker, K. F., *Du Pont Application Brief No.* TA 51.
140. Hassel, R. L., *Du Pont Application Brief No.* TA 46.
141. Cremer, M., and H. N. Elsheimer, *Anal. Chim. Acta*, 60, 183 (1972).
142. Kristoff, J., J. Inczedy, J. Paulik, and F. Paulik, *J. Thermal Anal.*, 15, 151 (1979).
143. Kristoff, J. and J. Inczedy, *J. Thermal Anal.*, 18, 111 (1978).
144. Kristoff, J., J. Inczedy, J. Paulik, and F. Paulik, *Thermochim. Acta*, 56, 285 (1982).
145. Onodera, S., *Bull. Chem. Soc. Jpn.*, 50, 123 (1977).
146. MacLaury, M. R. and A. L. Schroll, *Fire Flammab.*, 12, 203 (1981).
147. Chiu, J. and A. J. Beattie. *Thermochim. Acta*, 21, 263 (1977).
148. Chiu, J. and A. J. Beattie. *Thermochim. Acta*, 50, 49 (1981).

149. Chiu, J. and A. J. Beattie. *Thermochim. Acta*, 40, 251 (1980).
150. Gallagher, P. K., *Thermochim. Acta*, 26, 175 (1978).
151. Dyszel, S. M., *Thermochim. Acta*, 61, 169 (1983).
152. Tsuchiya, S., Y. Amenomiya, and R. J. Cvetanovic, *J. Catal.*, 20, 1 (1971).
153. Tsuchiya, S. and M. Nakamura, *J. Catal.*, 50, 1 (1977).
154. Smutzek, M., S. Cerny, and f. Buzek, *Adv. Catal.*, 24, 343 (1975).
155. COan, Y.-c. and R. B. Anderson, *J. Catal.*, 50, 319 (1977).
156. Luengo, C. A., A. I. Cabrera, H. B. MacKay, and M. B. Mapie, *J. Catal.*, 47, 1 (1977).
157. Cvclanovic, R. J., and Y. Amenomiya. *Adv. Catal.*, 17, 1031 (1967).
158. Phillips, D. C., and J. D. B. Smith. *Ind. Res.*, 18, 57 (1976).
159. Phillips, D. C., and J. D. B. Smith. *Chem. Instrum.*, 7, 261 (1976).
160. Phillips, D. C., J. D. B. Smith, I. F. Meier, and T. D. Kaczmarek. *Microchem. J.*, 23, 165 (1978).
161. Phillips, D. C., J. D. H. Smith, and J. F. Meier, *Anal. Lett.*, A11, 363 (1978).
162. Smith, J. D. B., D. C. Phillips, and T. D. Kaczmarek, *Anal. Chem.*, 48, 89 (1976).
163. Smith, J. D. B., D. C. Phillips, and T. D. Kaczmarek, *Microchem. J.*, 21, 424 (1976).
164. Smith, J. D. B., and D. C. Phillips, *Microchem. J.*, 21, 27 (1976).
165. Fischer, S. G. and J. Chiu. *Thermochim. Acta*, 65, 9 (1983).
166. Holdiness, M. R., *Thermochim. Acta*, 75, 361 (1984).
167. Simons, E. L., and A. E. Newkirk, *Talanta*, 11, 549 (1964).
168. Ashby, E. C., P. Calady, J. Bousquet, and J. Etienne, *J. Chem. Educ.*, 52, 618 (1975).
169. Wendlandt, W. W., and J. P. Smith. *Thermal Properties of Transition Metal Ammine Complexes*, Elsevier, Amsterdam, 1967.
170. Collins, L. W., W. W. Wendlandt, and E. K. Gibson. *Thermochim. Acta*, 8, 205 (1974).
171. Collins, L. W., W. W. Wendlandt, E. K. Gibson, and G. W. Moore, *Thermochim. Acta*, 7, 209 (1973).
172. Collins, L. W., W. W. Wendlandt, and E. K. Gibson. *Thermochim. Acta*, 8, 307 (1974).
173. Ref. 172, p. 315.
174. Ref. 172, p. 303.
175. Collins, L. W., E. K. Gibson, and W. W. Wendlandt, *Thermochimica Acta*, 9, 15 (1974).
116. Johnson, D. W., and P. K. Gallagher, *J. Am. Ceram. Soc.*, 54, 461 (1971).
177. Collins, L. W., E. K. Gibson, and W. W. Wendlandt, *Thermochim. Acta*, II, 17 (1975).
178. Krapf, G., J. L. Letzler, M. Meinick, and W. R. Bardi. *Thermochim. Acta*, 4, 257 (1972).
179. Ishikawa, T., and K. Inouye, *J. Thermal Anal.*, 10, 399 (1976).
180. Kuhas, J., and M. Szalkowicz in *Proc. 1rd ICTA VIII*, II. G. Wiedemann, ed., Vol. 2, Birkhauser, Basel, 1972, p. 447.
181. Morgan, D. J. in *First European Symposium on Thermal Analysis*, D. Dollimore, ed., Heyden, London, 1976, p. 355.

182. Balek, V. *J. Thermal Anal.*, 20,495 (1981).
183. Rutherford, E., *Pills. Z.*, 2, 429 (1901).
184. Kolovrat-Chervinskij, L. S., *Compt. Rend.*, 145, 425 (1907).
185. Balek, V., and J. Toigýessy, "Emanation Thermal Analysis and other Radiometric Emanation Methods," in *Wilson and Wilson's Comprehensive Analytical Chemistry*, G. Svehla, ed., Vol. XII, Part C., Elsevier, Amsterdam, 1984.
186. Balek, V., *Radiochem. Radioanal. Lett.*, 28,271 (1977).
187. Balek, V., *J. Mater. Sci.*, 4, 919 (1969).
188. Balek, V., *Anal. Chem.*, 42, 1M (1970).
189. Bniek, V., *Am. Lab.*, June 27, 1978.
190. Balek, V. *J. Thermal Anal.*, 20,495 (1981).
191. Balek, V., *Ind. Res. Dev.*, July 1981, p. 114.
192. Balek, V., *Powder Metal. Int.*, 14, 101 (1982).
193. Immerich, W. D., and V. Balek. *High-Temp.-High Pressure*, 5, 671(1973).
194. Függe, S., and K. E. Ziemens, *Z. Pills. Chem.*, B42, 179 (1939).
195. Balek, V., *J. Thermal Anal.*, 12, 1110977).
196. Balek, V., *J. Appl. Chem.*, 1970, 73.
197. Balek, V., J. Kroupa, and M. Prachar, *Radiachem. Radioanal. Lett.*, 28, 279 (1977).
198. Balek, V., H. Landspersky, and M. Voboril, *Radiochem. Radioanal. Lett.*, 28, 289 (1977).
199. Balek, V., *J. Radioanal. Chem.*, 30, 499 (1976).
200. Balek, V., and J. Dohnalek, *J. Marer. Sci.*, 17,2281 (1982).
201. Balek, V., and J. Dohnalek, *Chem. Conc. Res.*, 13, 1119831.
202. Bordas, S., M. Geli, V. Balek, and M. Voboril, *Thermal Analysis*, IeTA 80, Birkhauser, Basel, 1980, p. 403.
203. Balek, V., *J. Mater. Sci.*, 17, 1269 (1982).
204. Balek, V., M. VDboril, and V. Baran, *Vuel. Techiol.*, 50, 53 (1980).
205. Balek, V., *J. Mater. Sci.*, 5,166(1970).

CHAPTER

9

THERMOPHOTOMETRY

According to ICTA, thermophotometry is defined as "a technique in which the optical characteristics of a substance are measured as a function of temperature whilst the substance is subjected to a controlled temperature programme." Measurement of total light, light of a specific wavelength(s), refractive index, and luminescence lead to *thermophotometry*, *thermospectrometry*, *thermorefractometry*, and *thermoluminescence*, respectively. Observation under a microscope leads to thermomicroscopy, and so on. In this chapter, the optical properties of light emission, absorption, and reflectance of a substance as a function of temperature are discussed. This discussion includes high-temperature reflectance spectroscopy, dynamic reflectance spectroscopy photometric methods, thermomicroscopy, thermoluminescence, and oxylluminescence.

A. HIGH-TEMPERATURE REFLECTANCE SPECTROSCOPY AND DYNAMIC REFLECTANCE SPECTROSCOPY

1. Introduction

The measurement of the radiation reflected from a mat surface constitutes the area of spectroscopy known as diffuse reflectance spectroscopy. The difference between this technique and transmittance spectroscopy is shown in Figure 9.1. The reflected radiation is expressed as the ratio of I_r/I_i , where I_i is the incident and I_r the reflected radiation. The reflected radiation may be in the ultraviolet, the visible, or the infrared region of the electromagnetic spectrum. From a mat surface, the total reflected radiation, R_T , consists in general of two components: a regular reflectance component R (sometimes referred to as surface or mirror reflection), and a diffuse reflection component R_d (1, 2). The former component is due to the reflection at the surface of single crystallites, while the latter arises from the radiation penetrating into the interior of the solid and reemerging to the surface after being scattered numerous times.

According to the Kubelka and Munk theory (3), the diffuse reflection component for 1-3-mm-thick layers of a powdered sample (an increase in

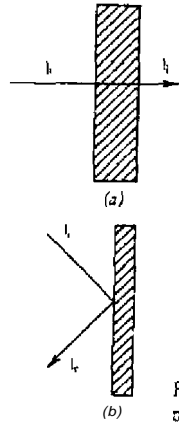


Figure 9.1. Reflectance and transmittance spectroscopy. (a) Transmittance mode; (b) reflectance mode.

thickness beyond this point has no effect on the reflectance) at a given wavelength is equal to

$$R_{\infty} = \frac{I_r}{I_0} = \frac{1 - [kl(k + 2s)]^{1/2}}{1 + [kl(k + 2s)]^{1/2}} \quad (9.1)$$

where I_r is the reflected radiation. I_0 is the incident radiation. k is the absorption coefficient, and s the scattering coefficient. The absorption coefficient is the same as that given by the familiar Beer-Lambert Law. $T = e^{-kd}$. The regular reflection component is governed by Fresnel's equation

$$R = \frac{I_r}{I_0} = \frac{(n - 1)^2 + n^2 K^2}{(n + 1)^2 + n^2 K^2} \quad (9.2)$$

where n is the refractive index and K is the absorption index defined through Lambert's law.

$$I = I_0 \exp\left(\frac{-4\pi Kd}{\lambda_0}\right) \quad (9.3)$$

The λ_0 denotes the wavelength of the radiation in vacuum, and d is the layer thickness.

With some algebraic manipulation, equation (9.1) can be rewritten into

the more familiar form

$$\frac{(1 - R_{\infty})^2}{2R_{\infty}} = \frac{k}{s} \quad (9.4)$$

The left-hand side of the equation is commonly called the *remission function* or the *Kubelka-Munk function* and is frequently denoted by $f(R_{\infty})$. Experimentally, one seldom measures the absolute diffuse reflecting power of a sample, but rather, the relative reflecting power of the sample compared to a suitable white standard. In that case, $k = 0$ in the spectral region of interest, $R_{\infty \text{ std}} = 1$ [from equation (9.4)], and one determines the ratio

$$\frac{R_{\infty \text{ sample}}}{R_{\infty \text{ std}}} = f(R_{\infty}) \quad (9.5)$$

from which the ratio k/s can be obtained using the remission function

$$f(R_{\infty}) = \frac{(1 - R_{\infty})^2}{2R_{\infty}} = \frac{k}{s} \quad (9.6)$$

Taking the logarithm of the remission function gives

$$\log f(R_{\infty}) = \log k - \log s \quad (9.7)$$

Thus, if $\log f(R_{\infty})$ is plotted against the wavelength or wave number for a sample, the curve should correspond to the absorption spectrum of the compound (as determined by transmission measurements) except for the displacement by $-\log s$ in the ordinate direction. The curves obtained by such reflectance measurements are, generally called *characteristic color curves* or *typical color curves*. Sometimes there is a small systematic deviation in the shorter-wavelength regions due to the slight increase in the scattering coefficient.

By use of modern double-beam spectrophotometers equipped with some type of a reflectance attachment, R_{∞} is automatically plotted against the wavelength. Many investigators replot the data as *percent reflectance* (%R), or plot by use of a remission-function table (4) $f(R_{\infty})$ or k/s as a function of wavelength or wavenumber. The most common method is probably the former procedure.

The preceding brief introduction to reflectance spectroscopy outlines the most elementary principles of the technique. As would be expected, the technique is widely used for the study of solid or powdered solid samples, although

it can be used for liquids or pastelike materials as well. The technique is a rapid one for the determination of the "color" of a sample, and is generally convenient to use since commercial instrumentation is readily available. Since only the surface of the sample is responsible for the reflection and absorption of the incident radiation, it is widely used in the study of the chemistry and physics of surfaces (5).

2. High-temperature Reflectance Spectroscopy

Practically all the studies in reflectance spectroscopy (it should be noted that the term reflectance spectroscopy used here will denote diffuse reflectance spectroscopy only) have been carried out at ambient temperatures, or in some cases at subambient temperatures. The latter would most probably be used in single-crystal studies for the elucidation of "hot bands," that is, transitions which originate from vibrationally excited ground states. However, in many cases, a great amount of additional information on a chemical system can be obtained if the reflectance spectrum of a compound is obtained at elevated temperatures. Normally, temperatures in the range from 100 to 300°C have been used, although there is no reason why higher temperatures could not be employed.

Two modes of investigation are used for high-temperature reflectance studies. The first is the measurement of the sample spectra at various fixed or isothermal temperatures; the second is the measurement of the change in reflectance of the sample as a function of the increasing temperature. The first procedure will be called the static method or *high-temperature reflectance spectroscopy* (HTRS) (6); the second is a dynamic method and has been termed *dynamic reflectance spectroscopy* (DRS) (7, 8). The two methods are illustrated in Figure 9.2. In (a), the HTRS curves, the spectra of the sample is recorded at increasing fixed temperatures, T_1 to T_4 . As can be seen, the curve maximum at wavelength λ_1 decreases with increasing temperature while a new curve maximum is formed at λ_2 . By measuring the spectra at small temperature increments, the minimum temperature at which the sample begins to undergo a thermal transition can be determined. By using the dynamic technique, these transition temperatures can be determined in a more precise manner, as shown in (b) and (c). Plotting reflectance of the sample versus temperature (b) as the sample temperature is increased at a slow fixed rate, at fixed wavelength λ_1 the reflectance is seen to decrease with an increase in temperature. With a fixed wavelength λ_2 , the DRS curve in (c) is obtained which shows the increase in reflectance of the sample with increasing temperature. These *isolumbic* curves reveal the temperatures at which sample thermal transitions begin and end, and also permit the investigation of only a single thermal transition: mass-loss and enthalpic effects do

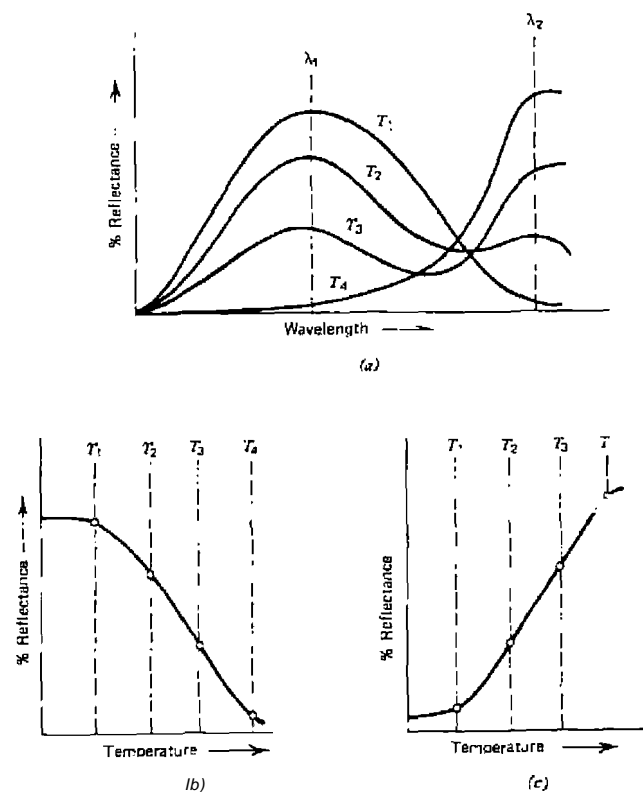


Figure 9.2. (a) High-temperature reflectance spectra curves; (b) and (c) dynamic reflectance spectra curves, at λ_1 and λ_2 , respectively (1).

not interfere with the measurements. The DRS technique is useful for determining the thermal stability of a substance, and also sample structural changes which are a function of temperature. Indeed, the technique shows great promise as a complementary method to other thermal techniques such as thermogravimetry, differential thermal analysis, high-temperature X-ray diffraction, and others (45).

3. Instrumentation

The use of a heated sample holder to contain the compound under investigation has been described by several investigators. Asmussen and Anders^{OT}.

(9) studied the reflectance spectra of several $M_2[HgI_4]$ complexes at various elevated temperatures in order to investigate their thermochromic $\beta \rightarrow \alpha$ form transitions. The heated sample container consisted of a nickel-plated brass block, 60 mm in diameter by 85 mm in height, the lower end of which contained a chamber in which a small light bulb was mounted. Regulation of the current through the bulb filament permitted temperature regulation of the block. The upper end of the block contained the sample chamber, which was 35 mm in diameter by 0.5 mm deep. A copper-Constantan thermocouple, embedded in the powdered sample, was used to detect the sample's temperature.

Kortum (2) measured the reflectance spectrum of mercury(II) iodide at 140° but did not describe the heated sample block or other experimental details. Another heated block assembly was described by Hatfield et al. (10). It consisted of a metal block in which a heating element was embedded. No other details are available, such as temperature detection or sample thickness.

In 1963, Wendlandt et al. (11) described the first of their heated sample holders for high-temperature reflectance spectroscopy. The main body of the sample container was 60 mm in diameter by 11 mm thick and was machined from aluminum. The sample itself was contained in a circular indentation, 25 mm in diameter by 1 mm deep, machined on the external face of the cell. Two circular ridges were cut at regular intervals on the indentation to increase the surface area of the holder and to prevent the compacted-powdered sample from falling out of the holder when it was in a vertical position. The sample holder was heated by coils of Nichrome wire wound spirally on an asbestos board and then covered with a thin layer of asbestos paper. Enough wire to provide about 15 Ω of resistance was used. The temperature of the sample was detected by a Chromel-Alumel thermocouple contained in a two-holed ceramic insulator tube. The thermocouple junction made contact with the aluminum block directly behind the sample indentation. To prevent heat transfer from the sample holder to the integrating sphere, a thermal spacer was constructed from a loop of 0.25-in. aluminum tubing and wet shredded asbestos. After drying, the thermal spacer was cemented to the sphere and the sample holder attached to it by a spring-loaded metal clip.

A modification of the preceding sample holder was described by Wendlandt and George (12) and by Wendlandt (13). The circular aluminum disk of the holder was heated by means of a cartridge heater element inserted directly behind the sample well. Two Chromel-Alumel thermocouples were placed in the block, one adjacent to the heater and the other in the bottom of the sample well so as to be in intimate contact with the compacted sample. The block thermocouple was used to control the temperature programmer.

while the sample thermocouple was used to detect the sample temperature.

Still another heated sample holder was described by Wendlandt and Hecht (1). It consisted of a block of aluminum, 50 mm in diameter by 25 mm thick, into which was machined a 25-mm by 1-mm deep sample well. A 35-watt stainless steel sheathed heater cartridge embedded in the main block of the holder was used as the heater. The same two-thermocouple system, one for the temperature programmer and the other for sample temperature, was employed. For samples which evolved gaseous products, a Pyrex or quartz cover glass was used to prevent contamination of the integrating sphere.

A heated sample holder, based on the design of Frei and Frodyma (14), which could be used for studying small samples, was recently described by Wendlandt (15). The sample is placed as a thin layer on glass fiber elate which is secured to the heated aluminum metal block by a metal clamp and a cover glass. Dimensions of the aluminum block are 4.0 by 5.0 cm. The block is heated by a circular heater element contained within the holder. Electrical connections to the heater and to the thermocouple are made by means of the terminal strip mounted at the top of the assembly. Both the aluminum block and the terminal strip are mounted on a 5.0 by 5.0-cm. transit block.

Generally, in the previously described heated sample holders, few attempts were made to control the atmosphere surrounding the sample as it was heated. A cover plate of Pyrex glass or quartz was employed but its main purpose was to prevent the sample from accidentally falling into the integrating sphere of the spectroreflectometer. In order to control the sample atmosphere, the sample holder shown in Figure 9.3 was constructed by Wendlandt and Dosch (16).

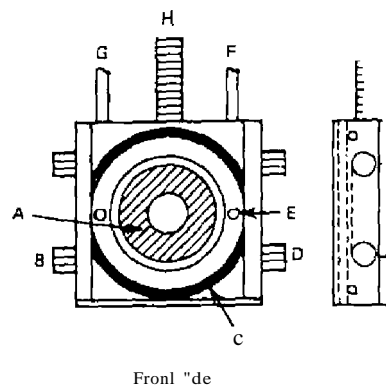


Figure 9.3. Schematic illustration of heated sample holder (16). A, silver sample block and heater; B, glass or quartz cover plate; C, O-ring; D, thumb screw (one of four); E, gas inlet to sample chamber; F, gas outlet tube; G, gas inlet tube and connecting cable.

The sample is contained in a 1 by 10-mm diameter indentation machined in the surface of a silver heater block. The circular block is 25 mm in diameter and it is heated by two 2.6-Q Nichrome wire heaters. It is contained in an enclosure, 55 mm square and 13 mm thick. The heater is thermally insulated from the main body of the sample holder by a thin layer of ceramic fiber insulation. The sample side of the holder is enclosed by a quartz plate, 50 mm on an edge by 2 mm thick, which is held firmly in place by two metal strips. Each metal strip is fastened to the holder by two thumb screws; they (and hence the cover plate) can easily be removed to facilitate sample

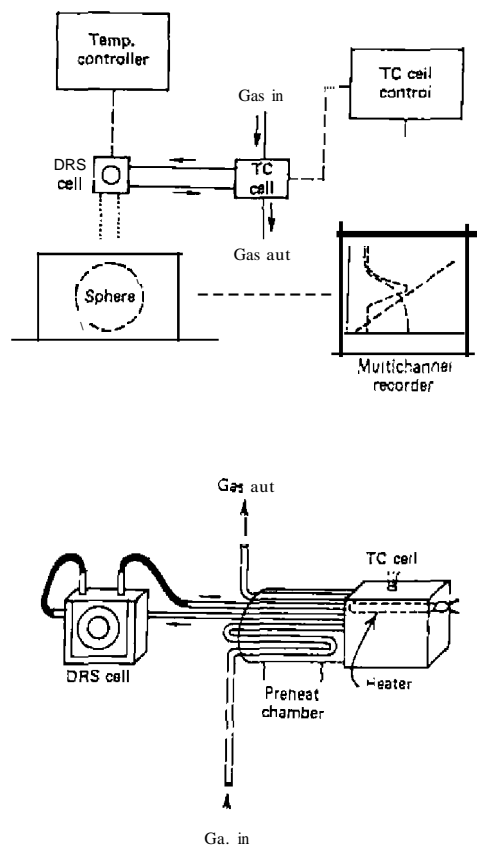


Figure 9.4. Schematic diagrams of DRS-EGD system (17)

loading and removal. A gas-tight seal between the cover plate and the sample holder is provided by a 44-mm-id O-ring. Two 0.125-in.-diameter aluminum tubes, located at the top of the holder, are used to control the gas inlet and outlet to the sample chamber.

With the controlled atmosphere heated sample holder, it was a simple matter to connect a thermistor-type thermal conductivity cell to the system and, by means of an external multichannel recorder, record the DRS and the evolved gas detection (EGD) curves simultaneously (17). This modification of the apparatus is shown in Figure 9.4. The cell was connected to a Carl Model 1000 Micro-Detector system by means of metal and rubber tubing. The thermal conductivity cell was enclosed by an aluminum block which was heated to 100°C by means of a cartridge heater. The block was connected to a preheat chamber, also operated at 100°C, which was used to preheat the helium gas stream before it entered the detector. The output from the detector bridge was led into one channel of a four-channel 0-5 mV Leeds and Northrup multipoint strip-chart potentiometric recorder. The temperature programmer from a Deltatherm III DTA instrument was used to control the temperature rise of the DRS cell. Output from the Beckman Model DK-2f

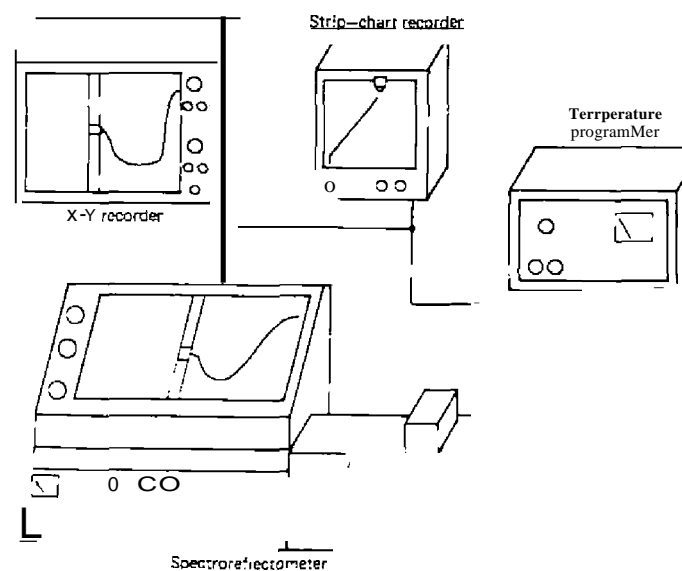


Figure 9.5. Schematic diagram of the DRS system

spectroreflectometer was also led into the multichannel recorder, as was the output from a thermocouple located in the DRS heater block.

The complete HTRS-DRS system is illustrated in Figure 9.5. The high-temperature sample holder is used in conjunction with a temperature programmer and two recorders. One recorder recorded the sample temperature versus time; the other, an X-Y recorder, was used to record reflectance versus temperature, as required for the DRS studies. A Beckman Model DK-2A or a Bausch & Lomb Spectronic 505 spectroreflectometer was employed for the spectral measurements.

4. Application of HTRS and DRS to Inorganic Compounds

a. The Octahedral \rightarrow Tetrahedral Transition in $\text{Co}(\text{py})_2\text{Cl}_2$

The octahedral \rightarrow tetrahedral structure transition of bis(pyridine) cobalt(II) chloride, $\text{Co}(\text{py})_2\text{Cl}_2$, has been the subject of a number of investigations (12, 22). Wendlandt and George (22) studied the transition using the techniques of high-temperature reflectance spectroscopy (HTRS) and dynamic reflectance spectroscopy (DRS). The thermal transition was found to begin at about 100° and was completed at about 135° . The color change reported for the transition was from violet (octahedral) to a dark blue (tetrahedral) color; it was stated that the change was nonreversible on cooling to room temperature.

Recently, Wendlandt (18) reported that the structural change was actually reversible. The blue form, after standing at room temperature for 24 hours, reverted to the original violet compound. The HTRS curves of $\text{Co}(\text{py})_2\text{Cl}_2$ at 20 and 120°C are given in Figure 9.6. At 20°C , reflectance minima were observed in the curve at 520 and 620 nm, with shoulders at 500 and 550 nm, respectively. The compound reflected rather strongly in the 350-450-nm region and at 580 nm. The blue tetrahedral form, at 120° , absorbed very strongly in the 500-700-nm region, with shoulders at 425, 480, and 510 nm, respectively. After standing 24 hours at room temperature, the reflectance curve of the blue form was again recorded at 20° . As can be seen, the curve obtained was almost identical with that of the original compound having the octahedral structure. Thus it is seen that the tetrahedral \rightarrow octahedral transition takes place rather slowly on standing; it does not even back to the octahedral form immediately upon cooling to room temperature.

The effect of heating rate on the octahedral \rightarrow tetrahedral transition is shown by the DRS curves in figure 9.7. The heating rate varied from 1.25 $^\circ\text{C}/\text{min}$ to $10^\circ/\text{min}$; the latter value is considered to be rather high for DRS studies. Surprisingly, the procedural transition temperature was greatest (107°) for the 1.25 $^\circ/\text{min}$ rate and lowest (95°) for the highest rate studied.

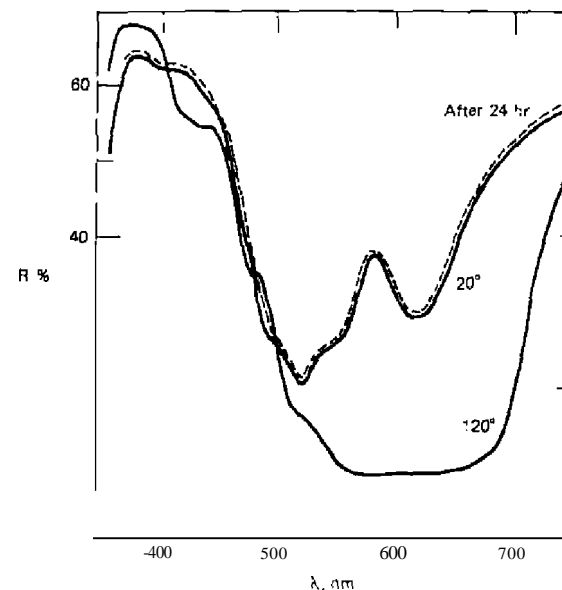


Figure 9.6. HTRS curves of $\text{Co}(\text{py})_2\text{Cl}_2$ at various temperatures ($^\circ\text{C}$).

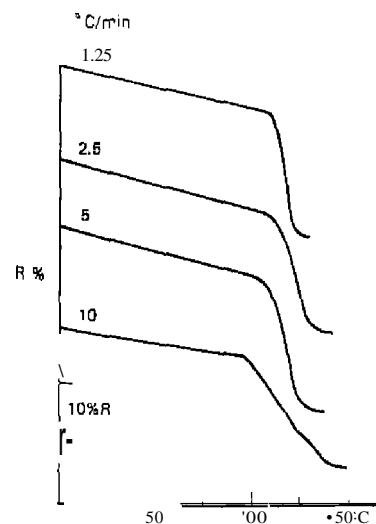


Figure 9.7. DRS curves of $\text{Co}(\text{py})_2\text{Cl}_2$ at various heating rates, curves recorded at 675 nm ($^\circ\text{C}$).

However, on increasing the heating rate, the reaction temperature interval increased, from 95–145° for the 10°/min rate to 107–123° for the slowest heating rate. This is just the opposite to that observed in dissociation reactions involving volatile products.

The spectra of $\text{Co}(\text{py})_2\text{Cl}_2$ in the visible and near-infrared regions (15) are shown in Figure 9.8. At room temperature, reflectance minima were found at 1140, 1670, 2150, and 2440 nm, respectively, for the α form. On heating to 125°, all these minima disappear except for a small minimum at 2440 nm. The β -form curve is practically identical to the curve obtained for tetrahedral $\text{Co}(\text{py})_2\text{Br}_2$.

b. $[\text{Cu}(\text{en})(\text{H}_2\text{O})_2]\text{SO}_4$

The deaquation of $[\text{Cu}(\text{en})(\text{H}_2\text{O})_2]\text{SO}_4$ was studied using HTRS and DRS by Wendlandt (15). This reaction, which takes place between 75 and 150°C, follows the equation

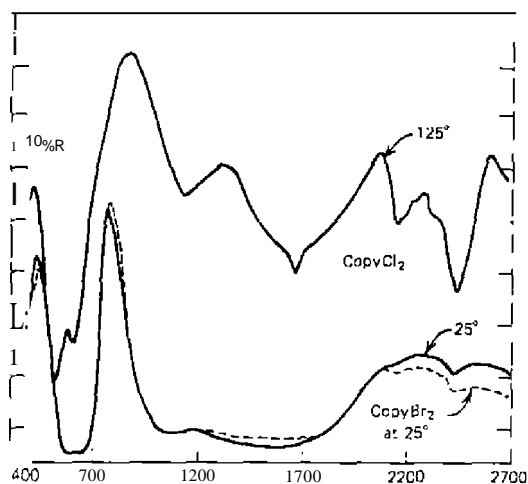
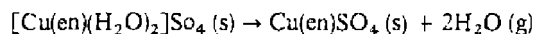


Figure 9.8. HTRS curves of $\alpha\text{-Co}(\text{py})_2\text{Cl}_2$ in the visible and near-infrared wavelength region (15).

The HTRS curves, from 25 to 180°C, are shown in Figure 9.9. Two sets of curves are shown, one set at 25 and 75°, and the other at 150 and 180°. The first set has a peak minimum at about 625 nm (corresponding to maximum absorption) and corresponds to the curves for the initial compound, while the second set has a peak minimum at 575 nm and corresponds to the curves for the deaquated compound, $\text{Cu}(\text{en})\text{SO}_4$. Thus, the deaquation reaction must have occurred between 75 and 150°.

To obtain the transition temperature for the deaquation reaction, the DRS technique was employed, as shown in Figure 9.10. The transition temperature dependence on the sample heating rate is readily seen; it varied from 115° at 6.7°C/min to 165° at 45.3°C/min. This behavior is not unexpected because it occurs with practically all the other thermal techniques where some physical property of the sample is measured as a dynamic function of temperature (13). In all DRS studies, the sample heating rate obviously must be specified.

Since the Beckman DK-2A spectrophotometer is capable of recording the sample spectra in the near-infrared wavelength region, the HTRS curve:

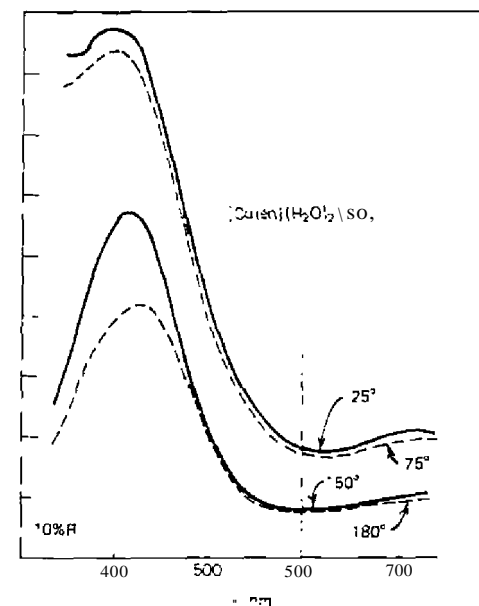


Figure 9.9. HTRS curves of $[\text{Cu}(\text{en})(\text{H}_2\text{O})_2]\text{SO}_4$ (15)

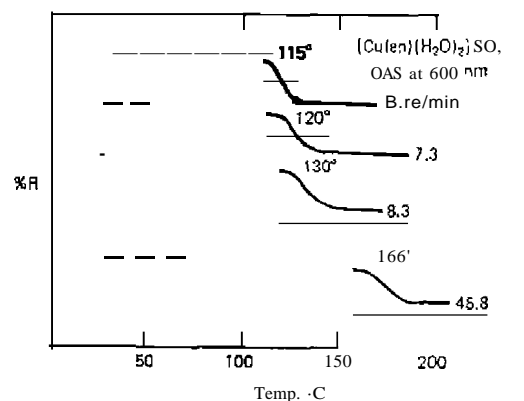


Figure 9.10. DRS curves of $[\text{Cu}(\text{en})(\text{H}_2\text{O})_2]\text{SO}_4$ at 600 nm (15).

were recorded to 2700 nm, as shown in Figure 9.11. At room temperature, the reflectance curve contained minima (absorption bands) at 1560, 1725, 2050, 2150, 2260, and 2500 nm, respectively. On heating the sample to 150°C, the bands at 1560, 1725, and 2050 nm remained unchanged, while the 2150 nm disappeared. The 2260-nm band shifted to 2280 nm, and the 2510-nm band shifted to 2525 nm. There were rather pronounced changes in intensity

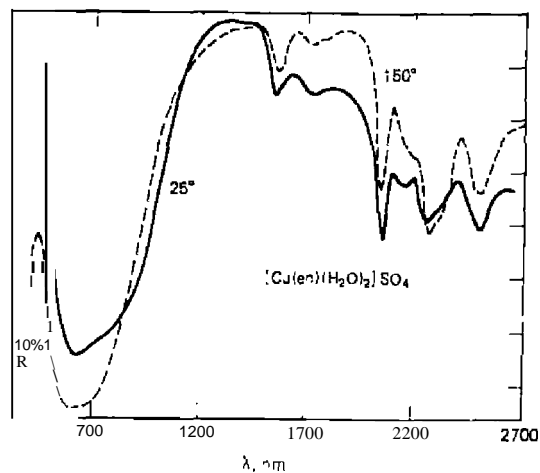


Figure 9.11. Visible and near-infrared reflectance spectra of $[\text{Cu}(\text{en})(\text{H}_2\text{O})_2]\text{SO}_4$. (15.)

for all of the bands discussed, which may be due to the sample-particle size changes.

c. $\text{CuSO}_4 \cdot 5\text{H}_2\text{O}$

The HTRS curves in the visible and near-infrared regions are given in Figures 9.12 and 9.13, while the DRS curve, at 625 nm, is given in Figure 9.14.

As in the case of $[\text{Cu}(\text{en})(\text{H}_2\text{O})_2]\text{SO}_4$, two sets of curves are shown for $\text{CuSO}_4 \cdot 5\text{H}_2\text{O}$ in Figure 9.12. At room temperature the reflectance minimum occurs at about 680 nm; on heating to 135°C the minimum shifts to 715 nm. In this temperature range, the compositional change of the compound is due to deaquation from $\text{CuSO}_4 \cdot 5\text{H}_2\text{O}$ to $\text{CuSO}_4 \cdot \text{H}_2\text{O}$. At still higher temperatures, such as 250°C, the last mole of water per mole of copper sulfate is evolved to give the anhydrous salt. In the near-infrared region at room tem-

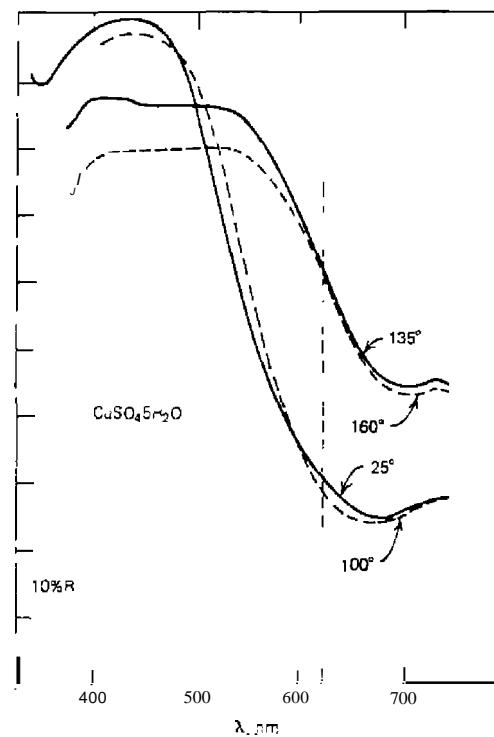


Figure 9.12. HTRS curves of $\text{CuSO}_4 \cdot 5\text{H}_2\text{O}$ in the visible wavelength region (15.)

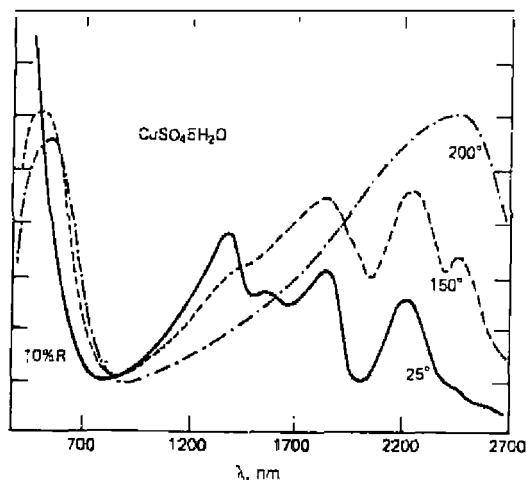


Figure 9.13. HTRS curves of $\text{CuSO}_4 \cdot 5\text{H}_2\text{O}$ in the visible and near-infrared waveT.gh region (15).

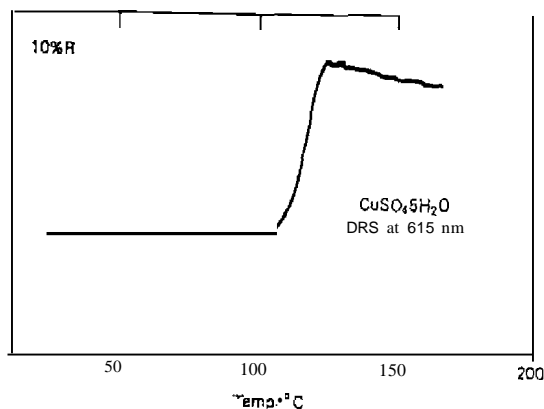


Figure 9.14. DRS curve of $\text{CuSO}_4 \cdot 5\text{H}_2\text{O}$ at 625 nm and a heating rate of 5.7 emir. (15)

perature, reflectance minima were observed at 1510, 1675, and 2000 nm, respectively. At 150°, the first two bands had disappeared while the 2000-nm band has shifted to 2060 nm. A new band, at 2400 nm, was observed at the higher temperature. At still higher temperatures, 200°, all of the bands in this region were absent.

The DRS curve in Figure 9.14, showed that a major increase in sample reflectance began at about 105°, although the reflectance was gradually increased from room temperature up to 100° about 0.1 a % R unit. At about 125°, the reflectance of the compound again decreased gradually until a maximum temperature of about 200° was attained.

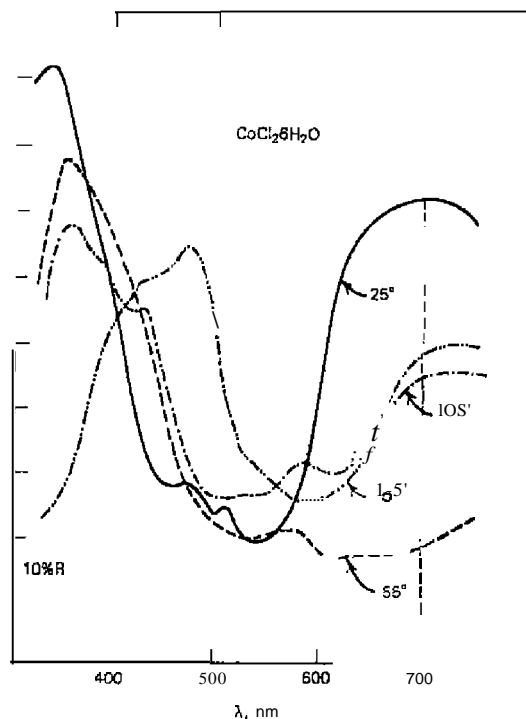
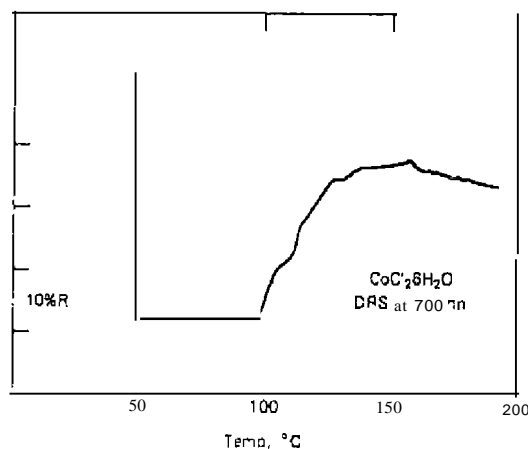
d. $\text{CoCl}_2 \cdot 6\text{H}_2\text{O}$

In an earlier investigation, Wendlandt and Cathers [26] studied the HTRS and DRS of the reaction between $\text{CoCl}_2 \cdot 6\text{H}_2\text{O}$ and KCl. The DRS curve revealed that the following structural and compositional changes occurred: *octahedral*- $\text{CoCl}_2 \cdot 6\text{H}_2\text{O} \rightarrow \text{tetrahedral } \text{CoCl}_4^{2-} \rightarrow \text{octahedral } \text{CoCl}_2 \cdot 2\text{H}_2\text{O} \rightarrow \text{tetrahedral } \text{CoCl}_4^{2-}$. The preceding reactions took place, of course, in the presence of an excess of chloride ion; hence, the final product was K_2CoCl_4 rather than anhydrous cobalt(II) chloride.

More recently, the deaquation of $\text{CoCl}_2 \cdot 6\text{H}_2\text{O}$ was investigated in the absence of potassium chloride. This compound is a rather difficult one to study because it fuses at about 50°, and since the heated sample holder is mounted in a vertical position on the spectroreflectometer, the liquid $\text{CoCl}_2 \cdot 6\text{H}_2\text{O}$ is impossible to retain on the sample holder. This problem was solved, however, by placing a thin layer of the powdered sample on a 25-mm-diameter round cover glass which was then contained on the glass fiber cloth by the rectangular cover glass. The viscous nature of the melt prevented the compound from leaving the sample area.

The HTRS and DRS curves of $\text{CoCl}_2 \cdot 6\text{H}_2\text{O}$ are shown in Figures 9.15 and 9.16, respectively. The HTRS curves reveal a rather interesting series of structural changes, both in the liquid and solid states. At 25°, solid $\text{CoCl}_2 \cdot 6\text{H}_2\text{O}$ has an *octahedral* structure with a reflectance minimum at 535 nm and shoulder minima at 460 and 500 nm, respectively. On heating the compound to 55°, it fused and gave a reflectance curve which had one minimum at 525 nm and a rather broad minimum between 600 and 700 nm. This latter curve is similar to the one previously observed for a mixture of *octahedral*- and *tetrahedral*-cobalt(II) complexes by Simmons and Wendlandt (27). Thus, a possible interpretation would be that the 55° curve is probably a mixture of *octahedral*- $\text{CoCl}_2 \cdot 6\text{H}_2\text{O}$ and *tetrahedral*- $\text{Co}(\text{CoCl}_4)$. On further heating, the mixture underwent further deaquation and gave, at 155°, anhydrous *octahedral*- CoCl_2 . This latter curve contained a peak minimum at 590 nm, with a shoulder minimum at 535 nm.

The DRS curve, Figure 9.16, showed a pronounced decrease in reflectance at 45° which was due to the formation of the *octahedral*-*tetrahedral* mixture. At 100°, the reflectance of the mixture began to increase, reaching a maximum value at about 150°, then decreasing slightly above this temperature. The

Figure 9.15. HTRS curves of $\text{CoCl}_2 \cdot 6\text{H}_2\text{O}$ (15).9.16. DRS curve of $\text{CoCl}_2 \cdot 6\text{H}_2\text{O}$ at 700 nm and a heating rate of $6.7^\circ\text{C}/\text{min}$, II (5)

curve reflects the various structural changes that have been discussed previously.

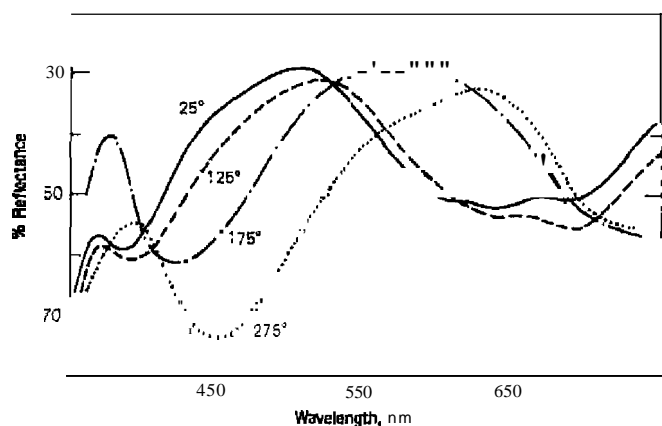
e. $\text{Ni}(\text{py})_4\text{Cl}_2$

Yang (28) studied the HTRS of the deamination of $\text{Ni}(\text{py})_4\text{Cl}_2$, the curves of which are illustrated in Figure 9.17. The spectrum at 25°C is that for the initial compound, $\text{Ni}(\text{py})_4\text{Cl}_2$. From 125 to 175°C , two moles of pyridine per mole of complex are lost, so that the spectrum at 175°C is that for the complex $(\text{Ni}(\text{py})_2\text{Cl}_2)$. From 175 to 275°C , another pyridine is evolved, so that the 275°C spectrum is that for $\text{Ni}(\text{py})\text{Cl}_2$. The loss of pyridine and the changes in the reflectance of the initial complex are shown in the 450-nm DRS curve in Figure 9.17. The transition, $\text{Ni}(\text{py})_4\text{Cl}_2 \rightarrow \text{Ni}(\text{py})_2\text{Cl}_2$, began at 145° and was completed at 160°C ; the loss of an additional pyridine began at 210°C and was completed at 220°C . The increase in slope throughout the DRS curve was due to the increasing sample temperature.

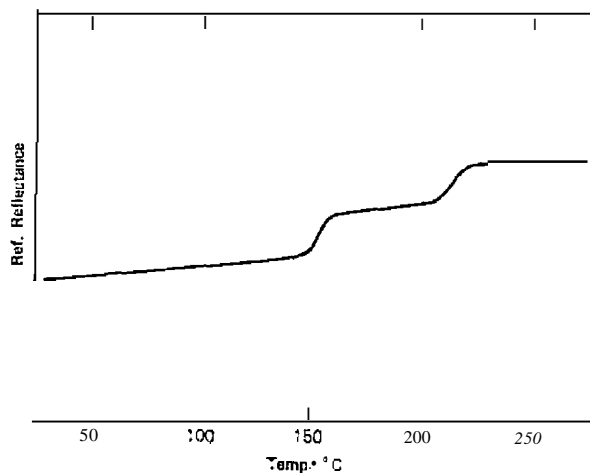
f. Thermochromism of $\text{Ag}_2[\text{HgI}_4]$

The thermochromism of $\text{Ag}_2[\text{HgI}_4]$ has been of great interest since its first preparation by Caventou and Willm (29) in 1870. The transition was first investigated in a thorough manner by Ketelaar using specific heat, X-ray, and electrical conductivity techniques (30, 33). Additional information concerning the color changes (34, 36, 39), dilatometry (35), crystal structure (37, 38), magnetic susceptibility (9), electrical conductivity (39, 40), and thermal stability (41) of the compound has been reported. The compound has been proposed as a temperature indicator (36, 42) and as a pigment for temperature-indicator paints (42-44).

The thermochromism of $\text{Ag}_2[\text{HgI}_4]$ is due to an order-disorder transition which involves no less than three phases. According to Ketelaar (33), both the yellow low-temperature β modification and the red high-temperature α form contain iodide ions which are cubic close-packed, while the silver and mercury ions occupy some of the tetrahedral holes. The β form has tetragonal symmetry, with the mercury ion situated at the corners of a cubic unit cell and the silver ions at the midpoints of the vertical faces. As the temperature is increased it becomes possible for the silver and mercury ions to occupy each other's lattice sites and also the two extra lattice sites (top and bottom face centers of the unit cube) which were unoccupied at lower temperatures. Above 52°C , the mercury and silver ions are completely disordered. The α modification has, therefore, averaged face-centered cubic symmetry. More recently, magnetic (39) and dielectric polarization (37, 39) measurements confirm the presence of a third phase, the β' modification. With an increase



(a)



(b)

Figure 9.17. (a) HTRS of $\text{Ni}(\text{py})_4\text{Cl}_2$ in an A_2O (50%) matrix; (b) DRS curve of $\text{Ni}(\text{py})_4\text{Cl}_2$ in an A_2O (50%) matrix recorded at 450 nm. (28).

in temperature, the silver ions become disordered, occupying at random $\frac{2}{3}$ of the face-centered positions of the unit cube during the $\beta \rightarrow \beta'$ transition. During the $\beta' \rightarrow \alpha$ transition, the silver and mercury ions become further disordered at random $\frac{2}{3}$ of the corners plus face centers of the unit cell (37) corresponding to two cubic (but not isotropic) cells stacked one on top of the other. The Patterson function suggests that a portion of the silver atoms

are disordered, having left sites surrounded tetrahedrally by iodide ions and appearing in interstitial (octahedrally occupied) sites. The interstitial silver ions would be expected to be rather labile, since the octahedral holes are large compared to those at the tetrahedral sites. This is also apparent from the low activation energy obtained (37) for the conduction process in $\beta\text{-Ag}_2[\text{HgI}_4]$, 12 kcal/mole below 20°C.

The reflectance curves for $\text{Ag}_2[\text{HgI}_4]$ from 23 to 100°C are shown in Figure 9.18. The yellow β form reflects rather strongly above 500 nm, with the maximum shifting to higher wavelengths during the transition to the red α form. The change in color is dependent on the rate of heating. At 2.5°C/min the transition is completed at a somewhat lower temperature than at the 10°C/min heating rate. This heating rate is extremely rapid compared to the temperature rise of 5°C/day used by Neubert and Nichols (39) in their magnetic studies. The transition temperature found here was not very well defined in that the color change appeared to take place over the temperature range from 30 to about 60°C. Reported transition temperatures include 50.7 ± 0.2 , 52.51, 50.5, and 52°C.

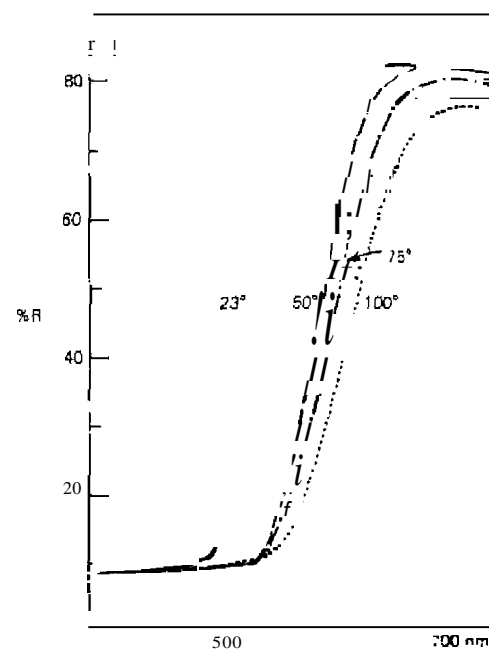
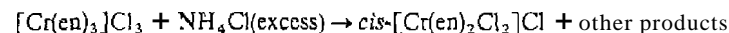


Figure 9.18. HTRS curves of $\text{Ag}_2[\text{HgI}_4]$ at 450 nm.

The DRS curves of a number of $M_n[HgI_4]$ complexes ($M = Pb, Cu, Hg, Ag,$ and Tl) are given in Figure 9.19. All the compounds exhibit rather sharp thermochromic transition, with the exception of $Tl_2[HgI_4]$. The latter compound is reported to have a transition at $116.5^\circ C$ (9); however, it is not evident from the DRS curve. The change in reflectance of the compound appears to decrease linearly with temperature.

g. Thermal Matrix Reactions

The techniques of HTRS and DRS were used by Wendlandt and co-workers (46-49) in the investigation of reactions between chromium(III) and cobalt(II) ammine complexes and ammonium salts (thermal matrix reactions). Such a reaction is illustrated by (46).



AI: 1 mass ratio of $[Cr(en)_3]Cl_3$ and NH_4X ($X = \text{fluoride, chloride, bromide, iodide, and thiocyanate}$) were heated up to $200^\circ C$ in a high-temperature sample holder. The HTRS mode was used to identify the reaction products, while the DRS mode was used to determine the temperature range at which the reaction took place. As a result of these studies, new synthetic procedures were developed for the preparation of $cis-[Cr(en)_2X_2]Cl$, $cis-[Cr(en)_2X_2]X$,

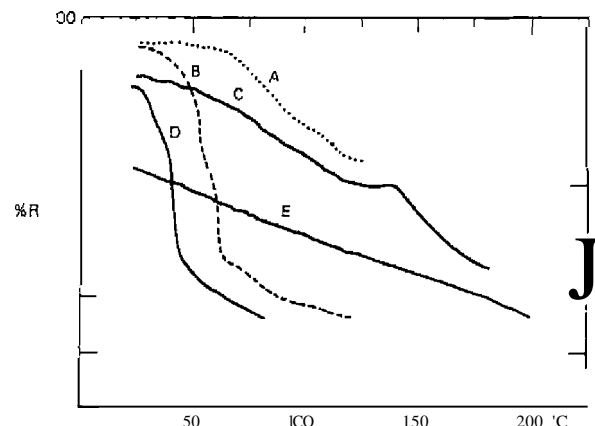


Figure 9.19. DRS curves of complexes ($5^\circ C/min$): A, $Pb[Cr(en)_3]$, 585 nm; B, $Cu_2[Cr(en)_3]$, 650 nm; C, $Hg[Cr(en)_3]$, 600 nm; D, $Ag_2[Cr(en)_3]$, 575 nm; E, $Tl_2[Cr(en)_3]$, 550 nm (45).

and $cis-[Cr(tm)_2X_2]X$ complexes ($pn = 1,2$ -propanediamine and $tm = 1,3$ -propanediamine).

Chang and Wendlandt (47-49) investigated several series of compounds of the types (1) cis - and $trans$ - $[Co(en)_2(H_2O)_2](NO_3)_3 \cdot NH_4X$ and (2) cis - and $trans$ - $[Co(NH_3)_4(H_2O)_2](NO_3)_3 \cdot NH_4X$. In all cases, a *trans* reaction product was obtained. Various mechanisms were proposed as well as synthetic procedures for the *trans* isomeric products.

B. PHOTOMETRIC METHODS

A simultaneous photothermal analysis (PTA) and DTA apparatus has been described by David (50). It was found after examining a large number of inorganic and organic compounds that the two techniques provided complementary information but that the PTA curves contained features which were not present in the DTA curves. Compounds investigated included limestone, clay, $CuSO_4 \cdot 5H_2O$, polystyrene, polyvinylchloride, and several other polymers.

The simultaneous PTA-DTA apparatus is illustrated in Figure 9.20. It consisted of a Stone-Premeo DTA cell which was modified by drilling a 0.275-in. opening in the cell cap and furnace chamber to permit sample viewing by the photomultiplier tube. With an "end-on" photomultiplier tube mounted on the top of the furnace, the sample in the ring thermocouple container could be viewed directly. Using a two-channel recorder, one channel recorded the output from the phototube and the other recorded the DTA curve.

In the case of several limestone samples that were examined, the DTA curves revealed small, broad exothermic peaks in the temperature range from 300 to $375^\circ C$, which coincided with the major glow peaks in the PTA curves. David concluded that DTA appeared to be as sensitive as or perhaps more sensitive than PTA for examining these types of materials and perhaps would be better suited to studies involving geological dating than thermoluminescent analysis. The lack of sensitivity in the PTA curves may be due to the slow heating rate that was employed ($10^\circ C/min$). Typical thermoluminescent curve determinations are made at heating rates from $10^\circ C/min$ to $16^\circ C/sec$. In the case of polymeric samples, David (50) found that melting and/or glass transitions were not detected by PTA but decomposition reactions were observed. Thus, the DTA-PTA technique permitted differentiation between these types of transitions. A PTA curve peak began at approximately the temperature where oxidation began, much like that observed in oxyluminescence. This behavior was observed even though the samples were heated in a flowing nitrogen atmosphere.

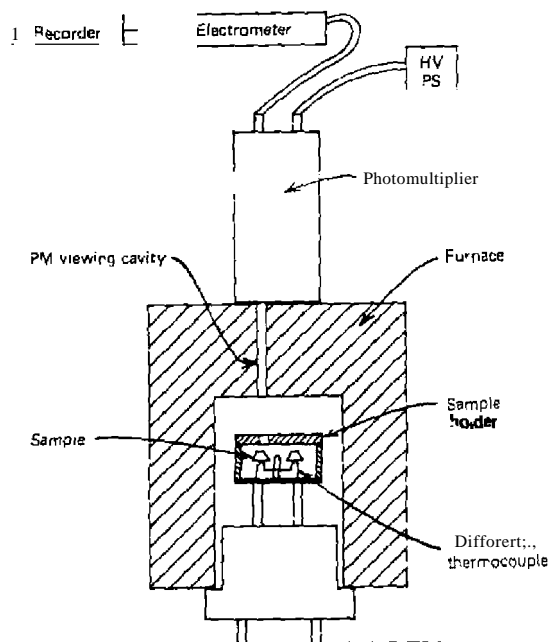


Figure 9.20. Simultaneous PTA-DTA apparatus (50).

A somewhat more sophisticated apparatus was described by Rupert (51) for observing phase transitions of incandescent materials. In this apparatus, a photomultiplier tube was used to follow the temperature changes of the heated sample. The phototube responds to the luminosity of the sample, which is proportional to the temperature. It is not necessary to know the exact relationship between the output of the phototube and the temperature of the sample because temperature calibration is accomplished by using a calibrated optical pyrometer which receives part of the light from the sample. The sample was contained in a crucible located within the current concentrator. The latter receives power from an induction heater whose output is controlled by an induction heater controller. Light from the sample emerges through a 0.070-in.-diameter hole in the top of the crucible, and travels upward through a Pyrex or quartz window into the lower end of a beam splitter. Part of the light is reflected at approximately 90° to the axis of the beam splitter, by a partially aluminized mirror, to the optical pyrometer used to measure the sample temperature. Typical cooling curves studied by

this technique include the freezing of a molybdenum carbide-carbon mixture at 2540°C, a cooling curve of the freezing of zirconium carbide-carbon eutectic mixture at 2855°C, and a solid-state transition of uranium dicarbide at 1800°C.

C. HIGH-TEMPERATURE INFRARED SPECTROSCOPY

Although the KBr disk technique in infrared spectroscopy is well known, few quantitative kinetic studies of solid-state chemical reactions in this medium have been reported. Hisatsune and co-workers (53-58) found that many chemical reactions were initiated by heating the disks to elevated temperatures and that the kinetics of these reactions could be conveniently followed by this technique. The disks were placed in an oven heated at the desired temperature for a specific period of time, and the IR spectrum of the disk was recorded after it was quenched to room temperature. A typical disk weighing about 0.5 g cooled from about 600°C to room temperature in less than a minute. Disks prepared from potassium salts could be heated in air to about 600°C, but above this temperature appreciable sublimation of the matrix salt occurred. Initial heating usually produced the greatest change in the appearance of the disks. They turned opaque, expanded, and often showed blisters on the surface when gaseous products were formed by the decomposition of the solutes. In some cases, the transparency of the disk could be restored by breaking it into small pieces and repressing. For quantitative studies the rim of the expanded disk was sanded off until it fitted the die cavity. Studies reported included the trapping of the BO_2^- ion (54), the carbon dioxide anion $[\text{CO}_2^-]$ free radical (55), the carbonate anion $[\text{CO}_3^-]$ free radical (56), the formate ion from the acetate ion (57), and the decomposition of the perchlorate ion (58).

The thermal decomposition kinetics of silver carbonate using the disk technique was reported by Wydcnen and Lebao (59). Continuous, *in situ* quantitative analysis of infrared active reactants and products of the decomposition reactions was made possible by use of a heated cell. The cell was constructed of stainless steel and could be heated to 500°C with the KRS-5 cell windows maintained at room temperature by cooling water. A similar approach was used by Wendlandt (60).

A heated temperature-programmable IR cell was used by Tanaka et al. (61) to study the thermal decomposition of a number of cobalt(II) ammine complexes. The disk matrix material was either KCl or KBr, and it was reported that they frequently became opaque to infrared radiation at elevated temperatures. A heated IR cell for use up to 200°C was also described by LeRoux and Montano (62).

D. THERMAL OPTICAL MICROSCOPY TECHNIQUES

1. Fusion Microscopy

The term "fusion microscopy" includes the methods and procedures that involve the heating of a compound or a mixture of compounds on a microscope slide (64). It includes all observations made during the heating of the preparation (description, sublimation, decomposition, melting, etc.) on the melt itself (refractive index, boiling point, critical solution temperature, etc.), the solidification of the melt (crystal angles, birefringence, rate of growth, etc.), and the cooling (polymorphic transformations, orthoscopic and conoscopic observations, composition diagrams, etc.). The most important applications appear to be (1) characterization and identification of pure compounds, (2) determination of purity, (3) analysis of binary mixtures, (4) determination of composition diagrams for binary and ternary systems, (5) elucidation of phase diagrams, and studies of (6) polymorphism, (7) crystal growth kinetics, and (8) crystal-lattice strain (63, 64). Identification of a fusible compound by this technique is very rapid, consumes only small quantities of material, and requires relatively little specialized training or equipment. The purity of a fusible compound is, in many cases, very quickly determined by fusion methods since impurities usually are visible as high-melting material, as liquid eutectic, or as early melting material. A mixed fusion gives a rapid and dependable means of determining whether two given samples are the same compound. Complete binary and ternary composition diagrams can be determined usually in a few hours' time. Recent reviews on this subject include those by Vaughan (65), Smith (66), Sommer (67, 68), and McCrone (63).

The various hot stages employed have been reviewed by McCrone (63, 64); the most successful appears to be that described by Kofler. It was first described in the 1930s and became commercially available in 1940. This instrument was successful mainly because it was reliable: temperatures indicated by the thermometer could be dependably associated with the temperatures of the preparation under investigation. A much more sophisticated instrument, the Mettler FP-2 hot stage, which was introduced in 1968, is schematically shown in Figure 9.21. In the control system, the temperature is detected by a platinum resistance thermometer placed in very close proximity to the sample. Power to the heating elements is proportionally controlled by the difference between the resistance of the resistance thermometer and the resistance of a motor-driven potentiometer. As long as the actual temperature and the required program temperature are in agreement with each other, the rotation of the program signal-generator motor will be a linear function of the temperature. Digital temperature readout is presented

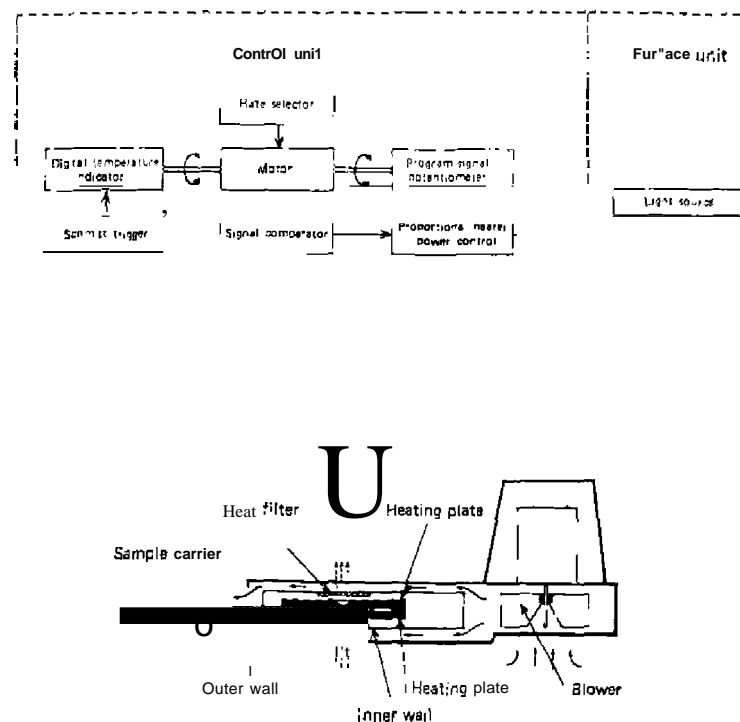


Figure 9.21 The Mettler FP-2 hot stage. (a) Schematic diagram of the control system; (b) schematic diagram of hot stage.

by connecting the program signal motor to a series of counter wheels. A choice of three heating rates may be preselected: 0.2, 2.0, and 10.0°C/min; the temperature range is from -20°C to 300°C. Temperature measurement and control accuracy is $\pm 0.1^\circ\text{C}$ below 100°C and $\pm 0.1\%$ above this temperature. The hot stage, which can be fitted to any standard microscope, consists of an adjustable sample carrier, two metal heating plates in which heating wires and the platinum thermometer are embedded, and a compact blower for circulating air within the chamber. The design of the hot stage is such that the sample is heated simultaneously from above and below and is thus maintained in a uniform temperature field.

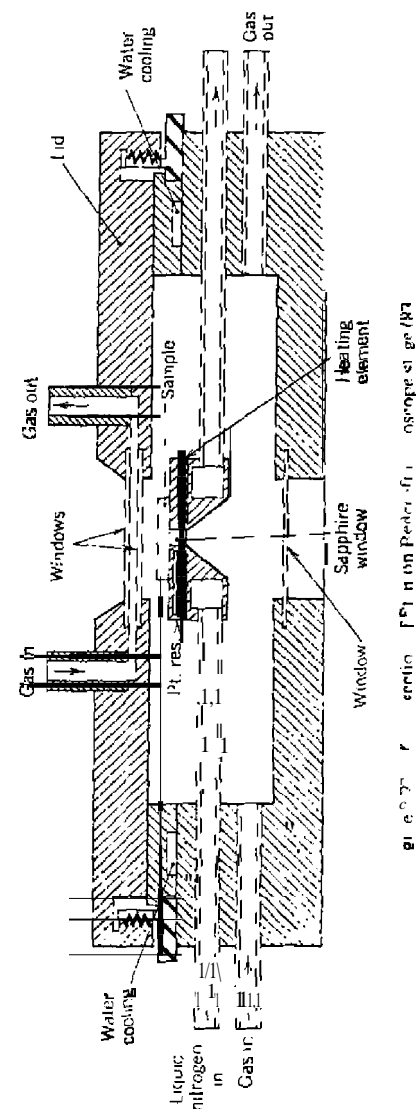
Microscope stages for use at low (-180°C) or high temperatures (1000°C)

have been described by numerous workers. Tynan and von Gutfeld (81) described a stage for use between 30 and 800 K that permits temperature cycling of a small area of the sample while monitoring it by an optical microscope. The sample can be illuminated by a laser beam directed on a small sample area, typically 25–50 μm in diameter, with sample heating by a small electrical heating coil, or cooling by circulation of cold gases in the cell. A mechanical vacuum pump and liquid N_2 trap permits the evacuation of the cell to $\sim 1 \times 10^{-5}$ Torr. Lower pressures can be achieved through use of a suitable diffusion pump. The stage was used to measure transverse thermoelectric voltages of thin films of Pd on an Al_2O_3 substrate.

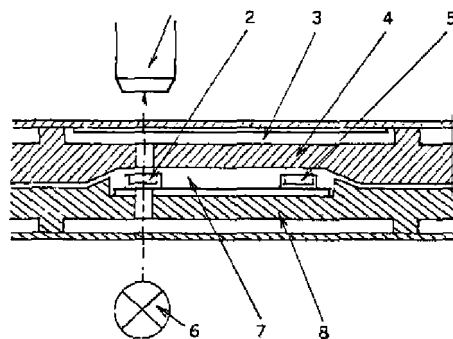
Hildebrandt and Cocks (82) described a low-temperature stage that permitted frozen samples to be etched by vacuum desiccation or sublimation in an inert gas atmosphere. Cooling rate and isothermal holding temperatures were controlled by regulating N_2 gas flow through a liquid N_2 bath and a cooling block in the device. Cooling rates from 1° to 7°/min were easily obtainable to -60°C. The stage was used to study frozen thin films of the $\text{NaCl}\text{-H}_2\text{O}$ binary system.

Charsley et al. (83) described a stage that permits observation of a sample by transmitted light, as it is heated or cooled at a controlled rate over the temperature range of -180° to 600°C. The sample can be viewed in normal or polarized light and the intensity of the transmitted light measured using a photocell and displayed on a recorder together with the sample temperature. A cross section of the stage is shown in Figure 9.22. The body of the device is made from anodized aluminum and is water cooled. The sample, normally placed between two cover glasses, is heated by means of a silver block containing a nichrome heating element. A sapphire window, approximately 2 mm in diameter, allows the viewing of the sample by transmitted light. Sample temperature is detected by a platinum wire resistor located in the block immediately adjacent to the sample. A temperature programmer permits heating rates from 1° to 99°C/min. Cooling is carried out by using liquid N_2 flowing through a coil in the block. A controlled flow of coolant used in conjunction with the heating program enables linear heating and cooling rates over the entire temperature range.

Morrow (51) has described a DTA-light photometer polarizing system for in-situ microscopy. Thermocouple wires, 0.003 in. in diameter, were used to detect the ($T_s - T_r$) temperature difference for simultaneous DTA measurements. Sample capsules were fabricated by bending small, identical stripes of Al foil over both sample and reference thermojunctions. A small hole in the foils permitted the viewing of the sample by transmitted light microscopy. The primary use of the apparatus was to study the thermal properties of thermally sensitive polymers (84).

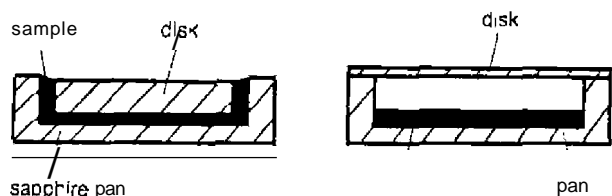


Wiedemann and co-workers (85-88) described several systems for simultaneous DTA-thermomicroscopy measurements. One of the systems is shown in Figure 9.23a. As with the stage shown in Figure 9.21, two-sided heating of the sapphire sample container is employed. The temperature differences between the sample and reference containers is detected by two vapor-



- | | |
|----------------------------------|--|
| 1 Microscope objective | 6 Microscope light source |
| 2 Sapphire sample crucible | 7 DSC measuring sensor |
| 3 J-lead protection filter | 8 Metal plate with heating wires and Pt100 resistance sensor |
| 4 Metal plate with heating wires | |
| 5 Sapphire reference crucible | |

(a)



(b)

Figure 9.23. Mettler DTA-thermomicroscopy FP 84 furnace and sample holder. (a) Cross section of device; (b) sapphire sample holders.

deposited, five-junction gold-nickel thermopiles. The system temperature is detected by a platinum resistance sensor located in the metal plate, which also contains the resistance wire heater. A special heat filter is used to cover the observation opening. The temperature range of the stage is -60 to 300°C with absolute temperature measurement accuracies of ± 0.4 to ± 0.8 degrees. Reproducibility of DTA enthalpy measurements is about 5%. Microscopic observations are at best performed at heating or cooling rates of less than $1^{\circ}\text{C}/\text{min}$.

Samples are contained in covered sapphire sample containers, as shown in Figure 9.23b. These containers are 5 mm in diameter with a cover 4 mm in diameter. Covered sample containers are used for volatile samples. For viscous melted samples, they can be enclosed between two glass disks for observation. Sealed aluminum crucibles can be used for nonsimultaneous measurements, that is, only those for DTA. Another technique that can be used for low-viscosity samples or liquid crystals is to place three small sapphire balls in the sample to support the sapphire lid (88).

A schematic diagram of the system is shown in Figure 9.24. Data may be obtained by recording on a strip-chart recorder or transferred via an RS-232 interface to a Hewlett-Packard Model HP87 microcomputer. In the latter, the data curve is displayed on a CRT screen or a printer/plotter.

Numerous applications of thermomicroscopy have been reviewed by McCrone (63, 64), Kuhnert-Brandstatter (89), and others. The use of these techniques in purity determinations of organic compounds is discussed in Chapter 12.

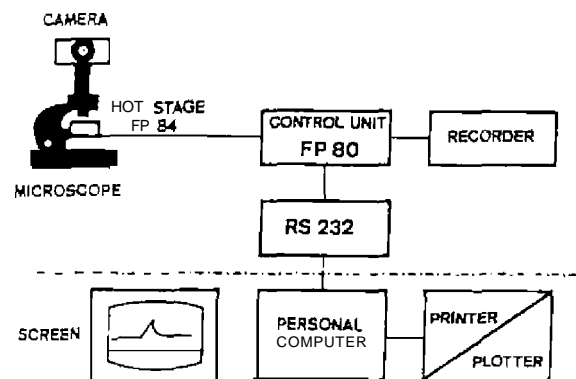


Figure 9.24. Mettler DTA-thermomicroscopy system, consisting of the FP 84 hot stage, FP 80 control unit, and a HP 87 microcomputer (88).

2. Depolarized Light Intensity and Photometric Thermal Microscopy

In the usual procedures used in fusion microscopy, thermal changes in the sample are visually observed; photomicroscopic techniques may be employed to obtain a permanent record of the thermal events. Because the eye is not particularly sensitive to subtle changes taking place over a period of several minutes, automatic devices have been used to detect these changes. One method is to use some type of photocell to measure changes in the sample light transmission or intensity of birefringence (45, 65, 69-78). Another method is to use an infrared scanning camera such as described by Hyzer (79). The former is primarily used for the accurate determination of melting points, polymorphic transitions, and crystallization rates, while the latter more sophisticated method can reveal the minute differences in temperature in the area under investigation.

The apparatus used for recording the changes in light transmission of a sample usually consists of the following components (65, 69, 73): (1) photodetector such as a photocell, photomultiplier tube or photoresistor; (2) hot stage; (3) temperature programmer; (4) microscope; (5) some type of sample holder; and (6) recorder (usually an X-Y plot). The output of the photodetector is recorded as a function of sample temperature as the sample is being heated at rates from 0.2-30°C/min. The sample preparation (69) for light-transmission methods consisted of placing it either melted between cover slips or mounted in a silicone oil and then covering with a cover slip. The oil cuts down light refraction and permits improved birefringence intensity measurements. For crystalline or partially crystalline polymers, an embedding technique may be used. The polymers are embedded in a thin layer (0.5 mm) of high-viscosity polydimethylsiloxane polymer spread over the microscope slide. Still another technique (65) is to use glass capillary tubes to contain the sample. Powdered samples are normally packed to a height of 3-4 mm in the bottom of the tube, while fats, oils, and waxes can be easily loaded into the tubes in their melted state by means of a long-needled syringe.

The photometric heating and cooling curves of ammonium nitrate (73) are illustrated in Figure 9.25. The four polymorphic transitions between 25 and 200°C are clearly indicated. The *orthorhombic* → *monoclinic* transition at 42° is observed as an increase in light intensity, while the *monoclinic* → *tetragonal* transition at 78°C is accompanied by a decrease in intensity. A sharp decrease in intensity indicates the *tetragonal* → *cubic* transition and then the fusion of the cubic form at 169°C. On cooling, the melt crystallizes to the cubic form at 175°C. Several large changes of light intensity are shown as the ammonium nitrate undergoes the various phase transitions. All these measurements were made under polarized light.

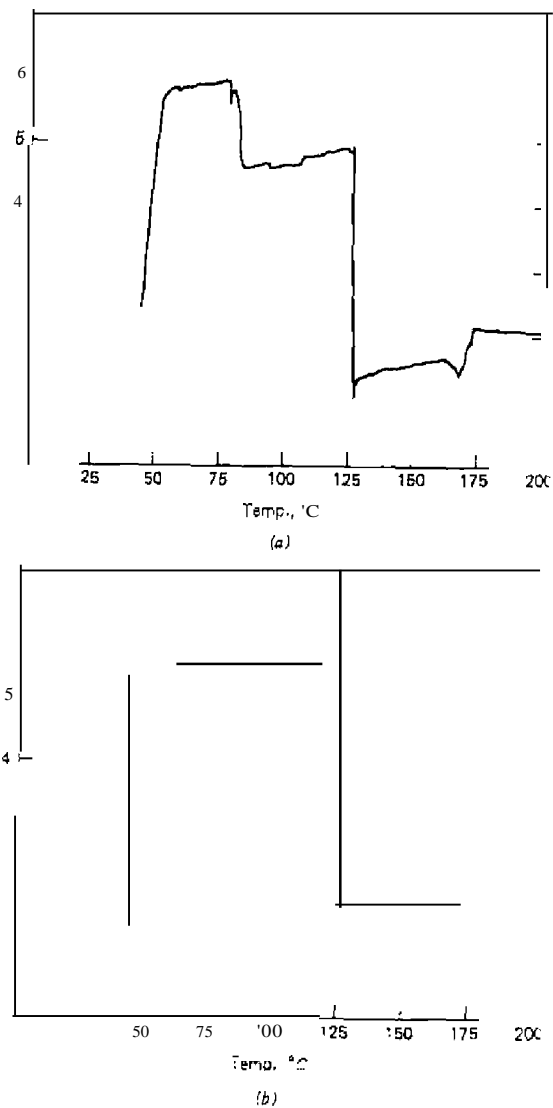


Figure 9.25. Photometric curves of ammonium nitrate (73). (a) Heating curve; (b) cooling curve.

The technique of depolarized light intensity (DLI) microscopy was introduced by Magill (80) in 1960. Basic elements of the apparatus were a light source, polarizers, a sample holder, an analyzer, and a suitable recording system. Barrall and Johnson (74) and Miller (75,76) have described applications of this technique to polymeric samples. Miller (75) prefers to call this technique *thermal polarization analysis* (TPA).

The DLI apparatus used by Barrall and Johnson (74) is illustrated in Figure 9.26. They found it convenient to use the recording system from a DuPont 900 DTA module. The intensity of the depolarized light was measured with a photoconductive cell used in conjunction with a Wheatstone bridge circuit. A hot stage, constructed from a copper block, could be used in the temperature range from -40 to 600°C at a heating rate of about $1^{\circ}\text{C}/\text{min}$ or in an isothermal operational mode. For faster heating rates, a low-thermal-mass furnace was used which contained a platinum heater and was usable up to Sooco.

The transmitted light intensity (TPI) curve of the melting and freezing of

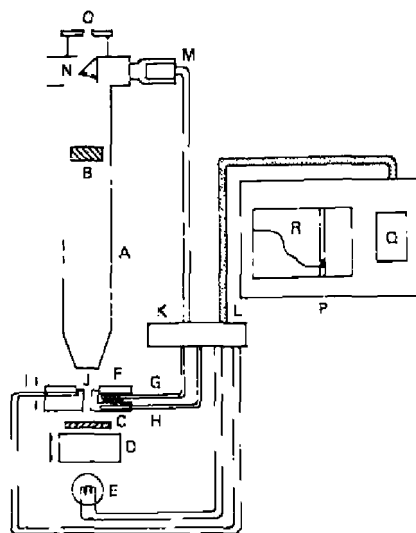


Figure 9.26. Schematic diagram of depolarized light intensity apparatus (74). A, uniron MPS microscope; B, analyzer sheet; C, polarizer sheet; D, movable cube condenser; E, tungsten lamp; F, movable hot stage; G, heater; H, program thermocouple; I, sample temperature thermocouple; J, sample well; K, pin plug terminal attached to microscope stand; L, shielded cable to Du Pont module; M, photocell; N, movable mirror; O, ocular; P, Du Pont 900 differential thermal analyzer module; R, X-Y recorder.

1,2-dichloroethane is shown in Figure 9.27 (83). On heating, the first change in the TPI curve is seen in the region of -35°C with a major change in the curve occurring in the range of -34.3 to -33.5°C . This transition compares favorably with the ICTA values of $-35.7 \pm 2.0^{\circ}\text{C}$ and $-31.4 \pm 4.3^{\circ}\text{C}$ for the extrapolated onset and peak temperatures, respectively. The TPI curve also shows the magnitude of the supercooling of this substance, which make it unsuitable for use as a standard in the cooling mode.

Wendlandt (45) used a microscopic method for the determination of the reflectance of the sample. The apparatus, as shown in Figure 9.28, consisted of a low-power (100x), generally reflection-type microscope, A, which is illuminated by means of a monochromator, B. The reflected radiation is detected by a photomultiplier tube, C, and amplifier, D, and recorded on either an X-Y recorder, E, or a strip-chart recorder, F. In order to heat the sample to 250°C , a Mettler Model FP-2 hot stage, G, is employed. Either isothermal ($\pm 1^{\circ}\text{C}$) or dynamic sample temperatures may be attained by this device. The sample is moved through the illuminated optical field by means of the reversible motor, H. The motor is reversed at preset intervals by a relay circuit and timer, J. Thus, it is possible to scan the reflectance from the sample, which may consist of a single crystal or a powdered mixture. Powdered samples may be placed directly on the heated microscope slide or

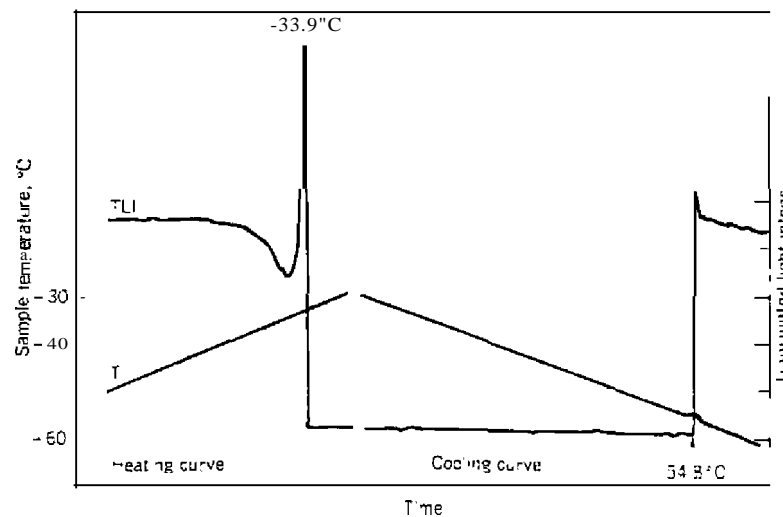


Figure 9.27. Transmitted light-intensity curve for 1,2-dichloroethane at $1^{\circ}\text{C}/\text{min}$ heating rate (83).

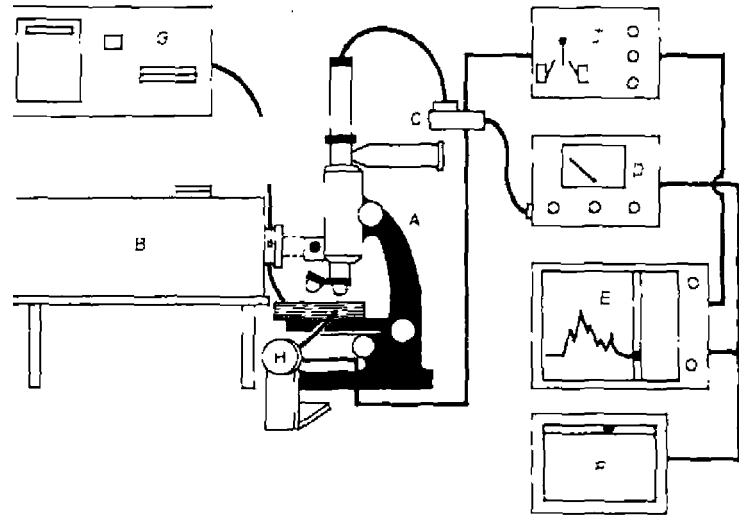


Figure 9.28. Microreflectance apparatus. A, B & L microscope; B, B & L monochromator and lamp; C, photomultiplier tube; D, amplifier and power supply; E, X-Y recorder; F, strip-chart recorder; G, Mettler hot stage; H, reversible motor; J, relay and timer (45).

else placed in 0.0-1.1-mm-id glass capillary tubes. In the latter case, it is possible to obtain the reflectance curve of a sample contained in a sealed tube.

Two modes of operation of the apparatus are possible: (1) The scanning mode in which the sample surface reflectance can be recorded as a function of scanning distance at ambient room temperature or at elevated temperatures and (2) the change in reflectance of the sample as a function of temperature can be recorded. The former mode is called *high-temperature scanning microreflectance (SMR)*, while the latter is called *dynamic microreflectance (DMR)*. The use of these two modes is illustrated by the acquisition of $\text{CuSO}_4 \cdot 5\text{H}_2\text{O}$.

The scanning microreflectance curves of a single crystal of $\text{CuSO}_4 \cdot 5\text{H}_2\text{O}$ (78) at room temperature are shown in figure 9.29. The curves represent the reflectance of the crystal surface at scans at points A, B, and C. Since the reflectance geometry or $90^\circ/90^\circ$ was used, the curve maxima represent maximum specular reflectance from the crystal surface. Thus, surfaces perpendicular to the incident beam reflect the strongest, giving the curve peak maxima. The curves are not very reproducible from crystal to crystal due to the different surfaces or the individual crystals.

The SMR curves of the same crystal at various temperatures are illustrated in Figure 9.30. The curves changed little on increasing the temperature of the crystal from 30–50°C. However, at 70°C, the specular reflectance maxima

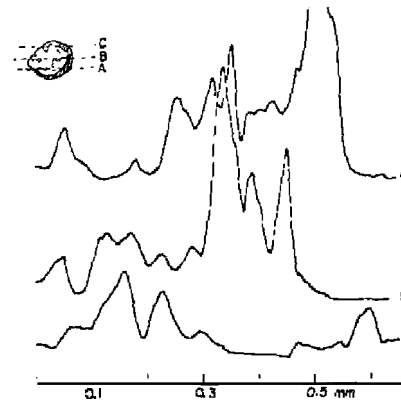


Figure 9.29. Scanning microreflectance curves of a single crystal of $\text{CuSO}_4 \cdot 5\text{H}_2\text{O}$ at a wavelength of 450 nm and at a temperature of 30°C (100 × magnification) (78).

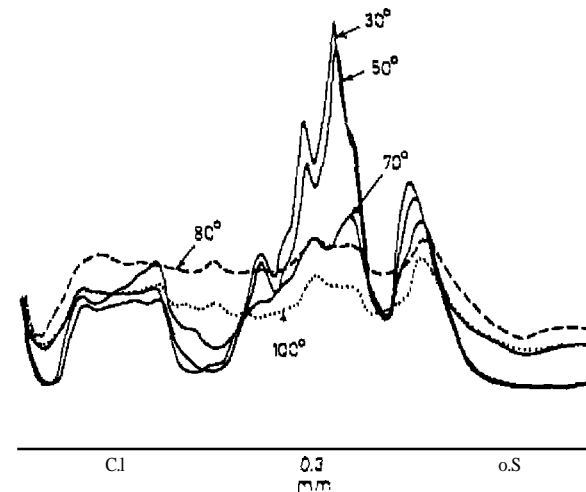


Figure 9.30. Scanning microreflectance curves of a single crystal of $\text{CuSO}_4 \cdot 5\text{H}_2\text{O}$ at various temperatures; wavelength of incident light 450 nm, 100 × magnification (78).

all showed a general decrease, which became more pronounced as the temperature was increased from 80° to 100°C. The decrease in the specular reflectance of the crystals was due to the formation of a surface layer of $\text{CuSO}_4 \cdot 3\text{H}_2\text{O}$ which is more opaque than the original compound. Thus, the formation of the former can easily be followed by the SMR technique.

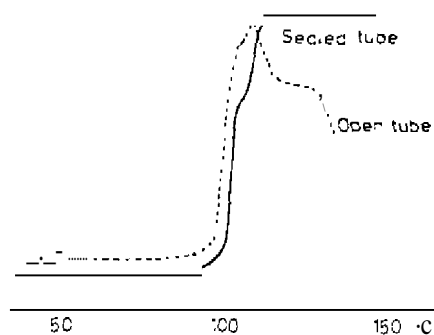


Figure 9.31. Microreflectance of sealed- and open-tube samples of $\text{CuSO}_4 \cdot 5\text{H}_2\text{O}$; heating rate of $10^\circ\text{C}/\text{min}$; wavelength of incident light, 450 m μ ; 80 \times magnification (78).

The evolution of liquid water in the deaquation of $\text{CuSO}_4 \cdot 5\text{H}_2\text{O}$ is illustrated by the microreflectance of powdered $\text{CuSO}_4 \cdot 5\text{H}_2\text{O}$ in sealed and open glass capillary tubes, as shown in Figure 9.31. In an open capillary tube, the sample reflectance of the samples decreased as the temperature was increased. However, since the liquid water was confined to the capillary tube, the reflectance did not increase again on further heating.

E. THERMOLUMINESCENCE

1. Introduction

Thermoluminescence (TL) is the light that is released from a crystalline material when it is heated from room temperature to 400–500°C. It is produced and stored when a crystalline material is irradiated with some kind of ionizing radiation any time prior to heating (90). Among the most effective sources of radiation are those originating from nuclear emissions such as α , β , and γ as well as from X-rays, cosmic rays, and so on. The total light emission is proportional to the overall radiation dosage the material has received. The TL curve or "glow curve" is the sum of all the measured light quanta emitted when the sample is heated. Upon cooling and reheating, no further TL light will be obtained until the sample receives an additional dose of ionizing radiation. TL is widely used in radiation dosimetry, archaeological dating, geological activity, catalyst evaluations, and so on.

The early applications of thermoluminescence to the analysis and identification of rocks have been made by Deribere (104), Garlick (105), Kohler and

Leitmeier (106), Royer (107), Saurin (108), and Northrup and Lee (109), Saunders (110), Parks (111), Daniels et al. (112), Lewis III (113), and Hose et al. (114). The applications of thermoluminescence to problems of geological thermometry and age determination have been discussed by Ingerson (115), Zeller (116), Cairns (117), and Zürer (92). General reviews on TL include those by Daniels et al. (112), Bose et al. (114), Lancaster (93), Manche (90), and others (117–121, 114).

2. The TL Process

A simple model of the thermoluminescence (TL) process is shown in figure 9.32 (130). In (a), ionizing radiation creates an electron and a hole in the crystal. The electron wanders in the conduction band until it falls into an electron trap, forming an F-center, and the hole moves in the valence band until it falls into a hole trap, forming a V-center. Upon heating, the electron (hole) is excited into the conduction (valence) band, where it wanders until it recombines with the hole (electron), giving off light. This simple model, however, does not take into account the dominant influence of impurities on the TL process (130). In the commonly used phosphor, LiF, for example, impurities are necessary to give highly sensitive TL.

Figure 9.32b shows schematically the TL process involving a divalent impurity. Again, electrons and holes are formed upon irradiation with ionizing radiation. The hole can now be trapped by the impurity cation. When the electron is released upon heating, it recombines with the hole at the impurity ion, exciting a characteristic luminescence. The impurity ions can also form complexes such as Z-centers that can trap electrons. As the crystal is heated, the traps are emptied—first the shallow traps at low energy and then deeper traps at higher energies, producing a number of TL peaks.

Other models and theories have been discussed by a number of investigators (112, 132, 133). These traps are often described and graphically illustrated as electron wells of different depths depending on their potential energy profiles, which may span a range of 0–4 eV (90).

The thermal ejection of relatively stable trapped electrons leads to the production of the TL curve and may be similar to the one shown in Figure 9.33. In this figure, the light intensity, I , is plotted as a function of sample temperature, T , during a linear programmed heating rate. Each trap is characterized by a frequency factor, s , and an activation energy for untrapping, E , as well as the temperature at the peak of curve, T_m . The latter temperature is dependent on the heating rate, and for second-order kinetics, it also depends on the fraction of traps populated. The part of the curve due to blackbody radiation is labeled BB.

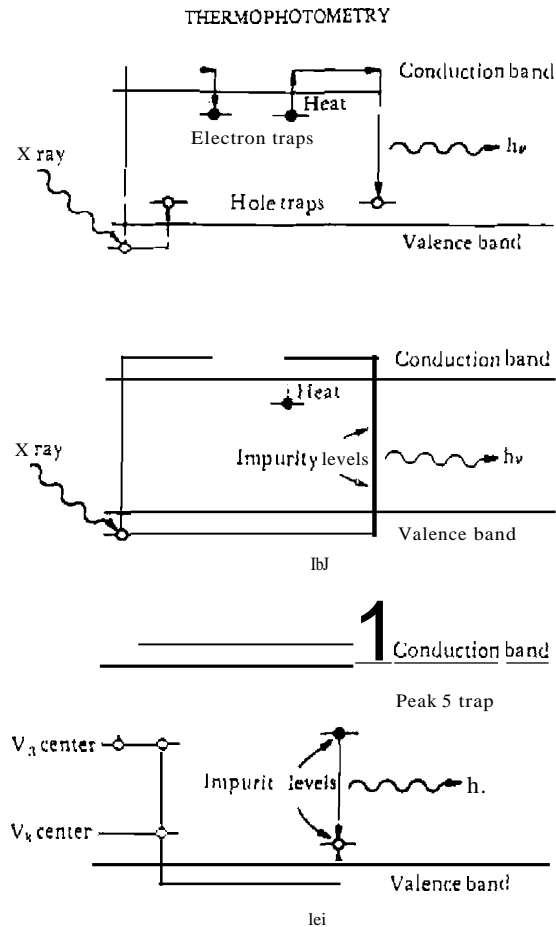


Figure 9.32. Schematic band models for thermoluminescence (41): (a) simple model; (b) model With Impurity present; (c) model involving electron and hole traps and impurity ion recombination centers.

3. Kinetics of TL

The kinetics of the TL process has been described by Randall and Wilkens (96), Boyd (122), Manche (90), Halperin and Branier (97), Chen (94, 95), and numerous others (98). The review by Chen (95) is a very comprehensive discussion of the subject. Only a simplified discussion will be included here.

THERMOLUMINESCENCE

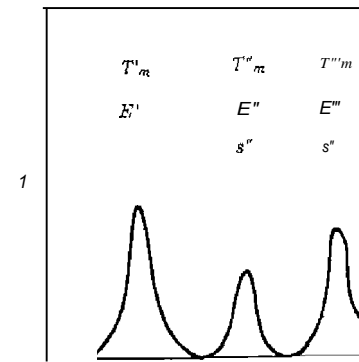


Figure 9.33. TL "glow curve" obtained on a substance with three different populations (90).

Under simplified assumptions, the rate of escape of trapped charges proportional to the intensity of emitted light, I , and can be written (90)

$$I = -\frac{dn}{dt} = ns \exp(-E/kT)$$

where J is the TL intensity in photons per unit time t , n the concentration of trapped charges at time t , s the frequency factor characteristic of the activation energy for thermal charge release, k the Boltzmann constant, and T the Kelvin temperature. Since the temperature is increasing with time, equation (9.1) can be integrated between the initial temperature, T_i , and final temperature, T_f to give the total intensity

$$I(T) = n_0 s \exp(-E/kT) \times \exp \int_{T_i}^{T_f} (s/t) \exp(-E/kT) dt$$

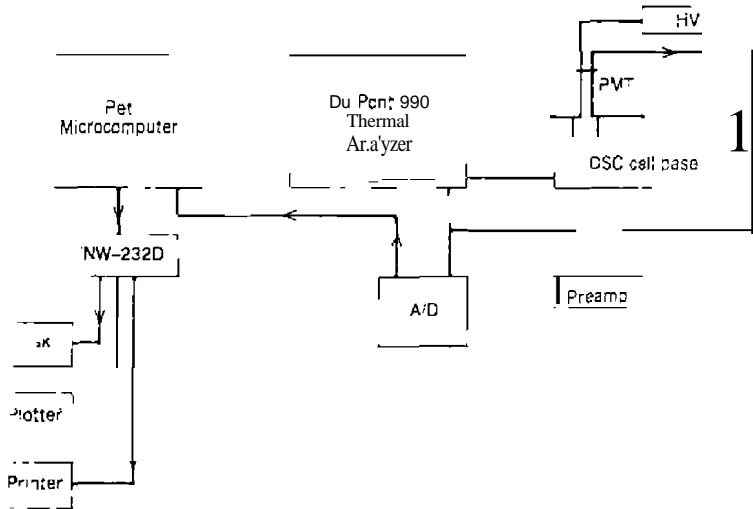
where n_0 is the trap charge concentration at T_i and $n(t)$ is the concentration under the TL curve. Each of the peaks in Figure 9.33 may be represented by equation (9.9), representing three different populations.

The activation energy, E , can be evaluated by calculations of charge in T_f with heating rate. Several methods have been used in the literature, each yielding various accuracies in the E values.

order kinetics, the TL curve peak is somewhat asymmetrical. whereas in the case of second-order kinetics, the peak is nearly symmetrical.

4. Instrumentation

Numerous instruments have been described for the measurement of the thermoluminescence of solid samples. Older instrumental arrangements have been described by Urbach (123), Randall and Wilkins (96), Boyd (122), Daniels et al. (112), Saunders (110), Parks (111), and Lewis (113). Basically, the apparatus consists of the following components: (1) a heated sample block. (2) a sample-temperature programmer or power supply, (3) a photomultiplier tube and power supply, and (4) a recorder, of either the two-pen strip-chart or the x-y function type. The TL curves are normally obtained at fairly fast heating rates of 1-20°C/sec. As the sample temperature is increased, the sample emits light that is detected by the photomultiplier tube whose output current varies linearly with the intensity of the emitted light. This output current is converted into a voltage signal and recorded on one channel of the strip-chart recorder. The other channel of the recorder is connected to a thermocouple embedded in the sample chamber and hence records the sample temperature. Thus, both light intensity emitted and temperature of the sample



THERMOLUMINESCENCE

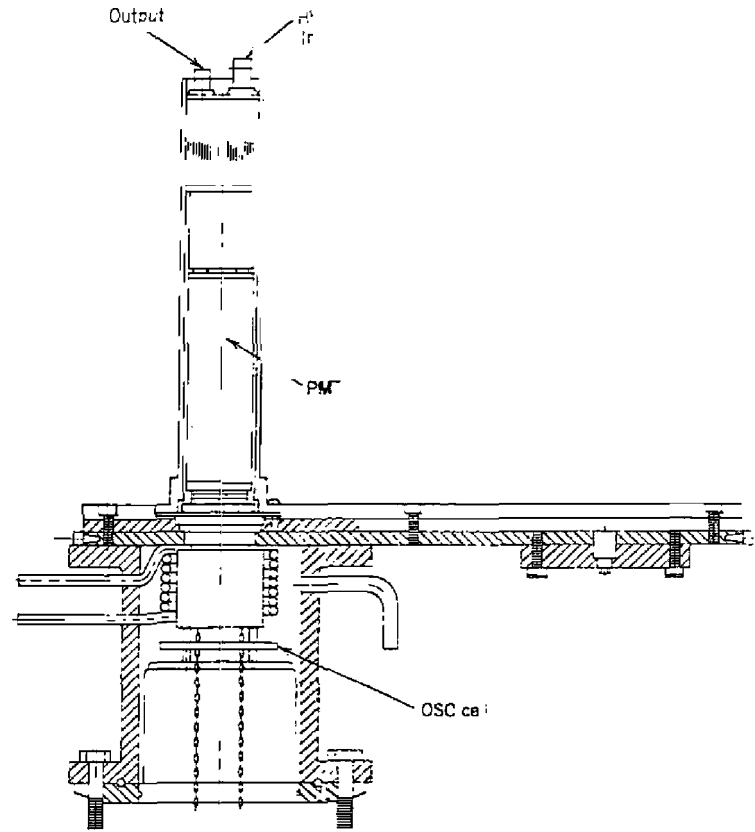


Figure 9.34. TL instrument described by Nuzzio (99). (a) Block diagram of instrument (b) Light-measuring system.

are recorded as a function of time. The temperature range of the apparatus is from ambient to 500°C. TL curves can be obtained on 50 mg of finely powdered sample.

Newer methods of obtaining the TL curve of a sample involve lock-in amplifiers, photon counting, and computer data reduction.

A recently described TL instrument, capable of obtaining reproducible TL curves, is shown in Figure 9.34 (99). The instrument can be used in an isothermal mode as well as the usual nonisothermal mode, and at subambient

temperatures or at reduced pressures. Since it uses a commercial DSC cell as the programmable furnace, it is capable of simultaneous TL-DSC measurements. The system consists of a Du Pont 990 thermal analyzer and DSC cell, a 9824A PMT, and a PET microcomputer. The PMT was chosen for its maximum sensitivity in the 390-420 nm spectral region. Included in the light-measuring system are filters that absorb heat and minimize the typical black-body radiation encountered all around 400°C. A specially designed low- and high-sensitivity amplifier was used to amplify the output from the PMT. The output from the amplifier was digitized and processed by the microcomputer and sent to peripheral devices such as a plotter and printer.

Manche and Carroli (100) used a Perkin-Elmer DSC-1B to obtain simultaneous TL-DSC measurements. The TL unit was capable of differential TL measurements; that is, two identical samples were employed but only one of them was heated (101). A two-channel recorder was used: one channel to record the TL signal and the other for the DSC curve. A block diagram and listing of component parts is given in Figure 9.35.

A representative set of TL-DSC curves obtained on the preceding instrument is shown in Figure 9.36 (101). The sample used was a 20.0 mg pellet of 40% (w/w) LiF in KNO_3 . The sample was irradiated with X-rays for 1.00 min at 36 kV and 16 mA. Normally, the heating rate of the furnace was 80°C/min in a N_2 atmosphere. The KNO_3 could also be used as an internal temperature standard. By integrating the peak areas, the investigators found that the intensity of TL of LiF and the enthalpy of transition of KNO_3 in the mixtures were linear functions of the weight fraction of the individual salts.

Commercial TL analyzers are available, such as the Harshaw Model 2000 thermoluminescence analyzer. It can be used for routine personnel dosimetry monitoring or for research purposes. The apparatus consists of a TL detector, an automatic integrating picoammeter, and a TL computer processing unit. Pia and Podgorsak (102) have recently described a computerized TL system based on this instrument and a PDP-8E minicomputer.

5. Applications

The types of substance that are thermoluminescent, either in their natural state or after radiation bombardment, include (112) the alkali metal halides, calcite, dolomite, fluorite, aluminum oxide, magnesium oxide, gypsum, quartz, glass, feldspars, feldspathoids, certain dried clays, and ceramic materials. Of over 3000 rock samples examined for thermoluminescence, some 75% showed visible light emission (112). Nearly all limestones and acid igneous rocks are naturally thermoluminescent, due mainly to the presence of trace elements of uranium, thorium, and so on. Calcium and magnesium

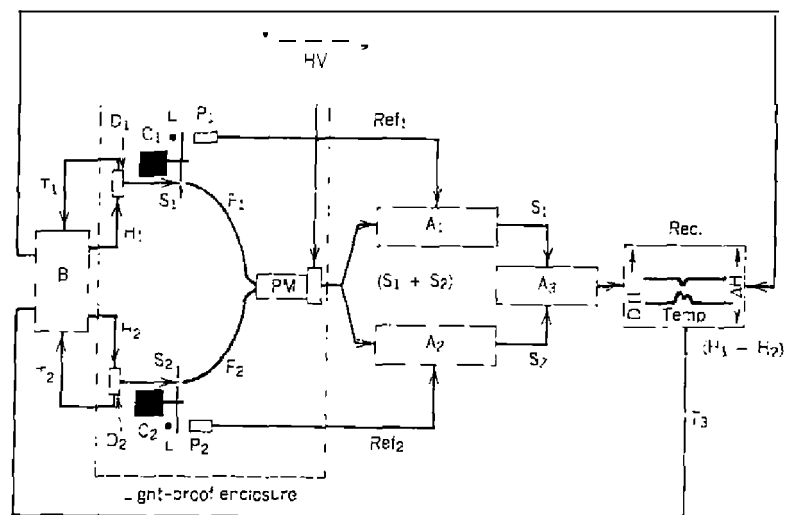


Figure 9.35. Block diagram for simultaneous TL-DSC apparatus (101). (A₁, A₂) clocked amplifiers tuned to frequencies REF₁ and REF₂, respectively; (A₃) differential amplifier; (B) temperature programmer and differential calorimeter; (C₁, C₂) choppers rotating at two different frequencies; (O₁, O₂) calorimeter cups with "sample" and "reference" materials; (HV) regulated high-voltage power supply; (L) lamps for reference signals; (F₁, F₂) matched fiber optics; (P₁, P₂) photocells for generating reference signals REF₁ and REF₂; (PM) photo-multiplier tube; (S₁, S₂) light signals originating from O₁ and O₂, respectively; (S₁ + S₂) signal output from the photomultiplier; (S₁ - S₂) thermoluminescence signal; (H₁, H₂) power input to calorimeter cups; (T₁, T₂) temperature signals from O₁ and O₂ at time *t*; (T₁) average temperature of calorimeter cups at time *t*; (H₁ - H₂) differential heat input, dH/dt ; (REC) two-channel recorder for the simultaneous display of the glow curve and thermogram.

carbonates show light yellow to orange light emission, whereas potassium and sodium feldspars exhibit white to blue-violet light emission.

The TL curves obtained are characteristic of a specific sample or substance and yield information concerning specific impurities present or indicate that the sample has had certain heat treatments or physical histories. However, glow curves are not suitable for the analysis of chemical compounds but are useful for identification and control purposes only. This is illustrated by the TL curves for several dolomite and calcite samples in Figure 9.37. The curves definitely show differences based on the composition of the sample but could hardly be used for the analysis of, say, the magnesium or calcium contents.

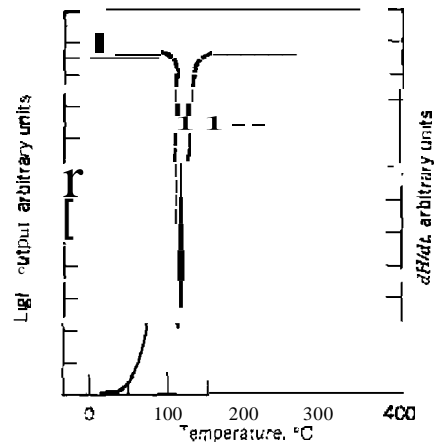


Figure 9.36. Simultaneous n-DSe curves of LiF in KNO_3 (100).

Saunders (110) has shown that the intensities of the peaks in the TL curves increased with increase in depth in a Niagara limestone deposit. The glow curves were useful for studying the various strata of the deposit. Parks (111) reported a similar study relating TL curves of the samples with the identification and characterization of a formation, the identification of the top and bottom of limestone formations, and the characterization of erosion or nondeposition of zones.

Garino-Canina and Cohen (125) used TL curves to characterize germanium oxide-aluminum oxide mixtures. It was found that after excitation by ultraviolet radiation, the peak positions, between 50 and 70°C, and the peak intensities of the curves varied with a change in alumina content introduced into the germanium oxide glass. The amount of alumina varied from 0 to 5%.

A rather interesting application of this technique is in the evaluation of the efficiency of surface catalysis (112,126). The TL curves for three commercial alumina catalysts are given in Figure 9.38; the relationship between TL Curve peak area and catalyst activity are given in Figure 9.38b. The total glow curve is composed of two peaks; the areas under peak number 2 were related to catalytic activity. As can be seen from Figure 9.38b, an excellent correlation exists between the peak areas and the activity of the catalyst. It should be noted that many catalysts do not give any thermoluminescence, and in other cases there is no apparent correlation. A number of catalysts that have been examined do exhibit such a correlation and hence suggest thermoluminescence as a useful tool for catalyst evaluation.

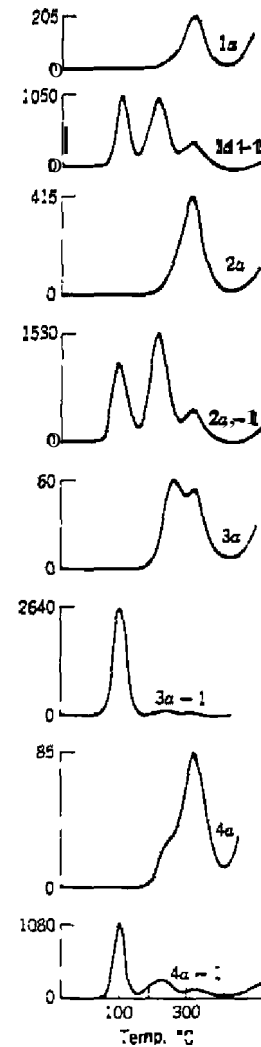


Figure 9.37. Natural and γ -ray activated glow curves of some calcite-dolomite samples. The -1 indicates γ -ray irradiated (113).

Sample	Dolomite, %	Calcite, %	Carbonate, %
1a	89.7	10.1	100.0
2a	92.2	7.9	92.5
3a	0.0	100.0	100.0
4a	48.6	51.4	100.0

The TL curves of samples of lunar material appear at 350°C for lunar fines and 400°C for crystalline rocks (134). The TL is probably the result of an equilibrium between gains from radiation by cosmic rays bombarding the moon's surface combined with the possible presence of radioactivity in the

lunar soil and losses from the thermal environment of the moon. Thermoluminescent results indicate that the temperature variation penetrates about 10.5 cm beneath the lunar surface.

Another application of a geological type is that of dating lava flows (135). At the time of a volcanic eruption, hot lava removes any past thermoluminescence, and after the lava cools the natural radioactivity present in the environment irradiates the lava over a period of years. The thermoluminescence intensity can then be recorded to determine the age of the lava flow, a calculation based on a number of factors.

a. Archaeological Dating

Archaeological dating of pottery sherds by TL has been comprehensively discussed by Cairns (91) and Manche (90). All clays contain a few parts per million of ^{238}U , ^{232}Th , and ^{40}K . When this clay is heated above 400°C , as in pottery manufacture, the natural TL is released and the TL clock is set back to zero. Over time, the radiation damage builds again within the clay. Reheating a sample of pottery and measuring its TL curve peaks gives an indication of how long it has been since the piece was fired. Although archaeologists once had great hopes for TL dating, it is now primarily used to expose modern ceramic fakes (92), where a high degree of accuracy is not needed. The TL method of dating has an error level of around $\approx 7\%$, too high for work done in historical times. Sometimes, however, it is the only dating method available for use by the archaeologists.

In principle, the age of a pottery sherd can be calculated by use of the equation (90):

$$\text{Age} = \frac{(\text{TL})_n \times (\text{dose})_a}{(\text{TL})_n \times (\text{dose rate})_n} \quad (9.10)$$

where $(\text{TL})_n$ is the natural TL; $(\text{TL})_a$ is the artificial TL; $(\text{dose rate})_n$ is the natural dose rate, in rads/yr; and $(\text{dose})_a$ is the artificial dose, in rads. In practice, however, many complications inherent in these measurements make the determination much more complicated. The age equation needs much modification due to the complicating factors.

The simplest model for dating pottery requires a minimum of three measurements (103):

1. The Natural TL. The stored TL is assumed to have accumulated linearly with time starting from the day the pottery was first fired.

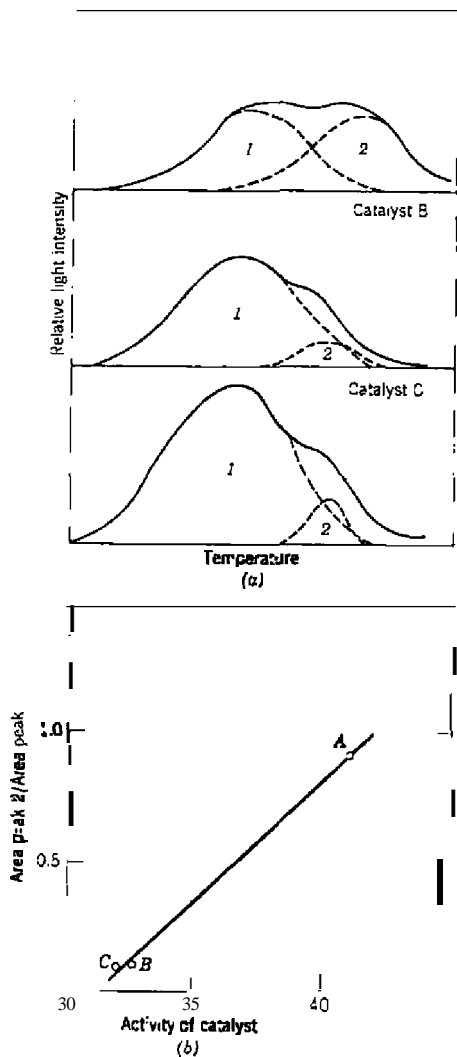


Figure 9.38. (a) TL curves of catalysts; (b) TL and catalytic activity (112).

2. *The artificial TL.* This measurement gives the TL susceptibility of the pottery sherd, and is obtained after it is heated, and then exposed to an artificial source.
3. *The annual dose rate.* A determination of the annual dose rate experienced by the sherd in its burial circumstances.

The TL curves of a pottery sherd are shown in Figure 9.39 (47); the ratio of natural thermoluminescence to sensitivity (TL_{nat}/S) plotted versus the age of the pottery is also shown. The ratio of natural thermoluminescence to

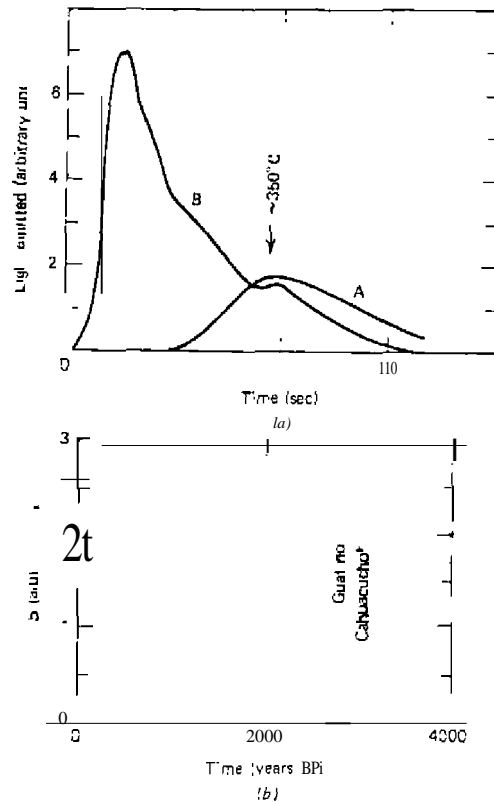


Figure 9.39. (a) TL curves from a pottery sherd, A, compared with the thermoluminescence induced by a standard X-irradiation: B, of a typical sherd; (b) ratio of natural thermoluminescence to sensitivity (TL_{nat}/S) plotted versus age of the pottery (36).

sensitivity is a fairly accurate indicator of archeologic age, especially when averaging is used to obtain a better mean for sherds from the same time level.

Using a relative dating method, one can calculate the age of a pottery sherd from

$$\text{Age} = K \frac{(TL)_{nat}}{(TL) \times R_x} \quad (9.11)$$

where $(TL)_{nat}$ and (TL) are the natural and artificial TL respectively, R_x is the α -particle count rate on a sample of pottery, and K is an empirical constant that is determined from a plot of the specific TL for each sample versus its known age.

Absolute dating methods are based on the fact that radioactivity within a sherd is nonuniform. The bulk of the TL comes from radioactive mineral inclusions such as quartz and feldspar and so on. Methods of employing this procedure are called the quartz inclusion technique, feldspar inclusion technique, and so on. The dating techniques all require a time-lapse period of at least 500 years since a young material lacks sufficient light output in the 300-500°C TL curve. The quartz pre-dose technique has a range of application of from present day to 1500 years. Normally, TL can be used to date pottery sherds and other ceramic materials from 10^1 - 1×10^4 years. The error limit is said to be at best $\pm 5\%$ but more realistically, $\pm 10\%$. The error of $\pm 7\%$, previously cited, appears to be too high to be very useful for serious applications of the technique.

b. Measurement of Ionizing Radiation

Perhaps one of the most important applications of thermoluminescence has been to the measurement of ionizing radiation (130, 133). Since the thermoluminescence intensity is proportional to the intensity of radiation striking the solid, crystals or powders can act as radiation dosimeters. The advantages of this method of radiation measurement are the small size and the large dose range of such solids. A small crystal of a thermoluminescent material is embedded in a small badge that is worn by the personnel. At periodic intervals, the crystal is placed in a detector (thermoluminescence apparatus) and heated. From the integrated intensity of the light emission, the amount of ionizing radiation can be determined.

For personnel dosimetry, the TL material, available in powder or solid form, consists of LiF , CaF_2 , Li borate, $CaSO_4$, Mg borate, and others. A typical TL curve of a LiF ribbon, shown in Figure 9.40, was determined using a Harshaw Model 2000 TL analyzer. When measured with LIF, a 10 mR exposure can be measured with a standard deviation of less than 10%.

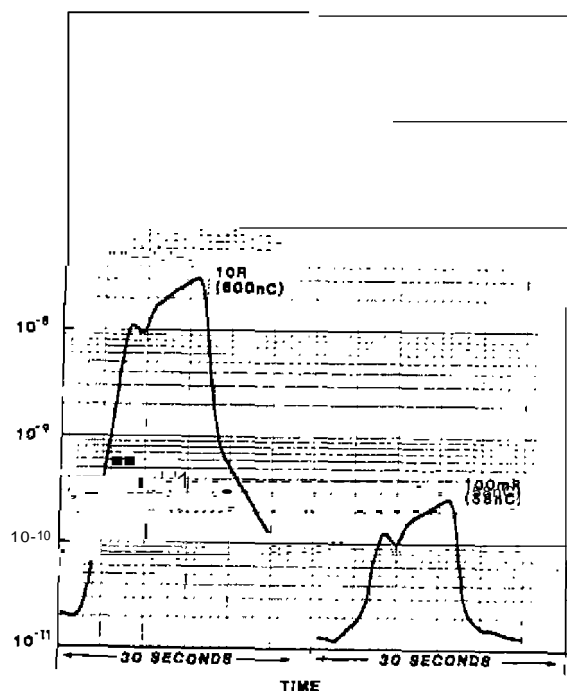


Figure 9.40. Typical TL curves of LiF TLD-100 dosimeters (137).

TL has been used to study radiation damage (38) and also the radioactivity of certain minerals (106, 111, 128, 129).

F. OXYLUMINESCENCE

1. Introduction

When many polymers are heated in air or oxygen in the temperature range 100–300°C, they exhibit a low-level light emission that is called oxyluminescence (OL). This phenomenon was first detected by Ashby in 1961 (136) who heated polypropylene in an oxygen atmosphere. It was noted that: (1) oxygen must be present for light emission to occur; (2) the intensity of the light was proportional to the concentration of oxygen in contact with the polymer

surface, and (3) the presence of stabilizers decreased the intensity of the light. Thus, a new tool was discovered that provided invaluable insight into the study of the oxidative degradation of polymers as well as to elucidate the effects of stabilizers on the polymer oxidation process. This technique is not widely used at the present time, although numerous investigations have studied the fundamental nature of the process, as well as its kinetics and other physical parameters. It has been found that OL is a general phenomenon that applies to many other organic compounds as well as to polymeric materials (24). The OL of polymers has recently been reviewed by Wendlandt (165), Stivala et al (160), and George (166).

There is not much agreement on the name for this phenomenon. Ashby (136) and others used the term oxyluminescence; Barker et al. (139) called it thermochemiluminescence (TCL); David (50) used photothermal analysis (PTA); Wynne and Wendlandt (142) called it light emission (LE); and Stivala (160) called it chemiluminescence (CL). The term employed here will be oxyluminescence (OI) although chemiluminescence would probably be just as appropriate.

2. Intensity and Spectral Distribution

The emitted OL light of most polymers is fairly low-level in that it requires a sensitive photomultiplier tube (PMT) and photometer circuit to detect it. Ashby (136) used a PMT and photometer in which the light emission was expressed in amp of anode current. It was estimated that 1 lumen generated 10 amperes of anode current for the PMT employed. The OL intensities, using this system, ranged from 10^{-10} – 10^{-5} lumens for all the polymers investigated. Nylon had the most intense OL in that at 200°C, it emitted enough light to be seen by the dark-adapted human eye. Schard and Russell (137) employed a PMT and photometer system with a luminous sensitivity of ~80 amp per lumen in the region of 400 ± 50 nm. The OI intensities, as described previously (136), were expressed in anode current from 10^{-10} – 10^{-8} amp. Barker et al. (139) stated that the OL of a Lexan resin and polypropylene at 250°C in air could be seen with the dark-adapted human eye. Wynne and Wendlandt (142) used a sensitive photometer; the OL was expressed in cpm in the range 10^2 – 10^5 . The PMT and photometer used by David (50) had a sensitivity of 2000 amp per lumen, in the spectral range 200–600 nm (See Section B).

The spectral distribution of the emitted light has been determined by a wavelength filter method. Ashby (136) found that the PMT anode current was attenuated about 50% by interposing a filter that absorbed light of the wavelengths shorter than 420 nm between the polymer and the PMT. No current could be detected if a filter was interposed that absorbed light of wave-

lengths shorter than 515 nm. It was concluded that in OL, 50% of the light emission had wavelengths between 420-515 nm and 50% between 300-420 nm. Barker et al. (139) also employed filters to determine the spectral distribution of the emitted light. Using a set of Corning filters, the SDCtrum of the OL of Lexan PC in air at 220-230°C was determined. If the overall response of the PMT and filters is F_i ($i = a, b, c, \dots, g$), the PMT signal should be

$$I_i = K \int_0^{\infty} F_i W_{\lambda} d\lambda \quad (9.12)$$

where W_{λ} is the radiant power density of the OL, and K a proportionality factor that depends on the sensor area and geometry. The filter output "areas" (I vs λ),

$$A_i = \int_0^{\infty} F_i d\lambda \quad (9.13)$$

were determined graphically and the OL spectrum, W_{λ} , was estimated by application of the mean value theorem in the form

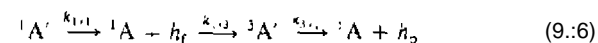
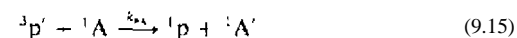
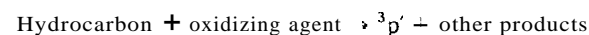
$$\text{Relative OL signal} \approx K \langle W_{\lambda} \rangle_{\text{av}} = I_i/A_i$$

The resulting spectrum consisted of a broad peak from 400-610 nm with a maximum at about 540 nm. A shoulder peak was observed at about 475 nm. Also using wavelength filters, de Kock and Hoi (140) obtained the OL spectrum of dicumyl peroxide in polypropylene. The OL curve extended from 360 nm to about 500 nm with a peak maximum at 420 nm. It was very similar to the phosphorescence spectrum of acetophenone dissolved in poly(methyl methacrylate); in fact, the peak maxima were exactly the same.

3. Mechanism of the OL process.

The origin of the OL process in polymers has been the subject of numerous investigations, with little agreement as to the mechanism of the light-emitting process. Ashby (136) found that for every photon of light emitted, 10^4 carbonyl groups were formed. This estimate indicated that the chemical reactions involved in OL occur with infrequency when compared to the reaction leading to carbonyl formation. Schard and Russell (137) indicated that as the number of tertiary hydrogen atoms increased, the OL increased. They stated that OL may be useful as a method for determining chain branching. It was

also noted that the species responsible for OL increased more rapidly in the case of nylon than in polypropylene and reached an equilibrium or steady-state condition much sooner. The rapid increase in luminosity, on changing from nitrogen to oxygen atmospheres, indicated that the OL process occurred principally on the surface of the polymer. There were no significant differences in the OL of polymers when the thickness of the sample varied from 7 to 70 mils. Barker et al. (139) calculated that for a 0.1 g sample of polypropylene, about 2×10^{-11} photons/reaction site were obtained. They postulated that the process may be similar to that proposed by Vassilev (146) to explain the chemiluminescence of substituted anthracenes in hydrocarbon solutions. This process consisted of the reactions



where the subscripts 1 and 3 denote singlet and triplet states, respectively, and the primes denote electronic excitation. Thus, the observed OL may be due to the fluorescence, ν_f , and/or phosphorescence, ν_p , of the acceptor materials. Spin orbit coupling is the mechanism leading to a measurable intermolecular energy transfer rate, k_{pA} .

de Kock and Hoi (140,147) argued that since the reaction of polypropylene with oxygen was too complicated to be used for verifying the origin of OL, a model system composed of dicumyl peroxide mixed with polypropylene could be employed. Heating this mixture in a nitrogen atmosphere would be expected to give rise to OL, and at the same time the nature of the reaction products could be ascertained. From the spectrum of the model system, which was almost identical to that of the phosphorescence spectrum of acetophenone (a decomposition product), it was stated that the observed OL of the former may result from the phosphorescence of the reaction product, acetophenone. Part of the cumyl radicals split off methyl radicals and the remaining compound may be an excited acetophenone molecule, which, via a phosphorescence process, deactivate to the electronic ground state. It was concluded that the OL reaction of polypropylene may possibly be interpreted as the phosphorescence of a carbonyl-group containing reaction product. Wynne and Wendlandt (142) suggested that the OL process involved polymer peroxy radicals, RO_2 , such as are involved in the thermal degradation of polymers (148). In the presence of oxygen, the polymer free radicals, R, formed hydroperoxide radicals, RO_2 , or molecules, RO_2H , giving the follow-

ing termination steps:

1. $2R' \rightarrow \text{products}$
2. $RO_2 + R \rightarrow \text{products}$
3. $2RO_i \rightarrow \text{products} + O_2$

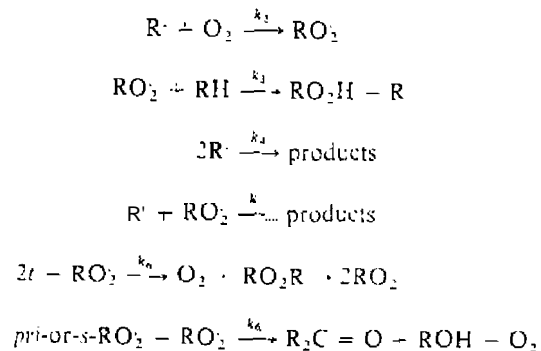
At high oxygen concentration, step (3), thought to involve ketonic intermediates, is the most significant, whereas at low oxygen concentrations, step (1) predominates. OL accompanies all three termination steps; however, that associated with steps (2) and (3) is considerably more intense than that arising from step (1). Wynne and Wendlandt (142) called the light emission from step (1) "chemiluminescence" since it occurred in a nitrogen atmosphere and Ot. from steps (2) and (3), which occurred in air or oxygen atmospheres.

Stivala et al. (160) have summarized the transitions of Ot as arising from free radical reactions, such as

4. $RO_2H \rightarrow (\text{products})^*$
5. $RO_2 \rightarrow (\text{products})^* + O_2$
6. $(\text{products})^* \rightarrow (\text{products})$

The asterisk denotes an excited state, such as an electronically excited ketone, which can undergo an electronic transition ($n \rightarrow \pi^*$) type. Although OL during oxidation of various polymers can be satisfactorily interpreted using step (5), recent investigators have invoked steps (5) and (6) (161). Step (5) appears to be the most probable origin of OL.

The basic autoxidation scheme of polymers that results in OL has been presented by Stivala et al. (160). This scheme involves the following reactions:



The OL intensity is assumed to be due mainly to recombination of peroxy radicals, thus

$$I = \eta k_6 [RO_2]^2 \quad (9.17)$$

where η = a coefficient.

4. Kinetics of Oxyluminescence

The kinetics of the OL process in polymers has been fairly extensively studied by several investigators. Schard and Russell (139) were the first to calculate apparent activation energies, E , for the OL reactions using Arrhenius plots of the light intensities measured at various temperatures. They found no relationship between E and the intensity of light emission. Polypropylene required a higher E (97.5 kJ mol⁻¹) than polyethylene (82.4 kJ mol⁻¹) but the former had a greater intensity of light emission. Poly(methylmethacrylate) had a sharp change in slope (for the log Ot. vs. $1/T$ curve) and hence different values for E were obtained. The average value of 97.5 kJ mol⁻¹ found for unstabilized polypropylene was reasonably close to the 109 - 113 kJ mol⁻¹ for the oxidation of both isotactic and amorphous polypropylenes found by other techniques. It is even closer to the 100 - 105 kJ mol⁻¹ that Manyasek et al. (149) found for the E of peroxide formation in atactic polypropylene. They reported an E of 113 kJ mol⁻¹ which could be interpreted as supposing the theory that light is emitted by the reaction of the $RO_2 \cdot$ radicals. Nylon 6, which undergoes an autoretardant reaction (2), had a lower E than did polyolefins.

Barker et al. (139) calculated an apparent E for polypropylene from Ashby's data [1]. The E values ranged from 23.4-73.6 kJ mol⁻¹ depending on the oxygen concentration. They reported that Ol. obtained in static atmosphere systems always tend to be low, thus the flow replacement of the boundary layer gases is important. Comparing the OL E for polypropylene ($E = 172$ kJ mol⁻¹) with the E for oxidation by O_2 absorption (121 kJ mol⁻¹) the authors found that the former was larger than the average value obtained by the other three methods. The E for Lexan consisted of three values: ~ 42 kJ mol⁻¹ at lower temperatures, ~ 138 kJ mol⁻¹ for intermediate temperature, and ~ 251 kJ mol⁻¹ for the higher temperature region. These values are in reasonable agreement with TG results. Cycling data indicated that in OL was approximately a decreasing linear function of the number of cycles n of heating and cooling. Results obtained in a CO atmosphere gave E values of about the same magnitude as in O_2 . The Williams-Eyring method (150) that was developed for thermoluminescence (TL) was applied to the OL process, giving an E for polypropylene of ~ 155 kJ mol⁻¹.

Wynne and Wendlandt (142) found a linear relationship between OL and the rate of reaction using

$$(R - R_0) = \alpha \phi \left(\frac{dn}{dt} \right) \quad (9.18)$$

where $R - R_0$ is the PMT response (photon counter), α is a constant, and ϕ is the quantum efficiency. For Alathon Z (polyethylene), $E \approx 80$ kJ mol⁻¹ in air, oxygen, and nitrogen atmospheres, between 385 and 460 K.

Chen (151, 159) described a general kinetics equation that was applied to a thermoluminescence "glow" curve but could possibly be employed to an OL curve as well. The basic equation is

$$I = -dn/dt = S'n^b \exp\left(-\frac{E_a}{kT}\right) \quad (9.19)$$

where b is the kinetic order and S' is the preexponential factor in sec⁻¹ cm^{3(b-1)}. The general theory of the TL process was also reviewed.

Wendlandt (152) described a method for evaluating the kinetics of OL employing a method developed by McCarter (153) for evolved gas detection (EGA). Using the corrected light emission curve, the rate of OL was given by

$$\text{Rate} = k \left(\frac{a}{A} \right) \quad (9.20)$$

where k is the specific rate constant in min⁻¹, a is the area of the Curve peak to temperature T (or time, t) and A is the total area minus a . The Arrhenius equation was then used to calculate E_a . An E of 100 kJ mol⁻¹ was calculated for poly(vinyl formal) using this method.

The OL E values obtained for selected polymers are listed in Table 9.1.

5. Oxy luminescence in Polymer Stabilizer Studies

It was pointed out by Ashby (136) that in the presence of stabilizers (antioxidants), the OL of the polymer was changed. Using polypropylene containing a 1:1 mixture of the stabilizer, 4,4'-thiobis(3-methyl-6-tert-butylphenol) with diacrylylthiopropionate, he greatly reduced the OL intensity for an initial time interval and the extent of this reduction was determined by the concentration of the stabilizer. When the stabilizer concentration was depleted, the OL returned to its original intensity. This suggested that the intensity of OL is reduced as the rate of oxidation was reduced by the stu-

Table 9.1. Oxy luminescence E of Selected Polymers

Polymer	E (kJ mol ⁻¹)	Reference
Nylon 66	63 (to 435 K)	7
	97 (>435 K)	7
	41 (to 460 K)	7
	199 (>460 K)	7
Alathon I	80	7
Polypropylene (Profax 6701)	44.4 (< 300°C)	4
	251 (> 300°C)	4
	55 ^a	4
	97	3
	73.6 ^b	1
Polyethylene (I.D.)	82.4 [above transition point]	3
	31 [below transition (Joint)]	J
Nylon 6	64.4	J
Polystyrene	50.6	3
Polyurethane	46.9	
Poly(methyl methacrylate)	85.8	3
	27 [below transition point]	3
Poly(caprolactone)	135	18
Polyethylene, 25% C	60	8
Polyethylene, 36% C	100	18
Polyethylene, 42% C	100	18
Polyethylene, 48% C	135	18
Poly(vinyl formal)	100	18

^aE-W method [16].

^bO₂/(O₂ + N₂) ratio = 0.

bilizer. A rapid method for determination of the concentration of the stabilizer in the polymer was also developed.

Schard and Russell (138) studied the OL change for polypropylene containing varying amounts of the stabilizer, 4,4'-thiobis(3-methyl-6-tert-butylphenol). The OL was delayed for a short period of time after admission of oxygen to the system to an extent depending on the stabilizer concentration. The rate of OL emission curve rise appeared to vary inversely as a function of stabilizer concentration. Preliminary studies showed that the effect of stabilizer on the OL of polyethylene was quite different from that in polypropylene. The time to maximum intensity of OL was a critical value in the former since with 0.1% of stabilizer present, the maximum intensity was attained almost instantly.

Collins and Wendlandt (155) used OL to determine the stabilizer concentration in polyethylene. The initial deviation of the curve from the baseline as well as the peak maximum temperature were both found to be a function of stabilizer concentration in the polymer. The method was compared to those using TG and DSC.

6. Instrumentation

The instrumentation used to follow the OL process in polymers is relatively simple. It generally consists of a light detection apparatus containing a sensitive photomultiplier tube and photometer; a furnace and temperature controller or programmer; an enclosed chamber surrounding the sample that is capable of a controlled static or dynamic atmosphere of oxygen or other gases; and a recording system. The output from the photometer is plotted versus time (isothermal mode) or temperature (nonisothermal mode). More sophisticated instruments have recently been described (162-164) in which the emitted light is collected by means of a lens system and focused on a cooled photomultiplier tube (PMT). The PMT output signal is analyzed by a photon-counting system to yield a digital record of the light intensity.

Most of the early studies used the isothermal mode (136-40) but more recent ones employed the nonisothermal mode (50, 141-142). Many of the early isothermal studies were carried out at a temperature of 150°C (136-139) but the nonisothermal mode has been used to study polymers up to a temperature maximum of 400°C. This is usually the upper temperature limit

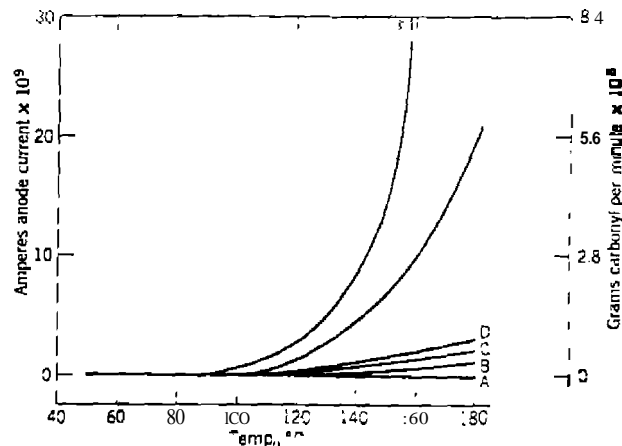


Figure 9.41. Effect of oxygen concentration on the intensity of OL for polypropylene (138).

because of radiation effects that mask the OL emission. However, Wendlandt (143) used a data center recorder that permitted the detection of the initial deviation of the curves giving only the OL versus temperature background curves. A system for low-temperature measurements down to -96°C has also been reported by Kaimin and Galefs (144). OL measurements at low pressures have been taken by Barker et al. (1139) who also analyzed the gaseous

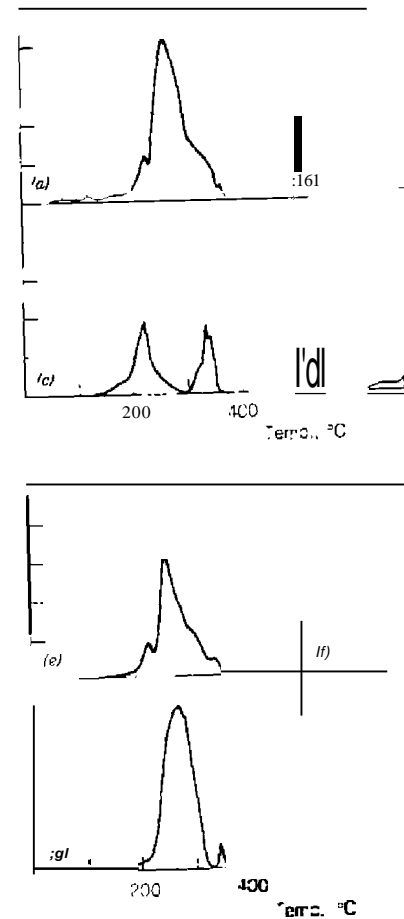


Figure 9.42. OL curves of various polymers (158): (a) nylon 6 x 10, (b) nylon 6, (c) nylon 6/10, (d) nylon 6/12, (e) nylon 6-T., (f) ...

and condensation and extractable pyrolysis products of the polymer using a gas chromatograph and mass spectrometer. To determine the OL spectral distribution, investigators (136, 140) have employed various *light* filters. Simultaneous OL and DTA measurements were obtained by David (50) using a commercial DTA apparatus, whereas OL-DSC data were recorded by Wynne and Wendlandt (141,142) using a du Pont or a Perkin-Elmer DSC instrument. Johnson and Chiu (145) also obtained light emission measurements coupled with smoke evolution detection and TG.

7. Applications of OL to Polymers

Many of the early studies on the OL of polymers involved the isothermal mode (136-138). More recent studies employed the nonisothermal mode of heating in which the furnace atmosphere was changed from argon, to oxygen + nitrogen, to oxygen, and so on. The effect of oxygen concentration on the OL of polypropylene is shown in Figure 9.41 (136). The intensity of the OL increases with oxygen concentration in the temperature range studied.

Using the nonisothermal mode, Figure 9.42 shows the OL of various nylon polymers, as determined by Wendlandt (156). The OL curves for nylon 6,6/12, 6/6, 11, and 12 are quite similar in appearance in that they all consist of a broad prominent peak with peak maxima between 250 and 300°C. The shoulder peaks on the leading and trailing edges of the main peaks are different. The OL curves for nylon 6/6, 6/9, and 6/10 are unique in that they consist of two or more curve maxima. For example, the curve peaks in nylon 6/9 have maxima at 225 and 335°C, respectively, whereas nylon 6/6 has a peak with a maximum at 375°C, the highest temperature recorded in any curve peak. The OL curves may be used for the characterization of the nylon polymers, supplementing other TA data. OL has been used to characterize other polymers as well (152, 156, 157).

A compilation of polymers known to exhibit OL is given in Table 9.2.

Table 9.2. Polymers Known to Exhibit Oxyluminescence

Polymer	Reference
Polypropylene	136-139
Polyethylene	50, 136-138, 155
Polyisobutylene	136
Polyurethane	136-138
Polychloroprene	136
Poly(methyl methacrylate)	50, 138-138
Polystyrene	50, 136-138
Poly(vinylidene chloride)	136
Polyhexamethylene adipamide (Nylon)	136

Table 9.2.

Polymer	Reference
Poly(vinyl chloride)	50, 136
Polyoxymethylene	136,137
Polyacrylonitrile	136,141
Polytetrafluoroethylene	137
Poly(ethylene terephthalate)	137
Nylon 6	137, 141, 152, 156
Nylon 6	137,140, 156,158
Nylon 6	137,156
Ethylene propylene rubbers	147
Dicumyl peroxide in polypropylene	140
Diathionite (polyethylene)	142
Lythene	141
Nalgene	141
Polycarbonate	139,141
Poly(vinyl pyrrolidone)	141, 152
Nylon 6/9	156
Nylon 6/12	156
Nylon 6/12	156
Nylon 6/12	156
Nylon 12	156
Poly(vinyl formal)	152
Poly(vinylidene fluoride)	152
Poly(vinyl fluoride)	152
Poly(vinyl acetate) 100% hydrolyzed	152
Poly(vinyl stearate)	152
Poly(vinyl butyral)	152
Chlorinated polyethylenes	152
Poly(diallyl isophthalate)	152
Poly(diallyl phthalate)	152
Polycaprolactone	152
Poly(lactide)	152
Polyacrylamide	152
Poly(1,4-cyclohexanedimethyleneterephthalate)	152
Poly(1,4-butylene terephthalate)	152
Poly(butyl methacrylate)	157
Cellulose acetate	157
Cellulose propionate	157
Ethyl cellulose	157
Cellulose acetate butyrate	157
Hydroxypropyl cellulose	157
Cellulose sulfate	157
Cellulose triacetate	157

Almost every polymer studied by this technique exhibits a weak emission of light in the presence of air or oxygen.

REFERENCES

1. Wendlandt, W. W. and H. G. Heche. *Reflectance Spectroscopy*, Interscience, New York, 1966, Chaps. 3, 4.
2. Kortum, G., *Trans. Faraday Soc.*, 58, 1624 (1962).
3. Kubelka, I. and F. Munk, *Z. Techn. Phys.*, 12, 593 (1931).
4. Ref. 1, pp. 275-279.
5. Ref. 1, Chap. 8.
6. Wendlandt, W. W., P. H. Franke, and J. P. Smith, *Anal. Chem.*, 35, 105 (1963).
7. Wendlandt, W. W., *Science*, 140, 1085 (1963).
8. Anon., *Chem. Eng. News*, April 15, 1963, p. 62.
9. Asmussen, R. W., and P. Anderson, *Acta Chem. Scand.*, 12, 939 (1958).
10. Hatfield, W. E., T. S. Piper, and C. Klabunde, *Inorg. Chem.*, 2, 629 (1963).
11. Wendlandt, W. W., P. H. Franke, and J. P. Smith, *Anal. Chem.*, 35, 105 (1963).
12. Wendlandt, W. W. and T. D. George, *Chem. Anal.*, 53, 100 (1964).
13. Wendlandt, W. W., *Thermal Methods of Analysis*, Interscience, New York, 1964, Chap. 10.
14. Frei, R. W. and M. M. Frodyma, *Anal. Chim. Acta*, 32, 501 (1965).
15. Wendlandt, W. W., in *Modern Aspects of Reflectance Spectroscopy*, W. W. Wendlandt, ed., Plenum, New York, 1968.
16. Wendlandt, W. W., and E. L. Doscl, *Thermochim. Acta*, 1, 1031 (1970).
17. Wendlandt, W. W., and W. S. Bradley, Ref. 16, p. 143.
18. Wendlandt, W. W., *J. Thermal Anal.*, 1, 469 (1970).
19. Cox, E. G., A. J. Shorter, W. Wardlaw, and W. J. R. Way, *J. Chem. Soc.*, 1556 (1937).
20. Dunnz, J. D., *Acta Cryst.*, 10, 307 (1957).
21. Mellor, D. P. and C. D. Coryell, *J. Am. Chem. Soc.*, 60, 1786 (1938).
22. Wendlandt, W. W., and T. D. George, *Chem. Anal.*, 53, 71 (1964).
23. Ocone, L. R., J. R. Soulen, and B. P. Block, *J. Inorg. Nucl. Chem.*, 15, 76 (1960).
24. Beech, G., C. T. Mortimer, and E. G. Tyler, *J. Chem. Soc.*, 925 (1967).
25. Murgulescu, I. G., E. Segai, and D. Fatu, *J. Inorg. Nucl. Chem.*, 27, 2677 (1965).
26. Wendlandt, W. W., and R. E. Cahers, *Chem. Anal.*, 53, 10 (1964).
27. Simmons, E. L., and W. W. Wendlandt, *J. Inorg. Nucl. Chem.*, 28, 2187 (1966).
28. Yang, W. Y., unpublished results.
29. Caventou E., and E. Willm, *Bull. Soc. Chim. Fr.*, 13, 194 (1870).
30. Ketelaar, J. A. A., *Z. Krist.*, 81, 436 (1934).
31. Ketelaar, J. A. A., *Z. Phys. Chem.*, B26, 327 (1935).
32. Ketelaar, J. A. A., *Z. Phys. Chem.*, B30, 35 (1938).
33. Ketelaar, J. A. A., *Trans. Faraday Soc.*, 34, 874 (1938).
34. Suchow, L., and P. H. Keck, *J. Am. Chem. Soc.*, 75, 518 (1953).
35. Thomas, D. G., L. A. K. Staveley, and A. F. Curtis, *J. Chem. Soc.*, 1727 (1952).
36. Bachman, C. H., and J. B. Maginnis, *Am. J. Phys.*, 19, 424 (1951).
37. Oisen, C. E. and P. M. Harris, *Phil. Rev.*, 86, 651 (1952); U.S. Department of Commerce, Office, Tech. Ser., PB Dept. 156, 106, 61 pages (1959).
38. Hahn, H., G. Frank, and W. Klinger, *Z. Anorg. Allg. Chem.*, 279, 271 (1955).
39. Neubert, T. J., and G. M. Nichols, *J. Am. Chem. Soc.*, 80, 2619 (1958).
40. Reihstein, J., *Phys. Rev.*, 98, 271 (1955).
41. Heintz, E. A., *J. Inorg. Nucl. Chem.*, 21, 64 (1961).
42. Andrews, W. S., *Gen. Elec. Rev.*, 29, 521 (1926).
43. Perez, H. G., *Quim. Ind. (Sao Paulo)*, 4, 137 (1936).
44. Horiguchi, Y. T., Funlyama, and T. Nakanishi, *Sci. Pap. Inst. Phys. Chem. Res. Jpn.*, 53, 274 (1959).
45. Wendlandt, W. W., *Pure Appl. Chem.*, 25, 826 (1971).
46. Wendlandt, W. W., and C. H. Stenbridge, *J. Inorg. Nucl. Chem.*, 27, 575 (1965).
47. Chang, F. C., and W. W. Wendlandt, *J. Inorg. Nucl. Chem.*, 32, 3535 (1970).
48. Chang, F. C., and W. W. Wendlandt, *Thermochim. Acta*, 2, 293 (1970).
49. Chang, F. C., and W. W. Wendlandt, *Thermochim. Acta*, 3, 69 (1971).
50. David, D. J., *Thermochim. Acta*, 3, 277 (1972).
51. Rupert, G. N., *Rev. Sci. Instrum.*, 34, 1183 (1963).
52. Morrow, S. L., *Microscope*, 21, 29 (1973).
53. Hisatsune, I. C., *Perkin-Elmer Instrument News*, 16, No. 2, 2 (1965).
54. Hisatsune, I. C., and N. Haddock Suarez, *Inorg. Chem.*, 3, 168 (1964).
55. Hartman, K. O., and I. C. Hisatsune, *J. Chem. Phys.*, 44, 39 (1966).
56. Hisatsune, I. C., T. Adl, E. C. Beahn, and R. J. Kempf, *J. Phys. Chem.*, 74, 3225 (1970).
57. Hisatsune, I. C., E. C. Beahn, and R. J. Kempf, Ref. 56, p. 3444.
58. Hisatsune, I. C., and D. G. Linnehan, Ref. 56, p. 4091 (1970).
59. Wydeven, T., and M. Leban, *Anal. Chem.*, 40, 363 (1968).
60. Wendlandt, W. W., and J. P. Smith, *Thermal Properties of Transition Metal Ammine Complexes*, Elsevier, Amsterdam, 1967, p. 35.
61. Tanaka, N., M. Sato, and M. Nango, *Rep. Tohoku Univ.*, 48, 1 (1964).
62. LeRoux, J. H., and J. J. Montano, *Anal. Chem.*, 38, 1808 (1966).
63. McCrone, W. C., *Mettler Technical Information Bulletin*, No. 3003, 1968.
64. McCrone, W. C., *Fusion Methods in Chemical Microscopy*, Interscience, New York, 1957.
65. Vaughan, H. P., *Thermochim. Acta*, 1, 117 (1970).
66. Smith, R. V., *Am. Lab.*, Sept. 1969, p. 85.
67. Sommer, G., *Thermochim. Acta*, 2, 10 (1965).
68. Sommer, G., and P. F. Joehens, *Mater. Sci. Eng.*, 3, 3 (1971).
69. Keith, A. K., C. L. Lee, and R. M. Till, *J. Chem. Phys.*, 39, 1206 (1961).
70. Vaughan, H. P., *Microscopy*, 17, 1 (1969).
71. Reese, D. R., P. N. Nordberg, S. F. Erickson, and J. V. S. Santos, *J. Polym. Sci.*, 50, 177 (1961).
72. Hoch, C. W., and J. E. Arbogast, *Anal. Chem.*, 33, 462 (1961).
73. Fairbrother, B. D., *Anal. Chem.*, 43, 24 (1971).
74. Barak, E. M., and J. F. Johnson, *Thermochim. Acta*, 5, 4 (1971).
75. Miller, G. W., *Thermochim. Acta*, 3, 48 (1967).

76. Miller, G. W., in *Analytical Calorimetry*, R. S. Porter and J. F. Johnson, eds., Vol. 2, Plenum, New York, 1970, p. 397.
77. Bruckner, H. P., and K. Heide, *Z. Chem.*, 10, 125 (1970).
78. Wendlandt, W. W., *Thermochim. Acta.*, 1, 419 (1970).
79. Hyzer, W. G., *Re.L/Dev.*, Feb. 1972, p. 61.
80. Magill, J. H., *Nature*, 187, 770 (1960).
81. Tynan, L. E., and R. T. von Gutfeld, *Rev. Sci. Instrum.*, 46, 569 (1975).
82. Hildebrandt, W. H., and F. H. Cocks, *Rev. Sci. Instrum.*, 47, 866 (1976).
83. Charsley, E. L., A. C. F. Kamp, and J. A. Rumsby, Application Note 254, Stanton Redcroft Ltd.
84. Morrow, S. L., *Am. Lab.*, April 1976, p. 54.
85. Van Tets, A., and H. G. Wiedemann, *Thermal Analysis*, R. F. Schwenker and P. D. Gam. eds., Academic, New York, 1969, p.
86. Perron, W., G. Bayer, and H. G. Wiedemann, *Thermal Analysis*, ICTA 80, ed., Birkhauser, Basel, 1980, p.
87. *Mettler Application Note F5J52S*, Mettler Instrument Corp., Griefensee, Switzerland.
88. *Mettler Application Note No. 806*, Mettler Instrument Corp., Griefensee, Switzerland.
89. Kuhnert-Brandstatter, M., "Thermomicroscopy of Organic Compounds," in *Comprehensive Analytical Chemistry*, G. Svehla, ed., Vol. XVI, Elsevier, Amsterdam, 1982.
90. Manche, E. P., *J. Chem. Educ.*, 56, A 273, A 303, A 341 (1979).
91. Cairns, T., *Anal. Chem.*, 48, 267A (1976).
92. Zurer, P. S., *Chem. Eng. News*, Feb. 1983, pp. 21, 26.
93. Lancaster, D. E., *Electron. World*, March 1969, p.
94. Chen, R., *J. Electrochem. Soc.* 116, 1254 (1969).
95. Chen, R., *J. Mater. Sci.*, 11, 1521 (1976).
96. Randall, J. J., and M. H. F. Wilkins, *Proc. R. Soc. (London)*, A184, 3, 66, 390 (1945).
97. Halperin, A., and A. A. Braner, *Phys. Rev.*, 117, 408 (1960).
98. Kivits, P., and H. L. L. Hagebeuk, *Luminescence*, 15, 1 (1977).
99. Nuzzio, D. B., *Thermochim. Acta.*, 52, 245 (1982).
100. Manehe, E. P., and R. Carroll, *Anal. Chem.*, 54, 1236 (1982).
101. Manche, E. P., *Rev. Sci. Instrum.*, 49, 715 (1978).
102. Pla, C., and E. B. Podgorsak, *Med. Phys.*, 10, 462 (1983).
103. Aitken, M. I., in *Thermoluminescence of Geological Materials*, D. J. McDougall, ed., Academic, New York, 1968, p. 369.
104. Deribere, M., *Argile*, 188, 5 (1938); *Rel. Sci.*, 76, 383 (1938).
105. Garlick, G. F., *Luminescent Materials*, Oxford University Press, London, 1949.
106. Kohler, A., and H. Leitmeir, *Z. Krist.*, 87, 87 (1934).
107. Royer, L., *Camp. Rend.*, 204, 602 (1937).
108. Saurin, E., *Camp. Rend. Soc. Geol. Fr.*, 209 (1939).
109. Northrup, M. A., and O. I. Lec, *J. Opt. Soc. Am.*, 30, 206 (1940).
110. Saunders, D. F., *Bull. Am. Assoc. Petro. Geol.*, 37, 114 (1953).
111. Parks, J. M., *Bull. Am. Assoc. Petro. Geol.*, 37, 125 (1953).

112. Daniels, F., C. A. Boyd, and D. F. Saunders, *Science*, 117, 343 (1953).
113. Lewis, D. R., *J. Phys. Chem.*, 60, 698 (1956).
114. Bose, S. N., J. Sharma, and B. C. Datta, *Trans. Bose Res. (in Hindi), Calcutta*, 20, 117 (1955).
115. Ingersoll, E., *Econ. Geol.*, 50th. Anniv. Vol., 341 (1956).
116. Zeler, E. L., *Congr. Geol. Int. Compt. Rend. 19^e Algiers*, 12, 365 (1952).
117. Mott, N. F., and R. W. Gurney, *Electronic Processes in Ionic Crystals*, Oxford University Press London, 1940.
118. Fonda, G. R., and F. Seitz, *Cornell Symposium of the American Physical Society*, Wiley, New York, 1948.
119. Kroger, F. A., *Some Aspects of the Luminescence of Solids*, Elsevier, Amsterdam, 1948.
120. Leverenz, H. W., *An Introduction to the Luminescence of Solids*, Wiley, New York, 1950.
121. Pringsheim, P., *Fluorescence and Phosphorescence*, Interscience, New York, 1949.
122. Boyd, C. A., *J. Chem. Phys.*, 17, 1221 (1949).
123. Urbach, F., *Sitzungber. Akad. Wiss. Wien. Math. Naturwiss. Kl., Abt.*, 139, 363 (1930).
124. Garino-Capina, V., and S. Cohen, *J. Am. Ceram. Soc.*, 43, 415 (1960).
125. Boyd, C. A., and J. Hirschfelder, U.S. Patent No. 2, 573, 245, October 30, 1951.
126. Morehead, F. F., and F. Daniels, *J. Phys. Chem.*, 56, 546 (1960).
127. EHsworth, H. V., *Can. Dep. Mines Geol. Surv. Econ. Geol. Ser. No. 11*, 55 (1932).
128. Alt, M., and H. Steinmetz, *Z. Angew. Mineral.*, 2, 153 (1940).
129. DeWard, L. A., and T. G. Stoebe, *Am. Sci.*, 60, 303 (1972).
130. Christy, R. W., N. M. Johnson, and R. R. Wilberg, *J. Appl. Chem.*, 38, 2 (191967).
131. Cameron, J. R., N. Sumharalingam, and G. N. Kenney, *Thermoluminescence Dosimetry*, University of Wisconsin Press, Madison, 1968.
132. Dalrymple, G. B., and R. R. Doell, *Science*, 167, 715 (1970).
133. McDougall, D. J., ed., *Thermoluminescence of Geological Materials*, Academic, New York, 1968.
134. Mazess, R. B., and D. W. Zimmerman, *Science*, 152, 347 (1966).
135. Harshaw Model 3000 TL Analyzer brochure, Harshaw Chemical Co., Solon, OH.
136. Ashby, G. E., *J. Polym. Sci.*, 50 (1961) 99.
137. Schard, M. P., and C. A. Russell, *J. Appl. Polym. Sci.*, 8 (1964) 985.
138. Ref. 137, p. 997.
139. Barker, R. E., J. H. Duane, and P. M. Rentzepis, *J. Polym. Sci. Part A*, 3 (1965) 2033.
140. de Kock, R. J., and P. A. H. M. Hoi, *Rec. Trav. (111m)*, 85 (1966) 102.
141. Wynne, A. M., and W. W. Wendlandt, *Thermochim. Acta.*, 13 (1975) 393.
142. Wynne, A. M., and W. W. Wendlandt, *Thermochim. Acta.*, 14 (1976) 61.
143. Wendlandt, W. W., *Thermochim. Acta.*, in press.
144. Kaimin, I. F., and Z. Galeis, *Vysokomol. Soedin. Ser. A*, 9 (1967) 245.
145. Johnson, B. B., and J. Chiu, *Thermochim. Acta.*, 50 (1981) 57.
146. Vassiliev, R. F., *Nature*, 200 (1963) 773.

147. de Kock, R. 1., and A. H. M. Hal, *Fourth International Synthetic Rubber Symposium, Lectures*, 1969, p. 53.
148. Reich, L., and S. S. Stivala. *Elements of Polymer Degradation*. McGraw-Hill New York, 1971, pp. 99, 161.
149. Manyasek, F., D. Berek, M. Michko, M. Lazar, and Y. Pabljnetz, *Vysokomol. Soedin.* 3 1:19611 : 104.
150. Williams, F. E., and H. Eyring, *J. Chem. Phys.* 15 (1947) 280.
151. Chen, R., *J. Marer. Sci.*, 11 (1976) 1521.
152. Wendlandt, W. W., *Thermochim. Acta.*, 71,1291\983).
153. McCarter, R. J., in *Syllabus of Thermal Analysis*, O. Meris, ed., NBS Special Pub. 338, OCI, 1970, p. 137.
154. Allen, N. S., J. F. McKellar, and D. Wilsor., *J. Photochem.*, 6 (1977) 337.
155. Collins, L. W., and W. W. Wendlandt, *Isr. J. Chem.*, 22 (1982) 233.
156. Wendlandt, W. W., *Thermochim. Acta.*, 68, 383 (1983).
157. Ref. 156, p. 387.
158. Wendlandt, W. W., unpublished results.
159. Chen, R., and Y. Kirsch, *Analysis of Thermally Stimulated Processes*, Pergamon, New York, 1981.
160. Stivala, S. S., J. Kimura, and L. Reich, in *Degradation and Stabilization of Polymers*, H. H. G. Jellinek, ed., Elsevier, Amsterdam, 1983, Chap. 1, Marisova-Rychla, L., L. Rychly, and M. Vavrekova, *Eur. Polym. J.*, 14, 1033 (1978).
162. George, G. A., *Polymer Degrad. Stab.*, 1, 217 (1979).
163. Mendenhall, G. D., *Angew. Chem. Inc. Ed. Engl.*, 16, 225 (1977).
164. Naito, K., and T. K. Kivei, *J. Polym. Sci. Polym. Chem. Educ.*, 17, 2935 (1979).
165. Wendlandt, W. W., *Thermochim. Acta.* 72, 363 (1984).
166. George, G. A., in *Developments in Polymer Degradation*, N. Grassie, ed., Applied Science Pub., London, 1981.

CHAPTER

10

CRYOSCOPIC AND DIFFERENTIAL SCANNING CALORIMETRY PURITY DETERMINATION

A. CRYOSCOPIC METHODS

1. Introduction

The purity of organic and inorganic compounds can be determined by a number of techniques ranging from simple physical methods of boiling- and melting-point determinations to more sophisticated instrumental methods such as absorption or emission spectroscopy. An attempt is made to summarize the principal instrumental techniques for purity (or impurity) determinations in Table 10.1. The figures cited are not very accurate and may vary widely, depending on the main component as well as the impurities present. The first six methods may each show a number of contaminants in one single experiment and permit the determination of each of them. Electrical conductance permits the estimation of ions in aqueous or nonaqueous solutions as well as the ionic components in semiconductors. Although the latter is a rather limited technique, it does approach the optimum purity-control method for group contaminants.

The method offering the widest potential for the determination of the purity of a substance is *thermal analysis* (1). It is applicable to all substances which are sufficiently stable at their melting points and permits the determination of the total quantity of impurity not soluble in the solid phase. Thermal analysis may be defined as a method for the determination of the amount of contaminant(s) in a substance from an analysis of the temperature-time or temperature-heat content curves at its melting point. Glasgow and Ross (38) prefer to use the broad term of "cryoscopy," which they define as the science of the determination of temperatures, from solid-liquid equilibria. If the freezing points of liquids and of the melting points of solids, and the uses of such measurements for analytical purposes. The terms *freezing point* and *melting point* are commonly accepted (38) as referring to the temperature where an infinitesimal amount of solid is in equilibrium with liquid when the measurements are performed in equilibrium with air at one atmosphere.

Various methods have been used to determine the temperature-time or

Table 10.1. **Methods** of Impurity Detenninalon of Chemical Compounds (1)

Method	Sensitivity ^a	Substance	
		Organic	Inorganic
Emission and X-ray spectroscopy	10 ⁻⁴ -10 ⁻⁵		x
Activation analysis	10 ⁻¹ -10 ⁻⁸	x	x
Polarography	10 ⁻⁶	x	x
Mass spectroscopy	10 ⁻³ -10 ⁻⁵	x	x
Chromatography	10 ⁻¹	x	x
Absorption spectroscopy	10 ⁻³	x	
Electrical conductance	10 ⁻⁸		x
Thermal analysis	10 ⁻⁵	x	x

^aSmallest fraction of impurity still detectable.

temperature-heat content curves of a substance. They include the following:

1. *Thermometric methods* (not to be confused with thermometric titrations) in which temperature-time curves are obtained at various intervals. Heat evolution or absorption occurs continuously and preferably at a constant rate. The amount of heat supplied per unit time is not measured directly but may be calculated as a fraction of the total heat of melting of the substance.

Calorimetric methods in which temperature-heat-content curves are obtained. An adiabatic calorimeter or a differential scanning calorimeter may be employed. The latter instrument is much more convenient to use and is capable of almost the same accuracy and precision as the former technique.

- J. *Dilatometry* (volume-temperature curves) and *dielectric constant*. The latter method appears to be as accurate as the other techniques, and, by virtue of use of an extensive property, it is not influenced by the amount of material used. These methods will not be discussed here.

Various reviews on the subject of thermal analysis as a means of purity determination of organic compounds have been published by Sturtevant (2), Cines (3), Mathieu (4), and Smit (1, 5), Glasgow and Ross (138), Skau and Arthur (39), and others (40-42).

2. Theory

The treatment of temperature-heat content curves from a theoretical viewpoint has been carried out by a number of investigators, starting with White (6) in 1920. Other early papers on the subject are by Andrews et al. (7), Skau (8), Mair et al. (9), Glasgow et al. (10), Malotau and Straub (11), and Thomas and Parks (12). More recent treatments have been given by Rossini (13), Mastrangelo and Domte (14), Badley (15), and Smit (1). The reader is referred to these references for a more comprehensive presentation than that given here.

To analyze the temperature versus time curve, we discuss the curves in Figure 10.1. The basic analysis of this curve has been described by White (6) and modified by Carleton (16). The resulting temperature versus time curve is based on the linear relationship of heat input to time added to the equation

$$N_2 = \frac{\Delta H}{RT^2} (T_0 - T) = A(T_0 - T) \quad (10.1)$$

where N_2 is the mole fraction of solute, ΔH is the heat of fusion of the solvent, T_0 is the freezing point of pure solvent, and T is the equilibrium temperature. This equation is restricted to those examples which are nearly pure and in

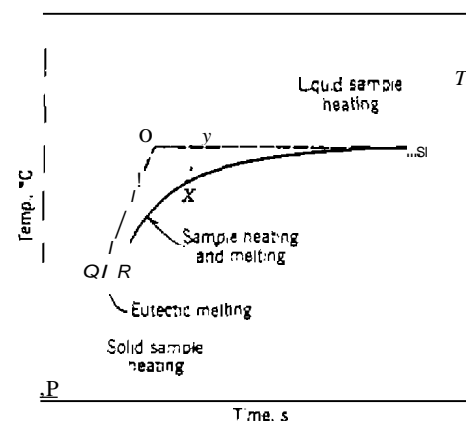


Figure 10.1. Melting-temperature curve for two-component system; - - - actual equilibrium curve; - - - idealized process, heating without melting (specific-heat component) (16).

which, on freezing, the pure major component solidifies, leaving the impurity in solution.

The linear relationship of heat input to time follows from the maintenance of a constant temperature interval between the sample and the bath. During melting, this heat input has two components: a specific-heat component which raises the temperature of the sample and the thermometer bulb, and a melting component. The separation of these two components on a time scale is illustrated in Figure 10.1. The initial straight-line portion, PQ , represents the heating of the solid sample and thermometer bulb. In the case of a two-component system, there is a flattening of the curve at the eutectic temperature, QR . Above this eutectic, melting and heating occur simultaneously, as indicated by RS . The curve arches and flattens out until all of the solid is melted and then the slope changes abruptly, where heating of the liquid sample begins, at ST .

The dashed line represents an idealized process in which all solid is heated to the freezing point and then all the sample is melted isothermally. The two lines, QO and OS , are thus separate specific-heat and melting components for the actual process. The flat line, AS , represents the melting of the two substances, solvent and solute, with different heats of fusion. However, for most substances studied, the amount of solute is always small so that on the central part of the curve, which is used for analysis, the fraction of material melted is proportional to the distance along OS .

Analysis of a temperature versus time curve depends on the construction of several projections, such as XY , from the actual curve to the ideal flat line, or, the sample slope as that of PQ could be used with negligible error. However, a run usually begins at a temperature at which some melting is already under way, so that the slope of the separate specific-heat component is not known. When the properties of the sample are known, a slope for XY may be approximated from the dimensions of the apparatus, the specific heat, the heat of fusion of the sample, and a rough estimate of the impurity, assuming ideal solution behavior. Usually, however, these properties will not be known, but either the properties or the slope may be estimated with sufficient accuracy to be useful.

If x represents the mole fraction of impurity in the original sample and T_1 the freezing point of the impure sample (temperature at point S), then equation (10.1) gives

$$N_2 = A(T_0 - T) \quad (10.2)$$

$$x = A(T_0 - T_1) \quad (10.3)$$

whence

$$N_2 = x + A(T_1 - T) \quad (10.4)$$

If f is the mole fraction of the solvent frozen at temperature T ,

$$f = \frac{N_2 - x}{N_2} = x \frac{A(T_1 - T)}{A(T_1 - T) + x} = \frac{A \Delta T}{x + A \Delta T} \quad (10.5)$$

If Δt represents the time difference from the point of complete melting, YS , and Δt_1 the total time represented by the ideal melting flat line, OS , then

$$f = \frac{\Delta t}{\Delta t_1}$$

Equations (10.5) and (10.6) are rearranged to

$$\Delta t = \Delta t_1 - \frac{x}{A} \left(\frac{\Delta t}{\Delta T} \right) \quad (10.7)$$

Thus, the theory predicts that a plot of Δt against $\Delta t / \Delta T$ will give a straight line whose slope is $-x/A$. The term A is equal to

$$A = \frac{\Delta H}{RT_0^2} \quad (10.8)$$

and is a characteristic property of the major component in the sample. When ΔH is not known, A may be determined from an additional run on the sample containing a known mole fraction of added solute. Alternatively, ΔH may be estimated by comparing the curve for the sample with a curve for a reference substance of known heat of fusion, obtained in the same apparatus. Then x is the product of A and x/A determined from the slope of the curve.

For the temperature-heat content curves, a similar expression can be derived. Rossini (13) has shown that the thermodynamic relation for equilibrium between a liquid phase, of the major and minor components, and a crystalline phase of the major component alone is given by

$$\ln N_1 = \ln(1 - N_2) = -A(T_0 - T)[1 + B(T_0 - T) + \dots] \quad (10.9)$$

where N_1 and N_2 are the mole fractions of the major and minor components, respectively, in the liquid phase. The temperature T_0 is the freezing point of

the pure major component ($N_1 = 1$), and T_i is the equilibrium temperature for the mixture. The quantity A is given by equation (10.8), while B is the other cryoscopic constant

$$B = \left(\frac{1}{T_0}\right) - \frac{(\Delta C_p)}{2\Delta H_f} \quad (10.10)$$

where C_p is the molar heat capacity of the liquid less that of the solid. For highly purified samples, T approaches T_0 and N_2 approaches zero, so that equation (10.9) can be written as

$$N_2 = A(T_0 - T) \quad (10.11)$$

If N_2 is the mole fraction of impurity in the liquid phase for a fraction F of the sample liquid, then

$$N_2 = N_2^* \frac{1}{F} \quad (10.12)$$

where N_2^* is the mole fraction of impurity in the sample. Combining equations (10.11) and (10.12) gives

$$T = T_0 - \left(\frac{N_2^*}{A}\right)\left(\frac{1}{F}\right) \quad (10.13)$$

A plot of T versus $(1/F)$ will give a straight line of slope $-(N_2^*/A)$ and the intercept at $(1/F) = 0$ will be T_0 . Thus, from the slope of the line, the purity of the sample can be determined. Such a curve of $(1/F)$ versus temperature for benzotrifluoride is given in Figure 10.2.

The previous procedure is based on the assumptions (17) that (1) the values of T are thermodynamic equilibrium temperatures, (2) an ideal solution is formed in the liquid phase, (3) the impurity is insoluble in the solid phase, and (4) N_2^* is very much less than 1. Departure from linearity in a plot of T versus $(1/F)$ may be taken as an indication that one or more of these assumptions is not met fully.

Gunn (37) has proposed for quantitative purity determination another method, which can also be used for the estimation of heat capacities and heats of fusion of the sample.

Assuming Newton's law, the heat transfer to the sample is

$$\frac{dH}{dt} = k(T_b - T_s) \quad (10.14)$$

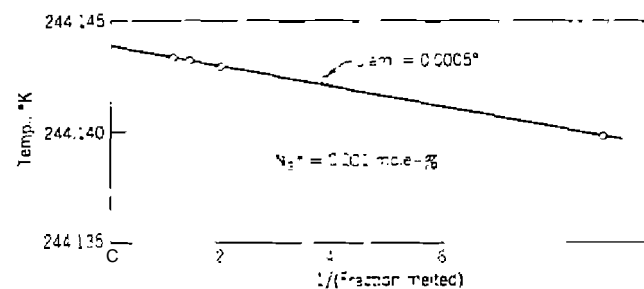


Figure 10.2. The melting curve of benzotrifluoride (7).

where T_b is the temperature of the block, T_s is the temperature of the sample, and k is the heat transfer coefficient. The rate of temperature change of the sample is

$$\frac{dT_s}{dt} = \frac{k(T_b - T_s)}{nC_s + C_g} \quad (10.15)$$

where n is the number of moles of sample, C_s is its molar heat capacity, and C_g is the heat capacity of the glass bulb, sample well packing, and part of the thermocouple. If T_b is increased at a constant rate, T_s will approach asymptotically and follow a parallel time-versus-temperature line such that

$$\frac{dl_s}{dt} = \frac{dT_b}{dt} = r \quad (10.16)$$

displaced in temperature at a given time by a thermal heat, h :

$$h = T_b - T_s = r(nC_s + C_g)/k \quad (10.17)$$

and displaced in time at a given temperature by a lag, i :

$$i = \frac{T_b - T_s}{r} = \frac{nC_s + C_g}{k} \quad (10.18)$$

Thus, h is a function only of the heat capacity and k , but h is also a function of heating rate, r :

$$h = ri \quad (10.19)$$

The treatment for purity determinations used by Gunn (37) assumes that k is a constant, but that its value need not be known; likewise, the values of n , C'' and C' need not be known.

In Figure 10.3 is illustrated an idealized melting curve to be described by this treatment. Curve AB represents the block temperature, increasing at an approximately constant rate, r . Curve CGF represents the sample temperature, t , being selected before this temperature departs from a line parallel to AB . From equation (10.14), it follows that the heat transferred to the sample in warming it from T_i to T_f is

$$H_f - H_i = k \int_{t_i}^{t_f} (T_b - T_s) dz = k(ABFGC) \quad (10.20)$$

If no latent heat were associated with the fusion, the sample would warm along path $CDEF$, where T_0 is the melting point and the curves CD and EF are separated from AB by the differentials, l and l' , which reflect the different heat capacities of the solid and liquid, that of the solid generally being lower. The absorption of heat would be $k(ABFEDC)$; hence, the molar heat of fusion, ΔH , of the sample is

$$n\Delta H = k(ABFGC) - k(ABFEDC) = k(CDEFG) \quad (10.21)$$

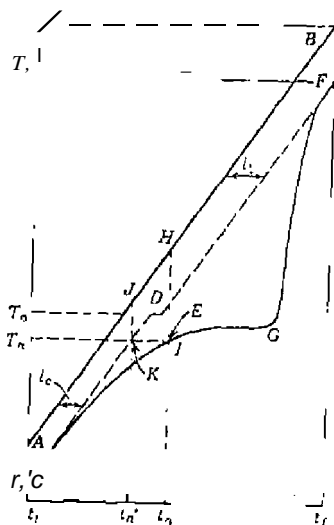


Figure 10.3. Idealized melting curve (17)

The area, $CDEFG$, will be called Z ; in practice, it is evaluated by graphical integration, that is, by dividing the area into several easily measured triangles which cover an area judged visually to be equal.

The heat transferred to the sample to warm it from T_i to T_n is $k(AHIC)$, and is denoted as W . The heat required to warm the solid from T_i to T_n in the absence of melting would be $k(AJKC)$, and is denoted as X . Instead of integrating X graphically, it is noted that

$$X = r(t_n' - t_i) = k_s(t_n' - t_i) \quad (10.22)$$

The amount of heat which has been used to melt part of the sample at time t_n is $k(W - X)$; the quantity $W - X$ is denoted as Y . The reciprocal of the fraction of the sample melted, F^{-1} , is

$$F^{-1} = \frac{Z}{Y} \quad (10.1J)$$

where F^{-1} may be calculated for as many points as desired on the melting curve.

For the ideal or sufficiently dilute solutions, the van't Hoff law of freezing-point lowering has the form

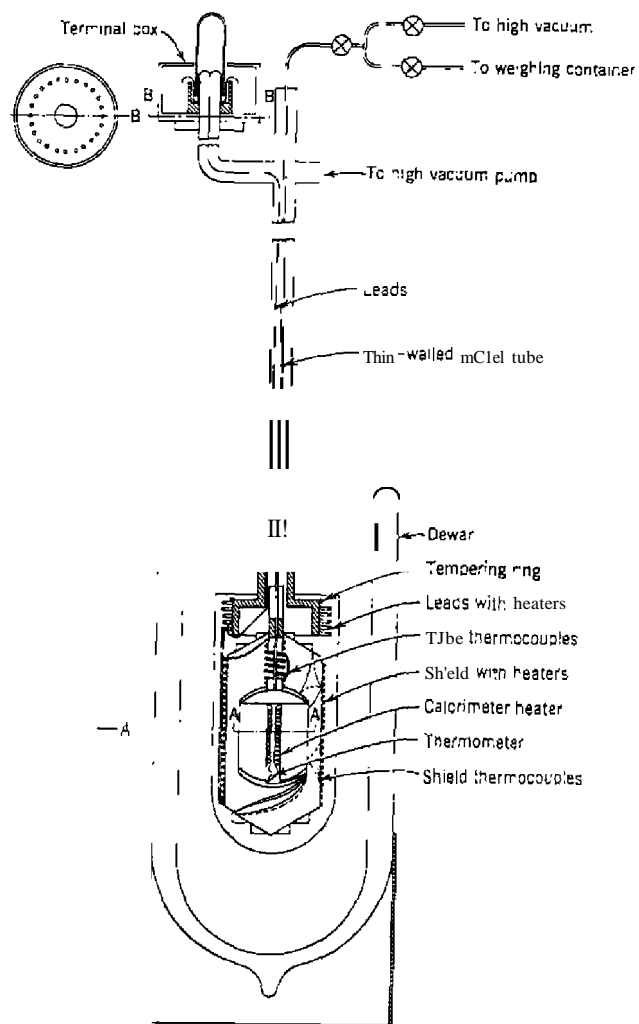
$$T = T_0 - \frac{N_2 F^{-1} R T_0^2}{\Delta H} \quad (10.24)$$

where T_0 is the melting point of the pure material and N_2 is the mole fraction of impurity. Hence, the values of T_n plotted against F^{-1} should lie on a straight line whose slope multiplied by the cryoscopic constant, $RT_0^2/\Delta H$, is equal to N_2 .

3. Experimental Techniques

For thermal analyses by the static method, a precise adiabatic calorimeter is required. Although many adiabatic calorimeters have been described in the literature, Glasgow et al. (18) have described a calorimeter which was used to determine the purity of benzene and other substances in the temperature range 10–300K. The calorimeter is illustrated schematically in Figure 10.4.

The sample container, suspended in the calorimeter by a small tube, was constructed of copper and had a capacity of about 106 ml. Tinned copper vanes were arranged radially from the central concentric well, containing a heater and a platinum resistance thermometer. On the outer wall of the



Adiabatic calorimeter for volatile compounds (18).

container. The vanes were held in place by means of a thin coating of tin. A thin copper thermal shell was attached to the upper periphery of the container to obtain a nearly isothermal surface. The outer surface of the container, the inner and outer surfaces of the shell, and the inner surface of the adiabatic shield were gold plated and polished to minimize heat transfer by

radiation. A high vacuum, 10^{-6} Torr, was maintained in the space surrounding the sample container and the adiabatic shield.

The resistance of the platinum thermometer was measured by means of a Mueller bridge. The electrical input energy was determined from the measurements of the current and potential across a 100Ω Constantan wire heater and the time interval of heating. The heater current and potential were measured by means of a Wenner potentiometer in conjunction with a resistor and a volt box. The time interval of heating was measured by means of a precise interval timer.

The calculations involved in the determination of the specific heat of a sample have been described by Stull (19). During a heat input, an electric current of I amperes flowed through the sample heater because of a voltage e impressed on the heater terminals for t seconds. The heat in calories, H , is then

$$H = \frac{Ier}{4.1840} \tag{10.25}$$

This heat input caused the temperature of the sample to go from its initial state, T_i , before the heat was applied, to T_f , the final temperature of the sample after the sample had reached a constant temperature. Thus, $T_f - T_i = \Delta T_s$, the rise in temperature due to H , and $\frac{1}{2}(T_f + T_i) = T_a$, the average temperature of the space heat input.

Now heat was absorbed by the sample container of weight w grams and specific heat C_{pc} at T_a as well as by the sample of W grams and specific heat C_{ps} at T_a . Expressed mathematically,

$$H = [wC_{pc} + WC_{ps}] \Delta T \tag{10.26}$$

and combining equations (10.14) and (10.15) one obtains

$$\frac{Ier t}{4.1840WT} - \frac{WC_{pc}}{W} = C_{ps} \tag{10.27}$$

Equation (10.27) is the basic equation used to calculate the heat capacity of the sample. By slight modification of the equation, the calculations can be made by an electronic digital computer.

Other calorimeters that have been used for melting determinations have been described by Clarke et al. (20), Aston and Fink (21), Pilcher (22), Mazze (23), and Ruehrwein and Huffman (24).

In the case of the dynamic method, the constant heat supply to the sample is obtained by maintaining a constant thermal head between the sample and

its surrounding. This may be done by two different methods: (1) by a constant-wall apparatus and (2) by an adapted-wall apparatus (I). A constant-wall apparatus maintains a constant temperature between the wall of the sample container and the sample. In an adapted-wall apparatus, a constant temperature is maintained between the wall of the sample container and the sample. In an adapted-wall apparatus, a constant heat supply to the sample is also maintained when the sample is surrounded by a mantle and its temperature is continuously adapted to the temperature of the sample in such a way that the difference between both temperatures remains constant.

The various constant- and adapted-wall apparatuses have been summarized by Smit (I). The former type have been built by White (6) and by Rossini and co-workers (9, 10), Instruments of the latter type have been described by Thomas and Parks (12), Malotau and Straub (11), Carleton (16), Smit and Kateman (25), Smith (26, 27), Glasgow and Tenenbaum (28), Glasgow et al. (18), Handley (29), and Barnard-Smith and White (30).

The applications of the constant wall instruments are mainly for the determination of cooling or freezing curves, and not for heating or melting curves. This is probably because when heat must be transported to the sample, the outer wall of the apparatus, and thus the isolating mantle, must be at a temperature much higher than when heat must be transported from the sample (I). Since due to radiation the isolating power of a vacuum jacket decreases rapidly at increasing temperatures, it is clear that the thermal head for heating a sample at a permissible rate will be lower than the opposite thermal head for cooling the sample at the same rate.

Depending on the temperature range to be covered, the wall of the adapted-wall instruments consists of a glass bulb immersed in a liquid bath or a thick cylindrical mantle made of metal. The temperature of the bath or of the metal mantle is adapted to the temperature of the sample so that the difference of the two temperatures remains constant. Between the wall and the measuring vessel containing the sample, there is an air space which provides the necessary insulation. The thermal gradient or difference usually amounts to about 2°C , and the rate of heating of the sample is quite low, about $0.1-0.3^{\circ}\text{C}/\text{min}$. This type of apparatus is not stirred.

A simple apparatus of the adapted-wall type has been described by Carleton (16) and is a modification of the apparatus described by Smit (26). The apparatus is schematically illustrated in figure 10.5.

The enclosure of the sample is in the form of a thin, uniform film surrounding the bulb of a 0.1°C graduated mercury thermometer. The thermometer was positioned by means of a bored cork in a glass sample tube drawn to the proper dimensions in the portion surrounding the thermometer bulb. To reduce the effects of temperature fluctuations, the sample tube was jacketed with a slightly larger tube retained by a plastic ring. The entire sample assembly was placed in a 300-ml round-bottomed flask, in such a

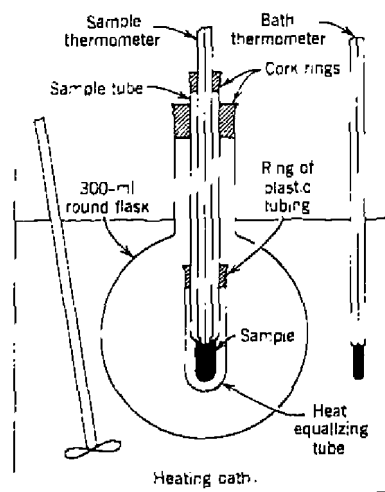


Figure 10.5. Apparatus for determination of melting temperatures (16).

position that the thermometer bulb was at the approximate center of the flask. The flask was immersed to the neck in a suitable heating bath which was provided with a stirrer, thermostat, and thermometer. The volume of sample required for a determination was about 0.3 ml. The outside bath was heated at a rate of 0.3°C per 100 sec or per minute. A plot of sample temperature versus time was started at $15-20^{\circ}\text{C}$ below the melting point of the substance.

Another apparatus which was similar to that described previously by Glasgow et al. (10), and modified by Barnard-Smith and White (30), is schematically illustrated in Figure 10.6. The sample, usually about 25 mL was frozen and melted in a double-walled tube, the rate of heat transfer from the refrigerant or heating bath to the sample being controlled by the vacuum between the walls of the tube. A rotating stirrer was used and, for smaller samples, an aluminum tube was inserted to reduce the volume of the sample chamber. The temperature of the sample was measured by a platinum resistance thermometer and a Mueller bridge. The instrument could also be used for heat-of-fusion measurements by insertion of a series of aluminum vanes. These vanes assisted in the even distribution of heat throughout the sample.

4. Errors, Limitations, and Other Factors Affecting Results

The errors in the determination of temperature versus heat content or time curves have been discussed in detail by Smit (31) and McCullough and

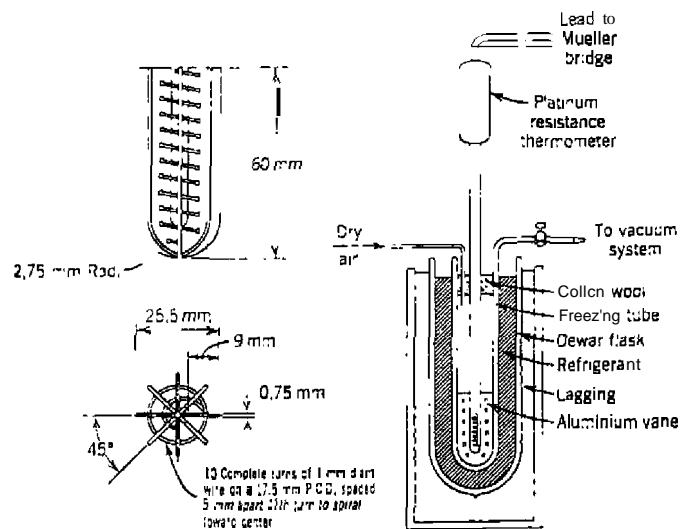


Figure 10.6. Freezing-point apparatus (30).

Vaddington (17). The former discussed the qualitative consideration concerning the rates of phase transitions, the rates of diffusion, and the temperature differences occurring with the "thin-film" method. The latter were concerned with the limitations of the calorimetric method based on the results of more than 125 melting-point studies.

a. Limitations of the Dynamic Method

Solid-Liquid Transitions. When heat is supplied to a system, its temperature will increase until the net rate of melting equals the rate of heat supply. When heat is withdrawn from the system, its temperature will decrease until the net rate of heat production by crystallization equals the rate of cooling. This is only possible below a temperature T_m , the temperature at which thermodynamic equilibrium exists. However, in this region, the rate of heat production may be low and may increase only slightly at decreasing temperatures. Consequently, the temperature obtained may differ appreciably from the equilibrium temperature. The temperature finally obtained remains constant so long as the rate of heat production of the system equals the rate of cooling. This is illustrated by the heating and cooling curves of antipyrine containing 0.1-mole-% acetanilide, as shown in Figure 10.7. The heating curve of pure

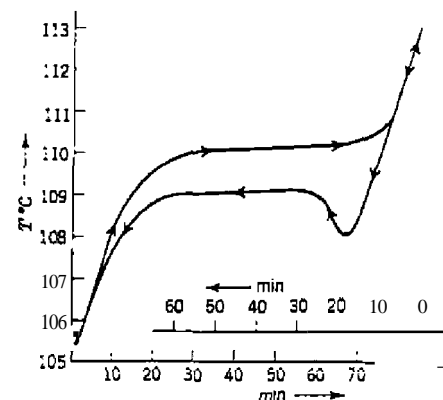


Figure 10.7. Heating and cooling curves of a sample of antipyrine containing 0.1 mole-% acetanilide. Upper curve is the heating curve (3 i).

antipyrine showed a range of constant temperature at 110.45°C, which appeared to be independent of the rate of heating. The cooling curve determined at a comparable rate of cooling showed a small undercooling peak and then the temperature rose to a maximum at about 109°C. The height of the maximum was dependent on the rate of cooling. The curves obtained by heating and cooling the antipyrine and 0.1-mole-% acetanilide mixture were comparable to those obtained with the pure antipyrine.

Similar analogous behavior has been observed with azobenzene, benzyl benzoate, and *p*-xylene, and slight differences with naphthalene.

Solid-Phase Transitions. A heating curve usually shows the existence of *solid* → *solid* or enantiotropic transitions. When melting occurs before the *solid* → *solid* transition is completed, the melting curve will obviously be unreliable. Smit (31) recommended that the sample be stored for a period of time at a temperature above the transition temperature before determination of the melting curve.

Rates of Diffusion. When the solid and liquid of a multicomponent system are in thermodynamic equilibrium, the composition of the solid will usually differ from that of the liquid. When the system is submitted to further melting or crystallization, the composition of at least one of the phases will change in the vicinity of the contact surface. Diffusion tends to equalize the concentration differences occurring both in the solid and in the liquid phases and should, therefore, be promoted,

Effect of Stirring. Stirring promotes the homogeneity of the liquid phase only and does not affect the inhomogeneities occurring in the solid phase. Thus, even when stirring is applied, thick layers may be disadvantageous. Stirring is an advantage at times in that it may cause disintegration of solid particles which may promote the bulk rate of crystallization. The advantage is rather dubious, according to Smit (11), because stirring can only be applied over a limited range of solid-liquid ratios.

Rate of Heat Transport. When heat is supplied or withdrawn from a calorimeter, temperature differences will occur throughout all parts of the calorimetric system, including the wall, the sample, and even the thermometer. These differences constitute a source of errors, the magnitude of which depend on the rate of heating, the sizes of the system components, and the heat conductivities of the construction materials. The magnitude of these errors has been calculated by Smit (31).

Temperature Differences During Melting. Melting, of course, starts at the inner wall of the sample container and subsequently proceeds to the thermometer bulb. As soon as melting starts, the flow of heat to the thermometer decreases appreciably. It is not reduced to zero, however, because the temperature of the thermometer is below the temperature of the melting zone. The difference between the temperature indicated by the thermometer and the temperature of the melting zone constitutes an error which gradually decreases with time. The deviations will be large at the start of the melting process and gradually approach zero as the curve is continued. It is important to know within what time this error has decreased to a value not exceeding the limit of accuracy of the determination. An attempt has been made by Smit (31) to calculate this exact time.

Influence of Contact Between Layers. Contact is never perfect between the glass wall, the sample, and the thermometer bulb. This imperfect contact can give rise to extra temperature differences. Heat can flow from the environment along the stem to the bulb of the thermometer and subsequently to the sample. The temperature of the thermometer will be high when imperfect contact exists between the sample and the bulb.

b. Limitations of the Static Method

The limitations of the static method undoubtedly apply to a greater or lesser extent to any melting-point method. These limitations are as follows (17).

Uncertainty of Impurity Values. Inhomogeneous distribution of impurity in the liquid phase may result in low values of ΔT because the slope of the

melting curve is usually decreased by this effect. A more important source of error, formation of solid solutions has long been recognized as a possible limitation of all melting-point purity methods, but it has not been realized that the phenomenon is so common.

Evidence of Solid-solution Formation. It is not unreasonable to expect that that solid solutions may be formed in highly purified samples, for the impurities may often be isomeric with the main component. About half the melting curves observed by McCullough and Waddington (17) showed moderate to pronounced deviation from linearity of the T versus $1/F$ plots, indicative of solid-solution formation. In fact, linear melting curves over the entire range of fractions melted are rare. Both the formation of solid solutions and inhomogeneous distribution melting-point studies to be too low. The calculations of impurity values from the slope of the melting curve at high fractions melted will minimize errors in most cases.

Applications of Solid-solution Theory. If a melting curve shows evidence of appreciable solid-solution formation, it may require application of a solid-solution treatment (14, 15) to give an accurate impurity value, although Smit (1) has criticized one of the treatments (14). Unfortunately, the method often has failed to give an adequate representation of observed melting curves. In some instances, the solid-solution treatment has given an excellent representation of experimental data, but the high sensitivity of the method to small thermometric errors makes the calculated impurity values unreliable. For example, the difference in temperatures observed with 70 and 90% of a sample melted may easily be in error by $\pm 0.0005^\circ\text{C}$. for the solid-solution treatment, such an error would correspond to an uncertainty of 500% in the impurity value for very pure compounds with normal cryoscopic constants, whereas the same 0.0005°C error corresponds to 150% uncertainty if solid insolubility is assumed.

c. Comparison of Results Obtained by the Static and Dynamic Methods

It is rather interesting to note that the impurity values determined by static methods are systematically lower than those determined on the same sample by dynamic methods (1, 4). However, an extremely careful study by Glasgow et al. (18) on a sample of very pure benzene contaminated by known amounts of *n*-heptane showed that the divergence between the two methods of determination was not so large as was formerly obtained. The results of this study are given in Table 10.2. It is suggested that the difference in values may be due to desorbed water as a source of contamination.

Table 10.2. Comparison of the Results from Dynamic and Static Methods (18)

Sample	Computed From Contamination	Purity (mole-%)	
		Dynamic	Static
A	100 ^a	99.994 ± 0.002	99.9937 ± 0.0010
B	99.9964	99.970 ± 0.004	99.958 ± 0.005
C	99.9610	99.940 ± 0.002	99.947 ± 0.005

^aThe "pure" sample was assumed to be pure beyond the sensitivity of the methods of analysis employed.

d. Recommendations

The following recommendations have been suggested by Smit (31) for thermal analysis:

1. When a static method is used, each period of heat supply to the substance should be followed by a period of "adiabatic conditions" of sufficient length so as to approach equilibrium to a desired extent.
2. For the dynamic method, heating curves are preferred to cooling curves.
3. Before starting a measurement of a heating curve, the sample should be kept at a temperature slightly below the initial melting point for at least 1 hour.
4. The stirring method for determining heating curves is not recommended.
5. The rate of heating of samples with small heats of fusion should be decreased as far as practical.
6. Subject each curve to an internal check and also select a reliable part of the curve for purity determination. Besides experimental checks on the technique, the curve should be checked to see if it obeys the equation (31)

$$T_y = T_a - \frac{C_f C_m}{C_f + Y(C_m - C_f)} \rho \quad (10.28)$$

where T_y is the temperature at which a fraction Y of the sample has

melted, T_a is the melting point of the absolutely pure substance, C_f and C_m are cor. constants, and ρ is the mole-% of contamination present in the sample.

Equations (10.17) can be rearranged to give

$$T = C_1 - \frac{C_2}{C_3 + Y} \quad (10.29)$$

where C_1 , C_2 , and C_3 are constants which can be resolved algebraically by selecting three pairs of corresponding values of T_y and Y . If the T_y values of the melting curve are plotted as a function of $1/(C_3 + Y)$, the plot should be a straight line with slope C_2 .

With all of the preceding distressing sources of error and limitations, thermal analysis has several incomparable advantages (1). Being a physical method, it may be applied without any knowledge concerning the chemical properties of the main component or the contaminants of the sample. It is sensitive, although not equally sensitive, to all types of contaminants. When the sample may be considered as a binary system, it certainly permits quantitative determination of its content of contaminants.

5. Applications to Impurity Determinations and Other Problems

The impurities in synthetic mixtures of naphthalene with anthracene or diphenyl were determined by the melting-curve method of Carleton (16). Melting curves for pure naphthalene alone and for naphthalene containing 1.45-mole-% diphenyl are given in Figure 10.8. The ideal melting flat lines extend across from T_0 , and diagonal lines representing heating without melting (specific-heat effect) are drawn in at selected values of f . Slopes of these lines are obtained by resolving the slope of the equilibrium curve at 70°C into separate specific-heat and melting components, calculated from the dimensions of the apparatus and the properties of naphthalene.

The calculation was as follows for pure naphthalene. The quantities J_0 and x were estimated as 79.7°C and 0.003, respectively. In the 10°C temperature interval 65-75°C, the change in fraction melted, $(1 - f)$, was calculated from:

$$(1 - f) = \frac{x}{T_0} = \frac{x}{79.7} \quad (10.30)$$

Because A is equal to 0.0184 for naphthalene, $(1 - f)$ is equal to 0.0226. The melting component for the 65-75°C temperature range is the product of 0.0226 and 35.6 cal/g (ΔH of naphthalene, 1.8 cal/g from the dimen-

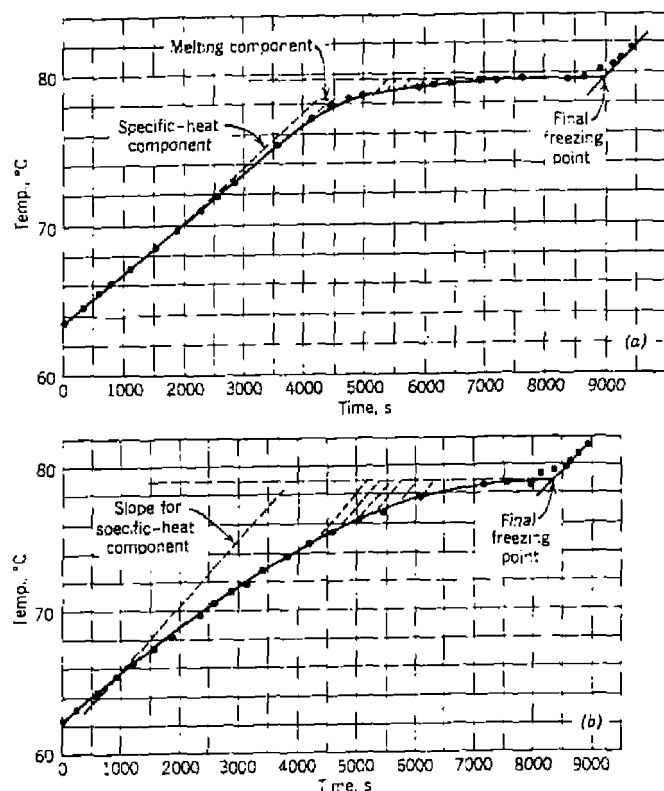


Figure 10.8. (a) Melting curve of pure naphthalene; (b) melting curve of naphthalene containing 1.45 mole-% biphenyl (115).

sions of the apparatus employed, the total value of the specific-heat component was 13.1 cal/g.

A triangle was constructed with the slope of the equilibrium curve at 70°C forming the long side as shown in Figure 10.8a. The other two sides represent the melting and specific-heat components, whose ratio was 0.81 to 1.0. The slope of the specific-heat component was used in the analysis. Lines having the slope of the specific-heat component were then drawn for selected values of ΔT , and the intersections with the ideal melting flat line gave the corresponding values of ΔT as shown in Figure 10.8b.

Figure 10.9 shows a plot of Δt against $\Delta t/\Delta T$ for the naphthalene-biphenyl mixture. The best straight line drawn through these points had a slope of -0.95; hence $x = 0.0175 = 1.75$ mole-% contaminant which includes the added biphenyl and the original impurity. From a similar analysis of the naphthalene by itself, $x = 0.34$ mole-% impurities. Thus, the mole-% biphenyl found experimentally was 1.41 compared to the 1.45 actually added.

In the method employed by Schwab and Wieners (32), the amount of contaminant originally present in a sample can be obtained by determining the freezing curve of the original sample and also the curve of the original sample plus a known amount of contaminant. The preceding comparative method is said to be applicable even if the fraction frozen does not vary linearly with time. Herington (33) has also described the use of this method employing a similar experimental apparatus as previously described.

A set of freezing curves used in the comparative method is given in Figure 10.10. The difference, ΔT , between the initial freezing temperature and the temperature at a time equal to half that required for complete freezing is found, as shown in curve 1. A known amount of impurity, x_1 mole-%, is then added and another freezing curve is obtained using the same rate of cooling as previously employed. A value, ΔT_1 , for the difference between the new initial freezing temperature and the temperature at a time equal to half that required for complete melting is thus obtained. The same procedure is carried out after the addition of a second amount of impurity, x_2 , and another ΔT_2 value is obtained.

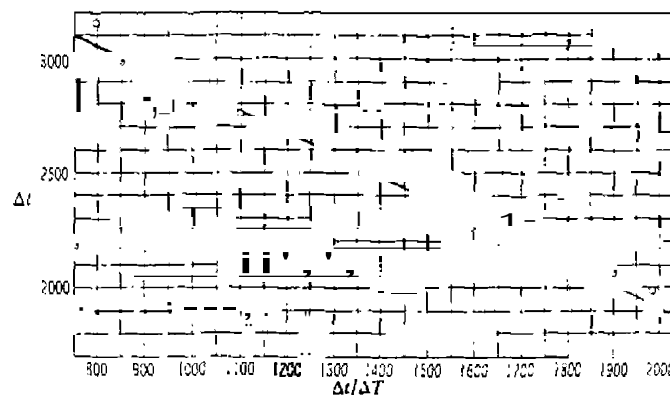


Figure 10.9. Derived line of Δt versus $\Delta t/\Delta T$ for naphthalene + 1.45 mole-% biphenyl (116)

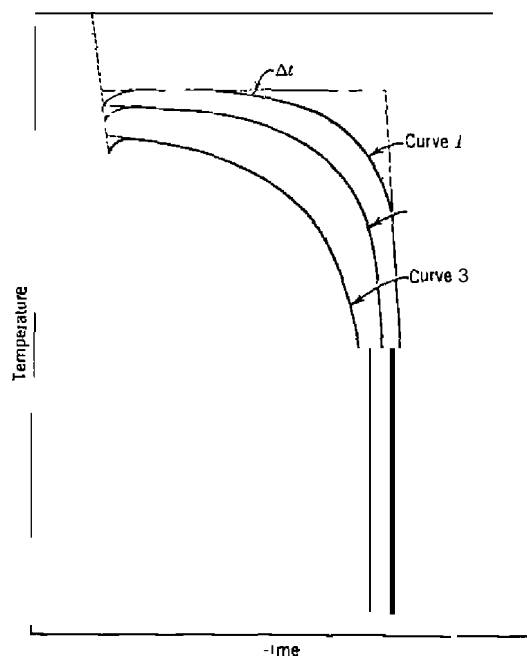


Figure 10.10. Temperature-time curves obtained in freezing experiments (33).

From the relationship

$$\frac{\Delta T_2 - \Delta T}{x_1} = \frac{\Delta T_2 - \Delta T}{x_2} \quad (10.31)$$

the amount of contaminant originally present, x , can be given by

$$x = \frac{x_2 \Delta T}{\Delta T_1 - \Delta T} \quad (10.32)$$

The experiments are carried out in duplicate or triplicate and the standard error computed. The standard error was found to vary from sample to sample, but the mean of several results indicated a value of approximately $\pm x/8$ for this quantity.

If this technique is used, it is important to choose a suitable substance to add to the system. In general, the melting point of this material should not be

higher than the melting point of the main material and should have a lower melting point. The chosen material should not form solid solutions, nor should it form a compound with the main component.

When a freezing curve is obtained, the values may vary at times, due to the nonlinearity of the temperature in the entire system, defects in the temperature detection, and so on. The determination of an actual curve to fit the experimental data presents a difficult problem. Various techniques, such as the use of a flexible spline, have been employed to draw this curve. An optical method, using a lantern projector, has been employed successfully by Saylor (34). Another method that has been suggested is that given by Kienitz (35). A hyperbola is constructed from certain values of time and temperature which best represent the measured curve. In this way, the freezing point of a sample is better obtained than with the analytical or geometrical methods of evaluation via three points on the equilibrium curve.

The purity of a n-pentane sample was determined by a calorimetric method by Clark et al. (20). The results obtained for pure n-pentane and for a synthetic n-pentane-iso-octane mixture are given in the resistance (temperature) versus time curve in figure 10.11. For purity determination, these data have been converted to the fraction melted after each equilibration period by allowing for the heat necessary to raise the temperature of the solid and liquid and for the amount of heat leak from radiation and conduction. The heat of fusion determined from this work was 2090 calories per mole, which gave a purity of 99.79 mole-% for the n-pentane.

To the sample of pure n-pentane, 2.40 mole-% of iso-octane was added. The melting curve so obtained showed considerable curvature, while that for the pure n-pentane was a straight line. From the slope of the line, a purity of 97.58 mole-% was obtained compared to a theoretical value of 97.53 mole-%.

The purity of two samples of pentaborane was also determined with this instrument. Sample I was 99.99 mole-% pure, while Sample II analyzed as 99.91 mole-%. When the two samples were mixed together to obtain a sample purity of 99.94 mole-%, the experimental calorimetric purity was 99.949 mole-%.

The purity of several highly reactive substances, such as titanium(IV) chloride, was obtained in a special freezing-point apparatus developed by Glasgow and Tenenbaum (28). The freezing point of titanium(IV) tetrachloride under saturation pressure with zero impurity was calculated to be -24.10 ± 0.01 T.

The thermal analysis of a number of normal alkanes was studied by Mazee (23). In the case of a binary mixture in which the components are completely miscible both in the liquid and solid states, the curves in Figure 10.12 were obtained. Curve (a) is the temperature-composition phase diagram, while

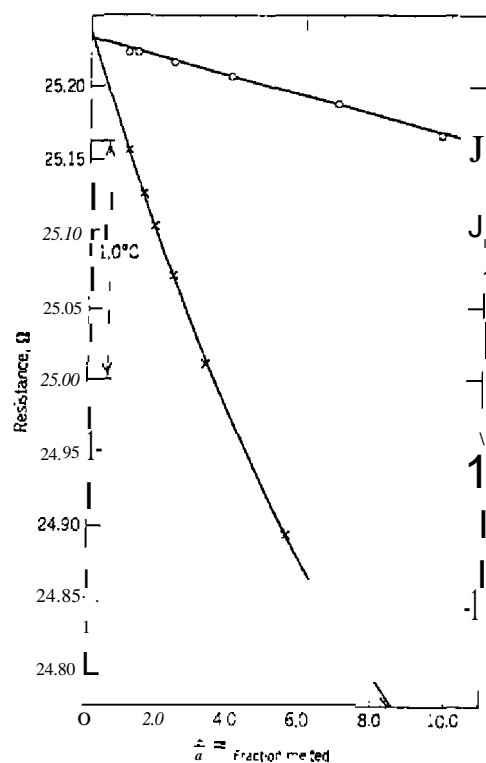


Figure 10.11. Melting curve for *n*-pentane (20). (O), *n*-pentane, 99.80% pure; (x) same — 2.26 mole-% *iso*-octane.

(b) is the heating curve so obtained on a 50-mole-% *n*-C₂₁H₄₄-50-mole-% *n*-C₂₃H₄₈ synthetic mixture. The heating curve is simple and easy to interpret and leaves no room for uncertainties. The amount of "impurity," in this case the amount of the second component, can be calculated with sufficient accuracy.

When certain organic salts, such as cyclohexylamine stearate, cyclohexylamine palmitate, and others, are melted, they undergo the probable double decomposition reaction

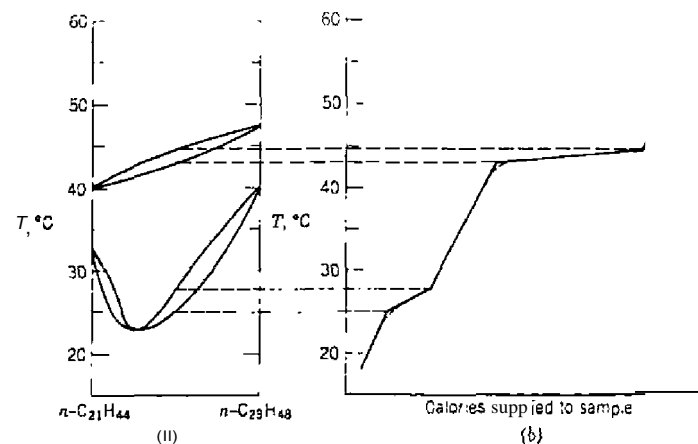
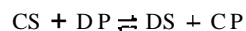


Figure 10.12. (a) *T*-*x* diagram of mixtures of *n*-C₂₁H₄₄ and *n*-C₂₃H₄₈; (b) heating curve for 50 mole-% *n*-C₂₁H₄₄ and 50 mole-% *n*-C₂₃H₄₈ (23).

where CS and DP are the amine salts. The system consisting of these four substances is a ternary system of the reciprocal or metathetical type. Systems of this type have been investigated by thermal analysis by Skau et al (36).

B. DIFFERENTIAL SCANNING CALORIMETRY METHODS

1. Introduction

In 1966, Gray (50) proposed a method for the determination of absolute purity of a compound using differential scanning calorimetry (DSC). This method was based on the fact that small amounts of impurity in the sample broadens its melting range and lowers the final melting point from T_0 , the melting point of the infinitely pure material, to a lesser temperature, T_m . An example of this effect is shown in Figure 10.13 for the DSC curves of benzoic acid of three different purities. As the impurity content increases (97.2%), the melting point decreases and the range of melting broadens. Very small impurity levels have a marked effect on the melting point and the melting range (98.6% primary standard). With proper sample preparation and instrument optimization, DSC is a rapid, accurate, and precise technique for the analysis of the purity of many different types of substances. It is estimated that over 75% of crystalline organic compounds can be analyzed by the DSC method if

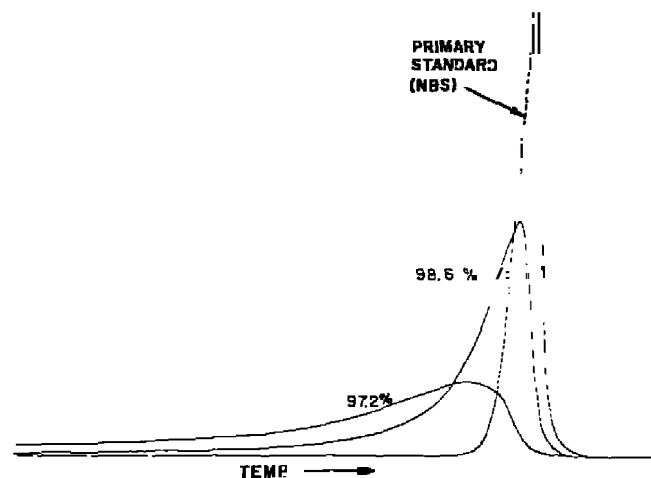


Figure 10.13. Effect of purity on the DSC melting-peak shape and melting temperature of benzoic acid (r).

they are sufficiently pure (4J). Because total impurity is measured, a relatively large experimental error does not appreciably alter the purity value in the first decimal place. Also, an experienced analyst can estimate the purity of an unweighed sample to within about 0.2 mole-% by visual inspection of the DSC curve produced in a 3-min. run.

A comparison between the DSC method (using the Perkin-Elmer DSC-1B instrument) and the pre-melting method of Johnston and Giaque (51) is shown in Table 10.3 (52). Johnston and Giaque (51) came to the conclusion that the nitric oxide used in their measurements contained less than 10^{-3} mole-% of eutectic impurities, or the so-called purity is of the order of 99.999%. The authors excluded the possibility of noneutectic impurities. It should be noted that the difference between the two methods is not in thermodynamics but rather in instrumentation and the properties of the methods of measurement. The disadvantage of the calorimetric method is the extremely long measurement time of 2-4 days, which is due to the large sample masses and the necessity for equilibrium to be attained at each temperature. The penalty for a shorter analysis time is, of course, a lower accuracy in purity measurements.

The DSC method for the purity determination of organic compounds has been extensively and critically reviewed by numerous authors. One of the most comprehensive reviews is that by Marti (52); others include those by

Table 10.3. Comparison of the Johnston and Giaque (51)-Pre-melting Method with the DSC Method (52)

Condition or Property Measured	Calorimetric Method of Johnston and Giaque (51)	DSC-1B* (Perkin-Elmer Corp.)
Weight of the sample	100 g	3 mg
Accuracy of the absolute temperatures	$\pm 10^{-2}$ K	$\pm 3 \times 10^{-1}$ K
Accuracy of the relative temperatures	$\pm 2 \times 10^{-3}$ K	$\pm 10^{-2}$ K
Accuracy of the measured heat of fusion	$\pm 2 \times 10^{-1}$	$\pm 5\%$
Accuracy in the purity value for high-purity substances	$\pm 10^{-3}\%$	$\pm 5 \times 10^{-2}\%$
Time for a pre-melting measurement	2-4 days	10 min

*DSC-1B refers to the instrument employed in the DSC measurements.

BarraH and co-workers (40, 42, 48); Joy et al. (41); Gray (50, 53, 54); Brennan et al. (55); Cisse et al. (56); Palermo and Chiu (57); De Angelis and Papariello (47); Plato and Glasgow (43); Plato (58); Staub and Perron (59); Brown (60); Gustin (61); Burroughs (62); and numerous others.

2. Principles of Measurement

All the DSC methods of purity determination depend on the applicability of the van't Hoff equation. This restricts the method to systems where the impurity forms a simple eutectic phase diagram with the major component; that is, the impurity or impurities are soluble in the melt and the components do not form solid solutions (53). Use of the van't Hoff equation assumes that the solution of impurity in major components above the melting point is an ideal solution in the thermodynamics sense. Also, the method assumes that the solid-liquid system is essentially in true thermodynamic equilibrium during the measurements. Failure to meet any of these conditions will lead to erroneous results. Other possible errors are associated with the instrumentation employed. This involves the use of the smallest possible sample size consistent with homogeneity (50), proper encapsulation to minimize temperature gradients within the sample, and the slowest possible heating rate to approach equilibrium conditions. It is recommended that the melting

curve *be* analyzed over a range of fraction melted from 10-50%, where the curve is least sensitive to gradients or lags in the instrument-sample system.

Brown (60) has reviewed the DSC method of purity determination in a comprehensive manner. A typical idealized DSC curve is shown in Figure 10.14. The fusion reaction is endothermic with T_0 the melting point (freezing point) of the sample with the area *ABC* proportional to the enthalpy of melting, ΔH_{melt} . As mentioned earlier, the presence of an impurity in the sample lowers the freezing point and broadens the melting range, giving a broader DSC curve peak such as is illustrated in Figure 10.15 (60). This illustrates a DSC curve of 0.01 mmol of an impure phenacetin sample at a heating rate of 1 K/min. The slope of *YB* is used to correct the programmed temperature, T_p to the sample temperature, T_s ($T_s = T_p - YW$). The freezing point is T_f and the area *ABC*, represents the enthalpy of melting, ΔH_{melt}^0 . The fraction melted, F_m , at temperature, T_m , is equal to area *AD*:area *ABC*. The maximum value of the apparent heat capacity of the sample is c_p .

A simple derivation of the van't Hoff equation has been given by Brown

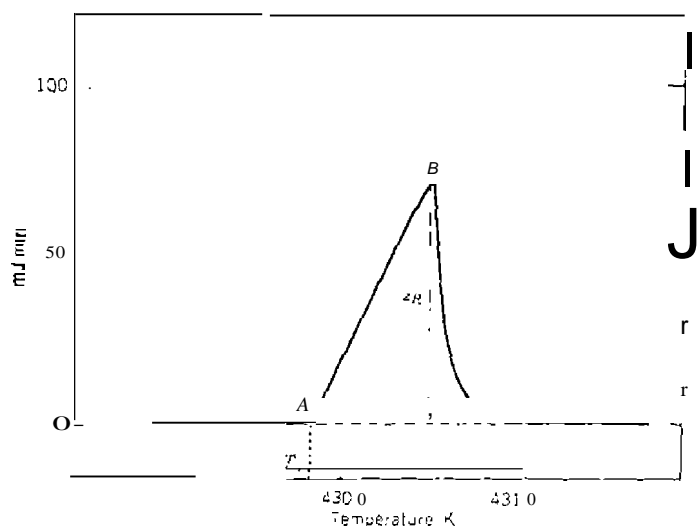


Figure 10.14 Idealized DSC curve of the melting of a pure substance at a heating rate, $\theta = 1 \text{ K min}^{-1}$. The slope of *AB* = $1/R\theta$ is used to correct the programmed T_p to the sample temperature, T_s . The area *ABC* represents the enthalpy of melting, ΔH_{melt}^0 . T_m is the maximum value of the apparent heat capacity, c_p is reference material.

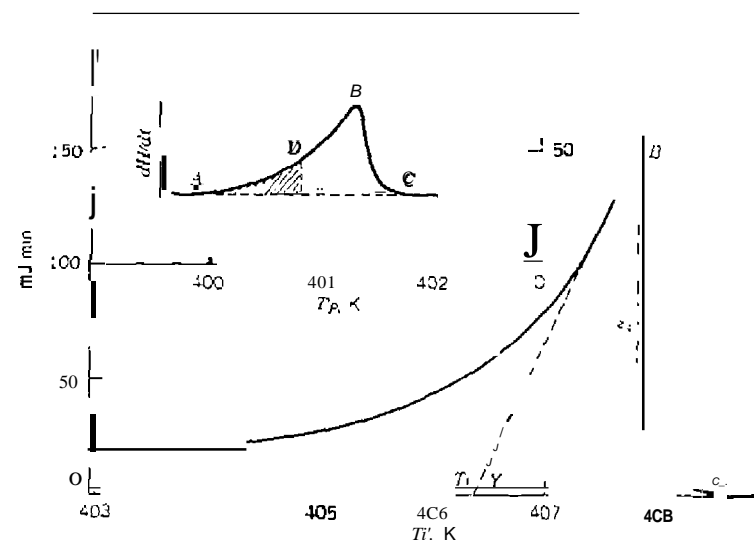


Figure 10.15 Idealized DSC curve of 0.01 mmol of an impure phenacetin sample at a heating rate of 1 K min⁻¹ (11).

(60). For a simple system in which a solid solution is not formed and an ideal solution in the melt is formed, the mole fraction of solute (impurity, component 2) in the solvent (component 1) is given by

$$x_2 = \frac{\Delta \bar{H}_{\text{melt},1}^0}{R} \left[\frac{1}{T} - \frac{1}{T_0} \right] \quad (10.33)$$

where T is the equilibrium melt temperature, T_0 is the freezing point of the pure solvent, and $\Delta \bar{H}_{\text{melt},1}^0$ is the standard molar enthalpy of melting of the pure solvent, assumed to be independent of temperature over the range. At the unique temperature $T = T_f$, the freezing point of the impure sample, the mole fraction of impurity is given by

$$x_2 = \frac{\Delta \bar{H}_{\text{melt},1}^0}{R} \left[\frac{1}{T_f} - \frac{1}{T_0} \right] = \frac{\Delta \bar{H}_{\text{melt},1}^0}{R} \frac{T_0 - T_f}{T_f T_0} \quad (10.34)$$

If the depression of the freezing point, ΔT_f , is small, $T_0 \approx T_f$ so that $T_0 T_f \approx$

T_0^* . Also,

$$x_2 = \frac{n_2}{(n_1 + n_2)} \approx \frac{mM_1}{1000} \quad (10.35)$$

where m is the molarity of solute and M_1 , the molar mass of the solvent. Then

$$\Delta T_f = \left[\frac{RT_0^*M_1}{\Delta \bar{H}_{\text{melt},1}^\theta (1000)} \right] m = K_f m \quad (10.36)$$

where K_f is the cryoscopic constant. These relationships apply to low impurity levels, $x_2 < 0.03$, that is, to the extremity of the liquidus curve of a simple eutectic phase diagram (60).

Only when the sample is completely melted, at $T > T_f$, is the mole fraction of impurity in the liquid, x_2 , the same as that in the original sample, x_2^* . Assuming a linear segment of the liquidus curve and using equation (10.33), one obtains

$$F = \frac{x_2^*}{x_2} = \frac{T_0 - T_f}{T_0 - T} = \frac{x_2^* R T_0}{\Delta \bar{H}_{\text{melt},1}^\theta (T_0 - T)} \quad (10.37)$$

which on rearrangement gives the van't Hoff equation:

$$T = T_0 - \left[\frac{x_2^* R T_0^2}{\Delta \bar{H}_{\text{melt},1}^\theta} \right] \frac{1}{F} \quad (10.38)$$

If F can be determined at various temperatures, T , a plot of T versus $1/F$ should yield a straight line, provided that $\Delta \bar{H}_{\text{melt},1}^\theta$ is independent of temperature. The quantity, x_2^* , can be determined from the slope of the resulting curve if values for T_0 and $\Delta \bar{H}_{\text{melt},1}^\theta$ are known.

3. The DSC Curve

Brown (60) also discussed the DSC melting curve. The output of the DSC is proportional to the heat capacity of the system, dH/dT , or

$$\frac{dH}{dt} = \frac{dH}{dT} \frac{dT}{dt} = \dot{\phi} \cdot \frac{dH}{dT} \quad (10.39)$$

where dH/dt is the thermal energy transfer to or from the sample as the temperature of the sample holder, T , is changed at a constant rate, $dT/dt = \dot{\phi}$.

For an absolutely pure compound with zero melting range, dH/dT would become infinite at the melting point, T_0 . For an impure compound, dH/dT is finite and a function of T .

When the fraction melted, F , is zero, the apparent heat capacity of the sample is that of the solid mixture, and when $F = 1$ the apparent heat capacity of the sample is that of the ideal solution. Intermediate behavior is obtained from

$$\frac{dH}{dT} = \frac{dH}{dF} \frac{dF}{dT} \quad (10.40)$$

where dF/dT is obtained from equation (10.37) as

$$\frac{dF}{dT} = \frac{x_2^* R T_0^2}{\Delta \bar{H}_{\text{melt},1}^\theta (T_0 - T)^2} \quad (10.41)$$

Assuming that

$$H(F) = \Delta \bar{H}_{\text{melt},1}^\theta \cdot F \quad (10.42)$$

and therefore

$$\frac{dH}{dF} = \Delta \bar{H}_{\text{melt},1}^\theta \quad (10.43)$$

combining these results yields

$$\frac{dH}{dT} = \frac{x_2^* R T_0^2}{(T_0 - T)^2} \quad (10.44)$$

This equation gives the variation of the apparent heat capacity of the sample during melting, as a function of T . The upper limit of the melting process is $T = T_f$ (when $F = 1$). The lower limit of the melting process is $T \ll T_0$, when

$$\frac{dH}{dT} \approx x_2^* R = C_p \quad (10.45)$$

Since dH/dt is proportional to dH/dT , plots of dH/dT against T represent the initial part of the idealized DSC melting curve.

The real DSC melting curve, because of factors such as thermal lag, looks more like the inset in Figure 10.15. The range of F values used in practice is usually restricted to $0.1 < F < 0.4$. Even in this restricted range, the linearity of plots of T against $1/F$ is often poor. Corrections must be made for thermal lag (49) and undetected premelting.

4. Thermal Lag and Undetected Premelting

The flow of thermal energy from the sample holder at the programmed temperature, T_p , to the sample at a slightly lower temperature, T_s , is governed by Newton's law of cooling (60).

$$1/F \cdot T_s = \frac{dH}{dt} R_0 \quad (10.46)$$

R_0 may be obtained from slope AB in Figure 10.16 by use of the relationship

$$\frac{d}{dT} \left(\frac{dH}{dt} \right) = \frac{1}{R_0} \quad (10.47)$$

The value of R_0 is then used graphically to correct the programmed temperature, T_p , to the true sample temperature, T_s . The latter is then plotted against $1/F$ in the van't Hoff equation.

Even with correction for thermal lag, the linearity of the plots of T_s against $1/F$ is not good (60). Melting actually begins at the eutectic temperature which may be far below the range of temperatures being examined. Corrections thus have to be made to the measured areas for melting that has occurred at lower temperatures and that is difficult or impossible to measure. Brown (60) has shown that the correction may be estimated from

$$1/F_n = \frac{(A + \epsilon)}{(a_n + \epsilon)} \approx \frac{A}{(a_n + \epsilon)} \quad (10.48)$$

where a_n is the partial area up to temperature T_n , A is the total area, and ϵ is a parameter whose value is adjusted so that a plot of T_s against the corrected $1/F$ is linear. The restraints are that the final value of $(A + \epsilon)$ should correspond to the correct value of ΔH_{melt}^0 (if known) and that the value of T_0 should be correct. The correction, ϵ , may be quite large and values of ϵ as much as 30% of the total area are not uncommon. Obviously, the approximation, $(A + \epsilon) \approx A$ cannot be used.

Another correction in the DSC curve is that of the baseline shift due to

heat capacity change (47, 50). The effect of this small correction is illustrated on the DSC curve of cyclohexane as shown in Figure 10.16a. The correct sample temperature, T_s , is the curve extrapolated to a true baseline (44). A small-area measurement (ABCD) must be added to the partial area under consideration. A typical pier of T_s versus $1/F$ is illustrated in Figure 10.16b. The raw data, as shown in the curve, do not define a straight line (44). This is because some peak area is missed before the instrument deviates measurably from the baseline due to the noise levels and sensitivity involved. That-and-error additions of small increments to both the partial area and the total area are carried out until a straight line is obtained.

One of the most serious limitations of the method is the assumption that no solid solutions are formed. For solid solution systems (63, 44)

$$T_s = T_0 - \frac{RT_0^2 X}{\Delta H_f} \cdot \frac{1}{K(1-K) + F} \quad (10.49)$$

where the distribution ratio of the impurity between the liquid and solid phases is $K = k/k'$ and is zero in the absence of solid-solution formation. There is no criterion, however, that permits solid solutions to be detected in the DSC curve.

Other linearization methods have been described by Sondack (63) and Wiedemann and Riesen (64). These methods are based on adding constant K to the total or partial areas

$$\frac{1}{F} = \frac{A_{\text{tot}} + K}{A_{\text{part}} + K} \quad (10.50)$$

by iterative linearization or simultaneous multiple linear regression (MLR). These graphical methods are shown by the curves in Figure 10.17 (64). In the MLR method, the equation is rearranged in a linear manner such as

$$A(T) = -K - T_0 \cdot \frac{AT}{T} + \left(T_0 K - \frac{RT_0^2 m}{M} \right) \frac{1}{T} \quad (10.51)$$

$$Z = a + b \cdot x + c \cdot y$$

The resulting equation gives the linear form Z as a function of x and y . One experiment gives a set of values for Z , x , and y , which permits the calculation of a , b , and c to give the best fit of the curve. Constant a gives the linearization constant, b determines the melting point of the pure substance, T_0 , and thus the impurity, x_2^0 , can be calculated from c . The total area need not be

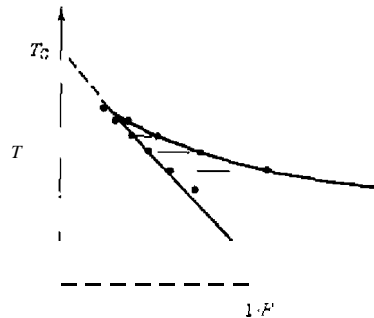
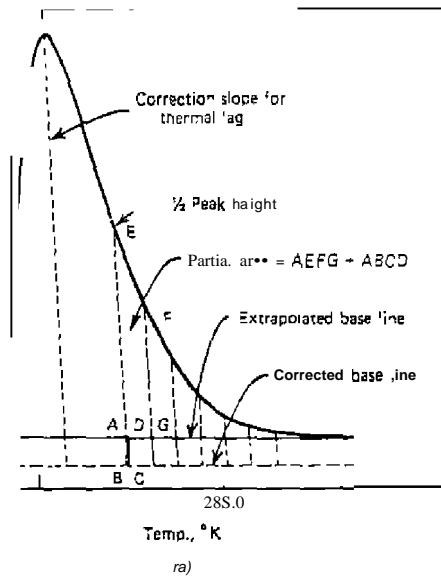


Figure 10.17. Linearization methods on the variable Hoff equation (5).

determined, hence, substances that decompose immediately after melting can still be measured using only the first portion of the curve.

Staub and Perron (65) proposed that instead of continuously heating the sample, heat is applied in steps until melting has been completed. This is similar to the older static method, but with smaller samples and shorter times. A typical stepwise heating curve is illustrated in Figure 10.18 (57). A temperature interval, say, 0.5 K, is selected, and heat is applied until the furnace temperature has increased by this amount. The heating is stopped and the curve permitted to return to the baseline. If no melting has occurred, an essentially constant area results from the difference in heat capacity between the reference and the sample. When melting occurs, this area increases and after correcting for background area, the isothermal step temperature, T_s ,

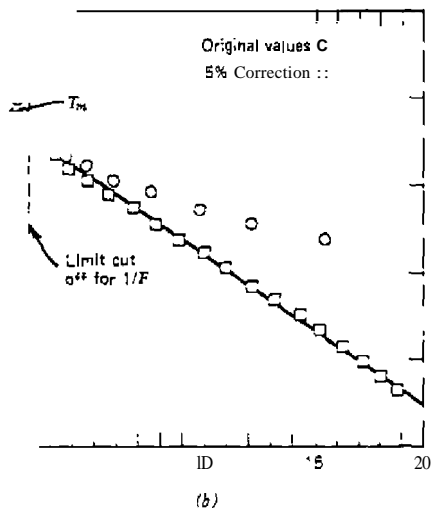


Figure 10.18. Stepwise heating method. Heating rate 5°C/min for 6 sec to obtain a ΔT of 0.5°C (8).

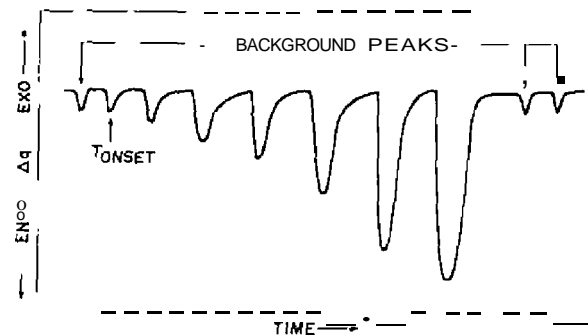


Figure 10.18. Stepwise heating method. Heating rate 5°C/min for 6 sec to obtain a ΔT of 0.5°C (8).

is plotted versus lIF to obtain the mole-% impurity. The heat of fusion is calculated by summing all the areas. Usually no correction is necessary to obtain linear T_i versus lIF plots. Staub and Perron (65) claimed that the nonlinearity in this curve results from an absence of thermodynamic equilibrium. Palermo and Chiu (57) believe that this is not true; they think that it is due mainly to instrument insensitivity. Gray (53) has also pointed out that this does not appear to be the case and suggests equations for its correction.

Ramsmond (66) described a modified expression for the van't Hoff equation that does not apply the usual approximations to the mole fraction impurity and T_0 and T_i . The new derived equation is

$$T_i = T_0 - \frac{RT_i T_0}{\Delta H_f} \ln \left[\frac{KX_1' - KF + F}{x_1' - 1 + K + F - KF} \right] \quad (10.52)$$

where K is a partition coefficient defined to be

$$K \equiv \frac{X_1^s}{X_2^s} \quad (10.53)$$

and X_1' is the mole fraction of component 1 in the original sample. Solving for T_i gives

$$T_i = \left(\frac{T_0}{(1 + RT_0/\Delta H_f)} \right) \ln \left[\frac{KX_1' - KF + F}{x_1' - 1 + K + F - KF} \right] \quad (10.54)$$

Procedures for solving for X_1' , K , and T_0 are given using an iterative, multiple regression method.

5. Experimental Measurements

To obtain usable data from DSC measurements, Barrall and Diller (42) recommended the following guidelines:

1. The sample size must be less than 3 mg.
2. The heating rate must be less than 1.25°/min.
3. The encapsulation in a volatile sample sealer must be modified to maintain good thermal contact.
4. The precise calibration of the temperature axis must be made. The area considered for lIF calculation must start at the first detectable

melting and finish with a point at the endothermic minimum and contain at least six points.

5. The heating rate and sample size must be adjusted so that the slope of the endotherm never exceeds the slope of the pure standard at half the peak height of the standard.
6. The thermal lag must be measured with a standard that melts near the sample.

Palermo and Chiu (57) recommended sample sizes from 2-4 mg; 5 mg sample sizes result in thermal equilibrium not being maintained. Heating rates should be less than 1°C/min; faster heating rates, up to 10°C/min, have been used for qualitative comparison, unstable compounds, or extremely broad melting peaks. If thermal equilibrium is maintained and a solid solution is not formed, curvature of the T_i versus l, F plot may result from the insensitivity of the instrument to detect early melting. To remove this curvature, a constant is added to the fractional and total areas until linear plots are obtained. This may be accomplished either manually or with a computer. The most common limits for lIF in the linearization procedure are 10-50% of the melt. If too little of the curve is used, the purity value will be too high; and if too much is used, the purity value will be too low.

The effect of sample size on the purity determination of benzene containing known amounts of cyclohexane is shown in Table 10.4 (57). With small samples, the method is accurate to about 1 mole-% impurity. With larger samples, thermal equilibrium is not easily maintained, especially for low-

Table 10.4. Dynamic DSC Method with Time-sharing Computations—Benzene-Cyclohexane Series (57)^a

Sample Size (mg)	Known Mole % Cyclohexane	Obtained Mole % Cyclohexane
2.2	<0.10	0.05
	0.64	0.61
	1.24	1.14
7.8	2.32	1.71
	<0.10	0.07
	0.64	0.62
	0.83	0.76
	1.24	0.96

^aHeating rate: 0.5°C/min. l, F limits: 2-10 (10-50% melt); scan rate: 1 point/3 sec; N : flow: 15 ml/min.

purity samples. Large sample size and high-heating rates are known to decrease the applicable purity range.

Brown (60) described the procedure for purity determination in the flowchart shown in Figure 10.19. Computer programs for these calculations have been described by a number of investigations and also are available for commercial instruments. A detailed procedure is outlined by Brown (60).

6. Applications

Differential scanning calorimetry as a purity determination technique has been applied to a large number of substances (41). Compounds studied include aliphatic hydrocarbons (44), amides, amines, and carbamates (43, 51), benzene derivatives (43,51,52), halogenated compounds (41,43,44), malic acid (52), organophosphates (43), pesticidal chemicals (43), pharmaceuticals (51, 52), steroids (52), benzoic acid (41), polycyclic hydrocarbons (41), urea (41), cholesterol (41), liquid-crystal-forming materials (46, 53, 54), and numerous others. *One* such investigation (43) determined the purity and heat of fusion of 95 high-purity organic compounds.

The estimation of purity of pharmaceutical compounds is one of the most important aspects of a drug profile (67). Use of the *Dse* method has significantly decreased the time necessary for such an analysis.

Impurities in liquid crystal materials can induce the appearance of a mesophore where none exists in a purer sample, or can inhibit the formation of a mesophore that would be present (68). Small amounts of impurity may broaden and shift the mesophore transition to lower temperatures by several degrees. Hence, the DSC method is useful for the determination of liquid crystal purity.

Marti (52) has reported his experience in analyzing over 10,000 melting curves for about 500 different compounds.

Joy et al. (41) compared the purity determination results obtained by *DSC* with those obtained by gas chromatography (*Ge*) and titrimetric assay values. For a number of polycyclic hydrocarbons purified by multipass zone refining followed by simple sublimation, the results obtained by *Dse* and *Ge* assay are given in Table 10.5. As can be seen, in most cases, the agreement between the two methods is good considering the quite different underlying phenomena. It should be noted that a value of 99.99 area-% was assigned for the *GC* assay whenever no impurity peak was detected.

A correlation of the purity determined by *DSC* and by the phase solubility method for several pharmaceutical samples is given in Table 10.6 (69). The correlation between these two methods is quite good. Seven independent determination of the purity of estradiol dipropionate sample gave a standard deviation of 0.04% purity.

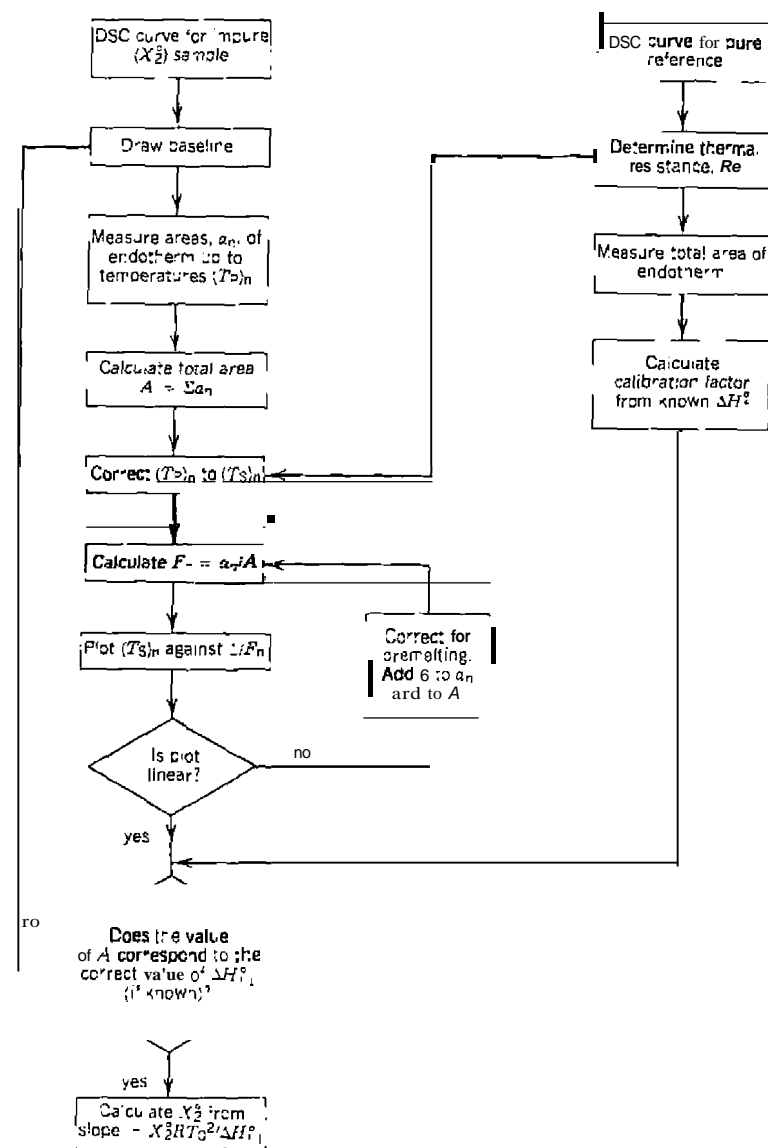


Figure 10.19. Flowchart representing the procedure used in purity determination by DSC: II.

Table 10.5. Comparison of GC Assay and DSC purity Values for Some Zone-refined Hydrocarbons (41)

Compound	J. T. Baker ULTREX Lot No.	GC Assay (area-%)	DSC Purity (mole-%)
Acenaphthene	UHC 322	99.99 (1701)	99.99; 99.99
Anthracene	UHC 123	99.99 (220)	99.95; 99.96
Bibenzyl		98.24(125)	99.97; 99.96
Biphenyl	UHC 124	99.99(1701)	99.99; 99.96
Durene	UHC 325	99.99 (75)	99.96; 99.98
Naphthalene	UHC 126	99.99 (140)	99.96; 99.93
	UHC 327	99.99 (140)	99.99; 99.97
Phenanthrene		99.99 (210)	99.75; 99.77
		99.99 (210)	99.71; 99.92
Pyrene	UHC 328	99.97 (250)	99.94; 99.94
	UHC 129	99.99 (250)	99.97; 99.98
Trans-Stilbene		99.97 (200)	99.97; 99.94
p-Terephenyl	UHC 310	99.99 (240)	99.97; 99.96

Table 10.6. Correlation of Purity Data from DSC and Phase Solubility (69)

Sample	DSC (%)	Phase Solubility (%)
Estradiol dipropionate, NF	99.33	99.2
Estradiol cypionate, NF	99.91	99.9
Chlorpheniramine maleate, USP	99.4	99.6
Dexchlorpheniramine maleate, NF	98.3	98.4
Methsuximid, NF	99.96	100.4

The DSC method for calculating purity is not universally applicable to all compounds. The material being studied should not undergo decomposition during melting. The DSC curves in Figure 10.20 represent cases in which the DSC purity method should not be applied (70).

7. Assessment

In view of its rapidity, use of milligram quantities of samples, and application to the purity region from 98.0-99.95 mole-% DSC is a most valuable tool for characterization of organic compounds (41). For a thermally stable compound, a low-purity value, based on a satisfactory run of the instrument, is

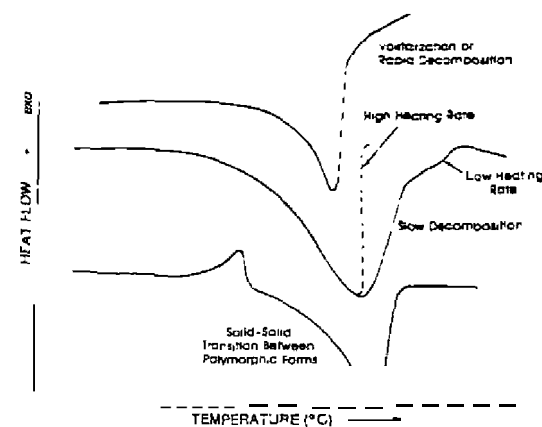


Figure 10.20. DSC curves of compounds that should not be studied by the DSC purity method (21).

clear evidence that the compound is not of high purity. In contrast, a high-purity value cannot be taken as conclusive evidence that the compound is indeed of high purity. Above 99.10 mole-% purity, the premelting behavior on which the DSC calculation is based, becomes progressively smaller and the purity value as assigned becomes strongly dependent on the assumption made in the calculation. The practical upper limit for absolute DSC measurements may therefore be about 99.95 mole-% with the presently available instrument and technique. However, it is possible to detect differences in impurity content of as little as 0.005 mole-%. If replicates are run, the relative purity of two lots of a single compound can be assessed up to 99.98 mole-%.

The lower limit of purity determination using the stepwise DSC method is about 95 mole-% without linearization and 92 mole-% with linearization (57). However, the time required is approximately 1-2 hours compared to about 30 min for the DSC method. Using only two peaks in the stepwise DSC method, the investigators concluded that this method could be used down to 90 mole-%. Palermo and Chiu (57) do not think that it can be used below this value because the van't Hoff approximation becomes invalid. The two-step method is independent of the heat of fusion and less time-consuming. It was cautioned that other analytical methods should always be used in conjunction with DSC methods, whenever possible. Once the applicability of the method is established, DSC may prove to be the most convenient one to use.

REFERENCES

1. Smit, W. M., *Z. Elektrochem.*, **66**, 779 (1962).
2. Sturtevant, J. M., in *Techniques of Organic Chemistry*, 2nd ed., A. Weissberger, ed., Vol. I, Part 1, Interscience, New York, 1949, p. 731.
3. Cines, M. R., "Solid-Liquid Equilibria of Hydrocarbons," in *Physical Chemistry of Hydrocarbons*, A. Farkas, ed., Vol. I, Academic, New York, 1950, Chap. 8.
4. Mathieu, M. P., *Acad. R. Belg. Classe Sci. Mem.*, **28**, No. 2 (1953).
5. Smit, W. M., *Thermal Analysis*, Elsevier, Amsterdam, 1959.
6. White, W. P., *J. Phys. Chem.*, **24**, 393 (1920).
7. Andrews, D. H., G. T. Kohmann, and I. Johnston, *J. Phys. Chem.*, **29**, 914 (1925).
8. Skau, E. L., *J. Am. Chem. Soc.*, **57**, 243 (1935).
9. Mair, B. L., A. R. Glasgow, and F. D. Rossini, *J. Res. Natl. Bur. Stand. (U.S.)*, **26**, 591 (1941).
10. Glasgow, A. R., A. J. Streiff, and F. D. Rossini, *J. Res. Natl. Bur. Stand. (U.S.)*, **35**, 355 (1945).
11. Maioletaux, R. N. M. A. and J. Straub, *Rec. Trav. Chim.*, **52**, 275 (1933).
12. Thomas, S. B., and O. S. Parks, *J. Phys. Chem.*, **35**, 2091 (1931).
13. Rossini, F. D., *Chemical Thermodynamics*, Wiley, New York, 1950.
14. Mastrangelo, S. V. R. and R. W. Dornte, *J. Am. Chem. Soc.*, **77**, 6200 (1955).
15. Badley, J. H., *J. Phys. Chem.*, **63**, 1991 (1959).
16. Carleton, L. T., *Anal. Chem.*, **27**, 845 (1955).
17. McCullough, J. P., and G. Waddington, *Anal. Chim. Acta*, **17**, 80 (1957).
18. Glasgow, A. R., G. S. Ross, A. T. Horton, D. Enagorio, D. D. Dixon, C. P. Saylor, G. T. Furukawa, M. L. Reilly, and J. M. Henning, *Anal. Chim. Acta*, **17**, 541 (1957).
19. Stull, D. R., *Anal. Chim. Acta*, **17**, 133 (1957).
20. Carke, I. T., II. I. Johnston, and W. De Sorbo, *Anal. Chem.*, **25**, 1156 (1953).
21. Astor, I. G., and H. L. Fink, *Anal. Chem.*, **19**, 218 (1947).
22. Pilcher, G., *Anal. Chim. Acta*, **17**, 144 (1957).
23. Mazec, W. M., *Anal. Chim. Acta*, **17**, 97 (1957).
24. Ruchwein, R. A., and H. M. Huffman, *J. Am. Chem. Soc.*, **65**, 1620 (1943).
25. Smit, W. M., and G. Kateman, *Anal. Chim. Acta*, **17**, 161 (1957).
26. Smit, W. M., *Chem. Weekbl.*, **36**, 750 (1939).
27. Smit, W. M., *Rev. Trav. Chim.*, **75**, 1309 (1956).
28. Glasgow, A. R., and M. Tenenbaum, *Anal. Chem.*, **28**, 1907 (1956).
29. Hancey, R., *Anal. Chim. Acta*, **17**, 115 (1957).
30. Barnard-Smith, E. G., and P. T. White, *Anal. Chim. Acta*, **17**, 125 (1957).
31. Smit, W. M., *Anal. Chim. Acta*, **17**, 23 (1957).
32. Schwab, F. W., and E. Wichers, *Temperature—Its Measurement and Control in Science and Industry*, Reinhold, New York, 1941, p. 256.
33. Herington, E. F. G., *Anal. Chim. Acta*, **17**, 151 (1957).
34. Saylor, C. P., *Anal. Chim. Acta*, **17**, 36 (1957).
35. Kienitz, H., Ref. 34, p. 43.
36. Skau, E. L., F. C. Magne, and R. R. Mod, Ref. 34, p. 107.
37. Gunn, S. R., *Anal. Chem.*, **34**, 1292 (1962).
38. Glasgow, A. R., and G. S. Ross, in *Treatise on Analytical Chemistry*, I. M. Kolthoff and P. I. Elving, eds., Vol. 8, Part I, Interscience, New York, 1968, p. 4991.
39. Skau, E. L., and J. C. Arthur, in *Physical Methods of Chemistry*, A. Weissberger and B. W. Rossiter, eds., Vol. 1, Part V, Wiley-Interscience, New York, 1971, p. 105.
40. Barrall, E. M., and J. F. Johnson, in *Purification of Inorganic and Organic Materials*, M. Zief, ed., Marcel-Dekker, New York, 1969, p. 77.
41. Joy, E. F., J. D. Ilonn and A. I. Barnard, *Thermochim. Acta*, **2**, 57 (1971).
42. Barrall, E. M., and R. D. Kiner, *Thermochim. Acta*, **1**, 509 (1970).
43. Plato, C., and A. R. Glasgow, *Anal. Chem.*, **41**, 330 (1959).
44. Driscoll, G. L., J. N. Duling, and F. Magnotta, in *Analytical Calorimetry*, R. S. Poner and I. M. Johnson, eds., Vol. 1, Plenum, New York, 1968, p. 271.
45. Barrall, E. M., and M. J. Vogel, *Thermochim. Acta*, **1**, 27 (1970).
46. Reubke, R., and J. A. Moilica, *J. Pharm. Sci.*, **56**, 822 (1957).
47. DeAngelis, N. J., and G. J. Pappalardo, *J. Pharm. Sci.*, **57**, 1868 (1968).
48. Barrall, E. M., J. F. Johnson, and R. S. Porter, *Mol. Cryst.*, **8**, 27 (1969).
49. Ennulat, R. D., *Mol. Cryst.*, **8**, 247 (1969).
50. Gray, A. P., *Thermal Analysis Newsletter*, Nos. 5, 6, Perkin-Elmer Corp., Norwalk, CT.
51. Johnston, H. C., and W. F. Giaque, *J. Am. Chem. Soc.*, **51**, 3194 (1929).
52. Marti, E. E., *Thermochim. Acta*, **5**, 173 (1972).
53. Gray, A. P., *Thermal Analysis Application Study No. 3*, Perkin-Elmer Corp., Norwalk, CT.
54. Gray, A. P., and R. L. Fyans, *Thermal Analysis Application Study No. 10*, Perkin-Elmer Corp., Norwalk, CT.
55. Brennan, W. P., M. P. DeVito, R. L. Fyans, and A. P. Gray, *ASTM Symposium on Purity Determination by Thermal Methods*, Baltimore, MD, April 25, 1983.
56. Cisse, Z. P., Clechet, M., Coter, J., Delafontaine, and H. Tachoire, *Thermochim. Acta*, **2**, 357 (1971).
57. Palermo, F. E., and I. Chiu, *Thermochim. Acta*, **14**, 1 (1976).
58. Plato, C., *Anal. Chem.*, **44**, 1531 (1972).
59. Staub, H., and W. Perron, *Anal. Chem.*, **46**, 128 (1974).
60. Brown, M. E., *J. Chem. Educ.*, **56**, 30 (1979).
61. Gustin, G. M., *Thermochim. Acta*, **39**, 81 (1980).
62. Burroughs, P., *Anal. Proc. (London)*, **17**, 231 (1980).
63. Sondack, D. I., *Anal. Chem.*, **44**, 888 (1972).
64. Wiedemann, H. G., and R. Riesen, *Merriar Application No. 806*, Mettler Instrument Corp., Greifensee, Switzerland.
65. Staub, H., and W. Perron, *Anal. Chem.*, **46**, 128 (1974).
66. Ramslard, A. C., *Anal. Chem.*, **52**, 1474 (1980).
67. Daly, K. F., *Am. Lab.*, **1**, 57 (1975), p. 57.
68. Brennan, W. P., and A. P. Gray, *Thermal Analysis Application Study No. 13*, Perkin-Elmer Corp., Norwalk, CT.
69. *Thermal Analysis Application Brief, "i," 900B35*, February 1973, Du Pont Co., Wilmington, DE.
70. Blaine, R. L., *Thermal Analysis Application Brief No. 1A-80*, Du Pont Co., Wilmington, DE.

CHAPTER
11
MISCELLANEOUS THERMAL
ANALYSIS TECHNIQUES

A. INTRODUCTION

Although the principal *thermal* analysis techniques are thermogravimetry, differential thermal analysis, and differential scanning calorimetry (see Chapter I), there are a number of other thermal techniques, besides those discussed elsewhere in this book, that are useful for solving chemical and technological problems. Some of these methods are of recent development and hence little used at the present time, but they possess the potential for wider use in the future. Many of these techniques are employed to supplement or complement the three principal techniques of TG, DTA, and DSC, either in the simultaneous (single sample) or concurrent (multiple samples) modes.

Perhaps all the analytical techniques that produce temperature-dependent data may be classified as *thermal techniques*. If these data are obtained as a function of temperature, the list of techniques might include X-ray diffraction, UV-VIS-IR spectroscopy, nuclear magnetic resonance, electron spin resonance, electron diffraction, and so on. Obviously, space limitations prevent taking such a broad viewpoint of thermal analysis. Thus, only a few of the more important miscellaneous thermal techniques will be discussed here. They include thermomechanical methods (TDA, TMA, and DMA), thermoelectrometry, thermosonometry, thermomagnetic methods, accelerating rate calorimetry (ARC), and other related calorimetric methods (SEDEX). The discussion on each technique is necessarily brief since entire monographs could, and have in certain cases, been written on each of them. However, each section does provide an insight into the principles, instrumentation, and applications of the technique.

B. THERMOMECHANICAL METHODS

I. Introduction

The changes of volume, shape, length, and other properties relating to the physical shape of a substance constitute the broad area of thermal analysis

known as thermomechanical methods. Three techniques are commonly included that are related by expansion behavior and viscoelastic effect (1): they are *thermodilatometry (TDA)* or dilatometry; *thermomechanical analysis (TMA)*; and dynamic *thermomechanometry (DMA)*. The difference among these three techniques lies in their methods of measurement. In thermodilatometry, the sample is allowed to expand or contract under its own mass and no dimensional changes are measured. For thermomechanical analysis, a stress is applied to the sample that is nonoscillatory and the deformation under load is measured. In the last case, dynamic thermomechanometry or dynamic mechanical analysis, an oscillatory stress is applied to the sample and dynamic modulus and/or mechanical damping of the sample is/are measured. Thus, the three techniques involve the measurement of dimension, deformation, and dynamic modulus or damping under no-load or non-oscillatory or oscillatory load, all recorded as a function of sample temperature while the sample is being heated at a linear heating rate.

Daniels (1) has correlated the behavior of a sample with the three techniques in the following manner: In TDA, the bulk effect of the sample's molecular response to changes in thermal energy is measured. These changes involve crystal structure, lattice vibrations, and physical and chemical states, all of which can result in the change of length of a solid sample. Similar changes occur in TMA when measurements are made under an applied stress but changes in shape or size may result. These result from either dissipation of energy by relative motion of molecules (viscous response) or storage of energy, which is released on removal of the stress (elastic response). Thus, TMA response is a combination of expansion behavior and the viscoelastic effect. The viscous response is time-dependent but the elastic response is independent of time. Hence, the viscoelastic effect can be resolved into its two components by use of a "time probe," the frequency in DMA. The resulting stress in a sample under a continuous oscillatory load will be oscillatory also at the same frequency but will be out of phase with the stress by an amount that depends on the relative elastic and viscous responses.

Classical dilatometry or TDA is generally used to detect volume or length changes caused by phase transitions of various types. The most common phase transition that is determined is the *solid₁ → solid₂*, although *solid → liquid* and *solid → gas* transitions can be determined. The technique can also be used to detect shrinkage and sintering of a sample upon heating to elevated temperatures. The linear coefficient of thermal expansion of a sample can be determined; other uses include the determination of the glass transition temperature, T_g , softening temperatures, distortion temperatures, and so on. Temperature ranges employed vary from -150 to 2500°C, and the sample can be heated or cooled during the measurement.

Gray (29) discussed the recording of the derivative of the TMA curve, or

derivative thermomechanical analysis (DTMA). This mode of recording is of value particularly in expansion measurements. The variation in length of a sample as a function of temperature is commonly expressed by the equation

$$l = l_0(1 + \alpha T) \quad (11.1)$$

where l is the sample length at T , l_0 is the sample length at 0°C, T is the temperature in °C, and α is the linear coefficient of thermal expansion. In the TMA mode, l is recorded as a function of temperature, and in the absence of a phase transition and assuming α is constant, the curve will be a straight line with slope α . If equation [11.1] is differentiated with respect to time, the following expression is obtained:

$$\frac{dl}{dt} = l_0 \alpha \left(\frac{dT}{dt} \right) \quad (11.2)$$

where dT/dt is the heating rate and is constant. Thus, in the DTMA mode of thermal expansion measurements, the pen displacement is directly proportional to the coefficient of thermal expansion, and by appropriate calibration, it can be read directly from the curve. Also, a first-order transition would appear as a peak in the curve, the area of which is Δl .

TMA and DMA are widely used to study the properties of polymers and other materials under various experimental conditions in the temperature range from -200 to approximately 850°C. The former usually gives limited information on viscoelastic responses as well as dimensional changes, whereas the latter is concerned with viscous responses.

2. Instrumentation

a. TDA and TMA

Compared to many other analytical techniques, the instrumentation involved in TDA and TMA is quite simple. A large number of TDA instruments have been described in a book by Valentich (2). The instrumentation of TDA and TMA has been discussed by Wermlandt (3), Daniel (1), Paulik and Paulik (4), Gill (5), Riesen and Sommerauer (6), and others.

Changes in the dimensions of a sample are detected by a mechanical, optical or electrical transducer although the transducer is usually a linear variable differential transformer (LVDT). The sample may be positioned either vertically or horizontally. The latter usually introduces friction between the sample and the support tube, which may be reduced to acceptable levels but never totally eliminated (1). Vertical dilatometers overcome the prob-

lem of friction, but achievement of zero loading is difficult. The LVDT core must make light but positive contact with the sample and its mass must be counterbalanced by flotation or spring loading. In TMA, the vertical arrangement is easily adapted for use under applied loads. The stress may be applied in tension, flexure, compression, or torsion.

The Perkin-Elmer Model TMS-2 TMA apparatus is shown in Figure 11.1. The system consists of an analyzer module, analyzer control module, and heater control module. In penetration and expansion modes, the sample is placed on the platform of a quartz sample tube. The appropriate quartz probe

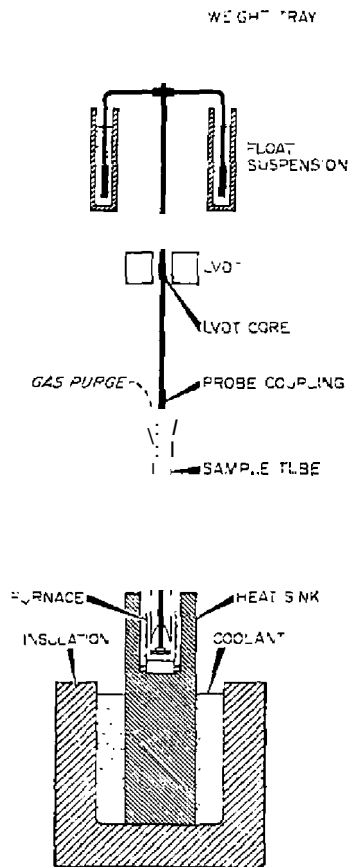


Figure 11.1. Perkin-Elmer TMS-2 TMA apparatus.

is fitted to the probe assembly which consists of a shaft upon which the LVDT core is mounted. Any change in position of the core in the annular space of the LVDT results in a change of voltage which can be recorded on a potentiometric or X-Y recorder (or computer data reduction system). The probe assembly includes a weight tray, which permits a choice of loadings on the sample surface. The entire assembly is supported by a plastic float rigidly fixed to the shaft and totally immersed in a high-density fluid. Using standard and optional furnaces, the temperature range of the system is -170 – 725°C . Sample probes for the system are shown in Figure 11.2. Probe (a), a flat tip of 0.140 in. in diameter is for coefficients of expansion. Probes in (b), flat and hemispherical tips, are for penetration and compressive modulus, respectively. Probe (c) is a wedge-tip probe and sample mount for flexural deformation and modulus measurements. Probe (d) is for tension studies of fibers and films, while probe (e) is a syringe-fit piston-cylinder for cubical coefficient of expansion of solids or liquids. An accessory, which permits deformation studies on drawn fibers, films, and so on, consists of a sample tube, sample clips, and a mounting tool. Samples of film are placed in a slot on the sample holder and clipped with a pliers.

The Mettler TMA 40 thermomechanical analyzer is illustrated in Figure 11.3. A measuring sensor applies a user-definable force to the sample of -0.05 – 0.5 N. The position of the sensor is continuously monitored by a LVDT. TMA measurements can be made in the temperature range -100 – 1000°C . This module is part of the Mettler TA 3000 thermal analysis system.

The Du Pont Model 943 TMA module is shown in Figure 11.4. The apparatus uses a LVDT to sense linear displacements of the sample probe. A thermocouple in direct contact with or in close proximity of the sample is used to detect the sample temperature. The sample and probe are surrounded by a temperature-controlled cylindrical heater and Dewar assembly. Various probe configurations allow the apparatus to be used in the expansion, compression, penetration, tension, stress relaxation, parallel plate rheometry, and fiber tension. The temperature range of the instrument is -180 – 800°C ; an optional furnace can be used to extend the range to 1200°C .

Two novel sample holders for the Du Pont apparatus are shown in Figure 11.5. In (a), volume coefficients of expansion can be determined, even of irregular shaped samples. A filling medium transfers the dimensional changes of the sample to the dilatometer probe. A film clamp assembly is shown in (b), which is used to secure a film sample and increase ease of operation (7, 8). The clamps slip over the fused quartz hooks of the tension probe after the film has been secured between them. Nominal sample size is 0.05×0.04 in. \times 0.0005 – 0.005 in. thick.

TMA instruments are also available commercially from Stanton Redcroft Ltd. and others. The Stanton Redcroft Model 791 can be used in the tempera-

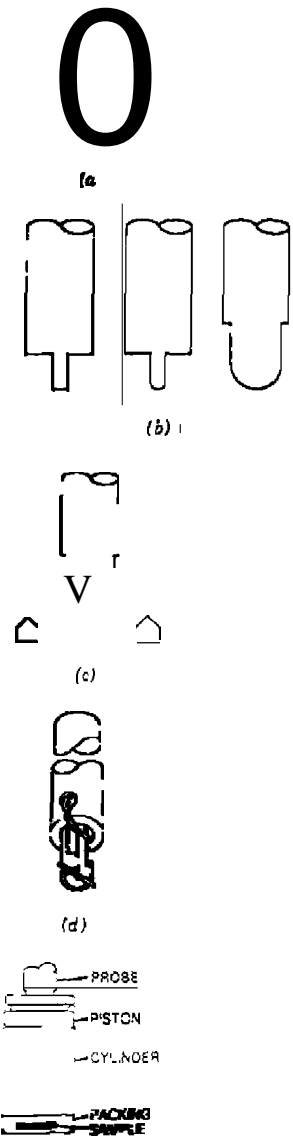


Figure 11.2. Perkin-Elmer TMA probes: (a) expansion; (b) compression; (c) flexure; (d) extension; (e) dilatometer.

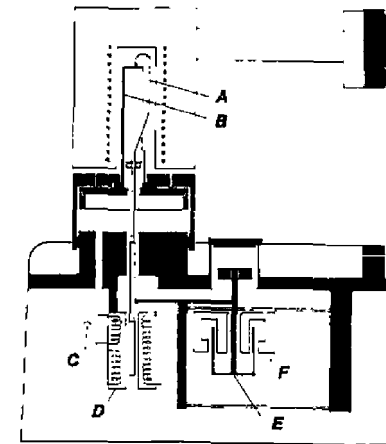


Figure 11.3. Mettler TMA 4Q-TMA apparatus: A, measuring sensor; B, sample support; C, purge gas inlet; D, linear variable differential transformer; E, linear motor coil; F, linear motor stator.

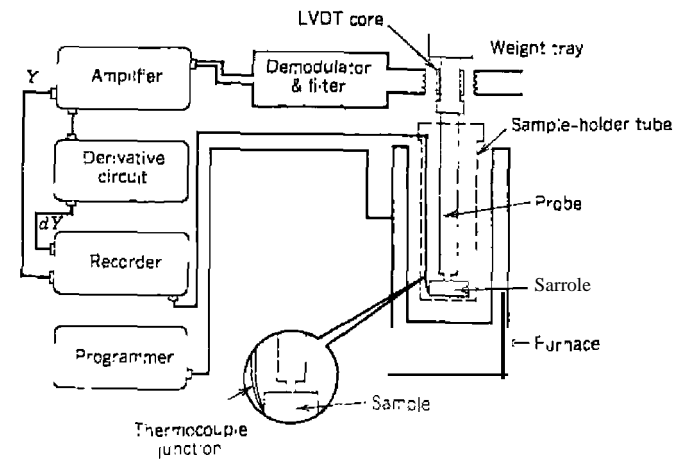


Figure 11.4. Du Pont Model 943 TMA module.

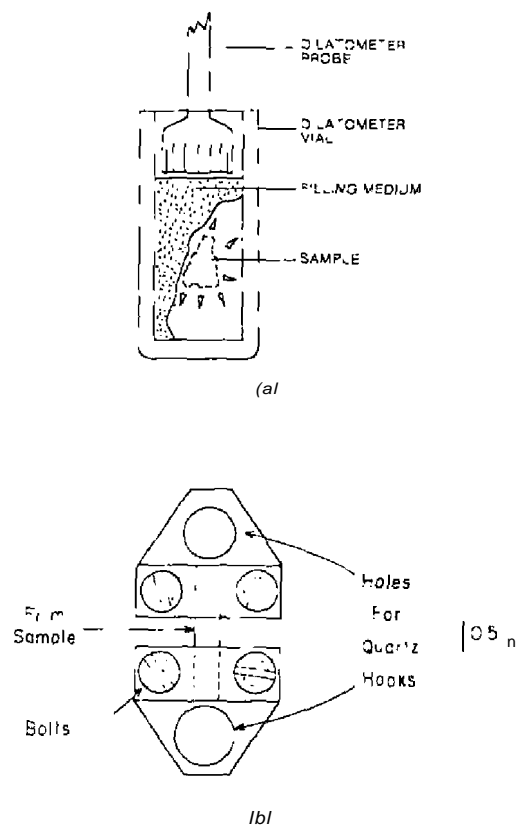


Figure 11.5. Two sample holders for Du Pont apparatus.

ture range $-180-500^{\circ}\text{C}$, whereas the Model 792 can be used from ambient room temperature to 1000°C .

b. DMA

DMA instruments use different principles to study the viscoelastic response of a sample under oscillatory load (1). They are: (1) the sample may be driven in forced oscillation or allowed to resume its natural frequency; (2) the stress may be applied in flexure, tension/compression, or torsion; and (3) the load may be applied continuously and the modified oscillatory re-

sponse of the sample measured. Numerous instruments have been designed to use the preceding principles, some of which are commercially available (1). In the free vibration instruments, the dynamic modulus is related to the natural frequency (maximum amplitude). This amplitude and peak width is related to the damping by

$$\text{Tan } \delta = \frac{\Delta f}{f} \tag{11.3}$$

where Δf is the peak width at maximum amplitude/ $\sqrt{2}$ and f is the resonant frequency. The Du Pont instrument applies a flexural stress of fixed amplitude to the sample. The modulus is related to the resonant frequency of the system and the damping to its power absorption. The torsional braid apparatus employs an intermittent stimulation by the application of a torsional strain. Decay of oscillation is measured, and the modulus related to the frequency of the oscillation and the damping to the decrease in amplitude.

The Du Pont Model 981 DMA apparatus is shown in figure 11.6. The sample arms are fixed to the rigid block via low-friction flexure pivots (9). A compound resonance system is formed by clamping the sample between the arms. The sample-arm-pivot system is oscillated at its resonant frequency by an electromechanical transducer. Frequency and amplitude of this oscillation are detected by a LVDT positioned at the opposite end of the active arm. The LVDT provides a signal to an electromechanical transducer, which in turn keeps the sample oscillating at constant amplitude. Sample resonant frequency, measured to 0.01 Hz, and damping, measured to 0.1 dB, are digitally displayed. Young's modulus, E , for the sample may be obtained

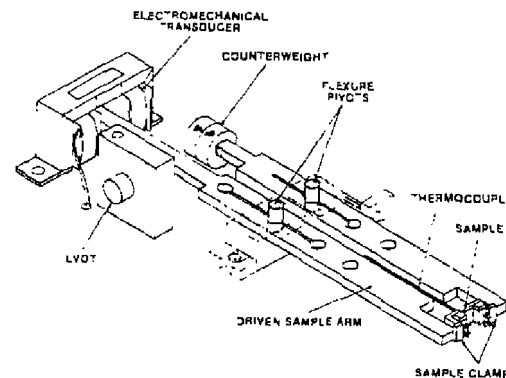


Figure 11.6. Du Pont Model 981 DMA apparatus

from the relationship

$$E = \frac{(4\pi^2 f^2 J - K)}{2w[L_r/2 - D]^2} \left(\frac{L}{T}\right)^3 \quad (11.4)$$

where j is the DMA frequency, J the moment of inertia of arm, K the spring constant of pivot, D the damping distance, W the sample width, T the sample thickness, and L the sample length. Specifications of the Du Pont DMA are given in Table 1U. The DMA module is used in conjunction with the Du Pont 1090 system.

A schematic diagram of the PI. DMA mechanical assembly is shown in Figure 11.7. In normal operation a bar sample is clamped rigidly at both ends and its central point is vibrated sinusoidally by the drive clamp. The stress experienced by the sample, via the ceramic drive shaft, is proportional to the current supplied to the vibrator. The strain on the sample is proportional to the sample displacement and is monitored by the nonloading eddy current transducer and the metal target on the drive shaft. The drive shaft is supported on light metal diaphragms that allow longitudinal but not lateral motion. Soft materials such as rubbers, adhesives, and fats can be measured in shear sandwich geometry by a special clamp. Films and fibers can be measured in bending by shortening the free length. Liquid polymers can be supported on films or absorbed into papers or braids, similar to the torsional braid method. The sample environment can be controlled with nitrogen, an inert gas, or controlled humidity air. Temperature of the sample area is detected by a platinum resistance thermometer.

Table 11.1. Specifications of DuPont DMA

Frequency Range and resolution	3-100 Hz \pm 0.01
Damping range	0.01-1.0 tan
Temperature range	-150-500°C (subambient temperatures require optional cooling accessory)
Heating rate	0.5-20°C min ⁻¹
Oscillation amplitude	0.05-1.0 mm (peak-to-peak)
Sample Size	0.01-1.6 mm. thickness 0.02-13 mm width 20-32 mm sample length 6-20 mm working length

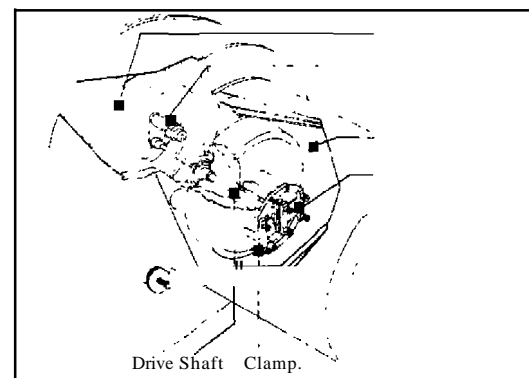


Figure 11.7. PI. DMA

3. Tors

The technique of *torsional braid analysis* (TBA) was introduced by Gillham (44,45). It permits thermomechanical "fingerprints" at particular temperatures in the temperature range -190 S(XYC in controlled atmosphere. The sample is prepared by impregnating a glass braid or thread with a solution of the material to be tested, followed by evaporation of the solvent. Upon the heating of the sample impregnated braid, it is subjected to sinusoidal oscillations. From these oscillations, the relative rigidity and damping index are used as a measure of the material's properties, where ρ is the period of oscillation, is used as a measure of rigidity, and $1/n$ is used as a measure of damping index, where n is the number of oscillations between two fixed boundary conditions in a series of waves. Changes in rigidity and damping index are interpreted as far as possible in terms of changes in the polymer. Major and secondary transitions, such as glass transitions, are readily revealed, as are the effect of many and degradative reactions. The technique has been the subject of a review by Gillham (10, 46).

The apparatus used in TBA is shown in Figure 11.8. The oscillation frequency (cps) and decay of the freely oscillating pendulum provide information on the modulus and mechanical damping of the polymer under test. An electrical analog of the decaying pendulum oscillation is used to attenuating light with a circular transmission disk, which varies the relationship between the light transmission and displacement.

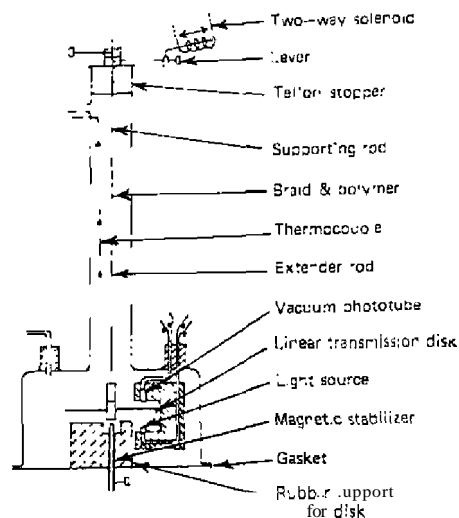


Figure 11.8. Torsional braid analysis apparatus (46).

4. Applications

a. TDA

According to Paulik and Paulik (4), TDA techniques have generally been neglected in thermal analysis yet they can provide useful information about changes occurring in the crystal structure of inorganic compounds, an area in which other TDA techniques have not been very useful. The TDA curve can reveal many processes occurring during the solid-state or decomposition reaction including crystal modification and recrystallization processes. One reason for this neglect is the difficulty in interpretation of the TDA curve, as in general it usually gives a more complicated picture than TG or DTA curves of the decomposition reaction. For example (4), in a thermal decomposition reaction, the sample decomposes and an amorphous or microcrystalline phase is formed. The recrystallization that usually follows is generally protracted and overlaps the previous process. DTA and TG indicate only the first process but TDA depicts both processes. Hence, TDA curves are frequently recorded simultaneously with TG, DTA, electrothermal, and emanation thermal analysis (ETA) techniques to aid in their interpretation.

TDA applications have been reviewed for inorganic compounds (4,11,13 clays (12), metallic glasses (14), metallurgy (15), ceramic science (16), and zeolites (17). Since numerous applications of this technique have been described, only a few illustrative examples will be discussed here.

The use of TDA to detect phase transitions (47) of various types of compounds are illustrated in Figure 11.9— $solid_1 \rightarrow solid_2$ phase transition

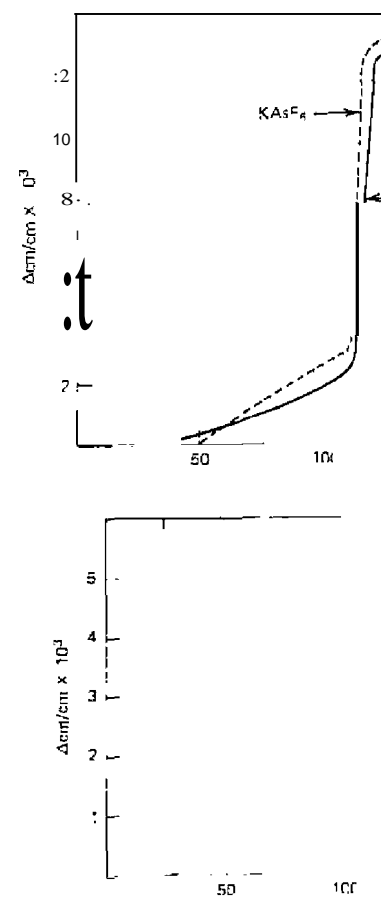


Figure 11.9. Same as

detected in $KAsF_6$, $KC_2H_3SO_4$, and $Co(py)_2Cl_2$; a decomposition reaction, $3AlCl_3 \cdot 2H_2O$ deaquation; and a *solid* \rightarrow *liquid* transition, the fusion of acetanilide.

Typical linear coefficients curves of aluminum, platinum, and Pyrex glass are shown in Figure 11.10. The loading on the probe is 5 g with various sizes of the samples indicated (18). Linear coefficients of thermal expansion for several metals and other substances, as determined by IDA, are given in Table 11.2 (19). Single crystals of the inorganic salts were used for all TDA measurements.

The quasi-isothermal dilatometric (QID) technique (13, 20) is useful for sintering studies since kinetic data, diffusion coefficients, as well as the optimum sintering conditions, can be determined by use of a single experiment. The sample is heated in a dilatometer at a constant rate until the dL/dt signal, which is proportional to the shrinkage rate, becomes larger than a preset limit, at which point the heating is stopped. Shrinkage then continues isothermally until the dU/dt signal again becomes smaller than a second preset limit, at which point heating is resumed. The whole sintering cycle takes place in isothermal segments at different temperatures as shown in Figure 11.11. The technique has been applied to the sintering of UO_2 pellets (20); the $Fe_2O_3 + ZnO$ mixture for spinel formation (13); and the thermal decomposition of $CaC_2O_4 \cdot 2H_2O$ and $BaCl_2 \cdot 2H_2O$ (13).

Simultaneous TDA curves with their corresponding TG and DTA curves are shown in Figure 11.12 (21). Kaolinite ($Al_2O_3 \cdot 2SiO_2 \cdot 2H_2O$) loses water between 400 and 800°C. At 950°C, a solid-state reaction occurs in which metakaolinite is first formed followed by the formation of mullite. In the

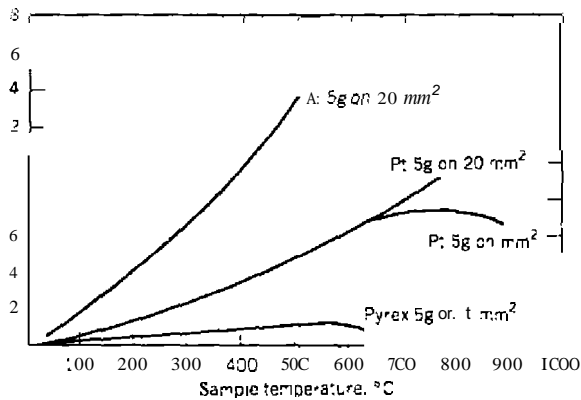


Figure 1.10. TDA curves of Al, Pt, and Pyrex glass (18).

Table 11.2. Linear Coefficients of Thermal Expansion (α) Determined by TDA (19)

Material	$\alpha \times 10^6 / ^\circ C$
Aluminum	22.5
Copper	16.6
Brass	23.8
Glass	7.6
NaCl	39.7
KCl	41.9
KBr	39.4
CaF ₂	22.0
SrF ₂	26.4
BaF ₂	23.9
Ni:	
(i) 30–180°C	39.0
(ii) 180–280°C	110.0

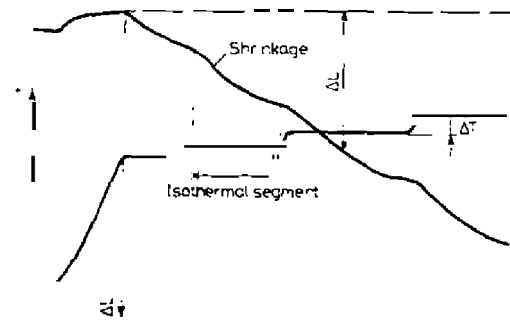


Figure 1.11. Principle of quasi-isothermal dilatometry (20).

case of $BaCl_2 \cdot 2H_2O$, water of crystallization occurs below 300°C which is followed by a recrystallization process which takes place from 350–850°C. Just before the substance fuses, an $\alpha \rightarrow \beta$ crystalline transition occurs at about 900°C.

TDA has provided useful information on the tempering process and the influence of individual alloying elements in steel (15). Complications arise due to the fact that while the decomposition of martensite produces a contraction, decomposition of any retained γ -iron is accompanied by expansion.

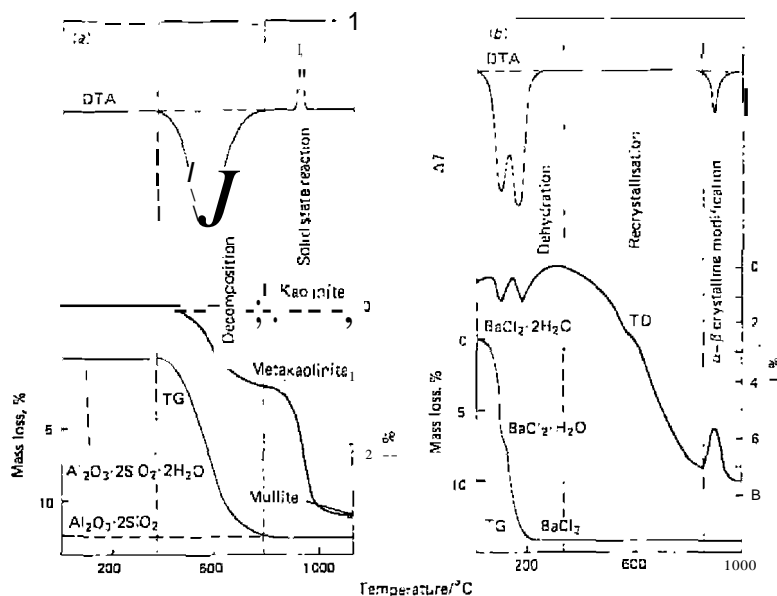


Figure 11.12. TDA and TG, DTA curves of (a) kaolinite and (b) BaCl₂ · 2H₂O (21).

sian. Secondary hardening that occurs on tempering can also be studied by this technique.

TDA is useful in ceramic materials development not only in ascertaining the expansion coefficient as such, but also in noting the gross volume changes that occur during the crystallization process (16). These act as a guide to phase changes and the influence they may have on processing variables such as heat-treatment rates and temperatures, as well as the ability to form *in situ* seals to other rigid materials without cracking. For measurement at very low coefficients of expansion, push-rod TDA is inadequate because the displacements to be measured are usually less than mechanical and thermal stability allows. An interferometric dilatometer accurate to several parts per million in thermal expansion must be employed.

b. TMA

Almost all the applications of TMA have been to polymeric systems. It is used to measure the thermal expansion characteristics of the polymer and hence to determine the glass transition temperature, T_g , a temperature at

which there is a characteristic increase in the thermal expansion coefficient (22). In practice, the T_g is a time-dependent phenomenon, and it is *atsD* dependent on the thermal history of the sample. It is a common practice to condition a sample above its T_g and then to quench it to a temperature well below the T_g to erase any "structure" in the glass resulting from any previous thermal history. Other uses include transition temperatures, modulus, viscoelastic properties, thermal stability, and liquid-solid interactions, as functions of temperature and time.

From penetration produced by a hemispherical quartz probe, Firsklin (23) showed that Young's modulus of the sample is given by

$$E = 3(1 - \nu^2)FRf/4H^3 \tag{11.5}$$

where ν is Poisson's ratio for the sample, F is the applied load, R is the radius of the probe tip, H is the sample height, and f is a polynomial function of the quantity Rd/H^3 , where d is the depth of penetration. The modulus of the probe must be much greater than the sample. With a cylindrical probe of radius equal to or larger than that of the sample, the compressive modulus can be obtained (24).

Reviews on the application of TMA to polymers include those by Miller (48), Chiu (25), Ogilvie (26), Barton (22), and numerous others. TMA has also been used to characterize oil shales (27) but its use in clay mineralogy appears to be slight (12).

A summary of TMA measurements on polymeric materials is shown in Table 11.3.

The thermoplastic melt viscosity can also be determined by TMA, using the Du Pont parallel plate rheometer accessory. Viscosity range of 10^2 - 10^8 poise can be measured with shear rates of 10^0 - 10^{-3} sec⁻¹. Viscosity data of polyethylene made by this method are shown in Figure 11.13 (29). Approximately 15 min are required to reach temperature equilibrium for a 60 mg sample.

Yanai et al. (30) demonstrated a definite correlation between data from Accepted ASTM methods and those obtained by TMA. These methods are the deflection temperature under load (DTUL) and the VICAT softening temperature. The DTUL is determined in the ASTM method by applying a load to the center of a sample that acts as a beam supported at both ends (31). The Young's modulus of this beam is calculated by

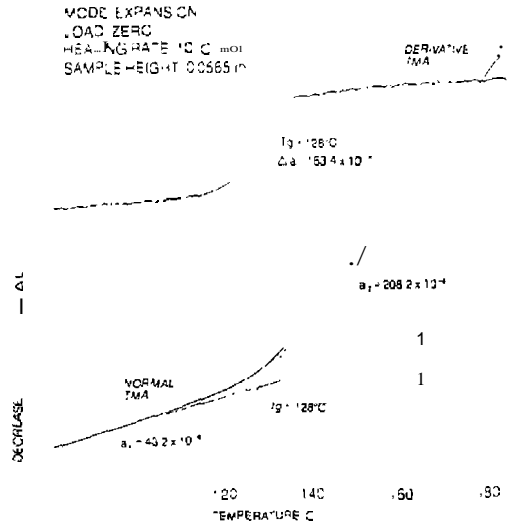
$$E = \frac{FL'}{4CD^3Y} \tag{11.6}$$

where C is the width of the sample, L is the length of the sample between beam supports, Y is the deflection of the sample under load, D is the thickness

Table 11.3. Types of TMA Measurements on Polymers (28)

TMA	Mode	Probe Type ^a	Sample	TMA Data
-----	------	-------------------------	--------	----------

Coefficient of linear expansion



Penetration

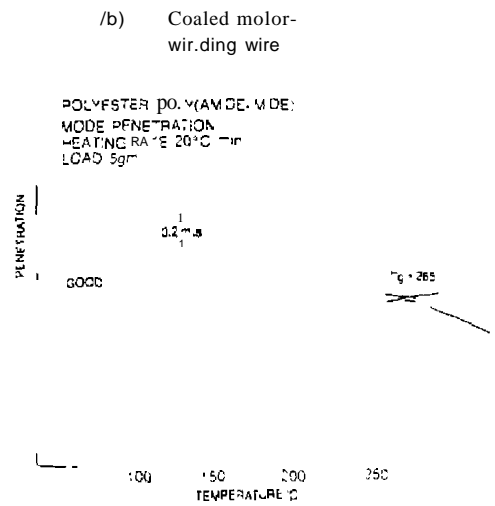
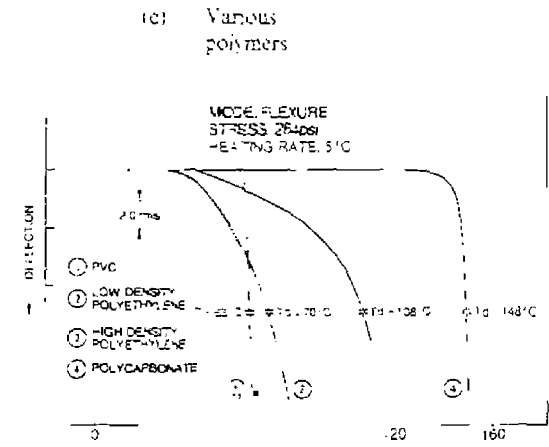


Table 11.3. (Continued)

TMA	Mode	Probe Type ^a	Sample	TMA Data
-----	------	-------------------------	--------	----------

Flexure



Creep compliance and modulus

(e) Plastic material
or (d)

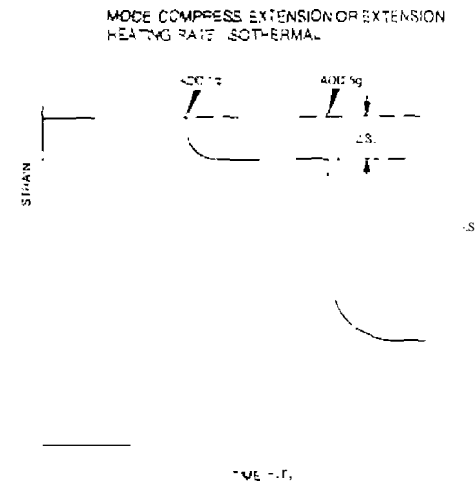
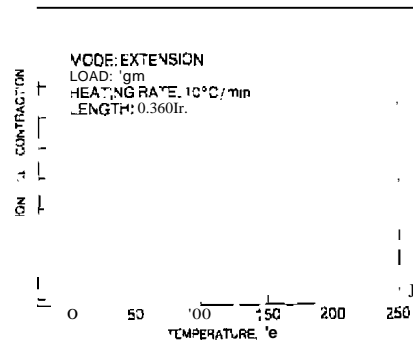


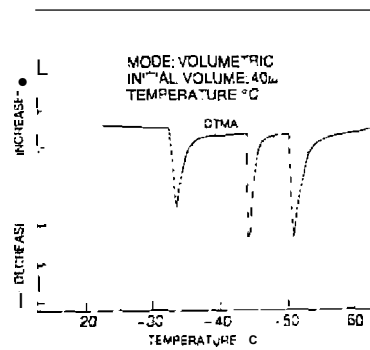
Table 11.3. (Continued)

TMA	Mode	Probe Type ^a	Sample	TMA Data
Extension		(d)	Nylon 5ber	



Volumetric

(e) CCl₄



^aSee Figure 11.2.

VISCOSITY OF POLYETHYLENE ISOTHERMAL AT 135 DEG.

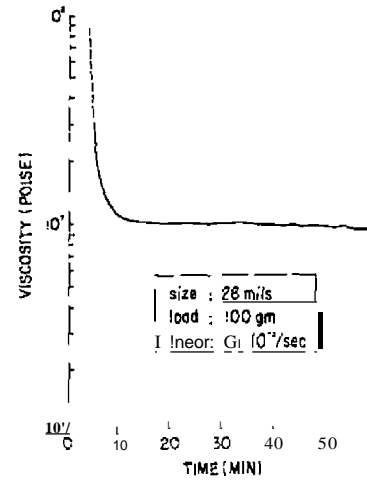


Figure 11.3. Viscosity curve of polyethylene determined by TMA (29).

of the sample, and F is the load on the sample. In TMA, Young's modulus is determined by a penetration mode procedure, using the equation

$$E = \frac{3F}{8Rd} (1 - 0.75 R/d) \quad (\text{for } D \gg R) \quad (11.7)$$

where R is the radius of the probe and d is depth of penetration. A comparison of the DTUL by TMA and the ASTM method is shown in Table 11.4 (32).

Table 11.4. Comparison of DTVL Obtained by TMA and ASTM Methods (32)

Sample	TMA (°C)	ASTM (°C)
Lr.modified PVC	73	75
Service temperature modified PVC	90	91
Impact modified PVC	77	73
Service temperature and impact modified PVC	78	80

The VICAT softening temperature is defined as the temperature at which a circular probe of 1.0 mm² cross section, under a load of 1000 g, penetrates 1.0 mm into a sample 12.7 mm thick (33). Using the same samples as were used for the DTUL tests, the correlation between TMA and VICAT softening temperatures are given in Table 11.5 (32).

TMA has been employed in criminalistic studies to characterize a single fiber of untextured cellulose triacetate (34). The normal thermal expansion of the material at low temperatures is followed by contraction as water is lost above 100°C. The 5% expansion associated with the T_g at 180°C is followed by contraction before melting/decomposition, properties that are diagnostic of the material. Other major classes of fibers such as Orion, Acrilon, rayon, or cotton show no distinctive features up to 300°C.

c. DMA

As in the case of TMA, almost all the applications of this technique are on polymeric substances. Methods for the measurement of DMA have been used for 40 years, but it is only during the past 10 years that commercial instrumentation has enabled a wider use of the technique. Commercially available instruments, in general, suffer from a restricted frequency range, the upper limit of which is in the region of 100 Hz (35). The lower end of the frequency is ideally suited to TA techniques but the upper frequency limit imposes severe restrictions for noise reduction applications where frequencies as high as 100 kHz are of interest. Although a single temperature scan can yield useful information about the structure of a sample, from a practical view, a more comprehensive method of evaluation is to step the temperature isothermally in 5°C steps (35). At each isothermal temperature, the frequency is scanned over the available frequency range. Scanning the frequency has the advantage in that time-temperature shift can be computed. These shift

Table 11.5. Comparison of VICAT Softening Temperatures by TMA and VICAT (32)

Sample	TMA (°C)	ASTM (°C)
Unmodified PVC	86	84
Service temperature modified PVC	106	101
Impact modified PVC	84	85
Service temperature and impact modified PVC	93	92

factors can then be used to predict the behavior of the sample at other frequencies and temperatures.

DMA applications to polymeric materials have been described by Wetton (36, 41) England et al (35), Gillham (10), Du Pont (37), Provder et al (9), Miller (38), Lofthouse and Burroughs (39), Gramelt (40), Murayama (42), and numerous other reviews on polymer characterization.

As in TDA and TMA applications, only a few uses of the DMA technique can be described here. Lofthouse et al (39) reported the DMA curves of linear and branched polyethylene, as given in Figure 11.14. The term *molecular spectroscopy* is illustrated by the curves for each of the compounds. The temperature scans start at -150°C, with an upper temperature limit of 100°C, at a programming rate of 5°C/min. Both samples exhibit damping peaks at around -100 and 50°C, which are due to long chain $1-\text{CH}_2$ crankcase relaxations in the amorphous phase and motion in the $(-\text{CH}_2)_n$ crystalline phases of the polymer, respectively. The temperature, position, and size of this latter damping peak are related to the crystallinity of the polyethylene. In Figure 11.14b, a third damping peak at -9°C, which is attributed to $(-\text{CH}_3)$ relaxations in the amorphous phase, indicates that the sample is a branched (low-density) polyethylene. This conclusion is supported by the rapid decrease in frequency (modulus) of that sample as a function of temperature. In fact, the sample becomes so flexible (low in modulus) at 90°C that it no longer contributes any restoring force to the compound resonance system; that is, it is pliant enough to be molded.

DMA can be used to evaluate the relative merits of inert fillers and reinforcing agents added to thermoplastics and thermosets to enhance the properties of the finished product. This technique can be used to study the amorphous properties of metal glasses (39). Common formulations of these glasses have the general formula approximating $M_{30}X_{70}$, where M may be Fe, Ni, Cr, Co, Pd, and Cu and X may be one or more from the group of P, B, C, Al, and Si.

DMA has been used to study a series of styrene-butadiene rubber (SBR) samples for automobile tires (37). SBR does not match the superior physical properties of natural rubber but has a lower cost and exhibits better heat aging and wear. The DMA curves for a styrene-butadiene rubber are shown in Figure 11.15, whereas a comparison of five different SBR samples is shown in Table 11.6. The damping maxima of styrene-butadiene rubber (SBR PB) in Table 11.6 occur at only a single temperature, -60°C. The highest temperature damping peak in every case corresponds to a large loss in modulus and is probably the T_g of the elastomer. The large polybutadiene content (samples that are 20 mole-% styrene) of the copolymer results in their T_g 's being closer to that of pure polybutadiene. Sample 1 is probably predominantly *cis*-polybutadiene. The absence of a well-defined damping peak in

j

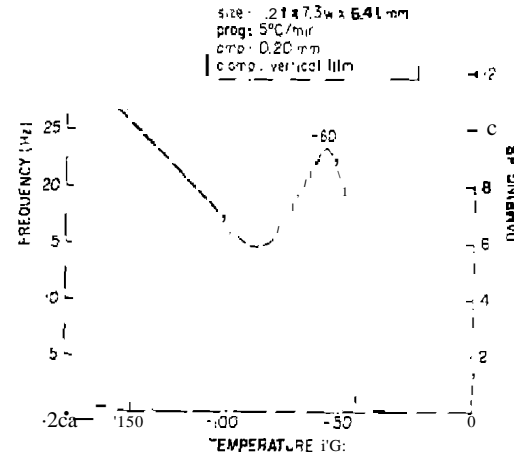
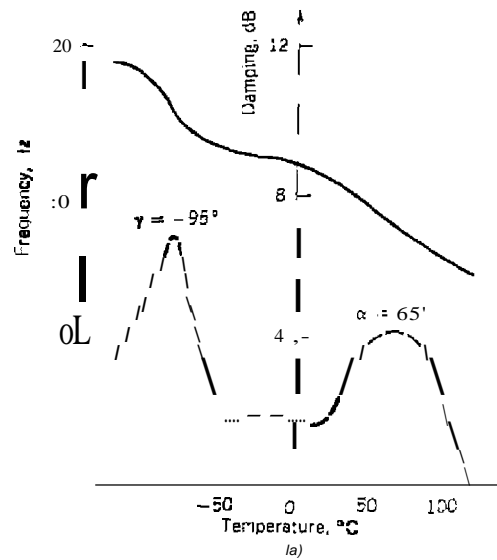


Figure 11.5. DMA curves of styrene-butadiene rubber (SBR/PB in Table 11.6) (37).

Table 11.6. Damping Maxima for a Series of SBR Samples (37)

Sample	Composition ^a	Damping Peak Maxima (°C)
	PB	-100
	SBR, PB	-60
3	SBR	-37, -80, -150 (broad)
4	SBR/PB/Carbon black	-52, -84, -100, -150 (broad)
	SBR/PB/Carbon black	-53, -94, -125, -149

^aSBR = styrene butadiene rubber; PB = polybutadiene.

all these samples in the temperature range -150-140°C is an additional indication that all (the polybutadiene is probably predominantly the *cis* configuration. Sample 3 has a high Mooney viscosity, indicative of a high molecular weight. This is reflected in its higher T_g temperature and higher modulus than are found in sample 2. Samples 3, 4, and 5 also have a large number of secondary damping peaks, particularly the broad one at low temperatures, which reflect additional structural interactions and motions. These additional damping peaks are to be expected since lower molecular weight rubbers have more cross-linking. Peaks observed in these latter formulations are particularly important since they may be related to heat

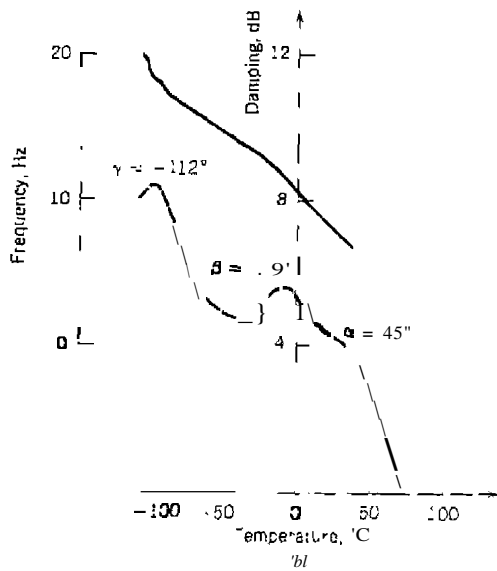


Figure 11.14. DMA curves of polyethylene (39). (a) Line: (b) Unannealed.

buildup, vibration, and road noises at road speeds in the lire. High-damping peaks have been correlated to favorable reductions in road vibrations and noises as well as to increased friction with the road. On the other hand, high damping has also been correlated to an unfavorable decrease in dimensional stability and an increase in heal buildup. The addition of carbon black as a reinforcing agent to SBR formulations also affects the damping behavior observed as seen in samples 4 and 5.

The DMA of a epichlorohydrin-bisphenol A epoxy resin cured using BF₃-ethylamine is shown in Figure 11.16(137).

The nomenclature for the DMA transitions observed in the epoxy systems, as described by Kacible 143), is as follows:

α Transition. Synonymous with the glass transition. It is associated with cooperative rotational motion normally involving 20-50 atoms along the main chain, and in cured epoxies is related to the rotational freedom of the segments between cross-links.

β Transition. Normally describes motion in the flexible side chains of polymers with short branches. In epoxies, this transition is related to the motion of the (-CH₂CH(OH)CH₂-O-) segment in the epoxy component of the resin. It is usually found in the region -60- -30°C.

γ Transition. Normally describes motion of a main chain segment containing 2, 3, or 4 carbon atoms. In epoxies, this transition is related to (-CH₂-) segments in aliphatic diamine curing agents. Usually appears in the region -120 -100°C.

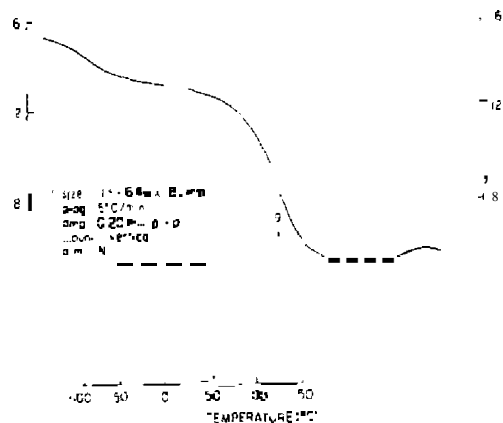


Figure 11.16. DMA curves of epoxy laminate (137).

There are three basic regions of interest in the damping curve of the epoxy laminate: the region [-150- -20°C) where the modulus of the sample is slowly decreasing; the region 110-210°C) where the modulus undergoes a precipitous drop and then levels off; and a region (210-330°C) where the majority of glasslike structure is gone and the modulus exhibits the rubberlike properties of increasing with temperature prior to decreasing as the sample thermally degrades. In the low-temperature region, there is a single broad damping peak with a maximum at -70°C, which is the β transition of the epoxy. Furthermore, the area under the peak is proportional to the degree of cure. Hence, the relative size of this peak and its temperature maximum can be used to evaluate the degree of cure of the epoxy. Probably more important is the fact that the presence and size of the β peak appears to be related to the toughness of the epoxy, being present in the tougher diamine cured epoxies but absent in the more brittle anhydride cured epoxies. The absence of an appreciable damping peak in the region -120-100°C indicates that this epoxy does not contain an aliphatic amine as its curing agent. The other major damping peak at 119°C represents the T_g of the epoxy.

C. THERMOELECTROMETRY

1. Introduction

According to the International Confederation of Thermal Analysis (ICTA), the thermal analysis technique of *thermoelectrometry* is defined as "a technique in which the electrical characteristics of a substance is measured as a function of temperature whilst the substance is subjected to a controlled temperature programme." (49) The most common measurements, according to ICTA, are of resistance, R , conductance, A , and capacitance, C . However, since $A = 1/R = I = F \cdot R$, and F is usually constant, $A = I = k/R$; thus, many investigators report the use of current, I , plotted as a function of temperature. Indeed, David (97) used the term *amperometric thermal analysis* (ATA) to describe the technique that he developed.

Thermoelectrometry techniques are not widely employed in thermal analysis, in fact, they may be described as "neglected" techniques in comparison with the widely used thermogravimetry (TG), differential thermal analysis (DTA), and differential scanning calorimetry (DSC) techniques. Nevertheless, they are important for certain specific applications, many of which will be discussed here.

In a recent thermal analysis technique survey of *Thermochemical Acta* (TCA) and *J. Thermal Analysis* (JTA), Wendlandt (50, 51) found that thermo-

electrometry (electrical properties) accounted for 2.2% of all the techniques used in TCA and 1.4% of the techniques used in JTA. The time period covered by this survey included volumes 24-29 of TCA and volumes 8-13 of JTA. This is quite small when compared to 22.0-29.1% for TG and 16.7-26.2% for DTA during the same time frame.

Thermoelectrometry has been reviewed in book chapters by Wendlandt (52,53) and Warfield (54), and reviews by Chiu (78), Paulik and Paulik (55), and Wendlandt (56, 98, 99). Since many of the thermoelectrometry studies involve simultaneous methods with other thermal analysis techniques, reference (55) is especially useful.

Since a number of different techniques are included under the broad term of thermoelectrometry, this discussion will be divided into three categories: (1) electrical conductance, current, and resistance; (2) dielectric constant and capacitance; and (3) miscellaneous electrical techniques that are of interest to thermal analysis.

2. Electrical Conductance, Current, and Resistance

Adeosun and co-workers studied the electrical conductance and other properties of molten lead dodecanoate and mixtures with lead acetate (57), dodecanoic acid (58), metal dodecanoates (59), and lead (II) oxide (60). Using the specific conductance of lead dodecanoate mixtures, they interpreted the curvature of these curves in terms of a simple dissociation theory involving lead dodecanoate (PbA_2):



Assuming that the major charge carrier is Pb^{2+} and that it moves by a simple activated process, the following expressions were obtained:

$$\log K = \log Q - \frac{\Delta H_k + \Delta H/3}{2.303RT} \quad (11.9)$$

and

$$\log Q = \log(NeA/2V_m) + \frac{1}{2.303R} \left(\Delta S_k^{\ddagger} + \frac{\Delta S}{3} \right) \quad (11.10)$$

where ΔH_k^{\ddagger} , ΔS_k^{\ddagger} , ΔH , and ΔS are the enthalpies and entropies of activation for movement of the Pb^{2+} ion and the dissociation reaction, respectively. Thus, plots of $\log K$ versus $1/T$ should be linear with slopes of $(\Delta H_k^{\ddagger} + \Delta H/3)/$

$2.303R$. For the mixtures of PbA_1 with $Pb(C_2H_3O_2)_2$, the values of $(\Delta H_k^{\ddagger} + \Delta H/3)$ ranged between 47 and 50 kJ mole⁻¹.

The dc electrical conductivity of a number of *N*-(2-pyridyl)benzamide and *N,N'*-dibenzoyl-2,6-diaminopyridine metal complexes, as a function of temperature (to 388 K) and radiation, was studied by Abou Sekkina et al. (61). Linear log versus $1/T$ plots were obtained for all the Cu(II) and Ni(II) complexes, from which the activation energy, E_a , and other parameters could be calculated, using the expression

$$\sigma = \sigma_0(\exp - E_a/2kT) \quad (11.11)$$

where σ is the specific conductivity, σ_0 is a constant independent of temperature, k is the Boltzmann constant, and E_a is the activation energy (eV). The behavior of a positive temperature coefficient of k indicates that semiconducting behavior or promotion of electrons from the ground state to excited states may occur. Carrier mobilities, μ , of the different complexes were found to be in the range of 10^{-5} - 10^{-10} cm²V⁻¹sec⁻¹ and to increase with an increase in temperature.

Simultaneous thermodilatometry-electrical conductivity measurements have been employed to determine the sintering or coalescence of powdered materials. An equation has been developed by Ramanan and Chaklader (62) that relates electrical conductance to density changes of powder compacts on sintering:

$$\Lambda = C/\Lambda_0[(D/D_0)^{2/3} - 1] \exp(-E_a/RT)$$

where Λ is the conductance at sample density D . D_0 is the initial density. C is a constant, Λ_0 is the preexponential factor, E_a is the activation energy, R is the gas constant, and T is the temperature. The equation predicts that on heating the powder compact, the conductance should increase rapidly after initial contact between the particles has occurred. To follow both the change in Λ and the shrinkage of the powder compact, the investigators employed simultaneous thermodilatometry-electrical conductance measurements (63-65). This simultaneous technique has been applied to vitreous materials such as glass, an epoxy resin, iron, $CuSO_4 \cdot 5H_2O$, coal ash, and others. The T_g of a vitreous material can be easily obtained using electrical resistance [R] data plotted as a function of $1/T$. The simultaneous dilatometric and electrical resistance curves of $CuSO_4 \cdot 5H_2O$ are given in Figure 11.17 (65). Using a compacted sample (to 1500 bars) of the compound, one can see that the first four water molecules are evolved in two distinct steps. In addition, the removal of the fifth "water" of hydration appears clearly on the thermodilatometric curve (as it does on the TG and DTG curves), as well as on the

electrical resistance curve. The fifth molecule is not present as water of hydration but is thought to originate from OH groups in the crystal.

Perhaps the most commonly used simultaneous technique involving electric conductivity is that with DTA. Burmistrova and Yitzeva (66) used this technique to study the reactions between alkaline earth metal oxide: (CaO, SrO, BaO) and selected Pb, Cu, and Ni halides. Electrical conductivity is useful in determining the appearance of a liquid phase at the moment of interaction between the solids. The interaction between BaO and CuBr, as shown in Figure 11.18, is exothermic, as revealed by the DTA curve peak at 360°C. This is accompanied by an increase in electrical conductivity also.

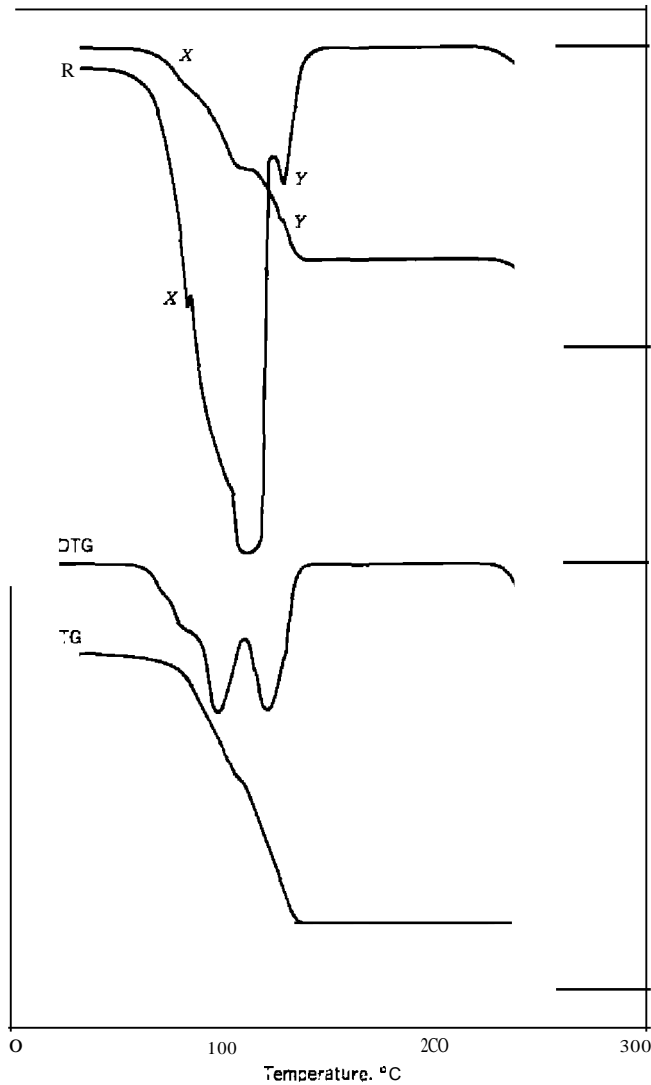


Figure 11.17. Simultaneous thermogravimetric (T) and electrical resistance (R) curves of $\text{CuSO}_4 \cdot 5\text{H}_2\text{O}$. DTG and TG curves are also shown (65).

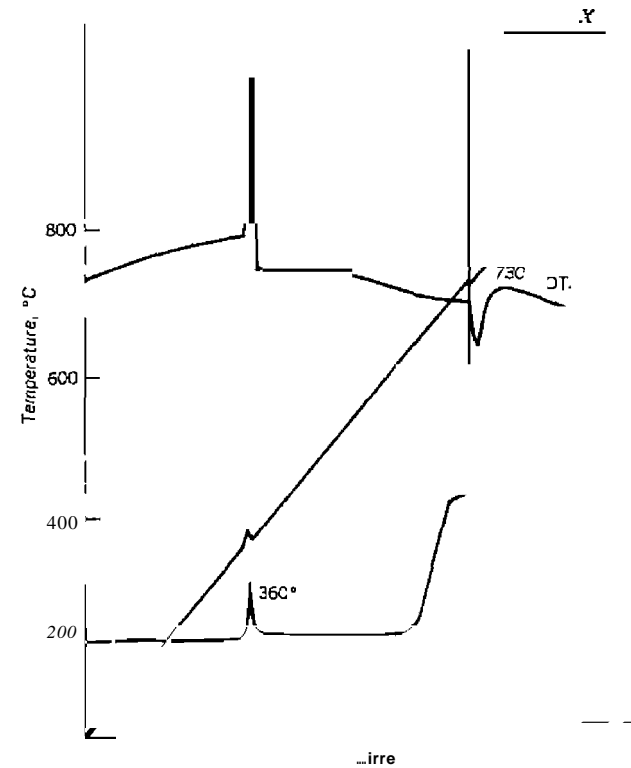


Figure 11.18. DTA and electrical conductivity curves for a mixture of BaO and CuBr (66).

forming a small peak in the curve. On further heating, the curve returns to its baseline until the reaction product, BaBr_2 , begins to melt 730°C , where it again increases rapidly. The 360°C peak, which is due to the melting of the $\text{Ba}(\text{OH})_2 - \text{BaO}$ eutectic, also appeared in a reaction mixture of BaO and PbBr_2 .

An apparatus for simultaneous DTA-ATA measurements (where ATA = amperometric thermal analysis) has been described by David (97). This apparatus, as shown in Figure 11.19, consisted of a 20-gauge platinum wire electrode, H, coupled to a small platinum-plated stainless steel cup, F, which constituted the other electrode in the electrical conductivity system. The small platinized cup received the same type of sample as was utilized in ring-type thermocouples. The upper electrode, E, was movable so as to maintain continuous contact with the sample during first-order phase transformations in which a reduction in bulk volume frequently occurred. A suitable dc voltage from 1 to 1000 V was applied to the sample and the current flow through the system was measured by an electrometer connected in series with the voltage source. Loss of evolved water in the dehydration of $\text{CuSO}_4 \cdot 5\text{H}_2\text{O}$ was followed by this technique as well as the fusion behavior of potassium nitrate and certain polymeric materials.

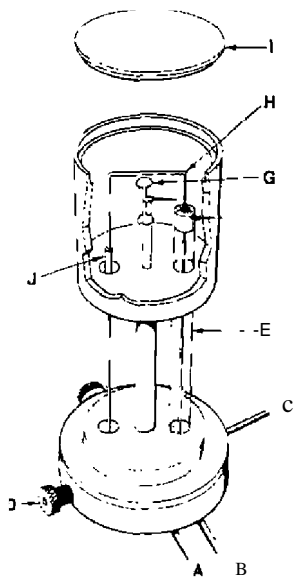


Figure 11.19. DTA-ATA sample holder developed by David (97). A, electrometer input lead; B, negative voltage input lead; C, thermocouple leads; D, cooling water connectors; E, Pyrex capillary voltage insulator; F, sample pan container; G, differential thermocouple; H, platinum electrode; I, sample-holder cover; 1, platinum electrode coupler.

Wendlandt (100) used electrical conductivity (EC) measurements to detect quadruple points in various metal salt hydrate systems. This was the first application of this technique to detect the presence of quadruple points that had previously been determined by DTA (101) techniques. Using DTA, the quadruple point is indicated usually as a shoulder peak on a larger endothermic peak. In the case of $\text{CuSO}_4 \cdot 5\text{H}_2\text{O}$, the four phases present at the quadruple point are $\text{CuSO}_4 \cdot 5\text{H}_2\text{O}$, $\text{CuSO}_4 \cdot 3\text{H}_2\text{O}$, $\text{H}_2\text{O}(\text{l})$, and $\text{H}_2\text{O}(\text{g})$. Due to the presence of a liquid phase in contact with the ionic solid, a low resistance or conducting solution is obtained so that a rapid increase in I is indicative of the quadruple point.

The apparatus used by Wendlandt (100) is illustrated in Figure 11.20. It consisted of a recording micro-microammeter, an X-Y recorder, a power supply capable of furnishing 3-25 V dc, a sample holder and electrode probe, and a metal block furnace whose temperature rise was controlled by a simple temperature programmer. Powered samples of the metal salt hydrates were contained in Pyrex glass tubes, 5 mm in diameter by 50 mm in length.

The EC-DTA curves of $\text{CuSO}_4 \cdot 5\text{H}_2\text{O}$ are illustrated in Figure 11.21 (100). The DTA was similar to that previously described except for the more pronounced resolution between the first and second peaks. The first began at about 91°C , with a ΔT_{min} of 101°C . The ΔT_{min} values for the second and

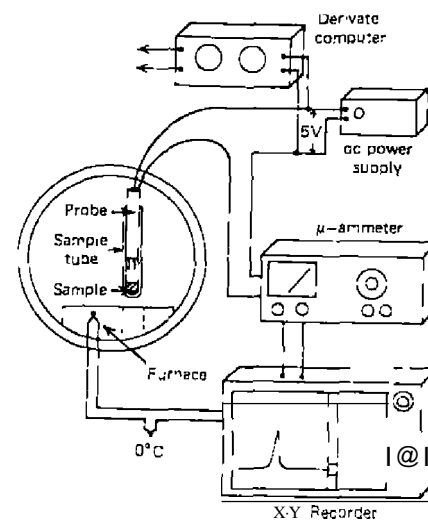
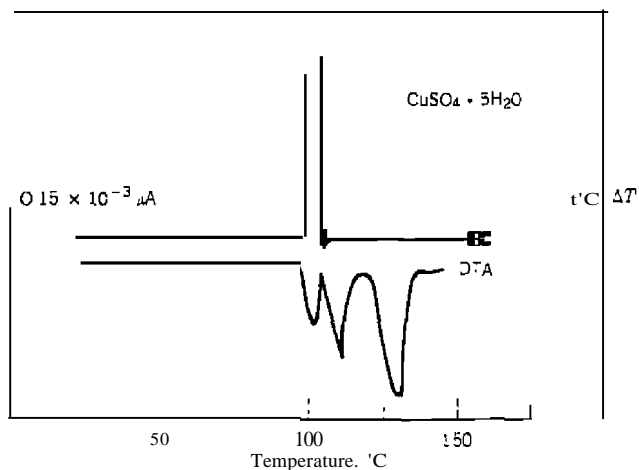


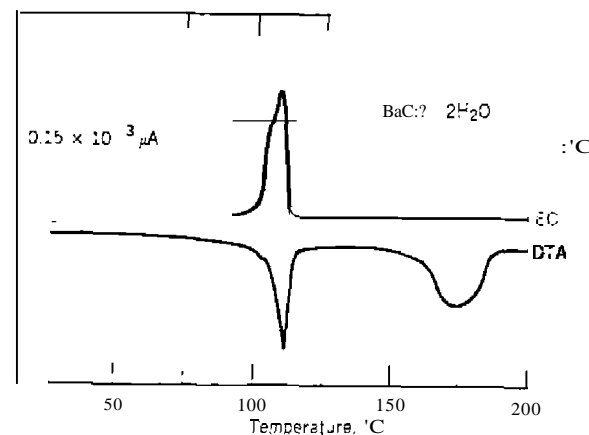
Figure 11.20. EC apparatus developed by Wendlandt (100).

Figure 11.21. EC-DTA curves of $\text{CuSO}_4 \cdot 5\text{H}_2\text{O}$ (100).

...ird peaks are 112 and 135°C, respectively. Formation of liquid water was readily shown by the EC curve in that the current flowing through the sample began to increase at about 95°C and obtained a maximum, EC_{max} , at 103°C. Rapid vaporization of the liquid water from the saturated salt solution was readily apparent by the steep slope of the descending portion of the curve. No EC peak was observed for the $\text{CuSO}_4 \cdot 3\text{H}_2\text{O} \rightarrow \text{CuSO}_4 \cdot \text{H}_2\text{O}$ transition.

For the $\text{BaCl}_2 \cdot 2\text{H}_2\text{O}$ system, as shown in Figure 11.22, the DTA curve contained two endothermic peaks, in agreement with previous studies. The first endothermic peak, which is of primary interest here, began at about 90°C with a ΔT_{min} of 112°C. The presence of a liquid phase was indicated by the appearance of a peak in the EC curve. The peak began at about 98°C, with an EC_{max} value of 108°C. The presence of the liquid phase in this system was not observed by Borchardt and Daniels (101). They stated that the relatively small difference between the vapor pressure of the salt hydrate at the quadruple point and atmospheric pressure required close adherence to equilibrium conditions if the formation of a liquid was to be observed. This condition, they stated, obviously was not met. On closer inspection of their DTA curve, however, a slight shoulder peak is observed in the curve. Perhaps if they had used a slower heating rate, a more pronounced peak would have been observed. This shoulder peak is observed also in the DTA curve in Figure 3 although the slower heating rate (2.5°C·min⁻¹) did not reveal another peak in this region of the curve.

As with other TA techniques, the electrical conductivity curve of a sample

Figure 11.22. EC-DTA curves of $\text{BaCl}_2 \cdot 2\text{H}_2\text{O}$ (100).

is influenced by the furnace heating rate. The EC curve of $\text{BaCl}_2 \cdot 2\text{H}_2\text{O}$ at various heating rates are shown in Figure 11.23. As the heating rate decreased from 20-1.25°C·min⁻¹, the slope of the peak changed rather drastically. At the high-heating rates, the peak was much smaller and broader; on decreasing (the heating rate, the peaks became sharper and of greater height. The area of the peaks varied also but much of this was due to the inability to pack the sample in a uniform, consistent manner. The effect of heating rate on the shape of the peaks is related to conditions previously discussed. At rather high-heating rates, the system is too far from equilibrium and condition 13 cannot be met. Low-heating rates would allow more time for the water vapor to diffuse away from the sample but with the enclosed sample chamber, the diffusion process is hindered. The EC peak maximum is also affected by the heating rate. At 20°C·min⁻¹, it had decreased to 103°C. Although the peak maximum temperature changed with heating rate, the temperature at which the peak began changed little. They all began in the temperature range 97-100°C. A more elaborate thermal analysis system was described by Chiu (102, 103) in which concurrent TG, DTG, DTA, and EC measurements were recorded. The sample-handling system of this apparatus is shown in Figure 11.24. One electrode, M, in the sample holder, is a 0.003-in.-thick piece of platinum foil wrapped around the ceramic insulation, T, of the sample thermocouple, Z. The other electrode, L, is made from platinum foil in the form of a cylinder to fit inside the quartz tube. K. The sample is packed tightly between the two electrodes; a spacer, S, located at the bottom of the tube, is used to prevent accidental shorting of the electrodes. Current flowing

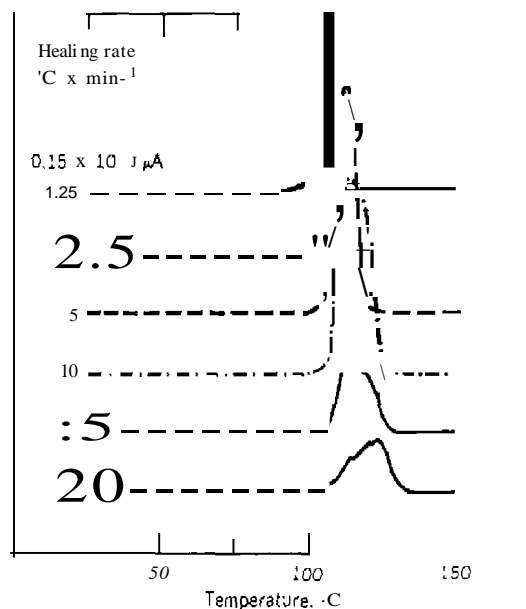


Figure 11.23. Effect of heating rate on the EC peaks of $\text{BaCO}_3 \cdot 2\text{H}_2\text{O}$ (100).

through the system, under an applied dc potential of 1-2 V, is detected with an electrometer and recorded on the Y axis of an X-Y recorder. Sample currents from 10^{-10} to 10^{-5} A, in five decades, were recorded.

To study the EC of several metal oxide systems, Rudloff and Freeman (104) used an apparatus in which an electrode, E_1 , inside a gas flow tube made of Vycor glass, was mounted on a glass disc fused to a sturdy glass capillary tube fixed at one side of the flow tube. The other electrode, E_2 , was fixed to a similar disk-capillary tube combination. A spring provided adequate pressure of the electrodes to the single crystal or powder pellets for good electrical contact. The flow tube is placed into a heated tube furnace and during operation, the entire system is carefully shielded to prevent noise pickup from the surroundings.

An apparatus for simultaneous electrothermal analysis (ETA) and dilatometry has been described by Judd and Pope (105) consisted of a thermal aluminous porcelain 525 tube mounted horizontally in a Kaothermal wire-wound tube furnace capable of operation up to a temperature of 1250°C. The tube is reduced to a narrow neck at one end to which a vacuum line is connected. Fixed to the other end of the tube is a metal bracket fitted with

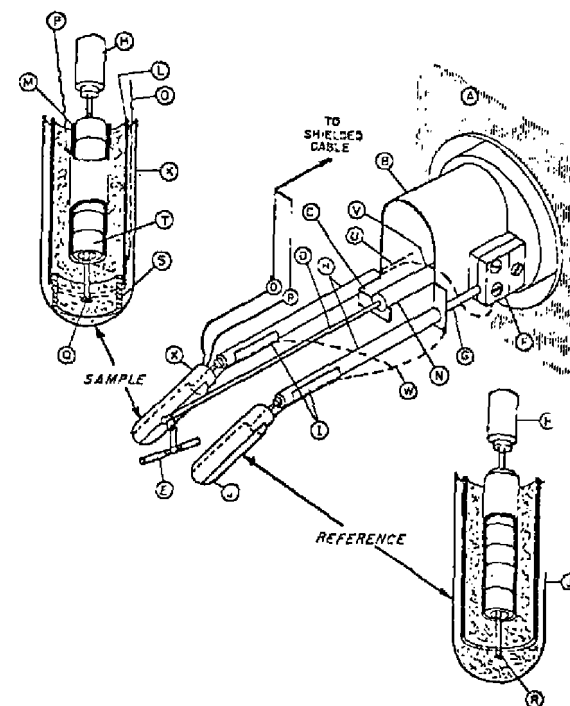


Figure 11.24. Apparatus used by Chiu (102) for parallel TG-DTG-DTA and ETA measurements. A. balance housing; B. balance beam sheath; C. beam stop; D. quartz beam; E. sample container; F. thermocouple black; G. sample measuring thermocouple; H. ceramic tubing; I. platinum jacket; J. reference quartz tube; K. sample quartz tube; L. outer platinum electrode; M. center platinum electrode; N. cold beam member; O, P. platinum lead wires; Q. sample thermocouple junction; R. reference thermocouple junction; S. spacer; T. ceramic insulation; U, V. sample thermocouple wires; W. platinum grounding wire.

two O-rings, giving a vacuum-tight connection. A spacer keeps the compacted sample in a fixed position near the center of the furnace. Electrical contact with the sample is made by means of two platinum disk electrodes pressed against the opposing faces.

Carroll and Mangravite (106) described an apparatus in which simultaneous EC and DSC measurements could be made on the same sample. They referred to their technique as simultaneous scanning calorimetry and conductivity (SSCC).

A highly sensitive EC-DTA apparatus was developed by Halmas and

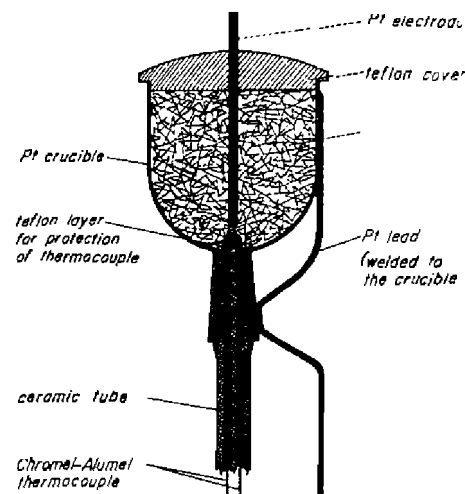
Wendlandt (107). A cross-sectional view of the sample holder is shown in figure 11.25a. The sample (and reference) container was constructed from a platinum crucible, 5 mm in diameter and 5 mm in height, which made contact with junction of a thermocouple on the bottom. Since the thermojunction was in direct contact with the sample, it was coated with a thin layer of Teflon (from an aerosol spray container). This limited the temperature maximum to about 320–340°C; however, without the Teflon the maximum temperature limit was about 550°C. To measure the electrical conductivity of the sample, the investigators welded one electrode to the sample container while the other was a platinum wire that was introduced into the sample through a hole in the Teflon cover. The depth of sample contact by this electrode was adjustable by means of a screw device. Two modes of operation were used: in one, no cover was used for the sample container, whereas the other was a tight-fitting cover for self-generated atmosphere studies. The reference holder was similar to the preceding holder in order to maintain the same heat capacity, but it contained aluminum oxide rather than a thermally active sample.

Details of the complete EC-DTA cell are shown in figure 11.25b. The heater block, which was machined from aluminum, contained a 500 W heater cartridge located in the center of the block. Two cylindrical chambers located on each side of the heater housed the sample and reference container, respectively. Care was taken to position each container at exactly the same distance from the heater. It was found from previous DTA studies that the diameter of the container cavities greatly influenced the DTA curves obtained. In this cell they were 18 mm in diameter by 38 mm in depth.

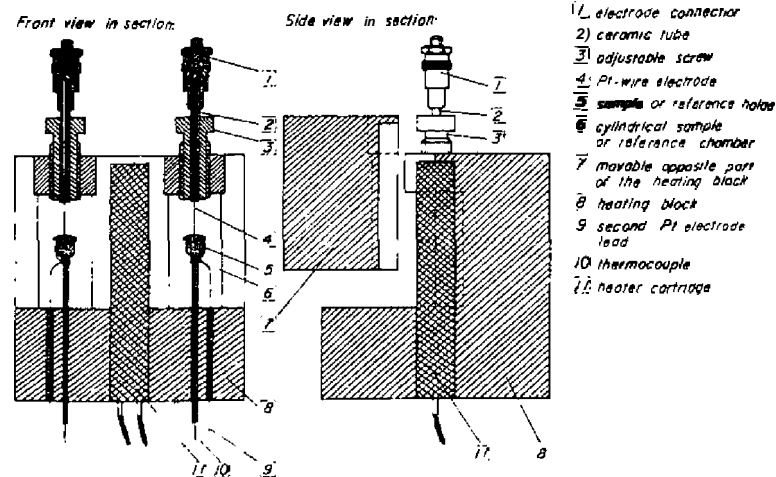
The upper electrode was electrically insulated from the block by a ceramic tube and sleeve and was attached to an adjustable screw device and an electrical connector. To aid in sample loading and to remove the spent sample, one half of the block was removable. It was always placed into position when EC-DTA measurements were made.

The cell block was supported by three 5-mm-diameter ceramic rods that were attached to a 12-mm-thick circular aluminum base. To insulate the cell, the experimenters used a Marinette enclosure which was approximately 10 mm thick. It could be placed over the entire cell during the heating cycle and removed to aid in the cooling of the cell back to room temperature. All electrical connections were made on a connector located on the base of the cell. Due to the cell construction, it was not possible to control the furnace atmosphere in any manner, hence, most of the runs were made in the self-generated atmosphere mode.

The order-disorder transition for a series of thermochromic M_nHgI_4 complexes, where M is Ag^+ , Cu^+ , Hg_2^{2+} , Tl^+ , and Pb^{2+} , were studied by the above ETA-DTA apparatus (108). As an example, the ETA-DTA curves for



(a)



(b)

Figure 11.25. Sensitive EC-DTA apparatus developed by Harro and Wendlandt (107). (a) Sample-holder cross section. (b) EC-DTA cell.

Cu_2HgI_4 are given in Figure 11.26. As is well known, the thermochromic transition of this compound occurs at about 70°C , at which temperature the color change is from red to brown-black. The color transition is reversible in that on cooling, the red compound is again obtained. In the DTA curves, in both the heating and cooling modes, only a single narrow endothermic peak was observed, which was due to the thermochromic transition. During both heating curves, the peak began at 64°C with a T_{min} temperature of 70°C . The peak was also observed during the cooling mode, indicating, as expected, that the transition is reversible. The ETA curve peak was not as well pro-

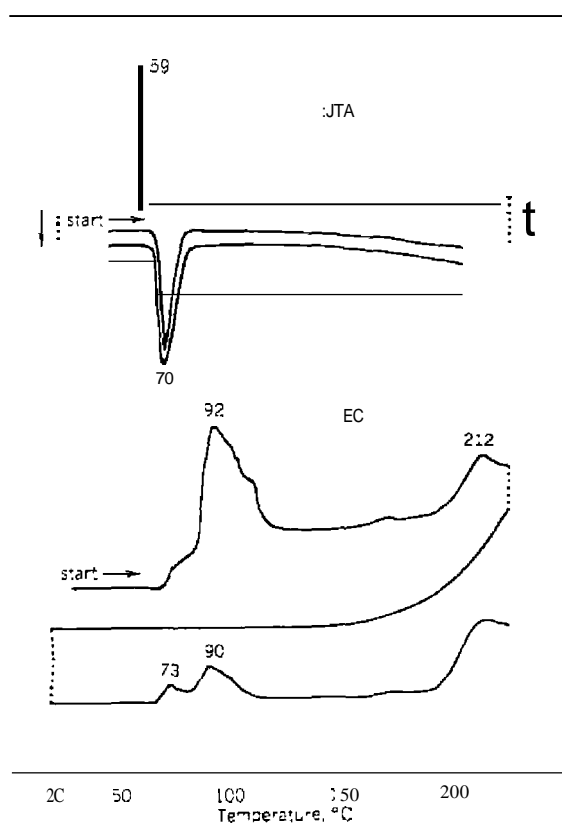


Figure 11.26 EC-DTA curves of Cu_2HgI_4 (108)

nounced during the thermochromic transition as was the DTA peak. Only a shoulder peak was observed simultaneously with the DTA curve peak but this was followed by a large asymmetric curve peak with a maximum at approximately 92°C . Apparently, an additional disorder occurs about 200°C which results in a curve peak with a maximum at about 212°C . On cooling, none of the initial ETA peaks were observed in the curve. Reheating the sample gave the same ETA curve peaks, but all of them were at a decreased peak height. From the preceding data, the ETA curves appear to indicate multiple disordering processes or transitions involving phases not previously reported. Similar behavior was noted for the other complexes as well as for HgI_2 and AgI .

Using the apparatus described earlier, Halmos et al. (109) made a more thorough investigation on the determination of the quadruple point of $\text{CuSO}_4 \cdot 5\text{H}_2\text{O}$. These results are summarized in Table 11.7. In (1), the effect of sample size is shown. As the mass of the sample decreased, the amplitude of both the EC and DTA peaks decreased, with the EC peak disappearing completely when a sample mass of less than 10 mg was employed. In (2), as the heating rate increased, the magnitude of the splitting of the first dehydration peak increased in the DTA curve. The EC peak also increased in amplitude, which indicates the formation of a more substantial/liquid phase in the system. The effect of particle size on the EC-DTA curves is shown in (3). All the DTA curves have the same general shape and the magnitude of the EC peaks did not change significantly with particle size. However, with large particle sizes, there is some distortion of the EC-DTA peaks which indicates that a more complicated diffusion process is probably occurring.

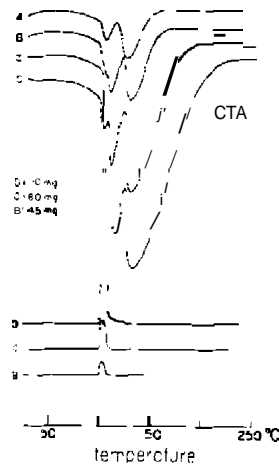
In conjunction with the development of a high-pressure thermobalance (122) and DTA apparatus (123), an ETA apparatus capable of operation from 1-170 atm in the temperature range of $25\text{-}500^\circ\text{C}$ was also constructed (124). The sample holder, electrode system, and furnace were enclosed by a stainless steel pressure vessel. Pressurization of the vessel was affected by use of compressed nitrogen gas obtained from a cylinder. The effect of pressure changes from ~ 170 atm on the ETA curves of $\text{BaCl}_2 \cdot 2\text{H}_2\text{O}$ are given in Figure 11.27. A moderately packed sample of the compound showed no change in current flow during heating at 1 atm. As the pressure increased, a slight change in the curve near 100°C was observed. With increasing system pressure, the magnitude of the peak height and also the area increased as did the temperature range of ETA. The increase in the peak height and area is thought to be due to the decrease in diffusion of water vapor from the sample as the pressure is increased. A second peak was not observed because the heat transfer through the metal sample cup wall was rapid enough to vaporize the liberated water and the short diffusion path was not as effective in retarding the escape of the vapor as in the previous sample

Table 11.7. Effect of Experimental Variables at the Quadruple Point of $\text{CuSO}_4 \cdot 5\text{H}_2\text{O}$ (109)

Experimental Variable

I. Sample mass

Effect on EC-DTA Curves



2. Heating rate

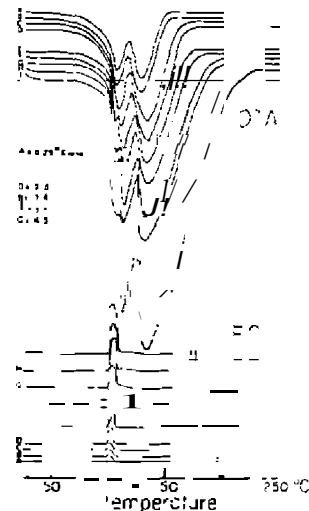
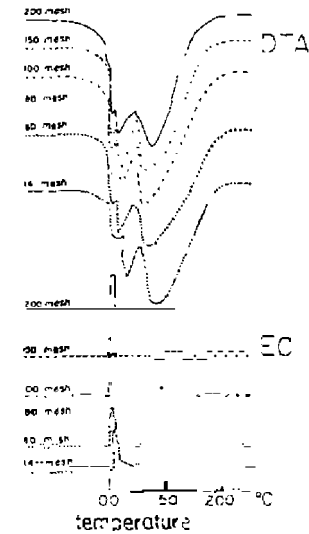


Table 11.7.

Experimental Variable

3. Particle size

Effect on EC-DTA Curves



holders. Additional ETA curves for $\text{BaCl}_2 \cdot 2\text{H}_2\text{O}$, $\text{BaBr}_2 \cdot 2\text{H}_2\text{O}$ and $\text{CoCl}_2 \cdot 6\text{H}_2\text{O}$ were given by Williams and Wendlandt (1125).

In order to investigate the ETA of pure substances or mixtures of pure substances with a matrix material such as KBr, KI or KCl, Wendlandt (110) developed an apparatus in which the sample, in the form a disk 5 mm in diameter by 1 mm thick, was placed between two circular metal electrodes. In order to assure efficient contact between the electrodes and the sample disk, he held the upper electrode in place by a spring-loaded mechanism. Also, instead of measuring a dc current through the sample, a variable frequency ac power supply was employed that permitted ac current measurements of the samples.

Wendlandt has also described an EC apparatus that can be incorporated into the furnace of a commercial thermobalance so that concurrent EC-TG measurements can be made (110). This sample holder was later modified so that concurrent EC-DTA measurements could also be carried out (112). A high-temperature EC furnace and sample holder, for use up to

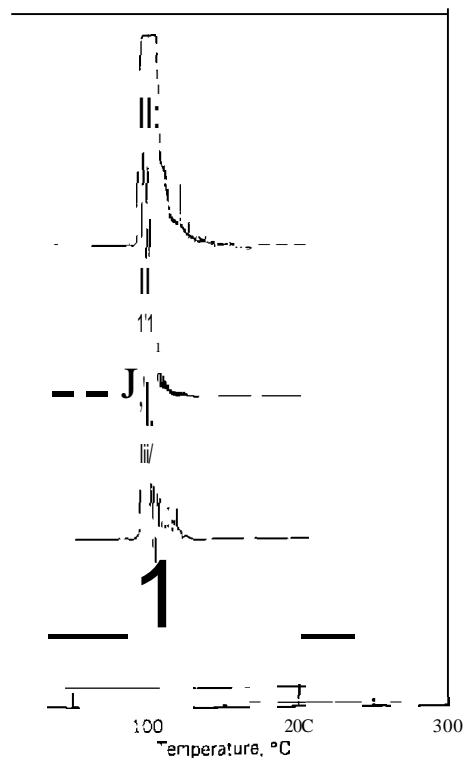


Figure 11.27. Effect of pressure on ETA curves of $BaCl_2 \cdot 2H_2O$. a. 1 atm; b. 7 atm; c. 15 atm; d. 42 atm; e. 170 atm (124).

has been described by Wendlandt (112). The sample holder and furnace arrangement are shown in Figure 11.28. The sample A, in the form of a compressed disk (1 x 5 mm) was placed between two platinum electrodes (1 mm in diameter). Leads to the electrodes were led out of the furnace area through one-holed ceramic insulator tubes. To maintain a constant tension on the sample disk by the electrodes, one electrode is spring-loaded at H. The furnace consists of a Nichrome resistance wire heater element on a Vycor tube, which is properly insulated with a ceramic material. A clamp G secures the tube furnace to the base. Furnace temperature, T_f , is detected by a Chromel-Alumel thermocouple located at D. The other components of the EC apparatus are the same as those previously described. The apparatus was used on pure

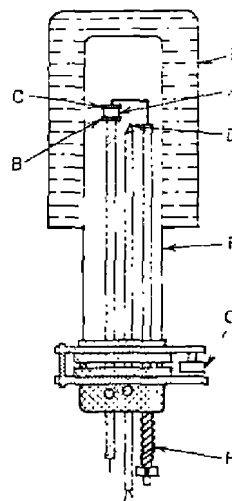


Figure 11.28. ETA sample holder and furnace for use up to 1000°C (112).

samples, compressed in the form of disks, or of a matrix mixture with KCl, KBr, or KI.

The EC technique was applied to the study of the thermal decomposition reactions of coordination compounds by Wendlandt (113). One such investigation (113) involved the ETA of selected $[Co(NH_3)_6]X_3$ and $[Co(en)_3]X_3$ complexes ($X = Cl^-, Br^-, I^-, NO_3^-, HSO_4^-$ and $\frac{1}{2}C_2O_4^{2-}$). These compounds, which had been previously studied by TG, DSC, MS, EGD, EGA, and thermomagnetic analysis techniques, were chosen because of questions concerning the intermediates formed during the thermal dissociation processes. Also, the reaction with various matrix materials such as KNO_3 , KBr, K_2SO_4 and so on, was also investigated.

The ETA curves of $[Co(NH_3)_6]Cl_3$ in various matrices are given in Figure 11.29. As can be seen, there is a wide variation in the ETA curve of $[Co(NH_3)_6]Cl_3$ with composition of the matrix material. The ETA increase begins at the following temperatures for each matrix: 250°C (KNO_3); 270°C (KBr and K_2CrO_4); 285°C (K_2SO_4), and 290°C (KCl). All the matrix materials exhibited intermediate peaks in the ETA curve except KNO_3 , which gave only a pronounced increase in EC to a maximum value of 1000 μA . The ETA curves all increased with temperature in the 400°C temperature range except that for the KCl matrix. Unfortunately, it is not possible at this time to interpret the reactions responsible for the occurrence of the ETA curve peaks in the KCl, KBr, K_2CrO_4 , and K_2SO_4 matrices. All the peaks are related, of

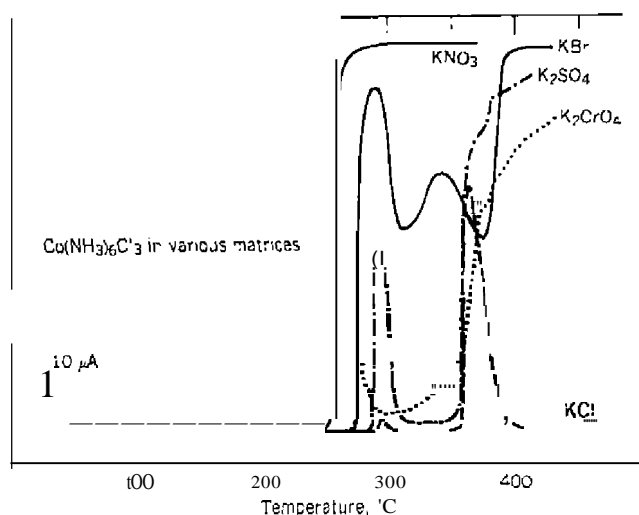


Figure 1. 29. ETA curves of $[\text{Co}(\text{NH}_3)_6]\text{Cl}_3$ in 1:1 matrices of KNO_3 , KBr , K_2SO_4 , and KCl (113).

course, to the formation of conducting phases formed as intermediates in the thermal dissociation reactions.

Simultaneous electrical conductivity-DTA was used by Romano¹ et al. (67) to study the thermal behavior of α -oxyalkylphosphonates. It was found that the thermal transformations of these compounds and their analogs are preceded by the ionization of the hydroxy group near the α -carbon atom. On the phosphonate-phosphate rearrangement of α -oxyalkylphosphonates containing electron-donor substituents near the α -carbon atom, no prior decomposition to the initial components takes place, and rearrangement proceeds by an intramolecular tricenter mechanism.

Electrical conductivity was used in conjunction with other thermal analysis techniques by Golunski et al. (68) to study the oxides of antimony. For orthorhombic Sb_2O_3 (valentinitel, in N_2 , the first thermal effect to be observed by electrical conductivity was a change in slope at about 225°C , which was not observed by any other technique used. This decrease was observed to be the loss of chemisorbed OH groups; the mass-loss being too small to be observed by TG. For cubic Sb_2O_3 (senarmontite), in N_2 , changes occurred in the electrical conductivity curve at temperatures well below those observed by DTA or TG. The slope of the electrical conductivity curve

increased above 230°C and further changes were observed at 350 and 530°C , respectively.

Due to the inherent problems of studying the thermal decomposition of NH_4VO by TG and DTA, Trau (69) found that electrical conductivity could be used to provide information relating to the changing concentration of crystal lattice defects. The formation of these lattice defects is connected with any formation process of a new solid phase. A decrease in the electrical conductivity curve in the temperature range 10 - 50°C was ascribed to the probable desorption of water vapor from the sample surface. Three maxima were observed at 150 , 190 , and 230°C , respectively, which corresponded well with the three stages of the thermal decomposition process of NH_4VO , as determined by other thermal analysis techniques. These maxima can be explained as a result of the decreasing number of lattice defects due to diffusion and combination reactions. A curve peak at 290 - 370°C was related to the recrystallization of V_2O_5 , as well as to the possible oxidation of V601.1 to V20S. The foregoing results show that this technique can be useful for detecting and/or confirming the existence of intermediate products of the thermal decomposition reaction.

This was also the case when Nandi et al. (70) used electrical conductivity and dielectric constants to study the deaquation reactions of single crystals of $\text{NiSO}_4 \cdot 6\text{H}_2\text{O}$ and $\text{NiSO}_4 \cdot 7\text{H}_2\text{O}$, as well as $\text{FeSO}_4 \cdot 7\text{H}_2\text{O}$ (73) and $\text{CuSO}_4 \cdot 5\text{H}_2\text{O}$ (72). The electrical conductivity curve of a $\text{NiSO}_4 \cdot 6\text{H}_2\text{O}$ crystal grown at 40°C contained four distinct peaks at temperature maxima of 100 , 142 , 186 , and 360°C , respectively. For $\text{NiSO}_4 \cdot 7\text{H}_2\text{O}$ crystals, melting and boiling of the evolved water were also observed in the electrical conductivity curve. One mole of water per mole of salt was evolved from the crystal and dissolved part of the NiSO_4 , creating Ni^{2+} and SO_4^{2-} ions in solution. These ions caused an increase in conductivity that decreased as boiling began. The number of charged particles, n , in the electrical conductivity curves of these compounds could be determined experimentally by calculating the area under the current versus time curves and dividing by e , the charge on the electron.

Sircar et al. (73) used electrical conductivity to study carbon-filled polymer compounds. Thermal transitions were observed by this technique that could not be detected by any other thermal analysis technique and it could also be used to predict the thermal stability of amorphous polymers. A modified Du Pont DSC cell was used for the electrical conductivity measurements. Employing electrical conductivity techniques, Rajeshwar et al. (74) showed that the Green River Oil shales decompose by a two-step process in which the rate-determining step is the III breakdown of an outershell polar bridge structure (180 - 350°C) and (2) cleavage of an inner naphthenic structure also involving polar groups (350 - 500°C). The observed trend in charge transfer

mechanisms in the decomposition behavior of thermally unstable materials may be indicative of how thermal and electrical properties of all solid materials in general are closely coupled.

The ac electrical conductivity of ammonium and alkali metal perchlorates was studied by Rajeshwar et al. (75-77). Plots of $\ln(\sigma T)$ versus $1/T$ were made for both heating and cooling cycles with results usually superimposable once the samples were subjected to an annealing treatment. Activation energies were obtained in the usual manner for the K, Cs, and Rb salts. The electrical conductivity of ammonium perchlorate is the subject of a major controversy concerning the mechanism-controlling charge transfer. One model is that of proton transfer, the other is a defect model in which interstitial NH_4^+ ions are believed to be the dominant charge-carrying species. The results of these investigations are consistent with an extrinsic defect-controlled behavior in the temperature range studied (ambient to 350°C). Identical charge conduction mechanisms were present in all the perchlorate salts studied. Electrical conduction in the low-temperature region is postulated to take place via temperature-activated jumps of interstitial cations ($E_a = 0.55\text{--}0.78$ eV). Anion vacancies, either free or bound to an impurity ion, contribute appreciably to the conductivity at higher temperatures ($E_a = 0.87\text{--}1.11$ eV).

Khilla and Hanna (88) measured the electrical conductivity of CrO_2 from 20-182°C. The conductivity decreased with temperature, which may have been due to the presence of OH groups adsorbed on the compound. The activation energy was calculated to be 4.32 eV, which may represent the value for the gap width of CrO_2 .

3. Dielectric Constant

The application of dielectric constant techniques to thermophysical measurement of solids has been used for a number of years (114, 115). The early uses of the technique involved isothermal measurements employing bridge methods. Recently, techniques have been developed that permit the measurement of the dielectric constant of a solid as a function of temperature, in a manner similar to other TA techniques. Chiu (116) used the term *dynamic electrothermal analysis* (ETA) to describe the measurement of both the capacitance and the dissipation factor of polymeric samples. Nottenburger et al. (117) developed an automated technique that permitted the rapid determination of the dielectric properties of a substance over a wide range of temperature and frequencies. This technique, which was called *dynamic dielectric analysis CDDA*, was modified to measure concurrently the DTA curve of the sample as well (117, 118). This new technique was called dynamic dielectric analysis-differential thermal analysis, DDA-DTA.

The experimental parameters of interest to the DDA technique are the following:

1. *Sample Capacitance*, C_s

$$C_s = \frac{1}{\omega Z_s} \sin \phi_s \quad (11.13)$$

where Z_s is the sample impedance and ω is $2\pi f$, the angular frequency.

2. *Phase Shift*, δ_s

$$\delta_s = \tan^{-1}(\omega R_s C_s) \quad (11.14)$$

where R_s is the resistance of the sample.

3. *Loss Tangent*, $\tan \delta_s$

$$\tan \delta_s = \frac{\epsilon''}{\epsilon'} \quad (11.15)$$

where ϵ' is the relative dielectric constant of the sample and ϵ'' , its loss factor which is related to the conductivity, σ_s of the sample by

$$\epsilon'' = \sigma_s / \omega \quad (11.16)$$

ϵ' can also be measured by a "sample in" and "sample out" measurement, according to the expression

$$\epsilon' = \frac{C_A' - C_g}{C_A - C_g} \quad (11.17)$$

where C_A is the capacitance of the empty dielectric cell and C_g is the stray capacitance.

The preceding expressions permit the calculation of the equivalent dielectric parameters of a sample from the measured attenuation and phase shift values.

Dielectric measurements, as a function of temperature, have been widely used to study the properties of semiconductors, insulation materials, plastics, elastomers, all shales, inorganic substances, and others. The dielectric constant technique provides more insight into the segmental motions of the molecule and relaxation phenomena (116) than does other electrical measurements such as electrical conductivity, resistivity, and so on.

a. Instrumentation

Although many instruments are commercially available for the measurement of dielectric constant, only several will be described here. A block diagram of the apparatus used by Chiu (116) is shown in Figure 11.30. The instrument was designed so that the control and data output could be used in conjunction with the Du Pont 900 thermal analysis system. The temperature of the sample-holder assembly was controlled by the temperature programmer of the thermal analyzer console through a thermocouple feedback loop. A General Radio automatic capacitance bridge provides digital output signals of both capacitance, C , and dissipation factor, D , or conductance, G , automatically and continuously. This bridge has three fixed frequencies of 120, 400, and 1000 Hz, and is available for use up to 1 MHz. The digital output of the bridge is converted to analog signals by a D/A converter and displayed on a $X-Y^1, y^1$ recorder on the console.

A schematic diagram of the sample holder, which was built around a Du Pont 941 thermomechanical analyzer, is shown in Figure 11.31. The electrode assembly contains two stainless steel electrodes that permit the use of sample disks having a diameter of about 1 cm. Contact of the electrodes with the sample is assured by placing a 10 g weight on the upper electrode. A thermocouple positioned close to one side of the sample provided measurement of the sample temperature. Purge gas can be applied through a glass tubing into the sample chamber. A glass Dewar flask was used to cool the sample for low-temperature measurements; the temperature range of the sample holder-furnace arrangement was said to be ~ 190 – 500°C .

The automated DDA-DTA apparatus described by Nottenburg et al. (117, 118) is shown in Figure 11.32. Two modes of operation of the DDA are: Mode A, which allows monitoring of the ac electrical properties of the sample

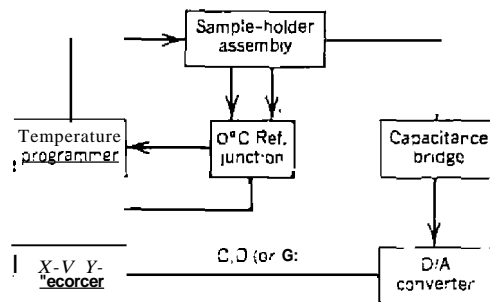


Figure 11.30. Block diagram of system used by Chiu (116)

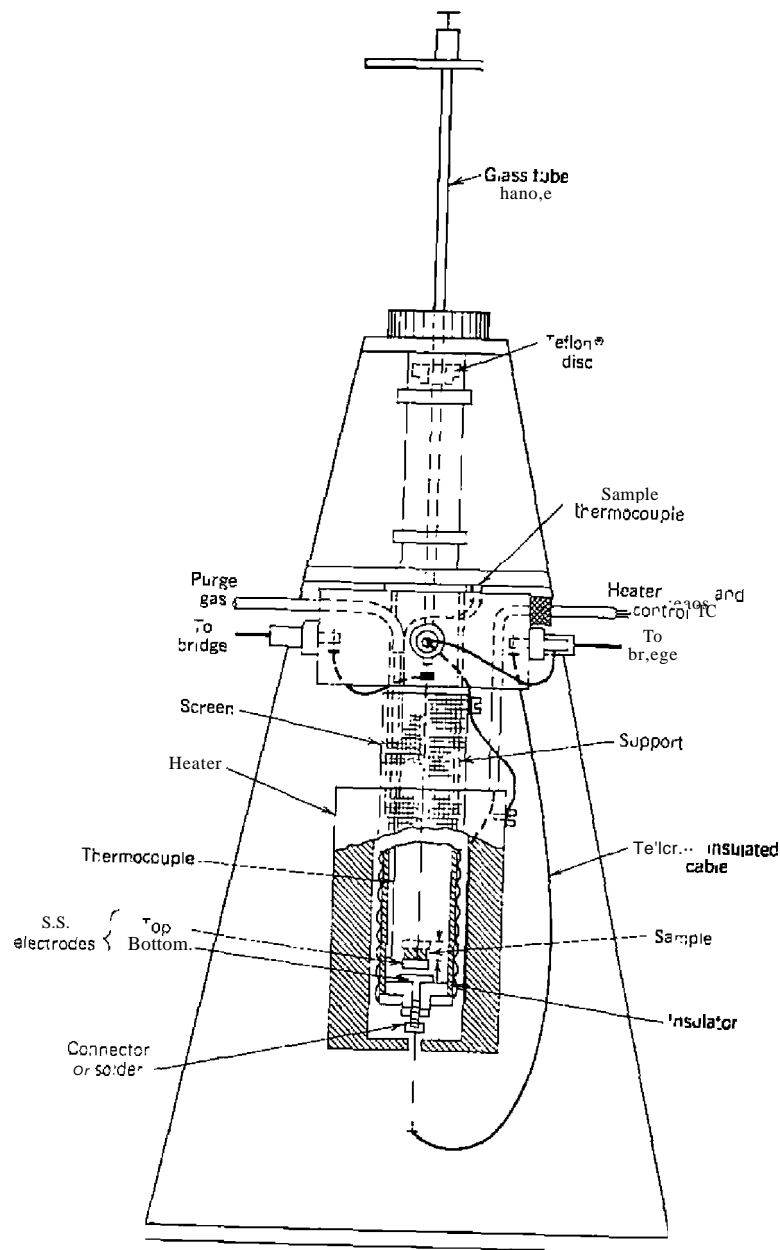


Figure 11.31. Sample-holder arrangement (116).

over a range of frequencies from 50-1 MHz at selected temperatures; and Mode B, which permits the measurement of dielectric properties from 25-800°C at selected frequencies.

The major component of the system is the Hewlett-Packard desk-top calculator, shown in Figure 1U2a, which provides digital control of the system components, acquisition of thermal and electrical data, and subsequent processing and storage on floppy-disks. A general-purpose interface bus links the calculator with various components of the control assembly. The major components of the system are a programmable frequency synthesizer and a network analyzer. Frequency coverage from 50-1 MHz is provided by the frequency synthesizer, with the network analyzer functioning mainly as a vector voltmeter.

The sample-holder arrangement consists of a nickel block 50 mm in diameter and 45 mm in length. This block is suspended from a vacuum flange

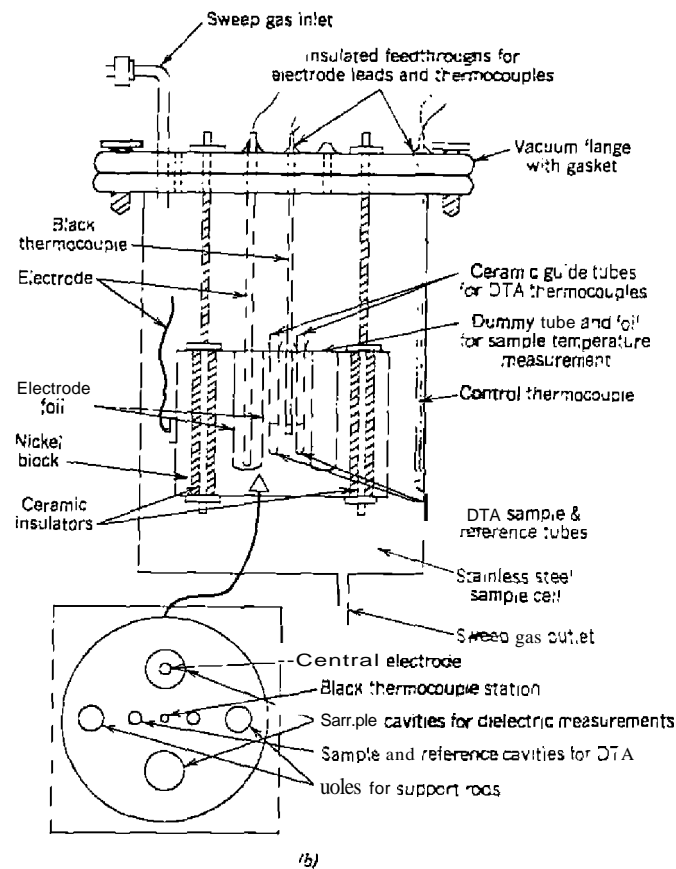
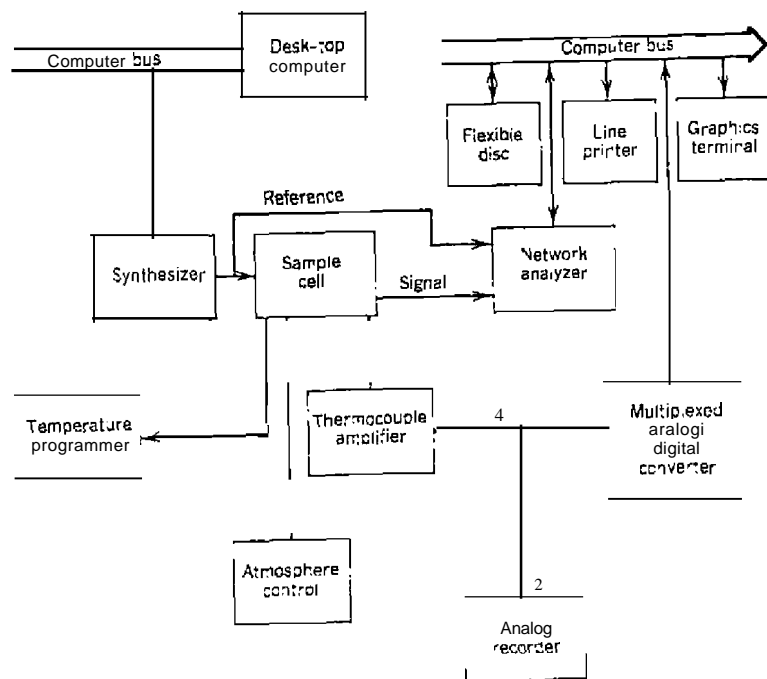


Figure 1U2. DDA-DTA apparatus described by Nottenburg et al. (117, 118). (a). Block diagram of system; (b). sample-holder arrangement.

by rods that are insulated from the nickel block with ceramic inserts. For dielectric measurements, two symmetrical holes in the block provide cavities for the two DTA and two DDA sample and reference materials. The entire assembly can be either flushed with an inert gas or evacuated. A coaxial-type two-terminal electrode configuration is used for the DDA measurements. The inner electrode is a solid silver rod 5 mm in diameter which is positioned symmetrically with respect to the outer electrode, comprised of a thin silver foil pressed to the outer walls of the 13.5-mm diameter cavity. The coaxial arrangement permits

measurements on liquids, powders, or machined samples and offers greater flexibility than the simple parallel-plate configuration. The other 13.5 mm cavity is used for temperature measurement of the block.

b. Applications

Chiu (116) used the apparatus previously described to study the thermal decomposition of selected polymers such as poly(ethylene terephthalate), poly(vinyl fluoride), poly(vinylidene fluoride), and others. The dielectric constant curves of a group of fluorocarbon polymers are shown in Figure 11.33. As illustrated, the more polar polymers such as poly(vinylidene fluoride) (PVDF) and poly(vinyl fluoride) (PVF) show characteristic dielectric loss peaks that are distinguishable from the relatively featureless and low-loss curves of the other polymers. For PVF, the low-temperature process is due

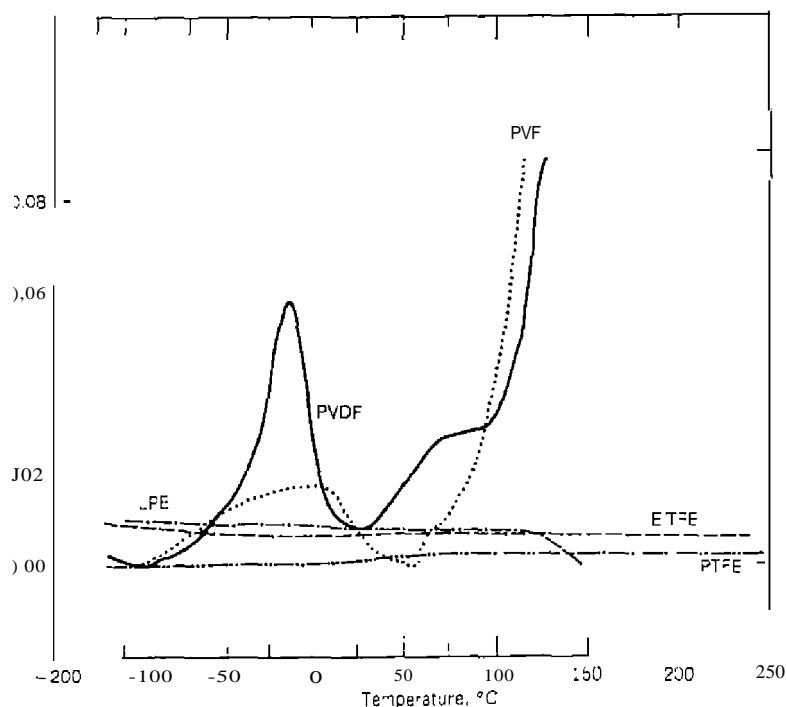
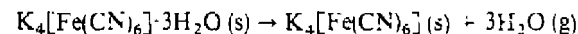


Figure 11.33. Dielectric constant curves of various polymers (116).

to a glass transition, whereas the higher-temperature peak is due to a dielectric relaxation mechanism.

Bristoti et al. (79, 80) used dielectric constant measurements, as well as other thermal analysis techniques, to study the thermal decomposition of various inorganic compounds. The DTA and dielectric constant curves for NaNO_2 both consist of a single peak. [In the DTA curve, a narrow endothermic peak centered at 165°C was observed, due to an order-disorder crystalline transition. The dielectric constant curve showed a well-defined Debye relaxation behavior for this compound. This relaxation is generally accepted to be due to a diffusion process of the nitrogen ions along the crystal *b* axis. It was found that the dielectric constant curve for the dehydration of $\text{CuSO}_4 \cdot 5\text{H}_2\text{O}$ was similar to the TG curve rather than the DTA curve of this compound. The dielectric constant curve for this compound did not show any significant Debye relaxation behavior and changed little during the dehydration reactions.

The dielectric constant curve versus temperature was also investigated for $\text{K}_4[\text{Fe}(\text{CN})_6] \cdot 3\text{H}_2\text{O}$ by Bristoti et al. (80) in the temperature range -80 to 150°C . Four peaks were observed in the curve from -80 to 25°C , due to the presence of the water of hydration. A single peak with a maximum at 105°C was due to a paraelectric order-disorder transition. [It is in this temperature region that the dehydration reaction



takes place.

Nottenburg et al. (117, 118) used the DDA-DTA technique to study the thermal properties of KClO_4 (118), Green River oil shales (83, 84), and oil sands (85). The weak dependence of ϵ' and ϵ'' on shale organic content at frequencies in the range of 50 to 1 MHz effectively rules out the application of dielectric techniques as an assay tool (35). The transparent behavior of oil-shale minerals to electromagnetic radiation in the microwave frequency could, however, facilitate possible determination of organic content at these frequencies. For oil sands (85), the ϵ' values showed an anomalous increase at temperatures above 200°C and reached a maximum at temperatures in the range 350 – 450°C . This increase is attributed to polarization effects arising from the thermal decomposition of oil sand bitumen. The dielectric loss tangent ($\tan \delta$) showed a temperature dependence similar in nature to that of ϵ' . This increase in $\tan \delta$ is due to the increased conductivity arising from the creation of mobile charges from thermal fragmentation of the oil sand bitumen. This anomalous increase is superimposed upon the usual exponential temperature dependence of the dc electrical conductivity. Dipolar relaxation effects were observed in $\tan \delta$ (or ϵ'') at temperatures above 150°C .

These relaxation effects arise from orientation of dipolar charges created by the thermal decomposition reaction.

The dielectric constant versus temperature curves of trans-stilbene and N-benzylideneaniline were determined by Kwatra et al. (86). As shown by the curve for the latter compound in Figure 11.34, the steep curvature of the curve just before melting is indicative of a premelting phenomenon involving a solid-solid transition, whereas the behavior in the supercooled region indicates the occurrence of a prefreezing transition in the liquid state. Such a phenomenon is not uncommon, particularly in molecules with a strong dipolar character, with groups involving torsional oscillations or rotational movements.

The dielectric constant at 1 MHz showed an anomaly near the phase transition point for K_2SO_4 (87). A gradual increase of the dielectric constant at 1 kHz for this compound was observed from 158 to 600°C; at 600°C, the dielectric constant at 1 kHz for this compound was observed from 158 to

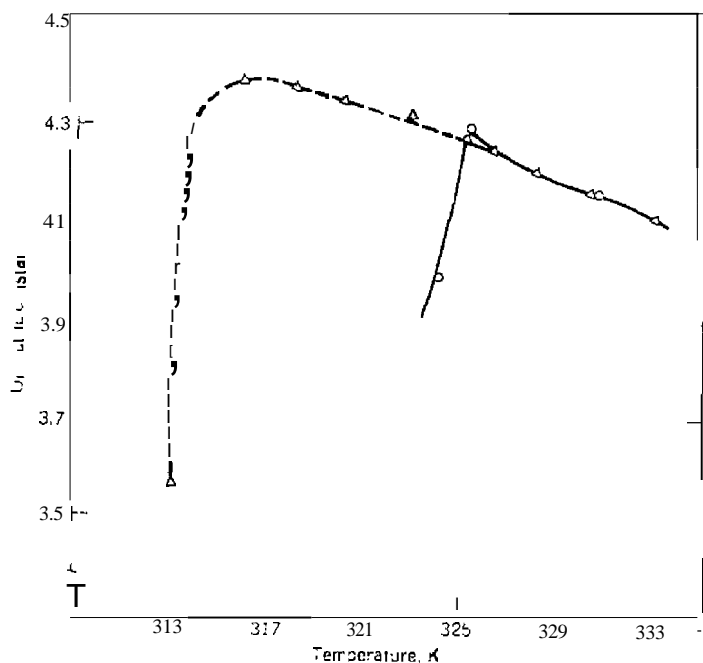


Figure 11.34. Dielectric constant of N-benzylideneaniline. (○) heating; (△) cooling (86)

600°C; at 600°C, the dielectric constant was 469. The temperature dependence of the dielectric constant at 1 MHz above and below 587°C revealed a Curie law behavior.

4. Miscellaneous Electrical Techniques

a. Current-Voltage

A current-voltage technique was developed by Rajeshwar (59) to study oil shales. When an electric field is applied to a solid substance, the current flowing through it is time-dependent. Two types of polarization mechanisms have been used to explain this time dependency: linear polarization and nonlinear polarization. A convenient method of distinguishing between these is to examine the $\ln J_{ss}$ versus $\ln V$ plots (where J_{ss} is current density and V is the voltage). Linear polarization will result in curves with a slope of +1, whereas nonlinear polarization will give linear $\ln J_{ss}$ versus $\ln V$ plots of slope $\neq 1$. The oil shales reveal a complex behavior involving both linear and nonlinear polarization effects.

A typical current density versus voltage curve for a Colorado oil shale is given in Figure 11.35. An increase in temperature enhanced the nonlinearity in the curve while an increase in the shale organic content (or oil yield)

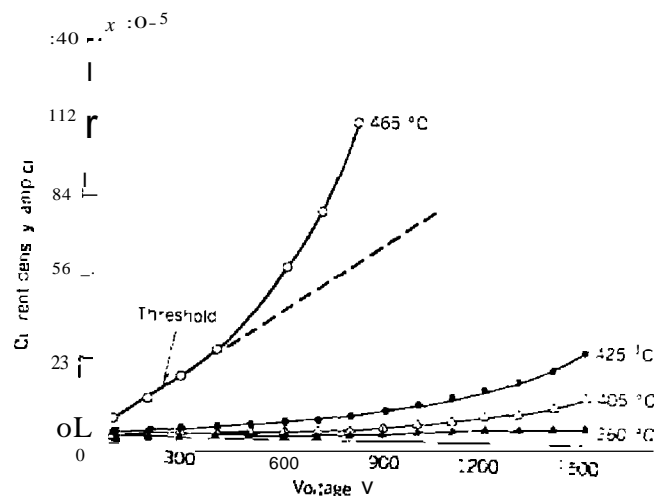


Figure 11.35. Variation of current density with voltage for a Colorado oil shale (oil yield = 100 Litons) (89).

tended to enhance the nonlinearity of the current-voltage behavior, This was manifested by the shift in the threshold voltage to lower values with increasing oil yield at a given temperature.

b. Thermally Stimulated Discharge (TDS)

A new simultaneous thermal analysis technique was reported by Weber and Vogel (90), which consisted of DSC or OTA combined with thermally stimulated discharge (TDS). For copolymers of methyl methacrylate, the molecular origin of the TSD-current at the low-temperature side of the T_g was related to the disorientation of small polar segments of the comonomer in the main chain of the polymer. The TSD-current of the α_2 -relaxation ($T \sim 80^\circ\text{C}$) increased with increasing comonomer content. The TSD₃-peak at $T > T_g$ could be attributed to trapped space charges that regain their freedom of motion. This simultaneous technique is recommended for the investigation of the relationship among the dipolarization of dipoles, carrier transport, trapping of real charges, and thermal transitions of polymers.

c. Current-Temperature and Voltage-Temperature

Pillai et al. (91) studied the current versus temperature curves that were obtained when certain polymers, in contact with two dissimilar metal electrodes, were heated to moderate temperatures. The magnitude of this current was proportional to the metal electrode work function, the liberated ions that reacted with the metal electrodes electrochemically, and the resistance of the cell. A plot of current versus temperature for cellulose, using Cu-Al electrodes, contained only a single peak in the 50–130°C temperature range. This peak was attributed to the water that was desorbed during the thermal degradation reaction. A second increase in the current above 150°C was attributed to water dehydrated from equatorial hydroxy groups in the cellulose units. Similar current-temperature curves were obtained on poly(vinyl alcohol) and $\text{NiSO}_4 \cdot 6\text{H}_2\text{O}$.

Wendlandt (119) has developed a similar technique but plotted the EMF versus temperature. Since this was potentially a new general thermal analysis technique, he proposed the name *thermoelectric detection* (TVD) for it. The EMF is generated by the sample undergoing a thermal transition (fusion, thermal dissociation, etc.) in contact with two dissimilar electrodes (usually platinum and aluminum, respectively). A schematic diagram of the electrode arrangement is shown in Figure 11.36 (119). The voltage of the electrodes during the thermal decomposition reaction of the sample varies from 0 to 1.2 V. This is rather surprising because in most TA techniques, the magnitude of the measured signals is of the order of microvolts or millivolts. Thus,

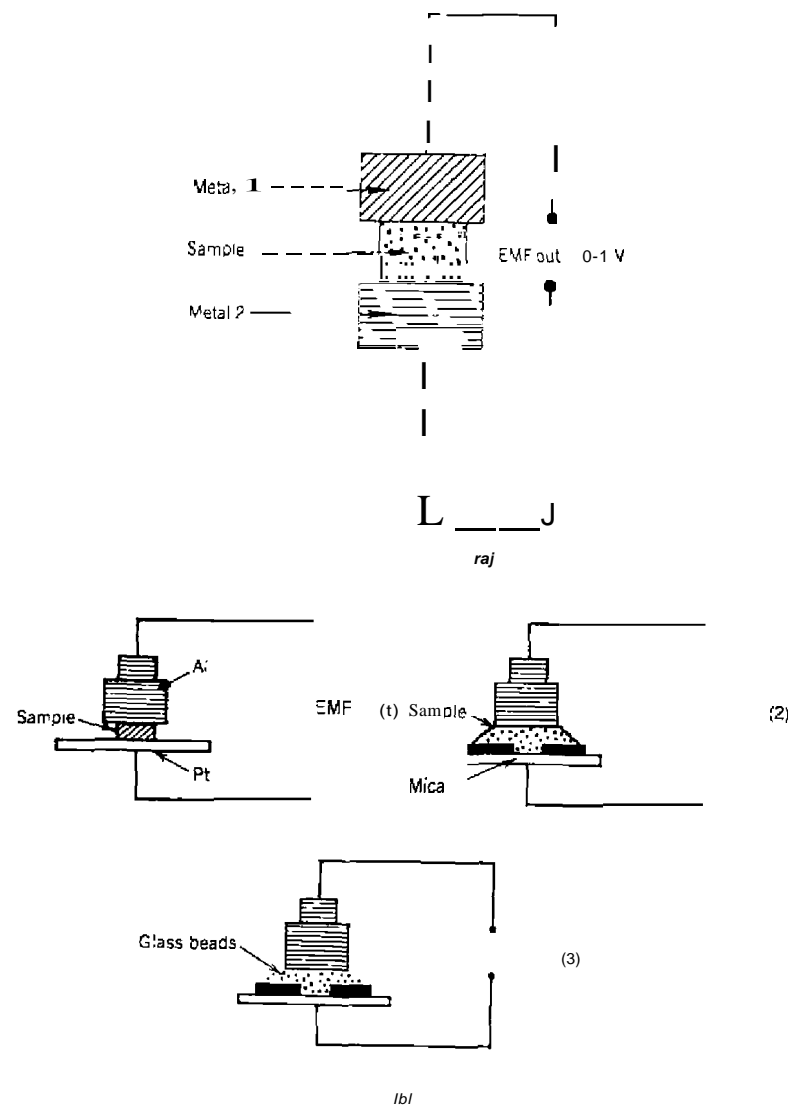


Figure 11.36. Schematic diagram of TVD electrode arrangements (119, 120). (a) Principle "TVD" detection; (b) types of sample holders—1, disk samples; 2, powdered samples; 3, liquid samples.

simpler voltage measuring recorders are needed to record the V-I curves. Vendlandt (119) employed a data center recorder that permitted storage of the digitized data on floppy disks.

TYD curves of three inorganic compounds, $\text{NiSO}_4 \cdot 6\text{H}_2\text{O}$, $\text{CoSO}_4 \cdot 7\text{H}_2\text{O}$ and $\text{Ni}(\text{py})_4\text{Cl}_2$ are shown in Figure 11.37 (119). Two of the compounds are metal salt hydrates, $\text{NiSO}_4 \cdot 6\text{H}_2\text{O}$ and $\text{CoSO}_4 \cdot 7\text{H}_2\text{O}$, whereas the third is a pyridine complex, $\text{Ni}(\text{py})_4\text{Cl}_2$. For $\text{NiSO}_4 \cdot 6\text{H}_2\text{O}$, a shoulder peak at 119°C and two peaks at 135 and 160°C , respectively, are observed in the curve. These peak maxima agree with the concurrent DTA curve (not shown) obtained on a disk sample at the same heating rate of $10^\circ\text{C min}^{-1}$. In the case of $\text{CoSO}_4 \cdot 7\text{H}_2\text{O}$, two major peaks are observed in the IVD curve, at 109 and 122°C , respectively. These two peaks occurred at a much lower temperature than those found in the corresponding DTA curve (136 and 150°C , respectively). The evolution of water is not necessary in order to generate an EMF from the electrode system employed, as is illustrated by the TVD curves of $\text{Ni}(\text{py})_4\text{Cl}_2$. Two peaks are observed in the curve at 144 and 165°C , respectively. In this temperature range the DTA curve (not shown) contained two endothermic peaks, with peak minima at 144 and 183°C , respectively.

The TVD curves of five organic acids are illustrated in Figure 11.38 (120). Each acid gives a characteristic curve that can be used for fingerprinting or

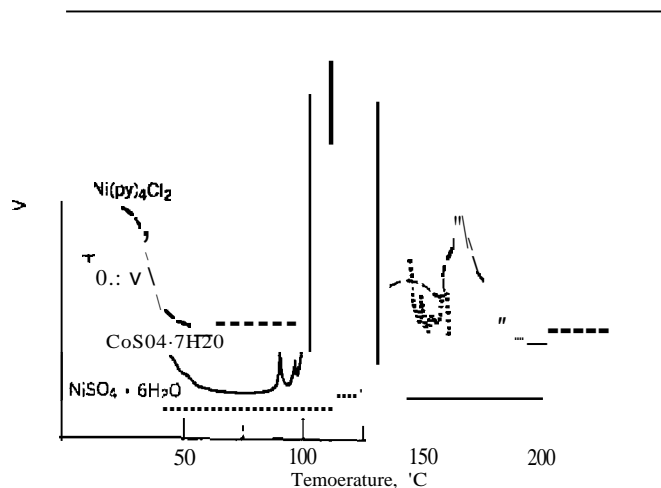


Figure 11.37. TVD curves of $\text{NiSO}_4 \cdot 6\text{H}_2\text{O}$, $\text{CoSO}_4 \cdot 7\text{H}_2\text{O}$, and $\text{Ni}(\text{py})_4\text{Cl}_2$ in N_2 and at $0.1^\circ\text{C min}^{-1}$ heating rate (119).

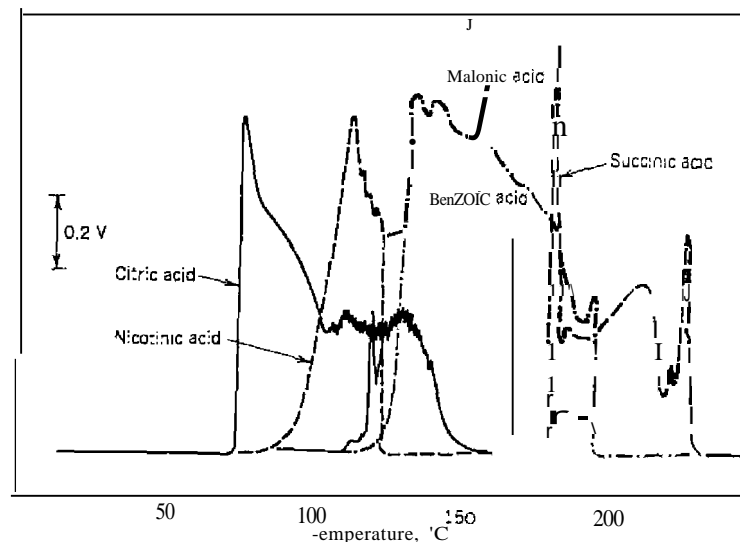
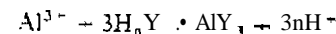
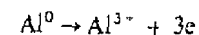


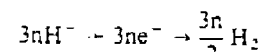
Figure 11.38. TVD curves of organic acids (120).

identification of the individual compound. All the acids generate a characteristic EMF curve during fusion and/or decomposition reactions. For these compounds, the probable electrode reactions that occur at the Al-Pt electrode system are:

Aluminum electrode (-)



platinum electrode (+)



At the end of the run, the aluminum electrode is covered with a deposit of the organic acid, necessitating polishing it before the start of the next run. The reproducibility of the TVD curves was demonstrated with malonic acid. Three curves, recorded under identical conditions, were within 3-4% of each

other. The reproducibility may be fortuitous when all the instrumental factors such as solid sample-electrode and liquid sample-electrode interfaces are considered.

The TVD curves of selected amino acids were determined by Contarini and Wendlandt (111). A comparison of the TVD and DSC peak temperature is shown in Table 11.8. The TVD peak temperatures are somewhat higher than those obtained by DSC. Obviously, the kinetics of the electrode-decomposition product(s) reaction are different from those of the decomposition reaction. These electrode reactions probably involve one or more diffusion steps between the electrode surface and the amino acid or amino acid decomposition product(s), which would be different from the decomposition kinetics themselves. The leading edge of the TVD curve peaks is reproducible to within $\pm 1-2\%$. However, after the peak maximum temperature is attained, the reproducibility falls to within $\pm 20\%$ in some cases. This is related to the electrode-amino acid decomposition products interface, which due to the nature of the reaction, would not be expected to be reproducible. The trailing edge portion of the curve also consists of several shoulder peaks that may be related to the consecutive and/or concurrent reactions previously described in the DSC curves. These reactions could produce decomposition products that would react with the aluminum metal electrode surface.

The primary amino acid-electrode reaction is probably similar to that

Table 11.8. DSC and TVD Peak Temperatures for Selected Amino Acids (121)

Amino Acid	DSC ΔT_{min} (°C)		T_{max} (°C)	
	This work	Refs. 3-6	TVD ^a	TG ^b
L-Arginine	248	246	265	285
L-Glycine	262	259	288	285
L-Glutamine	192	196	210	228
L-Histidine	287	288	308	322
DL-Lysine ^c He:	273	233 ^c	297	310
DL-Methionine	272	289	288	

^aPeak maxima temperature.

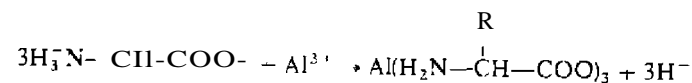
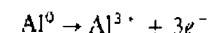
^bTemperature for maximum slope of TG curves.

^cFor L-lysine.

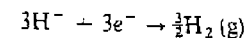
^dNot available.

previously described for succinic acid (120). Using a general formula for an amino acid, one finds that the electrode reactions are probably:

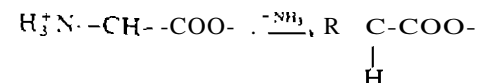
Aluminum electrode (-)



platinum electrode (+)



These would involve the primary electrode reactions with the amino acid; a possible secondary reaction could involve deamination reactions of the amino acid such as



which might also react with the aluminum electrode via various diffusion-type reactions. Decarboxylation reactions might also proceed via the aluminum electrode to give the amine, $R-CH_2-NH_2$. Also, at still higher temperatures, pyrolytic reactions may take place yielding carbon or carbonaceous residues.

d. Applied Electrical Fields

MacKenzie (95, 96) has developed a method for the TG study of solids in the presence of applied electrical fields. Electric fields of the order of $\sim 10^5$ V/cm lower the initial decomposition temperature for the dehydroxylation of kaolinite by 60° in some cases. The activation energy for the process is reduced by 3-12 kcal/mole. Rate constants for the material are increased by electrolysis but this effect falls off at higher temperatures as the normal processes begin to predominate.

D. THERMOSONOMETRY

1. Introduction

Thermosonometry (TS) is defined by the ICTA as "that technique in which the sound emitted by a substance is measured as a function of temperature whilst the substance is subjected to a controlled temperature programme." As a thermal analysis technique, TS is concerned with the detection and interpretation of the various acoustic emissions occurring prior to, during, and after thermal events (127). It can thus contribute to the elucidation of the thermal behavior of solid materials and to an understanding of the dynamic processes of the solid state. The technique has been developed for thermal analysis measurements principally by Lonvik (128, 143) with other applications described by Clark (127) and Rajeshwar et al. (129).

The specific origin of acoustic emissions are: (1) fracture mechanics, (2) release of inclusions, (3) phase transformations, and (4) dislocation processes and plastic deformation (128). Sonic noise-producing processes are obviously initiated by the strain-stress state of the crystalline state. Different thermal expansions of crystallites, mutual displacements of them, and so on, cause the material to rupture and shear. The sudden release of the thermally accumulated elastic energy can initiate measurable mechanical vibrations. Decrepitations, caused by exploding gas-liquid inclusions in minerals as they are heated, can initiate sonic shock waves. Certain phase transitions and volumetric effects of structure recrystallization, emit ultrasonic emission. Proposed sources of acoustic emission include dislocation slips, dislocation breakaway, activation of dislocation sources, twinning, grain boundary sliding, crack nucleation, and phase changes.

The technique of TS, although not widely used at the present time in thermal analysis, has the potential of being useful in many different areas of science and technology. It has been applied to problems in inorganic and organic chemistry, mineralogy, metallurgy, fuels, and so on.

2. Instrumentation

The components of a TS system are shown in Figure 1.39 (130). A resonance stethoscope is used to transmit crystalline vibrations in the sample to the audio frequency range where they are converted to electrical signals by use of a piezo-electric crystal. The stethoscope is constructed of quartz, which, because of its high Q value, operates mechanically both as a tuned pick-up sensor and as a self-exciting resonator. The unit incorporates a sample-holder head shaped as an acoustic transformer and fitted with a transmitter rod that mechanically matches the piezo-electric cell fixed on a heavy recoil

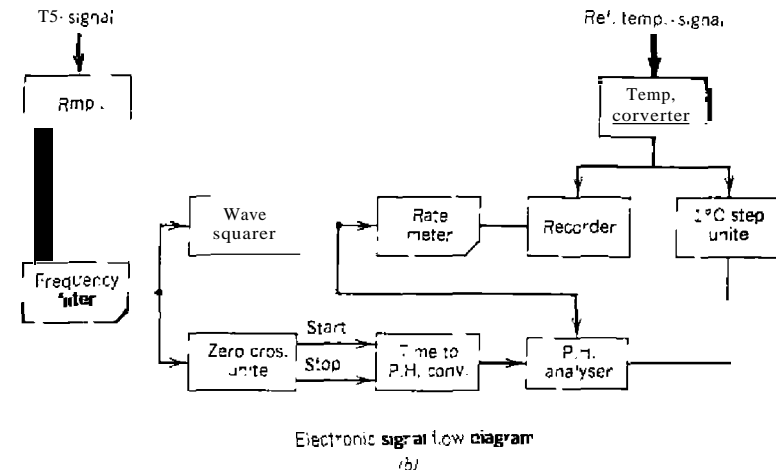
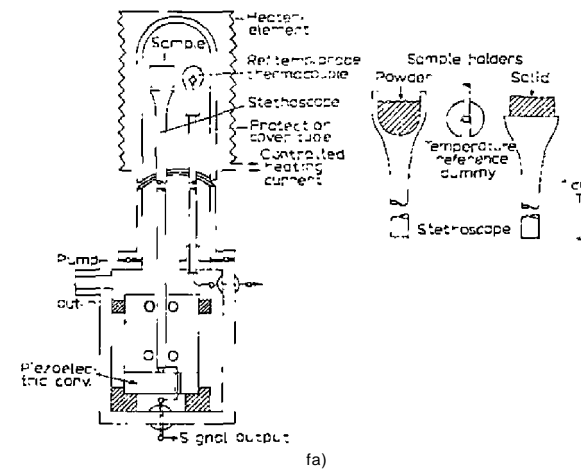


Figure 1.39 TS system as described by Lonvik (130). (a) Schematic diagram of furnace and sample holder; (b) signal processing and detection.

foundation. The entire assembly has a seismic mount to prevent noise interference from the outside. Mechanical distortions or perturbation in the sample create elastic oscillations in the stethoscope, the amplitude of which depend on the coupling efficiency between the sample and the stethoscope. The actual output is a charge signal converted from the elastic forces pro-

portional to the displacement appearing at the reflecting end of the transmission rod. The results of these electrical effects appear as damped ringing oscillations of the natural resonance frequencies of the stethoscope assembly. A full analysis of the signal is a rather complicated problem but two effects of fundamental importance are:

1. A series of instantaneous pulses, $S[N_s]$, with a period, $T(w)$, inserted on an oscillator system (w_0), which give an impact resonance if $n\omega = w_e'$ with amplitude, A , of $S/2mw_0(\sin \pi\omega_0/\omega)$.
2. An instability effect of a closed passive resonance system in a self-exciting oscillating amplitude because of a small perturbation of frequency, w , in the potential state given by

$$\omega_s^2 = \omega_0^2 (1 - p \cos(2x)) \quad (11.18)$$

with the parametric substitution of

$$x = \frac{1}{2}\omega t$$

The principal method of TS detection is based on the registration of the number of bursts (or waves) per second of the electrical signals. The electronic components include also a circuit to register the primary frequency components in the TS burst signal. The occurrence of the individual frequencies is stored and recorded as a distribution versus frequency curve. The output curves are a scan of the TS activity versus temperature and the pulse height analyzer output that gives the density distribution per 1°C of TS activity.

An apparatus similar to the one described by Lonvik (130) has been discussed by Clark (127). Improvements include a waveguide system that can be accurately and reproducibly positioned and the attachment of the piezo-electric crystal transducer. The system also includes a DTA sample holder for measurement of concurrent TS-DTA data. Furnace heating rates up to $100^\circ\text{C}/\text{min}$ are required for some studies although the normal heating rate is $40^\circ\text{C}/\text{min}$. The maximum furnace temperature is 1000°C .

Mraz et al. (129) have described an automated technique for the thermoacoustimetry of solids in which precise measurements of the transmission times of Sand P waves across a sample of known dimensions can be made.

3. Applications

The TS curve for $\text{Mg}(\text{OH})_2$ powder is given in Figure 11.40 (130). The curve is characterized by successive subpeaks around 400°C which is at the begin-

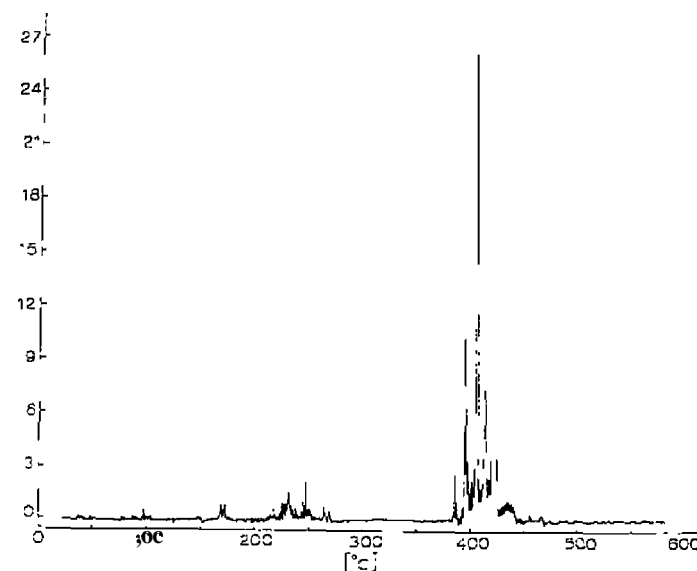


Figure 11.40 TS curve of $\text{Mg}(\text{OH})_2$ powder (130).

ning of the endothermic dehydroxylation peak in the DTA curve. The TS signals at the 400°C peak are lowered 50% on decreasing the heating rate from $10\text{--}2^\circ\text{C}/\text{min}$. From the TS curve it was concluded that the dehydroxylation reaction is stepwise.

The TS curves of four kaolinite samples are presented in Figure 11.4 (131). All the curves contain two areas of TS activity. The first region, from $500\text{--}600^\circ\text{C}$, corresponds to dehydroxylation, whereas the second region, $980\text{--}985^\circ\text{C}$, is due to the high-temperature solid-state phase transition. In the temperature region between them, the so-called metakaoлин region, several smaller TS activities are noted that have not been identified. The dehydroxylation peaks consist of numerous subpeaks and in some cases show a splitting into two separate regions. This indicates that this process may consist of two separate steps.

Four Green River oil shales were studied by TS (132). The TS curve of the sample with a low organic content, 54 L/ton, is shown in Figure 11.42. All the curves contained the same general features even though the organic contents varied from $10\text{--}400\text{ L}/\text{ton}$. Four regions of TS activity were noted in each curve although there was considerable overlapping in the $300\text{--}470^\circ\text{C}$ region. Most of the samples had a tendency to exhibit activity over a

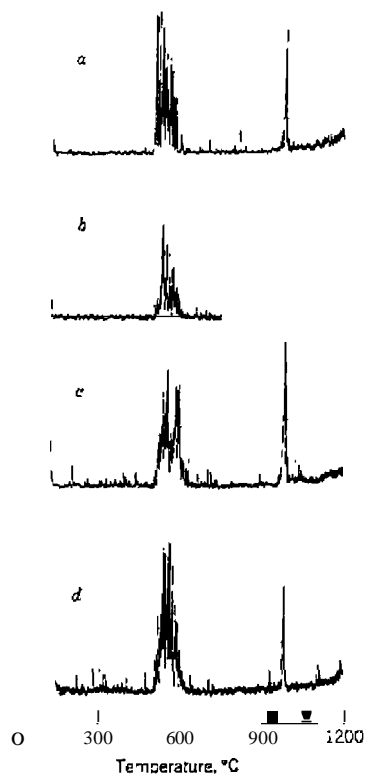


Figure 11.41. TS curves of kaolinite (131). Sources: a, Standard porcelain; b, Grolleg; c, NSC; d, LPC.

broad temperature range in this region. Very little TS activity was noted above 500°C.

Clark and Garlik (133) compared the TS peak temperatures with the DTA peak temperatures for the NBS-ICTA temperature standards. However, the precise relationship between the TS peak and the DTA peak for a given thermal event was not established.

The extrapolated onset temperatures for the NBS-ICTA standard materials are given in Table 11.9 (133). Three sets of data are presented, the JCTA (134) temperature; the DTA (model 673-4 DTA apparatus) temperature; and the TS-DTA apparatus temperature. Standard deviations between these onset temperatures and the ICTA mean extrapolated onset values (T_{ICTA}) are -1.5 and -6.5°C , respectively. The deviation of the DTA 673-4 is negligible

THERMOSONIMETRY

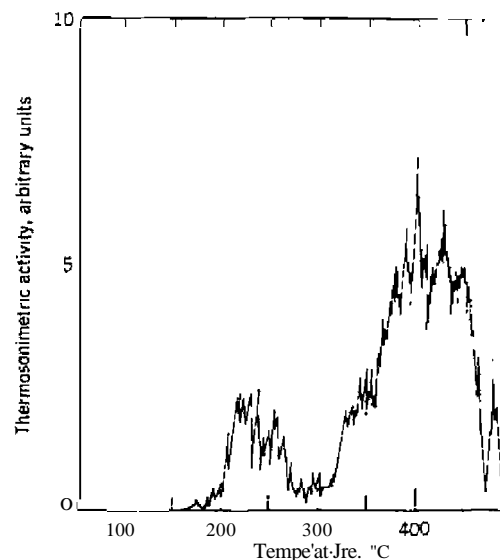


Figure 11.42. TS curve of Green River oil-shale assaying 54 L/100.

Table 11.9. Extrapolated Onset Temperatures of NBS-ICTA Standard Materials 759 and 760 (133)

Material	ICTA Mean Extrapolated Onset Temperature (8), T_{ICTA} (°C)	Observed Mean Extrapolated Onset Temperature, DTA 673-4 (°C)	Observed "Extrao" Onset Temperature, TS-DTA (°C)
KClO ₄	299	300	294
Ag ₂ SO ₄	424	427	416
SiO ₂	571	570	563
K ₂ SO ₄	582	579	576
K ₂ CrO ₄	665	663	661
BaCO ₃	808	806	800
SrCO ₃	928	923	921

and the TS-DTA values are within $\pm 5-8^\circ\text{C}$ deviation of the T_{ICTA} value.

Other materials studied by TS include alkali metal dichromates (i.e., CuSO₄·5H₂O (136); European and South American bauxites (137); K₂Cr₂O₇ (138); Ca₂SiO₄ and Na₂BeF₄ (139); CsCl-NaCl phase diagram (140); [use, salts (141); metallic glasses (142); quartz (143); and others.

E. THERMOMAGNETOMETRY

1. Introduction

Thermomagnetometry (TM) is defined by the TCTA as "a technique in which the magnetic susceptibility of a substance is measured as a function of temperature while the substance is subjected to a controlled temperature programme." The determination of the magnetic susceptibility of a substance at various temperatures has been used in inorganic chemistry for many years as a means of determining metal ion oxidation states, stereochemistry, Curie points, and so on. In thermomagnetometry, the changes in the TG, EGA, or other technique curves of a substance are determined in the presence or absence of a magnetic field gradient. The most common technique employed is TG, but EGA has also been used to study reduction reactions in reducing atmospheres. Numerous analytical applications have made use of this technique for the determination of magnetic materials in a nonmagnetic matrix. This discussion will include only those applications of TM as defined by ICTA and will not be a comprehensive review of the applications of magnetic techniques to inorganic chemistry or other fields.

2. Instrumentation

For TG-TM, the sample holder and furnace are in close contact with a magnetic field, supplied by either a permanent or electromagnetic magnet. The observed changes in mass are proportional to changes in sample mass and the magnetic susceptibility of the sample, both as a function of temperature. Either the classical Gouy or Faraday methods of determining the magnetic susceptibility of the sample may be employed. Instruments described in the literature include a helical-spring microbalance-Faraday or Guoy magnet apparatus (144, 164), Ainsworth semimicro recording balance-Faraday magnet apparatus (165), Perkin-Elmer TGS-1 thermobalance (145) and Cahn microbalance (146-149)-Faraday magnet systems. For EGA-TM studies, a magnet is located in close proximity to the furnace and sample holder (145, 150). A mass spectrometer or similar analytical device are used to monitor the evolved or reacted gases.

3. Applications

The TG curve of $[\text{Co}(\text{NH}_3)_6]\text{Cl}_3$, in the absence and presence of a magnetic field, are shown in Figure 11.43 (165). The deviations of the TG curve in the presence of the magnetic field are proportional to the magnetic susceptibility of the substance. From this curve, the changes in the magnetic suscep-

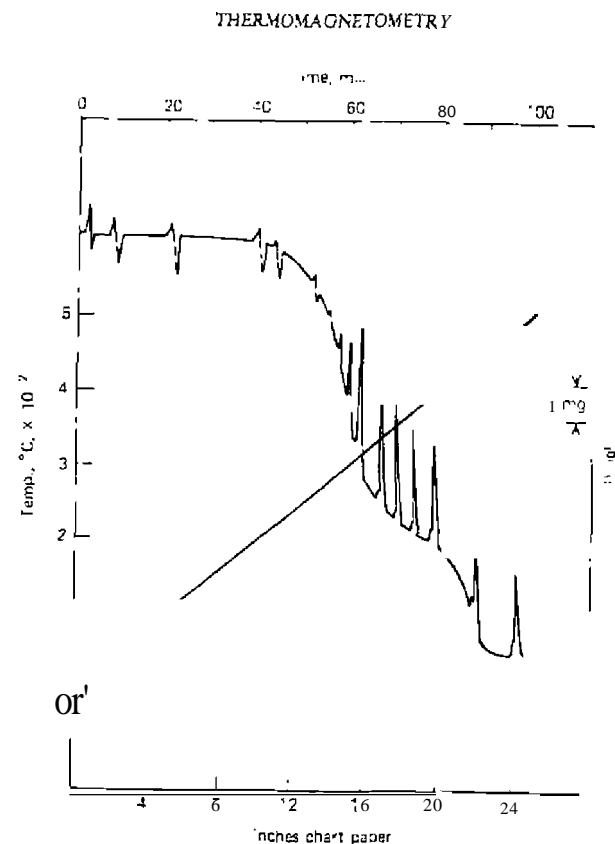
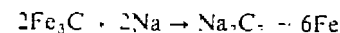


Figure 11.43. TG curve of $[\text{Co}(\text{NH}_3)_6]\text{Cl}_3$ in absence and presence of magnetic field (165).

tibility of the reacting mixture can be calculated and plotted as a function of system temperature to yield the TM curve. Such a plot is shown in Figure 11.44 (65), where the molar percent reduction of the $\text{Co}^{3+} \rightarrow \text{Co}^{2+}$ reaction, mass susceptibility, and mole-% cobalt(III) reduced curve are presented.

Charles et al. (166) used TM to study the reduction of Fe_3C with excess lithium or sodium metal. Decomposition of Fe_3C , shown in Figure 11.45, is rapid above 600 C, whereas the reaction with sodium metal indicates that no direct reaction such as



can take place in the temperature range at which the dissociation reaction is

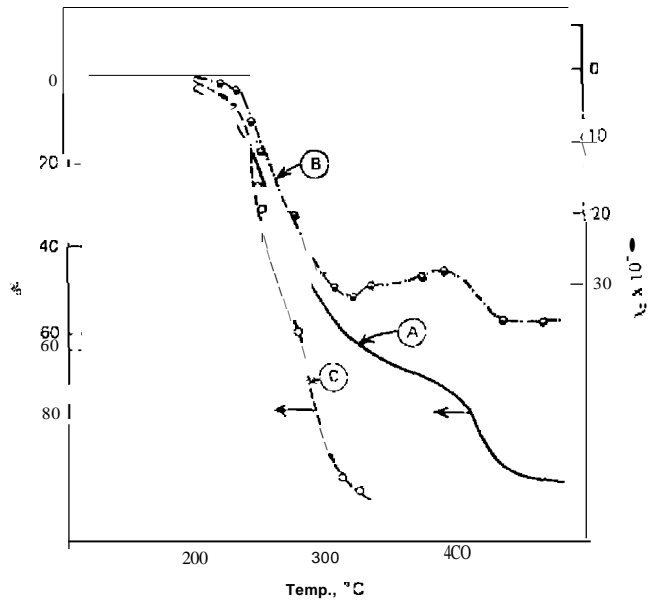


Figure 11.44. TG, mass susceptibility, and molar percent reduction of $[\text{Co}(\text{NH}_3)_6]\text{Cl}_2$. A, TG curve; B, mass susceptibility curve; C, mole-% cobalt(III) reduced curve (165).

important. Both the Curie point and the extent of interaction with the magnetic field at room temperature were found to be unaffected by the heating.

Thermomagnetometry was used by Gallagher et al. (151) to study the phase changes of Chromindur II (Fe-28 Cr -10.5Co) alloys having different thermal histories. The TM curves for this alloy at various heating rates are shown in Figure 11.46. Although various sample masses were used, the curves were normalized by using weight (mass)% as the Y axis. The fastest heating rate, 160°C/min, gave a curve the most representative of the pure α -phase. The sharpness of the transition at 640-650°C indicates a T_c (Curie point temperature) of 650°C for the alloy. As the heating rate is decreased, the extent of α_1 and α_2 formation should increase, resulting in the maximum variation in composition between the two phases. Since the spinodal decomposition results in phases of higher and lower chromium content than the parent, α , alloy, there should be apparent mass losses at higher temperatures depending on the magnetic properties of the various α_1 and α_2 phases.

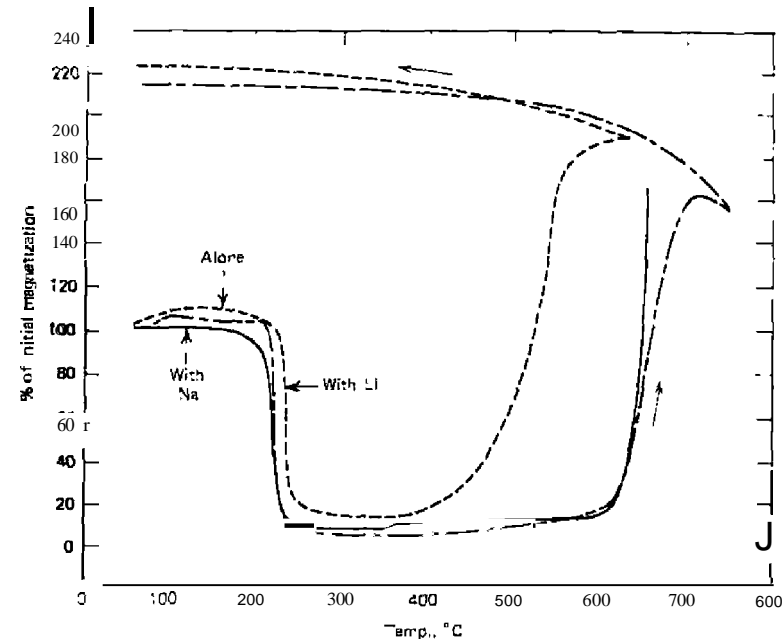


Figure 11.45. TM curves of reaction DfFe/C with Na or Li (166).

This is particularly evident for the alloy heated at the slowest rate, 0.62°C/min. Intermediate heating rates showed less of this resolved behavior. A rapid heating-rate TM curve will quickly reveal whether the alloy had previously undergone significant spinodal decomposition during its prior thermal history.

TM, along with TG, EGD, and X-ray diffraction, was used to study the thermal decomposition of siderite (145, 151). The TM curve for siderite, in nitrogen and oxygen, is presented in Figure 11.47. The decomposition in N_2 begins around 400°C as the wustite originally formed becomes oxidized by the CO_2 and magnetite is formed. These magnetite nuclei grow until they are of sufficient size and crystallite perfection to magnetically order. This gives rise to an apparent mass-gain in the magnetic field gradient because the sample is still below the T_c for the spinel phase. As the T_c in this phase is exceeded, the mass quickly adjusts to the mass-loss curve in the absence of a magnetic field. The T_c (-550°C) is in good agreement with literature values. In O_2 , however, the wustite is so rapidly oxidized to hematite that the

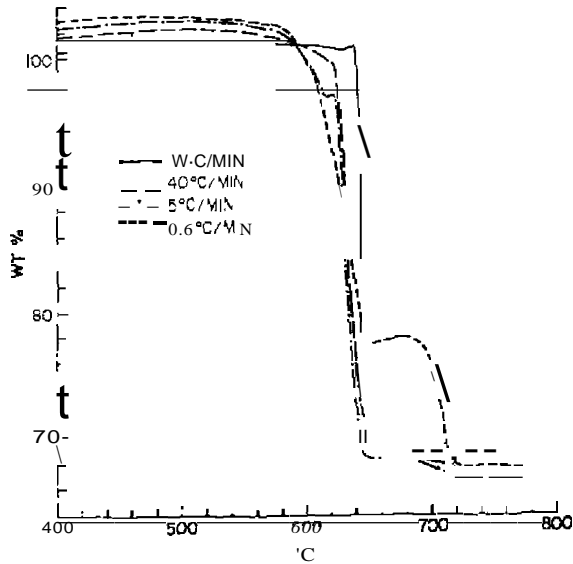


Figure 1.46. TM curves for Chromindur (II) at various heating rates (51).

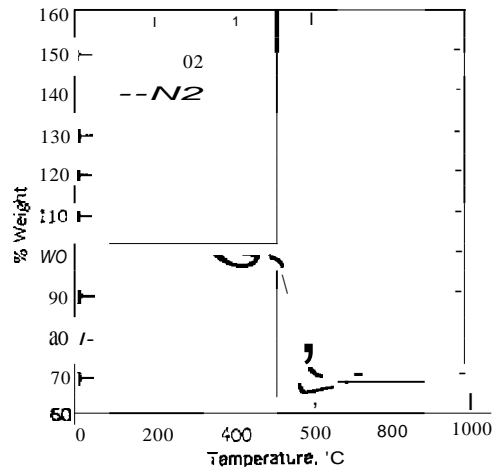


Figure 1.47. TM curves for siderite A in O₂ and N₂ (45).

strongly magnetic spinel phase never has a chance to form. Or by the magnetically induced perturbation evident in the slight drop at about 675°C is indicative of the parasitic ferromagnetism in hematite, TM was found to be a useful technique to detect the intermediate magnetic phases during the thermal decomposition reaction. If the T_c of the resulting spinel phase is depressed below the decomposition temperature of the siderite, then intermediate phases cannot be detected magnetically. The end product, however, can be evaluated by this technique to aid in determining the distribution of impurities.

There has been much interest and controversy regarding the influence of an external magnetic field on reaction rates below their magnetic transition temperatures. Skorski (153) found an increase in the reduction rate of hematite to metallic iron when Hz was used as the reducing agent in a 500-1400 O_e magnetic field. Rowe et al. (154) observed no difference in the reduction rate of NiO to Ni on the application of a strong magnetic field. On repeating the reduction reaction with Fe₂O₃, they found that the application of a magnetic field of 4200 O. resulted in a significantly slower reaction rate than when the reduction was carried out in the earth's magnetic field (155). In all cases, the product was more highly magnetic than was the reactant. The reduction rates varied as follows:

NiO → Ni	No observable effect
Fe ₂ O ₃ → Fe ₃ O ₄ → Fe	Reduction increased
Fe ₂ O ₃ → Fe	
Fe ₂ O ₃ → Fe	Reduction decreased

Using EGA in the presence of a magnetic field. Gallagher et al (150) could find no significant changes in the reaction rates for the reduction of Co₃O₄, NiO, or Fe₂O₃. Earlier TG experiments were probably erroneous due to distortions of the gravimetric measurements brought on by magnetic effects arising from, for example, amorphous to superparamagnetic to bulk crystalline transitions as the reaction zones grow and/or rearrange or align the particles during the reaction.

In still another study, using TM combined with TG and EGA, Aylmer and Rowe (159) concluded that a strong magnetic field affects the reduction rates of some metal oxides, in particular, those of CoO → Co, Fe₃O₄ → Fe, and FeO → Fe. Other reactions, such as NiO → Ni, Co₃O₄ → CoO, and Fe₂O₃ → Fe₃O₄ do not seem to be affected by strong magnetic fields. Obviously, the end to this controversy does not appear in sight.

Larson et al. (149, ISI, 156-158) used TM to study the composition of

known C1-C4 carbonaceous chondrites in meteorites. Certain magnetic phases can be identified and their mass percentages estimated. The only magnetic phase found in four of the C1 chondrites was magnetite containing less than 6% nickel. The RevLs:oke C1 chondrite contained essentially Ni-free Fe_3O_4 as the predominant phase, although only a small amount of thermally unstable iron compound (presumably FeS) was additionally present. Estimates of the mass percentages of magnetite, based on saturation moments, ranged from $5.3 \pm 0.4\%$ to $12.2 \pm 0.9\%$ for the various C1 chondrite samples.

Rowe et al. (144, 160-162) used TM and TG to determine the pyrite contents of coals and lignites. A TM curve of a coal ash used for analyzing the pyrite content of the coal is shown in Figure 1.48. The presence of initial Fe_2O_3 is first checked by inserting the magnetic field around the sample and sample holder; this results in a small change in mass, as shown in the TG curve. The temperature is then slowly increased to 400°C , in H_2 , whereby the Fe_2O_3 is reduced to metallic Fe, causing a large increase in the apparent sample mass. When all the Fe_2O_3 is reduced, the saturation magnetization due to the iron becomes constant indicating that the reaction is complete, and the furnace heater is turned off. An increase in apparent mass is observed as the sample cools due to the increase of saturation magnetization of the Fe with decreasing temperature. Again, the apparent mass will become constant as the temperature approaches room temperature. The magnet is removed

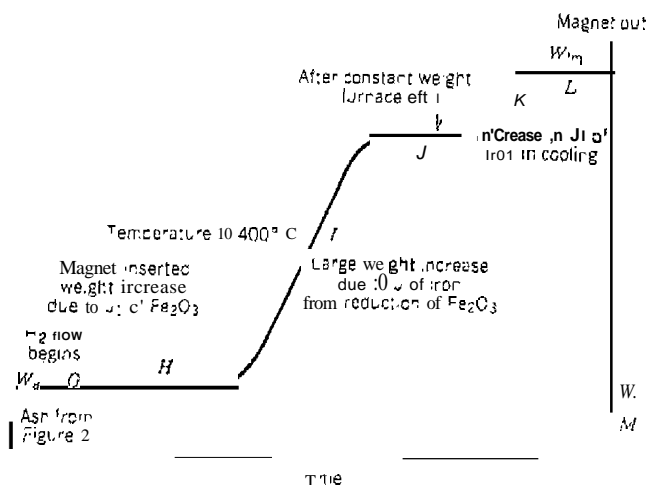


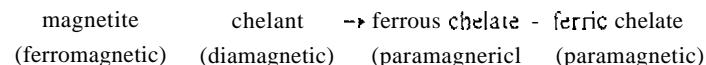
Figure 1.48. TM curve of coal ash (161).

and the final mass of the residue is recorded. The percent of FeS_2 (pyrite) in the sample can be calculated from

$$\% \text{FeS}_2 = (W_{fm} - W_f) \frac{100}{W_2 - W_1} \frac{W_1}{W_4} \quad (W_i \text{ or } W_d)$$

where W_{fm} is the final mass, magnet in place; W_f is the final mass in absence of magnet; W_1 is the molecular weight of Fe; W_2 is the molecular weight of FeS_2 ; and W_i or W_d is the initial mass or dry mass of the sample.

Charles et al. (163) used TM to follow the dissolution of magnetite-containing nuclear steam generator sludge deposits in a chelant-based water solution. The method is based on the ferromagnetic nature of magnetite and the loss of magnetism that occurs upon reaction with chelants:



Consumption of magnetite can be followed by this procedure whether the products of reaction remain in true solution or reprecipitate as separate solid phases.

F. ACCELERATING RATE CALORIMETRY

1. Introduction

The accelerating rate calorimeter (ARC) is an instrument that provides time(*t*)-temperature (*T*)-pressure (*P*) data for thermally initiated chemical reactions taking place under adiabatic conditions. The technique, which was developed by Townsend and Tou (167,168) in 1977 can determine the following parameters: (1) adiabatic rate of self-heating, (2) adiabatic time to explosion, (3) rate of pressure rise, (4) maximum rate of reaction, (5) kinetic data such as E_a , n , and preexponential term, and (6) heat of reaction, ΔH_r . Thus, potential hazards associated with the thermal behavior of substances can be evaluated to assure their safe handling, processing, and storage. Although DSC and other thermal analysis methods can evaluate the thermal stability of a substance, they have limitations as a realistic test for process hazards in a reaction vessel (169). ARC can be used to simulate and study self-heating reactions that can initiate runaway thermal reactions. A single experiment can provide ample thermokinetic data from *t*-*T*-*P* relationships that are applicable to the design and performance evaluations of batch reactors and storage vessels where agitation does not affect behavior.

2. Instrumentation

The ARC calorimeter jacket and sample system are shown in Figure 11.49 (168). A spherical bomb is mounted inside a nickel-plated copper jacket with a swagelok fitting to a 0.0625 in. tee, on which is attached a pressure transducer and a sample thermocouple. The jacket is composed of three zones, top, side, and base, which are individually heated and controlled by the Nisil/Nicrosil type N thermocouples. The thermocouples are cemented on the inside surface of the jacket at a point one quarter the distance between the two cartridge heaters. The point is halfway between the hottest and coldest spots of the jacket. The same type of thermocouple is clamped directly in the outside surface of the spherical sample bomb. All the thermocouples are referenced to the ice point that is designed to be stable to within 0.01°C. Adiabatic conditions are achieved by maintaining the bomb and jacket temperatures exactly equal. The sample holder has a capacity of 1-10g of sample. Pressure in the system is monitored with a Serotec 0-2500 psi TJE pressure transducer; pressure is limited in the vessel to 2500 psi. The maximum temperature of the system is 500°C.

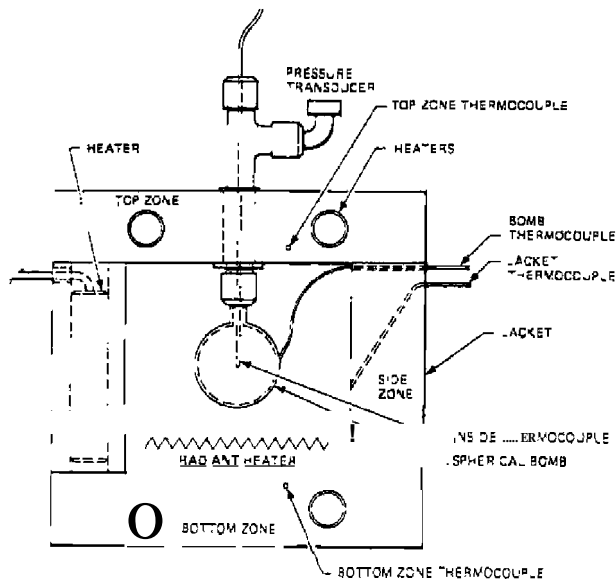


Figure 11.49. ARC jacket and sample system as described by Townsend and Tou (168)

A schematic diagram of the complete ARC calorimeter is shown in Figure 11.50 (170, 171). The logic to search for and follow an exotherm is programmed to permit use of a selection of run parameters and to provide an on-line display of critical variables such as time, temperature, and pressure. A search for a reaction exotherm is accomplished by elevating the sample temperature by a fixed increment (step-heat) and then checking to see if the sample self-heat rate exceeds a user-selected threshold. Once an exotherm is detected, automatic collection of time, temperature, and pressure data is carried out until the reaction has finished and the self-heat rate has dropped back below the threshold value. All operations are controlled by a microprocessor system with final data presentation presented via a built-in line printer.

The heat-wait-search operational logic of the ARC is shown in Figure 11.51 (168). The ARC is first heated to a desired starting temperature and held a period of time for thermal equilibrium to be achieved before a rate search is performed. If the rate is less than the preset rate, the ARC will proceed automatically to the preselected temperature step heat-wait-search sequence until a self-heat rate greater than the preset rate is detected.

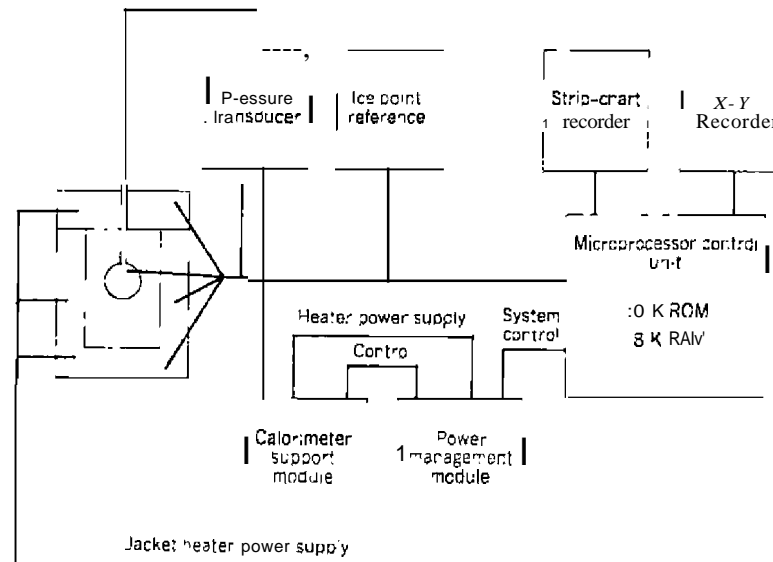


Figure 11.50. Analysis and microprocessor control system of ARC 1170, (171).

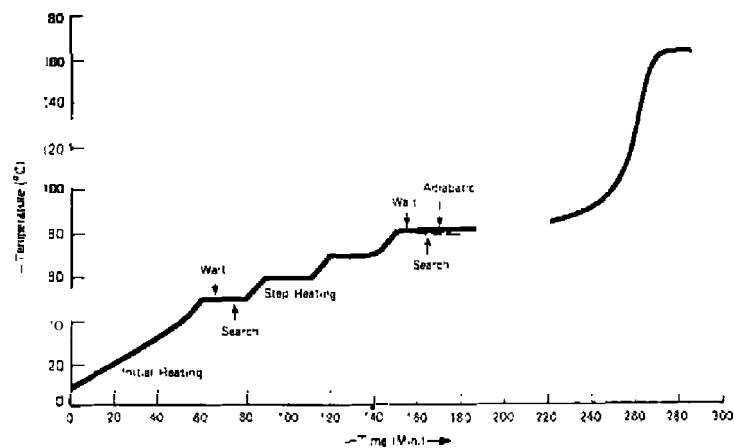


Figure 11.51. The heat-wait-search operator mode of the ARC (16&).

The calorimeter will be maintained at adiabatic conditions until the completion of the experiment. The stepwise heating is accomplished with a radiant heater located at the bottom of the jacket.

The performance of the ARC, as evaluated by the use of di-*t*-butyl peroxide, is shown in Table 11.10. Using a sample mass of ~ 2 g, the thermal inertia, ϕ , was ~ 7.0 . Literature values of E for di-*t*-butyl peroxide in various solvents range from 34.0-39.1 kcal/mol (168). Thus, the ARC values are somewhat lower. In order to evaluate the solvent effect, a 14.6 weight-% di-*r*-butyl peroxide in mineral oil was run in the ARC and an E of 38.9 kcal/mole was found.

Table 11.10. The Precision of the Thermokinetic Parameters for di-*t*-butyl Peroxide Evaluated from 16 Runs (168)

	Mean (\bar{X})	Standard Deviation (σ)	Relative Precision [$(\sigma/\bar{X}) \times 100\%$]
Adiabatic temperature rise, ΔT_{AB}	67.6 C	± 3.2 C	± 7.7
Frequency factor, A (in ln unit)	35.20	± 1.12	± 2.9
Activation energy, E	36.11 kcal/mol	± 0.82 kcal/mol	± 2.3
Reaction order, n	0.925	± 0.088	± 9.5

3. Theory

The expected $T-t$ curve for an adiabatic reaction system is given in Figure 11.52. For an exothermic reaction at adiabatic conditions, the heat generated from the reaction at an initial temperature T_0 will result in a temperature rise, which in turn accelerates the rate of the reaction. However, associated with the acceleration of the rate is the depletion of the concentration of the reactant. Therefore, the rate of the reaction is expected to decrease after reaching its maximum value at temperature T_m and finally diminishes to zero at the completion of the reaction at temperature T_f . At any T or t , the concentration of the reactant can be related approximately to the temperature of the system

$$C = \frac{T_f - T}{\Delta T_{AB}} C_0 \quad (11.20)$$

where ΔT_{AB} is the adiabatic temperature rise, $T_f - T_0$, and C_0 the initial concentration of the reactant. The heat of reaction, ΔH_x , can be calculated from

$$\Delta H_x = M \bar{C}_p \Delta T_{AB} \quad (11.21)$$

if the average heat capacity, \bar{C}_p , over the experimental temperature range and the mass of the sample, M , are known.

Substitution of equation (11.20) after differentiation with respect to T , into the Arrhenius equation, gives an equation relating the thermal measur-

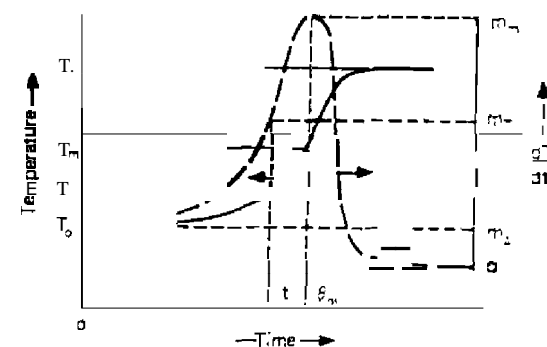


Figure 11.52. The $T-t$ and self-heat rate versus t of an adiabatic reaction (168)

able quality, T , to a kinetic event

$$m_T = \frac{dT}{dt} = k \left(\frac{T_f - T}{\Delta T_{AB}} \right)^n \Delta T_{AB} C_0^{n-1} \quad (11.22)$$

where m_T is the self-heat rate measured at T or t .

Rearranging equation (11.22) gives

$$k'' = \frac{C_0^{n-1} k}{\Delta T_{AB}^{n-1}} = \left(\frac{T_f - T}{\Delta T_{AB}} \right)^n \Delta T_{AB} \quad (11.23)$$

where k'' is a pseudo zero-order rate constant at T . Substituting the Arrhenius equation into equation (11.23), we obtain

$$\ln K'' = \ln C_0^{n-1} A - \frac{E}{R} \left(\frac{1}{T} \right) \quad (11.24)$$

A plot of $\ln K''$ versus $1/T$ is, therefore, expected to be a straight line, providing the order of reaction is correctly chosen. The Arrhenius kinetic parameters, E and A , can be calculated from this plot. A plot of the initial self-heat rate versus the reciprocal of the initial temperature gives

$$\ln m_0 = \ln \Delta T_{AB} C_0^{n-1} A - \frac{E}{R} \left(\frac{1}{T_0} \right) \quad (11.25)$$

and will yield a line with a slope $-E/R$. This is called a zero-order line.

As the initial temperature increases, the initial self-heat rate increases following the zero-order line. One very interesting phenomenon occurs when the maximum self-heat coincides with the initial self-heat rate. Above this temperature, the reaction decelerates, even though the temperature itself continues to increase. This temperature is designated as T^* and can be evaluated when $T_m = T_0 = T^*$ and $T_f = \Delta T_{AB} + T^*$:

$$T^* = \sqrt{\frac{E \Delta T_{AB}}{nR}} \quad (11.26)$$

providing that there is no mechanistic change in the temperature range of interest.

This equation indicates that, theoretically, there always exists a temperature, T^* , for a reaction, above which the concentration depletion effect on the

reaction rate is more drastic than the acceleration effect due to the temperature rise. This phenomenon can take place not only in a pure chemical system, but also in a system with thermal inertia, ϕ , which will lower the adiabatic temperature rise, ΔT_{AB} .

The time to maximum rate (TMR), θ_m , can be expressed as

$$\theta_m = \frac{RT^2}{m_T E} - \frac{RT_m^2}{m_m E} \quad (11.27)$$

where m_T is the self-heat rate at T and m_m is the self-heat rate at T_m . A plot of θ_m versus T^2/m_T is a straight line with a slope of R/E and intercept, $-RT_m^2/m_m E$.

Other expressions can be derived for the temperature of no return, T_{NR} , and the thermal inertia, ϕ (168).

The principles of ARC can be illustrated by the thermal decomposition of Diazald (N-methyl-N-nitroso-p-toluene sulfonamide). An ether solution of this compound gave a rate of 0.044 CC/min above the threshold, 0.02°C/min, set for the calorimeter, at 71.2°C. The calorimeter was maintained at an adiabatic condition until the completion of the reaction at 131.2°C.

The temperature and pressure recorded during the adiabatic reaction are shown in Figure 11.53. The amount of gas generated is about 0.4 mol mol⁻¹ of Diazald.

The temperature rate versus temperature plot is shown in Figure 11.54. A plot of pressure rate versus temperature revealed a linear relationship, as expected from the data presented in Figure 11.53. The experimental data and the calculated results are summarized in Table 11.11.

Using an average heat capacity, \bar{C}_p , of the reactant of 0.5 cal°C/g, the heat of reaction found was 230 cal/g which gives a molar heat of 50 kcal/mol. When the calculated pseudo zero-order rate constants, k'' , are plotted for three assumed reaction orders, a straight line was obtained for $n = 1$. The Arrhenius kinetic parameters, E and A , were calculated to be 27,860 kcal/mol and 4.58×10^{14} min⁻¹, respectively.

4. Applications

The kinetics of the thermal decomposition of di-*t*-butyl peroxide in toluene were determined by Tou and Whiting (172). They found the kinetic parameters to be $E = 37.8 \pm 1.1$ kcal/mol and $\log A = 16.15 \pm 0.6$ sec⁻¹. This compares favorably with $E = 37.78 \pm 0.06$ kcal/mol and $\log A = 15.80 \pm 0.03$ sec⁻¹ determined by Shaw and Pritchard (173) from a least-squares treatment of 177 data points obtained by various workers. The highest self-heat rates that the calorimeter can follow without deviation from the

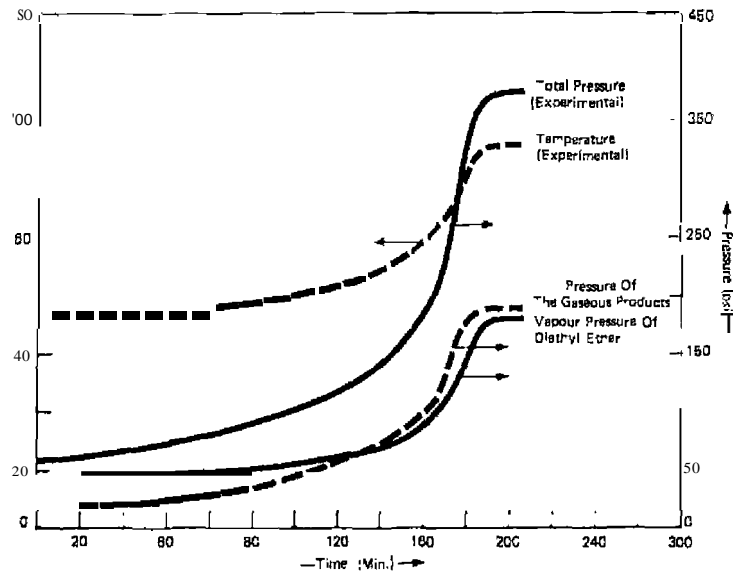


Figure 11.53. Temperature and pressure versus time curves of the thermal decomposition of Diazald in diethyl ether solution (168).

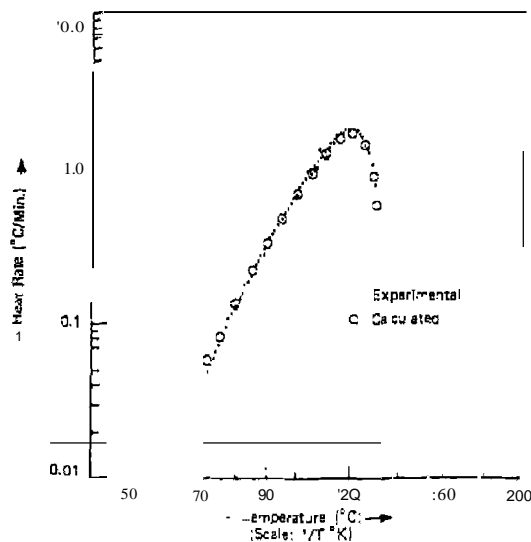


Figure 1.54. The experimental and calculated self-heat rate versus temperature curves of the thermal decomposition of Diazald (168).

Table 11.11. Experimental and Calculated Kinetic Data of the Diazald/Diethyl Ether Solution (16)

	Experimental	Calculated	
Thermal inertia	3.0	2.0	1.0
Initial temperature (°C)	71.2	71.1	71.2
Final temperature (°C)	131.2	131.2	191.2
Adiabatic temperature rise (°C)	60	60	120
Initial self-heat rate (°C min ⁻¹)	0.044	0.057	0.114
Maximum self-heat rate (°C min ⁻¹)	1.8	1.7	1.90
Temperature at maximum rate (°C)	120	120	177.2
Time to maximum rate (min)	199	191 ^a	87 ^a
		143 ^b	74 ^b
Activation energy (kcal mol ⁻¹)		27.860	
Frequency factor (min ⁻¹)		4.58 x	
Heat of reaction of Diazald (kcal mol ⁻¹) assuming C _v = 0.5 cal °C ⁻¹ g ⁻¹		50	

^aNumerical integration.

^bEquation (11.251).

expected self-heat curve were found to be dependent on the type of sample container and the sample itself.

Compounds studied by ARC include styrene (174), o-nitroaniline (169), di-(*n*-butyl) peroxide (171), and substances employed in the synthesis of explosives, detergents, bleaches, adhesives, fertilizers, resins, plastics, and many others.

A comparison has been made of the evaluation of thermal hazards by DTA, DSC, Dewar tests, and ARC (175).

G. SEDEX SYSTEM

I. Introduction

The SEDEX system (SEnsitive Detector of EXothermic processes) was developed by Hakl (176-178) for investigating the thermal decomposition of compounds undergoing exothermic processes. It features: (1) a high sensitivity; (2) a mode of operation conformable to plant conditions; (3) economy, for example, low cost of apparatus, simultaneous measurements, reliable data, and so on; and (4) a simple way to operate and interpret the results.

Z. Instrumentation

A schematic diagram of the apparatus is shown in Figure 11.55. The sample is heated in a suitable receptacle (50 ml glass beaker) by means of a gaseous medium whose temperature rises in a linear manner. Platinum resistance thermometer sensors are used to detect the heating medium and sample temperatures, which are displayed on a three-channel recorder. The difference in temperature between the heating medium and sample, at high sensitivity, is also recorded. If there are no exothermic processes taking place, the difference temperature remains constant. The temperature at which the temperature difference begins to decrease is the initial temperature of an exothermic process. Conversely, the temperature at which the difference begins to increase is the initial temperature of an endothermic process.

The oven must be capable of maintaining a homogeneous spatial distribution temperature using air or other gaseous atmospheres. Stirring the sample may not be necessary in all cases but is recommended when suspensions are being investigated. The stirrer has a stirring speed of 100-500 rpm.

A display of the three-channel recorder is shown in Figure 11.56. The sample, oven, and difference temperatures are indicated. An initial temperature of 315°C is shown for an exothermic process.

A comparison of SEDEX with other methods is given in Table 11.12. The SEDEX temperature is always lower than any of the other methods listed. The Sikarex is an adiabatic calorimeter developed by Sandoz.

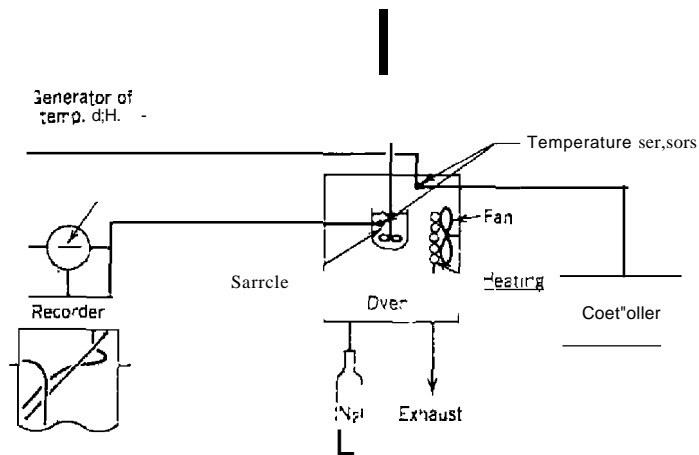


Figure 11.55 Schematic diagram of SEDEX (176).

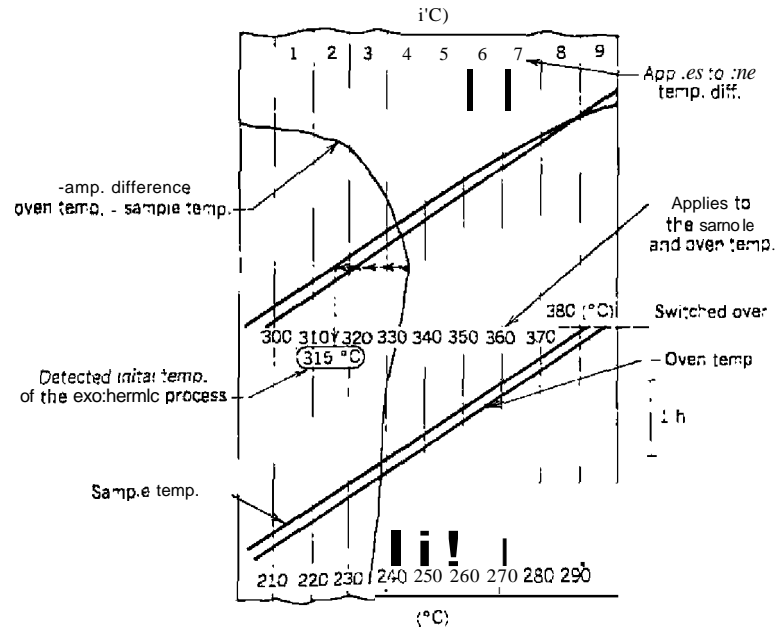


Figure 11.56. Chart recording of the thermal stability of 1,5-dinitroanthraquinone (176).

Table 11.12. Comparison of SEDEX with Other Thermal Hazard Evaluation Methods (176)

Substance	Initial Temperature of the Exothermic Process (°C)			
	Dynamic Decomposition Test	DSC	Sikarex	Sedex
p-Xyly; chloride + 0.02% Fe	110	80	80	55
1,5-Dinitroanthraquinone		> 370	330	320
Mixture of 1,5 and 1,8-Dinitroanthraquinone	340	330	285	290
1-Nitroanthraquinone	360		325	295
1-Nitroanthraquinone, raw material	370	380	305	295
Dodecyl nitrite		145	116	115
2,4-Dinitroaniline	310			250
p-Nitroaniline			273	272

*Not measured.

3. Theory and Applications

The sample is heated in a suitable container by means of an electric heater that is controlled by a constant power source. The ambient temperature of the sample is kept equal to that in the sample itself (adiabatic conditions). The temperature in the sample is measured and the first derivative of it with respect to time is recorded. If there is no process with heat effects taking place in the sample, the temperature rises in a linear fashion; that is, the first derivative remains constant and can be described by a simple differential equation:

$$\frac{dT}{dt} = S \quad (11.28)$$

where T is the temperature in K , t is the time, and S the linear rate of heating. At the temperature at which the reaction starts producing its own heat, the rise in temperature accelerates and can be described by a modified Arrhenius equation. The following equation is valid for the temperature rise under such overadiabatic conditions for a first-order reaction:

$$\frac{dT}{dt} = A(B + S - T) \exp\left(-\frac{C}{T}\right) + S \quad (11.29)$$

where S is the linear rate of heating from the equation (11.28). The determination of the heat of reaction is carried out on the basis of the knowledge of the adiabatic temperature rise and the heat capacity of the reaction mixture, assuming that the specific heat remains constant during the reaction and does not vary with the temperature. Equation (11.37) contains three parameters: parameter A comprises the frequency factor, initial concentration, heat capacity of the reaction mixture, and coefficients of proportion; parameter B has a physical significance: final temperature of the reaction mixture after the end of the reaction under adiabatic conditions; and parameter $C = E/R$, where E is the activation energy and R is the universal gas constant. These parameters can be estimated as follows: Parameter B is obtained directly from the course of the temperature curve. Parameters A and C can be calculated from the course of the dT/dt curve either graphically or, better, by a regression analysis. The measured parameters can then be used in the Arrhenius equation

$$\frac{dT}{dt} = A(B - T) \exp\left(-\frac{C}{T}\right) \quad (11.38)$$

to calculate the course of the temperature of the process being studied under ideally adiabatic conditions. The expression within the brackets, $(B + S - T)$, has the dimensions of temperature and describes the decrease of concentration during a reaction having first-order kinetics. For a reaction of second- (or third-) order, equations (11.27) and (11.38) must be extended accordingly, so that the changing concentration of all the reacting species can be taken into account.

REFERENCES

1. Daniels, T., *Anal. Proc.*, Oct. 1981, p. 412.
2. Valentich, L. *Tube Type Dilatometers*, Instrument Society of America, Research Triangle Park, NC, 1981.
3. Wendlandt, W. W., *Thermal Methods of Analysis*, 2nd ed., Wiley-Interscience, New York, 1974, Chap. II.
4. Paulik, F., and I. Paulik, *J. Thermal Anal.*, 16, 399 (1979).
5. Gill, P. S., *Am. Lab.*, 16, 39 (1984).
6. Riesen, R., and H. Somnemer, *Am. Lab.*, 15, 30 (1983).
7. Burks, H., *J. Appl. Polym. Sci.*, 18, 627 (1974).
8. Baker, K. F., Du Pont Application Brief No. TA 50.
9. Provder, I., R. M. Holsworth, and T. H. Grenzer, *Polymer Characterization: Spectroscopic, Chromatographic and Physical Instrumental Methods*, C. D. Craver, ed., American Chemical Society, Washington, DC, 1983, p. 77.
10. Gillham, I. K., *Anal. Proc.*, Oct. 1981, p. 424.
11. Paulik, I., and F. Paulik, "Simultaneous Thermoanalytical Examinations by Means of the Derivatograph," in *Comprehensive Analytical Chemistry*, G. Svehla, ed., Vol. XII, Elsevier, Amsterdam, 1981, p. 22.
12. Mackenzie, R. C., in *Advanced Techniques for Clay Mineral Analysis*, J. J. Lipia, ed., Elsevier, Amsterdam, 1981, Chap. 1.
13. Paulik, F., and I. Paulik, *J. Thermal Anal.*, 16, 399 (1979).
14. Scott, M. G., *Anal. Proc.*, Oct. 1981, p. 437.
15. Newall, R. IL, *Anal. Proc.*, Oct. 1981, p. 440.
16. Morreil, R., *Anal. Proc.*, Dec. 1981, p. 443.
17. Dyer, A., *Anal. Proc.*, Oct. 1981, p. 447.
18. TMA 790 Thermomechanical Analyzer brochure, Stanton-Redcroft, London.
19. Rao, K. V., and I. Maiti, *Indian J. Pure Appl. Phys.*, 15, 437 (1977).
20. El-Sayed Ali, M., O. T. Sorenson, and L. Haldahl, *J. Thermal Anal.*, 25, 75 (1982).
21. Paulik, F., and J. Paulik, *Analyst*, 103, 417 (1978).
22. Barton, J. M., *Anal. Proc.*, Oct. 1981, p. 421.
23. Finkler, E. F., *War.*, 19, 277 (1972).
24. Hwo, C., J. P. Bell, and I. F. Johnson, *J. Appl. Polym. Sci.*, 18, 2865 (1974).
25. Chiu, T., *J. Macromol. Sci.-Chem.*, A8, 3 (1974).

26. Ogilvie, G. D. *Anal. Proc.* Oct, 1981, p. 426.
27. Rajeshwar, K., R. Nottenburg, and J. DuBow. *J. Mater. Sci.*, **14**, 2052 (1979).
28. Blaine, R. L. *Du Pont Analysis Application Brief No. TA 60*.
29. Gray, A. P., *Perkin-Elmer Instr. News*, 20, No. 1, 10 (1969).
30. Yanai, H. S., W. I. Freund, and O. L. Carter, *Thermochim. Acta*, **4**, 199 (1972).
31. *ASTM Standards*, ASTM, Philadelphia, PA, Part 27, June 1969, D-648, p. 214.
32. Creedon, J. P., *Du Pont Thermal Analysis Application Brief No. TA 37*.
33. *ASTM Standards*, ASTM, Philadelphia, PA, Part 27, June 1969, D-1525, p. 527.
34. Davies, G., *Anal. Chem.*, **47**, 318A (1975).
35. England, J. C., R. F. Long, and D. J. Townsend, *Anal. Proc.*, Oct., 1981, p. 430.
36. Welton, R. E., *Anal. Proc.* Oct. 1981, p. 416.
37. *Dynamic Mechanical Analysis: Thermal Analysis Review*, Du Pont Instrument Corp., Wilmington, DE.
38. Miller, D. G., *Am. Lab.*, Jan. 1982, p. 80.
39. Lofthouse, M. G., and P. Burroughs, *J. Thermal Anal.*, **13**, 439 (1978).
40. Gramelt, C., *Am. Lab.*, **16**, 102 (1984).
41. Wetton, R. E., T. G. Croucher and J. W. M. Fursdon, in *Polymer Characterization: Spectroscopic, Chromatographic and Physical Instrumental Methods*. C. D. Craver, ed., American Chemical Society, Washington, DC, 1983, Chap. 5.
42. Murayarna, T., *Dynamic Mechanical Analysis of Polymeric Material*, Elsevier, New York, 1978.
43. Kaelble, D. H., in *Epoxy Resins*, C. A. May and Y. Tanaka, Eds., Marcel-Dekker, New York, 1973, pp. 342-371.
44. Gillham, I. K., *Appl. Polym. Sym.*, **2**, 45 (1966).
45. Lewis, A. F., and J. Gillham, *J. Appl. Polym. Sci.*, **6**, 422 (1962).
46. Gillham, J. K., in *Proceedings of the Second Toronto Symposium on Thermal Analysis*, H. G. McArdie, ed., Chemical Institute of Canada, Toronto, 1967, p. 79.
47. Wendlandt, W. W., *Anal. Chim. Acta*, **33**, 98 (1965).
48. Miller, G. W., in *Thermal Analysis*, R. F. Schwenker and P. D. Garn, eds., Vol. 1. Academic, New York, 1969, p. 435.
49. Lombardi, G., *For Belter Thermal Analysis*, ICTA, Rome, 1977, p. 19.
50. Wendlandt, W. W., *Thermochim. Acta.* **36** (1980) 393.
51. Wendlandt, W. W., *Natl. Bur. Stand. Spec. Publ. 580*, May 1980, p. 219.
52. Wendlandt, W. W., *Thermal Methods of Analysis*, Wiley-Interscience, New York, 1964, Chap. XII.
53. Wendlandt, W. W., *Thermal Methods of Analysis*, 2nd ed., Wiley-Interscience, New York, 1974, Chap. XII.
54. Warfield, R. W., in *Treatise on Analytical Chemistry*, [M. Kolthoff et al. eds., Vol. 4, Part III, Wiley, New York, 1977, 608.
55. Paulik, F. and J. Paulik, *Analyst*, **103**, 417 (1978).
56. Wendlandt, W. W., *Thermochim. Acta.* in press.
57. Adeosun, S. O., *Thermochim. Acta.*, **32**, 119 (1979).
58. Adeosun, S. O., and M. S. Akanni, *Thermochim. Acta.*, **39** (1980) 35.
59. Adeosun, S. O., M. O. Ilori, and H. A. Ellis, *Ref.* **58**, p. 125.
60. Adeosun, S. O., M. S. Akanni, and H. D. Buttows, *Thermochim. Acta.* **42** (1980) 233.

61. Sekkijna, M., M. Abou, T. M. Salem, M. F. El-Shazly, and A. El-Dissouky, *Thermochim. Acta.*, **48** (1981) 1.
62. Ramanar, I., and J. Chaklader, *J. Am. Ceram. Soc.*, **58** (1975) 476.
63. Raask, E., *Application Note 253*, Station Retkraft, London.
64. Karmazsin, E., M. Remand, and M. Murat, *Proceedings of Second European Symposium on Thermal Analysis*, D. Dollimore, ed., Sept. 1-4 1981, Heyden, London, p. 562.
65. Karmazsin, E., M. Romard, and M. Murat, *Thermochim. Acta.*, **55** (1982) 293.
66. Bur-nisuova, N. P., and R. G. Fieveva, *J. Thermal Anal.*, **4** (1972) 61.
67. Romanov, G. V., R. G. Fitzeva, I. V. Konova'ova, A. N. Pudovik, and N. P. Burmistrova, *J. Thermal Anal.*, **6** (1974) 119.
68. Golunski, S. E., T. G. Nevell, and M. L. Pope, *Thermochim. Acta.*, **51** (1981) 53.
69. Trau, J., *J. Thermal Anal.*, **6** (1974) 355.
70. Nandi, P. N., D. A. Deshpande, and V. G. Kher, *Thermochim. Aero.*, **34** (1979) 1.
71. Nandi, P. N., D. A. Deshpande, and Y. G. Kher, *Indian J. Pure Appl. Phys.*, **16**, 742 (1978).
72. Nandi, P. N., D. A. Deshpande, and V. G. Kher, *Proc. Indian Acad. Sci. Sect. A*, **55**, 113 (1979).
73. Sircar, A. K., T. G. Lamond, and J. L. Welis, *Thermochim. Acta.*, **37** (1980) 315.
74. Rajeshwar, K., M. Das, and J. DuBow, *Nature*, **287** (1980) 131.
75. Rajeshwar, K., R. Nottenburg, V. R. Pal Verneker, and J. DuBow, *J. Chem. Phys.*, **72**, 6678 (1980).
76. Nottenburg, R., K. Rajeshwar, V. R. Pal Verneker, and J. DuBow, *J. Phys. Chem. Solids*, **41**, 271 (1980).
77. Rajeshwar, K., R. Nottenburg, V. R. Pal Verneker, and J. DuBow, *Phys. Stat. Sol.*, **58**, 245 (1980).
78. Chiu, L., *Thermochim. Acta.*, **8**, 15 (1971).
79. Bonilla, I. R., P. R. Andrade, and A. Bristoli, *J. Thermal Anal.*, **8**, 387 (1975).
80. Bristoli, A., I. R. Bimila, and P. R. Andrade, *J. Thermal Anal.*, **9**, 93 (1976).
81. Nottenburg, R., M. Freeman, K. Rajeshwar, and J. DuBow, *Anal. Chem.*, **51**, 1149 (1979).
82. Nottenburg, R., K. Rajeshwar, M. Freeman, and J. DuBow, *J. Solid State Chem.*, **28**, 195 (1979).
83. Nottenburg, R., K. Rajeshwar, M. Freeman, and J. DuBow, *Thermochim. Acta.*, **31**, 39 (1979).
84. Rajeshwar, K., J. DuBow, and R. Thapar, *Can. J. Earth Sci.*, **17**, 1315 (1981).
85. Das, M., R. Thapar, K. Rajeshwar, and J. DuBow, *Can. J. Earth Sci.*, **18**, 742 (1981).
86. Kwa'ra, B., V. Ramakrishna, and S. K. Suri, *Thermochim. Acta.*, **48** (1981) 231.
87. Watanabe, T., K. Sakai, and S. Iwai, *Bull. Tokyo Inst. Technol.*, **117**, 13 (1973).
88. Khil'a, M. A., and A. A. Hanna, *Thermochim. Acta.*, **51**, 335 (1981).
89. Rajeshwar, K., *Thermochim. Acta.*, **54**, 59 (1982).
90. Weber, G., and B. Vogel, *Intern. Makromol. Chem.*, **86**, 215 (1980).
91. Pillai, P. K. C., S. F. Xavier, and M. Molah, *Thermochim. Acta.*, **35**, 385 (1980).
92. Wendlandt, W. W., *Thermochim. Acta.*, **37**, 121 (1980).
93. Wendlandt, W. W., and S. Conant, *Thermochim. Acta.*, **65**, 321 (1983).

94. Contarini, S., and W. W. Wendlandt, *Thermochim. Acta.*, 70, 283 (1983).
95. MacKenzie, K. J. D., *J. Thermal Anal.*, 5, 5 (1973).
96. MacKenzie, K. J. D., and N. Hadipour, *Thermochim. Acta.*, 35, 227 (1980).
97. David, D. J., *Thermochim. Acta.*, 1, 277 (1970).
98. Wendlandt, W. W., *Thermochim. Acta.*, 72, 1 (1984).
99. Wendlandt, W. W., *Thermochim. Acta.*, 73, 89 (1984).
100. Wendlandt, W. W., *Thermochim. Acta.*, 1, 11 (1970).
101. Borhardt, H. J., and F. Daniels, *J. Phys. Chem.*, 61, 917 (1957).
102. Chiu, J., *Anal. Chem.*, 39, 861 (1967).
103. Chiu, J., *J. Polym. Sci.*, (8), 27 (1965).
104. Rudloff, W. K., and E. S. Freeman, *J. Phys. Chem.*, 74, 3317 (1970).
105. Judd, M. D., and M. I. Pope, *J. Appl. Chem.*, 20, 380 (1970).
106. (arroll, R. W., and R. V. Mangravite, in *Thermal Analysis*, R. F. Schwenker and P. D. Garn, 005, Vol. I, Academic, New York, 1969, p. 189.
107. Halmos, Z., and W. W. Wendlandt, *Thermochim. Acta.*, 7, 95 (1973).
108. Ref. 107, p. 113.
109. Halmos, Z., L. W. Collins, and W. W. Wendlandt, *Thermochim. Acta.*, 8, 381 (1974).
110. Wendlandt, W. W., *Thermochim. Acta.*, 26, 19 (1978).
111. Wendlandt, W. W., *Thermochim. Acta.*, 37, 117 (1980).
112. Wendlandt, W. W., *Thermochim. Acta.*, 30, 359 (1979).
113. Wendlandt, W. W., *Thermochim. Acta.*, 37, 89 (1980).
114. Birks, J. B., and J. Hart, eds., *Progress in Dielectrics*, Vol. 3, Wiley, New York, 1961.
115. Hedvig, P., *Dielectric Spectroscopy of Polymers*, Wiley, New York, 1977.
116. Chiu, J., *Thermochim. Acta.*, 8, 15 (1974).
117. Nottenburg, R., K. Rajeshwar, M. Freeman, and J. DuBow, *J. Solid State Chem.*, 28, 195 (1979).
118. Nottenburg, R., M. Freeman, K. Rajeshwar, and J. DuBow, *Anal. Chem.*, 51, 1149 (1979).
119. Wendlandt, W. W., *Thermochim. Acta.*, 37, (21) (1980).
120. Wendlandt, W. W., and S. Contarini, *Thermochim. Acta.*, 65, 321 (1983).
121. Contarini, S., and W. W. Wendlandt, *Thermochim. Acta.*, 70, 283 (1983).
122. Williams, J. R., and W. W. Wendlandt, *Thermochim. Acta.*, 7 (1973) 253-260.
123. Ref. 122, pp. 269-274.
124. Ref. 122, pp. 261-268.
125. Ref. 122, pp. 275-285.
126. Wendlandt, W. W., *Thermochim. Acta.*, 21 (1977) 291-294.
127. Clark, G. M., *Thermochim. Acta.*, 27, 19 (1978).
128. Lonvik, K., *Proceedings of the Nordforsk Symposium on Thermal Analysis*, Haganand, Finland, Mar. 15-16, 1972.
129. Mraz, T., K. Rajeshwar, and J. DuBow, *Thermochim. Acta.*, 38, 211 (1980).
130. Lonvik, K., *Thermochim. Acta.*, 27, 27 (1978).
131. Hindar, J., J. L. Italm, J. Lindemann, and K. Lonvik, *Proceedings of the Sixth Conference on Thermal Analysis Bayreuth*, Birkhauser, Basel, 1980, p. 313.
132. Lonvik, K., K. Rajeshwar, and J. B. DuBow, *Thermochim. Acta.*, 42, 11 (1980).
133. Clark, G. M., and R. Garlick, *Thermochim. Acta.*, 34, 365 (1979).
134. McAdie, H. G., P. D. Gam, and O. Menis, *U.S. Nat. Bur. Stand. Spec. Publ.*, 260 40, 1972.
135. Lonvik, K., *Thermochim. Acta.*, 29, 243 (1979).
136. Clark, G. M., and R. Garlick, *Proceedings of Fifth Scandinavian Symposium on Thermal Analysis*, Trondheim, 1977, p. 3.
137. Holm, J. L., and K. Lonvik, *Proceedings of Seventh International Conference on Thermal Analysis*, B. Miller, ed., Wiley, New York, 1981, p. 306.
138. Clark, G. M., M. Tonks, and M. Tweed, *J. Thermal Anal.*, 12, 23 (1977).
139. Holm, J. L., and K. Lonvik, *J. Thermal Anal.*, 25, 109 (1982).
140. Lonvik, K., and T. Osrvold, *Proceedings of the Fifth Scandinavian Symposium on Thermal Analysis*, Trondheim, 1977, p. 57.
141. Lonvik, K., and T. Osrvold, *Proceedings of the Second International Symposium on Molten Salts*, J. Braunstein and J. R. Seama, eds., Electrochemical Society, Pennington, NJ, 1977, p. 207.
142. Hunderi, O., and K. Lonvik, *Rapidly Quenched Metals*, B. Cantor, ed., Vol. 1, Chameleon Press, London, 1978, p. 375.
143. Lonvik, K., *Proc. 4th ICF.A. Akademiai Kiado, Budapest, 1974*, p. 1089.
144. Rowe, M. W., *J. Geol. Edlle.*, 31, 5 (1983).
145. Gallagher, P. K., and S. St. J. Warne, *Thermochim. Acta.*, 43, 253 (1981).
146. Hyman, M., and M. W. Rowe, *J. Chem. Educ.*, 56, 835 (1979).
147. Hyman, M., and M. W. Rowe, *J. Geol. Educ.*, 27, 190 (1979).
148. Hyman, M., and M. W. Rowe, *J. Geophys. Res.*, 88, A736 (1983).
149. Larson, E. J., D. E. Watson, J. M. Herndon, and M. W. Rowe, *Earth Planet. Sci. Lett.*, 21, 345 (1974).
150. Gallagher, P. K., E. M. Gyorgy, and W. R. Jones, *J. Chem. Phys.*, 75, 3847 (1981).
151. Gallagher, P. K., E. Coleman, S. Jin, and R. C. Sherwood, *Thermochim. Acta.*, 37, 291 (1980).
152. Gallagher, P. K., and S. St. J. Warne, *Mat. Res. Bull.*, 16, 141 (1981).
153. Skorski, R., *Nature phys. Sci.*, 240, 15 (1972).
154. Rowe, M. W., R. Fanick, D. Jewett, and J. D. Rowe, *Nature*, 263, 756 (1976).
155. Rowe, M. W., S. V. Lake, and R. Fanick, *Nature*, 266, 612 (1977).
156. Herndon, J. M., M. W. Rowe, E. E. Larson, and D. E. Watson, *Earth Planet. Sci. Lett.*, 29, 283 (1976).
157. Watson, D. E., E. E. Larson, J. M. Herndon, and M. W. Rowe, *Earth Planet. Sci. Lett.*, 27, 101 (1975).
158. Rowe, M. W., *Geochem. J.*, 1(1), 215 (1976).
159. Aylmer, D., and M. W. Rowe, *J. Phys. Chem.*, 78, 2094 (1983).
160. Hyman, M., and M. W. Rowe, *J. Chem. Educ.*, 59, 424 (1982).
161. Aylmer, D., and M. W. Rowe, *Proc. 7th ICF.A.*, B. Miller, ed., Wiley, New York, p. 198.
162. Hyman, M., and M. W. Rowe, in *New Approaches in Coal Chemistry*, B. D. Blaustein et al., ed., American Chemical Society, Washington, DC, 1981, p. 389.

163. Charles, R. G., J. G. Cleary, and M. J. Wootten, *Nucl. Technol.*, **58**, 184 (1982).
164. Mulay, I. N., and L. K. Kes, *Anal. Chem.*, **36**, 2383 (1964).
165. Simmons, E. I., and W. Wendlandt, *Anal. Chim. Acta*, **35**, 461 (1966).
166. Charles, R. G., L. N. Yannopoulos, and P. G. Haveriak. *J. Inorg. Nucl. Chem.*, **32**, 447 (1970).
167. Townsend, D. I., *Chem. Engl. Prog.*, **73**, 80 (1977).
168. Townsend, D. I., and I. C. Tou, *Thermochim. Acta*, **37**, I (1980).
169. Duch, M. W., K. Marcali, M. D. Gordon, C. J. Hensler and G. J. O'Brien, *Plant Oper. Prog.*, **1**, 19 (1982).
170. Columbia Scientific Industries Corp., *Tech. Inform. Bulletin No. 1*.
171. Smith, D. W., M. C. Taylor, R. Yourd, and T. Stephens, *Am. Lab.*, June 1980, p. 51.
172. Tou, J. C., and L. f. Whiting, *Thermochim. Acta*, **48**, 21 (1981).
173. Shaw, O. H., and H. O. Prilchard, *Can. J. Chem.*, **46**, 2721 (1968).
174. Whiting, L. F., and I. C. Tau, *J. Thermal Anal.*, **24**, III (1982).
175. Columbia Scientific Industries Corp., *Tech. Inform. Bulletin No. 1*.
176. Hakl, J., *Thermochim. Acta*, **38**, 253 (1980).
177. Hakl, J., *Chem. Techn.*, **8**, 505 (1979).
178. Hakl, J., *Chem. Rundsch.*, **11**, 100 (1981).

CHAPTER

12

THE APPLICATION OF DIGITAL
AND ANALOG COMPUTERS
TO THERMAL ANALYSIS

A. INTRODUCTION

One of the important trends in chemical analytical instrumentation during the past decade has been the use of digital computers as data processing aids. Raw experimental data from an instrument is manipulated, displayed, and printed by use of a microcomputer or minicomputer. This trend has become very apparent in thermal analysis instrumentation. A small dedicated microcomputer is used to set the instrument's operating parameters as well as to process and display the experimental data. Unfortunately, the TA instruments such as thermobalances, DTA, DSC, and TMA units are of designs that are at least 20 years or more old. New instrument designs have not been developed but, rather, the emphasis has been on computerization.

This chapter attempts to summarize the important applications of digital, and, in certain cases, analog computers to thermal analysis instrumentation. No attempt has been made to make it comprehensive in scope, due to the voluminous literature on this subject. Instead, it is hoped that the discussion will provide a background on the general subject of computerization of TA techniques and an insight into what to expect from commercially available computer-assisted instruments. The latter subject changes at very short-time intervals due to the rapid advances in the technology of small computers.

B. THERMOGRAVIMETRY (TG)

One of the first applications of a digital computer to calculations of thermogravimetric data was that by Soulen III. Since the amount of computation required to obtain kinetics constants from TG is large, a computer program was developed for the calculation of temperature, mass, and rate of reaction from the devoltage generated by the thermobalance. A Remington Rand Univac computer was used, employing a Math-Matic compiling system, in which a 23-sentence English language program was used to compute 60 values each of temperature, mass, cumulative mass-loss, and rate of reaction, and to store these for subsequent computation of the kinetics constants.

Instead of a data-logging system, numerical values were manually taken from the strip-chart recordings at one-minute intervals and used as input into the computer. It was stated that an English language program was rather inefficient for this type of program and that a more efficient program could no doubt be developed using machine language.

Almost all the other applications of computers to thermogravimetry involved calculations pertaining to reaction kinetics. Schempf et al. (2) developed a program, POLY 2, for the determination of the preexponential factor of the Arrhenius equation and the activation energy. This program, designed to accept sample mass (w) and sample temperature (T) values as a function of time (t) was written for first-order reactions only, although with slight modifications it could be used for any order of reactions. It made use of a least-squares-of-polynomial fit of the time-sample mass values to the equation.

$$w = \sum_{i=0}^n C_{i+1} t^{i+1} \quad (12.11)$$

where n is the desired order polynomial, C the coefficient of the polynomial, and t the time. From the w - t curve thereby generated, an additional Fortran subroutine, FREEB, calculated the reaction rate constant for any point on the TG curve using the equation

$$k = \frac{-\sum_{i=0}^{n-1} [i+1] C_{i+2} t^{i+1}}{\sum_{i=0}^n C_{i+1} t^{i+1}} = \frac{dw/dt}{w} \quad (12.2)$$

where n is the desired order polynomial. A least-squares analysis of the values of $\log k$ versus $1000/T$ was obtained for the following first-order polynomial:

$$\log k = \log A - Ea/2.303 R (1000/T) \quad (12.3)$$

The complete program is illustrated by the flow diagram in Figure 12.1. The accuracy of the computer fit of the TO curve was 0.2 mg, while the limit of accuracy for reading a weight value was 0.1 mg.

Two programs for the algorithmization of kinetic-data computations from TG curves were developed by Sestak et al. (3) They make use of the basic equation

$$\frac{d\alpha}{dt} = \exp\left(\frac{-E}{RT}\right) (1-\alpha)^n \quad (12.4)$$

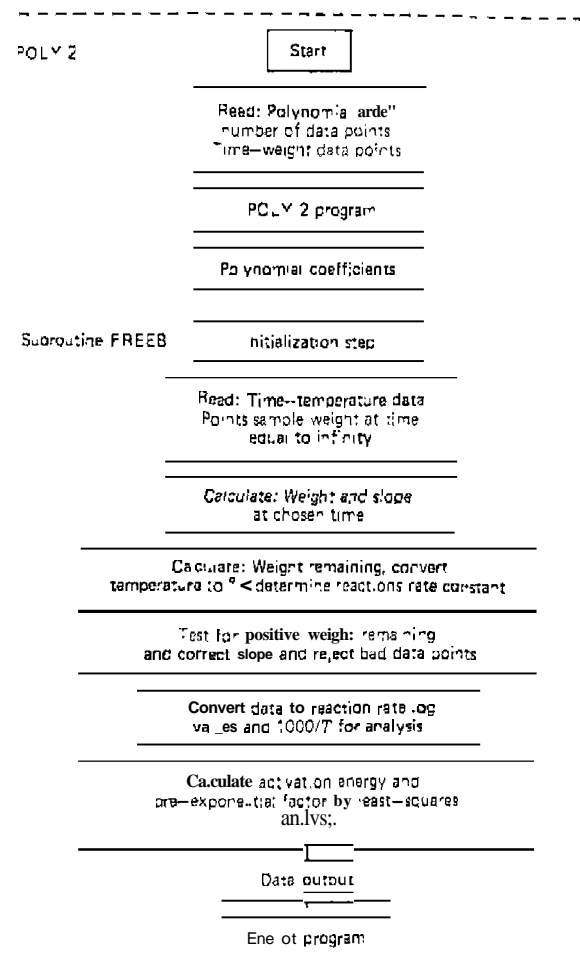


Figure 12.1. Flow diagram for calculation (12).

where α is the degree of decomposition, and n the order of reaction. The kinetics parameters, E , Z , and n , were evaluated by use of two differential methods. The first method utilized a least-squares polynomial fit of the TG curve with a j th-order polynomial:

$$\alpha = A_0 + A_1 x + \dots + A_j x^j \quad (12.5)$$

where) is about 13 and the A's are constants obtained from The least-squares fit of the experimental data. The second method attempted TO use the simplest means of obtaining a derivative of the observed TG curve by numerical derivation using the first three terms of the series.

$$\left(\frac{dx}{dt}\right)_i = \left\{ \frac{1}{2}(w_{j+1} + w_{j-1}) - \dots - \frac{1}{60}(w_{j+3} - 4w_{j+2} + 5w_{j-1} - 5w_{j-1} + 4w_{j-2} - w_{j-3}) - \dots \right\} / Qw_m \quad (12.6)$$

where w is the mass-loss and Q is a constant time interval of scanning. This program was written in ALGOL 60. The results obtained by computing data obtained from TG curves, with various programs and with those calculated manually, are shown in Table 12.1. The discrepancies which occur were said to be due to differences in the requirements for the input data. A flowchart for the second program used was also presented in detail.

Gallagher and co-workers have described several TG data-collection systems in which the data are obtained on magnetic tape or on punched paper tape. A block diagram or their first system (7) is shown in Figure 12.2. In this system, the outputs from the Cahn Model RG balance and the Chromel-Alumel thermocouple were converted to digital form and punched on paper tape for subsequent computer processing. The timing cycle for the counter was normally set to count the thermocouple channel for 1 sec and the mass channel for 99 sec. Switching time was relatively instantaneous and the data were punched while the counter was operating so that the dead time was negligible. The effective use of averaging each reading over these times leads to a reduction of noise, which is important for the computation of the time derivative.

The digital data were transferred from punched paper tape to cards and the EMF versus temperature tables for the compensated thermocouple were

Table 12.1. Comparison Between Manual and Computer Calculations (3)

Experimental Data Used	Manual Results			CL Computer Program
	Derivative (4)	Integral (5)	Frequency Factor (6)	
CaC ₂ O ₄ → CaCO ₃ + CO(g) (from Ref. 4)				
E = 74 kcal, n = 0.7	E = 67 ± 15 n = 0.6	74.1 ± 3.5 1		72.1 58.67 0.59t

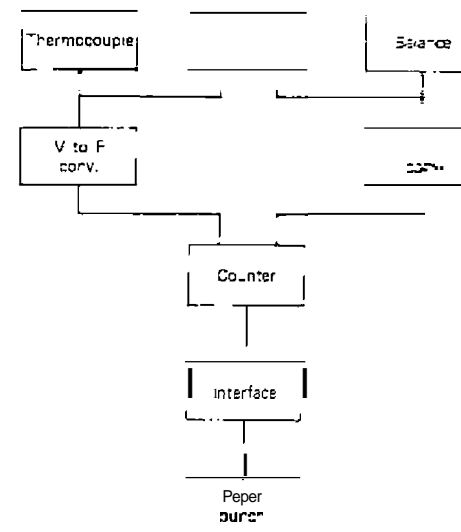


Figure 12.2. Block diagram of digital TG system of Gallagher and Schrey (7)

fitted by a least-squares technique to the equation

$$^{\circ}\text{C} = 22.2877 + 25,7003 (\text{mV})^2 + 0.0017 (\text{mV})^3 \quad (12.7)$$

which was satisfactory to ±1°C over the temperature region 200 to 1000°C. A program was developed to compute the average temperature for each pair of consecutive temperature readings and associate this temperature with the average mass readings in the interval between the thermocouple readings. A General Electric Model 600 computer then tabulated and plotted both the percent mass-loss and the rate of mass-loss (mg. min) as a function of temperature. The rate of mass-loss was obtained from the difference in mass of consecutive readings (100-sec intervals) and corrected to give milligrams per minute. No further refinement or smoothing of the differential data was necessary.

For isothermal measurements, using a Cahn Model RG thermobalance, the data acquisition system shown in Figure 12.3 was employed (11, 12). The system accepted up to four analog input signals, of which two were used for mass and temperature, respectively. The voltages were converted to frequency using a voltage-to-frequency converter, and four channels were simultaneously counted on four scalars for a predetermined time interval.

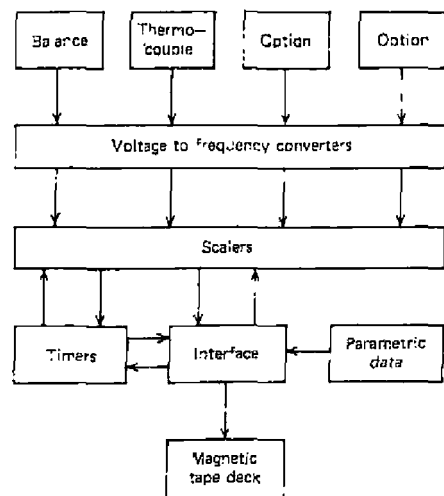


Figure 12.3. Data acquisition system of Gallagher and Johnson (11, 12).

The magnetic tape interface served as the control center. In the automatic mode, the data were scanned repeatedly at a preset time interval and placed on the magnetic tape along with channel identification numbers. A fifth channel could be created to insert a six-digit number for labeling or control purposes. Data processing consisted of transferring the data from tape onto the disk storage of a Honeywell Model 635 Computer in appropriate arrays corresponding to each channel. Computer-generated plots of each array as a function of time were then made with subsequent data processing as previously described (12).

Gallagher and co-workers (8-10, 13) also described a modification of the Perkin-Elmer thermobalance to obtain the data in digital form. In this instrument, the platinum furnace heater winding serves also as the temperature sensor. It forms one side of a bridge circuit, while the other side is driven by the output voltage from the programming potentiometer. This same voltage is used to supply the temperature portion of the digital equipment and is directly related to temperature by use of magnetic (Curie point) TG calibration standards.

The two input voltages were converted to frequency and counted for a predetermined time in the sequence shown in Figure 12.4. The temperature signal was counted for 0.1 sec and then automatically switched to the mass signal for 10 sec. The output data were constantly punched on paper tape for input into the computer.

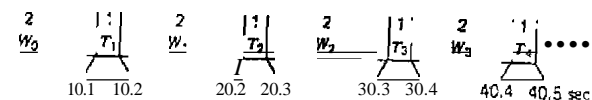


Figure 12.4. Timing sequence employed by digital thermobalance (8).

The first stage in the computer processing of the punched-tape data was to transfer the data to cards and to use these cards for the three steps in processing (9). The first step was to obtain a graphical output of the mass as a function of time, as shown in Figure 12.5. The second step of data handling consisted of utilizing the initial and final mass for each interval to determine values of α , the fraction reacted. The computer, having calculated the values of α for each point, then plotted these to conform to the 18 equations

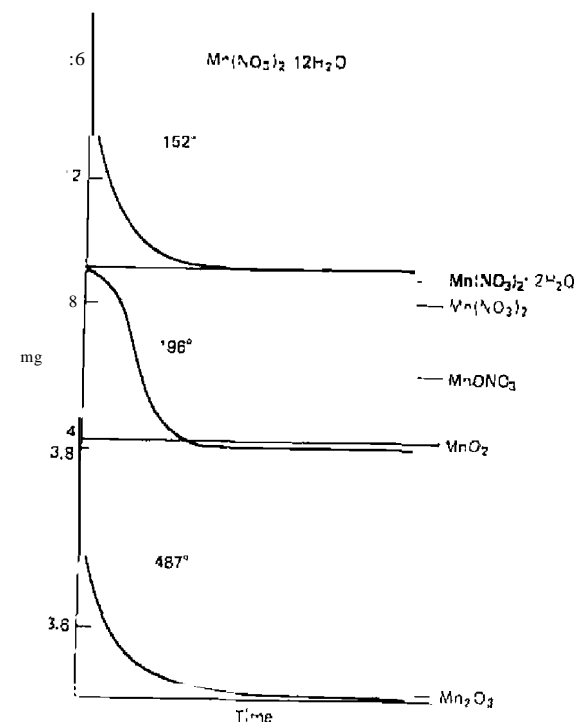


Figure 12.5. Mass versus time curves as reported by Gallagher and Johnson (9).

given in Table 12.2. Appropriate equations were determined by visual inspection of the computer output plots for their linearity. One such set of curves for the plot of $-\ln(1 - \alpha)$ versus time is shown in Figure 12.6. The choice of equation was then based on the exact degree of fit determined by the standard deviation arising from the calculation of k in the third stage of processing. This third stage consisted of the selection of the most likely

kinetic equation or equations and the plotting of the best values of $\log k$ versus the reciprocal of the absolute temperature, and a least-squares fit to determine the best straight line. The resulting activation energies, E , and the preexponential terms were printed out along with the plot.

Vachuska and Vobori (20) developed a program called VACHIVO 11 (21) for use on the GIER computer, in which the first-order and also the second-order derivations of the time dependencies of both sample mass and temperature are computed numerically with respect to time from experimental values of these quantities. A newer version of this program is VYRVACHVON 122, in which a certain polynomial function is laid through the experimental points and its course is determined by a least-squares method. The computer then calculates the "corrected" input data from a given expressed function and, using these data, numerically differentiates. Both programs were written in the GIER-ALGOL language.

Although the programs of techniques were not discussed in detail, a digital computer was used to analyze the kinetics data obtained from TG by a number of investigators (14-19). One of these studies (19) used a Hewlett-Packard Model 9100A programmable calculator.

Hughes and Hart (23) have developed an analog simulation program, BASE, which was used for the prediction of a TG curve. The calculation involved the plotting of the TG curve from the equation.

Table 12.2. Kinetic Equations Used in the Computer Analysis (9)

1. Power law	$\alpha^n; n = \frac{1}{2}, \frac{1}{3}, \frac{1}{4}, \text{ and } 2$
2. Contracting geometry	$1 - (1 - \alpha)^{1/n}; n = 2 \text{ and } 3$
3. 2D diffusion controlled	$(1 - \alpha) \ln(1 - \alpha) + \alpha$
4. Emfeev	$[-\ln(1 - \alpha)]^{1/n}; n = 1, \frac{1}{2}, 2, 3 \text{ and } 4$
5. 3D diffusion controlled	$(1 - \frac{2}{3}\alpha) - (1 - \alpha)^{2/3}$
6. Jander	$[1 - (1 - \alpha)^{1/3}]^2$
7. Prill-Thompkins	$\ln\left(\frac{\alpha}{1 - \alpha}\right)$
8. Second order	$1 - \alpha$
9. Exponential	$\ln \alpha$

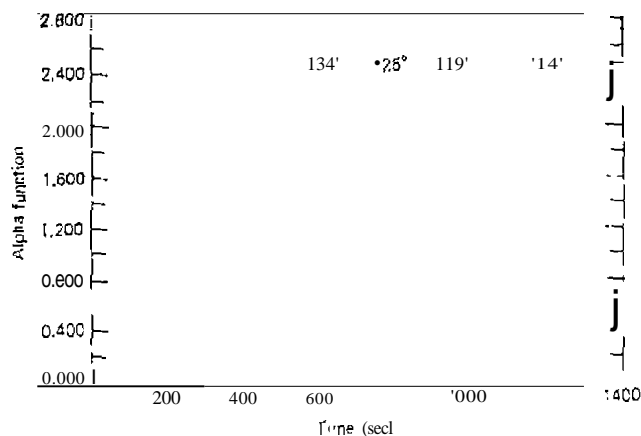


Figure 12.6. Plots of $-\ln(1 - \alpha)$ versus time for the dehydrations of aqueous manganese(II) nitrate (9).

$$f(\alpha) = \frac{A}{a} \int_{T_1}^{T_2} \exp\left(-\frac{E}{RT}\right) dt \tag{12.8}$$

where $f(\alpha)$ represents some description of the rate law for the fractional decomposition (α) of the solid; A is the preexponential factor; a is the heating rate (dT/dt), and E is the activation energy. In order to write a patch diagram for the program, they set

$$y = \exp\left(\frac{-E}{RT}\right) = e^z \tag{12.9}$$

where $z = -E/RT$ and $dz = (E/RT^2)dT$. Then

$$dy = e^z dz \tag{12.10}$$

$$dy = e^z \frac{E}{RT^2} dT = 2.4e^z \left(\frac{E}{RT^2}\right) dT \tag{12.11}$$

or

$$\dot{y} = 2.4 \exp\left(\frac{-E_1}{RT}\right) \left(\frac{E}{RT^2}\right) \quad (12.12)$$

Since the integral of \dot{y} is y and because $2.4 \exp(-E_1/RT)E/RT^2$ is identical with y , it is assumed that $E_1/RT^2 y$, where $y = \exp(-E_1/RT)$ and generate $f(y)$ (i.e., $2.4y E_1/RT^2$), the integral of this function will be y . This process is represented by the patch diagram in Figure 12.7. The computations were applied to the dehydration of $\text{CaC}_2\text{O}_4 \cdot \text{H}_2\text{O}$, a system which has been well studied by a number of investigators. Using the data given by Freeman and Carroll (4), the calculated and experimental curves are given in Figure 12.8. It is interesting to note that the curve calculated by integrated methods using Akahira's tables and the experimental parameters gave a curve which coincided nicely with the computed one.

The in-house differences between results for duplicate samples tested by different laboratories under supposedly similar conditions led to interest in the effects of the Tate and mode of beating, and also of fluctuations in temperature after heating, on the mass-loss curves. Because these problems did not lend themselves to direct solution with the experimental equipment on hand, Gayle and Egge (24) applied analog computation to study the importance of these variables. The calculations were performed on an analog computer where the heating-rate curves were programmed as the corresponding differential equations and the temperature integral of these were used as input into the Arrhenius equation. Integration of the latter provided the corresponding mass-loss curves. The treatment provided an estimate of the influence of constant thermal errors and of fluctuations about the programmed temperature level. It is noteworthy that symmetrical fluctuations did not result in a cancellation of errors when the rate behavior was exponential rather than a linear function of temperature. The analog computer provided a graphic, reasonably accurate picture of such effects.

Yllen et al. (5) have described an automatic data acquisition system for the simultaneous operation of two Mettler Model TA-1 Thermoanalyzers. A

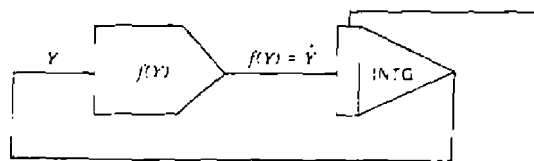


Figure 12.7. Patch diagram of Hughes and Han (23)

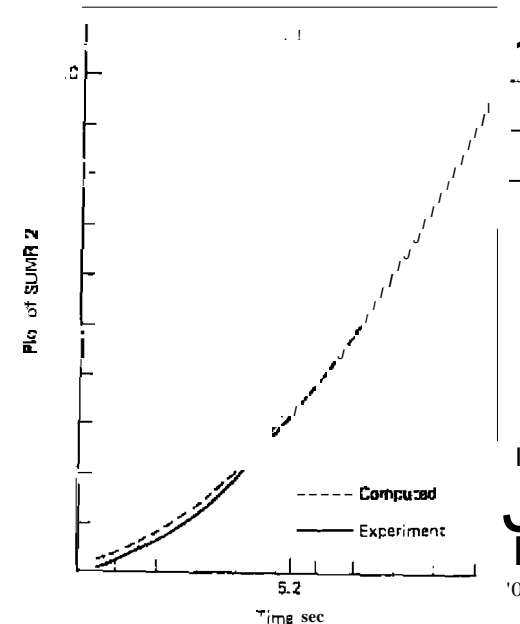


Figure 12.8. Calculated and experimental time (sec) TG curves for $\text{CaC}_2\text{O}_4 \cdot \text{H}_2\text{O}$ (23).

schematic diagram of the system is shown in Figure 12.9. The system uses an on-line Hewlett-Packard HP 9825 S desk-top computer equipped with a real-time clock and HP-1B interface options. The computer had 23 Kb of RAM and 42 Kb of ROM. Other components of the system included a HP 59500 A I/O interface, a HP 6940B multiprogrammer and a HP 9872A four-color plotter. A 12-bit analog-to-digital converter, relay output cards, a digital input card, and a custom-designed dynamic range expansion circuit are used with the multiprogrammer unit.

The system is designed to collect up to six channels of analog information as a function of time, from each thermobalance. Nominal collection rate is one data set logged alternately from each instrument every 5 sec for a per instrument rate of six sets per min. Data acquired from the two thermobalances is converted to actual units, such as temperature in °C, and so on, and stored in two arrays of 100 data sets, with one array being assigned to each instrument. The conversion of the thermocouple EMF into temperature is based on two polynomials, one for the PtRh10%-Pt system and the other for NiCr-Ni and stored in the data acquisition program. When the two arrays are filled, they are automatically recorded on tape.

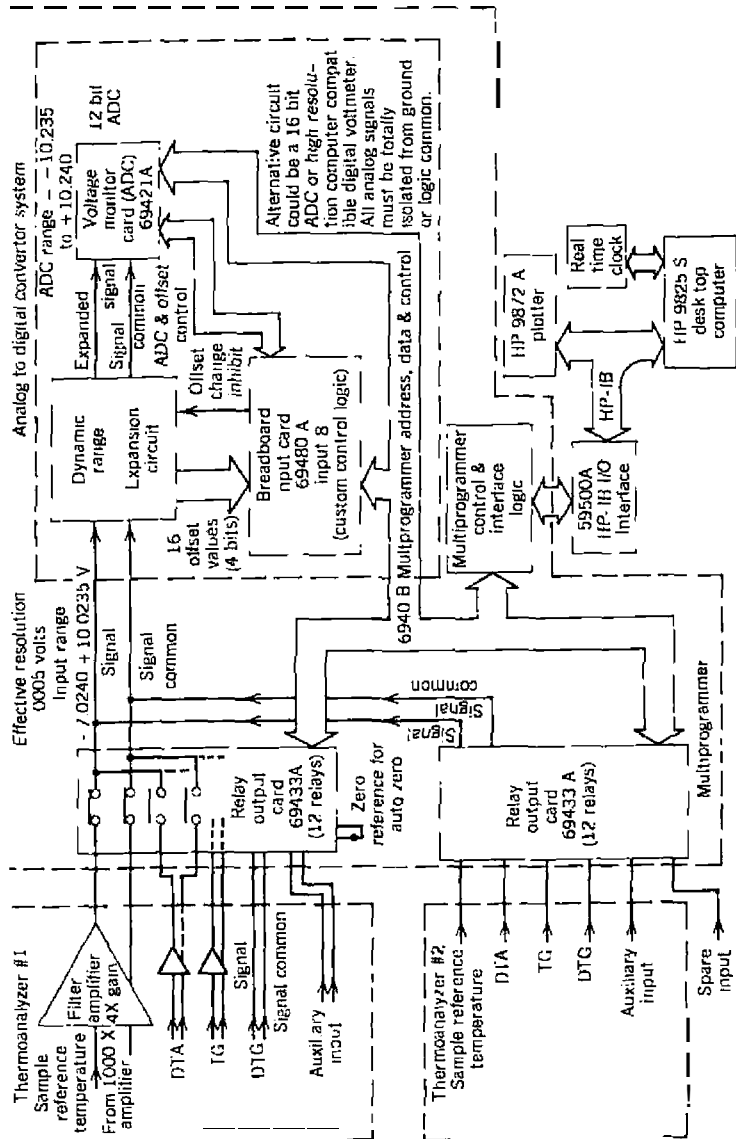


Figure 12.9. Block diagram of data acquisition system described by Yuen et al. (5).

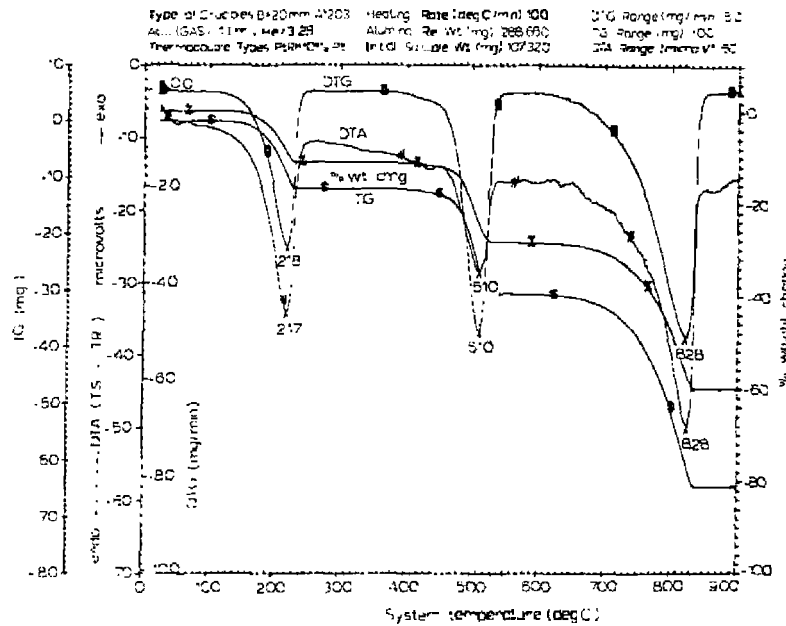


Figure 12.10. TG, DTG, and DTA curves of $\text{CaC}_2\text{O}_4 \cdot \text{H}_2\text{O}$ obtained by Yuen et al. (5).

Data reduction at the end of the sample run is handled by five programs: (1) weight off, (2) buoyancy correction, (3) plotting, (4) find peak, and (5) percent weight-change tabulation. The data reduction system permits data to be analyzed rapidly with a savings of 70-80% over the normal recording system of the thermobalances. A plot of the computer printout of the TG, DTA, and DTG curves of $\text{CaC}_2\text{O}_4 \cdot \text{H}_2\text{O}$ is given in Figure 12.10. A curve that required several hours to plot using the normal thermobalance recorders is now plotted in a matter of seconds using the computer system. The plot can also be made in four colors on a clear transparency for use in overhead projector presentation at a later time or reduction on photocopy machines.

Doelman et al. (6) described an on-line data acquisition system for TG using an IBM S/7 computer followed by data reduction on an IBM 360/195 computer. A DuPont Model 990 thermobalance was interfaced to the IBM S/7 computer using the system previously described for DTA data collection (53). The thermobalance must have the electrical zero (zero weight) signal established at the beginning of the run. Unlike DTA, the thermobalance does not have a completely linear temperature change with time. The con-

linearity of the temperature change is due to the thermal magnitude of endothermal or exothermal weight-loss or gain processes, which are usually larger than normal heats of fusion, solid \rightarrow solid phase transition, and so on.

The primary commands for data reduction were entered by means of an interactive display device, Tektronic 40J3 Scope, supported by the IBM 360/195. Data from the IBM 5/7 are transmitted to the IBM 360/195 on command. The program that reads the data file allows it to be combined with that of another run (at a different heating rate) or with an empty pan run. This combinatory function is required both to calculate an activation energy by the method of Gyulai and Greenhaw (55) and to correct any sample run for base- or zero-line drift. Prior to display, all weight-loss data are normalized on the basis of sample weight and the total measured weight-loss from zero to 100%. The program also calculated the DTG curve.

Three calculation functions are performed: (1) weight-loss, (2) kinetics, and (3) 2-INTM. Kinetics calculations are used to obtain the activation energy, E , from

$$\ln \left(\frac{-\text{rate}}{(\text{wt}_{\text{obs}} - X)} \right) = \frac{-E}{RT} + \ln(Z/a) \quad (12.13)$$

where rate is the rate of weight change or slope of the integral curve at any point; $(\text{wt}_{\text{obs}} - X)$ is the weight observed at time t minus the weight at any residue remaining after the reaction, E is the activation energy, and Z is the preexponential factor. The 2-INTM function calculates E using the double-heating rate method of Gyulai and Greenhaw (55). E values were calculated for the three-step decomposition reactions of $\text{CaC}_2\text{O}_4 \cdot \text{H}_2\text{O}$ and compared with other methods in the literature.

Vernon (56) has written computer programs to acquire and analyze TG and DSC data and to calculate reaction kinetics using DSC, isothermal DSC, and TG. A system was described in which the instrument analog signals were digitized using a Fluke 1600A-scanning digital multimeter and transferred to a Hewlett-Packard UP 9845T computer for data reduction and plotting. Ordinate data points were obtained by digitizing mV instrument outputs at a sensitivity selected by the operator. Abscissa data points were obtained as time from a real-time clock interfaced to the computer. Temperature was obtained as the product of time and heating rate.

Data points (X_j, Y_j) were curve-fitted using a precise continuous polynomial, or cubic spline, algorithm. Ordinate values were represented as

$$Y_j = \sum_{k=0}^3 M_{jk} X^k \quad (12.14)$$

where the coefficient matrix M is determined by demanding continuity of the polynomial, and its first derivative at each data point. Use of this algorithm permits facile differentiation and integration of the data curves and is relatively insensitive to noise in the instrumental output. A complete listing of all the programs has been given (56).

C. DIFFERENTIAL THERMAL ANALYSIS (DTA) AND DIFFERENTIAL SCANNING CALORIMETRY (DSC)

Nearly all the computer applications to DTA have been concerned with the calculations of reaction kinetics where they find the ideal means of simulating the DTA curve of a chemical reaction of known kinetics. One of the first of these applications was that by Reed et al. (25) in which the quantitative determination of kinetics by the methods of Borchardt and Daniels (26) and Kissinger (27) were evaluated and compared. The DTA curve was generated numerically by use of equations such as

$$-\theta_r \frac{d\psi}{d\theta_r} = \zeta \psi^\alpha e^{\varepsilon - \theta} \quad (12.15)$$

where ε is the activation energy and θ_r , $d\psi/d\theta_r$, the reaction order, ψ is N/N_0 (number of moles), $\zeta = \alpha A(N_0/V)^{\alpha-1}$, and θ_r is the dimensionless heating rate: in finite-difference form,

$$\psi(\theta_r) - \psi(\theta_r + h) = \frac{h\zeta}{\theta_r} \left[\frac{\psi(\theta_r - h) - \psi(\theta_r)}{h} \right]^\alpha \exp \left(\frac{-\varepsilon}{\theta_r} (\theta_r - h) - \theta(\theta_r) \right) \quad (12.16)$$

where h represents the mesh spacing, $\Delta\theta_r$. A typical computer-generated curve, in which the effect of activation energy ε on the DTA curve is plotted, is shown in Figure 12.11. Both the location and the shape of the curves is affected, but the dependence is inverse to that observed for the changes of the frequency factor.

The fraction of sample decomposed (α) from DTA curves was calculated by an algorithm made in ALGOL 60 language for a NCR Elliot Model 4130 computer by Skvara and Satava (28). This algorithm calculated α and $\log \theta(\alpha)$ and plotted the latter as a function of temperature. Comparison of the computed DTA data with the experimental values for several dissociation reactions indicated a good agreement and applicability of the method.

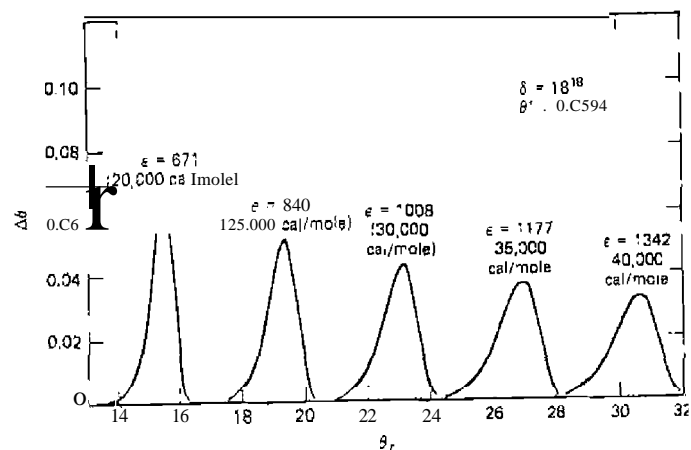


Figure 12.11. Effect of activation energy on DTA curve (25).

The use of a systems analog to improve the performance of a DTA apparatus and also to study the thermal effects in the DTA curve was investigated by Wilburn et al. (29, 30). A finite-difference procedure was used to relate the thermal gradients within the samples and to generate or absorb heat according to a known equation. The influence of such physical properties on the shape and peak temperature of a typical DTA curve was calculated on an ICT Model 1909 computer.

The application of computer calculations to DTA studies of the crystallization kinetics of polymers was described by Gornick (51). Calculations were made of the temperature of a polymeric sample during the cooling process using a Burroughs Model 5500 computer. Morie et al. (52) used an IBM Model 1130 computer to prepare standard vapor-pressure plots of $\ln P$ versus $1/T$, the vapor-pressure data being obtained from DTA or DSC curves. The heat of vaporization was calculated by the Haggemacher method as modified by Fishtine.

David et al. (31) used a digital temperature readout device in conjunction with an analog recorder for transition temperature measurements. Temperature resolution was about 0.05°C at a heating rate of $10^\circ\text{C}/\text{min}$.

Amstutz (32) described the Mettler data-acquisition system which is capable of handling eight-digit numbers of any format type or voltage level. A schematic diagram of the system is shown in Figure 12.12. Expansion capabilities include digital and analog multiplexers, keyboards and switch banks for manual entry of data, timers, and programmers. Applications to DTA include off-line recording of raw data on punched paper tape or mag-

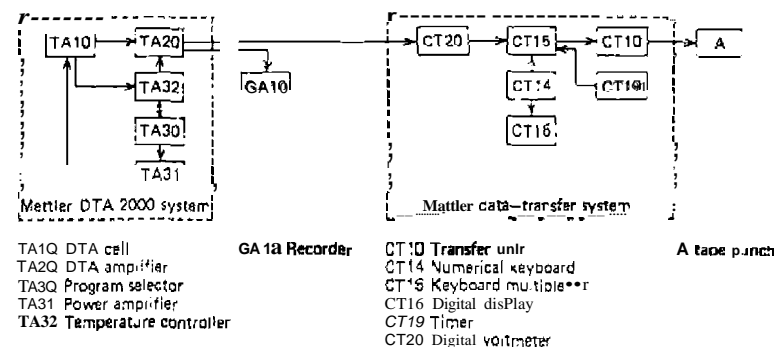


Figure 12.12. Mettler data transfer system connected to a Mettler DTA 1000 system (32).

netic tape, and on-line processing, ranging from simple peak area calculations by means of programmable desk-top calculators to the more complex numerical determinations of heat or reaction, kinetics, and purity analysis.

One of the major applications of computers to differential scanning calorimetry (DSC) is in the determination of the purity of organic and inorganic compounds. The precision and accuracy of purity determinations by this technique have been reviewed by Joy et al. (33). One of the first programs for purity determinations using DSC data was that developed by Driscoll et al. (34). Required input data are the sample mass and molecular weight, instrument constants, a reference temperature at a point where the curve is still on the baseline, and ordinate and abscissa measurements on the curve. One measurement should be at the melting curve peak, but the intervals need not be of uniform size. A maximum of 99 pairs of readings can be accommodated by the program.

The program divides the curve into 99 equal temperature intervals and integrates to obtain the ΔH_f . Temperature correction and baseline area correction are determined for each interval, and the partial area is calculated. The program then applies successive 0.5% area corrections on each partial area and the total area and calculates the $1/F$ values. A least-squares regression analysis is used in each corrected line until a minimum standard deviation of the points about the calculated line is reached. The "best values" are then used in the subsequent calculations. Output from the computer includes the ΔH_f , T_p , and T_m , the mole-% impurity, the $1/F$ limits used, the percent correction applied, and the cryoscopic constant. A corrected mole percent impurity assuming solid-solution behavior is also calculated. The "linearization" or the T_p versus $1/F$ curve has been discussed (35). Joy et al. (33) rewrote the preceding program from Fortran into a basic program operable on a

time-shared computer terminal. Other DSC purity determination programs have been developed by Barrall and Diller (36) and Scott and Gray (37).

Using an IBM Quiktran program, Ellerstein (38) performed calculations of DSC-curve data from the equation.

$$\frac{\Delta \log l}{\Delta \log A_r} = \frac{E}{2.303R} \frac{[\Delta(l_i)]}{[\Delta \log A_r]} \quad (12.17)$$

where l is the ordinate displacement between the baseline and curve and A_r corresponds to the area remaining at temperature T . Plotting the left-hand side versus the bracketed expression gives a curve whose slope is $E/2.303R$, and the intercept will be equal to n , the order of reaction. Results from the Quiktran program are then fed into all IBM Quiktran Common library program (FITLIN) which gives a "best" line fit of the calculated points.

Gray (39) developed a program which accepts the DSC sample and baseline data, matches the "isothermal," performs cumulative and total area integrations in units of cal/g, corrects the temperature for thermal lag, and tabulates and plots ordinate values in specific-heat units as well as cumulative area in enthalpy units. The analog data from the DSC instrument are digitized and transferred to paper tape with the use of the Perkin-Elmer ADS VI Analytical Data System for Thermal Analysis. The data are digitized every two seconds or every 0.133". A computer plotter then plots the DSC curve and also the cumulative peak area in specific enthalpy units, cal/g.

Crossley et al. (40) used a computer reduction technique for the DSC isothermal curve which was developed to replace the use of a planimeter. The data reduction was divided into two phases: (1) mechanism-independent solutions for the reactant fraction, α , and various functions of α (where α is the reactant fraction remaining at time t) and (2) solutions for mechanism-dependent rate constants. For the first phase, the DATAR program was developed, which consisted of the following: Ordinal points referred to a "coarse data," and evenly spaced in time over the time span of the DSC curve, are read directly into the computer. Up to 1000 points may be read, but 40-50 are usually sufficient for acceptable accuracy. The resultant fraction remaining at time t is calculated by the equation

$$\alpha(t) = \frac{\int_0^{t_{\max}} (\text{ORD}) dt}{\int_0^{t_{\max}} (\text{ORD}) dt} \quad (12.18)$$

A Simpson's rule procedure modified to handle odd numbers of intervals is used to evaluate the integrals. The program calculates and prints the time

in seconds and in minutes, α , $\ln \alpha$, $1/\alpha^2$, $(1 - \alpha)/\alpha$, and $\log 100 [(1 - \alpha)/\alpha]$. For the second stage, the PARACT program is used to determine the true rate constants, k_1 , and k_2 .

Other programs which can be used to calculate reaction kinetics from DSC data were formulated by Kauffman and Beech (41) and Rogers and Smith (42). Heuvel and Lind (43) used a computer to correct DSC data for effects due to thermal lag and heat capacity changes, while Sondack (44) developed a simple equation for the meanization of data in DSC purity determinations.

As described in section B, DTA and DSC data may also be acquired and processed by the systems previously discussed (5,6, 54, 56). Vernon (56) used the Borchardt and Daniels (26) and Kissinger (27) methods to calculate E and Z of explosive materials from nonisothermal DSC data. Roger's method (57) was used for these calculations from isothermal DSC data.

Dunn et al. (58) interfaced a DEC PDP 11-10 computer to a DuPont Model 990 thermal analysis system. The BCD-binary converter used a cascade of 15 6-bit BCD-binary ROMs to convert the 4.5-digit BCD output of the Hewlett-Packard Model HP 3430D digital voltmeter to bit binary for input to the DEC DR-11C general input-output device. All software was written in FOCAL, under the RT-11 operating system.

D. MISCELLANEOUS THERMAL TECHNIQUES

Analysis of isoperibol calorimetric data requires lengthy graphical procedures and tedious calculations to obtain corrected resistance changes for the reaction and calibration experiments. The reaction experiment graphically resolves into two linear portions, the initial rating period (IRP) and the final rating period (FRP), connected by a curve for which no analytical equation is known. A program was developed for these calculations by Gayer and Bartel (45).

Friedman and co-workers (46-48) have developed a digital converter for recording evolved gas analysis (EGA) mass spectrometric (MS) data on punched paper tape. The data collection system is shown in Figure 12.13. It is based on a very stable programmed power supply that steps the gate to preselected discrete, ionic mass peak locations. In practice, analog gate voltages are determined for about 20 peak centers from $m/e 1$ to about 203, as monitored by a digital voltmeter. These are then analyzed by a least-squares shared-turc program using a polynomial equation that includes five constants. If all the calculated points are within values equivalent to 10 nsec of the observed time delay, the fit is accepted and a printout is obtained for all analog gate voltages as a function of mass number, by interpolation and extrapolation. The punched paper tapes generated during a run are read by an optical reader and stored in a small computer. A large computer then

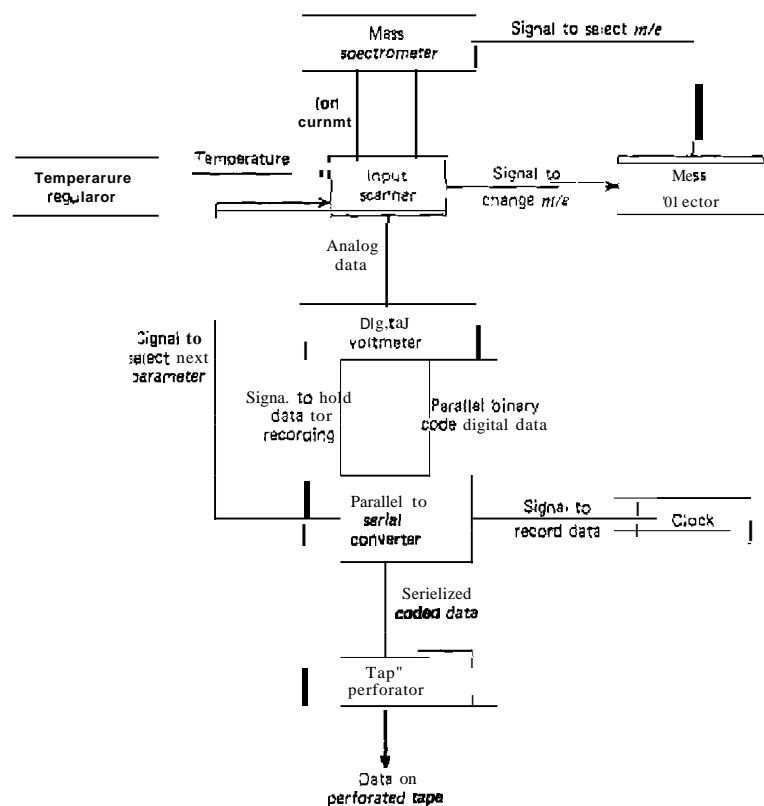


Figure 12.13. Data collection system for EGA-MS after Friedman et al. (47).

orts the data by mass number and plots the data on a graphic ploner. The Plotted data are corrected for background and instrument sensitivity, editorial corrections are made, and the data are normalized to 1 mg initial sample mass.

Gibson (49) described a TG-MS system which contained a PDP 8/L computer interfaced to the mass spectrometer for on-line control of the mass spectral data. A schematic diagram of the system is shown in Figure 12.14. The output analog signal from the mass spectrometer is integrated and converted to digital form by a 12-bit converter and transferred to magnetic tape. Two separate modes are possible: 1. data logging and 2. spectrum control; they differ only in the manner in which they acquire data. During operation

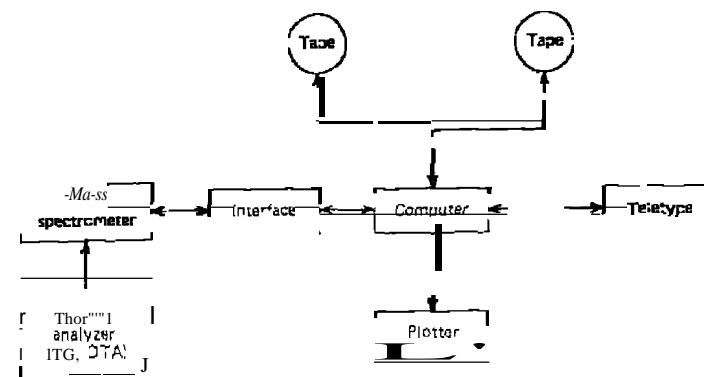


Figure 12.14. TG-MS computer system after Gibson (49).

of the mass spectrometer, the plotter gives a real-time gas release curve, which is simply a plot of the ion current from the electron multiplier at each recorded spectrum scanned. Other output routines include.

1. Reconstruction of a gas release pattern which normalizes the largest gas release peak or region to 100 and indexes the mass spectra during the run.
2. Printed or plotted spectra from any mass spectrum collected.
3. Plots of individual mass (e.g., $m/e = 18$) peaks as a function of temperature.
4. Spectrum plots or printouts with positively identified mass scales and numeric ion intensities.
5. Spectrum plots or printouts with the background spectra subtracted to eliminate the effect of contaminants or backgrounds.

Kinetics calculations on poly(methylmethacrylate) using mass-spectrometric thermal analysis (MTA) were described by Sakamoto et al. (53). Using the activation energy calculated from the experimental data, the computer plots the logarithm of the reduced rate, $dc/d\theta$, versus the logarithm of the reduced time, θ . A comparison is then made between this curve and a calculated theoretical curve for various reaction mechanisms, and the curve which fits best is that of the first-order reaction. Pfeil (50) discussed the application of digital computers to the statistical analysis of the TG measurements of edema. Computer graphics can also provide a useful and much-needed service in the thermal analysis of biological systems.

Yuen et al. (62) developed an automated system that permits DTA, TG, DTG, and mass spectrometry (MS) measurements to be performed simultaneously on a single sample in inert or oxidative atmospheres. A Hewlett-Packard 5992 quadrupole mass spectrometer was used to obtain the MS data. Software programs were developed for: (1) continuous MS monitoring of volatiles, (2) screening of the acquired MS data, (3) tabulation of mass spectra, (4) subtraction of mass spectra acquired at two different times, and (5) TA curves and mass ion profiles. This system was modified by the addition of a gas chromatograph so that it had GC/MS capability (62) as well as the aforementioned TA techniques.

Data acquisition from the Mettler TA-1 and the mass spectrometer were handled by two separate HP 9825 calculators with the MS data stored on a floppy disk.

E. COMMERCIAL THERMAL ANALYSIS INSTRUMENTATION

Perhaps the most important advance in commercial thermal analysis instrumentation during the past 10-12 years has been the use of microprocessors and/or dedicated microcomputers to control the operating parameters of the instrument and to process the collected experimental data. This innovation is by no means unique to thermal analysis instrumentation alone since these techniques have been applied to almost every type of analytical instrument. Unfortunately, the automation of thermal analysis has not become a commercial reality. Complete automation is defined here as automatic sample changing, control of the instrument, and data processing. Such instruments were first described by Wendlandt and co-workers in the early 1970s (See Chapters 3 and 5) although they lacked microprocessor control of the operating conditions.

Due to the rapid changing technology in microcomputers and microprocessors, data and control systems have evolved rapidly; a life time of 3-4 years is about the maximum for such a system. Thus, only the most current computer system will be described here for a particular type of thermal analysis system. No attempt will be made to give details on the software programs in use; these can be obtained from the commercial vendor of the system, if desired. Almost all the commercially available thermal analysis instrumentation employs a microprocessor for operating system control or a microcomputer for data processing. Either a proprietary or a commercially available microcomputer is employed to process the experimental data into conventional thermal analysis plots or to perform more sophisticated kinetics or purity determination calculations.

a. Perkin-Elmer Systems

The TADS (Thermal Analysis Data Station) system has been described by Brennan and DiVito (59). This is a modular system consisting of a microprocessor module of 64 Kbytes of RAM with a 32 Kbyte RAM available for graphics and interactive command entry; two double-sided floppy disk drives; a video display unit with a graphics resolution of 255 points vertical by 720 points horizontal; and a detachable keyboard. A graphics plotter, connected to the computer by a standard RS-232 interface, is used for hard copy. The plotter has a resolution of 0.001 in. as well as alphanumeric printing. The software consists of three types of programs: (1) standard, or routine for instrument control data acquisition, storage and recall, and routine data calculations and optimization; (2) DSC or TG advanced programs, such as kinetics, partial area, purity, specific heat, and other calculations; and (3) general-purpose, or BASIC programming. PFCOWRITER (a word processor), and others. A listing of the DSC standard software library programs is given in Table 12.3. A typical TADS plot of the fusion of Nylon is given in

Table 12.3. TADS DSC Standard Software Library (59)

MODIFY PARAMETERS	Displays and allows modification of the current program parameters.
CONDITIONS	Displays and allows modification of the current set-up conditions.
ZERO READY	Displays the current analyzer zero position. Sets up the Graphics Plotter for plotting during data acquisition.
START STOP	Begins data acquisition and storage. Allows for manual termination of data acquisition and storage.
QUICK-COOL	Terminates data acquisition and automatically cools the analyzer to the starting temperature.
OVERRIDE	Overrides the upper temperature limit during data acquisition.
GO TO ANALYSIS	Activates the library of programs for analyzing data.
GO TO SET UP	Activates the library of programs for setting up, acquiring and storing data.
CONTENT	Displays the files currently stored on the data disk on the CRT.
PLOT CONTENT	Generates a hard copy printout of the files currently stored on the data disk.
RECALL SAVE	Recalls and displays previously run data on the CRT. Saves a data file on the data disk.

Table 12.3. TADS DSC Standard Software Library (59)

DELETE	Deletes a data file from the data disk.
RESCALET	Rescales the temperature or time axis to user defined limits.
SLOPE	Changes the slope of the curve displayed on the CRT.
YSHIFT	Shifts the curve on the CRT along the Y axis.
RESCALE Y	Rescales the Y axis display on the CRT.
NORMALIZE	Normalizes a curve with respect to its sample weight for easy comparison of different data sets.
RECALL 2nd CURVE	Recalls a second curve to the screen for comparison with the first curve.
COMPARE	Shades in the differences between two curves for simple visual comparison.
SUBTRACT	Subtracts a second curve from a first curve and displays the difference.
RESTORE ORIGINAL	Restores a curve to the screen as it was originally stored on the disk.
TJG	Analyzes the onset, midpoint, and change in specific heat of a glass transition.
DERIVATIVE	Calculates and displays the first derivative of any curve.
PEAK	Analyzes peak area (ΔH), peak limits, onset temperature, and peak maximum of any peak.
PLOT SCREEN	Generates a hard copy printout of any screen display on the Graphics Plotter 2.
PLArCALC	Generates a hard copy printout of any calculation currently displayed on the screen.
OPTIONS	Displays a menu on the CRT of the currently active function key with a short description of each key.
RESULTS	Displays the results of any calculations performed and permits a hard copy printout of these results. <i>Optional</i>
TADSOFF	Allows the generation of user-defined programs for operation on TADS data.
AUTOMODE	Allows the development, execution, storage, and recall of a set of instructions for the automatic setup and analysis of samples (DSC-2C).
PARTIAL AREAS	Allows for advanced peak analysis of complex heating and cooling curves.
KINETICS	Allows for the determination of the kinetic parameters of a data curve.
PURITY	Allows for the determination of the absolute purity of highly crystalline compounds.

Figure 12.15 (60). The curve peak onset and maximum temperatures, 249.47 and 261.01°C, respectively, as well as the peak area of 16.82, are presented.

Perkin-Elmer 7500 Professional Computer. This computer system is used as an integral part of the Perkin-Elmer 7 Series Thermal Analysis System consisting of the DSC7 and TGA7 modules. The computer uses a M68000 8MHz microprocessor, 1.64Mbytes of RAM, 32 Kbytes of ROM, two double-sided, double-density 5.25 in. floppy disk drives, a 13-in. color or monochrome CRT, and a variety of different plotters or printers. One novel feature of the system is the multiple-tasking design permitting simultaneous operation of multiple thermal analysis instruments. An extensive library of thermal analysis and general-purpose software programs are available for use with this computer.

A partial list of TGA 7 software commands is as follows:

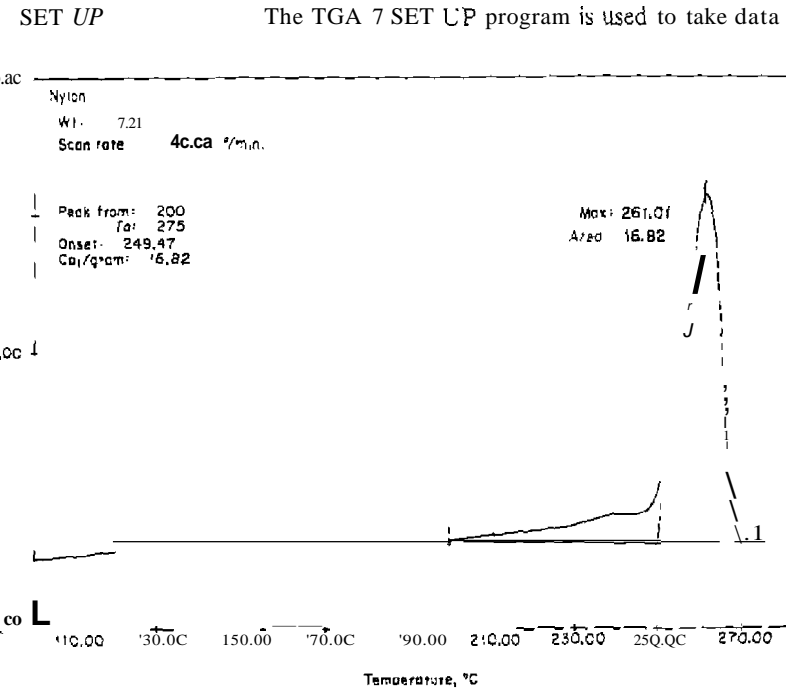


Figure 12.15 DSC curve of the fusion of nylon as plotted by the Perkin-Elmer TADS system (61).

	from the TOA 7. It includes routines for direct TOA control from the computer keyboard. Other options include heat, cool, and isothermal modes of operation, multistep program development, and operation in either temperature or time scales.
DELTA Y	The DELTA Y program permits the calculation of percent weight changes at any point on a TG curve. Options include the total percent weight change and the temperature or time limits over which the weight change has been calculated.
ONSET	The ONSET program permits the quantitative determination of the onset temperature or time of a weight loss or weight gain.
PLOT	The PLOT program is used to obtain a hard copy printout of TG data, results, and calculations.
OPTIMIZE	The OPTIMIZE programs are a series of software programs that are used to optimize TG data curves. Programs are available for rescaling the temperature or time axes, the ordinate axis, and shifting curves.
RECALL	The RECALL program is used to recall to the screen data, results, and run parameters that are stored on disk. Options include recalling a single curve, multiple curves, and curves of different techniques (i.e., TO and DSC curves).
SAVE	The SAVE program permits the storage of data, results, calculations, optimized curves, calculated curves, and comments on the disk.
CALIBRATE	The CALIBRATE programs permit automatic mass and temperature calibration of the TGA 7 analyzer.
CALCULATIONS	The CALCULATIONS programs permit a wide variety of calculations to be performed on TO data. Programs for curve subtraction and derivative calculations are available.
For the DSC 7, a partial list of some of the software programs include:	
SETUP	The SETUP program is used to set up and take data from the analyzer. It includes routines for direct instrument control from the computer keyboard. Other options include heat, cool, and isothermal

	modes of operation, multistep program development, and operation in either temperature or time scales.
PEAK	The PEAK program permits the calculation of the parameters of any peak. Options include peak area calculation, peak maximum, minimum temperature or time, peak onset temperature or time, and the calculation of the peak height.
GLASS TRANSITION	The GLASS TRANSITION program permits the calculation of the parameters of a glass transition. Options include the glass transition onset and midpoint temperature, as well as the change in the specific heat before and after the glass transition.
ONSET	The ONSET program permits the quantitative determination of the onset temperature or time of a transition, such as in oxidative stability testing or decomposition testing.
PLOT	The PLOT program is used to obtain a hard copy printout of DSC 7 data, results, and calculations.
OPTIMIZE	The OPTIMIZE programs are a series of software programs that are used to optimize DSC 7 data curves. Programs are available for rescaling the temperature- or time axis, the energy axis, shifting curves, resloping curves, and aligning curves.
RECALL	The RECALL program is used to recall to the screen data, results, and run parameters that are stored on disk. Options include recalling a single curve, multiple curves, and curves of different techniques (i.e., DSC and TO curves) for direct data comparison.
SAVE	The SAVE program permits the storage of raw data, results, calculations, optimized curves, calculated curves, and comments on the disk.
CALIBRATE	The CALIBRATE programs permit the automatic calibration of either the DSC temperature axis, the DSC energy axis, or both axes simultaneously.
BASELINE OPTIMIZATION	The BASELINE OPTIMIZATION program permits automatic baseline optimization of any DSC scan.
CALCULATIONS	The CALCULATIONS programs permit a wide variety of calculations to be performed on DSC data. Programs for curve subtraction, nonnormalization, and derivative calculations are available, and so on.

b. Du Pont Model 1090 Thermal Analysis System

The Du Pont Model 1090 thermal analyzer is a complete, multi-microprocessor-based thermal analysis system of modular design, with a complete library of software programs for data analysis. It is a compact unit consisting of a temperature programmer, printer/plotter, visual display, and two 8-in. floppy disks. Plug-in TA modules include a DSC cell, DTA cells, thermobalance, TMA and DMA modules, and so on. A built-in keyboard is used to enter one-stroke programming and operating commands; the status of these commands is visible on the plasma display. Data storage is on one or two 8-in. double-sided, double-density floppy drives of 500 Kbytes each. A RS-232 port permits bidirectional communication with external computers to permit off-line data handling as well as remote control of the instrument.

The instrument can perform four tasks simultaneously, as shown in Figure 12.16. They are:

- .. Collect data from a current experiment.
- Play back and plot data from a previous experiment, even if collected

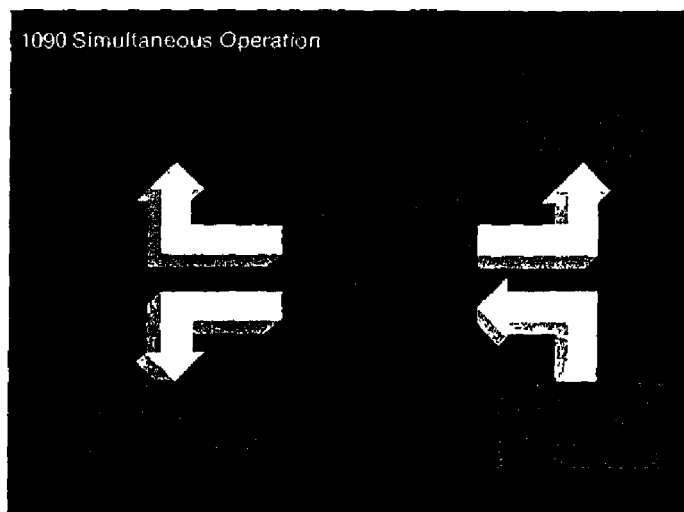


Figure 12.16. Simultaneous operation of the Du Pont Model 1090 thermal analyzer (12).

3. Analyze data from a third experiment.
4. Set up instrument conditions for a fourth experiment.

In addition, the RS-232 port can be used simultaneously during data collection and analysis to transmit data to an external computer and to receive commands from the computer to provide automated setup of instrument conditions.

A comprehensive library of module specific software programs are available, including:

1. Analysis of transitions.
 - a. Onset temperature: crystallization, melting point, and decomposition.
 - b. Onset time.
 - c. Peak temperatures: first-order transitions, derivative curves.
 - d. Peak time.
 - e. Step temperatures: second-order transitions, weight loss onset, penetration.
 - f. Step magnitude; change in heat capacity, weight loss.
2. Integration methods.
 - a. Peak integration: heat of fusion, DTG, heat of crystallization.
 - b. Partial integration: overlapping transitions, fractional areas.
 - c. Cumulative integration: enthalpy, liquid fraction.
3. File modification utility.
 - a. Curve subtraction, addition, and normalization.

c. Mettler TC10 TA Processor

The Telo TA Processor is the basic unit for all configurations of the Mettler TA3000 thermal analysis system. All control commands for the particular module, DSC cell, thermobalance, TMA unit, and so on, are entered via the 21-key splash-resistant plastic-covered keyboard. A 20-character alphanumeric display permits the use of a dialog mode between operator and instrument. All evaluation software and the standard programs are in ROM. Accumulated experimental data are stored in RAM and subsequently processed for display and other purposes. The unit has a data input connection for the measuring module but requires an additional data interface for a printer/plotter or an external computer. An analog output connector is provided for an external strip-chart recorder.

The following software programs are in ROM:

1. Dse
 - a. SCREEN: Complete curve with section expansion and first derivative.
 - b. INTEG: Peak integration.
 - c. PLRITY: Purity determinations.
 - d. OXSTAB: Oxidation stability (isothermal and dynamic).
 - e. CRYST: Crystallinity of polymers.
 - f. GTRANS: Glass transition temperature.
 - g. KINETIC: Reaction kinetics.
 - h. CP: Specific heat.
2. TG
 - a. SCREEN: Same as DSC.
 - b. STEP: Automatic determination and evaluation of weight steps in percent of absolute values.
 - c. KINETIC: Determination of reaction kinetics.

A typical DSC curve peak integration is shown in Figure 12.17. In the fusion of dimethyl terephthalate, the peak maximum temperature found was 139.4°C with a ΔH_f of 66.853 J/g.

d. Stanton-Redcroft System

The Stanton-Redcroft DAPS 2 on-line data processing system employs a four-channel IEEE 488 data acquisition unit connected between the TG, DTA, or TMA module and a Commodore PET 4032 microcomputer. The computer contains a dual-drive floppy disk system, a high-speed digital tape unit, a high-resolution graphics board, and a Hiplot 6-color plotter. A number of software programs are available for calculation of oxidative inductive stability, time-to-ignition, degree of cure, curve integration, and so on.

REFERENCES

1. Soulen, J. R., *Anal. Chem.*, **34**, 136 (1962).
- Schempf, J. M., F. D. Freeburg, D. J. Roger, and F. M. Angeloni, *Anal. Chem.*, **38**, 520 (1966).
3. Sestak, J., A. Brown, V. Rihak, and G. Berggren, *Thermal Anal.*, R. F. Schwenker and P. D. Gam. eds., Vol. 2, Academic, New York, 1969, pp. 1035, 1085.
4. Freeman, E. S., and B. Carroli, *J. Phys. Chem.*, **62**, 394 (1958).

```
PEAK INTEGRATION
DYN/ISO      2/2
ALTO LIMIT   011
START        136
END          :42
BASELINE TYPE 9
PLOT CM      :0
PLOT MODE    :C1
```

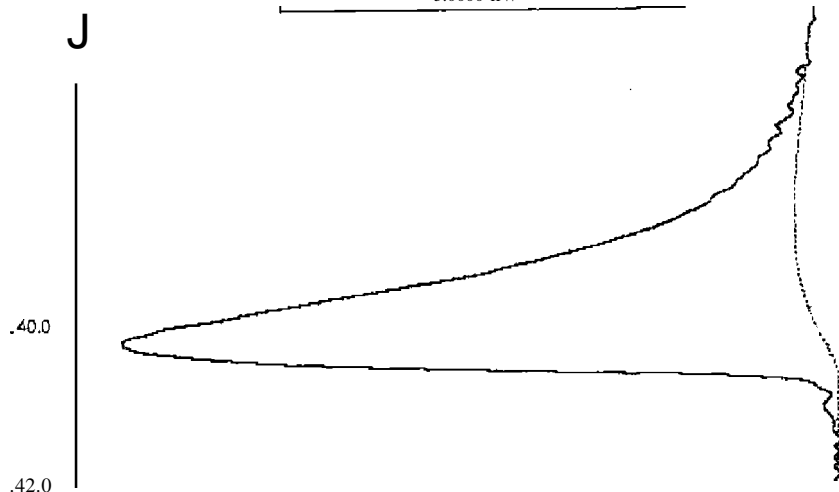
DIMETHYL TEREPHTHALATE

WARNING

TEMPERATURE °C

HEAT FLOW
EXOTHERMAL —

5.0000 mW



```
ΔH ENDO mJ      334.26
ΔH JIG         66.853
PEAK TEMP. °C  139.4
```

***** METTLER TA3000 SYSTEM *****

Figure 12.17. Curve peak integration for dimethyl phthalate using the Mettler TeO TA processor and the Mettler TA 3000 system.

5. Yuen. H. K., W. A. Grote. and R. C. Young, *Thermochim. Acta*, 42, 305 (1980).
6. Dodman, A., A. R. Gregges, and E. M. Barrall, *EBM J. Res. Dev.*, 22, 81 (1978).
7. Gallagher, P. K., and F. Schrey, *Thermal Anal.*, R. F. Schwenker and P. D. Garn, eds., Vol. 2, Academic, New York, 1969, p. 929.
8. Gallagher, P. K., and F. Schrey, *Thermochim. Acta*, 1, 465 (1970).
9. Gallagher, P. K., and D. W. Johnson, *Thermochim. Acta*, 2, 413 (1971).
10. Gallagher, P. K., and D. W. Johnson, *Thermochim. Acta*, 3, 303 (1972).
11. Gallagher, P. K., and D. W. Johnson, *Thermochim. Acta*, 5, 455 (1973).
12. Johnson, D. W., and P. K. Gallagher, *J. Phys. Chem.*, 75, 179 (1971).
13. Gallagher, P. K., F. Schrey, and B. Prescott, *Thermochim. Acta*, 2, 405 (1971).
14. Ozawa, T., *J. Thermal Anal.*, 2, 301 (1970).
15. Zsako, J., *J. Phys. Chem.*, 72, 2406 (1968).
16. Zsako, J., C. Varhelyi, and M. Agosescu, *Studia Babes-Bolyai Univ.*, 2, 33 (1970).
17. Zsako, J., Ref. 16, p. 113.
18. Sharp, I. H., and S. A. Wentworth, *Anal. Chem.*, 41, 2060 (1969).
19. Reich, L., W. Gregory, and S. S. Stivala, *Thermochim. Acta*, 4, 493 (1972).
20. Vachuska, J., and M. Voboril, *Thermochim. Acta*, 2, 379 (1971).
21. Vachuska, J., and N. Rykalo, *GIER Computer Library, NRI, Czech. Acad. Sci.*, No. 1064.
22. Rykalo, N., and J. Vachuska, *GIER Computer Library, NRI, Czech. Acad. Sci.*, No. 1399.
23. Hughes, M. A., and R. Hart, *LeTA III, Davos, Switzerland, August 23-28, 1971, paper No. 1-21*.
24. Gayle, I. B., and C. T. Egger, *Anal. Chem.*, 44, 421 (1972).
25. Reed, R. L., L. Weber, and B. S. Gottfried, *Ind. Eng. Chem. Fundam.*, 4, 38 (1965).
26. Borckardt, H. I., and F. Danieš, *J. Am. Chem. Soc.*, 79, 41 (1957).
27. Kissinger, H. E., *Anal. Chem.*, 29, 1702 (1957).
28. Skvara, F., and V. Satava, *J. Thermal Anal.*, 2, 325 (1970).
29. Wilburn, F. W., J. R. Hesford, and I. R. Flower, *Anal. Chem.*, 40, 777 (1968).
30. Meiling, R., F. W. Wilburn, and R. M. McIntosh, *Anal. Chem.*, 41, 1275 (1969).
31. David, D. I., D. A. Ninke, and B. Duncan, *Am. Lab.*, January 1971, p. 31.
32. Amstutz, D., *ICTA III, Davos, Switzerland, August 23-28, 1971, paper 1-39*.
33. Joy, E. F., I. D. Bonn, and A. I. Barnard, *Thermochim. Acta*, 2, 57 (1971).
34. Driscoll, G. L., I. N. Duling, and F. Magnotta, in *Analytical Calorimetry*, R. S. Porter and I. F. Johnson, eds., Vol. 1, Plenum, New York, 1968, p. 271.
35. Driscoll, G. L., I. N. Duling, and F. Magnotta, *Quart. (Sun Oil Co.)*, 3, 24 (1969).
36. Barrall, E. M., and R. D. Diiler, *Thermochim. Acta*, 1, 509 (1970).
37. Scott, L. R., and A. P. Gray, *Perkin-Elmer Instrument News*, 19, No. 3, 1 (1969).
38. Ellerstein, S. M., in *Analytical Calorimetry*, R. S. Porter and I. F. Johnson, eds., Vol. 1, Plenum, New York, 1968, p. 279.
39. Gray, A. P., *Perkin-Elmer Instrument News*, 20, 8 (1969).
40. Crossley, R. W., E. A. Dorko, and R. L. Diggs, in *Analytical Calorimetry*, R. S. Porter and I. F. Johnson, eds., Vol. 2, Plenum, New York, 1970, p. 429.
41. Kauffman, G. B., and G. Beech, *Thermochim. Acta*, 1, 99 (1970).
42. Rogers, R. N., and L. C. Smith, Ref. 41, p. 1.
43. Heuvic, H. M., and K. C. I. B. I., *Anal. Chem.*, 42, 1044 (1970).
44. Sondack, D. L., *Anal. Chem.*, 44, 888 (1972).
45. Gayer, K. H., and I. Bartel, *Thermochim. Acta*, 3, 337 (1972).
46. Friedman, H. L., *J. Macromol. Sci.*, A1, 57 (1967).
47. Friedman, H. L., G. A. Griffith, and H. W. Goldstein, in *Thermal Analysis*, R. F. Schwenker and P. D. Garn, eds., Vol. 1, Academic, New York, 1969, p. 405.
48. Friedman, H. L., *Thermochim. Acta*, 1, 199 (1970).
49. Gibson, E. K., *Thermochim. Acta*, 5, 243 (1973).
50. Pfeil, R. W., in *Proceedings of the Third Toronto Symposium on Thermal Analysis*, H. G. McAdie, ed., Chemical Institute of Canada, Toronto, 1969, p. 187.
51. Gornick, F., *J. Polym. Sci.*, Part C, 25, 131 (1968).
52. Morie, G. P., T. A. Powers, and C. A. Glover, *Thermochim. Acta*, 3, 259 (1972).
53. Sakamoto, R., T. Ota, and M. Kanazaski, Ref. 52, p. 291.
54. Doelman, A., A. R. Gregges, and E. M. Barrall, *Analytical Calorimetry*, R. S. Porter and I. F. Johnson, eds., Vol. IV, Plenum, New York, p. 1.
55. Gyulai, G., and E. I. Greenhow, *Thermochim. Acta*, 6, 239 (1973).
56. Vernon, G. A., *NWC TP 6337, Naval Weapons Center, China Lake, CA, August, 1982*.
57. Rogers, R. N., *Thermochim. Acta*, 3, 437 (1972).
58. Dunn, J. G., B. T. Sturman, and W. Van Bronswijk, *Thermochim. Acta*, 37, 337 (1980).
59. Brennan, W. P., and M. P. DiVito, *Am. Lab.*, Jan. 1984.
60. *Perkin-Elmer TADS Information Bulletin*, Perkin-Elmer Corp., Norwalk, CT, June 1980.
61. Du Pont (90 Thermal Analysis System), DuPont Co., Wilmington, DE.
62. Yuen, H. K., G. W. Mappes, and W. A. Grote, *Thermochim. Acta*, 52, 143 (1982).
63. Yuen, H. K., and G. W. Mappes, *Thermochim. Acta*, in press (1983).

THERMAL ANALYSIS NOMENCLATURE

A. INTRODUCTION

In 1967, McAdie (1) reported the recommendations of the committee on standardization of the International Confederation of Thermal Analysis for reporting DTA or *TO* data. To accompany each DTA or TG curve, the following information should be reported:

1. Identification of all substances (sample, reference, diluent) by a definitive name, an empirical formula, or equivalent compositional data.
2. A statement of the source of all substances, details of their histories, pretreatments, and chemical purities, so far as these are known.
3. Measurement of the average rate of linear temperature change over the temperature range involving the phenomena of interest.
4. Identification of the sample atmosphere by pressure, composition, and purity; whether the atmosphere is static, self-generated, or dynamic through or over the sample. Where applicable, the ambient atmospheric pressure and humidity should be specified. If the pressure is other than atmospheric, full details of the method of control should be given.
5. A statement of the dimensions, geometry, and materials of the sample holder, and the method of loading the sample where applicable.
6. Identification of the abscissa scale in terms of time or temperature at a specified location. Time or temperature should be plotted to increase from left to right.
7. A statement of the methods used to identify intermediates or final products.
8. Faithful reproduction of all original records.
9. Wherever possible, each thermal effect should be identified and supplementary supporting evidence stated.

In the reporting of TG data, the following additional details are also necessary:

10. Identification of the thermobalance, including the location of the temperature-measuring thermocouple.
11. A statement of the sample weight and weight scale for the ordinate. Weight loss should be plotted as a downward trend, and deviations from this practice should be clearly marked. Additional scales (such as fractional decomposition or molecular composition) may be used for the ordinate where desired.
12. If derivative thermogravimetry is employed, the method of obtaining the derivative should be indicated and the units of the ordinate specified.

When reporting DTA curves, these specific details should be presented:

10. Sample weight and dilution of the sample.
11. Identification of the apparatus, including the geometry and materials of the thermocouples and the locations of the differential and temperature-measuring thermocouples.
12. The ordinate scale should indicate deflection per *AC* at a specified temperature. Preferred plotting will indicate upward deflection as a positive temperature differential, and downward deflection as a negative temperature differential, with respect to the reference. Deviations from this practice should be clearly marked.

In 1969, Mackenzie (2), Chairman of the ICTA Nomenclature Committee, published the first definitive nomenclature report. These recommendations should be adhered to in all English-language publications in thermal analysis. The recommendations are as follows.

B. GENERAL RECOMMENDATIONS

1. *Thermal analysis* and not *thermography* should be the acceptable name in English, since the latter has at least two other meanings in this language, the major one being medical. The adjective should then be thermoanalytical (cf. physical chemistry and physicochemical); the term *thermoanalysis* is not supported (on the same logical basis).
2. *Differential* should be the adjectival form of difference; *derivative* should be used for the first derivative (mathematical) of any curve.

3. The term *analysis* should be avoided as far as possible, since the methods considered do not comprise analysis as generally understood chemically; terms such as *differential thermal analysis* are too widely accepted however, to be changed.
4. The term *curve* is preferred to *thermogram* for the following reasons:
 - a. Thermogram is used for the results obtained by the medical technique of thermography.
 - b. If applied to certain curves (such as thermogravimetric curves), "thermogram" would not be consistent with the dictionary definition.
 - c. For clarity there would have to be frequent use of terms such as *differential thermogram*, *thermogravimetric thermogram*, and so on, which are not only cumbersome but also confusing.
5. In multiple techniques, *simultaneous* should be used for the application of two or more techniques to the same sample at the same time; *combined* would then indicate the use of separate samples for each technique.
6. *Thermal decomposition* and similar terms are being further considered by the committee.

C. TERMINOLOGY

Acceptable names and abbreviations, together with names which were for various reasons rejected, are listed in Table 13.1. The committee is in accord

Table 13.1. Recommended Terminology

Acceptable Name	Acceptable Abbrev.	Rejected Name(s)
<i>General</i>		
Thermal analysis		Thermography Thermoanalysis
<i>Methods associated with weight change</i>		
I. Static		
Isobaric weight-change determination		
Isothermal weight-change determination		Isothermal thermogravimetric analysis

Acceptable Name	Acceptable Abbrev. ^a	Rejected Names ^b
2. Dynamic Thermogravimetry	TG	Thermogravimetric analysis Dynamic thermogravimetric analysis
Derivative thermogravimetry	DTG	Differential thermogravimetry Differential thermogravimetric analysis Derivative thermogravimetric analysis
<i>Methods associated with energy change</i>		
Heating curves ^c		Thermal analysis
Heating rate curves ^b		Derivative thermal analysis
Inverse heating rate curves ^b		
Differential thermal analysis	DTA	Dynamic differential calorimetry
Derivative differential thermal analysis		
Differential scanning calorimetry	DSC	
<i>Methods associated with evolved volatiles</i>		
Evolved gas detection	EGD	Effluent gas detector.
Evolved gas analysis ^d	EGA	Effluent gas analysis Thermovaporimetric analysis
<i>Methods associated with dimensional change</i>		
Dilatometry		
Derivative dilatometry		
Differential dilatometry		
<i>Multiplex techniques</i>		
Simultaneous TG and DTA, etc.		DATA. (Differential and thermogravimetric analysis) Derivatography Derivatographic analysis

^aAbbreviations should be in capital letters without full stops, and should be kept to the minimum to avoid confusion.

^bWhen determinations are performed during the cooling cycle these become cooling curves, cooling rate curves, and inverse cooling rate curves, respectively.

^cThe method of analysis should be clearly stated and abbreviations such as MTA (mass-spectrometric thermal analysis) and MDTA (mass spectrometry and differential thermal analysis) avoided.

with the suggestion, made during discussion of the report, that the limited number of abbreviations considered permissible should be adopted internationally, irrespective of language.

The committee did not wish to pronounce on nomenclature in borderline techniques (such as thermometric titrimetry or calorimetry) which are, to its knowledge, being considered by other bodies. Consideration of techniques not yet extensively employed has been deferred.

D. DEFINITIONS AND CONVENTIONS

1. General

Thermal analysis. A general term covering a group of related techniques whereby the dependence of the parameters of any physical property of a substance on temperature is measured.

2. Methods Associated with Weight Change

a. Static

Isobaric Weight-change Determination. A technique of obtaining a record of the equilibrium weight of a substance as a function of temperature (T) at a constant partial pressure of the volatile product or products.

The record is the isobaric weight-change curve: it is normal to plot weight on the ordinate with weight decreasing downward, and T on the abscissa increasing from left to right.

Isothermal Weight-change Determination. A technique of obtaining a record of the dependence of the weight of a substance on time (t) at constant temperature.

The record is an isotherm weight-change curve: it is normal to plot weight on the ordinate with weight decreasing downward, and t on the abscissa increasing from left to right.

b. Dynamic

Thermogravimetry (TG). A technique whereby the weight of a substance, in an environment heated or cooled at a controlled rate, is recorded as a function of time or temperature.

The record is the thermogravimetric or TG curve: the weight should be plotted on the ordinate with weight decreasing downward, and t or T on the abscissa increasing from left to right.

Derivative Thermogravimetry (DTG). A technique yielding the first derivative of the thermogravimetric curve with respect to either time or temperature.

The curve is the derivative thermogravimetric or DTG curve; the derivative should be plotted on the ordinate with weight losses downward, and t or T on the abscissa increasing from left to right.

E. METHODS ASSOCIATED WITH ENERGY CHANGES

Heating Curves. These are records of the temperature of a substance against time, in an environment heated at a controlled rate.

T should be plotted on the ordinate increasing upward, and t on the abscissa increasing from left to right.

Heating-rate Curves. These are records of the first derivative of the heating curve with respect to time (i.e., dT/dt) plotted against time or temperature.

The function of dT/dt should be plotted on the ordinate, and t or T on the abscissa increasing from left to right.

Inverse Heating-rate Curves. These are records of the first derivative of the heating curve with respect to temperature (i.e., dl/dn) plotted against either time or temperature.

The function of dl/dT should be plotted on the ordinate, and t or T on the abscissa increasing from left to right.

Differential Thermal Analysis (DTA). A technique of recording the difference in temperature between a substance and a reference material against either time or temperature as the two specimens are subjected to identical temperature regimes in an environment heated or cooled at a controlled rate.

The record is the differential thermal or DTA curve; the temperature difference (ΔT) should be plotted on the ordinate with endothermic reactions downward, and t or T on the abscissa increasing from left to right.

Derivative Differential Thermal Analysis. A technique yielding the first derivative of the differential thermal curve with respect to either time or temperature.

The record is the derivative differential thermal or derivative DTA curve; the derivative should be plotted on the ordinate, and t or T on the abscissa increasing from left to right.

Differential Scanning Calorimetry (DSC). A technique of recording the energy necessary to establish zero temperature difference between a substance and a reference material against either time or temperature as the two specimens are subjected to identical temperature regimes in an environment heated or cooled at a controlled rate.

The record is the DSC curve; it represents the amount of heat applied per unit time as ordinate against either t or T as abscissa.

F. METHODS ASSOCIATED WITH EVOLVED VOLATILES

Evolved Gas Detection (EGD). This term covers any technique of detecting whether or not a volatile product is formed during thermal analysis.

Evolved Gas Analysis (EGA). A technique of determining the nature and amount of volatile product or products formed during thermal analysis.

C. METHODS ASSOCIATED WITH DIMENSIONAL CHANGE

Dilatometry. A technique whereby changes in dimension(s) of a substance are measured as a function of temperature. The record is the dilatometric curve.

Derivative Dilatometry: Differential Dilatometry. These terms carry the connotations given in 1(b).

H. MULTIPLE TECHNIQUES

This term multiple techniques covers simultaneous DTA and TG and other techniques, and definitions follow from the preceding discussion.

Mackenzie et al. (3) protested the use of the term *thermogravimetric analysis* (TGA) as used by Still and Cluley (4). They suggested that this technique was simply a branch of evolved-gas analysis, for which the abbreviation EGA has been internationally accepted. The IeTA Nomenclature Committee regards the coining of abbreviations for what are variants of an accepted term as completely indefensible, and would urge all scientists to give serious consideration to the implications of introducing and publishing new abbreviations or complicated terminology.

In a second report of the Nomenclature Committee by Mackenzie et al.

(5), the following more definitive recommendations were published:

I. DTA

The *sample* is the actual material investigated, whether diluted or undiluted.

The *reference material* is a known substance, usually inactive thermally over the temperature range of interest.

The *specimens* are the sample and reference material.

The *sample holder* is the container or support for the sample.

The *reference holder* is the container or support for the reference material.

The specimen-holder assembly is the complete assembly in which the specimens are housed. Where the heating or cooling source is incorporated in one unit with the containers or supports for the sample and reference material, this would be regarded as part of the specimen-holder assembly.

A *block* is a type of specimen-holder assembly in which a relatively large mass of material is in intimate contact with the specimen holders.

The *differential thermocouple* or ΔT thermocouple is the thermocouple system used to measure temperature difference. Should another thermosensing device be used, its name should replace "thermocouple."

J. TG

A *thermobalance* is an apparatus for weighting a sample continuously while it is being heated or cooled.

The *sample* is the actual material investigated, whether diluted or undiluted. Samples used in TG are normally not diluted, but in simultaneous TG and DTA diluted samples might well be used.

The *sample holder* is the container or support for the sample.

K. DTA AND TG

The *temperature thermocouple* or T thermocouple is the thermocouple system used to measure temperature: its position with respect to the sample should always be stated. Should another thermosensing device be used, its name should replace "thermocouple."

The *heating rate* is the rate of temperature increase, which is customarily quoted in degrees per minute (on the Celsius or Kelvin scales). Correspondingly, the cooling rate is the rate of temperature decrease. The heating or cooling rate is said to be *constant* when the temperature-time curve is linear.

In simultaneous DTA-TG, definitions follow from those given for DTA and TG separately.

The following definitions are to be used in conjunction with those previously reported (1, 2) for DTA and TG data.

L. DTA

In DTA it must be remembered that although the ordinate is conventionally labeled ΔT , the output from the ΔT thermocouple will in most instances vary with temperature, and the measurement recorded is normally the emf. output, E , [the conversion factor, b , in the equation $\Delta T = bE$ is not constant; since $b = 1/(nJ)$. A similar situation occurs with other sensor systems.

All definitions refer to a single peak such as that shown in Figure D.1; multiple-peak systems, showing shoulders or more than one maximum or minimum, can be considered to result from superposition of single peaks.

The *baseline* (Figure 13.1, AB and DE) corresponds to the portions of the DTA curve for which ΔT is approximately zero.

A *peak* (Figure 13.1, BCD) is that portion of the DTA curve which departs from, and subsequently returns to, the baseline.

An *endothermic peak* or *endotherm* is a peak where the temperature of the sample falls below that of the reference material (i.e., ΔT is negative).

An *exothermic peak* or *exotherm* is a peak where the temperature of the sample rises above that of the reference material (i.e., ΔT is positive).

Peak width (Figure 13.1, $B'D'$) is the time or temperature interval between the points of departure from the return to the baseline.

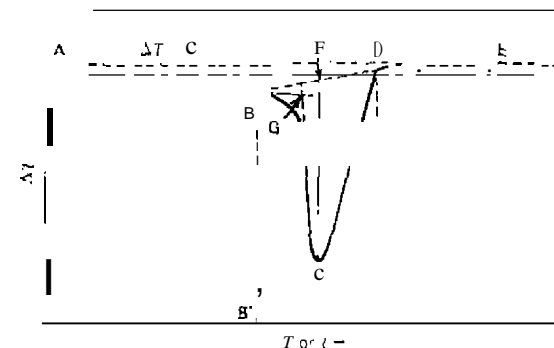


Figure 13.1. Normalized DTA curve (5).

1. CF is the distance, vertical to the time or on the interpolated baseline and the peak tip Figure

, $BCDB$ is the area enclosed between the peak line.

Figure 13.1, G is the point of intersection of the (greatest slope on the leading edge of the peak extrapolated baseline (Figure 13.1, BG).

M. TG

single-stage process such as that shown in Figure can be considered as resulting from a series of

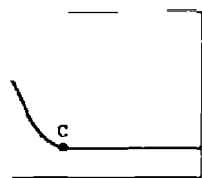
steps that part of the TG curve where the weight

Figure 13.2, B is that temperature (on the which the cumulative weight change reaches a value can detect.

Figure 13.2, C is that temperature (on the which the cumulative weight change reaches a

temperature difference between T_i and T_f as

the recommendations of IATA concerning TGA or evolved gas analysis (EGA) curves.



Typical TG curve (5).

1. Identification of all substances (sample, reference, diluent) by a definitive name, an empirical formula, or equivalent compositional data.
1. A statement of the source of all substances, and the details of their histories, pretreatments, and chemical purities, so far as these are known.
3. A clear statement of the temperature environment of the sample during reaction.
4. Measurement of the average rate of linear temperature change over the temperature range involving the phenomena of interest. Non-linear temperature programming should be described in detail.
5. A statement of the dimensions, geometry, and materials of the sample holder, and the method of loading the sample where applicable.
6. Identification of the abscissa scale in terms of time or temperature at a specified location. Time or temperature should be plotted to increase from left to right.
7. Identification of the ordinate scale in specific terms where possible. In general, increasing concentration of evolved gas should be plotted upward. For gas density detectors, increasing gas density should also be plotted upward. Deviations from these practices should be clearly marked.
8. A statement of the methods used to identify intermediate or final products.
9. Faithful reproduction of all original records.
10. Identification of the sample atmosphere by pressure, composition, and purity, and by whether the atmosphere is self-generated or dynamic through or over the sample. The flow rate, total volume, construction, and temperature of the system between the sample and detector should be given, together with an estimate of the time delay within this system.
- II. Identification of the apparatus used by type and commercial name, together with details of the location of the temperature-measuring thermocouple and the interface between the systems for sample heating and detecting or measuring evolved gases.
12. In the case of EGA, when exact units are not used, the relationship between signal magnitude and concentration of species measured should be stated. For example, the dependence of the flame ionization signal on the number of carbon atoms and their bonding, as well as on concentration, should be given.

REFERENCES

1. McAdie, H. G. • *Anal. Chem.* 39, 543 (1967).
2. Mackenzie, R. C. *Talanta*, 16, 1227 (1969).
3. Mackenzie, R. C., C. J. Keatch, A. A. Hodgson, and J. P. Redfern, *Chem. Ind.*, 272 (1970).
4. Still, J. E. and H. J. Cille, *Chem. Ind.*, 1771 (1969)
5. Mackenzie, R. C., C. J. Keatch, D. Dollimore, J. A. Forrester, A. A. Hodgson, and J. P. Redfern, *Thermochim. Acta*, 5, 71 (1972).
6. McAdie, H. G. • *Anal. Chem.* 44, 640 (1972).

INDEX

- Accelerating rate calorimetry, 747
 applications, 753
 instrumentation, 748
 theory, 75:
- Additive content of polymers, TO of, 195
- Alkaline earth oxalates, TO of, 148
- Alkaline earth salt hydrates, TG of, 147
- Alumina, specific heat of, 442
- Alumina whiskers, 152
- Aluminum oxide, TO of, 151
- Ammonium dichromate, 154
- Ammonium nitrate, DTA of, 396
- Ammonium perchlorate, DTA of, 390
- Analgesics, TG of, 184
- Anderson et al. equation, 291
- Anisaldazine, DTA of, 418
- Antacids, TG of, 186
- Aortic-GAG-LDL complex, DSC of, 368
- Applied electrical fields, 733
- Archaeological dating, 607
- Arrhenius equation, 59
- Aspirin, TG of, 184
- Automatic gravimetric analysis, 201
- Bascom Turner data center recorder, 108
- Benzoic acid, DTA of, 409
- Biphenyl, DTA of, 435
- Boersma equation, 218
- Borchert and Daniels equation, 285, 286
- n-Butane, DTA of, 411
- Cahn electrobalance, 92
- Calcium acetate, 161
- Calcium bromides hydrate, TG of, 148
- Calcium carbonate, TG of, 21
- Calcium chromate, TG of, 156
- Calcium silicate, TG of, 158
- Catalyst reactions, DSC of, 369
- Cellulose, DTA of, 388
- Chemical Abstracts*, 8
- Chevenard thermobalance, III
- Clausius-Clapeyron equation, 234
- Coal, TG of, 143
- Coal samples, DSC of, 385
- Cobalt complexes, TG of, 166
- Cobalt sulfate 7-hydrate, DTA of, 239
- Commercial thermal analysis instrumentation, 786
- Computers:
 application to DTA/DSC, 779
 application to EGA, 783
 application to TG, 765
- Coordination compounds, TG of, 164
- Copper (II) acetate, TG of, 160
- Copper sulfate 5-hydrate, DTA of, 261
- Copper (II) tartrate, TG of, 163
- Cryoscopic methods, 627
 instrumentation, 635
- Current-voltage, 727
- Davis et al. equation, 291
- Derivatograph, 113
- Diamonds, TG of, 168
- Dielectric constant, 718
 applications of, 724
 instrumentation for, 720
- Differential thermal analysis:
 automated, 333
 calibration of, 270
 constant sensitivity, 272
 definition, 213
 high pressure, 325
 quantitative aspects of, 269
 sample holders, 301
 sealed-tube, 320
 temperature calibration of, 309
 theoretical aspects of, 216
- Differential thermal analysis apparatus, 299
- Differential thermal analysis curve:
 operational parameters, 264

- Differential thermal analysis curves (*Continued*)
 sample characteristics, 258
 typical, 115
- Differential thermal analysis and differential scanning calorimetry, comparison of, 266
- Differential thermal analysis systems:
 DuPont, 349
 Eberbach, 353
 Mettler, 349
 Netzsch, 353
 Perkin-Elmer, 345
 SETARAM, 352
- Differential thermal analysis theory, 222
- Differential thermal analysis thermocouples, 306
 thin-film, 307
- Differential thermal gas analysis, 501
- Differential thermometry, 213
- Diffuse reflectance spectroscopy, 559
- Drying of analytical precipitates, 204
- Doyle's method, 62
- DSC purity determination:
 applications, 664
 experimental methods, 662
- DTNDSC:
 applications of, 361
 applications to biological materials, 363
 applications to catalysts, 369
 applications to clays, 373
 applications to petroleum products, 387
 applications to inorganic materials, 388
 applications to organic materials, 406
 applications to pharmaceuticals, 419
 applications to polymers, 424
 calibration standards, 276
 reaction kinetics methods, 282
 specific heat determination, 442
- DTA/DSC curve:
 factors affecting, 227
 origin of, 359
- DTG curves, comparison with TG, 55
- DuPont 1200 Deg. C. cell, 350
- DuPont high pressure DSC cell, 350
- DuPont Mode 11090 system, 792
- Dynamic thermomechanometry, 67B
- Elastomers, TG of, 195
- Ethanol, DTA of, 445
- Ethylene-vinyl acetate copolymer, TG of, 199
- Evolved gas analysis:
 definition of, 461
 water detection of, 509
- Evolved gas detection:
 automated, 504
 definition of, 461
 temperature calibration of, 500
- Evolved gas detection/evolved gas analysis:
 apparatus, 493
 applications, 533
 coupling with DTA, 489
 coupled with TG, 477
 current techniques, 470
 detectors for, 494
 multiple techniques, 473
- FGA-MS, 508
- Egyptian blue, TG of, 168
- Electrical conductivity, 698
- Emanation thermal analysis, 524
- Final temperature, 10
- Flame ionization detection, 512
- Freeman and Carroll method, 61
- Hectorite, DTA of, 377
- High temperature reflectance spectroscopy, 562
- Horowitz and Metzger method, 61
- HTRS/DRS, application of, 568
- Infrared spectroscopy, high temperature, 583
- Initial temperature, 10
- Journal of Thermal Analysis, 5
- Kaolinite:
 DTA of, 378
 TG of, 140
- Kissinger equation, 229
- Lignite, DTA of, 237
- Lithium glasses, DTA of, 449
- Magnesium acetate, DSC of, 397
- Magnesium sulfate 7-hydrate, DTA of, 238
- Manganese oxalate, DSC of, 396
- Master data method, 67
- Maycock equation, 288
- Magnetic transition temperatures, 106
- Mercury compounds, DSC of, 402

- Mercury (I, m compounds), TG of, 170
- Methanation reaction, DSC of, 371
- Methacqualone, DSC of, 423
- Mettler TC10 system, 793
- Microdistillation, TG use in, 147
- Microrreflectance technique, 594
- Microscopy, fusion, 384
- Miscellaneous sample effects in TG, 37
- Multiple sample holder, 304
- Multiple techniques, 805
- Murray and White equation, 283
- Naphthalene-benzoic acid phase diagram, 444
- National Physical Laboratory, 310
- Nemst quartz microbalance, 11
- Newkirk method, 60
- Nickel, Curie point of, 447
- Nickel-alumina catalyst, TG of, 139
- Nickel sulfide, TG of, 173
- Niobium nitride, TG of, 175
- Nylon 6/6, DTA of, 431
- Oil shale:
 DSC of, 382
 TG of, 145
- Organic acids, DTA of, 408
- Organic derivatives, DTA of, 415
- Organic particulate analysis, 517
- Oxyluminescence, 610
 applications of, 620
 instrumentation of, 618
 kinetics of, 615
 mechanism of, 612
- Ozawa method, 69
- Pacor equation, 220
- Papyrus sheets, DTA of, 448
- Peak temperature, variation with heating rate, 230
- Pentlandite, DTA of, 379
- Perkin-Elmer DTA 1700 system, 349
- Perkin-Elmer systems, 787
- Petroleum pitch, DSC of, 383
- PFHC-methanol, DSC of, 417
- Photothermal analysis, 581
- Pitoyan equation, 284
- Plaster of Paris, DTA of, 375
- Platinum cyano bromide, TG of, 165
- Platinum group oxides, TG of, 179
- Polyadipamide, DTA of, 434
- Polyethylene, DTA of, 429, 432
- Polymer mixture, DTA of, 426
- Polystyrene, TG of, 194
- Polyvinyl chloride, TG of, 196
- Potassium aluminum sulfate, TG of, 1711
- Potassium chlorate, DTA of, 391
- Potassium hydrogen phthalate, TG of, 177
- Potassium nitrate, DSC of, 400
- Potassium permanganate, TG of, 176
- Purity determination by differential scanning calorimetry, 651
- Pyrolysis-gas chromatography, 510
- Quantitative differential thermal analysis/differential scanning calorimetry, precision and accuracy, 280
- Quartz balances, 126
- 8-Quinolol, DTA of, 265
- Reaction interval, 11
- Reconline balances, 89
- Reich equation, 287
- Reich and Stivala method, 68
- Rogers equation, 289
- Rubber, TG of, 198
- Sample container buoyancy, 38
- Sample holder, vapor pressure, 95
- Sample holders, comparison of, 246
- Sample particle size, 35
- Sapphire, DSC of, 275
- SEDEX system, 755
- Sident, TG of, 14
- Silver acetate, 161
- Silver carbonate, DTA of, 401
- Silver citrate, DTA of, 261
- Sodium carbonate, TG of, 181
- Sodium penicillins, DSC of, 420
- Spell equation, 217
- Stanton-Redcroft system, 795
- Starch, DTA of, 365
- Steady state parameter jump method, 67
- Strontium carbonate, DTA of, 237
- Sulfathiazole, DSC of, 421
- Sulfur, DTA of, 395
- Temperature calibration, 100
 fusible link method, 104
- Temperature programmed reduction, 503
- Temperature programmer, DuPont, 311

- Tetramine platinum chloride, TG of, 164
Thénardite, DTA of, 262
Thermal analysis. *See* 1. 213
 definitions of, 803
 nomenclature, 799
 recommended terminology, 801
Thermal Analysis Abstracts, 8
Thermal conductivity of gases, 22
Thermal energy storage materials, 450
Thermal lag, 658
Thermally stimulated discharge, 728
Thermal matrix reactions, 580
Thermal microscopy, 590
Thermobalances, 87
 automated, 127
 DuPont, 112
 high pressure, 130
 Honda, 110
 Mettler, 114
 Perkin-Elmer, 118
 Rigaku, 121
 SETARAM, 123
 Stanton Redcroft, 119
 vapor pressure determinations, 13;
Thermochimica Acta, 8
Thermochromic compounds, 708
Thermocouples, 249
Thermogravimetry:
 applications of, 137
 applications to catalysis, 138
 applications to clays, 139
 applications to fuels, 143
 applications to inorganic compounds, 147
 applications to pharmaceuticals, 184
 applications to polymers, 191
 definition of, 9
 derivative, 52
 isothermal, 10
 mass changes detectable by, 138
 nonisothermal reaction kinetics of, 57
 quasiisothermal, 10
 recording systems, 105
 self-generated atmosphere, 46
 sources of error, 38
Thermogravimetry curves:
 effect of neat sinks on, 27
 errors in, 46
 factors affecting, 12
 optimum sensitivity, 32
Thermoelectrometry, 697
Thermoluminescence, 596
 applications of, 602
 instrumentation of, 600
 kinetics of, 598
Thermomechanical analysis, 672
 instrumentation, 67;
Thermomechanical methods, applications of,
 682
Thermomagnetometry, 740
Thermomolecular beam analysis, 23, 131
Thermoparticulate analysis, 515
Thermophotometry, 559
Thermopile, Mettler, 305
Thermosonometry, 734
 applications of, 736
 instrumentation of, 734
Thermovoltic detection, 728
 applications of, 730
Thin-layer chromatography, 514
Three wire thermocouple, 326
Titanium carbide, TG of, 184
Torsional braid analysis, 681
Tremolite, 270
Triamcinolone diacetate, DTA of, 422
Ugine-Eyraud B70 balance, J24
U.S. Bureau of Standards, J09
Uranyl oxalate, DTA of, 248
Vapor pressure determinations, 205
Vibrin 135 resin, DTA of, 428
Void equation, 217
Zinc hydroxide carbonate, X-ray of, 31